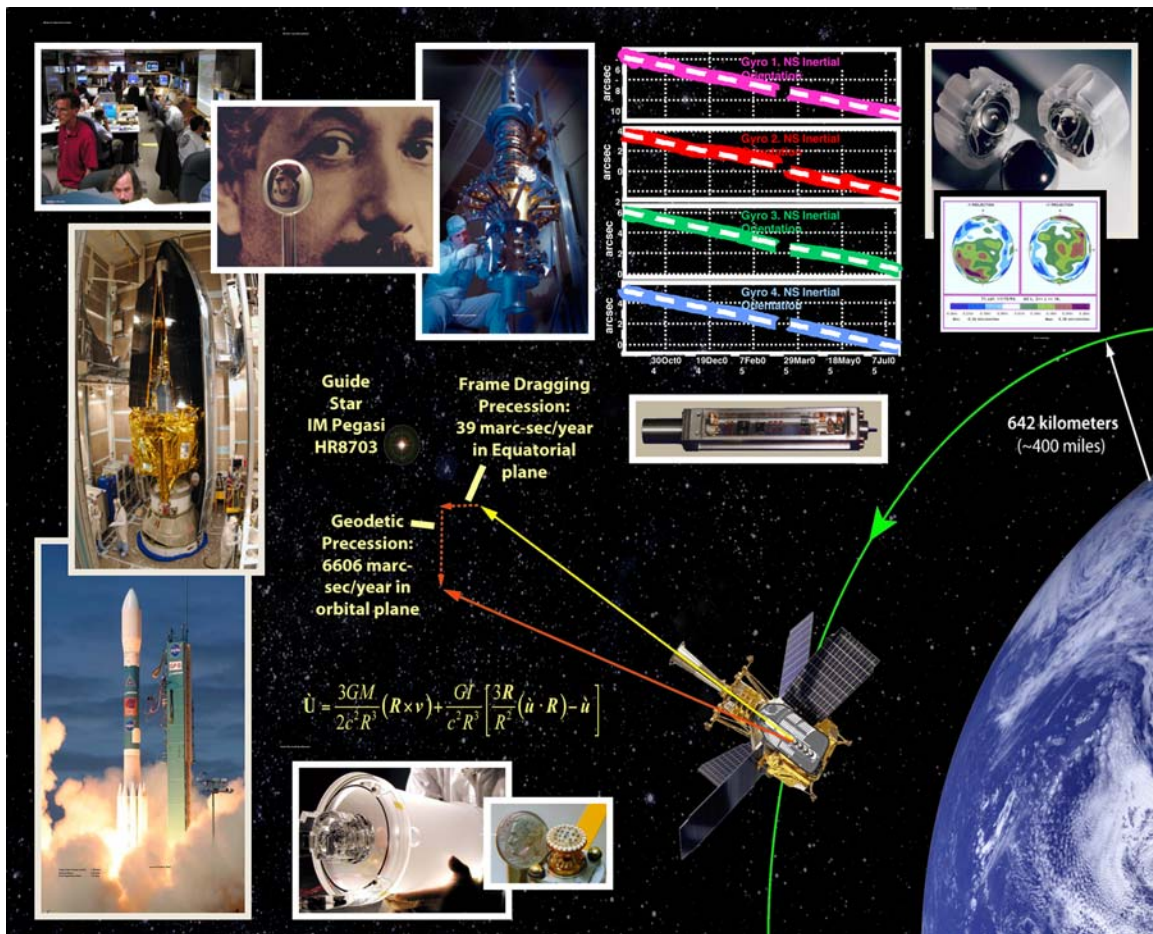


# The Gravity Probe B

## EXPERIMENT

" TESTING EINSTEIN'S UNIVERSE "



## Post Flight Analysis — Final Report

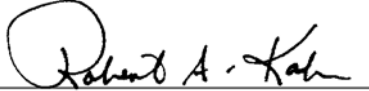
March 2007

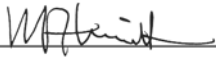


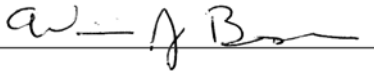


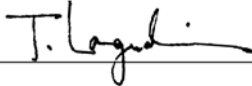
# Signatures & Approvals

---

Prepared by  Public Affairs Coordinator,  
Stanford University September 10, 2007  
Robert Kahn Date

Approved by  Principal Investigator,  
Stanford University September 10, 2007  
Francis Everitt Date

Approved by  Program Manager  
Stanford University September 10, 2007  
William Bencze Date

Approved by  Deputy Program Manager  
Stanford University September 10, 2007  
Tom Langenstein Date

Tom Langenstein: ITAR Assessment performed. ITAR Control required:  Yes  No





# Table of Contents

---

<b>Preface</b> .....	xxvii
<b>1 Executive Summary</b> .....	1
<b>1.1 What is Gravity Probe B?</b> .....	3
<b>1.2 A Quest for Experimental Truth</b> .....	3
<b>1.3 The GP-B Flight Mission</b> .....	4
<b>1.4 The Two Einstein Effects</b> .....	5
<b>1.5 Why Perform Another Test of Einstein?</b> .....	6
<b>1.6 Experimental Design &amp; “Near Zeroes”</b> .....	6
<b>1.7 Unique and Extraordinary Technologies</b> .....	7
1.7.1 The World’s Most Perfect Gyroscopes .....	7
1.7.2 Gyro Suspension System (GSS) .....	8
1.7.3 SQUID Magnetometers for Gyro Orientation Readout .....	9
1.7.4 The Pointing Telescope .....	10
1.7.5 Relating the Guide Star’s Motion to a Distant Quasar .....	11
1.7.6 The Dewar .....	11
1.7.7 Spacecraft Control—Nine Degrees of Freedom .....	13
<b>1.8 The Management Experiment</b> .....	13
<b>1.9 The GP-B Spacecraft</b> .....	14
<b>1.10 On-Orbit Operations</b> .....	16
<b>1.11 Anomaly Resolution</b> .....	18
<b>1.12 Managing Program Risks</b> .....	19
<b>1.13 A Successful Mission</b> .....	20
<b>1.14 The Broader Legacy of GP-B</b> .....	22
<b>2 Overview of the GP-B Experiment &amp; Mission</b> .....	23
<b>2.1 Gravity Probe B in a Nutshell</b> .....	25
2.1.1 A Brief History of GP-B .....	25
2.1.2 Einstein Stands on Newton’s Shoulders .....	31
2.1.3 Why perform another test of Einstein? .....	32
2.1.4 The Geodetic and Frame-dragging Effects .....	33
2.1.5 The Significance of the GP-B Experiment .....	34
2.1.6 The Basic GP-B Experimental Design .....	35
2.1.7 The GP-B Spacecraft .....	36
2.1.8 The Broader Legacy of GP-B .....	42
<b>2.2 Spacecraft Launch</b> .....	43
<b>2.3 Spacecraft Separation</b> .....	44

<b>2.4</b>	<b>Initialization &amp; Orbit Checkout (IOC)</b>	44
2.4.1	Overview of IOC	44
2.4.2	Weekly Summary of IOC Accomplishments	47
2.4.3	Overview of Main IOC Tasks	49
<b>2.5</b>	<b>Science Phase</b>	57
2.5.1	Overview of the Science Phase	57
2.5.2	Monthly Science Phase Highlights	59
<b>2.6</b>	<b>Calibration Phase</b>	61
2.6.1	Overview of the Calibration Phase	62
2.6.2	Weekly Calibration Phase Highlights	62
<b>3</b>	<b>Accomplishments &amp; Technology Innovations</b>	65
<b>3.1</b>	<b>Goals &amp; Accomplishments</b>	67
3.1.1	GP-B's Seven Near Zeroes	67
3.1.2	Noteworthy Accomplishments	68
<b>3.2</b>	<b>Extraordinary Technology of GP-B</b>	69
3.2.1	An Overview of GP-B Technology	69
3.2.2	Redundancy in GP-B Systems and Technology	78
3.2.3	GP-B's Unique Technological Challenges and Solutions	80
<b>3.3</b>	<b>GP-B Technology Transfer</b>	93
<b>4</b>	<b>GP-B On Orbit</b>	95
<b>4.1</b>	<b>Overview of On-Orbit Operations</b>	97
4.1.1	Three Mission Phases	97
4.1.2	Daily Operations Routine	97
4.1.3	NASA Group Achievement Award	98
<b>4.2</b>	<b>Mission Planning</b>	98
4.2.1	Function Charter: What is Mission Planning?	98
4.2.2	Critical Factor: Efficiency	101
4.2.3	Critical Factor: Flexibility	104
4.2.4	Critical Factor: Error-Free	106
<b>4.3</b>	<b>Data Processing</b>	107
4.3.1	General	107
4.3.2	Data Archiving	110
<b>4.4</b>	<b>Orbit Determination</b>	110
4.4.1	The GP-B Mission Orbit Design	111
4.4.2	Launch Requirements	112
4.4.3	Post-Launch Orbit Events	113
4.4.4	Orbit Determination Calculations	114
4.4.5	Conclusions	118
<b>4.5</b>	<b>Computer Hardware</b>	118
4.5.1	Reliability	119
4.5.2	Disk Storage Issues	119
4.5.3	System Design – MOC LAN	120
4.5.4	System Design – SCIENCE LAN	120
4.5.5	Performance	120
<b>4.6</b>	<b>The Integrated Test Facility (ITF)</b>	121

<b>5</b>	<b>Managing Anomalies and Risk</b>	123
5.1	The Spacecraft's Tale	125
5.2	Overview of GP-B Anomalies in Orbit	126
5.3	Anomaly Review Process	126
5.3.1	Anomaly Definitions	126
5.3.2	Anomaly Review Organization	127
5.3.3	Anomaly Assessment	129
5.3.4	Anomaly Room	130
5.3.5	Anomaly Identification and Response Plan	132
5.3.6	Overall Effectiveness of GP-B Anomaly Resolution Process	133
5.4	Risk Analysis	133
5.4.1	Forward to GP-B Risk Management Plan	133
5.4.2	Purpose	133
5.4.3	Risk Management Approach	134
5.4.4	Risk Metric and Items	134
<b>6</b>	<b>The GP-B Management Experiment</b>	139
6.1	The Phases of GP-B Program Management	141
6.2	The Early Years (1959-1984)	142
6.2.1	Concept Development	142
6.2.2	Initial Research	142
6.2.3	Technology Design and Prototyping	144
6.2.4	Transition to a NASA Flight Program	145
6.2.5	GP-B Formalizes Program Management	146
6.2.6	NASA Makes Stanford Prime Contractor on GP-B	148
6.3	Flight Hardware Development (1984-1997)	149
6.3.1	Incremental Prototyping	150
6.3.2	Re-Thinking STORE Post-Challenger	153
6.3.3	Selecting a Spacecraft Subcontractor	153
6.3.4	NASA Funds GP-B as a Flight Program	154
6.3.5	Flight Hardware and Electronics Development	155
6.4	Payload Integration, Testing and Repairs (1997-2002)	156
6.4.1	Devising a Work-around for the Dewar Axial Lock	156
6.4.2	Flight Probe C Integration & Testing	157
6.4.3	Repairing Flight Probe C & Replacing Gyro #4	158
6.4.4	Moving Towards Flight Readiness	158
6.4.5	Changing Focus from Maximizing R&D to Minimizing Risk	159
6.4.6	NASA/MSFC Management of GP-B	159
6.5	Final Integrated Testing, Launch & Science Mission (2002-2005)	163
6.5.1	The Thermal Vacuum Test	163
6.5.2	Six-Month Launch Postponement for ECU Repair	163
6.5.3	Successful Launch and Flight Mission	163
6.6	Data Analysis Period (2005-2007)	164
6.6.1	Final Management Transition at Stanford	164
6.6.2	Gallery of GP-B Program Managers/Deputies at Stanford	165
6.7	Some Observations on the Management Experiment	166

6.8	<b>Sources and References</b>	166
<b>7</b>	<b>Attitude &amp; Translation Control Subsystem Analysis</b>	169
7.1	<b>ATC Background and Overview</b>	171
7.1.1	ATC Hardware	171
7.1.2	Vehicle ATC Modes	172
7.1.3	GS Valid/Invalid	172
7.1.4	Guide Star Verification	173
7.2	<b>He Thruster Technology</b>	173
7.3	<b>ATC Performance</b>	175
7.3.1	Pitch/Yaw Pointing	175
7.3.2	Roll Phase Error RMS	183
7.3.3	Drag-Free Control System	184
7.3.4	Pressure Controller/Mass Flow	186
7.3.5	Calibration Phase	188
7.4	<b>Conclusions and Performance Summary</b>	189
7.5	<b>Flight Challenges/Solutions and Additional Accomplishments</b>	189
7.5.1	Quick vehicle stabilization off Delta II w/ failed thruster	189
7.5.2	Successful recovery from multiple CCCA reboots	190
7.5.3	Supporting higher science roll rate	190
7.5.4	Successful large-scale dither	190
7.5.5	ARP Motion Challenges	191
7.5.6	Proton Activity	195
7.5.7	Star Tracker Magnitude Updates	199
7.5.8	Dewar Slosh Control	199
<b>8</b>	<b>Other Spacecraft Subsystems Analyses</b>	201
8.1	<b>Commands &amp; Data Handling (CDH)</b>	203
8.1.1	Performance	204
8.1.2	Conclusion	206
8.2	<b>Thermal Control Systems (TCS)</b>	206
8.2.1	System Performance	208
8.2.2	QBS and SRE Temperature Control	218
8.2.3	TCS Accomplishments	223
8.2.4	TCS Summary	223
8.3	<b>Electrical Power Systems (EPS)</b>	223
8.3.1	System Features and Capabilities	223
8.3.2	Critical Mission Requirement	224
8.3.3	System Performance	224
8.3.4	EPS Accomplishments	224
8.3.5	Eclipse Cycle	225
8.3.6	Bus Power	225
8.3.7	Batteries	226
8.3.8	Solar Array Power	228
8.3.9	Solar Array Power Degradation Analysis	230
8.3.10	Conclusion	232

<b>8.4</b>	<b>Communications</b> .....	232
8.4.1	TDRSS Operations .....	234
8.4.2	Ground Network Operations .....	235
8.4.3	Communications Anomalies .....	235
8.4.4	Communications—Prime Mission and Beyond .....	239
<b>8.5</b>	<b>Flight Software (FSW)</b> .....	239
8.5.1	Requirements Satisfaction .....	239
8.5.2	Flight Software Statistics .....	241
8.5.3	Test It Like You Fly It .....	242
8.5.4	On-Orbit Software Changes .....	243
8.5.5	Safemode Discussion .....	246
8.5.6	CCCA Single Bit Errors .....	248
8.5.7	CCCA Multi-Bit Errors .....	252
<b>9</b>	<b>Gyro Suspension Subsystem (GSS) Analysis</b> .....	255
<b>9.1</b>	<b>GSS Hardware Description</b> .....	258
9.1.1	Low voltage drive amplifier .....	258
9.1.2	High voltage drive amplifier .....	258
9.1.3	Computer drive .....	259
9.1.4	Position Bridge .....	259
9.1.5	Analog Backup Controllers .....	259
9.1.6	Suspension arbiter .....	260
9.1.7	Mode Register .....	260
9.1.8	Forward Communication Link .....	261
9.1.9	RAD6000 Processor .....	261
9.1.10	Mux and Timing .....	261
9.1.11	Clock synchronization .....	262
9.1.12	Aft Comm Link .....	262
9.1.13	Power supply .....	262
<b>9.2</b>	<b>Suspension Controller Design</b> .....	263
9.2.1	Controller description and space of operation .....	263
9.2.2	Controller performance on Orbit .....	265
9.2.3	Drag-Free control .....	270
<b>9.3</b>	<b>GSS Software</b> .....	274
<b>9.4</b>	<b>References</b> .....	279
9.4.1	Engineering Documents .....	279
<b>10</b>	<b>SQUID Readout Subsystem (SRE) Analysis</b> .....	281
<b>10.1</b>	<b>Introduction</b> .....	283
<b>10.2</b>	<b>Hardware Description</b> .....	284
<b>10.3</b>	<b>Pre-Launch Ground-Based Tests</b> .....	288
<b>10.4</b>	<b>On-Orbit Performance Data</b> .....	293
10.4.1	SQUID Noise .....	293
10.4.2	SQUID Bracket Temperature Control .....	294
10.4.3	SRE Temperature Control Performance .....	296
<b>10.5</b>	<b>SRE Software</b> .....	297
<b>10.6</b>	<b>References</b> .....	306

<b>11 Telescope Readout Subsystem (TRE) Analysis</b> .....	307
<b>11.1 Telescope Readout Electronics Report Summary</b> .....	309
<b>11.2 Operational Performance and Overview</b> .....	310
11.2.1 Gain Levels .....	310
11.2.2 PID Temperature Controllers for DMAs .....	311
11.2.3 Signal Strengths .....	311
11.2.4 Telescope Operation with the Shutter Open .....	311
<b>11.3 Hardware Performance</b> .....	312
11.3.1 TRE Detector Dark Noise .....	312
11.3.2 Platform Temperature Stability .....	312
11.3.3 Temperature History and Detector High Levels .....	313
11.3.4 Daily Data Example .....	317
<b>11.4 Optically Related Performance</b> .....	318
11.4.1 Guide Star Brightness Variation and Period .....	318
11.4.2 Telescope Pointing Signal .....	319
11.4.3 Telescope Scale Factor .....	320
11.4.4 RMS pointing noise .....	321
11.4.5 Dither amplitude variation .....	326
11.4.6 Bias Variation .....	327
11.4.7 Snapshots Comparison to Science Slopes .....	331
11.4.8 Telescope and Windows operating temperature .....	331
<b>12 Cryogenic Subsystem Analysis</b> .....	333
<b>12.1 Cryogenic System Requirements</b> .....	335
<b>12.2 Temperature / pressure control of the Main Tank</b> .....	336
<b>12.3 Events and conditions related to Dewar performance</b> .....	336
12.3.1 Launch .....	336
12.3.2 Thermal transient events .....	337
12.3.3 Stuck thrusters .....	337
12.3.4 Heating events in the Probe .....	338
12.3.5 Drag-Free operation .....	338
12.3.6 Effect of Dewar shell temperature .....	338
12.3.7 Thermo-acoustic oscillations (TAOs) .....	338
<b>12.4 Lifetime projection</b> .....	339
12.4.1 Thermal models .....	339
12.4.2 Helium mass gauging .....	340
12.4.3 Initial lifetime estimate .....	340
12.4.4 Update of lifetime estimate .....	341
<b>12.5 Heat pulse measurement (HPM) operation</b> .....	341
12.5.1 Principle of operation .....	341
12.5.2 Results from HPM operations .....	342
<b>12.6 Dewar Vent Rate Measurement</b> .....	343
<b>12.7 Reconciliation of lifetime estimates</b> .....	344
<b>12.8 Comparison of lifetime prediction with final result</b> .....	345
<b>12.9 HPM Results: Conclusions</b> .....	347

<b>12.10 Magnetic Shielding Performance</b> .....	348
12.10.1 Rotor Trapped Flux .....	348
12.10.2 AC Shielding .....	349
<b>12.11 Probe Vacuum Performance</b> .....	349
<b>13 Other Payload Subsystems Analyses</b> .....	351
<b>13.1 Experiment Control Unit (ECU)</b> .....	353
13.1.1 ECU Hardware .....	353
13.1.2 ECU-Controlled Heaters & Temperature Sensors .....	353
13.1.3 ECU-Managed Subsystems .....	355
13.1.4 ECU Performance During Flux Reduction & Low Temperature Bakeout .....	358
13.1.5 ECU Heater Activity During IOC .....	360
13.1.6 ECU Heater Activity During the Science Phase .....	364
13.1.7 ECU transmission of Spacecraft Noise .....	366
<b>13.2 Proton Monitor</b> .....	367
13.2.1 GP-B Radiation Environment .....	367
13.2.2 Proton Monitor Features and Specifications .....	367
13.2.3 History of Performance .....	369
13.2.4 Data Collected .....	369
13.2.5 Correlating the PM with the Telescope .....	373
13.2.6 Possible Post-Science Missions and Analysis .....	375
<b>13.3 Payload Magnetometers</b> .....	375
13.3.1 About the Magnetometers .....	376
13.3.2 Other Applications for Payload Magnetometers .....	378
13.3.3 Lessons Learned Using Payload Magnetometers .....	378
<b>13.4 Global Positioning System (GPS)</b> .....	378
13.4.1 GPS Hardware .....	379
13.4.2 Hardware Modifications for GP-B .....	380
13.4.3 Pre-Launch Testing and Results .....	380
13.4.4 Time Reconciliation .....	382
13.4.5 Orbital Accuracy .....	385
13.4.6 On-Orbit Results .....	386
13.4.7 On-Orbit Events .....	387
13.4.8 References .....	389
<b>13.5 Gas Management Assembly (GMA)</b> .....	390
13.5.1 GMA Development and Operational Concept .....	390
13.5.2 Pre-Launch Ground Support .....	392
13.5.3 GMA Gas Consumption for Gyro #4 Spin-Up .....	395
13.5.4 Total GMA Gas Consumption for Gyro Spin-Up .....	395
13.5.5 GMA Science and Post-mission Status .....	396

<b>14 Data Collection, Processing &amp; Analysis</b> .....	397
<b>14.1 Collection and Processing GP-B Data</b> .....	399
14.1.1 Data Collection and Telemetry .....	399
14.1.2 Detecting and Correcting Computer Memory Errors in Orbit .....	403
14.1.3 GP-B Safemodes and Anomaly Resolution .....	406
14.1.4 Effects of Anomalous Events on the Experimental Results of GP-B .....	408
14.1.5 Aberration of Starlight—Nature’s Calibrating Signal .....	409
14.1.6 Telescope Dither—Correlating the Gyro & Telescope Scale Factors .....	414
14.1.7 Extracting the Gyro Signals from the Noise .....	416
<b>14.2 The GP-B Science Data Analysis Process</b> .....	418
14.2.1 Formal Data Analysis Phases .....	418
14.2.2 Independent Data Analysis Teams .....	420
14.2.3 Data Grading .....	420
14.2.4 Data Analysis “Standard Model” .....	421
14.2.5 Publication of Overall Results .....	422
<b>15 Preliminary Results</b> .....	423
<b>15.1 GP-B Successfully Collected the Data to Test Einstein’s Predictions About Gravity</b> ..	425
<b>15.2 The Effects of Relativity Are Clearly Visible in the Raw Data</b> .....	425
<b>15.3 A First Peek at the Results</b> .....	427
<b>15.4 The Two Surprises and Their Impact On The Experiment</b> .....	428
15.4.1 Time-Varying Motion in the Gyro Rotors .....	430
15.4.2 The Effects of Time-Varying Polhode Motion on the Experiment .....	431
15.4.3 Classical Misalignment Torques on the Gyros .....	433
15.4.4 Patch Effects—The Underlying Cause of Both Effects .....	434
<b>15.5 Next Steps—Moving Towards a Final Result</b> .....	437
<b>15.6 GP-B Data Archive to be Available Through the NSSDC</b> .....	439
<b>16 Lessons Learned and Best Practices</b> .....	441
<b>16.1 Lessons Learned</b> .....	443
16.1.1 Pre-launch lessons learned .....	443
16.1.2 Lessons Learned from On-orbit Operations .....	447
16.1.3 IOC Observations by Lewis Wooten of NASA MSFC .....	453
<b>16.2 Selected Best Practices</b> .....	454
16.2.1 Design team transition to mission operations .....	454
16.2.2 Mission planning flexibility .....	454
16.2.3 Control and communication of spacecraft configuration .....	455
16.2.4 Effective use of databases .....	455
16.2.5 Inclusion of operations experts in hardware development .....	455
16.2.6 Team member cross-training .....	455
16.2.7 Peer reviews in software development .....	456
16.2.8 Minimizing program risks with formal risk management plan .....	456



<b>16.3 Management Lessons from the Calder-Jones Report</b> .....	457
16.3.1 Working With Organizational Asymmetries .....	458
16.3.2 Recognizing and Managing Critical Transition Points .....	458
16.3.3 Adaptive Program Management. ....	458
16.3.4 Maintaining Aerospace Knowledge at Universities .....	458
16.3.5 Managing Risk .....	459
16.3.6 Funding Predictability .....	459
<b>A Gravity Probe B Quick Facts</b> .....	461
<b>B Spacecraft Data Chart</b> .....	465
<b>C Weekly Chronicle of the GP-B Mission</b> .....	469
C.1 Pre-Launch Mission Phase: 4/2/04 – 4/18/04 .....	471
C.2 GP-B Launch: 4/19/04 – 4/20/04 .....	472
C.3 IOC Mission Phase: 4/21/04 – 8/26/04 .....	473
C.4 Science Mission Phase: 8/27/04 - 8/12/05 .....	484
C.5 Instrument Calibration Phase: 8/19/05 – 9/30/05 .....	511
<b>D Summary Table of Flight Anomalies</b> .....	521
<b>E Flight Software Applications SLOC</b> .....	549
<b>F Acronyms &amp; Abbreviations</b> .....	569



# List of Figures

Figure 1-1.	GP-B Principal Investigator, Francis Everitt, receiving the NASA Distinguished Public Service Award at an awards ceremony at NASA Headquarters in April 2005	4
Figure 1-2.	Newton’s flat and fixed space and time (left) vs. Einstein’s warped and twisted spacetime (right)	5
Figure 1-3.	The GP-B spacecraft in orbit and the two measurements being made with the gyroscopes on-board	6
Figure 1-4.	A GP-B niobium-coated gyro rotor and housing (left), the Guinness Database record for roundness (center), and measuring the sphericity of a gyro rotor (right)	8
Figure 1-5.	A GP-B SQUID module (left) and a diagram of the magnetic pickup loop and London moment	9
Figure 1-6.	A pre-flight prototype of the GP-B telescope and diagram of its image-centering operation	10
Figure 1-7.	Guide Star IM Pegasi (HR 8703) sky location (left), photo (center) and proper motion (right)	11
Figure 1-8.	Clockwise, from top left: The dewar, a cross-section of the dewar, the porous plug, and one thruster	12
Figure 1-9.	The GP-B spacecraft and its main payload components	15
Figure 1-10.	The GP-B Mission Operations Center (MOC) during gyro spin-up (left) and end of helium (right)	17
Figure 1-11.	NASA GP-B Program Manager, Tony Lyons, from the Marshall Space Flight Center in Huntsville, AL, presents a NASA Group Achievement Award to the entire GP-B team in November 2005.	18
Figure 1-12.	The GP-B Anomaly Room in action	19
Figure 1-13.	Stanford GP-B/GPS graduate students and a faculty member pose next to a GPS-controlled tractor (left); Clark Cohen and Brad Parkinson receive awards from the Space Technology Hall of Fame	22
Figure 2-1.	GP-B Historical Time Line	26
Figure 2-2.	GP-B Co-founders and Nancy Roman. Clockwise from top left: Leonard Schiff (~1970), William Fairbank (~1988), Robert Cannon (2005), and Nancy Roman (2005)	27
Figure 2-3.	Clockwise from top left: GP-B Principal Investigator, Francis Everitt, and Co-PIs Brad Parkinson, John Turneure and Dan DeBra.	29
Figure 2-4.	GP-B Principal Investigator, Francis Everitt, receiving the NASA Distinguished Public Service Award at an awards ceremony at NASA Headquarters in April 2005.	31
Figure 2-5.	Newton’s universe: Space and time are absolute or fixed entities. Gravity is a force that acts instantaneously between objects at a distance, causing them to attract one another.	31
Figure 2-6.	Einstein’s Universe: Space and time are relative entities, interwoven into a spacetime fabric whose curvature we call gravity. Objects follow the straightest possible lines, called geodesics, through curved spacetime.	32
Figure 2-7.	The Missing Inch	33
Figure 2-8.	Illustration of frame-dragging	34
Figure 2-9.	Frame-dragging around a black hole	35
Figure 2-10.	Schematic diagram of the GP-B experiment	36
Figure 2-11.	Exploded diagram of the GP-B spacecraft & payload	37
Figure 2-12.	Final assembly of the Probe	38
Figure 2-13.	Looking inside the top hat down into the Probe	39
Figure 2-14.	The GP-B spacecraft	39
Figure 2-15.	Stanford GP-B/GPS graduate students and a faculty member pose next to a GPS-controlled tractor; Clark Cohen (left) and Brad Parkinson (right) receive awards from the Space Technology Hall of Fame.	42
Figure 2-16.	Photos of the GP-B Launch on April 20, 2004	43
Figure 2-17.	On-board video camera shows separation	44
Figure 3-1.	Gravity Probe B gyroscope rotor, with quartz housing halves.	69
Figure 3-2.	SQUID detector package, with housing cover	71
Figure 3-3.	Functional diagram of a SQUID pickup loop measuring the London Moment around a GP-B gyro rotor (left) and four SQUID readouts—one for each gyro (right).	72

Figure 3-4.	The GP-B dewar—one of the largest and most sophisticated dewars ever flown .....	72
Figure 3-5.	Cross sectional schematic of the dewar .....	73
Figure 3-6.	Proportional micro thrusters used for GP-B spacecraft attitude control .....	74
Figure 3-7.	A pre-flight prototype of the Cassegrain telescope on-board the GP-B spacecraft .....	75
Figure 3-8.	Tracking the guide star, IM Pegasi, with the GP-B telescope .....	76
Figure 3-9.	Schematic diagram of starlight image division in the GP-B telescope .....	78
Figure 3-10.	The porous plug .....	81
Figure 3-11.	Lead bag magnetic shield in GP-B flight probe .....	82
Figure 3-12.	GP_B proportional micro thruster assembly .....	83
Figure 3-13.	Polishing a gyro rotor .....	83
Figure 3-14.	Measuring the roundness of a gyro rotor and mapping the contours on its surface .....	84
Figure 3-15.	A gyro rotor and both halves of its quartz housing .....	85
Figure 3-16.	Top view of the Gas Management Assembly (GMA) .....	85
Figure 3-17.	The telescope Image Divider Assembly (IDA) and Detector Package Assemblies (DPA) .....	86
Figure 3-18.	Schematic diagram and photo of a SQUID gyro readout .....	87
Figure 3-19.	Checking the GP-B solar arrays on the spacecraft at Lockheed Martin & solar arrays deployed on a scale model of the spacecraft .....	88
Figure 3-20.	GP-B's annual orientation patterns with respect to the sun .....	89
Figure 3-21.	Window #4—the outer vacuum seal of the Probe .....	90
Figure 3-22.	GP-B—The first spacecraft with 6 degrees of freedom in position and attitude control .....	91
Figure 4-1.	NASA GP-B Program Manager, Tony Lyons, from the Marshall Space Flight Center in Huntsville, AL, presents a NASA Group Achievement Award to the entire GP-B team in November 2005. ....	98
Figure 4-2.	Example TISI visualization. ....	103
Figure 4-3.	Number of hours of re-planning required per day during IOC. ....	105
Figure 4-4.	Data flow through the GP-B's automated data processing. ....	109
Figure 4-5.	Pictorial depiction of $\eta$ . The circle represents the Earth, the vertical line is the orbit plane viewed edge-on, and the asterisk represents the guide star. $\eta$ is the angle between orbit plane and guide star at any point in the orbit plane. ....	112
Figure 4-6.	Eta and Eta-Average Histories (Degrees) Associated with GP-B .....	113
Figure 4-7.	Eta-Average Error Associated with GP-B Orbit as a function of IOC duration and science mission lifetime .....	114
Figure 4-8.	Usable GPS Points per Day (2005) .....	115
Figure 4-9.	Typical residual plot from daily GPS solution. ....	116
Figure 4-10.	SLR passes per day .....	117
Figure 4-11.	Comparison of GPS and SLR Cross-Track Errors. ....	118
Figure 4-12.	GP-B Computer Network. ....	119
Figure 4-13.	The Integrated Test Facility (ITF) flight simulator hardware in a Clean Room at Lockheed Martin ..	122
Figure 5-1.	Anomaly Review Team Organization .....	128
Figure 5-2.	GP-B Anomaly Room Layout .....	131
Figure 5-3.	For each risk, an assessment is completed by the identifying team or person .....	134
Figure 5-4.	Metric of risk item closure prior to launch of GP-B. All risk items were either accepted or closed prior to launch. ....	135
Figure 5-5.	(part 1 or 3). Open risk items during on-orbit science mission .....	136
Figure 5-6.	(part 2 or 3). Open risk items during on-orbit science mission .....	137
Figure 5-7.	(part 3 or 3). Open risk items during on-orbit science mission .....	137
Figure 6-1.	Clockwise from top left: GP-B Co Founders Leonard Schiff, William Fairbank, and Robert Cannon and former head of NASA's Office of Space Sciences, Nancy Roman. ....	144
Figure 6-2.	Clockwise from top left: GP-B Principal Investigator, Francis Everitt and Co-PIs Bradford Parkinson, John Turneure and Dan DeBra. ....	147

Figure 6-3.	The six GP-B Co-Investigators. Clockwise from top left: Sasha Buchman, George (Mac) Keiser, John Lipa, James Lockhart, Barry Muhlfelder, and Michael Taber. ....	148
Figure 6-4.	Probe C: testing in clean room (left), ready for integration with dewar (center) and connections inside the top hat interface (right). ....	150
Figure 6-5.	Left: Engineering Development Dewar (EDD); Middle & Right: Science Mission Dewar (SMD). ...	151
Figure 6-6.	Gyroscope rotor development and precision sphericity measurement. ....	151
Figure 6-7.	SQUID readout development prototypes and lithograph for SQUID chip. ....	152
Figure 6-8.	An early development telescope prototype (left), the pre-flight #2 prototype telescope (center), and a close-up of the Image Divider Assembly and Detector Assembly Package from the #2 pre-flight prototype. ....	152
Figure 6-9.	The Lockheed Martin GP-B Spacecraft Development Team circa 1995. Key managers from LM included: Norman Bennett, Hugh Dougherty, Bill Reeve, Robert Schultz, and Jeff Vanden Beukel. ...	154
Figure 6-10.	MSFC Program Managers/supporters of GP-B since 1995. Clockwise from top left: Rudolph Decher, Richard Potter, Joyce Neighbors, Rein Ise, Steve Richards, Rex Geveden, Tony Lyons, and Arthur Stephenson. ....	162
Figure 6-11.	MSFC resident and engineering managers. Left to right: Edward Ingraham, Todd May, Buddy Randolph, and Stephan Davis. ....	162
Figure 6-12.	GP-B Program Managers. Clockwise from top left: Bradford Parkinson, John Turneaure, Sasha Buchman, Ron Singley, Gaylord Green, and Bill Bencze and GP-B ....	165
Figure 6-13.	GP-B Deputy Program Managers. Left to right: Robert Farnsworth, Tom Langenstein, and Robert Brumley ....	165
Figure 7-1.	Schematic of Guide Star Valid (GSV) and Guide Star Invalid (GSI) periods ....	173
Figure 7-2.	12 hours of thruster pressure data from 2004 day 184 ....	174
Figure 7-3.	Science Telescope Components Schematic ....	176
Figure 7-4.	Normalized Telescope Signal vs Pointing Error ....	177
Figure 7-5.	Pitch and Yaw Pointing Performance during the science mission ....	178
Figure 7-6.	X-Axis RMS pointing performance correlation with solar angle ....	179
Figure 7-7.	Magnitude of the roll rate component of pitch yaw pointing performance ....	180
Figure 7-8.	Correlation of pointing roll rate component with telescope/sun angle ....	181
Figure 7-9.	Guide star capture performance before capture method update ....	182
Figure 7-10.	Guide star capture performance after capture method update ....	183
Figure 7-11.	Roll Phase Error over 4 orbits ....	184
Figure 7-12.	Drag-Free system diagram ....	185
Figure 7-13.	Drag-Free performance ....	186
Figure 7-14.	ATC Mass Flow Usage in drag-free Mode ....	187
Figure 7-15.	Mass flow effects of a Heat Pulse Meter Test and the Magnetic Torquing System ....	188
Figure 7-16.	Vehicle rotation rate damping after separation from the Delta II ....	189
Figure 7-17.	Large Scale Dither Performance (2004/197) ....	191
Figure 7-18.	GSV/GSI rate gyroscope bias offset ....	193
Figure 7-19.	Side view of partially assembled dewar showing primary structural elements except for forward PODS. ....	194
Figure 7-20.	Cutaway top view of dewar showing forward PODS and ARP post locations and details of the ARP post and flexure. (Representation of the ARP is schematic and not accurate.) ....	195
Figure 7-21.	Percentage of data corrupted by proton activity in the South Atlantic Anomaly ....	196
Figure 7-22.	South Atlantic Anomaly Region produced from telescope proton hit data ....	197
Figure 7-23.	Effects on telescope pointing from the solar flare on January 20, 2005 ....	198
Figure 8-1.	Physical Location of CDH boxes on GP-B ....	203
Figure 8-2.	Block Diagram of CDH communications. Green blocks belong to the CDH subsystem ....	204
Figure 8-3.	Commands sent by month ....	205
Figure 8-4.	Commanding loads sent to the vehicle by month ....	206

Figure 8-5.	The Seasons of GP-B .....	207
Figure 8-6.	The annual gamma angle and eclipse cycle of GP-B .....	208
Figure 8-7.	Battery 1 & 2 Temperature Trends for Mission Duration .....	209
Figure 8-8.	GSS1 Temperature Trends for Mission Duration .....	210
Figure 8-9.	Solar Array (Average) Temperatures for Mission Duration .....	211
Figure 8-10.	Forward Dewar Vacuum Shell Temperatures for Mission Duration .....	212
Figure 8-11.	Aft Dewar Vacuum Shell Temperatures for Mission Duration .....	213
Figure 8-12.	Forward +X Thruster Temperatures for Mission Duration .....	215
Figure 8-13.	Forward -X Thruster Temperatures for Mission Duration .....	216
Figure 8-14.	Aft +X Thruster Temperatures for Mission Duration .....	217
Figure 8-15.	Aft -X Thruster Temperatures for Mission Duration .....	218
Figure 8-16.	The temperature from of the SQUID Bracket (top), the QBS (middle) and the Cryo Pump .....	221
Figure 8-17.	Bus Ripple Metric (Ripple Value in Volts since Launch) .....	224
Figure 8-18.	Eclipse Length and Depth of Discharge Metric .....	225
Figure 8-19.	Space Vehicle Power Margin Metric .....	226
Figure 8-20.	Battery Voltage Metric .....	227
Figure 8-21.	Battery State of Charge Metric .....	228
Figure 8-22.	Solar array voltage and bus power performance metric .....	229
Figure 8-23.	Solar Array Temperatures Variations vs. Gamma Angle .....	230
Figure 8-24.	EPS Power Generation Capability Comparison 2004 Vs 2005 .....	231
Figure 8-25.	EPS Power Generation Capability Comparison (minus attitude discrepancies) .....	231
Figure 8-26.	GP-B Communications Block Diagram .....	232
Figure 8-27.	Location of antennae and transponder palette on spacecraft. ....	233
Figure 8-28.	Remote controlled operation of GRST from WSC .....	234
Figure 8-29.	The Svalbard Ground Station Network. ....	235
Figure 8-30.	Xpndr-A STDN (green), Xpndr-A TDRS (yellow), Xpndr-B STDN (red), Xpndr-B TDRS (white) ....	236
Figure 8-31.	Transponder B TDRS AGC (red) vs Transponder A TDRS AGC (green) .....	237
Figure 8-32.	Plot of TDRS AGC vs Temperature over a 20-minute time frame .....	238
Figure 8-33.	CCCA 1Hz CPU Usage (in %) averaged over ~4 hours. (Red = max; Blue = avg; Green = min): ...	240
Figure 8-34.	CCCA 10Hz CPU Usage (in %) averaged over ~4 hours. (Red = max; Blue = avg; Green = min) ..	241
Figure 8-35.	ITF Hardware and Interconnects .....	243
Figure 8-36.	Structure of a Safemode Test .....	247
Figure 8-37.	Excerpt from Safemode Status in March 2005 .....	247
Figure 8-38.	Excerpt from Test Description Table in Safemode Design Document .....	248
Figure 8-39.	Location of Single Bit Errors during Science Data Collection .....	249
Figure 8-40.	A-side CCCA Single Bit Errors from Oct. 10, 2004 to Nov. 10, 2004 .....	250
Figure 8-41.	B-side CCCA Single Bit Errors from Apr. 10, 2005 to May 10, 2005 .....	250
Figure 8-42.	Proton Flux measured by GOES11 satellite during January 20, 2005 solar flare .....	251
Figure 8-43.	A-side CCCA Single Bit Errors during January 20, 2005 solar flare .....	252
Figure 8-44.	Location of Multi-Bit Errors during the first year of on-orbit operations .....	253
Figure 8-45.	Cumulative CCCA MBE count from launch through end of May 2005. ....	253
Figure 9-1.	Block diagram of the payload electronics package showing the interconnect of the GSS units .	257
Figure 9-2.	Photograph of GSS units. Aft processor and power supply (left), forward quiet analog electronics (right). One pair is required for each gyroscope. During the mission, the temperature of the aft assembly ranges between 300 K and 320 K; the forward assembly range is 265 K to 300 K. ....	258
Figure 9-3.	Block diagram of the Forward Suspension Unit (FSU) .....	259
Figure 9-4.	GSS Arbiter State Transition diagram. ....	260
Figure 9-5.	Block Diagram of the Aft Suspension Unit (ACU) .....	261
Figure 9-6.	Block diagram of the GSS power system. ....	262

Figure 9-7.	Photograph of rotor and housing. Suspension electrodes and spin-up channel are clearly seen. . . .	263
Figure 9-8.	Block diagram of the LQE control architecture. . . . .	264
Figure 9-9.	Simulated response of adaptive LQE controller showing constant excursion for varying disturbance	264
Figure 9-10.	Suspension Controllers and Modes of Operation showing the 8 orders of magnitude of operation for this system. . . . .	265
Figure 9-11.	Initial suspension of gyroscope in analog backup mode (blue=A axis, green = B, red = C) . . . . .	266
Figure 9-12.	GSS step response in Science mode, showing control stiffness as a function of miscentering. . .	267
Figure 9-13.	Details of control response showing high-bandwidth (left) low-bandwidth (right) operation. . .	267
Figure 9-14.	GSS control efforts during full flow gyroscope spin-up operations (top plot: blue = A, green = B, red = C) . . . . .	268
Figure 9-15.	Simulated (L) and actual (R) spin axis alignment tracks for Gyro 3 coarse alignment . . . . .	269
Figure 9-16.	Predicted and measured drift rates for coarse and fine alignment modes. . . . .	270
Figure 9-17.	Unsuspended or "prime" drag-free control topology. . . . .	271
Figure 9-18.	Suspended or "backup" drag-free control topology. . . . .	272
Figure 9-19.	Drag-free transitions: Backup and prime . . . . .	273
Figure 9-20.	Representative drag-free performance together with gravity gradient acceleration on the space vehicle . . . . .	274
Figure 10-1.	Gyroscope SQUID Readout System . . . . .	285
Figure 10-2.	SQUID Readout Electronics (SRE) – Forward Units . . . . .	286
Figure 10-3.	SQUID Readout Electronics (SRE) – Aft Units . . . . .	287
Figure 10-4.	SQUID Readout Electronics (SRE) – Sub-system Architecture . . . . .	287
Figure 10-5.	SQUID Noise Data - Payload Test . . . . .	289
Figure 10-6.	AC Magnetic Shielding – Payload Test . . . . .	290
Figure 10-7.	SQUID Temperature Coefficient – Payload Test . . . . .	291
Figure 10-8.	Temperature Error of SQUID Bracket Temperature Control Test at August 8 2001 18:19-20:19 . .	292
Figure 10-9.	Square Root of Power Spectrum Magnitude of the Temperature Error . . . . .	292
Figure 10-10.	Quiescent SQUID Noise Data – On Orbit . . . . .	294
Figure 10-11.	SQUID Bracket Temperature Control – On-Orbit . . . . .	295
Figure 10-12.	SQUID Electronics Temperature Control – On-Orbit . . . . .	296
Figure 11-1.	Block diagram of TRE and associated aspects of the SRE system . . . . .	310
Figure 11-2.	CLL switch states during normal operation . . . . .	313
Figure 11-3.	CLL switch states during the reset interval. . . . .	314
Figure 11-4.	CLL switches locked for offset adjustment . . . . .	314
Figure 11-5.	Local box temperature and detector high signals since launch . . . . .	315
Figure 11-6.	High Gamma Angle Data Sample . . . . .	317
Figure 11-7.	Low Gamma Angle Data Sample . . . . .	318
Figure 11-8.	Guide Star intensity versus time . . . . .	319
Figure 11-9.	Point spread function of IM Peg image at the roof prism . . . . .	321
Figure 11-10.	Pointing angle . . . . .	321
Figure 11-11.	X-axis, A side RMS pointing noise equivalent due to detector noise . . . . .	322
Figure 11-12.	Y axis, A side RMS pointing noise equivalent due to detector noise . . . . .	323
Figure 11-13.	X axis, B side RMS pointing noise equivalent due to detector noise . . . . .	323
Figure 11-14.	Y axis, B side RMS pointing noise equivalent due to detector noise . . . . .	324
Figure 11-15.	X axis, A side current variation . . . . .	325
Figure 11-16.	Y axis, A side current variation . . . . .	325
Figure 11-17.	X axis, B side current variation . . . . .	326
Figure 11-18.	Y axis, B-side current variation . . . . .	326
Figure 11-19.	Dither amplitude as a function of time . . . . .	327

Figure 11-20.	Pointing angle difference between primary and redundant readouts	328
Figure 11-21.	The color variation of IM Peg. The sum of the detector current of one of the axis is also shown to indicate how star brightness varies.	328
Figure 11-22.	The scaled summed current for each of the four pairs of detectors.	329
Figure 11-23.	Comparison of four pairs of scaled summed current with each other and with R band of ground measurement.	329
Figure 11-24.	Scaled summed current compared with the values of channel XB. The ratios have been normalized for easy comparison.	330
Figure 11-25.	Comparison of estimated photocurrent based on Science slopes and on least square fit slope derived from TRE snapshots	331
Figure 11-26.	Temperature variation of telescope top plate	332
Figure 11-27.	Temperature variation of Window 1	332
Figure 11-28.	Temperature variation of Window 2	332
Figure 11-29.	Temperature variation of Window 4	332
Figure 12-1.	Integrated probe and dewar.	335
Figure 12-2.	Temperature spiking at probe station 200 (primary cryogenic probe/dewar interface).	337
Figure 12-3.	Helium flow rate predicted by dewar model based on both the measured shell temperatures and predicted temperatures.	340
Figure 12-4.	Main tank temperature in response to fourth heat pulse measurement with linear trendlines before and after heat pulse. Temperature increase is taken to be the difference in the two trendline values at the middle of the pulse.	342
Figure 12-5.	Plot of the remaining mass of liquid helium as a function of HPM measurement date with linear trendline. The fact that the trendline does not project backwards to the original quantity of liquid helium (taken to be 337 kg) is indicative of a scale factor error.	343
Figure 12-6.	Flow meter and ATC flow rates as a function of UTC date starting at launch. Data encompass periods of flow control (constant segments in the ATC data) as well as pressure control.	344
Figure 12-7.	Mass remaining estimated from integrated flow meter and ATC flow rates. Trendline fits are extrapolated to zero mass. Since depletion did not occur in early July, it is clear that the dewar flow meter results under-predicted lifetime.	344
Figure 12-8.	Flow meter data reduced by 10% and plotted with ATC flow rate and flow rate predicted by the dewar thermal model. Thermal model is based on measured shell temperatures rather than predicted shell temperatures.	345
Figure 12-9.	HPM data analyzed under three different assumptions together with extrapolated linear trendlines.	348
Figure 13-1.	Locations of Forward and Aft ECU boxes on the GP-B spacecraft	353
Figure 13-2.	ECU-operated heaters in the dewar & probe	354
Figure 13-3.	ECU-operated temperature sensors in the dewar & Probe	354
Figure 13-4.	ECU-operated heaters and temperature sensors in the Probe and Probe windows	355
Figure 13-5.	General locations of ECU-controlled subsystems on the spacecraft	355
Figure 13-6.	A six-inch Vatterfly leakage exhaust valve at the top of the dewar	356
Figure 13-7.	The Gas Management System (GMA)	356
Figure 13-8.	UV lamps and the gyro electrostatic discharge system	357
Figure 13-9.	The GP-B Proton Monitor box	357
Figure 13-10.	Performance during Low Temperature Bakeout	359
Figure 13-11.	ECU performance during IOC flux reduction	360
Figure 13-12.	ECU heater activity following launch	361
Figure 13-13.	ECU heater activity during first month of IOC	361
Figure 13-14.	ECU heater activity during the 2nd month of IOC	362
Figure 13-15.	ECU heater activity from mid June - mid July, 2004	363
Figure 13-16.	ECU heater activity during gyro spinup and other critical IOC procedures	363
Figure 13-17.	ECU heater activity during the last month of IOC	364



Figure 13-18. ECU heater activity during the first half of the Science Phase .....	365
Figure 13-19. ECU heater activity during the Science Phase, from January-May 2005 .....	366
Figure 13-20. Typical Month of Proton Monitor Data .....	369
Figure 13-21. Proton Monitor data in South Atlantic Anomaly .....	370
Figure 13-22. Twice Orbital Component .....	370
Figure 13-23. FFT of data from the horizontal detector .....	371
Figure 13-24. Histogram of Proton Events .....	371
Figure 13-25. Proton Monitor Data from November 2004 .....	372
Figure 13-26. Zoomed out view of <a href="#">Figure 13-25</a> .....	372
Figure 13-27. Increased Proton Flux during the November 2004 solar activity .....	373
Figure 13-28. Correlation between Vertical PM Detector and Science Telescope (PXA) .....	373
Figure 13-29. Correlation between Horizontal PM Detector and Science Telescope (PXA) .....	374
Figure 13-30. Correlation between Vertical PM Detector and Science Telescope (PYA). .....	375
Figure 13-31. GP-B payload magnetometer .....	376
Figure 13-32. Measurement axes of the payload magnetometers. ....	377
Figure 13-33. Mounting locations of the payload magnetometers. ....	377
Figure 13-34. Location of GPS equipment on GP-B .....	379
Figure 13-35. GPS Antennae Field of View .....	380
Figure 13-36. Rolling Rig .....	381
Figure 13-37. Master Antenna Switching .....	382
Figure 13-38. Histogram of PPS Data .....	383
Figure 13-39. Time difference between transmission and reception of GPS data packet. ....	384
Figure 13-40. Residuals of Least Square fitting algorithm with 2nd order model. ....	385
Figure 13-41. Coverage Curves for GPS simulator, rolling rig, and flight data. At GP-B's roll rate, the simulated coverage is 86%, while flight rate is better than 95% .....	386
Figure 13-42. Coverage rates during an increase in vehicle roll rate. ....	387
Figure 13-43. Percent Lock and data points used before and after the switch to the B-side receiver on March 4, 2005, day 64. ....	389
Figure 13-44. A Top View of the GMA Pallet with the Thermal Blanket Frame Attached .....	391
Figure 13-45. A Bottom View of the GMA Showing the Supply Tanks and Outlet Valves .....	392
Figure 13-46. GMA vent manifold and service GSE used to minimize cryogenic contamination and ensure regulator lock-up for launch .....	393
Figure 13-47. Service valve assembly (fill and drain valves) used to service the GMA to reduce the risk of cryogenic contamination during ground support .....	393
Figure 13-48. The GMA configuration on a vented honeycomb pallet .....	394
Figure 13-49. Schematic diagram of the GMA .....	394
Figure 13-50. Helium gas consumption for 10 hz and full spin-up of gyro #4 during IOC .....	395
Figure 13-51. Pressure Transducer GP-1 Snap-Shot of Actual Gas Consumed by the GMA .....	395
Figure 14-1. A drawing of the spacecraft communicating with ground tracking stations .....	399
Figure 14-2. A typical solid state recorder (SSR) manufactured by SEAKR Engineering .....	400
Figure 14-3. A NASA TDRSS Satellite .....	401
Figure 14-4. NASA ground stations at Svalbard, Norway (upper left), Poker Flats, Alaska (lower left), and Wallops Island, Virginia (right) .....	402
Figure 14-5. The GP-B building and Mission Operations Center (MOC) at Stanford University .....	403
Figure 14-6. ITF readout showing a discrepancy between the actual value (left) of memory location in the spacecraft's computer vs the correct value (right) stored in the ITF simulator. ....	405
Figure 14-7. Two members of the GP-B Mission Operations team discuss an MBE that triggered a B-Side (CCCB computer) reboot on March 18, 2005 .....	405
Figure 14-8. Uploading commands to the spacecraft from the MOC, following a B-side computer reboot. ..	406

Figure 14-9.	In the Anomaly Room, team members discuss a series of recovery commands that will be uploaded to the spacecraft. ....	407
Figure 14-10.	British Astronomer Royal, James Bradley .....	409
Figure 14-11.	Due to the motion of the Earth, the apparent position of a distant star viewed through a telescope differs from its actual position—Bradley called this difference the aberration angle. ....	411
Figure 14-12.	GP-B's Orbital aberration of light from the Guide Star, IM Pegasi .....	412
Figure 14-13.	GP-B's annual aberration of light from the Guide Star, IM Pegasi .....	413
Figure 14-14.	Schematic diagram of the GP-B telescope optics .....	414
Figure 14-15.	Normalized pointing values for the GP-B telescope .....	415
Figure 14-16.	Centering the telescope's light distribution .....	415
Figure 14-17.	The telescope dither pattern around Guide Star, IM Pegasi .....	416
Figure 14-18.	Components of the GP-B Data Analysis Standard Model (equations shown are significantly simplified and are of iconic value only) .....	421
Figure 15-1.	A photo montage of the GP-B spacecraft in orbit and a photo of the GP-B Mission Operations Center in action during the spin-up of gyro #4. ....	425
Figure 15-2.	A diagram of the GP-B experiment showing the predicted geodetic and frame-dragging effects. ...	426
Figure 15-3.	A slide from the GP-B plenary talk that Francis Everitt will deliver at the APS meeting on April 14, 2007. The plots on the left side of this slide clearly show the predicted geodetic effect in the unprocessed gyro data to an accuracy level of ~1%. A copy of this talk will be available on the APS page of the GP-B Web site: <a href="http://einstein.stanford.edu/content/aps_posters#talks">http://einstein.stanford.edu/content/aps_posters#talks</a> . ....	426
Figure 15-4.	A slide from the GP-B plenary talk that Francis Everitt will deliver at the APS meeting on April 14, 2007. This slide shows the changing polhode paths of gyros #1 and #4 and summarizes the issues of polhode rate variations in the gyros. ....	428
Figure 15-5.	A slide from the GP-B plenary talk that Francis Everitt will deliver at the APS meeting on April 14, 2007. This slide shows the misalignment torques discovered during a series of instrument calibration tests performed during the last six weeks of the mission, prior to depletion of helium in the dewar. ....	429
Figure 15-6.	Plots from different viewing angles showing the changing polhode path of gyro #1 over the life of the experiment. ....	430
Figure 15-7.	A poster on gyro polhode motion to be presented at the APS meeting in April 2007. You can view/download a larger and more readable PDF version of this poster on our GP-B APS Web page: <a href="http://einstein.stanford.edu/content/aps_posters#posters">http://einstein.stanford.edu/content/aps_posters#posters</a> . ....	431
Figure 15-8.	A slide from the GP-B plenary talk that Francis Everitt will deliver at the APS meeting on April 14, 2007. This slide shows how dither and aberration of starlight are used as calibrating signals in determining the gyro-telescope scale factor, $C_g$ . ....	432
Figure 15-9.	A poster on the effects of classical torques on the gyros to be presented at the APS meeting in April 2007. You can view/download a larger and more readable PDF version of this poster on our GP-B APS Web page: <a href="http://einstein.stanford.edu/content/aps_posters#posters">http://einstein.stanford.edu/content/aps_posters#posters</a> . ....	434
Figure 15-10.	A poster on the evidence for patch effects to be presented at the APS meeting in April 2007. You can view/download a larger and more readable PDF version of this poster on our GP-B APS Web page: <a href="http://einstein.stanford.edu/content/aps_posters#posters">http://einstein.stanford.edu/content/aps_posters#posters</a> . ....	435
Figure 15-11.	A slide from the GP-B plenary talk that Francis Everitt will deliver at the APS meeting on April 14, 2007. This slide shows the succession of investigative steps and observations that led to the determination that patch effects are the root cause of both the polhode variation and misalignment torques on the gyros. ....	436
Figure 15-12.	A slide from the GP-B plenary talk that Francis Everitt will deliver at the APS meeting on April 14, 2007. This slide shows the GP-B data analysis team, except for Principal Investigator, Francis Everitt. A copy of this talk will be available on our APS Web site: <a href="http://einstein.stanford.edu/content/aps_posters#talks">http://einstein.stanford.edu/content/aps_posters#talks</a> . ....	437

Figure 15-13. Map of the estimated magnetic flux trapped on the surface of the gyro rotors. Two methods are currently being employed—one mapping individual fluxons and the other mapping magnetic field strength. .... 438

Figure 15-14. A slide from a talk that Irwin Shapiro will deliver at the APS meeting on April 14, 2007, entitled: **Proper Motion of the GP-B guide star**. .... 439

Figure 16-1. Six interacting translational degrees of freedom ..... 452

Figure D-1. Anomaly Type Trends during the mission ..... 523

Figure D-2. Observation categories by subsystem ..... 524



# List of Tables

Table 1-1.	GP-B Seven Near Zeroes .....	7
Table 2-1.	Final gyro spin rates .....	46
Table 2-2.	Weekly summary of IOC accomplishments .....	47
Table 2-3.	Spin-up history of the GP-B gyros .....	55
Table 2-4.	Monthly highlights of the GP-B Science Phase .....	59
Table 2-5.	Weekly highlights of the 7-week final instrument calibration phase .....	63
Table 3-1.	GP-B Seven Near Zeroes .....	68
Table 4-1.	Mission Planning Mastery Index .....	101
Table 4-2.	Mission Planning Commercial Software .....	101
Table 4-3.	Mission Planning software developed by GP-B .....	102
Table 4-4.	Pre-TISI Mission Planning Challenges .....	102
Table 4-5.	Addressing mission planning needs with TISI .....	103
Table 4-6.	Features & benefits of Web delivery .....	104
Table 4-7.	Re-inventing the mission operations concept .....	104
Table 4-8.	Mission Planning workload volume—IOC & Science .....	106
Table 4-9.	Summary of Data Capture .....	108
Table 4-10.	Significant Events/Sources of Data Loss .....	110
Table 4-11.	ITF equipment list .....	121
Table 5-1.	Summary of Open GP-B risks at the end of IOC .....	135
Table 6-1.	GP-B Promised vs. Actual Funding History, FY '99 - FY '02 .....	155
Table 7-1.	Control System Equipment List .....	171
Table 8-1.	SRE Temperature Coefficients (in mV/K) .....	221
Table 8-2.	TDRS Command Modes .....	234
Table 8-3.	Ground Station Setup .....	235
Table 8-4.	SCRs Addressed in On-orbit S/W Change .....	243
Table 8-5.	Tests Executed and Passed to Verify SCRs .....	246
Table 9-1.	GSS Science Mission Mode (220Hz) CPU Utilization .....	275
Table 9-2.	GSS Spin-up Mode (660Hz) CPU Utilization .....	276
Table 9-3.	GSW application source lines of code (SLOC) metrics .....	276
Table 10-1.	Calculations of true noise for each of the four SQUIDs .....	289
Table 10-2.	Measured SQUID bias temperature coefficients .....	291
Table 10-3.	Thermal Power Density at Roll (C/(Hz))— Worst case estimate .....	296
Table 10-4.	RMS Temperature Variations in 3 mHz Band About Roll (C)— Worst case estimate .....	297
Table 10-5.	RE Bias Temperature Coefficients .....	297
Table 10-6.	Processor utilization and activation schedule for SQUID/Science telescope applications during Guide Start Valid and Invalid .....	298
Table 10-7.	SSW application source lines of code (SLOC) metrics .....	299
Table 11-1.	Gain code change times .....	311
Table 11-2.	Photo detector dark noise .....	312
Table 11-3.	Dates and UTC times when clamp commands were changed .....	316
Table 11-4.	Weighting factors used for processing data .....	320
Table 11-5.	On-orbit detector pair characteristics .....	324
Table 12-1.	Key cryogenic system flight requirements .....	335
Table 12-2.	Measured trapped field compared to the London moment equivalent field in each of the gyro rotors. ....	349
Table 13-1.	Proton monitor channel configuration .....	368
Table 13-2.	Technical Specifications .....	368

Table 13-3.	GP-B payload magnetometer performance characteristics. ....	376
Table 13-4.	Installed Position of GPS Antennae .....	379
Table 13-5.	Environmental Testing Highlights .....	381
Table 13-6.	Percent Lock for Various Scenarios .....	382
Table 13-7.	Raw and Processed Positions vs. Truth .....	385
Table 13-8.	Raw and Processed Velocities vs. Truth .....	385
Table 13-9.	Summary of Components for the Gas Management Assembly .....	391
Table 13-10.	Summary for Helium Gas Consumption for GMA Operations On Orbit .....	396
Table 16-1.	GP-B Risk categories and definitions .....	457
Table E-1.	Mission Support Software (MSS) Software Lines Of Code (SLOC) Detail .....	551

# Preface

---

Gravity Probe B (GP-B) is a test of Einstein's General Theory of Relativity based on orbiting gyroscopes. NASA technology funding commenced in March 1964. After a long development process, reaching completion in 2003 to 2004, the mission was successfully launched on April 20, 2004—almost exactly 40 years later. This Post-Flight Analysis Report provides a coherent overall final account of all aspects of GP-B, except the science results which are now planned for publication towards the end of 2007.

GP-B has been a collaborative program between two Stanford University Departments, Physics and Aeronautics-Astronautics. Since 1965, it has also involved a continuous collaboration between Stanford and George C. Marshall Space Flight Center in Huntsville, Alabama. A payload subcontract was let from Stanford to Lockheed Martin in November 1984; the spacecraft contract, also to Lockheed Martin, was let in October 1993. The GP-B story is, therefore, a complex one, in fact, seven interfolded stories:

1. About testing Einstein
2. About the invention of many new technologies
3. About a collaboration between university departments
4. About highly successful student involvement in a long-running space program
5. About a remarkable range of spin-offs, including drag-free technology, Autofarm® GPS-based precision tractor control, a novel quartz bonding technique, and the porous plug device for controlling superfluid helium in space which made possible the IRAS, COBE, WMAP and Spitzer missions
6. About collaboration between NASA and academia
7. About the challenge of managing a flight program with a very highly integrated payload and spacecraft which led the then-NASA Administrator, Mr. James Beggs, in 1984, to say that GP-B was not only a fascinating physics experiment but also a fascinating management experiment.

We, at Stanford, feel profound appreciation to NASA Marshall Center and also many friends at NASA Headquarters who have helped to make this challenging mission possible. Credit for coordinating, assembling, and editing this report goes to our GP-B Public Affairs Coordinator, Bob Kahn.

Francis Everitt & Bradford Parkinson

March 2007





# 1

## Executive Summary

---





## 1.1 What is Gravity Probe B?

Gravity Probe B (GP-B) is a NASA physics mission to experimentally investigate Albert Einstein's 1916 general theory of relativity—his theory of gravity. GP-B uses four spherical gyroscopes and a telescope, housed in a satellite orbiting 642 km (400 mi) above the Earth, to measure in a new way, and with unprecedented accuracy, two extraordinary effects predicted by the general theory of relativity (the second having never before been directly measured):

1. The geodetic effect—the amount by which the Earth warps the local spacetime in which it resides.
2. The frame-dragging effect—the amount by which the rotating Earth drags its local spacetime around with it.

The GP-B experiment tests these two effects by precisely measuring the precession (displacement) angles of the spin axes of the four gyros over the course of a year and comparing these experimental results with predictions from Einstein's theory.

GP-B is actually the second dedicated NASA physics experiment to test aspects of general relativity. The first, Gravity Probe A, was led in 1976 by Dr. Robert Vessot of the Smithsonian Astrophysical Observatory. Gravity Probe A compared elapsed time in three identical hydrogen maser clocks—two on the ground and the third traveling for two hours in a rocket, and confirmed the Einstein redshift prediction to 1.4 parts in  $10^4$ .

## 1.2 A Quest for Experimental Truth

The idea for testing Einstein's general theory of relativity with orbiting gyroscopes was suggested independently by two physicists, George Pugh and Leonard Schiff, in late 1959-early 1960. Schiff, then chairman of the Stanford University Physics Department, published a paper summarizing the experiment, "Possible New Experimental Test of General Relativity," in *Physical Review Letters* (March 1960). Also during this time, Schiff teamed up with two colleagues from the Stanford faculty: low-temperature physicist William Fairbank and gyroscope expert Robert Cannon of the Department of Aeronautics & Astronautics. Thus was born the collaboration between the Stanford Physics and Aero-Astro departments which has been essential to the success of GP-B.

In 1962, Professor Fairbank invited Francis Everitt to come to Stanford as the first full-time academic staff member on the experiment. NASA's Office of Space Sciences, under the leadership of Dr. Nancy Roman, provided research funding in 1964, with Fairbank and Cannon as Co-Principal Investigators and Schiff as Program Advisor. Initial funding was direct from NASA Headquarters to Stanford. In 1971, program oversight was transferred to NASA Marshall Space Flight Center (MSFC) where some engineering collaboration had already begun. Also in 1971, in parallel with the technology development, MSFC funded an in-depth Mission Definition Study by Ball Brothers Research Corporation (BBRC, now Ball Aerospace), performed in close collaboration with Stanford, the starting point of all future flight studies.

Between 1978 and 1984, following in-house Phase A and Phase B studies at MSFC, the experiment was re-structured as a NASA flight program. An important step between 1982 and 1984 was the definition of a technology development program for GP-B to be performed on the Shuttle in 1989—the Shuttle Test Of the Relativity Experiment (STORE), followed two years later by a satellite launch from the Shuttle. In 1981, Francis Everitt became Principal Investigator, the position which he still holds, and in 1984, Stanford Professor Bradford Parkinson (Aero-Astro) joined GP-B as Program Manager, and also as Co-PI, along with Co-PI's John Turneure (Physics) and Daniel DeBra (Aero-Astro).

NASA initiated funding of STORE in FY 1985, following receipt in November 1984 of a Stanford proposal, with Stanford as prime contractor, and Lockheed Missiles and Space Company (LMSC, now Lockheed Martin) as subcontractor to Stanford. In this proposal, Lockheed held principal responsibility for developing the unique 650-gallon dewar and probe—the cryogenic apparatus that houses the telescope and four gyroscopes. After the Challenger disaster in 1986 and the subsequent closure of NASA's West-Coast, polar-orbiting shuttle launch

facility, it was necessary to recast the mission as the launch of a dedicated satellite from its own expendable launch vehicle, without losing the technology funding. Eventually, after extended NASA review and two competitive industrial Phase A studies and proposals, Stanford selected LMSC to build the space vehicle and associated control systems that would contain the dewar and probe in orbit.

William Fairbank once remarked: “No mission could be simpler than Gravity Probe B. It's just a star, a telescope, and a spinning sphere.” However, it took the exceptional collaboration of Stanford, MSFC, Lockheed Martin and a host of others almost two more decades to finally bring this “simple” experiment to the launch pad in April 2004. Over this period, as construction of the payload and spacecraft commenced, the GP-B team expanded, reaching a peak of approximately 100 persons at Stanford, and eventually some 200 persons at Lockheed Martin. Six scientists, each with a different area of specialization, became Co-Investigators: Saps (Sasha) Buchman, George (Mac) Keiser, John Lipa, James Lockhart, Barry Muhlfelder, and Michael Taber. In 1998, Bradford Parkinson stepped aside as Program Manager, to be succeeded first by John Turneure, and then in turn, Sasha Buchman, Ronald Singley, and Gaylord Green for the flight program, and William Bencze for the data analysis phase of the mission. Throughout this period, Tom Langenstein served as the Deputy Program Manager, with responsibility for resources and procurements.



**Figure 1-1.** GP-B Principal Investigator, Francis Everitt, receiving the NASA Distinguished Public Service Award at an awards ceremony at NASA Headquarters in April 2005

However, if there is one person who, along with William Fairbank has proved to be the driving force of GP-B since his arrival in 1962, it is Francis Everitt. His leadership has markedly advanced the state of the art in the areas of cryogenics, magnetics, quantum devices, telescope design, control systems, quartz fabrication techniques, metrology and, most of all, gyroscope technology. The fact that GP-B survived no fewer than seven potential cancellations, finally launched in April 2004, successfully completed a 17-month flight mission, and is now in the final stages of analyzing the relativity data is a direct tribute to Everitt's leadership, tenacity, and dogged pursuit of the experimental truth. It was in recognition of these seminal contributions that, in April 2005, NASA awarded Everitt the Distinguished Public Service Medal—the highest award that NASA can confer upon a non-government employee.

### 1.3 The GP-B Flight Mission

On April 20, 2004 at 9:57:24 AM PDT, a crowd of over 2,000 current and former GP-B team members and supporters watched and cheered as the GP-B spacecraft lifted off from Vandenberg Air Force Base. That emotionally overwhelming day, culminating with the extraordinary live video of the spacecraft separating from the second stage booster meant, as GP-B Program Manager Gaylord Green put it, “that 10,000 things went right.” The orbital insertion was within a few meters of a perfect “bull's eye,” and thus no orbit trim was required during the initialization and checkout phase of the mission.

Once in orbit, the spacecraft first underwent a four-month Initialization and Orbit Checkout (IOC), in which all systems and instruments were initialized, tested, and optimized for the data collection to follow. The IOC phase culminated with the spin-up and initial alignment of each of the four science gyros early in August 2004.

On August 28, 2004, the spacecraft began collecting science data. During the ensuing 50 weeks, the spacecraft transmitted over a terabyte of science data to the GP-B Mission Operations Center (MOC) at Stanford, where it was processed and stored in a comprehensive database for analysis. On August 15, 2005, the GP-B flight team finished collecting science data and began a planned set of essential calibration tests of the gyros, telescope, and SQUID readouts that lasted six weeks, until the liquid helium in the dewar was exhausted on September 25, 2005. (The helium actually lasted about three weeks longer than expected, allowing for extra calibration tests to be made.)

In October 2005, the GP-B science team began a three-phase data analysis process. As of March 2007, the team has progressed through Phase I, Phase II, and much of Phase III, and is preparing to announce preliminary results on April 14-15, 2007\_ at the American Physical Society (APS) meeting in Jacksonville, Florida. In April-May, the team will be releasing the science data and a complete archive of GP-B documents to the National Space Sciences Data Center (NSSDC) at the Goddard Space Flight Center. Subsequently, the science team plans to spend several more months refining the analysis in order to achieve the most precise result possible. The analysis and results will then undergo a careful and critical review by the GP-B external Science Advisory Committee (SAC) and other international experts. During the latter part of 2007, the GP-B team will also be preparing scientific and engineering papers for publication, as well as working with NASA in planning an announcement of the final results of this unprecedented test of General Relativity.

## 1.4 The Two Einstein Effects

Newton believed that space and time were absolute or fixed entities and that gravity could be represented as an attractive force that somehow acted instantaneously between objects at a distance. In Newton's universe, the spin axis of a perfect gyroscope orbiting the Earth would remain forever fixed with respect to absolute space. Einstein determined that space and time are relative entities, interwoven into a “fabric,” which he called spacetime, and he realized that no force—not even gravity—could act faster than the speed of light. In Einstein's universe, the presence of celestial bodies causes spacetime to warp or curve; and gravity is the product of bodies moving in curved spacetime (Figure 1-2). Thus, in Einstein's universe, the spin axis of a perfect gyroscope orbiting the Earth will precess (change its orientation) over time with respect to the distant universe, as it follows the warping and twisting curvature of spacetime.

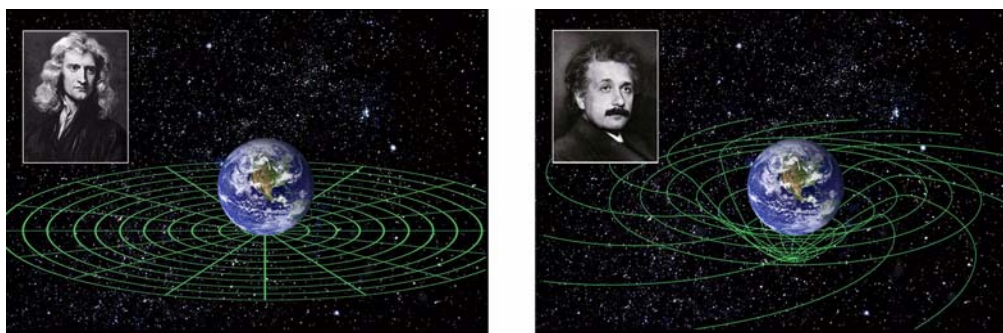


**Figure 1-2.** Newton's flat and fixed space and time (left) vs. Einstein's warped and twisted spacetime (right)

GP-B is measuring both the predicted geodetic effect, the amount by which the Earth's presence is warping its local spacetime. Concurrently, and even more important, GP-B is measuring the predicted frame-dragging effect, deduced in 1918 as a corollary to general relativity by Austrian physicists Josef Lense and Hans Thirring, and never before directly measured. It states that massive celestial bodies, like the Earth, drag their local



spacetime around with them as they rotate. This effect of a moving “gravitational charge” is often compared to the generation of a magnetic field by a moving electric charge, and is often referred to as *gravitomagnetism*. Physicists and cosmologists are particularly interested in frame-dragging because it may account for the enormous power generation in the most massive and explosive objects in the universe, such as black holes.

## 1.5 Why Perform Another Test of Einstein?

While it has become a cornerstone of modern physics, general relativity has remained among the least tested of all theories in physics, because, as Caltech physicist Kip Thorne once put it: “In the realm of black holes and the universe, the language of general relativity is spoken, and it is spoken loudly. But in our tiny solar system, the effects of general relativity are but whispers.”

And so, any measurements of the relativistic effects of gravity around Earth must be carried out with utmost precision. Over the past 90 years, various tests suggest that Einstein was on the right track. But, in most previous tests, the relativity signals had to be extracted from a significant level of background noise. The purpose of GP-B is to test Einstein’s theory by carrying out the experiment in a pristine orbiting laboratory, reducing background noise to extremely low levels and enabling the experiment to examine general relativity in new ways. If GP-B’s results corroborate the predictions of general relativity, we will have made the most precise measurement of the shape of local space-time, and confirmed the theory of general relativity to a new standard of precision. If on the other hand, the results disagree with Einstein’s theoretical predictions, theoretical physicists may be faced with the challenge of constructing a whole new theory of the structure of the universe and the motion of matter.

## 1.6 Experimental Design & “Near Zeroes”

Conceptually, the GP-B experiment is simple (Figure 1-3): Place a gyroscope and a telescope in a polar-orbiting satellite, 642 km (400 mi) above the Earth. (GP-B actually uses four gyroscopes for redundancy.) At the start of the experiment, align both the telescope and the spin axis of each gyroscope with a distant reference point—a guide star. Keep the telescope aligned with the guide star for a year, and measure the precession change in the spin-axis alignment of each gyro over this period in both the plane of the orbit (the geodetic precession) and orthogonally in the plane of the Earth’s rotation (frame-dragging precession).

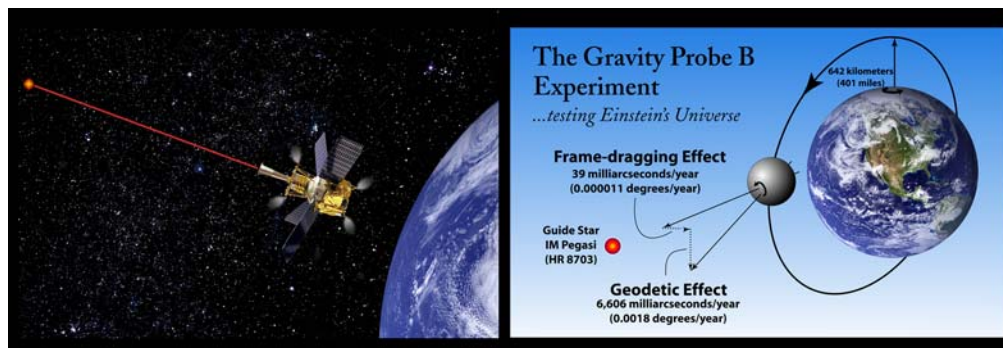


**Figure 1-3.** The GP-B spacecraft in orbit and the two measurements being made with the gyroscopes on-board

The predicted geodetic gyro-spin-axis precession is a tiny angle of 6,606 milliarcseconds (0.0018 degrees) in the orbital plane of the spacecraft. The orthogonal frame-dragging precession is a minuscule angle of 39 milliarcseconds ( $1.1 \times 10^{-5}$  degrees)—about the width of a human hair viewed from  $\frac{1}{4}$  mile away, or four feet at the Earth’s radius. GP-B’s measurement of the geodetic effect has an expected accuracy of better than 0.01%. The frame-dragging effect has never directly been measured, but Gravity Probe-B is expected to determine its accuracy to ~1%.

Designing a physics experiment involves a basic choice: maximize the effect to be measured, or minimize the “noise” that obscures it. For the Gravity Probe-B experiment, that choice was moot because Einstein’s relativistic effects that literally “roar” near black holes whisper almost inaudibly here on earth. Thus, implementing the experimental design described above required meeting seven near-zero design constraints—three near-zero constraints on the gyro rotors, which had to be near-perfect spheres, with uniform superconductive coatings and virtually no imperfections in shape and density, and four near-zero constraints on the pristine space-borne, cryogenic laboratory, which housed the gyros and shielded them from any sources of noise or interference that might distort the results—solar radiation, atmospheric friction, magnetic fields, electro-magnetic signals radiating from Earth, and so on. [Table 1-1](#) summarizes these seven near-zero constraints, showing the tolerance required and the tolerance actually achieved for each one during the mission.

**Table 1-1.** GP-B Seven Near Zeros

Experimental Variable	Tolerance Requirements	Tolerances Achieved During Mission
<b>Gyroscope Rotor Near Zeros</b>		
Mechanical Sphericity	50 nanometers (2 micro inches)	<10 nanometers (< 0.4 microinches)
Material Homogeneity	3 parts in 10 <sup>6</sup>	3 parts in 10 <sup>7</sup>
Electrical Sphericity	5 parts in 10 <sup>7</sup>	<5 parts in 10 <sup>7</sup>
<b>Probe Environment Near Zeros</b>		
Temperature	1.95 kelvin (-271.2° degrees Celsius or -456.2° degrees Fahrenheit)	1.8 kelvin (-271.4° degrees Celsius or -456.4° degrees Fahrenheit)
Non-Gravitational Residual Acceleration	Less than 10 <sup>-10</sup> g	Less than 5 x 10 <sup>-12</sup> g
Background Magnetic Field	10 <sup>-6</sup> gauss	Less than 10 <sup>-7</sup> gauss
Probe Pressure	10 <sup>-11</sup> torr	Less than 10 <sup>-11</sup> torr

## 1.7 Unique and Extraordinary Technologies

While the concept of Gravity Probe B is relatively simple, carrying out the experiment required some of the most accurate and sophisticated technology ever developed. In fact, scientists and engineers from Stanford, Lockheed Martin, and NASA had to invent about one dozen totally new technologies in order to meet GP-B’s near-zero constraints, because much of this technology simply did not exist when the experiment was first suggested in late 1959 - early 1960. Einstein, himself once a patent clerk, would have enjoyed reviewing these extraordinary technologies.

### 1.7.1 The World’s Most Perfect Gyroscopes

To measure the minuscule angles predicted by Einstein’s theory, the GP-B team needed to build a near-perfect gyroscope—one whose spin axis would not drift away from its starting point by more than one hundred-billionth of a degree each hour that it was spinning. By comparison, the spin-axis drift in the most sophisticated Earth-based gyroscopes, found in high-tech aircraft and nuclear submarines, is seven orders of magnitude (more than ten million times) greater than GP-B could allow.

To accomplish this exceptional challenge, the GP-B gyroscope rotors ([Figure 1-4](#)) had to be perfectly balanced and homogenous inside. They had to be free from any bearings or mechanical supports, and they had to operate in a near-perfect vacuum.

After years of work and the invention of new technologies and processes for polishing, measuring sphericity, and thin-film coating, the result was a homogenous 1.5-inch sphere of pure fused quartz, polished to within a few atomic layers of perfectly smooth. In fact, the GP-B gyro rotors are now listed in the Guinness Database of World Records as being the roundest objects ever manufactured; they are topped in sphericity only by neutron stars. The spherical rotors are the heart of each GP-B gyroscope. The raw quartz material was mined in Brazil, and then fused (baked) and refined in a proprietary process at Heraeus Amercil in Germany. The interior composition of each gyro rotor is homogeneous to within two parts in a million. On its surface, each gyroscope rotor is less than three ten-millionths of an inch from perfect sphericity. This means that every point on the surface of the rotor is the exact same distance from the center of the rotor to within  $3 \times 10^{-7}$  inches. If a GP-B gyroscope rotor were enlarged to the size of the Earth, its tallest mountain or deepest ocean trench would be less than eight feet!



**Figure 1-4.** A GP-B niobium-coated gyro rotor and housing (left), the Guinness Database record for roundness (center), and measuring the sphericity of a gyro rotor (right)

Finally, a GP-B gyroscope is freed from any mechanical bearings or supports by levitating the spherical rotor within a precisely machined fused-quartz housing cavity. Six electrodes, evenly spaced around the interior of the housing, keep the rotor levitated in the housing cavity. During the IOC phase of the mission, a stream of pure helium gas was used to spin up each of the four gyroscopes to approximately 4,000 rpm. After that, all but a few molecules of the helium spin-up gas was evacuated from the housings, and the gyroscopes were left spinning—a mere 32 microns (0.001 inches) from their housing walls, free from any mechanical or fluid supports. During the experiment, the near-perfectly spherical and homogeneous rotors, combined with the highly sophisticated Gyro Suspension System (GSS), resulted in an average spin-down time constant of approximately 15,000 years for the four GP-B gyros.

### 1.7.2 Gyro Suspension System (GSS)

The GSS, that electrostatically suspends the science gyroscopes within their housing cavities and enables them to spin freely with minimal friction and torque, is a marvel of engineering in its own right. To perform its mission successfully, the GSS had to satisfy a number of requirements:

1. Operate over 8 orders of force magnitude. The same system must be able to suspend the gyroscopes on Earth in a 1 g field as well as generate minimal disturbances at the  $10^{-8}$  g level during data collection.
2. Suspend or levitate the gyroscopes reliably. The system must *never* let a spinning rotor touch the housing. There is sufficient mechanical energy in a rotor spinning at 4,000 rpm to effectively destroy the rotor and housing in such an event.



3. Operate compatibly with the SQUID readout system. The SQUID magnetometers are extremely sensitive. Thus, the suspension system must not interfere with these sensors, both during ground and on-orbit operation.
4. Minimize electrostatic torques during science data collection. The suspension system must meet centering requirements with absolutely minimal control effort, and thereby with minimal residual torques on the rotors.
5. Apply controlled torques to the rotor for calibration and initial rotor spin-axis alignment.
6. Act as an accelerometer as part of the “drag-free” translation control system to further minimize classical torques on the rotors by another factor of  $10^6$ .

All of these requirements were met during the GP-B flight mission. Furthermore, the suspension systems continue to operate well following the depletion of helium from the dewar, since they do not require cryogenic electronics to function.

### 1.7.3 SQUID Magnetometers for Gyro Orientation Readout

How can one monitor the spin-axis orientation of a near-perfect spherical gyroscope without any physical marker showing the location of the spin axis on the gyro rotor? The answer lies in a property exhibited by some metals, called “superconductivity.” At temperatures slightly above absolute zero, many metals completely lose their electrical resistance and become superconductive. Furthermore, as predicted in 1948 by theoretical physicist Fritz London, a spinning superconductor develops a magnetic moment—created by the electrons lagging the lattice of the superconducting metal—which is therefore exactly aligned with its instantaneous spin axis.

What is wonderful about this phenomenon (and most fortunate for GP-B) is that the axis of this magnetic field lines up exactly with the physical axis of the spinning metal coating on each rotor. Here was the “marker” Gravity Probe B needed. Each spherical GP-B quartz gyroscope rotor is coated with a very thin layer of superconducting niobium (1,270 nanometers thick). When each niobium-coated gyroscope rotor is spinning, a small magnetic field surrounds it. By monitoring the axis of the magnetic field, Gravity Probe B knows precisely which direction the gyroscope's spin axis is pointing, relative to its housing. This is one of the many technologies invented and developed specifically for GP-B.

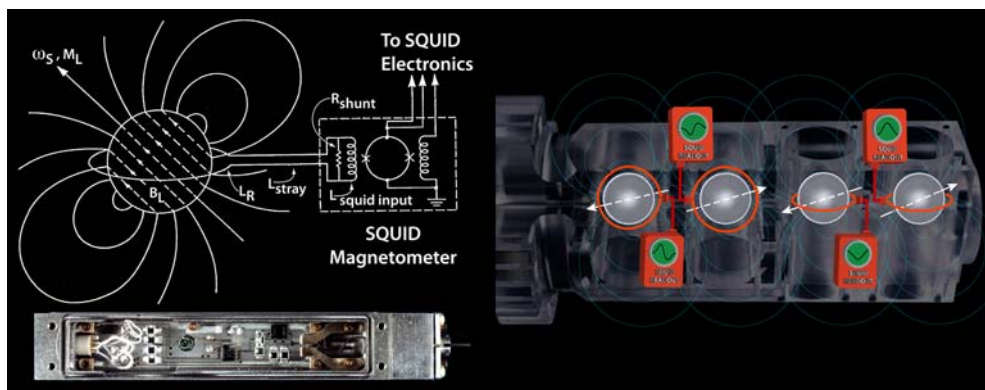


**Figure 1-5.** A GP-B SQUID module (left) and a diagram of the magnetic pickup loop and London moment

The spinning rotor’s magnetic field axis is monitored with a special type of magnetometer, called a SQUID (Superconducting QUantum Interference Device, shown in [Figure 1-5](#)). The SQUID is connected to a superconducting niobium pickup loop, deposited on the flat surface at the outer edge of one optically flat mating surface of the quartz housing in which the gyro rotor spins. Thus, the loop, which senses the gyro’s spin-axis orientation, is located on the planar surface where the two halves of the gyro housing are joined. When the spin

axis of a gyroscope rotor changes its orientation, the London moment magnetic field moves with it, passing through the superconducting loop. This causes a quantized current to flow in the loop, and the SQUID detects this change in magnetic field orientation. The SQUID magnetometers are so sensitive that a field change of only  $5 \times 10^{-14}$  gauss (one ten-billion<sup>th</sup> of the Earth's magnetic field) and corresponding to a gyro deflection of 0.1 milliarcseconds ( $3 \times 10^{-8}$  degrees)—is detectable.

### 1.7.4 The Pointing Telescope

A 36 centimeter (14 inch) long Cassegrain reflecting astronomical telescope (Figure 1-6) with a focal length of 3.8 meters (12.5 feet), mounted inside the GP-B Probe along the central axis of the spacecraft and dewar, provided the experiment's required reference to a distant "guide star." Any change in spin-axis orientation of each of the gyros, as they traveled through the warped and twisted spacetime around the Earth, was measured against this guide star reference to distant spacetime. During the science phase of the mission, the telescope's job (in conjunction with the ATC) was to keep the entire spacecraft precisely pointed at the center of the guide star with a pointing deviation in the range of approximately  $\pm 200$  milliarcseconds ( $\pm 6 \times 10^{-5}$  degrees).

To satisfy these precision pointing requirements, it was necessary to locate the optical center of the guide star image in the telescope to an accuracy of 0.1 milliarcseconds ( $3 \times 10^{-8}$  degrees). The diffraction limit size of the GP-B telescope is approximately 1.4 arcseconds, which is about 14,000 times larger than the required pointing accuracy, and this presented a formidable challenge to the GP-B team. The solution was to precisely split the image into equal x-axis and y-axis components, and then to divide each of the axis components into two half images whose brightness values could be compared.

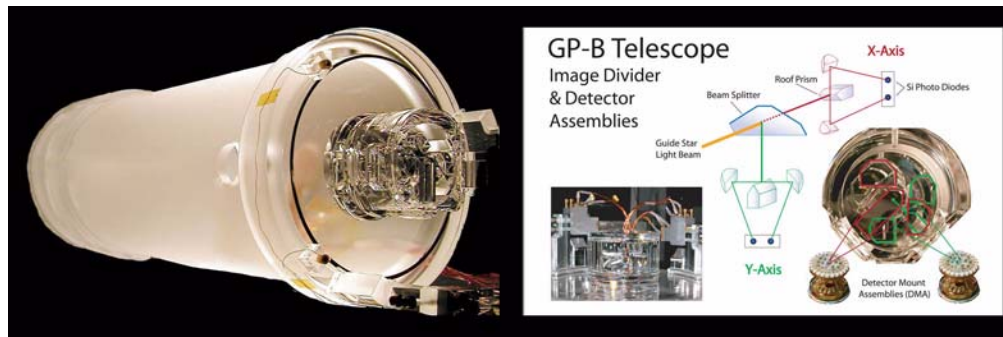


**Figure 1-6.** A pre-flight prototype of the GP-B telescope and diagram of its image-centering operation

GP-B accomplished this task by focusing the mirror-reflected starlight onto an Image Divider Assembly (IDA) at the telescope's front end. In the IDA, the starlight was first passed through a beam-splitter (a half-silvered mirror), that forms two separate images, one for the horizontal (x) axis and one for the vertical (y) axis. The half beam from each axis was then focused onto a roof-prism (a prism shaped like a peaked rooftop). Each roof prism sliced its portion of the starlight beam into two half-disks, which were focused onto a pair of silicon photo diodes.

The photo diodes converted the light signals from each half-disk to electrical signals which were then compared. If the signals were not equal, the roof-prism was not slicing the image precisely in half. The orientation of the entire spacecraft was then readjusted in real time until the signals were equal and the image was split right down the middle. When this was accomplished for both the x-axis and y-axis halves of the starlight beam, the telescope was locked on the exact center of the guide star. Once tuned up, the Attitude and Translation Control (ATC) system on-board the spacecraft was capable of locking the telescope onto the guide star in less than a minute each time the spacecraft emerged from behind the Earth over the North Pole and the guide star came into view. Once the telescope was locked onto the guide star, the telescope pointing signals were used to compensate for the small pointing deviation to an accuracy of better than 0.1 milliarcseconds ( $3 \times 10^{-8}$  degrees).

### 1.7.5 Relating the Guide Star’s Motion to a Distant Quasar

Ideally, the telescope would be aligned with a distant quasar, because quasars are so distant from the Earth that they appear to be fixed in their relative position and would thus provide an ideal, stable reference point for measuring changes in gyroscope spin-axis orientation. However, quasars are too dim for any optical telescope this size to track. So, instead, the telescope was focused on a brighter, nearby guide star whose motion could be mapped relative to quasars separately. As such, the frame of reference of the Gravity Probe B gyroscope measurements will ultimately be related to the far distant universe.

In order to precisely map the motion of a guide star relative to a quasar, it was necessary to select a guide star that was in the correct position for tracking by the on-board telescope, shines brightly enough for the on-board telescope to track accurately, can be tracked by radio telescopes on Earth, and is visually located within a fraction of a degree from a reference quasar. Out of 1,400 stars that were examined, only three matched all the necessary criteria, and the star that was chosen as the GP-B guide star is named IM Pegasi (HR 8703).

Thus, throughout the science phase of the mission, the GP-B science telescope was tracking a very slowly moving star, but the gyros were unaffected by the star's so-called “proper motion,” their pointing reference was IM Pegasi’s position in the celestial sphere. Consequently, in the gyro precession data, it is necessary to subtract out the displacement of the original guide-star orientation so that the angular displacements of the gyros can be related to the guide star’s initial position, rather than to its current position. For this reason, a very accurate map of the proper motion of IM Pegasi is required in order to complete the GP-B data analysis.

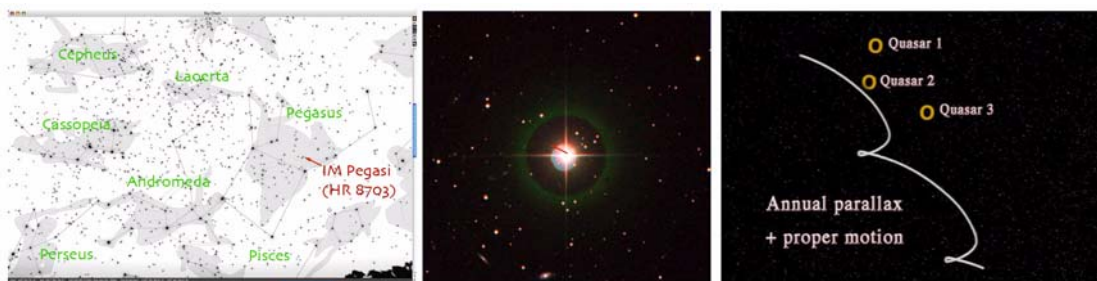


**Figure 1-7.** Guide Star IM Pegasi (HR 8703) sky location (left), photo (center) and proper motion (right)

Because IM Pegasi is a radio source, its proper motion can be tracked by a sophisticated world-wide network of radio telescopes, through a technique called Very Long Baseline Interferometry or VLBI. A team at the Harvard-Smithsonian Center for Astrophysics (CfA) led by astrophysicist Irwin Shapiro, in collaboration with astrophysicist Norbert Bartel and others from York University in Canada and French astronomer Jean-Francois Lestrade, have now mapped the motion of IM Pegasi with respect to a reference quasar over a number of years to an unprecedented level of accuracy. With these measurements the motions of the GP-B gyroscope spin axes can now be precisely related to the reference quasar in the far distant universe.

### 1.7.6 The Dewar

One of the greatest technical challenges for Gravity Probe B was keeping the probe and science instrument precisely at a designated cryogenic temperature, just above absolute zero, of approximately 2.3 kelvin (-270.9 degrees Celsius or -455.5 degrees Fahrenheit) constantly for 16 months or longer. This was accomplished by integrating the probe into a special 2,441 liter (645-gallon) dewar, or thermos (Figure 1-8), about the size of a mini van, that is filled with liquid helium, cooled to a superfluid state. This nine-foot tall Dewar comprised the main structure of the GP-B satellite itself.

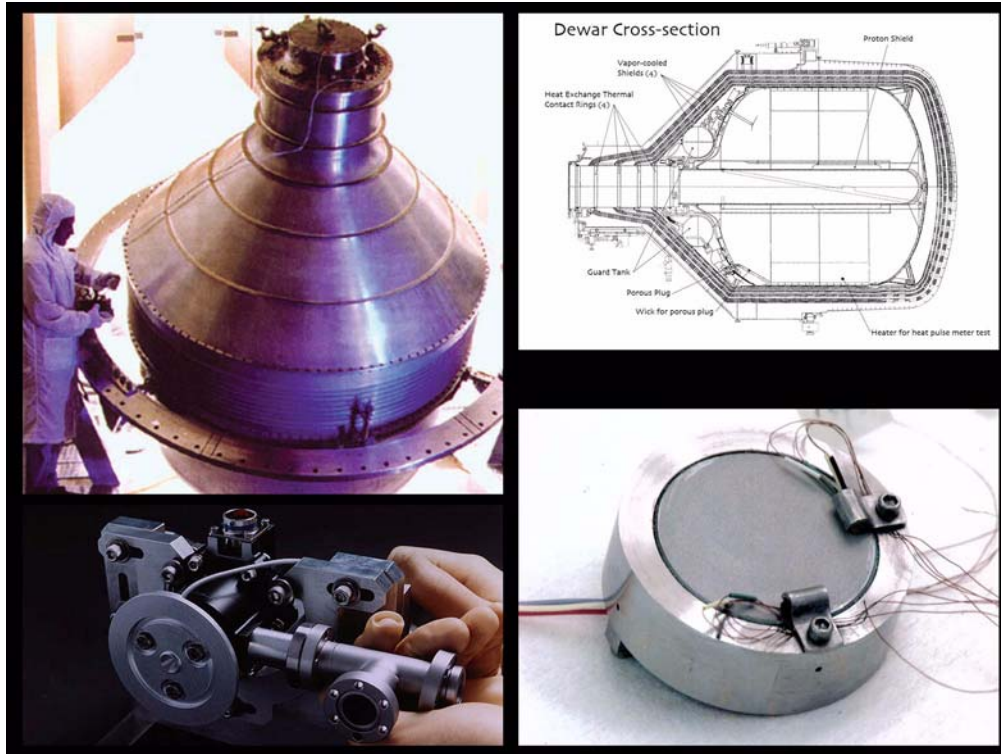


**Figure 1-8.** Clockwise, from top left: The dewar, a cross-section of the dewar, the porous plug, and one thruster

Through a combination of multi-layer insulation, vapor-cooled shields, and a unique porous plug, the dewar's insulating chamber was maintained in a cryogenic vacuum throughout the mission. While virtually no heat could penetrate from the outside wall through the vacuum and multi-layer insulation inside, a small amount of heat was continually conducted from the neck of the Dewar and from the heat-trapping windows inside the probe into the superfluid helium inside the dewar chamber. This very slight, but continual warming caused the superfluid helium to slowly vaporize into helium gas, which needed to be vented continually from the dewar chamber through the porous plug.

Invented at Stanford, and engineered for space at the NASA Marshall Space Flight Center, Ball Aerospace, and the Jet Propulsion Laboratory, the porous plug controls the flow of this evaporating helium gas, allowing it to escape from the Dewar, but retaining the superfluid helium inside. The plug is made of powdered titanium that has been sintered (heated) until it coalesces into a sponge-like pumice with very tiny pores. The evaporating helium gas climbed the side of the dewar near the plug and collected on the plug's surface, where it evaporated through the pores in the plug, much like sweating in the human body, drawing heat out of the liquid helium remaining in the Dewar, and thereby balancing the heat flow into the Dewar. The helium gas continually escaping through the porous plug was cycled past the shields in the outer layers of the Dewar, cooling them (thus the name, "vapor-cooled shields.") Moreover, it then was used as the propellant for eight pairs of micro thrusters, strategically located at the extremities of the spacecraft and used by the Attitude and Translation Control system (ATC) for high-precision pointing and positional control. Thus, not only did the dewar serve as the means of maintaining a cryogenic environment for the experiment, it was also the sole source of propellant for the ATC system.

### 1.7.7 Spacecraft Control—Nine Degrees of Freedom

GP-B is the first spacecraft ever launched requiring six degrees of freedom in active attitude control—three degrees of freedom in pointing control to maintain its guide-star pointing orientation (pitch and yaw) plus its constant roll rate, and three degrees of freedom in translational control (up-down, front-to-back, and side-to-side), to maintain a drag-free orbit throughout the 17-month flight mission. In addition, the Gyro Suspension System (GSS) for each gyroscope required three degrees of freedom in controlling the location of the spherical rotor within its housing. Thus, in total, the GP-B experiment required nine degrees of freedom for controlling the spacecraft—a truly demanding and remarkable accomplishment.

The term “drag-free” refers to a body that is moving without any friction or drag, and thus its motion is affected only by gravity. A drag-free satellite refers to a feedback system consisting of a satellite within a satellite. The inner satellite, often called a proof-mass, is typically a small homogeneous object, such as a spherical GP-B gyroscope, totally shielded from air drag and solar pressure. The position of the outer shielding satellite must be tightly controlled to prevent it from ever touching the proof mass. This is accomplished by equipping the outer satellite with sensors that precisely measure its position relative to the proof mass and a set of thrusters that automatically control its position, based on feedback from the sensors. Through this feedback system, the satellite continually “chases” the proof-mass, always adjusting its position so that the satellite remains centered about the proof mass, which is orbiting the Earth in a constant state of free fall—i.e, a purely gravitational orbit.

In the GP-B spacecraft, the drag-free feedback system was based on data from the Gyro Suspension System (GSS) for the science gyro that was serving as the drag-free proof mass. Based on this feedback, the ATC system metered the flow of the escaping helium gas through the 16 micro-thrusters in order to precisely control the spacecraft’s position. In fact, the location of the entire spacecraft was continually balanced around the proof-mass gyroscope by increasing or decreasing the flow of helium through opposing thrusters, to maintain a drag-free orbit. The drag-free feature of the GP-B spacecraft was critically important to the experiment because external drag on the spacecraft would otherwise cause an acceleration that would obscure the minuscule relativistic gyro precessions being measured.

GP-B’s ATC system, designed by Lockheed Martin, was truly an engineering “tour-de-force.” It took a considerable amount of time during the 4-month Initialization and Orbit Checkout (IOC) phase of the mission and part of the science phase of the mission for the GP-B and Lockheed Martin Mission Operations Team to master all the subtleties of this complex system.

## 1.8 The Management Experiment

GP-B was not a packaged experiment carried into orbit by a space-cargo vehicle. Rather, the GP-B spacecraft was a total system, comprising both the space vehicle and its unique payload—an integrated system dedicated as a single entity to making the measurements of unprecedented precision required by the experiment. To accomplish this goal, it was crucial that the whole system be developed by a strong and cohesive team.

In 1984, GP-B began the transition from program definition to payload and spacecraft design. Francis Everitt had become Principal Investigator in 1981, and with the anticipated increase in staff and activity required for design and development, he recruited Bradford Parkinson to join GP-B as Program Manager and also as a Co-PI, along with Co-PI’s John Turneure (Physics) and Dan DeBra (Aero-Astro). At that time, GP-B was defined as a two-phase Space Shuttle mission: first, a technology readiness demonstration (STORE—Shuttle Test of the Relativity Experiment) to be launched in 1989, followed two years later by the actual experiment, a satellite to be launched from a polar-orbiting Shuttle. For a number of reasons including the interdependency of the payload and spacecraft and the high level of technology development required, Samuel Keller, then Deputy Director of the NASA Office of Space Science Applications, decided to make Stanford NASA’s prime contractor on the GP-B mission. James Beggs, then the NASA Administrator, concurred with this decision and remarked that in addition to being a physics experiment that needed to be carried out in space, GP-B was equally interesting as a



“management experiment.” This was one of the first, and largest NASA missions, in which a university was given the prime role of managing the development of an entire space flight mission—science instrument, spacecraft, operations and data analysis.

Following the Challenger disaster in 1986 and the subsequent closure of NASA's West Coast, polar-orbiting shuttle launch facility, it became necessary to re-cast the GP-B mission as a satellite to be launched from its own expendable rocket. From 1992-1994, Stanford conducted a thorough source selection process from which LMSC was chosen to build the space vehicle into which the dewar and probe would be integrated. During the ensuing years, Stanford led the combined team, with oversight from NASA's Marshall Space Flight Center (MSFC), in developing and perfecting each of the components of the payload and spacecraft.

In the late 1990s, it was time to transition GP-B from a research and development program with limited NASA oversight to a classical NASA flight program that would culminate in the complete integration and testing of the payload-spacecraft system, followed by a successful launch, on-orbit operations, and subsequent data analysis. This shift in focus from maximizing advances in research and development to minimizing the risks in producing a flight-ready spacecraft was a difficult transition for GP-B. It took the exceptional insight and leadership of Rex Geveden, then NASA's GP-B Program Manager at MSFC (now Associate Administrator at NASA Headquarters), in collaboration with Principal Investigator Francis Everitt and other senior management at Stanford, LMSC, and NASA to arrive at an effective, minimum-risk-based management plan that would ready the GP-B spacecraft, payload and operations team for the flight mission.

Given the success of the GP-B launch and 17.3-month flight mission, the management experiment was also a success. It showed that a university, in close partnership with NASA and an experienced aerospace sub-contractor, can effectively develop and operate a sophisticated integrated satellite, and it provided NASA with invaluable management insights for future missions.

## 1.9 The GP-B Spacecraft

All of the Gravity Probe B technologies were integrated into one of the most elegant satellites ever launched ([Figure 1-9](#)). The spacecraft was built around the dewar. Embedded along the dewar's central axis was a cigar-shaped canister called the Probe which contained a series of heat-absorbing windows, a helium-adsorbing cryopump, and the Science Instrument Assembly (SIA)—the pristine space-borne laboratory for making the GP-B experimental measurements.

The SIA comprised the telescope and the quartz block, optically bonded together. The quartz block contains the four gyros and SQUIDs that monitor the spin-axis orientations of the gyros. The telescope and all four gyros were precisely aligned along the long, central axis of the spacecraft, around which the spacecraft rolled continuously at 0.77 rpm (77.5 seconds per revolution) throughout the science phase of the mission.

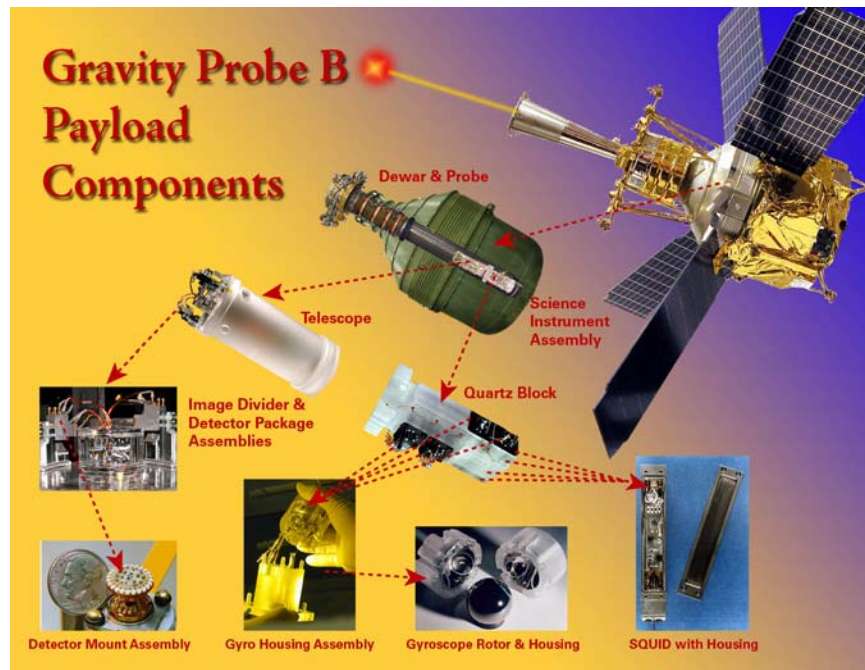


**Figure 1-9.** The GP-B spacecraft and its main payload components

Outside the dewar, mounted to the spacecraft frame are all the systems that provide power, navigation, communication and control of the spacecraft, including:

**Sun Shield.** This is a conical tube, attached to the probe, that kept stray light from entering the telescope.

**Proportional Micro Thrusters.** Eight pairs of balanced, proportional thrusters provided very precise attitude and position control in orbit during the flight mission. (Now that the helium is exhausted from the dewar, these micro thrusters are no longer functional, and only a set of magnetic torque rods control the spacecraft's attitude, with much less precision than the thrusters provided.)

**Solar Arrays.** These four arrays convert energy from the Sun into electrical power that is stored in the spacecraft's two batteries and then used to run the various electrical systems on board. Because the orbit plane of the GP-B spacecraft always contained the guide star, the position of each solar array was precisely canted to maximize the power output as the spacecraft rolled and changed position with respect to the Sun over the course of the mission.

**GPS Sensors & Antennae.** Four GPS (Global Positioning System) antennas on-board the spacecraft—two at the forward end of the spacecraft and two at the aft end—transmit information about both the spacecraft's position and its attitude.

**Telemetry & Communications Antennae.** These fore and aft antennae enable both inbound and outbound communications with the space vehicle, including communications with ground stations and with orbiting communications satellites in the Tracking Data Relay Satellite System (TDRSS).

**Two Star Trackers.** Basically, these are telescopes with cameras and pattern-matching systems that use constellations and stars to determine the direction in which the satellite is pointing. During the mission the star trackers functioned like "spotting scopes" for the science telescope. Once the star trackers had oriented the spacecraft within 60 arcseconds (0.017 degrees) of the guide star, the telescope took over the job of achieving and maintaining the precise alignment required for measuring gyroscope precession.

**Attitude-Control Gyroscopes.** Two pairs of standard, flight-qualified rate-sensing gyroscopes, equivalent to those found on other spacecraft (and also airplanes, ships, and other vehicles) were included as part of the general navigation system used for monitoring the orientation of the spacecraft.

**Electro-mechanical Control Systems.** Surrounding the dewar, a lattice of trusses forms the outer structure of the spacecraft. Attached to these trusses are a number of electrical and mechanical systems that control the operation of the spacecraft and enabled the relativistic measurements to be carried out. These control systems include the following:

- **Attitude & Translation Control System (ATC)**—Uses feedback from the gyro suspension system (GSS), the SQUID readout system (SRE), the telescope readout system (TRE), the star trackers, magnetometers, and rate-sensing navigational gyroscopes to control the proportional micro thrusters and magnetic torque rods that determine and maintain the spacecraft’s precise attitude and position relative to one of the science gyro rotors that serves as the drag-free proof mass.
- **Magnetic Torquing System (MTS)**—A set of long electromagnets that push or pull against the Earth’s magnetic field to orient the spacecraft’s attitude.
- **Mass Trim Mechanism (MTM)**—A system of movable weights that can be adjusted during flight to restore precise rotational balance of the space vehicle (similar to spin balancing the tires on an automobile)
- **Gyro Suspension System (GSS)**—The electronics that levitate and precisely control the suspension of the four gyroscopes at the heart of the Gravity Probe B experiment.
- **Gas Management Assembly (GMA)**—A very complex set of valves, pipes, and tubing that was used to spin up each of the four gyroscopes by blowing a stream of 99.99999% pure helium gas over them, through a channel built into one half of each gyroscope’s quartz housing. (Subsequently, all but a few molecules of the helium gas were removed from each housing; the gyro rotors spun in a near-perfect vacuum.)
- **Experiment Control Unit (ECU)**—The ECU controls many of the systems on-board the space vehicle, including the GMA, the ultraviolet light system used to remove electrostatic charge from the gyro rotors, and various thermal devices.

## 1.10 On-Orbit Operations

With a typical spacecraft, the mission operations team spends a considerable amount of time after launch learning how the spacecraft behaves and responds. Once the team has become comfortable operating the vehicle, the more sophisticated experimental operations are then attempted. In contrast, GP-B required that a number of very complex operations be carried out during the Initialization and Orbit Checkout (IOC) mission phase immediately following launch, because the dewar’s lifetime was limited to approximately 16-17 months and a year’s worth of experimental data had to be collected while there was still liquid helium in the dewar. With all of the unique features and cutting-edge technologies embodied in the GP-B spacecraft, it became apparent early on that the GP-B mission operations team would have to “hit the ground running.” To accomplish this goal, a sophisticated mission operations plan was created. Detailed procedures with contingencies, were developed, and the GP-B mission operations team went through rigorous training. One of the hallmarks of the GP-B mission operations team was “test it as you fly it, and fly it as you test it.” This meant that all of the ground test software and procedures used were essentially the same as those used in flight. The GP-B team also worked through a number of pre-launch simulations, with the test program being based on expected mission operations. Thus, by the time of launch, the team was already well-rehearsed and ready to tackle real issues and anomalies.



Launch operations proceeded like clockwork, with virtually perfect orbit insertion. The team then immediately set to work performing IOC initialization and checkout procedures. Activities during the IOC phase included tuning the ATC system to set the spacecraft's roll rate, capturing the guide star at the top of each orbit in less than one minute, and establishing and maintaining drag-free control. In addition, it was necessary to balance the spacecraft about its center of mass by adjusting the Mass Trim Mechanisms on the spacecraft frame and to uniformly wrap the helium bubble inside the dewar by briefly increasing the spacecraft's roll rate.

However, the most delicate and painstaking operations concerned the four science gyros, for which there were no precedents in any other space mission. First, the gyro suspension system had to be checked out and calibrated for each of the four gyros. Then, the gyros were spun-up, one by one, by blowing a stream of pure helium gas through a spin-up channel in each rotor housing. The spin-up was accomplished gradually, in three stages that lasted over a month, ultimately resulting in the final gyro spin rates averaging 4,000 rpm. The spin-up operations were among the most stressful and risky of the entire mission. Following gyro spin-up, it was necessary to “bake out” excess helium molecules remaining in the Probe from the spin-up gas. It was then necessary to align the spin axis of each gyro with the guide star—another set of painstaking procedures. Finally, gyro #3 was designated as the “proof mass” to be used by the ATC system to maintain the spacecraft in a drag-free orbit. At last, on August 28, 2004, the spacecraft and payload were ready to begin collecting science data.



**Figure 1-10.** The GP-B Mission Operations Center (MOC) during gyro spin-up (left) and end of helium (right)

The IOC phase was followed by an 11 month science-data-taking phase. In comparison to IOC, this period was relatively straightforward and routine. By the start of the science phase, the team was very well trained; each team member knew well his or her responsibilities, thus further easing the effort. Moreover, while most days were uneventful, an “all-hands” meeting was held every day to ensure that the team remained focused on the status of the total system—spacecraft and payload. The all-important science data were transmitted to the ground four times a day. The engineering and science teams reviewed the data on a daily basis and provided top-level feedback on the previous day's data at the daily meeting.

The science mission concluded with a 6-week instrument calibration phase. The purpose of this phase was to help evaluate sources of systematic experiment error and to allow the team to place limits on possible gyroscope torques. Although many operations were performed during this period, the implementation was performed nearly flawlessly.

Ever since the launch of the spacecraft in April 2004, the Mission Operations Center (MOC) at Stanford ([Figure 1-10](#)) was the lifeline to the spacecraft. Mission operations personnel in the MOC were always focused on the current vehicle status. Typically, the vehicle would be “green” and the MOC would verify this status with a real-time monitoring system. In a typical “green” day, the daily 10 am “all-hands” meeting would inform the team of the previous day's events and planned future operations. Following the all-hands meeting, mission planners would meet with subsystem specialists to develop the detailed plan for the next day. In practice, much of the planning already had been developed long before, and only rearrangement of the order of tasks was required. When new products were required, the Integrated Test Facility (ITF), a ground-based computerized model of all systems on-board the GP-B spacecraft, was used for verification prior to use on the vehicle.

Any significant deviation from “green” would immediately “trump” other program activities. An efficient electronic communication-information system allowed for rapid response. Telemetry information from the MOC, as well as information determined from off-line analysis, were in near-constant review. Deviations from a “green” or expected result would cause the immediate initiation of an in-house anomaly resolution process, described in the next section.

By the end of mission, the GP-B team had become very skilled at both operating the spacecraft and handling anomalies. Thus, there was some sadness—as well as the thrill of accomplishment—when the mission ended and members of this truly remarkable mission operations team moved on to new jobs and other missions in their careers.



**Figure 1-11.** NASA GP-B Program Manager, Tony Lyons, from the Marshall Space Flight Center in Huntsville, AL, presents a NASA Group Achievement Award to the entire GP-B team in November 2005.

At the end of November 2005, shortly after the successful completion of the GP-B flight mission, NASA’s GP-B Program Manager, Tony Lyons from the Marshall Space Flight Center, presented a NASA Group Achievement Award to the entire GP-B science mission team, including, of course, people from both Stanford and Lockheed Martin (Figure 1-11). The award reads: “For exceptional dedication and highly innovative scientific and engineering accomplishments leading to the successful execution and completion of the Gravity Probe B Science Mission.” The award is signed by NASA Administrator Michael Griffin, and an individual citation was given to each and every member of the team.

## 1.11 Anomaly Resolution

In space missions, there are always some problematic events—both anticipated and unexpected. The GP-B mission was no exception. We call these surprising events “observations” and “anomalies.” An important part of the pre-launch preparation for the mission was to set up a formal anomaly review process, including procedures for assembling a quick-response anomaly team at any time—day or night—to work through the anomaly, determine the root cause, and come up with a procedure for addressing the issues and returning the spacecraft to nominal operating mode.

A special room in the GP-B Mission Operations, called the Anomaly Room (Figure 1-12), was the home of the GP-B Anomaly Review Board (ARB), a select group of senior GP-B team members from Stanford, NASA, and Lockheed Martin, who managed the troubleshooting of anomalies and observations. The Anomaly Room, which was located across the corridor from the GP-B MOC, contained a set of spacecraft status monitors, communications and teleconference equipment, computer and voice hookups, a documentation library, white boards, a computer projection system, and an oval discussion table.



**Figure 1-12.** The GP-B Anomaly Room in action

During the flight mission, whenever an anomaly was in the process of being resolved, the Anomaly Room was staffed 24 hours a day, 7 days a week; at other times, it was staffed during normal working hours, with team members on call. When major anomalous events, such as computer reboots, occurred outside normal working hours, the Mission Director on duty activated the Anomaly Room and issued a series of pager and cell phone calls via computer, summoning key staff members on the ARB, along with a selected anomaly team, comprised of resident engineers and engineering specialists, to come in and work through the issue. The group used a technique called “fault tree analysis” to evaluate and determine the root cause of unexpected events.

The first anomaly in orbit occurred just two weeks into the mission at around 3:00 AM, when stray protons from a solar flare struck multiple critical memory cells in the main on-board flight computer, causing an automatic switch-over to the backup computer. The GP-B anomaly team was assembled by 4:30 AM that morning—within 90 minutes of the event—and they immediately began taking corrective action.

Over the course of the flight mission, the ARB successfully worked through 193 observations/anomalies. Of these, 23 were classified as true “anomalies,” five of which were sub-classified as “major anomalies,” including the B-Side computer switch-over and the stuck-open valve problems with two micro thrusters early in the mission, as well as subsequent computer and subsystem reboot problems due to radiation strikes. Of the remaining 18 anomalies, 12 were sub-classified as “medium anomalies” and 6 were sub-classified as “minor anomalies.”

The 170 other issues (88%) were classified—at least initially—as “observations.” These observations typically documented various unanticipated events, sub-optimal parameter settings, and other unusual results that were monitored until their root cause was understood. In several cases, observations were escalated to anomaly status, and then necessary actions were taken first to understand, and then to correct the problem. In all cases, the established anomaly resolution process enabled the team to identify the root causes and provide procedures that led to recovery.

Anomalies on orbit did cause some disruptions in the data collection. Methods of treating these had been identified prior to launch and are currently being systematically addressed in the data analysis.

## 1.12 Managing Program Risks

Through mission development, GP-B instituted a high-visibility risk steering committee, which program management used to evaluate and set overall program priorities. Risk groups met on a monthly basis; both Stanford and MSFC had independent risk evaluation teams, using different processes, that met regularly to share their assessments.

Hardware risks were evaluated on the basis of probability of occurrence, as well as the impact of potential failure, using a complete Failure Modes and Effects Analysis (FMEA) process. Other program risks (e.g., budget, schedule and personnel) were evaluated using a similar method. The committees solicited advice from independent councils of experts to ensure that our evaluations were correct. Five categories of risk were

established, ranging from Level 1 (not likely, little cost or critical path impact, and no compromise in mission performance) to Level 5 (Nearly certain likelihood, very large program cost and critical path impact and loss of mission).

Based on potential impact to the program, each risk was evaluated using a table of risk levels and consequences as a guideline. The risk action was then assigned to one of three categories:

- **Mitigate.** Eliminate or reduce the risk by reducing the impact, reducing the probability or shifting the time frame.
- **Watch.** Monitor the risks and their attributes for early warning of critical changes in impact, probability, time frame, or other aspects.
- **Accept.** Do nothing. The risk will be handled as a problem if it occurs. No further resources are expended managing the risk.

Risks were promoted or demoted as program needs or technical understanding evolved. This risk mitigation process was an exceptionally good example of the complementary skills of the MSFC and Stanford-Lockheed teams, as borne out by the success of the mission.

## 1.13 A Successful Mission

Managing a flight program such as GP-B, in which the spacecraft contained only a single, highly integrated payload proved to be a challenge for NASA, its government overseers, Stanford University as NASA's prime contractor, and Stanford's subcontractor, Lockheed Martin—so much so that in 1984, the then NASA Administrator, James Beggs, remarked that GP-B was not only a fascinating physics experiment, but also a fascinating management experiment. NASA thoroughly addressed these challenges, and the many years of planning, inventing, designing, developing, testing, training and rehearsing paid off handsomely for GP-B, culminating in a highly successful flight mission.

Beginning with a picture-perfect launch, bull's-eye orbit insertion, and breath-taking live video of spacecraft separation, the mission got off to a flawless start. The preparedness of the GP-B mission operations team immediately became evident in its deft handling of two major anomalies that occurred within the first month of the mission—the automatic switch-over from the main to the backup flight computer due to proton strikes induced by solar flares and two micro thrusters that had to be isolated due to stuck-open valves. In both cases, the team's knowledge and well-coordinated responses resulted in efficient mitigation of the problems and timely restoration of nominal spacecraft operations. Furthermore, the experience of working through major anomalies early in the mission provided invaluable experience that enabled the team to handle similar anomalies during the science phase of the mission with even more efficiency.

GP-B is arguably one of the most sophisticated spacecraft ever flown. It incorporated many new technologies—most notably the gyros, their suspension systems, the accompanying SQUID readouts, and the precision-pointing of the spacecraft-fixed telescope—whose debut performance in space occurred during this mission. It is remarkable, and a testament to the preparation, talent, knowledge and skill of the Stanford-NASA-Lockheed Martin development team, that all of these technologies performed exceedingly well on orbit, with some, such as the GSS and SQUID readouts, far exceeding their required performance specifications. Likewise, the GP-B mission operations team was one of the best ever assembled. During IOC, even the most difficult and risky operations, including gyro spin-up, low-temperature bakeout of the excess helium gas, and gyro spin-axis alignment all proceeded smoothly. The one system that required considerable fine-tuning well into the science phase of the mission was the Attitude and Translation Control (ATC) system. Due in large part to solar environment sensitivity of the external Attitude Reference Platform (ARP), on which the ATC's star trackers were mounted, parameters in the ATC system had to be seasonally adjusted in order for the spacecraft's required precision pointing to be maintained. By April 2005, all of the issues with the ATC had been identified and addressed, and from that time forward, the ATC system performance was quite good.

By the end of IOC in August 2004, GP-B team members had a masterful command and knowledge of the spacecraft's systems and its nuances, and they were well-primed to handle any situation or anomaly that might occur during the ensuing science (data collection) and instrument calibration phases. As it turned out, the helium in the dewar lasted 17 months and 9 days—a month longer than had been anticipated through numerous helium lifetime tests performed throughout the mission by the dewar team. This made it possible to collect science data for 50 weeks, just 14 days shy of the one-year data collection goal, and this was of great benefit to the GP-B science team. In fact the helium lasted long enough for the team to perform many extra calibration tests following the science data collection phase.

During the months after the flight mission, the team performed several feasibility tests of possible post-mission experiments, and then they readied the spacecraft for a hibernation state, from which it can be awakened at any time, in the event that there is interest and funding for post-mission experiments or uses of the spacecraft. (The spacecraft can remain functional in orbit for another ten years or more.)

Following is a list of some of the extraordinary accomplishments achieved by GP-B during the 17 months of its flight mission.

- Over the course of the 17.3-month mission, we communicated with the spacecraft over 4,000 times, and the Mission Planning team successfully transmitted over 106,000 commands to the spacecraft.
- GP-B is the first spacecraft ever to achieve nine degrees of freedom in control. The spacecraft itself maintained three degrees of freedom in attitude control (pitch, yaw, and roll), plus three degrees of freedom in translational drag-free control (front-to-back, side-to-side, and up-down). In addition, the Gyro Suspension System (GSS) for each gyro maintained three degrees of freedom in controlling the location of its spherical rotor within the gyro housing.
- The GP-B gyros, which performed extraordinarily well in orbit, have been listed in the Guinness Database of World Records as being the roundest objects ever manufactured.
- The spin-down rates of all four gyros were considerably better than expected. GP-B's conservative requirement was a characteristic spin-down period (time required to slow down to ~37% of its initial speed) of 2,300 years. Measurements during IOC showed that the average characteristic spin-down period of the GP-B gyros was approximately 15,000 years—well beyond the requirement.
- The magnetic field surrounding the gyros and SQUIDs (Super-conducting QUantum Interference Device) was reduced to  $10^{-7}$  gauss, less than one millionth of the Earth's magnetic field—the lowest ever achieved in space.
- The gyro readout measurements from the SQUID magnetometers had unprecedented precision, detecting fields to  $10^{-13}$  gauss, less than one trillionth of the strength of Earth's magnetic field.
- The gyro suspension system operated magnificently. It had to be able to operate both on the ground for testing purposes prior to launch, as well as in space. This meant that the suspension system had to operate over 11 orders of magnitude—an enormous dynamic control range—and its performance throughout the mission was outstanding.
- The science telescope on board the spacecraft tracked the guide star, IM Pegasi (HR 8703), to superb accuracy, and it also collected a year's worth of brightness data on that star. The brightness data we collected on IM Pegasi represents the most continuous data ever collected on any star in the universe.
- In November 2005, the entire GP-B team was awarded a NASA Group Achievement Award “For exceptional dedication and highly innovative scientific and engineering accomplishments leading to the successful execution and completion of the Gravity Probe B Science Mission.”



## 1.14 The Broader Legacy of GP-B

At least a dozen new technologies had to be invented and perfected to carry out this experiment. For example, the spherical gyros, at  $10^{-8}$  g, are better than ten million times more accurate than the best navigational gyros. The ping-pong-ball-sized rotors in these gyros had to be so perfectly spherical and homogeneous that it took more than 10 years and a whole new set of manufacturing techniques to produce them. They're now listed in the Guinness Database of Records as the world's roundest man-made objects. The SQUIDs are so sensitive that they can digitally detect a gyro tilt of 0.1 milliarcseconds ( $3 \times 10^{-8}$  degrees).

Over its 40+ year life span, spin-offs from the GP-B program have yielded many technological, commercial, and social benefits. For example, GP-B's porous plug for controlling helium in space was essential to several other vital NASA missions, including IRAS (Infrared Astronomical Satellite) and COBE (COsmic Background Explorer). Most important, GP-B has had a profound effect on the lives and careers of numerous faculty and students—graduate, undergraduate and high school—including 79 Ph.D. dissertations at Stanford and 13 elsewhere. GP-B alumni include the first U. S. woman astronaut, an aerospace CEO, and a Nobel laureate.



**Figure 1-13.** Stanford GP-B/GPS graduate students and a faculty member pose next to a GPS-controlled tractor (left); Clark Cohen and Brad Parkinson receive awards from the Space Technology Hall of Fame

One interesting GP-B spin-off story is automated precision farming. Under the supervision of GP-B Co-PI Brad Parkinson, centimeter-accurate Global Positioning Satellite (GPS) technology, originally developed for attitude control of the GP-B spacecraft, was re-purposed for other automated guidance and control applications in the early 1990's by Clark Cohen and a group of his fellow GP-B/GPS graduate students at Stanford. After receiving his Ph.D., Cohen founded a company, now Novariant Corporation, to develop precision GPS guidance and control applications, such as an automatic aircraft landing system and automated precision farming. In May 2006, Novariant's Autofarm technology was inducted into the Space Technology Hall of Fame, and individual awards were given to Cohen and several colleagues at Novariant, along with Parkinson and Stanford's GP-B and Hansen Experimental Physics Lab (HEPL) for their role in supporting this technology development.

# 2

## Overview of the GP-B Experiment & Mission

---







This chapter provides an overview of the Gravity Probe B experiment, the spacecraft and its associated technologies, a description of the mission and mission phases, including a summary and discussion of the activities, issues, and accomplishments that took place during the Initialization and Orbit Checkout (IOC), Science (data collection), and Instrument Calibration phases of the mission.

## 2.1 Gravity Probe B in a Nutshell

The Gravity Probe B (GP-B) mission is a physics experiment that uses four spherical gyroscopes and a telescope, housed in a satellite orbiting 642 km (400 mi) above the Earth, to measure, with unprecedented accuracy, two extraordinary effects predicted by Albert Einstein's general theory of relativity—our present theory of gravitation. The first measurement is the geodetic effect—the amount by which the Earth warps the local spacetime in which it resides. The other effect, called frame-dragging, is the amount by which the rotating Earth drags local spacetime around with it. The GP-B experiment tests these two effects by precisely measuring the drift angles of the spin axes of the four gyros over the course of a year and comparing these experimental results with predictions from Einstein's theory.

### 2.1.1 A Brief History of GP-B

The idea of testing general relativity by means of orbiting gyroscopes was suggested independently by two physicists, George Pugh and Leonard Schiff, in late 1959-early 1960. Pugh's **Proposal for a Satellite Test of the Coriolis Prediction of General Relativity** appeared in an unusual location: the U.S. Department of Defense *Weapons Systems Evaluation Group (WSEG) Memo #11* (November, 12, 1959). Schiff's **Possible New Experimental Test of General Relativity Theory** was published in the March 1, 1960 issue of *Physical Review Letters*. For an historical review and comparison, see C. W. F. Everitt: **The Stanford Relativity Gyroscope Experiment (A): History and Overview**, in *Near Zero: New Frontiers of Physics*, ed. J. D. Fairbank et. al., New York, W. H. Freeman, 1988.

Schiff, then chairman of the Stanford University Physics Department, discussed his developing ideas with two physics department colleagues, Professors William Little and William Fairbank, both low-temperature physicists. Fairbank, in turn, had an exchange with Professor Robert Cannon, who like Fairbank had just arrived at Stanford. Cannon had considerable experience with state-of-the-art gyroscopes, and he had come to Stanford to create a Guidance and Control Laboratory in the Department of Aeronautics & Astronautics. There followed an amusing and much publicized three-way meeting between Fairbank, Cannon and Schiff at the now-no-longer-existing swimming pool in the Stanford Men's Gymnasium. Thus began the essential collaboration between the Physics and Aero-Astro departments which has been fundamental to the success of GP-B.

Schiff's more extended paper, entitled **Motion of a Gyroscope According to Einstein's Theory of Gravitation** was then published in the June 15, 1960 issue of the *Proceedings of the National Academy of Sciences* (Volume 46, Number 6, pp. 871-882). Pugh's too-little-known article was finally published in *Nonlinear Gravitodynamics: The Lense-Thirring Effect*, ed. R. Ruffini and C. Sigmond, Singapore, World Scientific, 2003. An important feature of Pugh's paper was that it contained the first proposal and analysis of the concept of a drag-free satellite.

During the startup period of GP-B, at the 1961 meeting of the International Union of Theoretical and Applied Mechanics, Cannon presented the first engineering paper describing the planned orbital experiment: **Requirements & Design for a Special Gyro for Measuring General Relativity Effects from an Astronomical Satellite**, published in *Kreiselp Probleme Gyrodynamics, Symposium Celerina, August, 1962*, ed. H. Ziegler, Berlin, Springer-Verlag.

Copies of all the papers mentioned in this section, plus other historical GP-B papers, are available in Adobe Acrobat PDF format on the Web at: [http://einstein.stanford.edu/content/sci\\_papers/origins.html](http://einstein.stanford.edu/content/sci_papers/origins.html).

It is worth noting that earlier theoretical discussions of gyroscope tests of general relativity were given in the 1920's by J. A. Schouten and A. S. Eddington. In the 1930's, P. M. S. Blackett investigated the possibility of a ground-based experiment, concluding correctly that it was beyond the reach of technologies known at that time.

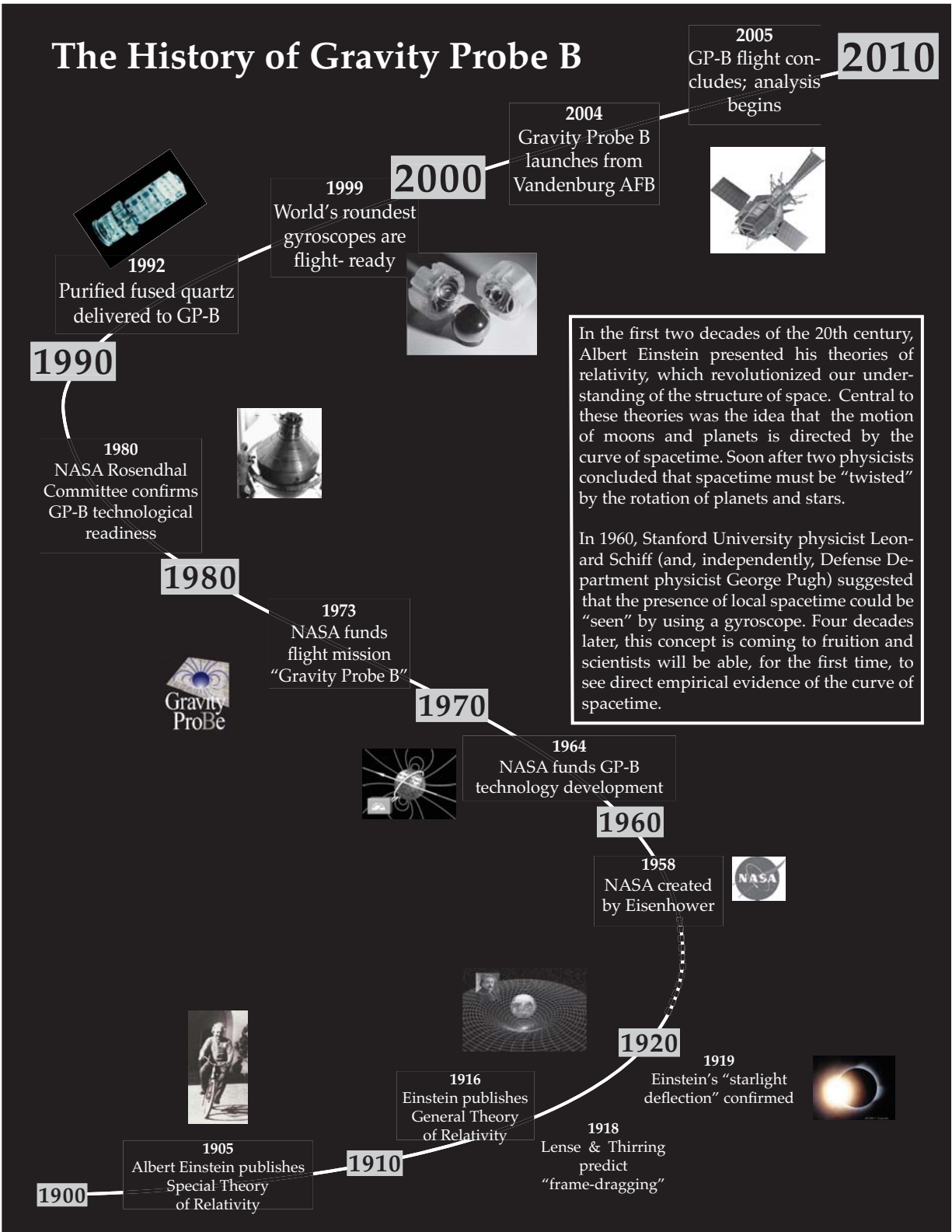


**Figure 2-1.** GP-B Historical Time Line

In the months following publication of Schiff's paper, Schiff, Fairbank and Cannon continued to develop and refine various aspects of the relativity gyroscope experiment. One early question was the feasibility of flying a reference telescope. Cannon, being familiar with NASA's forthcoming Orbiting Astronomical Observatory (OAO) from conversations with Dr. Nancy Roman of NASA Headquarters was able to dispel this concern. In January 1961, Schiff and Fairbank sent a two-page letter proposal to NASA's Office of Space Sciences, outlining a possible approach to the relativity gyroscope flight experiment.



**Figure 2-2.** GP-B Co-founders and Nancy Roman. Clockwise from top left: Leonard Schiff (~1970), William Fairbank (~1988), Robert Cannon (2005), and Nancy Roman (2005)

During Roman's first year at NASA, the Office of Space Sciences had received a number of proposals on space tests of general relativity, including this one. Roman and other NASA scientists were eager to support such research; however NASA realized that evaluating these proposals required input from scientists and engineers with highly specialized knowledge in this field. At Roman's initiative, a NASA-sponsored conference on experimental tests of relativity was held at Stanford under the chairmanship of the distinguished relativist H. P. Robertson of Caltech, on July 20-21, 1961, with a large attendance of physicists and aerospace engineers, including Schiff and Cannon.

Also present from Stanford's Aero-Astro Department were two of Cannon's graduate students: Daniel DeBra, who was finishing his Ph.D. while heading up the Dynamics & Controls Analysis Group at Lockheed Missiles & Space Company (LMSC, now Lockheed Martin), and Benjamin Lange, also from Lockheed, who was just starting his graduate studies in the Stanford Aero-Astro Department. Lange independently proposed the concept of a drag-free satellite during the course of the meeting, and it became the subject of his doctoral dissertation. DeBra, now a Professor Emeritus in Stanford's Aero-Astro Department, has been a Co-PI on GP-B since the late 1960's. Separately, in the early 1970s, he led the development, in collaboration with Johns Hopkins

Applied Physics Laboratory, of the first-ever drag-free satellite—the Disturbance Compensation System (DISCOS) drag-free controller for the U. S. Navy’s TRIAD transit navigation satellite, successfully launched in July 1973. It achieved  $5 \times 10^{-12}$  g throughout a one-year orbital test.

In 1962, Fairbank met Francis Everitt, then a research associate at the University of Pennsylvania, and encouraged him to come to Stanford as the first full-time academic staff member in the relativity gyroscope experiment, some graduate student research having already begun. NASA support commenced in March 1964, retroactive to November 1963, along with a supplemental grant from the U.S. Air Force, following receipt of a proposal “To develop a zero-G drag-free satellite and perform a gyro test of general relativity in a satellite,” with Cannon and Fairbank as Co-Principal Investigators and Schiff as Program Advisor. In 1968, Cannon left Stanford and GP-B to become Chief Scientist of the U. S. Air Force, and at this time, DeBra and Everitt were appointed Co-PIs, along with Fairbank.

NASA’s research funding lasted through July 1977—the longest running single continuous grant ever awarded by NASA. Initial funding was direct from NASA Headquarters to Stanford; in 1971, oversight was transferred to NASA Marshall Space Flight Center (MSFC) where some engineering collaboration had already begun. In 1971, in parallel with the technology development, MSFC funded an in-depth Mission Definition Study by Ball Brothers Research Corporation (BBRC, now Ball Aerospace), performed in close collaboration with Stanford, the starting point of all future flight studies. Two smaller follow-up studies by BBRC were performed later in the 1970’s. Between 1977 and 1984, the experiment was re-structured as a NASA flight program, following in-house Phase A and Phase B studies at MSFC, the latter being completed in 1982. The essential step between 1982 and 1984 was the definition of a ~\$70 M technology development program for GP-B to be performed on the Shuttle—the Shuttle Test Of the Relativity Experiment (STORE). In 1981, Everitt became Principal Investigator. In 1984, Bradford Parkinson, who had obtained his Stanford Ph.D. on GP-B-related gyroscope work in 1965, joined GP-B as Program Manager (later also a Co-PI) and concurrently as Professor of Aeronautics & Astronautics. Parkinson was previously program manager through successful deployment of the U.S. Global Positioning System (GPS). Also in that year, Stanford physicist John Turneaure was appointed Hardware Manager of GP-B, and two years later he also became a Co-PI.

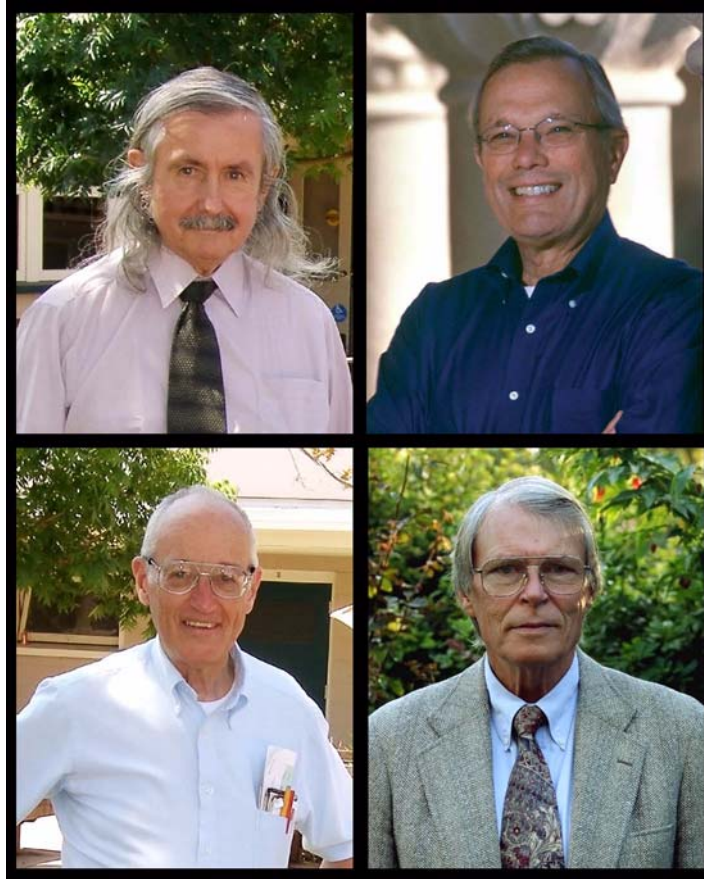


**Figure 2-3.** Clockwise from top left: GP-B Principal Investigator, Francis Everitt, and Co-PIs Brad Parkinson, John Turneure and Dan DeBra.

Coincident with the transfer from NASA HQ to MSFC, the HQ manager, C. Dixon Ashworth, coined the names Gravity Probe A (GP-A) for the Smithsonian Astrophysical Observatory relativity H-maser clock comparison experiment, headed by Dr. Robert Vessot and Gravity Probe B for the relativity gyroscope program. GP-A, like GP-B, became an MSFC program, performed with a sub-orbital Scout launch in 1976.

NASA initiated funding of STORE in FY 1985, following receipt in November 1984 of a Stanford proposal, with LMSC as sub-contractor. In this proposal, Lockheed held principal responsibility for developing the unique 650-gallon dewar and probe—the cryogenic chamber that houses the telescope and four gyroscopes. The original notion of STORE was a two-stage process:

1. Construct the complete GP-B payload, and perform a ten-day rehearsal on Shuttle.
2. Bring the payload back, address any issues, mount it on a space vehicle, to be deployed into polar orbit via a Shuttle launch from the Western test range (Vandenberg AFB, SL-6).

After the Challenger disaster in 1986 and the subsequent closure of SL-6, it was necessary to re-think the mission as a satellite launch from an expendable launch vehicle, without losing the technology funding. In a visit to GP-B, James Beggs, then the NASA Administrator, decided that NASA would make Stanford University the prime contractor for the mission. Eventually, after extended NASA review and two competitive industrial Phase B studies, Stanford then selected LMSC to build the space vehicle and associated control systems that would house the dewar and probe in orbit.



William Fairbank once remarked: “No mission could be simpler than Gravity Probe B. It’s just a star, a telescope, and a spinning sphere.” However, it took the exceptional collaboration of Stanford, MSFC, Lockheed Martin and a host of others almost two more decades to finally bring this “simple” experiment to the launch pad in April 2004. Over this period, as construction of the payload and spacecraft commenced, the GP-B team expanded, reaching a peak of approximately 100 persons at Stanford, and eventually some 200 persons at Lockheed Martin. Six scientists, each with a different area of specialization, became Co-Investigators: Saps (Sasha) Buchman, George (Mac) Keiser, John Lipa, James Lockhart, Barry Muhlfelder, and Michael Taber. In 1998, Bradford Parkinson stepped aside as Program Manager, to be succeeded first by John Turneure, and then in turn, Sasha Buchman, Ronald Singley, and Gaylord Green for the flight program, and William Bencze for the data analysis phase of the mission. Throughout this period, Tom Langenstein served as the Deputy Program Manager, with responsibility for resources and procurements.

As Brad Parkinson recently noted: “Optimism was rampant [in 1960, when GP-B began]. We didn’t have any idea how hard this was, and I would contend it was probably not until 30 years later that we brought [into existence] the technology to make perfect spheres, the coating technology, the readout technology, the cryogenic technology, the [telescope] pointing technology... None of this was possible in 1960.”

On April 20, 2004 at 9:57:24 AM PDT, Everitt, Parkinson, Rex Geveden, the MSFC Program Manager for GP-B, and a crowd of over 2,000 supporters and former GP-B team members watched and cheered as the GP-B spacecraft lifted off from Vandenberg Air Force Base. That emotionally overwhelming day, culminating with the extraordinary live video of the spacecraft separating from the second stage booster meant, as GP-B Program Manager Gaylord Green put it, “that 10,000 things went right.”

Once in orbit, the spacecraft first underwent a four-month Initialization and Orbit Checkout (IOC) phase, in which all systems and instruments were initialized, tested, and optimized for the experimental data collection to follow. The IOC phase culminated with the spin-up and initial alignment of the four science gyros early in August 2004. Beginning on August 28, 2004, the spacecraft began collecting science data. During the ensuing 50 weeks, the spacecraft transmitted over a terabyte of science data to the GP-B Mission Operations Center (MOC) at Stanford University, where it was processed and stored in a database for analysis. On August 15, 2005, the GP-B Mission Operations team finished collecting science data and began a planned set of calibration tests of the gyros, telescope, and SQUID readouts that lasted six weeks, until the liquid helium in the dewar was exhausted at the end of September.

In October 2005, the GP-B science team began a three-phase data analysis process. As of the final editing of this report in March 2007, the team has progressed through Phase I, Phase II, and much of Phase III, and is preparing to announce preliminary results on April 14-15, 2007 at the American Physical Society (APS) meeting in Jacksonville, Florida. In April-May, the team will be releasing the science data and a complete archive of GP-B documents to the National Space Sciences Data Center (NSSDC) at the Goddard Space Flight Center. Subsequently, the science team plans to spend several more months refining the analysis in order to achieve the most precise result possible. The analysis and results will then undergo a careful and critical review by the GP-B external Science Advisory Committee (SAC) and other international experts. During the latter part of 2007, the GP-B team will also be preparing scientific and engineering papers for publication, as well as working with NASA in planning an announcement of the final results of this unprecedented test of General Relativity.

If there is one person who, along with William Fairbank has proved to be the driving force of GP-B since his arrival in 1962, it is Francis Everitt. His leadership has markedly advanced the state of the art in the areas of cryogenics, magnetics, quantum devices, telescope design, control systems, quartz fabrication techniques, metrology and, most of all, gyroscope technology. The fact that GP-B survived no fewer than seven potential cancellations, finally launched in April 2004, successfully completed a 17-month flight mission, and is now in the final stages of analyzing the relativity data is a direct tribute to Everitt’s leadership, tenacity, and dogged pursuit of the experimental truth. It was in recognition of these seminal contributions that, in April 2005, NASA awarded Everitt the Distinguished Public Service Medal—the highest award that NASA can confer upon a non-government employee.



**Figure 2-4.** GP-B Principal Investigator, Francis Everitt, receiving the NASA Distinguished Public Service Award at an awards ceremony at NASA Headquarters in April 2005.

### 2.1.2 Einstein Stands on Newton’s Shoulders

In a letter of 1676, written to his lifelong enemy, Robert Hooke, Isaac Newton made the now famous remark: “If I have seen farther, it is by standing on the shoulders of giants.” In 1687, Newton published his three-volume *Philosophiæ Naturalis Principia Mathematica*—universally regarded as the most important work in the history of science—in which he fused the work of Copernicus, Galileo, Kepler, and others into the first comprehensive treatise on theoretical physics. In the *Principia*, Newton defined the three laws of motion and derived the formulae that, for practical purposes, describe the motion of celestial bodies, as well as the motion of everyday objects (e.g., apples falling from trees). Newton believed that space and time are distinct and absolute entities, and although he could not explain the mechanism by which it works, he thought that gravity is an attractive *force*, somehow acting instantaneously at a distance between bodies, as illustrated in [Figure 2-5](#) below.

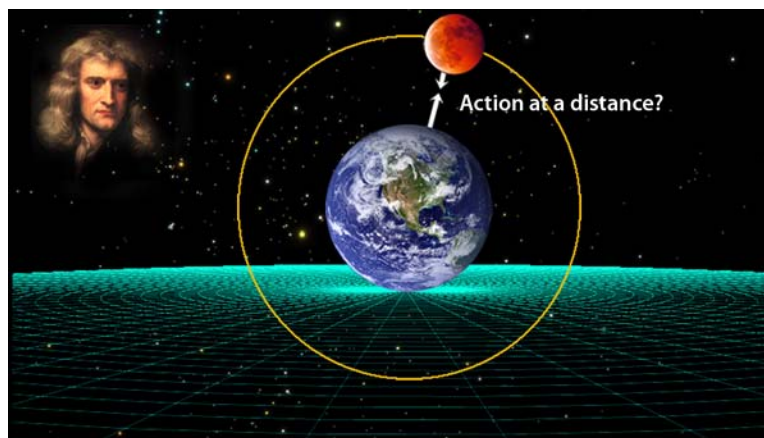


**Figure 2-5.** Newton’s universe: Space and time are absolute or fixed entities. Gravity is a force that acts instantaneously between objects at a distance, causing them to attract one another.

About two centuries later, in 1905, Einstein published his special theory of relativity, which is based on the premise that the speed of light is a universal “speed limit”—nothing can travel or propagate faster than the speed of light. Realizing that Newton’s idea of gravity violated this basic premise of his special theory of relativity, Einstein spent the next 11 years developing his general theory of relativity—his theory of gravity—which utilized the equivalence principle to go beyond the concepts of inertia and weight to describe how gravity makes things fall.

In Einstein's view, space and time are relative entities, inextricably woven together into a "fabric" which Einstein called "spacetime." Furthermore, spacetime and matter interact—spacetime tells matter how to move, and matter tells spacetime how to curve and twist. Thus, in Einstein's universe, gravity is not an attractive force, but rather the interaction of bodies moving through curved spacetime. This concept is illustrated in [Figure 2-6](#) below.

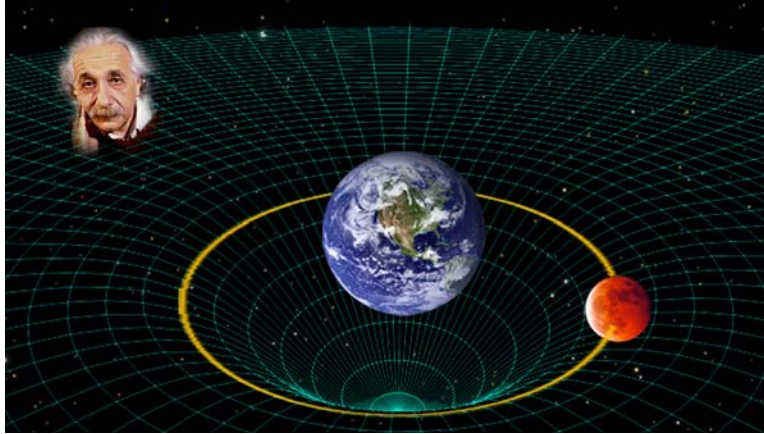


**Figure 2-6.** Einstein's Universe: Space and time are relative entities, interwoven into a spacetime fabric whose curvature we call gravity. Objects follow the straightest possible lines, called geodesics, through curved spacetime.

### 2.1.3 Why perform another test of Einstein?

With the general theory of relativity, acclaimed as one of the most brilliant creations of the human mind, Einstein forever changed our Newtonian view of gravity. However, even though it has become one of the cornerstones of modern physics, general relativity has remained the least tested of Einstein's theories. The reason is, as Caltech physicist Kip Thorne once put it: "In the realm of black holes and the universe, the language of general relativity is spoken, and it is spoken loudly. But in our tiny solar system, the effects of general relativity are but whispers." And so, any measurements of the relativistic effects of gravity around Earth must be carried out with utmost precision. Over the past 90 years, various tests of the theory suggest that Einstein was on the right track. But, in most previous tests, the relativity signals had to be extracted from a significant level of background noise. The purpose of GP-B is to test Einstein's theory by carrying out the experiment in a pristine orbiting laboratory, thereby reducing background noise to insignificant levels and enabling the Probe to examine general relativity in new ways.

Gravity is the most fundamental force in nature; it affects all of us all the time. But, gravity is still an enigma—we don't completely understand it. Einstein's 1916 general theory of relativity forever changed our notions of space and time, and it gave us a new way to think about gravity. If the Gravity Probe-B experimental results corroborate the geodetic and frame-dragging predictions of general relativity, we will have made the most precise measurement of the shape of local spacetime, and confirmed the theory of general relativity to a new standard of precision. If on the other hand, the results disagree with Einstein's theoretical predictions, we may be faced with the challenge of constructing a whole new theory of the universe's structure and the motion of matter.



Such rigorous experimental verification is essential to furthering our understanding of the nature of our universe, particularly about massive objects in space, such as black holes and quasars. As GP-B Physicist John Mester puts it,

“General relativity is our current theory of gravitation, and it has wide-ranging implications for our understanding of the structure of the cosmos. At present, Einstein’s theory of gravitation lies outside the other three forces of nature (the strong force, the weak force and the electromagnetic force), which are explained within a unified framework called The Standard Model. Attempts to unify all four forces of nature have eluded physicists from Einstein to the current day. Testing theories to high precision will help define their range of validity or reveal where these theories break down.”

Whatever the result, Gravity Probe B will provide us another glimpse into the sublime structure of our universe.

## 2.1.4 The Geodetic and Frame-dragging Effects

Gravity Probe B was designed to test, through a direct, controlled experiment, two predictions of Einstein’s general theory of relativity. The first, known as the geodetic —or as it is sometimes called, deSitter— effect, measures the size of the very small angle by which our Earth warps its local spacetime. One way to visualize this effect is to think of local spacetime as a trampoline and the Earth a bowling ball lying in the middle. The heavy ball warps or puts a dent in the trampoline, so that a marble (another celestial body) moving along the trampoline surface will be inexorably drawn down the warped slope towards the massive ball.

Another, and perhaps more useful way to visualize the geodetic warping of spacetime is the so-called “missing inch” shown in [Figure 2-7](#) below.

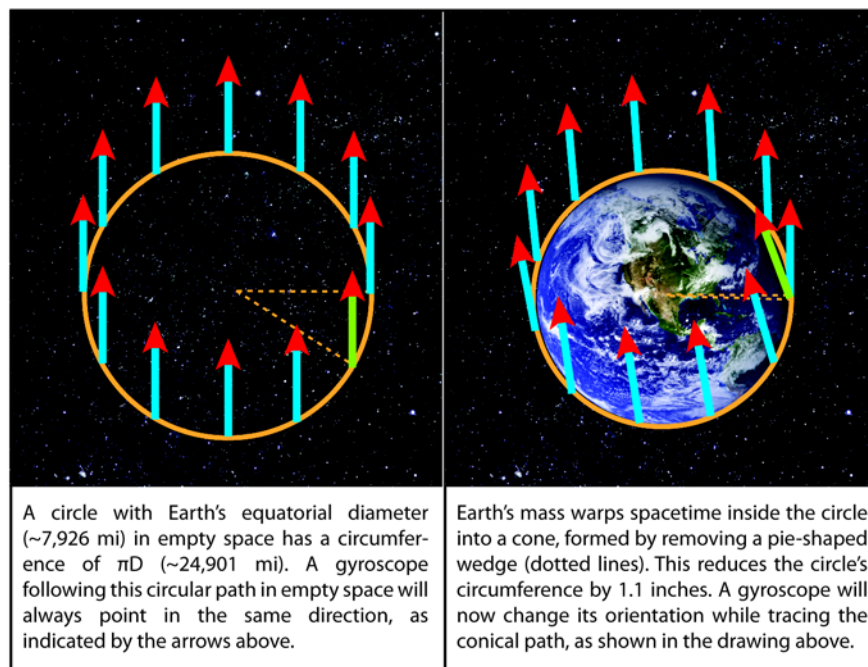


**Figure 2-7.** The Missing Inch

If you were to draw a circle with the same diameter ( $D$ ) as the Earth (~7,900 miles) in empty space, the circumference of this circle, calculated using standard Euclidian geometry, would be  $\pi D$  (~24,000 miles). Furthermore, a gyroscope following this circular path in empty space would always point in the same direction, as illustrated in the left side of [Figure 2-7](#). However, if you were then to slip the Earth inside this circle, Earth’s mass warps the spacetime inside the circle into a shallow cone, thereby shrinking the circumference of the circle

by a mere 1.1 inches. You can see this effect (not to scale) by cutting out a pie-shaped wedge from the circle and then closing the gap. The circumference of the resulting cone is slightly diminished, and the orientation of a gyroscope will now shift as it moves around the circular edge of the cone, as shown in the right half of [Figure 2-7](#). This shifting orientation of a gyroscope’s spin axis as it moves through warped spacetime is the essence of the GP-B experiment.

The other effect being measured by GP-B, known as “frame-dragging,” was postulated by Austrian physicists Josef Lense and Hans Thirring two years after Einstein published his general theory of relativity. It states that as a celestial body spins on its axis, it drags local spacetime around with it, much like a spinning ball in bowl of molasses would drag around some of the molasses as it spins. This concept is illustrated in [Figure 2-8](#).

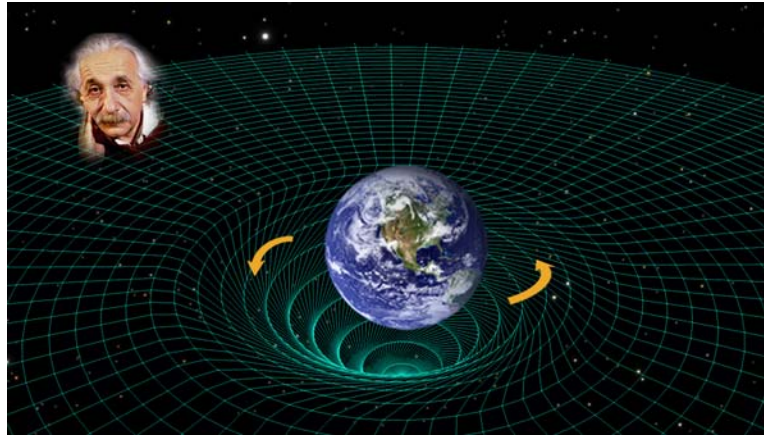


**Figure 2-8.** Illustration of frame-dragging

Particularly intriguing, the frame-dragging measurement probes a new facet of general relativity—the way in which spacetime is dragged around by a rotating body. This novel effect closely parallels the way in which a rotating electrically charged body generates magnetism. For this reason it is often referred to as the “gravitomagnetic effect,” and measuring it can be regarded as discovering a new force in nature, the gravitomagnetic force.

### 2.1.5 The Significance of the GP-B Experiment

Physics advances experimentally in two ways: 1) by measuring known effects with higher accuracy and 2) by investigating previously untested phenomena. The geodetic effect has previously been determined to ~1% in complex studies of the Earth-Moon system around the Sun. GP-B aims to measure it to about 0.01%. The frame-dragging effect, on the other hand, is so minuscule around a planet the size of our Earth that until GP-B, it has not been possible to measure this effect directly. However, the frame-dragging effect is of particular interest to physicists and cosmologists who study black holes, because like the air in a hurling tornado, the hurling space around a black hole has enormous destructive potential.

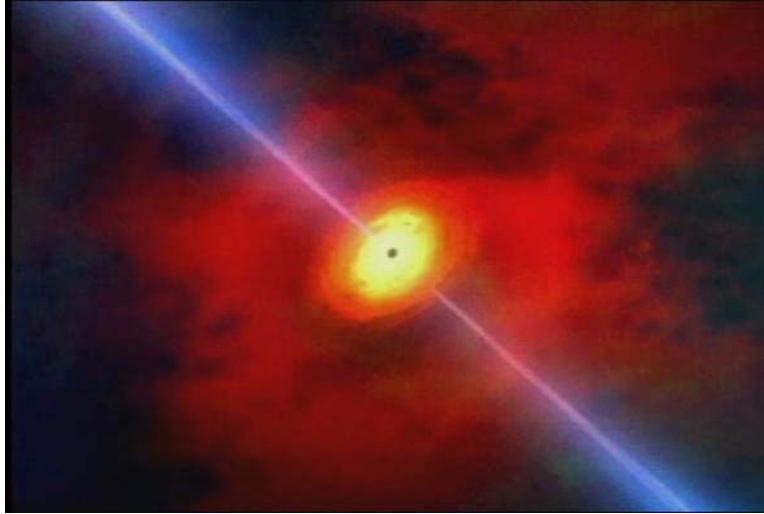


**Figure 2-9.** Frame-dragging around a black hole

At the GP-B press conference held at NASA Headquarters in April 2004, just prior to the GP-B launch, Caltech physicist Kip Thorne, one of the world's leading experts on black holes, made the following comments on the significance of the frame-dragging effect:

“The black dot in the center [of [Figure 2-9](#) above] represents a black hole. It is surrounded by an accretion disc of gas, shown in yellow, that we believe is forced into the equatorial plane of the black hole by the dragging of spacetime in that vicinity. Jets of energy [blue light in the figure] shoot out in both directions along the spin axis produced by frame-dragging around the black hole. Furthermore, the interaction of the frame-dragging around black holes with magnetic fields is responsible for the enormous and destructive power generation that produces the jets of energy streaming out of these objects.”

Thorne then concluded:

“The results of the GP-B experiment will enable us to verify that the frame-dragging effect does indeed exist, and that it is directly proportional to the angular momentum of our spinning Earth. Physicists and cosmologists will then be able to extrapolate these frame-dragging measurements around the Earth to much more massive celestial objects, such as black holes and quasars.”

### **2.1.6 The Basic GP-B Experimental Design**

Conceptually, the GP-B experiment is simple: Place a gyroscope and a telescope in a polar-orbiting satellite, about 642 km (400 mi) above the Earth. (GP-B actually uses four gyroscopes for redundancy.) At the start of the experiment, align both the telescope and the spin axis of the gyroscope with a distant reference point—a guide star. Keep the telescope aligned with the guide star for a year, as the spacecraft makes over 5,000 orbits around the Earth, and measure the change in the spin axis alignment of the gyros over this period in both the plane of the orbit (the geodetic drift) and orthogonally in the plane of the Earth's rotation (frame-dragging drift).

[Figure 2-10](#) below shows a conceptual diagram of the GP-B experimental design.

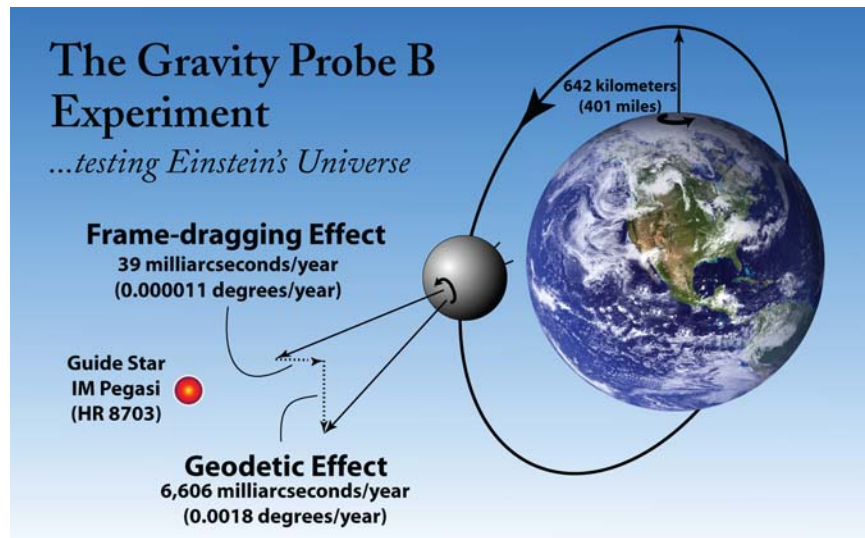


**Figure 2-10.** Schematic diagram of the GP-B experiment

According to Einstein's theory, over the course of a year, the geodetic warping of Earth's local spacetime should cause the spin axis of the gyroscope to drift away from its initial guide star alignment by a tiny angle of 6,606 milliarcseconds (0.0018 degrees). Likewise, the twisting of Earth's local spacetime should cause the spin axis to drift in a perpendicular direction by an even more minuscule angle of 39 milliarcseconds ( $1.1 \times 10^{-5}$  degrees), about the width of a human hair viewed from 1/4 mile away.

Gravity Probe-B's measurement of the geodetic effect has an expected accuracy of better than 0.01%—far more accurate than any previous measurements. The frame-dragging effect has never directly been measured, but Gravity Probe-B is expected to determine its accuracy to better than 1%.

## 2.1.7 The GP-B Spacecraft

All of the Gravity Probe B technologies are integrated into one of the most elegant and sophisticated satellites ever to be launched into space. The GP-B spacecraft is a marvel of engineering and truly a beautiful sight to behold. From its largest to smallest parts, it is filled with the cutting edge technologies and materials described throughout this report, many of which were invented specifically for use in the Gravity Probe B mission.

### 2.1.7.1 Inside the Dewar

The spacecraft is built around a 650-gallon dewar, one of the largest and most sophisticated ever flown in space. The dewar is nine-feet tall and forms the main structure of the spacecraft. The vacuum area just inside the dewar's shell contains multiple reflective surfaces that cut down on heat radiation. The dewar also contains vapor-cooled metal shields that help maintain its internal cryogenic temperature, and slosh baffles help suppress tidal motions in the superfluid helium inside. When cooled to nearly absolute zero temperature, liquid helium transforms into a state called "superfluid," in which it becomes a completely uniform thermal conductor. Only helium exhibits this, and other special properties of superfluidity.

Figure 2-11 shows the dewar's location in the center of the spacecraft, along with an exploded view of the main payload components inside the dewar.



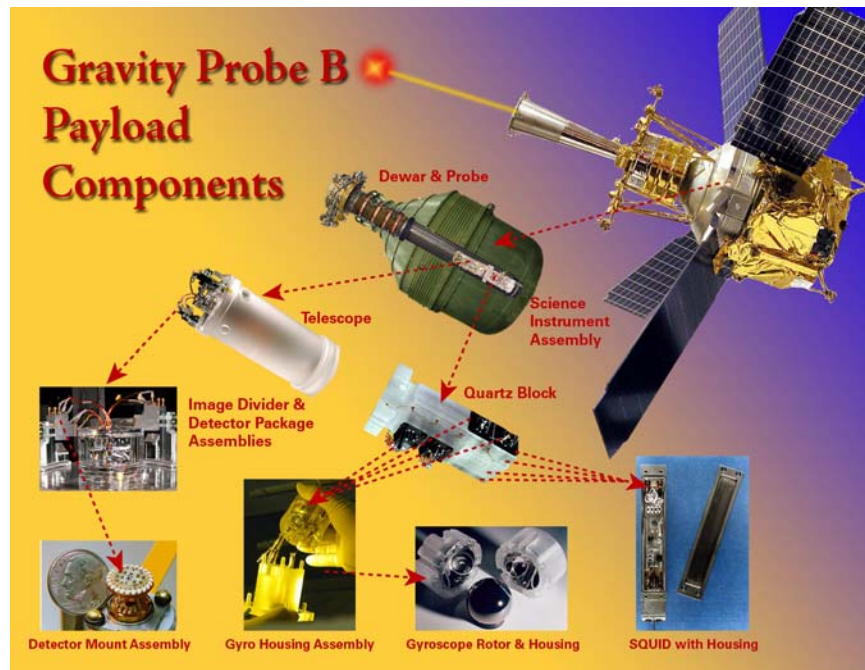


**Figure 2-11.** Exploded diagram of the GP-B spacecraft & payload

The Science Instrument Assembly (SIA) containing the quartz block and telescope forms the pristine spaceborne laboratory for making the measurements of the GP-B experiment. The SIA is located at the center of mass of the spacecraft/dewar, along its main axis. It is mounted inside a cigar-shaped vacuum canister called the Probe (described below).

The quartz block houses the four spherical gyroscopes and SQUID readout instruments (Super Conducting Quantum Interference Devices—the magnetometers that read the gyroscopes' spin axis orientation). Each spherical gyroscope rotor is enclosed in an elegant, two-piece cylindrical quartz housing, mounted in the quartz block and surrounded by antimagnetic shielding. The gyro rotors are electrically suspended by six round electrode pads—three in the top half of the housings and three in the bottom half—with only 32 microns (~0.001 inch) clearance from these pads, which are embedded in the housing walls. The average spin rate of the gyro rotors during the science phase of the mission was approximately 4,300 rpm.

Bonded to the top of the quartz block using a hydroxide catalyzed optical bonding process, is the quartz reflecting Cassegrain astronomical telescope, which focuses on the guide star, IM Pegasi. Hydroxide catalyzed bonding is a patented method of fusing together quartz parts, without the use of any glue or fasteners to ensure that the SIA did not distort or break when cooled to cryogenic temperatures. The line of sight of the telescope is rigidly aligned to the SQUID readout loop of each gyroscope. As such, the quartz telescope provided the frame of reference for measuring drift in the spin axes of the gyroscopes.

The SIA is mounted in a two-meter long cigar-shaped canister, called the “Probe,” which was inserted into the dewar prior to launch. The Probe is an amazing feat of cryogenic engineering, designed by Lockheed Martin in Palo Alto, California. It provided both mechanical and structural stability for the SIA. The Probe was designed to provide a free optical path for the telescope to view distant space through a series of four precisely manufactured windows, mounted in its upper section. Three of these windows served to reduce thermal conductivity into the dewar, and the fourth, which is made of sapphire, also forms the vacuum seal at the top end of the Probe.



**Figure 2-12.** Final assembly of the Probe

During the entire GP-B mission, the inside of the Probe was maintained at an extremely high vacuum—much greater than the vacuum of the thermosphere at the 642 km (400 mi) orbiting altitude of the spacecraft. The probe is surrounded by a superconducting lead bag, inserted between it and the dewar. The superconducting lead bag provided an impenetrable shield from electromagnetic signals that could disturb the gyroscopes. Taken together, all of these measures created an ultra-pristine cryogenic environment, free of any external forces or disturbances, in which the gyroscopes spun during the science phase of the mission.

At the upper end of the Probe, capping off the dewar, is the “top hat.” The top hat served as a thermal interface for connecting over 450 plumbing and electrical lines, that run from various electronics and control systems, mounted on the space vehicle’s truss system outside the dewar, to the cryogenic vacuum chamber inside the Probe and dewar.



**Figure 2-13.** Looking inside the top hat down into the Probe

Before the Probe was completely integrated into the dewar, each component went through years of testing and construction. Some parts even had to be de-constructed and rebuilt. The entire Probe was assembled in a Class-10 clean room, as any particles larger than a single micron would disrupt the precise structure.

### 2.1.7.2 Outside the Dewar

Outside the dewar are all of the systems that provide power, navigation, communication, and control of the space vehicle. [Figure 2-14](#) below shows a model of the spacecraft in orbit, with some of its key components labeled.

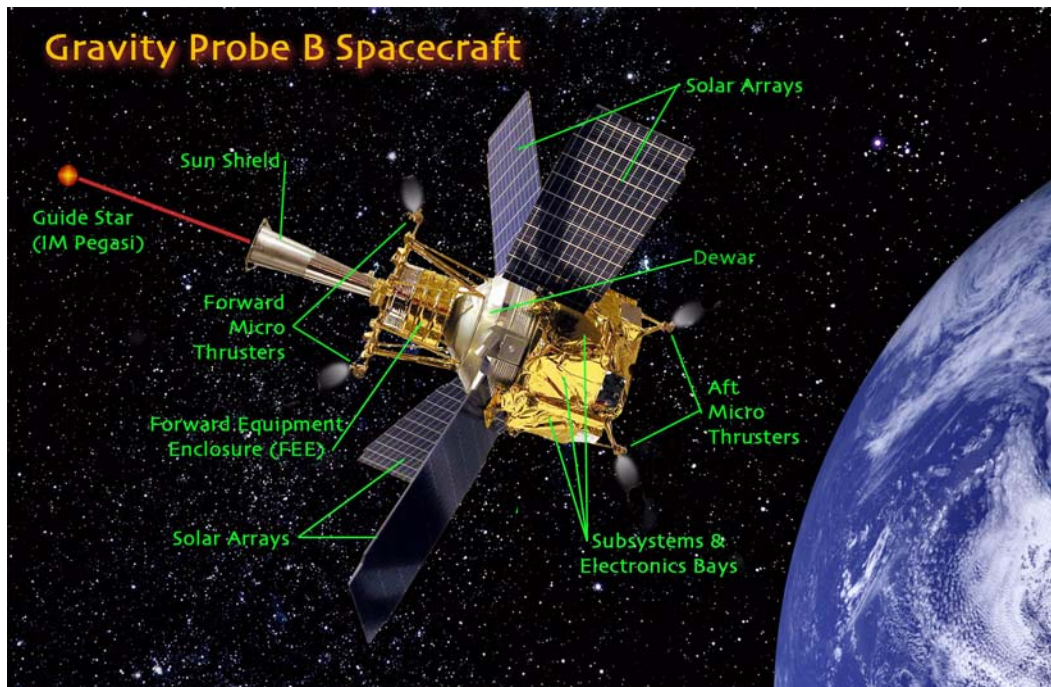


**Figure 2-14.** The GP-B spacecraft



**Sun Shield.** The sun shield is a long, conical tube that kept stray light from entering the telescope during the mission. Inside the sun shield are a series of black, metal baffles that absorb incoming stray light before it can reach the telescope. In addition to blocking out stray light from the Sun, the sun shield also blocked stray light from the Earth, Moon, and major planets.

**Proportional Micro Thrusters.** Until the helium in the dewar was expended at the end of the mission in late September 2005, the proportional micro thrusters on the spacecraft provided a very precise means of controlling its attitude or orientation in space. For the GP-B experiment, an unprecedented amount of on-orbit control was required for the vehicle to maintain its drag-free orbit. This was accomplished by harnessing the helium gas that continually evaporates from the dewar's porous plug and venting it as a propellant through eight pairs of opposing or balanced proportional micro thrusters.

Throughout the mission, these micro thrusters continually metered out a flow of helium gas—at the rate of about 1/100<sup>th</sup> the amount of a human “puff” exhalation that one might use to clean eyeglasses. This metered flow of helium kept the space vehicle's center of mass balanced around one of the gyroscopes, called a “proof mass.” During the flight mission, the spacecraft “chased” the proof mass, thus permitting the proof mass to follow a “free-fall” trajectory without the need for any support force. The thrusters are arranged in pairs, so that they counterbalanced each other. As long as the same amount of helium was flowing from two opposing thrusters, the space vehicle would not change its position relative to the proof mass along that axis. However, if the SQUID readout for the drag-free gyroscope or the telescope readout required the spacecraft's position or attitude to change, it was simply a matter of unbalancing the flow, ever so slightly, in the appropriate thruster pair to move the vehicle in the desired direction. These proportional micro thrusters also controlled the spacecraft's roll rate.

Now that the helium is exhausted from the dewar, these micro thrusters are no longer functional. Also, the on-board science telescope has much too narrow a focus to be used for determining the spacecraft's pointing direction. Instead, two star trackers mounted on the spacecraft frame, along with two magnetometers and standard navigational rate-sensing gyroscopes are used to determine the correct orientation of the spacecraft, and a set of magnetic torque rods are now used to control its attitude by pushing against the local magnetic field of the Earth.

**Solar Arrays.** These four arrays convert energy from the Sun into electrical power that is stored in the spacecraft's two batteries and then used to run the various electrical systems on board. The position of each solar array was precisely canted to maximize the power output as the spacecraft rolled and changed position with respect to the Sun over the course of a year. (The orbit plane of the spacecraft always contains the guide star.)

**GPS Sensors & Antennae.** Four GPS (Global Positioning System) antennas on-board the spacecraft—two at the forward end of the spacecraft and two at the aft end—transmit information about the spacecraft's position and attitude. The GPS system on the GP-B spacecraft provides positioning information that is better than 100 times more accurate than traditional ground-based GPS navigation systems. For example, a high quality handheld GPS receiver on Earth can locate your position to within about a meter, whereas the GPS receiver onboard the GP-B space vehicle can locate its position to within a centimeter. (This occurs because the GPS signals used do not have to travel through the Earth's lower atmosphere.)

**Telemetry & Communications Antennae.** These antennae enable both inbound and outbound communications with the space vehicle, including communications with ground stations and with orbiting communications satellites in the Tracking Data Relay Satellite System (TDRSS). Telemetry data from the space vehicle and science data from the experiment are transmitted to ground stations using these communications systems. These systems also enable the GP-B Mission Operations Center (MOC) to send batches of commands to the space vehicle. Communications between the space vehicle and orbiting satellites is limited to a 2K data format, whereas communications with ground stations use a 32K data format, enabling far more data to be transmitted per unit of time.



**Star Trackers.** A star tracker is basically a telescope with a camera and pattern matching system that uses constellations and stars to determine the direction in which a satellite is pointing. The GP-B spacecraft contains two star trackers (also called star sensors) for redundancy. The star trackers have a field of view on the order of eight degrees, and they can focus to a position within 60 arcseconds (0.017 degrees)—about the same as the whole field of view of the on-board telescope, which can pinpoint the guide star’s position to within a milliarcsecond. With such a small field of view, it would be nearly impossible to locate the guide star using only the onboard telescope, so the star trackers functioned like “spotting scopes” for initially pointing the spacecraft towards the guide star. During the mission, once the star tracker had oriented the spacecraft within 60 arcseconds of the guide star, the onboard telescope then took over the job of maintaining the precise alignment required for measuring gyroscope drift.

**Control Gyroscopes.** GP-B contains two pairs of standard, flight-qualified rate-sensing gyroscopes, equivalent to those found on other spacecraft (and also airplanes, ships, and other vehicles). These gyroscopes are part of the general Attitude & Translation Control System (ATC) of the spacecraft.

**Electro-mechanical Control Systems.** Surrounding the dewar, is a lattice of trusses that forms the structure of the space vehicle. Attached to these trusses are a number of electrical and mechanical systems that control the operation of the spacecraft and enable the relativistic measurements to be carried out. These control systems include the following:

- **Attitude & Translation Control System (ATC)**—Uses feedback from the gyro suspension system (GSS), the SQUID readout system (SRE), the telescope readout system (TRE), the star trackers, magnetometers, and rate-sensing navigational gyroscopes to controls the proportional micro thrusters and magnetic torque rods that determine and maintain the spacecraft’s precise attitude and position.
- **Magnetic Torquing System (MTS)**—A set of long electromagnets that push or pull against the Earth’s magnetic field to orient the spacecraft’s attitude. During the GP-B flight mission, the magnetic torque rods were used in conjunction with 16 proportional micro thrusters to control the spacecraft’s pointing with extreme precision. Following the mission, with no helium propellant remaining to operate the micro thrusters, these magnetic torque rods are the only means of controlling the spacecraft’s attitude and position in orbit.
- **Mass Trim Mechanism (MTM)**—A system of movable weights that can be adjusted during flight to restore rotational balance of the space vehicle (similar to spin balancing the tires on an automobile)
- **Gyro Suspension System (GSS)**—The electronics that levitate and precisely control the suspension of the four gyroscopes at the heart of the Gravity Probe B experiment. The GSS control boxes are mounted in the truss work, outside the dewar. The wiring goes through the top hat section of the Probe and down to each gyroscope.
- **Gas Management Assembly (GMA)**—A very complex set of valves, pipes, and tubing, that runs from a triangular assembly on the truss work, through the top hat and down the Probe to each of the gyroscopes. The critical job of the GMA is to spin up each of the four gyroscopes by blowing a stream of 99.99999% pure helium gas over them, through a channel built into one half of each gyroscope’s quartz housing.
- **Experiment Control Unit (ECU)**—The ECU controls many of the systems onboard the space vehicle, including the GMA, the UV system, and various thermal devices.

## 2.1.8 The Broader Legacy of GP-B

When the GP-B experiment was first conceived in late 1959- 1960, the United States had just created NASA, launched its first satellite, and entered the space race. Landing men on the Moon was still nine years away. At the time, this experiment seemed rather simple, but it has taken over four decades of scientific and technological advancement to create a space-borne laboratory and measurement instrument sophisticated and precise enough to carry out these minuscule measurements of relativistic effects around the Earth.

At least a dozen new technologies had to be invented and perfected in order to carry out the Gravity Probe B experiment. For example, the spherical gyroscopes have a stability that is more than a million times better than the best inertial navigation gyroscopes. The ping-pong-ball-sized gyroscope rotors in these gyroscopes had to be so perfectly spherical and homogeneous that it took more than 10 years and a whole new set of manufacturing techniques to produce them. They're now listed in the Guinness Database of Records as the world's roundest man-made objects.

The magnetometers, called SQUIDs (Super-Conducting Quantum Interference Devices), monitor the spin axis direction of the gyroscopes and can detect—digitally—a change in spin axis alignment to an angle of approximately  $1/40,000,000^{\text{th}}$  of a degree. These advances were only possible through GP-B's unique combination of cryogenics, drag-free satellite technology, as well as totally new manufacturing and measuring technologies.

Similarly, it took two years to make the flawless roof prisms in the GP-B science telescope that tracks the guide star. Some scientists have mused about how Einstein, himself once a patent clerk, would have enjoyed reviewing these extraordinary technologies. See [Chapter 3, GP-B's Unique Technological Challenges and Solutions](#) for descriptions of 12 key GP-B unique technological innovations.

Over its 40+ year life span, spin-offs from the Gravity Probe B program have yielded many technological, commercial, and social benefits. For example, optical-bonding and fused-quartz technologies pioneered for GP-B have subsequently been applied to commercial products, and photo-diode detector technology developed for use in the GP-B telescope has had ramifications for digital camera improvements. Another example is GP-B's porous plug for controlling helium in space. This cryogenic technology was essential to several other vital NASA missions, including IRAS (Infrared Astronomical Satellite) and COBE (COsmic Background Explorer).

One interesting GP-B spin-off story is the evolution of precision guidance control technology from testing Einstein to plowing fields. Under the supervision of GP-B Co-PI, Brad Parkinson, centimeter-accurate Global Positioning Satellite (GPS) technology, originally developed for attitude control of the GP-B spacecraft, was re-purposed for other automated guidance control applications in the early 1990's by Clark Cohen and a group of his fellow GP-B/GPS graduate students at Stanford. After receiving his Ph.D., Cohen founded a company, now Novariant Corporation, to develop precision GPS guidance control applications, such as an automatic aircraft landing system and automated precision farming.



**Figure 2-15.** Stanford GP-B/GPS graduate students and a faculty member pose next to a GPS-controlled tractor; Clark Cohen (left) and Brad Parkinson (right) receive awards from the Space Technology Hall of Fame.

In May 2005, Novariant's Autofarm technology was inducted into the Space Technology Hall of Fame, and individual awards were given to Cohen and several colleagues at Novariant, along with Parkinson and Stanford's GP-B and Hansen Experimental Physics Lab (HEPL) for their role in supporting this technology development.

Less tangible, but perhaps most important, the Gravity Probe B program has had a profound effect on the lives and careers of numerous faculty and students—both graduate and undergraduate, and even high school students, at Stanford University and other educational institutions. Nearly 100 Ph.D. dissertations have been written on various aspects of this program, and GP-B alumni include the first woman astronaut, the CEO of a major aerospace company, professors at Harvard, Princeton, Stanford and elsewhere, and a recent Nobel Laureate in Physics.

## 2.2 Spacecraft Launch



**Figure 2-16.** Photos of the GP-B Launch on April 20, 2004

The GP-B Space Vehicle launched on Tuesday, 20 April 2004, at 09:57:24 PDT. Following a smooth countdown, with excellent meteorological conditions, the GP-B spacecraft launched from the Launch Pad SLC-2W at Vandenberg Air Force Base (VAFB) in California aboard a Delta II 7920-10 rocket into a polar circular orbit of 640 km (400 mile) altitude. The Command/Control Computer Assembly (CCCA), Command and Data Handling (CDH) subsystem, and Attitude & Translation Control (ATC) electronics were powered on prior to launch, and command and telemetry links were established from the Mission Operations Center (MOC) at Stanford University when the fairing separated, five minutes after launch.

## 2.3 Spacecraft Separation

The Solar arrays deployed right on schedule, 66 minutes after launch, and the Boeing Delta II Launch Vehicle second stage released the Space Vehicle at the desired attitude, within 100 meters of a perfect orbit. Two on-board video cameras treated everyone watching the launch to a spectacular view of the spacecraft separating from the second stage rocket. The orbital insertion was indeed so precise that no orbit trim was required during the Initialization and Orbit Checkout (IOC) phase of the mission.

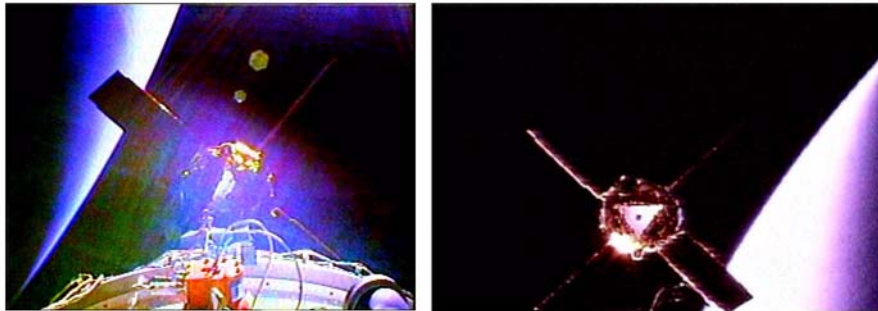


Figure 2-17. On-board video camera shows separation

## 2.4 Initialization & Orbit Checkout (IOC)

This section provides an overview of the IOC mission phase, a summary, week-by-week list of IOC accomplishments, and a discussion of the main tasks accomplished during IOC. A complete chronicle of the IOC mission phase, based on the weekly reports sent out via email and posted on the GP-B Web site by the GP-B Public Affairs Coordinator, is included in [Appendix C, Weekly Chronicle of the GP-B Mission](#).

### 2.4.1 Overview of IOC

During the IOC phase of the mission, the spacecraft underwent a complete initialization and shakedown of systems and subsystems.

#### 2.4.1.1 IOC Task Summary

Following is a list of the main tasks accomplished during IOC:

1. All subsystems that were not running during the launch were powered on and verified.
2. The spacecraft's ATC system was used for three main purposes:
  - To properly orient the spacecraft, enabling the science telescope to lock onto the guide star, IM Pegasi.
  - To establish and maintain the desired spacecraft roll rate.
  - To fly the spacecraft in a drag-free orbit around one of the science gyros.
3. The science gyros were digitally suspended, and the SQUID magnetometer gyro readouts were tested.
4. The spacecraft was balanced about its center of mass using the Mass Trim Mechanisms (MTMs) on the outside frame or shell of the spacecraft.
5. The spacecraft's roll rate was increased for a short time to uniformly wrap the bubble of superfluid liquid helium around the inside of the dewar wall.

6. Using the Gyro Suspension System (GSS), many tests were made to calibrate the positions of the four science gyro rotors in their housings.
7. In three spin-up stages, spread over a period of about a month, the spin rates of the gyros were gradually increased to their final science experiment levels, with many tests and calibrations performed at each stage.
8. A Low-Temperature Bakeout (LTB) procedure was performed to remove stray helium molecules from within the gyro housings and science probe.
9. The spin axes of the four gyros were aligned with the guide star,
10. Electrostatic charging of each gyroscope was controlled throughout the period using an ultraviolet light discharge system.

### **2.4.1.2 The Need to Extend The IOC Time Line**

Prior to launch, the estimated time line for the IOC phase, based on many tests and simulations conducted at Stanford University and Lockheed Martin, was between 42 and 60 days—42 days of tasks, plus 18 days contingency. An additional 15 days contingency, if needed, was also budgeted into the overall mission time line. In the actual mission, IOC required a little over twice the amount of time originally anticipated—the IOC phase officially concluded on Mission Day #129 (27 August 2004), with gyros #1, #2, and #3 in science mode, and gyro #4 continuing to undergo alignment of its spin axis. spin axis alignment of gyro #4 was completed on Mission Day #149 (16 September 2004), and it too then began collecting relativity data, along with the other three gyros.

Two main factors were responsible for most of the extension of the IOC phase of the mission:

1. Tuning the ATC system to perform correctly—complicated by the loss of two micro thrusters and a commanded increase in the spacecraft roll rate to more than twice its originally anticipated value
2. Full-speed gyro spin-up and gyro spin axis alignment—complicated by the gyros spinning at less than half the anticipated full-speed rates

### **2.4.1.3 Tuning The ATC System**

GP-B is the first spacecraft ever launched with a requirement to control all 6 degrees of freedom of the vehicle. It requires three axes of rotational control—pitch, yaw, and roll—and it requires three axes of translational drag-free positioning. Many other spacecraft, like the Hubble Space Telescope, control pitch, yaw, and roll, but they do not roll continuously. Also, GP-B is only the second satellite ever launched to achieve 3-axis drag-free control. In retrospect, these requirements were more difficult to achieve on orbit than had been anticipated.

### **2.4.1.4 Micro Thruster & Star Tracker Issues**

The initial IOC time line called for locking onto the guide star within the first four days in orbit. Successful locking onto the guide star was somewhat delayed due, in part, to the unexpected malfunction of two proportional helium-gas thrusters, which had to be identified, isolated, and taken out of service. These thrusters failed individually after two separate events 1) launch, and 2) Science Instrument Assembly (SIA) flux flushing operations. The likely root cause for both these failures has been identified as foreign particle contamination of the thruster mechanism. This problem was mitigated by revising the ATC software programming to perform with 14, instead of 16 thrusters and then uploading the revised software to the spacecraft's on-board computer. (The remaining 14 thrusters performed flawlessly throughout the entire experiment.)

The two conventional star trackers and associated processing software had difficulty properly identifying star fields while the spacecraft was rolling from the first day in orbit and this was formally declared Anomaly #5 by the Anomaly Review Board (ARB). (For a description of this anomaly, see [Appendix D, Summary Table of](#)



[Flight Anomalies](#).) Furthermore, a decision to reduce noise in the experimental data signal by increasing the spacecraft's roll rate from 0.52 rpm to 0.75 rpm (and ultimately, 0.774 rpm) made the ATC's star field identification more difficult.

### 2.4.1.5 Full Speed Gyro Spin-up Issues

The team, using a very thorough process, successfully completed the full-speed spin-up of the four science gyroscopes. Gyro #4, which showed the greatest spin-up helium leakage rate during low-speed testing was spun up to full speed first. The full-speed spin-up process, which lasted most of the day on 13 July 2004, went smoothly and resulted in a final spin rate of 105.8 Hz (6,348 rpm) for gyro #4. This rate was quite acceptable for collecting relativity data. Three days later, gyro #2 was spun up to full speed, also without incident. It reached a final spin rate of 87 Hz (5,220 rpm). Helium leakage from its spin-up caused gyro #4 to spin-down from 105.8 Hz to 91 Hz.

While both of these spin rates were acceptable for the science phase, the team decided to postpone the full-speed spin-up of gyros #3 and #1 for a little over a week in order to run both ground-based and on-orbit tests, in an attempt to both increase the spin rates of the final two gyro rotors and also reduce the helium leakage during the spin-up process. During the last week in July, gyros #3 and #1 were spun up to full speed. Each of these gyro spin-ups caused approximately a 15% decrease in spin rate of the other gyros, resulting in the final spin rates shown in [Table 2-1](#) below.

**Table 2-1.** Final gyro spin rates

Gyro #	Final Spin Rate (Hz)	Final Spin Rate (rpm)
1	80	4800
2	62.3	3738
3	82.7	4962
4	65.5	3930

### 2.4.1.6 Gyro Spin Axis Alignment

The final gyro spin rates were smaller than originally anticipated, but they were more than adequate for meeting our science requirements. However, these slower spin rates affected the process of spin axis alignment towards the end of the IOC period. Before beginning to collect spin axis precession data from the gyros, their spin axes must initially be aligned with the guide star. This alignment is accomplished by the Gyro Suspension System (GSS), in conjunction with the SQUID magnetometer readouts, by applying small torques to the gyro rotors to “nudge” their spin axis positions into alignment with the direction of the guide star, as indicated by the telescope readout.

The spin axis alignment algorithm was designed with the assumption that the gyros would be spinning in the range of 120-170 Hz (7,200-10,200 rpm). At these very high spin rates, the gyro develops a significant centrifugal bulge, and the GSS uses this bulge as a “handle” for applying the torque to nudge the rotor's spin axis. However, at slower spin rates, this centrifugal bulge is smaller than the natural out-of-round shape of the rotor, so the SQUIDs and GSS must apply the spin axis alignment torques to the natural, polhode modulated, shape of the rotor, rather than the more predictable centrifugal bulge of fast spinning rotor. The torques generated under these circumstances are very small, and they require ground processing of rotor information and manual adjustment of the phasing and timing of the torque commands. Thus, it takes more time to align the spin axes of the gyros when they are spinning slowly. In fact, the smaller the level of imperfections in the rotors, the longer it takes the GSS to complete the alignment. As an example, gyro #4 is apparently so perfectly spherical that it took over two weeks longer than the other three gyros to align its spin axis.

### 2.4.1.7 Proton Bombardment & Other Contingencies

While ATC tuning, gyro spin-up, and spin axis alignment accounted for most of the IOC time extension, other contingencies contributed as well. One of the most serious anomalies of the mission occurred in the second week, when the spacecraft was passing over the Earth's south magnetic pole and it was bombarded by proton radiation from the Sun. This radiation caused data errors in the spacecraft's primary (A-side) computer, which exceeded its capacity for self-correction. By design, the spacecraft automatically switched over to the backup (B-side) computer, placed the spacecraft in a safemode, and put the planned timeline of events on hold. The automatic switch-over from primary to backup computer worked flawlessly. The GP-B mission operations team re-booted and re-loaded the A-side computer and then switched back to it, using up a few days of contingency time in the IOC time line.

Another unexpected issue that required a few days of contingency time to work through occurred at the very end of the IOC period. The spacecraft had entered back-up drag-free mode in preparation for the transition to the science phase of the mission. However, the team noticed that excess helium was being expended by the micro thrusters to maintain drag-free flight, and this ultimately led to the discovery of an unexpected force along the roll axis of the spacecraft. This force was analyzed over a period of approximately two weeks and some components of this force, which were attributed to thruster bias were countered. Ultimately, the ATC was tuned to work around this force without excess expenditure of helium.

### 2.4.1.8 Science Phase Trade-off Decision

Because the dewar was launched with enough superfluid helium to support a total mission time line of 16-18 months, the extra time required by IOC resulted in a trade-off decision: More optimization/calibration of the instrument prior to entering science, with a shorter data collection period; or, less optimization/calibration, with a longer data collection period. At that time, we concluded that the best overall accuracy would be achieved by ensuring the science instrument was optimally calibrated from the start, even if this meant collecting data for a shorter period than hoped. An added benefit of this decision is that we gained a considerably better understanding of the spacecraft subsystems and science instrument than was originally anticipated at that stage of the mission.

## 2.4.2 Weekly Summary of IOC Accomplishments

Table 2-2 below provides a week-by-week list of the tasks and activities accomplished during the IOC phase. A more detailed chronicle of the entire GP-B flight mission, based on weekly updates/highlights sent out via email and posted on the GP-B Web site from 2 April 2004 through 30 September 2005 by the GP-B Public Affairs Coordinator, is included in [Appendix C, Weekly Chronicle of the GP-B Mission](#).

**Table 2-2.** Weekly summary of IOC accomplishments

Weekly Summary of IOC Accomplishments	
Week	Activities Completed
Week 1	Launch/Orbit Injection
	Turn on Payload
	SQUIDs (meet noise spec)
	Operate science gyroscopes in analog mode
	Operate science telescope electronics
	Turned off a stuck-open (but redundant) micro thruster
Week 2	Operate gyroscopes 1,2 and 4 in digital mode
	Sun-radiation-induced switch to B side computer and flawless recovery



**Table 2-2.** Weekly summary of IOC accomplishments (Continued)

<b>Weekly Summary of IOC Accomplishments</b>	
<b>Week</b>	<b>Activities Completed</b>
Week 3	All 4 gyroscopes digitally suspended for over 1 week Practiced Low Temperature Bakeout (Reduces residual He gas pressure) Resulted in 0.001-0.010 Hz science gyroscope spins
Week 4	Flew position drag-free for 1 <sup>st</sup> time (gyro 1) ATC system used roll stars to roughly align to guide star Began series of small maneuvers (dwell scans) to locate guide star
Week 5	Completed magnetic flux reduction: all gyroscopes have very low trapped magnetic flux (desirable situation) A second thruster was turned off due to stuck thruster caused indirectly by the magnetic flux reduction
Week 6	Sent a low flow of spinup gas (2 sccm for 90 seconds duration) to each gyroscope Each gyro spun to approximately 0.3 Hz MicroHz/Hr spindown rates confirm clean gyroscopes
Week 7	Locked onto IM Pegasi with the science telescope Began performing science calibration tests Successfully demonstrated the ability to discharge the science gyroscopes to spec (15 mV)
Week 8	Verified IM Pegasi by visiting two neighboring stars Successfully tested the control effort based drag-free system for 1 orbit
Week 9	Increased the spacecraft roll rate from 0.1 to 0.3 rpm allowing mass trim Performed updates on gyro biases to improve science performance
Week 10	Increased the spacecraft roll rate from 0.3 to 0.9 rpm (the maximum for the mission) for liquid helium bubble wrap Applied 120% of science gyro spinup voltages as a stress/health test: all gyroscopes worked perfectly Completed practice of science calibrations of gyroscopes
Week 11	Uploaded new ATC software to provide improved drag-free performance with the turned off thrusters Required turning off the flight computer and rebooting Procedure was perfectly executed
Week 12	Spun the 4 science gyroscopes to approximately 3 Hz Full flow rate of spinup gas for 90 seconds Reduced roll rate to 0.5 rpm Selected science roll rate to be 0.52 rpm
Week 13	Successfully demonstrated extended drag-free operation Full Speed Spin of Gyro #4 to 106 Hz Full Speed Spin of Gyro #2 to 88 Hz
Week 14	ATC Filter Tuning Coarse Spin Axis Alignment Gyros #2 and #4

**Table 2-2.** Weekly summary of IOC accomplishments (Continued)

<b>Weekly Summary of IOC Accomplishments</b>	
<b>Week</b>	<b>Activities Completed</b>
Week 15	Spinup of gyro 3 Spinup of gyro 1
Week 16	Coarse Spin Axis Alignment - all gyros drag-free and Science Mode Testing
Week 17	Roll up to 0.75 rpm ATC Adjustments
Week 18	ATC Adjustments Fine Spin Axis Alignment
Week 19	Roll up to .77419 rpm ( 77.5 sec period) Fine Spin Axis Alignment ATC Adjustments Gyros #1, #2, and #3 transition to science mode
Week 20	Spacecraft flying drag-free around gyro #3 Gyros #1, #2, and #3 in science mode, collecting data Gyro #4 continuing spin axis alignment
Week 21	Spacecraft flying drag-free around gyro #3 Gyros #1, #2, and #3 in science mode, collecting data. Gyro #4 spin axis slowly moving towards target alignment orientation
Week 22	Spacecraft flying drag-free around gyro #3 Gyro #4 completes spin axis alignment and transitions into science mode Gyros #1, #2, and #3 continue collecting data in science mode
Week 23	Gyro #3 transitioned out of drag-free mode to analog back-up; Drag-free flight re-established around gyro #1 All four gyros in science mode, collecting data. Heat pulse meter test on dewar indicates remaining mission lifetime of 9.9 months, or a total estimated dewar lifetime of 15.2 months. (The actual dewar lifetime was 17.3 months.)

### 2.4.3 Overview of Main IOC Tasks

Following are descriptions of the main tasks accomplished during the IOC phase of the mission.

#### 2.4.3.1 Orbit Trim Maneuver

The insertion of the GP-B spacecraft into orbit by the Boeing Delta II launch vehicle was so perfect that no orbit trim was required during IOC. Prior to launch, it was anticipated that orbit trim could have potentially been the longest running task during the IOC period. Instead, all of the superfluid helium that would have been required for trimming the spacecraft's orbit was available for IOC contingencies.

### 2.4.3.2 Guide Star Acquisition

About 24 hours after launch, the flight software, and specifically the ATC system, automatically began the process of acquiring the guide star, which, for a number of reasons, turned out to be more difficult and time-consuming than anticipated. As noted in section “[Micro Thruster & Star Tracker Issues](#)” above, it became apparent shortly after launch that the conventional star trackers, located on either side of the spacecraft, were not properly identifying reference stars, resulting in erratic spacecraft attitude control. This problem was logged by the ARB as anomaly #5 on Mission Day #1, and it was assigned a medium level of severity. (See [Appendix D, Summary Table of Flight Anomalies](#).)

This problem persisted throughout the first month of the mission. Through considerable analysis and testing, the ATC and ARB teams determined that space vehicle conditions (mass imbalance, alignments, and star tracker settings) were generating data that the star tracker processing algorithm was unable to successfully process. Actions taken to correct this problem included all of the following:

1. Switching to a magnetometer-based attitude determination algorithm.
2. Adjusting magnitude and error gate thresholds.
3. Tuning control gyro biases.
4. Updating star tracker alignment matrices.
5. Updating the guide star acquisition procedure based on ATC performance in orbit.

In addition, the process of locking onto the guide star was delayed by various other issues that arose on orbit, such as proton radiation that caused a switch over to the B-Side on-board computer, mechanical problems with two of the 16 micro thrusters, and thruster instability resulting from a pressure build-up in the dewar following a flux reduction procedure.

By the beginning of June 2004, the pointing error of the spacecraft had been reduced to within 385 arcseconds (0.11 degrees) of the guide star, allowing the science telescope to track IM Pegasi over a portion of a spacecraft roll cycle. Further fine tuning of the ATC continued over the following two weeks, and during the second week in June, the telescope finally locked onto IM Pegasi.

The process of locking the science telescope onto IM Pegasi started with star trackers on either side of the spacecraft locating familiar patterns of stars. Feedback from the star trackers was used to adjust the spacecraft's attitude so that it was pointing to within a few degrees of the guide star. The telescope's shutter was then opened, and a series of increasingly accurate “dwell scans” were performed to home in on the star. Since the spacecraft was rotating along the axis of the telescope, imbalance in the rotation axis could cause the guide star to move in and out of the telescope's field of view. Feedback from the telescope was sent to the ATC system, which adjusted the spacecraft's attitude until the guide star remained in view of the telescope throughout multiple spacecraft roll cycles. The ATC was then commanded to “lock” onto the guide star.

Finally, to verify that the telescope was locked onto the correct guide star, the spacecraft was pointed at a known neighboring star, HD 216635 (SAO 108242), 1.0047 degrees north of IM Pegasi. When the telescope was pointed at this location, the neighboring star appeared with anticipated brightness, and there were no other stars in the immediate vicinity. Thus, the sighting of the star, HD 216635, confirmed the correct relationship between the locations of the two stars, ensuring that the telescope was indeed locked onto the correct guide star. In a similar maneuver, the star HR Peg (HR 8714), a brighter and redder star, located less than half a degree to the west of IM Pegasi, was also seen in the telescope, further confirming that we had properly locked onto IM Pegasi.

During the week of 20 June 2004 (Mission Week #10), we increased the spacecraft roll rate from 0.3 rpm to 0.9 rpm in order to carry out mass trim and liquid helium bubble wrap procedures that balance the spacecraft around its center of mass. (See the following two sections for descriptions of these procedures.) Primarily as a result of the significantly increased spacecraft roll rate, the telescope came unlocked from the guide star, as

reported in the Anomaly Review Board (ARB) Observation #71. (See [Appendix D, Summary Table of Flight Anomalies](#).) In analyzing this situation, the ATC team, in consultation with the ARB, identified three factors that most likely contributed to the star trackers renewed failure to correctly identify star patterns:

1. Gyro bias errors—at the time we had rolled up to 0.9 RPM, roll and attitude errors are greatly magnified at this high roll rate, making the precise setting of control gyro hardware biases difficult. We did not spend enough time collecting data at this roll rate, in order to obtain an accurate prediction of gyro biases.
2. Incorrect gate strategy—this involves setting a software “gate,” in the flight database, that tells the star trackers (in degrees) how large a “window” to put around a potential star, and how big a region to search in the star catalog. At 0.9 rpm, it appears we had too large a gate.
3. Star attitude correction weighting gain—this sets how far the vehicle’s attitude reference “steers” away from a misidentified star, thereby preventing further star updates. Basically, the gain was set too low. During IOC, the vehicle was in mode 2A, using star trackers to help update the attitude error estimate. During the science mission, the star trackers update only the spacecraft roll; they have no effect on X/Y attitude. This is not an issue for the science mission, where the science telescope alone provides X/Y attitude error estimates.

Following the mass trim and liquid helium bubble wrap operations, the spacecraft’s roll rate was decreased to 0.52 rpm, and revised ATC software that addressed both star tracker and malfunctioning thruster issues was uploaded to the spacecraft and installed on the on-board computer. The revised software resulted in a significant improvement in attitude control, and on 3 July 2004, the science telescope re-locked onto the guide star, with the spacecraft rolling at 0.52 rpm.

Throughout the month of July, the ATC team continued to fine tune the ATC parameters in an attempt to optimize drag-free performance at 0.52 rpm, and also to decrease the amount of time required for the telescope to re-lock onto the guide star each time the spacecraft emerged from its eclipsed state behind the Earth. By the last week in July, ATC parameter tuning had reduced the time required to re-lock onto the guide star from as much as 15 minutes to less than one minute. In addition, the number of reference stars “seen” by the star trackers was increased from three to eight.

Finally, during the second week in August 2004, the spacecraft roll rate was increased from 0.52 rpm to 0.75 rpm (and eventually to 0.7742 rpm) in order to improve the signal-to-noise ratio of the science data with the gyros spinning more slowly than anticipated. This final increase in spacecraft roll rate was well tolerated by the revised ATC parameters, and since they were implemented, the telescope was more consistently able to re-lock onto the guide star as it emerged over the North Pole each orbit for the remainder of the mission.

### **2.4.3.3 Mass Trim Sequences**

After launch, the center of mass and products of inertia of the space vehicle can be corrected by moving some or all of the seven mass trim mechanisms (MTM). The process to operate the MTMs includes analysis on the ground of ATC data (to see what forces and torques are required to hold attitude), generation of commands, and then execution of special mass trim sequences. The mass trim procedures were conducted during the third week in June.

The mass trim procedure is somewhat similar to dynamically spin balancing an automobile tire. Weights mounted on long screw shafts are attached in strategic locations around the spacecraft frame, and small motors, under control of the spacecraft’s ATC, can turn these screw shafts in either direction, causing the weights to move back and forth by a specified amount. Based on feedback from the GSS, the spacecraft’s center of mass can thus be precisely positioned to place the vehicle’s center of mass on the desired vehicle roll axis. (A very limited capability exists to position the fore/aft mass center, but none of this trimming was performed)

A second mass trim operation had been scheduled after the spacecraft was placed in drag-free mode for the science phase of the mission, but this was not necessary. In fact, no further mass trim refinements were ever required.

#### **2.4.3.4 Space Vehicle Roll Up / Liquid Helium Bubble Wrap**

The space vehicle separated from the launch vehicle rolling at 0.1 rpm. During IOC the roll rate was incrementally increased to 0.9 rpm for two reasons:

1. To get better insight into adjusting the Mass Trim Mechanisms (MTM)
2. To mass balance the space vehicle by wrapping the liquid helium bubble uniformly around the inside of the dewar wall.

In addition to the mass trim operation performed mid-June, the so-called “bubble wrap” procedure was performed at the same time. During the bubble wrap procedure, the spacecraft’s roll rate was increased in incremental steps, from 0.3 rpm to 0.9 rpm. The increased roll rate begins to rotate the liquid helium, effectively pushing it outwards by centrifugal force. This process is intended to wrap the liquid helium uniformly around the inner wall of the dewar shell. Distributing the liquid helium uniformly along the spacecraft’s roll axis helps to ensure that the science telescope can remain locked on the guide star while the spacecraft is rolling.

Following the bubble wrap and mass trim procedures, the spacecraft’s roll rate was decreased incrementally from 0.9 rpm back to 0.5 rpm. During the first roll-down decrement to 0.7 rpm, we discovered that the distribution of the liquid helium in the dewar is less predictable during roll-down than it is during roll-up. When the spacecraft’s roll rate is slowed too quickly, the liquid helium begins to slosh around. The resulting displacement of the center of mass from the sloshing helium affects the micro thrusters, resulting in a significant increase in the time required to complete the roll-down.

#### **2.4.3.5 Drag-Free Operations**

Drag-free operations were first practiced during the third week of IOC. The term, “drag-free,” means that the entire spacecraft literally flies in its orbit around one of the gyros; this compensates for friction or drag in orbit. Signals from the Gyro Suspension System (GSS) are used by the ATC system to control the position of the vehicle, via the output of the micro thrusters, to fly the spacecraft around the selected gyro.

The GP-B spacecraft can fly using either a primary or a back-up drag-free mode. In primary drag-free mode, the GSS suspension control efforts are turned off on one of the gyros, so that no forces are applied to it. The ATC uses feedback from the position of the designated drag-free gyro in its housing to “steer” the spacecraft, keeping the gyro centered. Back-up drag-free mode is similar, but in this case the GSS applies very light forces on the gyro to keep it suspended and centered in its housing. The ATC uses the GSS to “steer” the spacecraft so that the required GSS forces are made very low.

The initial Drag-Free Control (DFC) checkout used the back-up drag-free mode and lasted 20 minutes, as planned. Then, a two-hour DFC session was tested, during which the spacecraft roll rate was increased and then returned to its initial rate, maintaining drag-free status throughout the test. Then, three weeks later in mid June 2004, after turning off the two malfunctioning micro thrusters, primary drag-free mode was successfully tested. Both drag-free modes continued to be tested periodically throughout July and August for varying lengths of time. When the gyros were spinning slowly, back-up drag-free mode yielded more stability.

Though primary drag-free control would be preferred due to the absence of forces acting upon a gyro and resulting in a data source free of any outside disturbance, analysis of on-orbit data confirmed that either primary or back-up drag-free mode would meet the science needs of the mission. Towards the end of IOC, exhaustive testing demonstrated that primary drag-free required more helium mass flow than desired, while back-up drag-free was both robust and reliable, and thus it was chosen to be used during the science phase.

### 2.4.3.6 Spinning Up the Gyros

Spinning up the Gravity Probe B gyroscopes is a delicate and complex process that required over half the IOC period to complete. Each of the science gyros underwent a series of incremental spin-up and testing sequences, gradually increasing its speed to the final spin rate for the science phase of the mission. Following is a summary of the whole process, as it actually happened during IOC.

Within the first three days of the mission, all four Gyro Suspension Systems (GSS) were activated, and each of the gyros underwent a “lift check” to ensure that the suspension systems were working properly. These were the first suspensions of the GP-B gyros in orbit, and all were successful. Within the first two weeks in orbit, the gyros were first suspended in analog mode, and then, one by one, they were digitally suspended. The analog suspension mode is used primarily as a backup suspension mode. With digital suspension, the GSS uses a computer to provide the primary gyro suspension.

Approximately one month into the mission, the team began spinning up the gyros. In preparation for spin-up, the digital suspension system for each gyro was first tested. This was accomplished by suspending each gyro in the center of its housing, electrically “nudging” it slightly off center in one of eight directions (the corners of a cube), and monitoring its automatic re-centering. This checkout was first performed under low-voltage conditions (fine control) and then under high-voltage conditions (secure hold).

To begin the actual spin-up process, ultra-pure helium gas was flowed over gyro #1 and gyro #4 for 15 seconds, which started them spinning at approximately 0.125 Hz (7.5 rpm). While these gyros were slowly spinning, the suspension test was repeated under high voltage conditions on gyros #2 and #3. During this high-voltage suspension test on gyro #3, the team discovered an error in its command template, which turned off the high-voltage amplifier to gyro #1 and caused it to lose suspension. There was no damage to gyro#1.

At this point in the mission, more than 1,000 commands had been sent to the Gyro Suspension System (GSS), and this was the first error found. Discovering an error in these numerous, intricate command templates was exactly the kind of situation that the painstaking gyro spin-up process was designed to identify; it enabled the team to correct the command template for gyro #3 without serious consequences. Also, as a further precaution, the team thoroughly reviewed the command templates for the remaining three gyros. By the end of May 2004, gyros #2 and #3 were spinning at 0.26 Hz (15 rpm) and 0.125 Hz (7.5 rpm) respectively, and gyro #1 was in the process of being spun-up.

The first week in June, the team started performing a highly methodical and painstaking series of calibration tests on the four science gyroscopes. These tests began at very low gyro spin rates of 0.333 Hz (20 rpm) or less and involved briefly applying voltages asymmetrically to the suspension electrodes on a given gyro, causing that gyro rotor (sphere) to move off center by a few micrometers -or less, and then re-centering it.

Carrying out these tests at very slow spin rates enabled the team to check out the software command templates that control the tests, without risk of damage to the gyro rotors or housings, which could occur at higher speeds. In fact, during these initial calibration tests, the team discovered that the performance characteristics of the gyros on orbit are slightly different from the simulator predictions on which the original command templates were based. As a result of these differences, during one of the initial tests, gyro #4 touched one of its electrodes and stopped spinning. A simple modification to the spin-up command templates corrected the problem.

Calibration testing of the gyros at spin rates less than 1 Hz (60 rpm) continued throughout the month of June. By the third week in June, the performance characteristics of each of the gyros was understood, and the results of this testing were used to fine-tune the GSS for each gyro. This significantly improved the suspension performance of all the gyros, especially gyro #2.

On Friday, 2 July 2004, the spin rates of gyros #1 and #3 was increased to 3 Hz (180 rpm), by streaming pure helium gas through their spin-up channels for 90 seconds each, and a few days later, gyros #2 and #4 were likewise spun-up to 3 Hz (180 rpm). Note that the exact spin rate of the gyros cannot be controlled. Rather, we control the length of time that ultra-pure helium gas flows through the spin-up channel for each gyro, and then the SQUID readouts tell us the resulting spin rates—which may differ slightly from one gyro to another.

During the week of July 4<sup>th</sup>, helium gas was flowed over gyro #4 for another 90 seconds, increasing its spin rate to approximately 6 Hz (360 rpm), and a number of tests were subsequently performed to ensure that gyro #4 and its suspension system were functioning properly in preparation for full-speed spin-up. Then, on 13 July 2004, Gravity Probe B achieved a major milestone with the successful spin-up of gyro #4 to a science-ready speed of 105.8 Hz (6,348 rpm). Second to the launch, the full-speed spin-up of the gyros was the next most long-awaited event in the history of GP-B. Members of the team were very attentive at their stations in the Mission Operations Center (MOC) here at Stanford for 3 hours and broke into applause when the final announcement came over the MOC intercom that the gyro #4 full spin-up had been completed successfully.

On July 16<sup>th</sup>, gyro #2 underwent the same spin-up procedure, reaching a final spin rate of 87 Hz (5,220 rpm). Spinning up the gyros to science-ready speed is a complex and dynamic operation that exercises the full capabilities of the Gyro Suspension System (GSS) and requires a high level of concentration and coordination on the part of the GP-B Team. Following is an overview of the full-speed spin-up process.

First, commands are sent to the GSS to move the gyro rotor (sphere) very close to the spin-up channel (about 1/100th of the edge of a sheet of paper) in one half of the gyro's housing. Ultra-pure (99.999%) helium gas is streamed from the Gas Management Assembly (GMA), mounted in a bay on the spacecraft frame, through tubing that enters the “top hat” (the thermal interface at the top of the Probe) and travels down to the gyro housings in the Science Instrument Assembly (SIA) at the lower end of the Probe. As the helium gas descends into the Probe, which is at a temperature of approximately 2.7 Kelvin, the gas cools down from 273 Kelvin to around 12 Kelvin.

Before entering the spin-up channel in one of the gyro housings, the gas is passed through a combination filter/heater. The filter, which is made of sintered titanium, removes any particles that may have been carried by the helium on its journey into the Probe. The heater enables the helium to be warmed slightly, which increases its adhesion to the ultra-smooth surface of the gyro rotor. The filtered and warmed helium then passes through the spin-up channel in one half of the gyro housing, and most of the gas evacuates into space through an exhaust system. However, some of the helium gas leaks into the housings of the other gyros, causing their spin rates to decrease up to 20% over a full spin-up period of 2-3 hours.

For this reason, the order in which the gyros are spun up is very important. Earlier in the IOC phase, the 3 Hz (180 rpm) spin-up provided information on the helium leakage rate of each gyro. Gyro #4, which had the highest leakage rate, was spun-up to full speed first, so that helium leaked from its spin-up would not affect other gyros that were already at science mission speed. The remaining gyros are then spun-up in decreasing order of their helium leakage rates—gyro #2, gyro #1, and finally, gyro #3.

Each full-speed spin-up takes most of a day. In the morning, helium gas is flowed over the gyro for 90 seconds, and tests are run to ensure that the helium leakage rate for that gyro corresponds to previous measurements. If everything checks out, the full-speed spin-up, in which helium gas is flowed over the rotors for 2-3 hours, commences early in the afternoon. The GP-B team controls the spin-up process by sending commands from the Mission Operations Center (MOC) here at Stanford to the spacecraft in real-time. For example, they send commands to open or close the GMA valves to flow helium through the gyro's spin-up channel. They also control the amount of heat applied to the gas before it enters the gyro spin-up channel, and they control opening and closing of exhaust valves. Real-time telemetry provides immediate feedback on the progress of the spin-up so that various parameters can be adjusted as necessary.



The successful spin-up of gyro #4 to full speed enabled us to spin-up gyro #2. Gyro #2 topped out at 87 Hz (5,220 rpm). Also, the helium gas leakage from the Gyro 2 spin-up slowed gyro #4 down to 91Hz (5,460 rpm). Based on these results, the team postponed the full-speed spin-up of gyros #3 and #1 for over a week, in order to run both ground-based and on-orbit tests, in an attempt to both increase the spin rates of the final two gyro rotors and also reduce the helium leakage during the spin-up process. From the results of these tests, the team determined that the gyro rotors could be positioned up to 30% closer to their spin-up channels during the spin-up process and still maintain a safe margin of clearance from the suspension electrodes and housings.

Using this finding, during the last week in July, gyros #3 and #1 were spun up to full speed. Each of these gyro spin-ups caused a 15% decrease in spin rate of the remaining gyros, resulting in the final spin rates ranging from approximately 60 – 80 Hz (3,600 – 4,800 rpm). [Table 2-3](#) below shows the history of the spin rates for all four gyros over the course of the entire spin-up process.

**Table 2-3.** Spin-up history of the GP-B gyros

GP-B's Gyro Spin-up Results (Hz)					
Date	13-Jul	16-Jul	28-Jul	30-Jul	Cumulative Avg Spin-down
Gyro #	Gyro 4 Spinup	Gyro 2 Spinup	Gyro 3 Spinup	Gyro 1 Spinup	
1	1.6	1.2	0.3	80.0	
2	1.6	87.0	75.7	62.3	
3	1.6	1.4	100.4	82.7	
4	105.6	90.5	79.5	65.5	
Spin-up Impact on other Gyros					
1	na	na	na	na	
2	na	na	-13.0%	-17.7%	
3	na	na	na	-17.7%	
4	na	-14.3%	-12.2%	-17.6%	
Average Spin-down	na	-14.3%	-12.6%	-17.7%	-15.4%

Although all four gyros ended up spinning at less than half the spin rates initially anticipated, their spin rates were more than adequate for collecting relativity data. Furthermore, several other accomplishments achieved by the GP-B subsystems during IOC—especially extremely low SQUID noise and higher than planned spacecraft roll rate—effectively reduced the error factor in the GP-B science experiment, thereby partially compensating for the reduced spin rates of the gyros.

### 2.4.3.7 Low Temperature Bakeout

Following gyro spin-up was the low temperature bakeout (LTB) process. The gyro spin-up process leaves residual helium gas in and around each of the science gyros. If not removed, this helium gas could reduce the accuracy of the experimental data collected during the Science Phase of the mission by providing a higher than desired gas pressure in the Probe, and thus causing the gyroscopes to spin down faster than requirements. The low temperature bakeout process involved applying a *very* mild heat cycle to the Science Instrument Assembly, briefly raising its temperature from 1.8 kelvin to approximately 7 kelvin. The net effect of this procedure was to remove nearly all of the residual helium. A cryogenic pump, comprised of sintered titanium, collected the remaining helium from the gyro housings. After low temperature bakeout, the SIA temperature was restored to 1.8 kelvin.

Low temperature bakeout was first practiced in May, during the third week of the mission. This practice LTB procedure had the added benefit of imparting a very small amount of spin-up helium gas to the gyros. Following the practice LTB, the SQUID gyro read-out data revealed that gyro #1, gyro #3, and gyro #4 were slowly spinning at 0.001, 0.002, and 0.010 Hz, respectively (1 Hz = 60 rpm). The Gyro Suspension Systems (GSS) were able to measure gas spin-up forces at the level of approximately 10 nano-newtons. This meant that the GP-B science team is able to interpret data from gyro spin rates four to five orders of magnitude smaller than what was planned for the GP-B science experiment.

The final low temperature bakeout procedure was performed during the first week in August, following the final high-speed spin up of all four gyros. This process yielded a post-LTB pressure inside the vacuum probe of  $1 \times 10^{-11}$  Torr, or 100,000 times less than  $1 \times 10^{-6}$  Torr in the external space vehicle low Earth orbit (LEO) environment.

#### **2.4.3.8 Spin Axis Alignment**

After gyro spin-up, the spin axis direction of each gyro had to be closely aligned to the guide star. This was performed using the Gyro Suspension System (GSS) in a special mode to slowly align each gyro spin axis to be in a certain orientation nearly parallel to the line of sight to the guide star. The gyroscopes were oriented a number of arc-seconds away from the apparent line of sight to the guide star so that over the mission, with the predicted relativistic precession and expected annual pointing aberration taken into account, the average misalignment of the gyroscopes would be zero. This minimized the possibility of disturbance torques on the rotors and enhanced the accuracy of the spin axis measurement process.

There were two phases to this alignment process—coarse and fine. During the coarse alignment, as much as one degree of spin axis orientation correction was achieved. The fine axis alignment then provided the final orientation accuracy of better than 10 arcseconds relative to the target orientation.

At the end of July 2004, after all four gyros had been spun-up to full speed, coarse spin axis alignment commenced. As noted in section 2.4.1.6 above, the lower than anticipated spin rates of the gyros, coupled with the nearly perfect sphericity of the gyro rotor surfaces, made the process of aligning the spin axes of some of the gyros—particularly gyro #4—more difficult and more time consuming.

Coarse spin axis alignment was completed on gyros #1 and #3 during the first week in August 2004, and the spin axes of gyros #2 and #4 were coarsely aligned by the middle of August. Fine spin axis alignment then commenced on all four gyros. Gyros #1, #2, and #3 completed their alignment and transitioned into science (data collection) mode during the last week in August. Gyro #4 required a little over two extra weeks to complete fine spin axis alignment and transition to science mode.

#### **2.4.3.9 Electrostatic Discharge of the Gyro Rotors**

An ongoing concern during the Gravity Probe B mission has been to minimize the build-up of electrostatic charges on the gyro rotors. The rotors build up a charge in two ways: 1) the process of suspending the rotors transfers some charge between the housing and rotor surface, and 2) protons from the sun are constantly bombarding the spacecraft, especially over the South Atlantic Ocean—the so-called “South Atlantic Anomaly”—and some of these protons strike the rotors and leave a deposit charge on them. Furthermore, various tasks such as gyro spin-up may impart a charge to the rotors.

Thus, periodically during the IOC phase, the team exercised an electrostatic discharge procedure, which uses ultraviolet light to reduce the electrostatic charge on the rotors. Each gyro housing is fitted with two fiber-optic cables that run from the gyro housings, up through the top hat of the Probe and out to an ultraviolet light source in the Experiment Control Unit (ECU) box, mounted on the spacecraft frame. UV light was beamed through the fiber optics onto the gyro rotors to discharge them. As a result of the light shining on metal surfaces in the rotor housing, electrons are liberated from the surface of the metal and create a cloud of electrons between the

housing and rotor surface. A charge control electrode, controlled via the Gyro Suspension System is biased to a certain voltage level to either drive electrons onto or off of the rotor surface, thus affecting the overall charge on the rotor. The suspension system then measures the charge on the rotor via a force balance technique, and the charging/discharging process stops when the rotors are within 15 mV of zero. Typically, the rotor charge is held to within 5 mV of ground potential during normal science operations. Reducing the level of charge was important because it increased the sensitivity and accuracy of the Gyroscope Suspension System (GSS) and reduced some disturbance torques on the rotors.

## 2.5 Science Phase

This section provides an overview and summary of the 5-week science phase of the mission which began on 27 August 2004 and ran through 14 August 2005.

### 2.5.1 Overview of the Science Phase

Following IOC, the mission transitioned into the science phase, where the essential science data were collected. This phase officially began on 27 August 2004 (Mission Day #129, Mission Week #20) with the transition of gyros #1, #2, and #3 into science mode. The gyroscopes were fully configured for the science phase once their axes had been aligned with the guide star, as described in section 2.4.3.8 and their rotors had been electrostatically discharged as described in section 2.4.3.9. Gyroscopes #1, #2, and #3 were all discharged and aligned by 27 August, 2004. However, gyro #4 required an additional 2 1/2 weeks to complete its spin axis alignment, which occurred on 16 September 2004 (Mission Day #149). Since each of the gyroscopes is independent of the others, gyros #1, #2, and #3 began providing science data at the end of August, and gyro #4 followed in mid-September.

#### 2.5.1.1 Mission Lifetime Determinations

During the week of 20 September 2004 (Mission Week #23), we performed a heat pulse meter operation on the dewar to determine its cryogenic lifetime, and in turn, the anticipated length of the science and subsequent instrument calibration phases of the mission. The results of this test, and several more performed at various times throughout the science phase, indicated that the helium remaining in the dewar would support approximately 10 months of science data collection and one month of instrument calibrations.

In fact, all of the heat pulse meter helium lifetime predictions that we made during the science phase of the mission turned out to be based on an incorrect assumption about the thermal connection between the liquid and gas phases of helium inside the dewar, leading to overly conservative helium lifetime predictions. We were actually able to collect science data for 11.5 months, followed by 1.5 months of instrument calibration testing.

#### 2.5.1.2 Transitioning from IOC to Data Collection

Upon commencement of the science phase, the science team began storing data with a “SCI” prefix so that it would be clear to all users this was valid science data. The anomaly team also separated its IOC record keeping from the new science documentation. Our daily 10 am meeting was moved to 11 am to allow the science team extra time to analyze the data, thereby making the meeting more meaningful.

The science phase was much quieter than the very busy IOC phase, although there still was important work each day requiring completion in a timely manner. The daily work load generally decreased as the science phase progressed. By the end of this phase, operations ran very smoothly, and were punctuated only by the occasional anomaly.

### 2.5.1.3 Lockheed Martin Team Phase-Out

An important shift in personnel took place when the IOC was completed. The Lockheed Martin team, which had supported the program as a very major contributor prior to launch, and as a co-contributor during IOC, phased out as IOC neared completion. Some of the subsystems, such as power, software, thermal, and others had been transitioned to Stanford personnel as IOC progressed. These systems were performing flawlessly, and required little or no commanding to maintain. The most challenging of the LM subsystems, the ATC system did require daily attention and very regular commanding. In this system, LM did remain on board with full-time support for a few months after the completion of IOC. In this very challenging system, Stanford was ramping up a 3-4 person team. Although the team members were young and less experienced than the LM team, their enthusiasm and capabilities of a Stanford Master's degree were quickly recognized. In addition to their innate strengths, the IOC period had been an exceptional training ground for the team.

### 2.5.1.4 Science Phase Routine Activities

After entering the science phase the team continued to monitor the gyroscopes and spacecraft very closely. Although all of the systems were working well, there were a small number of important updates required either on a weekly or more frequent basis. The biases on the spacecraft control non-science rate gyroscopes that required updating approximately twice a week. This process was important to minimize the guide star capture time for each acquisition. (It was thereby held to less than a minute.)

The spacecraft's stored program computer loads were transitioned from daily products to three uploads per week. This transition was possible because of the increasingly routine nature of the operations. This change was also important because of the reduced team size, and the need to allow adequate team rest. It should be repeated that the team had worked extremely long hours during IOC. It was important to provide a more reasonable work environment once the space vehicle no longer required intensive care.

### 2.5.1.5 Science Phase Anomalies

During the science phase, 3 major anomalies, 3 medium anomalies, 3 minor anomalies, and 65 observations were logged by the GP-B Anomaly Review Team. The relatively rare true anomalies that occurred during the science phase required immediate attention. The anomaly resolution process used during IOC was continued in the science phase. A discussion of the anomaly resolution process is described in [Chapter 5, Managing Anomalies and Risk](#), and a complete summary of all on-orbit anomalies and observations is available in [Appendix D, Summary Table of Flight Anomalies](#). During IOC, a significant effort was expended to minimize the recovery time from anomalies in order to expedite the overall IOC schedule. For some anomalies that occurred during the science phase, there was additional motivation to minimize anomaly recovery time, because mis-pointing, non-standard drag-free performance, and other non-science configurations not only put the validity of the data at risk, but also increased the risk of causing higher than nominal gyroscope torques. Thus, during the science phase, the team worked hard to minimize the recovery process, and these efforts paid off.

### 2.5.1.6 Early Calibration Tests During the Science Phase

It will be seen in the next section that like IOC, the calibration phase was on a very tight schedule and therefore was tension-packed. To help reduce the scope of work required for the calibration phase, and ultimately to improve the overall experimental error, many SRE tests were performed during the final month of the science mission. These tests were performed at this point in the mission for two main reasons:

1. These tests were of low technical risk.
2. The science data were not impaired by the impact of these tests.

In other words, the gyroscopes were maintained such that they could be returned to their science configuration after the SRE testing was complete. Although the science analysis of these tests is still ongoing at the time of the writing of this report, from an operational perspective no issues or problems arose.

## 2.5.2 Monthly Science Phase Highlights

Table 2-4 below provides a month-by-month overview of the science phase of the mission. For a more detailed, weekly description of activities that occurred during the science phase, see [Appendix C, Weekly Chronicle of the GP-B Mission](#).

**Table 2-4.** Monthly highlights of the GP-B Science Phase

<b>Monthly Highlights of the GP-B Science Phase</b>	
<b>Month</b>	<b>Activities &amp; Events</b>
September 2004	Gyros #1, #2, and #3 generating science data.
	Continued tuning of the ATC system.
	Drag-free gyro #3 transitions to analog suspension. Drag-free control transferred to gyro #1; identified cause as data spike in GSS, and re-suspended gyro #3 digitally.
	Gyro #4 completes spin axis alignment and begins collecting science data.
	Heat pulse meter test indicates ~10 months of helium available for the science phase
October 2004	Sympathetic resonance observed in drag-free controller due to sloshing wave on surface of helium in the dewar.
	All four gyros continue generating science data.
	Gyro #3 again transitions to analog suspension; bridge setting changed to increase signal-to-noise ratio. Cause determined to be GSS noise spikes that exceeded preset limits.
	Reduced gain on drag-free controller to mitigate harmonic coupling between ATC drag-free system and sloshing helium in the dewar.
November 2004	Drag-free gyro #1 transitions to analog suspension mode, just as gyro #3 had done. Switched drag-free control back to gyro #3 and changed bridge setting on gyro #1.
	All four gyros continue generating science data.
	Large geo-magnetic storm increases solar activity, with a corresponding increase in high-energy proton radiation.
	Proton strike causes the GSS computer to re-boot, sending all four gyros into analog backup suspension mode.
December 2004	Memory locations in SRE computer sustains multi-bit errors, causing the SRE to re-boot
	Spacecraft enters its second 15-day "full-sun" period of the mission towards the end of Nov.
	All four gyros continue generating science data.
	Dewar's helium flow rate adjusted for full-sun period.
	Warming of the Attitude Reference Platform (ARP) causes spacecraft pointing problems.
January 2005	Full-sun period ends.
	ATC adjusted to re-lock the telescope on the guide star after each GS-Invalid period.
	GPS triangulation problem causes computer overflow, triggering safemodes.
	All four gyros continue generating science data.
	Worst solar storm since 2003 results in saturation of telescope detectors, causing temporary loss of guide star and non-critical MBE in SRE computer.
Proton monitor stops working properly.	

---

## Monthly Highlights of the GP-B Science Phase

---

Month	Activities & Events
February 2005	All four gyros continue generating science data.
	Problematic sun spots from January return, but this time with no geo-magnetic storm; over the course of the month, solar activity returns to normal.
	ATC fine-tuning enable science telescope to lock onto guide star at the beginning of GSV periods in less than one minute.
	Another heat pulse meter test run to check helium life time; results consistent with previous test.
	Brief communications outages at Poker Flats and Wallops Ground Stations; data later recovered from Poker flats, but not from Wallops. Total data loss to date < 1%.
Star sensor magnitude tables updated.	
March 2005	All four gyros continue generating science data.
	Proton radiation strikes over South Pole, resulting in multiple MBEs in main CCCA computer and triggering automatic switch-over to B-Side (backup) computer.
	Experience from prior switch-over during 2nd week of mission, plus rehearsals enable Mission Ops team to cut recovery time from a week down to a weekend.
	3 MBEs in <0.2 sec period trigger 2nd computer re-boot, now in B-side (backup) computer; team again recovers within 2 days. SRE computer also sustains MBEs and is re-booted.
	Multiple MBE safemode response changed to stop time line, instead of re-booting computer.
	More proton strikes with accompanying MBEs in South Atlantic Anomaly (SAA) region trigger 3rd re-boot in B-side computer. This time, Mission Ops team able to recover in 12 hours.
ATC stored commands revised so that spacecraft doesn't roll down when computer re-boots.	
April 2005	All four gyros continue generating science data.
	Memory location in GSS computer sustains an MBE; location is subsequently patched via ground commands.
	ATC software is updated to enable spacecraft to remain in control of the science gyros during passes through the SAA.
	Investigated warming of Forward Equipment Enclosure as possible contributor to recent spate of MBEs.
	Discovered & corrected ATC problem that had been resulting in converted values exceeding a threshold, which had been causing ATC pointing problems in the SAA region. After the correction was implemented, ATC pointing was equally good in our out of the SAA region.
	UV light used to remove electrostatic charges from all four gyro rotors.
	Another heat pulse meter test performed to determine expected lifetime of helium in the dewar. Results suggest that helium will run out in late August or early September.
	GP-B celebrates anniversary of one year in orbit.
May 2005	All four gyros continue generating science data.
	Some non-torquing SRE calibration tests begin.
	Safemode response to MBEs in main computer changed to force re-boot if MBE occurs in memory location that increments the error counter.
	GP-B PI, Francis Everitt, presented NASA Distinguished Public Service Medal at NASA HQ.
	ECU turned off to reduce noise in SQUID readout system; ECU now turned on only once weekly to retrieve status data from various on-board systems.
	Spacecraft enters 3rd 15-day full-sun period of the mission.
May 2005 was one of the quietest and smoothest months in the science phase of the mission.	

---

## Monthly Highlights of the GP-B Science Phase

---

Month	Activities & Events
June 2005	All four gyros continue generating science data.
	Preliminary non-torquing SRE calibrations tests continue.
	Spacecraft full-sun period ends.
	Gyro #2 transitions to analog backup suspension mode and is subsequently re-suspended in digital mode.
	Benign MBEs discovered in SRE are patched via ground commands.
	Forward feed term of drag-free controller updated to improve accuracy based on 13 months of flight data.
	Another heat pulse meter test is run; results continue to indicate late August-early September helium depletion date.
July 2005	Switched drag-free control from gyro #3 to gyro #1 as part of ongoing calibration tests.
	All four gyros continue generating science data.
	With sun now shining on aft section of spacecraft, ATC performance now most stable of entire science phase.
	Benign MBEs in GSS computer patched via ground commands.
	Calibration tests on drag-free gyro #3 cause it to switch to analog suspension; gyro #3 is subsequently re-suspended digitally.
	Visit from Tony Lyons & Tony Lavoie from NASA MSFC; off-site management meeting held to discuss end-of-mission trade-offs between length of science and calibration phases.
	Poker Flats, AK ground station communication problems require temporary switch to McMurdo ground station at South Pole.
August 2005	UV light used once again to remove electrostatic charge from all four gyro rotors;
	Dr. Anne Kinney, Director of Universe Division in the Science Mission Directorate at NASA HQ spends a day visiting GP-B.
	All four gyros continue generating science data.
	Preliminary instrument calibration tests continue.
	A final heat pulse meter test is run and again confirms previous predictions of late August - early September helium depletion date.
	Based on the results of the heat pulse meter tests, as well as other helium lifetime estimates, science data collection concluded on August 12. In total, the mission collected science data for 352 days (11.6 months) during 7,000+ orbits, with a 99% data capture rate.
	Dr. Nancy Roman, retired Chief of Astronomy & Relativity Programs at NASA Headquarters from 1960-1979, who oversaw the early development of GP-B visited Stanford for two days.
Rex Geveden, former MSFC Program Manager for GP-B was appointed Associate NASA Administrator at NASA Headquarters.	
Final instrument calibration tests, which required pointing the GP-B telescope & spacecraft at neighboring stars in the vicinity of guide star IM Pegasi commenced.	

---

## 2.6 Calibration Phase

This section provides an overview and summary of the activities that occurred during the final 6-week calibration phase of the mission.



## 2.6.1 Overview of the Calibration Phase

The purpose of the post-science calibration phase was to perform tests to allow the placing of tight limits on systematic errors and gyroscope torques. A natural tension existed in choosing the correct moment to end the science phase and to begin the calibration phase. The technical underpinnings of this tension can be understood as follows. The total experiment error is the sum of three different types of error (plus the exact knowledge of the proper motion of the guide star). These three error sources are:

1. Statistical measurement error,
2. Systematic errors
3. Gyroscope torques.

The overall experiment measurement error improves as the duration of the science data taking is increased. Systematic errors, however, do not. Furthermore, some systematic errors and gyroscope torques may not be directly evident from the science data and may require on-orbit tests to set upper limits on their effect. Therefore a longer calibration phase reduces the impact of systematic errors and gyroscope torques at the expense of statistical measurement error. The purpose of the calibration phase was therefore to enhance various possible systematic error sources so that tighter limits could be placed on each, thereby reducing the overall experiment error. This technical balance had to be blended with an important programmatic issue; risk management.

During the science phase each of the gyroscopes had a spin rate of more than 60 Hz. or a stored kinetic energy of more than 1 joule. Based upon years of ground test, there was a concern that a de-levitation of a gyroscope would damage not only that gyroscope, but put the other gyroscopes at some risk as well. Since the calibration phase required a number of new commands to be performed, the sequence of testing was adjusted to perform the low risk operations first. Another risk involved the possibility that calibration phase would not be completed prior to the depletion of the liquid helium. The final schedule for this phase involved performing a number of GSS tests followed by a 2 week break. The purpose of the break was to allow the team to assess the adequacy of the tests and to allow time to generate new commands that were determined to be needed to support the science team.

In choosing to perform the GSS tests first, some of the gyroscopes could be kept in science mode while the others were GSS tested. Gyroscopes 2 and 3 entered the post-science calibration phase on July 7, 2005. Gyroscopes 1 and 4 entered the post-science calibration phase on August 15, 2005.

A series of ATC tests followed the GSS tests. (GSS tests on gyroscopes 1 and 4 were also completed during this final stage of the mission.) The most important of these ATC tests involved intentionally mis-pointing the space vehicle to allow investigation of resulting gyroscope torques. A series of these tests were performed. These tests were not believed to be of high hardware risk (i.e. the risk of a gyroscope de-levitation was thought to be low, there was a consensus that the risk of schedule slippage was significant. For many of the mis-pointing operations, the vehicle was to acquire a star other than IM Pegasi. There was a very real concern that finding these other stars could be problematic and time consuming. In practice, just like the GSS phase which preceded it, the operations went off without a hitch. By the end of this period, moving back and forth between stars had become almost routine. The team had learned a tremendous amount during the IOC and science phases.

## 2.6.2 Weekly Calibration Phase Highlights

[Table 2-5](#) below provides a month-by-month overview of the science phase of the mission. For a more detailed, weekly description of activities that occurred during the final calibration phase, see [Appendix C, Weekly Chronicle of the GP-B Mission](#).

**Table 2-5.** Weekly highlights of the 7-week final instrument calibration phase

<b>Weekly Highlights of the GP-B Final Calibration Phase</b>	
<b>Week</b>	<b>Activities &amp; Events</b>
Week ending 8/19	<p>Final calibration phase begins on Monday, August 14th when drag-free control on gyro #1 was turned off, and gyro preloads were set to IOC levels of 10 volts.</p> <p>The telescope &amp; spacecraft were maneuvered to point at the star HD216235, 1 degree away from IM Pegasi.</p> <p>The spacecraft returned to its guide star orientation, and drag-free control was restored for a day.</p> <p>The calibration excursions to HD216235 were repeated four more times over the course of this week.</p>
Week ending 8/26	<p>On Monday, the telescope &amp; spacecraft were maneuvered to the star Zeta Pegasi (HR 8634), located 7 degrees away from IM Pegasi. This pointing orientation was maintained for ~30 hrs.</p> <p>On Wednesday, the spacecraft's orientation was returned to IM Pegasi.</p> <p>On Thursday and Friday, DC mis-centering tests were performed on gyros #1, #2, and #4.</p> <p>At the end of the week, GSS torque calibrations were performed on gyros #1 and #4.</p>
Week ending 9/2	<p>Although heat pulse meter tests had suggested that the helium would be depleted by this day, some amount of liquid helium still remained in the dewar, and thus calibration tests continued this week.</p> <p>On Wednesday, the telescope &amp; spacecraft were maneuvered to point to the star HR Pegasi, 4 degrees away from IM Pegasi in the east-west plane (all previous slewing tests had been in the north-south plane).</p> <p>On Thursday &amp; Friday, several slewing tests were made to "virtual stars" less than one degree away from IM Pegasi in various directions. (Virtual stars don't actually exist; they are simply position markers at pre-determined distances from the guide star, IM Pegasi.)</p> <p>Tony Lyons, GP-B Program Manager from MSFC, joined the team at Stanford for this week of calibration tests.</p> <p>Various other slewing tests, in which the telescope/spacecraft was pointed at locations in the vicinity of IM Pegasi continued throughout the weekend.</p>
Week ending 9/9	<p>Heat pulse meter tests had predicted that the helium in the dewar would be depleted by the beginning of this week, but like the Energizer Bunny that keeps on running, the helium in the dewar kept on flowing. Thus, planned calibration tests continued.</p> <p>Over the weekend, we visited virtual stars located 0.1 degrees away from star HD216635, a neighbor of IM Pegasi, remaining pointed at the virtual star for 24 hours and then returning to IM Pegasi for 16 hours. We then repeated this procedure with a virtual star located 0.1 degrees in the opposite direction.</p> <p>On Tuesday, we visited a virtual star located halfway to the star HR Pegasi (HD216672), located to the West of IM Pegasi and remained pointed there for 24 hours. We then slewed the telescope/spacecraft back to IM Pegasi.</p> <p>On Thursday, we visited a virtual star 0.3 degrees towards HD216635 and remained there for 24 hours.</p> <p>We continued these "slewing" tests during the weekend, visiting virtual star locations within a 4 degree radius of IM Pegasi.</p>

---

## Weekly Highlights of the GP-B Final Calibration Phase

---

Week	Activities & Events
Week ending 9/16	<p>The virtual “helium level gauge” in the dewar was clearly in the “red zone,” but when the helium would actually run out was now anyone’s guess. So, planned calibration tests continued.</p> <hr/> <p>Over the weekend, after running more slewing tests, we locked back onto IM Pegasi and switched drag-free control from gyro #1 to gyro #3 in order to perform calibration tests on gyro #1.</p> <hr/> <p>During the gyro #1 calibration test, the pressure in the dewar dropped, causing thruster instability. To mitigate this situation, we switched the thrusters to “open-loop,” and they remained in this state for the duration of the calibration tests.</p> <hr/> <p>On Tuesday, we slewed the telescope/spacecraft to the very bright star, Alpha Pegasi (Markab or HD 218045), located 3.25 degrees South of IM Pegasi. We remained locked on Alpha Pegasi for 12 hours, before returning to IM Pegasi and switching drag-free control back to gyro #1.</p> <hr/> <p>On Wednesday, we sent commands to the spacecraft to decrease its roll rate from 0.7742 rpm to 0.4898 rpm and changed the frequency of a SQUID calibration signal that was causing interference at this slower roll rate. The spacecraft was then able to perform nominally at the new roll rate.</p> <hr/> <p>On Friday, we initiated procedures to remove electromagnetic flux from the SQUIDs.</p>
Week ending 9/23	<p>Because the helium in the dewar had now exceeded its expected lifetime by more than 3 weeks, the dewar team re-calculated the helium lifetime tests based on a new assumption—that there was weak, rather than strong thermal contact between the liquid and gas layers of helium in the dewar. This new assumption put an upper bound on the helium lifetime that was 5-6 weeks longer than the initial assumptions. Thus, it now appeared that the helium could last up to 3 weeks longer.</p> <hr/> <p>Over the weekend, we completed the process of removing electromagnetic flux from the SQUIDs.</p> <hr/> <p>On Tuesday, we visited a virtual star 0.1 degrees east of IM Pegasi and remained locked in that position for 48 hours. While the telescope was locked in this position, we performed some dark current calibration tests on the telescope.</p> <hr/> <p>During this week, we twice attempted to switch from backup to primary drag-free mode. Both attempts failed, and in each case, we returned to backup drag-free control, which had been used throughout the science phase of the mission. Analysis indicated that these failed switch-overs were due to configuration issues.</p>
Week ending 9/30	<p>This turned out to be the last week of the mission—the day the dewar “died.”</p> <hr/> <p>On Monday, we once again attempted to switch from backup to primary drag-free control, and once again, the attempt failed—but for a different reason than the two attempts made the previous week. Preliminary analysis indicated that this failed switch-over was similar to ones that occurred during IOC and was probably due to “un-modeled” forces between the gyro rotor and its housing.</p> <hr/> <p>On Tuesday and Wednesday, the team returned the spacecraft to its nominal science mode, pointing at IM Pegasi, and collected gyro data, later to be compared with similar data collected during the science phase of the mission.</p> <hr/> <p>On Thursday, 29 September 2005, at 1:55 pm PDT, the last of the liquid helium in the dewar transitioned to the gas phase, and the Science Instrument Assembly began to warm up.</p> <hr/> <p>The team correctly assessed the status of the dewar, based on a set of pre-approved indicators, and they initiated a planned helium depletion procedure.</p> <hr/> <p>On Friday morning, we held our last daily “all-hands” meeting, took a group photo of the team, and the GP-B flight mission was thus concluded.</p>

# 3

## Accomplishments & Technology Innovations





This section contains three main sub-sections: Goals & Accomplishments, Extraordinary Technology of GP-B, and GP-B Technology Transfer.

## 3.1 Goals & Accomplishments

This sub-section begins with a description of seven “near zeroes” that form the basis of the GP-B experimental method. The latter half of this sub-section lists a number of noteworthy accomplishments that GP-B has achieved during its flight mission, from launch in April 2004 through the final instrument calibrations in September 2005.

### 3.1.1 GP-B’s Seven Near Zeroes

Designing a physics experiment involves a basic choice: maximize the effect to be measured, or minimize the “noise” that obscures it. For the Gravity Probe-B experiment, however, that choice was moot because Einstein's relativistic effects, that literally “roar” near black holes and neutron stars, whisper almost inaudibly here on earth. Thus, GP-B had to turn the volume of the extraneous babble down as close to zero as possible in order to hear the whisper. It's like asking everyone in a football stadium to sit quietly to hear a bird sing.

The noise affecting near-earth relativistic effects comes. From the slightest amount of heat or pressure, the influence of any magnetic field, any kind of gravitational acceleration, or the tiniest amount of atmospheric turbulence or solar radiation, to the smallest imperfections in the instruments themselves, the tolerances must be at or very “near zero.”

It's hard to picture the precision of the Gravity Probe B instruments. The four gyroscopes, housings, and telescopes were all carved out of a single purified quartz block, grown in Brazil, refined in Germany, and delivered to GP-B as a trash-can-size crystal. From side to side, the crystalline structure of the quartz is identical and homogenous to within three parts per million. The gyroscope spheres are less than 40 atomic layers from a perfect sphere, the most perfectly round objects ever made by man, so they could spin for literally several thousand years without any significant drift. To put that in perspective, if the gyroscopes were enlarged to the size of the Earth, the highest mountain or the deepest ocean trench would be only 8 feet. The electrical charge at the gyroscopes' surfaces, known as the electric dipole moment, were likewise vanishing small, held to less than five parts in ten million.

The isolation of the instruments from their surroundings is equally impressive. For 17 months, from prior to launch until the helium in the dewar was depleted at the end of the post-science instrument calibration phase of the mission, the entire GP-B science instrument was maintained in a near-perfect vacuum, surrounded by superfluid liquid helium, cooled to a temperature of  $\sim 1.8\text{K}$  ( $-271.4^\circ\text{C}$  or  $-456.4^\circ\text{F}$ ). The helium's temperature was held constant, just above absolute zero, by the 650-gallon dewar, with its unique GP-B porous plug providing a controlled escape for the helium gas that boiled off continuously during the mission.

To zero out unwanted magnetic fields, the Probe was encased in a cascading succession of four lead bags within bags. After each of the first three bags was inserted, the outside bag was removed. Inside the remaining lead bag, remaining residual magnetic fields had been reduced to a negligible level, approximately  $10^{-11}$  of Earth's magnetic field. In other words, there was almost a total absence of any magnetic fields inside the probe that might affect the results.

Finally, and perhaps most impressive of all, is that throughout the flight mission, the GP-B spacecraft rolled continuously at a rate of 0.7742 rpm, pointing at the guide star, IM Pegasi, all the while maintaining a drag-free orbit. Using the helium gas that continuously sweated out through the dewar's porous plug as a propellant, eight opposing pairs of proportional micro thrusters enabled the spacecraft to precisely control its attitude and continually chase one of the science gyros, which was effectively circling the Earth in a perfect free-fall orbit.

It was in this pristine, near-zero disturbance environment, that the GP-B gyroscopes spun in lonely isolation for 50 weeks, collecting the data that has, at long last, put Einstein’s general theory of relativity to a rigorous and precise experimental test.

**Table 3-1.** GP-B Seven Near Zeroes

<b>Experimental Variable</b>	<b>Tolerance Requirements</b>	<b>Tolerances Achieved During Mission</b>
<b>Gyroscope Rotor Near Zeros</b>		
Mechanical Sphericity	50 nanometers (2 micro inches)	<10 nanometers (< 0.4 microinches)
Material Homogeneity	3 parts in 10 <sup>6</sup>	3 parts in 10 <sup>7</sup>
Electrical Sphericity	5 parts in 10 <sup>7</sup>	<5 parts in 10 <sup>7</sup>
<b>Probe Environment Near Zeros</b>		
Temperature	1.95 kelvin (-271.2° celsius or -456.2° fahrenheit)	1.8 kelvin (-271.4° celsius or -456.4° fahrenheit)
Non-Gravitational Residual Acceleration	Less than 10 <sup>-10</sup> g	Less than 5 x 10 <sup>-12</sup> g
Background Magnetic Field	10 <sup>-6</sup> gauss	Less than 10 <sup>-7</sup> gauss
Probe Pressure	10 <sup>-11</sup> torr	Less than 10 <sup>-11</sup> torr

### 3.1.2 Noteworthy Accomplishments

Following is a list of extraordinary accomplishments achieved by GP-B during the 17 months of its flight mission.

- Over the course of the 17.3-month mission, we communicated with the spacecraft over 4,000 times, and the Mission Planning team successfully transmitted over 106,000 commands to the spacecraft.
- GP-B is the first satellite ever to achieve both 3 degrees of freedom in attitude control (pitch, yaw, and roll), and 3 degrees of freedom in translational drag-free control (front-to-back, side-to-side, and up-down). Essentially, while orbiting the Earth, the whole spacecraft “chases” one of the science gyros while rolling continuously in its orbit.
- The GP-B gyros, which performed extraordinarily well in orbit, have been listed in the Guinness Database of World Records as being the roundest objects ever manufactured.
- The spin-down rates of all four gyros were considerably better than expected. GP-B’s conservative requirement was a characteristic spin-down period (time required to slow down to ~37% of its initial speed) of 2,300 years. Measurements during IOC showed that the actual characteristic spin-down period of the GP-B gyros exceeds 10,000 years—well beyond the requirement.
- The magnetic field surrounding the gyros and SQUIDs (Super-conducting QUantum Interference Device) was reduced to 10<sup>-7</sup> gauss, less than one millionth of the Earth’s magnetic field—the lowest ever achieved in space.
- The gyro readout measurements from the SQUID magnetometers had unprecedented precision, detecting fields to 10<sup>-13</sup> gauss, less than one trillionth of the strength of Earth’s magnetic field.
- The science telescope on board the spacecraft tracked the guide star, IM Pegasi (HR 8703), to superb accuracy, and it also collected a year’s worth of brightness data on that star. The brightness data we collected on IM Pegasi represents the most continuous data ever collected on any star in the universe.



- In November 2005, the entire GP-B team was awarded a NASA Group Achievement Award “For exceptional dedication and highly innovative scientific and engineering accomplishments leading to the successful execution and completion of the Gravity Probe B Science Mission.”

## 3.2 Extraordinary Technology of GP-B

This sub-section describes the extraordinary technologies, redundancy, and unique technological innovations that enabled the GP-B experiment to come to fruition.

### 3.2.1 An Overview of GP-B Technology

To test Einstein's theory of general relativity, Gravity Probe B must measure two minuscule angles with spinning gyroscopes, floating in space. While the concept of Gravity Probe B is relatively simple in design, the technology required to build it is some of the most sophisticated in the world. Scientists from Stanford University, NASA's Marshall Space Flight Center, and Lockheed Martin Space Systems have drawn from a diverse array of physical sciences, and have invented much of the technology that made the mission possible. In fact, much of the technology did not even exist when the experiment was first suggested in late 1959 - early 1960.

#### 3.2.1.1 World's Most Perfect Gyroscopes

To measure the minuscule angles predicted by Einstein's theory, 6,614.4 milliarcseconds (6.6 areseconds) per year and 40.9 milliarcseconds per year, Gravity Probe B needed to build a near-perfect gyroscope—one whose spin axis would not drift away from its starting point by more than one hundred-billionth of a degree each hour that it was spinning. This was an especially stiff challenge, given that the spin axes of all gyroscopes tend to drift slightly while they are spinning. Even the spin axis drift in the most sophisticated Earth-based gyroscopes, found in missiles and jet airplanes, is seven orders of magnitude greater than GP-B could allow.



**Figure 3-1.** Gravity Probe B gyroscope rotor, with quartz housing halves.

Each quartz rotor is coated with a sliver-thin layer of niobium, a superconducting metal. Inside each housing, six electrodes electrically suspend the gyroscope, allowing it to spin freely at up to 10,000 rpm. Channels are cut in the quartz housing to allow helium gas to start the rotor spinning. A wire loop, embedded in the housing, is connected to a SQUID (Superconducting Quantum Interference Device) magnetometer to detect any change in direction of the gyroscope's spin axis.

Three physical characteristics of any gyroscope can cause its spin axis to drift, independently of the general relativity precession predicted by Einstein's theory:

1. An imbalance in mass or density distribution inside the gyroscope
2. An uneven, asymmetrical surface on the outside of the gyroscope
3. Friction between the bearings and axle of the gyroscope.

This meant that a GP-B gyroscope rotor had to be perfectly balanced and homogenous inside, had to be free from any bearings or supports, and had to operate in a vacuum of only a few molecules.

After years of work and the invention of new technologies and processes for polishing, measuring sphericity, and coating, the result was a homogenous 1.5-inch sphere of pure fused quartz, polished to within a few atomic layers of perfectly smooth. In fact, the GP-B gyro rotors are now listed in the Guinness Database of World Records as being the roundest objects ever manufactured, topped in sphericity only by neutron stars.

The spherical rotors are the heart of each GP-B gyroscope. They were carved out of pure quartz blocks, grown in Brazil and then fused (baked) and refined in a laboratory in Germany. The interior composition of each gyro rotor is homogeneous to within two parts in a million.

On its surface, each gyroscope rotor is less than three ten-millionths of an inch from perfect sphericity. This means that every point on the surface of the rotor is the exact same distance from the center of the rotor to within  $3 \times 10^{-7}$  inches.

Here are two ways to imagine how smooth this is. First, compare the GP-B gyro rotor's smoothness with another smooth object—a compact disk. CD's and DVD's both appear and feel incredibly smooth. The pits on the compact disk's surface, which carry the digital information, are less than 4/100,000ths of an inch deep (one millionth of a meter). However, compared to the GP-B gyroscope, the surface of a CD is like sandpaper. The bumps and valleys on the surface of the GP-B gyroscope are 100 times smaller than those on a CD. Viewed at the same magnification, one could barely see any imperfections on the gyroscope's surface.

Alternatively, imagine a GP-B gyroscope enlarged to the size of the Earth. On Earth, the tallest mountains, like Mount Everest, are tens of thousands of feet high. Likewise, the deepest ocean trenches are tens of thousands of feet deep. By contrast, if a GP-B gyroscope were enlarged to the size of the Earth, its tallest mountain or deepest ocean trench would be only eight feet!

Finally, the gyroscope is freed from any mechanical bearings or supports by levitating the spherical rotor within a fused quartz housing. Six electrodes evenly spaced around the interior of the housing keep the rotor floating in the center. A stream of pure helium gas spins the gyroscopes up to 4,000 rpm or faster. After that, and with all but a few molecules of the helium spin-up gas evacuated from the housings, each gyroscope spins, a mere 32 microns (0.001 inches) from its housing walls, free from any interfering supports.

### **3.2.1.2 Spinning Superconductivity**

Each Gravity Probe B gyroscope is nearly perfectly spherical and nearly perfectly homogenous. While this ensures that the gyroscope will spin with near-perfect stability, its “near-perfectness” creates a daunting challenge—we cannot mark the gyroscope to see exactly which direction its spin axis is pointing.

For GP-B to “see” the shape and motion of local spacetime accurately, we must be able to monitor the spin axis orientation to within 0.5 milliarcseconds, and locate the poles of the gyroscope to within one-billionth of an inch.

How can one monitor the spin axis orientation of this near-perfect gyroscope without a physical marker showing where the spin axis is on the gyroscope? The answer lies in a property exhibited by some metals, called “superconductivity.”

Superconductivity was discovered in 1911 by the Dutch physicist H. Kammerlingh Onnes. He found that at temperatures a few degrees above absolute zero, many metals completely lose their electrical resistance. An electric current started in a superconductor ring would flow forever, if the ring were permanently kept cold. But, superconductors also have other interesting properties. In 1948, the theoretical physicist Fritz London predicted that a spinning superconductor would develop a magnetic moment—created by the electrons lagging the lattice of the superconducting metal—which is therefore exactly aligned with its instantaneous spin axis. In 1963, three different groups, including a GP-B graduate student, demonstrated the existence of this London moment experimentally.

What is remarkable about this phenomenon (and most fortunate for Gravity Probe B) is that the axis of this magnetic field lines up exactly with the physical axis of the spinning metal. Here was the “marker” Gravity Probe B needed. We coated each quartz gyroscope with a sliver-thin layer of a superconducting metal, called niobium (1,270 nanometers thick). When each niobium-coated gyroscope rotor is spinning, a small magnetic field surrounds it. By monitoring the axis of the magnetic field, Gravity Probe B knows precisely which direction the gyroscope's spin axis is pointing, relative to its housing.



**Figure 3-2.** SQUID detector package, with housing cover

The magnetic field axis is monitored with a special device called a SQUID (Superconducting QUantum Interference Device). The SQUID is connected to a superconducting niobium pickup loop, deposited on the flat surface at the outer edge of one half of the quartz housing in which the gyro rotor spins. Thus, the loop, which senses the gyro's spin axis orientation, is located on the planar surface where the two halves of the gyro housing are joined. When the gyroscope precesses or tilts, the London moment magnetic field tilts with it, passing through the superconducting loop. This causes a current to flow in the loop—a quantized current. The SQUID detects this change in magnetic field orientation. The SQUID magnetometers are so sensitive that a field change of only one quantum—equivalent to  $5 \times 10^{-14}$  gauss (1/10,000,000,000,000th of the Earth's magnetic field) and corresponding to a gyro tilt of 0.1 milliarcsecond ( $3 \times 10^{-8}$  degrees)—is detectable.

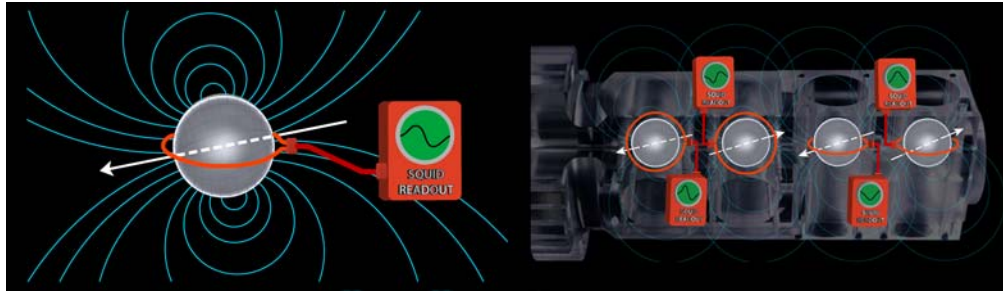


**Figure 3-3.** Functional diagram of a SQUID pickup loop measuring the London Moment around a GP-B gyro rotor (left) and four SQUID readouts—one for each gyro (right).

Using the London moment to monitor the gyroscope's orientation was the perfect readout scheme for Gravity Probe B—it is extremely sensitive, extremely stable, applicable to a perfect sphere, and—most important, it exerts negligible torques (forces) on the gyroscope.

### 3.2.1.3 The Dewar: A 9' Tall, 8' Wide Thermos

One of the greatest technical challenges for Gravity Probe B was keeping the science instrument just above absolute zero, at approximately 2.3 Kelvin (-270.9 celsius or -455.5 fahrenheit) constantly for 16 months or longer.



**Figure 3-4.** The GP-B dewar—one of the largest and most sophisticated dewars ever flown

The science instrument is kept at this supercold temperature, by placing it in a special 2,441 liter (645-gallon) dewar, or thermos, about the size of a mini van, that is filled with liquid helium in a superfluid state. This nine-foot tall Dewar is the main structure of the GP-B satellite itself. In its 640-kilometer (400-mile) high polar orbit, the GP-B satellite is low enough to be subjected to heat radiating from the Earth's surface, and it is also subjected to alternating hot and cold cycles, as it passes from intense sunlight into the Earth's shadow every ninety-seven minutes. Throughout the life of the mission, key portions of the science instrument had to be maintained at a constant temperature to within five millionths of a degree centigrade.

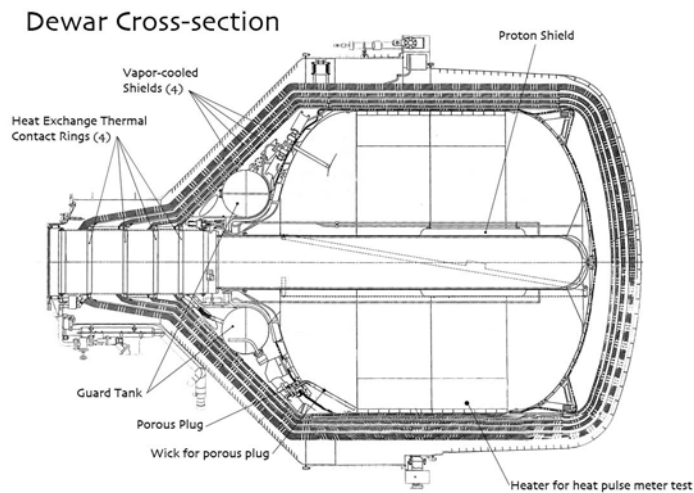


**Figure 3-5.** Cross sectional schematic of the dewar

During the mission, the dewar's insulating chamber remained a vacuum, which limited the amount of heat penetrating through the outside wall into the inner chamber containing the science instrument. In addition, it includes several other devices for maintaining the necessary cryogenic temperature:

1. Multilayer insulation—multiple reflective surfaces in the vacuum space to cut down radiation
2. Vapor-cooled shields—metal barriers, suitably spaced, cooled by the escaping helium gas
3. Porous Plug—invented at Stanford, and engineered for space at NASA Marshall Space Flight Center in Huntsville, AL, Ball Aerospace in Boulder, CO, and the Jet Propulsion Laboratory in Pasadena, CA. This plug allows helium gas to evaporate from the Dewar's inner chamber, while retaining the superfluid liquid helium inside. See section 3.2.3.1 for a more complete description of the porous plug.

When there was still helium in the dewar, virtually no heat could penetrate from the outside wall through the vacuum and multilayer insulation inside. However, a small amount of heat (about as much as is generated by the message indicator lamp on a cell phone) did leak into the Dewar from two sources:

1. Conduction of heat flowing from the top of the Dewar into the liquid helium
2. Radiation leaking down through the telescope bore into the liquid helium.

The porous plug controls the flow of this evaporating helium gas, allowing it to escape from the Dewar, but retaining the superfluid helium inside. The plug is made of a ground-up material resembling pumice. The evaporating helium gas climbed the sides of the inner tank near the plug and collected on its surface, where it evaporated through the pores in the plug, much like sweating in the human body.

The evaporating helium provided its own kind of refrigeration. As the helium gas evaporated at the surface of the porous plug, it drew heat out of the liquid helium remaining in the Dewar, thereby balancing the heat flow into the Dewar. You can feel this effect on your skin when you swab your skin with water. As the liquid evaporates off your skin, it draws heat energy with it, leaving your skin a tiny bit cooler than before.

The helium gas that escaped through the porous plug was cycled past the shields in the outer layers of the Dewar, cooling them (thus the name, “vapor-cooled shields”), and then it was used as a propellant for eight pairs of micro thrusters that are strategically located around the spacecraft.



Based on data from the on-board telescope and the gyroscope that was used as a proof mass for maintaining a drag-free orbit, the flow of the escaping helium gas was carefully metered through these thrusters in order to precisely control the spacecraft's position. In fact, the position of the entire spacecraft was balanced around the proof mass gyroscope by increasing or decreasing the flow of helium through opposing thrusters, creating a drag-free orbit. Thus, the Dewar and liquid helium served two critically important functions in the mission:

1. Maintaining a supercold temperature around the science instrument.
2. Providing a constant stream of gas propellant for precisely controlling the position and attitude of the entire satellite.

### 3.2.1.4 The Realization of Drag-Free Technology

Gravity Probe B is the first spacecraft ever launched requiring six degrees of freedom in active attitude control—three degrees of freedom in pointing control to maintain its guide star pointing orientation and constant roll rate (pitch, yaw, and roll) and three degrees of freedom in translational control (up-down, front-to-back, and side-to-side), to maintain a drag-free orbit throughout the 17-month flight mission.

The term “drag-free” refers to a body that is moving without any friction or drag, and thus its motion is affected only by gravity. Here on Earth, and even 642 km (400 miles) above the Earth where the GP-B satellite is in orbit, there is always some drag caused by the Earth's atmosphere, solar pressure, and other forces. However, a body can achieve drag-free motion if it is shielded by another body. A drag-free satellite, therefore, refers to a feedback system consisting of a satellite within a satellite. The inner satellite, often called a proof-mass, is typically a small homogeneous object, such as a spherical GP-B gyroscope. The position of the outer shielding satellite must be tightly controlled to prevent it from ever touching the proof mass. This is accomplished by equipping the outer satellite with sensors that precisely measure its position relative to the proof mass and a set of thrusters that automatically control its position, based on feedback from the sensors. Through this feedback system, the satellite continually “chases” the proof-mass, always adjusting its position so that the satellite remains centered about the proof mass, which is orbiting the Earth in a constant state of free fall. The drag-free feature of the GP-B spacecraft is critically important to the experiment because orbital drag on the spacecraft would cause an acceleration that might obscure the minuscule relativistic gyro precessions being measured.

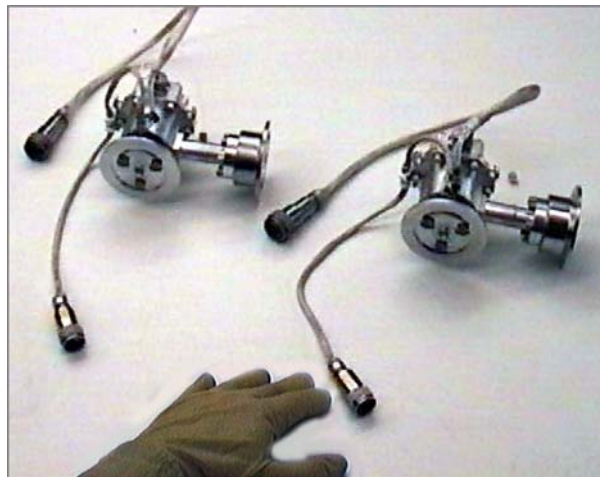


**Figure 3-6.** Proportional micro thrusters used for GP-B spacecraft attitude control

GP-B needs extremely sensitive thrusters to re-orient the satellite and keep it on its proper path. Here's where the escaping helium gas that slowly boils off from the liquid helium comes in handy. Minute amounts of gas, 1/10th of a human breath or a few millinewtons of force, provide just the right amount of thrust necessary to adjust the satellite's position.

The first, and only other 3-axis drag-free controller ever flown was called DISCOS (DISturbance COmpensation System). It was developed in the late 1960s as an offshoot of GP-B under the leadership of Professor Dan DeBra, then head of the Guidance & Control Laboratory in the Stanford Aero-Astro Department, and a Co-Principal Investigator on GP-B. DISCOS was the central drag-free control module in the three-module TRIAD I satellite, a test vehicle developed to improve the accuracy of the U. S. Navy's Transit satellite navigation system. Transit satellites enable ships to locate their positions on the Earth's surface by reference to orbit data stored on board the satellite, but earlier ones had been limited by uncertainties in orbit prediction arising from atmospheric drag. The DISCOS module was specifically designed to address this problem. The other two modules in the TRIAD I satellite were developed by the Applied Physics Laboratory (APL) at Johns Hopkins University, under the leadership of Robert Fischell. The TRIAD I satellite, with its central DISCOS module, was launched on September 2, 1972 and flew in a polar orbit at 750 km for a little more than a year and achieved drag-free performance of  $5 \times 10^{-12}$  g for the entire mission. Subsequently, the Navy built two more satellites in the TRIAD series, followed by three satellites in the NOVA series. All of these subsequent satellites contained only single-axis drag-free control, the development of which also included significant contributions by Stanford faculty and graduate students.

### 3.2.1.5 Telescope & Guide Star

In the GP-B science instrument, enclosed within the Probe, along the central axis of the dewar, a 36 centimeter (14 inch) long Cassegrain reflecting astronomical telescope, with a focal length of 3.8 meters (12.5 feet), is bonded, using a hydroxide catalyzed bonding process, to the end of the quartz block that houses the gyroscopes.

Together, the telescope and the quartz block form the Science Instrument Assembly (SIA). Hydroxide catalyzed bonding is a method of fusing together quartz parts, without the use of any glue or fasteners, that was developed and patented by the GP-B team at Stanford. This was necessary for the SIA not to distort or break when cooled to the cryogenic temperatures required for superconductivity used by the gyroscopes. The telescope's line of sight provided a reference for measuring any drift in the gyroscopes' spin axis over the life of the experiment.

During the science phase of the mission, the telescope had to remain focused on a distant stable reference point—a guide star. Furthermore, it had to remain fixed on the center of this guide star within a range of  $\pm 20$  milliarcseconds throughout the science phase of the mission. The resulting telescope signal was continuously subtracted from the gyroscope signal at the 0.1 milliarcsecond level to determine the amount of spin axis precession of each gyroscope.



**Figure 3-7.** A pre-flight prototype of the Cassegrain telescope on-board the GP-B spacecraft



Ideally, the telescope should have been aligned with a distant quasar (massive bodies, located in the most distant reaches of the universe, which put out powerful radio emissions), because they appear to be fixed in their position and would thus provide an ideal, stable reference point for measuring gyroscope drift.

However, quasars are too dim for any optical telescope this size to track. So, instead, the telescope was focused on a brighter, nearby “guide star.” But, like the Sun, nearby stars move relative to the other stars in our galaxy, and their light diffracts or scatters as it travels through the universe. This situation posed two difficult challenges to the experiment:

1. Choosing a guide star whose motion could be mapped relative to quasars separately, so that the Gravity Probe B gyroscope measurements can ultimately be related to the distant universe.
2. Creating a means for the telescope to find and remain focused on the exact center of a star whose light is widely diffracted.

### 3.2.1.5.1 Choosing a Guide Star and mapping its proper motion

In order to precisely map the motion of a star relative to a quasar, it was necessary to find a star that met all of the following criteria:

- Correct position in the heavens for tracking by the on-board telescope (for example, the sun never gets in the way)
- Shines brightly enough for the on-board telescope to track
- Is a sufficiently strong radio source that can be tracked by radio telescopes on Earth
- Is visually located within a fraction of a degree from the reference quasar

It so happens that stars that are radio sources belong to binary star systems. Because almost half the star systems in the universe are binary, it initially seemed that there would be many good candidates for the guide star. However, out of 1,400 stars that were examined, only three matched all four of the necessary criteria. The star that was chosen as the GP-B guide star is named IM Pegasi (HR 8703).



**Figure 3-8.** Tracking the guide star, IM Pegasi, with the GP-B telescope

Like all stars in our galaxy, the position of IM Pegasi as viewed from Earth and our science telescope changes over the course of a year. In fact, IM Pegasi moves around its binary partner in a spiraling pattern, rather than a linear path. The total motion of IM Pegasi in one year alone is 100 times larger than the smallest gyroscope spin

axis precession measurable with Gravity Probe B. Thus, throughout the science phase of the mission, the GP-B science telescope was tracking a moving star, but gyros were unaffected by the star's so called "proper motion;" their pointing reference was IM Pegasi's position at the beginning of the experiment. Consequently, in the gyro precession data for each orbit, it is necessary to subtract out the telescope's angle of displacement from its original guide star orientation so that the angular displacements of the gyros can be related to the telescope's initial position, rather than its current position each orbit. For this reason, a very accurate map of the proper motion of IM Pegasi is required in order to complete the GP-B data analysis.

Because IM Pegasi is a radio source, its proper motion can be tracked by a sophisticated system of radio telescopes, operating in conjunction with each other. This system is called Very Long Base Interferometry or VLBI. Using radio telescopes from New Mexico to Australia to Germany, acting as a single radio telescope the size of the Earth, a team at the Harvard-Smithsonian Center for Astrophysics (CfA) led by astrophysicist Irwin Shapiro, in collaboration with astrophysicist Norbert Bartel and others from York University in Canada and French astronomer Jean-Francois Lestrade have now mapped the motion of IM Pegasi with respect to a reference quasar over a number of years to an unprecedented level of accuracy. With these measurements the motions of the GP-B gyroscope spin axes can now be related to the reference quasar in the distant universe. However, to ensure the integrity of the GP-B experiment, we added a "blind" component to the GP-B data analysis by requesting that the CfA withhold the proper motion data that will enable us to pinpoint the orbit-by-orbit position of IM Pegasi until the rest of our GP-B data analysis is complete. Therefore, the actual precession angles of the GP-B gyros with respect to the distant universe, will not be known until the end of the data analysis process.

#### **3.2.1.5.2 Dividing the Guide Star Image**

Diffraction is a light-scattering phenomenon that spreads the image of a distant star when viewed through a telescope. Any finite sized telescope, even one with perfectly polished mirrors, focuses the light from a distant star to a non-zero spot size, known as the diffraction limit of the telescope. For the precision pointing measurements being made by GP-B, it was necessary to locate the optical center of the guide star image in the telescope to an accuracy of 0.1 milliarcsecond (0.001arcsecond or  $3 \times 10^{-8}$  degrees). The diffraction limit size of the GP-B telescope is  $\sim 1.4$  arcseconds, which is about 14,000 times larger than the required pointing accuracy, and this presented a formidable challenge to the GP-B team. The solution was to precisely split the image into equal x-axis and y-axis components, and then to divide each of the axis components into two half images whose brightness values can be compared.

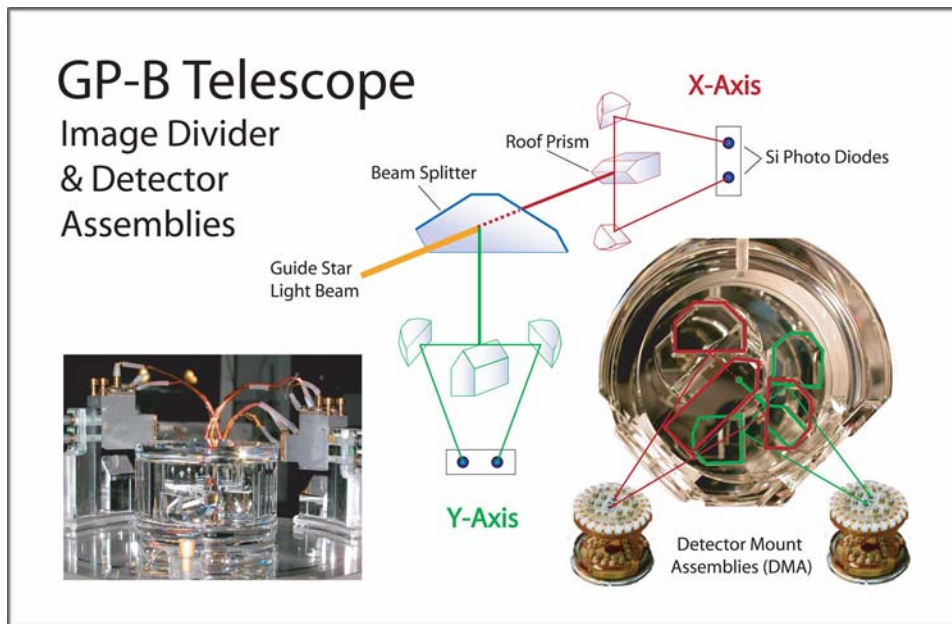


**Figure 3-9.** Schematic diagram of starlight image division in the GP-B telescope

As shown in [Figure 3-9](#), GP-B accomplishes this task by focusing the mirror-reflected starlight in the Image Divider Assembly (IDA) at the telescope's front end, and passing it through a beam-splitter (a half-silvered mirror). The beam-splitter forms two separate images, each of which falls on a roof-prism (a prism shaped like a peaked rooftop). The prism slices the star's image into two half-disks, which are focused onto two silicon photo diodes at opposite ends of the Detector Mount Assemblies (DMA), shown in [Figure 3-9](#).

On the DMA sensors, the light signals of each half-disk are converted to electrical signals and then compared. If the signals are not precisely equal, this means that the roof-prism is not splitting the image precisely in half. The position of the entire spacecraft is then adjusted until the signals are equal and the image is split right down the middle. When this is accomplished in both sensors for each (x and y) axis, then the telescope is locked on the exact center of the guide star. The flight telescope on-board the GP-B spacecraft was capable of pointing to the center of the guide star with an accuracy of 0.5 milliarcseconds ( $1.4 \times 10^{-7}$  degrees) per orbit.

## 3.2.2 Redundancy in GP-B Systems and Technology

Underlying the entire GP-B experiment is a philosophy of redundancy that has been built into the GP-B spacecraft and all of its subsystems. Following is a description of this redundancy.

### 3.2.2.1 Gyroscope Redundancy

At the highest level of the GP-B experiment, redundancy begins with the four gyroscopes. We actually need only one gyroscope to perform the GP-B experiment, but since it is unlikely that this experiment will ever be repeated, it seemed prudent to build redundancy into the experiment itself. Having four gyros obviously provides backup in case one, two, or even three gyros should fail during the mission. More important, however, having multiple gyroscopes provides built-in crosschecks on the relativity data. In other words, a high degree of correlation in data collected from four independent gyros provides greater confidence in the results than data collected from a single gyro, or even two gyros—especially if the results should differ from the predictions of general relativity.

### **3.2.2.2 Gyro Suspension System Redundancy**

An independent Gyro Suspension System (GSS) computer controls each of the gyros. Each GSS computer is connected to a single gyro, so they cannot be used interchangeably. Each of the GSS computers has two gyro suspension modes—analog and digital—that provide a form of redundancy in the gyro rotor suspension. The analog suspension mode is used primarily as a backup or safe mode for suspending the gyros. The digital suspension mode is computer-controlled; it puts less torque on the gyros than analog mode and enables their position to be controlled with extremely high precision. A failsafe mechanism, called the arbiter, is hard-coded into the GSS firmware (programming at the chip level) that automatically switches the suspension system from digital to analog mode under certain pre-set conditions.

### **3.2.2.3 Computer Redundancy**

The GSS computers comprise four of the eight computers on-board the spacecraft. In addition there are two flight computers and two SQUID Readout (SRE) computers. The main flight computer and its twin backup are called the A-Side (main) and B-Side (backup) CCCA (Command & Control Computer Assembly). Only one of these computers is running at any given time. If the A-side computer fails certain safemode tests, the B-side computer automatically takes over, as was the case in March 2005. However, when the backup computer failed these safemode tests, it was rebooted. We can only switch back to the main computer through manual commands.

### **3.2.2.4 SQUID Readout Redundancy**

Each of the twin SRE computers can control all four SQUID readouts, showing the spin axis orientations of all four gyros. Like the main computers, only one of the SRE computers is running at any given time. When the main CCCA computer automatically switched over to the B-side in March 2005, the SRE computer did not switch with it. However, in order to synchronize the timing between the B-side CCCA computer and the A-side SRE computer, we commanded the SRE computer to reboot. Also, to ensure that we remained on the A-side SRE computer, we disabled the safemode response that automatically switches from the A-side SRE computer to the B-side SRE computer.

### **3.2.2.5 Telescope Readout Redundancy**

Redundancy is also built into the Telescope Readout Electronics (TRE). The science telescope has two sets of detectors, designated A-side (primary) and B-side (backup). These detector packages, which are about the diameter of a dime, are comprised of pairs of silicon photo diodes that basically count photons from each half of the telescope's split beam, in both the X-axis (side-to-side) direction and the Y-axis (top-to-bottom) direction. Beam splitters and mirrors are used to redundantly direct all of these split light beams to the B-side detectors as well as the A-side detectors. For comparison sake, we collected the data from both the primary and backup detectors during telemetry communications passes, although we only used the data from one set of detectors to control the spacecraft's pointing direction through the ATC system.

### **3.2.2.6 Attitude Control System Redundancy**

The ATC uses the navigation control gyros (called “rate” gyros), star trackers, and magnetometers to control the spacecraft's attitude when the telescope detectors are not controlling the spacecraft's attitude (e.g., the portion of each orbit when the spacecraft moves behind the Earth, eclipsed from view of the guide star). The spacecraft contains two pairs of rate gyros, two star trackers, again designated A-side (primary) and B-side (backup), and two navigational magnetometers. The two rate gyros in each pair work together, independently controlling the X-axis and Y-axis position of the spacecraft; the redundant Z-axis position control from one of the gyros is not

used. The star trackers are essentially pattern-matching cameras, located on opposite sides of the spacecraft frame. The payload magnetometers are like three-dimensional compasses that determine the spacecraft's orientation with respect to the Earth's magnetic field.

During the 17-month GP-B flight mission, all of the above systems, in addition to data from the Gyro Suspension Systems were used to “steer” the spacecraft in its orbit. Moment to moment changes in the spacecraft's position were controlled by a combination of 16 micro thrusters (see below) and a set of magnetic torque rods—long electromagnets that push or pull against the Earth's magnetic field to change the spacecraft's orientation. After the helium was depleted from the dewar at the end of September 2005, these torque rods, controlled by feedback from the star trackers and magnetometers, are the only means of re-orienting the spacecraft in the post-mission phase.

### **3.2.2.7 Star Tracker Redundancy**

Both star trackers were turned on and have been running since the beginning of the mission, but only one pair of rate gyros was in use. During the science phase of the mission, we activated the other set of rate gyros, as well. Data from one set was sent to the ATC to control the spacecraft's position; data from the other set was collected during telemetry communications sessions and used for precise roll attitude calibrations to the science data. The B-side switch-over of the CCCA computer in March 2005 also triggered a switch to the B-side rate gyros and star tracker. We subsequently commanded the spacecraft to switch back to the A-side rate gyros and the A-side star tracker, both of which had been fine-tuned during the Initialization and Orbit Checkout (IOC) phase of the mission and were performing slightly better than their backup counterparts.

### **3.2.2.8 Micro Thruster Redundancy**

The final redundant spacecraft system is the micro-thruster system. The spacecraft is outfitted with 8 pair of opposing micro-thrusters, arranged in four clusters—two at the top of the spacecraft frame and two at the bottom. One thruster in each cluster is redundant, and a set of valves in the thruster system enables individual thrusters to be isolated and effectively disabled. This is precisely what we did early in the mission with two micro-thrusters, whose nozzles became stuck open, apparently due to particle contamination shortly after launch. The remaining 14 thrusters performed flawlessly throughout the science and post-science instrument calibration phases of the mission.

## **3.2.3 GP-B's Unique Technological Challenges and Solutions**

When the GP-B experiment was conceived late in 1959-1960, much of the technology had not yet been invented to accomplish this exacting test. Here are the some of GP-B's unique technology inventions and clever solutions to difficult challenges.

### 3.2.3.1 Porous Plug: A Stanford University/GP-B Invention

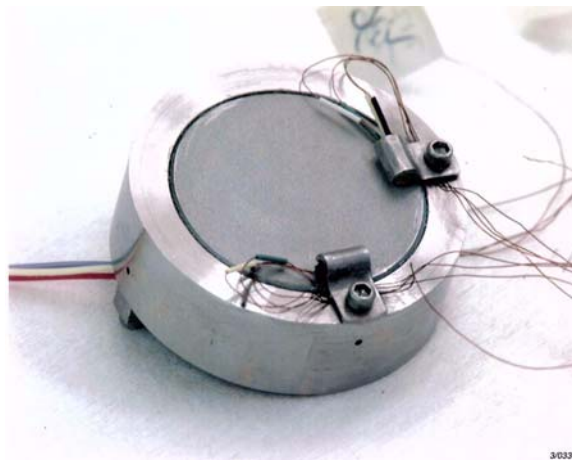


**Figure 3-10.** The porous plug

**Challenge:** On Earth, Dewars (Thermos bottles) function because of gravity. The liquid and gas naturally separate. In the zero gravity of space, a different method of separation is needed.

**Solution:** Release the evaporating helium while retaining the superfluid liquid helium.

Superfluidity is a characteristic of liquid helium that appears only when it is 2.18 kelvin or colder (during the mission, the temperature of the liquid helium in the dewar was held at 1.8K). When liquid helium is superfluid, it has no viscosity. This allows it to move about on a surface or through a porous substance without friction. A remarkable effect of this state is that if superfluid helium is left in an open beaker in a supercooled environment, the liquid will crawl up the inside of the beaker and down the outside until the beaker was empty!

The role of the porous plug was to control this flow of superfluid helium just enough to let some of it evaporate without letting the liquid leak out. A simple vent would not work because in a zero-g environment, the superfluid helium would simply migrate out of any opening in the Dewar, no matter how small we made it or how quickly we opened and closed it. Instead, we needed to make a porous plug.

The plug itself is made of stainless steel, but it has gone through a sintering process that makes it slightly porous (like a sponge). Sintering is a process of powdering a material into tiny granules and then heating the granules until they coalesce into a porous mass, without heating them so high that they melt together. The pores in the resulting mass are extremely small (in fact, invisible to the naked eye), but they are large enough for the superfluid helium to find its way through the plug.

Before the oozing superfluid helium leaks completely through the plug, it reaches a point where it begins to evaporate (called the liquid-vapor interface). When it evaporates, the helium vapor takes heat energy out of the liquid helium. Now the liquid helium near the outside of the plug is colder and it sinks back into the Dewar. At least, this is how it was supposed to work.

Choosing the right size for the porous plug was tricky. If the plug had been made too small, the liquid-vapor interface would have remained below it, choking the plug and preventing the release of helium vapor. If the plug had been made too large, the interface would have been above it, and the liquid helium would have oozed out of the plug before it had evaporated and would be lost. The proper size turned out to be a 6.9 cm disk, 0.635 cm thick with a permeability of  $3.8 \times 10^{-10}$  cm squared. The material for the plug is a low-carbon version of stainless steel provided by the Mott Corporation in Connecticut (which also produced our sintered titanium filters to purify the helium gas and the sintered titanium blades for the cryopump).

**Result:** By using the porous plug, we were able to maintain a steady pressure and temperature inside the Dewar. The liquid helium stayed within a few millikelvin of 1.8K throughout the mission. In turn, this allowed the science instrument to operate properly at superconducting temperatures and enabled us to collect 11.5 months of relativity data to test Einstein.

**Historical Note:** The porous plug was developed at Stanford specifically for the GP-B experiment, but it flew on both the NASA IRAS (Infrared Astronomical Satellite) and COBE (Cosmic Background Explorer) spacecraft prior to the launch of GP-B.

### 3.2.3.2 Nested Expanding Lead Bags

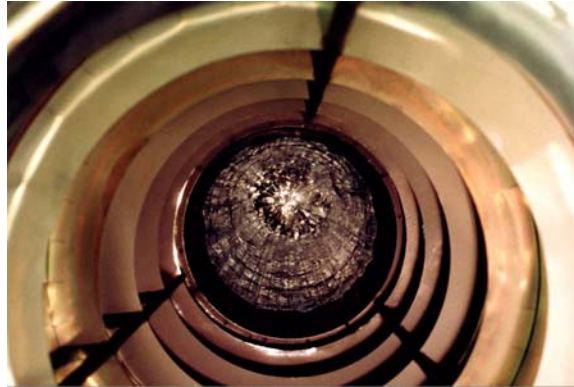


**Figure 3-11.** Lead bag magnetic shield in GP-B flight probe

**Challenge:** Earth’s magnetic field interferes with the hyper-sensitive magnetometer (SQUID), which reads each gyroscope’s orientation to within 0.5 milliarcseconds ( $1.4 \times 10^{-7}$  degrees).

**Solution:** Block out the ambient magnetic field by surrounding the science instrument with a “lead bag.” Four lead bags are actually used. The first one is inserted and expanded, partially reducing the magnetic field (by the ratio of final to initial volume.) Another bag is then inserted inside the first one and expanded, further reducing the magnetic field inside the second bag. The outer bag is then cut away. This process is repeated two more times, all but eliminating the magnetic field within the innermost bag. At this point the Probe, containing the gyroscopes and SQUIDS is inserted inside the final remaining lead bag.

**Result:** The series of four nested and expanded lead bags reduces the magnetic level to less than  $10^{-6}$  gauss. Then, magnetic shields surrounding each individual gyroscope and other local magnetic shields attenuate the magnetic variation down to  $10^{-14}$  gauss.



### 3.2.3.3 Proportional Micro Thrusters

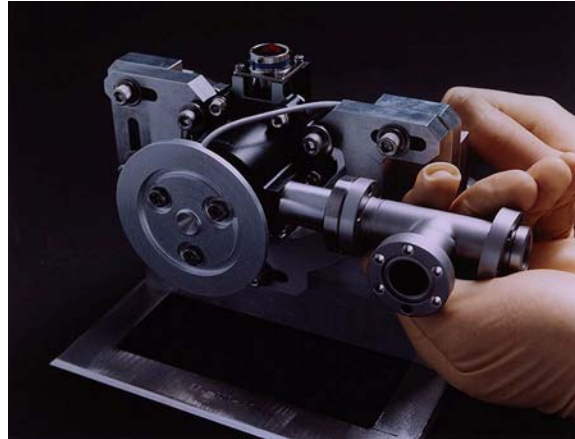


**Figure 3-12.** GP\_B proportional micro thruster assembly

**Challenge:** GP-B satellite's path is altered, ever so slightly, by solar radiation and atmospheric “wavytops”.

**Solution:** Re-orient the satellite with an extremely sensitive gas thruster system. Helium gas constantly flows out of eight pairs of opposing thrusters in balanced amounts. To alter the satellite's attitude, the gas flow in one or more pairs of opposing thrusters is unbalanced by 1/100<sup>th</sup> of a “puff” exhalation that one might use to clean eyeglasses, providing just a few millinewtons of force.

**Result:** These proportional micro thrusters precisely maintain the GP-B space vehicle's position to within 10 milliarcseconds ( $3 \times 10^{-6}$  degrees) of a perfect Earth orbit, and pointing to within 1 milliarcsecond ( $3 \times 10^{-7}$  degrees) of the exact center of the guide star.

**Bonus Fact:** This is the ultimate in recycling...the helium gas that continually evaporates through the porous plug from the superfluid liquid helium inside the Dewar, is harnessed as the propellant used by the proportional micro thrusters.

### 3.2.3.4 Polishing the Perfect Sphere

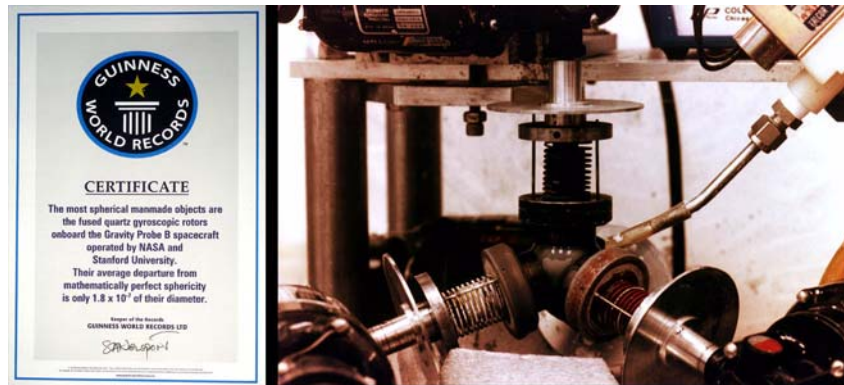


**Figure 3-13.** Polishing a gyro rotor

**Challenge:** Polishing a fused quartz sphere with standard methods creates “hills and valleys,” destroying sphericity.

**Solution:** Create a tetrahedral lapping and polishing machine that brushes the sphere with micro-inch abrasive slurry in random variations.

**Result:** Each fused quartz sphere deviates less than one micro-inch from peak to valley (25 nm), making them the roundest objects ever created on Earth.

**Bonus Fact:** In September 2004, GP-B received a certificate from Guinness World Records Limited, acknowledging that the GP-B gyroscope rotors had been entered into the Guinness Database of World Records. The certificate reads as follows: “*The most spherical man-made objects are the fused quartz gyroscopic rotors onboard the Gravity Probe B Spacecraft operated by NASA and Stanford University. Their average departure from mathematically perfect sphericity is only  $1.8 \times 10^{-7}$  of their diameter.*”

### 3.2.3.5 Precisely Measuring Sphericity (Roundness)

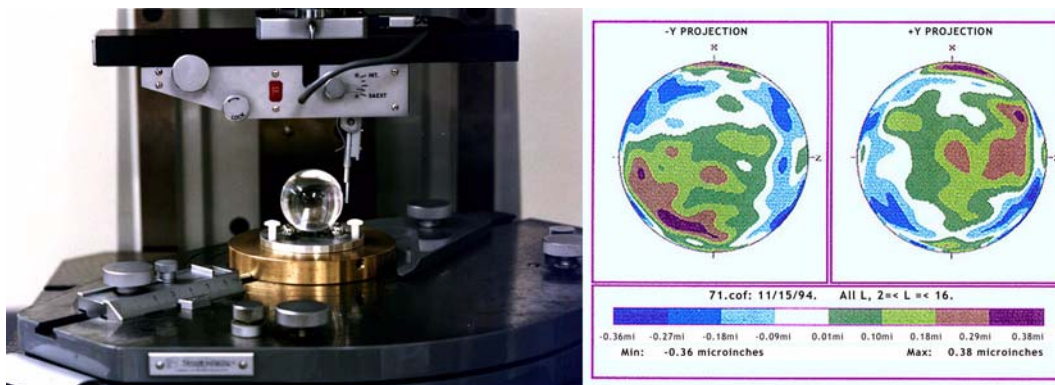


**Figure 3-14.** Measuring the roundness of a gyro rotor and mapping the contours on its surface

**Challenge:** How to measure the roundness of a sphere at the precision level of 1/10th of one millionth of an inch? The British instrument company, Rank, Taylor, and Hobson, created the Talyrond instrument for measuring the sphericity or roundness of GP-B gyroscope rotors using a stylus mounted on a round spindle to encircle a gyroscope rotor. However, they could not produce a spindle that was itself perfectly round, and thus the spindle introduced error into the measurement.

**Solution:** Combine the errors in the spindle’s roundness with the errors in the sphere being measured. Then, rotate the sphere to a new position and repeat the measurement. The measurement errors in the roundness of the spindle remain constant, while the measurement errors in the sphere change with each new position. After repeating this process several times, it is possible to separate out the constant spindle error. (The spindle roundness must be checked from time to time, to ensure that it has not changed.)

**Result:** The spindle roundness errors were calculated and stored in a computer, so they could be reused with different spheres. For each rotor, 16 great-circle measurements were made in the perpendicular plane and one final measurement was made around its equator, tying all the vertical measurements together. The spindle errors were subtracted out of the sphericity measurements, and then the sphericity measurements were translated into contour maps.

### 3.2.3.6 Gyroscope Suspension System



**Figure 3-15.** A gyro rotor and both halves of its quartz housing

**Challenge:** Suspend each spinning gyroscope in the exact center of its housing, a mere 32 microns or 1/1000<sup>th</sup> inch from the side of the housing.

**Constraint 1:** The suspension mechanism must be able to react instantly to misalignments, without overreacting and sending the gyroscope crashing into the side.

**Constraint 2:** The gyroscopes must maintain a spin rate greater than 3,500 rpm.

**Solution:** Six electrodes placed evenly around the gyroscope create a charge that electrically suspends the gyroscope. The charge attracts the gyroscope's niobium surface. Using a few millivolts, the gyroscopes are constantly balanced in the center of the housing with every electrode reacting dynamically to any adjustments by the other electrodes.

**Bonus Fact:** While in space it takes less than 100 millivolts to suspend the gyroscopes, whereas on Earth it takes nearly 1,000 volts to raise and balance the gyroscopes against the force of gravity.

### 3.2.3.7 Gas Management Assembly

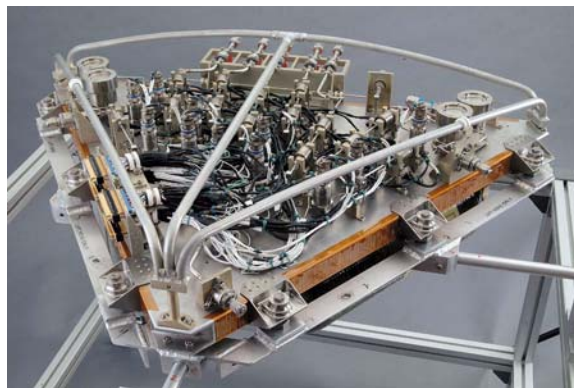


**Figure 3-16.** Top view of the Gas Management Assembly (GMA)

**Challenge:** Spin up an ultra-smooth gyroscope as fast as possible without crashing it into the sides of the housing with an electrical spark.

**Constraint 1:** Gas flowing into housing chamber can exit only as fast as the exhaust tube will allow.

**Constraint 2:** The exhaust tube must be very small (< 1/16th of an inch) to prevent outside heat from reaching the housing chamber and the gyroscope.

**Constraint 3:** If more gas flows into the chamber than flows out, the pressure inside the chamber will rise. As the pressure rises, the helium will ionize and possibly arc. The electrical spark could knock the electrically suspended gyroscope out of position and into the side of the housing.

**Solution:** A gas management system was designed specifically for spinning up the GP-B gyroscopes. It uses more than two dozen valves and numerous levels of redundancy to send ultra-pure helium gas into the chamber at 725 sccm (standard cubic centimeters per minute).

**Result:** The gyroscopes spin up to full speed, greater than 3,500 rpm, in less than three hours.

### 3.2.3.8 The IDA and DPA Inside the Telescope

(Image Divider Assembly & Detector Package Assembly)

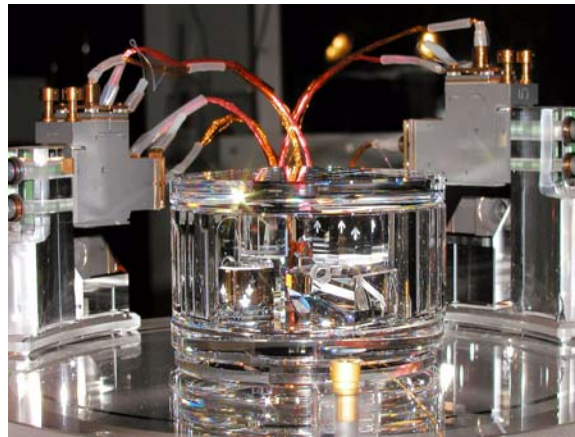


**Figure 3-17.** The telescope Image Divider Assembly (IDA) and Detector Package Assemblies (DPA)

**Challenge:** GP-B's telescope must locate the center of the guide star to within 0.1 milliarcseconds ( $3 \times 10^{-8}$  degrees). No existing telescope is accurate enough to accomplish this task.

**Solution:** Split the incoming light with a roof-prism (inside the IDA) and direct each half toward two sensors (inside the DPA). When each sensor registers an identical amount of electrical flux, the telescope is centered.

**Result:** Each sensor can detect the amount of light hitting it to within a few photons. The telescope can be adjusted to remain focused on the exact center of guide star, thereby precisely maintaining its original orientation.

### 3.2.3.9 Gyro Readout: Marking the Unmarkable

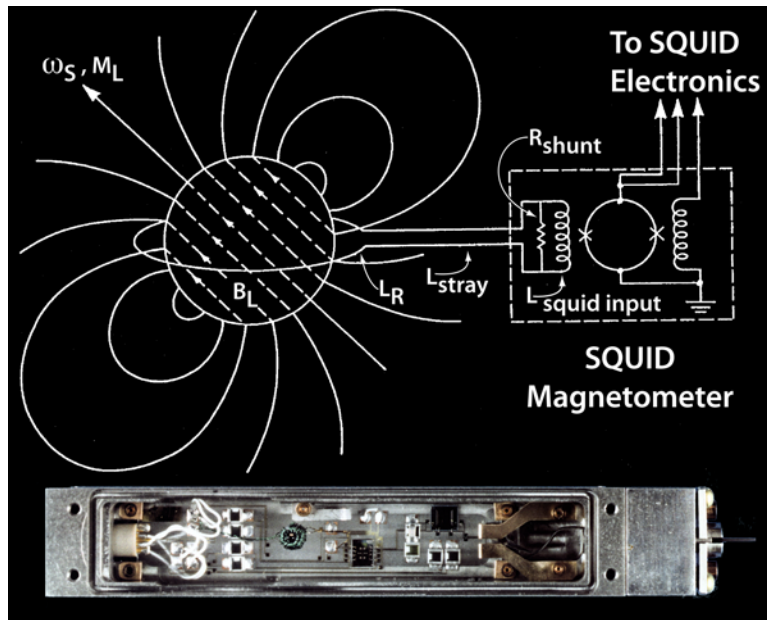


**Figure 3-18.** Schematic diagram and photo of a SQUID gyro readout

**Challenge:** How does one measure the direction of spin of a perfect unmarked sphere to 0.1 milliarcseconds ( $3 \times 10^{-8}$  degrees) without disturbing it?

**Solution:** The answer comes through the phenomena of superconductivity. Superconductivity provides a spin pointer which is neither optical nor mechanical as in conventional gyroscopes but magnetic. It also provides a sensitive non-interfering instrument to read the pointer, the Superconducting Quantum Interference Device (SQUID).

Superconductors have the property that when cooled below a specific temperature they completely lose their electrical resistance, hence their name. They become not just great conductors, but for steady currents, perfect ones. Additionally, when a superconductor—niobium, for example—spins, it generates a magnetic field (known as the London moment after physicist Fritz London) *which is exactly aligned with its spin axis*. Each circling positive charge bound in the metal lattice generates a magnetic field parallel to the rotation axis. The total field produced would be very large if not for the superconducting electrons themselves responding to it. Nearly all are forced to keep up with the lattice, generating a cancelling field of their own except in a shallow surface layer about 100 atoms thick. In this layer they lag slightly behind the charged lattice leaving a small difference field—the London moment—proportional to spin rate and exactly aligned with the spin axis. Here is our pointer.

To measure the spin direction, the rotor is encircled with a thin superconducting loop connected to a SQUID (Superconducting QUantum Interference Device) magnetometer. As the orientation of the spin axis of the gyro changes, the London moment follows, changing minutely the contribution of the London moment to the magnetic field through the loop. So sensitive is the SQUID that a field change of  $5 \times 10^{-14}$  gauss (1/10,000,000,000,000 of the Earth's magnetic field), corresponding to a gyro tilt of 1 milliarcsecond, should be detectable within 10 hours, and a 0.1 milliarcsecond deflection should be detectable in 42 days. Feedback electronics in the SQUID readout system allow for cancellation of reaction currents in the pick-up loop, thus reducing reaction torques on the gyro to an absolutely negligible level.

The London moment readout scheme is well suited to Gravity Probe B. It is sensitive, stable, applicable to a perfect unmarked sphere and does not exert any significant reaction force on the gyroscope.



**Result:** The on-orbit gyroscope spin rates were lower than baselined—70 Hz or 4,200 rpm on average, rather than 130 Hz or 7,800 rpm— which increased the integration time necessary to estimate the gyroscope spin direction to the desired precision. Partially in response to the low gyro spin rates, the final vehicle roll rate was set higher than baselined (12.9 mHz or 0.77 rpm rather than 5.5 mHz or 0.33 rpm) which decreased the integration time necessary. The net result is a decrease in measurement time needed. On-orbit noise floor data shows that the SQUID readout system is capable of measuring the gyro spin axis to a precision of 1 milliarcsecond in 6 hours, and to a precision of 0.1 milliarcseconds in 4 weeks.

### 3.2.3.10 Dual-Sided Solar Arrays



**Figure 3-19.** Checking the GP-B solar arrays on the spacecraft at Lockheed Martin & solar arrays deployed on a scale model of the spacecraft

**Challenge:** How do you provide continuous solar power to a spacecraft that has the unique requirements of always pointing at a single distant star, rather than the sun, while rolling continuously in orbit for 16 months or longer?

**Solution:** Most satellites are designed to face the sun year around, or they have moveable solar panels that can be re-oriented to face the sun, thus maintaining positive power throughout each orbit. This is not the case with GP-B. Due to the nature of the GP-B science mission, GP-B always points at the guide star, IM Pegasi; it never points directly at the Sun, because sunlight could overwhelm the telescope's ultra-sensitive photon detectors. Furthermore, the GP-B spacecraft itself must be as free as possible from any motion disturbances that could affect the gyros and SQUID readouts. Thus, once opened, the solar arrays on the GP-B spacecraft had to be locked into fixed positions. For these reasons, GP-B's solar arrays are unique, both in their design and in their positioning on the spacecraft.

GP-B is equipped with four fixed, double-sided solar array panels, canted at such angles as to always be able to receive some solar power regardless of the season. Additionally, these double-sided panels were designed to minimize the thermal effects of the spacecraft entering and exiting eclipses, when the Earth blocks the Sun's light for up to 36 minutes per orbit. Each GP-B array contains 9,552 individual single-junction Gallium Arsenide (GaAs) solar cells that convert sunlight into electrical power with 18.5% efficiency, the standard for this type of eclipsing satellite. As sunlight is absorbed by the solar cells, its photons, or bundles of energy, are

transferred to the electrons of the superconductive photo voltaic (PV) cells. The electrons in the PV cells become excited enough to escape their atoms and begin flowing, producing the current that powers the GP-B electronics.

Because the GP-B spacecraft always points at the guide star, rather than at the Sun, the angle between the spacecraft's main axis (also the telescope axis) and the Sun—called the gamma angle—varies throughout the year. Thus, the solar arrays do not receive consistent direct sunlight, and this is the reason for the unusual angles at which the solar arrays are canted.

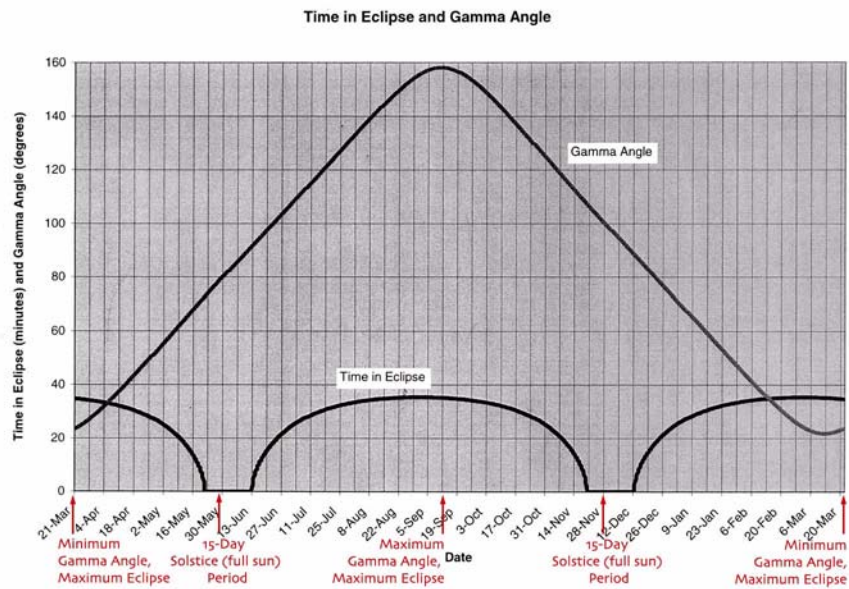


**Figure 3-20.** GP-B’s annual orientation patterns with respect to the sun

Engineers at Lockheed Martin, who designed and built the GP-B solar arrays, had to ensure that the arrays would produce sufficient electricity in the worst-case gamma angle of approximately 22 degrees, which occurred once during the mission, on 12 September 2004. The Lockheed Martin engineers also had to design and mount the solar arrays in such a way that there would be sufficient power during the maximum 36-minute eclipse times, which occur when the gamma angle is at its maximum and minimum values (158 degrees and 22 degrees, respectively). At these angles, GP-B’s orbit plane directly faces the sun—in other words, the Sun appears directly below the guide star, instead of off to one side or the other. This alignment only happened twice during the actual mission—on 12 September 2004 and 20 March 2005—and the greatest power usage and deepest depth of discharge (DOD) by the batteries occurred at these times.

Taking these worst-case alignments into account, the Lockheed Martin designers arranged the orientations of the solar panels on the spacecraft to optimize the amount of incident sunlight. Looking down on the spacecraft from the top of the telescope (that is, looking down the spacecraft’s z-axis), the arrays are arranged 90 degrees apart, forming an “X” pattern. Panels 1 and 3 are canted 90 degrees into the Z-plane of the spacecraft, so that you can only see their edges looking down on the spacecraft. Panel 2 is canted 25 degrees forward in the Z-plane, towards the top of the spacecraft, and Panel 4 is canted in the opposite direction, 25 degrees backwards in the Z-plane, towards the bottom of the spacecraft. Because of this asymmetry, the spacecraft is free to rotate about the Z-axis of the telescope with minimal perturbations due to the dragging or torquing of the solar panels.

GP-B maintains a Low Earth Orbit (LEO) at an altitude of only 640 km (400 miles) about the Earth's poles. At this altitude, it has an orbital period of 97.5 minutes, eclipsing behind the Earth 14-16 times a day--almost 5,000 times a year. While in these eclipses, GP-B relies on its Super NiCAD batteries to provide power for all of the



spacecraft's subsystems for the duration of each eclipse, lasting up to about 36 minutes during the peak eclipse seasons. This constant cycle of charging and discharging puts a large amount of strain on the batteries. Because of this high discharge and recharge rate, NiCAD batteries, which have been the standard in space since the 1960s, were chosen due to their extensive space heritage and robustness in high eclipse-cycle missions. GP-B's batteries have an expected lifetime of five years, and data analysis of battery performance throughout the mission has been consistent with this prediction.

**Result:** The solar arrays and batteries are capable of providing almost three times more power than the entire spacecraft requires, demonstrating the robustness of the system. The EPS has performed flawlessly since launch and has exceeded all expectations—not only by supporting all mission operations, but also doing so with more than ample margin.

**Bonus Fact:** In 1921, Einstein was awarded the Nobel Prize for his 1905 paper explaining the photoelectric effect, which is the principle on which the GP-B solar arrays function. Last year, 2005, was the 100th anniversary of Einstein's "Miracle Year"—the year in which he wrote not only his photoelectric paper, but also the special theory of relativity, and two other seminal papers.

### 3.2.3.11 Heat-Absorbing, Hermetically Sealed Outer Probe Window

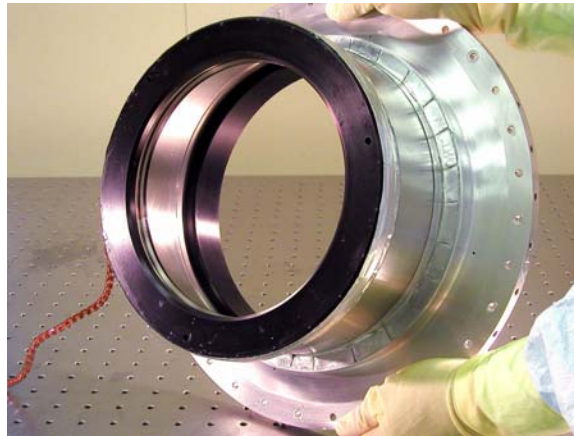


**Figure 3-21.** Window #4—the outer vacuum seal of the Probe

**Challenge:** Design a window at the outer end of the Probe that would meet all of the constraints listed below.

**Constraint 1:** This window forms the vacuum seal at the end of the Probe, and thus it had to be made of a material that was strong enough to withstand the pressure differential between the ultra high vacuum inside the Probe and normal atmospheric temperature and pressure outside the Probe without lensing or bulging.

**Constraint 2:** This window had to be a very good thermal conductor that would conduct heat uniformly in all directions from its center outward, with very little temperature rise in the center.

**Constraint 3:** The window had to be optically transparent, allowing the light from the guide star to enter the Probe and telescope undistorted, while at the same time, blocking electromagnetic radiation.

**Constraint 4:** This window had to satisfy all of the above constraints both in orbit and in extensive testing here on Earth, where the temperature and pressure differential inside and outside the Probe is much greater than in space.

**Solution:** That kind of window material meets all of these requirements? The answer is sapphire. Sapphire is extremely strong, it has very high thermal conductivity, it is an electrical insulator, and it is optically transparent. Sapphire has a crystalline structure, that could cause a phenomenon called birefringence or double refractions of a single light beam. However, due to the sapphire's strength, Window #4 could be made relatively thin, and birefringence was not a problem. In addition to an anti-reflective coating, which was also applied to the three fused quartz windows, Window #4 was treated with an electromagnetic interference (EMI) coating to attenuate the ambient low-frequency and microwave electromagnetic radiation leaking into the Probe through the wide open optical aperture, both in space and on the ground. Because EMI coatings use metal, which is opaque, they reduce the optical transmission of the window. Thus, there was a trade-off between the effectiveness of the EMI shield and optical transmission requirement. Finally, Window #4 also included a thermal emissivity or “low  $\epsilon$ ” coating that reduced the amount of heat it transmits into the Probe.

Perhaps the greatest challenge with Window #4 was its hermetic vacuum seal, which took many design iterations to arrive at a working solution. At the time Window #4 was constructed, rubber O-rings were typically used to create vacuum seals, but they would not have been able to withstand temperatures down to 200 K, which was a requirement for GP-B. Another option was to braze (very high temperature soldering) a metallic seal onto the outer edge of the sapphire window. However, brazing was deemed too risky, given thermal expansion issues and the very high cost of sapphire. Ultimately, the Stanford-Lockheed Martin engineering collaboration came up with a unique seal that had never before been tried: Window #4 was surrounded by an Indium-coated “C” seal, lined with a thin layer of gold against the sapphire, and held in place by a ring of springy nickel-chromium-iron alloy called Incline that is more typically used in formula race car exhaust systems.

**Result:** Window #4, along with its unique hermetic vacuum seal, was an engineering tour de force—a synergy of design constraints, ingenuity, and engineering prowess. This window and its hermetic vacuum seal have functioned flawlessly throughout months of pre-launch testing, and two years in orbit.

### 3.2.3.12 Precision Pointing Technology



**Figure 3-22.** GP-B—The first spacecraft with 6 degrees of freedom in position and attitude control

**Challenge:** Develop a spacecraft attitude and position control system that could meet the precision pointing and drag-free flight requirements of the GP-B experiment, including all of the following constraints:

**Constraint 1:** Provide precision attitude control for a minimum of 16 months on-orbit

**Constraint 2:** Maintain a continuous spacecraft roll at a selected rate, in a range of 0.1- 1.0 rpm.

**Constraint 3:** Keep the spacecraft pointed at a selected guide star (IM Pegasi) to within 50 milliarcseconds whenever the spacecraft has an unobstructed view of the guide star (Guide Star Valid periods). When the spacecraft moves behind the Earth so that the guide star is eclipsed from its view (Guide Star Invalid periods), maintain its pointing orientation so that when the guide star comes back into view, the spacecraft’s pointing can lock back onto the precise guide star pointing orientation within 1-2 minutes or less. This constraint requires very precise attitude control (pitch, yaw, and roll).

**Constraint 4:** Fly the entire spacecraft drag-free around one of the science gyroscopes, which have a clearance of only 32 micrometers (~0.001 inches) between the gyro rotor and its housing. In other words, the spacecraft must continuously “chase” this gyro in orbit without ever allowing the rotor to touch its housing wall. This requires that the attitude control system also have 3 degrees of translational control—thus the name *Attitude and Translation Control System* or “ATC.”

**Solution:** Many of the unique technologies described earlier in this section were combined to meet this challenge. The actual precision attitude control was provided by the 8 pairs of proportional micro-thrusters, described in section 3.2.3.3. These thrusters were arranged so that they could control the spacecraft in all three translational degrees of freedom, as well as three additional degrees of freedom attitude control.

The helium gas that constantly boiled off from the liquid helium in the dewar yielded a clever solution to providing the propellant for powering these micro-thrusters, and the porous plug, described in section 3.2.3.1 provided a means of controlling this helium gas as it escaped from the dewar. The design of the dewar, itself, was also part of the solution. It had to be large enough to hold the 650 gallons of liquid helium that would maintain the cryogenic environment for the gyros to spin for at least 16 months; yet the dewar had to be physically small enough to fit in the fairing of a Boeing Delta II rocket.

The science telescope, with its Image Divider Assembly, described in section 3.2.3.8, was also an important part of the solution, since it provided the precise pointing reference for the spacecraft throughout the mission. Likewise, the Gyro Suspension System (GSS) provided feedback on the rotor position of the “proof mass” gyro, around which the spacecraft was flown drag-free.

Finally, a number of more traditional spacecraft orientation and control devices, including the star trackers, navigational rate gyros, magnetometers, magnetic torque rods, and GPS receiver were all components of spacecraft’s attitude control system. (See section 2.1.7.2 for a description of these components.) Notably absent from the ATC system were reaction wheels and momentum wheels. The concern to the experiment was that these wheels could have a mass imbalance, which could interfere with the zero-g gyroscope performance.

**Result:** The attitude and translation control system (ATC) designed by Lockheed Martin for the GP-B spacecraft was truly an engineering “tour-de-force.” It took a considerable amount of time during IOC, and part of the science phase of the mission for the GP-B and Lockheed Martin Mission Operations Team to master all the subtleties of this complex system. But once it was properly tuned up, the GP-B ATC system was able to meet the mission requirements, and it enabled the GP-B program to collect over a terabyte of data during the science phase of the mission.

### 3.3 GP-B Technology Transfer

This section has outlined GP-B technologies demonstrated for the first time in space applications or technologies with novel and significant improvements over previous implementations. We summarize in the following chart these flight-proven technologies that are available for future missions.

Technology Category	Specific Implementation	Realization
<b>Precision quartz fabrication and metrology</b>	Roundness fab & metrology	20nm peak to valley
	Density homogeneity	parts in $10^7$
	Surface orientation	1 arc sec
	Flatness	better than $\lambda/20$
<b>Quartz stable reference</b>	Mechanical stability	Strain less than 1 part in $10^{10}$
	Robust precision bonding	OptoBond™ hydroxide catalyzed bonding
<b>Large Scale Cryogenic Systems</b>	Superfluid flight dewar	2441 liters, 17.3month hold time
	Guard Tank	90 day post-conditioning superfluid maintenance
	Porous plug phase separation	Flawless on-orbit operation. Also flown on IRAS and COBE after original GP-B development
<b>Cryogenic Electronics</b>	Superconducting thin film circuit technologies: patterning, contacting, multilayer transformers	No on-orbit failures
	DC SQUIDs	Noise PSD $2 \times 10^{-5} \Phi_0 / \sqrt{\text{Hz}}$ at 13 mHz
	Cryo JFET photo detectors	0.8 fA/ $\sqrt{\text{Hz}}$ noise current
<b>Magnetics Control</b>	AC shielding (superconducting)	1 part in $10^{12}$
	DC field reduction (Expanded superconducting shields)	$< 10^{-11}$ Tesla
	Precision field measurement	Absolute dc fields $< 10^{-12}$ T
	Non magnetic material control, and fab techniques	$< 10^{-10}$ Tesla at gyro position
	Comprehensive flight part testing	100% screening for parts within magnetic shields
<b>Attitude and Translation Control</b>		Control of all 6 spacecraft degrees of freedom
	Inertial sensing. Gyro (proof mass) suspension system.	Sub nm position noise. Sub $10^{-12}$ g acceleration measurement precision
	Attitude Sensing	Telescope pointing noise 0.48mas/orbit
	He proportional thrusters	Sub to milliNewton proportional controlled
	Attitude and roll	$\sim 200$ marc sec RMS, 5 marcsec at roll frequency
	Translation Control	Dragfree to $< 10^{-11}$ g; DC to 1Hz
<b>Non-contact Charge control</b>	Charge Measurement via GSS electronics	0.1 PicoCoulomb resolution
	UV fiber optic system	Control to $< 5$ PicoCoulomb; Discharge rate adjustable via electrode bias
	Mechanical fiber optic switch	No failures on-orbit
<b>Ultralow vacuum technology</b>	Low temperature bake-out techniques, 8 K cryopump	$< 10^{-11}$ Torr

<b>Technology Category</b>	<b>Specific Implementation</b>	<b>Realization</b>
<b>GPS system</b>	Orbit determination	MilliNewton force residuals in 30 hr integration
	Time transfer	< 0.1 millisecc uncertainty in science signal time relative to UTC
<b>Advanced Vehicle Control Simulation</b>		Successful on-orbit setup and control parameter optimization



# 4

## GP-B On Orbit

---







## 4.1 Overview of On-Orbit Operations

The preparation for on-orbit operations began long before launch. A series of simulations, generated by computer in the GP-B ITF (see “[The Integrated Test Facility \(ITF\)](#)” on page 121) were carried out to prepare the team. In preparation for launch, a number of changes were made to the program structure. The team was restructured to support the on-orbit needs. A number of additional capabilities were added in the final few years leading up to launch. The elements of the program included data processing, orbit determination, computer hardware, the Integrated Test Facility (ITF), anomaly resolution and risk management, and all of the technical payload and spacecraft subsystems. Although the program manager maintained overall responsibility for the vehicle, day to day responsibility for the vehicle was delegated to the mission directors. This clear and efficient program reporting and responsibility structure was a critical component of on-orbit operations and allowed for timely response to vehicle needs.

### 4.1.1 Three Mission Phases

The top level view of GP-B on-orbit consists of three phases: the initialization phase, the science phase, and the calibration phase. During the 4+ month initialization phase the vehicle was configured for science. This phase was extremely busy and at times very stressful for the team. Each part of the GP-B organization needed to perform efficiently, yet without error. Re-tasking of the spacecraft was carried out as needed and was based upon events on-board the vehicle. Large amounts of data were fed to the ground to provide information on these events. The computer hardware and data processing systems operated 24 hours a day, 7 days a week. Although the team had been through a series of very helpful pre-launch simulation exercises, the initialization phase was, in-effect, a 4+ month-long simulation. Many days of this period, many members of the team worked 60 or more hours per week. There were few easy days. In retrospect it is accurate to say that the team rose to the occasion, they remained focused on the vehicle throughout, and they succeeded in a very challenging task.

The initialization phase was followed by an 11 month science data taking phase. In comparison to IOC, this period was straightforward to implement. In addition, the team was very well trained by the start of science. Each team member knew well his or her responsibilities, thus further easing the effort. Most days were uneventful, although the daily “all-hands” meeting was maintained to ensure that the team remained focused on the vehicle status. The all-important science data were transmitted to the ground four times a day. The engineering and science teams reviewed the data on a daily basis and provided top level feedback on the previous day’s data at the daily meeting.

The science mission concluded with a 1.5 month long calibration phase. The purpose of this phase was to help evaluate sources of systematic experiment error and to allow the team to place limits on gyroscope torques. Although many operations were performed during this period, the implementation was performed nearly flawlessly.

### 4.1.2 Daily Operations Routine

Although a clear decision making process and clear definitions of personnel responsibilities are important in any organization, these aspects are particularly critical in an on-orbit environment. The overall description of the program can be described as follows: The Mission operations center was the lifeline to the vehicle. Personnel in the MOC were always focused on the current vehicle status. Typically, the vehicle would be “green” and the MOC would verify this status with a real time monitoring system. In a typical “green” day, a daily 10 am “all-hands” meeting would inform the team of the previous day’s events and planned future operations. Following the all-hands meeting, mission planners would meet with subsystem specialists to develop the detailed plan for the next day. In practice, much of the planning already had been developed long before, and only rearrangement of the order of tasks was required. When new products were required, the ITF was used for verification prior to use on the vehicle.

Any significant deviation from “green” would immediately “trump” other program activities. An efficient electronic communication-information system allowed for rapid response. Telemetry information from the MOC and information determined from off-line analysis were in near constant review. Deviations from a “green” or expected result would cause the initiation of our in-house anomaly resolution process. This process, which was developed and practiced prior to launch had the responsibility to determine root cause and to make recommendations to the mission director and program manager for an action plan/correction. The anomaly resolution team was comprised of a team lead, technical experts, NASA representation, Lockheed Martin representation, and anomaly support staff. The system worked extremely well. A more complete description of this process, as well as all of the other program elements described in this introduction, can be found in the sections and chapters following this one.

### 4.1.3 NASA Group Achievement Award

By the end of mission, the GP-B team had become very skilled at both operating the spacecraft and handling anomalies. Thus, there was some sadness when the mission ended and members of the mission operations team had to move on to new jobs and other missions.



**Figure 4-1.** NASA GP-B Program Manager, Tony Lyons, from the Marshall Space Flight Center in Huntsville, AL, presents a NASA Group Achievement Award to the entire GP-B team in November 2005.

At the end of November 2005, shortly after the successful completion of the GP-B flight mission, NASA’s GP-B Program Manager, Tony Lyons from the Marshall Space Flight Center, presented a NASA Group Achievement Award to the entire GP-B science mission team, including people from both Stanford and Lockheed Martin. The award reads: “For exceptional dedication and highly innovative scientific and engineering accomplishments leading to the successful execution and completion of the Gravity Probe B Science Mission.” The award is signed by NASA Administrator Michael Griffin, and individual copies were given out to each and every member of the team.

## 4.2 Mission Planning

This section discusses the Mission Planning function, which is part of the Mission Operations group.

### 4.2.1 Function Charter: What is Mission Planning?

The charter of Mission Planning at Gravity Probe-B is to program the spacecraft’s operations through a *spacecraft-executable timeline*, and to provide communications between it and the operators on the ground through a *communications schedule*.

### 4.2.1.1 The Operations Concept for Mission Planning

Part of the overall Operations Concept for the Gravity Probe-B was to divide the work of the crucial In-Orbit Checkout, or IOC phase of the mission into daily cycles. This is what a typical day would look like.

1. The overall plan for what the spacecraft would do—detailed down to the individual instruction—was created over years before the mission launched, and was called the Baseline Timeline.
2. Each day, project engineers, scientists, and managers would submit changes to the Baseline in the form of Timeline Change Requests, or TCRs.
3. Mission Planning would spend every morning receiving these TCRs and readying its products for review at the upcoming meeting.
4. Every day at 11:00 AM local time, a Timeline Meeting immediately after the Daily Status Meeting. At the timeline meeting, overall timeline strategy would be discussed, and TCRs would be dispositioned. A graphical version of the load for the day would be displayed to the group via laptop projection, and Adobe Acrobat software was used to mark up the timeline with requested changes in real time.
5. Also, at the Timeline Meeting Mission Planning would present the loads for the next day, and review the strategy for the next several days, so that major changes could be caught as early as possible—at least a day in advance. In any case, at the end of the meeting, Mission Planning would have its marching orders for the day in the form of TCRs, and also a visual representation of the changes.
6. Mission Planning would then begin the work of building the two loads for that day. Spacecraft memory was partitioned into two areas capable of holding executable instructions—what we called stored program command (SPC) loads, each of which could consist of several hundred SPC commands, each carefully timed down to the second. These two memory areas were called Ping and Pong.
  - The Ping load would carry out the bulk of the instructions designed to check out the payload and ready the experiment.
  - The Pong load would be the place where attitude and thruster control (ATC) initialization would occur, and other spacecraft systems would be initialized and fine-tuned.
7. Changes to the spacecraft SN and GN schedules would be implemented on a “best possible” basis. Since GP-B’s priority among other extant missions was middling, this often took a great deal of communication with elements at White Sands which manage the overall TDRSS and GN schedules. Furthermore, any change to the schedule had implications to the timeline, so once the final changes were made to the schedule, the revisions would need to be applied and accounted for by the Planner working on building the loads.
8. Once Mission Planning had a working draft of the Ping and Pong loads, they would be published to the Operations web site, “gpbops”, and a notification page would be sent to all the engineers, scientists, and managers responsible for approving the load so they could review the load as soon as possible, and report problems and errors.
9. At 4:30 PM local time (or whenever possible), a Final Review Meeting involving MP, mission managers, engineers, and scientists would occur. In this meeting, the final product was graphically reviewed, and compared to the TCRs and to the visually-marked-up baseline shown in the morning meeting. In addition, complete load packages would have been assembled and presented for approval. These printed

packages, one for each Ping load and one for each Pong load, were several hundred pages in length, and contained every MP product associated with that load, including the actual instructions (in human-readable code form) sent to the spacecraft.

10. Once the load packages are approved and signed off by all the sub-system engineers and mission managers, the loads could be sent to the Real-time Operations team in the MOC. Mission Planning would deploy the load products to both PODs (computer clusters capable of commanding the spacecraft) in the MOC, and would also deploy the final products to the web site for common availability to the entire mission.
11. Finally, an abbreviated load package would be produced containing high-level products. This small package would be photocopied and made available as the Ping and Pong loads were executing, so that anyone on-site could easily determine what the spacecraft's timeline and objectives were for the day. As a capstone to the day's events, a thematic and clever cartoon would be harvested from a book or the internet, and placed on the load package's cover sheet to provide much-needed levity.
12. Mission Planning was scheduled to leave for the day at 5pm.

In the Science Phase of the mission, things were planned to get a lot simpler – with only a few loads per week. And in the Calibration phase, we would have one load per day.

#### **4.2.1.2 Success Criteria**

Our success depends on three critical factors: (1) *efficiency* in the face of complex requirements, (2) *flexibility* in a dynamic environment, and (3) *error-free* results. Furthermore, the measure of our success is the quality of our two sets of products – the Timeline and the Schedule – which closely interlock and co-evolve throughout their creation on a daily basis. Mission Planners must:

- Coordinate all the essential input from mission researchers, spacecraft engineers, and program managers – even as situations change from morning to night
- Operate a rigorous set of quality assurance processes – to verify that the instructions received are precisely implemented as intended
- Operate a complex set of support software which facilitates the creation of timely, correct timelines and schedules – to meet the dynamic needs of spacecraft operations
- Deliver its output into production: the timeline must be delivered to the spacecraft, and the communications schedule must be synchronized between the Stanford Mission Operations Center (“MOC”) and the NASA communications elements around the world

#### **4.2.1.3 Coordination: the Primary Challenge**

Mission Planning drives the development of the timeline and the schedule through its contacts with all the operations, engineering, management, and NASA elements. The coordination required to develop a coherent product set – a spacecraft timeline and schedule – is extensive. The primary challenge of Mission Planning is to capture, coordinate and properly understand all the various inputs from these sources.

#### **4.2.1.4 Mission Planning in a University Setting**

Of special significance is Gravity Probe-B's implementation in a university setting. The Mission Planning team comprised a core group of two professional Mission Planners, supplemented by students. The core professionals were subject matter experts in the timeline, schedule, and software tools, while the students maintained expertise in niches and specific functions.

Three critical factors were essential to Mission Planning's success, and these are described in the three main sections that follow.

## 4.2.2 Critical Factor: Efficiency

The first critical factor was efficiency, and this section discusses the breadth of material that the Mission Planning team had to master in order to achieve maximum efficiency.

### 4.2.2.1 Subject Matter Expertise

For speed of product delivery, both general information and subject-matter expertise were required from Mission Planners at Gravity Probe-B. The following table illustrates the Mission Planning material that had to be mastered:

**Table 4-1.** Mission Planning Mastery Index

<b>Mission Planning Mastery Index</b>	
<b>Spacecraft Sub-Systems</b>	All the commandable sub-systems of the spacecraft must be understood.
<b>Safemodes</b>	Clear understanding of the safemode scheme, with its tests, masks, and macros is critical.
<b>CARD</b>	Internalizing the Constraints And Restrictions Document (CARD).
<b>Spacecraft Software</b>	The operating system and applications model of the spacecraft.
<b>Communications Systems</b>	Expertise with both the Space Network and Ground Network.

### 4.2.2.2 Software Expertise

In addition, Mission Planning had to master a great deal of software in order to implement its functions. Internally, we viewed software in two categories: externally-supplied software, including commercial software, and government software.

**Table 4-2.** Mission Planning Commercial Software

<b>Commercial Software</b>	
<b>GREAS for STK 4</b>	From Analytical Graphics, this software is used to build the spacecraft timeline and provide basic visualization.
<b>STK 4 (Unix) STK 6 (Windows)</b>	Mission Planning are able to perform a wide variety of orbit analysis functions through the use of STK products.
<b>STK VO</b>	Advanced, real-time three-dimensional visualization of the spacecraft in orbit was developed by Mission Planners through the use of the VO product from Analytical Graphics.
<b>SWSI</b>	NASA's interface to the Space Network scheduling system.

In addition to these software packages, Mission Planning used and developed many internal products:

**Table 4-3.** Mission Planning software developed by GP-B

<b>Internally-Developed Software</b>	
<b>TISI</b>	Software which provides SN and GN schedule visualization, timeline analysis, constraint checking, and reporting. Developed by Mission Planning itself.
<b>MP Toolkit</b>	Automation toolkit which automates almost every phase of product delivery. Developed by Mission Planning itself.
<b>Timeline Viewer</b>	Software which provides advanced timeline visualization. Developed by Mission Operations.
<b>Command Generation</b>	Developed by Lockheed-Martin for the GPB mission, this software compiles the timeline into spacecraft executable files.
<b>Parameter Generation</b>	Developed by Lockheed-Martin for the GPB mission, this software maintains a database of parameters which configure the spacecraft's sub-systems.

### 4.2.2.3 Showcase: TISI

TISI was the keystone software developed by Mission Planning to automate hours-long workflow and to provide features not available to Mission Planning through any other software available.

Early on, it was recognized that Mission Planning didn't have all the tools it needed to achieve its success criteria. We faced problems on all fronts of our workflow:

**Table 4-4.** Pre-TISI Mission Planning Challenges

<b>Mission Planning Challenges Pre-TISI</b>	
<b>Long Load Time Generation</b>	Building a single load was a long process, taking many hours.
<b>Schedule/Timeline Synchronization</b>	Keeping the spacecraft schedule and the timeline in sync, as both are changing, proved a serious challenge requiring many hours of work, and was prone to human error.
<b>SN Scheduling</b>	The raw work involved in space network scheduling using the SWSI interface made scheduling the number of contacts we required incredibly time consuming, and prone to human error.
<b>GN Scheduling</b>	NASA does not provide any tools to create a properly-formatted GN schedule, and these were done by hand. Incredibly prone to human error.
<b>Constraint Checking</b>	Something as simple as making sure we scheduled contacts within proper view periods was done by hand, and very prone to human error.
<b>Reports</b>	Our collaborators needed reports in a variety of formats, and all these were assembled by hand. Prone to human error!

In short, we faced a lack of tools which made our daily process long and error-prone. TISI was our answer. It was created in under 6 months prior to mission launch, and was validated in simulations and Proficiency Exercises. TISI simplified and automated vast stretches of workflow by delivering on a few key design objectives:



**Table 4-5.** Addressing mission planning needs with TISI

<b>TISI – Addressing Mission Planning’s Needs</b>	
<b>Easy Visualization</b>	TISI graphically displays planning data in a customizable viewer which can drill down to any time frame.
<b>STK Import</b>	TISI imports data from STK reports, providing it access to all the spacecraft views desired.
<b>Visual Scheduling</b>	The viewer window is interactive. Scheduling Space and Ground Network passes is a visual exercise, driven by simple clicking.
<b>Constraint Checking</b>	TISI analyzes both the spacecraft schedule and the current timeline for conformance to constraint rules.
<b>Reporting</b>	TISI creates a wide variety of reports, from those used by human operators, to GREAS, WOTIS, and SWSI bulk import formats. These reports are validated and error-free.
<b>Blackouts</b>	TISI can provide schedule avoidance through the use of blackout periods. In the case of GPB, we avoided JPL/DSN views to mitigate a transponder frequency problem.

TISI constantly evolved to meet changing needs. Since launch, TISI was upgraded over 30 times to add new features and to make more gains with automation.



**Figure 4-2.** Example TISI visualization.

#### 4.2.2.4 Showcase: Web Delivery

Based on the volume and frequency of delivering products to a large number of interested parties, Mission Planning developed a web-based product delivery system as part of its MP Toolkit. This system replaced a paper-based delivery system which was used in early simulations. The implementation of this system was instrumental in automating an entire section of mission planning workflow.

**Table 4-6.** Features & benefits of Web delivery

<b>Web Delivery — Features and Benefits</b>	
<b>Automation</b>	This software automated countless hours of photocopying and paper wrangling.
<b>Instant Access</b>	Products are available throughout the day in draft form so our collaborators can examine them before it's too late.
<b>Version Control</b>	All versions of the products are available to our customers.
<b>Global Access</b>	Products are available to all our customers around the world via a secure web site.
<b>Digital Formats</b>	By providing our products in digital form (rather than paper), our customers can (and have!) write tools to post-process the data.

### 4.2.3 Critical Factor: Flexibility

Having solved the problem of efficient product generation, the second challenge was how to adapt to the operational reality of planning a spacecraft, in which plans are made, scrapped, re-formed, and updated as information becomes available. The challenge here was planning for the next day's load, the next week's schedule, and trying to forecast weeks of schedule in advance, as well!

#### 4.2.3.1 On-Orbit Operations: Change is Constant

During early IOC, Mission Planning was required to re-implement its operations concept due to the demands on daily workflow, and problem mitigation strategies implemented by mission managers. The following table highlights the changes we made to adapt our concept to the reality of on-orbit operations:

**Table 4-7.** Re-inventing the mission operations concept

<b>Re-Inventing the Operations Concept</b>	
<b>From Baseline to Sequence Library</b>	As the 40-day baseline timeline experienced early deviations, Mission Planning transformed it into a "sequence library" which could be used in any day's load, with minor customization.
<b>From Change Control to Markup</b>	As we moved into the sequence library model, the highly structured change control process designed to capture slight deviations no longer made sense. We implemented a "markup" model using Adobe Acrobat, which was much more suitable for the kinds of changes we experienced.
<b>FWD Antenna Anomaly Mitigation</b>	The anomaly which resulted in a reduced-efficiency forward spacecraft antenna resulted in significant challenge to operations. Mission Planning had already laid the groundwork for solving this problem in the timeline, and was ready when operations needed the help!
<b>Extensive Coverage Requirements</b>	The coverage requirements from engineering and scientists far exceeded mission specifications. But with tools like TISI in place, Mission Planning was able to absorb the additional burden easily.
<b>Coverage Rebuilding</b>	Mission Planning was required to rebuild already-build spacecraft timelines constituting weeks of time, on many occasions. Mission needs were impossible to predict, and we needed to not only work on the day's loads, but also consistently rework and replan for the future.

#### 4.2.3.2 Commitment to the Mission

Mission Planning is proud of its performance during IOC, and nothing quite communicates this as well as the chart showing just how many hours we spent building our loads and schedules every day. The following diagram's vertical bars illustrate the number of hours our planners stayed late to get the job done during the heavy load days of IOC:



**Figure 4-3.** Number of hours of re-planning required per day during IOC.

In addition, these same mission planners were on-call 24 hours a day, 7 days a week during both the IOC and science phases of the mission, to support emergency changes in the SN and GN schedules, as well as on-orbit conditions which required middle-of-the-night load re-building.

#### 4.2.3.3 Flexibility Showcase: Timeline Automation

During the Calibration phase of the mission, MP designed and deployed a macro language for TCRs, building on our extensive experience with timeline design in the IOC and Science phases. The operations concept was simple:

- A Calibration baseline was created. This is a very simple, repeating structure where every week is the same.
- A TCR for each calibration activity was created – one per day. These TCRs were designed and discussed for months prior to use.
- The TCRs were “marked up” using a macro language developed by MP. These macros were also human-readable and intuitive.
- The macro TCR would be approved, and on the day of its use, it would be run through the processing software which would produce a GREAS file which contained the timeline instructions necessary to implement the TCR.
- A MP would then incorporate this GREAS file into the baseline GREAS file and massage the components into agreement. Some human work is still required, but hours of grunt work was eliminated, and human error removed!

This software added considerable efficiency to the MP workflow, but its real win was in the flexibility it gave us. Experience shows that timeline changes occurred often and late in the load design process, as operators and managers reacted to late-breaking spacecraft changes and results. By removing hours of planning and re-planning from this picture, the Timeline Automation software allowed us to incorporate bigger changes much later in the day than we could during the IOC or Science mission phases.

#### 4.2.4 Critical Factor: Error-Free

The third factor critical to Mission Planning’s success was delivering products that were completely error-free, and that met the intentions and operational objectives of the mission. To this end, Mission Planning set out a goal and a key mechanism to achieve it. Our goal was “no data loss”, and our quality assurance mechanism was “timeline verification.” This section discusses these elements.

##### 4.2.4.1 No Data Loss!

Our customers in the Science Group cared most about one thing: getting their data. And in this area, the goal of the Mission Planning team was simple: “Do everything we possibly could to ensure that no data loss occurred from anything we could control.” And, throughout the IOC and Science phases of the mission, we were successful! No data loss resulted from our scheduling and load generation products. This achievement was the result of solid processes that minimized the possibility for human error by employing direct human oversight and double-checking every step of the way.

The volume of the task was substantial. Consider:

**Table 4-8.** Mission Planning workload volume—IOC & Science

<b>Workload Volume over the Course of IOC and Science</b>	
<b>Months On-Orbit</b>	17.3 (April 20, 2004 – September 29, 2005)
<b>Space Network Passes</b>	9,000
<b>Ground Network Passes</b>	2,100
<b>Templates Executed during IOC</b>	34,856 1,891 templates per week (average)
<b>Templates Executed during Science</b>	89,207 1,774 templates per week (average)
<b>Total Number of Loads</b>	432

##### 4.2.4.2 Timeline Verification

During IOC, each spacecraft load was custom-built from the library of tasks and blocks of tasks Mission Planning created. This was a departure from our planned process of working from a constant, controlled baseline, and this meant that risk was injected into the load development process.

Mitigating that risk during IOC became critical, and our solution to this problem was in several parts:

- Implement software like TISI to do constraint checking among telemetry-critical tasks.
- Direct sub-system engineer panel review on each and every load, every day
- Flight Director and Mission Director oversight on each and every load, every day
- Complete load presentation sessions at the end of the day, visually charting the timeline, contact schedule, and orbital geometry variables such as Guide Star visibility, South Atlantic Anomaly presence, Sun-Eclipse periods, and so forth
- Rigorous version control of all load products, with hardcopy product sign-off of precisely the versions which would be sent to the spacecraft

During the Science phase of the mission, daily workflow became much more streamlined, to the point where we were able to have a baseline for each load during the week. This critical milestone allowed us to implement our TCR (“Timeline Change Request”) process, which we’d specified prior to launch. Using this system immediately resulted in a number of benefits:

- Web-based design: use anywhere, cut-and-paste from other electronic products eliminates typographical errors
- First-hand input: written directly by sub-system engineers
- Approval from managers: all TCRs must be approved by a Mission Director
- Peer review among all other sub-system engineers: eliminates unanticipated impacts in other sub-systems
- Post-implementation review during load sign-off to assure that each and every off-baseline change was as-intended

These safeguards proved to be very effective during both the IOC and Science phases of the mission. Timelines generated by the Mission Planning team never created a spacecraft emergency and never put the spacecraft in a degraded state.

In summary, the Mission Planning team was able to consistently deliver high quality products that:

- Met engineering specifications,
- Were thoroughly cross-checked for accuracy by software and a panel of engineers
- Were generated with increasing rapidity as the mission progressed
- Were available to our user community anywhere they might have been.

Mission accomplished!

## 4.3 Data Processing

### 4.3.1 General

Data processing greatly surpassed its nominal requirement of 95% data capture. The Data Processing team supported all vehicle operations and retrieved data in challenging situations, sleuthing out any additional data concerns. Data processing team members are currently addressing the task of archiving GP-B data for long-term access.

It is said that “an experiment is only as good as its data.” So, one might ask, “How useful are the actual data that were collected during the 50-week science phase of the GP-B experiment? Was it sufficient? For Gravity Probe B, the best gyro precession data were collected when the telescope was precisely pointing at the guide star, when the spacecraft was in Guide Star Valid (GSV) mode (that is, when the spacecraft was “In front” of the Earth, with a direct line of sight to the guide star), and when the spacecraft’s orbit was outside the South Atlantic Anomaly (SAA) region, located in the vicinity of the lower tip of South America. Since the Earth eclipses the guide star every orbit, these optimal conditions occurred only about 54% of the time. Data collected during the remaining 46% of the time was still useful to the experiment, but these data are not directly being used to calculate the gyro precession due to general relativity.

The data processing software and team can only process data that they actually received from the spacecraft. There are many reasons why data may not arrive. For example, ground-based experiments can lose data due to faulty collection techniques, decommutation errors, or inadequate storage methods. Satellites are prone to all these factors, and additionally, they can lose data because of temporary on-board data storage problems in the solid state recorder, communication problems or ground station errors. Fortunately, barring anomalies, many of these factors can be managed to minimize the amount of data this is lost.

For example, during ground contacts, streaming of data was re-routed from the solid state recorder to the transmitter, during which time the solid state recorder was not recording data. During the interval after the solid state recorder stopped recording, but before the ground station locked up with the transmitter, data was lost. By careful management of operational parameters, such as accurate vehicle position knowledge and ground station mask angle, data loss during that transition was minimized. Data was also lost whenever the spacecraft changed its data stream from the forward antenna to the aft antenna. For the GP-B spacecraft, loss of data during these antenna-switching periods was typically minimized to less than 40 seconds. These periods could not be managed by GP-B, since they were a function of the slew rate of the ground dish and the speed of the vehicle. By scheduling ground contacts during guide star invalid periods, we further minimized science data loss. Unfortunately, given the geometry of the GP-B orbit with respect to the ground stations, scheduling ground passes during Guide Star Invalid (GSI) periods (the period during each orbit when the spacecraft was “behind” the Earth, eclipsing its direct view of the guide star) was not always possible.

Management of the solid state recorder itself also mitigated data loss. Some ground station passes resulted in an unacceptably high number of data gaps— three or four is typical and acceptable, but occasionally ground passes generated more than 100 gaps. When data gaps were unacceptably high, the solid state memory location writer pointer had to be moved to prevent data from being over written. On these occasions, data processing worked with the operations team to prevent data loss.

For the Gravity Probe B mission, data loss was minimal. Mission specifications mandated that 95% of the data retrieved by the ground station had to be decommutated and stored in the GP-B L1 database. In fact, 99.62% of all 32K data, and 97.47% of 32K data collected during GSV periods was recovered and processed. [Table 4-9](#) summarizes the data capture statistics.

**Table 4-9.** Summary of Data Capture

<b>Sampling Period</b>	<b>Data Recovered</b>
Pre-launch Specification	95.00%
Total	99.62%
Guide Star Valid, outside SAA (“Optimal Science Data”)	97.47%



### 4.3.1.1 Automated Telemetry Data Processing

In addition to decommutation of the L0 data, an important function of the Gravity Probe B data processing algorithms was to clean up incoming data. Data had to be thoroughly vetted to remove redundant points and filler packets, along with noisy data caused by interference or antenna problems. While data integrity was paramount, high priority was also given to efficiency in this cleanup process. The data processing group is proud of its capability to process ten hours of spacecraft data in less than an hour—well within the specification.

A tremendous effort was made to automate data processing—to the extent possible—so that data was made available as quickly as possible. After data from the GP-B satellite was telemetered to the ground station, the files were sent to SAFS at Goddard Space Flight Center in Maryland. Data files were transferred via the NASA IOnet into the MOC, and detected by the automated data processing less than five minutes after arrival. TDP automatically checked for errors, filler packets and redundant data points, placing the cleaned data into the L0 database, and the decommutated data into the L1 database. L1 data could then be called by the various IDL and Matlab analysis tools used by the GP-B science and engineering team. All daily web plots, SAFS confirmation emails, user notification emails and data processing logbook entries were automated. More importantly, the system was designed with error handling in mind. For example, if data was expected at Stanford but had not arrived in a specified time, automated software alerted personnel on the data processing team. Furthermore, data with problems were rejected automatically before entering the Telemetry Database and staff was alerted via email.

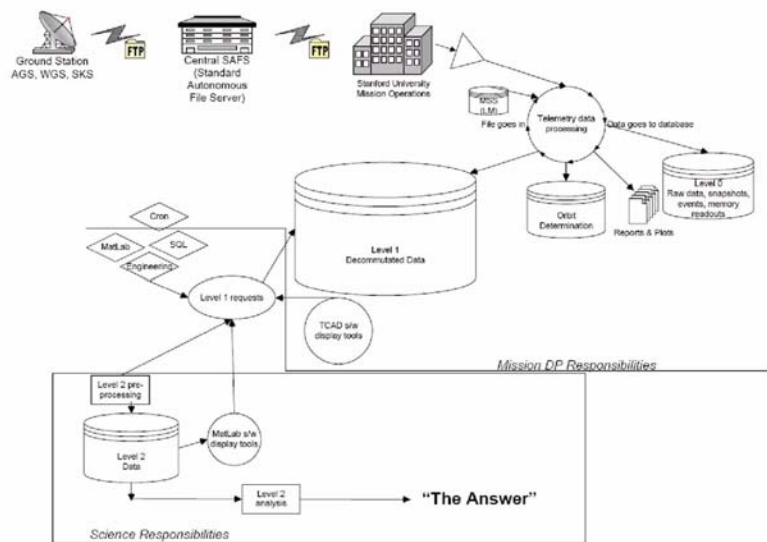


Figure 4-4. Data flow through the GP-B's automated data processing.

### 4.3.1.2 Data Capture

Data capture was excellent. The data processing group was able to process 100% of all the data received by the ground stations, keeping verifiable good data and not allowing corrupted or suspect frames. Since day 111, 2004, ~85 hours of data in total were not present. However, this was non-recoverable data—places where the recorder was not on or commanding wasn't possible. All data gaps over 10 seconds have been accounted for as either spacecraft antenna switch activity, or they have been correlated to a specific vehicle or command anomaly. Approximately 1,680 vehicle data files were processed between launch in April 2004 and the end of the post-science calibration phase in September 2005. Over 300 gigabytes of raw data was stored, in addition to database storage. Table 4-9 lists events and sources of lost data.

**Table 4-10.** Significant Events/Sources of Data Loss

Event/Source	Time (Hrs)
Anomaly 34 (CCCA Switch on 5/3/04)	0.76 **08:49:19.7
Day 125, 5/4/04	03:44:47.1
Day 130, 5/9/04	01:34:30.0
Anomaly 73 (MSS Reload on 6/30/04)	0.58
Day 240, 8/27/04	01:37:30.0
Day 260, 9/16/04	01:55:30.0
Day 268, 9/24/04	01:35:09.8
Anomaly 148 (CCCA Switch on 3/4/05)	7.09 **13:34:29.8
Anomaly 152 (CCCA Reboot on 3/15/05)	6.36 **08:13:57.2
Anomaly 156 (CCCA Reboot on 3/18/05)	3.11 **06:23:06.4
**Couldn't command to turn on recorder 2/22/05	2.6
Ground Station initial capture, antenna switch, and loss of signal (Typically 4 times per day)	17.25
Other –Please add cycle 13 data of 42h:28m:06.2s – partly in A34, 148, 152 & 156.	
Total	~37.6

#### 4.3.1.3 TCAD

The main tool for viewing L1 data was TCAD, a program originally written by University of Colorado's Laboratory for Atmosphere and Space Physics (LASP), and modified for Gravity Probe B by the data processing group. Since launch, TCAD had only one major upgrade to version 2.4.1, incorporating many unanticipated features desired by the engineering staff. The software, based on IDL version 5.4, was version controlled and underwent extensive regression testing prior release on February 11, 2005. Feedback to LASP is planned.

#### 4.3.2 Data Archiving

Plans are currently underway to archive the Gravity Probe B data in the National Space Science Data Center (NSSDC), located at Goddard Space Flight Center in Greenbelt, Maryland. Data archival is a contractual agreement, as described in S0331, Mission Data Management Plan.

### 4.4 Orbit Determination

There were two basic orbit requirements imposed by Gravity Probe-B science objectives. The first was to precisely align the initial orbit plane with respect to the guide star such that non-relativistic torques on each of the four gyroscopes would nearly average out during the science mission. The second was to determine the position and velocity with high accuracy continuously during the mission.

GP-B science requirements placed very strict limits on the placement and evolution of the GP-B orbit plane over the life of the mission. Over the course of a 10 - 14 month science mission, the average deviation of the line-of-sight to the guide star from the orbit plane was required to be under 0.025 degrees. Through proper design of launch vehicle insertion conditions, careful consideration of expected orbit perturbations, and plans to compensate for any launch dispersions with a limited capability to trim orbit inclination errors, the GP-B project has ensured that the established GP-B orbit will satisfy all science requirements.

At launch, GP-B's inclination was just  $5 \times 10^{-5}$  degrees away from the desired inclination, which corresponds to only about 6 m of error assuming a planned 60-day Initial Orbit Checkout (IOC). This small error eliminated the need to carry out orbit trim maneuvers. Even without trimming, the average orbit plane errors over the life of the science mission are expected to remain under 0.020 degrees - well within requirements.

GP-B operations also required accurate orbit determination (OD) in order to establish the GP-B position and velocity to within 25 m and 7.5 cm/sec RMS throughout the mission. GPS observations available at 10-second intervals were processed using the commercial Microcosm orbit determination program in daily 30-hour batch fits to satisfy those requirements.

#### 4.4.1 The GP-B Mission Orbit Design

The GP-B altitude was planned to be approximately 650 km, based on launch weight considerations and a desire to be above the region in which atmospheric drag could overpower the Helium thrusting that maintains the mission's drag-free status. The specific mean semi-major axis was finally chosen to be about 10 km lower, at 7018.0 km, in order to be between two repeat ground track resonances that would have complicated the IOC trimming process. In addition, it was desired that the orbit be nearly circular in order to minimize drag fluctuations around the orbit. The target mean eccentricity and argument of perigee were chosen to be 0.00134 and 90 degrees, the stable ("frozen") values at GP-B mission altitude.

The orbit plane was to have its descending node remain near the right ascension of the guide star, so that the spacecraft axis would remain nearly in the orbit plane to minimize gyroscopic torques. That implied a near polar orbit to minimize nodal precession and, after HR 8703 was chosen as the guide star, it implied a launch that was timed to place the right ascension of the orbit's descending node near 343 degrees.

The specific inclination and nodal values for the GP-B orbit plane were derived from the requirement that:

“[The] final target orbit shall be chosen such that the predicted angle between the line-of-sight to guide star and the orbit plane, averaged over an interval longer than 10 months and less than 14 months starting 2 months after launch, is less than 0.025 degrees.”

The specified angle in the preceding requirement, commonly known as  $\eta$  (eta), is illustrated in [Figure 4-5](#) below. The  $\eta$ -angle is significant because of its relationship to gyroscopic torque. Outside disturbances like gyroscopic torque must be kept to a minimum to improve the accuracy of measurements obtained by the GP-B science experiment. Since gyro torque is proportional to the distance between the gyroscope and the orbit plane, gyro torque is also proportional to  $\eta$ . The science requirement that  $\eta$  be  $< 0.025$  degrees when averaged over an interval of 10 – 14 months, allows the effects of gyro torque on precession rate to nearly cancel.

Mathematically, the angle  $\eta$  is obtained from the following equation:

$$\sin \eta = \cos i \sin \delta^* + \sin i \cos \delta^* \sin(\Omega - \Omega^*)$$

$$\eta \approx (90^\circ - i) \sin \delta^* - (\Omega - \Omega^* + 180^\circ) \cos \delta^*$$

where  $\delta^*$  and  $\Omega^*$  are declination and right ascension of the guide star, corrected for aberration and proper motion and expressed in true-of-date coordinates. Errors in  $\eta$ -average arise from errors in the histories of the orbit's inclination and right ascension of ascending node ( $i$  and  $\Omega$ ) during the mission, after the end of IOC.

The key issue here is that there can be no corrective thrusting after the drag-free mission begins, so the orbit parameters at the end of IOC must be established very accurately. In particular, the inclination then must be correct to within about  $\pm 0.00020$  degrees, a value much more precise than needed for most missions. In order to obtain that inclination accuracy, the mission profile allowed for almost continuous cross-track thrusting ("trimming") during the nominal 60-day IOC, using low-thrust Helium venting to remove the inclination errors made by the launch vehicle at insertion.

\*

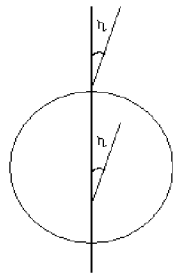


**Figure 4-5.** Pictorial depiction of  $\eta$ . The circle represents the Earth, the vertical line is the orbit plane viewed edge-on, and the asterisk represents the guide star.  $\eta$  is the angle between orbit plane and guide star at any point in the orbit plane.

#### 4.4.2 Launch Requirements

The orbit plane parameters that satisfy the requirement above depend on the launch day. That is, they depend on the motions of the orbit plane, which depend on the positions of the sun and moon during the mission.

For each potential launch day, an iterative process using semi-analytic integrations of orbit elements for 16 months was used to determine initial  $i$  and  $\Omega$  values that satisfy the  $\eta$ -average requirement. It was found that acceptable  $i$  and  $\Omega$  pairs filled a thin lens-shaped region. The center of the lens was chosen as the inclination and nodal target for each mission start day. (The lens boundaries are different for each start day, but the thinness of the lens is nearly constant, and that thinness limited the initial mission mean inclination values to  $\pm 0.00020$  degrees for maximum nodal launch errors). Launch vehicle requirements for each launch day were obtained by propagating the mission target elements backward to launch time.

Figure 4-6 illustrates an example of those computations. It shows the expected evolution of  $\eta$  and  $\eta$ -average (the pairs of curves with the same color) after a launch that takes place on 20 April 2004. The x-axis indicates time in months and includes the nominal 2-month IOC period as well as the 10 - 14 month science period (yielding a total duration of 12 - 16 months). The three cases shown represent the optimum and maximum/minimum allowable inclination limits, assuming in this case an ideal value of the right ascension of the ascending node. The max/min curves represent the worst-case initial inclination errors for which  $\eta$ -average would just remain within the  $\pm 0.025^\circ$  limits for a science mission lasting anywhere from 10 to 14 months.

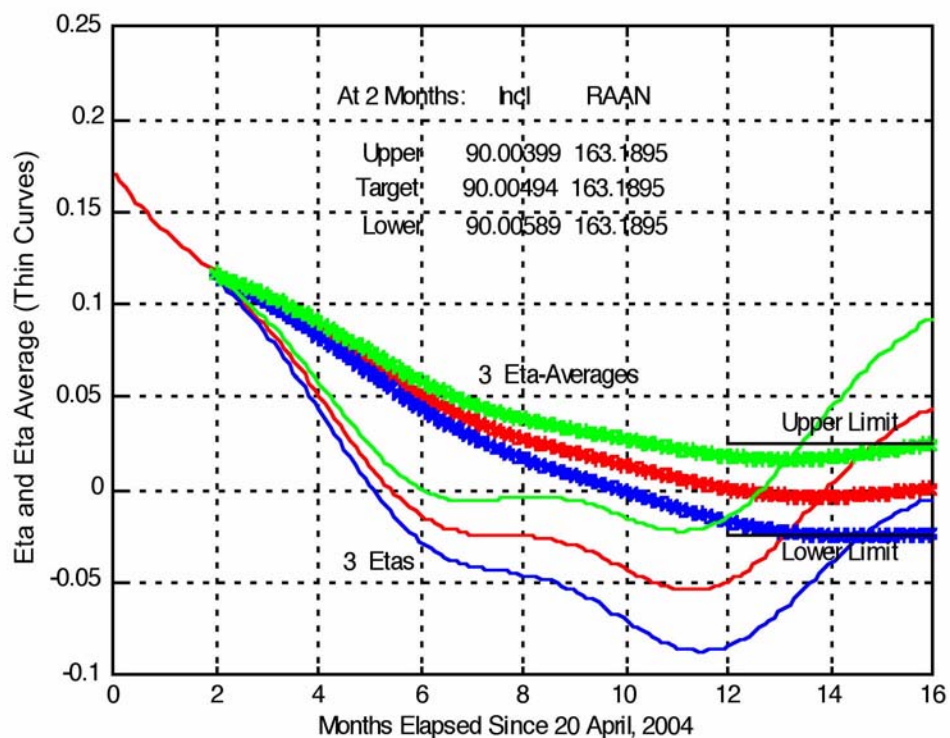


**Figure 4-6.** Eta and Eta-Average Histories (Degrees) Associated with GP-B

### 4.4.3 Post-Launch Orbit Events

On April 20, 2004, the Delta II 7920-10 launch vehicle injected the Gravity Probe-B satellite into an excellent orbit. The altitude, eccentricity, argument of perigee and ascending node were well within specifications and, most importantly, the inclination was almost perfect—within  $5 \times 10^{-5}$  degrees of the target (a cross track error of about 6 meters!) That was well within the  $\pm 0.00020$  degree inclination trimming goal, so it was decided that no trimming would be used during IOC.

However, the target values for inclination had been based on a 2 month IOC span, so as the need to extend the IOC period beyond 2 months arose, estimates of  $\eta$ -average errors for the current GP-B orbit for longer IOC spans were required. Figure 4-7 illustrates GP-B's computed eta-average histories for 60-, 90- 120- and 150-day IOC periods as a function of science mission duration. The red lines delineate the  $\pm 0.025$  deg limits on  $\eta$ -average imposed by science. It can be seen there that even with the actual 141-day IOC duration (for gyroscopes 1-3) and the 158-day IOC duration (for gyroscope 4), the GP-B orbit would satisfy the eta-average requirement for any science mission lifetimes lasting longer than two months. For the actual expected science mission lifetimes of 10 or 11 months the eta-average errors will be less than 0.020 degrees, well within the eta-average requirement.

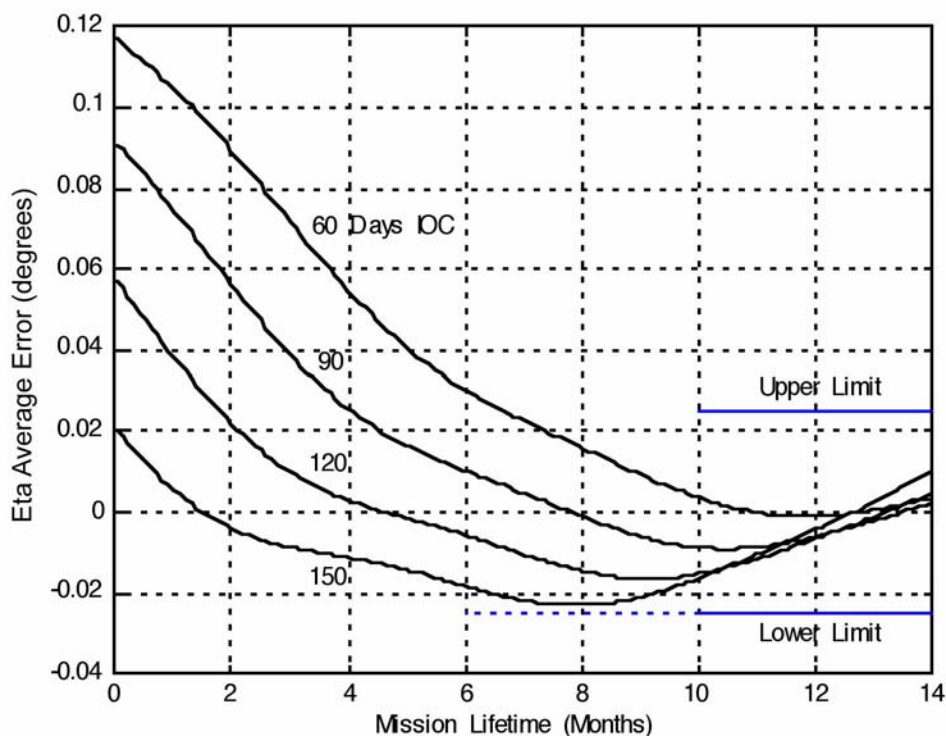


**Figure 4-7.** Eta-Average Error Associated with GP-B Orbit as a function of IOC duration and science mission lifetime

#### 4.4.4 Orbit Determination Calculations

GP-B operations also require an accurate knowledge of the satellite ephemeris throughout the mission. The most stringent requirements are for 25 m and 7.5 cm/sec RMS position and velocity accuracy, to permit accurate relativistic drift scaling and allow the computed aberration signature to be used for science signal calibration. There also is a looser requirement for regular three-week predictions for scheduling mission operations.

For those purposes, GP-B ephemeris segments have been generated every day using independent batch fits to 30-hour data spans centered on Greenwich noon. That allows for 6-hours overlap before and after each segment for consistency comparisons.

Global positioning system (GPS) measurements have been used as the primary means of orbit determination while Satellite Laser Ranging (SLR) measurements have been used as an independent means since late-July 2004. A similar procedure is used on both data sets to generate daily solutions.

##### 4.4.4.1 OD Using GPS Data

GPS data points are taken once every 10 seconds. Duplicate points and points with impossibly large or small radius values are removed from the data set before a GPS solution is generated. The result is a data set at around 7500-8500 time points in each 30-hour segment (Figure 4-5). The decrease in usable points available after day 66 reflects a switch from A-side to B-side GPS receiver.

Next, the commercial software package Microcosm was used to fit an ephemeris to the data. The 35 x 35 gravity model jgm3 was used for these fits, along with lunar-solar and earth-tide effects, a constant (shadowed) radiation pressure model and a Jacchia 71 atmospheric density model, both with adjustable scale factors.

After some initial experimentation a decision was made to solve for 9 parameters during each fit. Initially those were the 6 state variables (position and velocity) plus a drag coefficient and two sinusoidal in-track accelerations at orbital period to account for mis-modeled drag and eccentricity vector component rates. Because slowly varying constant and sinusoidal axial thrusting components persisted throughout the science mission, GP-B orbit determination continued to solve for those 9 parameters after IOC. The unconstrained drag coefficient absorbed the dominant in-track effects of the slow semi-major axis variations due to the sinusoidal axial thrusting term, and the in-track sinusoidal parameters modeled the eccentricity vector rate errors due to the constant axial thrusting term.

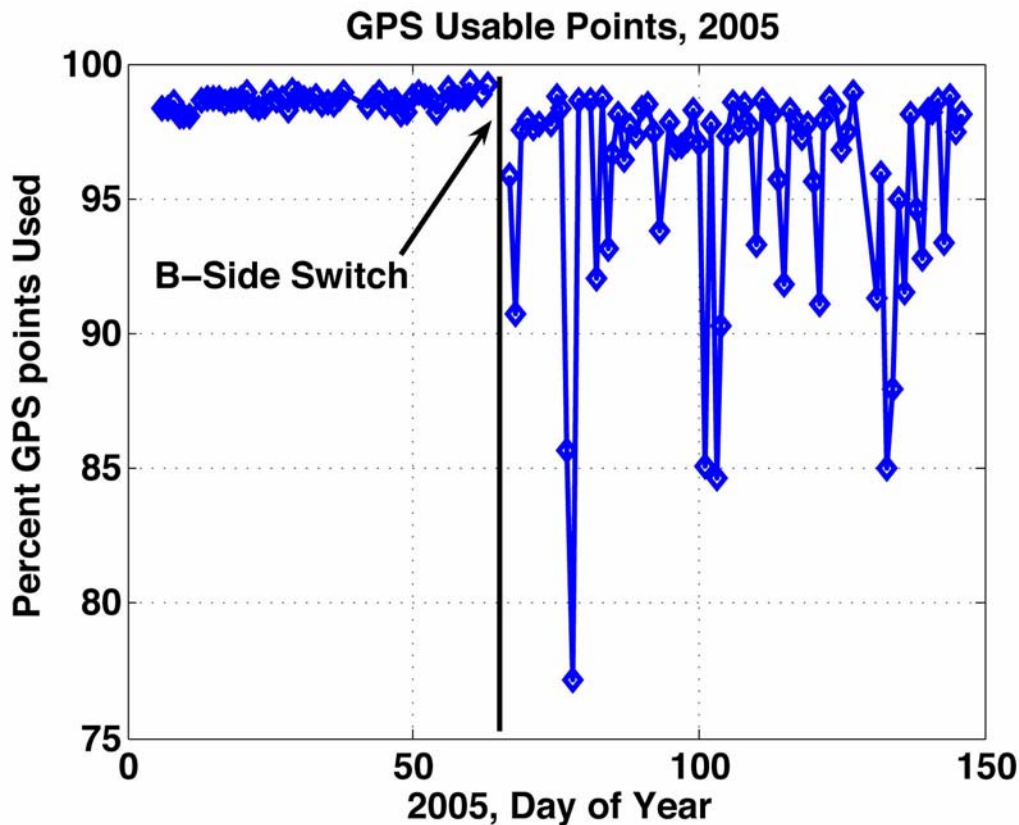


**Figure 4-8.** Usable GPS Points per Day (2005)

Daily residual plots (Figure 4-9) are generated to assess how well the ephemeris fits the data. Standard deviations for cross-track residuals are typically less than 5 meters, in-track residuals less than 10 meters, and radial residuals around 15 meters. It can be seen from Figure 4-6 that, for this solution, RMS values are primarily due to data noise – the ephemeris errors are far smaller. The corresponding overlap comparisons between successive daily 30-hr solutions are a better indication of actual orbit errors. Those daily orbit comparisons typically yield in-track and radial variations of just a few meters, and cross-track variations are often less than a meter.

There are exceptions to this general pattern of operations. On several days (for example, day 66 in Figure 4-5) there were gaps in the GPS data that prevented the use of a normal 30-hour fit span. When such gaps occurred, 2 or 3 days of GPS data were used to create an ephemeris segment spanning the gap. Also, on some days when the sinusoidal axial thrusting interacted with the orbital motion so as to generate in-track perturbations with a nearly daily period, the in-track effects could not be well approximated by fitting a drag coefficient alone. For those ephemeris segments, it is possible to reprocess the data with shorter fit spans and fit additional parameters as needed.



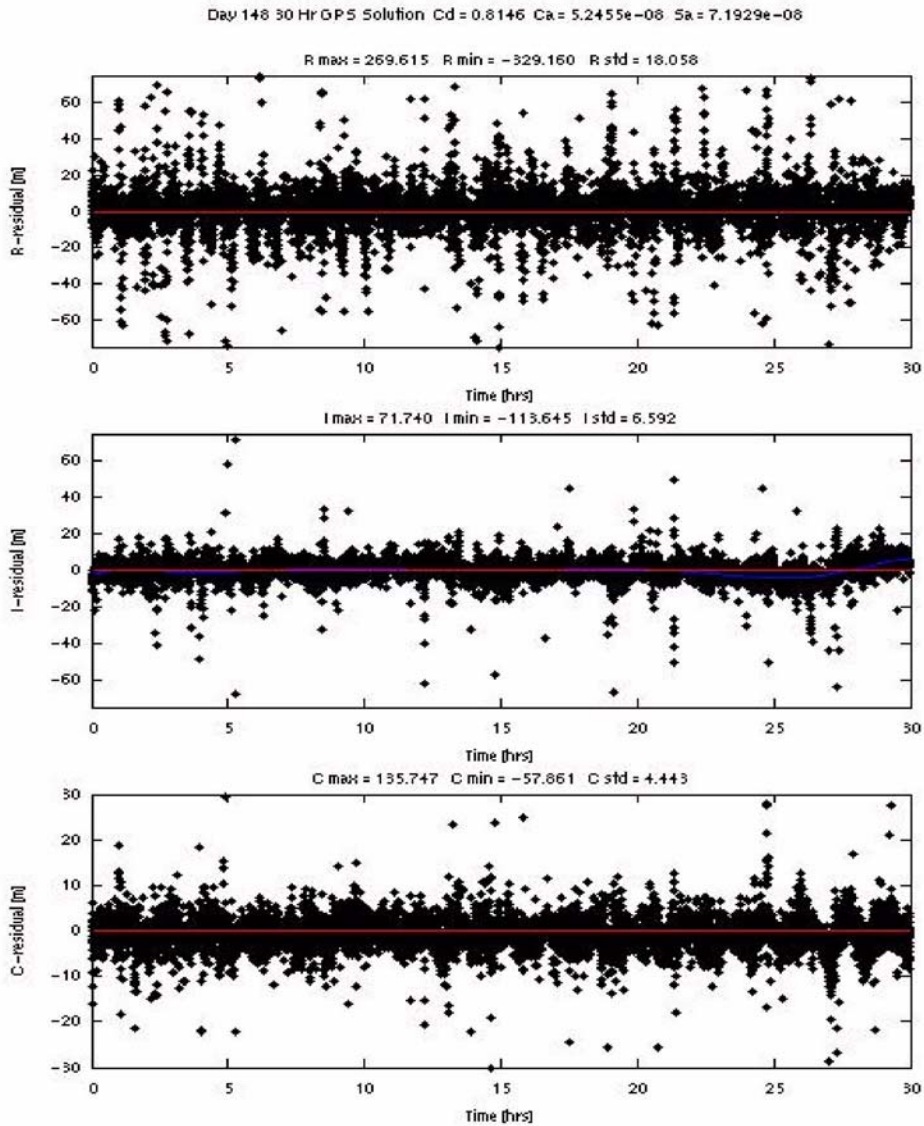


**Figure 4-9.** Typical residual plot from daily GPS solution.

#### 4.4.4.2 OD Using SLR Data

SLR data are available as a back-up to GPS data and also as an independent check of GPS ephemeris solution accuracy.

SLR data consist of round-trip range measurements to the GP-B spacecraft from an international network of laser ranging ground stations. Orbit determination accuracy from laser ranging measurements is dependent on the number of passes and the spatial distribution of those passes over the solution interval. Due to GP-B's inertial pointing attitude and the placement of its retro-reflectors (on only one end of the spacecraft) laser measurements can only be sampled on the portion of the orbit closest to the guide star and mostly only over the Northern Hemisphere. Consequently, SLR solution accuracy is limited by both geometry and sampling frequency.

There is significantly more variation in the amount of SLR data received each day than in the amount of GPS data received each day. Figure 4-10 shows a history of GP-B SLR passes to date. SLR tracking was initiated in late-July of 2004, and passes have varied from 0 to 17 passes per day (or 0 to 20 passes per day over the nominal 30-hour GP-B orbit determination solution interval). To date an average of about 5 SLR passes are collected per day. A minimum of 3 or 4 passes are typically required to obtain a valid solution. An attempt is always made to obtain as many observations as possible, but it is impossible to control factors such as weather. It is estimated that at some sites, cloud cover is too great for laser ranging 50% of the time.

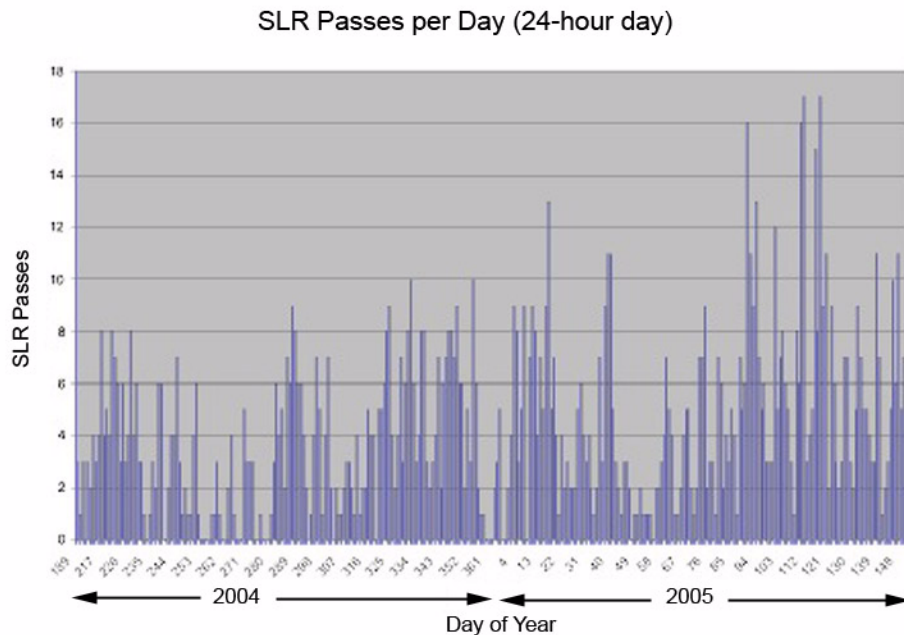


**Figure 4-10.** SLR passes per day

For comparison purposes, orbit determination using SLR data was performed in a manner identical to that using GPS data (i.e., Microcosm software is used along with a 35x35 jgm3 gravitational model, lunar-solar and earth-tide effects, a constant radiation pressure model and Jacchia '71 density model, and the solved-for state consisted of position, velocity, drag coefficient and two sinusoidal in-track accelerations at orbital period).

Two checks were performed to assess the accuracy of SLR orbit solutions. The first check compares each 30-hour SLR solution with the corresponding 30-hour GPS solution for that day. These 30-hour comparisons have yielded differences that ranged from  $\pm 0.5$  meters to  $\pm 20$  meters in the cross-track direction and from  $\pm 15$  meters to more than  $\pm 150$  meters in the in-track direction (although in rare cases of bad geometry and few passes they have been as large as  $\pm 1.5$  km).

The second check of SLR solutions consists of a 6-hour overlap compared with the previous day's SLR solution. To date, the 6-hour SLR overlaps for cross-track vary from a couple of meters at best to about 400 meters at worst. In-track errors vary from about 5 meters to over 100 meters. Maximum daily cross track overlap errors for SLR and GPS ephemeris segments are compared during part of 2004 in Figure 4-11.

Based on comparisons performed to date GP-B SLR orbit solutions have exhibited errors approximately 10 times larger than those using GPS data. If necessary, those SLR results could be much improved by fitting several days of SLR data together into longer ephemeris segments.

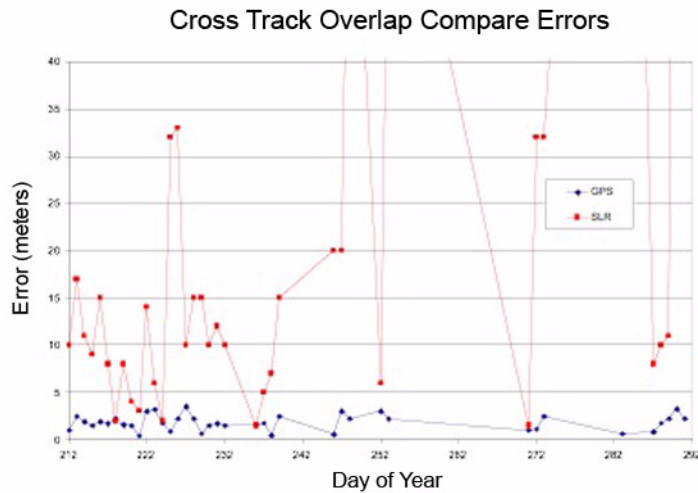


**Figure 4-11.** Comparison of GPS and SLR Cross-Track Errors.

#### 4.4.5 Conclusions

Detailed pre-launch planning for any launch day plus a precise launch on a Delta II 7920-10 allowed the Gravity Probe-B satellite to attain an orbit that satisfied all mission control requirements even though the IOC period was considerably extended.

Accurate and abundant GPS measurements used in the commercial Microcosm orbit determination program have allowed the GP-B ephemeris to be constructed to within all accuracy requirements throughout the mission.

### 4.5 Computer Hardware

The stability of the ground hardware played a vital role during all operational phases of the Gravity Probe B mission. The Stanford Mission Operations Center (MOC) computer network is a state of the art system used for ground commanding and real time telemetry. The Science network is used primarily for science analysis. Both networks are UNIX based and proved to be remarkably robust during all phases of the mission. [Figure 4-12](#) shows a block diagram of the hardware network

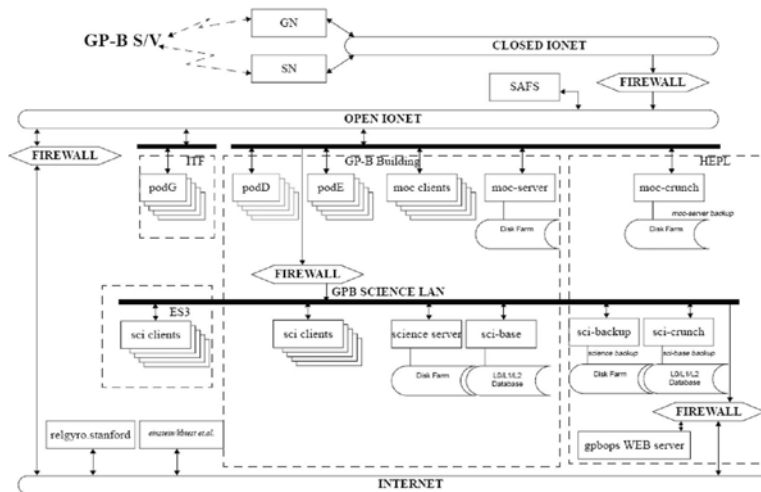


**Figure 4-12.** GP-B Computer Network.

### 4.5.1 Reliability

The computer hardware performed near flawlessly during the Gravity Probe B mission. The moc-server had an uptime of 290 days before a breaker was accidentally tripped during a routine cleanup causing a reboot.

During the IOC phase of the mission, two hardware malfunctions occurred, both involving hard drives. The POD E5 client disk failed, as did the Science server boot disk. Both disks were replaced within 45 minutes, and no data were lost.

During the science phase of the mission, several computer power supplies failed, but were replaced within 2 hours (MOC specifications require 24 hour turn around time). The SUN blade computers, the main class of computer on both the MOC and Science Networks, performed exceptionally well.

No problems were reported during the calibration phase of the mission.

Despite repeated attempts, neither network was ever compromised by hackers. Logs routinely showed hacker attempts on our clients connected to the open IONET. However, our firewall did an excellent job keeping hackers off our science net – not a single entry was recorded.

### 4.5.2 Disk Storage Issues

Disk storage proved a particular problem during the Gravity Probe B mission, with space requirements consistently underestimated.

The extension of the IOC phase did cause several problems for the hardware group, although more from a management standpoint than from equipment concerns. In particular, prior to launch, the decision was made to lock down all hardware modifications, even though disk usage was close to maximum. Considering a 44 day IOC, the decision to increase disk storage after IOC seemed reasonable. Unfortunately, increased storage needs due to an extended IOC caused disk usage to max out several times. User disk storage space was increased shortly after the end of IOC, and has been sufficient.

The GP-B database was similarly stressed, as storage requirements increased and necessary database maintenance postponed. Fortunately the database was fully checked out several weeks prior to launch, and efficiently managed during IOC. Prelaunch predictions underestimated the amount of data to be stored, requiring the acquisition of significantly more data base storage space.

Overall, the storage issues did not significantly affect users of the data, but serve as a valuable “lesson learned” for future missions.

### **4.5.3 System Design – MOC LAN**

The MOC as configured provided reliable support throughout the GP-B mission. It easily fulfilled all requirements; no systemic changes were needed. However, post launch two issues arose that would have impacted the system design had they been requirements: SN/GN desktop reconfiguration, and autonomous operation of MOC. These issues fall into the category of lessons learned, and are covered below.

#### **4.5.3.1 SN/GN Desktop Configuration**

The podD-podE design always assumed that should podD go down, the Mission Operations team would restart podE as the prime pod and continue with only a ~5min downtime. However, it turned out that changing an SN or GN site from connecting with podD over to connecting with podE took much, much longer (on the order of 30 minutes). Thus, the Mission Operations guideline was changed to fix podD, instead of attempting to swap in podE in its place. In hindsight, a simple hardware design of adding a firewall that allowed the use of “pseudo” IP addresses, so that the SN/GN stations would always connect to the same IP address, would have enabled a switch between podD and podE, without the outside stations ever knowing the difference, allowing the “5 min” switch-over to podE to be accomplished.

#### **4.5.3.2 Autonomous MOC operations.**

In the present hardware design, for S/W on podD to send a page for a RTworks out-of-limit violation requires 22 independent electronic boxes (over four separate LANs) be functional from the incoming T1 line to the outgoing SU internet router. A completely different approach to the pod design would have allowed this to be reduced to ~6 boxes for autonomous operation—two of which are redundant servers.

### **4.5.4 System Design – SCIENCE LAN**

Sybase servers are the only major components of the SCIENCE LAN that changed since launch, and this was due to the need to increase disk capacity by ~50%. The safest approach was to create an entirely new server (“sci-base”), and have the DBA run many regression/stress tests on it. After passing all the tests, the new server’s data were synchronized and then the new server was made the production server. Hence, the mission went from one server that had both NFS and Sybase responsibilities, to two servers—one with NFS server and the other as the primary Sybase server. Since Sybase recommends running the Sybase application program on its own server, the new configuration is preferable

### **4.5.5 Performance**

For operations, only one performance-related issue was noticed during the GP-B flight mission: On launch day, podE went down due to an OASIS “overload” situation.

All the MOC workstations were running 100Mbit/sec Ethernet. The highest real-time downlink rate from the S/V was 32Kbit/sec. So, the LAN had a maximum bandwidth ~3 orders of magnitude above the incoming bit stream. The incoming bit stream arrives at podE1, and from there it is sent to OASIS on podE2 and to RTworks on podE3. OASIS or RTworks displays can be “sent” to any MOC workstation, and this was accomplished via the “Xterminal” protocol. This protocol can require very extensive LAN bandwidth.

On the day of the launch, many of the Responsible Equipment Engineers had opened multiple RTworks displays, in order to best monitor their equipment. Early on launch day, so many displays were “sent” to other workstations that OASIS fell so far behind keeping up in real-time that it crashed. The impact was immediately noticed, and the work-around quickly determined— simply close displays. The team was alerted, and through continuing training, this problem never recurred.

A better distributed processing solution would have been to run OASIS on any workstation that needed OASIS displays, and simply pipe the low-bandwidth-telemetry to those workstations (i.e. do not use the Xterminal protocol, run multiple instances of OASIS instead).

## 4.6 The Integrated Test Facility (ITF)

The Integrated Test Facility (ITF) is composed of flight-equivalent electronics boxes, software, and hardware simulators which model the GP-B space vehicle. The Pods in the ITF are computers designed to run and operate the vehicle ground support software. In early phases of program development, the ITF is used to 1) test flight hardware for proper operation prior to being installed on the spacecraft, 2) test hardware interfaces, 3) resolve hardware discrepancies, and 4) develop and test flight software. Later in the program, the ITF is used to run test scenarios to verify software and operations sequences. The ITF also provides a flight-like space vehicle simulation for the operations team to use during mission rehearsals. During the on-orbit phase of the program, the ITF is used to test sequences prior to being run on the vehicle and troubleshoot flight anomalies. The ITF has been an important GP-B resource to reduce program risk

The electronic boxes in the ITF are listed in [Table 4-11](#) below. Each unit is categorized as a Engineering Unit (EU) or Functional Equivalent Unit (FEU). A photograph of the ITF hardware is shown in [Figure 4-13](#).

**Table 4-11.** ITF equipment list

EQUIPMENT	TYPE
Command / Control Computer Assembly (CCCA)	FEU
Command and Telemetry Unit (CTU)	FEU
Attitude Control Electronics (ACE)	-----
Aft Experiment Control Unit (Aft ECU)	FEU
Fwd Experiment Control Unit (Fwd ECU)	FEU
Interface Unit (IU)	FEU
Global Position System Receiver A (GPS “A”)	EU
Global Position System Receiver B (GPS “B”)	EU
Aft Gyro Suspension System 1 (AFT GSS1)	EU
Aft Gyro Suspension System 2 (AFT GSS2)	EU
Aft Gyro Suspension System 3 (AFT GSS3)	FEU
Aft Gyro Suspension System 4 (AFT GSS4)	EU
Fwd Gyro Suspension System 1 (Fwd GSS1)	EU
Fwd Gyro Suspension System 2 (Fwd GSS2)	EU
Fwd Gyro Suspension System 3 (Fwd GSS3)	-----
Fwd Gyro Suspension System 4 (Fwd GSS4)	-----
Aft Squid Readout Electronics A (Aft SRE A)	FEU
Aft Squid Readout Electronics B (Aft SRE B)	EU
Fwd Squid Readout Electronics A (Fwd SRE A)	FEU



**Table 4-11.** ITF equipment list

EQUIPMENT	TYPE
Fwd Squid Readout Electronics B (Fwd SRE B)	FEU
Star Sensor A (SS A)	-----
Star Sensor B (SS B)	-----
Solid State Recorder (SSR)	EU
Telescope Readout Electronics A (TRE A)	EU
Telescope Readout Electronics B (TRE B)	-----
Transponder A (XPDR A)	FEU
Transponder B (XPDR B)	-----

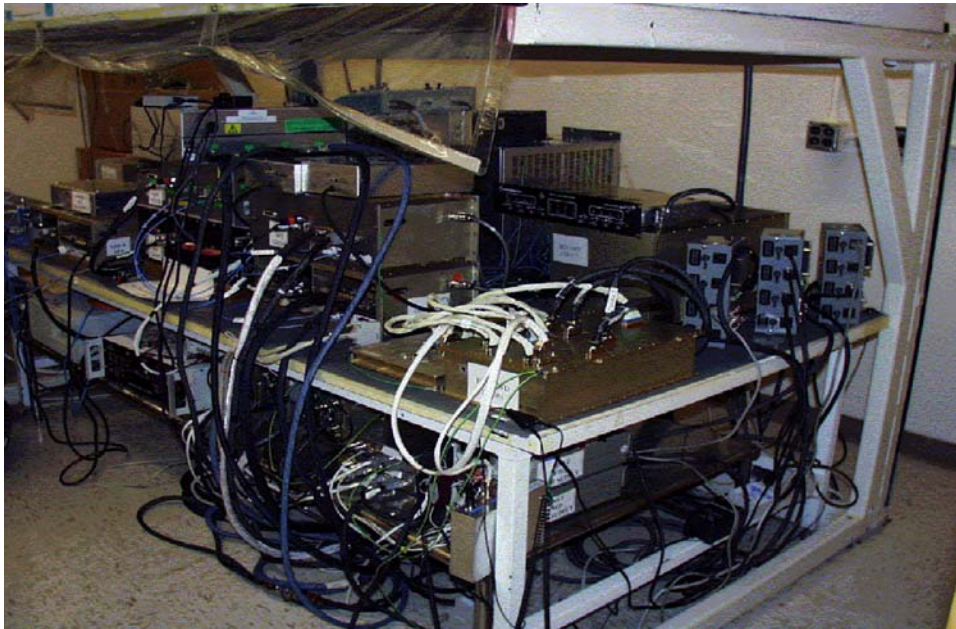


**Figure 4-13.** The Integrated Test Facility (ITF) flight simulator hardware in a Clean Room at Lockheed Martin

A detailed description of the ITF can be found in Integrated Test Facility (ITF) User's Guide (LM/P480818 1/20/2004).



# 5

## Managing Anomalies and Risk

---





## 5.1 The Spacecraft's Tale

We begin this chapter with a GP-B Mission News story entitled “The Spacecraft's Tale,” that was featured in our Weekly Status Update, posted on our GP-B Web site and sent out to our email subscriber list on December 10, 2004, following an anomaly with the spacecraft's GPS system that occurred over the South Atlantic Anomaly region of the Earth.

Last Saturday began as a rather “ho-hum” California winter's day. Orbiting the Earth every 97.5 minutes, the GP-B spacecraft passed directly over California around 6:30AM PST, but the Sun was already up, and the sky was too bright to see the satellite. In the GP-B Mission Operations Center (MOC), a skeleton crew, consisting of the on-duty Mission and Flight directors and one or two resident engineers, monitored several telemetry passes (communications sessions) during the morning hours. Most were 25-minute satellite passes, during which the spacecraft relays status information to the MOC through the NASA TDRS (Tracking and Data Relay Satellite) communications satellite system. And, during a 12-minute ground pass at 1:15PM PST, the spacecraft's solid-state recorder relayed relativity data to the GP-B science database through a high-speed telemetry connection with the Svalbard ground tracking station in Spitsbergen, Norway. All in all, it was a normal Saturday, and the atmosphere in the MOC was quite relaxed.

Following the successful ground pass with Svalbard, the spacecraft continued on its southward route. At around 1:30 PM PST, Pacific time, the spacecraft was flying over South America—heading towards the South Pole—when it entered the South Atlantic Anomaly (SAA). This is a region above the Earth where the fluxes of trapped protons and other particles, emitted by the Sun, are much greater than anywhere else on Earth, due to the asymmetry of the Earth's protective Van Allen Radiation Belts. Thus, spacecraft are more vulnerable to being struck by protons when flying through this region.

At 1:48PM, Pacific Time, an odd event silently occurred on-board the spacecraft, triggering four safemodes (pre-programmed command sequences designed to automatically place the spacecraft, its gyros, telescope, and other systems and instruments, in a stable and safe configuration in response to anomalous or out-of-limits feedback from various on-board sensors).

Back in the MOC, the next telemetry pass was not scheduled until 3:16 PM, so the operations staff was completely unaware of this change in the spacecraft's condition—for the time being. At 3:15PM, the MOC staff settled into their seats for the upcoming satellite status telemetry pass. As the spacecraft's antenna locked into the TDRSS satellite and began transmitting, one-by-one, status monitors around the MOC began turning red, signaling the spacecraft had triggered its safemodes. There is a problem on-board.

During the next 20 minutes, phones rang, pagers beeped, and soon, the MOC was teeming with activity. An assessment of the safemodes that were triggered indicated that an error—never seen before—had occurred in a module of the Attitude and Translation Control (ATC) computer system. The spacecraft's GPS had registered an off-the-scale velocity spike, which if correct, indicated that, for one brief moment, the spacecraft had traveled faster than the speed of light—or to use Star Trek terminology, it had “warped into hyperspace.” In fact, the GPS system had reported a single data point with an erroneously high velocity, which when squared, caused a computer overflow. The ATC computer module took exception to this data overflow and triggered a safemode test, which in turn activated a chain reaction response sequence.

The MOC staff immediately scheduled several extra satellite communication passes so they could communicate with the spacecraft more frequently. Then, over the ensuing 24 hours, they methodically worked through a series of tests and command sequences to return the spacecraft to its normal science operation mode. We initially assumed that the GPS receiver had suffered a proton hit in the SAA region, but further analysis suggests that this was not the case. Rather, this anomaly was apparently caused by one of the four accessible GPS satellites being in the wrong position for proper GPS triangulation. The ATC system usually catches situations of this kind and disallows the data; but, this one was out of range before the data reached the filter.

The spacecraft has returned to normal operations. This incident was not detrimental to the GP-B experimental data. And, once again, the fact that an anomalous event occurred while the spacecraft was flying through the SAA region appears to be a coincidence—or is it?

## 5.2 Overview of GP-B Anomalies in Orbit

The Spacecraft's Tale above typifies the anomaly discovery, review, and resolution process that our Mission Operations Team and Anomaly Review Board worked through time and again during all phases of the GP-B mission. The details were different in each case, but the discovery, analysis, and resolution process was always the same.

Over the course of the flight mission, the GP-B Anomaly Review Board (ARB) successfully worked through 193 anomalies/observations. Of these, 23 were classified as true “anomalies,” five of which were sub-classified as “major anomalies,” including the B-Side computer switch-over and the stuck-open valve problems with two micro thrusters early in the mission, as well as subsequent computer and subsystem reboot problems due to radiation strikes. Of the remaining 18 anomalies, 12 were sub-classified as “medium anomalies” and 6 were sub-classified as “minor anomalies.”

The 170 other issues (88%) were classified—at least initially—as “observations.” These observations typically documented various unanticipated events, sub-optimal parameter settings, and other odd results that were monitored until their root cause was understood. In several cases, observations were escalated to anomaly status, and then necessary actions were taken not only to understand, but also to correct the problem. In all cases, the established anomaly resolution process enabled the team to identify the root causes and provide recovery procedures.

Section [5.3 Anomaly Review Process](#) below provides a complete description of the GP-B anomaly review process that was used to work through all observations and anomalies. [Appendix D, Summary Table of Flight Anomalies](#), shows the complete list and status of all 193 observations and anomalies that were worked throughout the mission.

Section [5.4 Risk Analysis](#) below provides an overview of GP-B's risk management strategy, including a summary of current risk items and their planned mitigations.

## 5.3 Anomaly Review Process

Gravity Probe B uses a formal anomaly review process to assess, manage, and resolve vehicle or ground system anomalies when they occur. Processes and training of team members are in place to ensure that all identified issues are addressed in a uniform manner and the entire team (Stanford/Lockheed-Martin/NASA) are kept apprised of the status of all anomalies and associated mitigation efforts.

### 5.3.1 Anomaly Definitions

An anomaly is any unanticipated or undesired event, condition or configuration of the spacecraft or ground equipment. Anomalies are generally indicated by:

- Timeline execution via pre-programmed failure paths
- Safemode activations
- Real-time monitoring of subsystem behavior
- Off-line data analysis (engineering or science trending)

Anomalies are classified into 4 categories:

1. **Major Space Vehicle Anomalies**—Major Space Vehicle Anomalies endanger the safety of the spacecraft and/or the payload. These anomalies generally have contingency plans that have been pre-approved for immediate identification and response within the MOC at the direction of the Flight Director. Response to these anomalies is time-critical.
2. **Medium Space Vehicle Anomalies**—Medium Space Vehicle Anomalies do not endanger the safety of the space vehicle but may impact the execution of planned timeline. These are the most probable type of anomaly because the vehicle safing mechanisms are designed to allow the vehicle to be autonomous for 72 hours given any single failure. The response to these anomalies is not time-critical if addressed within the 72 hour window.
3. **Minor Space Vehicle Anomalies**—A Minor Space Vehicle anomaly does not endanger the safety of the space vehicle and does not stop the execution of the timeline. These anomalies also do not have any long-term implications to on-orbit operations. This category covers extremely low risk problems with the vehicle that are typically completely corrected by taking the appropriate corrective action.
4. **Space Vehicle Observations**—In addition to formal anomaly categories, the space vehicle may exhibit off-nominal or unexpected behavior that does not appear initially to be an operational or functional issue and does not violate any limits, but may warrant attention over time. Any team member who notices such issues contacts the anomaly room with the report. These items are designated an “observation” and will be reported daily to the Mission Director and the program on a daily basis, and are resolved on a time-available basis. Observation items may be elevated to an anomaly category if it is judged to be serious enough to warrant a high-priority investigation.

### 5.3.2 Anomaly Review Organization

The anomaly review process is organized into three different entities: the *Anomaly Resolution Coordinator*, the *Anomaly Review Board*, and a number of *Anomaly teams and Engineering Analysis teams*. The roles of these entities are outlined in [Figure 5-1](#) below.

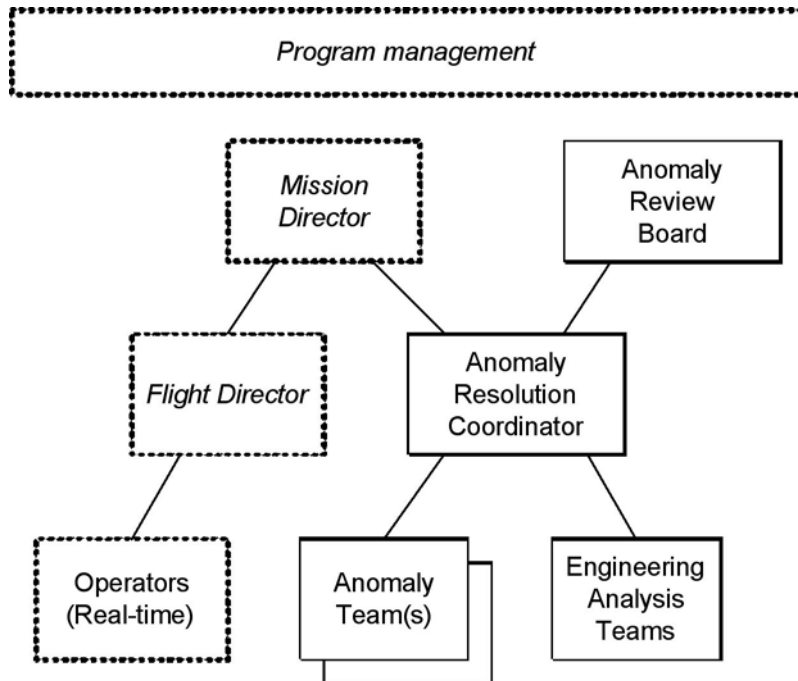


**Figure 5-1.** Anomaly Review Team Organization

### 5.3.2.1 Staff: Anomaly Resolution Coordinator

The *Anomaly Resolution Coordinator* function is staffed by a small team of system engineers to accomplish the following management and control functions:

- Receive, log, and track anomalies as reported by the Mission Director or Anomaly Review Board Chair
- Receive, log, and track real-time vehicle commanding requests; convene the Anomaly Review Board for screening and approval.
- Form and manage Anomaly Teams under direction of the Anomaly Review Board chair.
- Coordinate anomaly resolution activities with Anomaly Review Board.
- Report anomaly status to the program via a daily written summary report.

This position is a 7-day staffed position in a dedicated “Anomaly Room” near the Mission Operations Center (MOC) to enable rapid assessment of anomalies by the program. This position is staffed 24 hours by 7 days/week early in the mission, 16 hours by 7 days/week during the in-orbit checkout period (IOC), and 10 hours by 5 days a week during the science data gathering activities. Staffing levels are increased during critical vehicle operations or during the assessment and resolution phases of major or medium anomalies.

### 5.3.2.2 Staff: Anomaly Teams

An *Anomaly Team* is a group of technical experts assigned to investigate a particular anomaly. These teams report their status to the Anomaly Resolution Coordinator and to the Anomaly Review Board when requested. The teams operate on an on-call basis and the membership is ad-hoc based on the needs of a particular anomaly.

### 5.3.2.3 Staff: Anomaly Review Board

The *Anomaly Review Board*, or simply the *ARB*, oversees the program-wide anomaly assessment and root cause investigation. This board is composed of senior Stanford University, Lockheed-Martin, and NASA technical managers who have broad knowledge of the operation of the spacecraft, the payload, and the overall science mission.

Each day, an anomaly board member is designated as the anomaly room chairperson. The anomaly review board convenes during anomaly investigations; during non-anomaly periods the board members are generally engaged with other program activities. This board:

- Determines the membership of the anomaly teams.
- Assesses the technical approach of the anomaly teams.
- Oversees the progress of the investigations.
- Prioritizes program resources for the various investigations.
- Makes final recommendation to the program for anomaly resolution.

Members of the board are available on an on-call basis and will be available on a 24 hour, 7 day/week schedule.

### 5.3.2.4 Staff: Engineering Analysis Teams

The Engineering Analysis Teams are the program technical experts who monitor and assess the health and performance of the spacecraft and payload, but are not part of the real-time operations. These groups include teams from Stanford, Lockheed-Martin, and NASA MSFC.

All of these teams monitor the operation of the spacecraft and payload in both real time and through off-line data processing and analysis. In the event that an anomaly or issue is noted by any of these teams, the team lead contacts the anomaly room or the Mission Director to report the issue.

## 5.3.3 Anomaly Assessment

Upon receipt of a new anomaly report, the Anomaly Coordinator and the Anomaly Review Board evaluates the anomaly using a detailed checklist. In summary, the board will:

1. Assess vehicle safety issues.
2. Assess dewar lifetime implications.
3. Assess short and long term mission implications.
4. Estimate response time requirement.
5. Schedule an initial screening with the subsystem REs and Anomaly Board members.
6. Identify priority among other anomaly team activities
7. Identify near and long-term timeline flow implications.
8. Determine anomaly team membership
9. Develop fault tree to find root cause.
10. Formulate investigation schedule and identify key decision points.



### 5.3.3.1 Anomaly Investigation and Resolution

Once the vehicle is in a safe configuration the Anomaly Team lead, in consultation with the Anomaly Review Board and the Anomaly Resolution Coordinator, develops, tests, and implements a plan to isolate and correct the anomaly.

After an Anomaly Team has performed its analysis, they meet with the Anomaly Review Board and recommend any resolution options to correct the problem or any further investigative steps they feel need to be made to come to a resolution method.

The Anomaly Resolution Coordinator and the Anomaly Review Board then decides upon a resolution method and grants approval to implement the mitigation.

- If the resolution consists of an already-existing contingency procedure that the Anomaly Board approves for use as is, the procedure will be executed in the appropriate manner, usually by an SPC load
- If the contingency procedure does not exist, the Anomaly Team will develop the appropriate procedure, soliciting whatever additional help they need via the Anomaly Review Board. The procedure will undergo off-vehicle testing prior approval.

### 5.3.3.2 Management Reporting

In the event of a major space vehicle anomaly the Flight Director immediately notifies the Stanford University Program Manager in parallel with the Mission Director. The Mission Director and Program evaluates the anomaly and reports their findings to the MSFC Program Manager or his designee. Other classes of anomalies are reported to Program Management through the Mission Director as soon as practical aft the board's initial assessment.

### 5.3.3.3 Anomaly Closure

Once the root cause of the anomaly has been identified, and rectifying or mitigating activities are complete, the Anomaly Team and Anomaly Review Board will submit the anomaly for closure to the Mission Director. After review, the Mission Director will close the anomaly in the ARB database.

## 5.3.4 Anomaly Room

An *anomaly room* has been setup outside the MOC as a common meeting area for review and analysis of anomalies. The room has been designed to collect vehicle data from a variety of sources, act as a library of the key vehicle technical schematics and operations documentation, and permit multi-mode communication with both on-site and remote members of the GP-B team.

#### ***Mission Operations Data:***

- Non-commanding ops console set (POD) to shadow PODs in MOC for real-time data display.
- RTWorks display showing vehicle health and safety data.
- Access to post-processed vehicle database with a variety of tools.
- Copies of Lockheed-Martin SDRLs, engineering memos.
- Copies of Flight Ops Handbook.
- Safe mode logic, activation, and recovery plans.

***Space Vehicle Operations Data:***

- Schematics, specs for vehicle components.
- Software listings for flight software modules.
- Telemetry and telemetry formats lists.

***Communication and data analysis resources:***

- Conference phones.
- Voice loops to MOC, engineering analysis area.
- Secure network connections to Stanford, MSFC/VRC, and LM systems (via VPN).
- Secure web publishing of notes and anomaly data.
- Fast color scanner, photocopier, FAX machine.
- Web-based access to radio pagers/cell phones.

Figure 5-2 shows a photo of the anomaly room. Most of the information resources noted above can be seen.



**Figure 5-2.** GP-B Anomaly Room Layout

### 5.3.5 Anomaly Identification and Response Plan

The following is an outline of the steps to be followed in response to an anomaly. Note, iteration will likely be required within this plan as an anomaly investigation proceeds:

1. Any real-time operations team member that suspects an anomaly informs the current shift Flight Director.
2. The Flight Director, Mission Director, or Anomaly Review Board member collects information and recognizes it as an anomaly.
  - In the event of a major anomaly, the Flight Director uses pre-approved contingency procedures to safe the vehicle where possible.
  - In the event of a medium anomaly, the Flight Director consults with the Mission Director and Anomaly Review Board on a course of action.
  - In the event of a time minor anomaly, the Flight Director uses pre-approved contingency procedures or flight rules to recover from the anomaly.
  - In the event of an observation, the Anomaly Review Board informs the Mission Director and the system RE of the observation for evaluation.
3. The Flight Director notifies continues to assess the real-time operations issues and timeline impact of the anomaly.
4. The Anomaly Resolution Coordinator convenes the Anomaly Review Board, briefs the board on the anomaly, commissions an Anomaly Team, and coordinates with the board for resources, schedule, and milestones for investigation.
5. The Mission Director works with the Anomaly Review Board to assess short and long-term implications to the mission timeline.
6. The Anomaly Coordinator tracks the actions of the Anomaly Team and maintains the status documents (databases) for the program.
7. The Anomaly Review Board manages Anomaly Team's activities and augments the makeup of the team as needed to successfully understand the anomaly.
8. Once the anomaly is understood, the Anomaly Coordinator and the Anomaly Review Board proposes a plan for resolution. Should this anomaly require software changes or procedure changes, the Anomaly Resolution Coordinator will work with the Anomaly Team and the Flight Software Team to generate the appropriate change paperwork.
9. The Anomaly Review Board reviews and endorses recommended mitigations from the Anomaly Teams and coordinates their insertion into the timeline with the Mission Director. The interface between the Board and Mission Planning is via the Timeline Change Request (TCR) process. If real-time commanding is required, a Pass Plan Change Request (PPCR) is coordinated with the Flight Director.
10. The Anomaly Coordinator briefs the Flight Director of the chosen course of action.
11. The Anomaly Team monitors and assesses the effects of the mitigations via flight telemetry and reports results to the ARB.
12. The ARB and Anomaly Team assesses downstream implications of anomaly and possible operational changes to mitigate any negative effects.
13. The Anomaly Resolution Coordinator completes the post anomaly report.
14. The Mission Director closes the anomaly when mitigations are complete.

These steps are used to address all issues, from simple observations to major anomalies. This ensures that all issues are addressed in a uniform manner, that open vehicle issues are communicated to entire team on a regular basis, and that the issues are properly documented.

### 5.3.6 Overall Effectiveness of GP-B Anomaly Resolution Process

The anomaly resolution process described above was developed and perfected during seven pre-launch mission simulations and proficiency exercises. Lessons learned from each simulation were incorporated into the anomaly plan to create an effective and efficient process for the GP-B mission.

Since launch, 193 anomalies/observations have been identified (through 13 October 2005): 5 major anomalies, 12 medium anomalies, 5 minor anomalies, and 170 observations. This process was used to deal with all of these issues, and we have found that this anomaly resolution process is:

<b>Effective:</b>	Anomalies are understood and corrected with little long term mission impact. The technical teams were able to use the tools and structure provided to identify the root causes of the issues and mitigate them as appropriate.
<b>Efficient:</b>	Heavy staffing, extensive training, and good communications technology brings teams together rapidly and allows for efficient communications. The concentrated information resources in the anomaly room allowed the vehicle state to be determined rapidly and hypotheses to be checked quickly during the assessment phase of investigations.
<b>Transparent:</b>	All anomaly data made available “instantly” to the entire GP-B team via a secure web server. This allowed team members around the world to follow progress and contribute their expertise
<b>Robust:</b>	Good training of members allows team members to work a variety of ARB roles when necessary. The process does not rely on a few “key” members; it allows a significant group of people to fill the individual roles effectively.

In summary, the process has been very effective and may serve as a model for other spaceflight programs. A detailed summary of all mission anomalies and observations is found in [Appendix D, Summary Table of Flight Anomalies](#).

## 5.4 Risk Analysis

The GP-B Risk Management Plan (S-O423) documents the approach that was successfully implemented on GP-B.

### 5.4.1 Forward to GP-B Risk Management Plan

Risk management process involves open communication among our organizations, with the customer, our suppliers and other external interfaces. It is imperative that management create an atmosphere which welcomes risk identification without fear of personal consequence.

### 5.4.2 Purpose

The establishment of a risk management process provides a disciplined approach to the identification, analysis, and resolution of risk factors which may adversely affect ultimate program success. The goal of the risk management effort is to provide the proper balance between risk and the elements of cost, schedule, and technical performance thus assuring program success.

### 5.4.3 Risk Management Approach

The risk management process (Figure 5-3) is a continual process that assesses both the evolving state of the program (technical, cost, schedule) and the progress against active risk mitigation activities. The risk management process begins by identifying potential program risks.

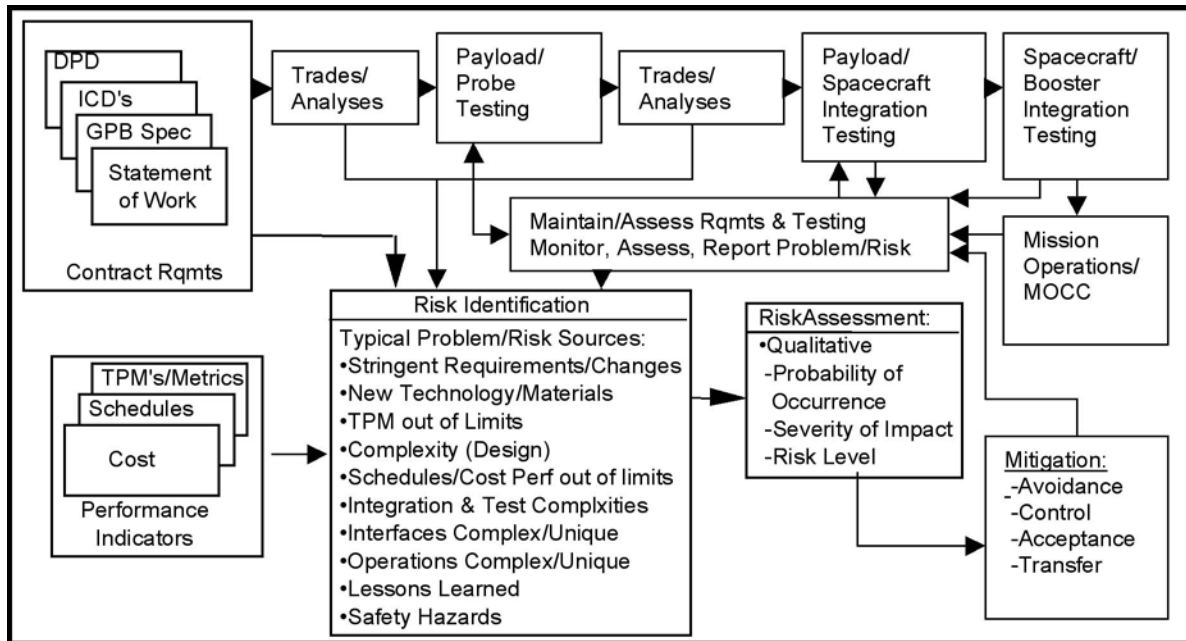


Figure 5-3. For each risk, an assessment is completed by the identifying team or person

Risk mitigation plans are developed and executed for risks comprised of one or more of the following strategies (1) avoidance: requirements relaxation and/or elimination; (2) control: testing, training, procedures, margin allocation, second source, parallel design; (3) acceptance: monitor only; and (4) transfer: move the risk to another area. Mitigation plans are implemented by the affected team, who establish monitoring methods which ensure that new problems are identified and resolved.

Program risk is monitored by the Risk Steering Group chaired by the Stanford program manager and includes participation from Lockheed Martin program manager, MSFC resident manager, and other senior managers on the GP-B program.

### 5.4.4 Risk Metric and Items

Formal GP-B risk management was started in October 2000. A metric showing the rate at which risk items were identified and closed is shown in Figure 5-4. All risk items were either closed or accepted prior to launch.

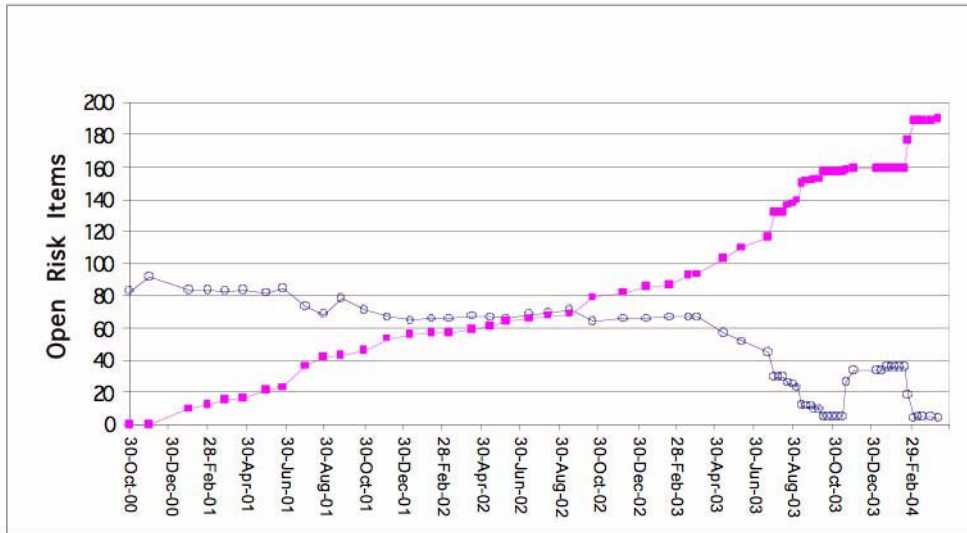


**Figure 5-4.** Metric of risk item closure prior to launch of GP-B. All risk items were either accepted or closed prior to launch.

During the on-orbit phase of the mission, we continued the risk management approach on GP-B. [Table 5-1](#) provides a summary of the open risk items at the end of the IOC phase. [Figure 5-5](#), [Figure 5-6](#), and [Figure 5-7](#) provide the open risk items at the end of the science mission phase.

Risk management was successfully implemented on GP-B and provided a disciplined process to identifying and managing program risk.

**Table 5-1.** Summary of Open GP-B risks at the end of IOC

Risk #	Subject	Owner	Mitigation
5	B side switch impact to attitude and recovery to star. SV rolls down to 0.1 rpm on b-side switch.	Barry	Draft B-side safemode recovery procedure completed. Walk-through scheduled for 9/14/04. Close risk when procedure and training are completed. On-call team available for recovery. Reassess the limits for DBE test activation. Plan B-side table top rehearsal and additional FD & MD training for initial actions to stop roll down.
22	Maintain ATC attitude control for science	Kirschenbaum	Recent improvements made in pointing performance. Roll phase variation improvement expected by star tracker alignment implemented on 9/10/04. Monitor ATC attitude performance. RTWorks upgrade in work for loss of star identification. Watch.
25	Loss of suspension due to untested post spin up operations	FD,MD,ARB	Continuous mitigation - Increased vigilance on PPCR's and changes. Maintain constant MOC discipline. Minimize GSS commanding.
29	Roll Frequency Accelerations at Rotor. SI at roll. Variation is sum of the squares of voltages on one electrode axis.	Keiser	Open – Watch – continue to monitor. Preliminary look by Alex advises we are OK.

**Table 5-1.** Summary of Open GP-B risks at the end of IOC

33	Drag-free control.	Bencze	Open – Mitigation in work (obs 98 & 110). Mitigation is more on-orbit assessment and parameter tuning. On-going investigation into cause. Develop methods to improve.
35	Double bit errors	Perry	<p>The following actions will be taken to mitigate and improve response to MBE's:</p> <p>Colin Perry will lead the closure of the following and will brief ARB and MD when complete:</p> <ol style="list-style-type: none"> <li>1. Obtain a complete memory dump of the freshly-rebooted MSS in the ITF, make that available at SU for rapid comparison.</li> <li>2. Expand upon MJ's email of 8 Sept to define sections of MSS memory to functionality, attempt to attach criticality to those sections.</li> <li>3. RTWorks limit checking of double bit diag monitor BC_TlmDiag06. MJ, could we use "set io_directive" to write x#000000 to that location after clearing this error.</li> <li>4. Training of FD, MD personnel in the detection and repair of this type problem. (Maggie to provide areas of MBE of concern). MD to be immediately notified of MBE's. (Steve Larsen to look at MBE impact on GSS).</li> </ol>



**Risk Overview**

GP-B Ops  
Flight Projects Directorate

Rank	ID	Risk Statement	Planned Closure	Status	Approach	Owner	Management Comments
				L/C	Active Plan		
1	GP-B Ops-01	<b>Early End of Mission because of Inadequate Safemode Response</b> Description: The Space Vehicle must recover from safe mode quickly in order to prevent excessive disturbances on the science gyros from loss of attitude and drag-free control. Impact: Early end of science mission, but with science collection consequence diminishing with time.	08/01/05	Open	Mitigate	Tony Lyons	All safemode tests and responses have been reviewed and the results implemented. State-tracking checklist has been developed to improve situational awareness and aid science team. Flight Director and Mission Director have been given authority for initial actions to stop roll down. Limits for multi-bit error test activation have been reassessed.
	<b>M</b>			L: 2 C(c): 1 C(s): 1 C(t): 4	Scrub/update safemode procedures. Practice simulations for B-side recovery. Increase communication requirements. Patch over multi-bit errors. Develop state-change checklist for recovery.		
2	GP-B Ops-02	<b>Degraded Science because of Degraded Attitude Control</b> Description: Build-up of attitude errors and biases causes excessive disturbances on the science gyroscopes. Impact: Degraded science, but diminishes with time	08/01/05	Open	Mitigate	Tony Lyons	The roll-notch filter has been implemented successfully. Pointing performance and roll phase variation has improved.
	<b>M</b>			L: 2 C(c): 1 C(s): 1 C(t): 4	Monitor attitude performance continually. Conduct ground simulations and analyses. Update control gyro biases and other parameters weekly. Implement roll-notch filter.		
3	GP-B Ops-08	<b>Degraded or Interrupted Science because of Flight Computer Reboots</b> Description: The flight computer has rebooted several times on-orbit because of multi-bit errors (MBE's) and may reboot more. Impact: Minor interruption of science data most likely, without long term consequences, but the potential for a devastating multi-bit error (MBE) exists.	08/01/05	Open	Mitigate	Tony Lyons	The contingency plan for a rapid reboot recovery, including an EEPROM update to prevent vehicle roll-down, has been developed and used successfully. The safemode response has been updated to "stop timeline" for sequential MBE's. A-side pointing performance has been restored on the B-side, by using A-side control gyros. Reboot fault tree has been developed. Operations Team quickly identifies MBE location and impact. MBE's are corrected via CSTOLs
	<b>M</b>			L: 3 C(c): 1 C(s): 1 C(t): 2	Develop a contingency plan for a rapid reboot recovery. Update the safemode response to "stop timeline" for sequential multi-bit errors (MBE's). Restore A-side pointing performance on B-side. Develop fault tree to determine root cause of reboots and additional mitigations.		

Top 10 Risks As of 5/20/2005

Report Generated by ePORT on May 20, 2005

**Figure 5-5.** (part 1 or 3). Open risk items during on-orbit science mission





## Risk Overview

Rank	ID	Risk Statement	Planned Closure	Status L/C	Approach Active Plan	Owner	Management Comments
4	GP-B Ops-07	<b>Science Interruption because of a Large Solar Flare</b> Description: A large solar flare could blind the science telescope, causing loss of the guide star, and increase the rate of multi-bit errors. Impact: Minor interruption of science data, with no long term consequences.	08/01/05	Open	Mitigate L: 2 Increase the Flight Team's awareness for solar flare activity. Develop a contingency to capture the guide star over the equator. C(c): 1 C(s): 1 C(t): 2	Tony Lyons	The Flight Team continually monitors solar flare activity. The contingency to capture the guide star over the equator has been developed and successfully used to recover from a solar flare.
5	GP-B Ops-03	<b>Degraded Science because of Loss of Drag Free Capability</b> Description: The Space Vehicle already has lost two thrusters. Four remaining thrusters now have no redundancy (#5, 7, 10, 12). The loss of either of these non-redundant thrusters will increase gyro torques and end the Vehicle's ability to fly drag-free. Impact: Degraded science.	08/01/05	Open	Mitigate L: 1 Monitor thruster performance. Maintain stable Dewar flow rate to reduce stress on thruster. Prepare a contingency plan for partial Thruster Isolation Valve (TIV) closure. C(c): 1 C(s): 1 C(t): 4	Tony Lyons	Thruster performance is being monitored continuously. Stable helium flow rate is being maintained. A contingency plan for partial TIV closure has been prepared.
6	GP-B Ops-05	<b>Science Interruption because of Untested Post Spin-up Operations</b> Description: The Science Gyroscopes may lose suspension after spin-up, if untested commands are sent to the Gyro Suspension System, or because of other untested vehicle commanding. Impact: Interrupted science data collection.	08/01/05	Open	Mitigate L: 1 Minimize Gyro Suspension System (GSS) commanding. Implement health and safety checks during each telemetry pass. C(c): 1 C(s): 1 C(t): 4	Tony Lyons	Vigilance has been increased on Pass Plan Change Requests (PPCR's) and changes. Emphasis on constant Mission Operation Center (MOC) discipline has been increased. Health and safety checks during each telemetry pass have been implemented. Additional mitigations will be planned for the post-science calibration phase.

Top 10 Risks As of 5/20/2005

Report Generated by ePORT on May 20, 2005

Figure 5-6. (part 2 or 3). Open risk items during on-orbit science mission



## Risk Overview

Rank	ID	Risk Statement	Planned Closure	Status L/C	Approach Active Plan	Owner	Management Comments
7	GP-B Ops-04	<b>Noise in Science Data because of Excessive Electronics Temperature Variation</b> Description: Excessive temperature variation in forward SQUID Readout Electronic (SRE) introduces noise into science gyroscope data. Impact: More analysis of science data required.	08/01/05	Open	Mitigate L: 1 Monitor the SRE temperature continually and control the temperature set points, especially in hot seasons. C(c): 1 C(s): 1 C(t): 3	Tony Lyons	A process has been implemented to monitor the SRE temperature continually and to adjust the set points as necessary.
8	GP-B Ops-06	<b>Science Interruption from Loss of Both Control Gyros</b> Description: GP-B uses the same control gyros as the Chandra x-ray telescope and one of Chandra's gyros is failing. Impact: Loss of primary Space Vehicle control and interrupted Science	08/01/05	Open	Accept L: 1 Chandra's gyros have lasted longer than the GP-B planned mission and the GP-B gyros have performed flawlessly. Therefore, this risk is accepted. C(c): 1 C(s): 1 C(t): 3	Tony Lyons	Trends of gyroscope currents are being tracked and remain nominal.
9	GP-B Ops-09	<b>Experiment Control Unit (ECU) Not Turning Back On after Power Off</b> Description: The ECU has been turned off, except for a few hours a week, to reduce its noise contribution to the readouts of science gyros #1 and #3. Impact: The ability to monitor the proton monitor, payload magnetometers, GMA heaters, flow meters, and QBS temperature control will be lost while the ECU is powered off. Also, failure of the ECU to turn back on when commanded would cause loss of gyro discharge capability, loss of the ability to perform another heat pulse measurement, no control over QBS temperature, and loss of flow meter helium mass flow rates for end-of-mission predictions.	08/01/05	Open	Accept L: 1 The ECU will be turned back on once a week for a few hours to obtain telemetry. C(c): 1 Pressure telemetry still is available continuously from the Attitude and Translation Control (ATC) system for trending. Contingency procedures are available to turn on the ECU immediately if pressure shows any anomalous behavior. Also, no science impact is expected if the ECU fails to turn back on. Therefore, this risk is accepted. C(s): 1 C(t): 2	Tony Lyons	The appropriate weekly or continuous telemetry is being obtained and trends remain nominal.

Top 10 Risks As of 5/20/2005

Report Generated by ePORT on May 20, 2005

Figure 5-7. (part 3 or 3). Open risk items during on-orbit science mission







The GP-B spacecraft was a total system, comprising both the space vehicle and its unique payload—an integrated system dedicated as a single entity to making the measurements of unprecedented precision (eight orders of magnitude more accurate than the best navigational gyroscopes) required by the experiment. To accomplish this goal, it was necessary for the total, tightly-integrated system to be developed by a strong and cohesive team. This chapter provides an overview of some of the important issues, challenges, trade-offs and practices that were involved in managing GP-B over a period of more than four decades to a successful performance of its mission.

## 6.1 The Phases of GP-B Program Management

NASA generally divides programs into six phases:

- Phase A-Preliminary Analysis
- Phase B-Definition
- Phase C-Design
- Phase D-Fabrication, Assembly and Testing
- Phase E-Mission Operations
- Phase F-Data Analysis & Results Determination

To some degree, all NASA programs progress through these phases. However, often—and especially in the case of GP-B, NASA's oldest continuous research program, whose origins date back NASA's infancy—there is much overlap between phases, and it is difficult to assign these phase labels to distinct chronological periods. Instead, it is more useful to describe GP-B's development and program management in terms of the following five main time periods:

1. **The Early Years (1959-1984)**. During this period, the relativity gyroscope experiment was conceived at Stanford and became a NASA-funded, university research program. The relativity gyroscope experiment evolved into a NASA mission, and was given the name “Gravity Probe B.”
2. **Flight Hardware Development (1984-1997)**. For reasons described in this section, NASA made Stanford its prime contractor in 1984, with NASA Marshall Space Flight Center provided the program's nominal oversight. This decision was dubbed “the GP-B Management Experiment” by James Beggs, the NASA Administrator at that time. Following a rigorous selection process, Stanford contracted with Lockheed Missiles and Space Corporation (LMSC, now Lockheed Martin Space Systems Company or LMSSC<sup>1</sup>) as principal subcontractor for constructing the integrated payload (dewar and probe). In a later, separate selection process, Stanford also selected LMMS for constructing the spacecraft. Towards the end of this period, GP-B made the challenging transition from maximizing research and technology development advances to minimizing risk as the payload and spacecraft were readied for launch.

---

1. The aerospace division of Lockheed Martin Corporation has undergone a number of name changes over the life of GP-B. In 1984, when Stanford first contracted with the company to build the GP-B dewar and probe, it was then called Lockheed Missiles and Space Company (LMSC). In 1995, the parent Lockheed Corporation merged with the Martin Marietta Corporation to become the Lockheed Martin Corporation, and the aerospace division became Lockheed Martin Missiles and Space (LMMS). A few years later, the Lockheed aerospace division underwent yet another name change to the current Lockheed Martin Space Systems Company (LMSSC). Throughout the development of the dewar, probe and other payload systems, GP-B subcontracted with the Lockheed Palo Alto Research Lab (LPARL), located next to Stanford. The spacecraft fabrication and assembly was carried out at the company's nearby Sunnyvale, CA facility. For the sake of simplicity, we have chosen to use “Lockheed Martin,” or the acronym “LM” for all further references to Lockheed Martin Space Systems Company in this chapter.



3. **Payload Integration, Testing and Repairs (1997-2002)**. During this five year period, a few critical problems surfaced during the integration and testing of the payload, including the dewar, probe, and Science Instrument Assembly. These problems were addressed, the payload was integrated into the spacecraft, along with several electronics systems, and the Gas Management Assembly. The presence of these problems caused NASA to significantly increase its management oversight of the program. This led to communications issues between Stanford, NASA, and Lockheed Martin that were successfully addressed towards the end of this time period.
4. **Final Integrated Testing, Launch & Science Mission (2002-2005)**. During the pre-flight integrated testing of the GP-B spacecraft, two final problems emerged which postponed the launch from 2002 to 2003, and then to 2004. GP-B finally launched on April 20, 2004, followed by a successful 17.3-month flight mission, which concluded on September 29, 2005.
5. **Data Analysis Period (2005-2007)**. Following the successful GP-B flight mission, focus shifted from spacecraft operations to science data analysis and results determination. As planned, this shift resulted in a considerable reduction in staff, of which the spacecraft operations team was a large component, as well as a final change in program management.

These five time periods provide the main organizational structure for discussing GP-B program management in this chapter.

## 6.2 The Early Years (1959-1984)

The early history of GP-B is covered in Chapter 2, Section 2.1.1 “A Brief History of GP-B”. To preserve context, parts of the current chapter are somewhat redundant to the history in Chapter 2; however this section focuses primarily on the program management aspects of GP-B.

### 6.2.1 Concept Development

The idea of testing general relativity by means of orbiting gyroscopes was suggested independently by two physicists, George Pugh and Leonard Schiff, in late 1959-early 1960. Pugh's **Proposal for a Satellite Test of the Coriolis Prediction of General Relativity** appeared in an unusual location: the U.S. Department of Defense *Weapons Systems Evaluation Group (WSEG) Memo #11* (November, 12, 1959). Schiff's **Possible New Experimental Test of General Relativity Theory** was published in the March 1, 1960 issue of *Physical Review letters*. What was then called the Stanford Relativity Gyroscope Experiment (later dubbed Gravity Probe B) began in late 1959-1960 as a research collaboration among Schiff, a theoretical physicist and then Chairman of the Physics Department, and two other professors at Stanford University—William Fairbank, a low-temperature physicist, and Robert Canon, a gyroscope and guidance control expert, and later Chairman of the Aeronautics & Astronautics Department. In June 1960, Schiff published an expanded paper, more completely defining the experiment, while Fairbank and Cannon focused on the cutting-edge technological innovations that would be necessary to actually carry it out. What became apparent early on, and proved critical to the eventual success of the experiment, was the necessity for collaboration—both inter-departmental collaboration within Stanford and also collaboration between Stanford, NASA, and eventually, Lockheed Martin. GP-B was a fundamental physics experiment that had to be performed in a spacecraft. As such, it required cutting-edge knowledge and expertise from both physicists and engineers—especially aerospace engineers.

### 6.2.2 Initial Research

Realizing the need for such aerospace collaboration, Schiff and Fairbank approached NASA in 1961 with a short, non-funding proposal outlining an experiment to be performed in an orbiting spacecraft. At that time, Dr. Nancy Roman was Chief of Astronomy and Relativity Programs in the NASA Office of Space Science at

NASA Headquarters. Roman was quite influential in creating astronomical research satellites such as the Orbiting Space Observatory (OSO), the Cosmic Background Explorer (COBE) and the Hubble Space Telescope (HST). In July 1961, under Roman's direction, NASA sponsored a conference at Stanford on the topic of experimental tests of general relativity. This conference, which was attended by many of the leading relativistic physicists and aerospace engineers of the day, helped crystallize various issues that needed to be addressed in order to carry out the relativity gyroscope experiment.

One important result of that conference was the idea of developing a “drag-free” satellite—a satellite that could orbit the Earth exactly as if acted upon by gravity alone—not by solar pressure or atmospheric drag. This feature was critical to the relativity gyroscope experiment because the effects of orbital drag on the gyroscopes would obscure the minuscule relativistic effects being measured. At the conference, Benjamin Lange, a Stanford Aero-Astro graduate student (and later a professor in the Stanford Aero-Astro Department) had an “aha moment,” in which he figured out how to create a “drag-free” satellite. This became the topic of his doctoral dissertation and several other dissertations to follow in the Stanford Aero-Astro department, under the supervision of Professor Robert Cannon.

Meanwhile, William Fairbank and his graduate students had begun investigating various cryogenic topics related to gyroscope composition, as well as gyro suspension, readout, and spin-up systems. In 1962, Fairbank invited Francis Everitt to come to Stanford as the experiment's first full-time academic staff member. Working with Fairbank, Everitt proposed using the London Moment property of spinning superconductors as the basis of a gyroscope readout system, and he helped redefine several other aspects of the experiment, such as the electrostatic gyro suspension system.

During the years 1963-1967, GP-B grew slowly as a university research program, with William Fairbank and Robert Cannon each managing research teams in their respective departments. Late in 1963, Stanford submitted a proposal to NASA entitled: **Proposal To Develop a Zero-G Drag Free Satellite and Perform a Gyro Test of General Relativity in a Satellite**. In March 1964, NASA's Office of Space Science funded this proposal in the amount of \$180,000, with Roman serving as NASA Program Manager. The proposal named William Fairbank and Robert Cannon as Co-Principal Investigators, with Leonard Schiff as Project Advisor. Once funded, the research program began to expand rapidly. Pictured in [Figure 6-1](#) below are GP-B co-founders Leonard Schiff, William Fairbank, Robert Cannon, and Nancy Roman, former Chief of Astronomy and Relativity Programs in the NASA Office of Space Sciences.





**Figure 6-1.** Clockwise from top left: GP-B Co Founders Leonard Schiff, William Fairbank, and Robert Cannon and former head of NASA's Office of Space Sciences, Nancy Roman.

Furthermore, the U.S. Air Force was interested in the drag-free and guidance control portion of this research and provided supplementary funding for this work. To further this effort, Robert Cannon invited Daniel DeBra, a recent Stanford Aero-Astro Ph.D., who was then heading up the Guidance and Control team for the Lockheed Discoverer spacecraft, to return to Stanford as a professor in the Aero-Astro Department. With DeBra, Lange, and two other researchers on his team and funding from NASA and the Air Force, Cannon helped lay the groundwork for the development of the first successful drag-free satellite, as noted below.

During this same period, Francis Everitt had become involved in all research aspects of the relativity gyroscope experiment, and his work, along with that of Fairbank and other physics faculty, graduate students, and staff, began to demonstrate that the relativity gyroscope experiment, as then defined, would be capable of reaching the one-milliarcsecond accuracy desired.

### **6.2.3 Technology Design and Prototyping**

For the next decade from 1967-1978, the size of the research teams grew gradually, as the focus shifted from conceptual design to the prototyping and development of various technologies required for the experiment. In the Physics department, this prototyping encompassed all of the technologies required to carry out the experiment—the gyroscopes, the gyro readout and suspension systems, a pointing telescope and artificial star simulator, ultra-low magnetic field technology, a helium dewar and porous plug and proportional thrusters for controlling the escaping helium, and other related technologies.

In parallel, a major focus of the Aero-Astro Department remained fixed on the development of a drag-free satellite. In December, 1969, the Stanford Aero-Astro Department submitted a proposal to Johns Hopkins Applied Physics Laboratory (APL) for a subcontract to **Develop and Build a [drag-free] Disturbance Compensation System (DISCOS) for the [U.S. Navy] TRIAD II and III Satellites**. This important early space experiment was developed and managed jointly by Daniel DeBra of Stanford and Robert Fischell of the Johns Hopkins APL, who was granted Navy funding for the project because it could (and did) make possible extreme accuracy at low cost for submarine navigation system updates which the transit satellite system provided. The TRIAD II transit navigation satellite, with DeBra's drag-free DISCOS unit as its centerpiece, was successfully launched in 1972—the only 3-axis drag-free satellite to be operated successfully until the launch of GP-B in 2004. It achieved control to  $5 \times 10^{-12}$  g throughout a one-year orbital test flight.

With the success of DISCOS, Stanford was able to procure funding for drag-free technology research from sources other than NASA, and GP-B's NASA funding was thus refocused solely on development and prototyping of the technology and control systems needed to perform the relativity gyroscope experiment.

In 1968, Robert Cannon left Stanford to become Chief Scientist for the U.S. Air Force. In the wake of his departure, Fairbank promoted Daniel DeBra to the status of Co-Principal Investigator for the Aero-Astro portion of the GP-B program, and he promoted Francis Everitt to the status of Coordinating Co-PI for the whole program. Leonard Schiff continued his role as Program Advisor, in frequent communication with Fairbank, Everitt, and DeBra until his death in 1971.

During these years, Stanford began collaborating on the development of several technologies with NASA's Marshall Space Flight Center (MSFC), and MSFC provided oversight assistance on Stanford subcontracts to aerospace companies for the development and testing of prototype gyroscopes, telescope hardware, the dewar, and other key technology elements.

NASA Headquarters formally transferred oversight responsibility for the relativity gyroscope program to MSFC in 1971. Coincident with this transfer, C. Dixon Ashworth, then the NASA HQ manager overseeing the relativity gyroscope experiment, renamed it “Gravity Probe B,” noting that it was to be the second NASA gravitational physics experiment. The first one, which he named “Gravity Probe A,” was a Hydrogen-maser clock comparison experiment, headed by Dr. Robert Vessot of the Smithsonian Astrophysical Observatory and also overseen by MSFC. (The Gravity Probe A experiment was successfully performed with a sub-orbital Scout launch in 1976.)

In December 1971, MSFC funded an in-depth “Mission Definition Study” of GP-B, performed by Ball Brothers Research Corporation (BBRC, Now Ball Aerospace), in close collaboration with Stanford—the starting point for all future flight studies. This study provided an initial spacecraft design and program plan. Two follow-up studies by BBRC were performed in 1973 and 1975, respectively. The results of these studies indicated that GP-B was ready to make the transition from exploratory research and technology development to a NASA flight program.

## 6.2.4 Transition to a NASA Flight Program

In January 1977, the original NASA research grant to Stanford was closed out—the longest running continuous research grant ever awarded by NASA—symbolically marking the end of the exploratory phase of the program, during which much of the key technology needed was developed. In its place, NASA's Office of Space Sciences awarded a new contract for the purpose of defining a flight program. A year later, funding support at NASA Headquarters for the program switched from the Office of Space Science under Nancy Roman to the Advanced Program Development Office under Jeffrey Rosendhal.

MSFC conducted an in-house Phase A study of GP-B in preparation for defining a flight program in 1980. Later that year, under the chairmanship of Jeffrey Rosendhal at NASA Headquarters, NASA convened a special committee to assess the technological readiness of GP-B for becoming a NASA flight mission. The Rosendhal Committee concluded that:

*...the remarkable technical accomplishments of the dedicated Stanford experiment team give us confidence that, when they are combined with a strong engineering team in a flight development program, this difficult experiment can be done.*

By 1981, Francis Everitt had become the single person most knowledgeable about all aspects of the GP-B experiment. For this reason, he was promoted to the job of Principal Investigator, challenged with bringing the experiment to fruition—a job that would ultimately take another 25 years to accomplish. Encouraged by the results of the 1980 Phase A study, MSFC, with support from Stanford, undertook a much more in-depth Phase B study in 1982. The Phase B study yielded a spacecraft that was too large and a program that was too expensive, with an unacceptable level of risk. Thus, in 1983, Everitt and the Stanford team, in collaboration with MSFC, undertook an extensive restructuring of the program, with a goal of reducing the weight and power requirements of the spacecraft, reducing overall costs, and reducing program risks to an acceptable level—all without sacrificing any essential science goals.

The result of this restructuring effort was a two-phase Space Shuttle mission. The first phase was to be a technology readiness demonstration called STORE (Shuttle Test of the Relativity Experiment). In this phase, the dewar and science instrument would be tested during a shuttle flight to be launched in 1989. At the end of the test, this equipment would be brought back to Earth by the shuttle, refurbished, and then integrated into a satellite for performing the actual experiment. Two years later, the GP-B satellite would be placed in orbit by a polar-orbiting Shuttle, which could be launched only from NASA's West Coast Shuttle Facility at Vandenberg AFB, in Southern California.

## **6.2.5 GP-B Formalizes Program Management**

Shortly after becoming Principal Investigator in 1981, Everitt realized that he was going to need a person with strong aerospace engineering background to help him manage the unique technology development challenges facing GP-B. In 1982, he began trying to recruit Bradford Parkinson (1966 Stanford Aero-Astro Ph.D whose dissertation research on spherical gyroscopes was carried out in the early GP-B labs) to return to Stanford from private industry to serve as both a Co-PI and the first formal Program Manager of GP-B. Parkinson is credited with creating the U.S. Air Force Global Positioning System (GPS) and had previously been Program Manager for its successful deployment. This experience, coupled with his aerospace background, ideally suited him for this new position. Parkinson agreed to serve as a consultant to GP-B until NASA funding for the GP-B flight program was imminent, and then to come on board as Program Manager and Co-PI of GP-B. In the interim period, Everitt recruited Robert Farnsworth to move to Stanford from the University of California, San Diego, where he had been managing other aerospace engineering projects and to serve as Deputy/Acting Program Manager until Parkinson arrived.

By 1984, with the newly restructured two-phase Shuttle-based plan completed, the stage was set for NASA to fund the GP-B flight program and for Parkinson to assume the role of GP-B Program Manager and Co-PI. Concurrently, Cannon, then chairman of Stanford's Department of Aeronautics and Astronautics, offered Parkinson a full professorship in that department—an equally strong incentive for Parkinson to return to Stanford. For about a year, Farnsworth served as Deputy Program Manager under Parkinson. He then accepted a new position as Associate Director of Stanford's Hansen Experimental Physics Lab (HEPL), under whose auspices the GP-B program was administered at Stanford. Farnsworth remained Associate Director of HEPL until his retirement some years later.

Parkinson's arrival at GP-B ushered in a 16-year period of flight hardware development that will be described in more detail in the next few sections. The Calder-Jones independent report to NASA, pages 31-32, makes the following comments about Parkinson's tenure as Program Manager:

*Professor Parkinson's tenure turned out to be one of the most influential and productive times of GP-B. Significant strides were made and a very high precedence was set despite the fact that some tremendous obstacles needed to be overcome. Again, technologically GP-B is an extremely difficult program; however, the [challenges] associated with Professor Parkinson's tenure [extended far] beyond technical hurdles. It was under his purview that Lockheed Martin (LM) was selected as the subcontractor to help build and integrate the payload and later selected again to build the spacecraft. Therefore, all original contract negotiations between the university prime and their private-industry subcontractor were performed under his guidance.*

(See Section 6.8 [Gravity Probe B: A Management Study](#) for more information about the Calder-Jones Report to NASA.)

To round out the new GP-B senior management team, Daniel DeBra continued as a Co-PI from the Aero-Astro Department, as did William Fairbank in the Physics Department, until his death in 1989. Furthermore, physics Professor John Turneure was promoted to Hardware Manager (and two years later, he also became a Co-PI). In addition, after Farnsworth's move to HEPL, Tom Langenstein was hired as GP-B's new Deputy Program Manager, with responsibility for the NASA contract, the Lockheed Martin subcontract, and resources. A full GP-B senior management team was now in place. Pictured in [Figure 6-2](#) below are Principal Investigator, Francis Everitt and his three Co-PIs, Bradford Parkinson, John Turneure, and Daniel DeBra.

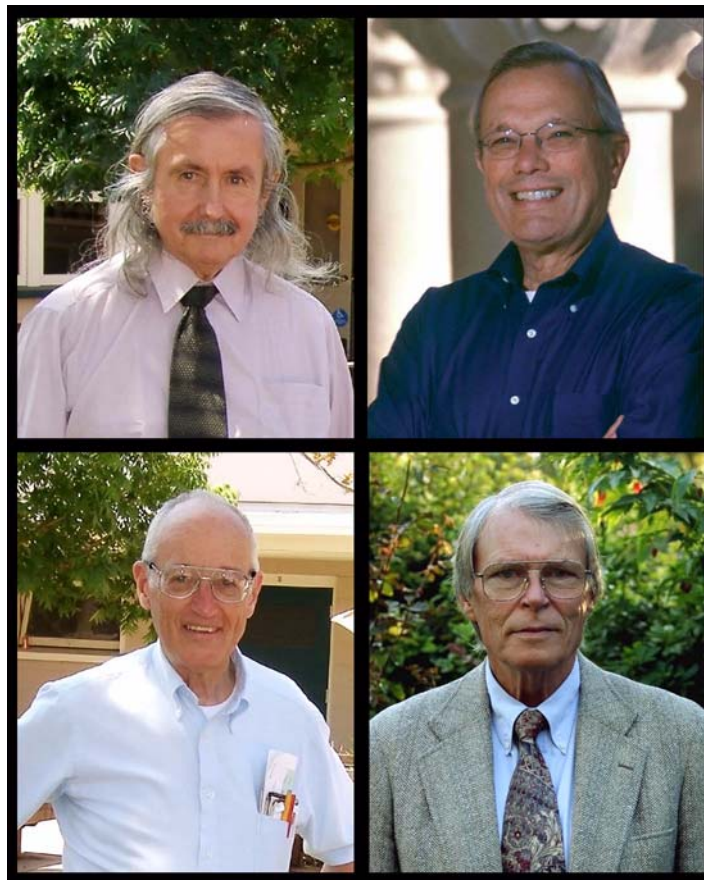


**Figure 6-2.** Clockwise from top left: GP-B Principal Investigator, Francis Everitt and Co-PIs Bradford Parkinson, John Turneure and Dan DeBra.

It is important to note that from this point through 1998, GP-B was actually managed by a three-person team, comprised of Program Manager Parkinson, Hardware Manager Turneure, and Principal Investigator Everitt. Each of these men had knowledge and skills complementary to the other two, so that together, the three formed a synergistic, and very effective management team. In terms of division of responsibility, it was often the case that Everitt and Parkinson dealt with top-level program issues, while Turneure managed the day-to-day hardware development.

Furthermore, during the 15-year period from 1985 through 2000, six Stanford experimental physicists, each with a different area of specialization, were promoted to the position of Co-Investigator, forming a strong second tier of management to aid in various aspects of hardware development and experimental design and testing. Pictured in [Figure 6-3](#) below are the six GP-B Co-Investigators: Sasha Buchman, George (Mac) Keiser, John Lipa, James Lockhart, Barry Muhlfelder, and Michael Taber.



**Figure 6-3.** The six GP-B Co-Investigators. Clockwise from top left: Sasha Buchman, George (Mac) Keiser, John Lipa, James Lockhart, Barry Muhlfelder, and Michael Taber.

The next few subsections provide a more detailed discussion of GP-B accomplishments, challenges, and issues that occurred during Professor Parkinson's term as Program Manager, which lasted until August 1998.

### **6.2.6 NASA Makes Stanford Prime Contractor on GP-B**

In the process of reviewing and preparing to fund the revised GP-B flight plan, Samuel Keller, then Deputy Director of the NASA Office of Space Science Applications, decided to make Stanford NASA's Prime Contractor on the GP-B mission. This was one of the first NASA missions, and at that time, the largest, in which a university was given the prime role of managing the development of an entire space flight mission—science instrument, spacecraft, mission operations and data analysis.



Among the reasons for NASA's decision to make Stanford the prime contractor on GP-B were the following:

1. The payload and spacecraft were intimately interdependent. That is, the payload sensor was the key control element to the space vehicle system. One of the four science gyros was also used as the drag-free sensor, and the helium gas escaping from the dewar was used by proportional micro-thrusters to maintain drag-free and attitude control. The total-system mass center location was also critical.
2. The development process and specification derivation were integrated. Because the payload drove most of the spacecraft requirements, the specifications were linked. They were developed together and verified in an integrated fashion.
3. Many of the technologies associated with the science Instrument Assembly—namely, the gyroscopes and their suspension systems, the SQUIDs, and the pointing telescope—were entirely new and unique technologies that could only have been developed in a very advanced academic research environment.
4. The Science Instrument Assembly had to be integrated into the probe, the probe was then integrated into the dewar, and finally, the dewar-probe unit was integrated into the spacecraft, so that all of these components functioned together as a unified system. This total integration of payload and spacecraft was crucial to the success of the mission.
5. The scientists and engineers at Stanford understood points 1-4 above, and they were the logical people able to oversee the technical trade-offs associated with designing and constructing this unique spacecraft.

In November 1984, following a by-the-book competitive bidding process, Stanford selected Lockheed Martin to build the flight dewar and probe that would house the Science Instrument Assembly, the heart of the experiment being developed and constructed at Stanford. GP-B then sent MSFC/NASA Headquarters a proposal, with Stanford as the prime contractor and LM as Stanford's subcontractor, for implementing the restructured flight plan and building the required flight hardware. In 1985, MSFC/NASA Headquarters accepted the Stanford-Lockheed Martin STORE proposal and funded this technology development plan. The fact that the technology plan included LM as Stanford's industry subcontractor represented a significant increase in management responsibility for Stanford. However, under Parkinson's experience and leadership, Stanford was prepared for this challenge, and "The Management Experiment" commenced.

## 6.3 Flight Hardware Development (1984-1997)

James Beggs, the NASA Administrator in 1985, concurred with Samuel Keller's decision to make Stanford the Prime Contractor on GP-B, and he remarked that in addition to being a physics experiment that needed to be carried out in space, GP-B was equally interesting as a "management experiment."

As stated in the Calder-Jones Report to NASA, page 7:

*The Management Experiment was an agreement between NASA Headquarters, NASA MSFC, and Stanford University that established Stanford as the prime contractor, managing the entire program with minimal NASA oversight. The decision followed a recommendation from the Space Studies Board (SSB) to NASA Headquarters in mid-1983, after the SSB had reviewed the MSFC Phase B Study. The view of the SSB, endorsed by NASA Headquarters, was that in a mission such as GP-B where the instrument and spacecraft are much more closely integrated than in typical space programs, separating the two would be gravely detrimental. It was predicated on Stanford University's agreeing to set up a much stronger management structure than is typical in universities.*

The flight hardware development period continued for about 15 years, at which time it became necessary to transition GP-B from a research and development program with minimal NASA oversight to a classical NASA flight program that would culminate in a successful launch, on-orbit operations, and subsequent data analysis, leading to the determination of the experimental results.

### 6.3.1 Incremental Prototyping

The period from 1985-1995 yielded significant advances in GP-B hardware development, due in large part to Bradford Parkinson's decision to use a methodology called "incremental prototyping." Incremental prototyping involved the rapid development and testing of increasingly more prototypical hardware. Developing GP-B's unique and cutting-edge technology required an approach that would maximize the capability of the hardware and software, while minimizing costs and development time. In the classical, aerospace hardware development approach, a number of years would first be spent defining a requirements specification, and then an aerospace contractor, such as Ball Aerospace, Lockheed Missiles and Space, Fairchild Aerospace, or General Electric Aerospace would spend more years designing and building hardware to meet the specifications. This would be a time-consuming and expensive process. Furthermore, this process would not necessarily yield the desired results, and more iterations would often be required.

During the flight hardware development years, GP-B required technology development consistent with a suitable flight readiness level. Thus, rather than adhering to the classical development model, one of Professor Parkinson's major contributions was to use incremental prototyping for developing the novel and complex technology required by the experiment. Hardware was rapidly prototyped and tested in order to determine how close it would come to meeting specified requirements and also to determine how difficult it would be to manufacture and test. Incremental prototyping allowed the team to develop new technologies by building actual hardware, while learning valuable lessons in the process. When the time was right, the team knew what they could build and how to build and test it. Eventually these "lessons learned" were applied to the development of actual flight hardware, allowing the team to build flight hardware more efficiently, in less time, and more accurately than would have been possible using the classical "build-to-requirements" approach.

Incremental prototyping was used to develop the technologies described in each of the five subsections below.

#### 6.3.1.1 Probes A, B, and C

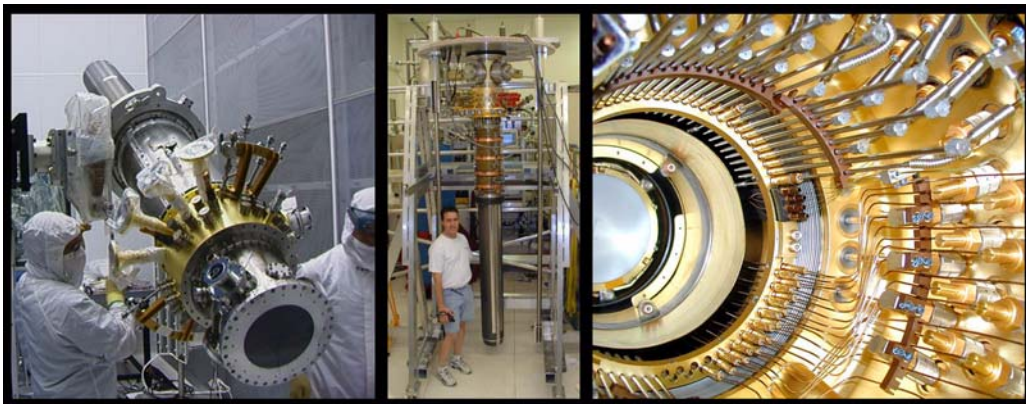


**Figure 6-4.** Probe C: testing in clean room (left), ready for integration with dewar (center) and connections inside the top hat interface (right).

The cryogenic Vacuum Probe, when inserted into the dewar, includes the science experiment. The Probe must maintain an internal temperature of 2.0K, while interfacing to external systems at ambient temperature. The Probe contains a sequence of four windows that enable the telescope to view the guide star. The Probe also had to minimize heat leakage, while providing an interface for ~600 cables to the external ambient temperature environment. [Figure 6-4](#) shows various views of Probe C, the final flight probe.



### 6.3.1.2 Engineering Development Dewar & Science Mission Dewar

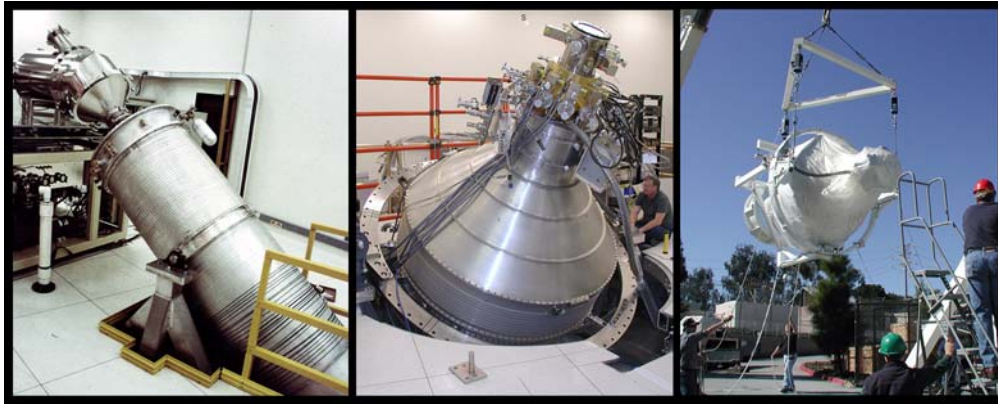


**Figure 6-5.** Left: Engineering Development Dewar (EDD); Middle & Right: Science Mission Dewar (SMD).

The dewar is a thermos-like reservoir that holds the supply of liquid helium to maintain the Probe at a tightly-specified cryogenic temperature for 16 months or more. Once filled, the dewar was never allowed to warm up, because it included a special lead-bag that formed a superconducting magnetic shield which was an integral part of the dewar well and was required for the experiment. The prototypical Engineering Development Dewar not only allowed early integrated-system testing, but also was the vehicle for early development of the critical probe-dewar integration procedure. [Figure 6-5](#) shows various views of the Science Mission Dewar or SMD.

### 6.3.1.3 Spherical Gyroscopes and Gyro Suspension System



**Figure 6-6.** Gyroscope rotor development and precision sphericity measurement.

Several types of gyros were prototyped, including ceramic, fused quartz engineering model, prototype/shuttle, and the final flight gyros. The gyros had to sustain heavy flight vibration environments, while maintaining their perfect shape for the experiment. [Figure 6-6](#) shows some of the gyro rotors in various stages of development and testing.

The Gyro Suspension System (GSS), that electrostatically suspends the science gyroscopes within their housing cavities and enables them to spin freely with minimal friction and torque. To perform its mission successfully, the GSS had to satisfy a number of requirements: Operate over 8 orders of force magnitude, suspend or levitate the gyroscopes reliably, operate compatibly with the SQUID readout system, minimize electrostatic torques during science data collection, apply controlled torques to the rotor for calibration and initial rotor spin-axis

alignment, and act as an accelerometer as part of the “drag-free” translation control system to further minimize classical torques on the rotors by another factor of  $10^6$ . See Section 6.3.5 below for a further discussion of the GSS development process.

### 6.3.1.1 SQUID Magnetic Gyro Readout

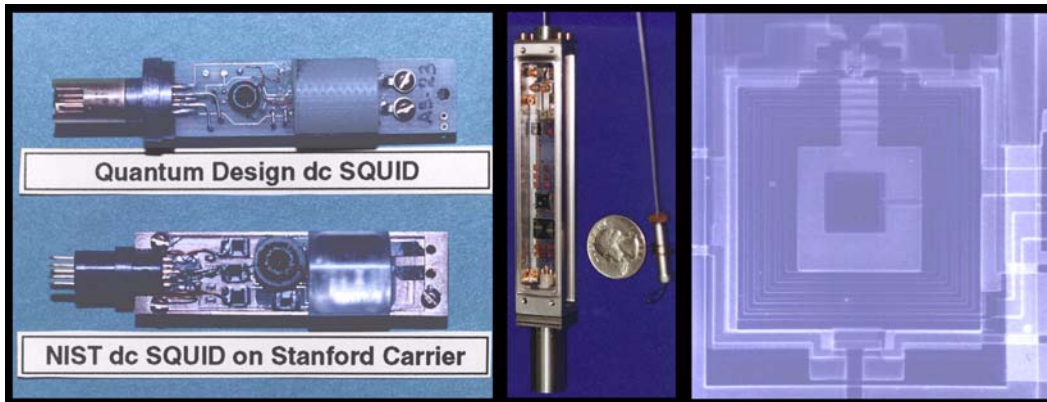


**Figure 6-7.** SQUID readout development prototypes and lithograph for SQUID chip.

Several types of SQUID (Super-conducting QUantum Interference Device) readouts were prototyped, including Quantum Design DC SQUID, NIST DC SQUID, and DC Flight SQUID). The cryogenic SQUID readout system provides a gyro spin axis orientation readout, with a precision of 0.1 milliarcsecond operating over a resolution range of  $\pm 60$  arc seconds. Figure 6-7 shows some of the SQUID prototypes, as well as the lithograph for a SQUID chip.

### 6.3.1.2 Telescope, Image Divider Assembly, and Detector Package Assembly

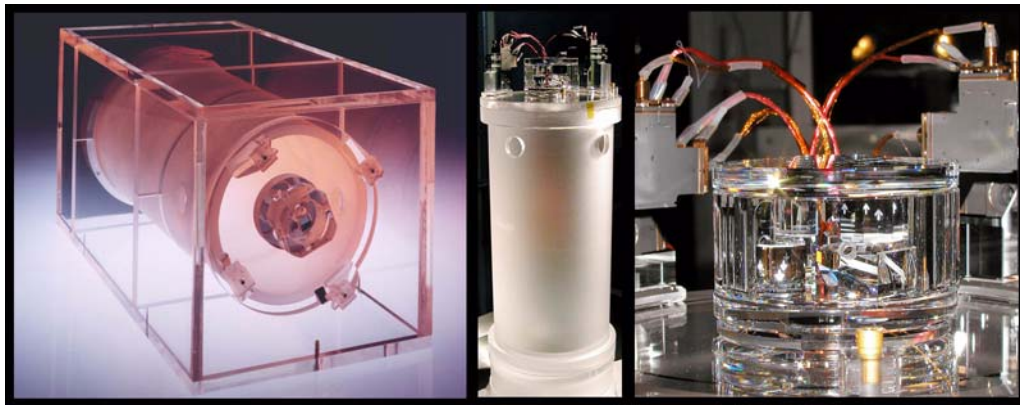


**Figure 6-8.** An early development telescope prototype (left), the pre-flight #2 prototype telescope (center), and a close-up of the Image Divider Assembly and Detector Assembly Package from the #2 pre-flight prototype.

Two early models of the science telescope were built in order to determine the technology requirements for the actual flight telescope. Later, three complete telescopes were incrementally prototyped, and 95% of the parts were manufactured for a fourth one. The first of the later prototype telescopes was manufactured primarily for testing optical performance. The second and third flight prototypes were both completed to flight qualification standards, and the third was integrated into the SIA in Probe C and flown on the mission. Assembly was started

on a fourth flight-ready prototype, but halted when it was determined that the third met all necessary flight qualifications. [Figure 6-8](#) above shows an early telescope prototype, plus the pre-flight #2 prototype telescope and its IDA.

### **6.3.2 Re-Thinking STORE Post-Challenger**

In the wake of the Challenger disaster in 1986, NASA closed its West Coast, polar-orbiting shuttle launch facility at Vandenberg AFB in California, and it became necessary to re-cast the GP-B mission as a satellite to be launched there by its own expendable rocket. Thus, in parallel with the incremental prototyping of GP-B flight hardware, the team also began redesigning the STORE experiment. In 1988, a new shuttle-based test of GP-B technology was proposed, designated Shuttle Test Unit (STU), and it was planned to take place in the mid-1990s. STU represented a substantial de-scoping of STORE. It was to be a room-temperature test of gyro suspension and spin-up in a micro-gravity environment. There were no cryogenics, no read-out, and no telescope. Gaylord Green, a retired Colonel from the U.S. Air Force who had worked with Parkinson on the GPS development, was brought on-board the GP-B team as the STU Project Manager. The STU experiment remained part of the GP-B plan until 1995, when NASA concurred with Stanford's recommendation that a Shuttle test of the technology was of limited overall value and would no longer be necessary. The testing performed during incremental prototyping of the flight hardware had already demonstrated the flight readiness of several key hardware components, and thus the funds that had been designated for the STU Program could better be used directly preparing GP-B for flight.

### **6.3.3 Selecting a Spacecraft Subcontractor**

By the early 1990s, it had become apparent that regardless of whether the STU Shuttle test of GP-B technology was carried out, the final experiment would require a space vehicle (satellite) that would house the dewar and probe as an integrated system, and that a subcontractor needed to be selected to develop this space vehicle. In 1992, Stanford received approval from NASA to begin this selection process.

Stanford sent out a Request For Proposal (RFP) and received preliminary proposals from three aerospace companies: General Electric, Fairchild Aerospace, and Lockheed Martin. During the initial round Stanford narrowed the selection to Fairchild Aerospace and Lockheed Martin. Then, in 1993-1994, Stanford funded both companies to develop competing Phase A proposals. The two proposals were closely competitive, each having superior aspects, and GP-B team members were divided as to which company should be awarded the contract. After a thorough review of both proposals, it was decided that LM's existing software for attitude control, inherited from the Hubble Space Telescope program, gave LM an advantage over Fairchild, and thus, Stanford selected LM to build the space vehicle. The contract gave LM responsibility for acquiring and building the spacecraft subsystems, integrating the spacecraft assembly, integrating the payload with the spacecraft upon the space vehicle, performing integrated testing, supporting pre-launch operations and supporting mission operations from initialization and on-orbit checkout (IOC) through the science data collection and post-science instrument calibration phases of the flight mission. Pictured in [Figure 6-9](#) below are members of the GP-B Spacecraft Development Team at Lockheed Martin circa 1995.





**Figure 6-9.** The Lockheed Martin GP-B Spacecraft Development Team circa 1995. Key managers from LM included: Norman Bennett, Hugh Dougherty, Bill Reeve, Robert Schultz, and Jeff Vanden Beukel.

### 6.3.4 NASA Funds GP-B as a Flight Program

By 1994, all of the pieces of a GP-B flight mission were at last coming together: flight-ready prototyping of the gyros, analog gyro suspension system, and gyro readout system at Stanford, development of the flight dewar and probe at LM, and the competitive selection of LM to construct the space vehicle. During this time period, extensive exchanges took place between NASA/MSFC, NASA HQ and Stanford as to the most appropriate method of going forward. An earlier decision (1993) by the then Associate Administrator of the Office of Space Sciences and Applications (OSSA) led to an unusual funding arrangement. In contrast to the standard NASA funding profile for flight programs, where there is a substantial increase in annual budget during the two or three years prior to launch to minimize risk and contingency, GP-B would receive a level funding of \$50M/year with schedule as contingency. While this was recognized as non-optimal, it was deemed most acceptable option in the constrained overall OSSA budget plan.

Prior analyses, including the independently reviewed FY '95 Program Funding Plan (PFP), had provided for a mission with an October 2002 launch and an overall program cost including the launch vehicle, full Phase E and tracking/data costs, and \$147.8M already invested for technical development and STORE, amounting to \$743.8M. The plan included fabrication of two flight dewars and four dewar probes. The \$743.8M was the bottom line figure in the Program Commitment Agreement (PCA) signed August 23, 1994 by the NASA Program Associate Administrator, the NASA Administrator, and NASA Comptroller. Prior to that (and noted in the PCA), MSFC, the Office of Space Sciences, and Stanford had recommended a de-scoped program, eliminating the Shuttle Test Unit (STU) and cancelling the development of a third flight dewar and a fourth probe (having deemed that the second dewar and third prototype probe were satisfactory for flight), with a target launch date of October 2000. By way of 'schedule contingency', an additional 15% (1 year) reserve (i.e. an October 2001 launch) was identified to be held at NASA HQ. The total runout costs to October 2001 including mission operations and data analysis - but excluding the launch vehicle (~\$62M), tracking/data (~\$20M), and

any HQ costs - was \$410.7M, or including the \$147.8M prior sunk costs, a total \$558.5M. (A footnote in the PCA identified this “recent re-baselining” and indicated an expected reduction of the “BTC and runout costs of about \$90 million”.)

Following the July 1994 letter exchange and signed PCA, GP-B went rapidly ahead with continuation of Stanford/Lockheed Martin payload activities and the release of the separate competitively selected space vehicle subcontract to Lockheed Martin. Funding continued at the assigned PCA level of \$50M/year (plus inflation) through FY '98. On November 16, 1996, however, the MSFC GP-B Program Manager (R. Geveden) found it necessary to sound the alarm in a memorandum to NASA HQ headed “Impact of Gravity Probe B Funding Cuts.” He noted that the NASA HQ budget submission to the OMB showed a \$1M reduction in FY '98 and an \$11M reduction in FY '99. The proposed budget cuts “jeopardize our ability to carry the program to the committed launch date and severely limit our ability to manage outyear contingencies.” The situation was alleviated in July 1998 by the addition of some additional year-end funding (\$10.3M) to compensate for the shortfall over FY '98/'99. But, heavily reduced funding in FY '00, '01, and subsequent years below the level funding commitment caused acute difficulties for GP-B. During the most critical phase of development, the program faced the shortfalls shown in [Table 6-1](#) below.

**Table 6-1.** GP-B Promised vs. Actual Funding History, FY '99 - FY '02

<b>\$M to Stanford</b>	<b>FY '99</b>	<b>FY '00</b>	<b>FY '01</b>	<b>FY '02</b>
<b>Program Commitment</b>	52.8	55.8	58.2	59.0♦
<b>Actual Funding</b>	54.2*	36.4	35.6	48.2
<b>Annual Shortfall</b>	<1.4>	19.4	22.6	10.8
<b>Cumulative Shortfall</b>	—	18.0	40.6	51.4

\*Includes \$10.3M from the FY '98 year-end increment; ♦per PCA

The impact was a greatly delayed start on the payload electronics systems which in turn complicated the diagnosis of other probe and dewar issues (noted below), and ended by delaying the GP-B launch by at least two years.

Issues of funding are not always within NASA's full control. Recognizing this, we judge that a critical evaluation of the level-funding concept is in order. The difficulties become far more acute when even level-funding is not maintained. Given the circumstances, the MSFC/Stanford/Lockheed teams' performance was more than commendable. It may be observed that after the large number of puts and takes for de-scoping, budget shortfalls, and hardware challenges during development, the actual cost of the program to date (\$767M) is very close to the estimate in the original PCA (\$744M).

### 6.3.5 Flight Hardware and Electronics Development

Streamlining of the program scope in 1994 hastened the completion of the SMD (Science Mission Dewar), the second dewar developed for GP-B by LM, which was delivered to Stanford in November 1996. Probe C, the third and final probe developed by LM was delivered to Stanford in 1998. Then, as planned, the development effort on the spacecraft began to ramp up. Also at this time, development of three key electronics systems—The SQUID Readout Electronics (SRE), the Telescope Readout Electronics (TRE) and Experiment Control Unit (ECU)—commenced as a collaboration between Stanford and LM. These electronics systems were originally included in Stanford's dewar/probe contract with LM, but since development of these electronics systems had been postponed to hasten delivery of the dewar and probe, their development was now folded into the LM spacecraft contract.

Furthermore, a fourth electronic system, the Gyro Suspension System (GSS), underwent a complete transformation in 1996. Development of what was originally called the Gyro Suspension Unit (GSU) had begun a number of years earlier under the leadership of Richard Van Patten at Stanford. The original design was based on a laboratory gyro suspension system using analog, rather than digital electronics, and a number of issues, including weight, power consumption, adherence to GP-B torque requirements and compatibility with the GP-B SQUID readout electronics, needed to be addressed in order to use this system in a spacecraft. As a result, the analog suspension system was becoming increasingly complex, and senior GP-B managers were concerned about the reliability and accuracy of this mission-critical system on orbit. With the GP-B launch date only four-six years away, the senior program managers made the difficult decision to start over—that is, they decided to design and construct a digital, rather than analog suspension system. A new collaborative GSS team, including engineers and scientists from Stanford and Lockheed Martin was assembled at Stanford, under the leadership of Bill Bencze (who became post-flight GP-B Program Manager in 2005).

It is a testament to the immense dedication and collaboration of the Stanford and LM teams that the three most mission-critical electronics systems—the GSS, SRE and TRE—all performed flawlessly throughout the entire mission.

## **6.4 Payload Integration, Testing and Repairs (1997-2002)**

In addition to continued development of the spacecraft, the Gyro Suspension System, and three key electronics systems described in the previous section, the years from 1997 through 2002 were primarily focused on payload integration and testing. This included integrating the gyros, SQUIDs, telescope, etc. into the Science Instrument Assembly (SIA), the SIA into the probe, and the probe into the dewar. The whole payload was then tested as a unified system. These years represented a critical period for GP-B, in which engineering design came face-to-face with the realities of technology fabrication. Not surprisingly, some unexpected design and assembly issues began to surface during tests of the integrated payload system. Addressing these issues used up the savings in time and money gained from streamlining the scope of the program, postponed the launch date from 2000 to 2002 (then to 2003 and ultimately 2004), and resulted in greater NASA management oversight during this period.

### **6.4.1 Devising a Work-around for the Dewar Axial Lock**

The first of these issues was a problem with the dewar's axial locks, a set of three deployable clamps located around the circumference of a pair of mating flanges in the center of the dewar—one flange at the top of the cryogenic portion of the probe and the other at the top of the dewar's helium-filled main tank. Each axial lock clamp had a bolt, that when tightened down, compressed the probe and dewar flanges together, ensuring positive thermal contact between the lower, cryogenic portion of the probe and the dewar main tank.

When Lockheed Martin delivered the final SMD to Stanford late in 1996, work began in 1997 testing and preparing it to accept Probe C, which was also nearing completion. Preparation activities included filling the dewar with liquid helium and a painstaking process of inserting a sequential series of four nested lead bags, three of which were removed as part of the process, leaving a single, very effective cryogenic, superconducting, magnetic shield lining the probe cavity. Once lead bag installation was completed in the summer of 1997, Probe B—the second prototype probe that had previously been delivered to Stanford—was inserted into the dewar as a test to ensure that the dewar-probe interface would function as expected when Probe C was delivered and integrated into the dewar.

In testing the SMD before delivery to Stanford, engineers at LM discovered some galling in the threads of one of the axial lock bolts, causing the bolt to seize up. At the time, LM engineers felt that this problem was isolated to that individual bolt and that if it were not used, the remaining two axial locks could adequately hold the flanges

together. Thus, when the Stanford engineers inserted Probe B into the SMD for testing, they did not tighten the faulty bolt, but they soon discovered that the same problem was occurring with the second axial lock, and they became concerned that if the bolts in either of the remaining two axial locks seized up completely, it would not be possible to remove Probe B from the SMD.

This was a critical issue, for which there were basically two solutions:

1. Send the SMD (dewar) back to LMSC to be modified and re-built.
2. Abandon the axial lock system entirely and modify Probe C, which was still at LMSC, to provide positive thermal contact between the two flanges using Belleville spring cup washers at the top (warm region) of the probe.

It was clear that the latter solution, which became known as the Belleville Preload System (BPS), would be faster, less expensive, and less risky to implement. Thus, work began at LMSC to modify Probe C to use the BPS, delaying its delivery to Stanford by about eight months. This delay, and later others, required the dewar to be maintained at a cryogenic temperature for over eight years, through the end of the mission—an amazing feat in its own right.

## 6.4.2 Flight Probe C Integration & Testing

Throughout Bradford Parkinson's tenure as Program Manager, Co-PI, John Turneure, served as the GP-B Hardware Manager, with responsibility for managing the day-to-day development of the GP-B flight hardware. In 1998, Parkinson decided to step aside as Program Manager to become acting CEO of Trimble Navigation Ltd., a Silicon Valley navigation technology company, although still maintaining his position as a Co-PI, and also a senior advisor to GP-B. Given his intimate knowledge about GP-B flight hardware and close working relationship with Parkinson, it was a natural transition for Turneure to take over as Program Manager.

Lockheed Martin delivered Probe C to Stanford in mid 1998, with Turneure now serving as Program Manager, and immediately, testing began on the fit of Probe C into the SMD. The new BPS hardware was then used to spring-load the probe into the dewar, and tests were performed to verify thermal contact between the SIA portion of the probe and the dewar's main tank.

Once it was established that the BPS dewar-probe locking interface was performing properly, it was necessary to extract Probe C and move it to a clean room at Stanford, where the Science Instrument Assembly (SIA), comprising the gyros, SQUIDs, and telescope, was then to be integrated into the lower, cryogenic cavity of the probe. This work proceeded smoothly for several months, and by mid 1999, Probe C (also called the Science Mission Probe or SMP) was ready to be inserted into the SMD for integrated payload testing.

Testing of the integrated payload system commenced in August 1999, and during these tests, another unexpected thermal contact issue surfaced, as well as an unrelated problem with the pickup loop for gyro #4. Temperature measurements taken at various points in the probe and dewar revealed that a set of four copper bands, each attached to a corresponding window inside the neck of the probe, were not making thermal contact with a matching set of copper bands on the outside of the probe neck, thereby preventing the probe windows from intercepting thermal radiation propagating down the neck of the probe. The thermal interface between the inner and outer copper bands had worked well in the Probe A and B prototypes, but during the assembly of Probe C, there apparently had been problems with the epoxy tape that secured these bands in position. Because interception of thermal radiation in the probe neck was essential for maintaining a cryogenic environment in the SIA, failure of this thermal interface was a serious problem that had to be solved. Consequently, the probe had to be removed from the dewar once again, further delaying the launch and mission.

Collaborating closely, Turneure and LM Lead Probe Engineer, Gary Reynolds devised a solution. They determined that carefully drilling a series of holes through the outer bands and probe wall, into—but not through—the inner bands and then cementing small copper pegs into these holes with epoxy, would yield



positive thermal connections between the inner and outer bands, thus meeting the needs of the experiment. Rather than returning Probe C to LM for this modification, it was decided that the work would be done at Stanford so that members of the Stanford gyro team could replace gyro #4 at the same time.

### **6.4.3 Repairing Flight Probe C & Replacing Gyro #4**

Having devised a conceptual solution for the repair of Probe C, Turneure, who had been working tirelessly on GP-B hardware development since the mid 1980s decided to step back from the role of Program Manager. Everitt then appointed Sasha Buchman, a GP-B physicist and Co-Investigator who had been working closely with Turneure, as the new Program Manager, and Turneure took a well-deserved sabbatical. Thus, Buchman's first task as GP-B Program Manager was to oversee the retrofitting of Probe C with copper pins to solve the thermal contact problem, and to supervise the replacement of gyro #4 and the reintegration of Probe C into the dewar.

At a Probe C repair review, held in March 2000, it was determined that the team was ready to implement the Turneure/Reynolds copper pin solution, and the repairs to Probe C commenced. The repair work was carried out in a Stanford clean room by the LM spacecraft team, under the supervision of Jeff Vanden Beukel. In parallel, while the copper pins were being inserted in the upper portion of the probe, the vacuum cover was removed from the lower half of the probe, and gyro #4 was replaced by the Stanford gyro team. The copper pin thermal repairs were completed in May, and the replacement of gyro #4, along with some other minor repairs to the probe were completed in September. Then, during the fall of 2000, Probe C was reintegrated into the SMD for the last time.

Parkinson's transition in 1998 from Program Manager to Co-PI and Program Advisor resulted in his spending much less time at GP-B thereafter, and this left the GP-B senior management team in need of an experienced aerospace engineer on-site at Stanford. Early in 2000, a NASA Independent Review Team (IRT) mandated that GP-B acquire a management-level consultant with considerable aerospace experience. To this end, Ron Singley, who had worked for many years at Lockheed Martin, was hired by GP-B later that year to serve in this capacity, helping Stanford improve their interactions with LM and aiding in the efficient development of the space vehicle.

### **6.4.4 Moving Towards Flight Readiness**

By early 2001, all of the major GP-B flight hardware problems had been solved, except for the Gas Management Assembly (GMA). Realizing that its team lacked the expertise to build a flight-ready gas management system, Stanford (with strong support from NASA) decided to contract out the development of this hardware. Stanford conducted a brief, but thorough source-selection process, and in June 2001, selected Moog, Inc. in East Aurora, New York, to design and build a GMA system for GP-B. Moog had considerable experience building such systems, and they delivered a flight-certified GMA system just 13 months later, in August 2002. Much credit goes to Stanford's lead engineer, Chris Gray and to Lockheed Martin engineering manager, Jeff Vanden Beukel, for making this happen in an extremely responsive manner.

Many other milestones were also accomplished in 2001-2002, including an acoustic vibration test of the integrated payload, completion of the space vehicle at LM, and integration of the payload with the spacecraft. In addition, the payload electronics boxes—TRE, SRE, and ECU—were completed and installed in mid 2002, as was the new GSS electronics system. Equally important, work had begun in 2000 setting up the GP-B Mission Operations Center at Stanford, from which the spacecraft and payload would be monitored and controlled once it was in orbit. Likewise, work on mission operations procedures, training, and simulations commenced in 2000 and continued through mid 2003.

In January 2002, Sasha Buchman had to step down as Program Manager due to health issues, and Ron Singley took over as Interim Program Manager for most of 2002. Singley led the Stanford/Lockheed Martin team in completing the payload-spacecraft integration and testing activities.

### 6.4.5 Changing Focus from Maximizing R&D to Minimizing Risk

During the years from 1995-1999, GP-B was in the process of making a critical program transition in which it was necessary to shift focus from maximizing advances in research and development to minimizing the risks in producing a flight-ready spacecraft. This was a difficult transition, exacerbated by the critical problems with the dewar and probe and the program delays resulting from addressing those issues.

To address the risk issues in all facets of the program, a risk management system was developed by Robert Schultz of Lockheed Martin. Schultz served as the Chief Systems Engineer for both LM and Stanford, and having a “crossover” person in this position turned to be a great advantage to the GP-B mission. The GP-B Risk Management Plan, which is described in more detail in Chapter 5, Section 5.4 “Risk Analysis”, was based on a risk management plan used at the Jet Propulsion Labs (JPL) in Pasadena, California on other NASA missions. The Stanford/LM risk management plan for GP-B was developed during the first half of 2000 and implemented in October of that year. Likewise, engineers at MSFC came up with a parallel and similar risk management plan which they followed for GP-B. On page 19 of their report, Calder and Jones note:

*...A risk management system was finally implemented on GP-B around fiscal year 2000 and the productivity of the program increased tremendously. Additionally, the nature of the relationship between SU/LM teams and their NASA colleagues improved. GP-B developed a predictable process of scaling the support based on the level of risk, i.e., the higher the risk the more support imparted by NASA. This ensured that the appropriate amount of support was provided and empowered the space vehicle team with the knowledge of what to expect from NASA for any given problem.*

### 6.4.6 NASA/MSFC Management of GP-B

During the early years, GP-B was a NASA-funded university research program, managed from NASA Headquarters with minimal oversight, first by Nancy Roman and later by Jeffrey Rosendhal. In 1971, NASA Headquarters formally transferred management oversight responsibility for GP-B to the Marshall Space Flight Center, where Richard Potter provided guidance and support through 1993. During the last 10 years of Potter’s term as the nominal program manager for GP-B, other MSFC managers shared the management responsibilities, including Joyce Neighbors, then Rein Ise, and finally Steve Richards. From 1990-1993, GP-B management oversight transitioned from Potter to Ise, and then to Richards. Ise and Richards had joint responsibility from 1993-1995, at which time Rex Geveden took over as the first formal program manager for GP-B. Towards the end of 1995, Tony Lyons joined the GP-B program as Chief Engineer from NASA/MSFC. Furthermore, Rudolph Decher provided guidance to the GP-B from 1965 until his death in June 2004, just a few weeks after GP-B’s launch.

Because GP-B was viewed as a “management experiment,” with Stanford University serving as NASA’s prime contractor, NASA Headquarters and MSFC provided minimal management oversight—essentially monthly advice and consent—to GP-B management at Stanford throughout the flight hardware development period from 1984-1996. However, in monitoring the hardware issues and schedule delays that occurred from 1997-2002, as GP-B transitioned from an R&D program to a NASA flight mission, upper management at NASA Headquarters became increasingly concerned about the viability of the GP-B mission, and this ultimately led to NASA taking a much more active role in the management of GP-B as it was readied for launch.

In 1998, following a recommendation from one of the NASA independent annual reviews, Francis Everitt assembled an external GP-B Science Advisory Committee (SAC), comprised of eight distinguished scientists, with expertise in various areas of relativistic and gravitational physics, low-temperature physics, and

astrophysics/cosmology. Many of the committee members were associated with other NASA missions related to GP-B. Clifford Will, a world-renowned expert in relativity and gravitational physics, was invited to chair this committee. The purpose of the SAC was to review and advise the GP-B management team on all aspects of the mission, including the functioning of the probe and spacecraft, possible sources of error, as well as the final data analysis. As of the time this chapter was written, the SAC has met 16 times and is scheduled to meet again late in 2007 to review the final experimental data analysis and results.

Even before the Probe C thermal disconnect problem, it had become apparent that the GP-B launch date would need to be pushed back. The discovery of the Probe C thermal problem and the pickup loop problem with gyro #4 in mid-1999 increased NASA's concern about the program's viability. As a result, Dan Golden, then the NASA Administrator, commissioned an independent review team (IRT) comprised of outside scientists and aerospace experts to examine the progress that had been made on the program to date, and to advise NASA as to whether the mission should be terminated or continue to proceed towards launch. GP-B senior management successfully defended the program, but there was an issue with the program funding. Because of budget constraints, NASA was unable to honor GP-B's level-funding plan. (See [Section 6.3.4, NASA Funds GP-B as a Flight Program.](#)) Consequently, the program was never able to increase the electronics and spacecraft development efforts to desired levels, and the result was further delays in the completion of those systems.

At the beginning of 2000, Stanford and Lockheed Martin management prepared a plan, including a revised time line and budget, for addressing the issues with Probe C and gyro #4 and for moving GP-B to the launch pad. The following month, Golden, convened another top-level review of GP-B at NASA Headquarters. Everitt, Parkinson, Buchman and other senior management from Stanford, as well as senior management from LM and MSFC were all present at this meeting. At this point, NASA's main concern was the viability of the GP-B mission, minimizing of risk, and constraining the remaining time and cost of completing the mission. Once again, Everitt, Parkinson, and Buchman prevailed, and GP-B was given a green light to proceed, with launch now anticipated in May 2002. However, at this point, Ed Weiler, the head of the Science Mission Directorate at NASA Headquarters, under which GP-B was managed and funded, placed full responsibility for the successful launch and completion of the GP-B mission in the hands of Arthur Stephenson, then the Director of MSFC. Stephenson interpreted this directive as meaning that a team of MSFC managers, scientists, and engineers, led by Geveden, needed to get actively involved in the day-to-day activities of GP-B.

Thus began a difficult two-year period from 2000-2002, during which the three entities involved—MSFC, Stanford, and LM—had to figure out how to communicate and work together effectively and harmoniously. Each of these entities had its own “culture” and ways of doing things that were successful for each entity respectively. These differences were an advantage in the early stages of the program when innovation and technology development were most important. However, in the focused environment of meeting a launch schedule while trying to minimize the risk of failure, these three divergent cultures collided. For example, the Stanford scientists and engineers, who excelled at innovating technology, were unaccustomed to the rigorous, methodical, procedural nature of the aerospace industry. Likewise, seasoned aerospace managers were frustrated by the tendency of university researchers to continue tinkering with and perfecting technologies past a stage that would be “good enough” to meet necessary milestones in a tight schedule.

In addition to the differences in culture, the Stanford management team, particularly with Parkinson's reduced involvement after 1998, had little collective experience with the intricacies of launching a satellite. At this stage in the program, they often needed help from NASA and from LM. The issue was that Stanford needed to learn how and when to request help from MSFC and LM. Likewise, MSFC, in particular, needed to learn when and how best to respond to such requests.

Furthermore, unlike the Chandra Telescope mission in which MSFC was actively involved in every step of the design and development, MSFC scientists and engineers had minimal involvement in the development of GP-B hardware and technology, since most of the development was done at Stanford and Lockheed Martin, under the

supervision of the Stanford GP-B management team. Thus, when Stephenson and Geveden began sending teams of NASA personnel to Stanford to support the program, this proved to be problematic. As stated in the Calder-Jones Report, page 33:

*...The Stanford and Lockheed Martin teams were unprepared for this influx from NASA and initially it slowed GP-B's progress even further. Engineers and scientists were now not only attempting to solve their own technical issues but were being forced to meet, brief, and report their activities at a level [of detail] far beyond what they were accustomed to...*

The situation was also frustrating for the MSFC engineers, who originally felt that they had a mandate from Stephenson to gain as much insight into GP-B as they had with Chandra. Eventually Stephenson clarified that while he recognized that Chandra-level insight was not possible, he still wanted MSFC to have an appropriate level of insight, and he directed Geveden to find a more productive solution. It fell to Lead Systems Engineer Buddy Randolph to devise a risk-based oversight system, based on a risk management system and a 5-level insight system developed by the MSFC Engineering Directorate.

Other factors served to improve the working relationships, including the constant efforts of Resident Manager Ed Ingraham, a communications plan negotiated and signed by Geveden, Buchman, and Hugh Dougherty (LM Program Manager), additional systems engineering personnel brought in by LM, and efforts by Stanford personnel, in many cases with LM support, to adopt such NASA and industry practices as risk management systems, fault tree analyses, and requirements verification. Others who contributed significantly to these efforts included LM Lead Systems Engineer Bob Schultz, LM systems Engineer Rich Whelan, and MSFC systems engineer Brian Mulac.

The Space Vehicle Acceptance Review (SVAR) in June 2003 was a significant, and much-improved, contrast to the Payload Acceptance Review (PAR). While the PAR issues took a long time to close (almost until the SVAR, in some cases), the noticeably-fewer SVAR issues closed within weeks. The entire team had clearly stepped up to the job of getting the space vehicle ready for transport to Vandenberg AFB for launch.

Unfortunately, in late 2003 there was a need for one last launch delay, to April 2004. This meant one more review with NASA Headquarters to establish a new launch date. The competence of the Stanford-LM-MSFC team clearly showed, with convincing and viable plan being presented to NASA managers. The result was a smooth, non-controversial review that established April 17 as the target launch date. The GP-B team successfully held to this schedule throughout the pre-launch processing until launch vehicle delays moved the launch to April 20. (See Sections 6.5.2 and 6.5.3 for further discussion of this launch delay.)

In July 2002, Geveden became Deputy Director of the MSFC Science Directorate, and in July 2003, he became Deputy Director of MSFC, but he remained Program Manager for GP-B through August 2004, when GP-B completed its Initialization and Orbit Checkout (IOC) phase. In October 2004, Geveden moved from MSFC to NASA Headquarters to become the NASA Chief Engineer, and in August 2005, he was promoted to the position of NASA Associate Administrator. In September 2004, Tony Lyons became Program Manager for GP-B, a position which he still holds. Arthur Stephenson stepped down as Director of MSFC in May 2003, and he subsequently retired from NASA in January 2004.

Pictured in [Figure 6-10](#) below are eight persons as MSFC who guided and/or supported the GP-B program since 1965, including: Rudolph Decher (1965-2004), Richard Potter (1971-1996), Joyce Neighbors (1981-1993), Rein Ise (1985-1996), Steve Richards (1990-1995), Rex Geveden (1995-2004), Tony Lyons (1998-Present), and MSFC Director, Arthur Stephenson (1998-2003).



**Figure 6-10.** MSFC Program Managers/supporters of GP-B since 1995. Clockwise from top left: Rudolph Decher, Richard Potter, Joyce Neighbors, Rein Ise, Steve Richards, Rex Geveden, Tony Lyons, and Arthur Stephenson.

In addition to the NASA/MSFC managers/leaders above, four other persons pictured below in [Figure 6-11](#) played important roles in the success of GP-B. They include NASA Resident Manager, Edward Ingraham, Integration Manager, Todd May, Chief Engineer/Lead Systems Engineer, Buddy Randolph, and Chief Engineer/Subsystem Manager, Stephan Davis.



**Figure 6-11.** MSFC resident and engineering managers. Left to right: Edward Ingraham, Todd May, Buddy Randolph, and Stephan Davis.

Among many at NASA Headquarters who helped make GP-B happen, in addition to Nancy Roman and Jeffrey Rosendhal, were Dixon Ashworth, George Albright, Colleen Hartman, Samuel Keller, Anne Kinney, Frank Martin, Frank McDonald, Ernest Ott, and Charles Pellerin. The current GP-B program executive at NASA Headquarters is Alan Smale.



## **6.5 Final Integrated Testing, Launch & Science Mission (2002-2005)**

In November 2002, Gaylord Green became Program Manager. During 2001-2002, Green, who had considerable prior spacecraft operations experience—including working with Parkinson on the development and deployment of the U.S. Air Force's Global Positioning Satellite System—had been responsible for organizing the ground support operations for GP-B at the Vandenberg Air Force Base launch site on the southern California coast. At the time he assumed the job of Program Manager, the spacecraft was being prepared at Lockheed Martin for a thermal vacuum test—a ground simulation of the conditions that the spacecraft would encounter in orbit.

### **6.5.1 The Thermal Vacuum Test**

Before the thermal vacuum test began, the LM mechanical team inadvertently left some unshielded wires resting against the spacecraft. Then, on the next shift, when the electronics team powered up the spacecraft for the electronics test, four fuses blew, preventing heater strips from being powered. Thus, during the thermal vacuum test at the cold temperatures of space, the associated heaters were not turned on and certain parts of the spacecraft were too cold. Also, a vent on the dewar's guard tank leaked into the thermal vacuum chamber, degrading the vacuum.

With the launch date now set for December 2003, and what appeared to be yet another possible problem with the spacecraft, NASA Headquarters convened yet another program review to determine whether to proceed towards launch or cancel the program. Both the NASA Independent Review Team and the GP-B Science Advisory Committee recommended that GP-B continue with launch preparations. To ensure minimal risk, NASA decided to repeat the thermal vacuum test following a spin balance test early in 2003. The second thermal vacuum test was performed in May 2003 without issue. Shortly thereafter, in July 2003, the spacecraft was loaded aboard a special truck and driven to the launch complex at Vandenberg Air Force Base.

Back at Stanford, throughout the latter part of 2002 and most of 2003, the GP-B Mission Operations Center and the mission operations team worked very hard, preparing for launch. Under Green's management, a total of seven procedural simulations were held to rehearse the GP-B mission operations team both for launch and for an unusually sophisticated initialization and orbit checkout period. Rehearsals for dealing with a number of potential anomalies that could occur on orbit were included in these simulations.

### **6.5.2 Six-Month Launch Postponement for ECU Repair**

In early November 2003, as part of a final spacecraft acceptance review, a grounding problem was discovered in a voltage converter on the Experiment Control Unit (ECU). The ECU was essential for gyro spinup and dewar monitoring, but not for collecting experimental data. Stanford's recommendation was to turn off the ECU during the actual science experiment, but LM recommended repairing it. NASA Headquarters then had to make a difficult go/no-go decision. This was the ultimate risk management decision, and not wanting to possibly jeopardize the experimental results, NASA Headquarters reluctantly decided to postpone the launch for 5-6 months so that the ECU could be returned to LM for correction of the voltage converter problem.

### **6.5.3 Successful Launch and Flight Mission**

Modifications to the ECU were completed in March 2004, and the ECU was then shipped back to Vandenberg and reinstalled on the spacecraft frame. A new launch date was set for mid April, and a pre-launch press conference was held at NASA Headquarters at the beginning of April. The GP-B team, which at that time included people from LM and NASA and totaled close to 200 people was primed and ready when GP-B finally launched on April 20, 2004. It was a flawless launch.

As described in Chapter 2, the flight mission lasted for 17.3 months, including a 4-month initialization and orbit checkout (IOC) phase, a 50-week science (data collection) phase, and a 6-week post-science instrument calibration phase. During the flight mission months, Green organized the mission operations team with rotating Mission Directors and Flight Directors, so that the Mission Operations Center could be staffed 24 hours a day, seven days a week. Every weekday, all-hands status meetings were held at 10:00 AM to brief the entire team on the status of the spacecraft and payload and to address any issues that may have arisen during the previous day or weekend. A more detailed description of mission operations is included in Chapter 4, Section 4.1.2 “Daily Operations Routine”. Green’s management style was an excellent fit for the 17.3-month flight mission. He was able to achieve extraordinary performance from the GP-B mission operations team, which led to the entire team being given a NASA Group Achievement Award, presented by Tony Lyons from MSFC, in November 2005, shortly after the mission concluded.

## 6.6 Data Analysis Period (2005-2007)

Throughout the flight mission, the GP-B team numbered approximately 150 people, a large percentage of whom were dedicated to mission operations activities. Naturally, as the flight mission began to wind down in August-September 2005, the focus of the GP-B began to shift from operating the spacecraft to analyzing the experimental data that had been collected. Between August and November 2005, GP-B said farewell to all but a handful of mission operations personnel. Some of the departing team members had worked on GP-B for ten years or more, and thus the mood at farewell gatherings was a mixture of triumph and sadness.

### 6.6.1 Final Management Transition at Stanford

By the end of November 2005, the GP-B team had shrunk to approximately 30 full-time scientists, engineers, mathematicians, with a small management team and associated support personnel. Gaylord Green, whose strong expertise was managing flight programs, had limited experience and little interest in managing the data analysis team, and thus he began reducing his involvement in the program, as did Deputy Program Manager, Tom Langenstein. Realizing that GP-B had reached another management transition point, Francis Everitt announced in March 2006 the appointment of Bill Bencze to assume the role of GP-B Program Manager for the duration of the data analysis period. Bencze had demonstrated his leadership skills as manager of the GSS development team. His strong organizational skills, coupled with his broad knowledge of the program and his ability to communicate effectively with scientists, engineers, and management, made him an excellent choice to manage the final phase of GP-B. In his announcement of Bencze’s promotion to Program Manager, Everitt also praised Gaylord Green for his superb leadership during the flight mission years:

*This is the moment to record our tremendous admiration and respect to Gaylord for the brilliant job he did in the four and a half years as Program Manager since November 2002. As we look back, we will all agree that those have been the most stirring years in the history of GP-B. It is an immense tribute to Gaylord that we came through them so successfully. I am confident that with Bill we will have corresponding success in the different, but no less stirring, time leading to our final result.*

Bencze was one of the key architects of the GP-B three-phase data analysis plan, and thus he is intimately familiar with the process and the issues that the team is working through. His chief management challenge for the remainder of the data analysis phase is to synthesize the various threads of the analysis process into a coherent picture, keep the team focused on the important issues, keep the analysis on track, and ensure that the final results will have the lowest margin of error possibly attainable within the time and budget constraints of the analysis phase.



## 6.6.2 Gallery of GP-B Program Managers/Deputies at Stanford

Pictured in [Figure 6-12](#) below are the six people who served as GP-B Program Manager over its 47-year history.



**Figure 6-12.** GP-B Program Managers. Clockwise from top left: Bradford Parkinson, John Turneaure, Sasha Buchman, Ron Singley, Gaylord Green, and Bill Bencze and GP-B

Pictured in and [Figure 6-13](#) below are three of the GP-B Deputy Program Managers. (Other people who also served as Deputy Program Manager are pictured elsewhere in different roles.)



**Figure 6-13.** GP-B Deputy Program Managers. Left to right: Robert Farnsworth, Tom Langenstein, and Robert Brumley

## 6.7 Some Observations on the Management Experiment

We have strong and deep reason to believe that the GP-B management experiment concept—NASA with skillful oversight, university as prime contractor, aerospace company as major subcontractor—was absolutely crucial to the success that the GP-B mission achieved. Following are some observations about the key ingredients that led to this success.

**NASA's Oversight Role** The management experiment concept enabled the building of a GP-B team that could both develop the many new and unique technologies required by the experiment—efficiently and effectively—and also take the mission through its full lifetime. Stanford and Lockheed Martin required only minimal oversight from NASA during the technology development phase. Then, as the program approached launch, NASA provided the increased oversight and assistance necessary to minimize risk and ensure flight readiness of the spacecraft and the team. Once the spacecraft was in orbit and the IOC phase completed, Stanford and LM once again required only minimal NASA oversight in successfully completing the flight mission. Finally, during the equally-critical data analysis period, the LM team members moved on to other aerospace projects, as the Stanford team carried out the final phase of the GP-B program.

**Subcontractor Selection** Following a thorough, by-the-book selection process to find the very best possible talent, spacecraft experience, and matching team spirit in an aerospace subcontractor for integration with the university's science and engineering team was an essential ingredient in the success of GP-B through every stage of the program.

**Incremental Prototyping** The incremental prototyping method enabled the development of unique technologies—the very essence of GP-B—from initial conception to flight readiness much faster and more efficiently than the traditional final-design specification-to-contractor approach would ever have been able to do.

**Highly Competent People and a Cohesive Team** The first ingredient for program success was the forming of a synergistic senior management team. Next came the cultivation of knowledgeable and skilled second-level managers for the various development areas and the selection of the best program manager for each phase of the program. It was concurrently essential to find and attract truly talented and competent people—including some outstanding university students—to provide the deep expertise needed in so many first-time-ever areas of research and technology development. Finally, it was essential to bond all these people—independent of their home groups—into a cohesive team, in which everyone knew each other well, and each respected the knowledge and judgment of each other person. (When a team member speaks in a status review meeting, every other person in the room listens carefully. This was inspiringly true through every day of the seventeen-month flight mission.)

**NASA Personnel at Stanford** The decision to place specific NASA personnel directly on the GP-B program at Stanford was both cost-effective and a win-win strategy for both NASA and Stanford. This practice enabled Stanford to assimilate at once team members having critical experience in areas ranging from management to science without the long and involved process of university hiring. Conversely, this practice enabled key NASA people to work in a cutting-edge flight mission—an invaluable experience that they could bring to their next NASA program assignment.

## 6.8 Sources and References

Following are the main source and references consulted in writing this chapter.

**The GP-B Green Book** A Report on a Program to Develop a Gyro Test of General Relativity in a Satellite and Associated Control Technology, June 1980, pp. 1-10.

***Near Zero: New Frontiers of Physics*** J. D. Fairbank et al., Editors. New York, W. H. Freeman and Company, 1988, pp. 587-608.

From the preface: [Near Zero is] a book detailing the work of a group of physicists associated with William Fairbank who explored the regions of physics opened up by making one or more of the variables of physics very nearly zero. The idea of the book was conceived in August 1981 during the 16th International Conference on Low Temperature Physics, at which time about twenty people, mostly former students and associates of Fairbank, met to plan a scientific conference to honor him on the occasion of his 65th birthday....

The conference was held at Stanford in March 1982, with nearly 150 participants. This book, which includes an entire chapter on GP-B, was one of the outcomes of this conference.

***Gravity Probe B: Countdown to Launch*** by C.W.F. Everitt, S. Buchman, D.B. DeBra, G.M. Keiser, J.M. Lockhart, B. Muhlfelder, B.W. Parkinson, J.P. Turneure and other members of the Gravity Probe B team. Included in *Gyros, Clocks, Interferometers...: Testing Relativistic Gravity in Space* (Lecture Notes in Physics), Edited by C. Lammerzahl, C.W.F. Everitt, F.W. Hehl, Springer, 2000, pp. 52-82.

This paper provides a summary of the history of GP-B and a detailed progress report on the development and testing of Probe C, as of spring 2000. An Adobe Acrobat PDF copy of this paper is available for downloading from our GP-B Web server at: [http://einstein.stanford.edu/content/sci\\_papers/papers/Everitt\\_et\\_al-Cntdwn-launch-2000.pdf](http://einstein.stanford.edu/content/sci_papers/papers/Everitt_et_al-Cntdwn-launch-2000.pdf)

***Gravity Probe B: A Management Study*** A report to NASA by Edward S. Calder and Bradley T. Jones, April 21, 2006.

Because some aspects of GP-B program management were unique among NASA programs, and because GP-B was viewed as a management experiment as well as a scientific experiment, in 2005, NASA Headquarters commissioned two former GP-B team members, Ned Calder from the Engineering Systems Division at MIT and Brad Jones, from the Aeronautics & Astronautics Department at Stanford University to research and prepare an independent study on the management of GP-B. In the spring of 2006, Calder and Jones presented their finished report to NASA. An Adobe Acrobat PDF copy of the complete Calder-Jones GP-B Management Study Report is available for downloading from the GP-B Web server at: [http://einstein.stanford.edu/pao/pfar/cj\\_report-apr2006.pdf](http://einstein.stanford.edu/pao/pfar/cj_report-apr2006.pdf).

Some of the information in this chapter—especially in the latter sections—was drawn, in part, upon observations from this report, and a few excerpts from the report have been quoted directly. (The quoted excerpts have been identified accordingly.) In addition, a summary of lessons learned from the GP-B management experiment, as described in the Calder-Jones report, is included in [Section 16.3, Management Lessons from the Calder-Jones Report](#).

***Personal Conversations*** In the process of writing this chapter, all of the following people were interviewed: Bill Benze, Sasha Buchman, Robert Cannon, Daniel DeBra, Francis Everitt, Gaylord Green, David Hipkins, Tom Langenstein, Barry Muhlfelder, Bradford Parkinson, Mike Taber, and John Turneure.



# 7

## Attitude & Translation Control Subsystem Analysis

---







## 7.1 ATC Background and Overview

The Attitude and Translation Control System (ATC) controls all proportional micro thrusters and magnetic torque rods that determine and maintain the spacecraft's precise position relative to the science gyro serving as the drag-free proof mass and the spacecraft's pointing direction. The position, acceleration, attitude and rotation rates of the space vehicle are measured by several redundant sensors. These sensors include both the control and science gyroscopes, star sensors, magnetometers, coarse sun sensors, GPS receivers, and the science telescope. The choice of which set of sensors are used at a given time depends on the configuration of the ATC subsystem. Feedback control logic takes the measured position, acceleration, attitude and rotation rates and computes commands sent to the thrusters and magnetic torque rods in order to maintain the space vehicle in the desired position and attitude.

The requirements for the Attitude and Translation Control subsystem are twofold. First, the position of the space vehicle must be accurately centered about one of the Science Gyroscopes so that the forces (control efforts) and torques applied to the science gyroscopes are rigorously minimized during the Science Mission. Second, the GP-B space vehicle must remain accurately pointed at the Guide Star IM Pegasi, during gyroscope spin up and throughout the Science Mission phase to provide the distant inertial reference and to minimize torques due to mis-pointing.

### 7.1.1 ATC Hardware

The ATC subsystem consists of a network of sensors, actuators, and computer/data management hardware and software, with the purpose of maintaining the spacecraft's pointing and position within the orbit to very strict tolerances. Of all the metrics to measure the ATC's performance, the ability to maintain pitch/yaw attitude on the guide star, the ability to maintain the spacecraft's position in roll phase and roll rate, and helium gas mass flow usage are of primary importance. In the table below is a list of the control system equipment used on orbit.

**Table 7-1.** Control System Equipment List

**Table 1. Control System Equipment List**

Component	Number Required	Size (cm)	Supplier
Control gyro	2	28x18x14	Kearfott Guidance and Navigation
Star sensor	2	27x17x11	Hughes Danbury Optical Systems (HDOS)
Magnetometer	2	4.8x6.7x11.9	Macintyre Electronics Design Associates (MEDA)
Coarse sun sensor	3	6x5x5	LMMS
Dewar pressure transducer	2	2x0.8 dia	Endevco
GPS Receiver (CFE)	1	12x27x8	Trimble
Antenna (CFE)	8	10x10x2	
Thruster	16	N/A	LMMS
Attitude Control Electronics	1	31x20x51	Spectrum Astro
Magnetic torque rods	3	91x 3	Ithaco

## 7.1.2 Vehicle ATC Modes

There are essentially 6 vehicle ATC modes (1A, 1B, 1C, 2A, 2B, 3A). Mode 1B is the science mode, with pitch/yaw attitude reference (“pointing”) supplied by the guide star and the TRE/Science Telescope package. Mode 2A is a telescope acquisition mode with pitch/yaw attitude reference updates supplied by reference star trackers. Mode 2A is also used when the telescope is unavailable such as during gyro spin-up and flux flush.

### 7.1.2.1 ATC Mode 1B

- Actuators – Thrusters (plus MTS optional)
- Pitch/Yaw “pointing” attitude – Science Telescope
- Pitch/Yaw rate – Control Gyros
- Roll Attitude – Star Trackers updates Control Gyros
- Roll Rate – Control Gyros

### 7.1.2.2 ATC Mode 2A

- Actuators – Thrusters
- Pitch/Yaw “pointing” attitude – Star Trackers update Control Gyros
- Pitch/Yaw rate – Control Gyros
- Roll Attitude – Star Trackers updates Control Gyros
- Roll Rate – Control Gyros

## 7.1.3 GS Valid/Invalid

During the science mission when the Guide Star is obscured by the Earth or other bodies (Guide Star Invalid, see [Figure 7-1](#) below), ATC Mode 1B automatically reconfigures to Gyro Hold. In this mode, the vehicle pointing is held fixed by integrating the control gyros. Until such time that the obstruction to the Guide Star is gone, slight drift of the control gyros takes place. When line of sight to the Guide Star returns as predicted by the onboard ephemeris, the attitude reference is turned back on, and the ATC recaptures the Guide Star by using polarity information from the telescope.

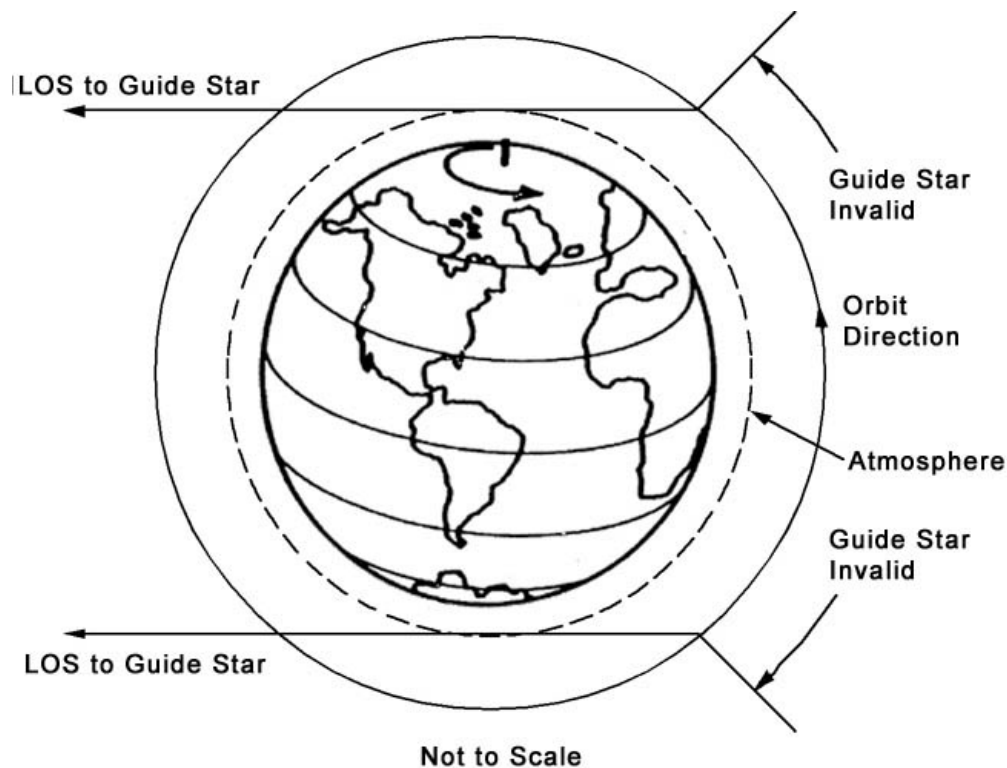


**Figure 7-1.** Schematic of Guide Star Valid (GSV) and Guide Star Invalid (GSI) periods

### 7.1.4 Guide Star Verification

Guide Star verification was performed by visiting two neighbor stars during IOC. On 2004/162, Neighbor Star 1 (HD 216635) was acquired and held in the FOV for approximately 15 hours. On 2004/167, Neighbor Star 1 was acquired again and held for approximately 3 hours. On 2004/169, HR Pegasi was acquired and held in the FOV for approximately 1 hour. Additionally, the Science Team was able to confirm the identity of these neighbor stars through inertial location in space, and by star brightness.

## 7.2 He Thruster Technology

Translation and attitude control of Gravity Probe-B is achieved primarily through the use of sixteen thrusters. The thrusters use helium boil-off from GP-B's dewar for propellant. Since the rate of boil-off in the dewar is on the order of milligrams per second, each thruster is capable of imparting a very small amount of force on the space vehicle (the requirement for maximum thrust is 8 mN per thruster using  $6.9 \times 10^{-6}$  kg/s or less of helium).

The purpose of this section is to show the level of minuteness that the amount of thrust produced by these thrusters can be controlled to. A quantitative measure for this is derived from on-orbit telemetry and ground testing. Furthermore, several analogies are made between this numerical figure and figures commonly encountered in everyday life in order to provide the reader with a qualitative feel for this parameter.

The amount of thrust produced by each thruster can be linearly regulated. Ground testing has revealed a directly proportional relationship between thrust and pressure in the restrictor of the thruster.

Pressure in the restrictor is controlled by movement of the piston and measured by an Endevco Model 8510B-1 sensor. The sensor is a piezoresistive type transducer with a range from 0 psig to 1 psig (or equivalently, 0 torr to 51.706 torr).

The output of the pressure transducer as read by the onboard computer and sent to the ground through telemetry is in mV. The conversion from mV to psig (or torr) varies from transducer to transducer, but is guaranteed by the manufacturer to fall in the range of  $200 \pm 50$  mV/psig. Thus, each mV measured by the sensor corresponds to roughly 0.20684 torr to 0.34473 torr.

Figure 7-2 is a plot of twelve hours of restrictor pressure data recorded on-orbit in Thruster 5.

A prominent feature of this plot is a lower bound on the pressure (at roughly 1.4 mV), which is sustained for nearly the full duration of the time period examined (Note: this behavior can also be observed in Thruster 7). There are occasional dips below this bound due to noise and perhaps transient conditions, but the overall inference to be made is that the thrusters can consistently control the restrictor pressure to a reading of 1.4 mV.

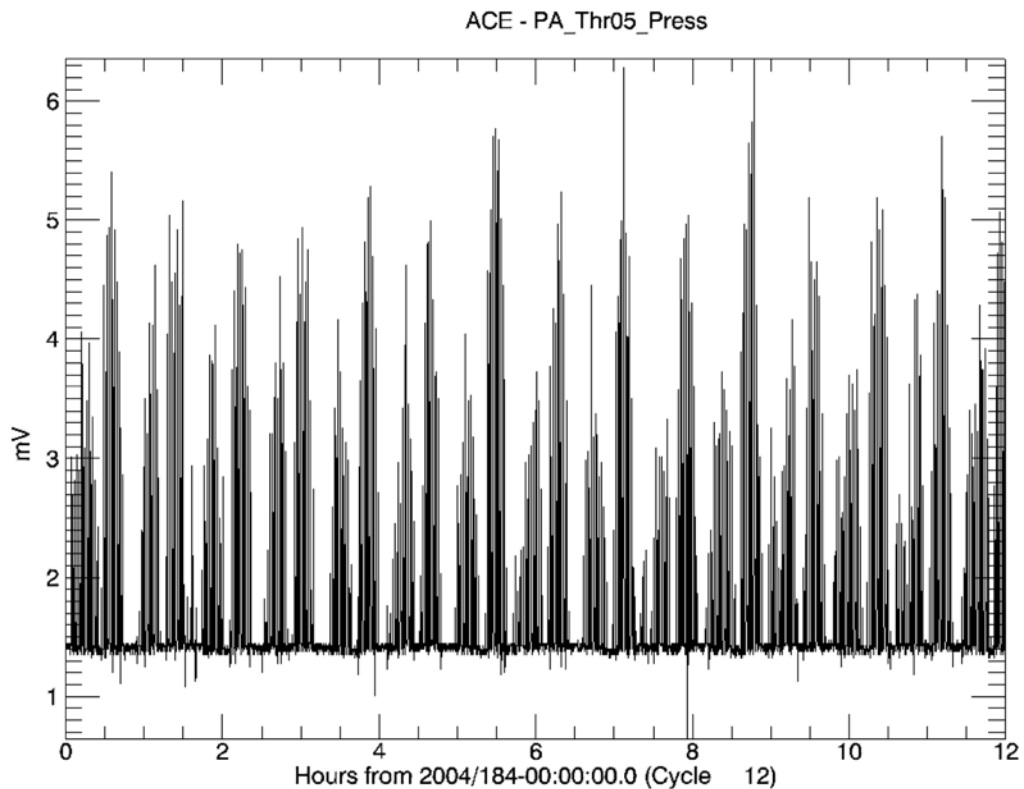


**Figure 7-2.** 12 hours of thruster pressure data from 2004 day 184

Since people in general do not think in terms of mN it is helpful to draw several analogies to put the figure of 1 mN of thrust into perspective. For instance, a 1 lb weight produces a force equivalent to 4,442.8 mN and the average American male in his twenties weighs 168 lbs. or roughly 745,000 mN. Furthermore, a male body builder capable of bench-pressing 500 lbs. could be shrunk to  $1/2,200,00^{\text{th}}$  of his normal size and still be able to bench press a 1 mN weight. Also, if everyone at a sold out game in 3 Com Park (which has a maximum capacity of 64,450) held a 1 mN thruster underneath a 15 lb bowling ball, they would still need an extra 2,300 thrusters to lift it off the ground.

In summary, ground testing and flight data indicate that the helium thrusters on Gravity Probe-B can be linearly controlled down to roughly 1 mN of thrust. This is a number that is so incredibly small, that it takes creative use of analogies for one to truly appreciate it and its role in the demanding task of testing Einstein.

## 7.3 ATC Performance

Data gathered from the GP-B space vehicle throughout the mission shows that the ATC system is performed well. The back up drag-free control mode, which minimizes gyro control effort, is used as the translation control mode throughout the Science Mission phase. Drag-free operations have proven to reduce control forces applied to the gyroscopes by a factor of 10 and generates a cross track control force on the order of a mere nanonewton at the roll rate frequency. Also, the attitude control system has proven to maintain the pointing of the GP-B Science Telescope to within a few hundred milliarcseconds of the Guide Star IM Pegasi. More importantly, the Science Telescope signal is kept in the linear range roughly 95% of the time while the Guide Star is not eclipsed by the Earth. Finally, the roll rate component of the attitude error signal has generally been at or below 10 milliarcseconds rms while the notch filter on the rate path error is enabled.

### 7.3.1 Pitch/Yaw Pointing

At the start of the science phase of the Gravity Probe B mission, the Science Telescope and gyroscope spin axes are aligned with the Guide Star IM Pegasi. Over the course of the Science Mission, the GP-B Science Telescope remains precisely pointed at the Guide Star.

If the predictions based on Einstein's theory are correct, the gyroscopes' spin axes should slowly drift away from their initial Guide Star alignment, in both the space vehicle's orbital plane, due to the curvature of local spacetime, and perpendicular to the orbital plane, due to the frame-dragging effect. These relativistic effects in the vicinity of a small planet like the Earth are barely noticeable. For example, the spin axis deflection due to the frame-dragging effect corresponds to the width of a human hair as seen from 100 mile away. In order to detect such minute deflections in the gyroscopes' spin axes, the GP-B Science Telescope must remain pointed at the Guide Star with equivalent accuracy.

The Guide Star pointing error is computed using the Science Telescope signals. The telescope measures the Guide Star position in the  $x$  and  $y$  orthogonal directions independently. The GP-B Science Telescope focuses the starlight in the "lightbox" at the telescope's front end. [Figure 7-3](#) is a general schematic of the Science Telescope components. Light from the Guide Star enters the telescope and is separated into two signals with a beam splitter. One signal is used to measure the Guide Star position in the  $x$  direction, and the other is used to measure the Guide Star position in the  $y$  direction. In each direction, the Guide Star's image is sliced into two half disks which are directed to hit opposite ends of a tiny sensor. The sensors convert each half signal into voltages  $S^+$  and an  $S^-$  corresponding to each half disk image. The difference between these two signals is then a measurement of how well the Guide Star image is centered on the roof prism, and hence provides the ATC system with attitude (pointing) error during Guide Star Valid periods. A Guide Star Valid period refers to the period of time when the view from the GP-B space vehicle to the Guide Star IM Pegasi is not blocked by the Earth.

# GP-B Telescope

## Image Divider & Detector Assemblies

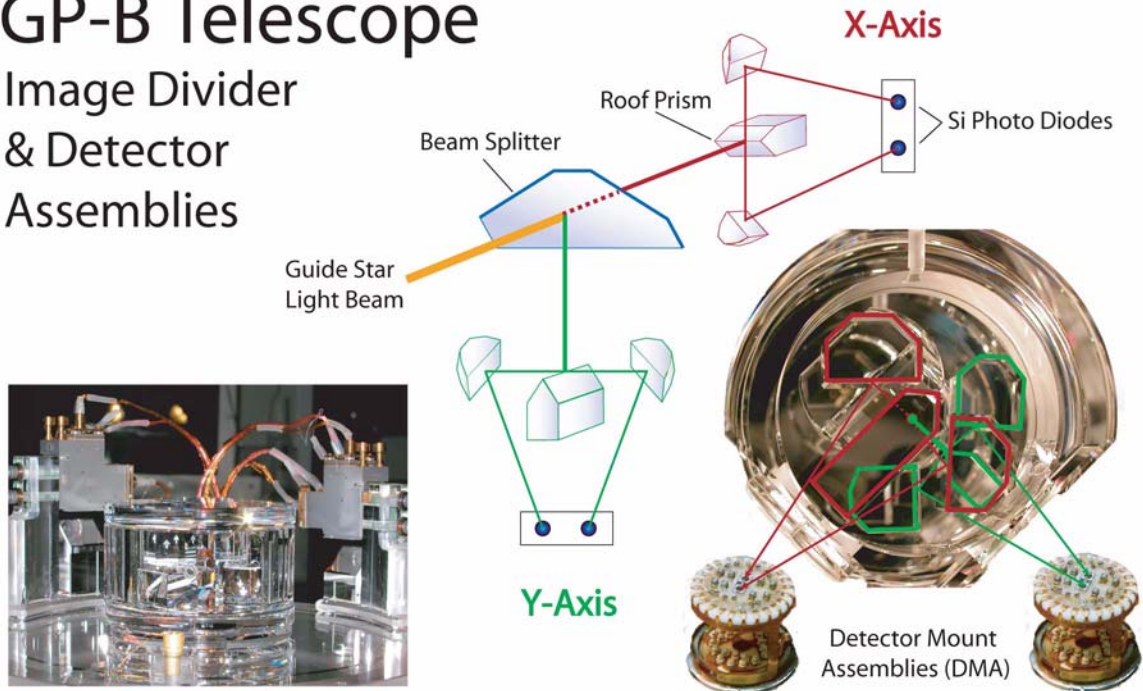


**Figure 7-3.** Science Telescope Components Schematic

The  $S^+$  and  $S^-$  telescope signals are differenced and normalized as follows.

$$S_N = \frac{S^+ - wS^-}{S^+ + wS^-}$$

Here,  $w$  is a weighting coefficient that accounts for differences between the  $S^+$  and  $S^-$  telescope detector biases. The resulting quantity  $S_N$  is the normalized telescope signal.  $S_N$  varies from +1 to -1 where a zero value indicates zero pointing error. In general,  $S_N$  is a nonlinear function of pointing error. However, for small values of  $S_N$ , the relation is nearly linear. Figure 7-4 shows qualitatively the relation between  $S_N$  and pointing error.

The onboard software also allows a constant to be used to minimize noise in the denominator, representing the detector sum signal. A constant is used based on the measured data from the detectors, rather than calculating the denominator for each measurement. Since the denominator is essentially the total light entering on one axis, the value used onboard is the mean value of the total signal on each axis.



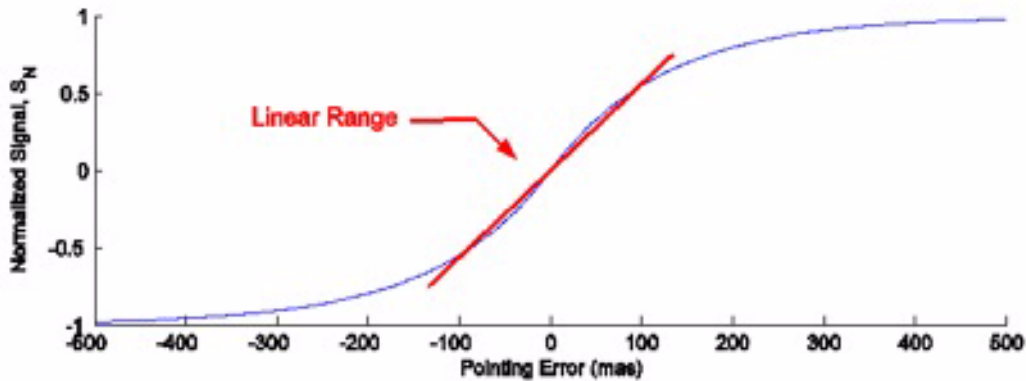


**Figure 7-4.** Normalized Telescope Signal vs Pointing Error

### 7.3.1.1 Pointing Accuracy Requirements for Science Data Analysis

In order to determine the direction of the spin axes of the Science Gyroscopes relative to distant space, the orientation of the GP-B space vehicle must be known accurately. The normalized telescope signal is used to precisely determine the pointing error of the vehicle. The pointing error is subtracted from the gyroscope spin axis direction, measured in the vehicle frame, to provide the spin axis orientation relative to the Guide Star. Therefore, the vehicle pointing error must be known at the same level of accuracy as the gyroscope spin axes. This can be accomplished when the normalized pointing signal is in the linear range.

Also, the pointing error at the roll rate frequency must remain especially small. As we have already seen, any cross track control forces applied to the Science Gyroscopes at the roll rate frequency and cause the gyroscopes to precess or drift. Therefore, we require that the pointing error of the vehicle be especially small at the roll rate frequency so that unwanted gyro suspension forces are not amplified.

The attitude (pointing) control system requirements for science data analysis can be summarized as follows:

- Vehicle pointing error must remain small enough so that the normalized telescope signal  $S_N$  remains in the linear range.
- Pointing error at the roll rate frequency must be especially small so that gyroscope control forces at the roll rate frequency do not generate significant torques.

### 7.3.1.2 Overall RMS

Figure 7-5 below shows the individual pitch and yaw errors over the science mission. The data points are calculated over each individual guide star valid period by taking the rms value of the attitude error, omitting the initial data points (~2 minutes) corresponding to the time required to capture, and damp out accumulated gyro hold drift errors. The individual pitch and yaw pointing error standard deviations have ranged between 100-300 milliarcseconds on the X-Axis and between 150-325 milliarcseconds on the Y-Axis. The corresponding estimate of the telescope noise during this time period using a method outlined by J. Turneure, is approximately 150 marcs per axis.

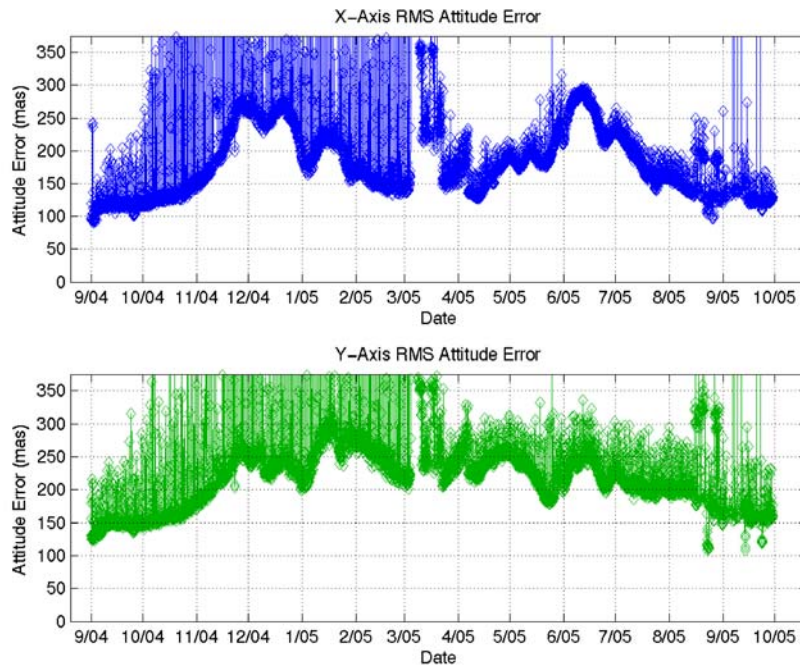


**Figure 7-5.** Pitch and Yaw Pointing Performance during the science mission

There are several events throughout the mission where there is a discontinuity in the more slowly trending data. Most of these outlying points occur during safemodes, where the vehicle switches from mode 1B to mode 2A or 3A in order to ensure a safe recovery from an unexpected error in memory.

The slower trends in these plots are believed to be mostly due to the orbital geometry of the sun. They are somewhat dependent on the gamma angle, the angle the sun vector makes with the boresight of the telescope. Evidence of this can be seen in the mirrored comparison of the pointing at corresponding gamma angles on either side of the telescope. [Figure 7-6](#) below shows a comparison between corresponding gamma angles on either side of the telescope. On March 12, the sun was directly in the orbital plane. After March 12, the pointing essentially retraces its behavior over the first half of the science mission as the sun moves away from the telescope boresight.

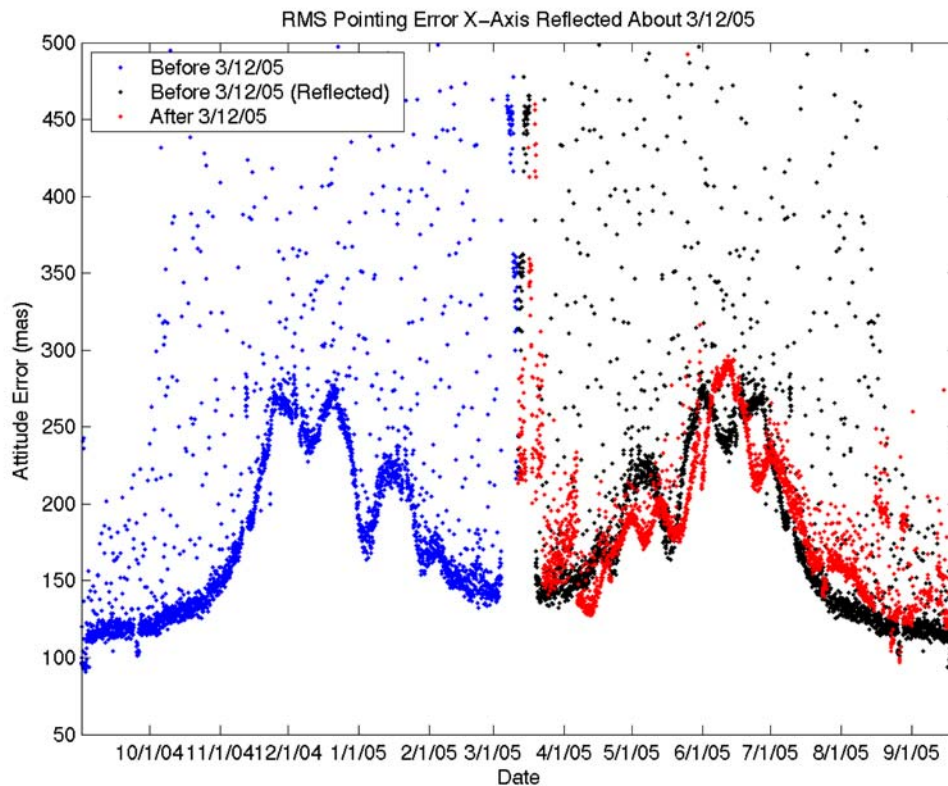


**Figure 7-6.** X-Axis RMS pointing performance correlation with solar angle

While it is difficult to exactly quantify the ATC pitch/yaw pointing performance and its relationship to T003 requirements, the performance does meet the needs of the Science Team and is sufficient for the science mission.

### 7.3.1.3 Roll component RMS

As the mission has progressed throughout the science part of the mission, the orbital geometry has yielded a large disturbance at roll rate due to the roll rate thermal cycle of the ARP. Since the disturbance comes in through the rate gyroscopes and is precisely at the roll frequency, a notch filter on the rate error signal has been very effective at removing the roll rate disturbance from the attitude error. It appears that most of the error at roll rate is transferred to twice roll and higher harmonics. While the overall RMS value of the pointing error increases slightly with the notch filter on, it is the roll component that most heavily affects the science data. The roll component of the pointing error is shown in the following chart, [Figure 7-7](#).

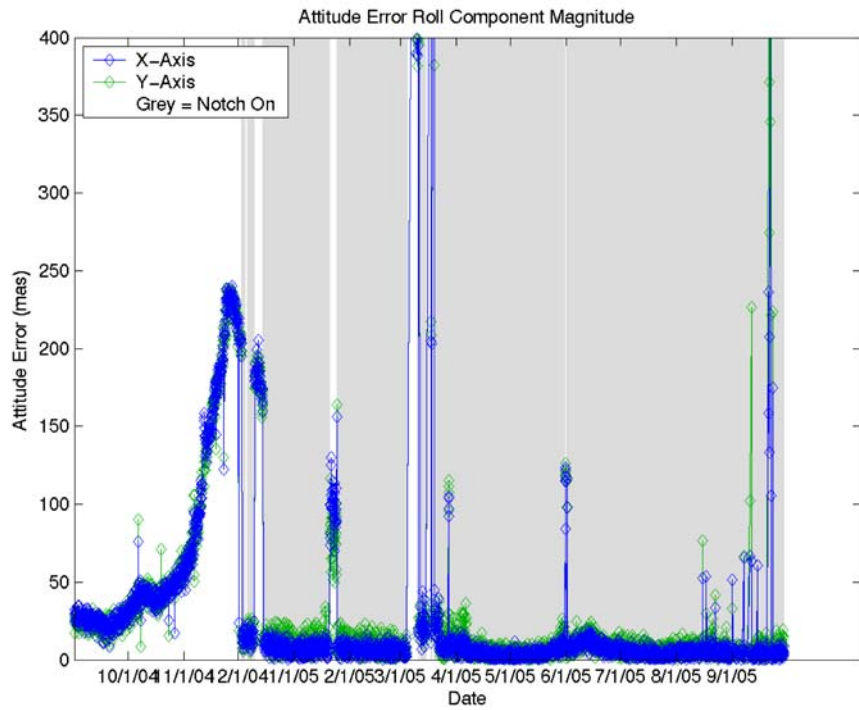


**Figure 7-7.** Magnitude of the roll rate component of pitch yaw pointing performance

Figure 7-8, again shows the correlation between pointing performance and the angle between the telescope axis and the sun vector. The notch filter was implemented in December 2004, and the roll component of the pointing error was only slightly affected by the sun's position following that date.

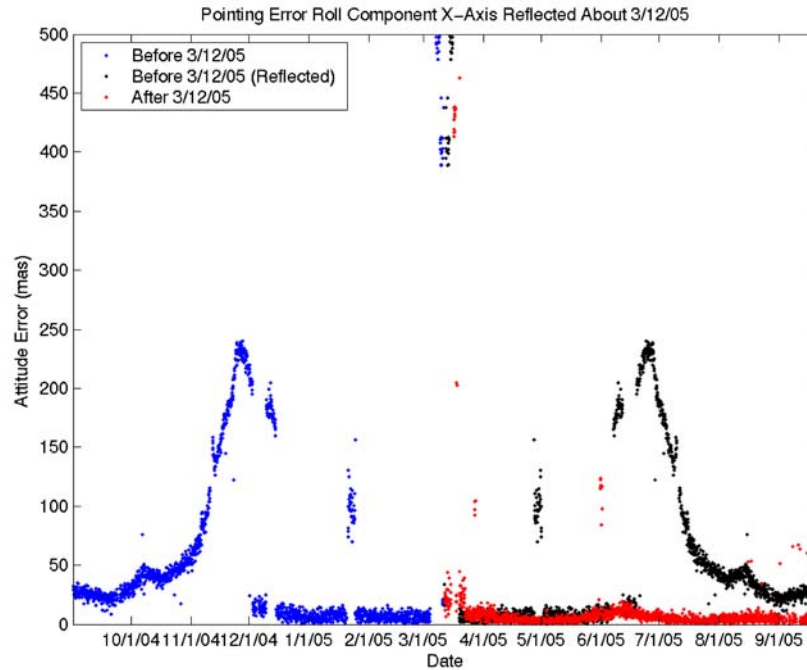


**Figure 7-8.** Correlation of pointing roll rate component with telescope/sun angle

### 7.3.1.4 SAA Behavior

The configuration of the ATC has been slightly adjusted to allow for continued pointing toward the Guide Star during periods of South Atlantic Anomaly (SAA). This was done at the request of the Science Team, and while excessive noise to the telescope detectors is noticed during these periods, much of the noise is filtered out by ATC filters and limits. The remaining noise which does slightly effect high-precision pointing during SAA is found to be a manageable risk as compared to the large benefit of greater mission duration in GSV (an additional 70 minutes, approximately, per day of GSV). Further improvement of the pointing accuracy through the SAA has been achieved by setting the TRE gains and clamp settings to avert the effects of a compilation error in the exception handling of the ATC slopes. This is discussed in more detail in a section below.

### 7.3.1.5 Guide Star Capture Times

Figure 7-9 and Figure 7-10 below show yaw errors immediately at the beginning of a GSV period, taken from two different dates (07 July 2004 and 27 Aug. 2004, respectively). First, one may note that the overall “capture” duration, the time required to damp out gyro hold errors accumulated during the previous GSI period, has been substantially reduced from approximately 13 minutes (07 July 2004) to about 3 minutes. This has been accomplished through the judicious selection of ATC controller gains and limits, and by removing the 7th order polynomial fit for ATC slope in favor of a truncated linear fit. The immediate benefit of this reduced capture duration (10 minutes shorter, approximately) is an additional 10 minutes of science data during a typical 55 minute GSV period. This represents nearly a 20% gain in usable science data per GSV period.

In addition to the gain and limit changes that have been made, we have also expanded the definition of the linear range of the telescope to more heavily weight the proportional term even outside the linear range. Part of the reason the guide star captures were so long, was the rate capture mode was actually driving the telescope away from the guide star before the integrator caught up to the error in the rate gyros due to the motion of the ARP.

Changing the method by which the gyro biases are determined has yielded further improvement. Early in the mission, the ATC system estimated the gyroscope biases onboard by averaging the signal measured while pointed at the guide star. This is a robust, self-calibrating method that served its purpose well during the highly dynamic period of IOC, but is not the most effective way to capture the guide star. Setting the gyro biases manually so they are optimal at the beginning of the guide star valid period has decreased the transient attitude behavior at the guide star valid transition and further shortened guide star captures.

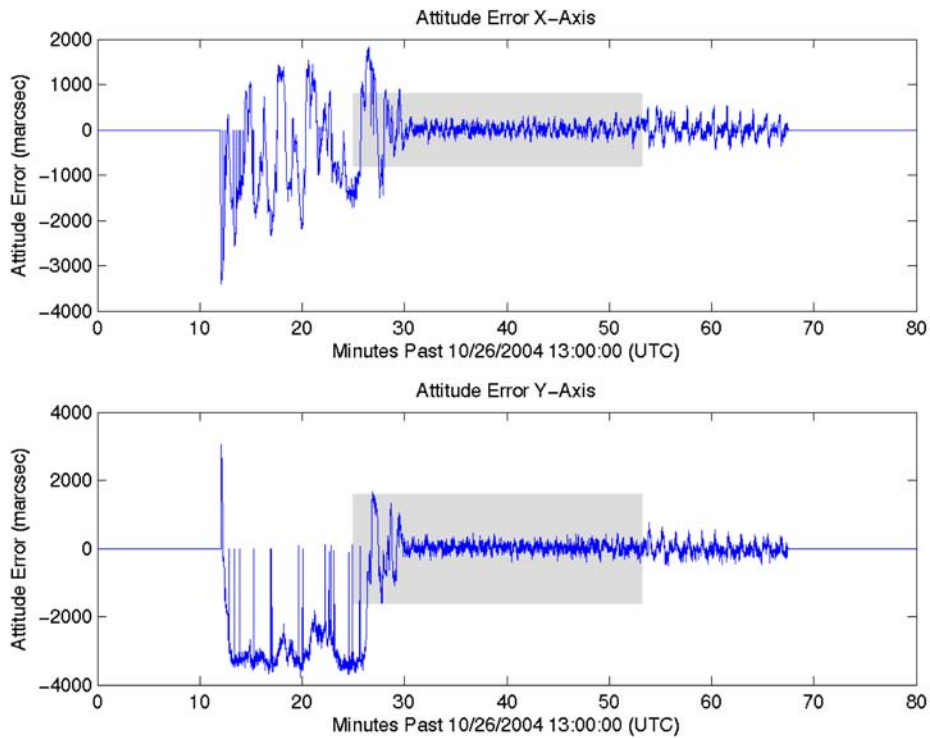


**Figure 7-9.** Guide star capture performance before capture method update



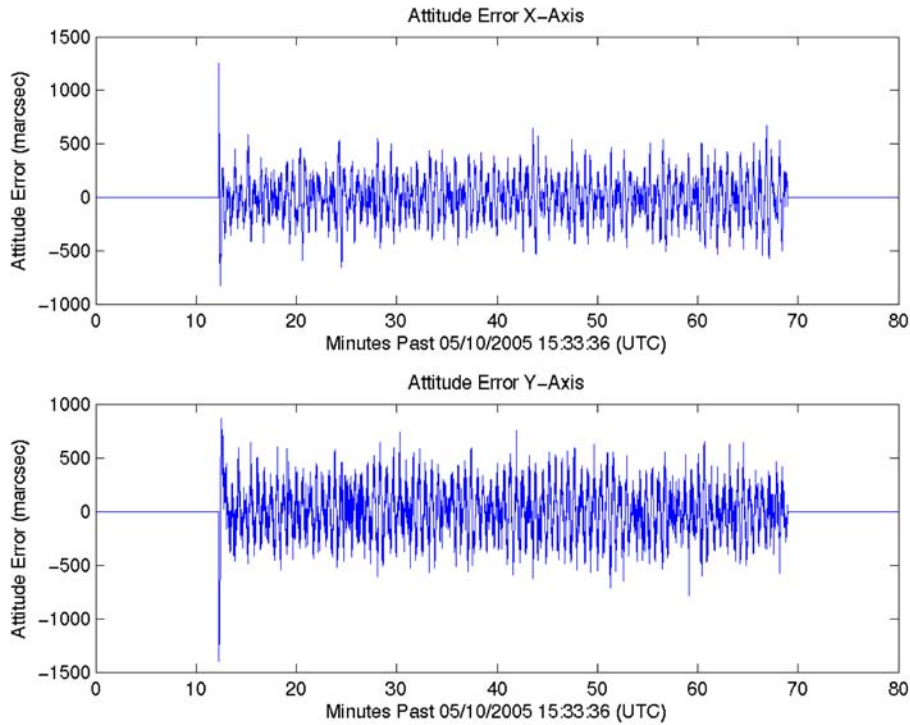


**Figure 7-10.** Guide star capture performance after capture method update

### 7.3.2 Roll Phase Error RMS

Figure 7-11 shows the Z-axis, or roll phase error (RF\_AttErr\_Z) estimate for a nominal period of 4 orbits (6.5 hours). The computed RMS roll phase error is 30 arcs. Note that the prelaunch estimated science roll rate was intended to be 0.3 RPM, and that final science roll rate is 0.7742 RPM. Furthermore, as roll rate increases, misalignments and gyro biases are greatly magnified. Throughout the science mission, the vehicle roll rate has remained 0.7742 RPM.

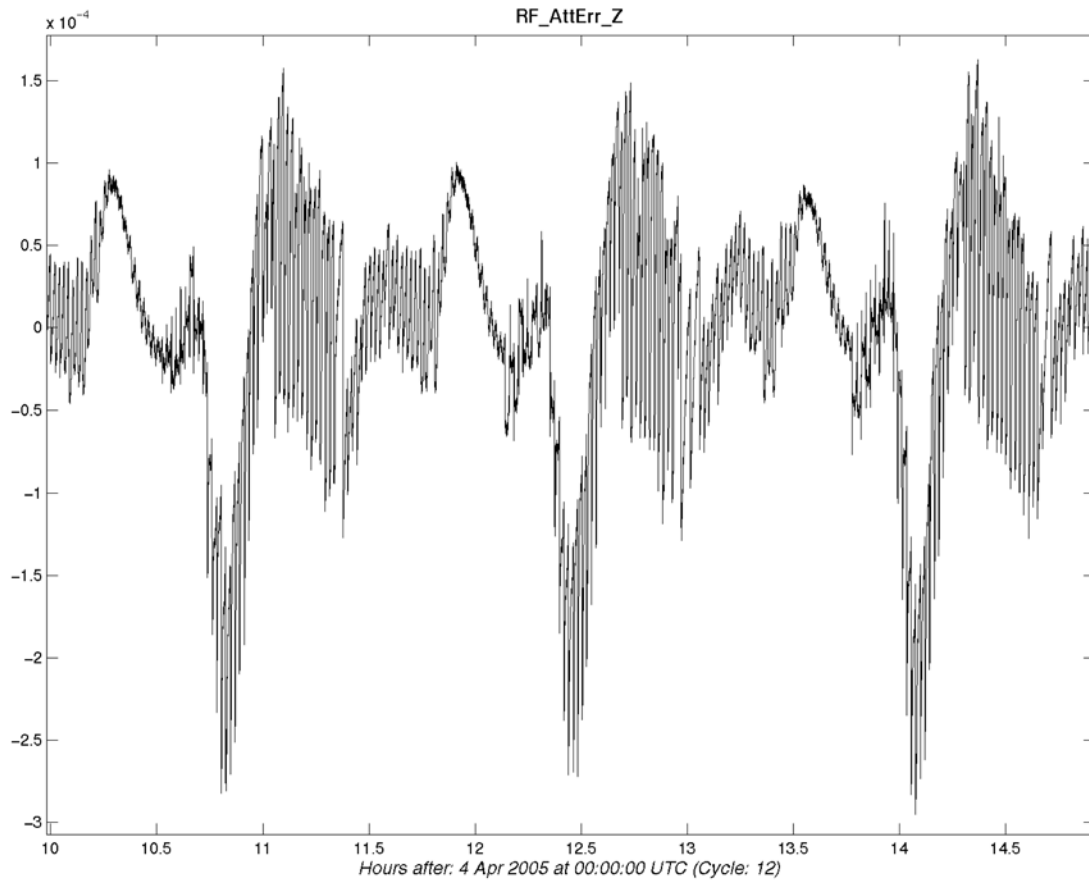


**Figure 7-11.** Roll Phase Error over 4 orbits

### 7.3.3 Drag-Free Control System

Control forces applied to the science gyroscopes can generate unwanted torques on the gyros. The geometric center (C.G.) of the gyroscopes is slightly different ( $\sim 10$  nanometers.) than the center of mass (C.M.) of the gyros. As a result, control forces acting perpendicular (cross track) to the spin axis can generate unwanted torques on the gyroscopes. These torques can cause the gyroscope spin axes to precess or drift, which could corrupt the relativistic signal. [Figure 7-12](#), depicts the geometry of the gyroscope and control forces that could generate torques.

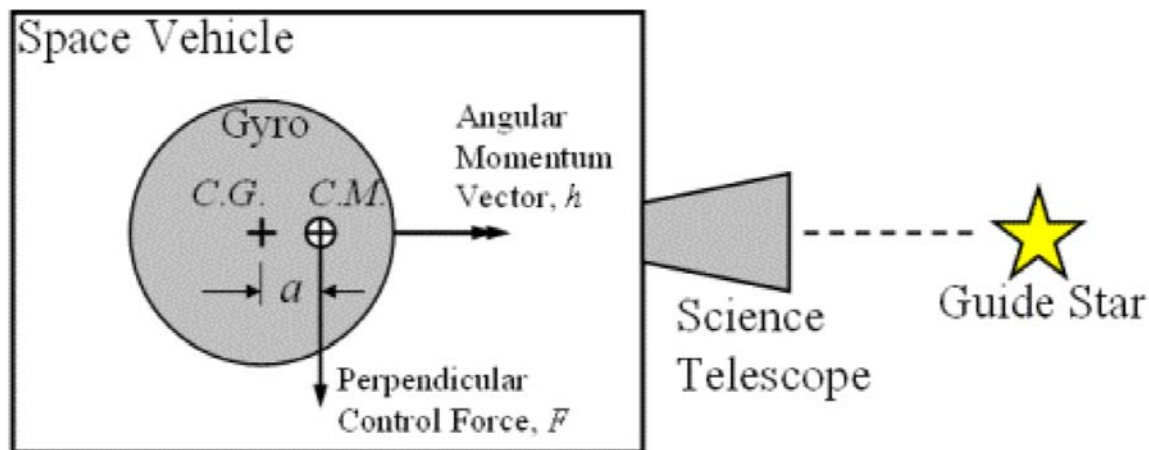


**Figure 7-12.** Drag-Free system diagram

Since the GP-B vehicle is rolling at 0.77 rpm, cross track control forces at the roll rate frequency (0.0128 Hz) are the dominant long-term gyro drift contributor. Cross track forces at frequencies other than the roll rate frequency will average out due to the vehicle roll and will not cause gyroscope drift. Cross track control forces at the roll rate frequency must be small enough so that resulting torques do not cause significant gyroscope precession or drift.

During the Science Mission phase of the Gravity Probe B mission, one of the four Science Gyroscopes inside the space vehicle acts as a drag-free sensor. In primary drag-free, this gyroscope is following a near perfect gravitational free-fall orbit around the Earth, and is spinning inside its housing a mere millimeter from the edge. GP-B uses sensors inside the housing and proportional micro thrusters to keep the space vehicle perfectly oriented around the spinning gyroscope therefore, following the drag-free sensor around the Earth in a near-perfect orbit.

For the most part, the space vehicle stays on course by following the same free-fall orbit. However, outside the space vehicle, two factors can alter its path: solar radiation pressure streaming from the Sun and atmospheric drag.

GP-B uses extremely sensitive proportional micro thrusters to reorient itself and keep it on its proper path. The thrusters utilize escaping helium gas that slowly boils off from the liquid helium inside the dewar as propellant. This minute amount of gas, roughly equivalent to 1/10<sup>th</sup> of a human breath or a few millinewtons of force, provides just the right amount of thrust necessary to adjust the space vehicle's position.

The Gravity Probe B drag-free control system has two control configurations. The first is primary drag-free control which senses the science gyro's relative position inside its housing, and the second is back up drag-free control which measures the control forces, known as "control efforts" applied by the GSS.

Since the back up drag-free control configuration attempts to minimize the gyroscope control efforts and not the measured position of the gyroscope, drag-free performance must be based on the size of the forces applied to the proof mass gyroscope instead of the proof mass' position relative to its housing. Furthermore, control force levels are an especially relevant performance metric because the primary purpose of the GP-B drag-free control system is to minimize gyro suspension forces that cause gyro torques.

There has been one major change to the control algorithm used in the drag-free system. Since the controller is coordinated in the nadir frame, the body-fixed roll components are shifted to lower frequency. By increasing the gain at orbit, improved performance has been observed.

### 7.3.3.1 DFS – Performance

The GP-B drag-free control system has for most of the mission performed nominally. Drag-free control reliably activates and deactivates on command and has operated essentially without fail. Drag-free control has been shown to reduce control forces by a factor of 10 or more. The rms control efforts applied to the proof mass gyroscope are on the order of 10 nanonewtons, and the cross track control force at the roll rate frequency, which can generate gyro torques, is roughly 1 nanonewton. Figure 7-13 shows the control effort time history before and during a six hour drag-free run on August 15, 2004, with gyroscope 3 acting as the drag-free sensor. Gyroscope 3 and 1 were used as the drag-free sensor gyroscopes throughout the Science Mission phase. The control efforts are clearly reduced once drag-free control is activated.

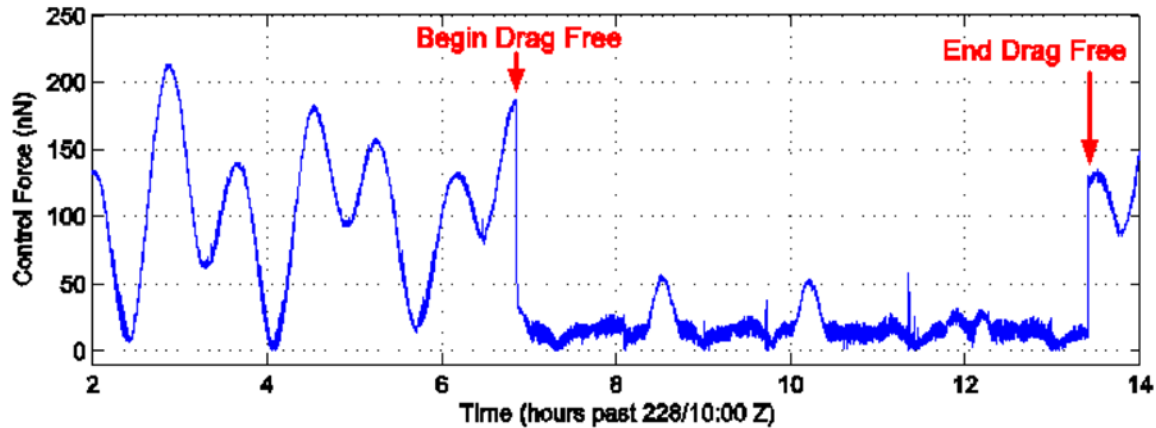


Figure 7-13. Drag-Free performance

Because the performance of the back up drag-free control system has typically been superior to that of the prime drag-free control system at low gyro spin rates, the back up drag-free configuration was selected for use during the Science Mission phase.

Since the science mission has started, the spacecraft was configured in backup drag-free on gyro 3 for most of the time. There is one stretch of time where the spacecraft used gyro 1 instead of gyro 3, due to an unexpected drop out of drag-free on gyro 3. There have also been several instances where the vehicle dropped out of drag-free entirely to enter a safe mode, but the cause has been something external most of the time. Furthermore, most of these periods have lasted for only a matter of hours, short enough that negligible effects on the science results are expected.

### 7.3.4 Pressure Controller/Mass Flow

The helium mass flow rate from the dewar is set with the primary function of maintaining the dewar at a constant temperature and pressure. That is, the flow rate is set to match the seasonal heat input to the dewar. The ATC uses mass flow as required to maintain attitude and a drag-free orbit. Short periods may exceed the average heat input do not appreciably change the tank temperature. Any excess mass flow output by the dewar, but not required for ATC control, is null dumped by adding equal flow to thruster pairs, thrusters aligned in opposite directions. Should the ATC require more flow than output by the dewar, the ATC may demand a brief additional amount of gas flow beyond the dewar setpoint. This is termed “negative excess mass flow”.

In Figure 7-14, mass flow data is shown starting on 2005/239. At this time, the commanded dewar flow rate is 7.0 mg/s (although the dewar temperature controller can adjust this amount as needed by 10- 20%). In the figure, the flow rate data spanning from 0-2 days, represents two days of testing drag-free on science gyro #3, in a 2-axis control mode (the Z-axis is not under drag-free control). During this time, the average ATC mass flow is approximately 3.0 mg/s, with the remaining 4.0 mg/s null dumped to space. The flow rate data spanning from

2-3.5 days represents the final Science Mission configuration of drag-free on science gyro #3, in a 3-axis control mode (Z-axis is under drag-free control). Note occasional peaks exist where the ATC mass flow exceeds the budget of 6.9 mg/s, and even the dewar set point of 7.0 mg/s. However, these durations of negative excess mass flow are brief in duration, and on average do not contribute to an overall cooling of the dewar. Additionally, adjustments to a Z-axis force bias between the ATC and the GSS, have allowed for further reductions in net mass flow usage by the ATC. After 2004/251 the bias had been adjusted such that the ATC no longer dips into negative excess mass flow usage, and the overall ATC mass flow usage was calibrated to be sufficient for the Science Mission.

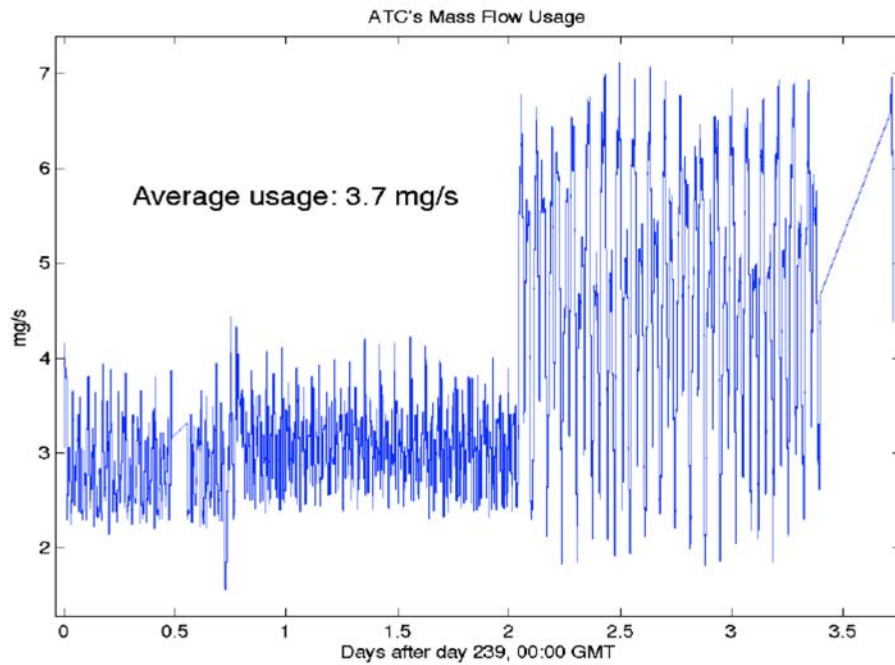


**Figure 7-14.** ATC Mass Flow Usage in drag-free Mode

Figure 7-15 shows the effect of both a heat pulse meter test as well as augmenting the thrusters with the magnetic torque rods for torque control. Throughout the mission, the heat pulse meter tests were used to measure the amount of helium left in the dewar. The torque rods were used during the science mission to give the vehicle more excess mass flow margin.

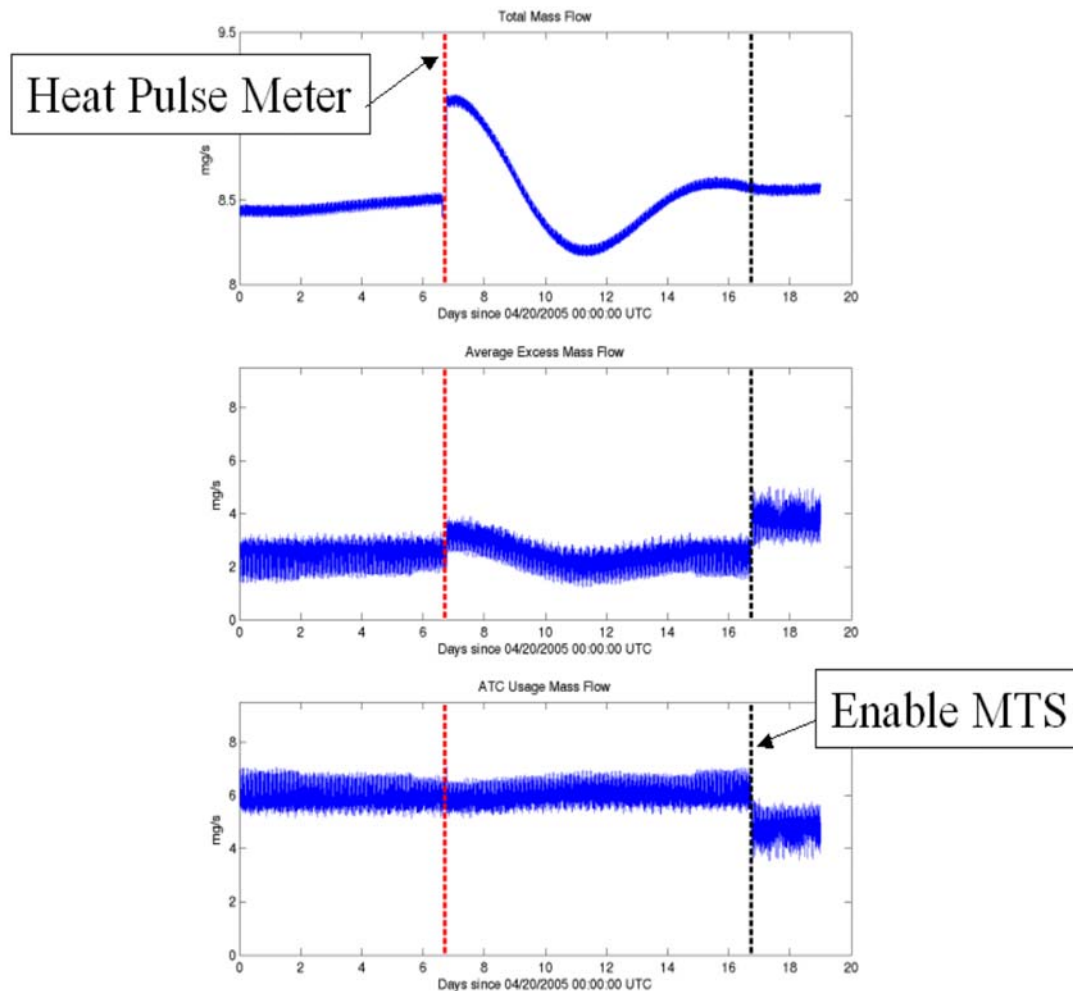


**Figure 7-15.** Mass flow effects of a Heat Pulse Meter Test and the Magnetic Torquing System

### 7.3.5 Calibration Phase

After the science phase of the mission ended, there was a period of data collection called the calibration phase of the mission. Several ATC operations were done during the calibration phase. The most intense operation was maneuvering the spacecraft to point at neighbor stars, other visible stars varying from 0.4 degrees away from IM Pegasi to 7 degrees away. Over the course of a few weeks, three different stars were visited multiple times.

Each maneuver consisted of a vehicle reconfiguration, a vehicle reorientation, and another vehicle reconfiguration that includes finding the new telescope target star. During the maneuver and neighbor star location, the star tracker was used for attitude reference. The planned neighbor star location procedure was to maneuver to the expected location of the star, then dwell around in a spiral if the star was not seen in the telescope field of view. However, during every neighbor star visit, the star was found and locked onto using only the predicted position. Thus, no costly time was used dwelling for the stars, and a more aggressive calibration schedule was achieved.

The other ATC calibration phase operations consisted of drag-free system testing. Drag-free biases were put into the drag-free system in order to measure the torque effects on the gyroscope pointing.



## 7.4 Conclusions and Performance Summary

The Attitude and Translation Control system of the Gravity Probe B space vehicle has performed well over the Science Mission phase. The drag-free control system operating in back up drag-free control mode has proven to maintain control forces applied to the gyroscopes within acceptable limits for the Science Mission. Drag-free control has been shown to reduce rms control forces by at least a factor of 10. During drag-free, the rms control efforts applied to the proof mass gyroscope are on the order of 10 nanonewtons.

The attitude control system has kept the pointing accuracy during Guide Star Valid periods within the limits required for the Science Mission. The rms normalized telescope signal is consistently around 0.1, or at 10% of the total range of  $S_N$ , and the telescope signal at the roll rate frequency is consistently around 0.01, or a mere 1% of the total range of  $S_N$ . The attitude control system has proven to keep the normalized telescope signal within the linear range 95% of the time allowing for accurate pointing determination.

## 7.5 Flight Challenges/Solutions and Additional Accomplishments

The following sub-sections of this chapter detail eight major accomplishments of the GP-B ATC system.

### 7.5.1 Quick vehicle stabilization off Delta II w/ failed thruster

The vehicle rotation rates were damped out quickly even with a failed thruster, shortly after separation from the Delta II. [Figure 7-16](#) below is a plot of the vehicle pitch and yaw rates (RF\_SensRate\_X and RF\_SensRate\_Y respectively).

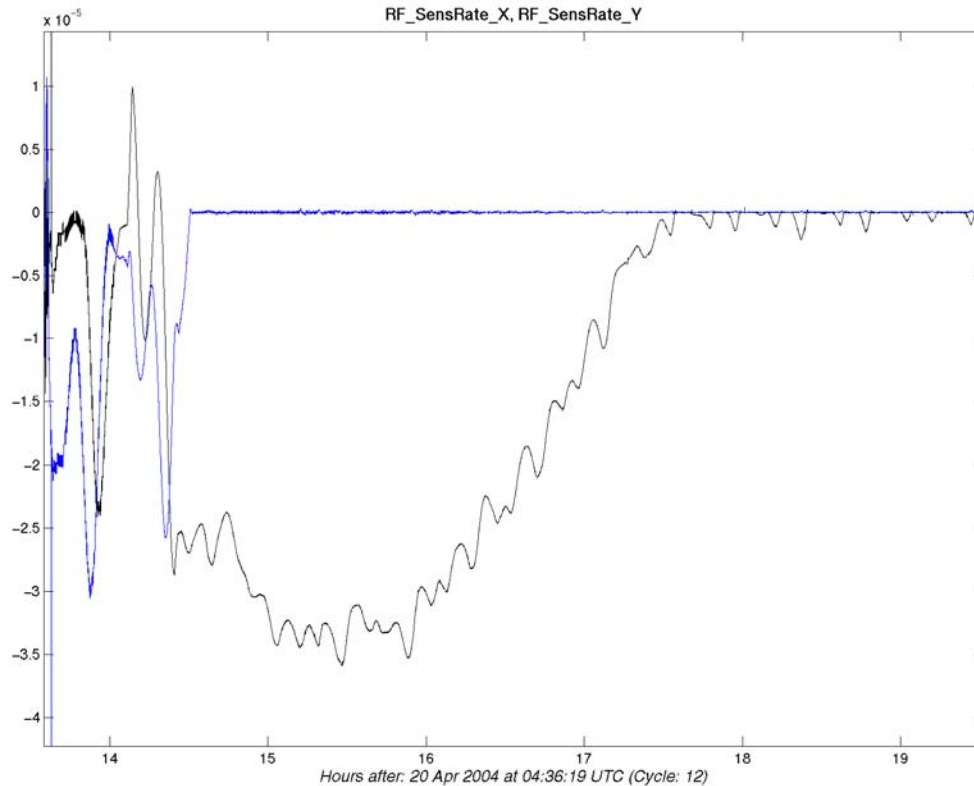


**Figure 7-16.** Vehicle rotation rate damping after separation from the Delta II

## 7.5.2 Successful recovery from multiple CCCA reboots

For several different reasons, the CCCA, the main processor for the satellite, has rebooted several times. Each time a reboot occurs, the vehicle attitude and translation control is off for a short time. Furthermore, all control software and parameter updates since the latest software installation on July 1, 2004 are cleared from the memory. All of the improvements and fixes are lost and must be reloaded. Through a series of automated load commands and manual commands, the vehicle is brought back to a nominal state over a period ranging from one day to one week.

A system of safemode operations has been developed that has left the vehicle in a predictable and recoverable state for each reboot. The recovery time for a reboot has been reduced from approximately one week to less than one day. More importantly, the vehicle is typically returned to drag-free operations and pointed to within arcseconds of the guide star in a matter of hours. A quick recovery time is necessary not only to ensure the safety of the spacecraft, but also the integrity of the science data.

## 7.5.3 Supporting higher science roll rate

Originally, the GPB spacecraft was optimized for a nominal roll rate of 0.3 rpm. After a request by the science team for a higher roll rate, the team determined that the vehicle could perform sufficiently at a higher roll rate. The team then developed an ATC configuration that supports a roll rate of 0.77 rpm, more than twice as fast as the baselined roll rate prior to launch. However, the system has performed well and has shown no significant deficiency due to the higher roll rate.

## 7.5.4 Successful large-scale dither

[Figure 7-17](#) below shows a plot of the large-scale dither operation from the IOC phase of the mission.

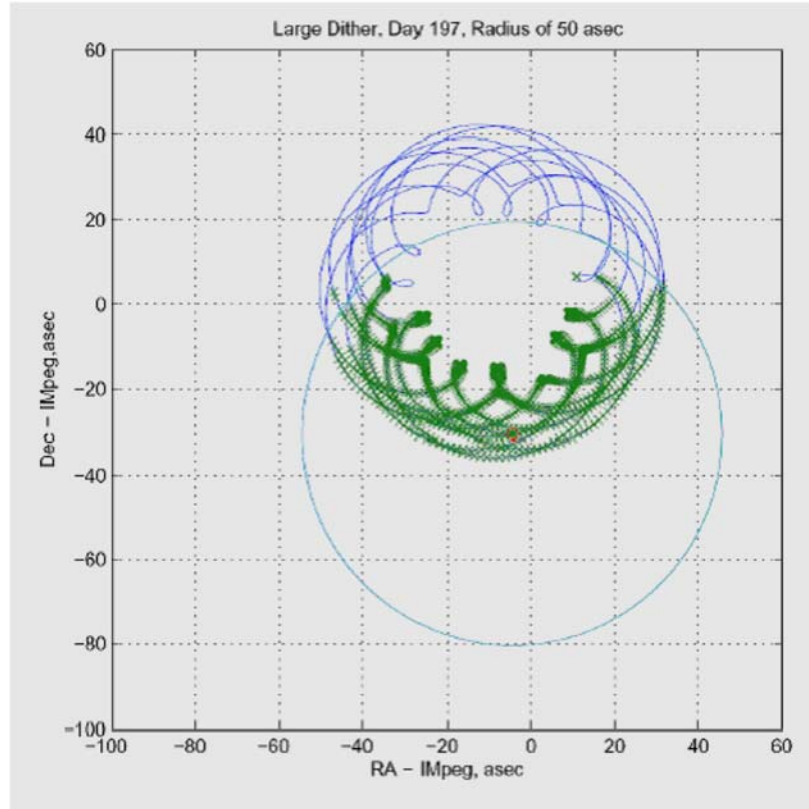


**Figure 7-17.** Large Scale Dither Performance (2004/197)

## 7.5.5 ARP Motion Challenges

The Attitude Reference Platforms (ARPs) are the mounting location of the control rate gyroscopes, as well as the roll star trackers. At one time, one set of gyroscopes and one star tracker are used in the control loop that maintains the attitude of the vehicle. While thermal effects were expected, the motion of the ARP and rate gyroscope housing have introduced disturbances into the rate signal that have presented challenges throughout most of the mission. The ARP moves with components of motion at annual, orbit, and roll rates, and all three of these components have provided unique challenges to overcome to arrive at the pointing performance the vehicle now achieves.

### 7.5.5.1 Mode 1A vs 1B

One of the most significant operational decisions resulting from ARP motion analysis is that Mode 1B (direct mode) was chosen as the science configuration, instead of Mode 1A (observer mode) while pointing at the guide star. The dependence on the gyroscope signal of the observer would lead to the telescope tracking the ARP motion rather than keeping the guide star centered in the field of view.

As the vehicle rolls around the telescope boresight (the z axis in the body frame), the ARP is heated and cooled in an almost sinusoidal fashion at precisely roll rate. As the ARP deforms, the orientation of the gyroscope housing changes with respect to the z axis, causing the roll rate of the vehicle to project onto the pitch and yaw axes. This effect shows up in the gyroscope output and yields a fictitious sinusoidal rate signal in both the pitch and yaw axes.

If the vehicle control system were in the observer mode (1A), the sinusoidal signal in the rate gyroscopes would dominate the observer, and the vehicle would point in a sinusoidal pattern, rather than staying centered on the guide star. Pointing error in this setup would be much larger than the error resulting from the telescope noise that enters the system in the direct pointing mode (1B).

As a result, mode 1B has been used where no estimation is done on the proportional control term. The attitude error is sent straight from the telescope data to the controller with no signal processing other than a straight gain. Although this leaves the vehicle susceptible to the noise in the telescope signal, the overall pointing disturbance is smaller. More importantly, the random telescope noise causes a disturbance much closer to white noise, rather than error at roll rate, the frequency that is most detrimental to science data.

### **7.5.5.2 GS captures (rate capture mode)**

The method of capturing the guide star called the rate capture mode has also been more challenging than originally thought due to the ARP motion. The rate capture mode, intended for guide star capture when the star is outside of the linear range of the telescope, is essentially a commanded rate in the direction of the guide star. In this case, the controller is commanded a constant rate in the correct direction, based on the telescope output. Once the star returns to the linear range of the telescope, the controller returns to PID control.

A problem arises, however, when the gyroscope housing is misaligned with the telescope boresight, due to ARP motion. There were cases where the ARP had moved so that when the gyros measured the commanded rate, the vehicle was actually moving in the wrong direction. This led to guide star captures in the worst case of over 20 minutes.

The solution to this problem has been to essentially stop using the rate capture mode. The implementation in place is an expanded definition of the linear range of the telescope. It has been more successful to use the proportional term and modify the integral and rate path limits, even when the star is outside of the actual linear range of the telescope.

### **7.5.5.3 Roll rate disturbance/rate notch filter**

The roll rate signal that enters through the gyroscopes causes another problem for the science data. The same roll rate ARP motion that led to using mode 1B, still causes a problems in this mode, since the gyroscope signal still enters the control law through the derivative term in the controller. Because the motion of the ARP is at roll rate, there is an artificial signal in the gyroscope output causing erroneous torque commands at roll frequency. This output is seen clearly in the spectral analysis of the attitude error and rate path error.

The solution to this problem is to attack the roll rate signal in the gyroscope data directly. There is a filter on the rate error path, between the gyroscopes and the control command generator. A notch filter at the roll rate has been implemented to attenuate the signal at roll by 10X, basically throwing out as much of the false signal as is deemed safe. Although the signal cannot be eliminated completely, this has been a very successful way of reducing the roll rate output of the vehicle pointing.

### **7.5.5.4 Gyro hold offset**

The orbit rate motion of the ARP has also provided challenges to the ATC system in the form of a large transient error while the guide star is captured at the beginning of every guide star valid period. At the end of every guide star valid period, the vehicle goes into gyro hold mode, where the telescope attitude error-nulling controller is off. The vehicle controls its attitude using gyroscope data for rate and attitude.

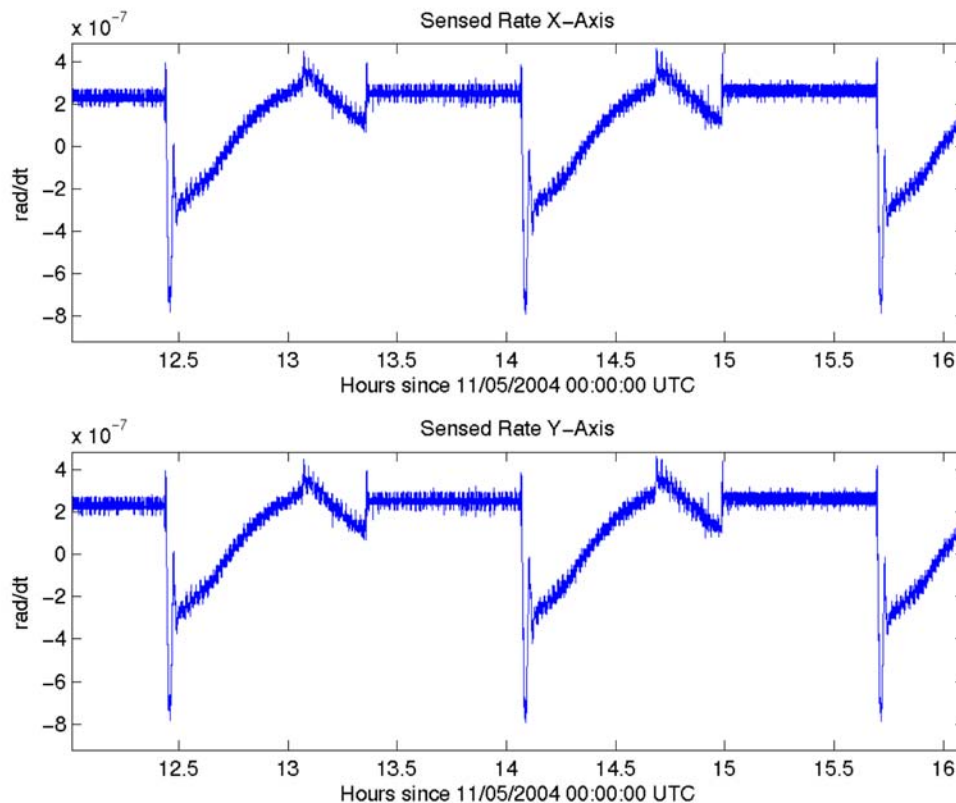


**Figure 7-18.** GSV/GSI rate gyroscope bias offset

While the guide star is out of the field of view and the vehicle is nulling its rates using only gyroscope signals, the controller tries to null out the pitch and yaw rates. However, as the ARP moves at orbit rate, the projection of the roll rate onto the pitch and yaw axes changes over the orbit. If the orientation of the ARP at the end of one guide star valid period does not match that of the beginning of the next, the vehicle effectively changes roll axes in order to keep the gyroscope signals nulled out. Thus, at the beginning of the next guide star valid period, the telescope will not be pointed in the same direction, and it is this initial error that must be damped out to center the guide star in the telescope.

The alignment of the ARP with the telescope axis can be corrected for by setting hardware bias settings. It has become regular maintenance on the vehicle, often multiple times per week, to set the biases so that the ARP is lined up correctly at the beginning of guide star valid. Bias errors on the order of one arcsec/sec can cause an increase in the guide star capture time by as much as 100-500%.

### 7.5.5.5 Effects of Dewar Shell Temperature Variation on ARP motion

One of the challenges of dewar design is to provide adequate mechanical support for the cryogenic region while maintaining low thermal conductance between the exterior and the interior. In the case of the GP-B dewar, this is accomplished by means of twelve low-thermal-conductivity composite strut tubes (PODS), six forward, and six aft. (See [Figure 7-19](#) and [Figure 7-20](#) for a depiction of the support system.) In the case of GP-B, there is an additional complicating factor: In order to acquire accurate roll phase and pointing information for the ATC system and science, there are two external Attitude Reference Platforms (ARPs) located on opposite sides of the dewar shell, near the Y axis, which provide mounting surfaces for control gyros and star trackers. These ARPs should maintain a stable angular relationship to the science instrument deep inside the dewar. In order to

accomplish this, the ARPs are mounted on posts that, in turn, are mounted on a pair of very stiff graphite-epoxy rings that provide the warm termination points for the forward PODS. The graphite rings are mounted just inside the dewar vacuum shell at the top of the vacuum shell cylinder by means of nine titanium flexures (See Figure 7-20 below). Nominally, the flexures provide radial compliance to provide isolation from thermally induced expansion and contraction of the dewar vacuum shell, but are stiff in other directions. The graphite-epoxy rings, for their part, have a high modulus and are designed to have a coefficient of thermal expansion that is near zero relative to that of aluminum. The aft end of the vacuum shell cylinder is bolted in turn to the dewar support ring, which provides the attach points for the spacecraft truss on the outside and termination points for the aft PODS on the inside. The ARP posts pass through openings in the vacuum shell cylinder and are sealed to the vacuum shell by flexible bellows.

The foregoing arrangement is intended to meet the requirement that the drift of the boresight of the star sensor in the roll direction relative to the science instrument be less than 10 arcseconds per year and not be correlated with any periodic behavior of the satellite. Evidence from the ATC system (section 8.1.1) indicates, however, that significant relative motion does occur at roll, orbit, and annual rates. This motion is correlated with the temperature of the dewar vacuum shell in a complex way: the short-term correlation (orbital period) has the opposite sign of the long-term correlation (seasonal time scale). Although other mechanisms may exist, it appears that the most likely explanation is that thermally-induced expansion and contraction of the dewar vacuum shell cylinder is being coupled to the graphite rings via the flexures and causing them to distort. The details of the mechanism and, in particular, the mechanism underlying the time-scale-dependent nature of the correlation are currently not well understood.

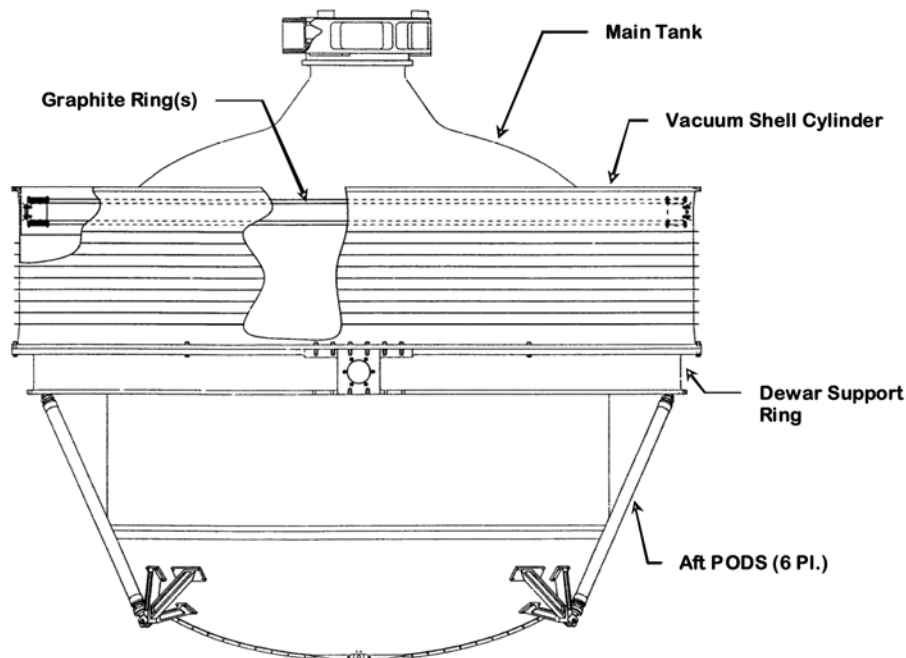


**Figure 7-19.** Side view of partially assembled dewar showing primary structural elements except for forward PODS.



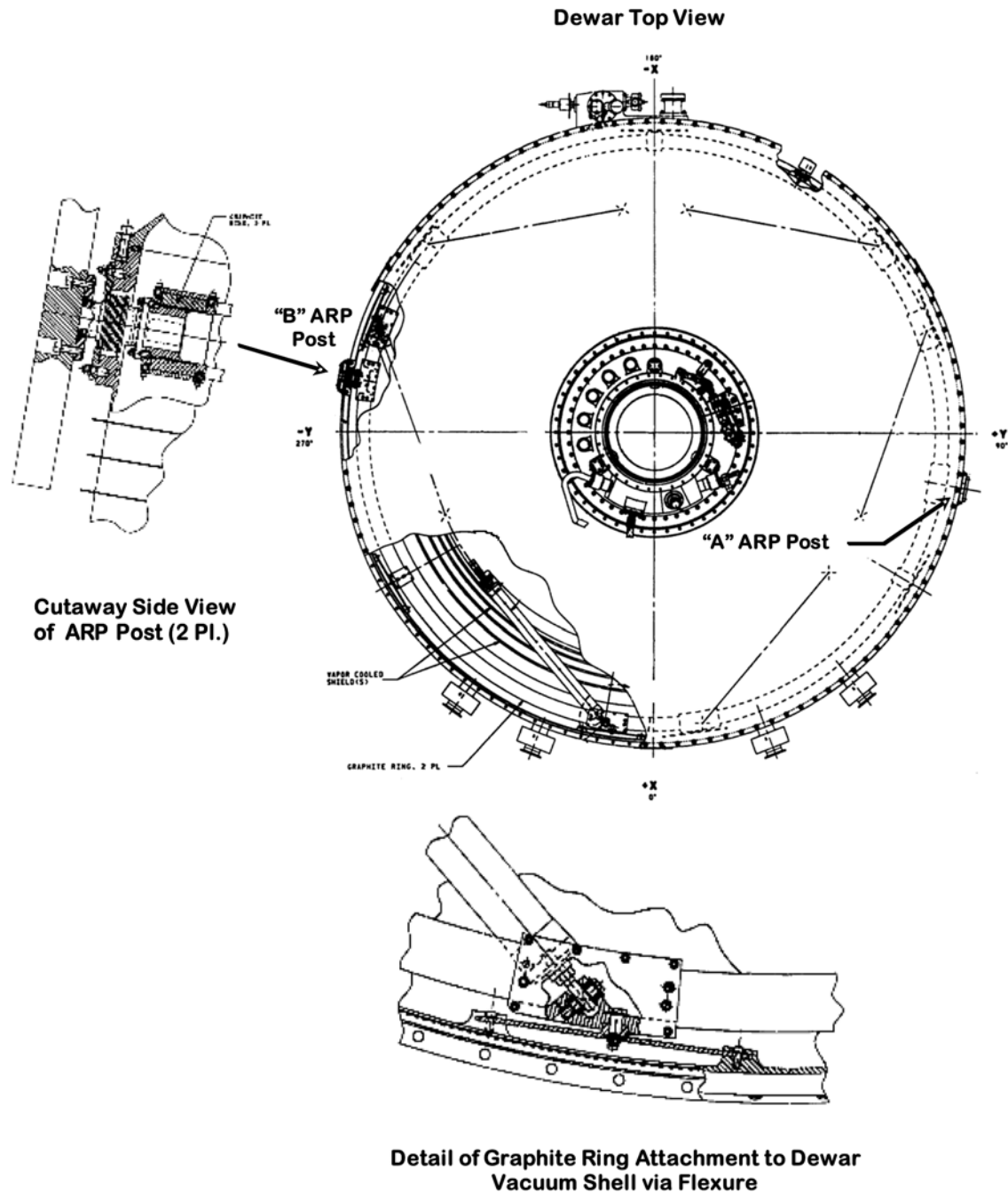


**Figure 7-20.** Cutaway top view of dewar showing forward PODS and ARP post locations and details of the ARP post and flexure. (Representation of the ARP is schematic and not accurate.)

### 7.5.6 Proton Activity

The GP-B ATC system had to deal routinely with increased proton activity in the South Atlantic Anomaly region, where protection by Earth's magnetic field is weakest, and also from increased proton radiation due to several strong solar flares.

### 7.5.6.1 South Atlantic Anomaly

Proton activity in the South Atlantic Anomaly (SAA) has provided challenges to the ATC configuration over a wide range of areas from the telescope settings to the range of times where we can have the rate notch filter enabled. The telescope settings are affected by the presence of proton hits to the detectors that lead to abnormally large signal readings. The large data values are interpreted by the telescope as a very strong light source entering one side of the telescope. The offset of the signal in the telescope field of view looks, to the controller, like a mis-centering of the telescope axis with the guide star and causes erroneous control commands to the thrusters. There is exception handling, a telescope sanity check and a sum magnitude limit in place intended to filter out these signals, but due to an error in the Ada exception handling compiler, the signals are not properly filtered. See ATC Slope Exception Handling section below for more details.

A new telescope configuration has been implemented to eliminate the exception handling problem, but even with this fix in place, the telescope is still essentially blinded for several minutes while passing over the South Atlantic Anomaly. While traveling through the center of the SAA, up to 90-100% of the data is filtered out due to proton activity corruption as shown in Figure 7-21 below. Thus, during this brief period of time, the ATC system is essentially controlling without any proportional term data that is generally used to keep the guide star centered.

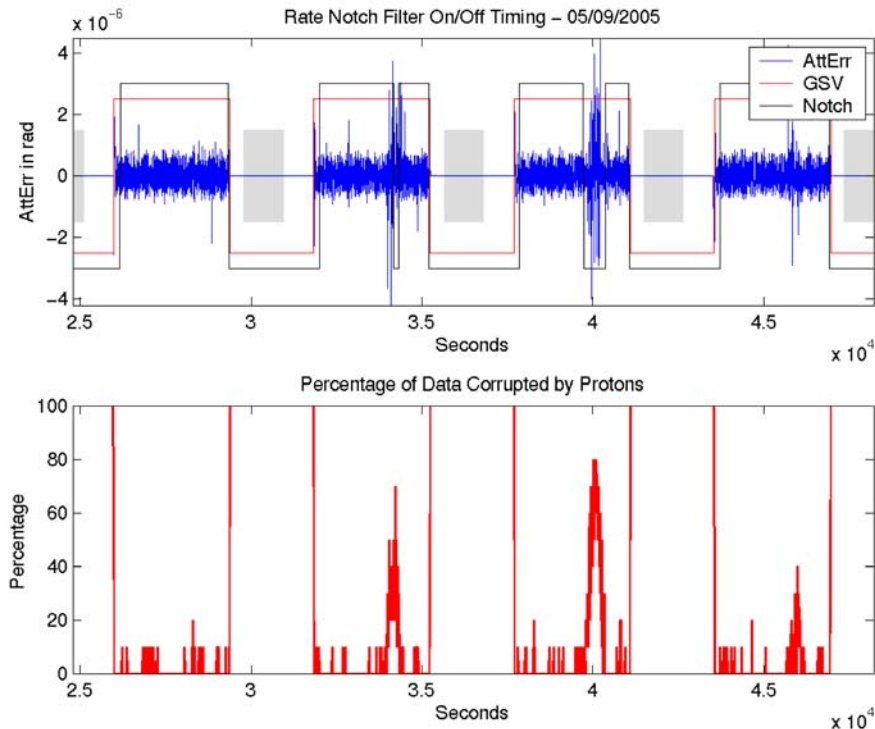


**Figure 7-21.** Percentage of data corrupted by proton activity in the South Atlantic Anomaly

During this period, the controller relies mostly on rate damping to keep from wandering too far off the guide star. However, as discussed earlier, there is a rate notch filter that strongly attenuates the body roll rate, or inertial signal. It has been deemed too much of a risk to keep the filter on through the strongest parts of the SAA, because the system would be controlling without proportional or inertial rate damping data. Therefore, the notch filter is turned off just before entering the SAA, and the roll rate disturbance from the ARP motion is not attenuated during passes through the SAA.

Furthermore, as a result of the transient behavior from the initial conditions while turning on the filter after the SAA, during parts of the year, the notch filter must remain off even after the SAA. This affects data on one or two orbits out of every day, or one or two out of every fifteen orbits. On orbit data has been used to map out the strongest section of the SAA, where more than 50% of the attitude error data points are lost due to proton activity, as shown in [Figure 7-22](#) below.

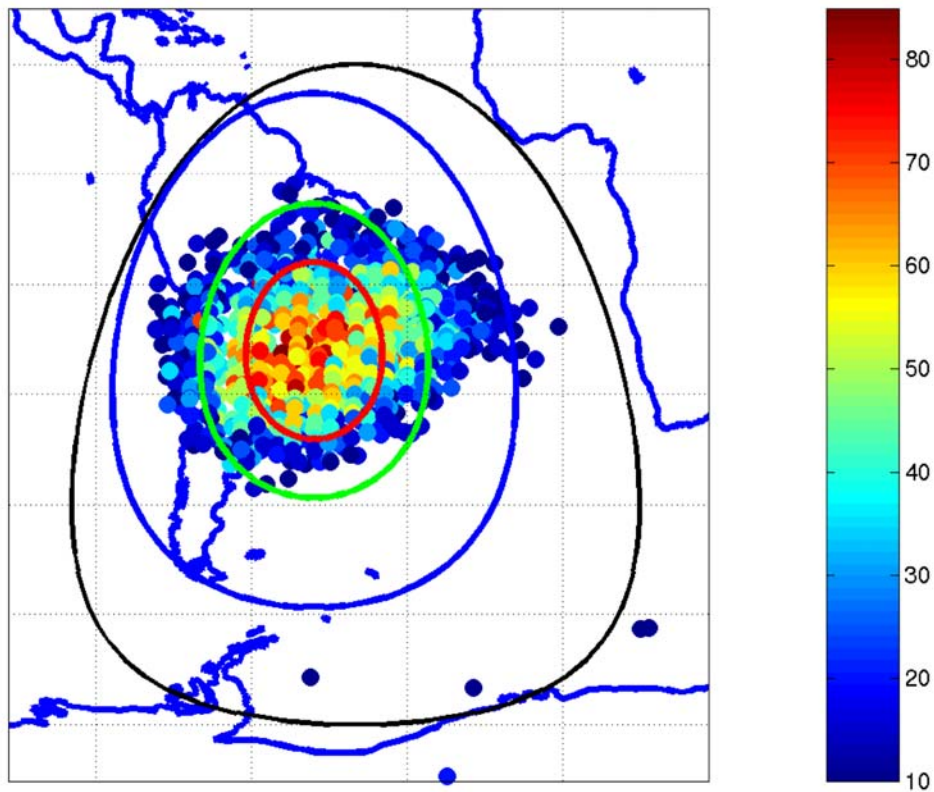


**Figure 7-22.** South Atlantic Anomaly Region produced from telescope proton hit data

### 7.5.6.2 Solar Flares

Solar flares have increased the proton activity that the satellite has observed in much of its sensitive equipment. The ATC system has been affected most by solar activity in the telescope detectors. Specifically, the January 20, 2005 solar flare charged up the north pole strongly enough to corrupt 90-100% of the telescope data. The data loss lasted long enough for the satellite to drift far enough to lose the guide star. Several hours of science data were lost while the team reacquired the guide star. Most other solar flare activity has been weak enough so the control system performance has been unaffected. The telescope data corruption and subsequent spacecraft attitude error is shown in [Figure 7-23](#) below.

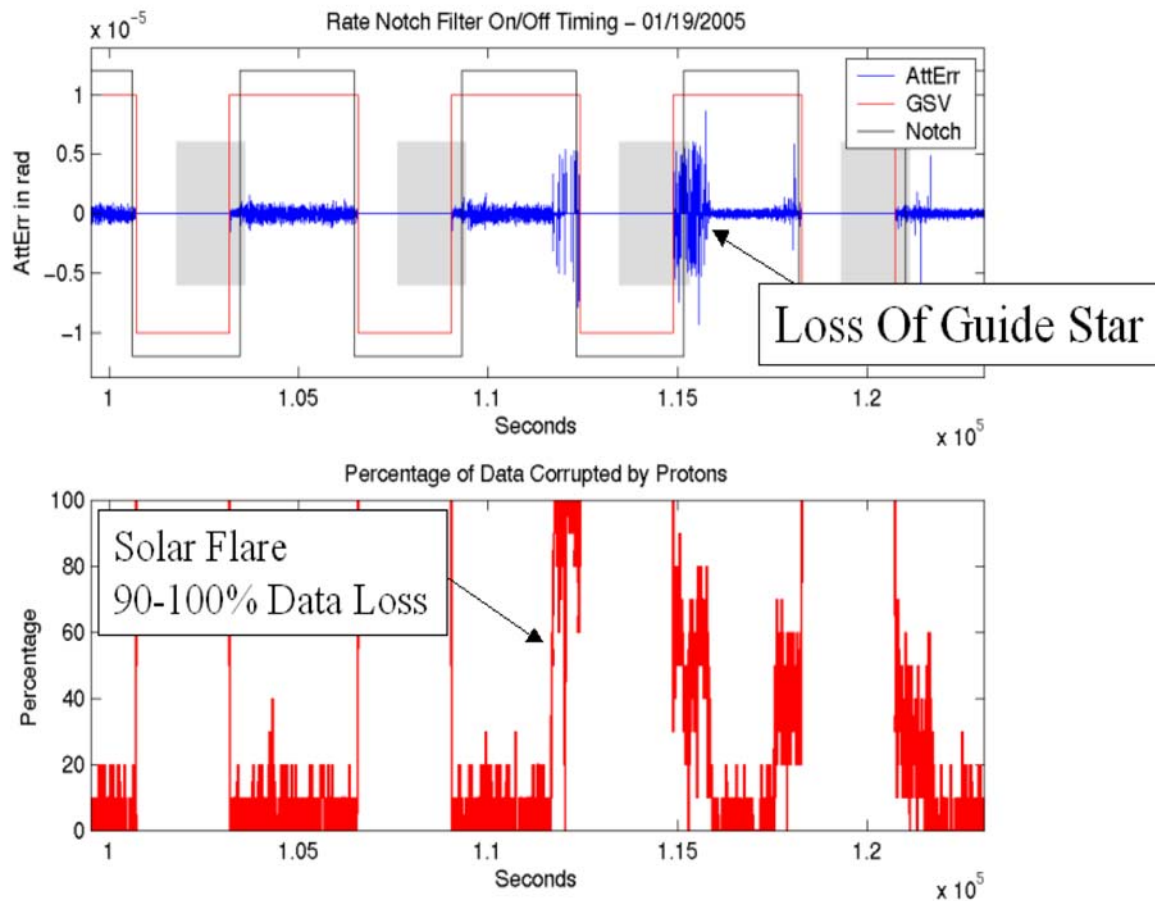


**Figure 7-23.** Effects on telescope pointing from the solar flare on January 20, 2005

### 7.5.6.3 ATC slope exception handling

There appears to be an error in the proton filter in the telescope detectors that remained unexplained for almost half of the science mission. The error is now believed to be a compile-time error where the programmed algorithm is correct and the compiled code is incorrect. The problem lies in the size of the largest number allowed in the exception handling. Basically, numbers twice as big as the intended threshold pass through the exception handler without causing an exception. However, the ATC slope algorithm still runs on the assumption that the numbers can be no larger than the threshold.

The resulting behavior is a “wrap-around” effect where negative numbers of larger magnitude than the threshold wraps around and are interpreted as a very large positive number. Due to this error, proton activity is especially potent in the SAA. The large data points getting through to the control system pushed it just about to its limits and resulted in large attitude error oscillations coming out of the SAA.

This could have been fixed by changing the onboard code, but a much simpler solution was implemented. The vehicle is now set up so that only half of the range of the telescope detectors is used. Since, we only use half of the detector range, we are guaranteed that the largest negative number will still have a smaller magnitude than the “wrap-around” threshold.

### **7.5.7 Star Tracker Magnitude Updates**

The star tracker has worked well after the initial setup and configuration. The majority of the updates to the star tracker operations have been updates to the magnitudes in the onboard star catalog. The variation of the measured magnitudes of the stars identified by the trackers is larger than the magnitude threshold that has been chosen in order to minimize the probability of mis-identification. Some stars have been identified on the order of once per day. Upon further investigation, it was determined that the magnitude in the catalog did not match the measured magnitude and the star was only identified when the outliers landed in the acceptable range according to the magnitude threshold. Updates to the magnitude in the onboard catalog have solved the problem of infrequent star identifications for a number of the stars that were seen regularly, but infrequently.

### **7.5.8 Dewar Slosh Control**

The drag-free control system and control efforts began to grow in an unstable manner at one point during the mission. The cause of this behavior is believed to be slosh occurring in the liquid helium in the dewar. The behavior observed was a slowly growing magnitude in the control efforts at the estimated slosh frequency and was likely caused by an attempt to change the roll rate of the vehicle too quickly. After a period of time out of drag-free and some changes to the drag-free controller, the system settled down, and the vehicle was returned to drag-free operations. Since the occurrence, a slower rollup/rolldown rate has been used, and no further slosh problems have been observed.

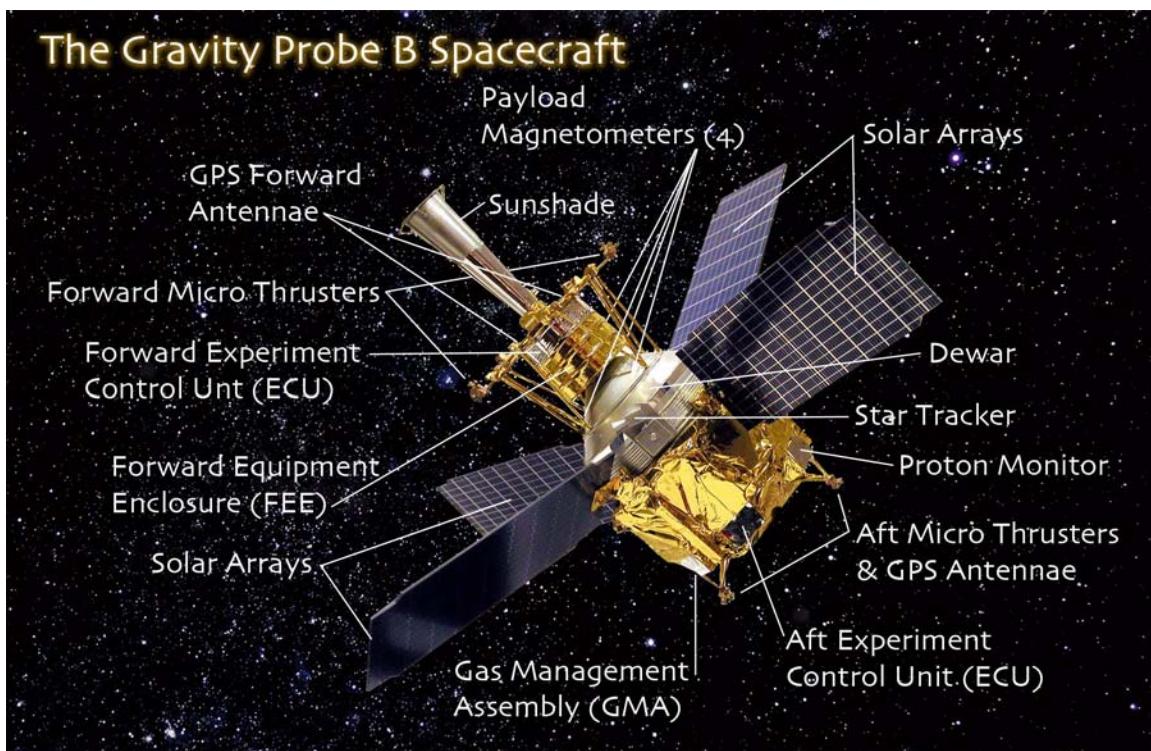




# 8

## Other Spacecraft Subsystems Analyses

---





## 8.1 Commands & Data Handling (CDH)

The Command and Data Handling subsystem (CDH) manages commands to and telemetry from the GP-B space vehicle as well as some communication on board the space vehicle. It consists of the Flight Computer (CCCA), Solid State Recorder (SSR), Command & Telemetry Unit (CTU), Watchdog Timer (WDT), and the Interface Unit (IU). These components are discussed in detail below. The CDH also provides the interface between the CCCA and the RF transponders, as well as the Control Gyro and GPS receiver. [Figure 8-1](#) below shows the physical locations of these boxes. The region in green shows the locations of the CCCA, SSR, IU, and CTU. The regions in blue show the transponders and antennas.

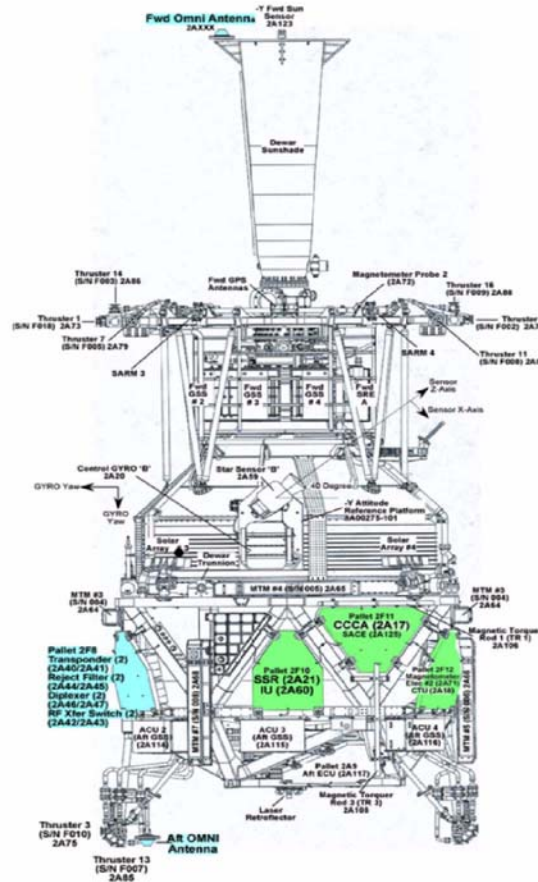


**Figure 8-1.** Physical Location of CDH boxes on GP-B

[Figure 8-2](#) is a block diagram showing the interactions between various components. The blocks with a green background belong to the CDH system.

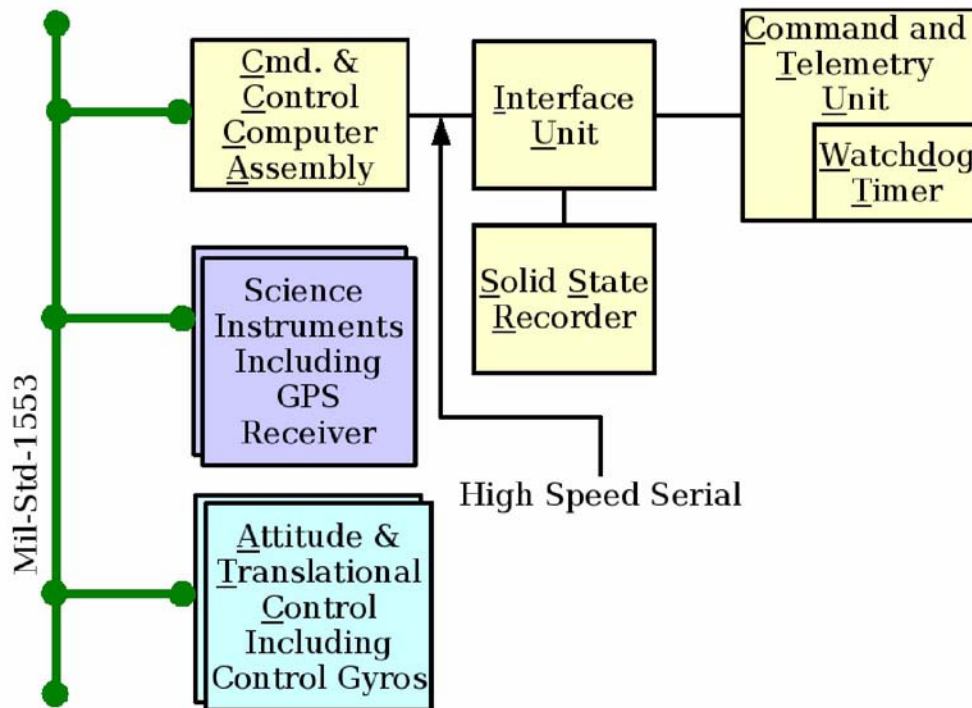


**Figure 8-2.** Block Diagram of CDH communications. Green blocks belong to the CDH subsystem

The CCCA communicates with the rest of the space vehicle via the 1553 bus, while the individual components of the CDH communicate via high-speed serial bus.

The CDH subsystem provides the following:

1. Verification and distribution of commands from the uplink data stream and the CCCA
2. Acquisition of data in response to CCCA requests
3. Generation of the downlink data stream
4. Data management and routing between the CCCA, SSR, GPS and Control Gyros
5. Receipt and distribution of 10 Hz synchronization
6. Watch Dog Timer (WDT) redundancy management

## 8.1.1 Performance

The CDH performance on-orbit has been nominal. All components have performed well without exception.

### 8.1.1.1 CCCA

See Section 8.5 for an in depth discussion of the CCCA.

### 8.1.1.2 SSR

The SSR stores telemetry for download to the ground. It has the capacity to store up to ~15 hours of data. During each ground contact the vehicle dumps approximately half its capacity, depending on the length of the contact.

### 8.1.1.3 CTU & IU

One of the functions of the CTU is to process commands received from the ground. Figure 8-3 shows the number of commands sent to the CTU. The total for the mission was approximately 106,000 commands. The spike observed in March 2005 is related to the recovery from the CCCA reboots. After a fail-over to the B-side, more real time commanding is needed to reconfigure the space vehicle. The increase observed at the end of the mission is due to calibration phase activities, starting in July 2005. Also note that after the IOC period, the need for real time commanding dropped significantly.

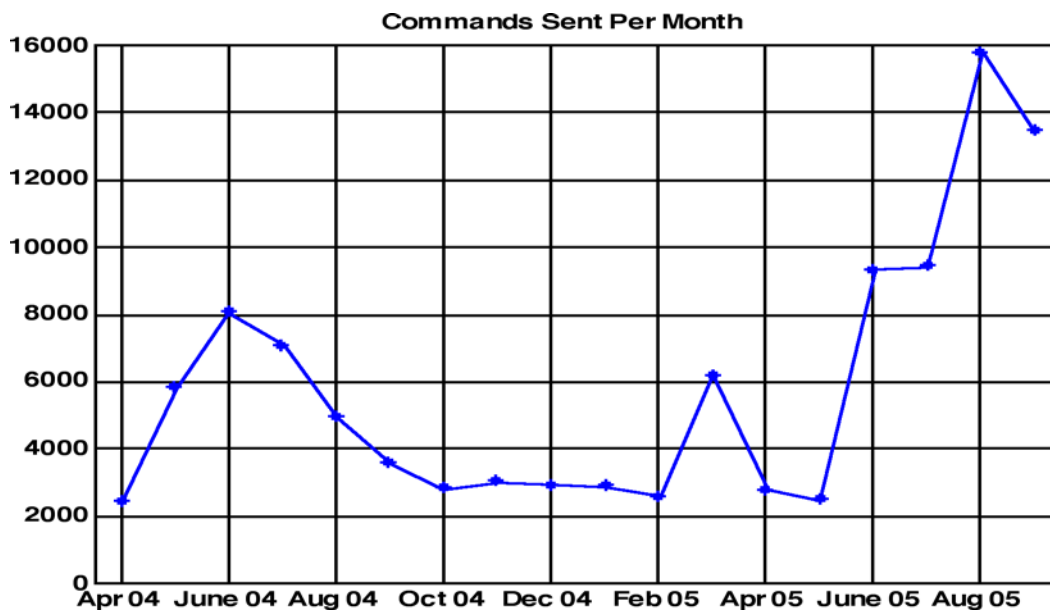
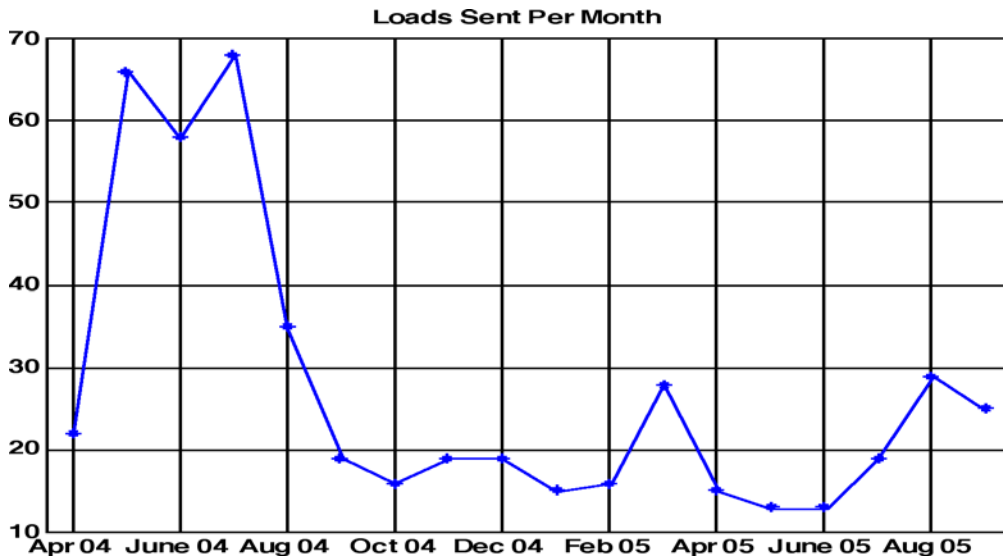


Figure 8-3. Commands sent by month

Routine vehicle commanding is accomplished by loads; sequences of commands stored for later use. In most cases, these sequences are run on the main flight computer. Figure 8-3 shows the number of loads sent to the space vehicle per month—almost 450 loads total. The spike observed in March is related to the recovery from the main flight computer reboots (Anomalies 148, 152, and 156). After such a reboot, updates to the flight software are uploaded, accounting for the spike. At the beginning of the mission, during the IOC phase, a new load was needed every day and sometimes more than once a day. Towards the end of the mission, a single load spanned 2 or more than 2 days. During the calibration phase the number of loads increased, consistent with increased vehicle activity.



**Figure 8-4.** Commanding loads sent to the vehicle by month

#### 8.1.1.4 WATCH DOG TIMER

The reboot of the CCCA associated with anomaly 156 has been attributed to the Watch Dog Timer (WDT). The WDT does not receive a heartbeat from the flight computer, software forces a hard reboot. It is believed that this was the reason for anomaly 156, but there is some speculation that a well placed multi-bit error in the WDT rather than the CCCA could have also caused an unnecessary reboot of the CCCA. Testing is underway to confirm the root cause.

#### 8.1.2 Conclusion

The CDH has performed nominally throughout the GP-B mission. The CDH system has supported and continues to support the GPB mission adequately.

### 8.2 Thermal Control Systems (TCS)

The temperatures of all GP-B space vehicle components are maintained within the minimum and maximum operating/survival temperatures. A margin of at least 11°C is carried at the hot and cold extremes for each component. Components with survival heaters have a minimum command authority of 25%.



Throughout the mission, all essential elements performed nominally with one possible exception. More specifically:

- All thermal systems have been and continue to be within tolerances.
- The TCS thermal monitor limits were developed early and the used extensively during the pre-flight testing of GP-B. All essential elements remained inside their limits for the duration of the mission.
- The success of the TCS during the mission was due to a qualified, certified and highly motivated TCS team. Notable contributions were made by Kevin Burns, as well as many others.
- The TCS's success can be directly attributed to extensive thermal modeling, limit development and thermal vacuum testing.
- The dedication, ability and willingness of the LMMS TCS team to develop limit updates and thermal model additions throughout the mission was exemplary and contributed in no small part to the GP-B mission success.

The thermal system for the GP-B spacecraft has an extremely robust design. GP-B, more than any other spacecraft, requires this robustness due to the large temperature swings the vehicle experiences during the different seasons. The science mission mandates that GP-B point in a fixed direction at a distant guide star throughout its mission. It is due to this fixed pointing in local inertial space that the spacecraft experiences different seasons as the sun appears to “walk” around the vehicle. The seasons of GP-B are illustrated in [Figure 8-5](#) below.

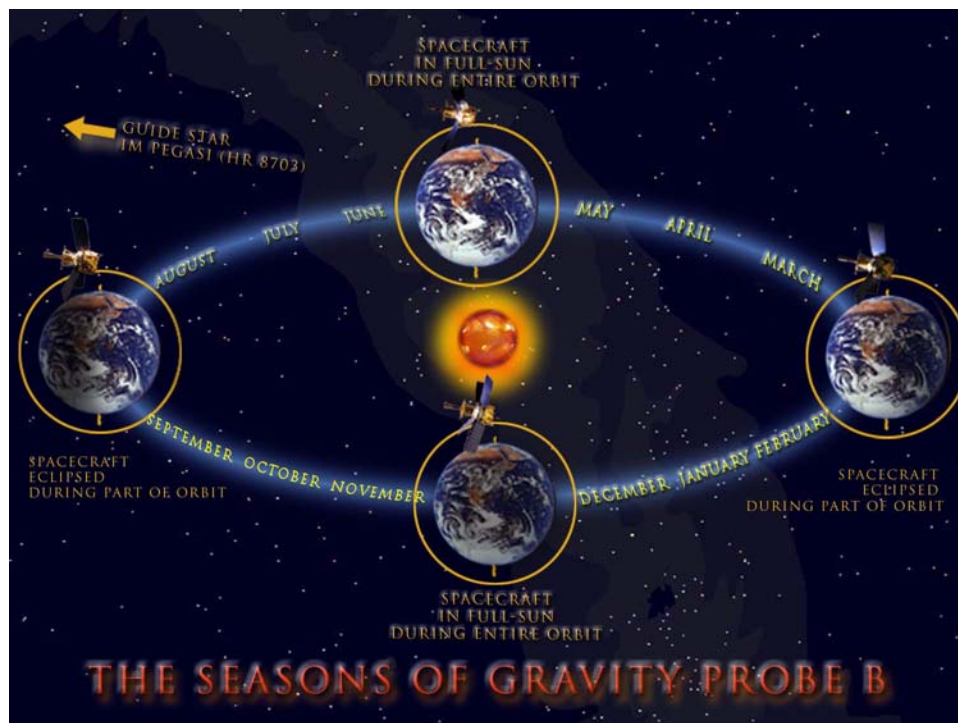


**Figure 8-5.** The Seasons of GP-B

This effect is also shown in the variation of the spacecraft's gamma angle throughout the year. The gamma angle is defined as the angle to the sun from the bore sight of the telescope. Also adding to the thermal complexities of the spacecraft is the fact that GP-B is in a low Earth polar orbit; therefore the vehicle experiences a high number

of eclipses each day (approximately 15-16 per day). [Figure 8-6](#) graphically shows the annual variation of the gamma angle, in conjunction with the spacecraft's corresponding time in eclipse. Accordingly the thermal data is highly cyclical and dependent on the eclipse cycle of the vehicle as well as the seasonal variations.

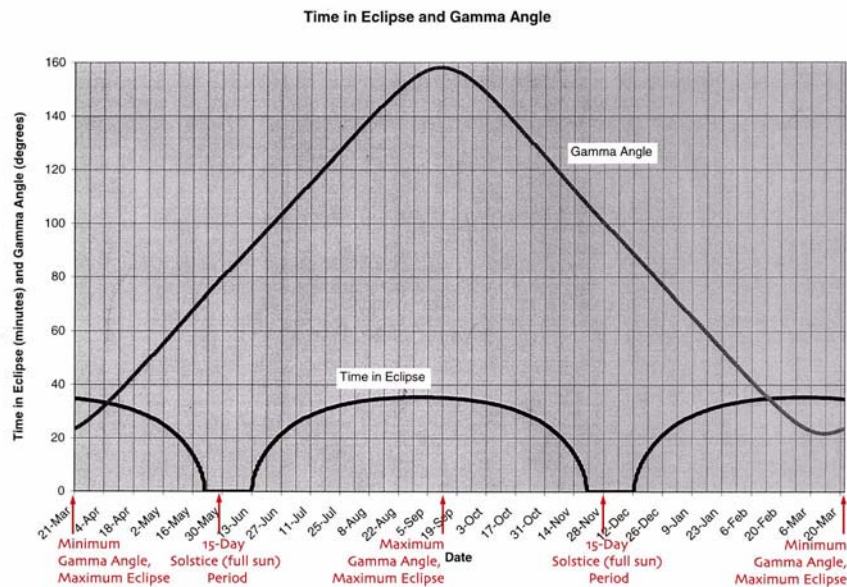


**Figure 8-6.** The annual gamma angle and eclipse cycle of GP-B

Despite the thermally complicated nature of GP-B's mission, there were no unexplained thermal transients or limit violations. It should be noted, however, that the dewar vacuum shell temperatures deviated 25–30 degrees from model predictions. [Chapter 12, Cryogenic Subsystem Analysis](#) explains the reason for this deviation in detail. However, it is important to note that although the temperatures are higher than predicted, the dewar met its mean-mission-duration requirement of 16.5 months.

## 8.2.1 System Performance

The Gravity Probe B Thermal Control System has performed exceptionally well from launch through the completion of the mission. All major TCS elements have demonstrated flawless performance and stability since launch. The following series of plots are intended to graphically display the thermal trending of the spacecraft's major components throughout the duration of the mission.

The spacecraft batteries are located on the battery pallet at the aft end of the vehicle. Each battery has an associated heater which keeps the temperature around 0 degrees Celsius. The battery temperatures are cyclic due to the oscillation of the heaters turning on and off. Additionally, the batteries have some seasonal variation in their temperature. As the sun moves to the front of the vehicle, the batteries become more dependent on their heaters to maintain their 0 degree average temperature. Where as, when the sun is on the aft end of the vehicle, the heaters turn off. [Figure 8-7](#) below, graphically displays the both batteries temperatures for the duration of the mission along with their associated yellow and red limits. It can easily be seen that the average temperature stayed around the desired 0 degrees Celsius and no limits were violated.

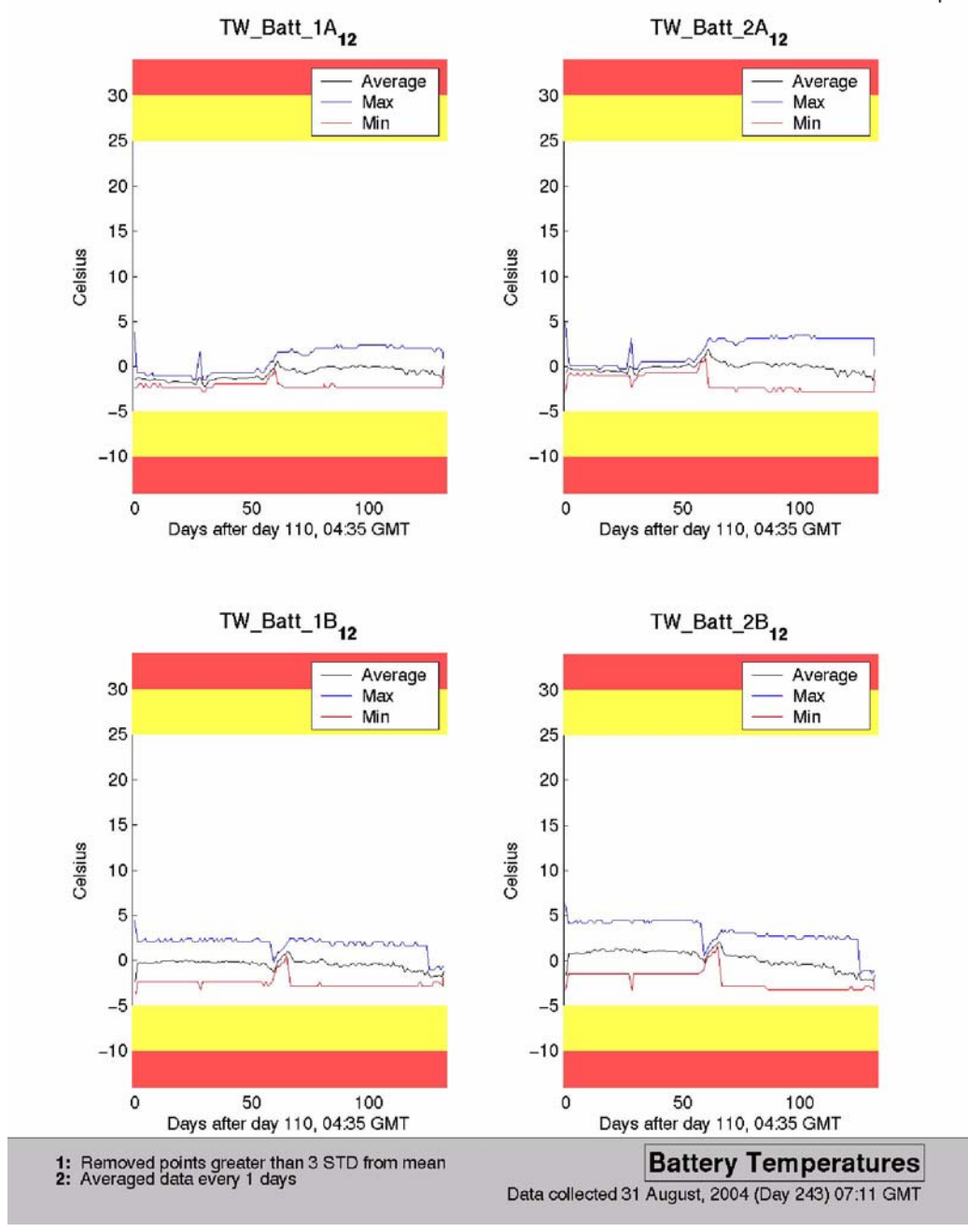


**Figure 8-7.** Battery 1 & 2 Temperature Trends for Mission Duration

The Gyro Suspension System (GSS) has maintained a steady range of temperatures. The largest variation occurred when the GSS dropped out of high voltage. The box is located in the Forward Equipment Enclosure (FEE) and is therefore thermally protected. Although its location allows for some thermal protection the changing of seasons is evident in the analysis of trended data. [Figure 8-8](#) below, displays all the mission data for GSS1. The other three boxes (GSS2, GSS3 and GSS4) all performed in almost identical fashion to box #1. It is interesting to note that temperature drops as the sun moves to the aft end of the vehicle and when science data acquisition began (GSS dropped out of high voltage).

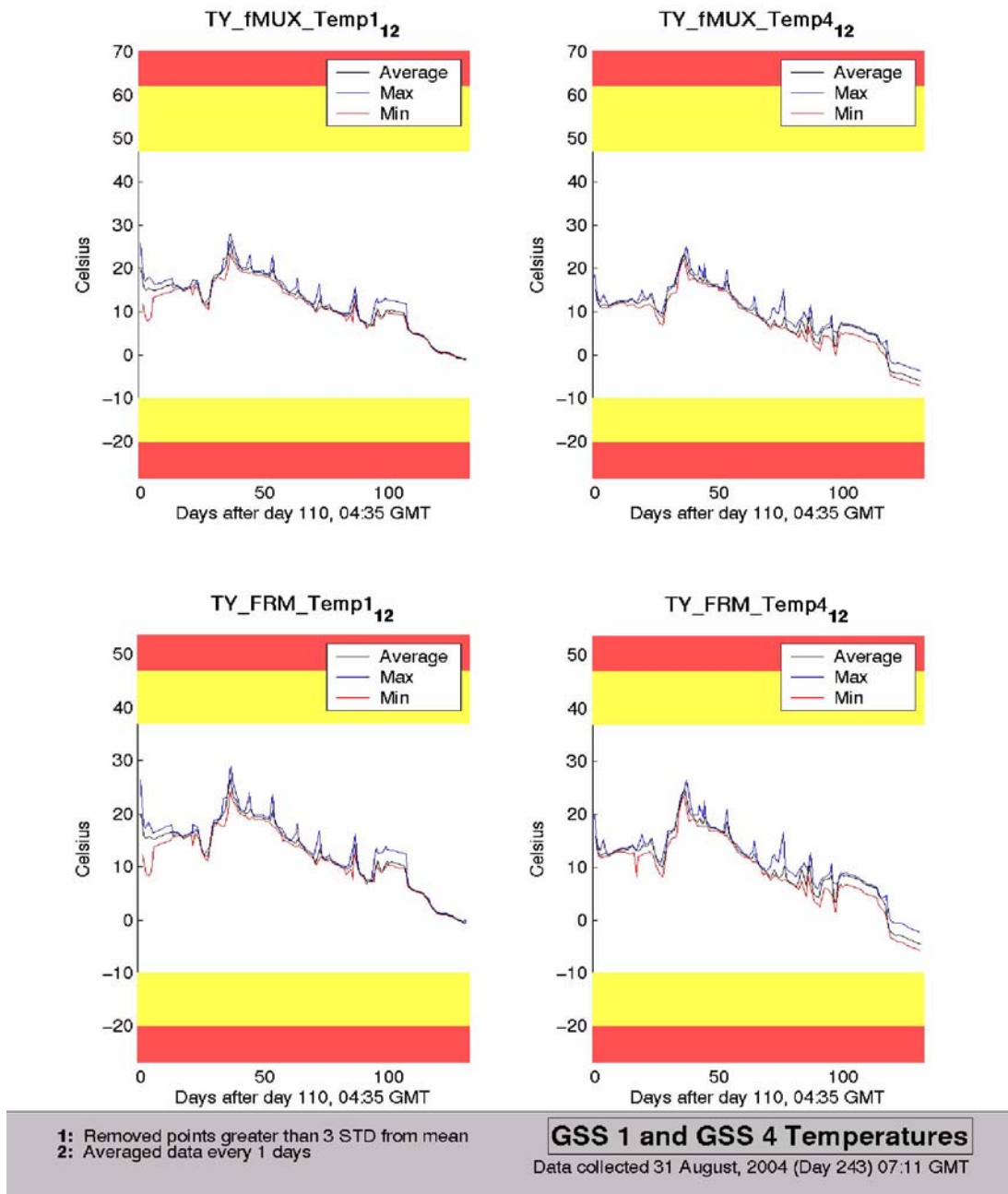


**Figure 8-8.** GSS1 Temperature Trends for Mission Duration

In order to maintain positive power throughout the year, GP-B had to develop a very unique design for its solar arrays. This design is discussed in much greater detail in the Electrical Power System (EPS) section of this report. However, the arrays are canted in such a manor to allow them to receive at least some sunlight year around. Due to similar canting, the array's temperatures tend to track each other in pairs. In other words array 1 & 3 have the same temperature as do arrays 2 & 4. Large temperature swings (~80 degrees Celsius) can be seen between full sunlight and eclipse. [Figure 8-9](#) graphically displays all 4 array average temperatures throughout the mission as well as the associated gamma.

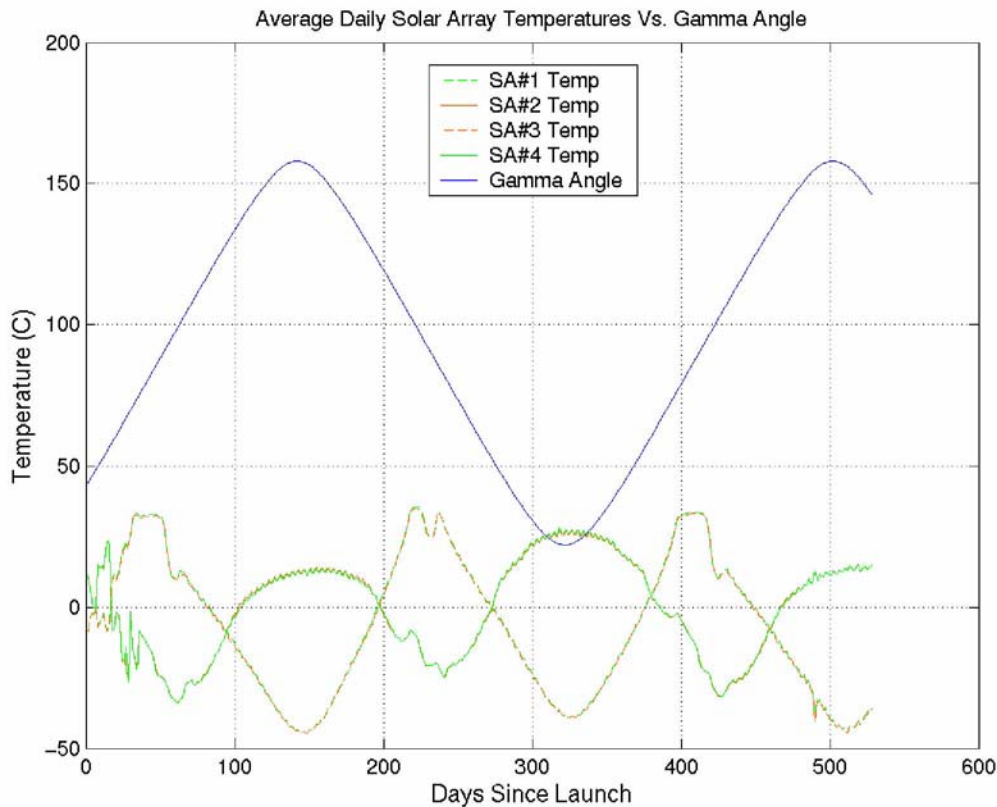
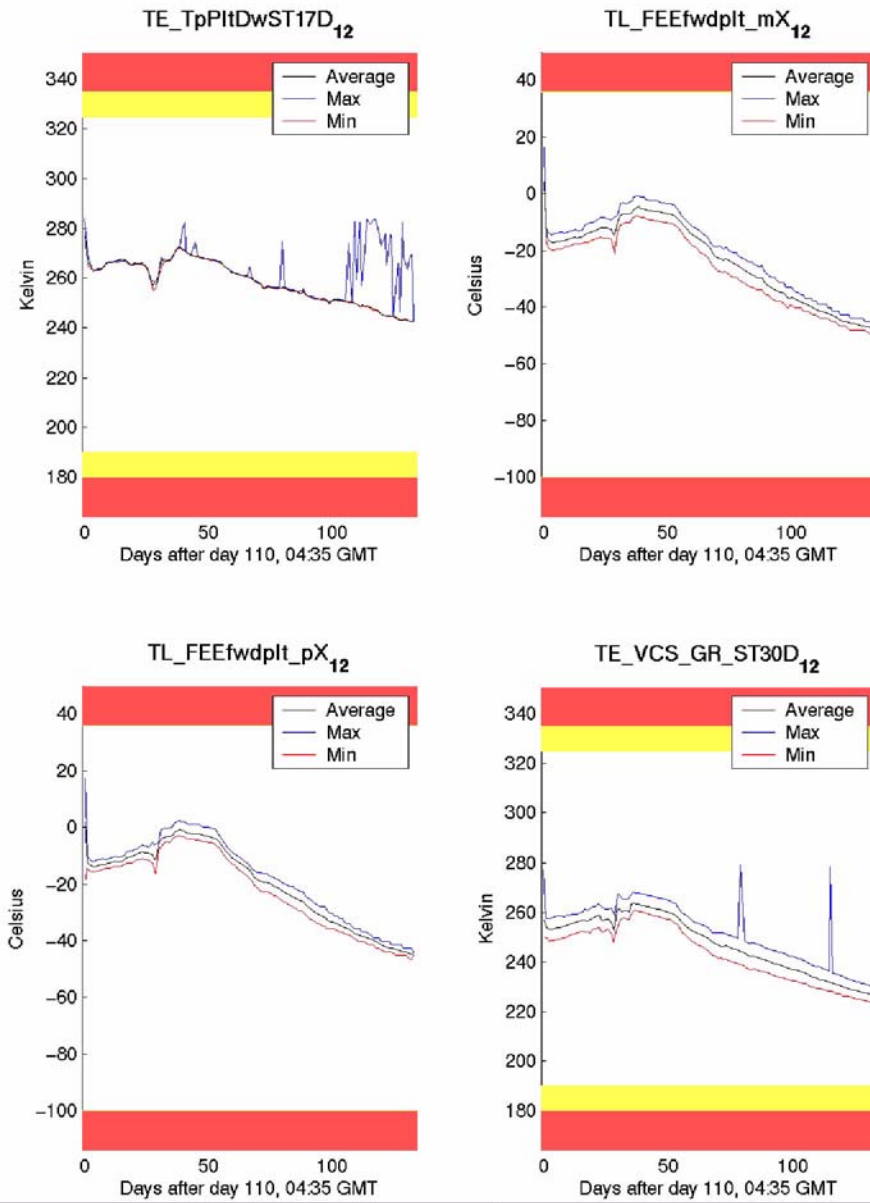


**Figure 8-9.** Solar Array (Average) Temperatures for Mission Duration

There are many thermal sensors located throughout the spacecraft; however, some of the most important ones for estimating the lifetime of the mission are located on the dewar Vacuum Shell. A thermal model was developed by Lockheed Martin for the entire spacecraft. This model produced estimates for temperatures of key systems for the different sun angles the vehicle would experience. During the mission these estimates were continually compared with the actual temperatures experienced on orbit. For the most part the actual and predicted temperatures matched up quite well. The one exception lies in the dewar vacuum shell temperatures. As mentioned earlier, the differences between the thermal model and the actual on orbit values has been extensively studied and is discussed in detail in [Chapter 12, Cryogenic Subsystem Analysis](#). [Figure 8-10](#) displays the actual temperature data taken over the course of the mission for the forward dewar vacuum shell, and [Figure 8-11](#) displays the temperature data for the aft dewar vacuum shell.



- 1: Removed points greater than 3 STD from mean
- 2: Averaged data every 1 days

### Dewar Shell FWD Temperatures

Data collected 31 August, 2004 (Day 243) 07:11 GMT

**Figure 8-10.** Forward Dewar Vacuum Shell Temperatures for Mission Duration



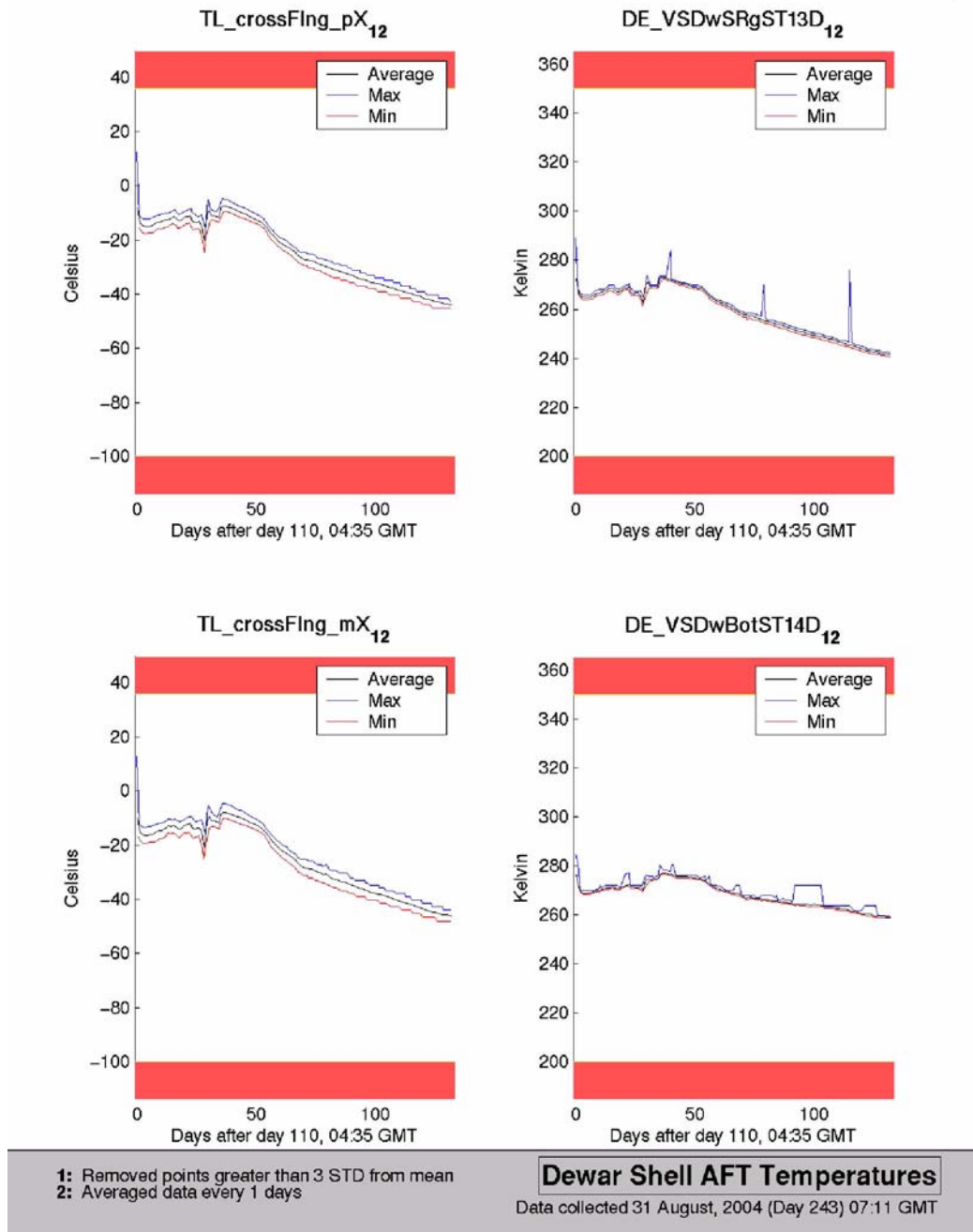


**Figure 8-11.** Aft Dewar Vacuum Shell Temperatures for Mission Duration

The Gravity Probe B spacecraft has forward and aft thrusters to maintain attitude control and for drag-free flight. The thrusters are mounted in clusters of four, with eight total thrusters on the forward and eight total on the aft. Having sixteen thrusters was a robust design, which allowed for redundancy throughout the thruster system. During the Initial Operation and Checkout (IOC) Phase one of the thrusters failed. This failure, although unfortunate, had little effect to the overall attitude control due to the redundancy of the system. A discussion of this failure is thoroughly discussed in [Chapter 7, Attitude & Translation Control Subsystem Analysis](#). However, as a result of this failure, four thrusters became “single-string” thrusters. Meaning that if one of these four thrusters were to now fail, some functionality in the attitude control system would be lost. All 16 thruster temperatures were monitored throughout the mission and due to their single-string nature, four of the thrusters were monitored with special care and a little more visibility. The four single-string thrusters are: Thrusters 5, 7, 10, & 12. [Figure 8-12](#), [Figure 8-13](#), [Figure 8-14](#), and [Figure 8-15](#) display the forward and aft thruster temperatures for the duration of the mission. It can easily be seen that the yellow and red limits were never violated and the seasonal variations in the thruster temperatures are evident as well. The forward thrusters cool as the gamma angle increases and the aft thruster cool as the gamma angle decreases.

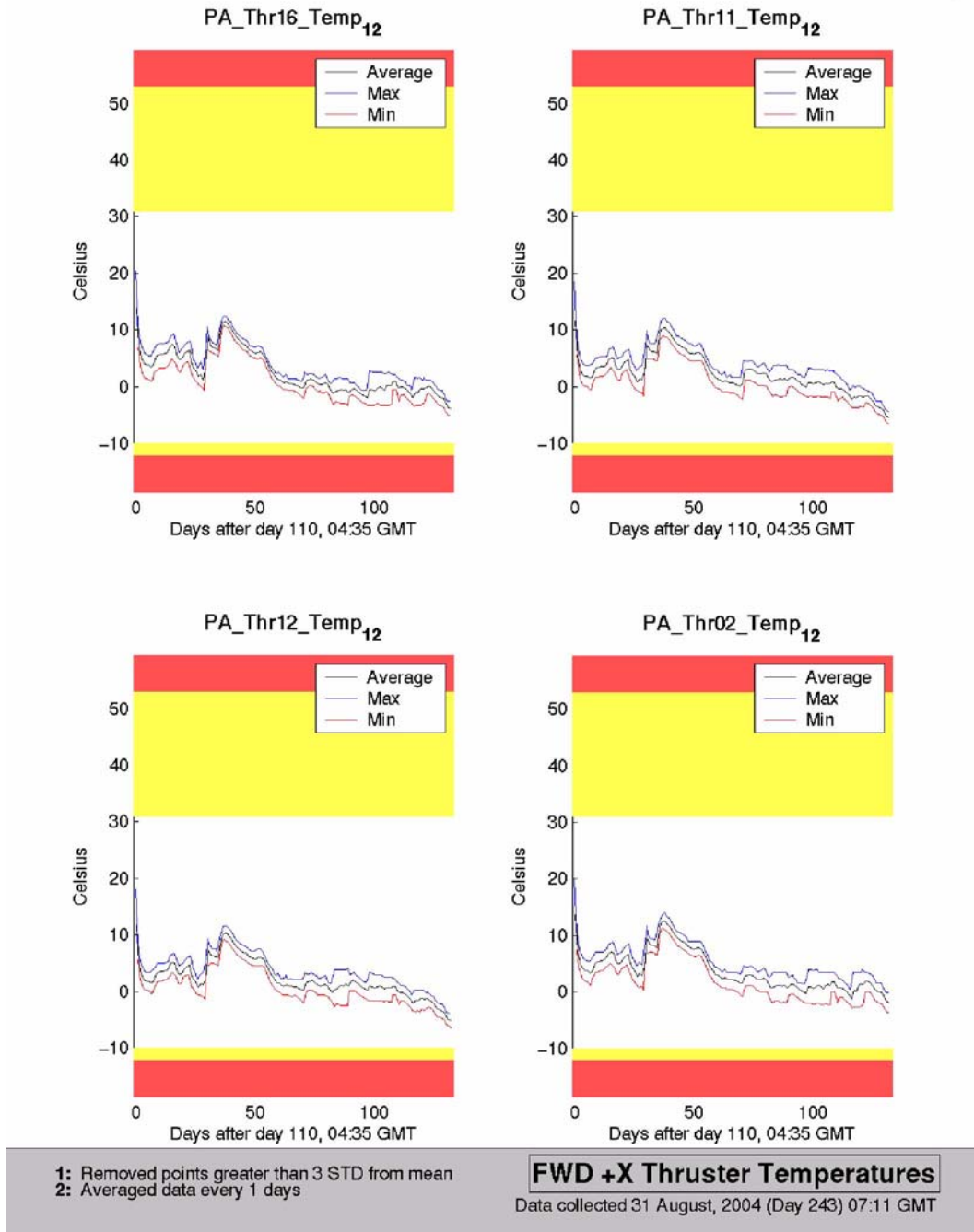


**Figure 8-12.** Forward +X Thruster Temperatures for Mission Duration

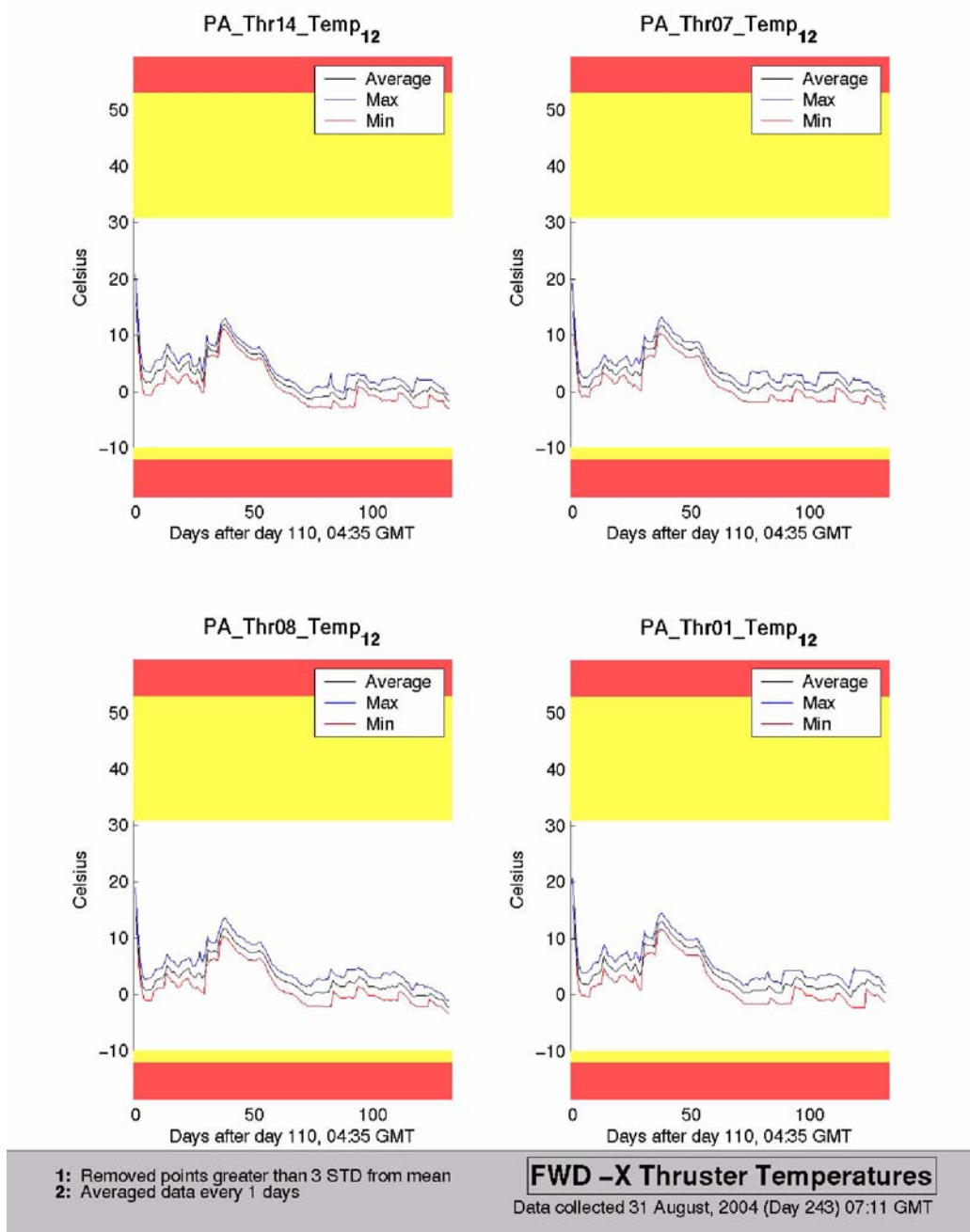
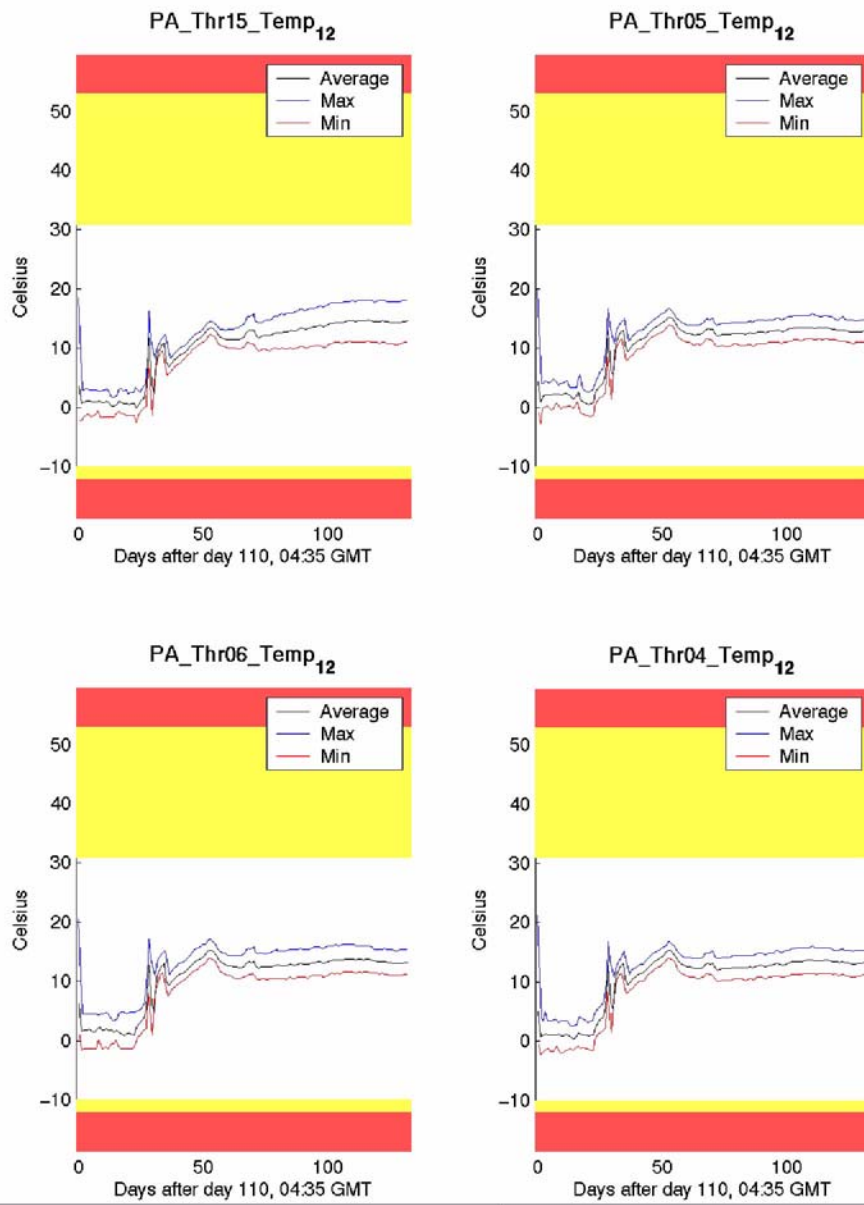


**Figure 8-13.** Forward -X Thruster Temperatures for Mission Duration



- 1: Removed points greater than 3 STD from mean
- 2: Averaged data every 1 days

**AFT +X Thruster Temperatures**

Data collected 31 August, 2004 (Day 243) 07:11 GMT

**Figure 8-14.** Aft +X Thruster Temperatures for Mission Duration

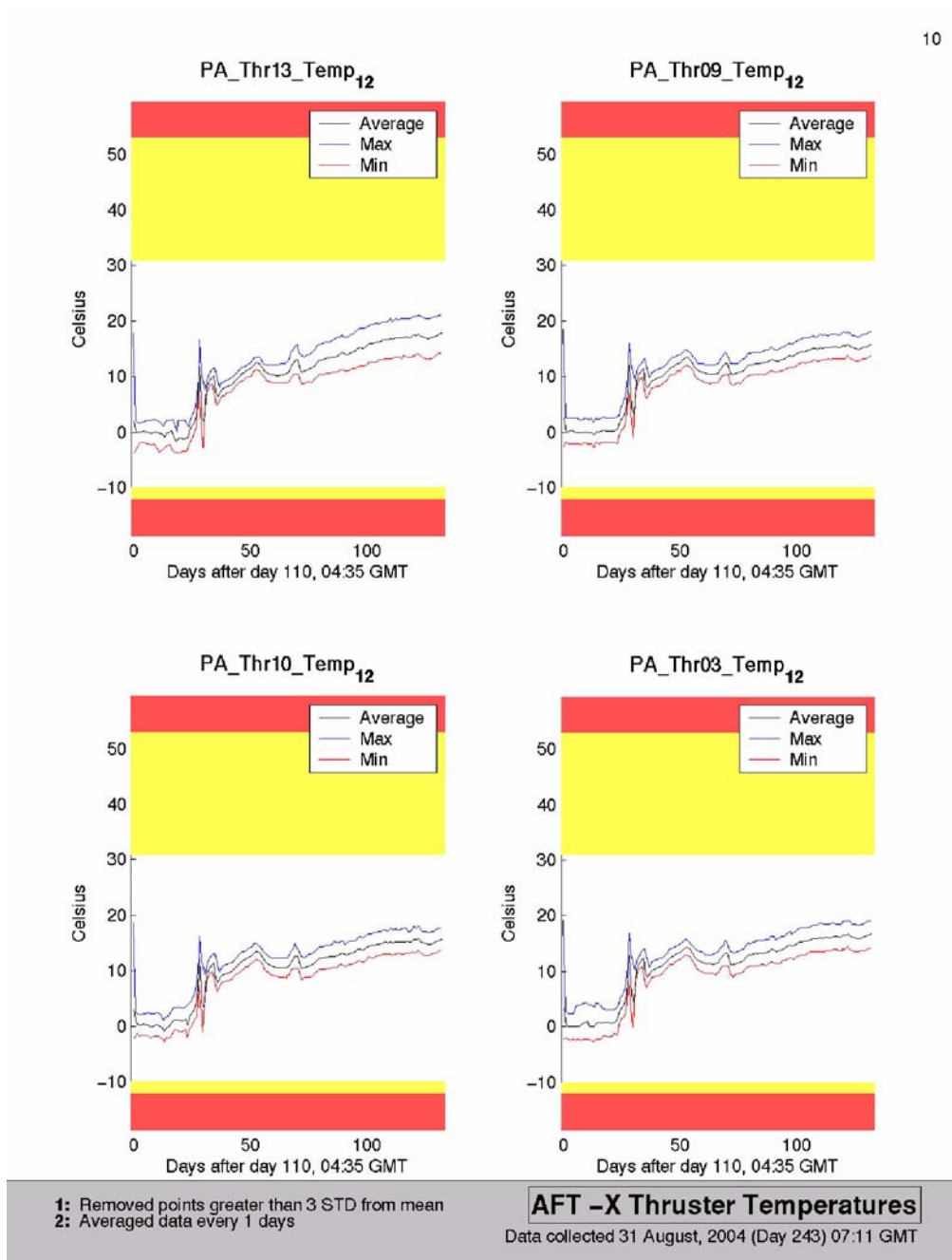


**Figure 8-15.** Aft -X Thruster Temperatures for Mission Duration

## 8.2.2 QBS and SRE Temperature Control

Because of the extremely precise nature of the GPB experiment there are several parts of the spacecraft that require exact temperature control to eliminate any thermal biases in the experiment. These parts are the Quartz Block Support and SQUID Brackets inside the Probe and the SQUID Readout Electronics outside the Probe. The temperature control of the parts inside the Probe is especially impressive: the QBS has 1 mK control while the SQUID Brackets have 5  $\mu$ K rms thermal stability with a 1mK disturbance.



Precise temperature control is achieved through a several control loops that link heaters to temperature sensors and increase or decrease the heater voltage according to the temperature readout. The QBS, SQUID Brackets, and SRE boards (FLL, DAC, DAS and a board controlling the SQUID Bracket temperature) all have their own heater, temperature sensor and control loop. The temperature control on these parts of the spacecraft limits the thermal bias of the gyroscope readout to less than 12  $\mu$ arcs—an extraordinary achievement.

### 8.2.2.1 QBS Temperature Control

The SQUID Bracket, which is thermally coupled to the QBS, requires the QBS to have a peak-to-peak thermal stability of 1 mK so that the SQUID Bracket will be able to meet its own thermal stability requirements.

Thermal stability of the QBS is achieved through two PI (Proportional Band, Integral) control circuits that operate the QBS heaters: A-side controller (QBS heater A in conjunction with an A-side GRT located on the QBS) and B-side controller (QBS heater B in conjunction with a B-side GRT located on the QBS). Each controller has three modes of operation:

1. Analog closed-loop, 80 Hz sinusoidal AC excitation;
2. Open-loop, 80Hz AC excitation;
3. Open-loop, DC voltage excitation.

However, under normal conditions only the analog closed-loop is used to achieve temperature control. It works as follows:

The desired QBS temperature (the heater set point) has a corresponding GRT resistance.

$$\text{GRT resistance} \times \text{current source level} \times \text{amplifier gain} = \text{GRT voltage}$$

A D/A Converter with 8-bit resolution is programmed to produce the desired GRT voltage. The analog PI controller heats the QBS to maintain the GRT voltage equal to the DAC voltage and thus control the QBS temperature.

It is important to note that because the controller can only add heat to the system, the controller must bias the QBS to a small delta above its sink temperature in order to achieve temperature control.

### 8.2.2.2 SQUID Bracket and SRE Temperature Control

SQUID Bracket and SRE temperature control is important because it is necessary to keep the electronic boards at a stable temperature to ensure precise SQUID measurements with little error.

As stated earlier, the SQUID Bracket requires a 5  $\mu$ K thermal stability with a 1mK disturbance. This is achieved through a control circuit which is located on the SRE boards (outside the Probe) and is itself temperature controlled.

The SRE boards are located outside the Probe and have to overcome much greater thermal variations than the QBS and SQUID bracket do inside the Probe. The temperature controls for the SRE boards were built to handle the following expected thermal environment variations (although they are capable of handling higher variations):

1. Roll temperature variation: less than 30 mK (peak-to-peak).
2. Orbital Temperature Variation: less than 0.5 K (peak-to-peak).
3. SRE Annual Temperature Variation: less than 15 K (peak-to-peak).

There is one DAS, FLL and DAC for each of the four gyros. Each of these has its own temperature control circuit that links its temperature sensor to a heater in order to provide temperature control.

Because there are only two SQUID brackets inside the Probe (each one holding two gyros) there are also only two boards outside the Probe where the control circuits for the SQUID bracket temperatures are. Each of these boards has a primary and backup heater and sensor. A PI algorithm controls the heaters and attempts to keep the temperature of the SRE bracket at its set temperature. There are two modes: Coarse Mode (750 ohms/volt) and Fine Mode (10 ohms/Volt).

The specification for temperature control of the SRE is given only in terms of the FLL. It states that, “The thermal-induced bias drift shall be less than 20 PPM of full scale per K for FLL ranges 1 and 2.” In other words, a 1 K temperature change of the FLL will result in less than a 0.4 mV change in the SQUID readout. This is roughly equivalent to 0.54 marcs, quite large by GPB’s standards. However, the average orbital temperature variation of the FLLs under temperature control is only 1mK so the thermal induced bias drift of the SQUID signal at orbital frequency is only 0.54  $\mu$ arc. An astoundingly small effect.

### 8.2.2.3 Verifying QBS Temperature Control Specifications

Analyzing a typical 24 hr. period of telemetry data from the monitor TE\_QBS\_a\_GT10P (the QBS temperature) shows that 1mK temperature control is achieved a majority of the time. More specifically: 85% of the time the QBS temperature was within +/- 0.5 mK of the average temperature over the 24 hr period.

65% of the time the temperature was within +/- .25 mK of the average temperature over the 24 hr period. 96% of the readings were within +/- 1 mK of the average temperature. 99.3% of the readings were within +/-1.5 mK of the average temperature.

The QBS temperature control loop must overcome temperature fluctuations caused by orbital, annual and roll cycles. The most rapid and drastic change in temperature is caused by an orbital cycle and this prevents the QBS from maintaining its specified thermal stability of 1 mK 100% of the time.

When the telescope shutter is open while the earth is between the guide star and GPB, light from the sun can reflect off the earth and travel down the telescope, heating the Probe. Areas of the earth covered in ice, snow or clouds reflect more light from the sun than other parts of the earth, so when the telescopes viewing field is over one of these areas, there is a larger increase in temperature of the QBS.

The PI control loop cannot respond (change the heater voltage) quickly enough to keep the QBS temperature within the control range when light reflecting off the earth travels down the telescope. Closing the telescope shutter during Guide Star Invalid periods would solve this problem. However, this was deemed an unacceptable solution as constantly opening and closing the shutter would cause vibrations in the Probe that could disturb the gyros. Another possible solution would be to use a PID (Proportional Band, Integral, Derivative) control loop that would be able to react fast enough to keep the QBS temperature within the desired range. However, this solution is not feasible as it is not possible to change the control loop after launch.

### 8.2.2.4 Verifying SQUID Bracket and SRE Temperature Control Specifications

Through telemetry, it was easy to verify that the thermal stability of the SQUID bracket met its specifications except during the time period when sunlight reflected off the earth traveled down the telescope, heating up the QBS. The chart in [Figure 8-16](#) below shows the temperature from of the SQUID Bracket (top), the QBS (middle) and the Cryo Pump, which is not under temperature control but was included to contrast temperature control against no temperature control (bottom).

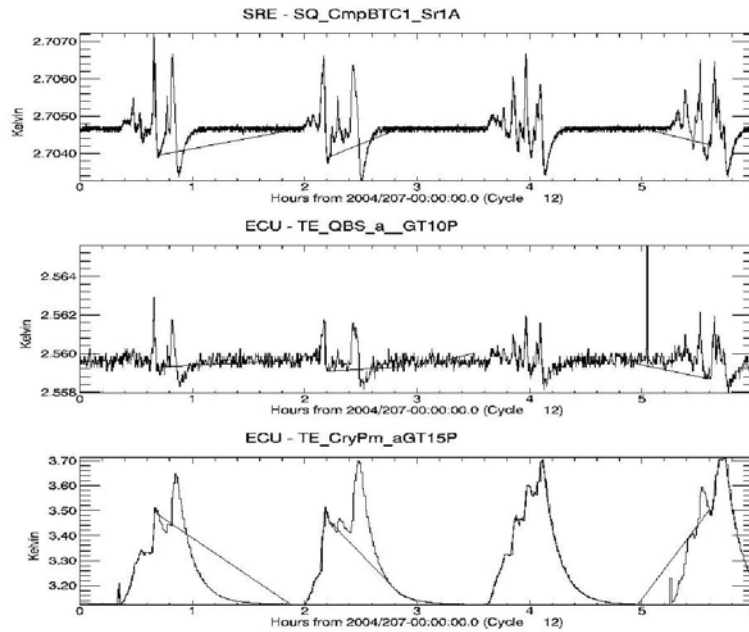


**Figure 8-16.** The temperature from of the SQUID Bracket (top), the QBS (middle) and the Cryo Pump

The thermal stability specification for the SRE was tested by purposely and individually modulating the temperature of all the SRE boards and observing the effect this had on the readout of the SQUID associated with that board. The temperature controller setpoint on the board being tested was alternated between 0 C and 75 C with a 90 second dwell at each value.

The results were given as Bias Temperature Coefficients in mV/K (in other words, the amount that changing the temperature of each board or bracket 1 K affected the readout of the SQUID associated with that board or bracket). The results are shown in [Table 8-1](#) below.

**Table 8-1.** SRE Temperature Coefficients (in mV/K)

	FLL1	FLL2	FLL3	FLL4	DAC1	DAC 2	DAC 3	DAC 4
<b>SQUID 1</b>	0.47 +/- 0.20				?			
<b>SQUID 2</b>		0.39 +/- 0.14				0.28 +/- 0.18		
<b>SQUID 3</b>			0.51 +/- 0.08				?	
<b>SQUID 4</b>				0.72 +/- 0.11				0.54 +/- 0.11

	DAS A	SQ Br EI A	DAS B	SQ Br EI B
<b>SQUID 1</b>	1.30 +/- 0.08	1.03 +/- 0.43		
<b>SQUID 2</b>		no data (SQ railing)	1.40 +/- 0.04	
<b>SQUID 3</b>	0.32 +/- 0.09			(no corr., bad SQ signal)
<b>SQUID 4</b>			0.24 +/- 0.05	0.54 +/- 0.67

Because the specifications for SRE thermal stability only pertained to the temperature of the FLL, they are the only Bias Temperature Coefficients necessary to verify that the specifications have been met. The average BTC for the FLLs is 0.52 mV/K. This is slightly higher than the specification of 0.4 mV/K, but with the superb temperature control of the FLLs the effect on the SQUID readout is minimal.

Using these thermal coefficients it is possible to determine the bias of the SQUID readouts caused by thermal fluctuations of the SRE boards. To do this, the temperature variations of each board at orbital and roll frequency were multiplied by that board's BTC to determine the bias that the thermal variation produced on the SQUID readouts. It was found that at roll frequency, the average effect on all the SQUIDS was 6 nV. This correlates roughly to an angle of 8  $\mu$ arcs.

### **8.2.2.5 Tangible Comparisons to Understand GPB Temperature Control**

GPB is a macro project in terms of depth and importance yet the experiment itself is on a micro level and it can be difficult to grasp some of the extremely small numbers involved in the experiment. The following are a few allegories that will hopefully enlighten the reader as to how precise temperature control on GPB truly is.

#### **8.2.2.5.1 QBS Comparisons**

There are two allegories that can be made to demonstrate the excellence of QBS temperature control. The first is by comparing it to the human body and the second is by comparing the temperature inside a room to the QBS temperature and the temperature outside the room to the Cryo Pump, which is near the QBS but not under temperature control.

1. The “nominal” range for an adult’s body temperature is 36.4 to 37.1° C (97.6 to 98.8° F). Control range of 7° C (1.2° F). The QBS temperature control is 700 times more precise!
2. Imagine the temperature outside the room you are in ranging from -63° C to 808° C (-81° F to 1486° F). To give you an idea, this ranges from the coldest temperature ever recorded in Canada (breathe hisses and turns to ice crystals) to the temperature of freely burning jet fuel. Now, if the room you are in had the temperature control of the QBS, it would be a comfortable 24 +/- 0.5° C (75 +/- 0.9° F) 85% of the time and 24 +/- 1° C (75 +/- 1.8° F) 96.5% of the time.

#### **8.2.2.5.2 SRE and SQUID Bracket Comparisons**

1. The SQUID Bracket temperature control is 140000 times as precise as the human bodies
2. The disturbance in the SQUID readout at roll frequency due to the thermal variation of the SQUIDS was extremely small. To be precise, it was 8  $\mu$ arcs. To get a better idea of the size of this angle let’s project it onto the moon, which is 384,400 km away. The projection would only be 50 m on the moon. This is 1 / 69520 of the moon’s diameter.

### **8.2.2.6 Conclusions**

The temperature control technology aboard GPB is superb. It nearly meets the extremely rigid specifications and ensures that thermal bias in the experiment will be minimal and easy to eliminate from the results, thus yielding a true test of Einstein’s Universe.

### 8.2.3 TCS Accomplishments

- No major thermal limits violated throughout mission duration
- Thermal model matched extremely well with on orbit temperatures
- Robust designs allowed for harsh thermal environment to have little effect on spacecraft operations or mission lifetime
- Well set limits can be attributed to extensive preflight testing and modeling
- Outstanding mission operations team training for monitoring the system health and data trending
- All thermal transients identified have been explained, as were any small limit violations

### 8.2.4 TCS Summary

The GP-B spacecraft is complex in many regards, the thermal control system is no exception. With seasonal variations experienced by all subsystems combined with the high number of eclipses each day, made designing a thermal system is no minor feat. With that in mind one can look back over the data from the mission and easily conclude that the thermal design was indeed robust and a success. Very few thermal transients were experienced during the mission and even fewer limits were violated. Most importantly the thermal system performed almost exactly as expected with no effect to science data or data collection.

## 8.3 Electrical Power Systems (EPS)

The Electrical Power System (EPS) is one of the most critical subsystems on the Gravity Probe B space vehicle and performs vital functions essential to achieve the vehicle science objectives during vehicle on orbit lifetime. The EPS primary objective is to maintain positive power supplied to the vehicle bus elements throughout the orbital eclipse and sun periods and ensure the flight batteries are fully charged when exiting the orbit eclipses. In addition, the electrical power system provides functions for sustained communication and tracking with the vehicle during all mission orbits.

### 8.3.1 System Features and Capabilities

Due to the nature of the science mission, the GPB EPS design introduced unique technologies and methods developed to meet the vehicle requirement of pointing in a fixed direction at a distant guide star which requires for the satellite to be free from disturbances as possible. GP-B's unique design includes four fixed double-sided solar array panels, canted at such angles to average solar power as a function of the orbital seasons. Most satellites that are designed to face the sun year around have moveable solar panels in order to maintain positive power during orbit conditions (sun; eclipse; and gamma angle). The unique GP-B design also featured double-sided panels to minimize the thermal effects of entering and exiting eclipses with no noticeable effects of thermal snapping.

The EPS bus design demonstrated outstanding efficiency and stability showing little bus ripple levels beyond the vehicle requirements vital to mission science payloads and instruments and has proven reliability and robustness throughout the entire mission.

The GPB EPS has met all requirements with flawless performance since launch supporting all mission operations and objectives providing ample power margin necessary to plan and support any contingency operations, if required.

### 8.3.2 Critical Mission Requirement

The GPB EPS primary function is to supply the required power to vehicle loads and science instruments necessary to support mission Science Mode and precious data collection during mission lifetime with no interruptions or dropouts. Additionally, the GPB science telescope must stay locked on the guide star IM Pegasi to within 100 milliarcseconds with no disturbances to the science instruments. The GPB EPS design demonstrated exceptional on-orbit performance with bus the ripple levels well below vehicle requirements of 2 volts peak-peak. Figure 8-17 below, displays the daily peak bus ripple measurements for the duration of the mission.

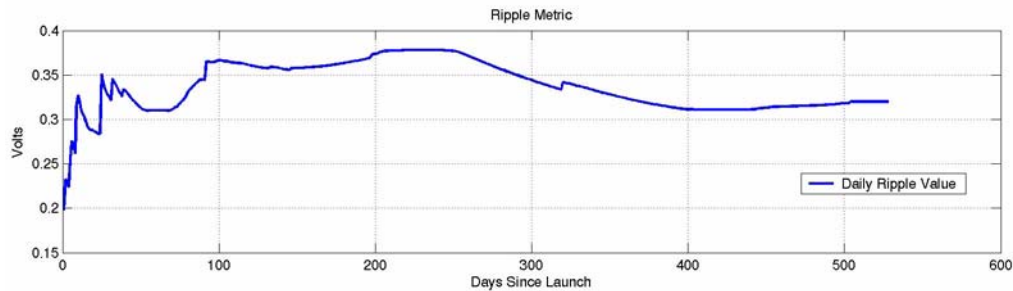


Figure 8-17. Bus Ripple Metric (Ripple Value in Volts since Launch)

### 8.3.3 System Performance

The Gravity Probe B Electrical Power System has performed exceptionally well from launch through mission completion with all EPS elements demonstrating flawless performance and stability. Immediately after spacecraft liftoff, the GPB EPS system delivered on-time exceptional performance with superb solar array deployment and continuous support to vehicle loads and mission operations during Initial and Orbit Checkout (IOC) phase. Successful on-orbit performance can be attributed to maintaining positive power to vehicle loads during vehicle mission operations and continuous system health and performance monitoring. It is also attributed to well-trained mission teams who effectively provided accurate data trending and comparison of real time data to predicted analyses and models. At the completion of the mission, the EPS system was performing well and continuing to support all science data collection and calibration activities. In fact over the mission lifetime, the system showed little degradation and could support extended missions if needed.

### 8.3.4 EPS Accomplishments

1. At vehicle launch, flawless solar array deployment in support of vehicle on-orbit initial operations
2. Positive power to the space vehicle bus and its payloads during orbit seasonal periods
3. Nominal and consistent performance during and post space vehicle Initial Operations and Orbit Checkout (IOC)
4. Stable bus telemetry during all vehicle operations
5. Very low bus ripple values better than specifications
6. Successfully supported vehicle Science and Calibration Mode, and any required contingency operations
7. Superb battery performance throughout all mission phases maintaining margin above minimum voltage and SOC thresholds for Safe mode.
8. Consistent performance agreed and matched predicted analyses and models
9. Outstanding mission operations team well trained to monitor system health and data trending



### 8.3.5 Eclipse Cycle

GP-B has an eclipse cycle that ranges from a maximum eclipse of ~36 minutes per orbit to no eclipses during its solstice season (full sunlight season). From launch through the end of mission, GP-B experience three (3) solstice seasons, all-lasting close to twenty one (21) days. Figure 8-18 below summarizes the variation of eclipse length for the entire mission. Additionally, it displays the associated depth of discharge on the batteries over that same time frame.

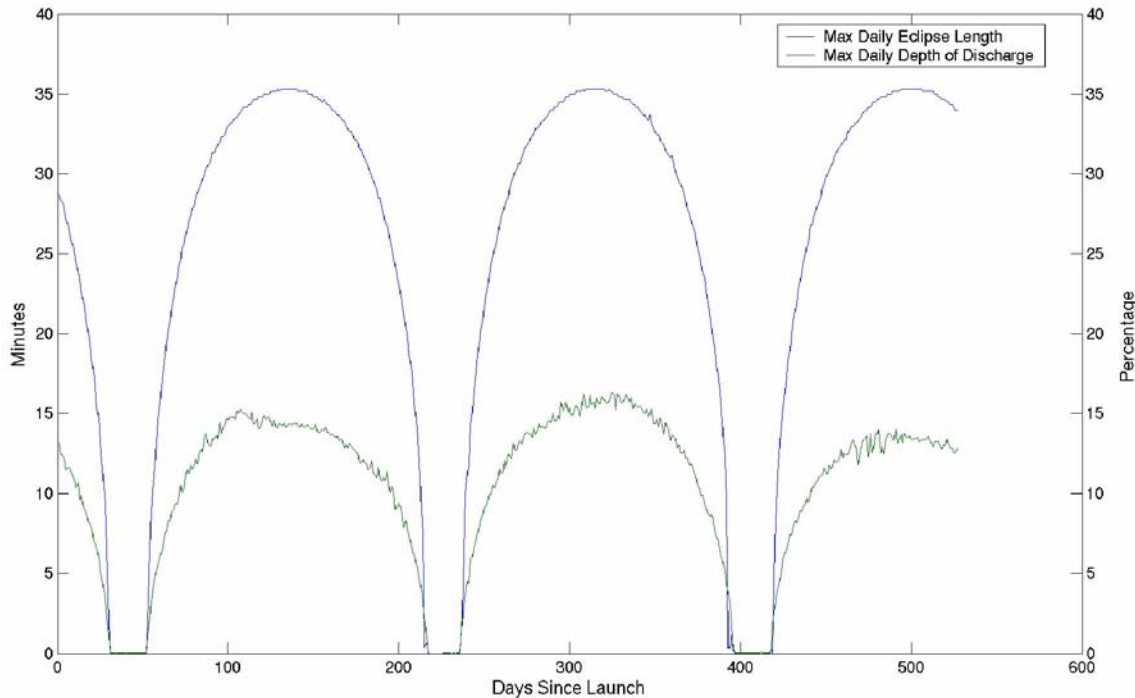


Figure 8-18. Eclipse Length and Depth of Discharge Metric

### 8.3.6 Bus Power

The space vehicle bus power performed nominally throughout the mission:

- All bi-levels & analogs are nominal
- SPRU was commanded to VT Level 4 prior to launch and has not changed since.
- Bus voltage and current are well within limits
- Very low bus ripple values better than specifications

Power generated by the solar arrays is regulated by the Standard Power Regulator Unit (SPRU) and distributed, through the Power Distribution Unit (PDU), to vehicle loads and two on-board 35 Amp-Hour (AH) Super NiCad batteries. The SPRU sole function is to supply regulated power to the bus and ensure batteries are fully charged. At eclipse exit, the SPRU provides the spacecraft with maximum power (peak power) to satisfy the vehicle loads and fully charge the batteries in preparation for the next eclipse orbit period. Throughout the mission, the system power margin has been trended and monitored (system power margin is defined as the additional power available from the system after satisfying vehicle loads and fully charge the two batteries).

Figure 8-19 is a plot of the power margin over the entire mission. The calculation of this margin combines many aspects of the EPS system, including the average power produced over 1 roll cycle immediately after eclipse, the predicted average power over 1 roll cycle immediately after eclipse and the average actual power being used by the vehicle load.

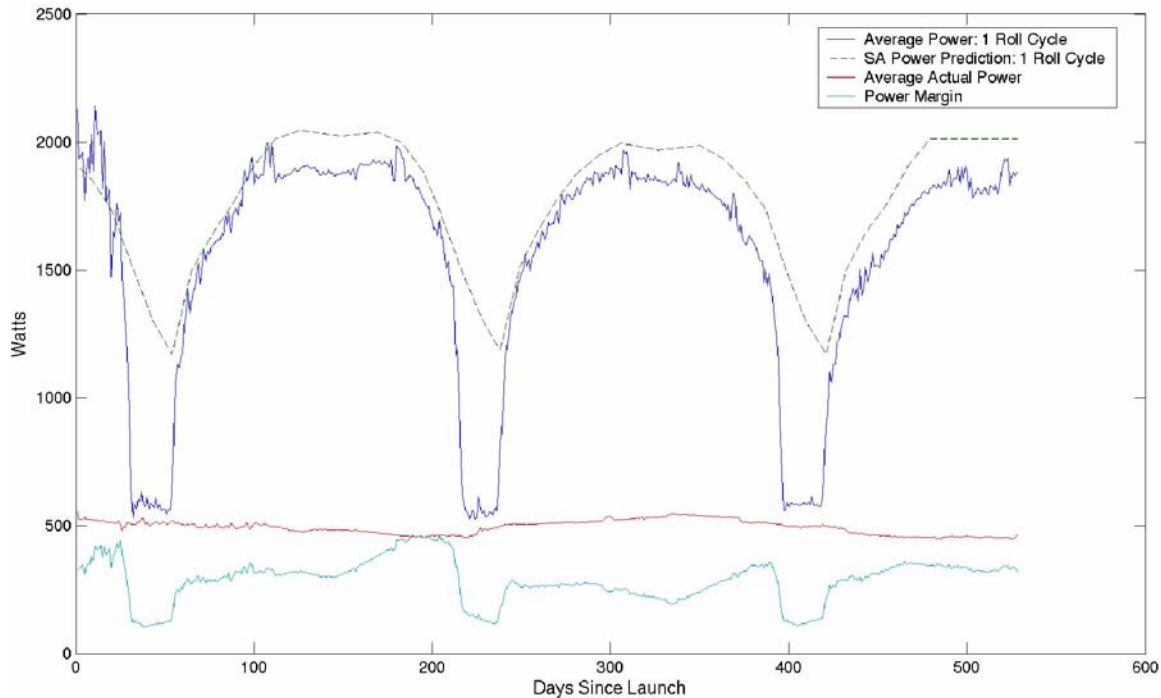


Figure 8-19. Space Vehicle Power Margin Metric

### 8.3.7 Batteries

GP-B maintains a Low Earth Orbit (LEO) at an altitude of only 640 km about the Earth's poles. At this altitude, it has an orbit time of 98 minutes, completing 14.6 orbits per day. GP-B LEO orbit has two solstice seasons of full sun for approximately 21 days each. For remaining times of the year, GP-B experiences 14.6 eclipses per day, total of 4800 eclipses per year. Maximum eclipse duration is 36 minutes during peak of each eclipse season. GP-B's batteries provide power for all of the spacecraft's subsystems for duration of each eclipse. Total eclipses required for the GP-B mission is approximately 7200.

GP-B's battery dominated bus is supported by two 35 Ah Super Nickel Cadmium batteries in parallel. Predicted power levels before launch were approximately 700 Watts, corresponding to 20% DOD for nominal two-battery mission. Cycle Life Analysis for nominal mission with two batteries in parallel cycling to constant 20% DOD at worst case temperature results in a cycle life margin of 24,000 cycles. This is equivalent to >5 years of cycling beyond the 1.5 year mission requirement. For mission scenario with one failed battery, Cycle Life Analysis for one battery cycling to constant 40% DOD at worst case temperature predicts margin equivalent to >1.2 years of cycling beyond the 1.5 year mission requirement.

Extensive ground testing was used to determine charge control levels for flight and confirmed GP-B battery capabilities. The nominal two battery-mission scenario was tested by subjecting test batteries to maximum 20% DOD mission eclipse profile over one year in real time. Minimum battery voltage observed from test was 26.4 Volts at maximum eclipse. Battery capacity sustained by charge control levels for flight was > 32 Ah, which is

more than adequate to meet mission requirements. Ability of single battery to support GP-B was also demonstrated. Minimum battery voltage at 40% DOD was 26.1 Volts, and capacity to meet mission requirements was also confirmed through worst-case eclipse season.

Actual loads in flight have not been as high as those used for analysis and test. Highest battery DOD experienced has been about 16% throughout the first year of the mission. [Figure 8-20](#) and [Figure 8-21](#) below display the variation (end of charge and discharge) of the battery voltage and state of charge over the entire mission. [Figure 8-3](#) shows that both batteries exhibit minimum voltage = 26.8 Volts. This is higher than the 26.4 Volts from ground testing due to the shallower DOD in flight. State of Charge for each battery is calculated from integration of measured currents. Both batteries exhibit same SOC throughout the mission. This is due to excellent current sharing between the two batteries.

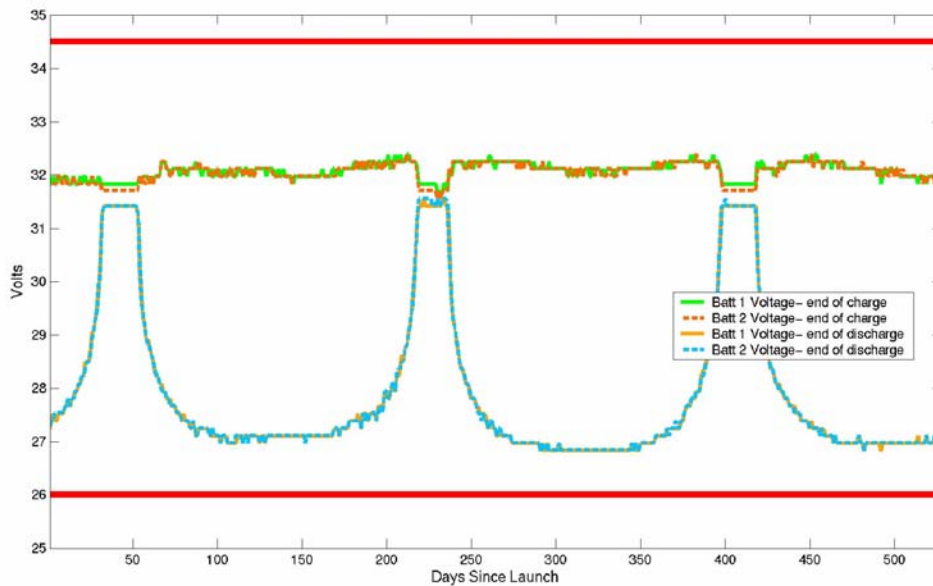


**Figure 8-20.** Battery Voltage Metric

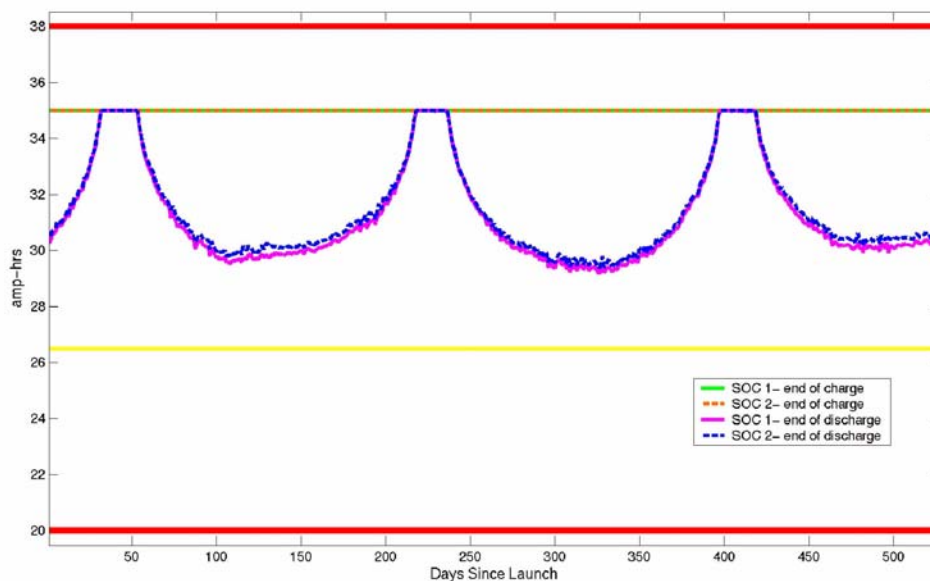


**Figure 8-21.** Battery State of Charge Metric

Battery Performance Summary:

- Charge control determined by ground testing has proven to be satisfactory throughout the mission.
- Battery Voltages in flight remain higher than from ground testing. This is due to lower DOD in flight (16% max) than was used in test (20% max).
- Current share between batteries is excellent, as evidenced by identical Voltage and State of Charge profiles throughout the mission.
- Spontaneous voltage rise at eclipse season exit indicates no degradation of the batteries since launch.

### 8.3.8 Solar Array Power

As previously mentioned, GP-B always points in a fixed direction at a distant guide star. Power source to the GPB spacecraft is supplied by the solar arrays that are designed and fixed positioned to receive average power over seasonal gamma angles. Engineers at Lockheed Martin considered worst-case scenarios for the gamma angle—the angle of the sunlight to the Z-axis of the spacecraft. The worst-case gamma angle of  $\sim 22^\circ$  occurs once throughout the mission lifetime. Another consideration was the maximum 36-minute eclipse time, which occurs when the gamma angle is at its maximum and minimum values ( $158^\circ$  and  $22^\circ$ ). At this angle, GP-B's orbit plane directly faces the sun. While this only occurs a few times throughout the mission, it represents the most usage and deepest depth of discharge (DOD) by the batteries

The orientations of the panels are arranged to optimize the amount of incident sunlight. Panels 1 and 3 are rotated  $90^\circ$  with respect to the X-Y plane of the spacecraft. Panel 1 is located  $45^\circ$  with panel 3 opposite it at  $225^\circ$  with respect to the positive X-axis. Panels 2 and 4 are rotated  $25^\circ$  and respectively located at  $135^\circ$  and  $315^\circ$  from the positive X-axis. Because of this asymmetry, the spacecraft is free to rotate about the Z-axis of the telescope with minimal perturbations due to the dragging or torquing of the solar panels.

Additionally GP-B is in a low Earth polar orbit, which causes it to have a high eclipse cycle (~15 per day). [Figure 8-22](#) and [Figure 8-23](#) display the bus power generated through the Standard Power Regulator Unit (SPRU) and solar array voltage and temperature variations respectively. It is interesting to note the consistency of the voltage input and current output as well as the consistent temperature tracking for each similarly canted pair of arrays.

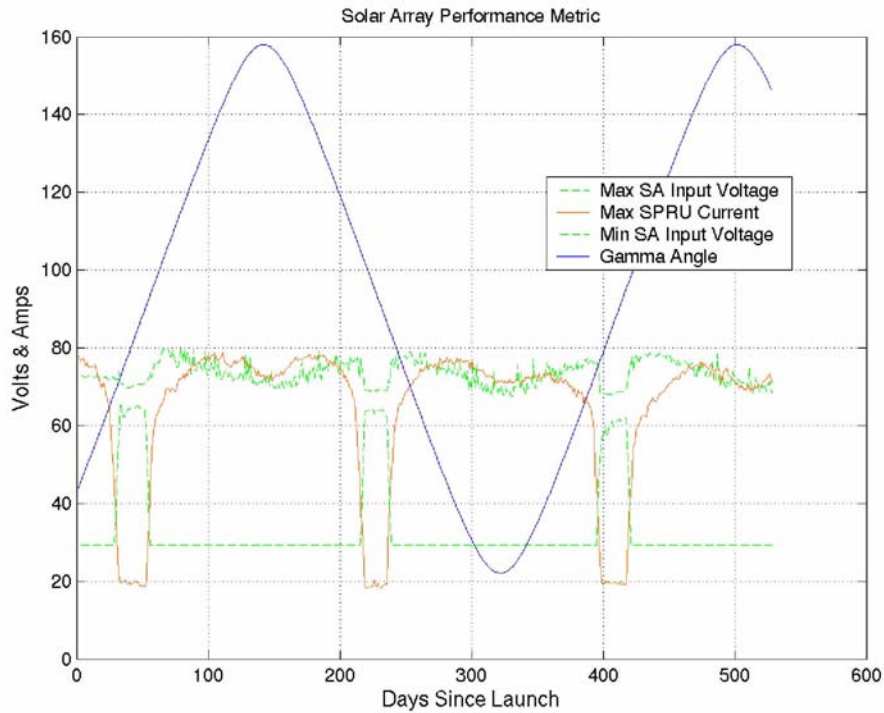


**Figure 8-22.** Solar array voltage and bus power performance metric

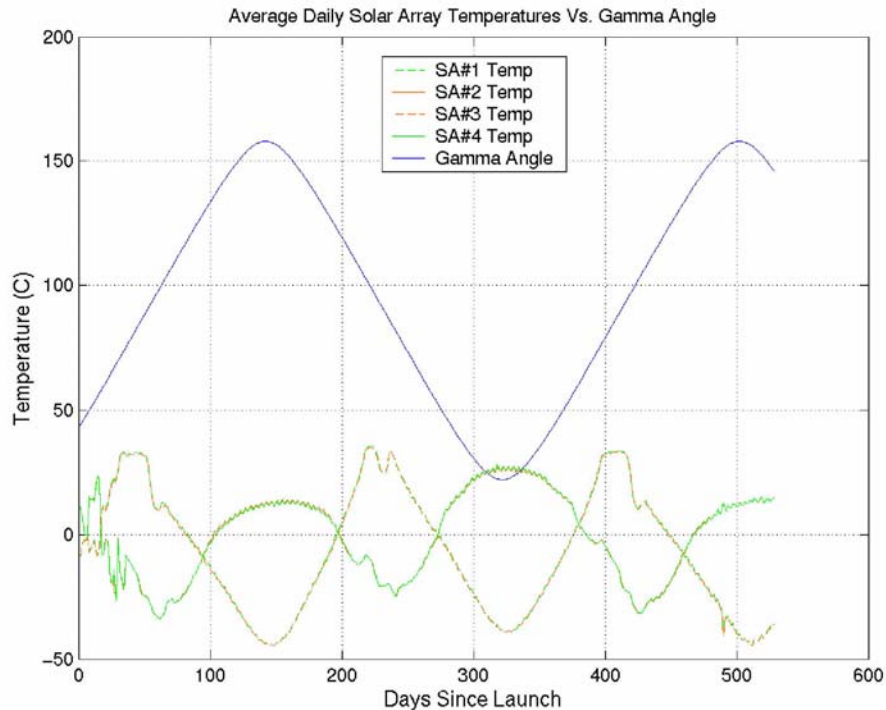


**Figure 8-23.** Solar Array Temperatures Variations vs. Gamma Angle

### 8.3.9 Solar Array Power Degradation Analysis

A detailed power analysis was performed by a team of Stanford Analysts supported by the Lockheed Martin power experts to determine the solar array power degradation over the mission lifetime and compare results with power margin calculation performed by the operation team using vehicle telemetry. The power analysis modeled the solar array panels including the panel temperature, solar intensity fluctuations, and the decay of the Gallium Arsenide (GaAs) cells. These factors have been added into the decay analysis and several efficiency factors have been determined to account for each of these effects. A formula to predict power generation in the course of the mission lifetime was developed and from which power values during 2004 and 2005 were calculated from the vehicle telemetry. A detailed power analysis is available for interested parties.

Results from analysis showed a drop of approximately 80 watts between 2005 and 2004, equating to 3.62% degradation in the power production over the mission lifetime (Figure 8-24 depicts the EPS peak power data comparison between 2004 and 2005). The analysis also showed ample power margin produced by the EPS system which would be sufficient to support mission extension, if required.

As mentioned, Figure 8-24 displays the peak power produced in 2004 and 2005. Additionally, the difference between the two curves was calculated and represents the power degradation of the arrays over the year. Figure 8-25, below, displays only the portion of the data prior to post science calibrations. During these calibrations the vehicle's attitude was purposely adjusted, which in turn changed the perceived gamma angle and likewise the peak power generated. Additionally, the data from 2004 was eliminated which included a vehicle anomaly resulting in an unplanned maneuver (gamma angle change) and roll down of the space vehicle. Therefore, Figure 8-25 provides the most consistent comparison of 2004 to 2005 and likewise the most accurate assessment of solar array degradation. Results from this analysis showed a decrease of approximately 86 watts, equating to 3.89% degradation in power production.

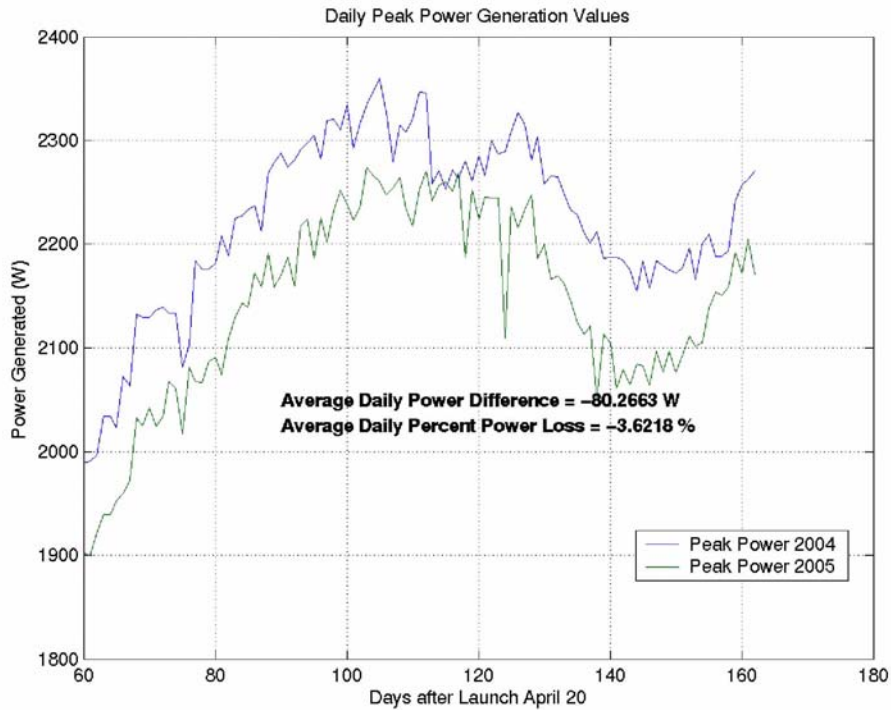


**Figure 8-24.** EPS Power Generation Capability Comparison 2004 Vs 2005

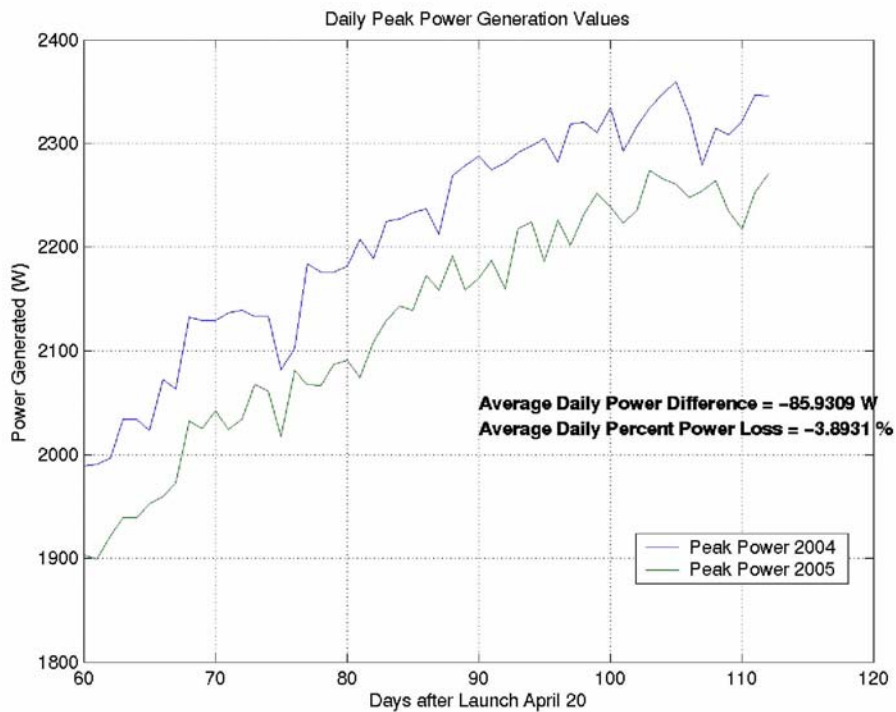


**Figure 8-25.** EPS Power Generation Capability Comparison (minus attitude discrepancies)





The Aft and Forward mounted omni-directional transponder configuration provide communications capability for all attitudes of the spacecraft with respect to the TDRSS and GN (except for the constraints imposed by the location of TDRS satellites and GN sites). The redundant receivers on both transponders are on active standby and are on direct power (unswitched) from the Power Distribution Unit (PDU). Both receivers acquire and track the forward carrier and are actively ready to receive command data from the ground via Multiple Access (MA) or S-Band Single Access (SSA) TDRSS service.

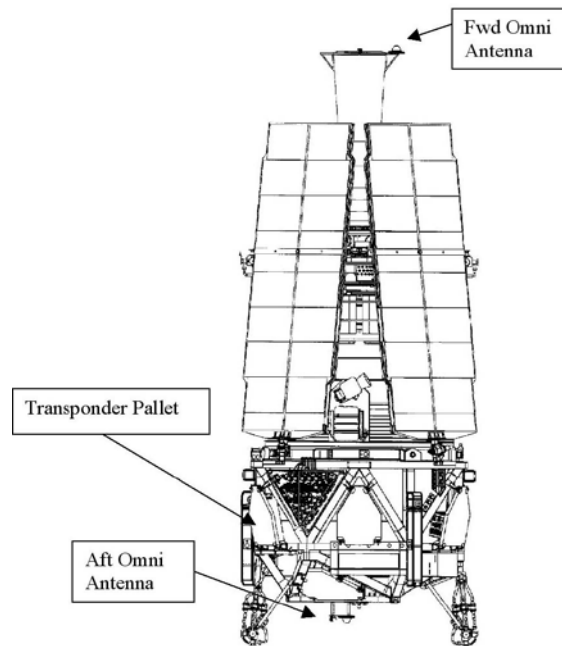


**Figure 8-27.** Location of antennae and transponder pallet on spacecraft.

The command decoders, part of the Command and Telemetry Unit (CTU) subsystem, receive the detector lock signal from the receivers and accept command data from the first receiver with the detector lock indication. The nominal transponder and antenna configuration is with the Transponder-A on the Fwd (Z-Axis) Omni Antenna, and Transponder-B on the Aft Omni. However, in the event of a problem with the nominal configuration, the receiver/antenna configuration can be cross-strapped with a single command.

## 8.4.1 TDRSS Operations

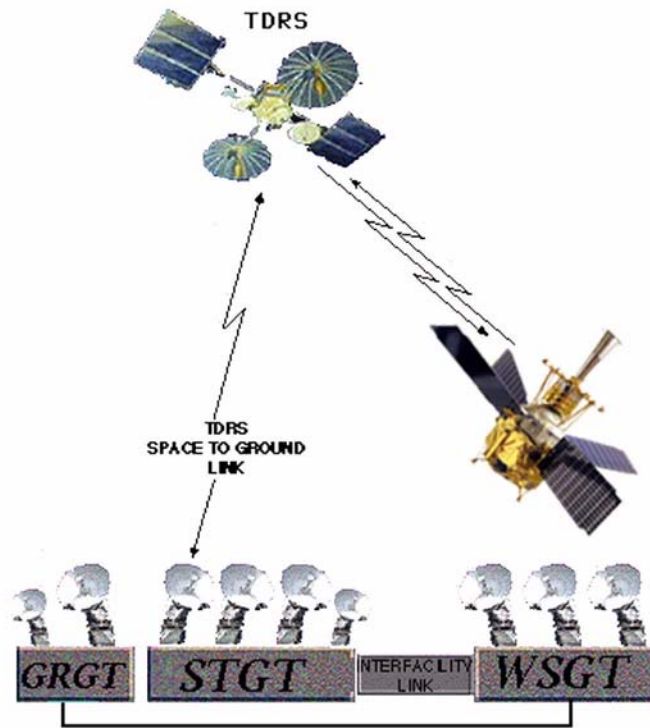


**Figure 8-28.** Remote controlled operation of GRST from WSC

The Space Network (TDRS) configuration is composed of various modes as shown below. Only one, safemode is automatically configured by the safemode system, the others are operated via command templates or command macros that are executed via the SPCs or ground commands. Selection of the Antenna to use is made by view angles based on spacecraft attitude and view angles (line-of-sight) to the various TDRS.

**Table 8-2.** TDRS Command Modes

Command (bps)	Telemetry (bps)	Coherency Mode	Service Type	Antenna Used	Condition
125	1024	Non	TDRS (MA/SSA)	Fwd	Safemode
2000	2048	Coh	TDRS (SSA/SMA)	Aft	Nominal
2000	1024	Coh	TDRS (SSA/SMA)	Aft	Nominal Format Loads
125	2048	Coh	TDRS (SSA/SMA)	Fwd	Transponder-A anomaly

## 8.4.2 Ground Network Operations



**Figure 8-29.** The Svalbard Ground Station Network.

The transponder mode for the GN is only one, as shown below. In the event of a safemode, the GN cannot be used, as the transponder is switched into a TDRS mode. However, it is possible to command (uplink only) during a GN while the vehicle is in a safemode, but this has not been necessary. Ground sites are scheduled as predicted by line-of-sight, based on the GP-B attitude (for antenna use), orbit and site location over the rotating Earth.

**Table 8-3.** Ground Station Setup

Ground Stations used by GP-B		Alaska, Wallops, Svalbard Ground Station			
Command (bps)	Telemetry (bps)	Coherency Mode	Service	Antenna Used	Condition
2000	2.56 M	Non	All GN Sites	Fwd/Aft	Nominal

## 8.4.3 Communications Anomalies

The Gravity Probe B Spacecraft, when using the Forward Antenna Transponder-A has a reduced forward link performance on TDRSS contacts. In addition, during the mission various issues with ground communications also occurred. To date, GP-B has experience no problems due to mutual interference with other spacecraft, but this could potentially be an issue in the future, as discussed at the end of this section.

### 8.4.3.1 Transponder-A Communication Anomaly

The anomalous behavior, which became apparent after GP-B began on orbit operations, effectively reduces the received Signal to Noise by 15 to 20 dB. It is believed that the reduced performance is due to an increase in the transponder noise floor, which rises at temperatures below 30 degrees C and increases as the transponder cools. The most likely root cause is a low level out-of-band oscillation in the second Low Noise Amplifier, which was induced during the retrofit to a new assigned frequency in October 2002.

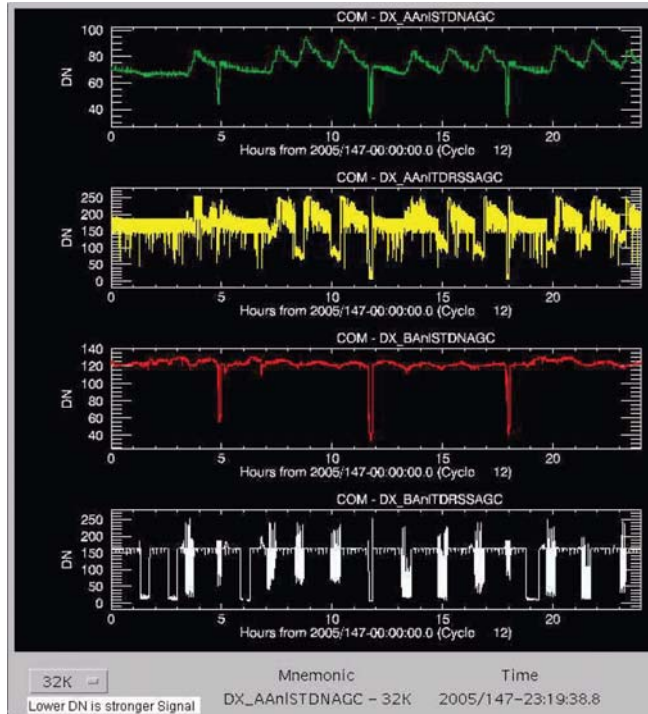


**Figure 8-30.** Xpndr-A STDN (green), Xpndr-A TDRS (yellow), Xpndr-B STDN (red), Xpndr-B TDRS (white)

The plots in [Figure 8-30](#) above show a significant difference between Transponder-A (first and second plots from top) and Transponder-B (third and fourth) raw Signal Level (AGC). The Transponder-A, STDN mode AGC shows large fluctuations and increased noise floor as compared to that of Transponder B.

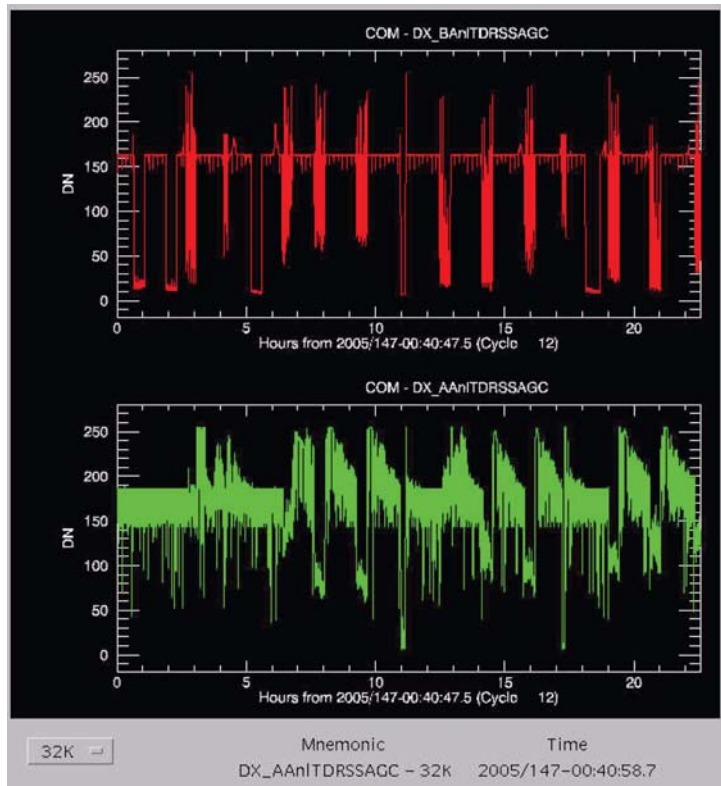


**Figure 8-31.** Transponder B TDRS AGC (red) vs Transponder A TDRS AGC (green)

Transponder A TDRS mode AGC is also very noisy, compared with Transponder B TDRS mode AGC, as shown in [Figure 8-31](#) above.

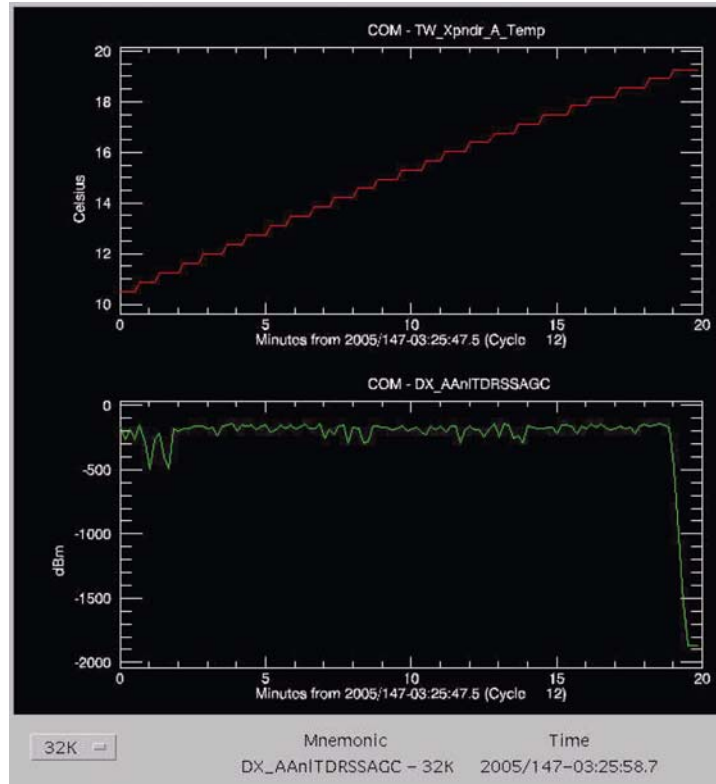


**Figure 8-32.** Plot of TDRS AGC vs Temperature over a 20-minute time frame

Figure 8-32 above shows the increase in the signal level (better Signal to Noise) as transponder temperature increases. The sample above shows an improvement of AGC from  $-264.0$  dBm to  $-171.0$  dBm in a twenty-minute period.

### 8.4.3.2 Transponder-A Anomaly Mitigation

To mitigate the reduced SNR, the GP-B transponder configuration macros were modified to operate the Fwd Antenna connected Transponder-A at the command data rate of 125 bps. This in turn provides an increase of 12 dB above the nominal command rate of 2000 bps, which the Aft Transponder's nominal command rate. In addition, the TDRSS supports that can provide high power on the forward link (SSA) are routinely operated in that mode, providing an additional increase in the link margin (5 dB better than low power). With both procedures in place, the command ability and reliability with the use of the forward transponder has not been a major issue during the GP-B science mission phase.

### 8.4.3.3 Ground Network Communication Anomalies

The Ground Network has had few problems with the transponder, as the transponder configuration (mode) is different and the GN uplink is of higher power. During the month of April of 2005, the Svalbard Ground Station was shut down for Antenna work, so the schedule shifted to the Svalbard commercial site (SKS). In addition, during the same month, Poker Flat Alaska commercial site (PF1) began to be scheduled more frequently. During this time period, the project experienced noisy data from these sites. Because of the compressed data dump, one-minute of data, lost due to noise, results in the loss of one hour and twenty minutes of 32K data. Whenever this kind of problem occurs, the operations team has to reconfigure the Solid State Recorder to repeat the playback during the next scheduled GN. Although, this was/is a good way to recover the data, it was not the



best solution. After a relatively short time however, the start and end time for the data dumps was changed to reduce the low elevation start and stop times (increased the masking); this reduced the dump time, but resulted in better quality data. GP-B is now using all sites without major concerns in the quality of the data.

#### **8.4.3.4 Mutual Interference Anomaly Potential**

Mutual Interference (MI) has not been a problem on GP-B. There are some incidences when another vehicle has affected the TDRSS supporting GP-B, but the MI's duration has not been very long and so are of no consequence. However, GP-B does have MI potential to other projects (S-Band Frequencies) supported by NASA's Deep Space Network (DSN). GP-B's mission planning, with predictions provided by the DSN has successfully managed the control of the GP-B downlink over DSN sites.

#### **8.4.4 Communications—Prime Mission and Beyond**

The GP-B Communications subsystem provides the command and control reliability as per the pre-launch system requirements. With the exemption of the Transponder-A anomaly, the system has functioned as expected, within or better than the expected link margins. The project has successfully sent approximately 106,000 commands over the 17.3-month mission and has retrieved 99% of the SSR data.

The management of the on-orbit problems, such as that of the transponder has given the project the ability to successfully complete the mission and go beyond. The project would like to acknowledge the assistance in resolving many of the COM issues on GP-B; members from Stanford, NASA Goddard and Marshall, Lockheed Martin and General Dynamics (with the issue of the transponder).

### **8.5 Flight Software (FSW)**

The Gravity Probe B Flight Software (FSW) consists of all Mission Support Software (MSS) running on the Command and Control Computer Assembly (CCCA). This software performs a wide range of duties, including but not limited to maintaining the spacecraft attitude and drag-free orbit, monitoring critical health and safety statistics, and supporting the transfer of telemetry to the ground. This software is distinct from the codes running in the payload computers, namely the Gyroscope Suspension Software (GSW) and the SQUID Readout Electronics Software (SSW); these payload packages are described in their respective payload sections.

This section will give an overview of the on-orbit performance of the flight software, as well as the steps taken by the FSW team to both prepare for mission operations and make adjustments to the software and procedures as a result of on-orbit events. The discussion will show that the FSW proved to be an efficient and robust piece of the complicated GPB system, and that the FSW team successfully guided the software through pre-launch preparations, on-orbit modifications, and several anomalous events.

#### **8.5.1 Requirements Satisfaction**

The GPB Flight Software (FSW) played an important role in achieving mission success. The mission level role of the FSW included the capability to provide functions to support all on-orbit activities of both the spacecraft and payload, perform autonomous health and safety monitoring of critical subsystems, and ensure proper processing of telemetry data and ground commands. The Flight Software successfully performed these goals, configuring the vehicle and science payload to a state appropriate for data taking, safing the vehicle from unexpected events on a number of occasions, and supporting the accurate transfer of > 95% of collected data to the ground. The on-orbit performance of GPB, from system initialization through science data collection, is a testament to the satisfaction of high-level FSW requirements.

The FSW also met its subsystem level performance specifications. A major requirement of the FSW was to provide all mission level capabilities mentioned above, while allowing the spacecraft computer (CCCA) to operate with acceptable usage margins. This requirement was stated in LM SCSE-15 (Flight Software Requirements Specifications): “Computer timing margins shall be defined as: PDR is 60% or less usage; CDR is 65% or less usage; vehicle acceptance review is 95% or less usage”

FSW performance was measured by the time duration (or percentage of allotted time) required for 1Hz and 10Hz task processing. Data for a typical week during science data collection are shown in Figure 8-33 and Figure 8-34. Processing times were averaged over ~4 hour periods for this plot. Red lines represent the maximum processing time over the averaging interval, blue lines represent the average processing time, and green lines represent the minimum processing time. The 1Hz processing times (Figure 8-33) show a maximum of about 35% (350 milliseconds), which exceeds the performance specification of both 60% (PDR) and 95% (vehicle acceptance). The 10Hz processing times (Figure 8-34) show maxima under 90% (90 milliseconds) with an average of just over 65% (65 milliseconds), also meeting performance specifications.

Additionally, watchdog timers were used to ensure that 1Hz and 10Hz processing tasks finished within the allotted time. This provided a means of monitoring the software performance and tracking the number of cycles that “timed out” before the processing task was complete. Based on flight data analyzed near the end of the GPB science mission, the FSW incurred zero (0) 1Hz processing timeouts during the first 400 days of the GPB mission. Eleven (11) 10Hz processing timeouts were recorded over this same time span (an average of ~36 days on-orbit per 10Hz timeout). Processing overload caused negligible (if any) interruption to on-orbit activities or science data collection.

Overall, the design and implementation of the GPB Flight Software met or exceeded all high-level system requirements, and most importantly, contributed to the realization of mission goals.

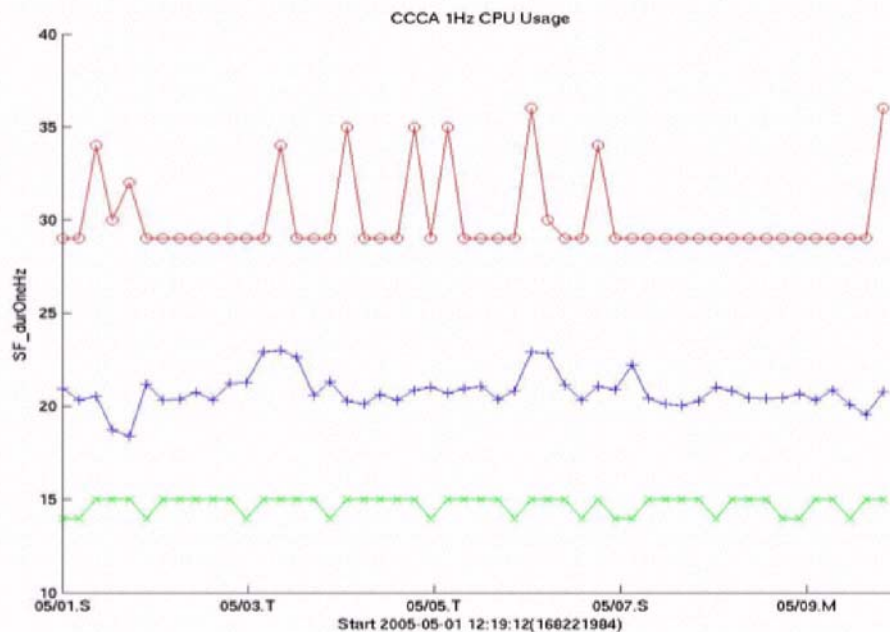


**Figure 8-33.** CCCA 1Hz CPU Usage (in %) averaged over ~4 hours. (Red = max; Blue = avg; Green = min):

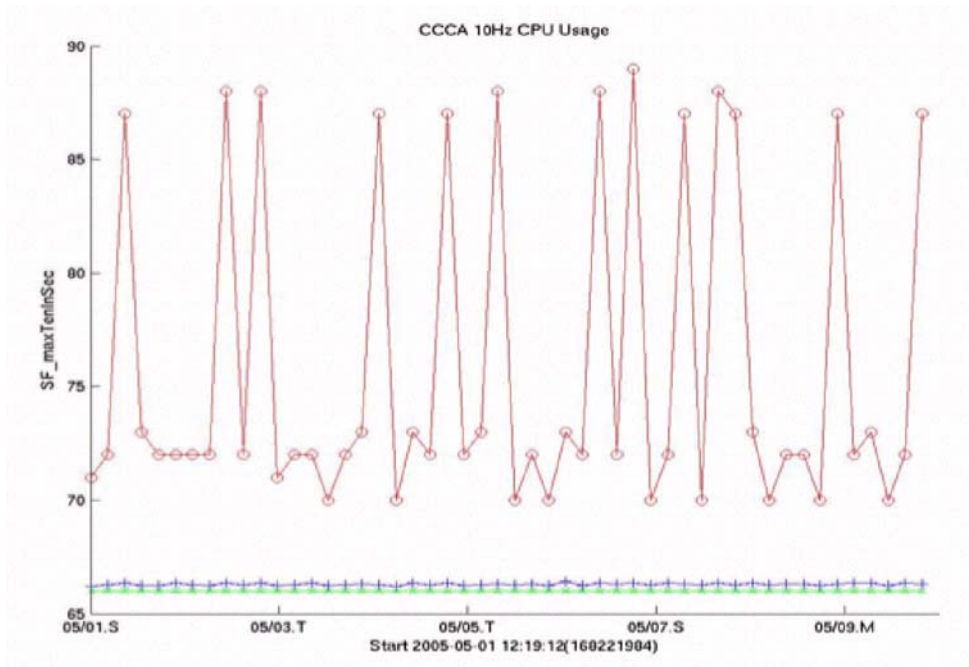


**Figure 8-34.** CCCA 10Hz CPU Usage (in %) averaged over ~4 hours. (Red = max; Blue = avg; Green = min)

## 8.5.2 Flight Software Statistics

The Mission Support Software (MSS) implements the following applications on the space vehicle:

1. Process uplink commands implementing CCSDS.
2. Command handler processes real time and Stored Program Commands.
3. CCSDS programmable telemetry, events, data base readout
4. Spacecraft computer memory load / dump
5. Attitude determination and control
6. Translation and dewar pressure / temperature control
7. Electrical power and thermal processing support
8. Route validated payload commands to payload processors
9. Route telemetry from payload processors to ground and mass memory device
10. Mass memory device record and playback management
11. Safemode (redundancy management and layered control modes)
12. Memory scrubbing

Start Up Software (SUS) extended boot loader

1. Loads flight software from mass memory device
2. Memory scrubbing

[Appendix E, Flight Software Applications SLOC](#) lists the source lines of code (SLOC) for the various FSW applications and their sub-components. 59,000 lines of ADA and 2.3 MB of memory were required to implement the FSW features required by GP-B. At run time, the FSW expands to 3.5 MB in the CCCA SRAM after heap, stack, an other dynamic storage is allocated.

Detailed requirements and functional descriptions of the FSW components can be found in **Lockheed Martin Document #P086580: SCSE-15, Gravity Probe B Flight Software Requirements Specification**.

### 8.5.3 Test It Like You Fly It

All of the GP-B software (Mission Support, Payload, and Ground) was tested in the Integrated Test Facility (ITF) during the Formal Qualification Test (FQT) phase of the mission; one of the requirements to pass the Flight Readiness Review prior to launch approval. The ITF is a static, on-ground spacecraft simulator that contained engineering models or flight equivalents of spacecraft and payload subsystem, a vehicle dynamics simulator computer to test the attitude and translation control system, and a communications downlink processor to permit the vehicle to communicate with the MOC our flight interfaces. [Figure 8-35](#) shows a picture of the ITF hardware as configured late in the mission.

The FQT was performed using the flight approved command templates (except where ITF-specific versions were required to account for differences between the ITF and the on-orbit Space Vehicle environment) in an approved manner in a series of about 15 comprehensive tests. The testing process of loading a series of command templates and executing them sequentially based on time-tags was the same process used during on-orbit operations. The same tools are used to construct the command loads for testing as for operations. The same ground station software is used to uplink commands and command loads, to start execution of the command loads, and to monitor and record the telemetry for testing as for operations.

The ITF was used prior to launch to test the flight software and to test the command templates used for on-orbit operations. After launch it was used to test any new or changed command templates as well as to check the operation of all new real-time command scripts, such as those used to clear multi-bit errors. Also after launch the ITF played a key role in the regression testing necessary to confirm that the post launch software change worked as specified with no surprises. It also was used to test the process of loading and rebooting the flight software prior to using the process on the space vehicle.



**Figure 8-35.** ITF Hardware and Interconnects

### 8.5.4 On-Orbit Software Changes

Between launch and May 17, 2004 thruster 6 and then 8 had gone unstable and were shut off using the Thruster Isolation Valves (TIVs). The existing thruster control software needed to be updated to provide proper control with some redundancy whilst using only 14 of the original 16 helium thrusters. Several Software Change Requests (SCRs) were written to address the control software changes plus related changes to the safemode application. Since launch two software discrepancies had been identified and several more changes that would either improve the spacecraft performance or its safemode response had been found, including some that were only to the ground system limits to improve recognition of anomalous behavior. [Table 8-4](#) below lists the SCRs that were addressed by the flight software team from mid-May 2004 to late-July 2004.

**Table 8-4.** SCRs Addressed in On-orbit S/W Change

SCR #	Date	Title	Reason for Change
3240	5/11/2004	Rtworks checks additions for multi-bit upset	The telemetry monitors in the attachments should be added to the Rtworks checks page "CDH_C". They should initially all be set to "skip". Once in use operationally, the limits and "verify" will be adjusted to detect multi-bit upset events in the on-board computers.
3241	5/11/2004	Post-launch calibration and limit update #1	Update the real time system to reflect the attached calibration and limit changes. See SCR3240 folder for change requests.
3242	6/4/2004	Simultaneous use of mag torquers and thrusters	At the request of Stanford because of the 2nd thruster failure, make the modifications necessary to provide the capability to simultaneously use magnetic torque rods and thrusters for ATC control.

**Table 8-4.** SCRs Addressed in On-orbit S/W Change

3243	6/4/2004	Modified thruster distribution algorithm	<p>Due to 2nd thruster failure, and the possibility of losing additional thrusters, modify the MSS to include Geometric Logic algorithm to mitigate this problem. Provide commands and data base readout capability to determine the configuration. This capability will co-exist with the current pseudo-inverse approach, and a control flag which can be verified by DBRO will be used to select which approach to use. The default will be the Geometric Logic approach.</p> <p>See attachment</p>
3244	6/11/2004	Modification to null dumping scheme	The null dumping scheme needs to be modified due to the thruster distribution change. Ref. SC3243
3245	6/11/2004	Mode 1B bias estimate update	During Mode 1B operations it was discovered that the gyro bias estimate was only correct for one vehicle axis. Modify the code to make it correct for x and y axes.
3246	6/11/2004	Update hard-coded star sensor db	<p>The star sensor data base has the following hard-coded parameters (Jon-TBD)</p> <p>Star_Mag_Limit_Comp(1)=3.0</p> <p>Star_Mag_Limit_Cat(1)=3.0</p> <p>It was determined from flight experience that system efficiency is increased if they are updated. A CSTOL patch was used to update them via release message, but with MSS3.4.3 the CSTOL will no longer have valid addresses.</p>
3247	6/11/2004	Modifications to drag-free safemode test	<p>Stanford has requested two new capabilities</p> <ol style="list-style-type: none"> <li>1) In primary drag-free mode, provide a return to drag-free option for 3 attempts in the event drag-free is dropped.</li> <li>2) In backup drag-free, stop translation control in the event of return to analog</li> </ol> <p>In a requirements review meeting held on Thursday, 6/10/04, it was decided that modifying this safemode test was the favored approach. The test will check the following, and each check can be independently enabled or disabled by command, with DBRO verification:</p> <ol style="list-style-type: none"> <li>1) RSS of error above a limit</li> <li>2) Arbiter state - analog</li> <li>3) DF_state (not=) DF_cmd</li> </ol> <p>There will also be macro changes as specified in SCR3248 and 3249</p>
3248	6/11/2004	Modify loss of drag-free safe mode macro	<p>As part of SCR3247, the loss of drag-free safe mode macro needs to be modified to accommodate the options specified in SCR3247.</p> <p>[6/14/04 O. Chan] The safing responses for drag-free Test as below:</p> <p>SMACRO07 to mask for GSS arbiter state check</p> <p>SMACRO29 to mask for drag-free data limit and status checks</p> <p>[7/22/04 O.Chan] No further implementation on Automatically reentry to primary drag-free.</p>

**Table 8-4.** SCRs Addressed in On-orbit S/W Change

3250	6/14/2004	Change sanity check axis indices	Ref SCR3168. The ATC slope sanity check requires the same change to the axis designation.
3251	7/9/2004	Post-launch VMS macro changes	<p><b>Add GV45 to skip star present in guide star valid VMS macros</b> if star not present, branch spcp f to mode 2a and branch the current spcp to 0</p> <p><b>Add GV46 to skip shutter commands in guide star valid and invalid VMS macros</b> Cycle (command) shutter open/closed (GV46 = 0) Do not cycle shutter open/closed (GV46 = 1) Set GV46 to 1 in FSW Initialization</p> <p><b>Add GV47 to skip star acquisition in mode 2A or 2B VMS macros</b> Default to no star acquisition to leave in gyro hold (GV47 = 0) Star acquisition (GV47 = 1)</p> <p><b>Set Observer to gyro hold in mode 3A VMS macro</b></p> <p><b>Add star present command to Guide Star Valid to detect loss of star</b> Perform ST present at beginning of GS valid macro if star not present branch to Mode 2A (GV45 = 1)</p> <p><b>Fix SAA_In macro to be like Guide Star Invalid macro</b> Don't use Telescope data when in SAA</p> <p><b>Fix SAA_Out macro to be like Guide Star Valid macro</b> Use Telescope data when out of SAA</p> <p><b>Add local variables 5, set LV5 = 1 in GS Valid and SSA_Out macros, set LV5 = 0 in GS_Invalid and SSA_In macros</b> LV5 = 0, don't reconfigure Observer and Att_Control modes Note: Deliver command template and CSTOL procedures to set GV45, 46, 47</p>
3252	7/12/2004	Update special macros for 125 bps uplink	Updates special macros to include 125bps uplink.
3253	7/12/2004	Post launch safemode macro changes	<p>Update to reflect desired safemode responses, and deletion of content of macros no longer required for flight operations.</p> <p>Thruster Current 2 test monitors the open loop thrusters (1,5,6,7,8)</p> <p>Thruster Pressure 2 test monitors the closed loop thrusters</p> <p>Thruster Pressure 1, Current 1 tests must be always disabled (CARD)</p> <p>Star sensor aliveness and reasonableness autonomous switch to mode 2A gyro hold</p> <p>Revise response to control gyro saturation and body rate tests</p>



The software and macro changes resulting from these SCRs were verified and validated using the tests summarized in the [Table 8-5](#). The testing was, naturally, all performed in the ITF to provide the highest fidelity environment possible.

**Table 8-5.** Tests Executed and Passed to Verify SCRs

Test ID	Test Description
TFSW0013	Gyro Uncage / drag-free, Backup drag-free, drag-free Sensor Failure
TMSSSCR3242	Drag-free Control Performance Verification
TMSSSCR3243	Thruster Distribution Algorithm Performance Verification
TMSSSCR3243_2	Additional Thruster Failure
TMSSSCR3243_3	MSS version 3_4_3_0 Unit Testing
TMSSSCR3245	Mode 1B Bias Calculation
TMSSSCR3246	GndRT v5.1.3 Real-Time Ground System Testing
TMSSSCR3247	Loss of drag-free Safemode Response
TMSSSCR3251	VMS Macros v2.11 Test
TMSSSCR3252	Special Macros v2.11 Test
TMSSSCR3253	Safemode Macros v2.11 Test

The implementation of these SCRs took place in two sessions: first the software changes to the ATC and Safemode tests, then the VMS and Safemode macro changes. On June 25, 2004 the ATC S/W Change Flight Readiness Review (FRR) was held and approved pending closure of a few tests still in analysis.

The process of changing the software in the CCCA is a lengthy one. It is possible to implement patches or overlays to the RAM but any changes implemented this way would vanish if the computer rebooted and reloaded itself from EEPROM. Instead the EEPROM has to get updated and the preferred, most reliable way to achieve that is to start by loading a new image into the Solid State Recorder (SSR, where there are several memory boards dedicated to holding images of the FSW) and then from there into the CCCA EEPROM while the CCCA is operating under the Start-UP ROM (SUROM).

This was an impressive process. From problem identified in 17 May to software solutions developed, coded, tested, and loaded onto the spacecraft by 30 June with the corresponding VMS, Safemode, and Special macros coded, tested, and loaded by 3 August. All of this was achieved while the operations team (and note that the development team was also part of the on-call operations support team) continued with the IOC testing and calibration on the vehicle.

Given an uplink rate of 1024 bps at best and 128 bps at worst the process of uplinking several megabytes of code is tedious. 3 days was required to load and verify the new CCCA image on the vehicle. The new image was started via a commanded A-side reboot on 29 July 2004 and the final VMS, Safemode, and Special macros were installed on the vehicle by 3 August.

### 8.5.5 Safemode Discussion

All spacecraft must face the possibility that some critical hardware element will fail, putting the long term safety of the spacecraft and the mission at risk. The GPB Flight Software mitigates this risk with its Safemode application. This basic idea of this application is to perform tests on selected telemetry monitors from the hardware or software; tests which compare the measured values of these monitors against limits that can be

configured on-orbit as required. If a test fails then a failure counter is incremented, otherwise the failure counter is set to 0. If the failure counter exceeds a limit (also configurable on-orbit) then a configurable set of predefined and preloaded safemode macros are activated. Breaking it down we get:

- There are 98 tests across the C&DH, ATC, Payload, EPS, and Thermal subsystems. Each test can be enabled or disabled by real-time or stored commands. The test failure limits and the consecutive failure limit for each test can be altered by real-time or stored commands. The safemode macros to activate when the test exceeds its consecutive failure limit are also configurable via real-time or stored commands.
- There are 47 safemode macros that do everything from switching to the backup computer to doing nothing (allows notification of the hardware failure status to be quickly noticed but leaves the response to the GPB staff).
- Once a test has been activated it will not activate again until re-enabled preventing an “infinite loop” of safemode responses. Further, once a safemode macro has been activated it won’t activate again until re-enabled.

Figure 8-36 illustrates the structure of a safemode test.

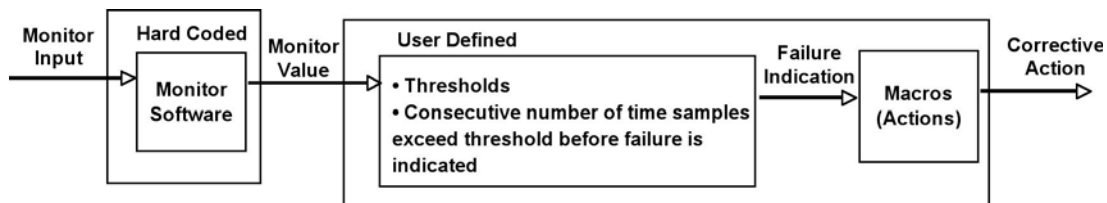


Figure 8-36. Structure of a Safemode Test

Figure 8-37 is an excerpt from a table made during March 2005 while the Safemode configuration was being evaluated. Note that some tests are disabled, primarily the secondary tests that would get enabled when the primary test failed.

Test	Status	# Macros	Macros							
ACE Aliveness	E	4	2	8	11D	59				
Btry 1 Prim Htrs T Up Lim	E	4	2	11D	50	59				
Btry 1 Bckup Htrs T Up Lim	E	4	2	11D	50	59				
Btry 2 Prim Htrs T Up Lim	E	4	2	11D	53	59				
Btry 2 Bckup Htrs T Up Lim	E	4	2	11D	53	59				
Btry 1 Prim Htrs T Lwr Lim	E	4	2	11D	51	59				
Btry 1 Bckup Htrs T Lwr Lim	E	4	2	11D	52	59				
Btry 2 Prim Htrs T Lwr Lim	E	4	2	11D	54	59				
Btry 2 Bckup Htrs T Lwr Lim	E	4	2	11D	55	59				
Battery SOC 1st Limit	E	6	2	3	11D	15	48	59		
Battery SOC 2nd Limit	Dis	8	2	5	7	11D	15	17	49	59
Battery SOC 3rd Limit	Dis	1	1							
BRE Chk High Mode	E	5	2	4	7	11D	59			
BRE Chk Low Mode	E	4	2	9	11D	59				
Bus Voltage	E	1	1							
CDH Built In Test	E	1	1							
CDH Telemetry Check	E	1	1							
CCCA B CR Monitor	E	4	2	6	11D	59				
CCCA Self Check	E	1	1							
CG Sat 1st Limit	E	4	2	9	11D	59				
CG Sat 2nd Limit	E	4	2	10	11D	59				
CG Disp 1st Fail	E	4	2	10	11D	59				
CG Disp 2nd Fail	Dis	5	2	5	7	11D	59			
CRC Error	E	1	1							
CSS Rsnblns	Dis	1	64A							
EDAC Error	E	1	1							
Gen SPC Error	E	4	2	3	11D	59				

Figure 8-37. Excerpt from Safemode Status in March 2005

Figure 8-38 below is an excerpt from the Test Description Table in the Safemode Design Document. It provides for each test a concise description of the test and the Safemode response to the test failure.

Sub-system	Test	Failure	Safing Action
C&DH	CCCA Self-Check	<p>Self_Check_failure Error flag in MSS_Status is set if</p> <ul style="list-style-type: none"> <li>• An error message, 1553 received BC error, is returned from the 1553 driver.</li> <li>• An error message, HSS message queue error, is returned from the HSS driver.</li> </ul> <p>If a message is received from either of these calls, it will be logged in a memory resident error log permanently located at hex'2020'.</p> <p>Test fails if 1553 or HSS error for 5 consecutive 10 Hz cycles.</p>	<p><b>SMACRO01:</b> Stop CCCA/CDHS Keep-Alives Upon restart, switch to redundant unit of CCCA/CTU/IU/ACE/GPS</p> <p>Interrupt Mission Timeline, Close GMA Valves and Set 125 bps uplink/1Kbps downlink sequences are set to activate from Recover Load; disabling or enabling SMACRO02, SMACR011 and SMACR059 will not have any effect on the responses.</p>
C&DH	Unrecoverable Ada Exception 1	<p>Separate error flags indicate Ada exception occurrence in 10 Hz and 1 Hz processing tasks.</p> <p>Test fails if Ada exception for 50 consecutive cycles.</p>	<p><b>SMACRO02:</b> Stop Mission Timeline (see Table 10.3.1-1)</p> <p><b>SMACRO03:</b> Switch to mode 2A gyro hold, (SS mode: CG/SS/Thruster control in low mode)</p> <p><b>SMACRO11:</b> Close GMA valves sequences (see Table 10.3.2-1)</p> <p><b>SMACRO59:</b> Set 125 bps uplink and 1 Kbps downlink Select Forward antenna</p>
C&DH	Memory Scrub	<p>Error flag indicates EDAC multi-bit failure in CCCA memory (SRAM, EEPROM, or machine code checks) by the BAE scrub task</p> <p>Test fails when CCCA EDAC multi-bit count error increases by 3.</p> <p>Note: Each RAD6000 processor allocates 5% of the CPU to read each location of memory and perform EDAC correction.</p>	<p><b>SMACRO01:</b> Stop CCCA/CDHS Keep-Alives Upon restart, switch to redundant unit of CCCA/CTU/IU/ACE/GPS</p> <p>Interrupt Mission Timeline, Close GMA Valves and Set 125 bps uplink/1Kbps downlink sequences are set to activate from Recover Load; disabling or enabling SMACRO02, SMACR011 and SMACR059 will not have any effect on the responses.</p>

Figure 8-38. Excerpt from Test Description Table in Safemode Design Document

The general health and safety of the GPB spacecraft is monitored by the Safemode application.

### 8.5.6 CCCA Single Bit Errors

One obstacle that must be overcome by any spacecraft is the space radiation environment that has noticeable adverse effects on electronic equipment. This radiation is the result of charged particles, some of which can be attributed to cosmic events or solar activity, interacting with the Earth's magnetic field and colliding with orbiting spacecraft. Collisions with electronic circuitry are commonly manifested as Single Event Upsets (SEUs) or Single Bit Errors (SBEs).

Due to the shape of the Earth's magnetic field and the orbital altitude of GPB, a majority of charged particle interactions occurred either over the North / South poles or over the South Atlantic Anomaly (SAA).

Figure 8-39 shows the locations of SBEs aboard GPB during a typical period of the science data collection phase.

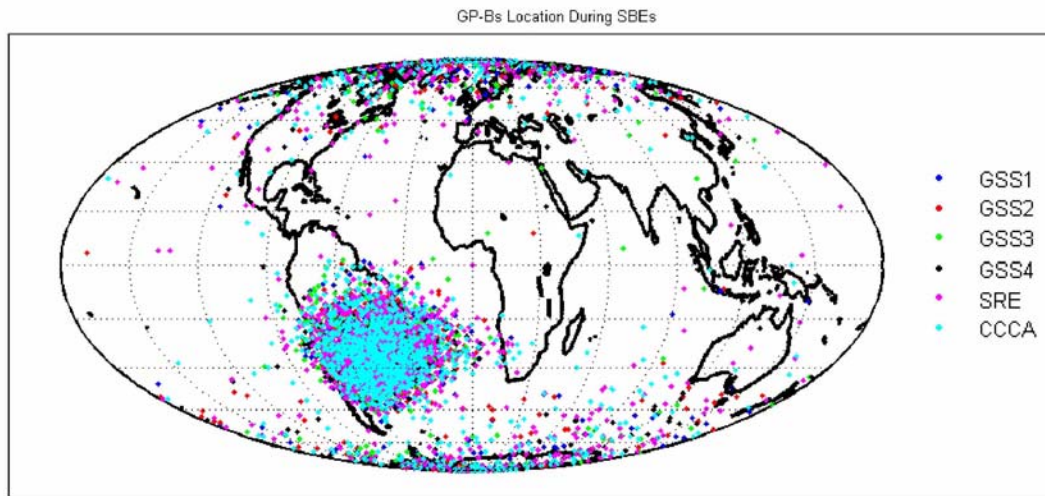


**Figure 8-39.** Location of Single Bit Errors during Science Data Collection

The GPB Flight Software together with Error Detection and Correction (EDAC) circuitry in the CCCA are responsible for monitoring the effect of this radiation on the memory components of all subsystems. A portion of the overall processing is dedicated to a continuous memory scrub that cycles through all onboard memory every 2.5 seconds. This function is able to detect and correct Single-Bit Errors (SBEs) automatically. The EDAC circuitry can also detect Multi-Bit Errors (MBEs)—the corruption of more than one bit within the same 64-bit memory word—but MBEs must be corrected manually. See section “[CCCA Multi-Bit Errors](#)” on page 252 for more information about the autonomous detection and manual correction of MBEs.

SBEs occurred at a relatively consistent rate throughout the GPB mission, subject to increases and decreases depending on solar activity and variations in the Earth's magnetic field. Data from typical one month periods during science data collection using both the A and B side CCCA are plotted in [Figure 8-40](#) and [Figure 8-41](#). These plots represent common SBE rates during periods of normal solar activity. The CCCA A-side ([Figure 8-40](#)) experienced about 8.7 SBEs per day during the period between October 10, 2004 and November 10, 2004. The CCCA B-side ([Figure 8-41](#)) detected about 7.6 SBEs per day during the period between April 10, 2005 and May 10, 2005. In general, a slightly higher SBE rate was observed during operation on the A-side CCCA as compared to the B-side CCCA.

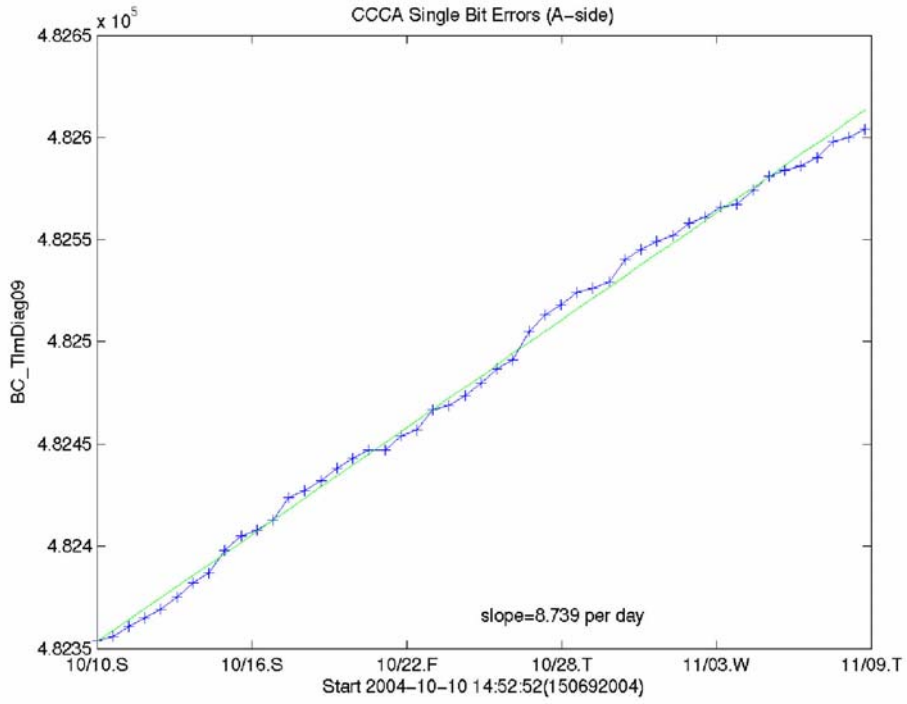


**Figure 8-40.** A-side CCCA Single Bit Errors from Oct. 10, 2004 to Nov. 10, 2004

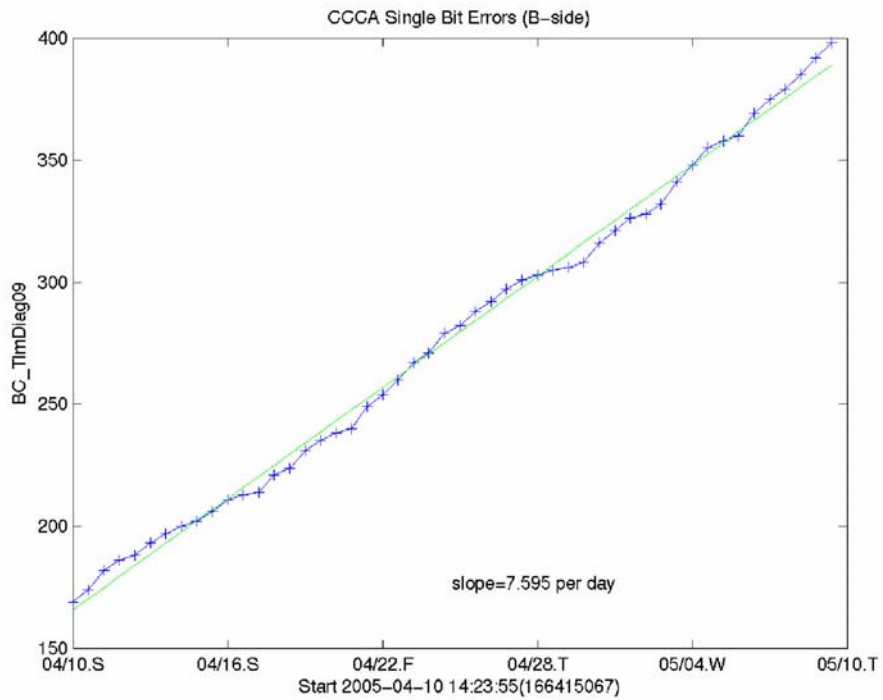


**Figure 8-41.** B-side CCCA Single Bit Errors from Apr. 10, 2005 to May 10, 2005

Increased SBE rates were observed during the periods of high solar activity that resulted from solar flares and coronal mass ejections. The best example of this occurred on Jan. 20, 2005 when a powerful X7 solar flare erupted into what was considered the strongest radiation storm since October 1989. Figure 8-42 shows proton flux data measured by the GOES11 satellite during the 3-day period from January 19 to January 22, 2005. The strength of this particular solar flare was due to the large number of high energy (>100 MeV) particles detected, represented by the green line in Figure 8-42. High-energy proton flux increased to a level four orders of magnitude greater than normal. Onboard SBE data over the same time span (January 19 to January 22) is displayed in Figure 8-43. At the peak of the solar event, the FSW detected and corrected over 60 SBEs in a period of 5 hours, a rate 40 times greater than standard levels.

Successful error detection and correction was an important function of the GPB flight software, functionally insulating sensitive GPB electronics from the harmful space radiation environment. The FSW memory scrub routine adequately protected the spacecraft from any hazardous conditions that could result from corrupted memory caused by single bit errors.

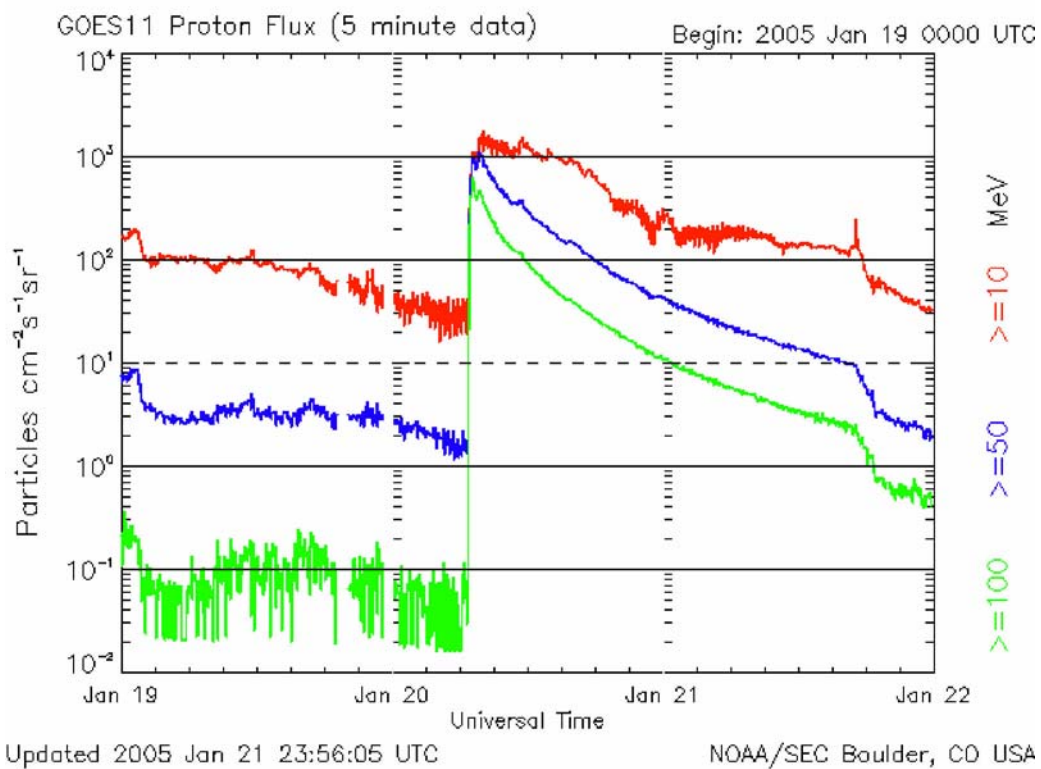


**Figure 8-42.** Proton Flux measured by GOES11 satellite during January 20, 2005 solar flare







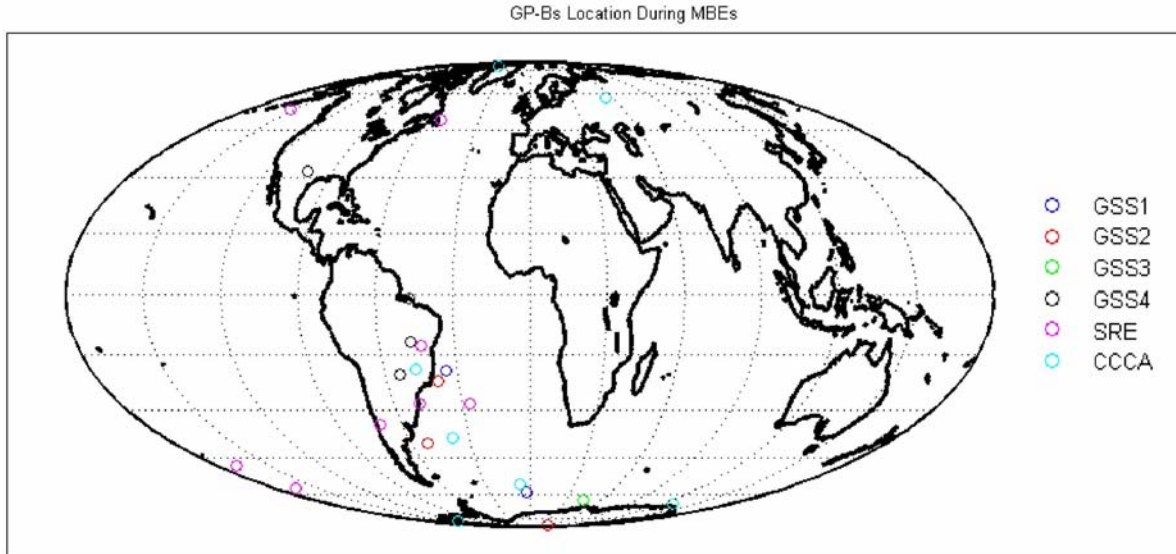


**Figure 8-44.** Location of Multi-Bit Errors during the first year of on-orbit operations

Built-in safemode protection against multiple CCCA MBEs in the same memory scrub cycle was exercised more than once on-orbit. When activated, this safemode response resulted in either a B-side “block switch”, with the redundant B-side CCCA / C&DH system taking over for the A-side equipment, or a reboot of the B-side CCCA. While disruptive to any ongoing activities, including science data taking, this response resulted in the autonomous clearing of any MBEs in the system, ensuring vehicle safety. The first time this safemode response activated, during IOC, the software team successfully recovered the spacecraft back to the A-side equipment. Per plan, when this safing action occurred during science data collection, the CCCA was kept on the B-side for the remainder of the mission. [Figure 8-45](#) shows the cumulative MBE count (in the CCCA only) from launch through the end of May 2005. The pink shaded regions represent operation on the B-side CCCA.

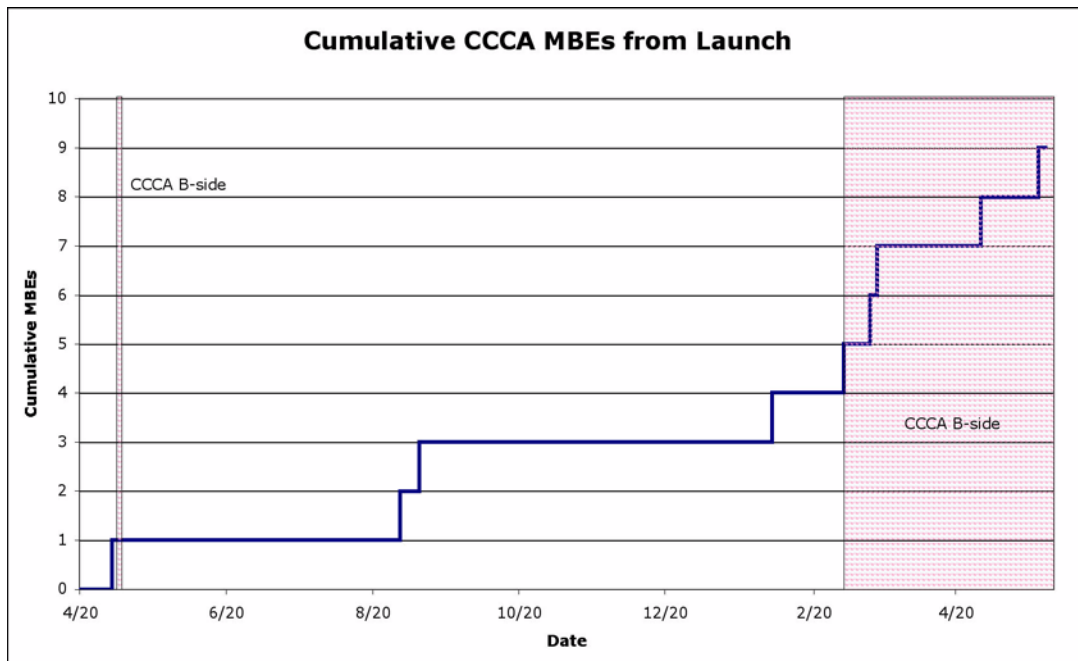


**Figure 8-45.** Cumulative CCCA MBE count from launch through end of May 2005.

When single MBEs did not result in autonomous safemode response, affected memory locations were manually patched in order to avoid executing corrupted code or accessing corrupted memory values. The software team developed a valuable set of tools that allowed rapid identification, diagnosis, and correction of MBEs. These tools consisted of realtime diagnostic commands that displayed the address of affected locations in memory and the (corrupted) value of that memory location. This information allowed software engineers to assess the operating risk imposed by the MBE, and to verify that the memory location had not been overwritten since the MBE was detected. Occasionally, MBEs would corrupt areas within a data buffer that were overwritten soon after corruption—these became known as “self-clearing MBEs”. After diagnostic data was collected and it confirmed that an MBE had occurred, the FSW team utilized the Integrated Test Facility to develop realtime commands to manually rewrite the affected memory locations to their expected value. The entire process, from detection through patching, was routinely performed in less than 6 hours throughout the GPB mission. The planning and forethought that resulted in this efficient set of tools for correcting MBEs ensured minimal science data loss due to corrupted onboard memory.

# 9

## Gyro Suspension Subsystem (GSS) Analysis

---





The Gyroscope Suspension System's (GSS) role in Gravity Probe B is to electrostatically suspend the science gyroscopes within their housing cavities so that the gyroscopes may spin freely with minimal friction and torque so that they may perform their role as local inertial space references.

To perform its mission successfully, the GSS must satisfy a number of core requirements:

1. Operate over 8 orders of force magnitude; the same system must be able to suspend the gyroscopes on Earth in a 1 g field as well as generate minimal disturbances at the 108 g level during data collection.
2. Suspend the gyroscopes reliably; the system must never let a spinning rotor touch the housing. There is sufficient mechanical energy in a rotor spinning at 60 Hz to effectively destroy the rotor and housing in such an event.
3. Operate compatibly with the SQUID readout system. The SQUID magnetometers are very sensitive, thus the suspension system must not interfere with these sensors during ground and on-orbit operation.
4. Minimize electrostatic torques during science data collection. The suspension system must meet centering requirements with minimal control effort and thus with minimal residual torques on the rotors.
5. Apply controlled torques to the rotor for calibration and initial rotor spin axis alignment.
6. Act as an accelerometer as part of the “drag-free” translation control system to further minimize classical torques on the rotors.

All of these requirements were met during the GP-B mission, and the suspension systems continue to operate well following the depletion of helium from the dewar since they do not require cryogenic electronics to function.

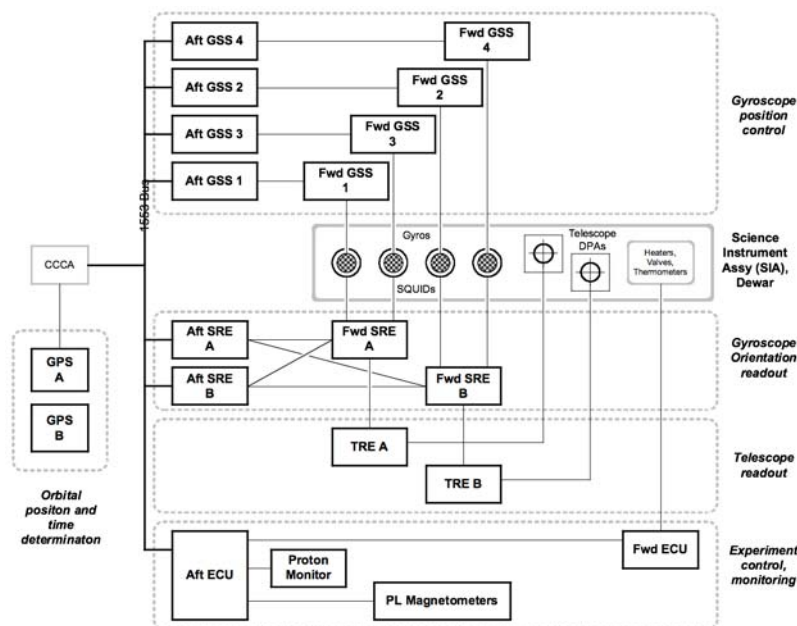


**Figure 9-1.** Block diagram of the payload electronics package showing the interconnect of the GSS units

## 9.1 GSS Hardware Description

Figure 9-1 shows the four GSS units and their relationship to the rest of the payload electronics package. Each gyroscope has a dedicated GSS system, and each GSS system comprises two electronics enclosures: forward and aft (see Figure 9-2).

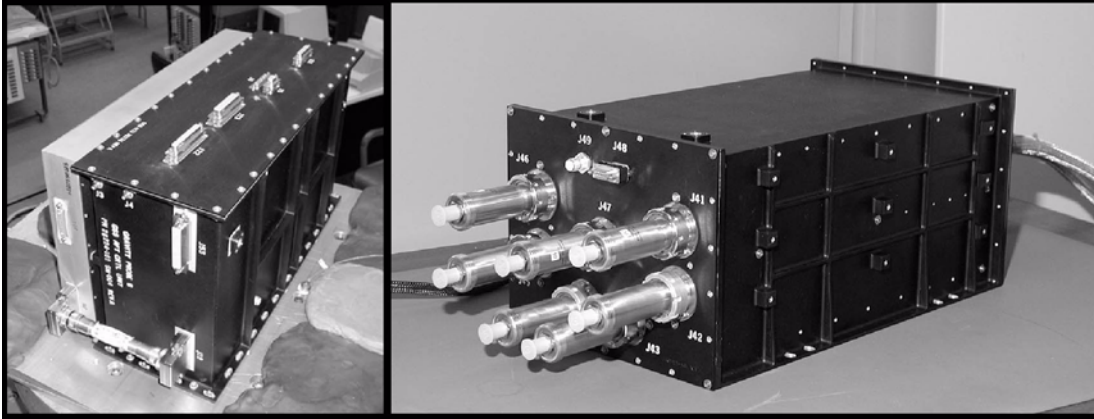


**Figure 9-2.** Photograph of GSS units. Aft processor and power supply (left), forward quiet analog electronics (right). One pair is required for each gyroscope. During the mission, the temperature of the aft assembly ranges between 300 K and 320 K; the forward assembly range is 265 K to 300 K.

The forward electronics unit (FSU) resides in the spacecraft's forward equipment enclosure (FEE), that is passively thermally controlled to a range of 300-320K over the mission. The FSU contains the sensitive analog electronics that are used to sense the position of the rotor and apply suspension voltages. A block diagram of this system is shown in Figure 9-3. The main components of this system are described in the following subsections:

### 9.1.1 Low voltage drive amplifier

During nominal science operation, voltages are applied to the electrodes through six  $\pm 50\text{V}$  low noise amplifiers; the bandwidth of these amplifiers was set by design to 100 Hz. Each amplifier has a input filter set that allows two modes of operation: 1) constant gain to DC, and 2) a band pass mode that rolls off the gain below 1 Hz to 10% of the nominal peak. The DC mode is provided to simplify the design and operation of the backup analog control loops. The band pass mode is used to limit the electrostatic force noise on the gyroscope by allowing only signals in the neighborhood of the 30 Hz AC science drive carrier to make their way to the gyroscope.

### 9.1.2 High voltage drive amplifier

A  $\pm 1600\text{ V}$  set of amplifiers is used during ground test and gyroscope spin-up to provide enough electrostatic force on the gyroscopes to suspend them in a 1g field or while spin-up gas is flowing in the channel. 1g ground suspension requires approximately 650V to maintain suspension once centered, and roughly twice that to pick up the rotor from the housing wall. Gas spin up requires  $\sim 150\text{V}$  per axis to hold the gyroscope in the spin-up channel. Nominal bandwidth of these amplifier is 2 kHz and power draw during spin-up is 0.8 W per channel.

The output of the low and high voltage amplifiers is switched to the gyroscope by a 3 HV RF vacuum relay, one per electrode. Switch time is approximately 1 ms, during which the rotor is not under active suspension control. During the mission, many checks are made on vehicle activity prior to making the switch to ensure the gyro will not move significantly during this uncontrolled period.

### 9.1.3 Computer drive

Six parallel 16-bit digital to analog (D/A) converters are controlled by the GSS processor (mounted in the aft enclosure) and control algorithms running in his processor send voltage commands through the D/A converters to both the high and low voltage amplifiers. Nominal update rate for the system is 220 Hz in science mode and 660 Hz during spin-up.

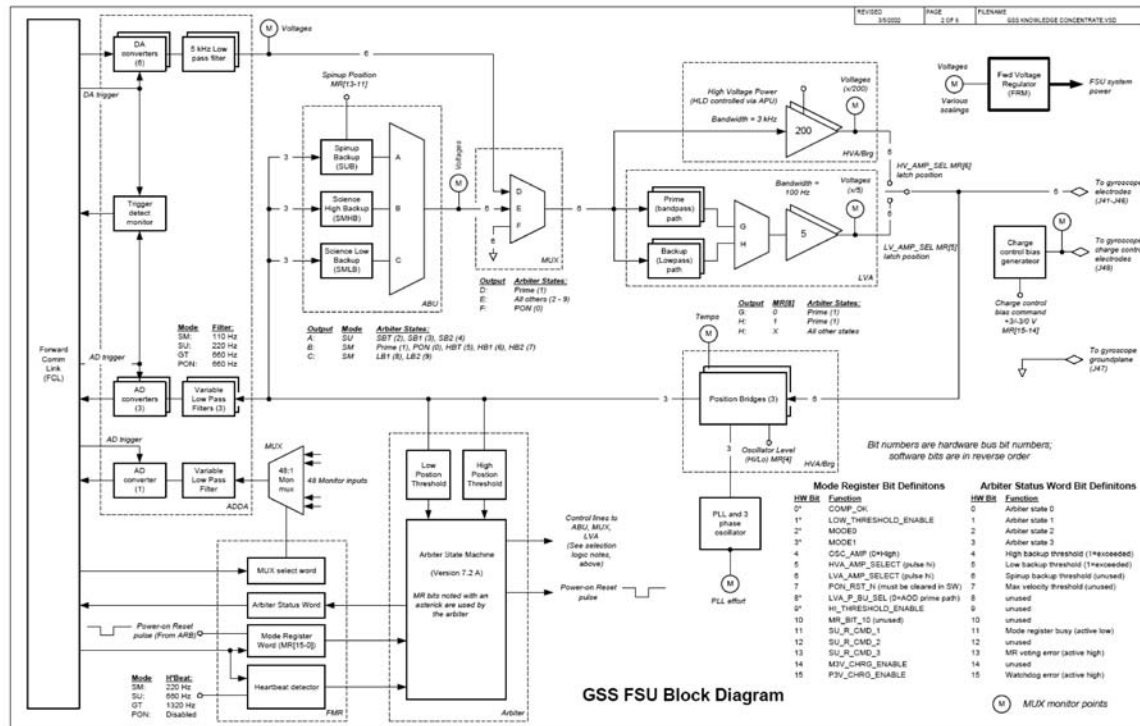


Figure 9-3. Block diagram of the Forward Suspension Unit (FSU)

### 9.1.4 Position Bridge

A 3 phase, 34.1 kHz sinusoidal position bridge is used to measure the position of the rotor in the housing. The ridge sense signal amplitude is selectable between 20 mV-pp and 200 mV-pp. The nominal bridge noise is 1 nm/rHz and the bandwidth is approximately 1 kHz. Each bridge channel is digitized by a 16-bit successive-approximation analog to digital converter and this information is sent at the control sample rate to the GSS processor.

### 9.1.5 Analog Backup Controllers

Three all-analog backup controllers are provided to cover all flight operational modes. These controllers are proportional-derivative (PD) architecture and are designed to center the gyroscope in the event of a failure of the computer to maintain positive control of the gyroscopes. During science data collection, two controllers are available: science mission high backup (SMHB) and science mission low backup (SMLB). The high backup controller is designed to have sufficient gain and bandwidth to allow re-centering of the under a worst-case 1 km-m/sec micrometeoroid strike. This controller can use most of the 50 V range of the low voltage amplifier and is needed primarily to insure gyroscope safety, but will subject the rotor to higher suspension forces and torques than the experiment error budget allows. The low backup controller is much less aggressive and is designed to emulate the normal science mission suspension voltages. In this mode, forces and torques are



significantly reduces and thus preserves to a much larger extent the science mission configuration while computer control is re-established. In spin-up mode, a similar controller is provided to hold the rotor in position in the spin-up channel while gas is flowing if the computer control should fail during this critical phase.

## 9.1.6 Suspension arbiter

An autonomous state machine in the FSU is used to monitor the health of the digital suspension algorithm and immediately switch to a backup system should a fault be detected. The arbiter monitors the health of the GSS processor via a heartbeat keep-alive circuit and the gyro position via radius-from-center position thresholds. Should either of these tests fail the backup system is engaged. In science mode, initially the control is passed the high authority backup controller (SMHB). Once the gyro position is stable for 30 seconds, control is passed to the low authority (SMLB) controller until the computer is ready to take control. In the event of a position excursion greater than the position threshold ( $> 10 \mu\text{m}$ ), the high authority controller is used until the position settles again. Before control may be passed back to the flight computer, a handshake set of commands must be sent to the FSU to convince the arbiter that the computer is healthy and read to take back control. A state transition diagram for this arbiter is shown in Figure 9-4.

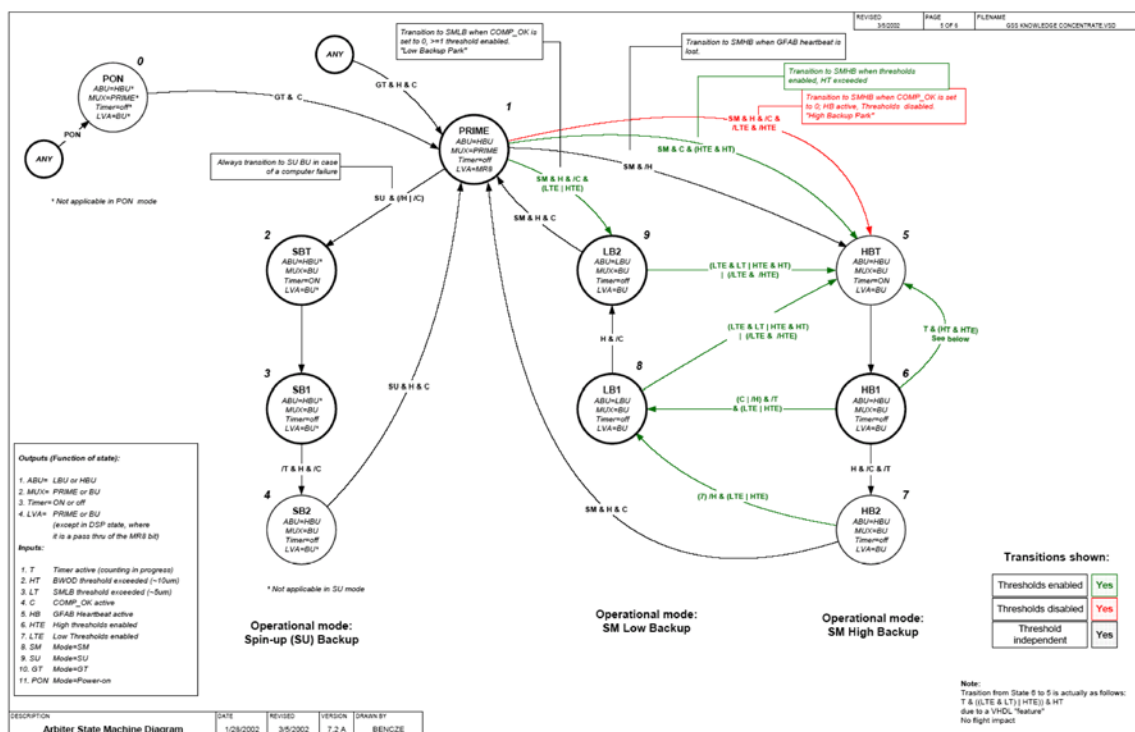


Figure 9-4. GSS Arbiter State Transition diagram.

## 9.1.7 Mode Register

A bank of 16 latching relays are used to hold the configuration of the FSU (bridge amplitude, suspension mode, low voltage amplifier configuration, threshold enables, etc.). This set of relays are highly radiation tolerant and retain their state should power be removed, thus they are a very stable source of configuration information should the aft computer need to be rebooted during the mission (this was never necessary, however).

## 9.1.8 Forward Communication Link

The forward unit communicates with the aft unit via a pair of unidirectional parallel data busses, one aft-to-forward and one forward-to-aft. Timing signals, including the 34.1 kHz bridge excitation signal is provide via this link.

The GSS aft control unit (ACU) houses the GSS flight processor card, associated support circuitry, and the power supply for the GSS string. A block diagram of this unit is shown in [Figure 9-5](#). This unit is mounted on the aft truss of the spacecraft, and thus is subject to wider temperature swings, approximately 265K to 300K

## 9.1.9 RAD6000 Processor

Each GSS employs a dedicated Lockheed-Martin Federal Systems (now BAE) RAD6000 processor, running at 16.368 MHz. On board is 1 MB of EEPROM and 3 MB of static RAM. The processor communicates with the spacecraft via a Mil-Std-1553 serial link and with the GSS electronics via a parallel port on the processor card. This processor hold the gyro suspension system software and telemetry processing needed to receive commands and send measurements to the ground via the spacecraft processor (CCCA). The telemetry system continuously provides data at 2 to 5 second intervals of gyro position, control effort, suspension voltages applied, system state, analog monitor points, box temperatures, and other engineering information. Also available are high-speed snapshots consisting of 12 seconds of full rate suspension control loop measurements and commands.

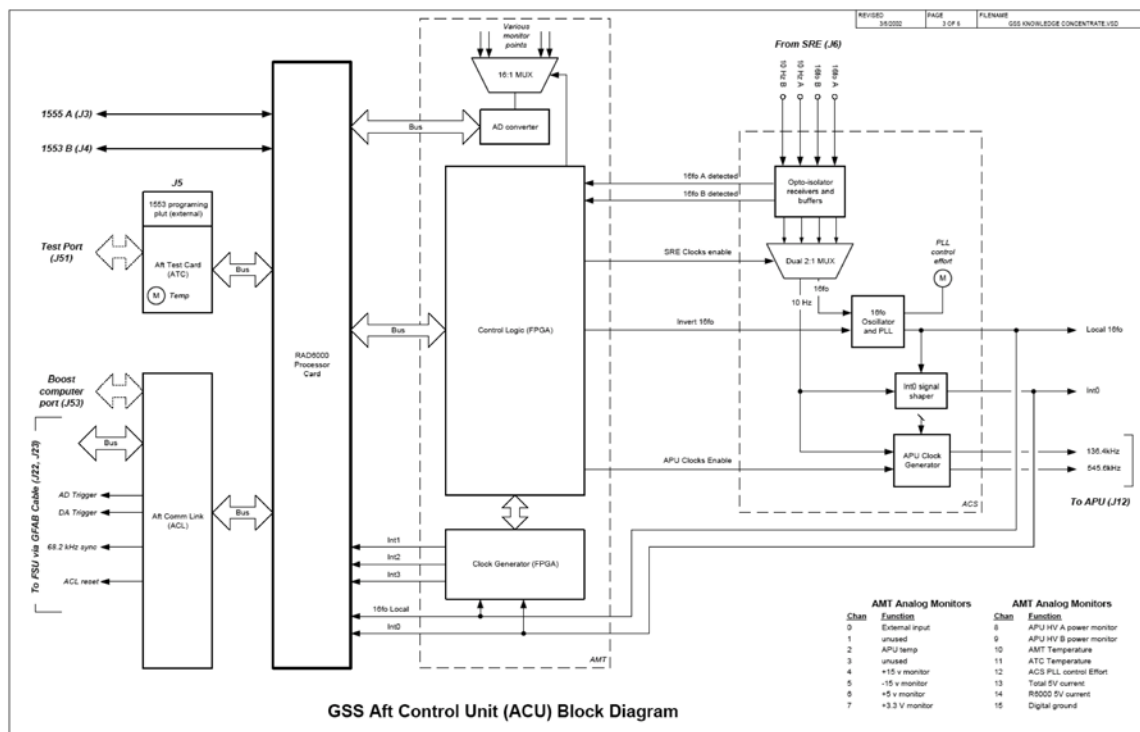


Figure 9-5. Block Diagram of the Aft Suspension Unit (ACU)

## 9.1.10 Mux and Timing

The aft multiplexer and timing (AMT) card collects analog telemetry monitors from the aft box (power supply voltages, temperatures, etc) and generates the suite of timing signals for the GSS string.

### 9.1.11 Clock synchronization

The aft clock support card (ACS) receives the master 16.368 MHz clock from the spacecraft, as well as the 10 Hz timing strobe, and uses a phase locked loop to synchronize a local oscillator to this timing source. This permits the GSS string to operate in perfect clock synchronization to the spacecraft and thus prevent any EMI clock beating effects that are possible with non-synchronized clocks. Should the external source be lost, the local oscillator will free-run and allow the suspension system to function without interruption.

### 9.1.12 Aft Comm Link

The Aft communications link (ACL) is the mate to the forward communications link (FCL) and enables the two subsystems to communicate.

### 9.1.13 Power supply

Mounted external to the ACU enclosure is the GSS power supply, a custom designed DC/DC converter set to supply the required voltages to the system. This is the lighter colored box to the left of the black ACU box in Figure 9-2. This system supplies single-string +3.3, +5.0 and ±15.0 volts to the ACU as well as redundant +5, ±12, and high voltage (either ±800 or ±1200) to the forward suspension unit. A block diagram of the power system is given in Figure 9-6. In addition to supplying electronics power, the system also supplies voltages for survival heaters used when the boxes are unpowered. Normal operation generates sufficient heat naturally to eliminate their need during the IOC and science data gathering phase of the mission.

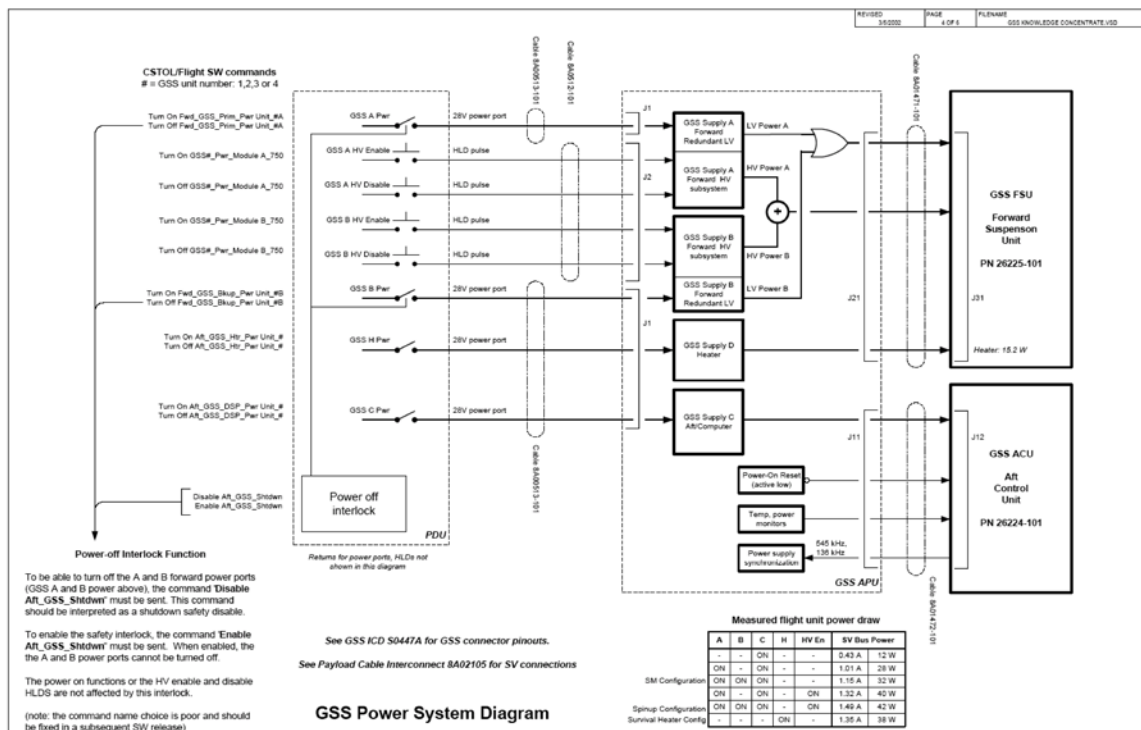


Figure 9-6. Block diagram of the GSS power system.

## 9.2 Suspension Controller Design

This section describes the design and operation of the gyro suspension controller.

### 9.2.1 Controller description and space of operation

The position of each gyroscope rotor in its housing is sensed through and electrostatic centering forces are applied via six circular electrodes located on the gyroscope housing wall (Figure 9-7). This non-contact suspension eliminates gimbal and bearing torques evident in other mechanical gyroscopes. The residual electrostatic torques that do remain are proportional to 1) the rotor's spherical asymmetry, 2) the rotor's mass-imbalance, 3) spin axis misalignment from the vehicle roll axis, and 4) the magnitudes of the electrostatic suspension fields. The GSS is designed to minimize the electrostatic suspension fields while keeping the rotor centered against external disturbances.



**Figure 9-7.** Photograph of rotor and housing. Suspension electrodes and spin-up channel are clearly seen.

Low-torque operation requires the control authority (bandwidth) of the controller to be minimized. The disturbance environment, however, is characterized by random micrometeoroid strikes that can apply impulsive disturbances as large as 10,000 times the nominal acceleration environment. A fixed control scheme that can handle these impulses produces gyroscope disturbance torques far in excess of mission requirements.

An adaptive Linear Quadratic Estimator (LQE) control algorithm has been developed to meet the high dynamic range requirements for the mission's electrostatic suspension. The controller architecture is novel because it uses estimates of the plant's state, rather than estimates of the plant's parameters, as inputs for adaptation (Figure 9-8). This allows the algorithm to dynamically increase its control authority and bandwidth to the level needed to respond to large impulsive disturbances while continuously minimizing control authority - and torques - during nominal operation. The net result of this scheme is that the control system performs like a high-bandwidth and high authority controller with respect to disturbances that move the rotor far from the commanded position, but performs like a low-bandwidth, low-authority control system with respect to gyroscope disturbance torques. Figure 9-9 shows the simulated response to variously sized micrometeoroids; this performance has been verified in orbit. This variable bandwidth control scheme, in part, allows the GP-B mission achieve its goal for the non-relativistic residual gyroscope precession rate of less than  $1.6 \times 10^{11}$  deg/hr.

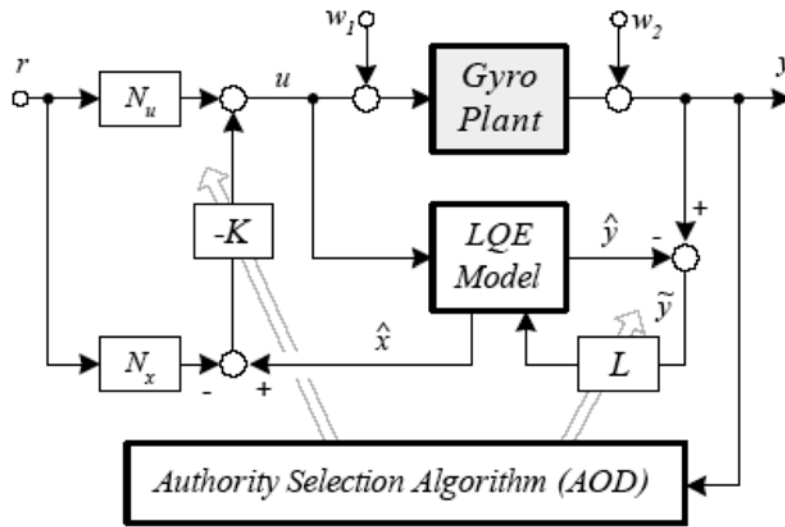


**Figure 9-8.** Block diagram of the LQE control architecture.

This algorithm is implemented in a radiation-hardened digital computer based on a Power PC-derived British Aerospace (formerly Lockheed-Martin Federal Systems) RAD6000 processor running at 16.368 MHz within the suspension electronics package. To achieve maximum performance from the processor, a custom single-thread, non-preemptive real time operating system was written for this application. During peak demand periods during spin-up operations, the processor is loaded to 96% of its capacity; science operation requires approximately 65% of capacity. The code for this application is small, however, only occupying 500 kB of memory. The range of external accelerations that can be handled by the digital control algorithm is shown in Figure 9-10.

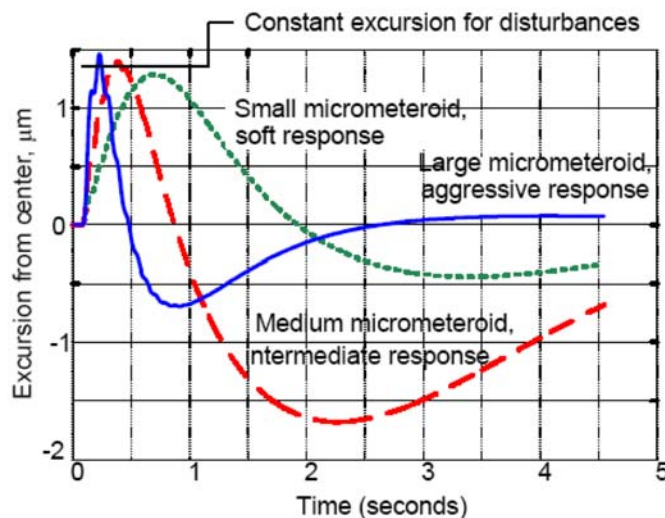


**Figure 9-9.** Simulated response of adaptive LQE controller showing constant excursion for varying disturbance

The digital controller is able to operate over 8 orders of magnitude of force disturbances while minimizing the torques on the gyroscope rotors. The primary science mode digital suspension operates over a specific force range from  $10^7$  m/s<sup>2</sup> to  $10^2$  m/s<sup>2</sup> and bandwidths of 1.5 Hz to 8 Hz, respectively, at a sample rate of 220 Hz. The

spin-up controller bandwidth is not adaptive, has a 660 Hz sample rate, and has been designed to reject the disturbances from the spin-up gas flow. During spin-up, electrostatic torques are not a concern, thus a computationally simpler, fixed control scheme is used. This system is also able to suspend a gyroscope in the laboratory in 1 g conditions, and can apply up to 1600 VDC to provide the required electric fields to suspend on the ground for performance testing. Computer systems are notoriously unreliable in a space radiation environment. Three all-analog backup control systems are also provided to suspend the gyroscope in the event of a computer fault.

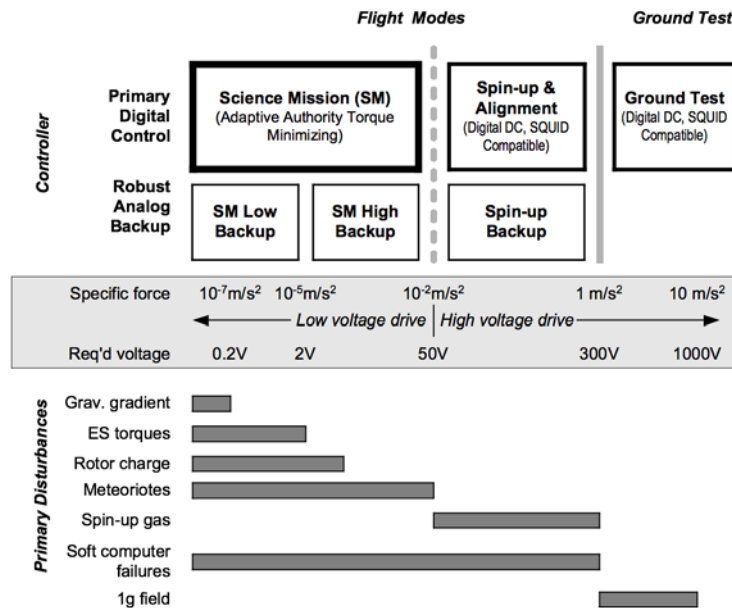


**Figure 9-10.** Suspension Controllers and Modes of Operation showing the 8 orders of magnitude of operation for this system.

The spin-up backup controller is used during gas flow operations, and the two science mode backups are active during the remainder of the mission. The all-analog controllers are robust proportional/derivative (PD) designs with a force-to-voltage nonlinearity inversion circuit to allow good control over the range of motion of the rotor in the housing. The primary role of these controllers is to prevent the rotor from contacting the housing wall, thus an integral term in the controller is not needed which significantly simplifying the design of these compensators. An analog arbiter (see the FSU block diagrams above) monitors computer health and rotor position and will autonomously switch into the appropriate backup controller in the event of a computer fault or a large position excursion of the rotor. This architecture permits the controller to operate over the required 8 orders of force magnitude, providing reliable suspension of the rotors (via prime and backup systems), and minimize electrostatic torques on the rotor via the variable bandwidth adaptive control law.

## 9.2.2 Controller performance on Orbit

The GSS system performed very well on orbit and was able to successfully suspend, support spin-up, and align the spin axes of the gyros to mission requirements.

### 9.2.2.1 Science Suspension

Because of the robustness and simplicity of the control algorithms, the gyroscopes were initially suspended using the analog backup control system. Figure 9-11 shows a snapshot of the trajectory of the Gyro 2 position on its inaugural on-orbit suspension. The gyro was initially sitting on the housing wall in the C electrode axis

direction (transverse to the space vehicle roll axis). Suspension voltage was applied at 0.5 seconds and remained on until 6.0 seconds, after which the rotor was left unsuspended and it began to “fall”. The kinks in the trajectory after the 6 second mark are points where the rotor “bounced” on the housing wall. The rotor is driven here by centrifugal acceleration of the housing with respect to the rotor. (This test was done prior to the final mass trim of the spacecraft roll axis.) This test and others verified the functioning of the analog backup control system on orbit.

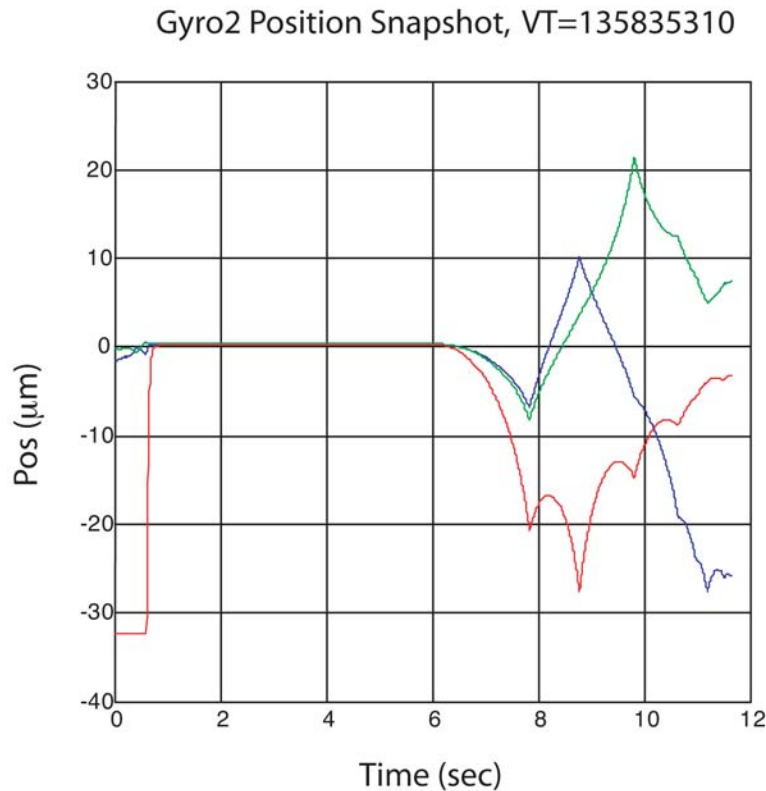


**Figure 9-11.** Initial suspension of gyroscope in analog backup mode (blue=A axis, green = B, red = C)

The performance of the digital LQG controller was demonstrated by a series of step responses starting at 8 μm from the center of the housing. As is seen in Figure 9-12 and in more detail in Figure 9-13, the step response show high frequency (high bandwidth) overshoot oscillations when away from center and well damped (low bandwidth) overshoot for steps near the center of the housing. The bottom plot in Figure 9-12 shows the bandwidth that the controller automatically selected during this run, ranging from 50 rad/sec (8 Hz) when the rotor was far from center, down to 10 rad/sec (1.6 Hz) at the end of the snapshot. The controller bandwidth bottoms out at 3 rad/sec (0.5 Hz) during normal science operation.



Gyro3 Position Snapshot, VT=138493151.5

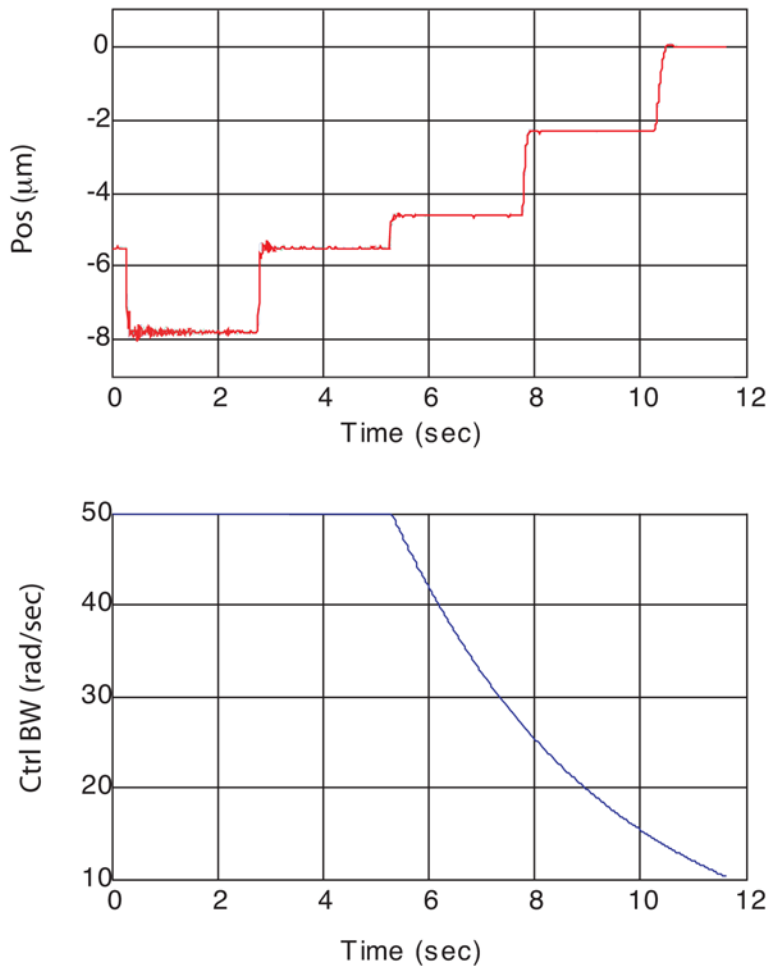


**Figure 9-12.** GSS step response in Science mode, showing control stiffness as a function of miscentering.

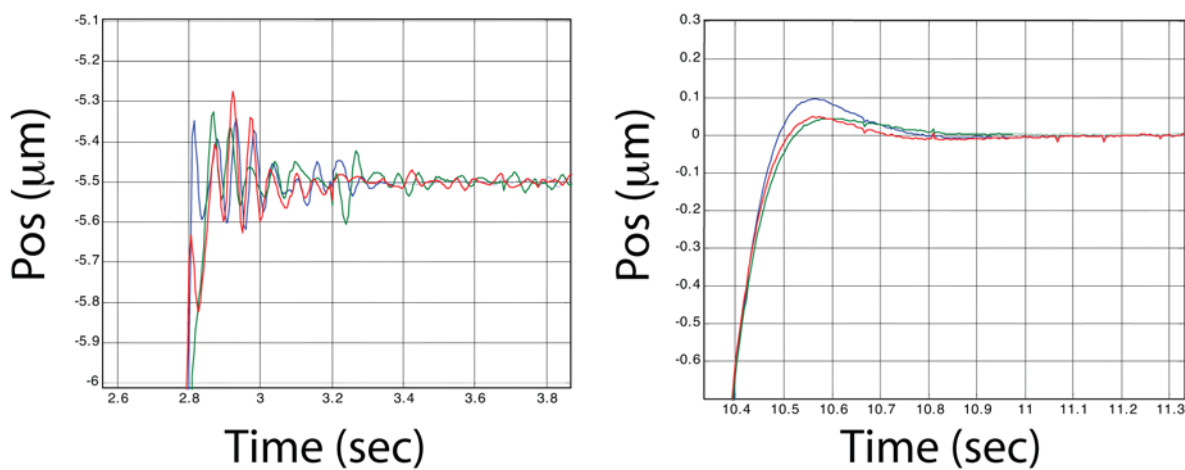


**Figure 9-13.** Details of control response showing high-bandwidth (left) low-bandwidth (right) operation.

### 9.2.2.2 Spin-up Suspension

During spin-up operations, much higher suspension voltages and control efforts are required to suspend the gyroscope against the spin-up gas. Figure 9-14 shows the control effort exerted by the suspension system (top) and the required electrode voltages to produce the force (bottom). A peak voltage of 150 VDC is required to suspend the rotor against the push of the spin-up gas at full flow rate – 40 mN peak (0.06 g equivalent acceleration). Nominal flow rate is 725 sccm at a temperature 6 K. To apply these DC high voltages, the GSS high voltage amplifier system and 660 Hz spin-up controller was required.

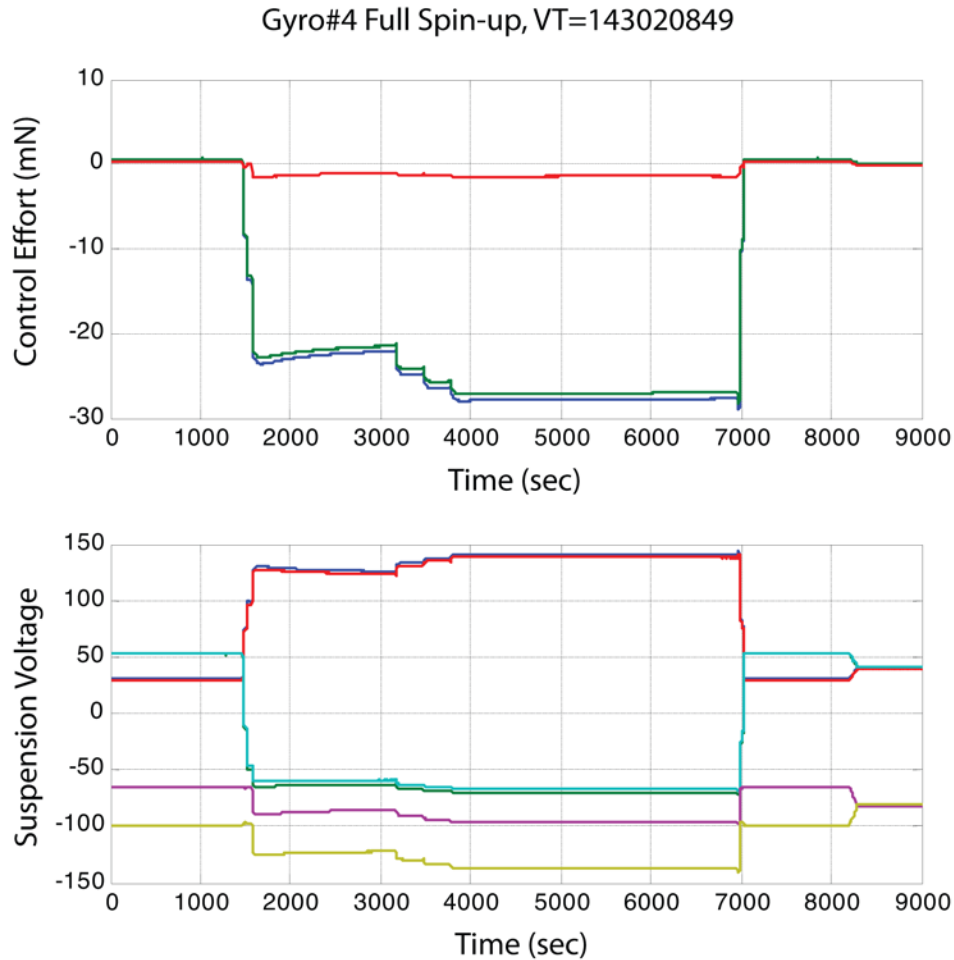


**Figure 9-14.** GSS control efforts during full flow gyroscope spin-up operations (top plot: blue = A, green = B, red = C)

### 9.2.2.3 Spin axis alignment

Though a core requirement of the experiment is to minimize GSS-induced disturbance torques on the gyroscope rotor, it is desired to align the spin axis of the rotor after gas spinup to within 1 arc-sec ( $2.8 \times 10^4$  deg) of a target orientation near line of sight of the guide star. This alignment establish the initial conditions for the experiment.

In the GSS, the electric fields used to suspend the rotor can be chosen to either enhance or minimize electrostatic torques on the gyroscope. By judicious choice of electrode voltages, the net electric field intensity on one axis can be made preferentially larger or smaller than the other axes, while staying consistent with the force constraints needed to hold the rotor centered in the cavity. When the interaction of this electric field

imbalance with non-spherical component of rotor shape (centrifugal bulging due to spin plus natural 10 nm level out-of-roundness terms) it is found that the gyroscope will tend to precess around the electrode axis with the largest preload electric field

During science data gathering, the suspension electric fields are reduced to the levels needed to meet the gyroscope centering and safety requirements which results in approximately 200 mV on the electrodes. During alignment, however, the electric fields are increased by a factor 300 over the science levels and explicit imbalances are introduced to increase the torques on the rotor by a factor of approximately 100 million over the nominal science levels.

Using the SQUID output as a measure of the gyroscope's orientation, a bang-bang control scheme is used to switch the dominant preload between two electrode axes that are oriented at a 45 degree angle from the vehicle roll axis, the A and B electrode axes. Proper phasing of this signal allows the spin axis orientation to be moved from the post spin-up orientation — up to 500 arc-sec from the vehicle roll axis — to a final, specified, orientation within 10 arc-sec of the roll axis.

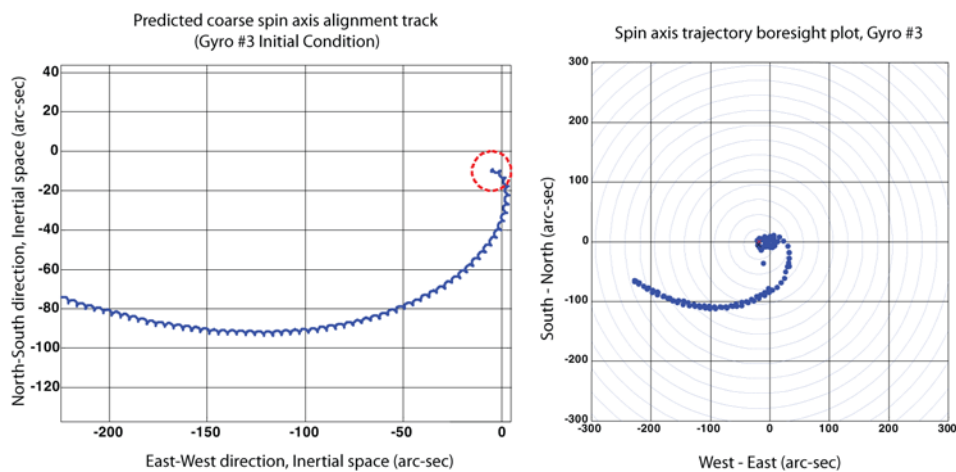


**Figure 9-15.** Simulated (L) and actual (R) spin axis alignment tracks for Gyro 3 coarse alignment

Figure 9-15 (left) shows the trajectory of a gyro spin axis during the alignment process; the goal is the circle near the origin. With this system, alignment rates on the order of 3 arcsec/hr can be generated when driven by the high voltage amplifier using 50 V common mode on the electrode axes (coarse alignment mode), while rates of 0.1 arc-sec/hr with a 8 V drive from the low voltage amplifiers (fine alignment mode); see Figure 9-16. The spiral shape of the predicted trajectory is expected because a convenient, though sub-optimal, switching surface was used in the bang-bang controller: the pickup loop on the gyroscope parting plane.

Figure 9-15 (right) shows the actual performance for the spin axis alignment of Gyro 3; note that the gyroscope follows a similar curve to the prediction. All four gyroscopes were aligned successfully using this method.

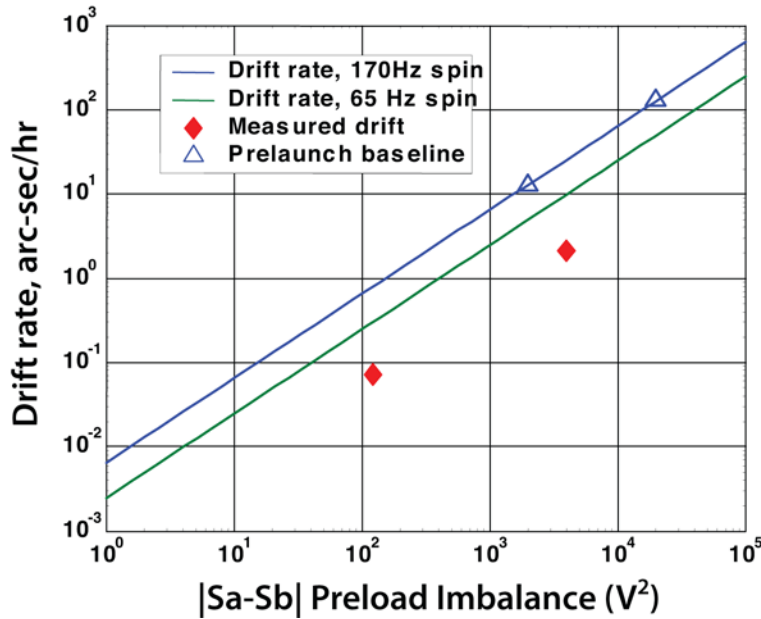


Figure 9-16. Predicted and measured drift rates for coarse and fine alignment modes.

### 9.2.3 Drag-Free control

In addition to gyroscope suspension, the GSS system interacts with the vehicle's ATC system to permit drag-free control of the vehicle to eliminate the effects of environmental forces on the vehicle. There are two equivalent ways of canceling the spacecraft disturbances: First, the spacecraft can fly to follow an internal unsupported proof mass by minimizing the relative position of the spacecraft with respect to the proof mass (this is called a "primary" or "unsuspended" drag-free), and second by suspending the internal proof mass and controlling the spacecraft to keep the suspending forces a minimum (called "backup" or "suspended" drag-free). These are equivalent in function, but the backup mode is more robust especially when the clearance between the spacecraft and the proof mass must be minimized to achieve an accurate relative orientation measurement, as is necessary in the GP-B case.

Both "prime" and "backup" drag-free modes were part of the ATC design and have been exercised on orbit. Implementation details for both modes are given below:

#### 9.2.3.1 Unsuspended or "prime" drag-free mode:

In this mode, the suspension system of the drag-free reference gyroscope is placed in a standby mode and the rotor is allowed to freely float while the vehicle flies to keep the rotor at the center of the housing cavity. The GSS monitors the position of the gyroscope in the housing and only allows rotor position excursions of approximately  $\pm 4\mu\text{m}$  from center of the  $32\mu\text{m}$  rotor/electrode gap prior to disabling the drag-free mode and re-centering the gyroscope electrostatically. At 4500 RPM, there is sufficient mechanical energy in the rotor to destroy the gyroscope assembly should the rotor come into contact with the housing wall. Therefore, conservative limits have been built into the suspension system to preclude this possibility during normal operation.

The ATC system regulates the position of the inertial mass of the spacecraft,  $\mathbf{R}$ , with respect to the position of the gyroscope,  $\mathbf{r}$ , as shown in Figure 9-17. The GSS passes rotor position information to the ATC controller through the interface gain  $\mathbf{K1}$ . The controller is implemented as a 3-axis PID controller with sufficient gain at the space vehicle roll frequency to meet its  $1 \times 10^{-11} \text{ m}\cdot\text{sec}^{-2}$  residual acceleration requirement. Calculations are performed in the nadir frame and are rotated into the vehicle body frame for application.

All drag-free sensors are subject to a gravity gradient force since the center of mass of the space vehicle is approximately 23 cm away from the location of the first gyroscope; each subsequent gyroscope is 8.8 cm further from the vehicle mass center along the vehicle roll. The gravity gradient acceleration is on the order of  $4 \times 10^7 \text{ m/s}^2$  on the rotor closest to the vehicle mass center (Gyroscope 1) and increases linearly with distance to the other gyroscopes. Drag-free operation in effect moves the vehicle point of free fall to the location of the drag-free gyroscope, thereby reducing the gravity gradient acceleration on the other gyroscopes as well.

To aid the controller in rejecting this significant disturbance, a gravity gradient feed-forward signal, scaled by the distance from the vehicle center of mass to the center of the gyroscope housing, is generated and added to the thrust commands sent to the space vehicle. In this case, the controller works primarily to reject the effects of vehicle resonance modes (minimal) and external disturbances from atmospheric drag, solar pressure, and other environmental disturbances.

The main advantage of this mode is that the rotor is free-floating, and thus it represents the purest implementation of a drag-free system and, in principle, to the greatest extent minimizes the torques on the rotors – a great value for this experiment. However, this topology does have some particular disadvantages for GP-B.

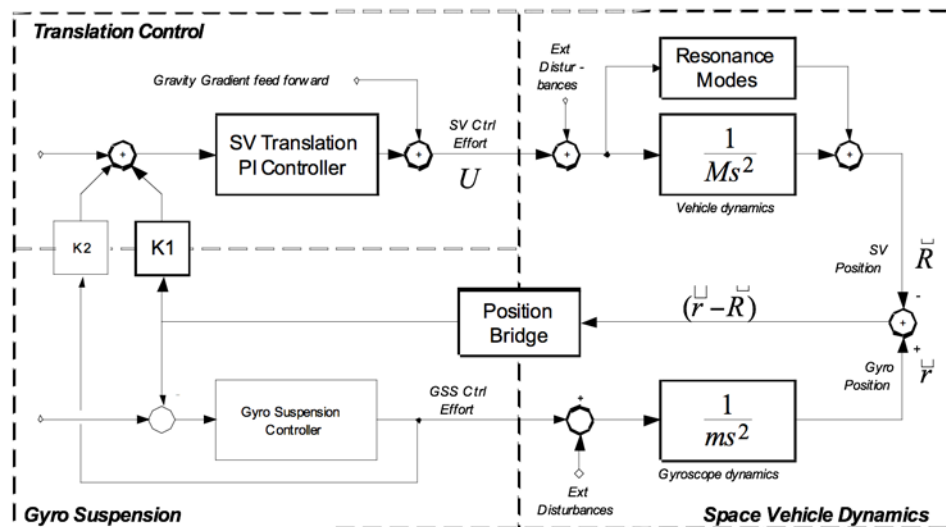


**Figure 9-17.** Unsuspended or “prime” drag-free control topology.

Because of the need to protect the spinning rotor, the drag-free system is only allowed to operate in a relatively narrow dead band around the center of the housing. This leads to more frequent drag-free shutdowns by the GSS when the vehicle encounters external environments that temporarily overwhelm the capability of the ATC system, approximately 5 mN per vehicle axis.

This mode also does not allow for acceleration bias compensation in the sensor since it relies on relative position of the rotor and housing as its input. Any force (due to an electrical patch charge, for example) between the rotor and housing will cause the rotor to accelerate toward the housing. In turn, the vehicle will accelerate to follow. To hold the rotor at a fixed position in the housing, the ATC system would need to apply a constant acceleration the vehicle which would change the orbit over time.

### 9.2.3.2 Suspended or “backup” drag-free mode:

In this mode, the gyroscope is suspended in science configuration by the GSS and the drag-free system flies the vehicle to minimize the measured suspension forces on the gyroscope. The ATC system works to drive the measured control effort on the proof mass,  $u$ , to zero via translation control commands,  $U$ , as shown in

Figure 9-18. The GSS passes rotor control effort information to the ATC controller through the interface gain  $K_2$ ; any accelerometer biases are removed on the translation control side of the interface. At low frequency, near space vehicle roll rate, the transfer function from  $U$  to  $u$  is simply a constant, and in principle, a simple integral control is all that is required to minimize  $u$ . The controller is implemented in the same structure as the suspension-off drag-free mode, but with different coefficients. Gravity gradient feed forward is again applied to compensate for known large disturbance acceleration.

The chief advantage of this mode is that the spinning gyroscope is always actively centered by the GSS, and thus is at minimal risk of contacting the housing wall. In addition, acceleration is measured directly and thus a post-measurement accelerometer bias adjustment can be readily made in the ATC system; this feature was exercised on orbit as noted below.

The disadvantage to the science measurement is that the drag-free gyroscope is always suspended, and thus is subject to greater electrostatic torques than a free-floating gyroscope due to the active suspension. However, this is not a significant disadvantage, since three of the four gyroscopes in primary drag-free mode need to be suspended against gravity gradient in any case, and the experiment error due to these residual forces has been shown to be well within the requirements.

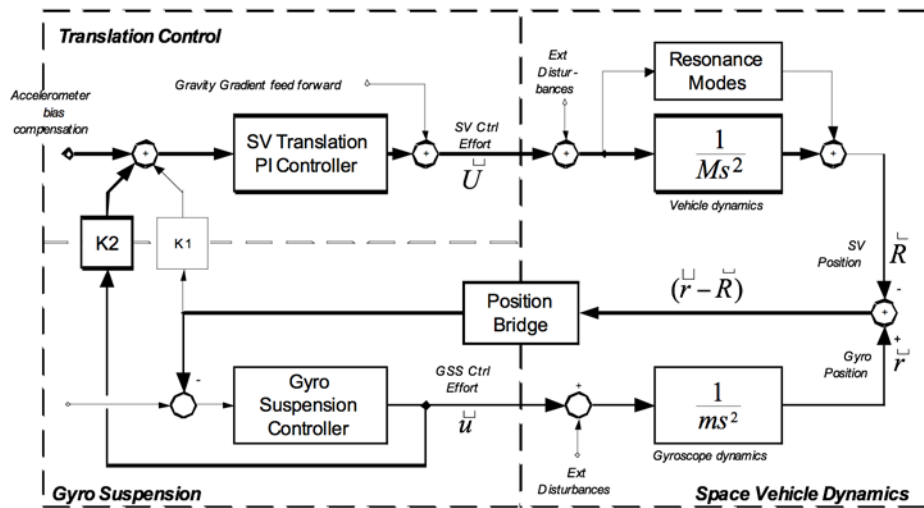


Figure 9-18. Suspended or “backup” drag-free control topology.

### 9.2.3.3 Drag-free Flight Performance

The design of the space vehicle permits any gyroscope to act as the drag-free reference; on orbit, the selection of the gyroscope to serve as the drag-free sensor was largely driven by practical, operational concerns. To minimize the overall residual gravity gradient acceleration the gyroscopes, Gyroscopes 2 or 3 (near the center of the linear array) are preferable. Gyroscope 4 is the furthest from the center of mass of the vehicle, and thus would require the most thrust – helium usage – to force the space vehicle to free fall around its center. Gyroscope 2, early on, required some control system tuning to optimize suspension performance and thus was not used for drag-free control during testing. Thus, drag-free testing and optimization was done with Gyroscopes 3 and 1.

Both the primary and the backup drag-free control modes were tested on the vehicle. Figure 9-19 shows an example transition sequence from non-drag-free, to suspended (backup) drag-free to free-floating (primary) drag-free control. During these transitions, the transfer of the gravity gradient acceleration moves from the gyroscope to the space vehicle ATC system as the space vehicle is forced to free-fall about the drag-free sensor. In prime drag-free mode, the suspension control efforts are disabled, so the vehicle must fly around the position of the rotor. Additional control effort activity in the ATC system is seen during this period.

Though prime drag-free is the preferred operational mode, it was not used during the science data gathering phase of the mission. After on-orbit calibration, it was found that some gyroscopes exhibited a small acceleration bias, up to 20 nN, that the prime drag-free system would track; though this bias would have no effect on the drift performance the gyroscopes, the ATC control action over time would slowly change the space vehicle's orbit. The backup drag-free system could properly compensate for these biases and showed acceptable performance for the mission during testing, thus it was selected as the baseline drag-free mode during science data collection.

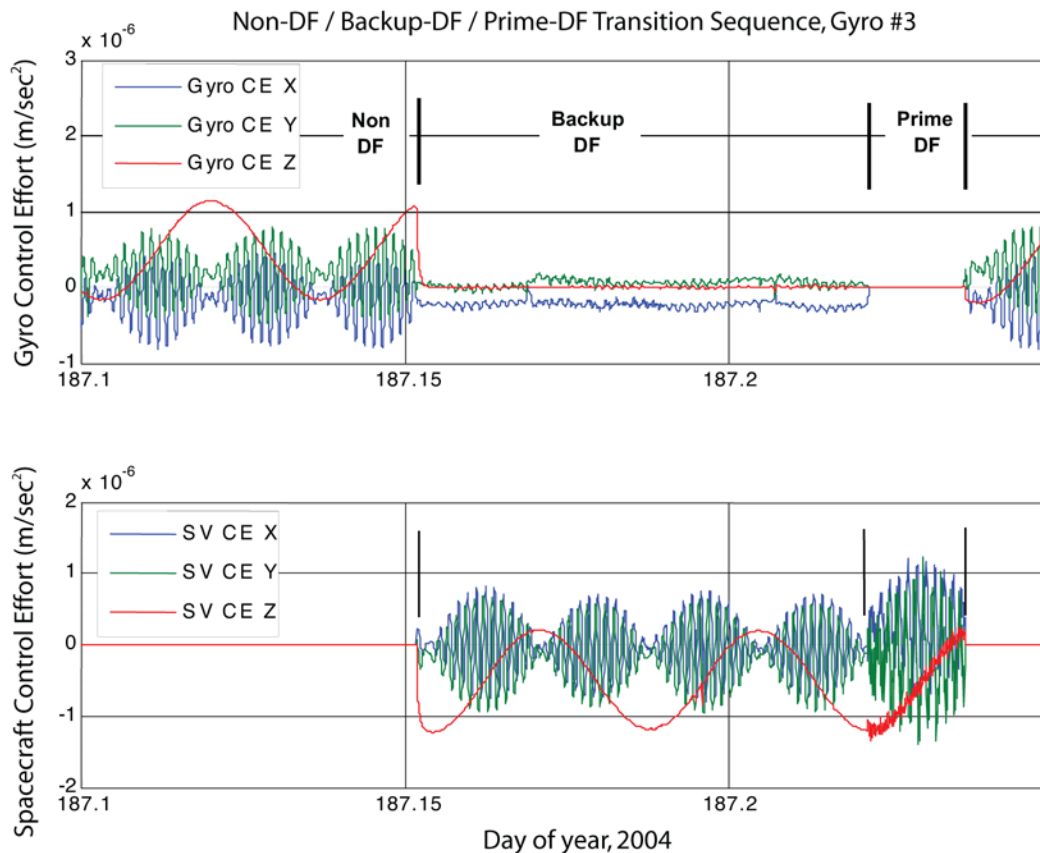


**Figure 9-19.** Drag-free transitions: Backup and prime

Representative backup drag-free performance is shown in [Figure 9-20](#). The top curve shows the spectrum of the space vehicle translation control effort showing the twice-orbit frequency gravity gradient signature at  $3.4 \times 10^4$  Hz (red line); the peak at  $1.7 \times 10^4$  Hz is the suspension system measuring the 10 nm rotor asphericity as modulated by rotor's polhode motion. The residual acceleration on the rotor is  $4 \times 10^{11} \text{ m/s}^2$  from  $< 0.01$  mHz to 10 mHz in inertial space (averaging period: 24 hours). If the gyroscope is viewed as an accelerometer, the acceleration measurement noise floor is  $1.2 \times 10^9 \text{ m/s}^2 \cdot \text{Hz}^{1/2}$  in inertial space. Performance of the gyroscopes as accelerometers is limited by noise introduced through coupling from the spacecraft's pointing system and the low signal-to-noise ratio on position sensing bridge, as required for compatibility with the SQUID readout system. A GPS receiver on board the spacecraft measures the position of the vehicle in orbit and is used, together with ground-based laser ranging data, to confirm that the resulting vehicle orbit is indeed drag-free. This orbit data has been used to identify and remove force biases in both the ATC and GSS systems



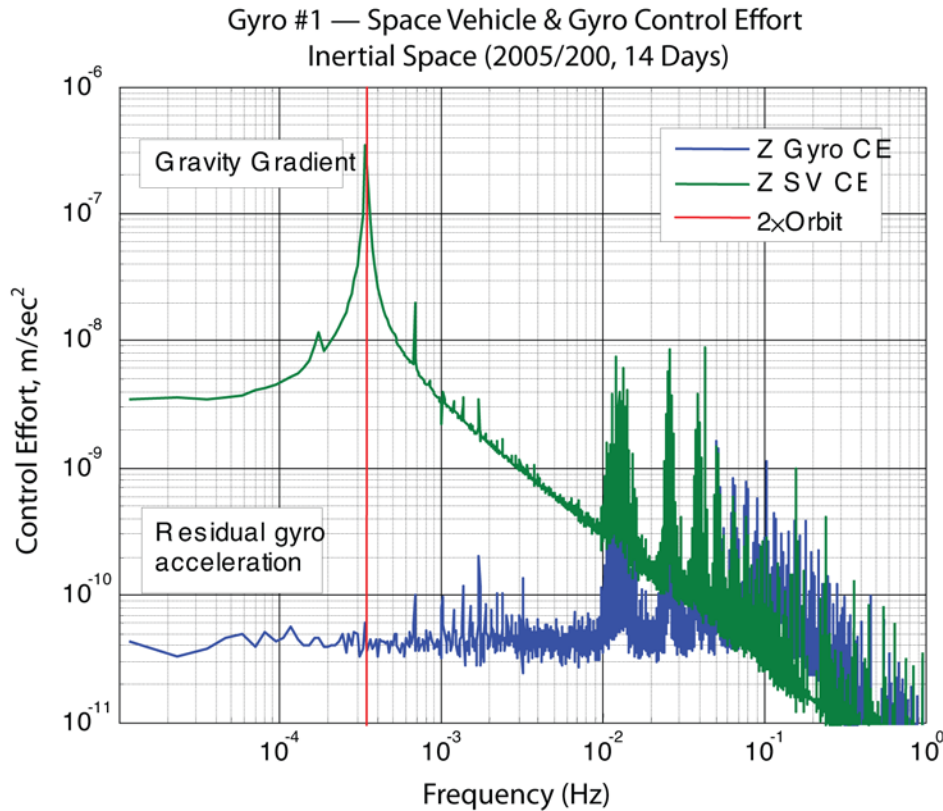


**Figure 9-20.** Representative drag-free performance together with gravity gradient acceleration on the space vehicle

### 9.3 GSS Software

The GSS software (GSW) residing in the RAD6000-based processors in each chain performs the control calculations and telemetry processing required to operate the suspension for each gyroscope. The code itself was written in the C language, rather than ADA used on the CCCA and the SRE systems, for two reasons: 1) compatibility with prototype code developed at Stanford prior to the design of the GSS, and 2) efficiency in execution to allow the flight system to suspend a gyroscope on the ground. To this end, the VxWorks operating system used on the CCCA and SRE subsystems was replaced with a single thread, non-preemptive real time operating system with a fixed scheduler. Since the GSS processor needed to execute a real-time control loop at high speed without hiccups, the software team could control explicitly the priority of the control calculations with other less-critical telemetry or housekeeping functions. This level of explicit control also made the coding of the transitions between spin-up and science configurations much more tractable.

The code image is relatively small at 480 kB; with data storage and scratchpad space, the code occupied about 37% of the 3 MB static RAM aboard the RAD6000 processor.

A number of different applications ran on the processor during the mission.

1. **I/O and Scheduler.** Communication with the GSS hardware via a parallel port and the CCCA via the MIL-STD-1553 link. Processor management via the scheduler with cycle times of 220 Hz in science suspension mode, 660 Hz in spin-up suspension mode, and 1320 Hz in ground-test mode.
2. **Gyro Suspension.** Implements the bandwidth on demand LQR control algorithm noted above, in either spin-up or science mode.
3. **Summit RAM Refresh.** Performs scrubbing of radiation induced errors in the MIL-STD-1553 interface that is not covered by the main processor error correction circuitry.
4. **RAM Scrub.** Performs scrubbing of radiation induced errors in the main processor SRAM. Detects multi-bit errors.
5. **Snapshots.** Collects 12 seconds of full suspension rate (220 Hz) snapshots of gyro position and control effort data. Not available in spin-up mode due to processor loading constraints.
6. **ATC Filter.** Low pass filter for drag-free data being send to the CCCA.
7. **Charge Measurement.** Presents excitation voltages to the gyro electrodes and performs on-board filtering to assess the charge on the rotor.
8. **Charge Control.** Manages the charge control electrode drive during rotor discharge operations.
9. **Science Filter – Electrode voltage.** Low pass filter that computes the mean and square of the 6 suspension voltages and passes the data to telemetry.
10. **Science Filter – Gyro position.** Low pass filter that computes the gyro position along the 3 suspension axes and passes the data to telemetry.
11. **Science Filter – Gyro control effort:** Low pass filter that computes the control effort applied to the gyro along the three suspension axes passes the data to telemetry.
12. **Database Readout:** Used for reading and updating user-configurable software parameters.

Table 9-1 and Table 9-2 present the processor loading for various operational configurations in science and spin-up modes used during the mission. Table 9-3 lists the source lines of code (SLOC) for the various applications; 21,600 lines of C code were required to implement the suspension features required by GP-B.

**Table 9-1.** GSS Science Mission Mode (220Hz) CPU Utilization

Application	All applications Off	Suspension only	Steady state in Science Mission	Peak load during database dump
I/O and Overhead	20.3	20.3	20.3	20.3
Gyro Suspension	—	36.5	36.5	36.5
Summit RAM Refresh	—	—	0.6	0.6
RAM Scrub	5.0	5.0	5.0	5.0
Snapshot	—	—	6.5	6.5
ATC Filter	—	—	0.1	0.1
Charge Measurement	—	—	2.2	2.2
Charge Control	—	—	0.3	0.3
Science Filter – Electrode voltage	—	—	2.0	2.0
Science Filter –Gyro position	—	—	0.9	0.9

**Table 9-1.** GSS Science Mission Mode (220Hz) CPU Utilization

Application	All applications Off	Suspension only	Steady state in Science Mission	Peak load during database dump
Science Filter – Gyro control effort	—	—	0.9	0.9
Database Readout GIO parameters	—	—	—	4.7
CPU Utilization%	25.3	61.8	75.3	80.0

**Table 9-2.** GSS Spin-up Mode (660Hz) CPU Utilization

Application	All applications Off	Suspension only	Steady state with Science Filters	Spin Axis Alignment	Peak load during command
I/O and Overhead	40.9	40.9	40.9	40.9	40.9
Gyro Suspension	—	38.8	38.8	40.2	40.2
Summit RAM Refresh	—	0.6	0.6	0.6	0.6
RAM Scrub	5.0	5.0	5.0	5.0	5.0
Snapshot	—	—	—	—	—
ATC Filter	—	—	—	—	—
Charge Measurement	—	—	—	—	—
Charge Control	—	—	—	0.2	0.2
Science Filter – Electrode voltage	—	—	2.8	2.8	—
Science Filter –Gyro position	—	—	2.2	2.2	—
Science Filter – Gyro control effort	—	—	2.2	2.2	—
Set gyro position vector command	—	—	—	—	7.1
CPU Utilization%	45.9	85.3	92.5	94.1	94.0

**Table 9-3.** GSW application source lines of code (SLOC) metrics

Reqs paragraph	GSW Application	Sub-Application	Req ID	Unit source filename	SLOC		Sec	Memory size
5.1.6.1	GSW Scheduler		SHG	shg.c	775	11948	.text	11948
				shg.common	91	168	.rodata	168
				shg.h	138	100	.data	100
				dT_10Hz.c	129	1316	.text	1316
				dT_10Hz.com	13	32	.rodata	32
				mon	18	20	.data	20
				dT_220Hz.c	439	5568	.text	5568
				dT_220Hz.com	13	32	.rodata	32
				mon	60	12	.data	12
				dT_220Hz.h				

**Table 9-3.** GSW application source lines of code (SLOC) metrics (Continued)

Reqt paragraph	GSW Application	Sub- Application	Req ID	Unit source filename	SLOC		Sec	Memory size
				dT_660Hz.c dT_660Hz.com mon dT_660Hz.h	880 13 134	13124 32 12	.text .rodata .data	13124 32 12
				dT_summit.c dT_summit.co mmon dT_summit.h	135 13 18	1316 32 20	.text .rodata .data	1316 32 20
5.1.6.2	Initialization		GIN	gin.c gin.h	66 5	156	.text	156
5.1.6.3	GSS Data Management		GD M					
5.1.6.3.1		GSS Cmd Router	GCR	gcr.c gcr.common gcr.h	120 18 29	984 28 28	.text .rodata .data	984 28 28
5.1.6.3.2		GSS TIm Proc	GTP	gtp.c gtp.common gtp.h	456 43 109	4896 40 12	.text .rodata .data	4896 40 12
5.1.6.3.3		GSS Cmd Proc	GCP	gcp.c gcp.common gcp.h	311 23 41	3348 48 68	.text .rodata .data	3348 48 68
5.1.6.4	I/O Processing		GIO	gio.c gio.common gio.h	222 41 23	2800 104 100	.text .rodata .data	2800 104 100
5.1.6.4.1		1553 Interface	GIF	gif.c gif.common gif.h	586 120 79	6828 28 76	.text .rodata .data	6828 28 76
5.1.6.4.2		Expansion Bus I/F	GSB	gsb.c gsb.common gsb.h	446 85 393	7608 192 164	.text .rodata .data	7608 192 164
				gswBIC.c gswBIC.commo n gswBIC.h gswSTIC.h	235 7 217 11	2428	.text	2428
5.1.6.5	Checks		GCK	gck.c gck.common gck.h	85 25 10	1052 28 4	.text .rodata .data	1052 28 4
5.1.6.5.4		RAM Scrub	GRS	grs.c grs.common grs.h	30 19 15	348 28 8	.text .rodata .data	348 28 8
5.1.6.5.6		SUMMITRAM Refresh	GSR	gsr.c gsr.common gsr.h	37 17 13	424 28 16	.text .rodata .data	424 28 16
5.1.6.6	GSS Support Processing		GPP					

**Table 9-3.** GSW application source lines of code (SLOC) metrics (Continued)

Reqs paragraph	GSW Application	Sub-Application	Req ID	Unit source filename	SLOC		Sec	Memory size
5.1.6.6.1		GSS ATC Proc	GPA	gpa.c gpa.common gpa.h	288 15 23	3324 104 128	.text .rodata .data	3324 104 128
5.1.6.6.2		GSSSnapshot Processing	GSP	gsp.c gsp.common gsp.h	1566 26 255	33896 56 25104	.text .rodata .data	33896 56 25104
5.1.6.6.3		Gyro Control Processing	GYP	gyp.c gyp.common gyp.h	1564 96 190	25288 288 1252	.text .rodata .data	25288 288 1252
				aod1.c aod1.h	223 27	3580 168 4	.text .rodata .data	3580 168 4
				aod1imp.c aod1imp.h	780 186	17308 1008 4	.text .rodata .data	17308 1008 4
				control1.c control1.h	344 120	3864 96 12	.text .rodata .data	3864 96 12
				inl1impl.c inl1impl.h	349 48	5024 368 4	.text .rodata .data	5024 368 4
				cvecmath.c cvecmath.h	705 112	14532 304	.text .rodata	14532 304
				aod_smm_cpf.c	177	2188 504 4	.text .rodata .data	2188 504 4
				aod_sum_cpf.c	177	2146 512 4	.text .rodata .data	2146 512 4
				aod_gtm_cpf.c	178	2196 496 4	.text .rodata .data	2196 496 4
				aod_ctm_cpf.c	178	2164 496 4	.text .rodata .data	2164 496 4
5.1.6.6.5		GSS Diagnostics	GDP	gdp.c gdp.common gdp.h	2118 92 417	31708 496 376	.text .rodata .data	31708 496 376
5.1.6.6.6		Gyro Charge Control	GCC	gcc.c gcc.common gcc.h	72 12 11	672 24 8	.text .rodata .data	672 24 8
				gmp.c gmp.common gmp.h fir880.h fir9600.h	621 19 20 4 4	8672 328 42680	.text .rodata .data	8672 328 42680

**Table 9-3.** GSW application source lines of code (SLOC) metrics (Continued)

Reqts paragraph	GSW Application	Sub-Application	Req ID	Unit source filename	SLOC		Sec	Memory size
5.1.6.6.7		GSS Hardware Command	GH W	ghw.c ghw.common ghw.h	820 25 119	10400 123 168	.text .rodata .data	10400 123 168
5.1.6.7	Science Suppot Processing		SCS	scs.c scs.common scs.h	228 22 11	2872 56 8	.text .rodata .data	2872 56 8
5.1.6.7.1		Electrode Volt Filter	EVF	evf.c evf.common evf.h	183 12 15	2908 56 3768	.text .rodata .data	2908 56 3768
5.1.6.7.2		Position Signal Filter	PSF	psf.c psf.common psf.h	173 10 15	2664 56 3584	.text .rodata .data	2664 56 3584
5.1.6.7.3		Control Effort Filter	CEF	cef.c cef.common cef.h	173 10 15	2664 56 3584	.text .rodata .data	2664 56 3584
	Utilities			newtRaphRoot.c newtRaphRoot.h	67 7	676 40	.text .rodata	676 40
				timeFuncs.c timeFuncs.h	44 36	720 80	.text .rodata	720 80
				taylorSeriesTrig.c taylorSeriesTrig.h	50 6	1080 128	.text .rodata	1080 128
				Total SLOC	21603			

## 9.4 References

### 9.4.1 Engineering Documents

W.J. Bencze. **Gyroscope Spin Axis Direction Control for the Gravity Probe B Satellite**. Ph.D. Dissertation, Dept. of Electrical Engineering, Stanford University. December, 1996.

M.L. Eglinton, **Authority-on-Demand Adaptive Suspension Control for the Gravity Probe B Gyroscopes**. Ph.D. Dissertation, Dept. of Aeronautics and Astronautics, Stanford University. August, 2000.

**An Electrostatic Suspension and Orientation Control System for the Gravity Probe B Relativity Mission's Science Gyroscopes** by William J. Bencze, Yueming Xiao, David N. Hipkins, Bradford W. Parkinson, and Gene F. Franklin which was presented at the *3rd International Conference on Motion and Vibration Control (3rd MOVIC)*, September 1996, Chiba, Japan.

**Gyroscope Spin Axis Direction Control for the Gravity Probe B Satellite** by William J. Bencze, Yueming Xiao, David N. Hipkins, Bradford W. Parkinson, and Gene F. Franklin which was presented at the *1996 IEEE Conference on Decision and Control*, December 1996, Kobe Japan.

**The Design and Testing of the Gravity Probe B Suspension and Charge Control Systems.** S. Buchman, W. Bencze, R. Brumley, B. Clarke, G.M. Keiser. LISA Symposium. in William M. Folkner, Ed. *Laser Interferometer Space Antenna, Second International LISA Symposium on the Detection and Observation of Gravitational Waves in Space*, Pasadena, California, July 1998, AIP Conference Proceedings 456, American Institute of Physics, Woodbury, New York, 1998.

**Precision Electrostatic Suspension System for the Gravity Probe B Relativity Mission's Science Gyroscopes** by W.J. Bencze, R.W. Brumley, M.L. Eglington, S. Buchman, *SICE Annual Conference*, August 2003, Fukui, Japan.

**On-orbit Performance of the Gravity Probe B Gyroscopes and Electrostatic Suspension System.** W.J. Bencze, D.N. Hipkins, Y. Ohshima, T. Holmes, G.M. Keiser, B. Muhlfelder, S. Buchman, C.W.F. Everitt. *SICE Annual Conference*, August 2005, Okayama, Japan.

W.J. Bencze, D.B. DeBra, L. Herman, T. Holmes, M. Adams, G.M. Keiser, C.W.F. Everitt, **On-Orbit Performance of the Gravity Probe B Drag-Free Translation Control System.** *29th AAS Guidance & Control Conference*, Breckenridge, CO, February 4-8, 2006. AAS 06-083.

Software Design Documents

**SCSE04-6 Rev C: Flight Computer Memory and Timing Analysis.** Lockheed Martin, April 2003 (LM/P086705C)

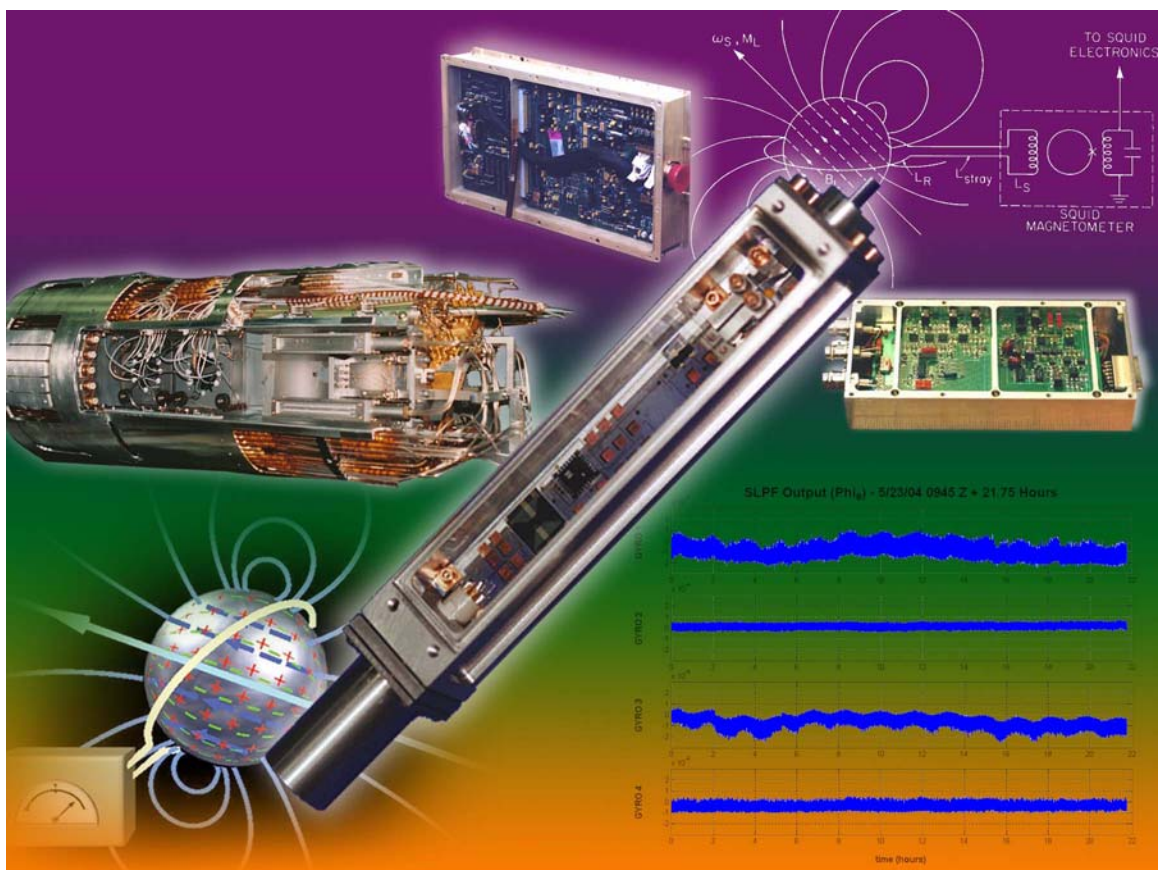
**SCSE16-8 Rev B: Flight Software Design Specification; GSS Software.** Lockheed Martin, April 2003 (LM/P086919B)

**SCSE16-9 Rev H: Flight Software Design Specification; External Interface Detailed Design.** Lockheed Martin, April 2003 (LM/P086868H)



# 10

## SQUID Readout Subsystem (SRE) Analysis





The SQUID gyroscope readout system is used for measuring the spin axis orientation of the Gravity Probe B (GP-B) gyroscopes to a precision of 1 milliarcsecond ( $3 \times 10^{-7}$  degrees) in 10 hours of integration time. The cryogenic portion of the readout system uses a dc SQUID to measure the gyroscope's London magnetic moment. Room temperature electronics appropriately bias the dc SQUID allowing the detection and amplification of the gyroscope signal. We describe the system hardware including improved electronics and packaging. We present payload test and flight performance data.

## 10.1 Introduction

The GP-B experiment requires a determination of the gyroscope precession rate with an error of less than 0.3 milli-arcsec/yr. The readout system provides this function. The basis of the readout system is as follows: The spinning gyro rotor generates a magnetic dipole, known as the London moment, which is perfectly co-aligned with the spin axis of the rotor. Any change in the orientation of the spin axis causes a change in the orientation of the London moment. A pickup loop, placed in very close proximity to the rotor, intercepts this changing London moment. A superconductive signal cable connects the pickup loop to a dc SQUID (Superconducting Quantum Interference Device). Since the magnetic flux threading the pickup loop is conserved, a current is generated when the London moment changes orientation. Also, because the pickup loop is tied to the spacecraft body, all of the gyroscope spin axis orientation information is upconverted to the spacecraft's roll frequency. Using a conventional, flux-locked loop configuration, the SQUID detects and amplifies the current signal.

The coupling between the gyroscope and SQUID is (Lockhart, 1986):

$$\text{SQUID\_FLUX} = \frac{M \cdot N^* \cdot B_L \pi r^2 \sin(\theta)}{L_T}$$

**Equation 10-1**

where  $M$  is the mutual inductance between the SQUID and its input coil,  $N^*$  is the effective number of turns in the pickup loop,  $B_L$  is the equivalent magnetic field associated with the London moment,  $r$  is the radius of the rotor,  $\theta$  is the angle formed by the gyroscope's spin axis and the pickup loop and  $L_T$  is the sum of the pickup loop inductance, SQUID input coil inductance and any stray inductance. For the GP-B configuration, the gyroscope spin axis lies nearly in the plane of the pickup loop and  $\sin(\theta)$  can be approximated by  $\theta$ , yielding a simple, linear relationship between gyroscope angle and SQUID flux.

Readout noise is a significant component of the total measurement error of the GP-B experiment. Computer simulations (Haupt, 1996) predict that the gyroscope's readout noise must be better than about 0.2 arcsec/ $\sqrt{\text{Hz}}$  or equivalently, a resolution of 1 marcsec in 10 hours of integration time. Using the linear relationship between gyroscope angle and SQUID flux, we can express the gyroscope readout noise as a SQUID magnetic flux noise. Doing so, we find that the SQUID flux noise must be  $\leq 50 \mu\Phi_o/\sqrt{\text{Hz}}$ . This noise performance must be achieved at the roll rate of the spacecraft,  $\geq 5.5 \text{ mHz}$ .

In addition to SQUID noise as described above, readout gain and bias variations contribute to readout error. Spurious bias variations synchronous with the relativistic signals must be limited to 0.1 marcsec or  $20 \text{ n}\Phi_o$  (Haupt, 1996). As discussed below, we have considered various environmental factors which might lead to small biases. We have designed and tested the hardware to ensure that these bias effects are kept adequately small. Gain variations must also be controlled. The initial gyro signal (due to spin axis misalignment) will be of order 10 arcsec. A slow, constant drift in readout gain would mimic a constant drift rate in the gyroscope. We must limit or measure gain variation in the readout system to 1 part in  $10^5$  per year (equivalent to 0.1 marcsec/yr drift

rate uncertainty). Although we have designed and tested the hardware to limit gain drift, we have also implemented a readout calibration system to measure the system's gain, and if necessary, to compensate for gain drift.

The performance attributes of noise, bias stability and gain stability have played a central role in developing the hardware. To achieve adequate performance, several environmental factors must be considered including magnetic and electromagnetic interference, thermal variations, and proton bombardment. As will be discussed in the next section, the hardware has been designed to tolerate these conditions.

## 10.2 Hardware Description

The SQUID carrier lies at the heart of the readout system and contains a Quantum Design dc SQUID die, an output transformer, a thinfilm feedback transformer, blocking resistors, and a resonance damping network. Photolithographically patterned Nb traces allow for superconductive connections. Au-Nb pads located near the SQUID and feedback transformer allow ultrasonic wedge bonds using Pb-In-Au wire. At other locations on the carrier, Cu-Nb pads allow us to solder resistors, a damping network and an output transformer onto the carrier. The resistors isolate the SQUID from cable capacitance. The RC damping network helps to control parasitic interactions between the SQUID and its input coil. Finally, the output transformer matches the output impedance of the SQUID to the input impedance of the room temperature electronics. The SQUID carrier is housed inside a SQUID package. Through use of Ge resistance thermometers, heaters and high thermal conductivity sapphire and niobium construction materials, precision temperature control is possible.

The pickup loop is a thinfilm structure and is fabricated on the parting plane of the gyroscope's housing. A niobium coating, 400 nm thick, is sputtered onto the housing using a dc magnetron system and patterned into a 4 turn loop using photolithographic techniques. The signal cable connects the loop to the SQUID using spring-loaded joints at each end. These joints have been designed to remain loaded during launch and thermal cycling. The signal cable has a solid Nb shield and passes through a 10 nF feedthrough filter to protect the SQUID from EMI.

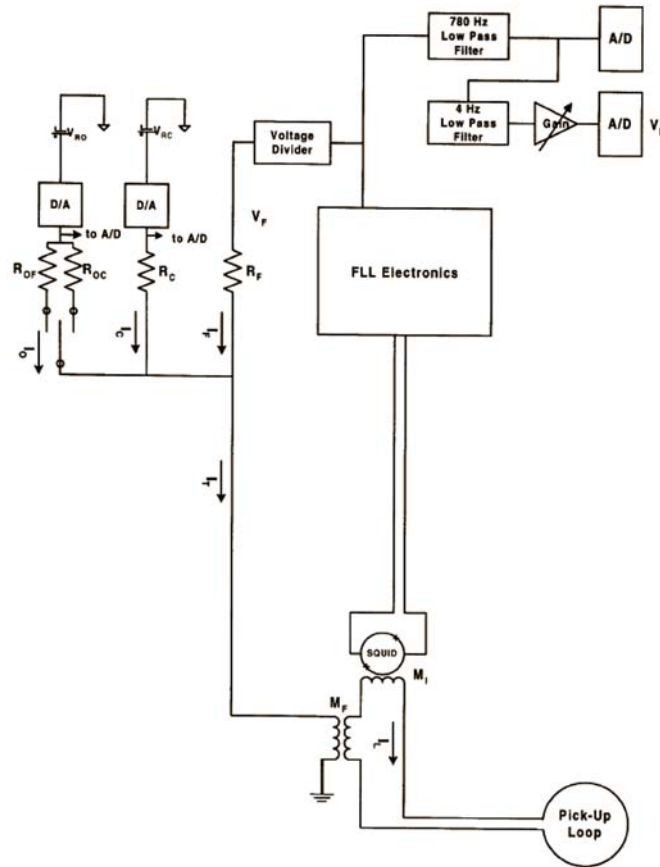


**Figure 10-1.** Gyroscope SQUID Readout System

As illustrated in [Figure 10-1](#) above, changes in magnetic flux through the pick-up loop induce a current ( $I_L$ ) in the superconducting pick-up circuit, which is coupled to the SQUID through the mutual input inductance ( $M_I$ ). The SQUID converts this current to a voltage which is read by the FLL electronics which provide a feedback current ( $I_F$ ) coupled to the pick-up circuit through mutual inductance ( $M_F$ ) in order to null changes in the input current ( $I_L$ ). Offset and calibration currents ( $I_O$  and  $I_C$ ) are also coupled to the input circuit through  $M_F$ . The FLL voltage output provides a measure of the changing flux through the pick-up loop, the low-passed component of which provides measure of the London Moment.

The SQUID is operated in a flux-locked loop using low noise, analog electronics. Four circuits are used with each SQUID to provide flux modulation current (at 420 kHz), dc bias current, feedback current (100 kHz bandwidth), and to receive the SQUID's output voltage. A constant amplitude ac current source is summed into the feedback line to provide a calibration of the system's gain. The feedback current contains the relativity and other information. A signal proportional to this current is filtered, digitized, stored, and ultimately sent to the ground. The electronics are located within a large Forward Equipment Enclosure (FEE) to prevent direct exposure to the sun. The FEE has been designed to passively stabilize the temperature without causing excessive heat build-up. In addition, key electronic components are temperature controlled.

A previous paper (Lockhart, 1986) describes a multi-layered shield design to reduce both dc and ac magnetic fields at the GP-B gyroscope. This shield has been designed to limit the magnetic field trapped in the rotor to a uniform equivalent field of  $\leq 1 \mu\text{G}$ . This shield also attenuates ac magnetic fields, which are coupled into the pickup loop as it passes through the earth's magnetic field, by a factor greater than  $10^{12}$ .

All of the GP-B electronics have been designed to be as quiet as possible to limit the amount of EMI reaching the readout system. The readout system itself is very well shielded; its cables are filtered and are nearly light tight. We have also considered EMI sources external to the experiment. Although the Probe and dewar make an excellent electrostatic shield, a window is provided for the telescope to view the guide star. We reduce the leakage through this window by metalizing it and by using EMI absorbing materials in the telescope's sunshade. Together, these measures provide at least 40 dB of attenuation to 10 GHz.

The payload electronics includes two forward SREs in order to provide readout system redundancy and ensure overall reliability. Figure 10-2 below shows a schematic diagram of the forward SRE units.

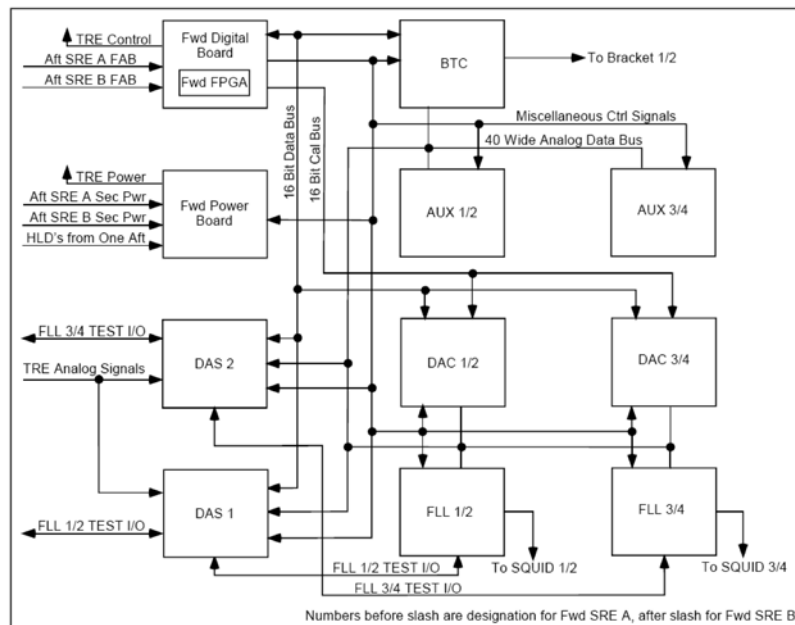


**Figure 10-2.** SQUID Readout Electronics (SRE) – Forward Units

Both forward units are operated simultaneously. FWD SRE A controls the SQUIDs for gyroscopes 1 and 3 and the SQUID bracket temperature control for SQUIDs 1 and 2 while FWD SRE B controls the SQUIDs for gyroscopes 2 and 4 and the SQUID bracket temperature control for SQUIDs 3 and 4. The sub-blocks located with the FWD SRE include; FLL = Flux locked Loop electronics, DAC = Digital to Analog conversion electronics, DAS = Data Acquisition System and BTC = Bracket (SQUID) Temperature Control electronics as well as power management, auxiliary analog test ports and communications blocks. The SRE subsystem also provides power, digital communications and digital processing for the Telescope Readout Electronics (TRE).

The payload electronics also includes two AFT SREs (A and B) in order to provide readout system redundancy and ensure overall reliability. Figure 10-3 below provides a schematic diagram of these aft SRE units.

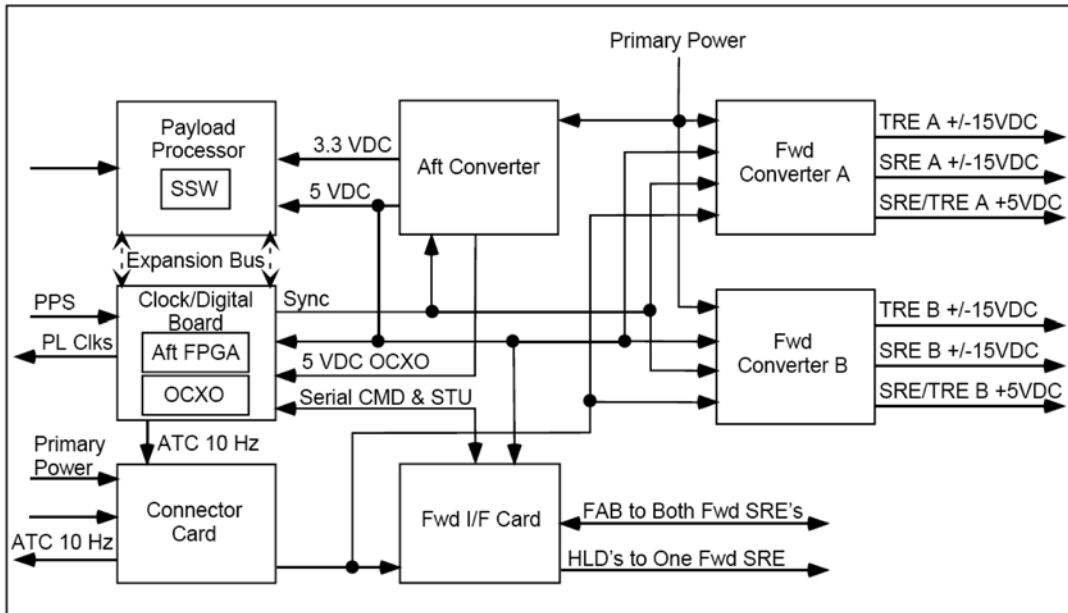


**Figure 10-3.** SQUID Readout Electronics (SRE) – Aft Units

At most one AFT SRE is operated at any one time. The AFT SREs manage power and communications for the forward SRE/TRE units. They also contain a payload processor running software particular to the SRE/TRE and an oven controlled crystal oscillator (OCXO), which provides a single accurate timing to all the payload electronics.

Figure 10-4 below contains a diagram of the SRE sub-system architecture.

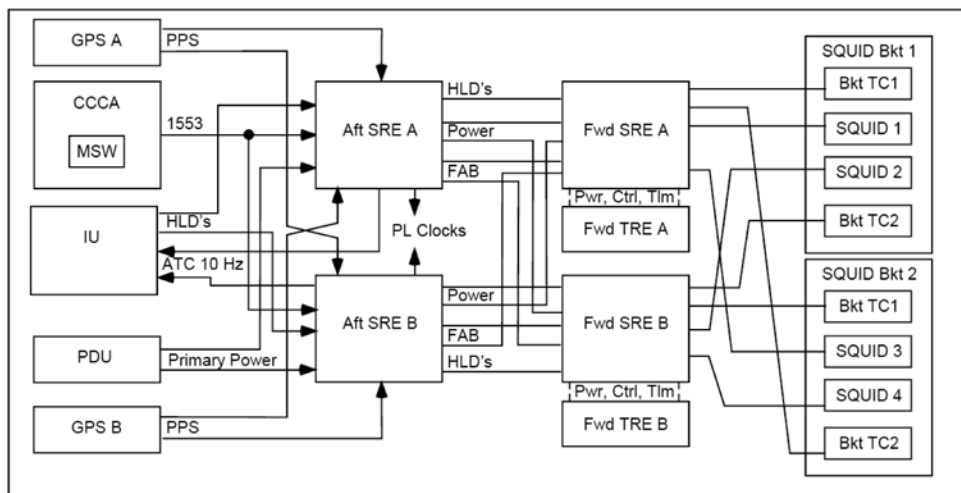


**Figure 10-4.** SQUID Readout Electronics (SRE) – Sub-system Architecture

The cross-strapping shown in Figure 10-4 above provides full redundancy of the AFT electronics and partial redundancy of the forward boxes. In the event of a failure of a single forward SRE, SQUID temperature control (BTC) may be maintained on both remaining SQUIDs using the remaining forward unit.



## 10.3 Pre-Launch Ground-Based Tests

We performed ground-based readout system noise measurements in both isolated, quiescent conditions as well as in the full GP-B payload configuration. Several years ago (Lockhart *et al.*, 1994), we achieved a single-sided SQUID noise of  $30 \mu\Phi_o/\sqrt{\text{Hz}}$  (equivalent to  $120 \text{ marcsec}/\sqrt{\text{Hz}}$ ) at a frequency of 5.5 mHz. The readout noise requirement of  $190 \text{ marcsec}/\sqrt{\text{Hz}}$  (equivalent to  $50 \mu\Phi_o/\sqrt{\text{Hz}}$ ) was met in the full GP-B configuration during payload testing. Improved EMI rejection allowed us to eliminate a lossy SQUID input filter which had been used in earlier tests. Removing this filter reduced SQUID noise and increased gyroscope coupling efficiency. Both of these effects translate into improved readout noise performance. In addition, the SQUID packages were temperature controlled to limit thermally induced drift and the use of normal metal near the pickup loop was limited to minimize Johnson noise.

Ground tests confirmed the coupling between the rotor's London moment and the output of the readout system, thus confirming [Equation 10-1](#). Furthermore, on-orbit environments were simulated to ensure that the readout system would continue to perform adequately. Specifically, we tested the readout system for magnetic and electromagnetic effects, thermal sensitivities, proton induced upsets and nonlinear behaviors.

The earth's magnetic field could couple into the readout system to mimic the science data. There are separate impacts for AC and DC fields. We demonstrated flux trapping in the gyro rotor of less than  $1 \mu\text{G}$  (uniform dc field equivalent). This performance met our needs at dc. Some of our earlier tests had shown that the attenuation of ac magnetic fields was limited by leakage into the SQUID package. In tests of an isolated SQUID package, a Pb-Sn gasket placed between the SQUID package and lid reduced this leakage by a factor of 50 yielding a residual leakage of approximately  $1 \text{ m}\Phi_o/\text{G}$ . An end-to-end readout system ac shielding test demonstrated adequate performance.

[Figure 10-5](#) shows a plot of SQUID noise data obtained during a payload test of the SRE system. The data were collected through the SRE DAS. The sampling rate was 1 Hz but the low pass digital filter was not active. Even without the low pass filter active, SQUIDS 2, 3 and 4 meet spec. SQUID 1 is 20% above spec. Proper filtering brings all SQUIDS into spec (see the third column of data shown directly below the figure).

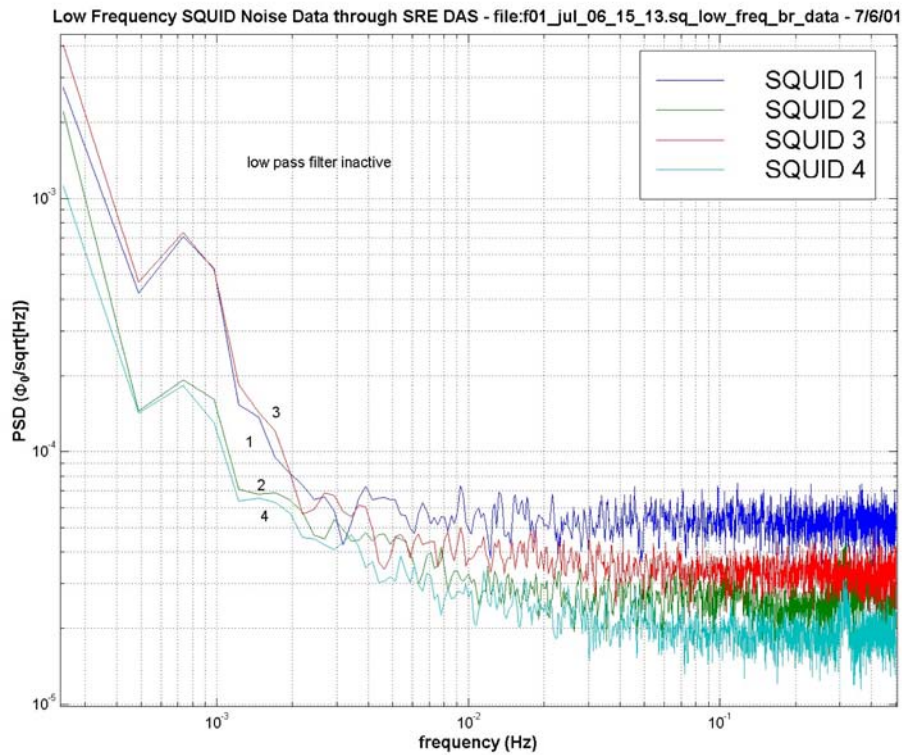


**Figure 10-5.** SQUID Noise Data - Payload Test

**Table 10-1.** Calculations of true noise for each of the four SQUIDs

SQUID	Noise @ 5.55 mHz ( $\mu\Phi_0/\sqrt{\text{Hz}}$ ) <b>measured</b>	White Noise ( $\mu\Phi_0/\sqrt{\text{Hz}}$ ) <b>measured level at 0.5 Hz</b>	Noise at 5.55 mHz ( $\mu\Phi_0/\sqrt{\text{Hz}}$ ) <b>after subtraction of aliased noise</b>
1	56	50	30
2	45	28	37
3	46	33	34
4	36	19	31

To calculate the true noise at 5.55 mHz the excess (aliased) white noise in the data above must be subtracted from the measured noise at 5.55 mHz. The amount of noise to be subtracted from each FFT bin is the noise between the Nyquist sampling frequency (0.5 Hz) and the filter passband frequency (4 Hz). This is 7/8 of the power as measured at 0.5 Hz. After subtraction of this aliased noise all four SQUIDs meet spec.

In [Figure 10-6](#) below, external AC magnetic fields applied to the payload show a response in the SQUIDs at the applied frequency. For reference, the applied field is indicated on the charts in [Figure 10-6](#) at the allowed amplitude at the roll frequency (nominally 5.5 mHz). This amplitude is below the SQUID noise floor at 5.5 mHz so measurements were performed at higher frequencies of 100 mHz and 50 mHz. The SQUID response at these frequencies shows the expected attenuation dependence on frequency and is consistent with meeting the AC shielding requirement at the roll frequency.

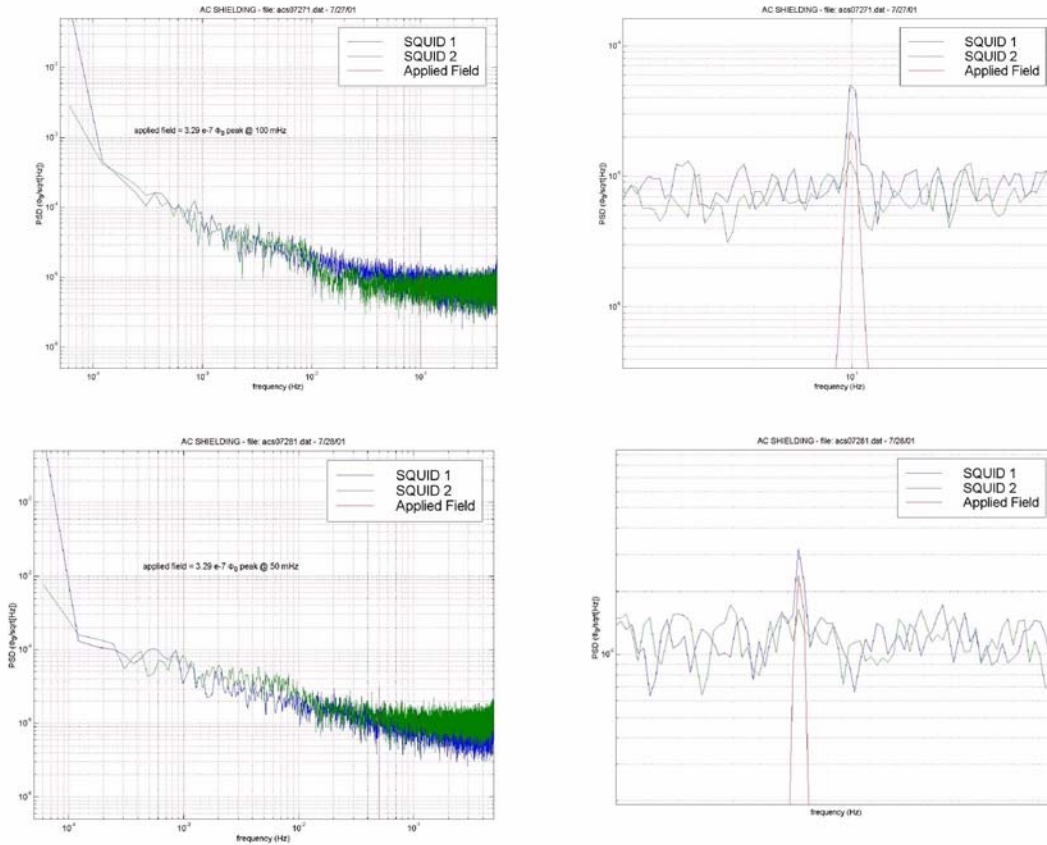


**Figure 10-6.** AC Magnetic Shielding – Payload Test

Thermal fluctuations of both the SQUID and its electronics correlate with bias variations of the readout system; we therefore control the temperature of both. (Thermal fluctuations also correlate with gain fluctuations, but the associated requirements are straightforward to meet). In addition, we minimize the sensitivity of the system to any residual thermal variations. We must limit to  $20 \text{ n}\Phi_0$  the bias variations which mimic the science data. We have measured the thermal sensitivity of isolated SQUIDs and have found a coefficient of approximately  $10 \text{ m}\Phi_0/\text{K}$ . Although we do not fully understand the cause, in some cases the thermal sensitivity of the complete readout system can be as much as  $1 \text{ }\Phi_0/\text{K}$ .

Temporarily raising the temperature of the superconductive signal cable above its transition temperature restores the sensitivity to approximately  $10 \text{ m}\Phi_0/\text{K}$ . Furthermore,  $2 \text{ }\mu\text{K}$  temperature control of the SQUID has been achieved using two nested feedback control loops. In addition, the temperature of the liquid helium bath is regulated and there are various passive control elements. We have measured the electronics sensitivity to thermal fluctuations. We achieved an electronics temperature coefficient of  $50 \text{ }\mu\Phi_0/\text{K}$  during early testing and have reached  $20 \text{ }\mu\Phi_0/\text{K}$  by selecting electronic components with little temperature sensitivity. A  $20 \text{ }\mu\Phi_0/\text{K}$  temperature coefficient implies a  $1 \text{ mK}$  temperature control requirement for the electronics at roll frequency.

For each SQUID, the measured bias temperature coefficient is less than the required  $0.01 \text{ }\Phi_0/\text{K}$ , as shown in [Table 10-2](#) and [Figure 10-7](#) below. The trend in the data taken between  $2.92 \text{ K}$  and  $4.35 \text{ K}$  indicates the bias temp-co will meet specification for all four SQUIDS over the full science range of  $2.7$  to  $3.0 \text{ K}$ .

**Table 10-2.** Measured SQUID bias temperature coefficients

SQUID	Bias Temp-co ( $\Phi_0/K$ )
1	0.00049
2	0.00180
3	0.00089
4	0.00095

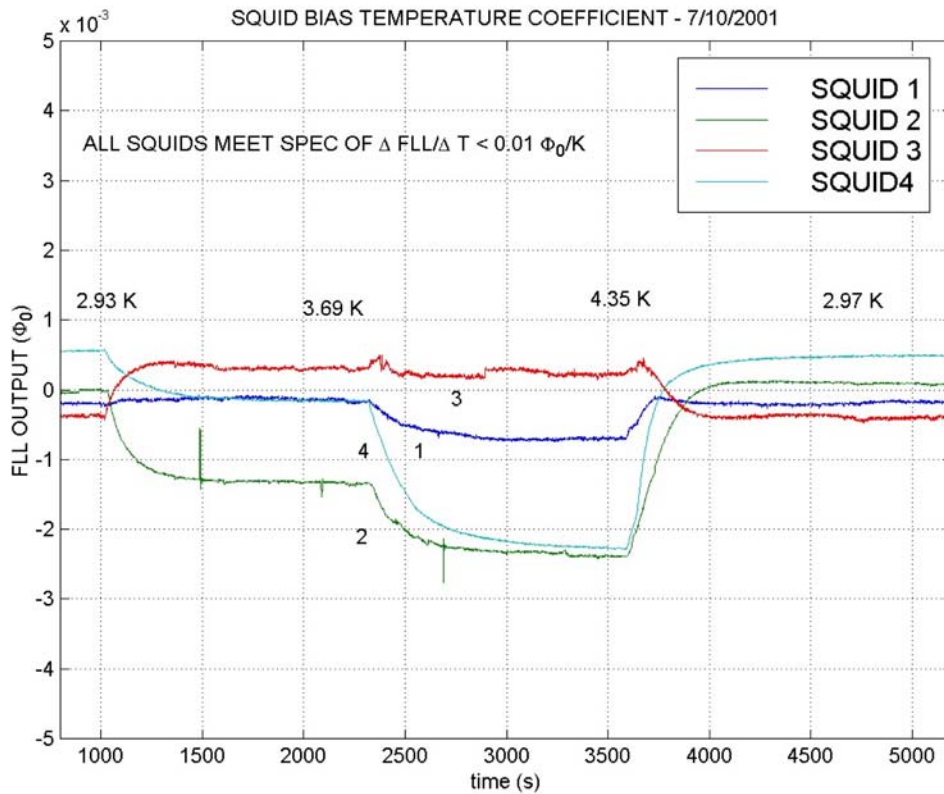


**Figure 10-7.** SQUID Temperature Coefficient – Payload Test

In Figure 10-8 below, the vertical axis scale multiplier is  $\times 10^{-3}$  (overwritten by chart title). No temperature control was used until vehicle time  $2.225 \times 10^4$  s, then coarse mode control until  $2.310 \times 10^4$  s, then fine mode control. The peaking filter was turned on at  $2.440 \times 10^4$  s.

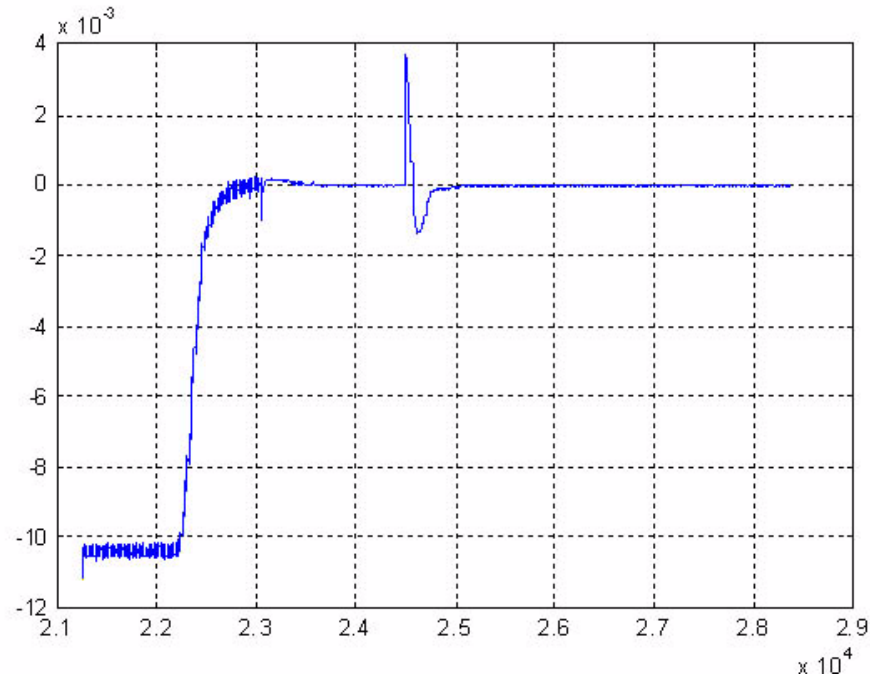


**Figure 10-8.** Temperature Error of SQUID Bracket Temperature Control Test at August 8 2001 18:19-20:19

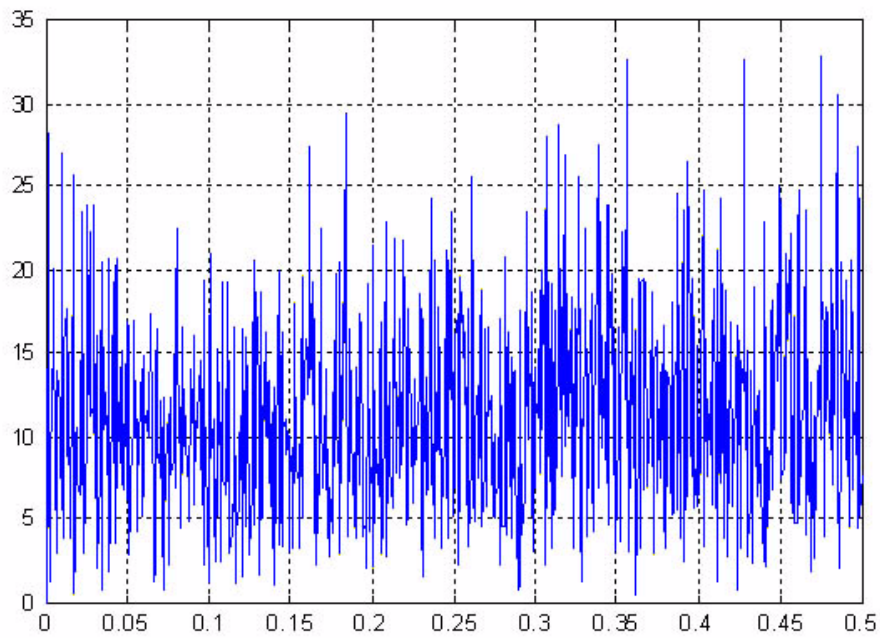


**Figure 10-9.** Square Root of Power Spectrum Magnitude of the Temperature Error

Nonlinear readout behavior can cause biases which mimic the relativity signals. The signal from the gyroscope is detected by the SQUID and since there is finite gain in the electronics, only a portion of this signal is nulled by the feedback electronics. The associated error interacts with the SQUID's nonlinear voltage vs. flux curve and causes the signal to be distorted and aliased to dc. We have analyzed this phenomenon (Gutt *et al.*, 1993) and have achieved adequate readout system performance by requiring and attaining adequately linear SQUID

voltage vs. flux characteristics (less than 1% deviation from a straight line over the expected operating range of  $0.02 \Phi_o$ ) and by requiring and achieving sufficiently high open-loop gain of the electronics (greater than 100 at 1 kHz).

Tests were also performed to evaluate the readout system's performance in the presence of EMI. We divided the EMI into 2 broad frequency ranges: below and above 1 GHz. EMI below 1 GHz was coupled via pickup on cables entering the Probe. We were able to reduce readout EMI sensitivity for these frequencies by implementing a variety of cable upgrades including 2 layers of electrostatic shielding, solid cable shields, and improved cable filters. Signals above 1 GHz were found to pass through the telescope window reaching the Probe interior. Shielding the window significantly reduced high frequency EMI related effects.

On orbit the GP-B spacecraft made repeated passes through the South Atlantic Anomaly (SAA). While in the SAA, as many as  $10^4$  protons/cm<sup>2</sup>/s with energies in excess of 10 MeV passed through the spacecraft. During component level ground testing we bombarded SQUIDS (Muhlfelder *et al.*, 1995) with high energy protons to simulate this environment. The flux-locked loop electronics showed no observable sensitivity to the proton bombardment. Some of the SQUIDS that we tested did show step-like bias shifts. For the SAA situation described above, these shifts corresponded to a few  $m\Phi_o$  every 5 minutes. We analyzed the impact of these bias shifts upon the determination of the relativistic drift rates and found that the predicted bias shifts should not cause significant degradation. We also subjected the SQUIDS and electronics to approximately 10 times the total proton dose we expect for the GP-B mission. Neither was damaged by this exposure.

The as-built GP-B readout system performed to its design specifications during ground testing. Its noise at 5.5 mHz was  $< 0.2$  arcsec/ $\sqrt{\text{Hz}}$ . The SQUID temperature coefficient was  $< 10 m\Phi_o/\text{K}$ , and the SQUID temperature was stabilized to 2  $\mu\text{K}$  at the spacecraft's roll frequency. The temperature coefficient of the electronics was  $< 20 \mu\Phi_o/\text{K}$  and the temperature of the electronics was controlled to 1 mK at roll frequency. The system had undergone thermal, proton, magnetic and EMI testing. Improvements in the SQUID's input filter and improvements in the shielding of the telescope window allowed us to meet the EMI requirement. All of the performance and environmental tests showed that the GP-B readout system met the flight requirements. On-orbit data indicate that the flight performance is similar.

## 10.4 On-Orbit Performance Data

This section summarizes on-orbit performance of the SRE system in terms of SQUID noise, SQUID bracket temperature control, and SRE temperature control.

### 10.4.1 SQUID Noise

Figure 10-10 below shows that SQUID noise data collected shortly after launch and initial system set-up are consistent with pre-launch results. The gyroscopes were electrostatically caged in their housings in order to minimize magnetic flux motion in the input circuit and make a measurement of only the SQUID sensor noise. The green horizontal line indicates the noise requirement at the roll frequency; the red line is a least squares fit to a power law tail. All SQUIDS meet the noise requirement at the roll frequency. The spectra for SQUIDS 2 and 4 also confirm that the ac magnetic shielding meets the requirement at the roll frequency.



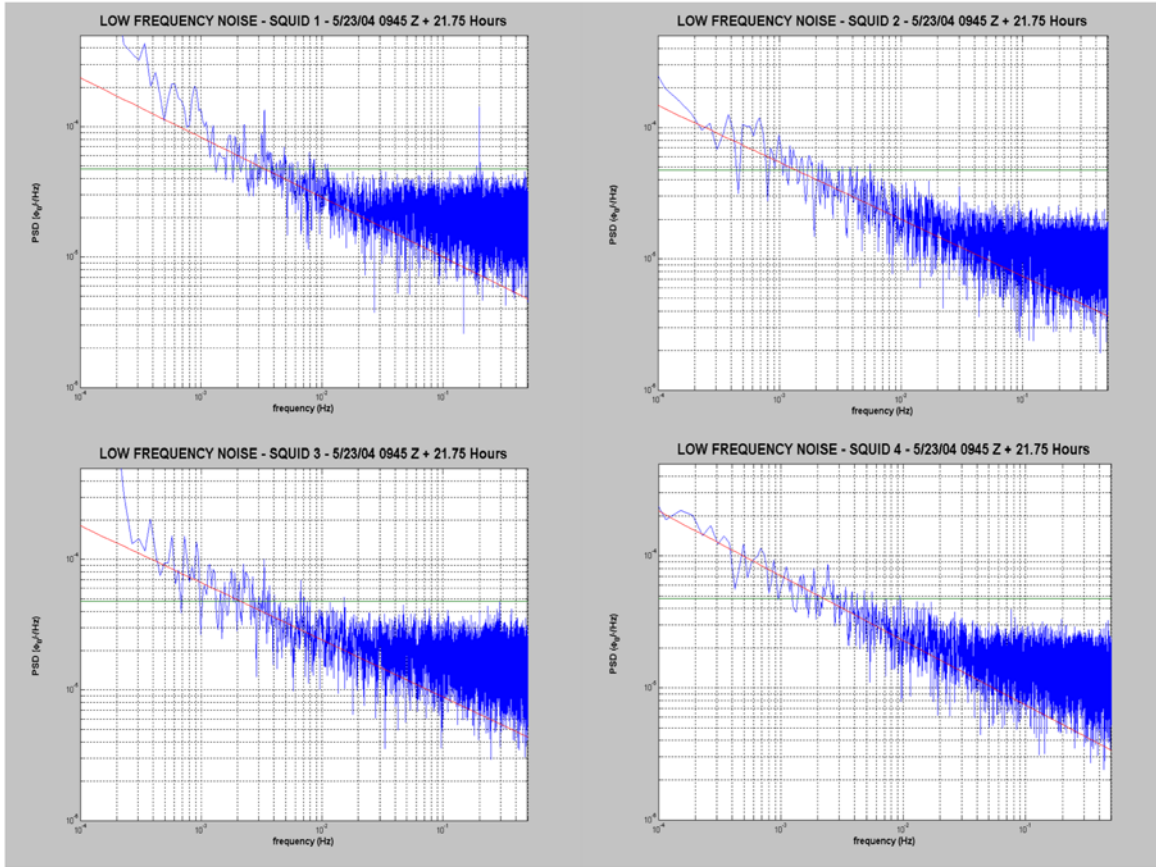


**Figure 10-10.** Quiescent SQUID Noise Data – On Orbit

### 10.4.2 SQUID Bracket Temperature Control

The two charts in [Figure 10-11](#) below show the performance of the SQUID bracket temperature controller on orbit. Using the Bracket Temperature Control algorithm, the SQUID sensor temperature was controlled to 1.6 micro K rms in a 3 mHz band about roll frequency. This is a factor of three below the required value of 5 micro K rms, providing margin in the overall experiment error budget. This performance was achieved without implementing the peaking filter at roll.



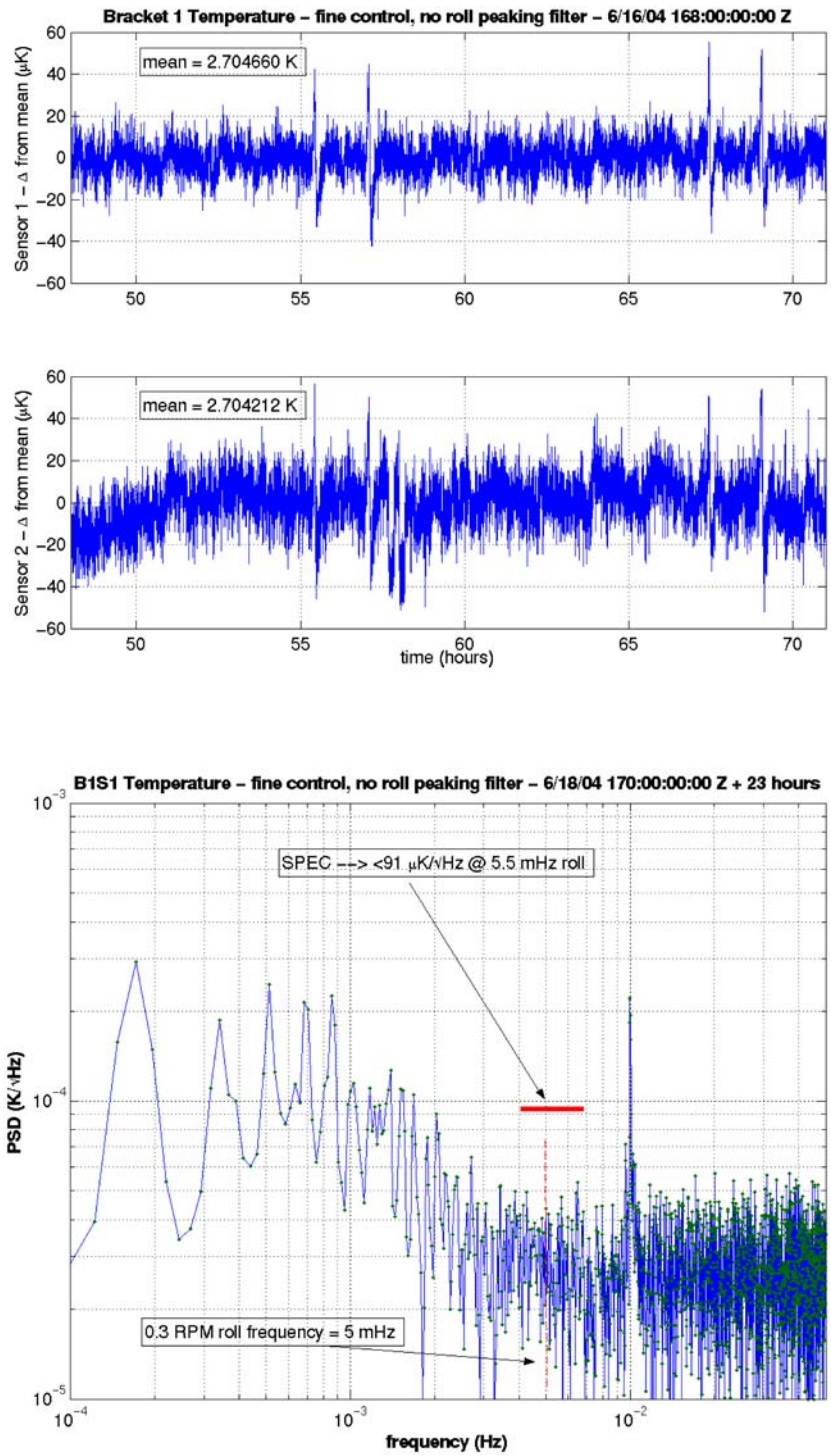


**Figure 10-11.** SQUID Bracket Temperature Control – On-Orbit

Analog control loops on the electronics boards in the forward SREs are optimized to remove thermal disturbances on annual time scales (i.e. bias drifts over the course of the year). There is no active temperature control at higher orbital (1.7 e-4 Hz) and roll (12.9 mHz) frequencies. However, the passive thermal attenuation of the FEE minimizes the thermal disturbances at roll to a few mK rms. Spectra for the FLL boards are shown in Figure 10-12 below. The other boards are similar.

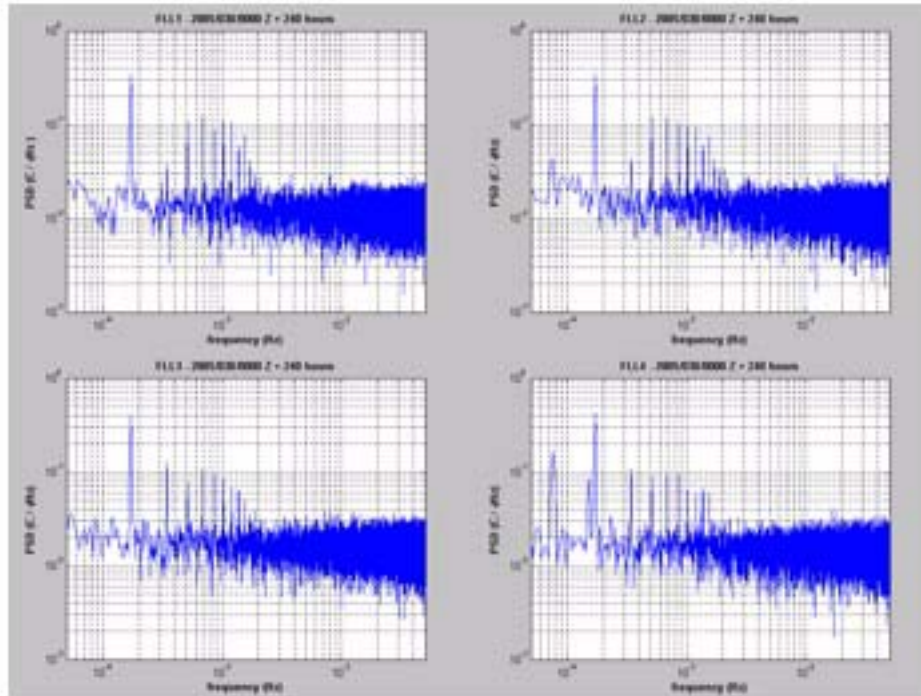


**Figure 10-12.** SQUID Electronics Temperature Control – On-Orbit

### 10.4.3 SRE Temperature Control Performance

The three tables below summarize the SRE temperature performance on orbit. The measured thermal stability at roll combined with the measured on-orbit bias temperature coefficients gives the bias contributions due to temperature fluctuations at roll. The measured amplitudes of the thermal disturbances are as expected pre-launch. The temperature coefficients of the electronics are a factor of 10 larger than expected, while the SQUID sensor temperature coefficients (BKT) are a factor of 10 smaller, keeping the end-to-end contribution as specified. Further study of the on-orbit temperature coefficient measurement data may be required.

**Table 10-3.** Thermal Power Density at Roll (C/(Hz))— Worst case estimate

	FLL	DAC	DAS	BKT_ELEC	BKT
<b>SQUID 1</b>	0.02	0.02	0.04	0.02	0.00030
<b>SQUID 2</b>	0.02	0.02	0.04	0.02	0.00030
<b>SQUID 3</b>	0.02	0.04	0.05	0.02	0.00030
<b>SQUID 4</b>	0.02	0.03	0.05	0.02	0.00030

**Table 10-4.** RMS Temperature Variations in 3 mHz Band About Roll (C)— Worst case estimate

	FLL	DAC	DAS	BKT_ELEC	BKT
<b>SQUID 1</b>	0.00155	0.00155	0.00310	0.00155	0.0000023
<b>SQUID 2</b>	0.00155	0.00155	0.00310	0.00155	0.0000023
<b>SQUID 3</b>	0.00155	0.00310	0.00387	0.00155	0.0000023
<b>SQUID 4</b>	0.00155	0.00232	0.00387	0.00155	0.0000023

**Table 10-5.** RE Bias Temperature Coefficients

Per A001 (Heifetz, Silbergliet) - May 2004					
R1G1 equivalents (mV/K)					
	FLL	DAC	DAS	BKT_ELEC	BKT
<b>SQUID 1</b>	0.47	0.25	1.30	0.0158	3.11
<b>std. error</b>	0.20	0.09	0.08	0.0066	0.06
<b>SQUID 2</b>	0.39	0.28	1.40	no data	8.02
<b>std. error</b>	0.14	0.18	0.04	no data	0.12
<b>SQUID 3</b>	1.50	0.05	0.94	no data	4.23
<b>std. error</b>	0.24	0.22	0.27	no data	0.08
<b>SQUID 4</b>	2.12	1.59	0.71	0.0125	9.71
<b>std. error</b>	0.32	0.32	0.15	0.0155	0.15
		=RANGE 2			=GAIN 6
		=GAIN 5			

## 10.5 SRE Software

The SQUID and Science Telescope Software (SSW) residing in the RAD6000-based processor performs the instrument control functions and telemetry processing required to operate the SQUID electronics instrumentation in the forward SRE boxes as well as the Telescope Readout Electronics (TRE) subsystem. The code is written in ADA and runs in the processor on a VxWorks real time operating system.

The code image is 750 KB; with data storage and scratchpad space, the code occupied about 79% of the 3 MB static RAM aboard the RAD6000 processor.

The primary functions performed by the SSW are:

1. Handshake interface with MSS
2. Command router sends commands to applications
3. SQUID and science telescope science and ATC data processing
4. Commands to SQUID and ST
5. Raw / processed telemetry from SQUID / ST
6. Payload Processor checks and memory scrub

The science support applications running on the processor include:

1. **SQUID signal FFT (SQ01).** The fftnd package calculates the SQUID fft in normal and decimated modes. It receives data from the fwd\_sre package and prepares data for the PIT.
2. **Science lowpass filter (SQ02).** A digital lowpass filter which operates on the output of the 20 Hz analog low pass filter, sampled at 2200 Hz and produces a filtered, decimated 5 Hz rate value for transmission to the ground.
3. **Squid\_Calibration (SQ04).** This application is a 10 Hz process whose purpose is the computation of the bias, amplitude and phase of reference calibration signals
4. **Sq\_Bracket\_Temp\_Ctrl (SQ05).** This application is a 10 Hz process which uses closed loop control to heat the two SQUID brackets to a target temperature specified in a database
5. **Slope\_Est. Slope\_Est (ST02).** This application performs a sanity check on the science telescope 2.2 kHz data and calculates the ATC slope fit.
6. **St\_Eng\_Data\_Filter (ST01).** This application is a 10 Hz process that gathers various TRE hardware housekeeping data and places it in telemetry. Values are updated every 2 seconds.
7. **Estimation of slope for science telescope (ST03,04).** This application is a 10 Hz process which computes estimates of the slope and intercept of the photo diode charging that is used to point the telescope to the guide star
8. **Tre\_Temp\_Control (ST05).** TRE Digital Temperature Control. This algorithm uses PID to keep the DMA temperature constant at a given setpoint (nominally 72 K)
9. **Snapshot Processing (ST07, SQ06).** These applications provide the capability to collect and transmit raw SQUID and ST data to the CCCA for deferred transmission to the ground.
10. **GPBPP Checks.** The purpose of this processing is to report hardware and software errors that occur in the payload processor. The following types of errors are covered: Un-handled application exceptions, Processing rate time-outs, CCCA 1 Hz sync failure, MIL-STD-1553 bus errors, processor expansion bus (EBI) errors, Memory errors

During testing, it was found that the processor was loaded to 90+% of its capacity with all science applications enabled and running. To mitigate this load, a set of applications were turned on or off at the Guide Star Valid/invalid transition points. A measure of the processor loading with this schedule in place is given in [Table 10-6](#). [Table 10-7](#) lists the source lines of code (SLOC) for the various applications; 16,341 lines of ADA code were required to implement the SQUID and Science Telescope processing required by GP-B.

**Table 10-6.** Processor utilization and activation schedule for SQUID/Science telescope applications during Guide Start Valid and Invalid

<b>SQUID/ST Flight Software: Standard Science scenarios</b>	<b>Guide star valid</b>	<b>Guide star invalid</b>
ATC 10Hz processing	36%	32%
Science 10Hz processing	84%	83%
Science 1Hz processing	10%	60%
Overall CPU usage (includes 5% for memory scrub)	59%	64%
<b>Application status</b>		
Data validation	None	None
SQUID & ST commanding	Enabled	Enabled
Science_Lowpass_Filter (SQ02)	X	X

**Table 10-6.** Processor utilization and activation schedule for SQUID/Science telescope applications during Guide Start Valid and Invalid

<b>SQUID/ST Flight Software: Standard Science scenarios</b>	<b>Guide star valid</b>	<b>Guide star invalid</b>
SQ_Bracket_Temp_Ctrl (SQ05)	X	X
TRE_Temp_Control (ST05)	X	X
ST_Snapshot (ST07): mode 6	X	
SQUID snapshot (SQ06)		X
SQUID_Calibration (SQ04)	X	
ST_Eng_Data_Filter (ST01)	X	X
Science_Slope (ST02)	X	
Slope_Est (ST03, ST04), w/ sanity checks	X	X
FFTs (SQ01): normal mode		X
<b>Notes:</b>		
<ol style="list-style-type: none"> <li>1. ST DMA balance is only used before spin-up and does not impact science mode usage. When it is being used, the CPU usage is no worse than shown above</li> <li>2. Includes 5% worst-case estimate for SQUID bracket temperature controller</li> <li>3. Includes 4% worst-case estimate for SQUID bracket temperature controller</li> <li>4. The worst-case scenario CPU usage before and during spin-up is no worse than shown above.</li> <li>5. The individual processing rates are shown because they need to finish within their time allotment, in addition to the overall CPU usage requirement. ATC usage percentage is based on 25ms available and Science usage percentage is based on 75ms available</li> <li>6. SQUID snapshot is not shown because ST snapshot is higher CPU usage, and only one type is commanded active at a time.</li> </ol>		

**Table 10-7.** SSW application source lines of code (SLOC) metrics

<b>Level 1</b>	<b>Level 2</b>	<b>Level 3</b>	<b>Level 4</b>	<b>Req ID</b>	<b>Unit source filename</b>	<b>SLOC</b>	<b>Memory size</b>
Mission Support SW				MSS			
	Data Mgmt Processing			DMP			
		Telemetry Processing		TMP			
			Application DB Readout	ADB	database_dump.1.ada	31	64
			Application DB Readout	ADB	database_dump.2.ada	86	4600
		Mathematical Functions		MFU	generic_utilities.1.ada	124	
		Mathematical Functions		MFU	generic_utilities.2.ada	162	
		Mathematical Functions		MFU	gnc.1.ada	63	

**Table 10-7.** SSW application source lines of code (SLOC) metrics

Level 1	Level 2	Level 3	Level 4	Req ID	Unit source filename	SLOC	Memory size
		Mathematical Functions		MFU	gnc.2.ada	97	
		Mathematical Functions		MFU	utility.1.ada	75	
		Mathematical Functions		MFU	utility.2.ada	122	
Operating System SW							288244
SQUID/ST Support SW				SSW	build_version.1.ada	4	
SQUID/ST Support SW				SSW	debug_io.1.ada	81	
SQUID/ST Support SW				SSW	debug_io.2.ada	74	
SQUID/ST Support SW				SSW	flt_io.1.ada	3	
SQUID/ST Support SW				SSW	generic_datatypes.1.ada	100	200
SQUID/ST Support SW				SSW	generic_datatypes.2.ada	99	376
SQUID/ST Support SW				SSW	int_io.1.ada	3	128
SQUID/ST Support SW				SSW	short_int_io.1.ada	5	
SQUID/ST Support SW				SSW	squid.1.ada	128	
SQUID/ST Support SW				SSW	sre.1.ada	188	448
SQUID/ST Support SW				SSW	sre_utilities.1.ada	96	
SQUID/ST Support SW				SSW	sre_utilities.2.ada	73	1828
SQUID/ST Support SW				SSW	time_io.1.ada	8	24
SQUID/ST Support SW				SSW	time_io.2.ada	14	144
SQUID/ST Support SW				SSW	tre.1.ada	68	232
SQUID/ST Support SW				SSW	tre.2.ada	42	328
	Scheduler			SHS	ccca_status.1.ada	17	168
	Scheduler			SHS	ccca_status.2.ada	19	308
	Scheduler			SHS	ccsds_time.1.ada	71	
	Scheduler			SHS	ccsds_time.2.ada	195	352

**Table 10-7.** SSW application source lines of code (SLOC) metrics

Level 1	Level 2	Level 3	Level 4	Req ID	Unit source filename	SLOC	Memory size
	Scheduler			SHS	ebi_interrupts.1.ada	10	24
	Scheduler			SHS	ebi_interrupts.2.ada	54	1056
	Scheduler			SHS	event_trace.1.ada	9	24
	Scheduler			SHS	event_trace.2.ada	17	1308
	Scheduler			SHS	p10hz_atc.2.ada	48	1608
	Scheduler			SHS	p10hz_science_1.2.ada	28	1176
	Scheduler			SHS	p10hz_science_2.2.ada	104	3360
	Scheduler			SHS	p10hz_science_3.2.ada	20	848
	Scheduler			SHS	p1hz_science.2.ada	48	1496
	Scheduler			SHS	processor.1.ada	9	24
	Scheduler			SHS	processor.2.ada	33	1280
	Scheduler			SHS	scheduler.1.ada	4	24
	Scheduler			SHS	scheduler.2.ada	180	3948
	Scheduler			SHS	ssw.2.ada	19	764
	Scheduler			SHS	ssw_status.1.ada	14	48
	Scheduler			SHS	ssw_status.2.ada	3	
	Scheduler			SHS	task_priorities.1.ada	7	
	GPBPP Initializatio n			SIN	initialize_ssw.2.ada	3	48
	GPBPP Initializatio n			SIN	initialize_mailboxes.2.ada	50	576
	GPBPP Data Mgmt			SDM			
		SQUID/ST Command Router		SCR	ccca_pit.1.ada	86	112
		SQUID/ST Command Router		SCR	command_class.1.ada	210	1368
		SQUID/ST Command Router		SCR	command_class.2.ada	434	10148
		SQUID/ST Command Router		SCR	command_envelope_class.1.ada	32	268
		SQUID/ST Command Router		SCR	command_envelope_class.2.ada	23	



**Table 10-7.** SSW application source lines of code (SLOC) metrics

Level 1	Level 2	Level 3	Level 4	Req ID	Unit source filename	SLOC	Memory size
		SQUID/ST Command Router		SCR	command_router.1.ad a	20	40
		SQUID/ST Command Router		SCR	command_router.2.ad a	96	3040
		SQUID/ST Command Router		SCR	payload_command_d ataset.1.ada	24	176
		SQUID/ST Command Router		SCR	payload_command_d ataset.2.ada	226	7608
		SQUID/ST Command Router		SCR	sw_mailbox_class.1.ad a	64	104
		SQUID/ST Command Router		SCR	sw_mailbox_class.2.ad a	182	6592
	GPBPP I/O Processing			SIO	bicpfns.1.ada	61	48
	GPBPP I/O Processing			SIO	bus_1553_device_driv er_interface.1.ada	209	
	GPBPP I/O Processing			SIO	ebifns.1.ada	30	
	GPBPP I/O Processing			SIO	rscfns.1.ada	55	
		SQUID/ST 1553 Interface		SIF	payload.1.ada	113	1184
		SQUID/ST 1553 Interface		SIF	payload_message.1.ad a	13	152
		SQUID/ST 1553 Interface		SIF	payload_message.2.ad a	44	4104
		SQUID/ST 1553 Interface		SIF	payload_message_tra nsfer.1.ada	13	72
		SQUID/ST 1553 Interface		SIF	payload_message_tra nsfer.2.ada	112	3212
		SQUID/ST 1553 Interface		SIF	read_packets.2.ada	30	1056
		SQUID/ST 1553 Interface		SIF	sre_pit_constructor.1.a da	8	24

**Table 10-7.** SSW application source lines of code (SLOC) metrics

Level 1	Level 2	Level 3	Level 4	Req ID	Unit source filename	SLOC	Memory size
		SQUID/ST 1553 Interface		SIF	sre_pit_constructor.2.ada	671	34344
		SQUID/ST 1553 Interface		SIF	sre_pit_format.1.ada	402	
		SQUID/ST Expansion Bus I/F		SSB	ebi.1.ada	81	160
		SQUID/ST Expansion Bus I/F		SSB	ebi.2.ada	65	1388
		SQUID/ST Expansion Bus I/F		SSB	engr_data.1.ada	34	312
		SQUID/ST Expansion Bus I/F		SSB	engr_data.2.ada	60	672
		SQUID/ST Expansion Bus I/F		SSB	fab_command_block.1.ada	108	400
		SQUID/ST Expansion Bus I/F		SSB	fab_command_block.2.ada	282	8308
		SQUID/ST Expansion Bus I/F		SSB	fwd_sre.1.ada	115	88
		SQUID/ST Expansion Bus I/F		SSB	fwd_sre.2.ada	319	30104
		SQUID/ST Expansion Bus I/F		SSB	fwd_sre_mux.1.ada	8	
		SQUID/ST Expansion Bus I/F		SSB	science_telescope_command.1.ada	138	84
		SQUID/ST Expansion Bus I/F		SSB	science_telescope_command.2.ada	547	23748
		SQUID/ST Expansion Bus I/F		SSB	send_fab_commands.2.ada	18	568
		SQUID/ST Expansion Bus I/F		SSB	squid_cmd.1.ada	243	80
		SQUID/ST Expansion Bus I/F		SSB	squid_cmd.2.ada	950	38940

**Table 10-7.** SSW application source lines of code (SLOC) metrics

Level 1	Level 2	Level 3	Level 4	Req ID	Unit source filename	SLOC	Memory size
		SQUID/ST Expansion Bus I/F		SSB	squid_test_data.1.ada	15	72160
		SQUID/ST Expansion Bus I/F		SSB	squid_test_data.2.ada	39	1912
		SQUID/ST Expansion Bus I/F		SSB	st_test_data.1.ada	10	3520
		SQUID/ST Expansion Bus I/F		SSB	st_test_data.2.ada	19	1080
		SQUID/ST Expansion Bus I/F		SSB	squid_science_data.1.ada	36	48
		SQUID/ST Expansion Bus I/F		SSB	squid_science_data.2.ada	239	136232
	Checks			SCK			
		GPBPP Checks		SGC	memory_scrub.1.ada	12	24
		GPBPP Checks		SGC	memory_scrub.2.ada	19	160
		GPBPP Checks		SGC	scrubfns.1.ada	33	
	SQUID Support Processing			SQS	dedicated_squid_cmd.1.ada	2	
	SQUID Support Processing			SQS	dedicated_squid_cmd.2.ada	211	4584
		SQUID ATC Processing		SQA	squid_atc.1.ada	43	256
		SQUID ATC Processing		SQA	squid_atc.2.ada	221	9468
		SQUID Snapshot Processing		SQT	squid_snapshot.1.ada	105	9112
		SQUID Snapshot Processing		SQT	squid_snapshot.2.ada	166	7536
		Science Lowpass Filter		SFP	science_lowpass_filter.1.ada	76	35264
		Science Lowpass Filter		SFP	science_lowpass_filter.2.ada	492	142924

**Table 10-7.** SSW application source lines of code (SLOC) metrics

Level 1	Level 2	Level 3	Level 4	Req ID	Unit source filename	SLOC	Memory size
		SQUID FFT Processing		FFT	fft1.1.ada	2	80932
		SQUID FFT Processing		FFT	fft2.1.ada	2	80996
		SQUID FFT Processing		FFT	fft3.1.ada	2	80996
		SQUID FFT Processing		FFT	fft4.1.ada	2	80996
		SQUID FFT Processing		FFT	fft_utilities.1.ada	17	
		SQUID FFT Processing		FFT	fft_utilities.2.ada	3	
		SQUID FFT Processing		FFT	fftad.1.ada	97	147664
		SQUID FFT Processing		FFT	fftad.2.ada	105	6136
		SQUID FFT Processing		FFT	fftnd.1.ada	108	
		SQUID FFT Processing		FFT	fftnd.2.ada	396	
		SQUID Cal Signal		SCF	squid_calibration.1.ada	60	104
		SQUID Cal Signal		SCF	squid_calibration.2.ada	266	228648
		SQUID Digital Bracket Temp Control		SBT	sq_bracket_temp_ctrl.1.ada	79	2048
		SQUID Digital Bracket Temp Control		SBT	sq_bracket_temp_ctrl.2.ada	1262	62244
	ST Support Processing			STS			
		ST ATC Processing		STC	slope_est.1.ada	96	136
		ST ATC Processing		STC	slope_est.2.ada	427	13732
		ST Snapshot Processing		STT	st_snapshot.1.ada	152	8024
		ST Snapshot Processing		STT	st_snapshot.2.ada	413	11020
		ST Sanity Check		SSC			
		ST Engineering Data Filter Processing		EDF	st_eng_data_filter.1.ada	228	456

**Table 10-7.** SSW application source lines of code (SLOC) metrics

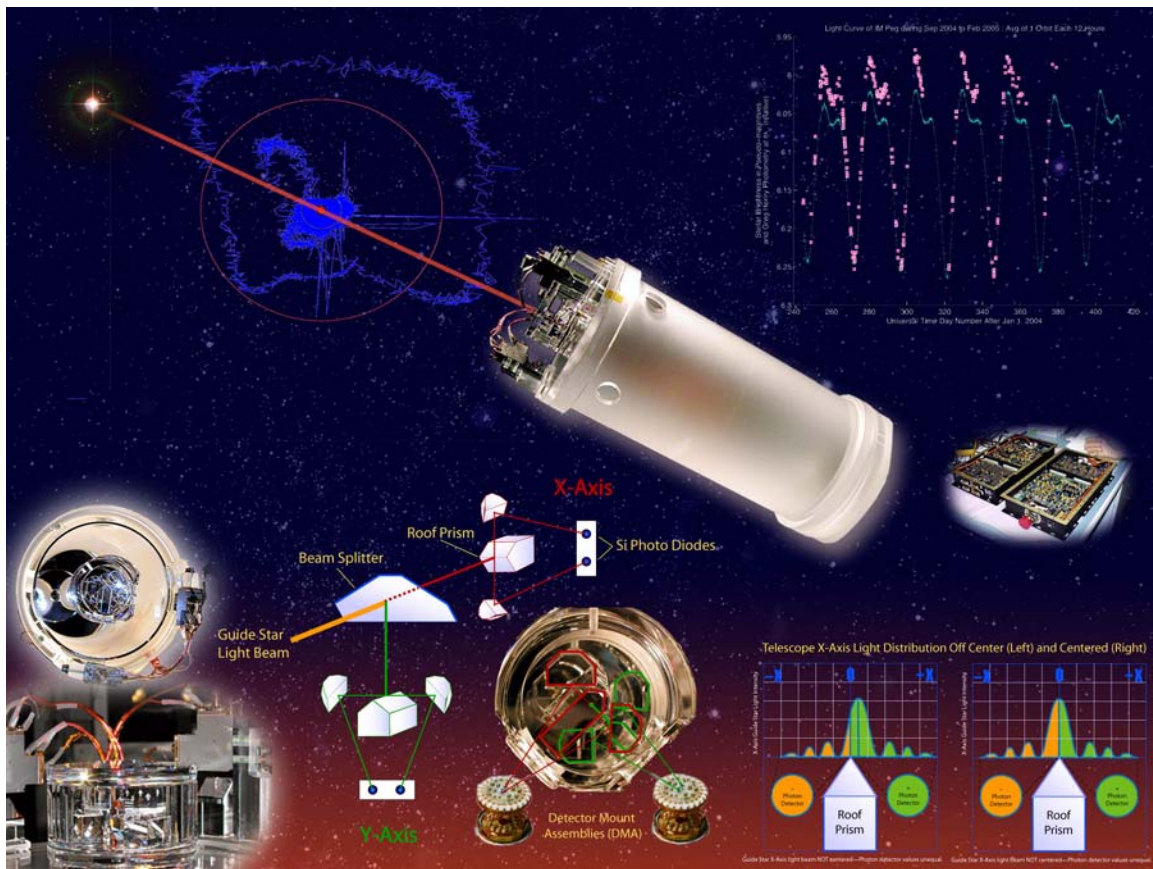
Level 1	Level 2	Level 3	Level 4	Req ID	Unit source filename	SLOC	Memory size
		ST Engineering Data Filter Processing		EDF	st_eng_data_filter.2.ad a	297	6552
		Science Slope Processing		SSL	science_slope.1.ada	154	21152
		Science Slope Processing		SSL	science_slope.2.ada	715	49948
		ST Digital Temp Control		SDC	tre_temp_control.1.ad a	45	672
		ST Digital Temp Control		SDC	tre_temp_control.2.ad a	291	14772
		ST DMA Balancing		SDB	dma_balancing_interf ace.1.ada	14	
		ST DMA Balancing		SDB	dma_balancing_interf ace.2.ada	91	512
		ST DMA Balancing		SDB	st_dma_balance.1.ada	23	32
		ST DMA Balancing		SDB	st_dma_balance.2.ada	422	30816
<b>Total SLOC</b>						16341	

## 10.6 References

- Gutt, G.M., N.J. Kasdin, M.R. Condrón II, B. Muhlfelder, and J.M. Lockhart, **A Method for Simulating a Flux-Locked DC SQUID**, *IEEE Trans. Superconductivity*, 3, 1837 (1993).
- Haupt, G. T., **Development and Experimental Verification of a Nonlinear Data Reduction Algorithm for the Gravity Probe B Relativity Mission**, Ph.D. Thesis, Stanford University (1996).
- Lockhart, J.M., **SQUID Readout and Ultra-low Magnetic Fields for Gravity Probe-B (GP-B)**, *SPIE*, 619, 148 (1986).
- Lockhart, J.M., D.N. Hipkins, G.M. Gutt, B. Muhlfelder, and N. Jennerjohn, **Comparative Study of Bias-Reversing Schemes for Low Frequency Noise Reduction in dc SQUIDs**, *Physica B*, 194, 89 (1994).
- Muhlfelder, B., G.M. Gutt, J.M. Lockhart, P. Carelli, A. Zehnder, *et al.*, **Effect of High Energy Proton Bombardment (50-280 MeV) on dc SQUIDs**, *IEEE Trans. Superconductivity*, 5, 3252 (1995)

# 11

## Telescope Readout Subsystem (TRE) Analysis







## 11.1 Telescope Readout Electronics Report Summary

Here we provide a brief overview of the telescope pointing readout system. The science telescope and the 4 probe windows constitute the sensor for pointing of the science metrology reference, and the telescope readout electronics (TRE) provide the readout for the telescope.

The light from the guide star passes through the 4 probe windows, which to first order does not disturb the wavefront of this light. The telescope brings the light to a focus on two roof prisms, one for each rotation axis (X and Y). When the telescope is directly pointed at the guide star the intensities of light that are reflected off of each side of the roof prisms are equal (after compensation by weighting factors). When the intensities are not equal, their normalized difference is a measure of the pointing of the telescope with respect to the guide star.

The telescope readout electronics measures the light reflected from each side of the roof prisms. The light from the two sides of a roof prism is transported to two pairs of photo detectors, a primary pair (A-side electronics) and a redundant pair (B-side electronics). Each photodetector pair is located on a sapphire platform with their JFET pre-amplifiers. The platforms are mounted on a thermal standoff on the front plate of the telescope (at about 3 K) so the platforms can be operated at 72 K, where the JFET pre-amplifiers work well. The platforms are temperature controlled. There are a total of 4 detector pairs (8 detectors) located on 4 platforms.

The TRE measures the current of each photo detector with a charge-locked loop using a feedback capacitor to the photo detector. The voltage across the feedback capacitor is read out after appropriate scaling by an analog-to-digital converter with a range from +10 V to -10 V at a rate of 2200 samples/second, and it is quickly reset every 0.1 s. This provides 220 A to D samples for each charge ramp. Only the even samples between 22 and 220 of the ramp are used to determine the science slope (photo detector current after appropriate scaling). The first few samples are ignored to avoid the transient associated with the reset, and only the even samples are used to reduce the on-orbit computation time for the slope. Little information is lost in using only the even samples since adjacent samples have a moderate degree of correlation.

The diagram shown in [Figure 11-1](#) indicates the relationship of the TRE and portions of the SQUID Readout Electronics (SRE) which provides power and control information to the TRE and digital-to-analog conversion, data handling, and signal processing for the TRE output signals. The four channels of the TRE are very independent of each other, with four identical sets of circuit boards that are housed in two boxes in intimate contact with a corresponding SRE forward unit. There are two identical aft SRE units, but one is always powered off while the other is active, so the unused unit is not shown in the diagram.

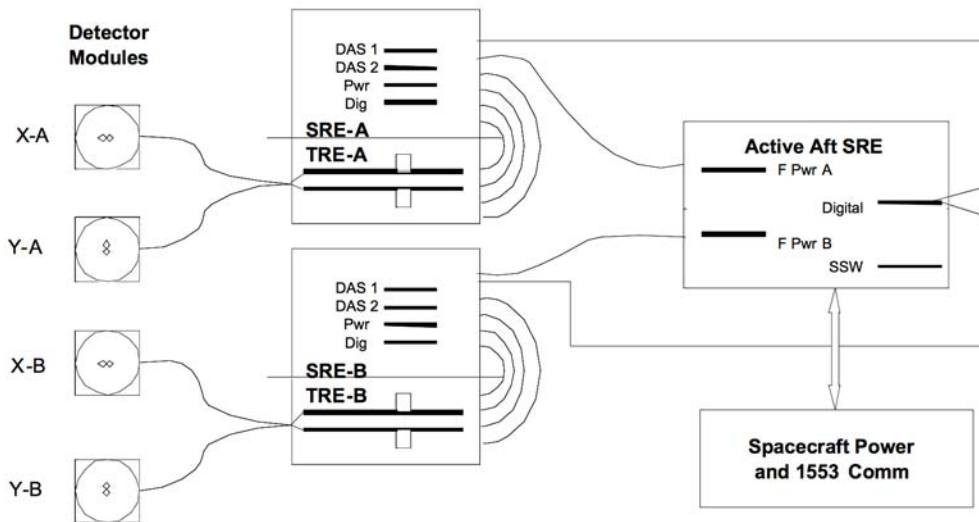


**Figure 11-1.** Block diagram of TRE and associated aspects of the SRE system

The telescope Readout System performed well during initial on-orbit checkout (IOC). Most of the templates worked as intended. The detector balancing algorithm, which is intended to adjust the operating point of the detector preamplifiers and the signal level at the A/D converter, underwent a minor adjustment to change the limits of acceptable completion for the clamp adjustment. As a result of less than optimal automated adjustment performance, a CSTOL procedure was created, and used to make manual adjustments of the clamp command level to optimize the voltage level at the A/D converter.

## 11.2 Operational Performance and Overview

The Operations personnel had little to monitor or change with the Telescope Readout Electronics. Most of the timeline events were related to managing the CPU utilization by the SQUID/ST Software. Three specific areas of interest, other than initial power on and setup did require some operator intervention, and these are highlighted in the next few sections.

### 11.2.1 Gain Levels

Two overall signal gain levels were used during IOC, Gain 12 and Gain 11. These correspond to approximately 870 and 615 V/V between the charge-locked loop preamp output and the A/D converter of the SRE. It has been determined that the lower gain level achieves good performance and is easier to adjust with the balancing procedure. During Science, it was determined that there might be an advantage to using even lower gain levels. [Table 11-1](#) lists the times of gain changes on the two sides from just after launch until the end of the Science data collection on 15 August 2005. The gain changes during the post-Science calibration phase are not given in the table.

**Table 11-1.** Gain code change times

A-side		B-side	
UTC Time	Gain Code	UTC Time	Gain Code
4/20/04 22:30	12	4/20/04 22:30	12
5/14/04 7:15	11	5/14/04 7:15	11
3/31/05 21:20	10	3/26/05 7:36	10
4/4/05 21:24	9	3/29/05 9:10	9
		3/31/05 8:00	11
		5/21/05 8:01	9

Gain codes are the commands to select specific taps on a resistive ladder attenuator. Following the attenuator selector is a large amount of linear gain and a 500 Hz low-pass filter. The net gain between the charge locked loop and the A/D converter for various gain codes is as follows:

- Gain code 9 commands gain value of 307 V/V, or 0.353 relative to gain 12.
- Gain code 10 commands gain value of 434 V/V, or 0.499 relative to gain 12.
- Gain code 11 commands gain value of 614 V/V, or 0.706 relative to gain 12.
- Gain code 12 commands gain value of 870 V/V.

### 11.2.2 PID Temperature Controllers for DMAs

The detector platform temperature for each of the four DMAs is controlled by PID controllers that sense the temperature and provide commands for the heater voltage. These controllers maintain the platform temperatures at 72 K. The controllers were used to purposely vary the platform temperatures during a stability test to allow determination of a pointing sensitivity to the platform temperature. Performance results are shown in section “[Platform Temperature Stability](#)” on page 312.

### 11.2.3 Signal Strengths

The currents of the 8 photo detectors ranged from about 6 to 12 fA. Weighting factors are used in the signal processing to match the pointing sensitivities from the plus and minus detectors for each axis.

### 11.2.4 Telescope Operation with the Shutter Open

The GP-B system was designed with the expectation that a shutter would open and close once per orbit to prevent sunlight reflected from the earth from affecting the detectors. Unfortunately, the shutter mechanism included a spring loaded mechanism and its operation resulted in un-damped contact with an end stop. The resulting disturbance gave a small acceleration shock to the gyroscopes, so the decision was made to operate with the shutter open continuously. Such operation did not cause damage to the detectors, however a few unexpected features arose. The earthshine resulted in an optical input several thousand times larger than the guide star, which caused significant unbalance in the four-JFET preamplifier circuits and saturation in most of the analog amplifiers in the signal chain of the warm electronics. The unbalance of the preamp currents effectively reduced the power dissipation of the circuit, so in order to maintain the cold platform temperature at the 72 K operating temperature, the PID controller increases the heater power until the earthshine subsides. This is followed by an under damped recovery transient to the normal steady-state condition observed in a time history of the heater voltage engineering monitor. The recovery response time depends on the thermal time constant of the DMA and the characteristics of the PID temperature controller. There was observable damping during the first 15 minutes of guide star valid, but this did not adversely affect the TRE contributions to the pointing error.

Additionally, the warm electronics power dissipation is increased when most of the amplifiers are driven to saturation. The signal level from the output of the charge locked loop is normally within a few mV of zero with guide star illumination, but increases to nearly -10 V during earth shine. The power dissipation in the resistive attenuator and the feedback resistors of the amplifiers increases, and it is distributed over much of the analog printed wiring board (PWB). The board temperature is measured using the temperature output of the REF-02 voltage reference mounted on the PWB and appears in the local box temperature monitor. The degree of heating changes with season, and the disturbance went through a long period during which earth shine was observed for nearly the entire guide star invalid period.

## 11.3 Hardware Performance

Hardware performance will be discussed in greater detail with examples, long term plots and a typical look at daily data.

### 11.3.1 TRE Detector Dark Noise

The TRE detector dark noise is difficult to measure separately from the effects of pointing ambiguity when the guide star is in the field of view. On May 31, 2005, when the guide star was lost for about three hours, there was a whole guide star valid interval during which the science slope processing was active and there was no star in the field of view. This provided 58 minutes of dark detector data in a normal operating environment. The effects of particle hits were removed, and the standard deviations of the remaining signals were calculated after scaling the data to fA using the appropriate factor for gain level 9. Each detector sample noise calculation used 33546 samples out of a total of 34801 available during the interval, indicating that 1255 samples or 3.6% were discarded due to particle hits. Using this data, [Table 11-2](#) is a listing of the resulting RMS dark current noise for each of the eight photo detectors, which are labeled with the detector designations P/M, X/Y, and A/B. A later section shows the effect on pointing noise as the star brightness varies.

**Table 11-2.** Photo detector dark noise

Detector Dark Noise
PXA: 0.297 fA
MXA: 0.255 fA
PYA: 0.252 fA
MYA: 0.257 fA
PXB: 0.249 fA
MXB: 0.379 fA
PYB: 0.264 fA
MYB: 0.248 fA

### 11.3.2 Platform Temperature Stability

The temperatures of the detector platforms are maintained using a computer algorithm with proportional, integral, and derivative (PID) gain coefficients. The temperature controller compares the temperature measured by the silicon diode sensor on the platform with a commanded set point temperature, usually 72 K. The PID algorithm output controls a DAC in the TRE warm electronics that provides the voltage to the heater resistors on the platforms. The platform temperatures are maintained at 72 K with a standard deviation of approximately 23 mK.

### 11.3.3 Temperature History and Detector High Levels

The small detector signals must have a large gain applied to match them to the input range of the A/D converter. There also needs to be a means to adjust the DC level of the signal within that range. The sensitivity of the adjustment changes with a different amount of net gain, and there is a small temperature drift of this offset as the temperature of the warm electronics changes. All of these features were considered in the system design, and several operational consequences and results will be discussed. The normal detector signal is reset to an initial condition, and then as photocurrent integrates on the capacitor, a negative going voltage ramp is produced. The slope of this waveform contains the information of interest, but it is also desired to know the region of the A/D converter range used.

The detector signals are digitized in the forward SRE using an A/D converter scaled to accept signals in a 20 V range centered about 0 V. Each detector signal is sampled at a rate of 2200 samples per second, to provide 220 samples during the tenth second signal interval. The TRE provides a set of selectable gains by which the signal output of the CLL preamplifier is increased to provide a better utilization of the range. The Science Slope algorithm calculates the slope of the detector ramp, but also reports three other signals of interest: detector high, detector mean, and detector low. The detector high signal provides the maximum value of detector sample 14 over a 2 second interval (20 consecutive signal integrations). The detector high signal indicates where the beginning of the ramp will occur, and is usually maintained near 0 V.

Timing of the TRE and SRE signals is synchronized using a 10 pps signal called the ATC strobe. The reset of the CLL begins upon the receipt of the ATC strobe and takes a total of approximately 3.5 ms of the 100 ms interval.

The charge locked loop is a reset integrator that uses a distributed operational amplifier. A portion of the amplifier is located adjacent to the cold detectors, and the remainder of the amplifier is located in the warm electronics. There is a solid state switch in the warm area prior to the final stage of the amplifier that is activated during the reset interval [Figure 11-2](#) shows the simplified schematic of the detector, feedback capacitor, and switch states during the signal integration period of operation.

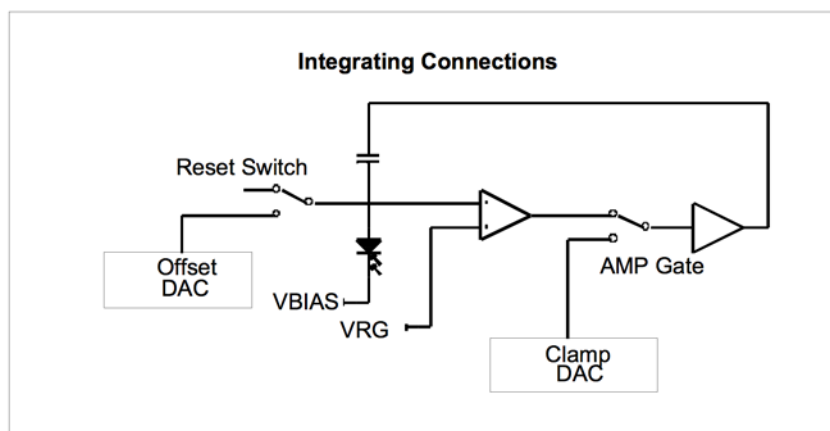


**Figure 11-2.** CLL switch states during normal operation

During the reset interval, the feedback capacitor is charged to a uniform voltage by switching its terminals to two low impedance voltages, both of which are adjustable over a small voltage range by changing the eight bit command value to the DACs which control the voltages. The detector, feedback capacitor, amplifier input node is switched using a reset JFET to a voltage source adjustable approximately  $\pm 20$  mV from the -4 V amplifier reference node. This DAC is called the offset DAC. See [Figure 11-3](#) for switch states.

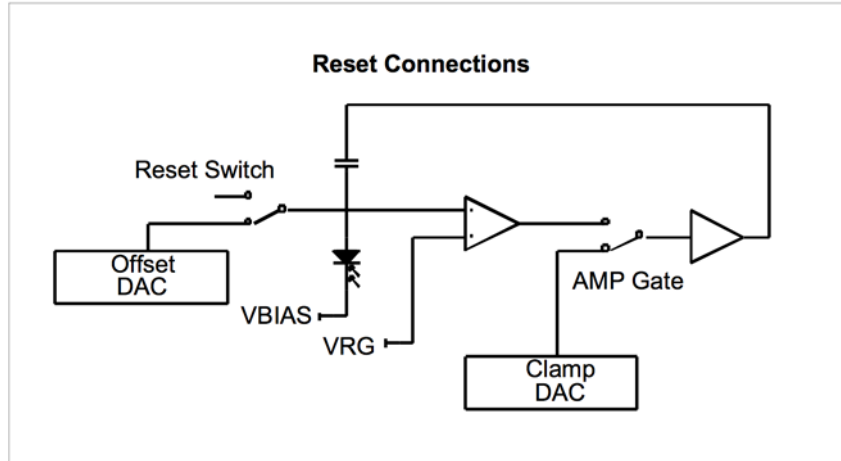


**Figure 11-3.** CLL switch states during the reset interval.

The input of the final amplifier in the charge locked loop is switched during the reset interval to another DAC that provides CLL output voltages between zero and -3.92 V with 256 steps of resolution. This DAC is called the clamp DAC because it clamps the capacitor to a fixed voltage during the reset operation.

An adjustment procedure is used to optimize the settings of the two DACs to assure that the preamplifier is reasonably well balanced, and that the DC level of the amplified output is appropriate for the A/D converter.

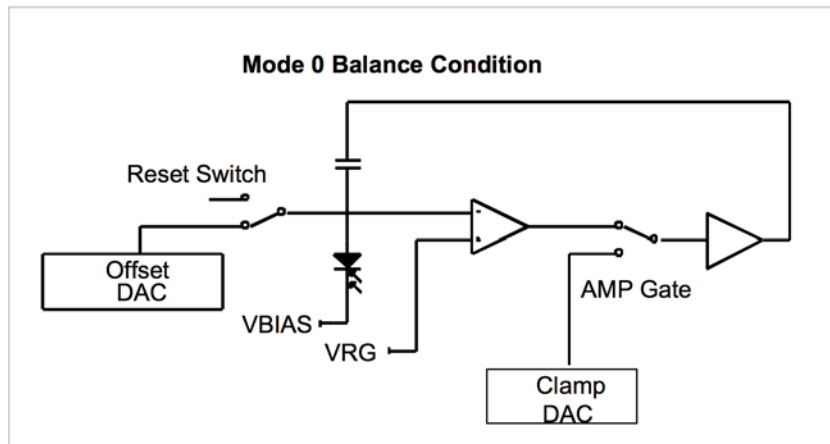


**Figure 11-4.** CLL switches locked for offset adjustment

In practice, the offset DAC is adjusted with the reset JFET in an ON state as shown in [Figure 11-4](#). Then the offset DAC is adjusted to provide the smallest positive voltage output within its resolution. The normal reset clocking is then re-enabled and the clamp DAC is adjusted to provide an operating point within a selectable range of the A/D converter. Once the adjustments are completed the same command values for the two DACs are used for long periods of time.

The cold preamplifiers are each biased using current sources in the warm electronics. As the warm electronics temperature changes, the 100  $\mu\text{A}$  current sources vary approximately  $0.159 \mu\text{A}/^\circ\text{C}$ , so over the  $\pm 10^\circ\text{C}$  operating range, the current would change by  $\pm 1.6\%$ . While this sensitivity has little effect on the pointing signals derived from the telescope, it causes a minor operational requirement to readjust the clamp command a few times during the mission lifetime. The operational results of these adjustments are shown in the figure below.

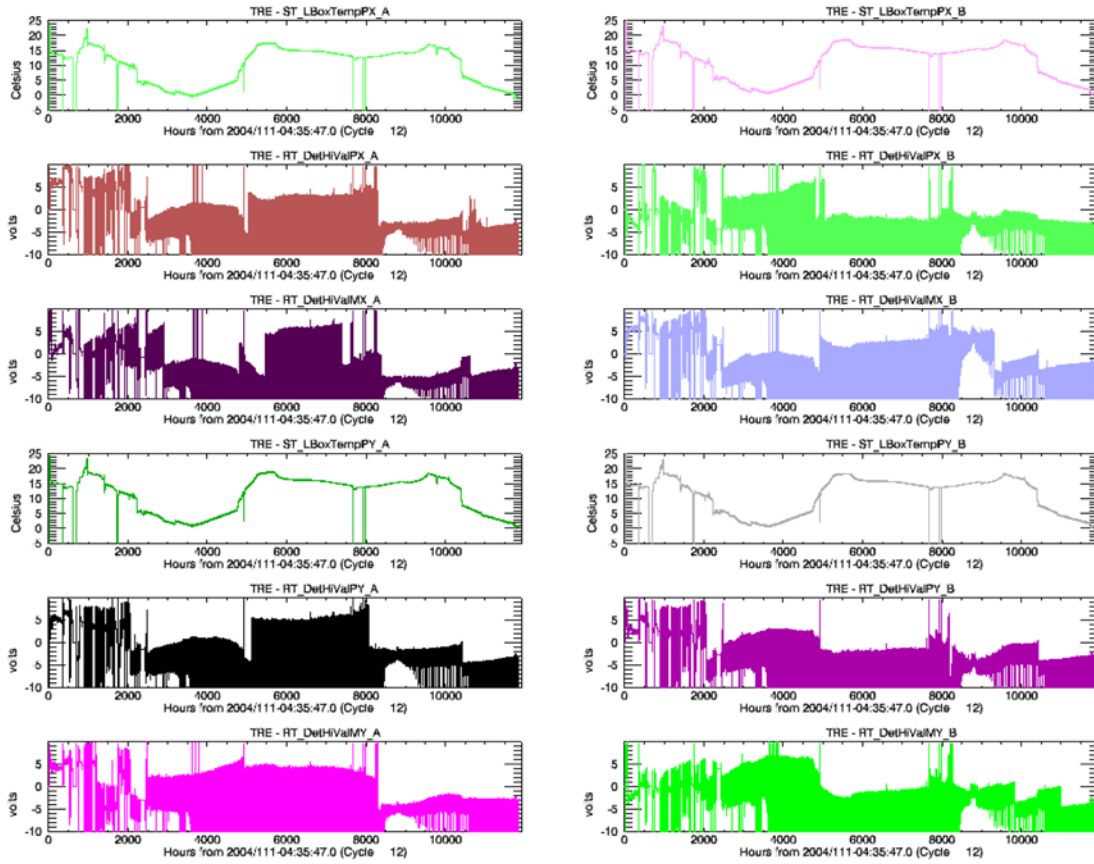


**Figure 11-5.** Local box temperature and detector high signals since launch

Figure 11-5 shows a very long time history of the eight detector high signals grouped in pairs below the corresponding box temperature plot. It is interesting to note that while the four temperature plots are very similar, there is some degree of variation in the shape of the detector high levels. In the range of time between about 2500 and 4500 hours, where the temperature tends toward a minimum and then increases smoothly, the shape of the detector highs for the bottom plot in the left column and the second from the top plot in the right column are quite different in character from the other six detector high plots. The steps in the detector high plots generally occur when an adjustment in the level was made.

Table 11-3 below contains a tabulation of when each of the clamp adjustments were made, and the command value to which they were set. Valid command values range from 0 to 255. There were some cases where a value was set, and then the system re-initialized for some reason such as an SRE processor re-boot. These resets are not included in the listing.



**Table 11-3.** Dates and UTC times when clamp commands were changed

Refer to plots in [Figure 11-5](#). All times listed are converted from vehicle time to UTC.

<i>Left Column Plot 2</i>	
<b>PT_STxClampPCdA</b>	<b>Switched to</b>
20-Apr-2004 22:28:29	176
14-Jul-2004 15:26:17	177
15-Nov-2004 19:13:31	176
31-Mar-2005 23:07:52	177
28-Jun-2005 16:07:30	178
<i>Left Column Plot 3</i>	
<b>PT_STxClampMCdA</b>	<b>Switched to</b>
20-Apr-2004 22:28:29	184
23-Apr-2004 09:59:09	185
22-Jul-2004 19:34:57	186
01-Aug-2004 16:32:53	185
20-Aug-2004 01:04:13	186
06-Nov-2004 23:12:39	185
03-Dec-2004 16:48:31	184
22-Feb-2005 01:31:39	185
04-Mar-2005 00:36:49	184
06-Mar-2005 06:15:59	185
04-Apr-2005 21:35:42	186
06-Jul-2005 18:22:30	187
<i>Left Column Plot 5</i>	
<b>PT_STyClampPCdA</b>	<b>Switched to</b>
20-Apr-2004 22:28:29	177
21-May-2004 08:04:11	178
31-Jul-2004 22:38:03	177
01-Aug-2004 16:34:13	179
19-Nov-2004 17:36:31	178
21-Mar-2005 23:53:22	179
28-Jun-2005 16:07:30	180
<i>Left Column Plot 6</i>	
<b>PT_STyClampMCdA</b>	<b>Switched to</b>
20-Apr-2004 22:28:29	186
09-Jun-2004 02:45:50	187
31-Jul-2004 22:38:53	186
01-Aug-2004 16:34:53	187
31-Mar-2005 23:08:12	188

<i>Right Column Plot 2</i>	
<b>PT_STxClampPCdB</b>	<b>Switched to</b>
20-Apr-2004 22:28:29	166
23-Apr-2004 09:59:09	167
21-May-2004 08:04:07	166
14-Jul-2004 15:27:57	167
31-Jul-2004 22:39:13	166
01-Aug-2004 16:31:03	167
06-Nov-2004 23:13:29	168
26-Mar-2005 08:35:32	169
26-Mar-2005 20:16:42	168
27-Mar-2005 05:12:02	167
29-Mar-2005 21:17:32	169
30-Mar-2005 23:34:22	168
<i>Right Column Plot 3</i>	
<b>PT_STxClampMCdB</b>	<b>Switched to</b>
20-Apr-2004 22:28:29	178
14-Jul-2004 15:28:27	179
11-Nov-2004 17:34:11	178
26-Mar-2005 08:36:12	179
26-Mar-2005 20:17:22	178
29-Mar-2005 21:17:52	179
30-Mar-2005 23:34:52	178
12-May-2005 22:54:52	179
28-Jun-2005 16:07:30	180
<i>Right Column Plot 5</i>	
<b>PT_STyClampPCdB</b>	<b>Switched to</b>
20-Apr-2004 22:28:29	192
23-Apr-2004 09:59:09	191
14-Jul-2004 15:29:07	192
01-Aug-2004 16:33:33	193
26-Mar-2005 08:36:33	192
26-Mar-2005 20:17:53	193
27-Mar-2005 05:12:13	194
30-Mar-2005 23:35:13	193
28-Jun-2005 08:22:30	194
<i>Right Column Plot 6</i>	
<b>PT_STyClampMCdB</b>	<b>Switched to</b>
20-Apr-2004 22:28:29	197
23-Apr-2004 09:59:09	198
26-Mar-2005 08:37:13	197
26-Mar-2005 20:18:33	198
27-Mar-2005 05:12:32	199
30-Mar-2005 23:35:43	198
03-Jun-2005 17:37:30	199
21-Jul-2005 18:12:30	200

### 11.3.4 Daily Data Example

It is unusual to look at data for time periods of greater than a few days duration; a 12 or 24 hour time span frequently shows many useful and interesting characteristics. Typical data for the TRE includes a look at how well the temperature control system is working, whether the detector high levels need adjusting, and a look at the ATC slopes to verify that the guide star is still in the field of view. These plots usually are done for all of the A-side and all of the B-side channels available. Usually the more boring the better, but shown here are two plots made from two distinctly different seasons that show how the sun location and the orbit affect the TRE (with the shutter open continuously). Both plots contain the same four signals, with a similar scaling range. The limits are different to accommodate the seasonal difference. The first plot, [Figure 11-6](#), is from 20 August 04 when the gamma angle was near its maximum value. The uncontrolled warm electronics box temperature is at a few degrees Celsius and the platform heater is supplying additional heat to the detector platforms during most of the guide star invalid period. During the guide star invalid period, the box warms, due to amplifier saturation, and then during guide star valid, it cools again. A noticeable slope exists in the detector high level waveform. The TRE gains were set at gain code 11 for both plots.

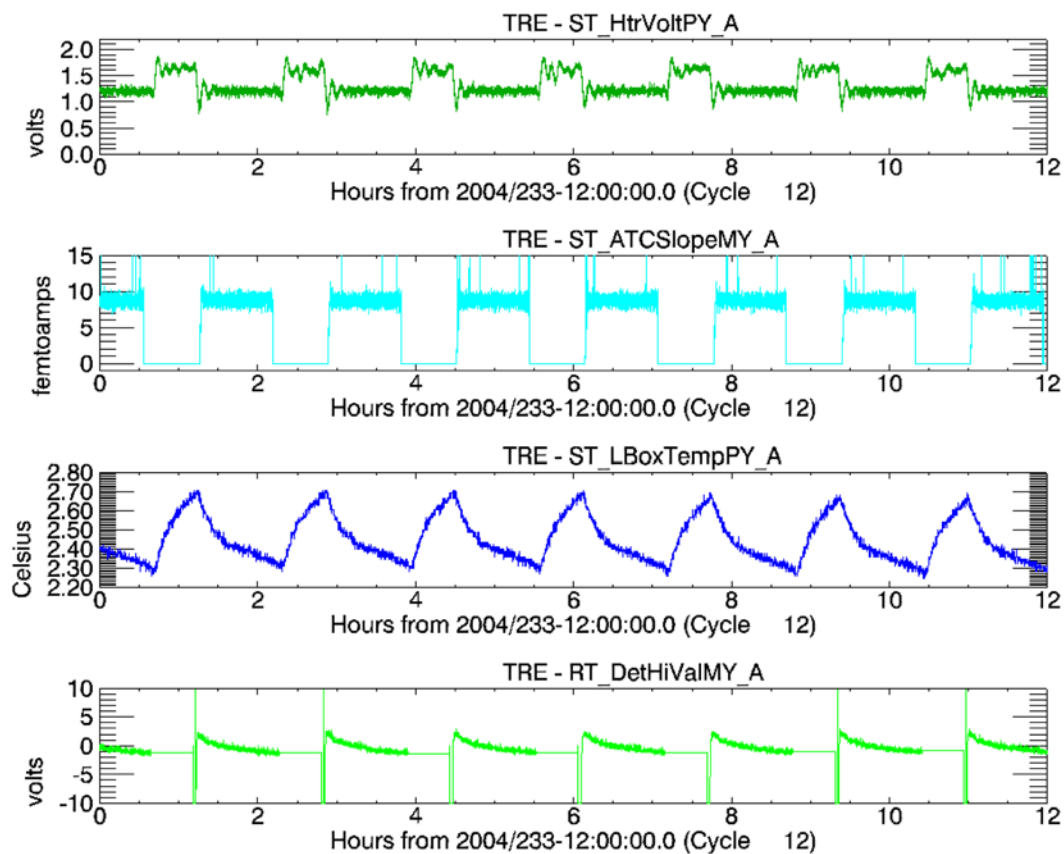


**Figure 11-6.** High Gamma Angle Data Sample

The second plot, [Figure 11-7](#), is from 12 February 05 when the gamma angle was near its minimum. The heater voltage shows only small blips at the beginning and end of guide star invalid, the box temperature is near 15 °C with much smaller excursions, and the detector high levels show much less sloping.

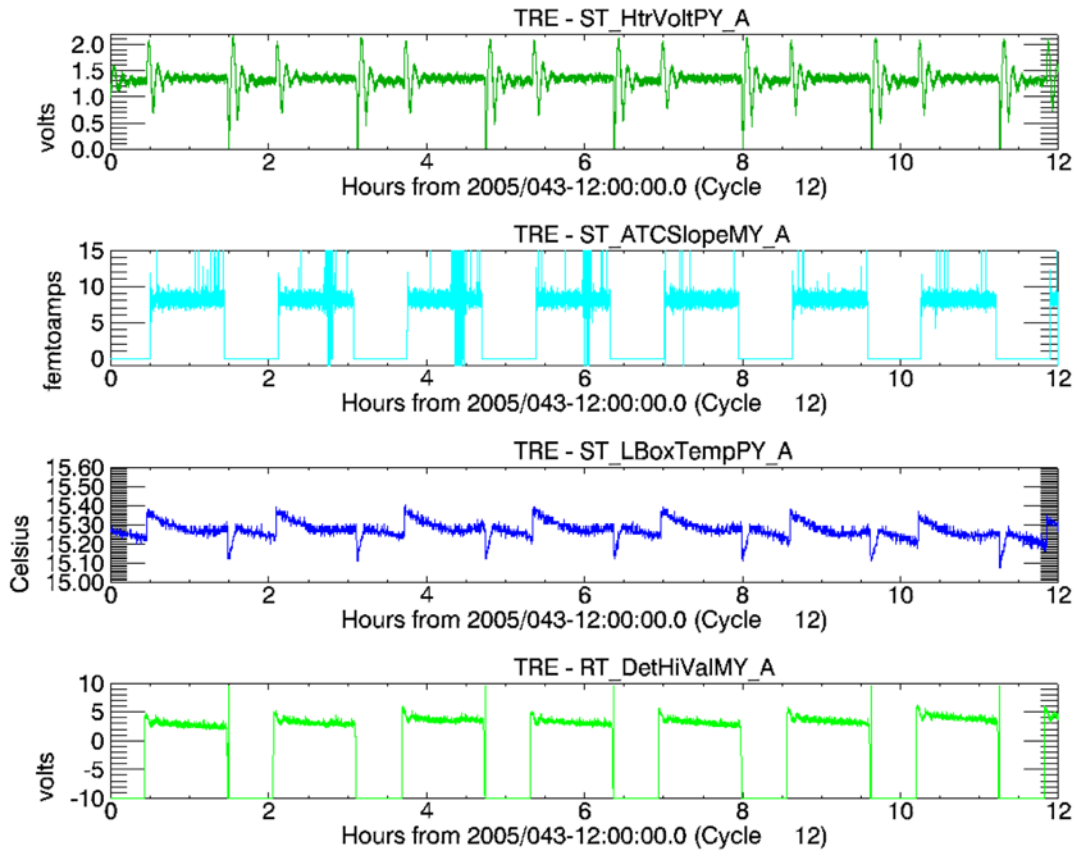


**Figure 11-7.** Low Gamma Angle Data Sample

The ATC slope signals are included in these plots as an indicator of photocurrent as well as a timing reference since they are active only during the guide star valid periods of each orbit. Similarly, the detector high signals are generated by the science slope algorithm, which is usually cycled off during guide star invalid as part of the load management of the SRE processor.

## 11.4 Optically Related Performance

Many of the telescope performance characteristics are influenced by the optical properties of the telescope, beam splitters, windows, and guide star. Several of these characteristics are discussed in this section.

### 11.4.1 Guide Star Brightness Variation and Period

Figure 11-8 displays the history of IM Peg's light intensity as measured by the summed current of all eight telescope detectors during the course of the Science Mission beginning on 1 September 2004 and ending 31 August 2005. Each point of intensity is an average of about 50 minutes continuous observation, the equivalent of one orbit's guide star valid period. Some cleaning and censoring of the data was required. The intensity is from the summation of all eight guide star telescope detectors in units of fA. Errors are derived from the standard deviation and the number of samples. The signal-to-noise ratio ranges from 5,000 to 10,000. Typically, 2 to 6 orbits were analyzed every day to create this plot.

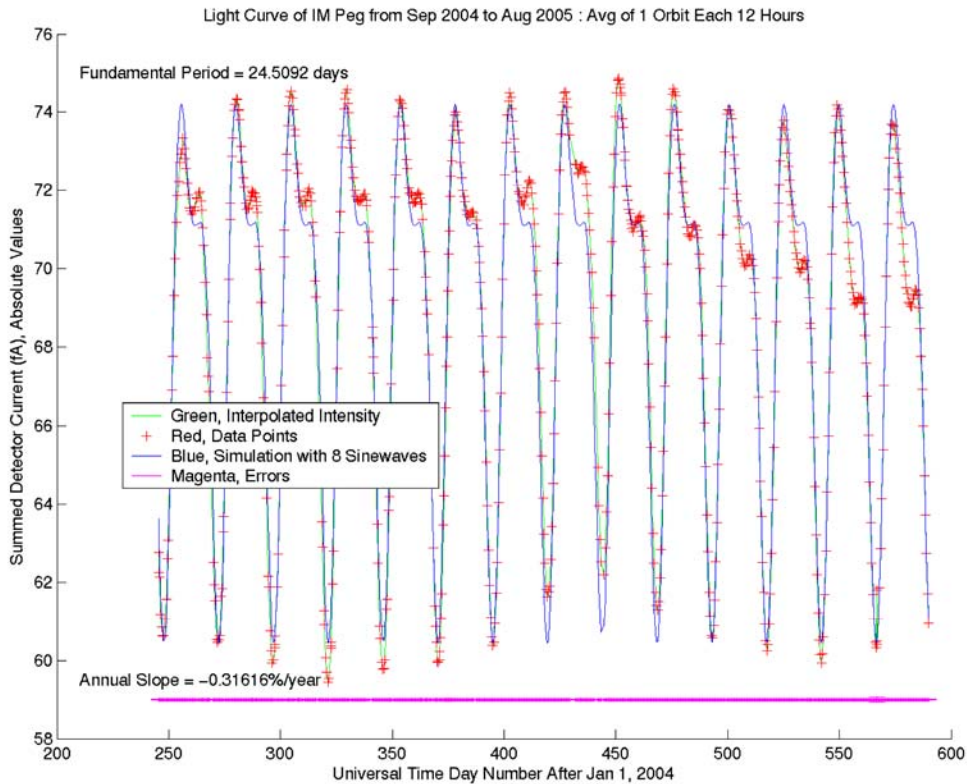


**Figure 11-8.** Guide Star intensity versus time

The dominant feature in the light curve is the 24.51 day period associated with star spots synchronized by the tidal and elliptical distortion wave forced by an unseen binary companion. The stellar rotation and orbital periods are tidally locked. Occasionally these systems flare, although during the GP-B mission no flaring was observed. RS CVn class stars, of which IM Peg is a member, display photospheric spots that modulate the light curve and they are also magnetically active. Doppler Imaging and Zeeman Doppler Imaging are used for mapping stellar surfaces of the RS CVn components.

The annual linear drift in guide star brightness is less than the 10% requirement that was specified at the beginning of the mission. Fortunately, we observed the star during a stable period when no flares or sudden changes in brightness occurred. The comparison waveform is composed of an 8 term Fourier trigonometric series with coefficients chosen by a least squares method (Matlab). The residual linear variation component of stellar brightness was -0.31616%/annum.

## 11.4.2 Telescope Pointing Signal

The telescope pointing signals for science are derived from the telescope detector slopes, which are calculated on-board the space vehicle and telemetered to the ground where they are converted to detector currents  $i^{+/-, X/Y, A/B}$ , where +/- refers to the +/- detectors of a pair, X/Y to the X or Y-axis, and A/B to the A or B side electronics. A normalized telescope pointing signal  $S_N^{X/Y, A/B}$  is found using the detector currents and weighting factors  $w^{+/-, X/Y, A/B}$ , which account for the different efficiencies for each of the optical and electronic paths for the eight telescope detectors. For simplicity the X/Y and A/B designations are not included in the expression. The symbol *sign* is plus for the X-axis, and minus for the Y-axis.

$$s_N = \text{sign} \frac{w^+ i^+ - w^- i^-}{w^+ i^+ + w^- i^-} \quad \text{Equation 11-1}$$

Note that the X-axis uses the detector currents designated by Y, and the Y-axis uses the detector currents designated by X, which is the result of the detector axes being designated by their spatial location and the pointing angles by the X and Y rotation axes.

The pointing signal  $s_p$  in units of marcsec is found with a scale factor, which is approximately  $3.3 \times 10^3$  marcsec/normalized pointing signal for both axes.

$$s_p = 3.3 \times 10^3 s_N \quad \text{Equation 11-2}$$

The weighting factors that are used to determine the ATC pointing signal on orbit are listed in [Table 11-4](#). Normally the same weighting factors are also used to calculate the science normalized pointing signal, although different weighting factors can be used in principle for science since the processing of the science slope data takes place on the ground.

**Table 11-4.** Weighting factors used for processing data

Electronic Side	A-Side		B-Side	
	+	-	+	-
Detector Designation \ Polarity				
X	0.9931	1.0070	1.0005	0.9995
Y	0.9421	1.0655	0.9245	1.0890

### 11.4.3 Telescope Scale Factor

From ground measurements, the scale factor, which converts the normalized pointing signal to pointing angle, as estimated in S0619 (J.P. Turneure, M. Heifetz, “Flight telescope/window system analysis of wavelength dependent properties”, GP-B S-Doc S0619 Rev. -, 3-Mar-02), was measured to be about 2.0 arcsec per normalized pointing signal. This estimate was based on measurements of the telescope in its Payload configuration (flight telescope at liquid helium temperature and with the 4 flight windows at temperatures close to those of flight) made with Artificial Star #3, see S0570 (R. Bernier, T. Acworth, J.P. Turneure, D. DeBra, “Flight telescope/window system verification”, GP-B S-Doc S0570 Rev. -, 20-November-01).

Room temperature and low-temperature measurements of the telescope indicated that the bare telescope was very close to focus with little wavefront error. However after the telescope was integrated into the payload, which included the four windows, the telescope/window system was found to be out-of-focus. When Artificial Star #3 was adjusted to compensate for the telescope/window system defocus, which amounted to a focal position shift of 5.2 mm, a good quality focus occurred with very little astigmatism. The knowledge in the quality of the focus was limited by the uncertainty in the wavefront error introduced by Artificial Star #3, which had an estimated Strehl ratio of 65%. Flight data shows that both telescope pointing axes have a scale factor of about 3.3 arcsec per telescope normalized pointing signal, which is consistent within error to the defocus measured on the ground.

The lack of focus has an advantage: namely that the linear range of the telescope is larger and thus larger RMS pointing errors are acceptable in the data analysis. The non-linearity of the telescope has been explored analytically using optical theory and experimental data. Initial analysis indicates the telescope is 0.17 inches (4.3 mm) out of focus, which within error agrees with the value measured on the ground when considering

wavefront errors. Figure 11-9 is a plot of the estimated intensity distribution function at the roof prism of the telescope, and Figure 11-10 is a plot of the calculated scale factor as a function of pointing angle for this intensity distribution. The small difference between two curves in the figure is due to the change of color of IM Peg.

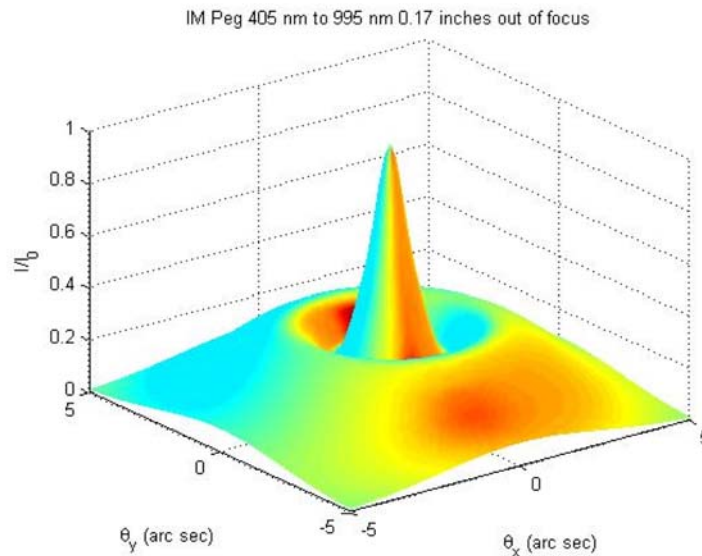


**Figure 11-9.** Point spread function of IM Peg image at the roof prism

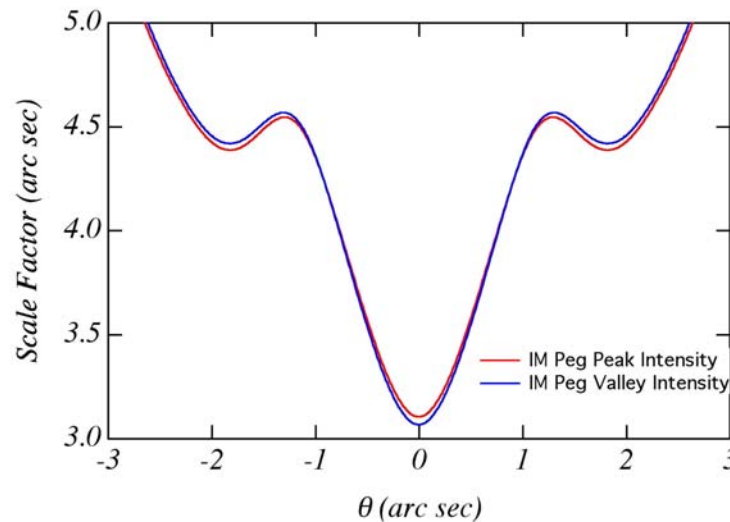


**Figure 11-10.** Pointing angle

#### 11.4.4 RMS pointing noise

We observe both common mode noise and statistically independent noise in the slopes for +/- detector pairs. Some of the common-mode noise is known to be associated with pick-up from switching noise due to the temperature control currents on the detector platforms. There may also be other unknown sources of common-mode noise. We observe that the common-mode noise is to first order Gaussian with zero mean. This allows us to use an average value over one guide-star valid period for the denominator in the normalized pointing signal



expression, which otherwise on a point-by-point basis would add about 2% to the pointing noise. The common-mode noise is removed to first order in the numerator of the normalized pointing signal since it is a difference between the + and – detector currents, which each contain the common-mode noise.

We find the resulting RMS noise in units of marcsec using the fact that the noise is Gaussian and the fact that the actual pointing can not change a significant amount compared to the noise from sample to sample (only 0.1 s). This allows the noise to be estimated using the first differences between adjacent samples.

$$\sigma_T = \sqrt{\frac{\sum_{i=1}^{N-1} (S_{P,i+1} - S_{P,i})^2}{2(N-1)}} \quad \text{Equation 11-3}$$

Figure 11-11 through Figure 11-14 are plots of the calculated noise for the four detector pairs as a function of time. The time is in days, where day 1 begins on January 1, 2004 at 0 hours. Each noise point is the average noise during one guide star valid period.

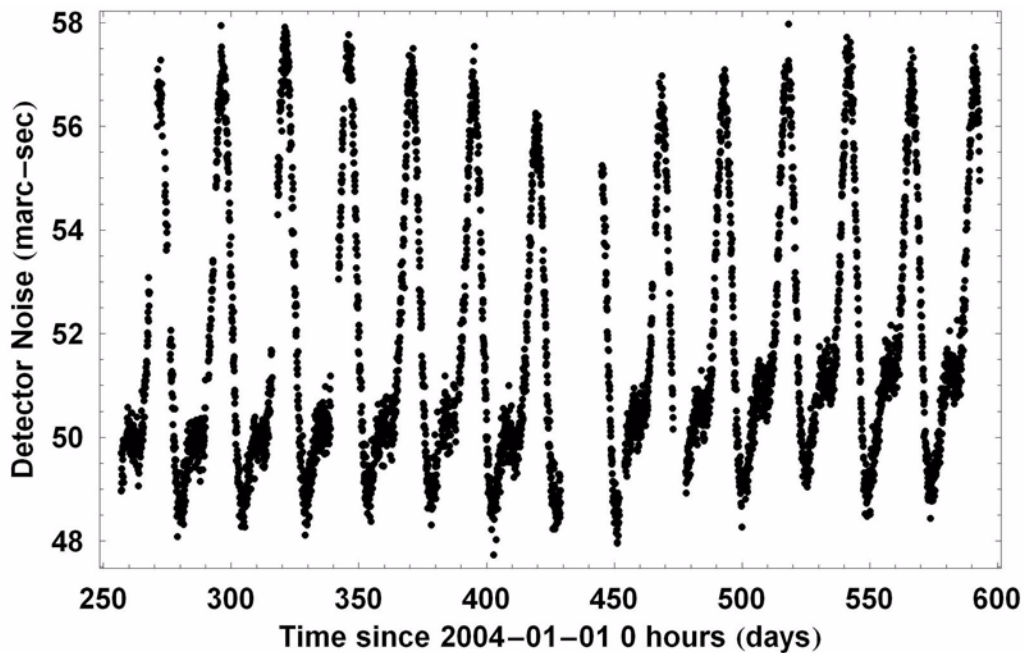


Figure 11-11. X-axis, A side RMS pointing noise equivalent due to detector noise



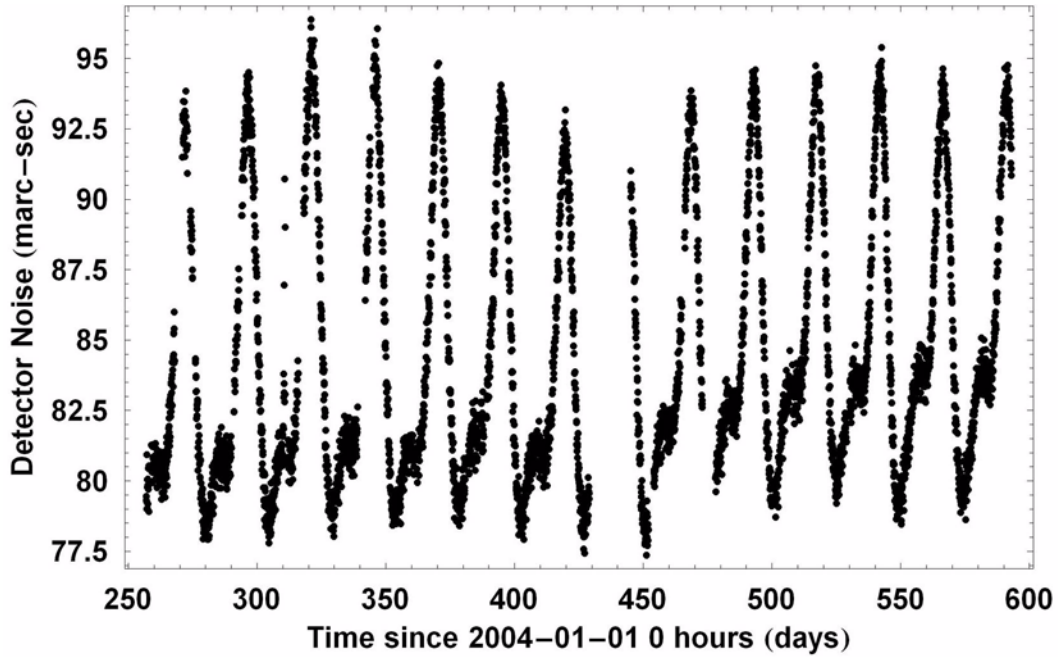


Figure 11-12. Y axis, A side RMS pointing noise equivalent due to detector noise

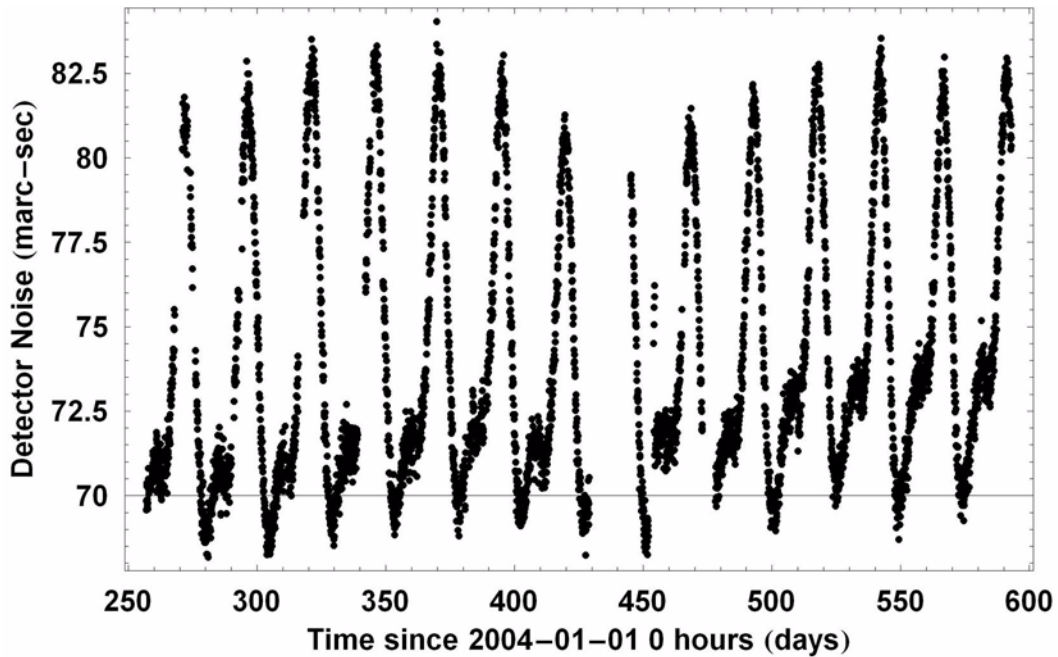
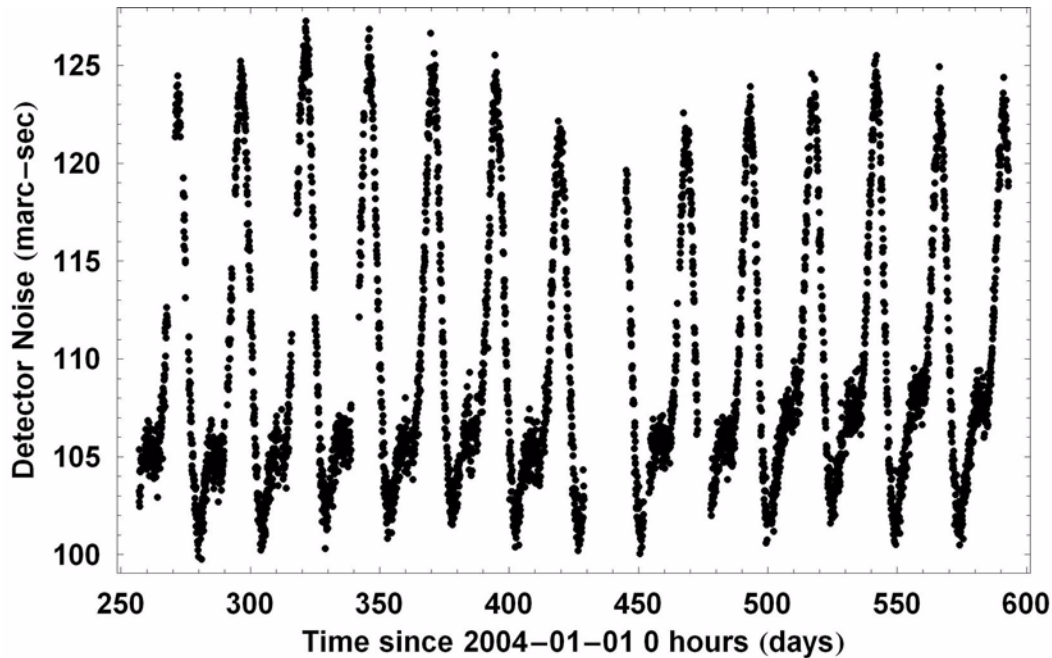


Figure 11-13. X axis, B side RMS pointing noise equivalent due to detector noise



**Figure 11-14.** Y axis, B side RMS pointing noise equivalent due to detector noise

The average, maximum, and minimum noise for the four channels are given in [Table 11-5](#). The noise variations with time are clearly correlated with the summed weighted currents (the denominator of the normalized pointing signal), which vary with the intensity of the guide star. Requirement 7.5.2 of T003 requires that the RMS noise, as defined in the equation above, be less than 75 marcsec. This is met only for the X-axis for the A-side electronics and the X-axis for the B-side electronics. The average noise for the Y-axis for the A-side electronics is 83.8 marcsec, just 12% above the requirement.

**Table 11-5.** On-orbit detector pair characteristics

Channel (Rotation Axis/ Electronic Side)	Average Summed Weighted Current (fA)	Average Noise (marcsec)	Maximum Noise (marcsec)	Minimum Noise (marcsec)	Ratio $n_S/n_E$
X-Axis, Side A	23.7	51.8	58.0	47.7	1.07
Y-Axis, Side A	13.4	84.4	96.4	77.4	0.74
X-Axis, Side B	15.4	74.0	84.0	68.2	0.82
Y-Axis, Side B	16.7	109.7	127.3	99.8	0.46

We can estimate the contribution of the photon/electron pair shot noise  $n_S$  and of the electronic noise  $n_E$  with the following expression and the knowledge of the summed weighted currents of each of the detector pairs, which vary with the brightness of the star. The summed currents  $i_S$  are plotted in [Figure 11-15](#) through [Figure 11-18](#) as a function of time, again in days. The fit assumes the following model.

$$n_T = \sqrt{n_S^2 + n_E^2} = \sqrt{\frac{c_S}{i_S} + \frac{c_E}{i_S^2}} \quad \text{Equation 11-4}$$

Using the on-orbit data, the ratios of shot noise to electronic noise are given in [Table 11-5](#). The first three channels in the table have ratios of  $n_S/n_E$  that correlate in an expected way with the summed current, *i.e.* the ratio increases as the summed current increases. The channel for the Y-axis, *B-Side*, however, appears to have a larger electronic noise than the other three channels.

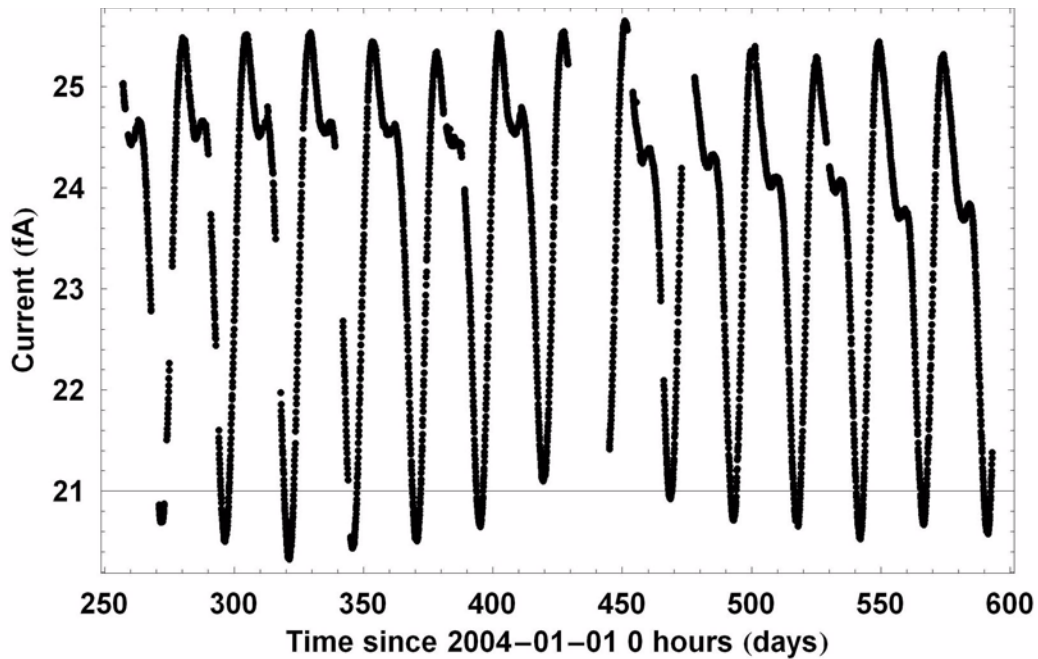


Figure 11-15. X axis, A side current variation

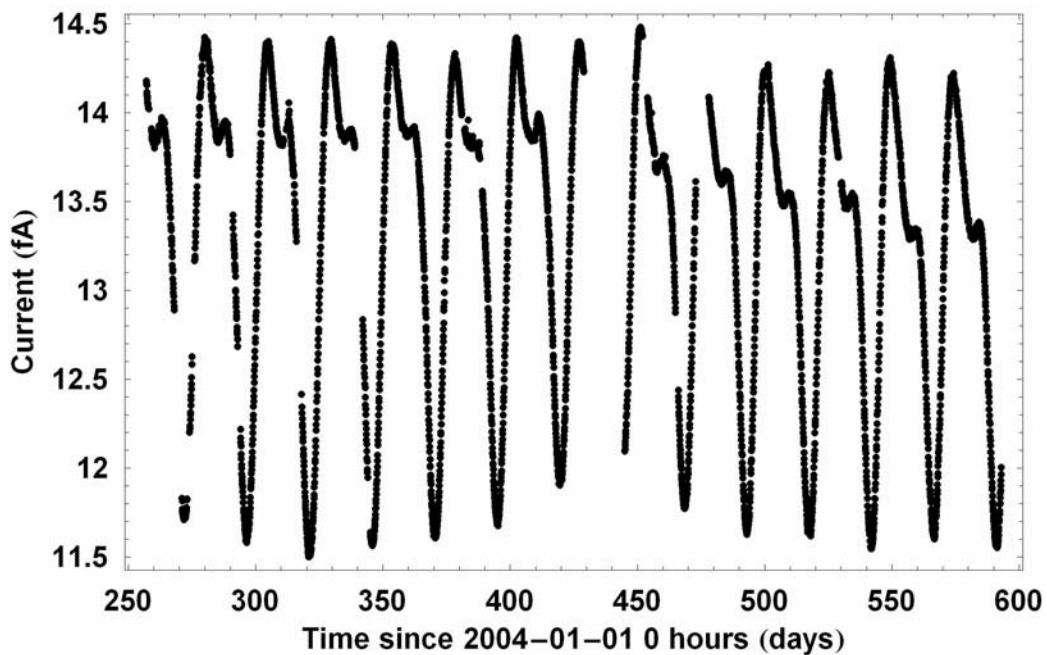


Figure 11-16. Y axis, A side current variation

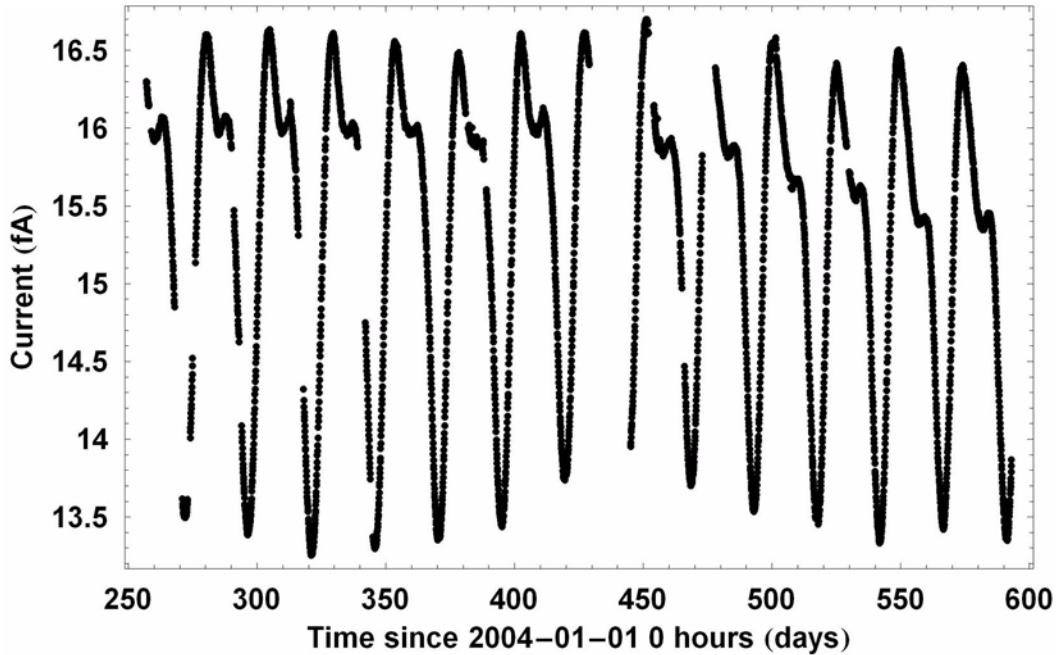


Figure 11-17. X axis, B side current variation

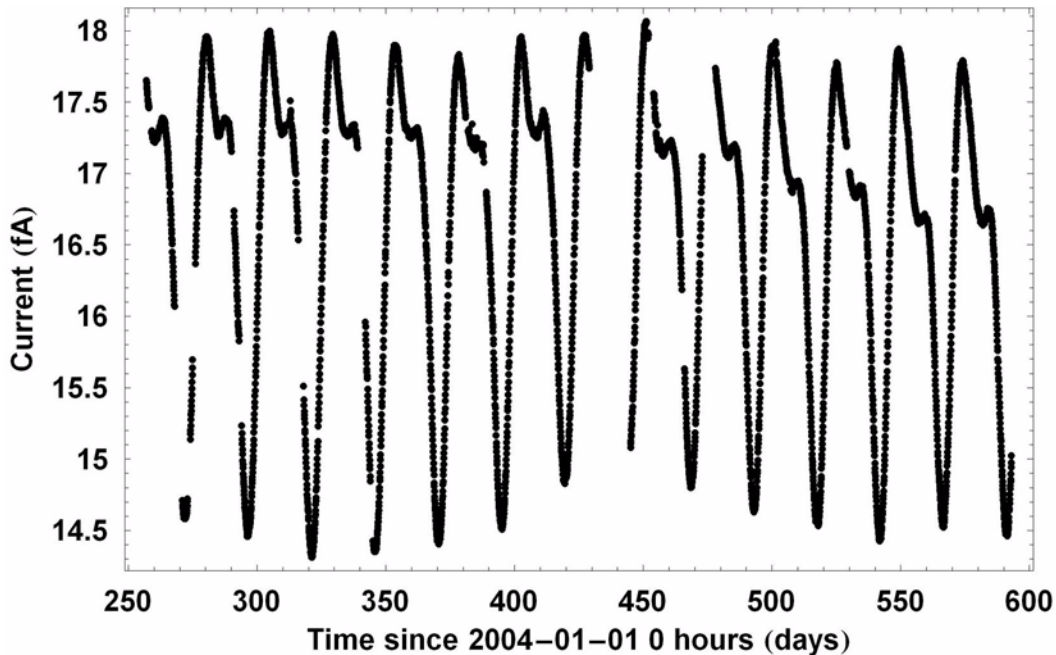


Figure 11-18. Y axis, B-side current variation

### 11.4.5 Dither amplitude variation

The telescope scale factors for both axes are matched to the gyroscope scale factors by sinusoidally dithering the space vehicle at two dither frequencies, nominally one about the  $X$  axis and one about the  $Y$  axis. Initially the dither periods were 30 s and 40 s. They were changed to 29 s and 34 s in December 2004 (Vehicle Time 156484800.0 s) to prevent the 2<sup>nd</sup> harmonic of roll frequency being too close to the second dither period when it was 40 s. The commanded dither amplitude, when it is on, is kept at a constant amplitude.



Figure 11-19 is a plot of the dither amplitude as a function of time in days beginning at 0 hours, 1 January 2004. The most notable feature in this figure is the ~10% variation in the dither amplitude at the rotation period of the guide star, IM-Peg. This same feature is also observed in the telescope X-axis dither amplitude. A similar correlation with the guide star brightness is also seen in the variation of the dither amplitude observed in the gyroscope pointing signals. This variation with the guide star brightness is the result of the detailed implementation of the attitude controller. The attitude controller in the ATC system assumes a constant denominator in the determination of the telescope normalized pointing signal. This results in the attitude controller injecting dither amplitudes into the pointing that vary with the guide star brightness. The change in the average dither amplitude at about 350 days is associated with the change in dither frequencies.

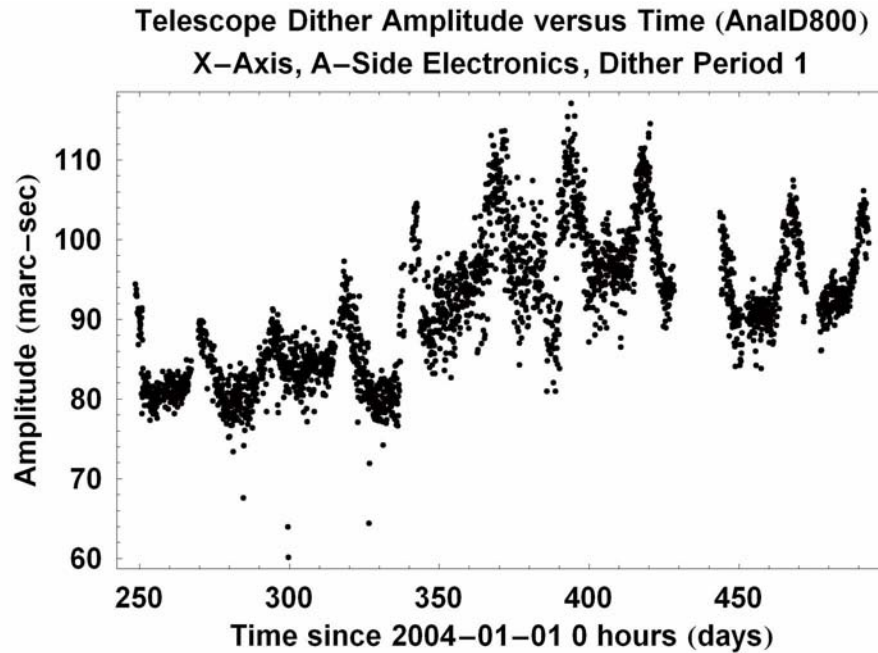


**Figure 11-19.** Dither amplitude as a function of time

#### 11.4.6 Bias Variation

It was observed that the difference between the pointing angle as read by the primary channels and redundant channels vary as a function of time. The variation correlates with the star intensity variation. Figure 11-20 shows such variation from 1 August 2004 to 31 May 2005. The top graph is the summed detector current of TRE-XA channels. Each data point is an average of all data points over one orbit in guide star valid period. The raw data is based on level 1 data with a radiation event removal filter. The bottom graph is the pointing angle difference between primary and redundant channels. Here again, each data point is an average over one orbit with the guide star valid. In both graphs, the nominal weighting factor is used.

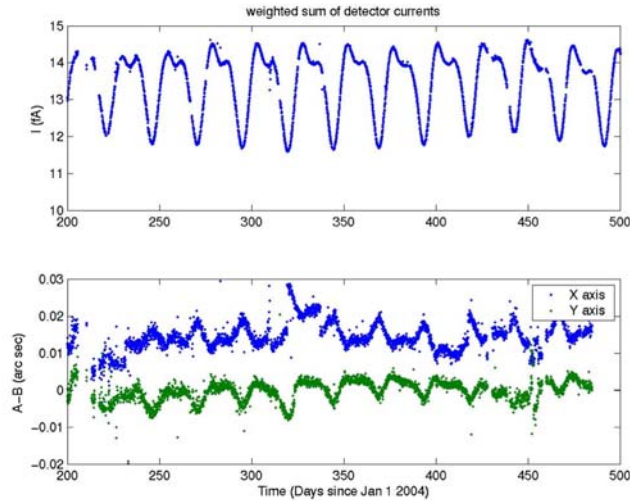


**Figure 11-20.** Pointing angle difference between primary and redundant readouts

One possible explanation for such a variation is the variation of the weighting factor. The mechanism for such a weighting factor variation could be that the light transmission efficiencies from the two roof prisms to each of the eight photo detectors have different spectral responses. It was found from ground observations by Greg Henry from Tennessee State University that the color of IM Peg also varies with the same period as the star brightness. [Figure 11-21](#) shows the color variation of IM Peg based on Greg Henry's data.

Based on the data shown in [Figure 11-21](#), a model based on the guide star spectrum and spectral properties of the light transmission through the optical system with a correction term for the color response difference between + and - detectors, a preliminary calculation indicates that the color variation could cause the weighting factor to vary so as to cause a pointing angle change of 50 marcsec.

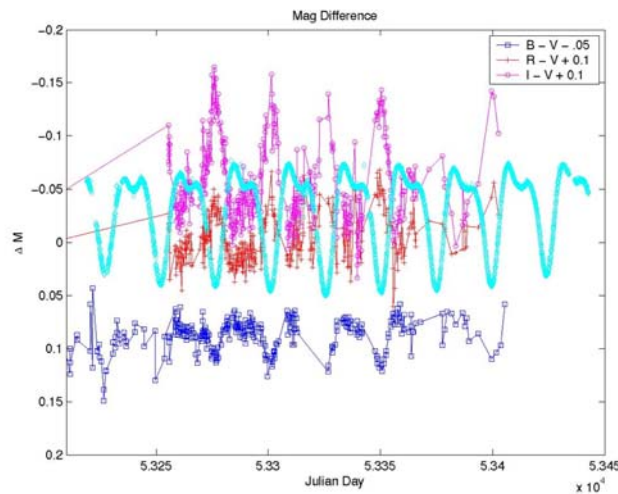


**Figure 11-21.** The color variation of IM Peg. The sum of the detector current of one of the axis is also shown to indicate how star brightness varies.

The weighted summed current for each of the four detector pairs were calculated and averaged from orbit to orbit in the guide star valid periods. [Figure 11-22](#) shows such a plot from 1 July 2004 for each of the four pairs. Most points for the pair XB are hidden below those for YB. These data were then scaled to the data on 30 May

2004 and converted to the instrument magnitude for each pair of detectors. [Figure 11-23](#) shows the data comparison with ground measurement by Greg Henry in the R band. Considering IM Peg is a red star, and the pass band of the telescope optics peaks in the red region, the comparison to the R band is thus justified. The agreement between the two measurements is striking.

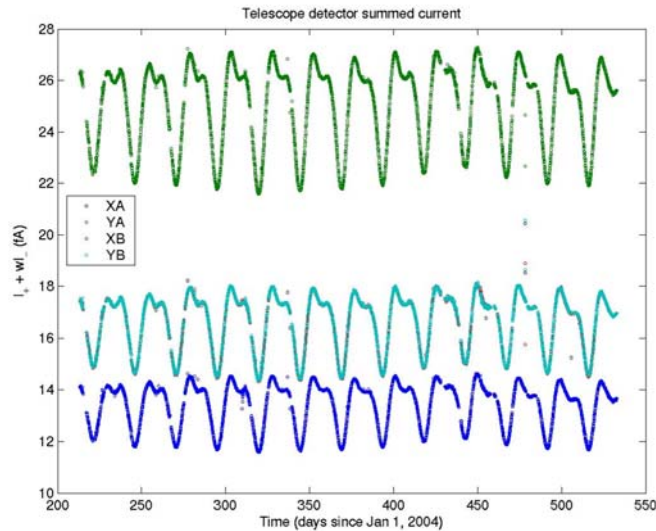


**Figure 11-22.** The scaled summed current for each of the four pairs of detectors.

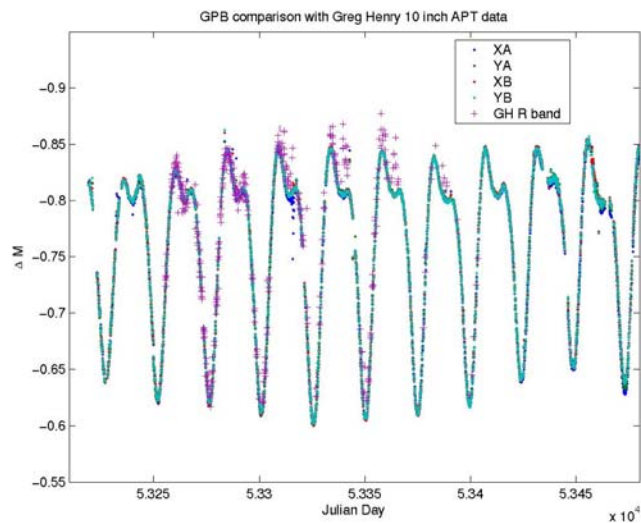


**Figure 11-23.** Comparison of four pairs of scaled summed current with each other and with R band of ground measurement.

In [Figure 11-23](#), there is reasonable agreement of the relative intensity change in all four pairs of detectors. To examine the comparison in more detail, summed currents in XA, YA and YB channels are scaled against XB channel. The scaled values are then normalized near unity. [Figure 11-24](#) show the scaled comparisons.



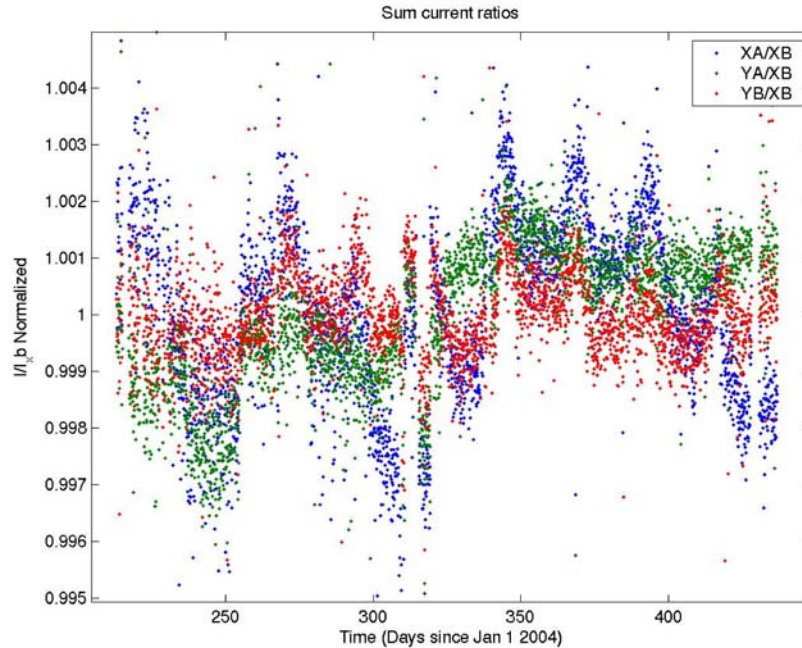


**Figure 11-24.** Scaled summed current compared with the values of channel XB. The ratios have been normalized for easy comparison.

Here, again one sees a variation which correlates with the pattern of the star intensity variation. This provides yet another indirect evidence for weighting factor variation with star intensity. This also provides an estimate of the reliability of the weighted summed current at no worse than  $\pm 0.5\%$ .

Since the transmission to each of the eight detectors has a different color dependence, and IM Peg becomes bluer when brighter, the weighting factor varies with time with the same period of IM Peg. Such variations are typically less than 1%. During the post calibration phase, we observed both Zeta Peg and HR Peg for an extended period of time. Preliminary analysis confirms the weighting factors do depend on the color of the star. Further analysis is in progress to estimate the impact of the weighting factor variation.

Other parameters affecting the pointing bias include the settings of the TRE clamp voltages, the thermal environment of the detector platforms as well as the thermal environment of the TRE box. These effects are also under analysis.

The direct impact of the weighting factor variation is a pointing bias variation in the body fixed frame. To the 1st order, such variation has no impact on the science signal as long as the variation is within the linear region. A detailed analysis is underway to evaluate the ultimate effect on the gyro readout.

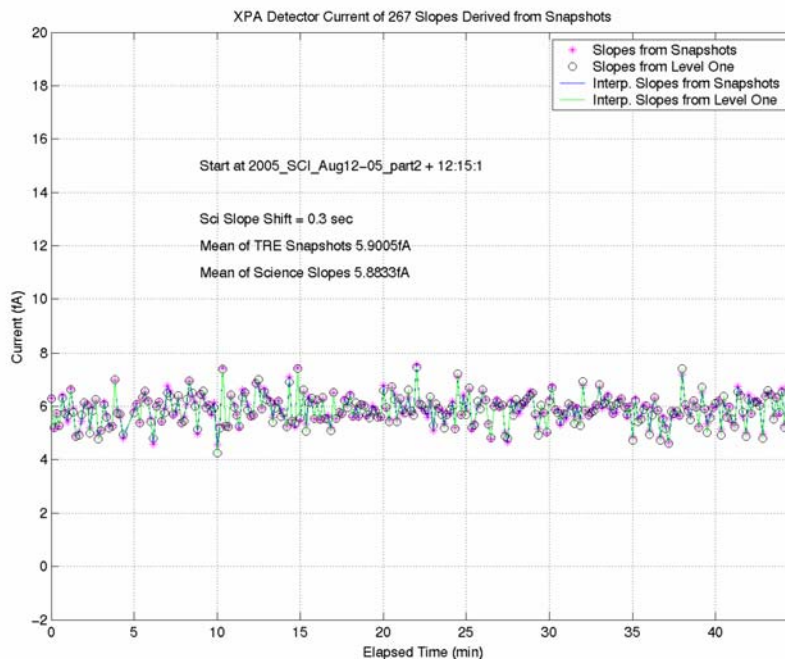


**Figure 11-25.** Comparison of estimated photocurrent based on Science slopes and on least square fit slope derived from TRE snapshots

### 11.4.7 Snapshots Comparison to Science Slopes

The telescope signals are processed by two on-board algorithms, which are named ATC Slopes and Science Slopes. Both the ATC slopes and the Science slopes are calculated at the rate of 10 per second (for all eight detectors); the ATC slopes are used in near real time by the attitude control system to point the telescope at the guide star. Typically, the Science slopes are in the telemetry formats at the highest rate of 10 per second, while the ATC slopes are at a rate of one per second. Intermittently the raw A/D converter samples, which are at a rate of 2200 samples per second, are also in the telemetry data stream called Snapshots. Snapshots need to be manually scheduled, and they are telemetered at a maximum rate of one frame of 300 contiguous A/D samples per ten seconds. There is a 0.3 s offset between vehicle times for Snapshots and Science slopes.

The snapshot data have been processed on the ground for a fidelity comparison between the ground-based Snapshot slope (calculated with a least squares algorithm using the same points as used by the onboard Science slope algorithm) to the slope estimated and reported by the Science slope algorithm. Figure 11-25 shows the result of 267 snapshots compared with Science slopes, where the resulting slopes have been scaled to detector photocurrent in fA. This comparison verifies that the on-board Science filter and a simple least square filter produce similar results with a correlation coefficient of 0.97364. Hence the Kalman filter derived Science slopes differ somewhat from the least squares estimate. This difference is attributed to the choice of Kalman filter coefficients that were optimally derived from a similar comparison early in IOC part of the mission. The Kalman filter provides an optimal estimator for the slope since the charge integrated signal contains both electronic white noise and photon/electron shot noise.

### 11.4.8 Telescope and Windows operating temperature

The temperatures of the window mounts and telescope top plate were monitored continuously until the ECU was turned off on 28 April 2005. After that date, the temperature was measured once a week.

Figure 11-26 through Figure 11-29 show the temperature variations of these platforms from the start of the mission.

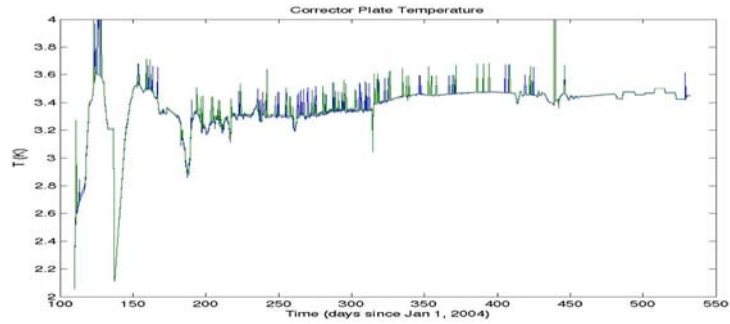


**Figure 11-26.** Temperature variation of telescope top plate

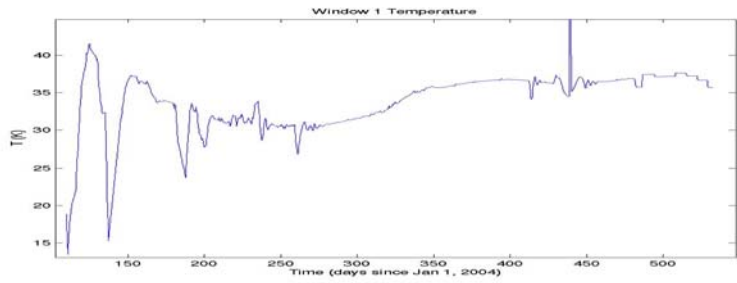


**Figure 11-27.** Temperature variation of Window 1

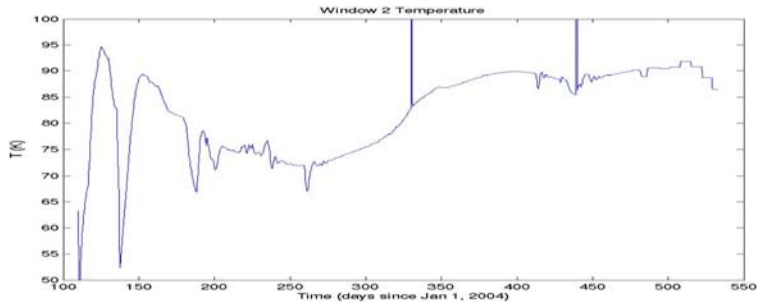


**Figure 11-28.** Temperature variation of Window 2

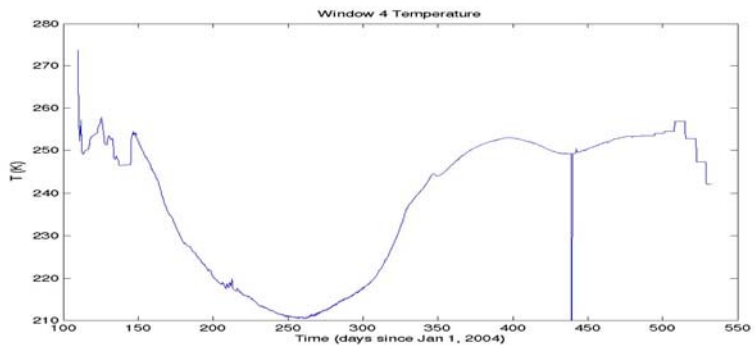


**Figure 11-29.** Temperature variation of Window 4

# 12

## Cryogenic Subsystem Analysis

---





This subsystem provides the cryogenic, mechanical, and magnetic environments required by the science instrument together with a view to the guide star (Figure 12-1). In this section, we focus primarily on dewar performance, particularly lifetime, and on the performance of the magnetic shielding as well as the Probe vacuum.

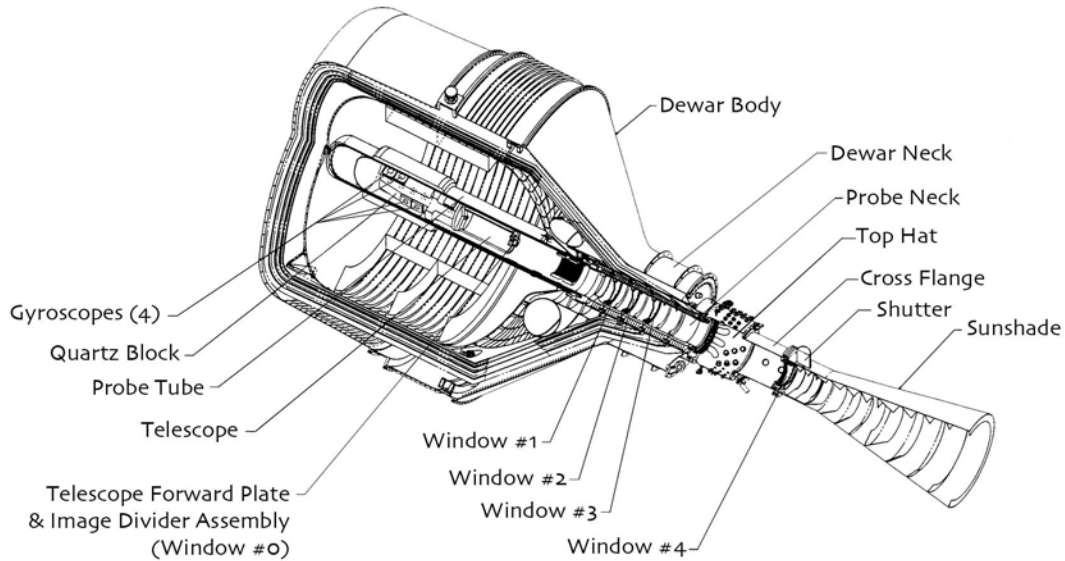


Figure 12-1. Integrated probe and dewar.

## 12.1 Cryogenic System Requirements

Some of the key flight requirements for the dewar, probe, and the magnetic shield system are summarized in Table 12-1 below. Actual flight performance relative to these requirements is discussed in the referenced sections.

Table 12-1. Key cryogenic system flight requirements

Requirement	Section No.	Doc. Reference
Maintain a liquid helium bath temperature < 1.85 K controlled to within 30 mK		T003, PLSE-12
Cryogen lifetime of 16.5 months		T003, PLSE-12
Liquid helium mass measurement to within 5%		PLSE-12
Vent flow measurement to within 5%		PLSE-12
Steady state field / gyro trapped flux < 9E-6 G		T003, PLSE-12
Magnetic field attenuation factor <=2E-12		T003, PLSE-12
Ability to perform flux flush and bakeout		PLSE-12
Alignment stability of roll phase sensor location (Attitude Reference Platform)		PLSE-12

## 12.2 Temperature / pressure control of the Main Tank

The primary function of the dewar is to maintain a tank of superfluid helium at approximately 1.8 K so that the science instrument can be maintained at its operating temperature of ~2.5 K. Thermal stability can be maintained by allowing the heat leaking into the main tank to evaporate the liquid helium at an appropriate rate. This evaporation occurs at the external surface of a sintered porous plug, which acts as a phase separator that retains the superfluid liquid helium in the tank. (The porous plug was invented and developed by GP-B and has been utilized by other flight programs requiring superfluid helium, e.g., IRAS, COBE.) The vapor thus produced is then vented through a chain of four heat exchangers that warm the gas to the external boundary temperature. The heat used to warm the gas is intercepted heat that otherwise would be conducted or radiated to the liquid helium. By this means, the rate of evaporation of the liquid is significantly less than what it would otherwise be. After traversing the heat exchangers, the gas enters the thruster manifold and then is supplied to the sixteen thrusters.

The ATC subsystem controls the gas flow from each thruster according to the needs not only for attitude and translation control but also to maintain the appropriate pressure in the main tank. In general, the boil-off rate of the dewar exceeds the amount of gas needed for thrusting, and, in that circumstance, the excess gas is “null dumped” such that no net torque or force is produced. When there is positive excess gas flow, the ATC pressure control algorithm controls the total gas flow in such a way as to maintain a constant pressure in the thruster manifold. If, on the other hand, the demand for thrusting exceeds the amount dictated by the pressure control loop (negative excess mass flow), ATC allows the needed flow regardless of the pressure control loop.

If the negative excess gas flow is such that on average the flow exceeds that provided by the main tank under normal heat load, the pressure will decrease in the main tank causing the temperature also to drop. This is accompanied by excessive cooling of dewar heat exchangers due to the high flow rate. If this condition were to persist, it could be compensated for by applying electrical heat to the main tank. It was not necessary to do this, however. In fact, except for special events and circumstances, ATC did maintain the main tank within a 5 mK temperature band, well within the 30 mK requirement.

## 12.3 Events and conditions related to Dewar performance

The liquid helium consumption rate is not only determined by long-term conditions, but also by various events and conditions. Most of these events occur during the IOC (Initialization and On-Orbit Checkout) because they are either part of planned IOC activity or because most unanticipated events occur early in the mission as part of the shakedown process. In fact, no significant additional thermal events occurred during the remainder of the mission.

### 12.3.1 Launch

Launch occurred with the main tank 95.5% full (337 kg) and at a temperature of approximately 1.8 K. These meet the requirements of launching at least 95% full and at a temperature less than or equal to 1.9 K. The guard tank was maintained at 4.2 K with normal boiling point liquid helium in order to reduce the heat rate to the main tank and avoid any need for servicing the main tank on the launch tower. During ascent the guard tank vented through a flow restrictor and a check valve that fully opened in zero-g. (The flow restriction was requested by Boeing in order to ensure that the cold gas would not damage the fairing on ascent.) This blow-down and depletion of the guard tank caused a substantial sub-cooling of the guard tank, heat exchangers, and vapor-cooled shields. This temporarily maintained a heat rate into the main tank that was below the steady-state value, which, if anything, is beneficial to the performance of the system. (The guard tank normally runs in the 25 – 30 K range when cooled only by vent gas from the main tank.) The flow restrictor prolonged the complete depletion of the guard tank, but this had no material impact on the performance of the cryogenic subsystem.



### 12.3.2 Thermal transient events

About a week into the mission, large thermal transient events (temperature spikes) were observed at probe and dewar station 200 and elsewhere in the Probe (Figure 12-2). These events were logged as Observation 029, and were noted to have a period of about 24 minutes and an amplitude of 20 - 40 mK at probe station 200. After five days, the amplitude had increased to 150 mK with a period of 40 minutes as measured at probe station 200, and an adverse impact on SQUID readout performance was noted. Although no direct evidence was available to confirm it, it was felt that the only feasible explanation for this phenomenon was periodic desorption and adsorption of residual helium gas in the dewar well. (A small long-term leak through cold valve RAV5 allowed helium to leak into the well during guard tank fill operations prior to launch. A special well pumping line had been installed to allow the well to be evacuated after fill operations. Normally pumping operations would extend for about a day, but due to prelaunch schedule limitations, this was curtailed to a few hours after the last fill operation prior to launch.) Because the well was slowly venting to space through an opened pyrovalve, it was felt that this problem would eventually resolve itself. Indeed, the period between spikes continued to lengthen and the phenomenon was self-extinguishing by the time the flux reduction operation (see below) was initiated. The heating that occurred during the flux flush operation undoubtedly caused additional gas desorption and removal from the well, and the phenomenon was never observed again. It should be noted that although this phenomenon had a significant adverse impact on SQUID readout noise performance, it did not have a significant impact on dewar thermal performance.

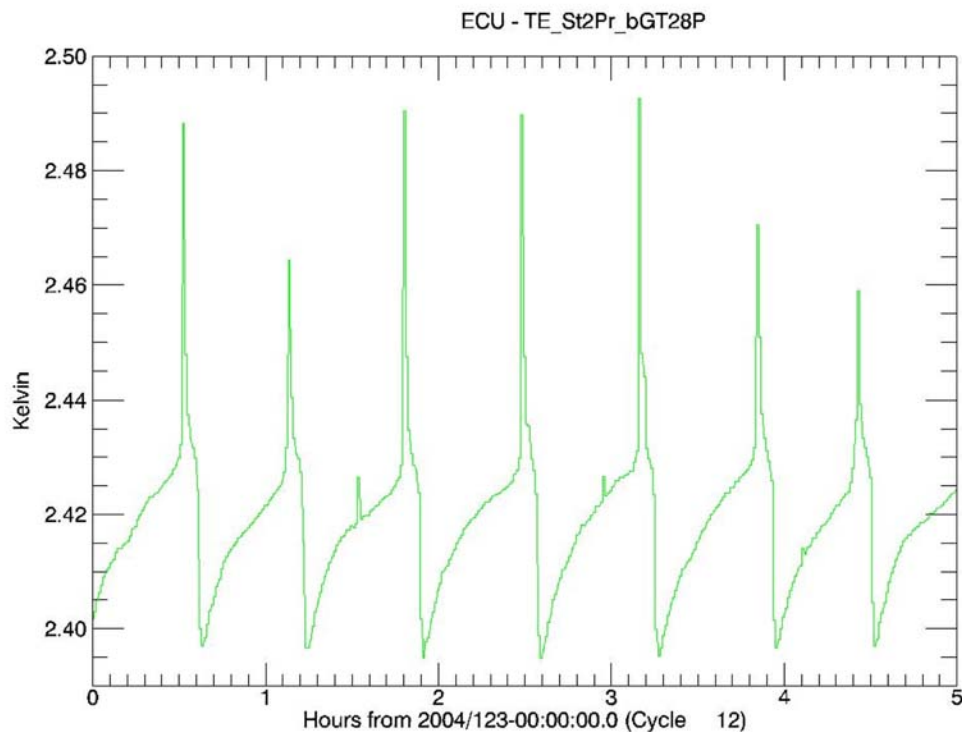


**Figure 12-2.** Temperature spiking at probe station 200 (primary cryogenic probe/dewar interface).

### 12.3.3 Stuck thrusters

On two separate occasions, after launch and near the end of the flux-reduction operation, one thruster (numbers 6 and 8, respectively) failed in a high-flow configuration. In each case, the problem was corrected by closing the appropriate thruster isolation valve (TIV). (There is sufficient redundancy in the thruster system to

control the space vehicle without these two thrusters.) As a result, there was excessive loss of liquid helium. Some of this loss is recoverable (sub-cooling of the heat exchangers and vapor-cooled shields temporarily reduced the heat rate; flow rate can consequently be reduced to allow temperatures to recover to normal values), but there is also some permanent loss.

### 12.3.4 Heating events in the Probe

There were three heating events in the Probe. These events added additional heat load to the main tank primarily through the station 200 interface, but also to some extent through residual gas conduction in the dewar well. These events were 1) low temperature bakeout rehearsal, 2) trapped flux reduction, and 3) low temperature bakeout (post gyro spinup). The first and third events were relatively mild with maximum temperatures in the 6–7 K range and durations of less than a day. The trapped flux reduction process produced temperatures up to 13 K and lasted for 36 hours. This event warmed the main tank over 1.9 K as the maximum vent rate (limited by choking of the porous plug) was not high enough to maintain heat balance. Functionally, however, all the heating events met their requirements and accomplished their purposes.

### 12.3.5 Drag-Free operation

After gyro spinup and at the commencement of drag-free operation, it was found that there was sufficient negative excess flow rate (i.e., demand by ATC for flow in excess of that called for by the pressure control loop) to cause the main tank to cool. Compared to the stuck-thruster incidents, however, this incident was rather minor with the negative excess occurring only during a fraction of each orbit. If this matter could not be resolved, however, it had the potential for shortening mission lifetime. It was subsequently discovered that if the pressure control loop were given additional control authority (a total range of 3 mg/s instead of 0.6 mg/s) the subsequent reduction in null dumping was sufficient to make up for the periods of negative excess flow and stabilize the tank temperature in the long run. The main tank has enough heat capacity that it does not react noticeably to orbital period flow variations.

### 12.3.6 Effect of Dewar shell temperature

The parasitic heat rate into the main tank (i.e., the heat rate in excess of that imposed by the science instrument) is ultimately a function of the dewar vacuum shell temperature. The exposed portion of the dewar vacuum shell (the cone and cylinder) is passively cooled by use of a FOSR (flexible optical solar reflector) film. This film reflects visible solar radiation while being an effective radiator to space in the infrared wavelengths. In general, shell temperatures followed seasonal trends as expected (colder when the sun was aft and illuminating the spacecraft, and warmer as the sun moved forward). On some occasions, however, the dewar shell temperature would run warmer than predicted (see discussion on lifetime estimation below), and this would have the tendency to elevate the heat rate into the main tank.

### 12.3.7 Thermo-acoustic oscillations (TAOs)

A TAO is a pressure oscillation that can occur in any gas-filled line that traverses a large thermal gradient, for example, the vent line of a cryogenic system. It is driven by the thermal gradient, and can sometimes cause a dramatic increase in heat rate to the cryogen. TAO activity has been previously observed in the main tank vent line in some non-flight configurations, and the question naturally arises as to whether it has affected heat rate on orbit. The answer is *no* for two reasons: The entire GP-B vent system was analyzed by Dr. Sidney Yuan, a recognized authority on TAO analysis, who determined that it was unconditionally stable against TAO. Secondly, the short-term peak-to-peak variation in the unfiltered thruster manifold pressure data during flight was approximately 0.1 torr. (Some of this is undoubtedly electronic noise since the analog circuitry before the

A/D converter is broadband. Also, operation of the thruster system contributed to pressure fluctuations.) Our experience has indicated that TAO activity at the 0.1 torr level or less is completely inconsequential compared to the normal parasitic heat rate. Thus, there is no evidence that TAO activity played a role in flight performance.

## 12.4 Lifetime projection

Most missions that use expendable cryogenics are typically observational in nature. Lifetime prediction is useful for planning and prioritization. In the case of GP-B, however, lifetime prediction is a bit more significant in nature. This is because the mission plan calls for a post-science calibration phase to apply known perturbations and measure their effects. This allows the quantification of various systematic errors. Many of these tests are done at the end of mission because they involve perturbing fully spun-up gyros, effectively ending science and entailing some degree of risk. As a consequence, it is important to monitor dewar performance and periodically make updated predictions of the time of cryogen depletion.

### 12.4.1 Thermal models

Because the dewar shell temperatures vary somewhat throughout the year, the heat rate to the main tank also varies. In order to predict future heat rates, it is useful to have a thermal model of the space vehicle that predicts the dewar shell temperatures and a thermal model of the payload that estimates heat rate into the main tank as a function of the dewar shell temperatures. The payload model correlates well with both ground measurements and with on-orbit measurements when measured dewar shell temperatures are utilized. There is some discrepancy, however, with the ability of the space vehicle model to predict dewar shell temperatures on orbit. This model predicts shell temperatures on the dewar forward cylinder that are as much as 10 K lower when measured in the warm season (sun forward). Likewise, the model under-predicts the dewar top plate temperature by as much as 10 K during the cold season (sun aft). Discrepancies at other locations and seasons are not as severe. The net effect of these discrepancies on payload performance, however, is not major. The average flow rate predicted on the basis of measured shell temperatures is 7.68 mg/s, whereas the value predicted for calculated shell temperatures is 7.84 mg/s, a 2.1% discrepancy (Figure 12-3). It should be noted, however, that cryogen lifetime easily exceeds one year. That being the case, once the launch anniversary is reached, it is possible to look at the previous year's data to aid in prediction. The perturbations occurring during the IOC phase tend to limit the utility of this approach, however.

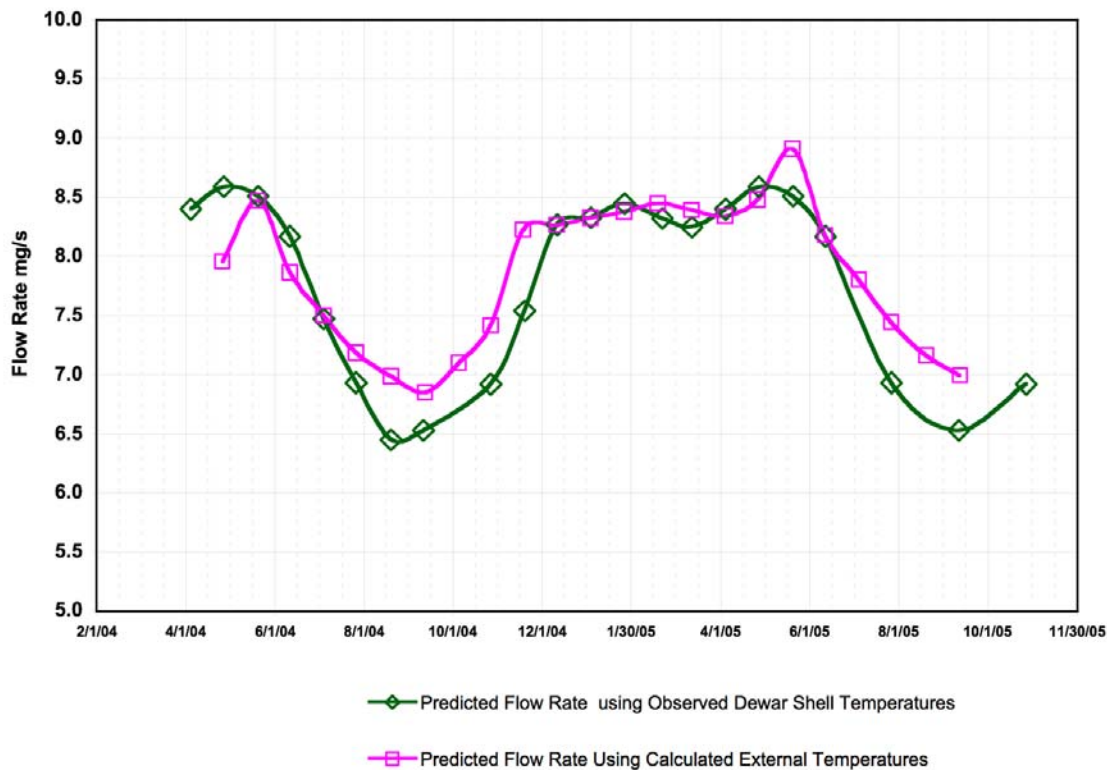


**Figure 12-3.** Helium flow rate predicted by dewar model based on both the measured shell temperatures and predicted temperatures.

### 12.4.2 Helium mass gauging

There are three independent ways of determining helium usage. Two of the three, the flow meter and the heat pulse measurement system, are instruments built into the dewar. The remaining is a mass flow rate estimate generated by the ATC software, based on commanded control force and the nominal specific impulse of each thruster. The two flow rate measurements must be integrated downward from the initial quantity of liquid helium (337 kg at launch as determined by a superconducting liquid level sensor coupled with a solid model of the interior of the main tank), whereas the heat pulse measurement yields a direct measurement of remaining liquid. Other factors involved in these measurements will be reviewed below.

### 12.4.3 Initial lifetime estimate

The prediction for on-orbit performance made prior to launch was 18.8 months with no contingency. This result did not include impacts of planned thermal events. For purpose of a prediction near the end of IOC, vacuum shell temperatures were adjusted upward by a fixed temperature increment. This was a conservative way to incorporate elevated dewar shell temperatures. Using this approach, the payload model predicted an annual average boil-off rate of 8.3 mg/s. Based on the heat pulse measurement result of 269 kg on 28 June 2004, we expected a remaining life of 10.5 months as of 8/23/04 (near the end of IOC). Total predicted lifetime was 14.7 months from launch compared to the mission requirement of 16.5 months. According to the Program Chief Scientist, however, this was deemed sufficient to meet mission needs.

## 12.4.4 Update of lifetime estimate

After the passage of over a year since launch, six HPM measurements (see below) had been made and other information became available that caused a significant change in our lifetime estimate. Our new estimate was for depletion to occur on September 1, 2005, for a total lifetime of 499 days or 16.4 months, an increase of 1.7 months over the initial estimate. This corresponds to an average boil-off rate of 7.8 mg/s. The reason for the change was that early in the mission there were insufficient HPM operations to establish a trendline and it was assumed that the flow meter results were accurate. As more HPM data, which correlated well with ATC flow rate values, became available, it became clear that the flow meter results were too high, and they were consequently discounted.

## 12.5 Heat pulse measurement (HPM) operation

This section discusses the heat pulse measurement (HPM) procedure that was used to determine the amount of liquid helium remaining in the dewar at various points in the mission.

### 12.5.1 Principle of operation

The HPM operation is a calorimetric technique involving the addition of a known amount of thermal energy to the main tank and measuring the resulting temperature rise to determine the mass of liquid helium. This can be done to a reasonable degree of accuracy for three reasons: 1) The heat capacity of the main tank is dominated by that of the liquid helium, 2) the thermodynamic properties of liquid helium are well known, and 3) the fact that the measurement involves superfluid helium means that the liquid is highly isothermal and that its thermal relaxation time is virtually instantaneous. (This is true of even separate pockets of liquid but not true of the vapor phase, as will be discussed below.) In order to make the most accurate measurement, however, it is useful to defeat the ATC pressure control loop and maintain a constant flow rate throughout the entire heat pulse period. The amount of heat added is chosen such that it is expected that the temperature rise will be on the order of 10 mK. This is a large enough temperature rise to allow a reasonably accurate measurement of the temperature rise yet not so large as to significantly affect dewar lifetime. Because of the potential to adversely affect lifetime, the hardware used to supply power to the heat pulse heaters is designed with redundant shutoff mechanisms. In addition, they are limited in number (four in a year vs. typically four a day for the flow meter) in order to limit impact on lifetime and risk.

There is another issue that should be noted. The amount of helium deduced from the HPM for a given temperature rise is proportional to the amount of thermal energy deposited into the main tank. The intention was to infer the energy from the measurement of the voltage across the heater resistance in conjunction with the measured current or known heater resistance. The measurement was to be made with a standard four-terminal technique. This is important because the electrical leads that traverse the thermal gradient of a dewar are made of a relatively resistive material (manganin) in order to limit thermal conductance. Unfortunately, due to a design oversight, the input of the op-amp used to measure the voltage was referenced to ground, as was the current source. This meant the measured voltage included the voltage drop across some of the electrical leads, which, in turn, introduces a potential scale factor error. This also meant that the inferred quantity of helium could be in error by some factor and the consumption rate could also be off by the same factor. It is essential to note, however, that since this is a scale factor error, it does not affect the zero intercept, the projected time of depletion.

The only effect that is likely to cause a bias error, which does affect the projected time of depletion, is a source of heat capacity in addition to that of the liquid helium. Additional, unaccounted for, heat capacity would lead to over-estimation of the quantity of liquid and the lifetime. There are two candidates in this regard: the main tank assembly and the helium vapor. The former is completely negligible: The main tank, taken as 250 kg of aluminum, has a heat capacity approximately equal to one part in  $10^4$  of 100 kg ( $\sim 1/3$  of initial fill) of liquid

helium at 1.8 K. It does not appear, however, that the effect of the vapor is quite so negligible: When the main tank is at 10% of capacity, the heat capacity of the vapor is nearly 6% of that of the liquid. In the analysis of the HPM results, it was therefore assumed that the vapor was in equilibrium with the liquid, and its contribution to the overall heat capacity was taken into account. This turned out to be a questionable assumption, as will be discussed below.

## 12.5.2 Results from HPM operations

Six HPM operations have been performed with the first being on 6/28/04, and the last on 7/29/05. In each case, the duration of heater operation was selected to yield a temperature increase of approximately 10 mK with a heater power of 1.44 W. This was chosen to yield a good signal-to-noise ratio for the temperature rise ( $\sim 1\%$ ) without perturbing the system too greatly or significantly reducing lifetime ( $\sim 15$  hours for the first measurement and proportionately less for subsequent measurements). An example of the data produced by such a measurement is shown in Figure 12-4, and the results of all six measurements are shown in Figure 12-5 together with a linear fit and extrapolation to depletion. Also shown in the latter figure is the fact that a backward extrapolation of the linear fit to the date of launch disagrees with the initial quantity of 337 kg by about 13%. This disagreement is indicative of a possible scale factor error, discussed above, which does not alter the zero intercept on the time axis (end of life).

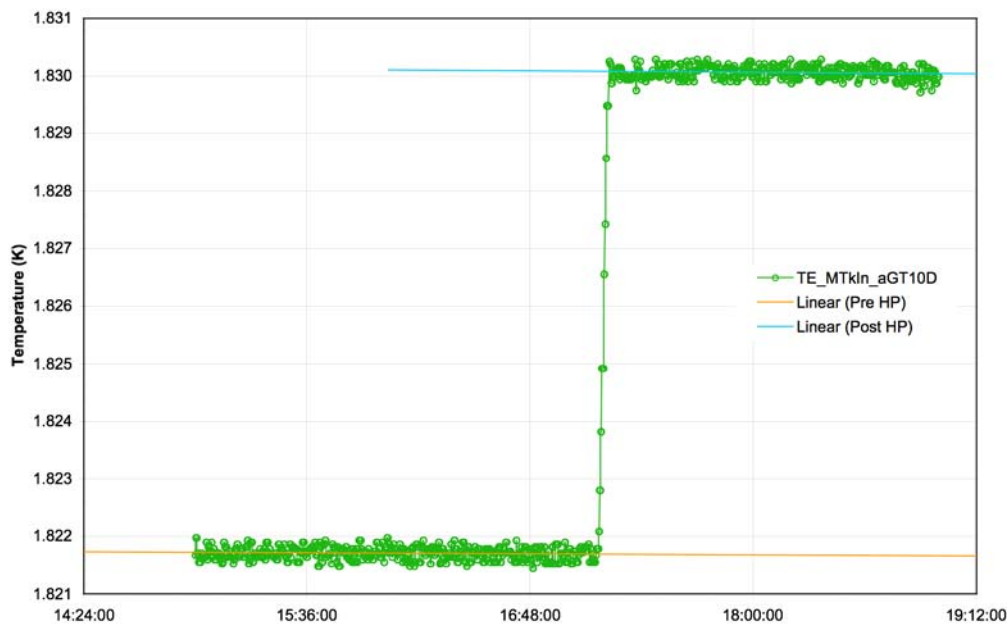


**Figure 12-4.** Main tank temperature in response to fourth heat pulse measurement with linear trendlines before and after heat pulse. Temperature increase is taken to be the difference in the two trendline values at the middle of the pulse.

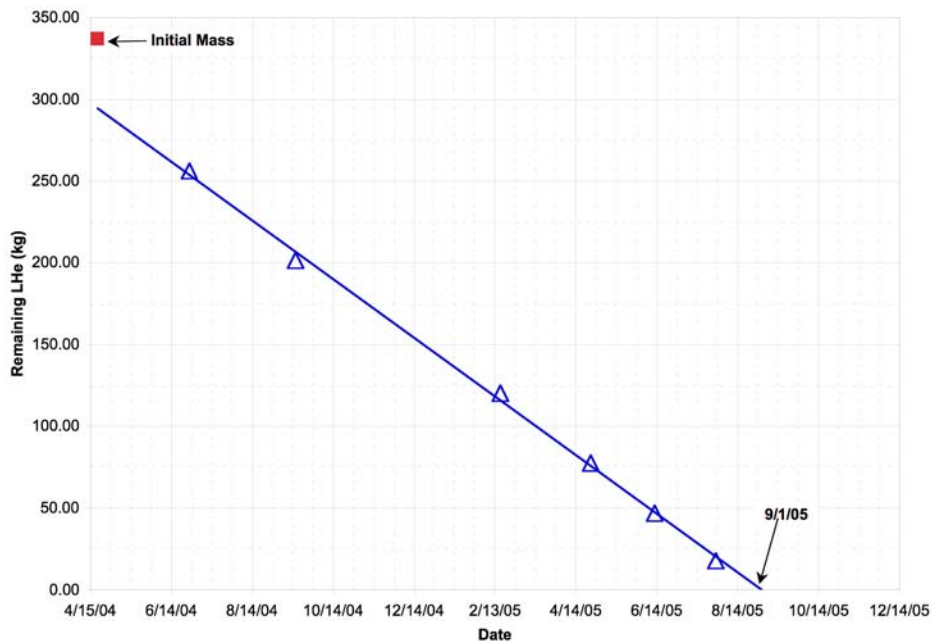


**Figure 12-5.** Plot of the remaining mass of liquid helium as a function of HPM measurement date with linear trendline. The fact that the trendline does not project backwards to the original quantity of liquid helium (taken to be 337 kg) is indicative of a scale factor error.

## 12.6 Dewar Vent Rate Measurement

The mass flow meter measures temperature rise of gas stream resulting from a constant heater power input. It consists of a combination of a heater and thermometer located on the main tank vent line between HEX0 (Heat Exchanger-0) and HEX1. In general, the higher the flow rate, the lower the temperature rise. The thermal response to flow is typically nonlinear and is calibrated during ground test with a wet test meter. Because of the heat added to the cryogenic region (80.6 mW), the heater is operated intermittently with typical flow meter operation being performed generally four times a day for the first year of the mission. (After that the Experiment Control Unit, ECU, which operated the flow meter, was turned on only once a week due to interference with two of the SQUID readout systems.) By integration of the flow data from a time when the quantity of helium is otherwise known, it is possible to estimate the current quantity of remaining helium.

As noted previously, ATC also continuously estimates flow rate for control purposes using pressure transducers at each of the thrusters. A plot of both measurements is shown in Figure 12-6. Figure 12-7 shows the remaining mass estimate obtained from integrating both of these flow rate measurements together with linear least-squares fits for both curves. The ATC flow rate result is typically about 10% lower than the dewar flow meter. This shows up as a difference in slopes in Figure 12-7. Since both curves start with the presumption of 337 kg, there is approximately two months of difference in the projected times of depletion from the linear fits. This points up an inherent problem with the integration of a flow rate measurement: any systematic error, whether bias or scale factor, ends up affecting the end point estimate.



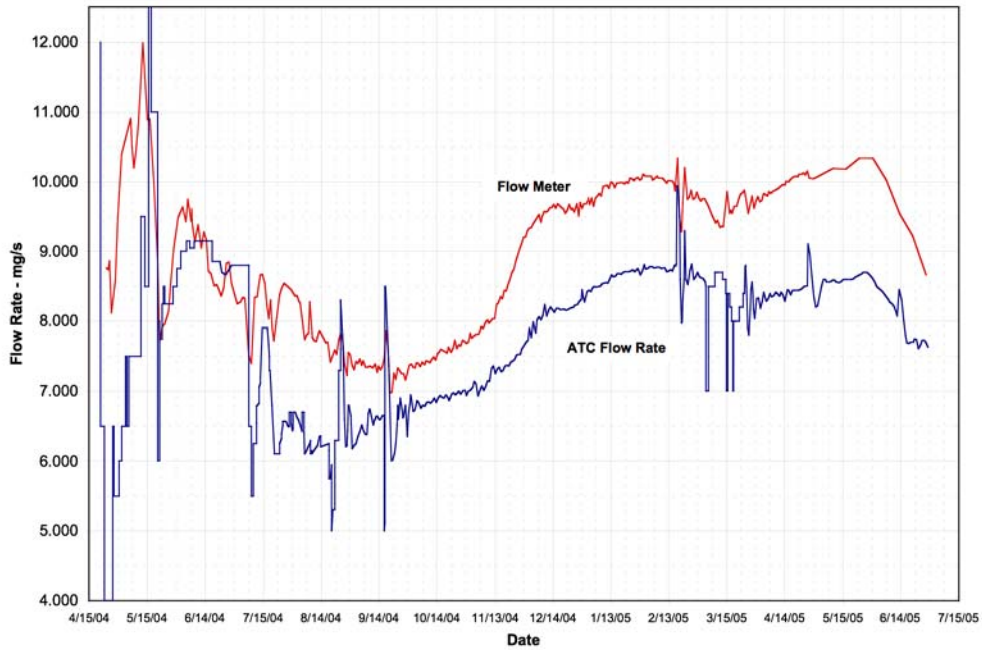


**Figure 12-6.** Flow meter and ATC flow rates as a function of UTC date starting at launch. Data encompass periods of flow control (constant segments in the ATC data) as well as pressure control.

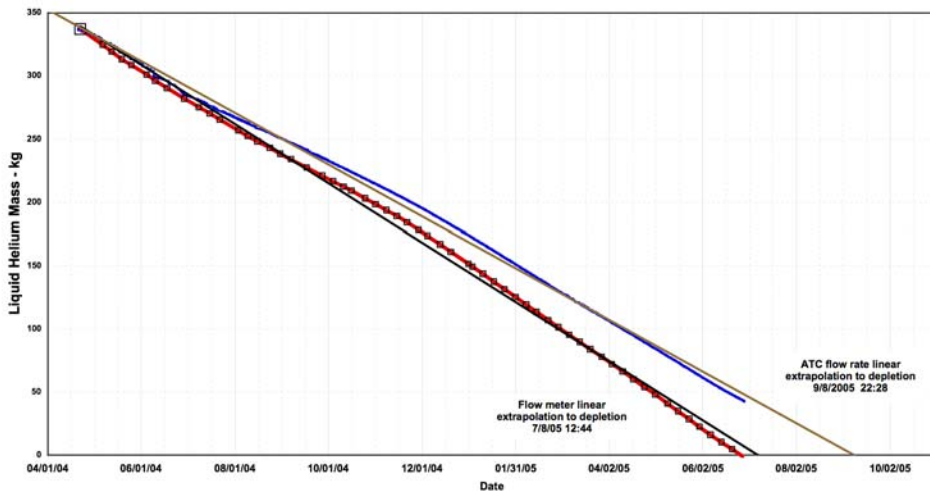


**Figure 12-7.** Mass remaining estimated from integrated flow meter and ATC flow rates. Trendline fits are extrapolated to zero mass. Since depletion did not occur in early July, it is clear that the dewar flow meter results under-predicted lifetime.

## 12.7 Reconciliation of lifetime estimates

A comparison of [Figure 12-5](#) and [Figure 12-7](#) indicate that the three different measurements yield three different predictions for end of life. However, the HPM and ATC results disagree only by eight days out of 16.4 months (1.6%). Of the three, the HPM was probably the most credible for the reasons that have been noted.

This implied that the dewar flow meter results were about 10% too high. It should be noted that there is a reason to be concerned about the dewar flow meter calibration: The calibration of the flow meter was performed during payload test and prior to a replacement of a dc-dc converter in the ECU after the vehicle had been shipped to Vandenberg. Thus there is a possibility that the power being applied to the flow meter heater is different than that used during calibration. There is a provision for four-terminal voltage measurement on this heater, but unfortunately this monitor circuit suffers the same problem as the HPM heater monitor.

In addition, there is one other piece of evidence in support of the conjecture that the dewar flow meter results are about 10% too high. If the ATC flow data are plotted together with the dewar flow meter data reduced by 10%, and the dewar thermal model results (based on measured dewar shell temperatures) are also plotted, all three results are in reasonable agreement. This is illustrated in Figure 12-8. Also, by using the 13% scale factor correction on the HPM results and inferring an average flow rate, the HPM results can be brought into the comparison: The average flow rate thus inferred from the HPM is 7.80 mg/s, which compares to the long-term ATC average of 7.72 mg/s. Hence, it would appear that although there were some unresolved issues, the various gauging techniques could be reconciled with each other in a consistent way by making some reasonable assumptions.

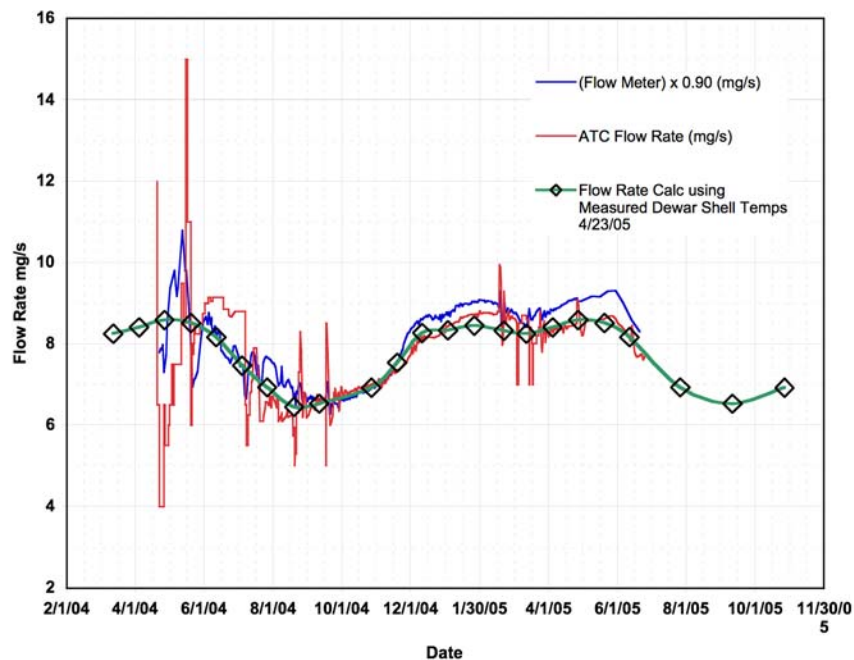


**Figure 12-8.** Flow meter data reduced by 10% and plotted with ATC flow rate and flow rate predicted by the dewar thermal model. Thermal model is based on measured shell temperatures rather than predicted shell temperatures.

## 12.8 Comparison of lifetime prediction with final result

Subsequent to the last HPM operation, updated EOL predictions were made by integrating the ATC flow downward from the last HPM result (17.8 kg) to the then-current date, and then integrating to zero using a projected flow rate based on the flow rate measured a year ago. The resulting EOL predictions varied a little but

were generally within a day or so of September 2, 2005. The actual time of depletion turned out to be 20:50 Z on September 29, 2005 (527.2 days or 17.3 months into the mission). This represents a mission duration prediction error of -5%.

Although a 5% error in duration does not seem too bad, in fact it represents a substantial error in the latter HPM results. For example, HPM #6 (on day 465 of the mission) yielded a liquid mass estimate of approximately 20 kg. (This includes the 13% correction for the probable scale factor error noted previously.) If one were to assume a constant boiloff rate of 337 kg over 527 days, one would expect that there would have been approximately 39.6 kg on day 465. HPM #6 was therefore likely to have been 49% too low. It should also be noted that the sign of the error (underestimation of liquid) is such that the problem is not that there is heat capacity missing from the analysis, but rather there is too much non-liquid heat capacity being assumed in the analysis. (This turned out to be fortunate because it caused the program to start the calibration phase earlier than it would have otherwise. The extra time in the calibration phase turned out to be very valuable.)

The most likely source of this problem is an assumption made in the analysis of the HPM data: that the entire contents of the main tank, liquid and vapor, were in equilibrium both before and after the heat pulse. This is probably not correct. The contact between vapor and liquid comes in two forms: thermal and mechanical. When power is applied to the HPM heater, which is in contact with the superfluid, its temperature and saturated vapor pressure increase immediately. (The roll of the vehicle at a rate of 12.9 mHz forces the liquid to reside against the outside wall of the main tank and the vapor to form a central vapor bubble surrounding the well during most of the mission. The HPM heaters are mounted on the slosh baffles, which are located at the outer wall and thus are kept in good contact with the liquid.) The pressure increase propagates at the speed of sound throughout the vapor and can maintain even isolated pockets of superfluid (if any were to exist) in equilibrium through the process of evaporation and recondensation. This effect has been clearly demonstrated by M. Wanner for the ISO program. [Ref.: M. Wanner, *Adv. Cryo. Eng.* **33**, 917 (1988).]

Thermal transfer within the bulk of the vapor phase is of a different nature, however. Since the vapor is a classical gas, there are two mechanisms that transfer heat: thermal conduction and convection. It will be shown that the vapor is convectively stable so that the primary thermal transfer mechanism is conduction, wherein the temperature distribution is governed by the diffusion equation together with the relevant boundary conditions. The relevant diffusion coefficient to be used in this equation is the thermal diffusivity, which is the ratio of the thermal conductivity of the gas to its heat capacity per unit volume (i.e., the specific heat times the density). It is equal to approximately  $1 \times 10^{-6} \text{ m}^2/\text{s}$  for saturated helium vapor at 1.85 K. The key question now is how the equilibration time scale compares to the post-heat-pulse measurement time. An order-of-magnitude estimate of the equilibration time is reciprocal of the thermal diffusivity times the square of a relevant dimension ( $\sim 0.5 \text{ m}$ ), which is on the order of  $10^5 \text{ s}$ . The post-pulse measurement time was always less than  $10^4 \text{ s}$  (see [Figure 12-4](#)). Although the numbers are rough, they definitely do support the picture that true thermal equilibration is slow compared to the measurement time and consequently that the vapor is essentially adiabatically compressed by the change in vapor pressure induced by the heated liquid.

As noted above, all the initial HPM analysis was done assuming liquid-vapor equilibrium. This is the assumption made on the SHOOT program [Ref.: M.J. DiPirro, P.J. Shirron, and J.G. Tuttle, *Adv. Cryo. Eng.* **39**, 129 (1994)], although it was noted that this assumption did not apply during ground test when stratification would occur. In our case, when approximately three weeks had passed after the predicted depletion date without depletion actually occurring, it was decided that the liquid-vapor equilibrium assumption needed rethinking. This was done by re-analyzing the HPM results under the assumption that the vapor phase underwent no change of state during the measurement period subsequent to the heat pulse. This assumption essentially has the effect of ignoring the presence of the vapor and is the one used in the Wanner paper cited above. The result of the re-analysis was to extend the EOL estimate by over a month to 10/11/05, which turned out to be in error by +2.3% (total mission duration). Although this was an improvement over the original estimate (duration prediction error of -5%), it was realized that this was a untenable assumption except as a simple mathematical approximation: Even though it is reasonable to assume that the vapor is thermally decoupled from the liquid for

the time scales under consideration, it is not reasonable to assume that it is mechanically decoupled. As noted above, over short time scales the evaporating liquid will adiabatically compress the vapor, and this will cause both a density and a temperature increase throughout the bulk of the ullage vapor. In fact, an estimate (based on thermodynamic data) of the effect of heating 1.85 K liquid by 10 mK indicates that the vapor will be compressionally heated by 24 mK, or over twice as much as the liquid! It is for this reason that the vapor is most likely to be convectively stable, as was asserted previously. In order to test this hypothesis, the HPM data were re-analyzed a third time under the assumption of adiabatic compression of the vapor. Since this assumption takes the vapor off the saturated vapor pressure curve, the density and specific internal energy changes in the vapor were calculated using the adiabatic compressibility parameter derived from tabulated thermodynamic data. [Ref.: V.D. Arp, and R.D. McCarty, NIST Technical Note 1334, 1989.] The results of the analyses of the HPM data using each of the three assumptions together with the actual depletion date are shown in [Figure 12-9](#). It can be seen that the case where adiabatic compression has been assumed yields results that are intermediate between the other two. This is not surprising since adiabatic compression by a given pressure increment takes less energy than equilibrium compression (which is more nearly isothermal) thereby causing the analysis to produce a larger liquid mass estimate. The reduction in mission duration prediction error achieved by assuming adiabatic compression rather than equilibrium compression is fairly modest, however, -3.8% instead of -5.3%. It is not clear why the systematic error is this large (implied error of -31% for HPM #6 after correcting for the 13% scale factor error), but it is clear from the algebraic expression used to calculate the amount of liquid that the problem is likely to involve an error in the presumed properties of the vapor, either the density or the specific internal energy, or both.

## 12.9 HPM Results: Conclusions

The following appear to be reasonable conclusions based on our experience with the HPM technique:

1. The calorimetric HPM technique is well (and uniquely) suited for use in measuring the quantity of remaining superfluid liquid helium and in estimating time of depletion. Unlike an integrated flow meter technique, the end-of-life estimate obtained from a sequence of HPM operations is insensitive to scale-factor (e.g., heater calibration) errors. If the initial quantity of superfluid is known with confidence, it can be used to detect and correct errors of this sort.
2. For 1.8 K operation, the largest source of systematic error in the EOL estimate appears to be in accounting for the effect of the ullage vapor. We analyzed our data using three different assumptions regarding the post-HPM state of the vapor: a) the vapor stays in complete equilibrium with the liquid; b) the vapor is completely decoupled from the liquid and does not change state as a result of heat applied to the liquid; and c) the vapor is adiabatically compressed by the increase in vapor pressure (i.e., the vapor is mechanically coupled to the liquid, but is thermally isolated). The first assumption is implausible because the thermal equilibration time of the vapor is much longer than the measurement time. It led to a 5.3% underestimate of lifetime. The second assumption is implausible because mechanical coupling does cause rapid change in the state of the vapor when the liquid is heated. This assumption led to a 2.3% overestimate of lifetime. The last assumption is plausible if the ullage volume is large enough that the thermal diffusion time is long compared to the measurement time. This assumption led to a 3.8% underestimate of lifetime. It should be noted that one would logically expect that the actual result should lie somewhere between the predictions based on the first and third assumptions since, in reality, the system should be somewhere between isothermal and adiabatic. The fact of the matter, however, is that the actual result was between the second and third assumptions. Why this should be the case is not clear.
3. Ultimately the vapor does re-equilibrate with the liquid so that, in principle, it should be possible to wait long enough after the HPM operation for the equilibrium assumption to be true. Unfortunately this is rarely a viable option. In a passive vent system (the most common configuration), the change in flow rate caused by the HPM will cause long-term instability in the vent system (including the vapor-cooled

shields) and subsequent instability in the bath temperature that will disturb the vapor equilibration process. Even in a system such as ours, where the vent rate is actively controlled, the long-term stability is rarely adequate due to environmental variation over various time scales (roll, orbital, diurnal) and due to electronics and sensor drift.

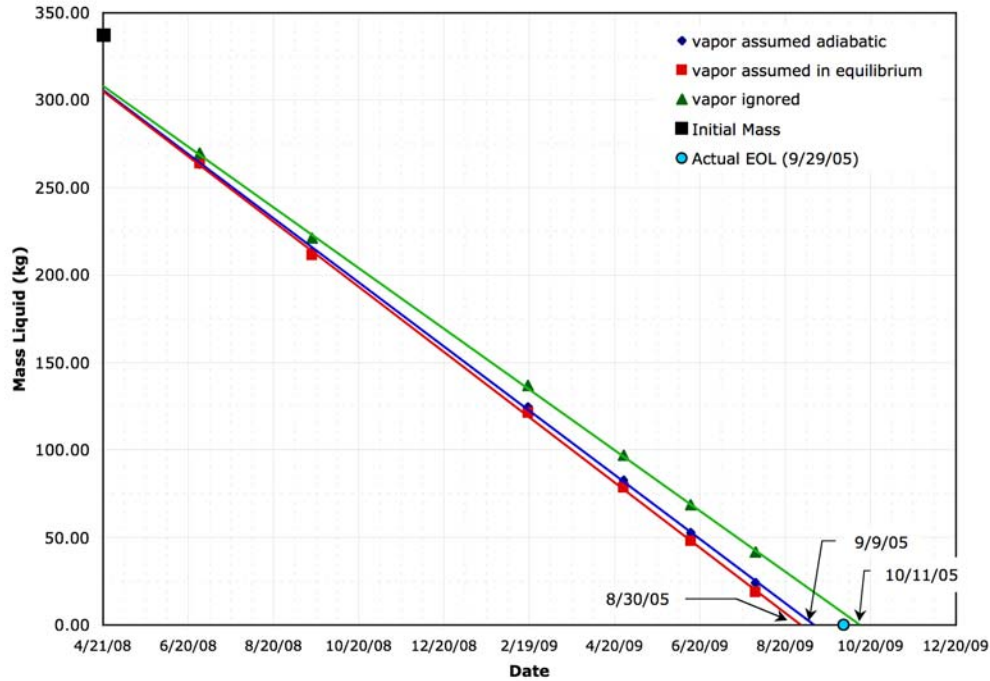


**Figure 12-9.** HPM data analyzed under three different assumptions together with extrapolated linear trendlines.

## 12.10 Magnetic Shielding Performance

This section describes two aspects of GP-B's magnetic shielding performance that are related to the cryogenic system: trapped flux in the gyro rotors and AC shielding.

### 12.10.1 Rotor Trapped Flux

GP-B has a unique magnetic shield system that provides an ultra-low magnetic field environment for the science instrument. Considerable effort was also made to ensure that the materials used in constructing the Probe and the science instrument did not degrade this environment. The primary reason for this requirement is the need to keep the magnetic flux in the gyro rotors below 9 microgauss (0.9 nT) uniform field equivalent.

The trapped flux in the gyro rotors measured on orbit is smaller than 4  $\mu\text{G}$  for all gyroscopes as shown in [Table 12-2](#). (The readout system is only capable of measuring the component of trapped flux that threads the pickup loop and varies in time as the rotor rotates.) The trapped field in gyro 4 is more than an order of magnitude smaller. The table also compares the trapped field to the magnitude of the equivalent London moment field for each rotor. These results indicate that the superconducting shield is nominal and that there was no degradation of the shield as a result of launch conditions.

**Table 12-2.** Measured trapped field compared to the London moment equivalent field in each of the gyro rotors.

Gyro No.	Trapped field ( $\mu\text{G}$ ) (Uniform field equivalent and as aligned late in mission)	London moment equiv. field ( $\mu\text{G}$ )	Ratio of trapped field to London moment
1	3.1	57	0.055
2	1.3	44	0.029
3	0.859	59	0.014
4	0.2	47	0.005

### 12.10.2 AC Shielding

The second function of the magnetic shielding system is to prevent time-varying fields from coupling to the readout pickup loops and contaminating the science signal. In this regard, the shields built into the dewar are supplemented by superconducting cylindrical local shields around each gyro and by the diamagnetic effect of the superconducting rotors themselves. As it turns out, the limits on the AC magnetic shielding derived from the data while the gyros were caged early in the mission were not as tight as the limits obtained from the ground verification, which were  $2 \times 10^{-12}$  (-234 db) attenuation. In any case, no evidence of a signal with the signature of a leakage field was observed above the noise. In addition, the fact that the ambient dc field is nominal is good prima facie evidence that the AC shielding has not been degraded from the ground test result.

## 12.11 Probe Vacuum Performance

Vacuum in the Probe is important during science data acquisition because of the damping effect residual helium has on the gyro rotors. Of particular concern is differential damping wherein the component of spin along the roll axis decays at a different rate than the component transverse to the roll axis. This can cause a precession if the spin and roll axes are not exactly aligned. In order to keep this effect to an acceptable level, there is a requirement that the Probe pressure be less than or equal to  $2 \times 10^{-10}$  torr after the low temperature bakeout. In the absence of other damping torques, residual pressure can be determined by measurement of the spin-down decay time. In actuality, the spin-down decay time varied between 7,000 years for gyro 3 and 25,700 years for gyro 4, however. This variability, along with other evidence, supports the contention that the spin-down rates were dominated by some other mechanism (possibly patch effect) rather than by gas damping. By using the longest decay time, however, an upper limit of  $\sim 1.5 \times 10^{-11}$  torr (2 nPa) can be placed on the residual gas pressure—a result that is an order of magnitude below the requirement, demonstrating ample margin.





# 13

## Other Payload Subsystems Analyses

---





## 13.1 Experiment Control Unit (ECU)

The Experiment Control Unit (ECU) performed nominally during GP-B Operations. All tasks were completed on schedule and without error. The ECU's success can be directly attributed to extensive software and hardware development and testing, anomaly identification, analysis, resolution and when necessary, rework prior to launch. Instrumental to the ECU's operational success was the early insertion of experienced operations personnel into the development process with a "test it like you fly it" mentality as developed by Gaylord Green. Finally, the development of a modular Flight Timeline prior to launch created an environment where re-planning and anomaly resolution was done with carefully thought out command sequences resulting in error-free implementation.

The dedication, ability and willingness of the Lockheed Martin ECU software team to develop last minute software updates and additions during IOC was exemplary and contributed in no small part to the GP-B mission success.

### 13.1.1 ECU Hardware

Figure 13-1 below shows the relative location of the forward and aft ECU boxes on the spacecraft frame.

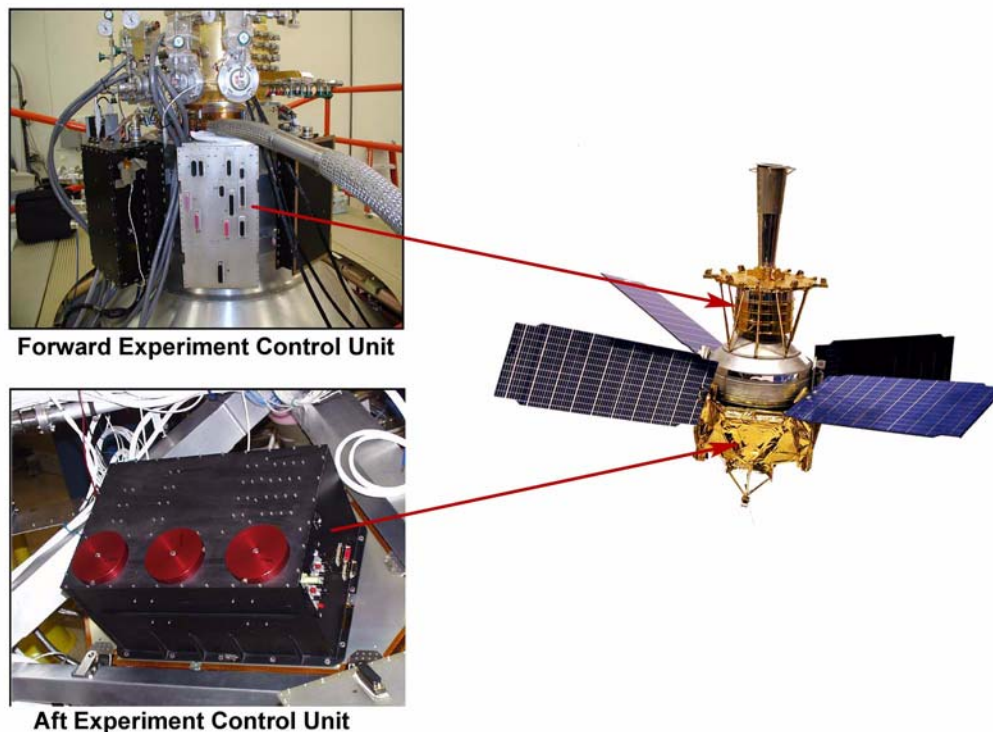


Figure 13-1. Locations of Forward and Aft ECU boxes on the GP-B spacecraft

### 13.1.2 ECU-Controlled Heaters & Temperature Sensors

The ECU controls a number of heaters and temperature sensors inside the dewar and inside the Probe. Figure 13-2 shows the locations of ECU-operated heaters.





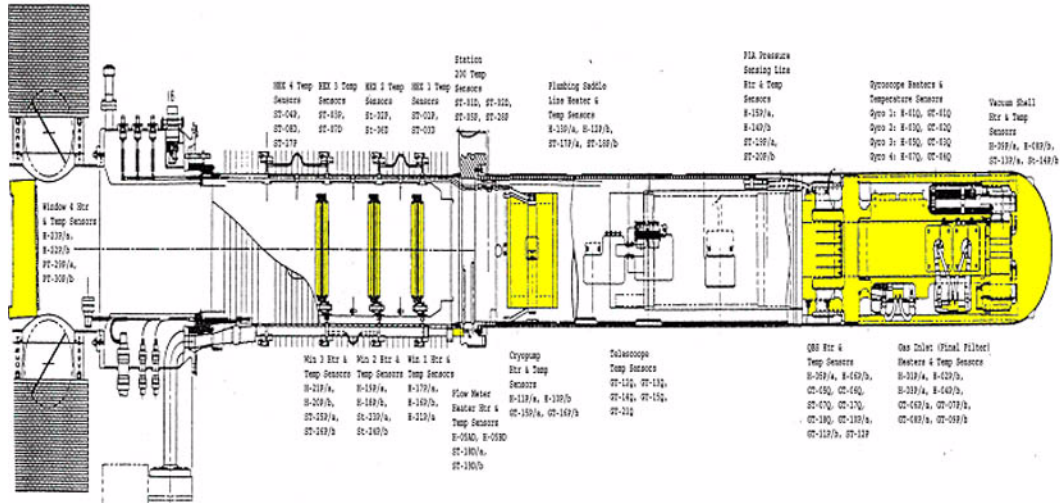


Figure 13-4. ECU-operated heaters and temperature sensors in the Probe and Probe windows

### 13.1.3 ECU-Managed Subsystems

In addition to controlling various heaters and temperature sensors, the two ECU boxes on the spacecraft control nine subsystems on-board the spacecraft. Figure 13-5 below shows the names and general locations of these subsystems on the spacecraft frame. A brief description of each ECU-controlled subsystem follows the diagram.

### ECU-Controlled Subsystems on the GP-B Spacecraft

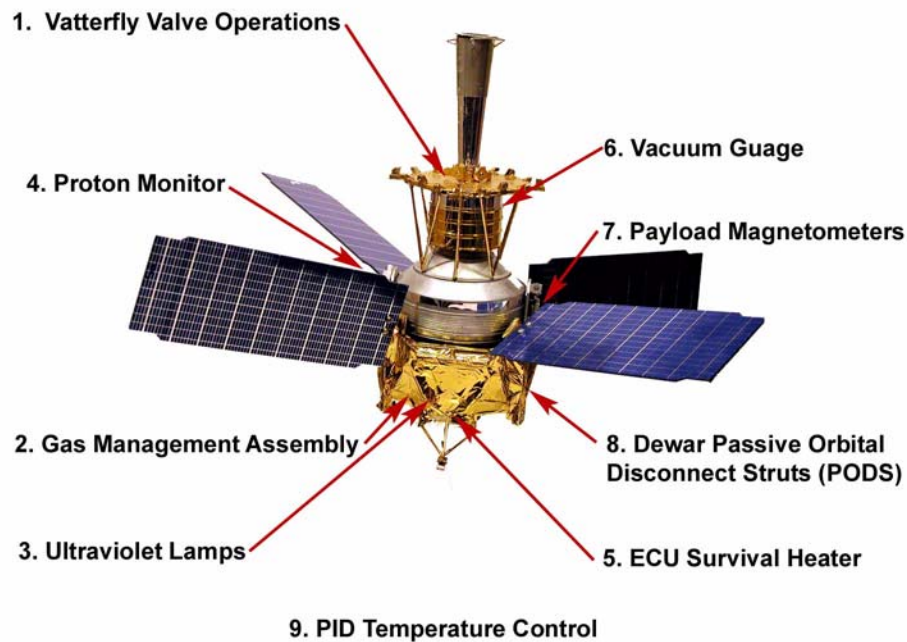


Figure 13-5. General locations of ECU-controlled subsystems on the spacecraft

### 13.1.3.1 Vatterfly Valve Operations



**Figure 13-6.** A six-inch Vatterfly leakage exhaust valve at the top of the dewar

There are 6 Vatterfly Valves operated by the ECU. Two (2) 6-inch Leakage Valves, used for exhaust from the top of the dewar. Four (4) 2.5-inch Exhaust Valves, used for exhaust from each Gyro and plumbed up and out near the top of the dewar.

### 13.1.3.2 Gas Management Assembly (GMA)

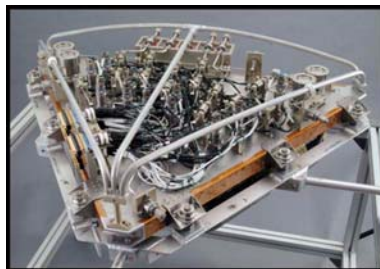


**Figure 13-7.** The Gas Management System (GMA)

The ECU provides heater control, temperature monitoring, and valve control for the Gas Management Assembly (GMA). The GMA is located in one bays on the lower spacecraft frame. It provides ultra-pure helium gas for spinning up and flux flushing the four science gyros.

### 13.1.3.3 Ultraviolet Lamps

The ECU operates two UV lamps and their optical switches. These UV lamps are used for controlling the build-up of electrostatic charge on the science gyros.

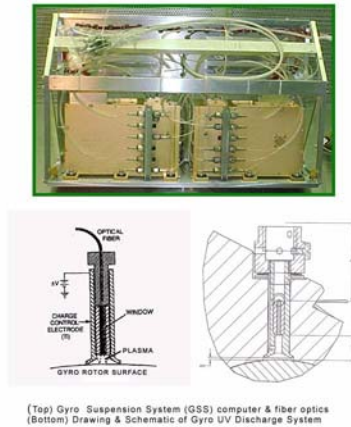


**Figure 13-8.** UV lamps and the gyro electrostatic discharge system

The two UV lamps are located on the lower spacecraft frame, and their light is carried to the gyro housings, inside the Probe, through fiber optic cables.

### 13.1.3.4 Proton Monitor

The Proton Monitor is a modifiable system designed to monitor the GP-B's environment and detect and distinguish in between protons, electrons and other charged particles/cosmic rays.



**Figure 13-9.** The GP-B Proton Monitor box

The ECU sends and receives 16-bit proton monitor commands from the spacecraft's main computer (CCCA/CCCB) via the 1553 bus at a rate up to and including 10.0 Hz.

### 13.1.3.5 ECU Survival Heater

Designed to maintain the Aft ECU Operational Temperature Range, the Aft ECU baseplate survival heater protects the UV Lamps from low temperature damage. They thermostatically maintain a temperature in between 0 and 4 Celsius.

### 13.1.3.6 Vacuum Gauge

The ECU provides +30V, 3W max. power and 2 channels of telemetry for each of two high vacuum gauges, used to measure probe pressure during high probe pressure events.



### 13.1.3.7 Payload Magnetometers

The ECU houses control circuitry for four external 3-axis magnetometers, and it provides three channels of analog telemetry.

### 13.1.3.8 Dewar Passive Orbital Disconnect Struts

The ECU senses the status of the dewar Passive Orbital Disconnect Struts (PODS), which are used to thermally isolate the dewar from the spacecraft structure surrounding it.

### 13.1.3.9 PID Temperature Control

The spacecraft's main computers (CCCA and backup CCCB) use a closed loop temperature control (PID) algorithm to control all of the following ECU heaters:

1. Gas Inlet (Final Filter) 1&2
2. Gas Inlet (Final Filter) 3&4
3. Quartz Block Structure (QBS)
4. Cryopump
5. Vacuum Shell
6. Heaters for each of the four windows in the Probe

A set of parameters, including the activity duration and a temperature profile is uploaded to the CCCA/CCCB computer, and the PID algorithm then maintains the PID heaters at their specified temperature until the parameters are changed. The PID algorithm runs autonomously and is designed for controlling complex heater operations in orbit. Performance of the ECU during two of these complex operations, flux flushing and low temperature bakeout of the Probe, is summarized in the next section.

## 13.1.4 ECU Performance During Flux Reduction & Low Temperature Bakeout

This section describes the flux reduction and low temperature bakeout procedures that were executed during the Initialization and Orbit Checkout (IOC) phase of the mission. For each of these procedures, the accompanying chart shows how well the ECU met the specified requirements and success criteria.

### 13.1.4.1 Low Temperature Bakeout

The low temperature bakeout process involves heating the interior surfaces of the Probe while open to space in order to desorb and remove the helium which has condensed and been adsorbed onto the Probe interior surfaces during spinup of the Gyroscopes. The major components used during this operation are the ECU, the ECU's Thermal Control PID Algorithm, the ECU Operated, Closed and Open Loop SIA Heaters and their associated Temperature Monitors.

**Requirements:** This operation will assist in reducing the measured probe pressure below X Torr. SCIT-01 Para. 8.2.3

**Success Criteria:** Heating the Probe to 6-7 K and then lowering the temperature in a ramp until the pressure within the Probe is within requirements.

Figure 13-10 below shows the performance of the ECU during the low temperature bakeout procedure carried out during the IOC phase of the mission.

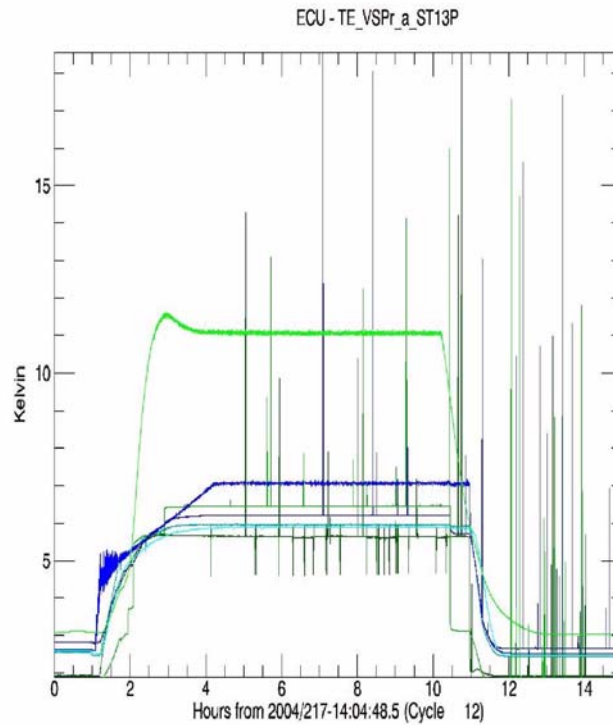


**Figure 13-10.** Performance during Low Temperature Bakeout

#### 13.1.4.2 Flux Reduction Operation

The purpose of this operation is to reduce the Science Gyroscope's trapped magnetic flux. The major components used during this operation are the ECU, the GMA, the ECU's Thermal Control PID Algorithm, the QBS (H-05P & H-06P) and Vacuum Shell (H-08P & H-09P) Heaters and their associated temperature monitors.

**Requirements:** This operation will assist in reducing the measured trapped flux on the science gyroscopes below 9 microgauss. SCIT-01 Para. 8.2.3

**Success Criteria:** Heating the QBS to 13 K and then lowering the QBS temperature in a ramp until the Gyro's are below superconductive temperature.

Figure 13-11 below shows the performance of the ECU during a flux reduction operation carried out early in the IOC phase of the mission.

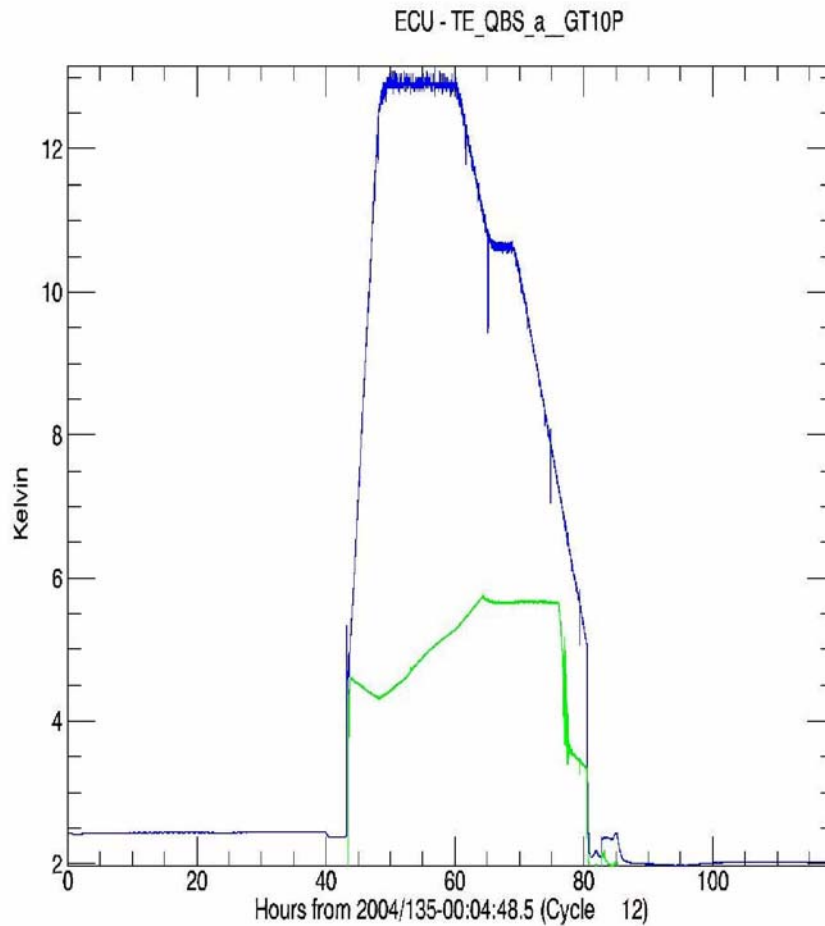
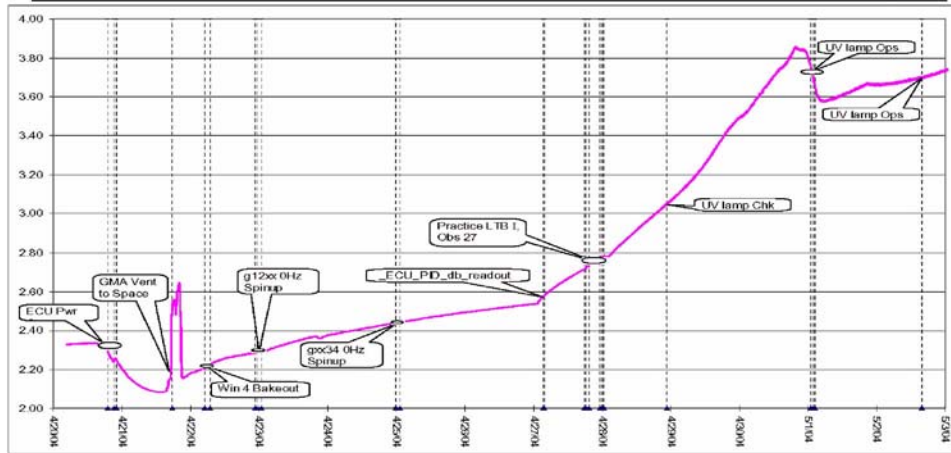


**Figure 13-11.** ECU performance during IOC flux reduction

### 13.1.5 ECU Heater Activity During IOC

During early orbit operations, The ECU was involved in Power on and Initialization of itself and it's subsystems, the initial Gyroscope spinup practice, the Window Bakeout to remove particulate from the outer window due to pre-launch and launch and the initial UV Lamp Operations. [Figure 13-12](#) below shows the ECU heater activity during the spacecraft's first 12 days in orbit, as a function of temperature in kelvin, as measured by the temperature sensor in the Cryopump.

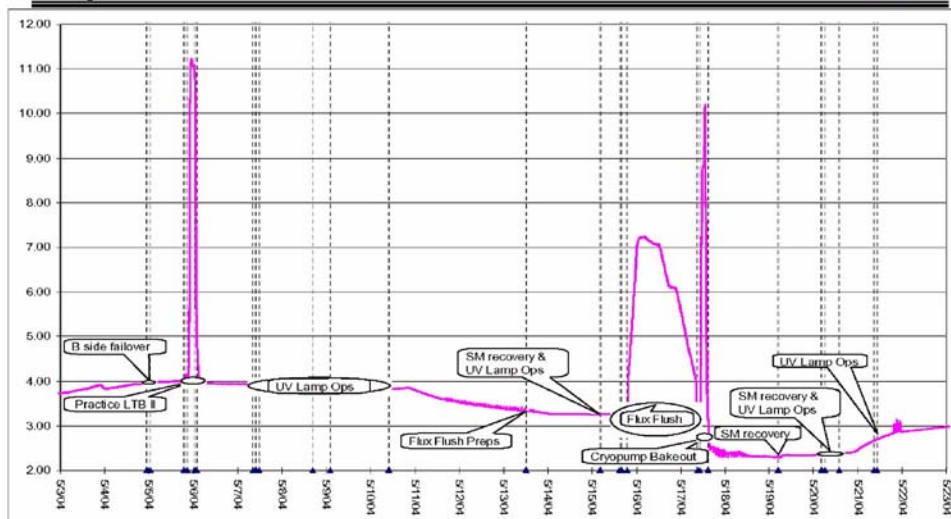


1/28/2005

3

**Figure 13-12.** ECU heater activity following launch

During early orbit operations, The ECU continued UV Lamp Ops, a practice Low Temperature Bakeout, Helium Flow rate analysis using the Flow Meter Heater and Gyroscope Flux Flushing. [Figure 13-13](#) shows this ECU heater activity as a function of Cryopump temperature for mission day#13 – mission day #33.



1/28/2005

4

**Figure 13-13.** ECU heater activity during first month of IOC

As we entered the second month of orbital operations, the focus again was on charge control with the UV Lamp, Helium Flow rate analysis using the Flow Meter Heater and increasingly sophisticated Gyroscope spinup routines. Figure 13-14 shows the continued ECU heater activity as a function of temperature for the three-week period from May 23, 2004 – June 12, 2004.

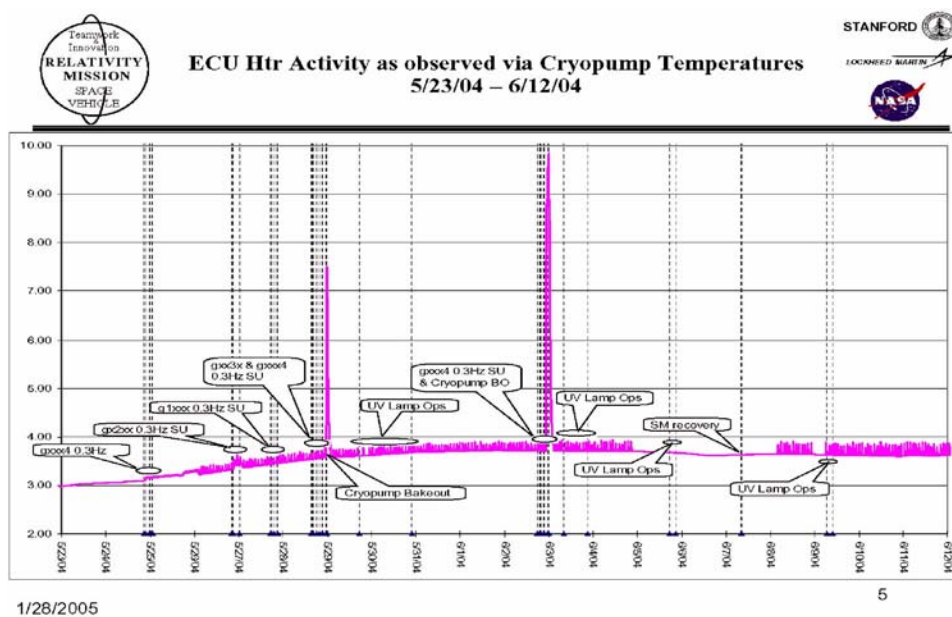
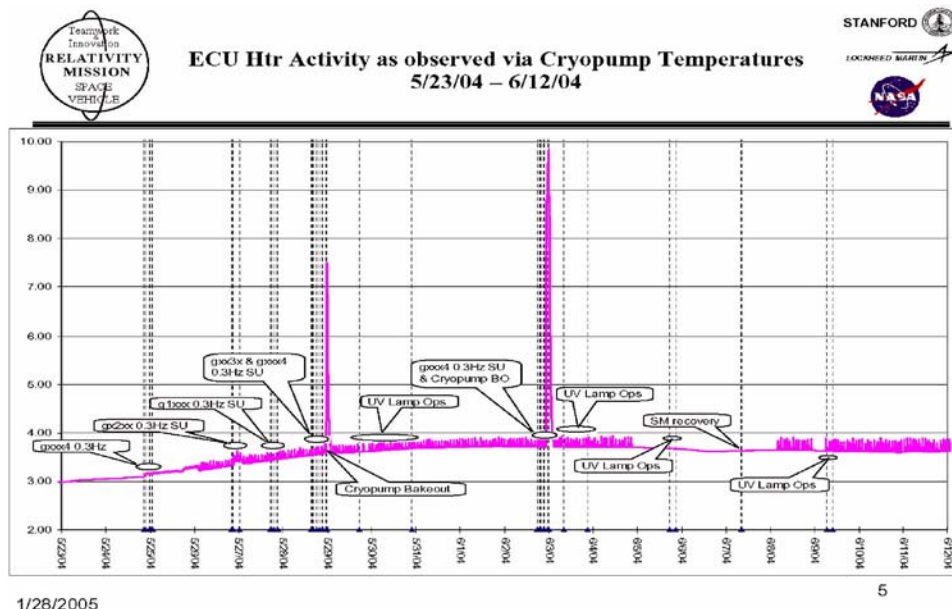
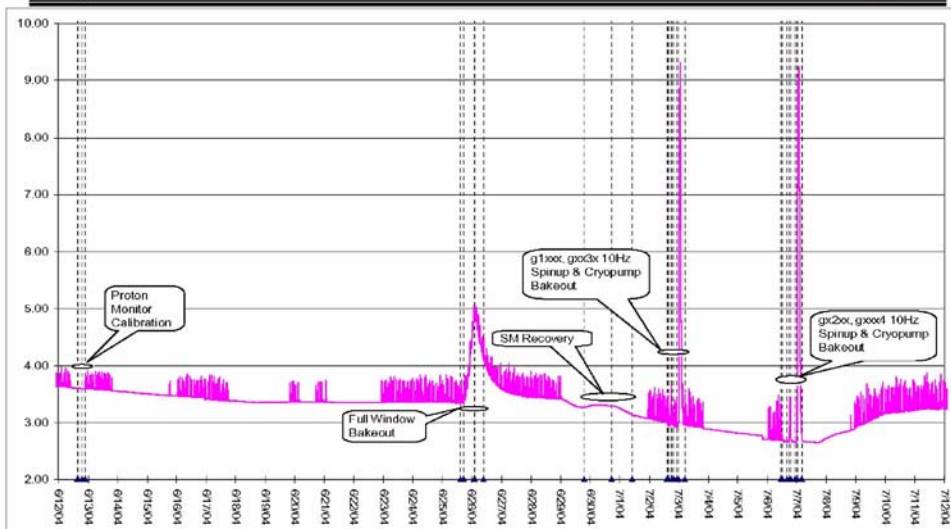


**Figure 13-14.** ECU heater activity during the 2nd month of IOC

For the month of June 2004, the ECU was involved in initializing the Proton Monitor, Helium Flow rate analysis using the Flow Meter Heater and a Full Window Bakeout, heating up all four Windows to remove any condensation interference with the telescopes view of our guide star IM Pegasus and further, increasingly complex Gyroscope spinup operations. Figure 13-15 below shows the continued ECU heater activity as documented by the Cryopump temperature sensor in June-July, 2004.

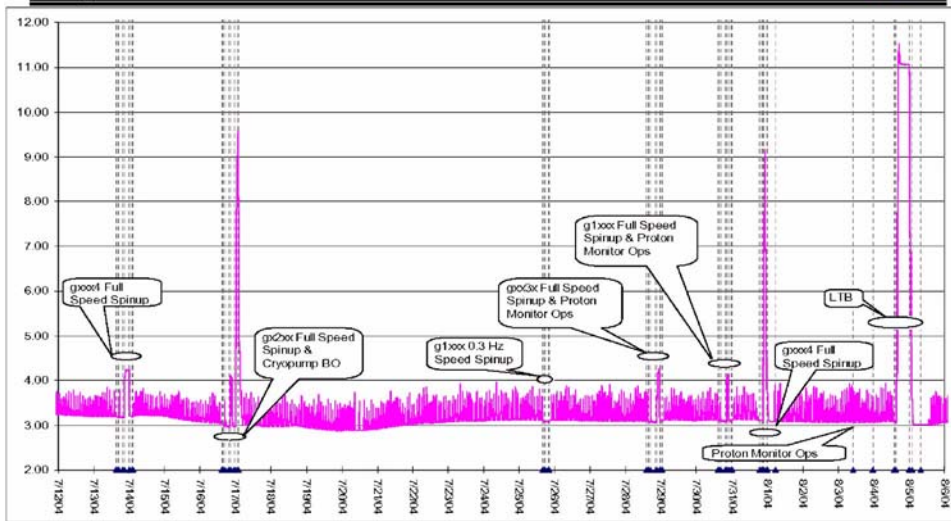


1/28/2005

6

**Figure 13-15.** ECU heater activity from mid June - mid July, 2004

As July turned to August, we entered the heart of the GP-B IOC phase, with full-speed gyroscope spinups, the low temperature bakeout, and helium flow rate analysis, using the Flow Meter heater. Figure 13-16 shows the ECU heater activity during these critical IOC procedures.



1/28/2005

7

**Figure 13-16.** ECU heater activity during gyro spinup and other critical IOC procedures



During the last month of IOC, preparing to enter the Science phase of the mission, the ECU heater activity slowed dramatically. During this period, the focus was on Quartz Block Support temperature stabilization using the closed loop QBS Temperature control, Charge Control use of the UV Lamps, Helium Flow rate analysis using the Flow Meter Heater and the health and safety monitoring of temperatures and pressures. [Figure 13-17](#) documents the ECU heater activity during this period.

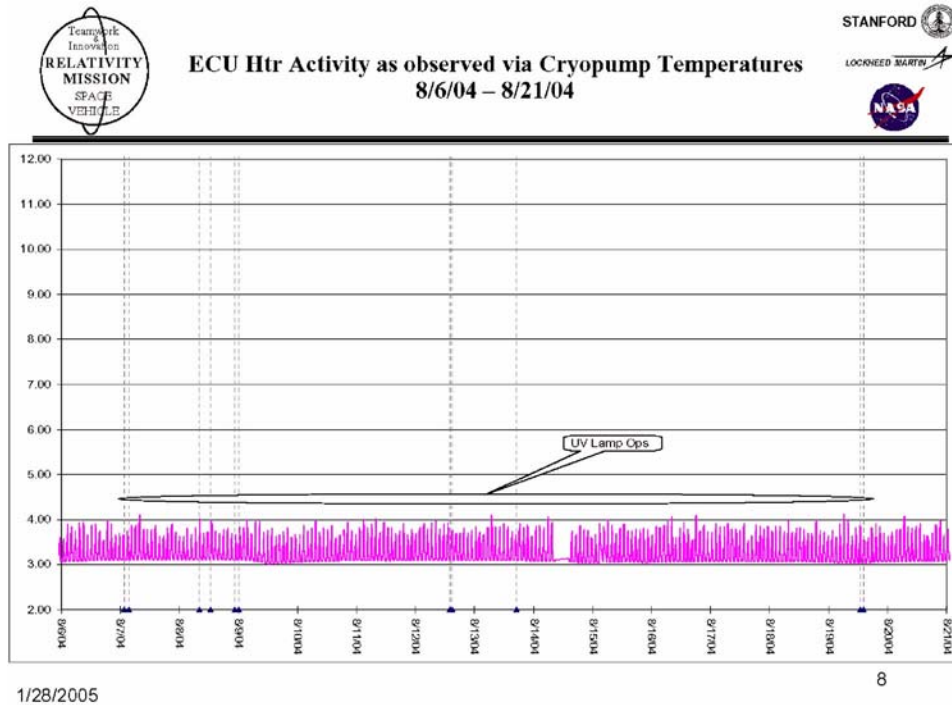


**Figure 13-17.** ECU heater activity during the last month of IOC

### 13.1.6 ECU Heater Activity During the Science Phase

During the first six months of the Science (Data Collection) Phase of the mission, we continued with health and safety monitoring of temperatures and pressures, Quartz Block Support temperature stabilization using the closed loop Temperature control, and Helium Flow rate analysis using the Flow Meter Heater. During this period, we also performed the first of several Heat Pulse Meter Heater tests to determine the amount of Helium remaining in the dewar. [Figure 13-18](#) documents the ECU heater activity during this period.





### ECU Htr Activity as observed via Cryopump Temperatures 8/21/04 – 1/24/05

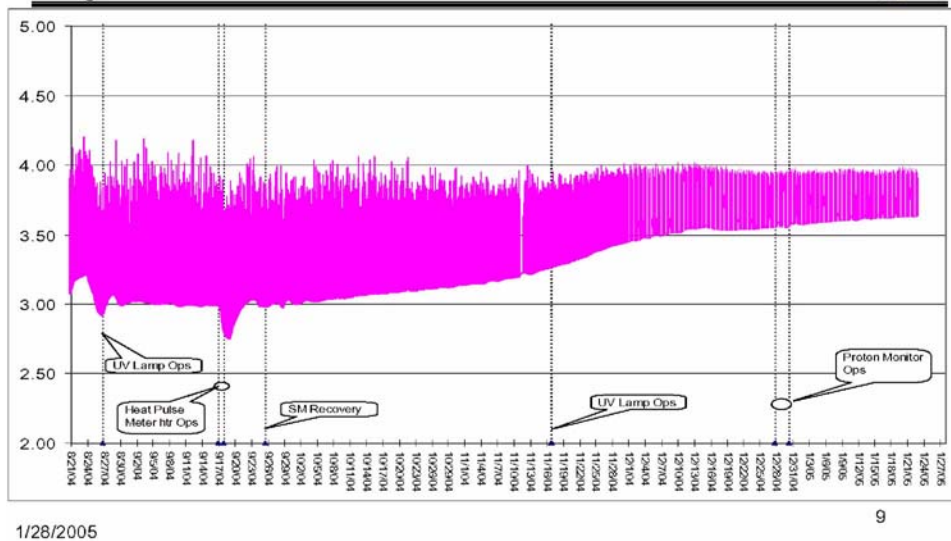


**Figure 13-18.** ECU heater activity during the first half of the Science Phase

As we continued through the remainder of the Science phase of the GP-B Operations, the activity on the ECU was used primarily for Charge Control use of the UV Lamps and Heat Pulse Meter Heater tests for a helium lifetime calculations. In April 2005, we determined that the ECU was contributing noise to the SQUID Readout System. To mitigate this issue, we kept the ECU turned off throughout the remainder of the Science phase, except for a few hours each week, when we powered-on the unit to check the status of various telemetry values. [Figure 13-9](#) below documents the ECU heater activity from January 2005 through the end of May 2005.

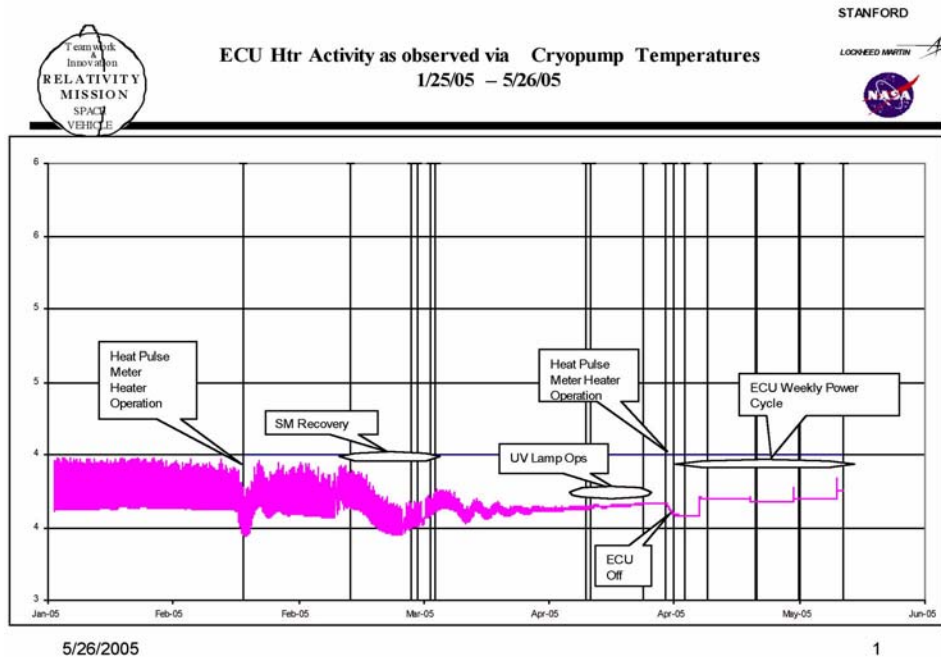


**Figure 13-19.** ECU heater activity during the Science Phase, from January-May 2005

### 13.1.7 ECU transmission of Spacecraft Noise

Noise coupling has been an ongoing issue with the ECU, both prior to launch and during flight. Following is a summary of this issue.

#### 13.1.7.1 Pre-Launch ECU Noise Coupling

Prior to launch, GP-B processed DR446 that addressed a noise-coupling path between the ECU and the SRE subsystems. Ultimately, this led to a launch delay from December 2003 to April 2004 to replace a faulty power supply in the ECU. However, the coupling path between the ECU and the SRE that allowed the detection of the faulty ECU power supply was not able to be isolated and repaired during this time, and it was deemed acceptable for the performance of the science instrument.

#### 13.1.7.2 ECU Noise Coupling On Orbit

Once on orbit, we found that the ECU would occasionally generate coherent noise at a slowly changing frequency that would couple to the SQUID outputs—primarily to SQUID#1. SQUID#1 and SQUID#3 have consistently exhibited a greater sensitivity to external sources of EMI due to the relatively long cables from the top hat to the forward SRE. Similar noise was observed on the SQUID#1 outputs in early 2005, and it was decided then that the ECU could be turned off for extended periods to eliminate this noise source from the SQUID data. The ECU was turned off on April 28, 2005 and was occasionally turned on for system monitoring and heat pulse measurements to the end of helium point on September 29, 2005. Following the depletion of helium, the ECU was turned back on permanently.

The effect of this coupled noise source on the science data is still to be determined in the post-mission science data analysis effort, but at this time the effect is expected to be small to insignificant.

## 13.2 Proton Monitor

The proton monitor (PM) aboard GP-B is a sophisticated electronic measurement instrument that is capable of detecting, counting, and measuring flux and energies of protons in the range 35MeV-525MeV. The purpose of this instrument is to provide valuable information about the radiation environment surrounding GP-B, especially the flux of high-energy protons, which can affect or disrupt the performance of sensitive electronics and science instruments and may contribute to charge build-up on the gyroscopes. This data can also be used to study the proton flux density in GP-B's low-earth orbit, as well as variations in flux that occur with changing geomagnetic field and geographic location of the spacecraft. Furthermore, there are potential experiments that the proton monitor can be used for during the post-science phase of the mission. This report describes the capabilities, summarizes the to-date performance, and discusses possible post-science applications of the proton monitor.

### 13.2.1 GP-B Radiation Environment

The Earth's geomagnetic field acts as a shield, blocking out much of the radiation from the sun and deep space. The shielding effect is strongest over the equator and low latitudes and weakest over the poles and the SAA, where the radiation belt shows a "pothole", a dip, which scientists explain as a result of the eccentric displacement of the center of the magnetic field from the geographical center of the Earth as well as the displacement between the magnetic and geographic poles of Earth. Over the poles, the shielding effect is weaker due to the orientation of the magnetic field. Thus, whenever GP-B passes over the poles or the SAA it is exposed to much higher particle flux than outside of these regions.

The radiation environment at the altitude of GP-B's orbit (640km) is dominated by the flux of trapped particles in the Earth's inner radiation belt. Most of these particles are low-energy protons and electrons, but there is a significant flux of higher energy particles, especially over the SAA and the polar regions and it is the high energy protons that the GP-B PM is designed to detect.

Trapped protons mirror between the magnetic poles, following spiral trajectories around magnetic field lines. Because of this spiral motion, the velocity vector of a trapped proton is approximately perpendicular to the magnetic field vector. This effect makes determining the originating direction of the proton flux more difficult because the direction of the source, e.g. the Sun, is not necessarily the direction from which the detector sees the highest proton flux.

Energetic protons can affect the performance of onboard electronics by impacting transistors and flipping one or more bits. Single and multi-bit errors of this kind can have a severe effect on critical spacecraft electronic systems, which is why it is important to understand when and how they happen.

### 13.2.2 Proton Monitor Features and Specifications

The GP-B PM has 16 channels and is capable of detecting protons in the energy range 35MeV-525MeV, which exceeds the range and resolution of most past and current satellite detectors in low-earth orbit (POES satellite detectors have a max of 275MeV, CPA - ~200MeV, SOPA - 50 MeV.) The monitor features two identical 4-layer silicon detectors with 45 degree view angles. The detectors are orthogonal, with one oriented along the -Z axis and the other along the -Y axis of the spacecraft. As the protons enter a detector, they are counted and sorted by energy level into 16 channels, whose configuration is shown in [Table 13-1](#).

**Table 13-1.** Proton monitor channel configuration

Channel	Energy Range (MeV)
1	34-40
2	40-48
3	48-57
4	57-68
5	68-81
6	81-96
7	96-114
8	114-135
9	135-160
10	160-190
11	190-225
12	225-266
13	266-315
14	315-373
15	373-442
16	442-525

The default integration period of the PM is 12.8s. This period is adjustable and can be set to 3.2s, 6.4s, 12.8s, 25.6s, or 51.2s. Other adjustable features include electron suppression, noise threshold, and minimum ionization. [Table 13-2](#) summarizes technical specifications.

**Table 13-2.** Technical Specifications

Specification	Value
Maximum Power Consumption	3.5 W
Mass	3.5 kg
Dimensions	17 x 15 x 10 cm
Science Data Rate	160 bps
Time Resolution	Programmable, 12.8s default
Energy Resolution	2 x 16 energy channels (see <a href="#">Table 13-1</a> )
Measurement Range	35 – 525 MeV protons
Configuration	Two orthogonal proton detectors

As mentioned above, the view angle of each detector is 45 degrees. However, since the horizontal detector is rolling with the spacecraft, its effective view angle is 45 degrees plus the angle that it rolls through in one integration period. For the default value of the integration period, 12.8s, that angle is  $0.7742\text{rpm}/60\text{s} \times 12.8\text{s} \times 360\text{deg}$  or about 59.5 degrees. Therefore, the effective view angle adds up to ~104.5 degrees, which is much greater than the view angle of the detector. This does not apply to the vertical detector since it is always pointed in the same direction. The effective view angle of the horizontal detector can be decreased by reducing the integration period or the roll rate of the spacecraft. On the other hand, increasing the integration period or roll rate will result in a wider effective view angle, which, if increased to 360 degrees, will result in an omni-directional detector. These considerations are important to keep in mind for the post-science phase of PM operations.

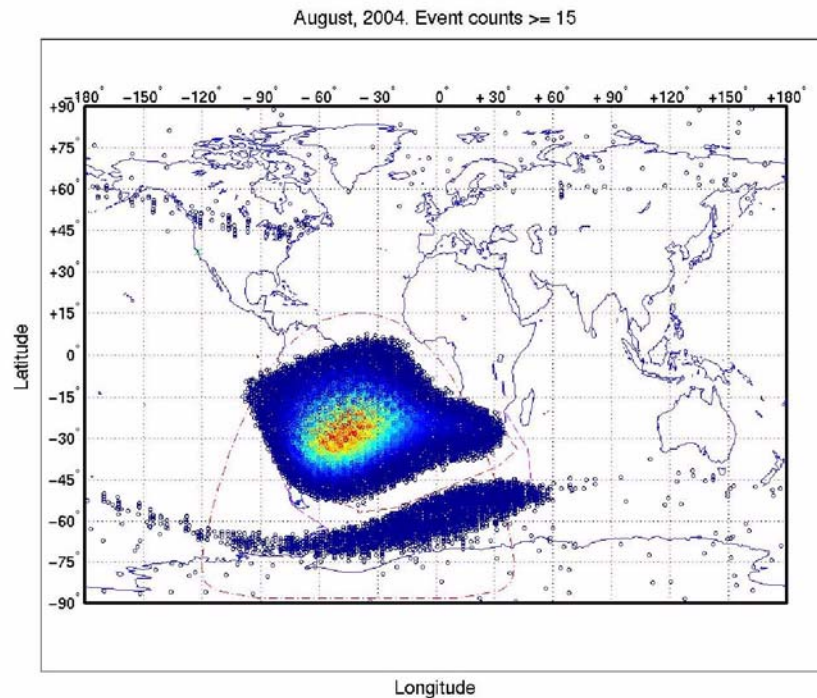
### 13.2.3 History of Performance

The PM operated nominally from the beginning of the mission until Nov. 16, 2004 when we began receiving corrupt telemetry data. After a couple of days, telemetry went back to normal. On December 14, 2004 the PM telemetry data became corrupt again. No good data was available for the following two weeks. In early January, 2005, the PM came back online, but stopped sending data shortly before the major peak of solar activity on Jan. 20, 2005. After that, the data from the PM appeared invalid and there was a period when no data was received.

On April 25, we discovered that if we apply a different parsing method to the incoming telemetry data, we see much more good data coming from the PM. Using this new parsing method, we went back and saw that the PM appeared to operate nominally starting on March 17, 2005.

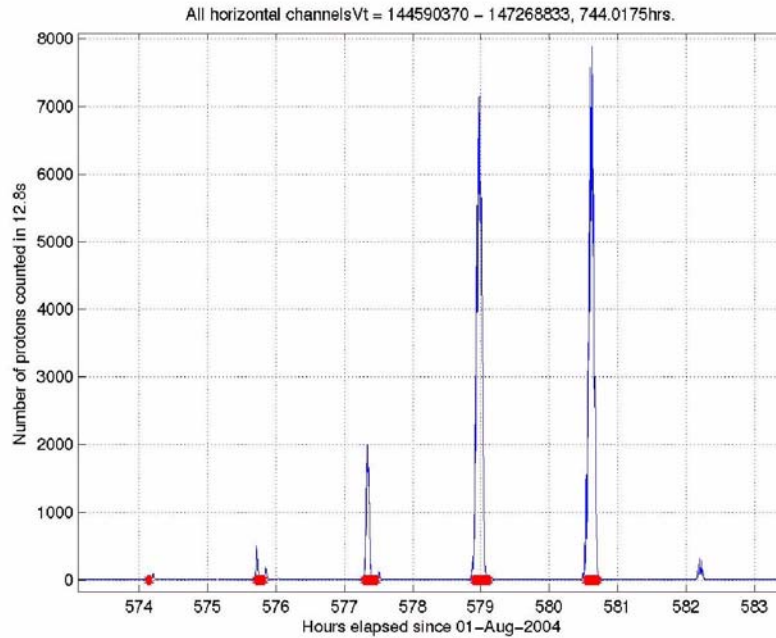
### 13.2.4 Data Collected

Figure 13-20, shown below, illustrates data collected on all horizontal channels over a one-month period, August 1 – September 1, 2004. The figure also shows the AP8min SAA model, ATC SAA model, and SLAC SAA model for GLAST contours [1]. Features of interest are active areas over the SAA, the poles and a band between the south-east SAA boundary and the South pole.



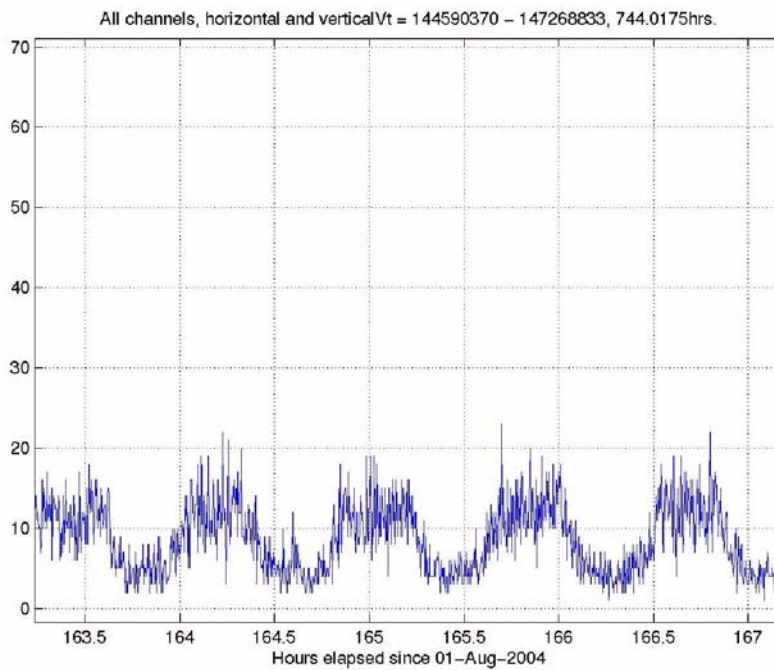
**Figure 13-20.** Typical Month of Proton Monitor Data

Figure 13-21 shows proton monitor data versus time. Levels of increased activity over the SAA are clearly visible as sharp spikes. Passes over the SAA are marked by red asterisks.



**Figure 13-21.** Proton Monitor data in South Atlantic Anomaly

Looking closer, we see a cyclic twice-orbital component to the signal, which shows increased proton flux as GP-B passes over the poles.



**Figure 13-22.** Twice Orbital Component



The main harmonics of the proton flux measurements can be seen by taking a fast Fourier transform (FFT) of the horizontal detector data, shown in Figure 13-23. The three vertical red lines mark the orbital, roll, and twice roll frequencies, from left to right. The roll and twice roll components are clearly present in the FFT of the horizontal detector data, since its boresight rolls with the spacecraft. The FFT of the vertical detector data is dominated by the orbital component.

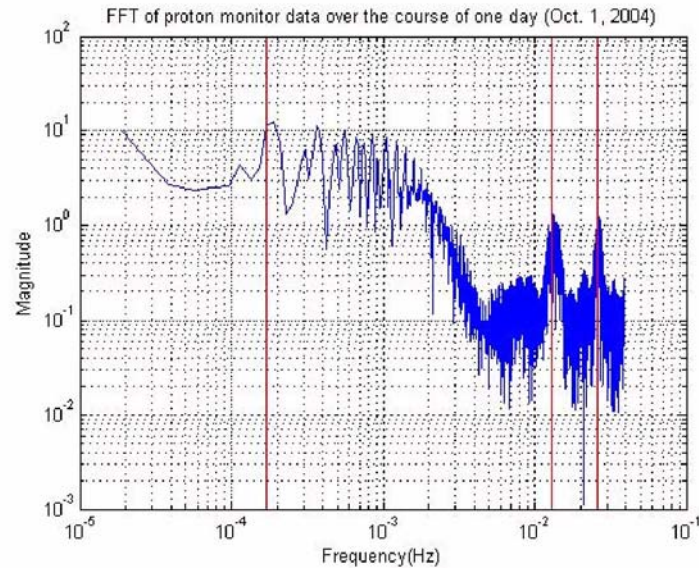


**Figure 13-23.** FFT of data from the horizontal detector

The next plot, Figure 13-24, is a histogram of proton events detected by each horizontal channel over the same one month period of August 1 – September 1, 2004.

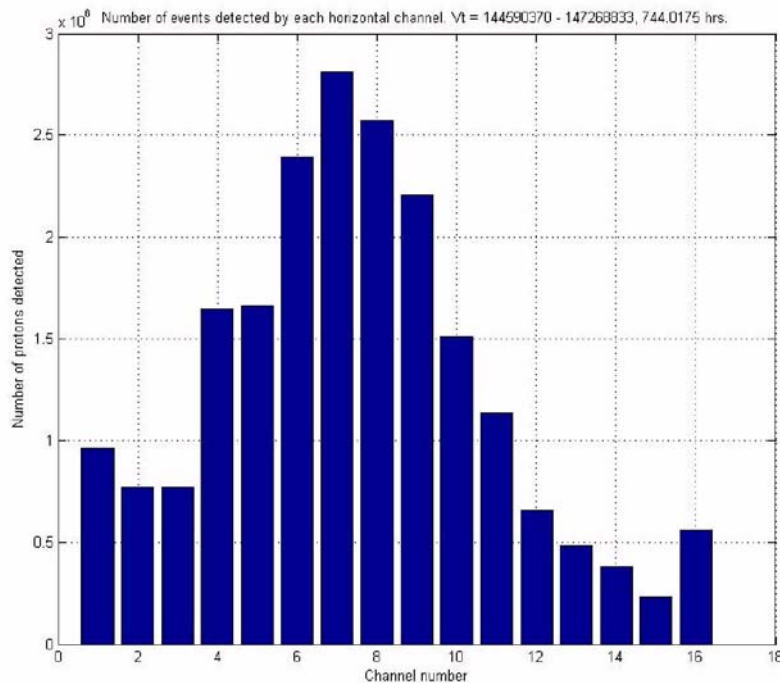


**Figure 13-24.** Histogram of Proton Events



In November, 2004 there was a large solar mass ejection accompanied by class X and M solar flares, which lasted for several days. This event was promptly picked up by the GP-B PM. [Figure 13-25](#) shows the increased flux on both the horizontal and the vertical detector during this event.

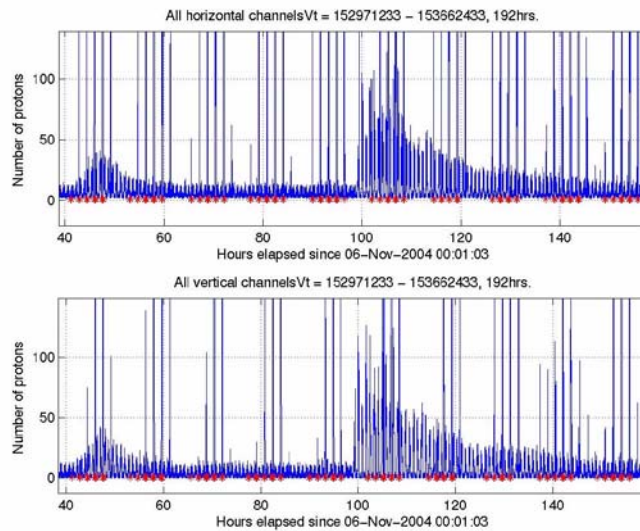


**Figure 13-25.** Proton Monitor Data from November 2004

[Figure 13-26](#) is a zoomed-out view of [Figure 13-25](#). It is interesting to note that the maximum flux over the SAA was slightly smaller during the times corresponding to the two peaks in [Figure 13-25](#). At first, this might seem unusual, but Katherine Harine from NASA's Marshall Space Flight Center explains this phenomenon, "After a solar event, the trapped proton flux should actually drop a bit. The slight atmospheric heave due to solar energy will increase the loss mechanism of protons more than the number of protons created by the event. Typically during a solar event the proton flux will increase at the Earth's magnetic poles due to the absence of geomagnetic shielding, but may decrease slightly at lower latitudes due to the atmospheric heave loss mechanism mentioned above."

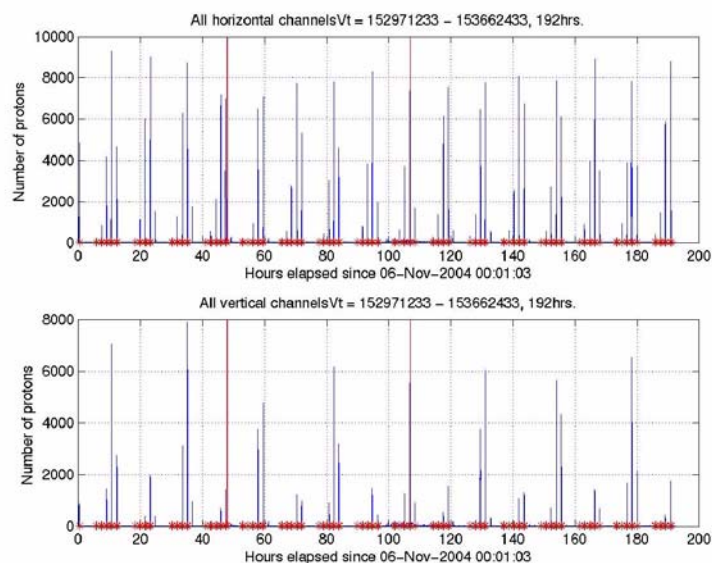


**Figure 13-26.** Zoomed out view of [Figure 13-25](#)

This is precisely what we observe in [Figure 13-27](#), which shows increased polar proton flux at the times of the flares.

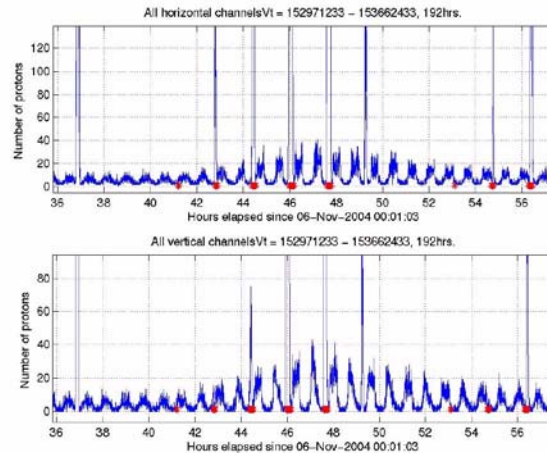
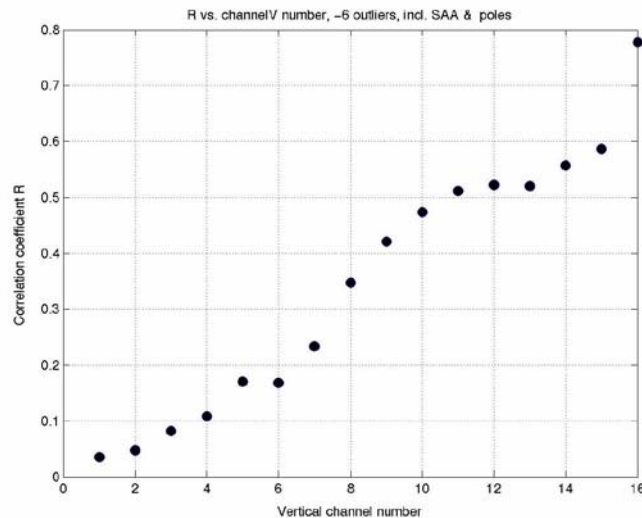


**Figure 13-27.** Increased Proton Flux during the November 2004 solar activity

### 13.2.5 Correlating the PM with the Telescope

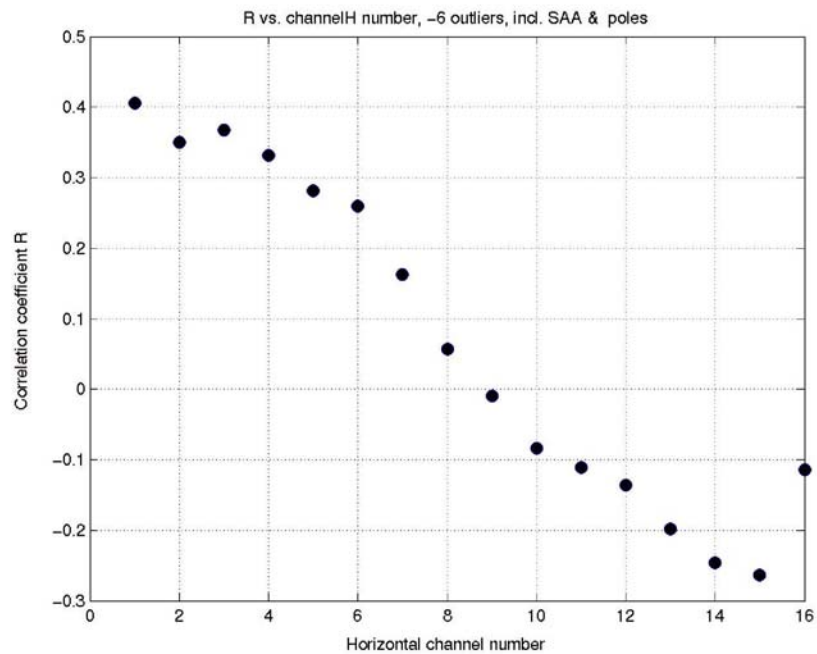
The pointing telescope onboard the GP-B has photo detectors which register hits from high energy protons. These protons contribute to the noise in the science slope measurements. To better understand the mechanism by which protons reach the photo detectors, I used the PM to determine the correlation between the proton flux and the noise in the science slope. The results of this analysis are summarized below.

For each channel of the proton monitor, a correlation coefficient was calculated between the daily number of protons detected on that channel and the daily number of proton hits detected by different telescope detectors. Two months of data were used. [Figure 13-28](#) shows the correlation coefficient vs. vertical channel number. Here, the data from the positive TRE-A X-Axis (PXA) detector was used.



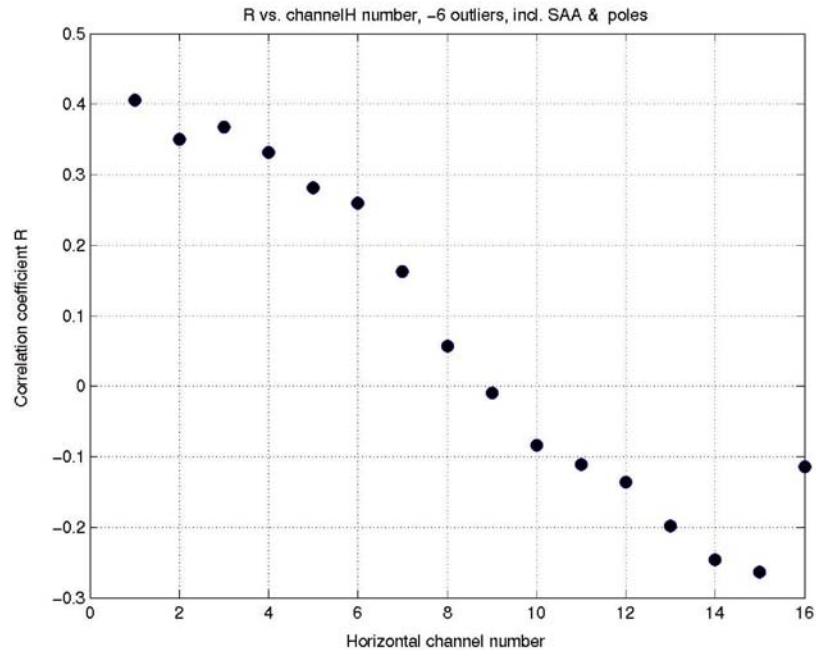
**Figure 13-28.** Correlation between Vertical PM Detector and Science Telescope (PXA)

Figure 13-28 shows a correlation that increases with channel number and, equivalently, energy level. One possible explanation for this is that higher energy protons are more likely to penetrate through the spacecraft structure to reach the detector. Figure 13-29 shows a similar plot using the data from the horizontal channels. In this case, the correlation function is inverse, meaning that the more high energy protons are seen by the PM, the fewer are seen by the telescope. Considering that the boresights of the two instruments are perpendicular, this can be explained knowing that direction of the trapped proton flux is approximately perpendicular to the magnetic field lines. Thus, if the telescope boresight is aligned with the magnetic field, many more protons will be traveling perpendicular to it and parallel to the horizontal PM detector.



**Figure 13-29.** Correlation between Horizontal PM Detector and Science Telescope (PXA)

Figure 13-30 depicts the correlation coefficient vs. vertical channel number, but this time the data from the positive TRE-A Y-axis detectors was used. A similar trend emerges.



**Figure 13-30.** Correlation between Vertical PM Detector and Science Telescope (PYA).

A more detailed analysis of the correlation will be done, taking into account the orientation of the telescope detectors and the magnetic field, and possibly other factors that affect the proton flux through the spacecraft.

### 13.2.6 Possible Post-Science Missions and Analysis

GP-B’s useful life does not end with the completion of the science mission. During the post-science phase of the mission, we can carry out experiments utilizing the numerous onboard instruments and sensors.

There are several possible experiments that would involve the proton monitor. For example, by changing the attitude and roll rate of the spacecraft, as well as the integration period of the proton monitor, we can effectively control the view angle and direction of both detectors, pointing them wherever the experiment commands. Using the data from the magnetometers, we can measure the proton flux at specific angles relative to the magnetic field lines. We can also combine the proton monitor data with the gyroscope charge measurements to study the contribution of high energy protons to gyroscope charge build-up. An ongoing effort that can and most likely will be continued in the post-science phase is understanding how energetic protons contribute to multi-bit errors (MBEs) that disrupt the onboard electronics.

## 13.3 Payload Magnetometers

As described in 13.2.2 (“Proton Monitor Features and Specifications”) of this report, a lead bag is used to attenuate the magnetic field around the Probe and gyroscopes within. In order to make an estimate on how strong this field is after attenuation, it is helpful to have measurements of the original field around the spacecraft. This information is collected by four fluxgate magnetometers mounted around the cone of the dewar.

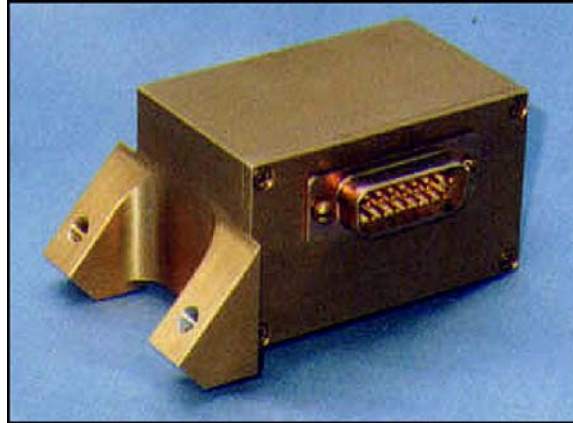


**Figure 13-31.** GP-B payload magnetometer

### 13.3.1 About the Magnetometers

Each of the GP-B payload magnetometers, manufactured by E. J. Iufer & Associates Inc. and shown in [Figure 13-31](#), have a mass of 0.133 kg and are 3.21 inch x 1.89 inch x 1.4 inch in length, width, and height, respectively. Measurements are taken along three orthogonal axes of the magnetometer, each of which contains a coil that creates an electrical current in response to the characteristics of the magnetic flux lines in the Earth's field. The key performance parameters for these magnetometers are listed in [Table 13-3](#) below.

**Table 13-3.** GP-B payload magnetometer performance characteristics.

	Axis	Unit 1	Unit 2	Unit 3	Unit 4
Offset (Volts)	X	4.997	4.998	5.011	4.983
	Y	5.001	4.995	4.981	4.968
	Z	4.995	4.994	5.012	5.001
Sensitivity (Volts/Gauss)	X	4.9421	4.9181	4.9707	4.8868
	Y	4.5815	4.4776	4.5545	4.4781
	Z	5.0248	4.9139	4.8913	4.9137
Range (Gauss)	X	-0.8 to 0.6	-0.8 to 0.6	-0.8 to 0.6	-0.8 to 0.6
	Y	-0.8 to 0.7	-0.8 to 0.7	-0.8 to 0.7	-0.8 to 0.7
	Z	-0.8 to 0.6	-0.6 to 0.6	-0.8 to 0.6	-0.7 to 0.6
Linearity* (%)	X	0.06	0.07	0.06	0.085
	Y	0.03	0.08	0.05	0.13
	Z	0.12	0.12	0.11	0.03
Noise (Gauss)	X	$<2 \times 10^{-5}$	$2 \times 10^{-5}$	$5 \times 10^{-6}$	$<2 \times 10^{-5}$
	Y	$<2 \times 10^{-5}$	$4 \times 10^{-5}$	$7 \times 10^{-5}$	$<2 \times 10^{-5}$
	Z	$<2 \times 10^{-5}$	$5 \times 10^{-5}$	$4 \times 10^{-6}$	$<2 \times 10^{-5}$
* Linearity is defined as the maximum deviation from the expected value					

As stated above, the magnetometers are mounted around the top of the dewar (the forward end of the spacecraft). This is illustrated in [Figure 13-32](#) below (Note: the +X and +Y axes are spacecraft fixed axes).

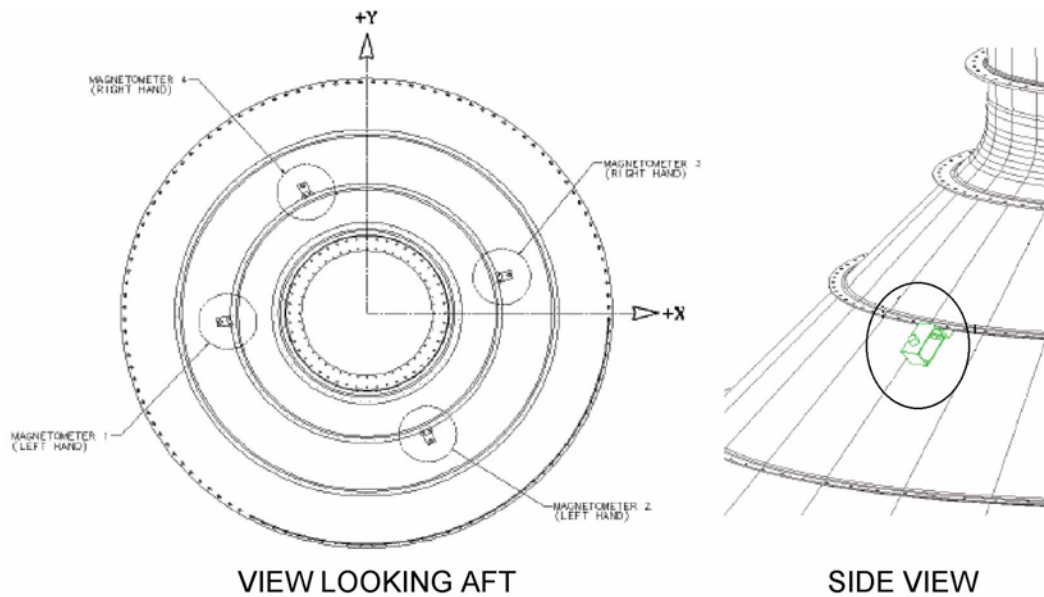


**Figure 13-32.** Measurement axes of the payload magnetometers.

Power and data signals are routed between the ECU and payload magnetometers through a 15-pin connector on the side of each unit. The measurement coils for the magnetometers are mounted on the side plate containing the power/data connector as shown in [Figure 13-33](#).

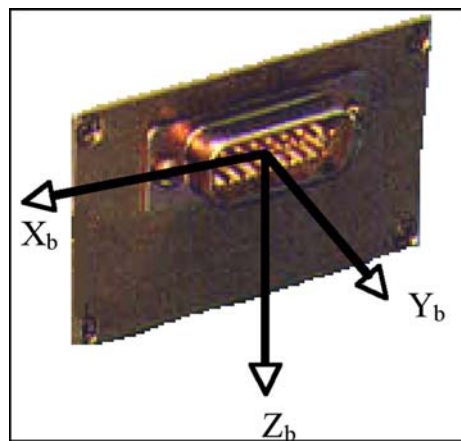


**Figure 13-33.** Mounting locations of the payload magnetometers.

The orientation of these coils determines the measurement axes of the magnetometer. For magnetometers 1 and 2, this plate is mounted on the left side of the unit as seen from the front end (the end opposite of the end that contains the mounting structure). Thus, these magnetometers are said to be “left-handed”. For magnetometers 3 and 4, this plate is mounted on the right side of the unit, and thus these magnetometers are said to be “right-handed”.

Data is sampled by each magnetometer unit every five seconds and transmitted down to Earth in counts (each volt corresponds to 3276.7 counts). The GP-B science team then performs several processing functions on this data. First, the data is converted from counts to volts. Next, crosstalk in the data, the interference that each measurement coil receives from the other coils, is eliminated through multiplication with a matrix of ground measurements. Finally, the measurements are converted from the magnetometer frame to the spacecraft frame through multiplication with direction cosine matrices.

### 13.3.2 Other Applications for Payload Magnetometers

While the data from the magnetometers is collected to provide a reference for estimating the magnetic field attenuation inside of the spacecraft, it can also be used for several other applications. For instance, the direction of the flux of ionized particles in the environment that the spacecraft flies in over the mid-latitudes of Earth is strongly influenced by the Earth's magnetic flux lines. These particles occasionally strike and flip digital bits in spacecraft computer memory (this is known as an upset event). Therefore, data gathered by the magnetometers on the strength and orientation of magnetic flux lines during upset events provides insight into the direction that these particles impact the memory board. This information can and has been used to identify vulnerabilities in both the shielding and layout of memory bits on the memory boards used in GP-B, and thus, will be helpful in selecting more robust shielding and memory board configurations in future missions.

Another application for the payload magnetometer data is the detection of ionospheric field aligned currents in the Earth's polar regions. These currents disturb the magnetic field and heat up the Earth's atmosphere, causing it to rise locally. This rise in the atmosphere should cause a small, temporary deceleration of GP-B (due to an increase in drag), which should be detectable in the GSS units. This phenomenon has been observed on other satellites and is of interest to the geophysics community for future study. In order to detect it on GP-B, GSS data will have to be processed to calculate the drag experienced by the vehicle. Then, if there are any noticeable instances of deceleration that could be linked to ionospheric field aligned currents, the magnetometer data corresponding to this period of time will to be compared with a model of the Earth's magnetic field to determine the presence and scale of such currents.

### 13.3.3 Lessons Learned Using Payload Magnetometers

The data produced by the magnetometers require a good deal of processing due to the fact that measurements are not taken in the spacecraft body axes or for that matter, axes common to all magnetometer units. As it turns out, this processing is nontrivial and has initially produced counter-intuitive results, which have proven difficult to verify. The lack of commonality in the sensors' measurement axes creates ambiguity as to whether discrepancies among the magnetometers' measurements are due to physical phenomena or errors in the calibration, numbering, positioning, and/or wiring of the individual units. Furthermore, if the spacecraft were not equipped with separate magnetometers for attitude control, the only way to verify that the conversion to the spacecraft body axes was correctly performed would be to compare the final results with a model of the Earth's magnetic field (note: this would require a conversion to Earth-Centered, Earth-Fixed axes). In future designs, these problems can be avoided by configuring the measurement axes of all magnetometer units so that they align with each other and the spacecraft body axes.

## 13.4 Global Positioning System (GPS)

When the notion of using GPS on GP-B was conceived in 1982, GPS had limited use in space applications. Nevertheless, GPS was selected as the best method to obtain precise position and velocity data. While the original goal of using GPS for closed loop navigation proved too ambitious, the GPS subsystem has surpassed its mission goal of providing real time Position, Velocity, and Time (PVT) solutions at better than 100 meter rms accuracy. Additionally, GPS time telemetry from the receiver has been successfully used to accurately reconcile vehicle time with Coordinated Universal Time (UTC). See section 8.2.5.2.9 for a list of selected GP-B GPS papers.

While laser ranging solutions has augmented GPS measurements during the mission, GPS telemetry is the primary source of PVT information. The receiver was powered on two hours after launch. Real time position and velocity telemetry provides relatively coarse orbit solutions. Post processed telemetry provides precise orbit



solutions. Accurate orbit solutions was needed both to determine the extent of orbit trim required during the initialization phase of the mission, and for precise vehicle position and velocity knowledge during the science phase of the mission.

### 13.4.1 GPS Hardware

The GPS equipment is divided into two fully redundant sets. Each set is composed of a Trimble TANS Vector III GPS receiver and four matching Trimble antennas. Originally built for battlefield GPS attitude applications, a modified TANS Vector III flew successfully on STS-77 in 1996, as part of the GPS Attitude and Navigation Experiment (GANE).

The Trimble TANS Vector III is a six channel L1 receiver which calculates position, velocity, and time (PVT) every 1.7 seconds. The receivers are mounted on the spacecraft superstructure. Each receiver has inputs for four antennae, two of which are mounted each fore and aft, as shown in Figure 13-34, and are placed as to maximize antenna baseline and optimize sky view, as delineated in Table 13-4. The forward antennae's field of view are obstructed slightly by the telescope sun shade, as depicted in Figure 13-35, but otherwise the antennae enjoy a full view of the sky.

**Table 13-4.** Installed Position of GPS Antennae

	<b>Azimuth angle</b>	<b>Elevation angle</b>
<b>Antenna 1</b>	90°	45°
<b>Antenna 2</b>	270°	45°
<b>Antenna 3</b>	0°	-45°
<b>Antenna 4</b>	180°	-45°

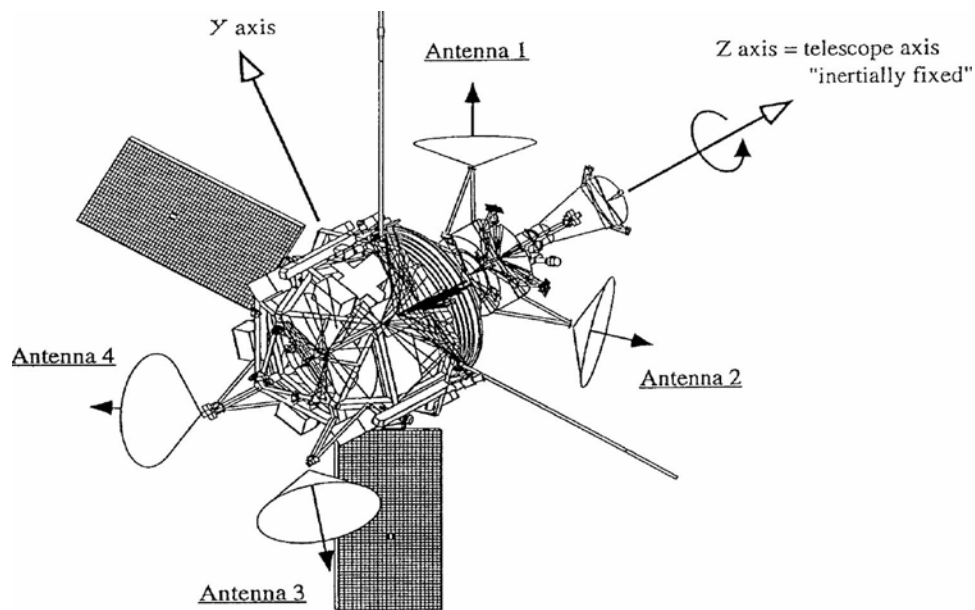


**Figure 13-34.** Location of GPS equipment on GP-B

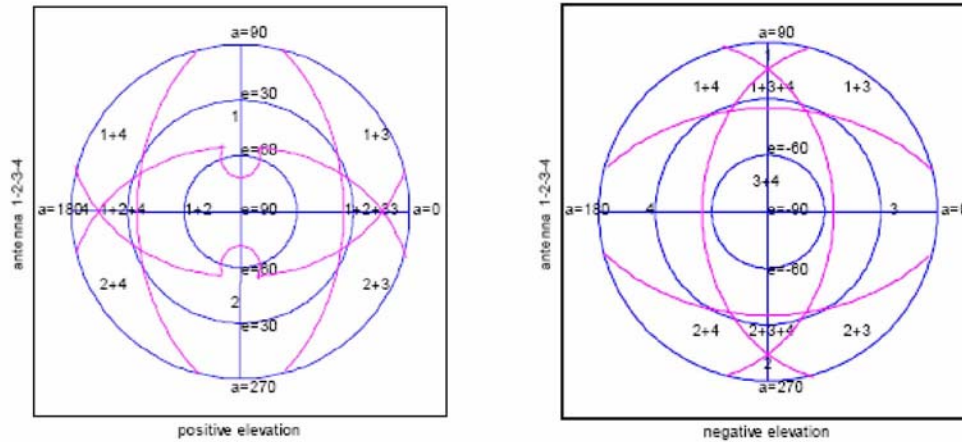


**Figure 13-35.** GPS Antennae Field of View

### 13.4.2 Hardware Modifications for GP-B

Despite the equipment's rugged heritage, pre-launch testing revealed hardware modifications were required to increase robustness. Non-stainless steel screws were replaced with stainless steel equivalents. Resistor and capacitor components were replaced with space compatible versions, as were connectors. Copper heat sinks were added to better facilitate heat transfer in orbit. Thicker aluminum housing covers replaced the original covers to provide increased radiation shielding and more stiffness. As is typical in space applications, all electronic boards were conformal coated.

The receivers were also retrofit with Pulse Per Second (PPS) circuitry, which outputs a 5V pulse every second, on the GPS second. The PPS signal is used to reconcile vehicle time with UTC time.

The majority of modifications involved changes to the receiver's software. The receiver's search algorithm was modified for space. To find a GPS satellite, the receiver must compare the incoming signal with the matching satellite PRN code. A terrestrial receiver looks through a Doppler shift range of ~10 kHz. Because the environment of GP-B is more dynamic, the Doppler shift window was increased to ~80 kHz. This increased search capability allows the receiver to do a "cold" search in space. While bootstrap acquisition is a definite plus, Ephemeris Aiding allows the receiver to acquire the constellation typically within ten minutes. After power up, or receiver reset, the receiver is initialized with Keplerian orbital elements, as well as a complete set GPS ephemerides.

Other modifications enhance communication with the GP-B flight computer. For example, while the flight computer interface operates at 10 Hz, a complete set of GPS telemetry occurs only every 10 seconds. The introduction of a Solution Quality Index (SQI) provides information about the receiver's acquisition status between successive sets. SQI has proved invaluable for understanding GPS telemetry, and is particularly useful as a filter during post processing.

### 13.4.3 Pre-Launch Testing and Results

The modifications necessitated strenuous qualification testing. Environmental testing focused on hardware modifications, and included the normal regimen of space qualification tests: EMI, thermal vacuum cycling, random vibration, etc. All tests were completed and data thoroughly reviewed prior to the equipment's installation on the vehicle in September 2002. Selected highlights are given in [Table 13-5](#). Integration testing was successfully completed by August 2003. Prior to launch, the GPS subsystem was routinely used to accurately time tag ground testing data.

**Table 13-5.** Environmental Testing Highlights

Test	Receiver	Antenna
Survival Temp High (C)	+85	+ 85
Survival Temp Low (C)	-55	-55
Operational Temp High (C)	+20	+30
Operation Temp Low (C)	-9	-34
Base Pressure (Torr)	$3.2 \times 10^{-7}$	$3.2 \times 10^{-7}$
VibroAcoustic (G rms)	6.1	9.7

Perhaps more interesting were the tests accomplished to verify software modifications. In particular, two competing effects needed to be investigated: rolling and orbiting.



**Figure 13-36.** Rolling Rig

Stanford University used a WellNav GPS Simulator to show that the software modifications allowed the receiver to acquire and maintain position fixes while in the simulated GP-B Orbit. But because the WellNav simulator cannot model a rolling, orbiting vehicle, a rotating platform (Figure 13-36) was designed and fabricated. The rig, which can rotate over the entire range of predicted roll rates (0.1 – 2 rpm), showed that the antenna switching algorithm would work up to 2 rpm, although slower rates yield better results.

The receiver calculates the Signal to Noise Ratios (SNRs) for up to six tracked GPS vehicles. The antenna selection algorithm compares the SNR values every 15 seconds. The antenna with the GPS satellite with the highest SNR is selected as the master antenna. The pattern should exactly repeat at the roll period. However, if the algorithm calculation occurs when the antenna with the best visibility is ascending, the next best antenna will erroneously be selected. Figure 13-37 shows the master antenna assignment for one channel at three different roll rates, plotted vs. time. The top plot shows the master antenna switching occurring more or less periodically, as expected. Errors increase as the roll rate increases (middle and bottom plots). Nevertheless, and most importantly, the receiver is able to maintain a lock in all cases.

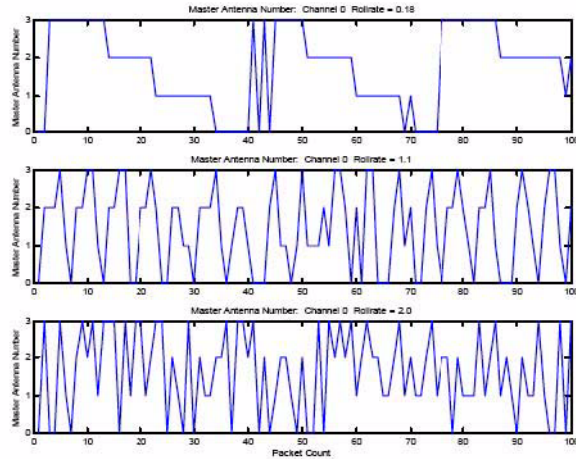


**Figure 13-37.** Master Antenna Switching

Testing the receiver under flight-like conditions, orbiting and rolling simultaneously, required the use of an advanced simulator. The Spirent GPS simulator at Marshall Space Flight Center (MSFC) was able to perform a variety of simulations, modeling the static scenario as well as the orbiting case at several different roll rates. [Table 13-6](#) presents the results. As can be seen, the percent lock is never 100%. While the GPS equipment on GP-B does not have an on-orbit coverage requirement, the informal goal has been 70%. All the tested scenarios, as well as on-orbit results, yielded more than acceptable coverage.

**Table 13-6.** Percent Lock for Various Scenarios

Scenario	Percent Lock (%)
Static	99.0
Rolling Rig (Typical of 50 data sets with roll rates less than 1 rpm)	98.0
Orbiting, Inertial Pointing, No Roll	96.6
Orbiting, Rolling (0.33 rpm)	96.6
Orbiting, Rolling (0.5 rpm)	98.1
Orbiting, Rolling (1.0 rpm)	72.6

### 13.4.4 Time Reconciliation

The addition of PPS circuitry allows vehicle time to be reconciled with UTC. But is the PPS signal dependent upon roll rate? The rolling rig provided an excellent platform to investigate this possibility.

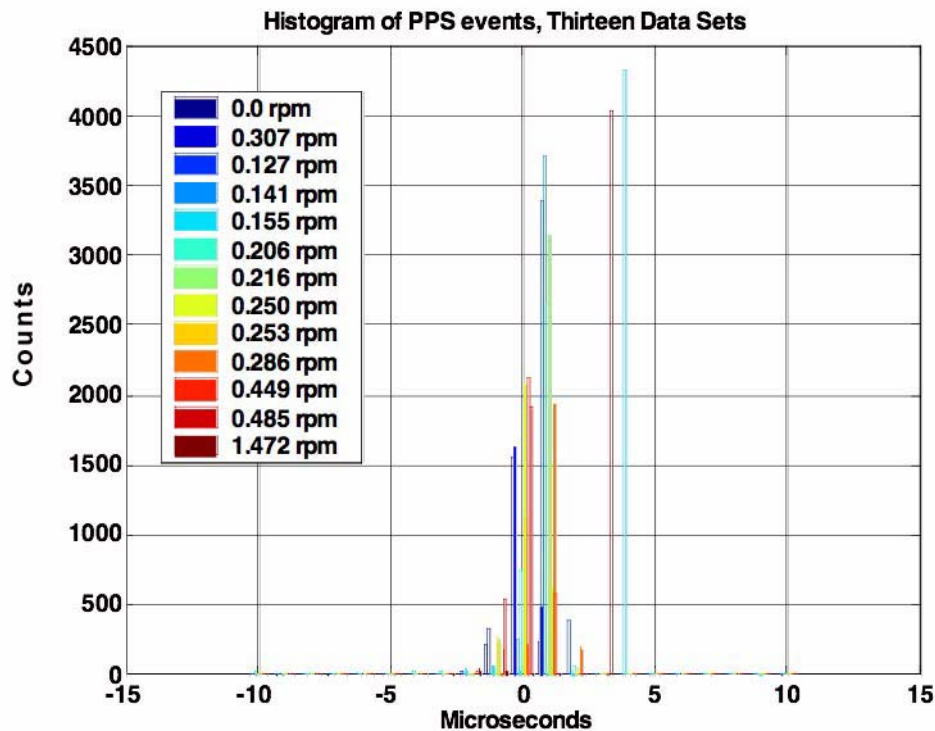


**Figure 13-38.** Histogram of PPS Data

A histogram of the data is shown in [Figure 13-38](#). Data for twelve different roll rates was used, in addition to a data set for the static case. Three data points were outside the plus/minus ten microsecond requirement range, 99.88% of the data is within a plus/minus five microsecond range. No correlation was discovered between the output PPS signal and roll rate.

A comprehensive set of tests verified that science telemetry could be time tagged to better than the 10  $\mu$ s requirement, and showed that the GPS PPS signal allows telemetry to be reconciled with UTC time without introduction of further measurable time error.

Details regarding the time reconciliation method can be found in [5], but an example of challenges overcome is useful for appreciating the complexity of the GP-B spacecraft as well as its detailed design. In addition to providing a 10 Hz timing strobe for vehicle hardware, the space flight computer's master clock drives a 31 bit counter at 16.368 MHz. Registers capture the value of the counter when a PPS or a 10 Hz strobe pulse is detected. The values are included in telemetry. Since there is no a priori way of differentiating one PPS signal from its neighbor, the GPS receiver telemetry includes transmission time: the time at which the GPS data packet leaves the receiver. Another telemetry mnemonic captures the time the GPS data packet was received by the flight computer. By design the interval is minimized. [Figure 13-39](#) shows the difference between the transmission and reception time. The figure shows that the interval is always less than 0.6 seconds.

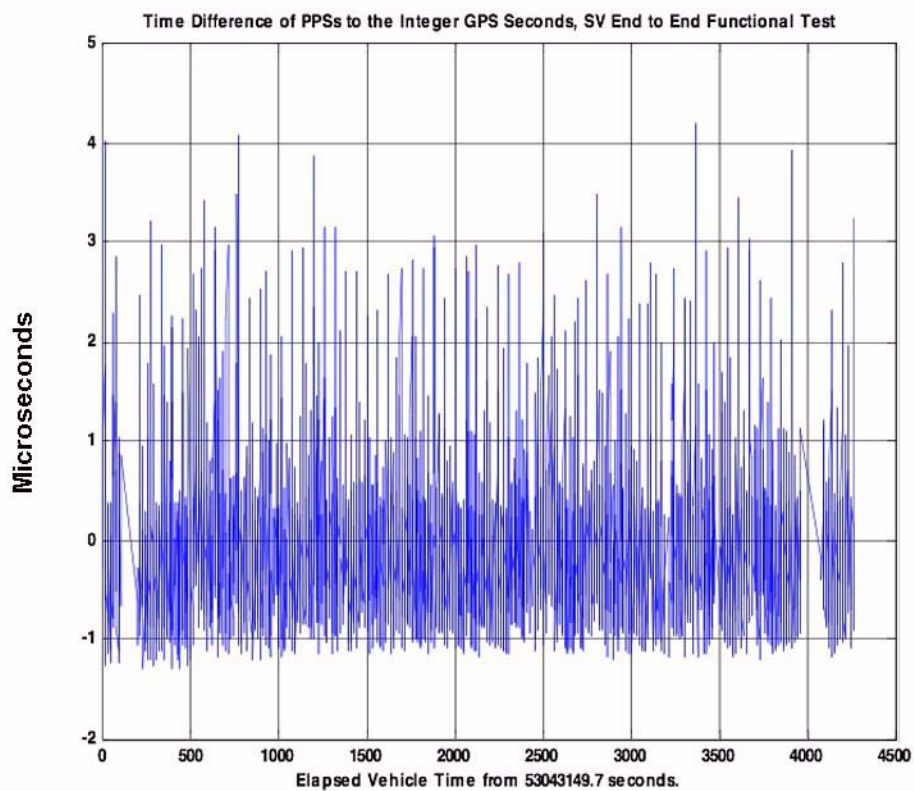


**Figure 13-39.** Time difference between transmission and reception of GPS data packet.

After determining the time difference, an algorithm fits the PPS signal to the integer GPS second. [Figure 13-40](#) shows the residuals using a second order model. Note that the residuals are less than 5 microseconds. Recent improvements to the algorithm enable piecewise parabolic or cubic polynomial fits [6].



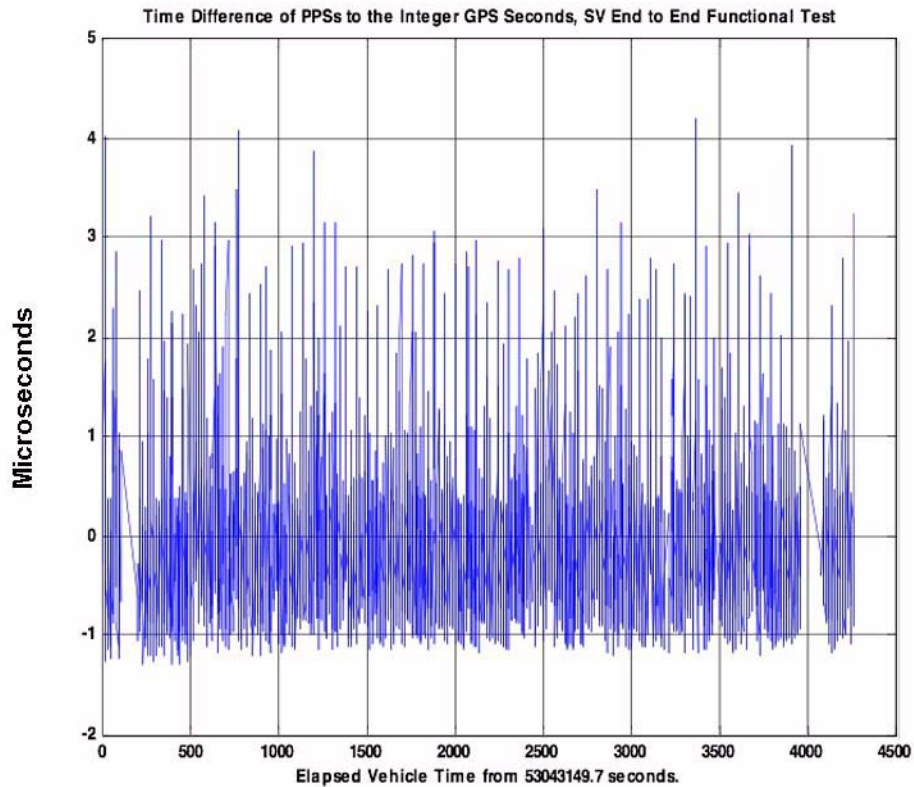


**Figure 13-40.** Residuals of Least Square fitting algorithm with 2<sup>nd</sup> order model.

### 13.4.5 Orbital Accuracy

Truth tables output by the GSSI simulator were compared to the receiver’s position and velocity solutions. [Table 13-7](#) and [Table 13-8](#) show the results, where the truth data is compared against both the raw and post processed telemetry.

**Table 13-7.** Raw and Processed Positions vs. Truth

Position	Spec	X	Y	Z
Real Time (m)	100	14.5	18.0	26.0
Post Processed (m)	25	3.7	6.9	4.6

**Table 13-8.** Raw and Processed Velocities vs. Truth

Velocity	Spec	X	Y	Z
Real Time (cm/s)	100	7.1	7.4	10.3
Post-Processed (cm/s)	7.5	0.4	0.7	0.5

In most cases, the real time solutions exceed the post-processed mission requirements. The post processed differences are well within mission specifications.



### 13.4.6 On-Orbit Results

The GPS components on GP-B have exceeded performance expectation through-out the GP-B mission.

In particular, coverage has been significantly better than ground tests predicted. At a roll rate of 0.77 rpm, simulator testing suggests that the coverage rate should be 86% (see [Figure 13-41](#)). Nevertheless, the receiver has enjoyed an average coverage rate of better than 97%.

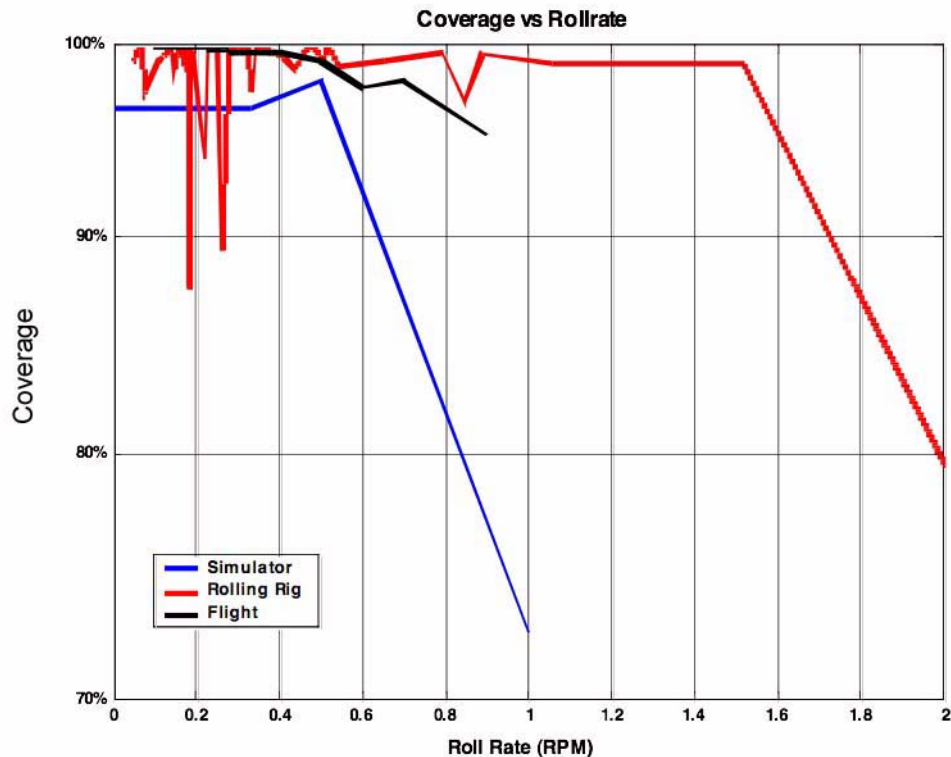


**Figure 13-41.** Coverage Curves for GPS simulator, rolling rig, and flight data. At GP-B's roll rate, the simulated coverage is 86%, while flight rate is better than 95%

The receiver also did well whilst changing roll rate, as shown in [Figure 13-42](#), where the roll rate was increased from 0.6 to 0.9 rpm in 8 hours; the receiver maintained a coverage of better than 95%.

The GP-B orbit modeling software, Microcosm, uses 30 hours of GPS solutions to compute a best fit orbit model. By comparing overlapping 30 hour data sets, accuracy of orbit position and velocity solutions can be estimated. The estimates are consistent with simulated orbit modeling done prior to launch and shown in [Table 13-7](#) and [Table 13-8](#), and suggest that on-orbit positions are known to better than 10 meters, and velocities are known to better than 2 cm/s.

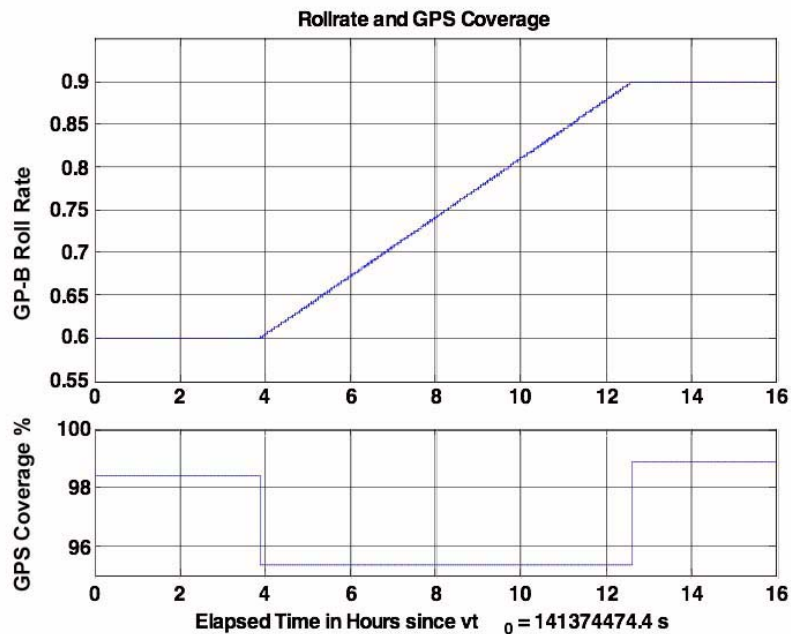


Figure 13-42. Coverage rates during an increase in vehicle roll rate.

## 13.4.7 On-Orbit Events

Several on-orbit events bare mention.

### 13.4.7.1 Delay in Initial Acquisition

While pre-launch validation testing suggested that the time to first fix after GPS power-on would be less than the required ten minutes, the actual initial acquisition after the first on-orbit power-on took 110 minutes. Since then the receiver has been power cycled four times, and in each case the time to first fix has been less than ten minutes. As the launch data was delayed one day, one likely explanation of the increased acquisition time is that initialized Keplerian orbital elements were sufficiently stale that a cold search was necessary to acquire the GPS constellation. The explanation is consistent with telemetry. Furthermore, simulated cold searches typically take about 90 minutes.

### 13.4.7.2 Possible Memory Leakage Anomaly

A second observation is that the A-side receiver performance fell dramatically on day June 16<sup>th</sup> of 2004, 55 days after a reset, recorded in the ARB notes as Observation 68. Symptoms included a drastic increase in the clock bias, and a severe decrease in coverage rate. Resetting the receiver's memory cleared the issue. A flight equivalent receiver set up on the ground to test the hypothesis that the receiver locked because of real time operating system limitations with limited memory locked up after 40 days, with similar symptoms. While memory leakage, as this phenomenon is called, appears the most likely explanation, an operational process was developed for early detection. Fortunately, the event did not reoccur.

### 13.4.7.3 GPS Constellation Geometry Anomaly

On December 4th, 2004, the ATC experienced an ADA exception error, which caused the vehicle to enter safe mode, with loss of both drag-free and Guide Star. Details regarding this event have been tracked by the ARB as Anomaly 129. The cause of the exception error was determined to have been exceptionally high vehicle position

and velocity values erroneously calculated by the GPS receiver. The cross product of the position and velocity solution calculated by the receiver resulted in a value with of  $3e19$ . The magnitude function takes the root sum squared,  $3e19^2 = 9e38$  which exceeded a short float range of  $1.7014e+038$  ( $2^{127}$ ). Typically all divisions, squares etc. are protected in the ATC code, but multiplications are not. The result caused a stack overflow, which in turn caused the safemode activation. The erroneous position and velocity solution was caused by poor geometry of the GPS constellation. The operational solution was to increase the exception counter.

#### **13.4.7.4 Channel Alignment Issues Due to Computer Memory Errors**

On two occasions, August 12<sup>th</sup>, 2004 (Observation 102) and Jan 10<sup>th</sup>, 2005 (Observation 135), telemetry indicated that a GPS error flag, channel alignment error, had toggled to the true state, indicating a problem with the receiver. A detailed analysis of GPS solutions ruled out an actual error state, suggesting that the error bit flipped as a result of a single bit or multi-bit event. While rebooting the receiver would have cleared the error, in both cases the decision was made to leave the receiver as is. In both instances, the receiver was eventually rebooted as part of other vehicle operations.

#### **13.4.7.5 Switch to B-Side GPS Receiver**

The last observation regards the switch to the B-side receiver. Since the GPS receivers are not cross strapped, when the vehicle switched from the A-side to the B-side on March 13, 2005, the GPS subsystem switched from the A-side to the B-side components as well. While the average percent lock by the B-side components is only slightly less than the A-side average (95% vs 98%), [Figure 13-43](#) clearly shows that the day-to-day values vary greatly. [Figure 13-43](#) also shows the percentage of GPS solutions used by the orbit determination group to calculate the GP-B orbit also dropped after the switch to the B-side hardware. The decrease in usable points is due to the increase in “stale” data—data from a previous solution still in the GPS memory buffer. When the receiver is locked and outputting valid GPS solutions, stale data is overwritten by new data. Stale data should only occur when the receiver is reacquiring the GPS constellation. Analysis of the solution quality index telemetry shows that the SQI is slightly, but consistently, higher on the B-side than on the A-side receiver, an observation consistent with the decrease in percent lock seen. Further insight is gleaned by observing that jitter in the clock bias is higher on the B-side. The most likely hypothesis is that the difference is caused by slight differences in the performance of the GPS internal oscillators, used to track time between successive PVT solutions. While only a detailed analysis of the GPS internal oscillators can verify the root cause, available telemetry is consistent with this hypothesis. Pre-launch sanity testing did not reveal performance differences between the two oscillators.

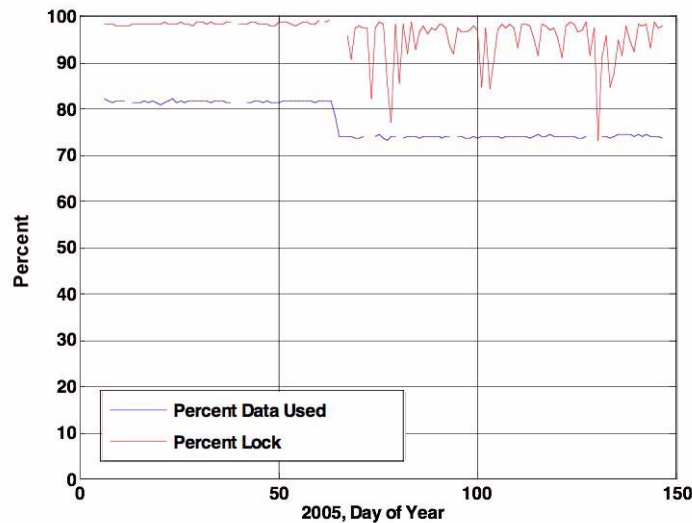


**Figure 13-43.** Percent Lock and data points used before and after the switch to the B-side receiver on March 4, 2005, day 64.

Regardless of the root cause, it is important to note that while the percentage of GPS solutions used by the Orbit Determination group has decreased since the switch to the B-side receiver, the quality of the solutions has not decreased. The orbit solution calculated by the group continues to meet mission requirements. Although a performance difference between the A-side and B-side components is clear, the GPS subsystem has easily exceeded all mission requirements and pre-launch expectations.

### 13.4.8 References

- J. Ceva, B. W. Parkinson, **Multiple Interference in Orbiting Receivers Due to Earth Surface Reflections**, *ION GPS-93*, Salt Lake City, Utah, September 1993.
- C. E. Cohen, B. W. Parkinson, **Mitigating Multipath Error in GPS Based Attitude Determination**. Reprinted from *Guidance and Control 1991*, Vol. 74, Advances in Astronautical Sciences.
- C. E. Cohen, B. W. Parkinson, **Expanding the Performance Envelope of GPS-Based Attitude Determination**, *ION GPS*, Albuquerque, N. M. September 1991.
- P. Axelrad, B. W. Parkinson, **Closed Loop Navigation and Guidance for Gravity Probe B Orbit Insertion**, *Journal of The Institute of Navigation*, Vol. 36, No. 1, Spring 1989.
- J. Li, G.M. Keiser, J.M. Lockhart, P. Shestople, **Time Transfer between UTC and Local Vehicle Time for the Gravity Probe B Relativity Mission**. *Proceedings of both Annual Meetings of Institute of Navigation*, pp.560-570, 2004.
- J. Li, A. Ndili, L. Ward, S. Buchman, **GPS Receiver Satellite/Antenna Selection Algorithm for the Stanford Gravity Probe B Relativity Mission**. *Proceedings of 1999 Institute of Navigation National Technical Meeting*, pp.541.
- J. Li, A. Ndili, L. Ward, S. Buchman, M. Keiser, **Analysis of Field-of-View of GPS Antennas and Constraints of the Antenna Transfer Time**, Stanford University, *GP-B Memo, SDOC 344, Rev -, 1998*
- D. Yale, A. Ndili, J. Li, E Ng, E. Bean, S Buchman, **Rolling GPS Receiver Development and Verification Testing for Space Application**, *Institute of Navigation GPS-99 Conference*, Nashville, Tennessee, Proceedings of the 12th International Technical Meeting, p. 857.

E. G. Lightsey, C. E. Cohen, B. W. Parkinson, **Development of a GPS Receiver for Reliable Real-Time Attitude Determination in Space**, *Proceedings of 7th International Technical Meeting of the Satellite Division of the Institute of Navigation*, 1994, p. 1677-1684.

## 13.5 Gas Management Assembly (GMA)

The GMA performed nominally during both the IOC and science (data collection) phases of the mission. All tasks were completed on schedule and without any errors.

All sub-systems of the GMA, including pressure and temperature were “green” throughout the mission, with the exception of a few hours during the second week after launch, when the spacecraft sustained a proton strike, causing a switch-over from the main “A-side” computer and systems to the backup “B-side” systems. During gyro spin-up procedures, the GMA performed “as expected” with respect to spin-up manifold pressure vs. time plots.

No anomalies and only two observations were attributed to the GMA during the mission. The two observations were for silicone diode temperature spikes that did not affect the thermal control of the GMA and an increased pressure down stream of the pressure regulators due to gas leakage through the GMA latch valves. This was expected based on ground testing.

### 13.5.1 GMA Development and Operational Concept

The GMA was a late delivery sub-assembly that was fabricated, environmentally tested, and delivered to Stanford in 13 months. At Stanford, the GMA was functionally verified by spinning up a low temperature (4° Kelvin) gyroscope. It was mated to the space vehicle at Lockheed Martin in Sunnyvale, California just prior to the space vehicle thermal vacuum testing. The GMA passed functional testing for both pre and post thermal vacuum testing.

The GMA has three main operating parts:

- Two high-pressure storage vessels filled with 10.4 liters of helium at 2000psia.
- Two redundant gas manifolds that lead to each gyro inlet, a probe inlet, and a vent path to space. Each gas manifold has two redundant pressure regulators, two flow controllers (725 sccm and 2 sccm), 15 latch valves, and 7 pressure transducers.
- Two heater strips to heat the GMA pallet to 20°C ±8°C during valve operations.

Ultra-pure (99.9999%) helium gas is streamed from the Gas Management Assembly (GMA), mounted in a bay on the spacecraft frame, through tubing that enters the “top hat” (the thermal interface at the top of the Probe) and travels down to the gyro housings in the Science Instrument Assembly (SIA) at the bottom of the Probe. As the helium gas descends into the Probe, which is at a temperature of approximately 1.8 Kelvin, the gas cools down from 273 Kelvin to around 12 Kelvin.

The GMA was used to perform the “flux reduction” and all phases of gyroscope spin-ups - 0Hz, 5Hz, 10Hz, and the final “Full” spin. Flux reduction was performed through an inlet into the Probe with a helium gas flow at 2 sccm while the Probe leakage valve was open.

The GMA consists of the components shown in [Table 13-9](#) below. Note the redundancy some of the components.

**Table 13-9.** Summary of Components for the Gas Management Assembly

Component	Qty	Redundancy	Comments
Regulators	4	2 Pairs	2 regulators in series
Latch Valves	30	15	Gyro outlet branches included 2 of 4 valves that were in an open state for electrical redundancy
Flow Control Orifices	5	2	10 SCCM flow control for flux reduction was in place to reduced the risk of over pressurizing the Probe
Filters	4	0	Filters were primarily for filling the GMA with He gas
Fill and Drain Valves	4	0	Used to fill GMA w/He gas and servicing the regulators (lock-up).
Pressure Sensors	14	0	Pressure sensors were primarily used to evaluate the status of a latch valve (open or closed)
Gas Bottles (5.2 liters each)	2	0	Gas bottles were in parallel and not isolated from each other (total gas - 2000psia / 99.9999% helium)

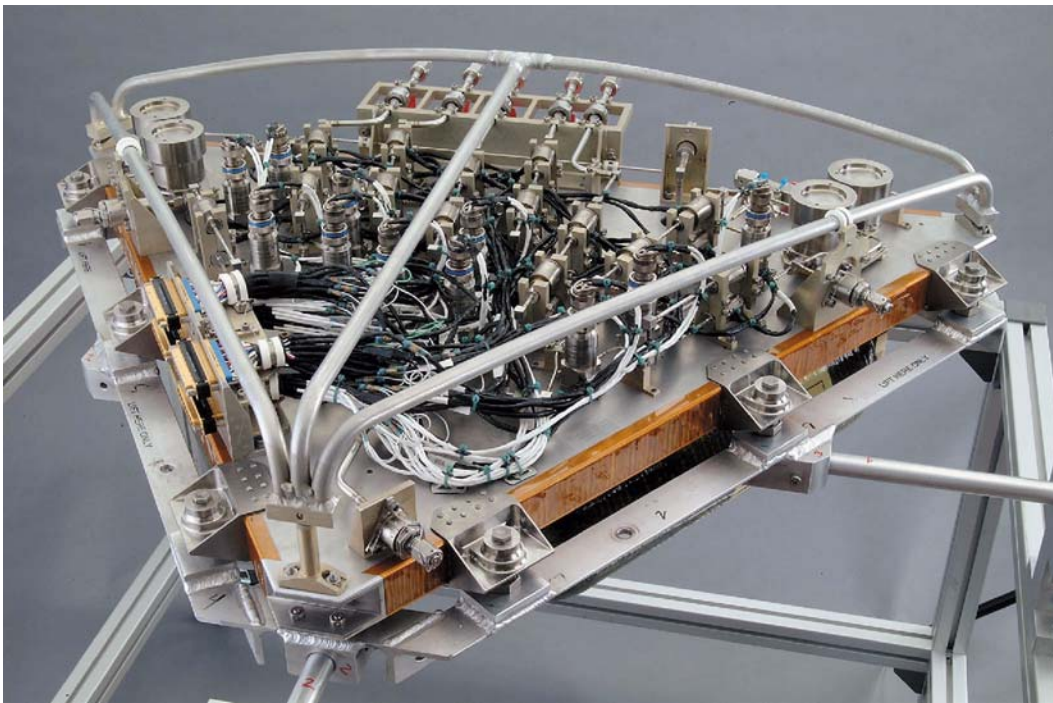


**Figure 13-44.** A Top View of the GMA Pallet with the Thermal Blanket Frame Attached



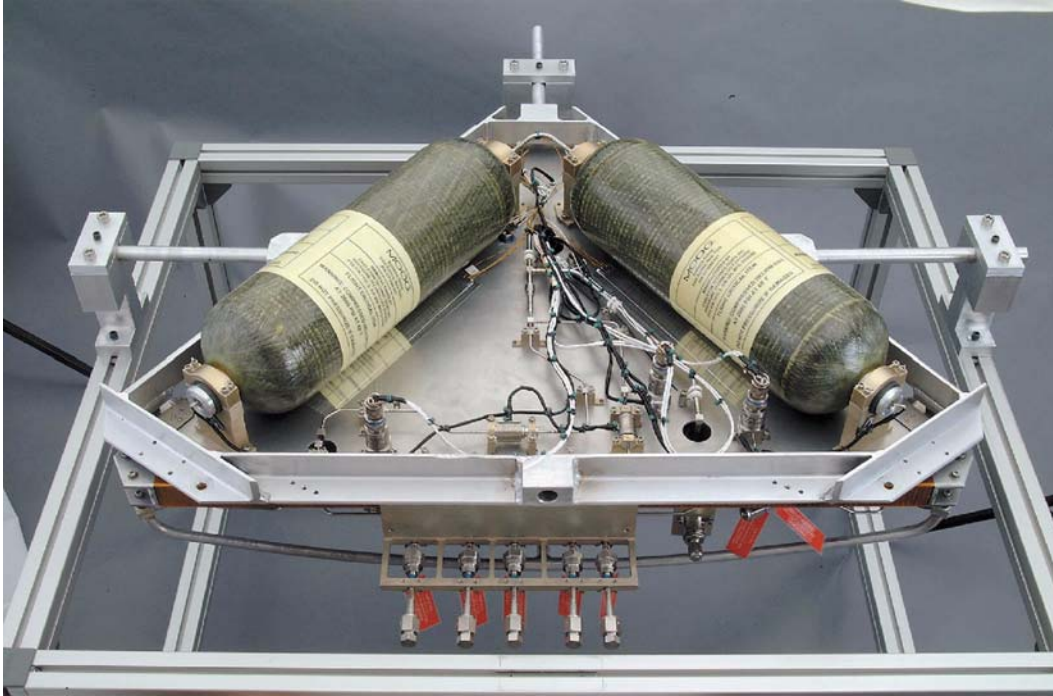


**Figure 13-45.** A Bottom View of the GMA Showing the Supply Tanks and Outlet Valves

### 13.5.2 Pre-Launch Ground Support

The GMA was built by Moog, Inc. in Buffalo New York. The latch valves had a gas leakage specification of  $< 1 \times 10^{-7}$  std cc/second. Most of the latch valves met this requirement, though some valves leaked at as high as  $1 \times 10^{-4}$  std cc/second. Some of the valves that did not meet the specification were the four vent valves that vented the GMA to space. The concern of these valves leaking on the ground was that “air” could leak back into the GMA that would contribute cryogenic contamination into the science probe during spin-up. A mitigation plan was developed by Stanford to back fill the GMA with 300 psia of ultra pure helium (See [Figure 13-46](#) below) up to the pressure regulators to ensure a minimal risk of cryogenic contamination of the SIA (science instrument assembly). Fill and Drain valves, as shown in [Figure 13-48](#) below, were installed between the GMA and the Probe inlets to minimize cryo contamination from entering into the Probe.



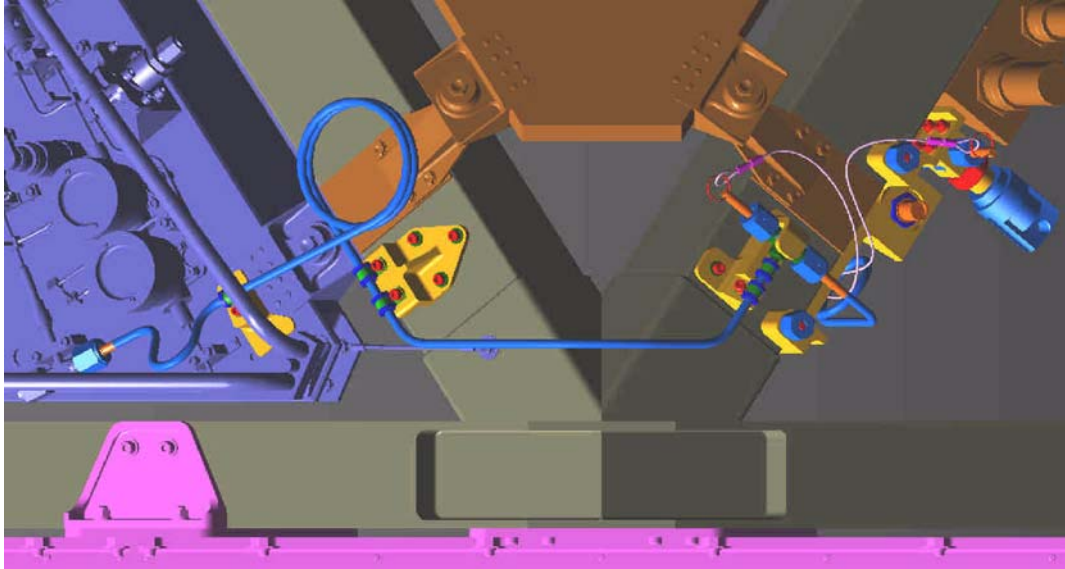


**Figure 13-46.** GMA vent manifold and service GSE used to minimize cryogenic contamination and ensure regulator lock-up for launch

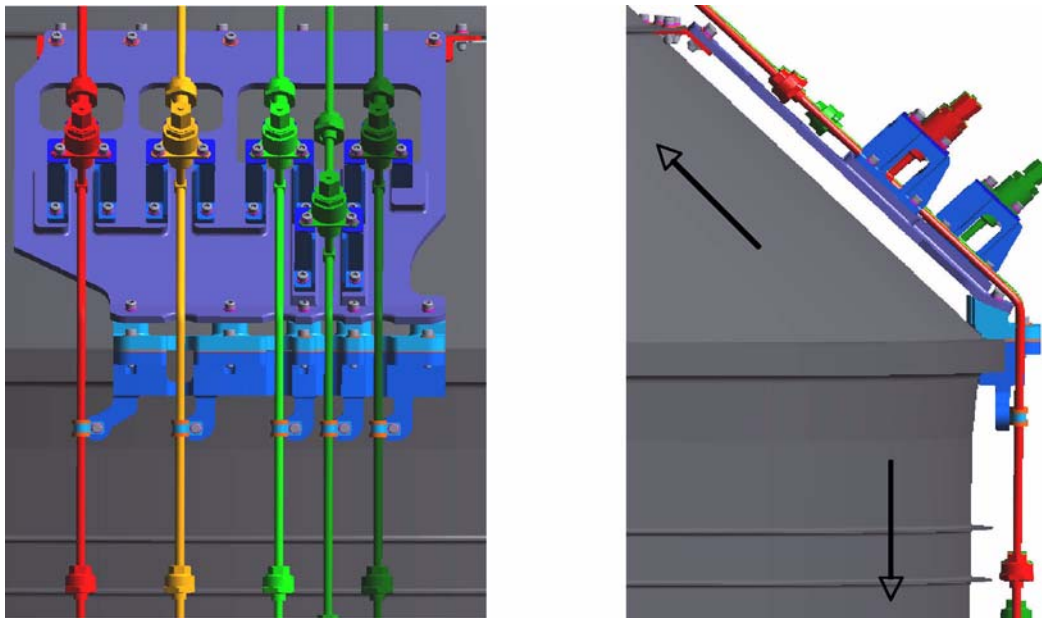


**Figure 13-47.** Service valve assembly (fill and drain valves) used to service the GMA to reduce the risk of cryogenic contamination during ground support

Cryogenic contamination could have resulted in a mission failure due to not having the ability to spin-up the gyroscopes. The mitigation plan included exhaustive ground support operations that took place until 12 hours prior launch to avoid cyro contamination. All this effort for ground support operations led to a successful GMA operation on orbit. The GMA configuration with component names is shown in [Figure 13-48](#) below, and a schematic diagram of the GMA, configured for Gyro #4 spin-up, is shown in [Figure 13-50](#).

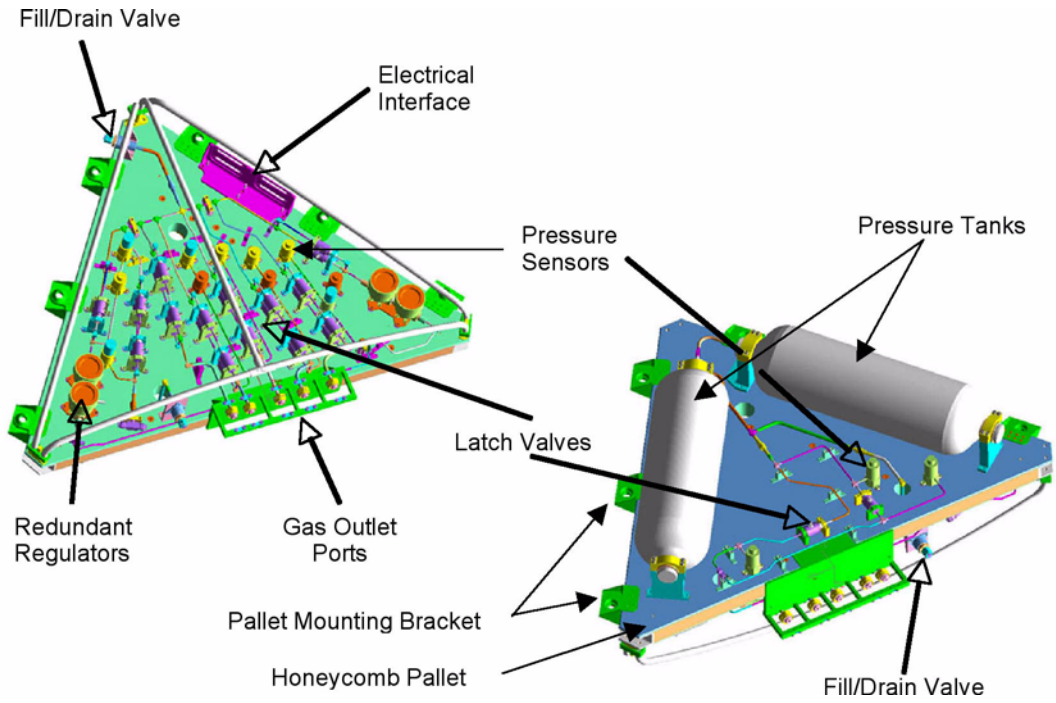


Figure 13-48. The GMA configuration on a vented honeycomb pallet

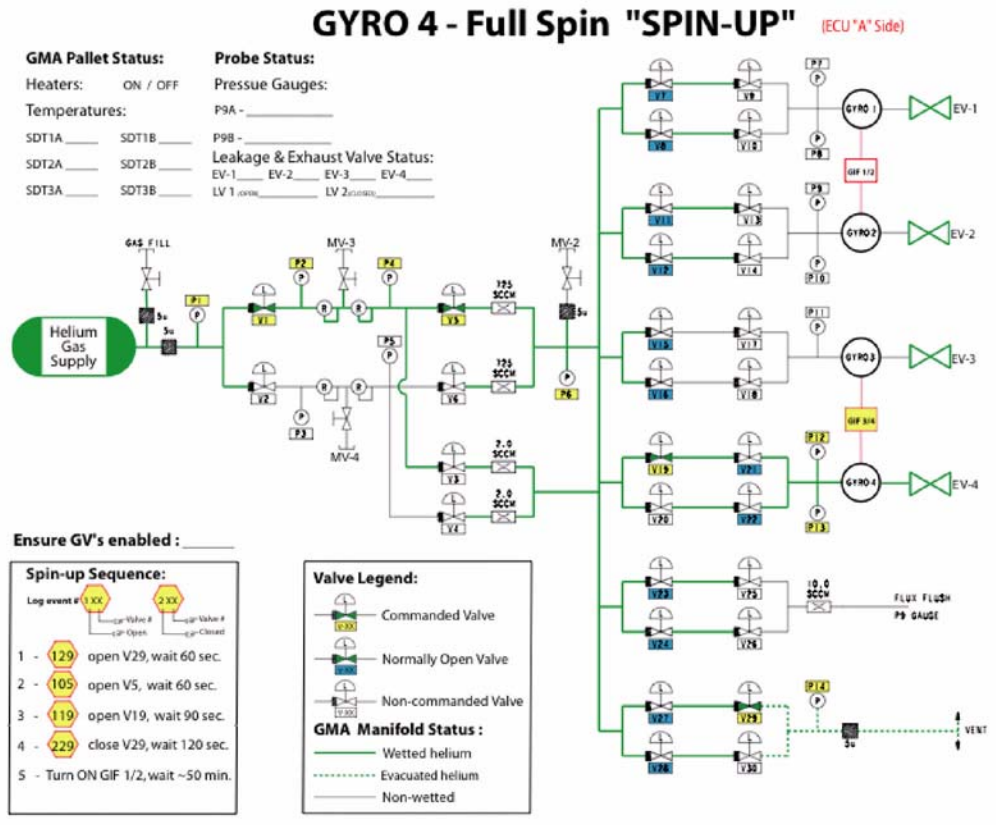
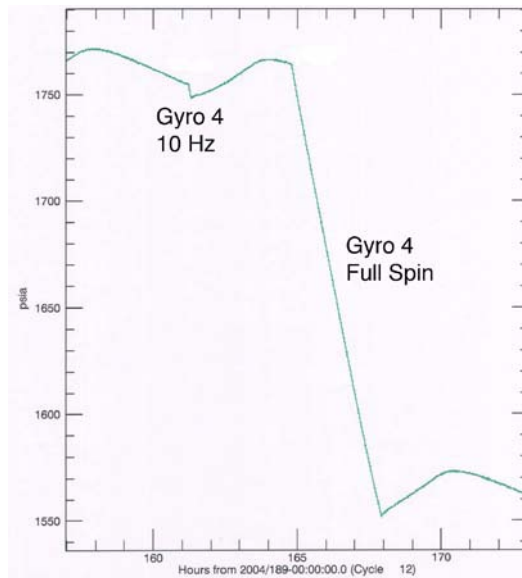


Figure 13-49. Schematic diagram of the GMA

### 13.5.3 GMA Gas Consumption for Gyro #4 Spin-Up

The graph in [Figure 13-50](#) below shows helium gas consumption for spinning up gyroscope #4 during IOC. This GMA gas consumption performance was typical for all four gyros.



**Figure 13-50.** Helium gas consumption for 10 hz and full spin-up of gyro #4 during IOC

### 13.5.4 Total GMA Gas Consumption for Gyro Spin-Up

Approximately 450 psia of ultra-pure helium gas was used during IOC. The He gas was used to perform the flux reduction, as well as gyroscope spin-ups. The GMA was used during briefly during post-mission still has an ample supply of helium gas remaining for post mission gyroscope spin-ups, if this is deemed desirable.

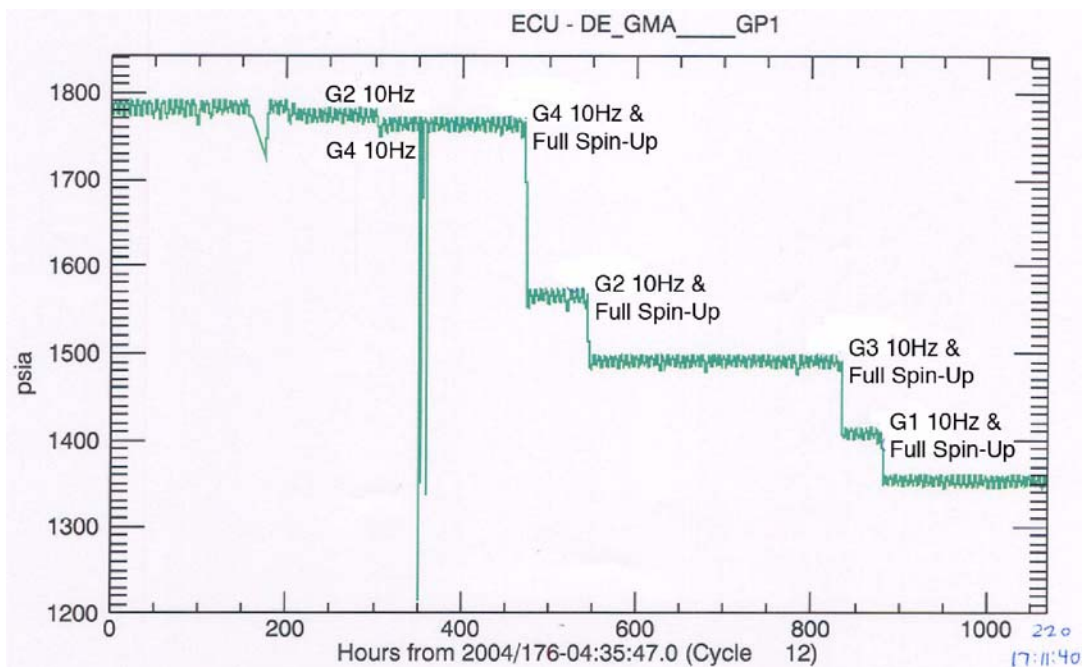


**Figure 13-51.** Pressure Transducer GP-1 Snap-Snapshot of Actual Gas Consumed by the GMA

**Table 13-10.** Summary for Helium Gas Consumption for GMA Operations On Orbit

Gyroscope Number	Helium Gas Consumption
1	~ 50 psia
2	~ 90 psia
3	~ 80 psia
4	~ 220 psia
Flux Reduction	~ 10 psia

### 13.5.5 GMA Science and Post-mission Status

The GMA was secured for the science phase of the mission. The vent path and all gyro inlet valves were closed. The redundant (normally open) valves for the flux flush inlets remained open. GMA heaters were turned off and the safe-modes to activate any GMA valves were disabled. During the science phase of the mission, there was no evidence of the GMA leaking any gas into the science gyroscopes that would affect any science data. There is an ample supply of helium remaining to spin up the gyros again for use in post-mission analyses or new experiments.



# 14

## Data Collection, Processing & Analysis





This chapter provides an overview of the collection, processing and analysis of data collected from the GP-B spacecraft and science instrument. The chapter includes two main sections:

1. “[Collection and Processing GP-B Data](#)” —Several vignettes excerpted from GP-B Mission News stories that were posted to our GP-B Web site and also sent out to over 2,400 GP-B Email Update List subscribers during the 17 months of the GP-B flight mission.
2. “[The GP-B Science Data Analysis Process](#)” —A brief description of the procedures that are currently being used to analyze the science data and determine the experimental results that will be announced and published in the spring of 2007.

## 14.1 Collection and Processing GP-B Data

This section contains a series of vignettes describing how GP-B data were collected and stored, how safemodes protected the spacecraft, science instruments and data, how anomalies such as computer memory errors were handled, and how intentional telescope dither and stellar aberration were used to calibrate the science data signals received. These vignettes were originally written to answer the question most asked throughout the mission by people around the world who have been following GP-B: “Why is it that proton hits to the spacecraft, computer memory errors, and other anomalies and glitches that occurred during the science phase of the mission will have little, if any effect on the final experimental results?”

### 14.1.1 Data Collection and Telemetry

Our GP-B spacecraft has the capability of autonomously collecting data—in real time—from over 9,000 sensors (aka monitors). Onboard the spacecraft there is memory bank, called a solid-state recorder (SSR), which has the capacity to hold about 15 hours of spacecraft data—both system status data and science data. The spacecraft does not communicate directly with the GP-B Mission Operations Center (MOC) here at Stanford. Rather, it communicates with a network of NASA telemetry satellites, called TDRSS (Tracking and Data Relay Satellite System), and with NASA ground tracking stations.

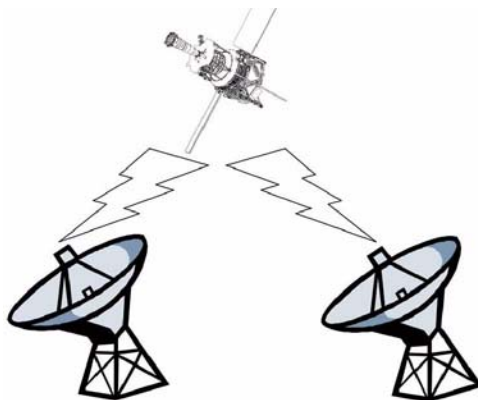


**Figure 14-1.** A drawing of the spacecraft communicating with ground tracking stations

Many spacecraft share these NASA telemetry facilities, so during the mission, GP-B had to schedule time to communicate with them. These scheduled spacecraft communication sessions are called “passes,” and during the flight mission, the GP-B spacecraft typically completed 6-10 TDRSS passes and 4 ground station passes each day. During these communications passes, commands were relayed to the spacecraft from the MOC, and data were relayed back via the satellites, ground stations, and NASA data processing facilities. The TDRSS links have



a relatively slow data rate, so we could only collect spacecraft status data and send commands during TDRSS passes. We were able to collect science data only during the ground passes. That's the "big picture." Following is a more detailed look at the various data collection and communication systems described above.

### 14.1.1.1 The Solid State Recorder

An SSR is basically a bank of Random Access Memory (RAM) boards, used on-board spacecraft to collect and store data. It is typically a stand-alone "black box," containing multiple memory boards and controlling electronics that provides management of data, fault tolerance, and error detection and correction. The SSR onboard the GP-B spacecraft has approximately 185 MB of memory—enough to hold about 15.33 hours of spacecraft data. This is not enough memory to hold all of the data generated by the various monitors, so the GP-B Mission Operations staff controlled what data were collected at any given time, through commands sent to the spacecraft.



A typical solid state recorder, manufactured by SEAKR Engineering

**Figure 14-2.** A typical solid state recorder (SSR) manufactured by SEAKR Engineering

Many instruments on-board the spacecraft have their own memory banks. Data rates from these instruments vary—most send data every 0.1 second, but some are faster and others slower. The data from all of these instruments are collected by the primary data bus (communication path) and sent to the central computer, called the CCCA. The CCCA then sends the data to the SSR.

The data were categorized into five subtypes:

1. **Sensor programmable telemetry**—High data rate of 0.1 seconds, greater than 9000 monitors, mostly used for science & engineering)—this is GP-B's "primary" useful data, including most science data.
2. **Event data**—For example, whether the vehicle is in eclipse (tells when we entered eclipse behind the earth and when we emerged)
3. **Database readouts**—Used to confirm that the on-board database is the same as the ground folks think it is – use this to verify that say, filter setting commands, were received and enacted.
4. **Memory readout (MRO)**—Used to ensure that the binary memory on-board is the same (error free) memory we think it is—this is where single & multi-bit errors occur (this is not collected data, but only programmable processes—i.e., the spacecraft's Operating System). If we find errors in the MROs, we can re-load the memory. Solar wind (proton hits), for example, can cause errors here.
5. **Snapshot data**—This is extremely high-speed data (1/200th of a second) from the SQUID (Super-Conducting Quantum Interference Device), Telescope and Gyro readout systems. The CCCA does some on-board data reduction, performing Fast Fourier Transforms (FFT) on some of the incoming SRE data. This on-board reduction is necessary, because we do not have room in our SSR, nor the telemetry bandwidth, to relay the high-rate data back to the MOC all the time. (Perhaps we should upgrade to DSL...) However, like all numerical analysis methodology, an FFT can become "lost" because an FFT is

not always performed from the same starting abscissa (x-axis) value. The Snapshot allows us to see some of the original data sets being used for the FFTs and confirm that they are not lost—or if they are, we can fix them by making a programmed adjustment on-board. Other systems—the Telescope Readout (TRE) and Gyro Suspension System (GSS)—use their snapshots for similar instrumentation and data reduction validity checks.

Data were stored to the SSR in a “First in, First out” queue. Once the memory is 15.33 hours full, the new data begins to overwrite the oldest data collected. That’s why it was a good idea to dump the SSR to the ground at least every 12 –15 hours (for safety!), which is exactly what we did.

#### 14.1.1.2 Telemetry—TDRSS and Ground Stations

So, how did we talk to the spacecraft and retrieve our data? NASA communicates with its spacecraft in several ways. Its highest availability is through TDRSS, two communications satellites in orbit, just waiting for communications. These two satellites can’t handle much data at a time, and we could transmit to them only at a 1K or 2K (kilobit per second) rate. For GP-B, this rate is only fast enough to exchange status information and commands; it was not fast enough for downloading science data.

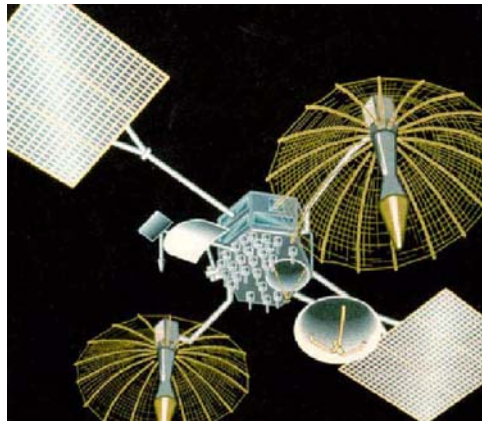


**Figure 14-3.** A NASA TDRSS Satellite

NASA also uses ground-based stations. There are several around the world, but each ground station network used is determined by satellite type and orbit. Because GP-B is in a polar orbit communicating primarily at 32K (32kilobits per second), we used the NASA Goddard “Ground Network”. This network includes stations in Poker Flats, Alaska; Wallops, Virginia; Svalbard, Norway; and McMurdo station, Antarctica. Communication with the South Pole station was not as reliable as the others, but we did use the McMurdo ground station on a few occasions during the mission.

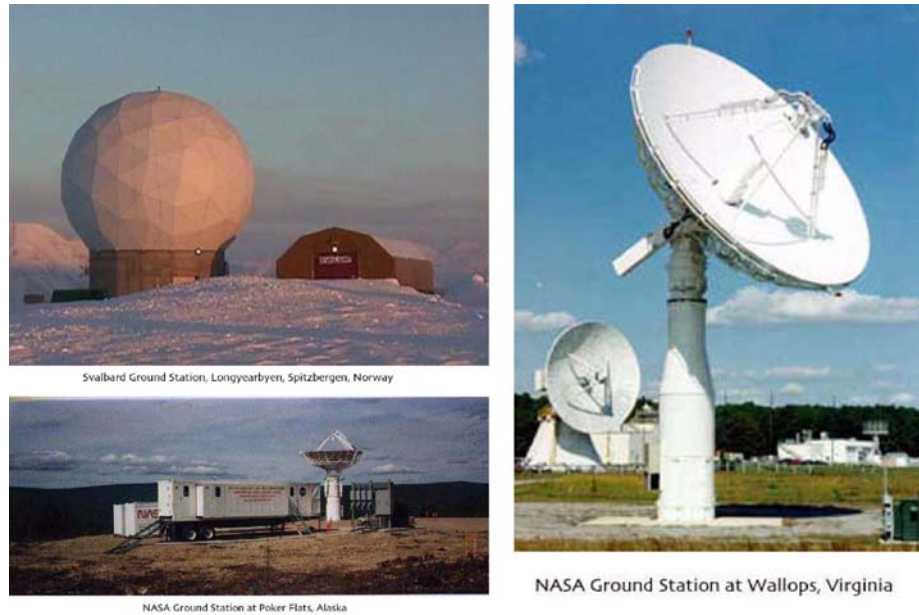


**Figure 14-4.** NASA ground stations at Svalbard, Norway (upper left), Poker Flats, Alaska (lower left), and Wallops Island, Virginia (right)

Usually, we scheduled a ground pass at one of the four ground stations every six hours or so. We talked to TDRSS about six times per day. Communications must be scheduled and arranged, and like all international calls, these communications passes are not cheap! Interspatial (satellite-to-satellite) calls are most expensive, and ground-to-space calls are slightly less costly. We could have talked to TDRSS and the ground stations more often, but it would have cost more money, so we generally followed our regular schedule, unless there was an emergency. During safemodes or other anomalies, we scheduled extra TDRSS and ground passes as needed. We were not in contact with the spacecraft at all times.

While streaming 32K SSR data to the ground, we cannot record to the SSR. Our data collected by the sensors during the transmission were therefore enfolded into the transmission, bypassing the SSR. Also, it was necessary to change antennas (switching from forward to aft antenna) midway through each ground pass. During these antenna changes, we lost about 30 seconds of the real-time data because it was “beamed into space”. Our overall data capture rate for the entire mission was 99.6%, significantly exceeding the 90% data capture specification in our contract with NASA. Thus, we did just fine in terms of data capture, despite the data losses during antenna switches and anomalous events. On average, it took about 12 minutes to download the entire contents of the SSR.

#### **14.1.1.3 Relaying Data to the GP-B MOC at Stanford**

When the spacecraft data were sent through TDRSS, they were then transmitted directly to the Stanford University GP-B MOC through our data link with NASA, in real time. We recorded the data on our computers in a format similar to the ground station data, and then processed it in our data processing center at Stanford.



**Figure 14-5.** The GP-B building and Mission Operations Center (MOC) at Stanford University

However, data relayed through ground stations went through an intermediate step, before being sent to our Mission Operations Center. When data arrives at a ground station, 32 byte headers are put on each data packet to identify it. The identifiers include our spacecraft ID, the ground receipt time, whether or not Reed-Solomon encoding was successfully navigated, the ground station ID, and several error correction checks. The data were stored at the local station and a copy was sent to a central NASA station. After it passed transmission error checks at NASA, it came to us at Stanford. The average 15-hour file took between 1.5 and 4 hours to arrive here.

#### **14.1.1.4 Uncompressing and Formatting the Data**

Once the data were received here at Stanford, a laborious process began. Spacecraft data, by its very nature, must be highly compressed so that as much data as possible can be stored. While we have over 9,000 monitors on-board, we cannot sample and store more than about 5,500 of them at a time. That's why our telemetry is "programmable"—we could choose what data we wanted to beam down. However, in order to get as much data as possible, we compressed it highly.

The data were stored in binary format, and the format included several complexities and codes to indicate the states of more complex monitors. For example, we might encode the following logic in the data: "if bit A=0, then interpret bits B and C in a certain way; but if bit A=1, then use a very different filter with bits B and C." The data were replete with this kind of logic. In order to decompress and decode all of this logic, we used a complex map. Our software first separated the data into its five types (described above). Then, type one underwent "decommutation." Once all of the data in a set was translated into standard text format and decommutated, that set was stored in our vast database (over one terabyte). This was the data in its most useful, but still "raw" form; we called this "Level 1 data." It took about an hour to process 12 hours of spacecraft data. It was the Data Processing team's job to monitor this process, making sure files arrived intact, and unraveling any data snarls that may have come from ground pass issues.

Our science team took the Level 1 data sets, filtered them, and factored in ephemeris information and other interesting daily information (solar activity, etc). The science team also performed several important "pre-processing" steps on the data sets. Once that initial science process was complete, a data set was stored in the "Level 2" database. From there, more sophisticated analysis could be performed.

#### **14.1.2 Detecting and Correcting Computer Memory Errors in Orbit**

The computer and electronics systems on-board every spacecraft must undergo special "ruggedization" preparations to ensure that they will function properly in the harsh environment of outer space. GP-B's on-board computers and other electronics systems are no exception. For example, the components must be radiation-hardened and housed in heavy-duty aluminum or equivalent cases. Furthermore, the firmware (built-in hardware-level programming) must include error detection and correction processes that enable the

electronic components to recover from the effects of solar radiation bombardment and other space hazards. Following is a brief description of GP-B's on-board computers and the techniques used to detect and correct single and multi-bit errors.

#### 14.1.2.1 Overview of Computers On-Board the GP-B Spacecraft

GP-B has several computers on-board the spacecraft. The main flight computer and its twin backup are called the CCCA (Command & Control Computer Assembly). These computers were assembled for GP-B by the Southwest Research Institute. They use approximately 10-year old IBM RS6000 Central Processing Units (CPUs), with 4 MB of radiation-hardened RAM memory. These computers, along with ruggedized power supplies are encased in sturdy aluminum boxes, with sides up to 1/4" thick.

In addition to the A-side (main) and B-Side (backup) flight computers, the GP-B spacecraft has two other special-purpose computers—one for the Gyro Suspension System (GSS) and one for the SQUID Readout Electronics (SRE). Each of these specialized computers contains 3 MB of radiation-hardened RAM memory and custom circuit boards designed and built here at Stanford University. Because of the custom circuit boards, these computers are housed in special aluminum boxes that were also built at Stanford.

#### 14.1.2.2 Memory Error Detection & Correction (EDAC) Logic

The RAM memory in these computers is protected by Error Detection and Correction logic (EDAC), built into the computer's firmware. Specifically, the type of EDAC logic used is called SECDED, which stands for "Single Error Correction, Dual Error Detection." Here's how it works. For every 64 bits of RAM in the computer's memory, another 8 bits are reserved for EDAC. This produces a unique 64-bit *checksum* value for each RAM location. A firmware process called *memory scrubbing* runs continually in the background, validating the checksums for the entire bank of RAM memory locations every 2.5 seconds.

If the EDAC detects an error in which only one single bit is incorrect—a *single-bit error* (SBE)—in a memory location checksum value, it sends an interrupt signal to the CPU, and the CPU automatically fixes the error by writing the correct value back into that memory location. However, if the EDAC detects an error involving more than one bit—a *multi-bit error* (MBE)—it generates a different type of interrupt signal causing the CPU to store the address of the bad memory location in a table that is transmitted to our mission operations center (MOC) during each telemetry communications pass.

#### 14.1.2.3 Correcting Multi-Bit Errors

Whenever the computer engineers on our operations team discovered the presence of one or more MBEs, they immediately looked up the use of that memory location in a map of the computer's memory. If that location was in an area of memory that was not being used, the MBE was said to have been "benign." In fact, most, but not all, of the MBEs we experienced during the mission occurred in benign memory locations. In these cases, one of the computer engineers traveled to the Integrated Test Facility (ITF),—then located at Lockheed Martin Corporation's Palo Alto office, about 15 minutes away from the GP-B MOC, but now located at Stanford—to determine what value was supposed to be contained in the corrupted memory location. The ITF is a very sophisticated flight simulator that maintains a ground-based replica of all the systems running on the spacecraft.



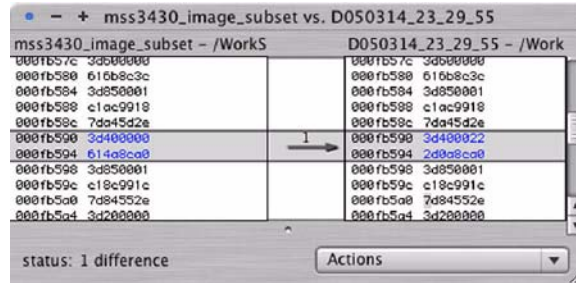


**Figure 14-6.** ITF readout showing a discrepancy between the actual value (left) of memory location in the spacecraft's computer vs the correct value (right) stored in the ITF simulator.

Once the engineer determined the correct value of a bad memory location in the spacecraft's computer, he created a set of commands that were manually sent to the spacecraft during a telemetry pass to patch the bad location with the correct value. Figure 14-6 shows a screen capture from the ITF comparing the correct and incorrect values for a memory location from the spacecraft's computer.



Two of GP-B's gyro experts having a discussion in the ADC during recovery from the recent B-side computer reboot.

**Figure 14-7.** Two members of the GP-B Mission Operations team discuss an MBE that triggered a B-Side (CCCB computer) reboot on March 18, 2005

On the other hand, if the engineer determined that the MBE was located in an active part of the computer's memory—a location containing a command that the CPU would be executing—he would ask the mission operations team to manually issue a command to the flight computer, stopping the timeline of instructions that was being executed, until the bad memory location could be patched. However, it turns out that there was one scenario in which an MBE in a critical part of memory could be missed by the EDAC system.

#### 14.1.2.4 Computer Reboots Triggered by a Watchdog Timer Failure

The 2.5 seconds that it takes the EDAC to scrub the entire memory may seem like a very short time in human terms, but an RS6000 CPU can execute a great many instructions in that time frame. Because the CPU is executing instructions while EDAC memory scrubbing is in process, it is possible for the CPU to access a memory location that was, say, struck by a stray proton from the sun near the SAA region of the Earth, before the EDAC system detected the error. And, if that memory location contains a corrupted instruction that the CPU tries to execute, it can cause the CPU to hang or crash. Communications hardware in the interface box connected to the computer includes a so-called “watchdog timer.” This is basically a failsafe mechanism that, like the deadman switch on a bullet train, awaits a signal from the CPU at regular intervals. If the watchdog timer expires without receiving a signal, it automatically triggers a reboot of the computer.

By a process of elimination, the GP-B Anomaly Review Team concluded that this is probably what happened in the backup CCCA (main computer) on-board the spacecraft on Friday, March 18, 2005. The flight computer maintains a history of completed instructions up to within one second of executing an instruction in a bad memory location. However, once the watchdog timer expires and the computer reboots, this history is lost. Thus, the occurrence of such an event can only be deduced by eliminating other possible causes.

### 14.1.3 GP-B Safemodes and Anomaly Resolution

Consider the following: GP-B is a unique, once-in-history experiment. Its payload, including the gyroscopes, SQUID readouts, telescope and other instrumentation took over four decades to develop. Once launched, the spacecraft was physically out of our hands, and typically, we only communicated with it about every two hours via scheduled telemetry passes. Thus, we entrusted the on-board flight computer (and its backup) with the task of safeguarding the moment-to-moment health and well-being of this invaluable cargo. How did the GP-B flight computer accomplish this critically important task? The answer is the safemode subsystem.

#### 14.1.3.1 The GP-B Safemode System

Most autonomous spacecraft have some kind of safemode system on-board. In the case of GP-B, Safemode is an autonomous subsystem of the flight software in the GP-B spacecraft's on-board flight computers. The GP-B Safemode Subsystem is comprised of three parts:

1. Safemode Tests—Automatic checks for anomalies in hardware and software data.
2. Safemode Masks—Scheme for linking each safemode test with one or more safemode response sequences.
3. Safemode Responses—Pre-programmed command sequences that are activated automatically when a corresponding test fails to provide an expected result.



Uploading commands to the spacecraft from the MOC during recovery procedures following the B-side computer reboot.

**Figure 14-8.** Uploading commands to the spacecraft from the MOC, following a B-side computer reboot.

These tests and response commands are designed to safeguard various instruments and subsystems on the spacecraft and to automatically place those systems in a known and stable configuration when unexpected events occur.

For example, one of the tests in the GP-B Safemode Subsystem checks to ensure that the communications link between the on-board flight computer and the GP-B MOC here at Stanford is alive and active. The requirement for this test is that the flight computer must receive some command from the MOC at least once every 12 hours. If the flight computer does not receive a command within that time frame, we assume that normal telemetry is not working, and the pre-programmed response commands cause the computer to automatically reboot itself and then re-establish communication. This test is a variation of the “deadman switch” test used on high-speed



bullet trains. To ensure that the train's engineer is alive and awake while the train is traveling at high speed, the engineer is required to press a button or switch at regular intervals. If the train does not receive the expected human input within each time interval, the train automatically throttles down and comes to a halt.

Not all of the tests and responses in the GP-B Safemode Subsystem were enabled at any given time. For example, some of the tests were specifically created for use during the launch and/or during the Initialization and Orbit Checkout (IOC) phase and were no longer needed during the science phase of the mission. Also, active tests and responses could be re-programmed if necessary. For example, the response commands for the safemode that triggered a computer reboot on Monday, March 14, 2005, were changed in the ensuing days to simply stop the mission timeline, rather than rebooting the flight computer, as originally programmed.

### 14.1.3.2 Responding to Anomalous Events On Orbit

When anomalous events occurred, automatic responses ensured that the spacecraft and its subsystems remained in a safe and stable condition. This enabled our mission operations team to become aware of the issue on-board, identify and understand the root cause, and take appropriate action to restore normal operations. GP-B employed a formal process, called “anomaly resolution,” for dealing with unexpected situations that occurred in orbit. This process was thoroughly tested and honed during a series of seven pre-flight simulations over the course of two years.

GP-B anomalous events were evaluated and classified into one of four categories:

1. **Major Space Vehicle Anomalies**—Anomalies that endangered the safety of the spacecraft and/or the payload. Response to these anomalies was time-critical.
2. **Medium Space Vehicle Anomalies**—Anomalies that did not endanger the safety of the space vehicle but could have impacted the execution of the planned timeline. Response to these anomalies was not time-critical if addressed within a 72-hour window.
3. **Minor Space Vehicle Anomalies**—Anomalies that did not endanger the safety of the space vehicle. These were low risk problems with the vehicle that were resolved by taking the appropriate corrective action.
4. **Observations**—In addition to formal anomaly categories, the space vehicle often exhibited off-nominal or unexpected behavior that did not appear initially to be an operational or functional issue and did not violate any limits, but warranted attention over time. Observation items were sometimes elevated to an anomaly category if they were judged to be serious enough to warrant a high-priority investigation.



In the GP-B Anomaly Room, team members discuss a set of recovery commands that are about to be sent to the spacecraft.

**Figure 14-9.** In the Anomaly Room, team members discuss a series of recovery commands that will be uploaded to the spacecraft.

A special room in the GP-B Mission Operations, called the Anomaly Room, was the home of the GP-B Anomaly Review Board (ARB), a select group of senior GP-B team members from Stanford, NASA, and Lockheed Martin, who managed the troubleshooting of anomalies and observations. The Anomaly Room, which was located across the corridor from the GP-B MOC, contained a set of spacecraft status monitors, communications and teleconference equipment, computer and voice hookups, a documentation library, white boards, a computer projection system, and an oval discussion table.

During the flight mission, whenever an anomaly was in the process of being resolved, the Anomaly Room was staffed 24 hours a day, 7 days a week; at other times, it was staffed during normal working hours, with team members on call. When major anomalous events, such as computer reboots, occurred outside normal working hours, the Mission Director on duty activated the Anomaly Room and issued a series of pager and cell phone calls via computer, summoning key staff members on the ARB, along with a selected anomaly team, comprised of resident engineers and engineering specialists, to come in and work through the issue. The group used a technique called “fault tree analysis” to evaluate and determine the root cause of unexpected events.

The GP-B Safemode Subsystem and anomaly resolution process worked very well throughout the mission. Over the course of the flight mission, the ARB successfully worked through 193 anomalies/observations. Most of these issues (88%) were classified as observations, and about 9% were classified as minor to medium anomalies. But five (3%) were classified as major anomalies, including the B-Side computer switch-over and the stuck-open valve problems with two of the 16 micro thrusters early in the mission, as well as subsequent computer and subsystem reboot problems due to solar radiation strikes. In each case, the established anomaly resolution process enabled the team to identify the root causes and provide successful recovery procedures in every case. You can read a detailed description of the GP-B Anomaly Resolution Process in [Chapter 5, Managing Anomalies and Risk](#). Also, [Appendix D, Summary Table of Flight Anomalies](#) contains a table summarizing the complete set of anomalies and observations from launch through the end of the post-science calibrations in October 2005.

#### 14.1.4 Effects of Anomalous Events on the Experimental Results of GP-B

Whenever anomalous events occurred on-board the GP-B spacecraft in orbit, such as computer switch-overs and reboots, we received numerous inquiries asking about the effects of these events on the outcome of the GP-B experiment. These events have resulted in a small loss of science data. In and of itself, this loss of data will have no significant effect on the results of the experiment. If it turns out that some of the lost data was accompanied by non-relativistic torques on the gyros (measurable drift in the gyro spin axes caused by forces other than relativity), we believe that there will probably be a perceptible, but still insignificant effect on the accuracy of the end results. We really will not be able to quantify the effect of these events until the full data analysis is completed early in 2007.

We have long anticipated and planned for dealing with possible lapses in the data and non-relativistic torques on the gyros during the mission. In fact, this subject was explicitly discussed in Dr. Thierry Duhamel's 1984 PhD thesis entitled **Contributions to the Error Analysis in the Relativity Gyroscope Experiment**. (This was one of 79 Stanford doctoral dissertations sponsored by GP-B over the past 42 years.) Chapter 4 of Dr. Duhamel's dissertation is entitled “Effect of Interruptions in the Data.” In this chapter, Dr. Duhamel modeled various hypothetical cases of an undetermined amount of gyro spin axis drift due to non-relativistic torques (forces) on the gyros, accompanying data interruption periods of varying lengths. Each of Dr. Duhamel's hypothetical scenarios models these effects over a 12-month data collection period, showing the effect of gyro drift and data loss as a function of when in the mission (month 1, month 2, etc.) the event occurs.

In a nutshell, the results of Dr. Duhamel's research showed that lapses of data in which the gyros do not experience any non-relativistic torques would have no significant effect on the outcome of the experiment. Lapses of data that are accompanied by gyro drifts of unknown size due to non-relativistic forces would have a

perceptible, but still relatively small effect on the experimental results. Furthermore, Dr. Duhamel's research indicates that in most cases, the effects of gyro drift and data loss tend to be larger if they occur at the beginning or end of the science phase, rather than in the middle.

Based in part on Dr. Duhamel's prescient research over 20 years ago, the GP-B science team has developed and perfected a comprehensive, state-of-the-art data analysis methodology for the GP-B experiment that, among many other things, takes into account data lapses and the possibility of accompanying non-relativistic torques on the gyros. Also, many improvements have been made in the GP-B technology since Dr. Duhamel did his research. These improvements provide us with more extensive data and extra calibrations that enable us to further refine the original error analysis predictions.

Dr. Thierry Duhamel now lives in France (his native country), where he works for EADS Astrium, a leading European aerospace company.

### **14.1.5 Aberration of Starlight—Nature's Calibrating Signal**

GP-B Principal Investigator, Francis Everitt, once said: "Nature is very kind and injects a calibrating signal, due to the aberration of starlight, into the GP-B data for us." This phenomenon actually provides two natural calibration signals in the relativity data that are absolutely essential for determining the precise spin axis orientation of the gyros over the life of the experiment. However, the word "aberration" typically refers to behavior that departs or deviates from what is normal, customary, or expected—and usually, such behavior is not welcome. So, what does aberration have to do with starlight? And, why would we want to use something aberrant as a calibration signal? To answer the first of these questions, we must first travel back in time to the 18th century.

#### **14.1.5.1 18<sup>th</sup> Century British Astronomer James Bradley Discovers Stellar Aberration**

At the beginning of the 18th century, astronomers were still seeking some form of direct proof of the Copernican theory that all the planets in our solar system orbit around the Sun. One such person was British Astronomer James Bradley, who in 1718 was recommended by the Astronomer Royal Edmund Halley to become a Fellow of the Royal Society, and who eventually succeeded Halley as British Astronomer Royal in 1742.



**James Bradley (1693-1762)**  
**British Astronomer Royal**

**Figure 14-10.** British Astronomer Royal, James Bradley

Starting on 3 December 1725, Bradley observed the star, Gamma Draconis, through his telescope and noted its position in the heavens. He was planning to observe the star's position periodically for a year, anticipating that in six months, he would be able to view a shift in the star's position due to stellar parallax caused by the Earth having moved around the Sun to the opposite extreme of its orbit. In Bradley's time, the prevailing wisdom was that the distance across the long axis of the Earth's orbit—approximately 300,000,000 km (186,000,000 miles)—would provide a sufficient baseline to view a parallax shift in the star's position. What the astronomers of Bradley's day did not know is that even the closest star to our solar system is nearly 150,000 times further away than the distance across Earth's orbit, and thus the parallax effect between December and June observations of Gamma Draconis only amounts to about 1.5 arcseconds (0.00042 degrees). This is an angle about the size a pea, viewed from one kilometer away—much too small to be measured with instruments of Bradley's day. It would be another 100 years before stellar parallax was actually detected by Friedrich Bessel, director of the Konigsberg Observatory in Germany.

As a result of a year's worth of periodic observations of the star, Gamma Draconis, Bradley was surprised to discover that the pattern traced out by the star's motion was an ellipse. Moreover, the major axis of the ellipse coincided not with the long axis across Earth's orbit from December to June as would be expected for a parallax measurement, but rather with the short axis from March to September. Bradley pondered these seemingly mysterious results for two more years, discovering that all other stars he observed also traced out identical elliptical patterns over the course of a year. One morning in 1728, he had an “aha” moment while sailing on a boat, watching the motion of a wind vane flying from a mast. He noticed that the vane kept changing directions as the boat turned to and fro, and that it did not necessarily point directly opposite the boat's direction of travel. He thought this might be due to a shifting wind, but upon querying the boat's captain, he learned that the wind's direction had remained constant. At that point, he realized that the vane's direction was resulting from a coupling of the boat's motion with the wind direction.

At this point, Bradley made a profound connection: he likened the Earth to the boat and the light from a star to the wind. He then realized that the apparent position of the star was changing as the Earth moved in its orbit. Bradley described this phenomenon in a letter to Halley, which was read to the Royal Society in January 1729. In his letter, he named the phenomenon “aberration of starlight,” because the stars appeared to be in a different position than they actually were, due to the fact that they were being observed from a moving body.

Bradley further realized that since his telescope was moving through space along with the Earth, in order for the starlight to hit the eyepiece in the center of his telescope, he would have to tilt the telescope in the Earth's direction of motion, towards the apparent position of the star. He determined that the angle at which the telescope must be tilted represents the ratio of the speed at which the Earth is moving around the Sun divided by the speed of light. Nowadays, thanks to Einstein's special theory of relativity, we now know that a relativistic correction factor must be added to the speed of light in the denominator of the stellar aberration ratio.

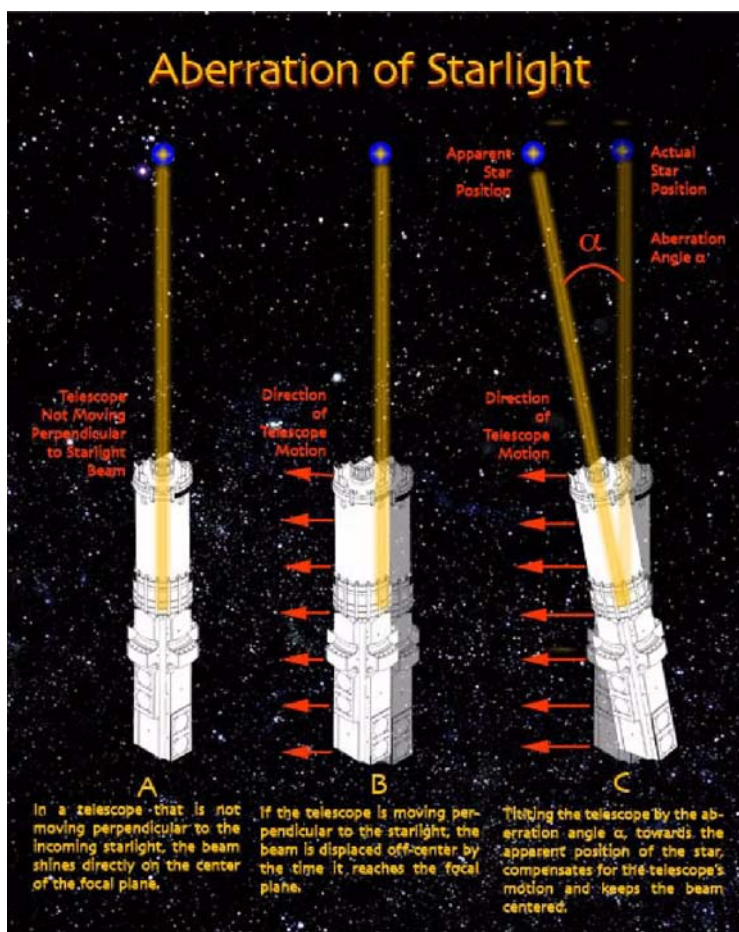


**Figure 14-11.** Due to the motion of the Earth, the apparent position of a distant star viewed through a telescope differs from its actual position—Bradley called this difference the aberration angle.

From his observations of Gamma Draconis, Bradley knew that the maximum angle at which his telescope had to be tilted was tiny—approximately 20 arc-seconds. Using this angle, and the velocity of the Earth moving around the Sun, known in his day to be  $\sim 30$  km/sec ( $\sim 18.6$  miles/sec), he calculated the speed of light to be about 10,000 times faster than the orbital velocity of Earth or  $\sim 300,000$  km/sec ( $\sim 186,000$  miles/sec).

### 14.1.5.2 The Role of Stellar Aberration in the GP-B Experiment

You can now see why the aberration of starlight played a role in the GP-B experiment. While constantly tracking the guide star, IM Pegasi, the telescope on-board the spacecraft was always in motion—both orbiting the Earth once every 97.5 minutes and along with the Earth, the spacecraft and telescope have been orbiting the Sun once a year. These motions result in two sources of aberration of the starlight from IM Pegasi. The first is an orbital aberration, which has a maximum angle of 5.1856 arcseconds, resulting from the spacecraft's orbital speed of approximately 7 km/sec, relative to the speed of light. (In the case of orbital aberration, the relativity correction is insignificant.). The second is the now familiar annual aberration due to the Earth's orbital velocity around the Sun, which when corrected for special relativity, amounts to an angle of 20.4958 arcseconds.

In the GP-B experiment, the signals representing the precession in the gyroscope spin axes over time are represented by voltages that have undergone a number of conversions and amplifications by the time they are telemetered to Earth. These conversions and amplifications imparted a scale factor of unknown size into the data, and early on in the development of the GP-B experimental concept it was apparent that there needed to be a means of determining the size of this gyro scale factor in order to see the true relativity signal. Initially, it



seemed that aberration of starlight was going to be a source of experimental error bundled into the scale factor. But upon examining this issue more closely, it became clear that, quite to the contrary, the orbital and annual aberration of light from the guide star actually provided two built-in calibration signals that would enable the gyro scale factor to be calculated with great accuracy.

### 14.1.5.3 The Orbital Aberration Signal

To see how this works, let's first take a closer look at how the orbital aberration of the starlight from the guide star, IM Pegasi, is "seen" by GP-B spacecraft.

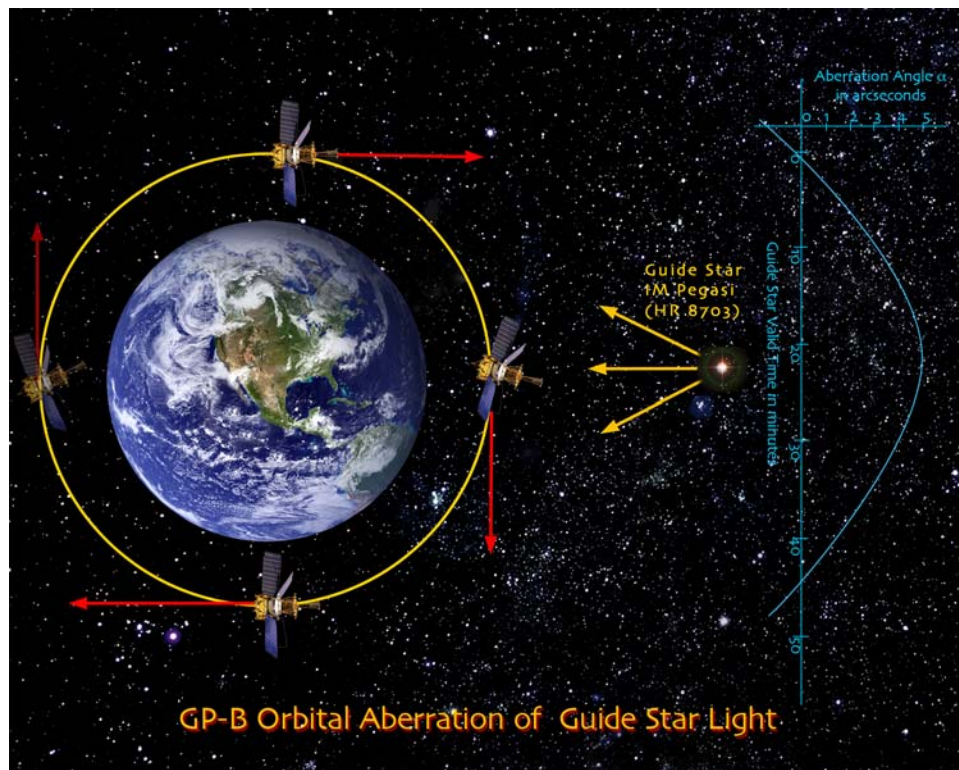


**Figure 14-12.** GP-B's Orbital aberration of light from the Guide Star, IM Pegasi

As mentioned earlier, the spacecraft orbits the Earth once every 97.5 minutes. During the mission, as the spacecraft emerged over the North Pole, the guide star came into the field of view of the science telescope, and the telescope then locked onto the guide star. This began what was called the "Guide Star Valid (GSV)" phase of the orbit. At this point in its orbit, the orientation of the spacecraft's velocity was directly towards the guide star, and thus, there was no aberration of the star's light—it traveled straight down the center of the telescope. However, as the spacecraft moved down in front of the Earth, the orientation of its velocity shifted in the orbital direction until it became perpendicular to the direction of the light from the guide star, slightly above the equator. This is the point of maximum aberration since the telescope was then moving perpendicular to the guide star's light. As the spacecraft moved on towards the South Pole and then behind the Earth and directly away from the guide star, the aberration receded back to zero. At this point, the telescope unlocked from the guide star, transitioning into what was called the "Guide Star Invalid (GSI)" phase of the orbit. The navigational rate gyros on the outside of the spacecraft maintained the telescope's orientation towards the guide star while the spacecraft was behind the Earth, but we did not use the science gyro data collected during the GSI phase.

During the GSV portion of each orbit, the telescope remained locked on the guide star, with the spacecraft's micro thrusters adjusting the telescope's pointing for the aberration of the guide star's light. This introduced a very distinct, half-sine wave pattern into the telescope orientation. This sinusoidal motion was also detected by the gyro pickup loops that are located in the gyro housings, along the main axis of the spacecraft and telescope. Thus, this very characteristic pattern, generated by the telescope and thrusters, appeared as a calibration signal in the SQUID Readout Electronics (SRE) data for each gyro.

#### 14.1.5.4 The Annual Aberration Signal

The annual aberration of the guide star's light works the same way as the orbital aberration signal, but it takes an entire year to generate one complete sine wave.

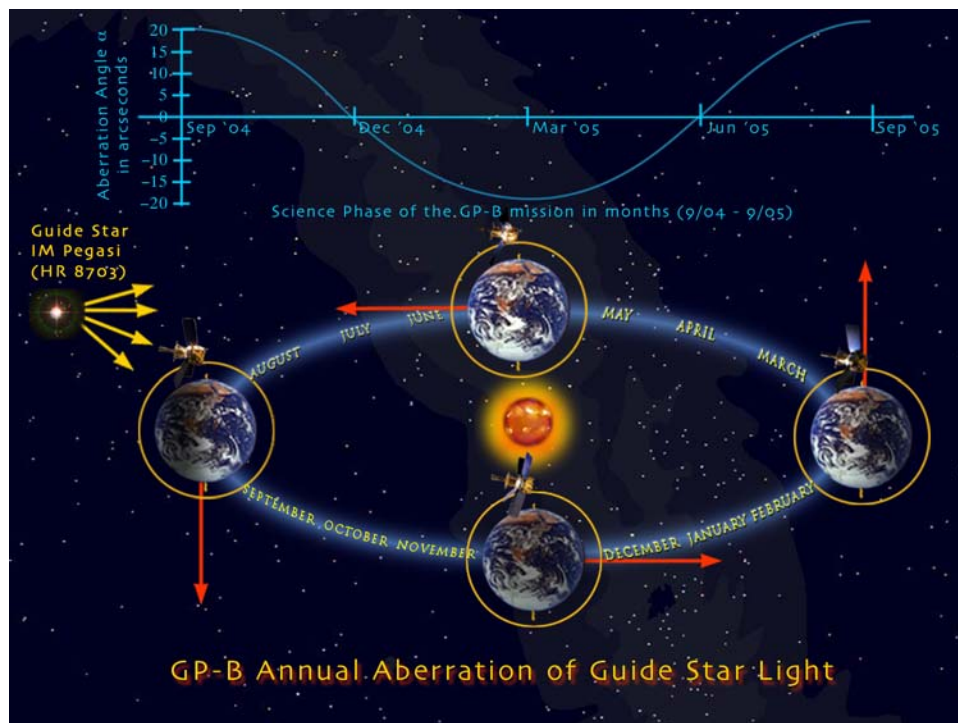


**Figure 14-13.** GP-B's annual aberration of light from the Guide Star, IM Pegasi

Using the spacecraft's GPS system, we can determine the orbital velocity of the spacecraft to an accuracy of better than one part in 100,000 (0.00001). Likewise, using Earth ephemeris data from the Jet Propulsion Lab in Pasadena, CA, we can determine Earth's orbital velocity to equal or better accuracy. We then used these velocities to calculate the orbital and annual aberration values with extremely high precision, and in turn, we used these very precise aberration values to calibrate each of the gyro pointing signals. It is interesting to note that the amplitude of the sine wave generated by the annual aberration is four times as large as the orbital aberration amplitude, with peaks occurring in September and March. Because we launched GP-B in April and started collecting science data in September, the effect of the annual calibration signal did not become apparent in the data until February-March 2005, six to seven months into the science phase of the mission. Thus, from March 2005 - August 2005, both the annual and orbital aberration signals were used in the ongoing analysis of the science data.



## 14.1.6 Telescope Dither—Correlating the Gyro & Telescope Scale Factors

When used in reference to technology, the term, *dither*, generally refers to the seemingly paradoxical concept of intentionally adding noise to a system in order to reduce its noise. For example, a random dithering technique is used to produce more natural sounding digital audio, and another form of visual dithering enables thousands of color shades, used on Internet Web sites, to be derived from a limited basic palette of 256 colors. With respect to the GP-B spacecraft, the dither refers to an oscillating movement of the science telescope and spacecraft that was activated whenever the telescope was locked onto the guide star. This intentional telescope movement produced a calibration signal that enabled us to relate the signals generated by the telescope photon detectors to the signals generated by the SQUID magnetometer readouts of the gyro spin axis positions.

### 14.1.6.1 Science Telescope—Centering on the Guide Star

The sole purpose of the GP-B science telescope was to keep the spacecraft pointed directly at the guide star during the “guide-star-valid” portion of each orbit—that is, the portion of each orbit when spacecraft was “in front of” the Earth relative to the guide star and the guide star was visible to the telescope. This provided a reference orientation against which the spin axis drift of the science gyros could be measured. The telescope accomplished this task by using lenses, mirrors, and a half-silvered mirror to focus and split the incoming light beam from the guide star into an X-axis beam and a Y-axis beam. Each of these beams was then divided in half by a knife-edged “roof” prism, and the two halves of each beam were subsequently focused onto a pair of photon detectors. When the detector values of both halves of the X-axis beam were equal, we knew that the telescope was centered in the X direction, and likewise, when the detector values of both halves of the Y-axis beam were equal, the telescope was centered in the Y-axis direction. (The telescope actually contains two sets of photon detectors, a primary set and a backup set for both axes.)

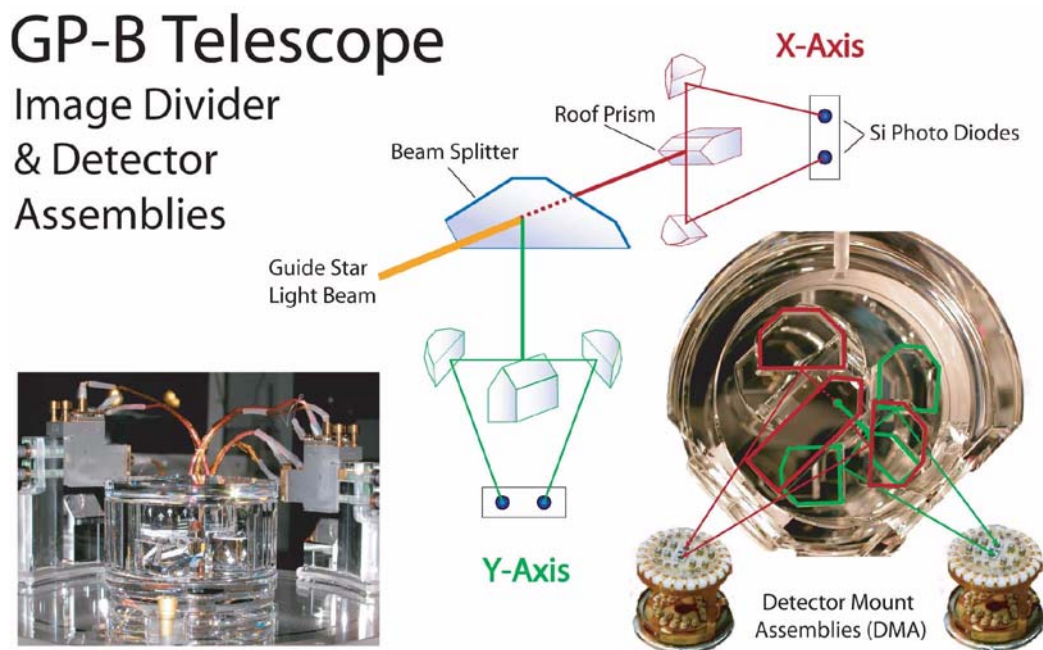
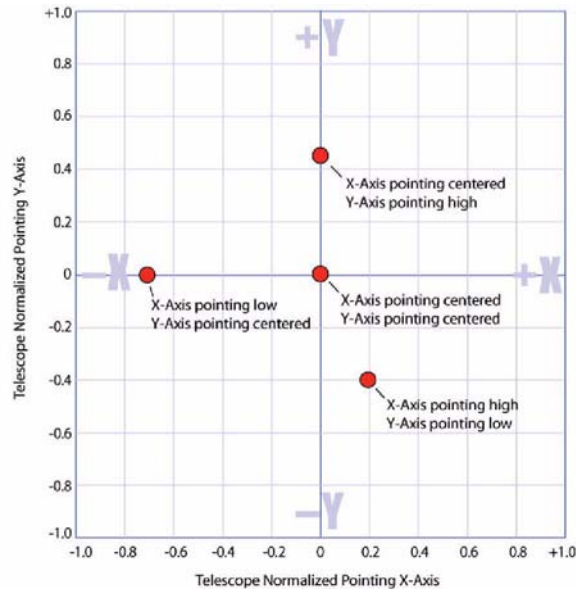


Figure 14-14. Schematic diagram of the GP-B telescope optics

### 14.1.6.2 Normalized Pointing

The telescope detector signals were converted from analog to digital values by the Telescope Readout Electronics (TRE) box, and these digital values were normalized (mapped) onto a range of -1 to +1. In this normalized range, a value of 0 meant that the telescope was centered for the given axis, whereas a value of +1 indicated that all of the light was falling on one of the detectors and a value of -1 indicated that all of the light was falling on the other detector.



**Figure 14-15.** Normalized pointing values for the GP-B telescope

In actuality, the light beam for each axis was distributed in a bell-shaped curve along this scale. When the telescope was centered, the peak of the bell curve was located over the 0 point, indicating that half the light was falling on each detector. If the telescope moved off center, the entire curve shifted towards the +1 or -1 direction. You can think of this as a teeter-totter of light values, with the 0 value indicating that the light was balanced, as shown in Figure 14-16.

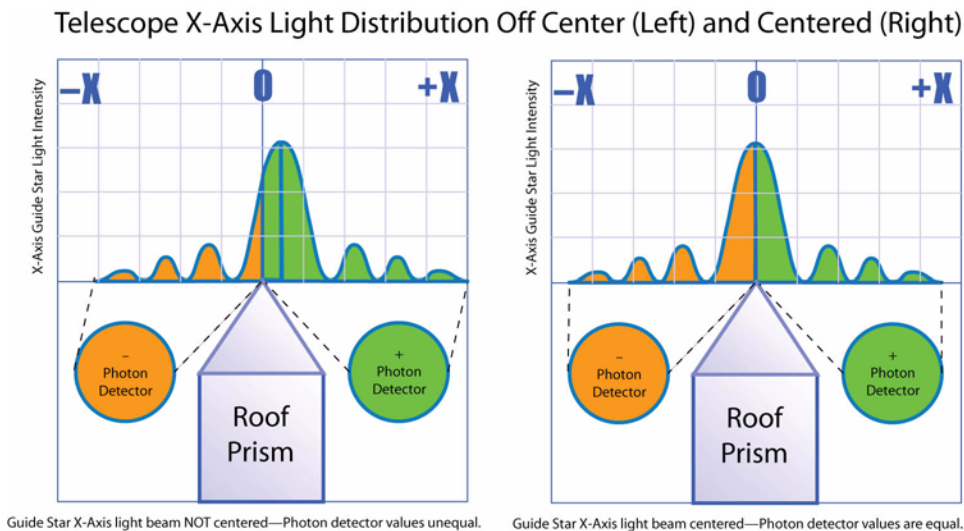


**Figure 14-16.** Centering the telescope's light distribution

### 14.1.6.3 The Telescope Dither Pattern

A telescope scale factor translated the values on this normalized scale into a positive or negative angular displacement from the center or 0 point, measured in milliarcseconds ( $1/3,600,000$  or  $0.0000003$  degrees). Likewise, a gyro scale factor translated converted digital voltage signals representing the X-axis and Y-axis orientations of the four science gyros into angular displacements, also measured in milliarcseconds. We then had both the telescope and gyro scale factors defined in comparable units of angular displacement. The telescope dither motion was then used to correlate these two sets of X-axis and Y-axis scale factors with each other.

The telescope dither caused the telescope (and the entire spacecraft) to oscillate back and forth in both the X and Y directions around the center of the guide star by a known amount.

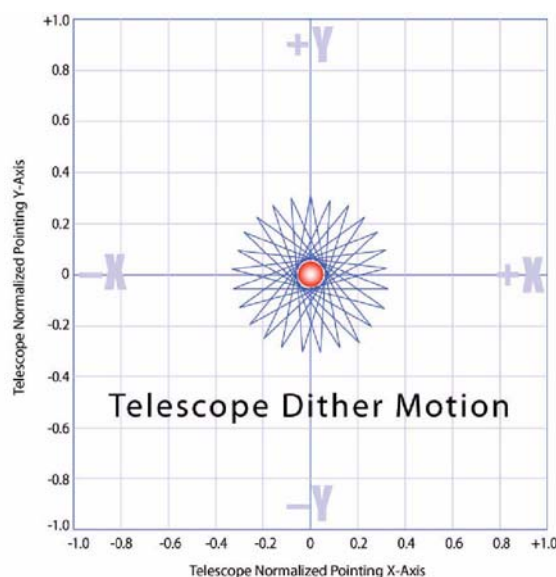


**Figure 14-17.** The telescope dither pattern around Guide Star, IM Pegasi

Because this motion moved the entire spacecraft, including the gyro housings that contain the SQUID pickup loops, the SQUIDs detected this oscillation as a spirograph-like (multi-pointed star) pattern that defined a small circle around the center of the guide star. This known dither pattern enabled us to directly correlate the gyro spin axis orientation with the telescope orientation. The result was a pair of X-axis and Y-axis scale factors that were calculated for the guide-star-valid period of each orbit. At the end of the data collection period on August 15, 2005, we had stored approximately 7,000 sets of these scale factors, representing the motion of the gyro spin axes for the entire experiment.

At the beginning of May 2005, we turned off the dither motion for a day to determine what effect, if any, the dither itself was contributing to our telescope pointing noise and accuracy. The results of this test indicated that the navigational rate gyros, which were used to maintain the attitude of the spacecraft and telescope during guide-star-invalid periods (when the spacecraft was behind the Earth), were the dominant source of noise in the ATC system, whereas the science gyro signals were stronger than the noise in the SQUID Readout Electronics (SRE) system.

### 14.1.7 Extracting the Gyro Signals from the Noise

Conceptually the GP-B experimental procedure is simple: At the beginning of the experiment, we initially pointed the science telescope on-board the spacecraft at the guide star, IM Pegasi, and we electrically nudged the spin axes of the four gyroscopes into the same alignment. Then, over the course of a just under a year, as the

spacecraft orbited the Earth some 5,000 times while the Earth made one complete orbit around the Sun, the four gyros spun undisturbed—their spin axes influenced only by the relativistic warping and twisting of spacetime. We kept the telescope pointed at the guide star, and each orbit, we recorded the cumulative size and direction of the angle between the gyroscopes' spin axes and the telescope. According to the predictions of Einstein's general theory of relativity, over the course of a year, an angle of 6,606 milliarcseconds should have opened up in the plane of the spacecraft's orbit, due to the warping of spacetime by the Earth, and a smaller angle of 39 milliarcseconds should have opened up in the direction of Earth's rotation due to the Earth dragging its local spacetime around as it rotates. In reality, what went on behind the scenes in order to obtain these gyro drift angles was a very complex process of data reduction and analysis that is taking the GP-B science team more than a year to bring to completion.

#### **14.1.7.1 GP-B Data Levels**

Throughout the science phase of the GP-B mission, we continuously collected data during all scheduled telemetry passes with ground stations and communications satellites, and these telemetered data were stored—in their raw, unaltered form—in a database here at the GP-B Mission Operations Center. This raw data is called “Level 0” data. The GP-B spacecraft is capable of tracking some 10,000 individual values, but we only captured about 1/5 of that data. The Level 0 data include a myriad of status information on all spacecraft systems in addition to the science data, all packed together for efficient telemetry transmission. So, our first data reduction task was to extract all of the individual data components from the Level 0 data and store them in the database with mnemonic identifier tags. These tagged data elements were called “Level 1” data. We then ran a number of algorithmic processes on the Level I data to extract ~500 data elements to be used for science data analysis, and this was called “Level 2 data.” While Level 2 data include information collected during each entire orbit, our science team generally only uses information collected during the Guide Star Valid (GSV) portion of each orbit when the telescope was locked onto the guide star. We do not use any gyroscope or telescope data collected during the Guide Star Invalid (GSI) portion of each orbit—when the spacecraft is behind the Earth, eclipsed from a direct view of the guide star—for science data analysis.

#### **14.1.7.2 Gaps in the Data**

Analyzing the data collected in the GP-B experiment is similar to fitting a curve to a set of data points—the more data points collected, the more accurate the curve. If there were no noise or error in our gyro readouts, and if we had known the exact calibrations of these readouts at the beginning of the experiment, then we would need only two data points—a starting point and an ending point. However, there is noise in the gyro readouts, so the exact readout calibrations had to be determined as part of the data collection and analysis process. Thus, collecting all of the data points in between enables us to determine these unknown variables. In other words, the shape of the data curve itself is just as important as the positions of the starting and ending points.

All measurements we collected were time-stamped to an accuracy 0.1 milliseconds. This enables our science team to correlate the data collected from all four gyros. If one gyro's data are not available for a particular time period, such as the first three weeks of the science phase when gyro #4 was still undergoing spin axis alignment, that gyro is simply not included in the analysis for that particular time period. In cases where all science data are lost for an orbit or two, the effect of these small data gaps on the overall experiment is very small. Examples of such data gaps include the March 4, 2005 automatic switch-over from the A-side (main) on-board computer to the B-side (backup) computer, and a few telemetry ground station problems over the course of the mission.

#### **14.1.7.3 Sources of Noise**

Another important point is that the electronic systems on-board the spacecraft do not read out angles. Rather, they read out voltages, and by the time these voltages are telemetered to Earth and received in the science database here in the Stanford GP-B Mission Operations Center, they have undergone many conversions and

amplifications. Thus, in addition to the desired signals, the GP-B science data include a certain amount of random noise, as well as various sources of interference. The random noise averages out over time and will not be an issue. Some of what appears to be regular, periodic interference in the data is actually important calibrating signals that enable us to determine the size of the scale factors that accompany the science data. In Section 14.1.5, “[Aberration of Starlight—Nature’s Calibrating Signal](#)” above, we described how the orbital and annual aberration of the starlight from IM Pegasi is used as a means of calibrating the gyro readout signals. Likewise, in Section 14.1.6, “[Telescope Dither—Correlating the Gyro & Telescope Scale Factors](#)” above, we described how the telescope dither motion is used to calibrate the telescope signals. In addition, over the course of the mission we have discovered a few unexpected sources of interference that must be appropriately modeled and removed from the data. The error analysis is well in hand, but careful and painstaking cross checks are required by our science team to ensure the validity of the final experimental results.

#### **14.1.7.4 Proper Motion of IM Pegasi—The Final Data Element**

Finally, there is one more very important factor that must be addressed in calculating the final results of the GP-B experiment. We selected IM Pegasi, a star in our galaxy, as the guide star because it is both a radio source and it is visually bright enough to be tracked by the science telescope on-board the spacecraft. Like all stars in our galaxy, the position of IM Pegasi, as viewed from Earth and our science telescope changed over the course of the experimental year. Thus, the GP-B science telescope was tracking a moving star, but the gyros were unaffected by the star’s so-called “proper motion;” their pointing reference was IM Pegasi’s position at the beginning of the experiment. Thus, for each orbit, we must subtract out the telescope’s angle of displacement from its original guide star orientation so that the angular displacements of the gyros can be related to the telescope’s initial pointing direction, rather than its actual pointing direction each orbit. The annual motion of IM Pegasi with respect to a distant quasar has been measured with extreme precision over a number of years using a technique called Very Long Baseline Interferometry (VLBI) by a team at the Harvard-Smithsonian Center for Astrophysics (CfA) led by Irwin Shapiro, in collaboration with astrophysicist Norbert Bartel and others from York University in Canada and French astronomer Jean-Francois Lestrade. However, to ensure the integrity of the GP-B experiment, we added a “blind” component to the data analysis by requesting that the CfA withhold the proper motion data that will enable us to pinpoint the orbit-by-orbit position of IM Pegasi until the rest of our data analysis is complete. Therefore, the actual drift angles of the GP-B gyros will not be known until the end of the data analysis process.

## **14.2 The GP-B Science Data Analysis Process**

In this section we first provide a brief overview of what is involved in analyzing the GP-B science data. Data analysis actually began before launch. The science data analysis team built prototype computer codes to process simulated science data in preparation for the actual data from the spacecraft. Following on-orbit checkout, the team used real data to test and refine these routines and to take into account the anomalies the mission has encountered (i.e. the time varying polhode period) that were not part of the initial simulations. These activities all preceded the formal data analysis effort.

### **14.2.1 Formal Data Analysis Phases**

Following acquisition and archiving of the science data from the satellite, the formal analysis of these data is broken into three phases; each subsequent phase builds upon the prior toward the final science results.

### 14.2.1.1 Phase 1: Short-term (day-by-day) analysis

Initially, the data are analyzed primarily over a short time period, typically a few orbits or a day, with the goal to understand the limitations of data analysis routines and to improve them where necessary. The major activities of this phase include:

- Final instrument calibrations are completed, based on the IOC, the Science Mission, and the Post-Science Calibration tests run on the vehicle.
- Refinements are made to the subsystem performance estimates (i.e. GSS, ATC, TRE, SRE subsystems). The performance of these systems sets lower bounds on the quality of the results we expect to obtain from the experiment.
- Through the data analysis, known features are removed—for example, aberration and pointing errors were removed from the science signals.
- A data grading scheme is implemented to flag and optionally ignore patches of the data set that are not of science quality due to spacecraft anomalies or off-nominal configuration of the instrument.

The overall goals of this phase are to improve the quality of the science data analysis package, calibrate out instrumentation effects, and produce an initial “orientation of the day” estimate based on the tuned-up data analysis package. It does not attempt at this stage to remove systematic errors that span many days or months. In addition, this analysis focuses on each gyros’ performance individually and does not attempt to combine the four measurements, and it does not attempt to estimate the gyroscope precession (due to either relativistic or classical effects)

### 14.2.1.2 Phase 2: Medium-term (Month-to-month) analysis

In this second phase, the analysis team’s attention turns to understanding and compensating for long-term systematic effects that span many days or months, such as those that arise from the time-varying gyro polhode period or drifts in the calibrations of the on-board instrumentation.

- Identify, model, and remove systematic errors and improve instrument calibrations.
- Understand causes and implications of spacecraft anomalies. Model and remove effects resulting from these anomalies.
- Assess the magnitude of residual Newtonian torques on the gyroscopes and compare with pre-launch estimates.

The primary products from this phase are a “trend of the month” per gyroscope, which is the initial estimate of the measured gyroscope precession over a medium time scale (approximately 1 month) after the compensation of identified systematic error sources. This phase will also produce a refined “orientation of the day” per gyroscope. Here, too, the focus is on individual gyroscope performance.

### 14.2.1.3 Phase 3: 1 Year perspective

In the final phase, the data from all four gyroscopes are combined with the guide star proper motion measurements, provided by our partners at the Smithsonian Astrophysical Observatory (SAO), to generate an overall estimate of the gyroscope precession rates over the mission. These estimates form the basis of the primary science result: the precession of the gyroscopes due to the effects of general relativity. This process will naturally produce a third, improved, “orientation of the day” for each of the gyroscopes.

## 14.2.2 Independent Data Analysis Teams

The Stanford team has formed two independent, internal teams to attack the data analysis task. This was done primarily for internal quality control: two teams, processing the exact same data, should produce very similar results. The results are compared formally on a regular basis where discrepancies are noted and investigated. These comparisons will unearth subtle software coding errors, which may go undetected if only a single analysis package is used. Each team, while working under the constraint of using the same source data, has considerable latitude in what methods of analysis to apply during each of the data analysis phases. This has the beneficial effect of better understanding the nature of the source data and what signal processing techniques are most effective in estimating the performance of the four science gyroscopes.

To provide a benchmark for both of the teams, sets of “truth model data” are constructed and are run on the two data analysis packages. In these truth model cases, the signal structure, instrument calibrations, and noises are precisely known and can be analyzed in a relatively straightforward way without sophisticated signal processing tools. Both data analysis packages should return identical results when run on such truth data; if they do not, this test reveals a fundamental difference in the algorithms that may be rectified quickly. Once the algorithms agree on “truth”, they will be re-benchmarked regularly to ensure that evolutionary changes in the codes do not compromise their ability to correctly analyze straightforward data sets.

## 14.2.3 Data Grading

The Gravity Probe B science data consists of approximately 5300 guide star valid intervals during which the instrument is able to measure the orientation of each of the four gyroscopes with respect to the line of sight to the guide star. Due to vehicle anomalies or environmental effects, not all of these intervals contain valid science measurement data. If these data are used in the analysis algorithms, significant errors in the overall results may be introduced.

Consequently, a data grading scheme is used to separate the compromised data from the clean science data. The grading system does not remove data from the set, but simply flags segments of the data that do not meet an established grading criteria. Roughly 20 criteria have been set to flag sub-standard data on a gyro-by-gyro basis. The criteria chosen are primarily a function of vehicle state, such as “guide star out of view,” “vehicle in eclipse,” “loss of drag-free control,” “SQUID unlocked;” these all directly affect the validity of the data being sent from the spin axis readout system.

During data analysis runs, the analyst selects the grading criteria that will apply during the run. Then, database extraction tools will then return the data that meet the grading criteria. Immediately, the same algorithm can be run with different grading criteria to assess the sensitivity of the result to various types of low quality data.



### 14.2.4 Data Analysis “Standard Model”

The data analysis effort revolves around a “standard model” for how the vehicle operates and how vehicle configuration affects the performance of the gyroscopes. This model evolves as the team’s knowledge of the operation and performance of the vehicle increases during the analysis efforts. In addition to the 1) Independent Analysis teams, 2) the Truth Modeling Efforts, and 3) the Data Grading system, the data analysis team focuses its efforts on six primary areas of vehicle performance (Figure 14-8):

1. Precession dynamics and torques: Understand the overall drift of the gyroscope and how it relates to relativistic effects and classical (Newtonian) effects.
2. Orbital and Annual Aberration: Model and compensate for the apparent motion of the guide star due to space vehicle motion.
3. Vehicle Pointing: Assess the pointing of the space vehicle during guide star valid (GSV) and guide star invalid (GSI) periods using all on-board sensors (ATC, telescope, science gyroscopes). Determine relative scale factor between telescope readout of pointing and science gyroscope readout of pointing.
4. Roll Phase Measurement: Measure and quantify errors in the roll phase of the vehicle over the mission (time history of the clocking of the vehicle with respect to the orbital plane).
5. Spin Axis Orientation Measurement: Model and calibrate the SQUID readout system and compensate for effects of vehicle pointing in the science signal.
6. Polhode and Scale Factor Modeling: Model and remove the effects of the time varying polhode period on the SQUID scale factor. Compensate for systematic errors in gyro orientation measurements due to the slow damping of the gyroscope polhode path.

<b>Independent Core Analysis + Support</b>	
$\frac{dS_{NS}}{dt} = R_{NS} \left[ \frac{d\phi_r}{dt} + \delta\phi_r \right] S_{EW}$ $\frac{dS_{EW}}{dt} = R_{EW} S_{NS}$ <p><b>Drift Dynamics and Torques</b></p>	$\begin{bmatrix} \theta_P^{NS} \\ \theta_P^{EW} \end{bmatrix} = \begin{bmatrix} \cos(\phi_r + \delta\phi_r) & \sin(\phi_r + \delta\phi_r) \\ \sin(\phi_r + \delta\phi_r) & \cos(\phi_r + \delta\phi_r) \end{bmatrix} \begin{bmatrix} \theta_P^X \\ \theta_P^Y \end{bmatrix}$ <p><b>Roll Phase</b></p>
$\begin{bmatrix} \delta_{NS} \\ \delta_{EW} \end{bmatrix} = \begin{bmatrix} \frac{dR_{NS}(t)}{dt} + \frac{dR_{EW}(t)}{dt} \\ \frac{dR_{EW}(t)}{dt} \\ 0 \end{bmatrix} \begin{bmatrix} Z_{SQ1,3}^{SV} \\ Z_{SQ2,4}^{SV} \\ GSI \end{bmatrix}$ <p><b>Orbital and Annual Aberration</b></p>	$Z_{SQ1,3} = C_G \left\{ \begin{array}{l} [\delta_{NS} - S_{NS}] \cos(\phi_r + \delta\phi_r) + \\ [\delta_{EW} - S_{EW}] \sin(\phi_r + \delta\phi_r) \end{array} \right\} + b + n$ $Z_{SQ2,4} = C_G \left\{ \begin{array}{l} [-\delta_{EW} - S_{EW}] \sin(\phi_r + \delta\phi_r) + \\ -x_1''\theta_x - x_2''\theta_y \end{array} \right\} + b + n$ <p><b>Spin axis orientation measurement</b></p>
$\theta_P^x = \frac{1}{C_{19}} Z_{19}^x$ $\theta_P^y = \frac{1}{C_{19}} Z_{19}^y$ $\theta_S^x = C_{G3} Z_{SQ3} - C_{G4} Z_{SQ4}$ $\theta_S^y = C_{G4} Z_{SQ3} - C_{G3} Z_{SQ4}$ <p><b>Vehicle Pointing GSV and GSI</b></p>	$C_G \left[ \frac{d\phi_r}{dt} + \delta\phi_r \right] \begin{bmatrix} \cos(\phi_r + \delta\phi_r) & \sin(\phi_r + \delta\phi_r) \\ \sin(\phi_r + \delta\phi_r) & \cos(\phi_r + \delta\phi_r) \end{bmatrix}$ <p><b>Gyroscope: Polhode and Scale Factor</b></p>
<p><b>Data Grading</b></p>	<p><b>Truth Modeling</b></p>

**Figure 14-18.** Components of the GP-B Data Analysis Standard Model (equations shown are significantly simplified and are of iconic value only)

Phase 1 activities focus primarily on improving the accuracy of all the terms that go into the standard model, based on vehicle data, and setting performance limits on the ultimate resolution of the experiment. Phase 2 and 3 activities focus on the precession dynamics, effects of anomalies, and polhode models that span weekly or

monthly time scales. Though only shown in a simple outline here, the standard model gives a convenient frame of reference for the whole team in which to discuss results and propose new explanations and models for observed phenomena.

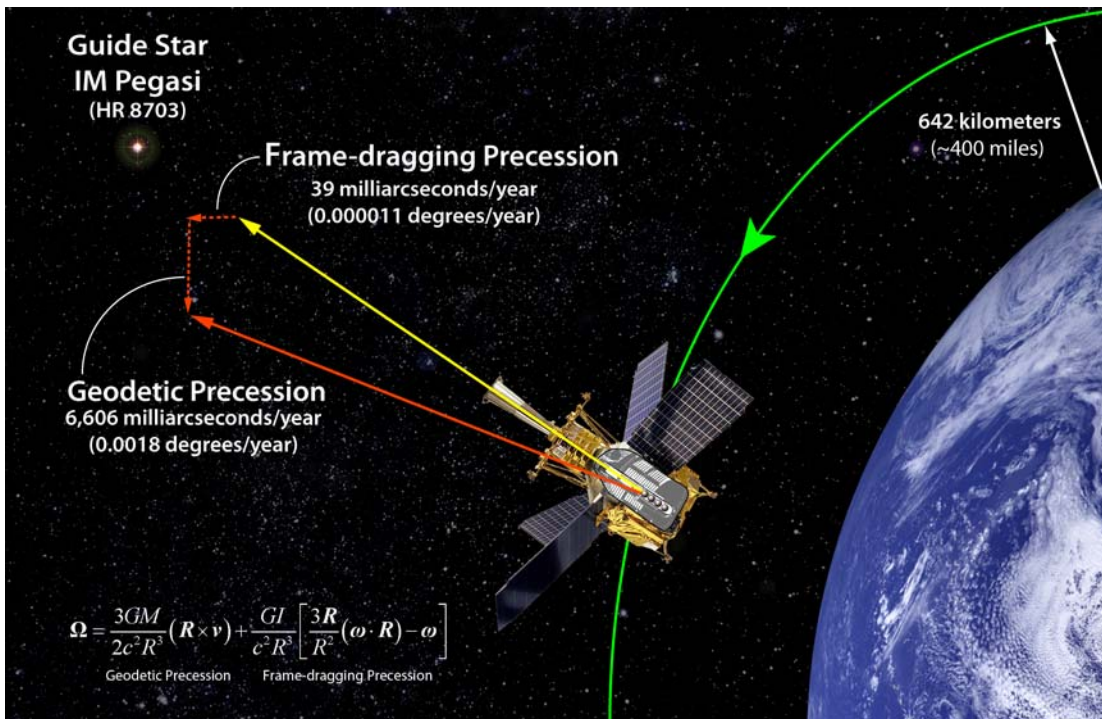
### **14.2.5 Publication of Overall Results**

Based on the successful results announcement strategies for the COBE and WMAP missions, the Gravity Probe B project will announce the results of the experiment only after the internal data analysis effort is complete (Phases 1, 2, and 3, above), and after critical and detailed peer review of the results from the gravitational physics community. No data or preliminary results will be released prior to this point. This is done to insure the integrity of the result and maintain credibility within the wider scientific community.

Once this work is complete and both the internal and external review teams are satisfied with their reviews, the results will be presented, along with a coordinated set of papers on the design and operation of the mission, at a major physics conference.

# 15

## Preliminary Results





This chapter summarizes the preliminary results announcement that the GP-B team will be presenting at the meeting of the American Physical Society (APS) in Jacksonville, Florida, on April 14-17, 2007. To learn about the current status of the mission, and to view a summary of the final results once they have been announced towards the end of 2007, please visit the GP-B Web site at: <http://einstein.stanford.edu>.

## 15.1 GP-B Successfully Collected the Data to Test Einstein's Predictions About Gravity

Over four decades of planning, inventing, designing, developing, testing, training and rehearsing paid off handsomely for GP-B. The 17.3-month flight mission succeeded in collecting all the data needed to carry out this unprecedented, direct experimental test of Einstein's general theory of relativity—his theory of gravity.



**Figure 15-1.** A photo montage of the GP-B spacecraft in orbit and a photo of the GP-B Mission Operations Center in action during the spin-up of gyro #4.

GP-B is arguably the most sophisticated spacecraft ever flown. It incorporated many new technologies—most notably the gyros, their suspension systems, the accompanying SQUID readouts, and the precision-pointing of the spacecraft-fixed telescope—all of whose debut performances in space occurred during this mission. It is remarkable, and a testament to the preparation, talent, knowledge and skill of the Stanford-NASA-Lockheed Martin development team, that all of these technologies performed exceedingly well on orbit, with some, such as the Gyro Suspension System and SQUID readouts, significantly exceeding their required performance specifications.

As Gaylord Green, the GP-B Program Manager during launch operations, remarked after the spacecraft was in orbit and all systems were functioning nominally: "...10,000 things went right!"

## 15.2 The Effects of Relativity Are Clearly Visible in the Raw Data

The GP-B satellite was designed as a pristine, space-borne laboratory, whose primary task was to use four ultra-precise gyroscopes to measure directly two effects predicted by general relativity. One is the geodetic effect—the amount by which the mass of the Earth warps the local space-time in which it resides. The second effect, called frame-dragging, is the amount by which the rotating Earth drags local space-time around with it. Because the spacecraft is in a polar orbit, the two effects occur at right angles to each other, giving a clean separation between them. Furthermore, the gyros are arranged such that each measures both effects.



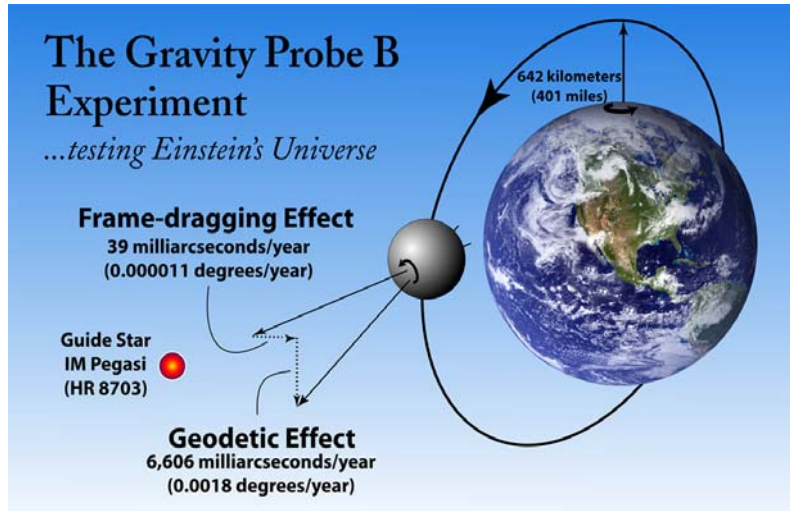


**Figure 15-2.** A diagram of the GP-B experiment showing the predicted geodetic and frame-dragging effects.

According to Einstein's theory, over the course of a year, the geodetic warping of Earth's local space-time should cause the spin axis of each gyroscope to shift from its initial alignment by a minuscule angle of 6.606 arc-seconds (0.0018 degrees) in the plane of the spacecraft's orbit. Likewise, the twisting of Earth's local space-time should cause the spin axis to shift by an even smaller angle of 0.039 arc-seconds (0.000011 degrees)—about the width of a human hair viewed from a quarter mile away—in the plane of the Earth's equator.

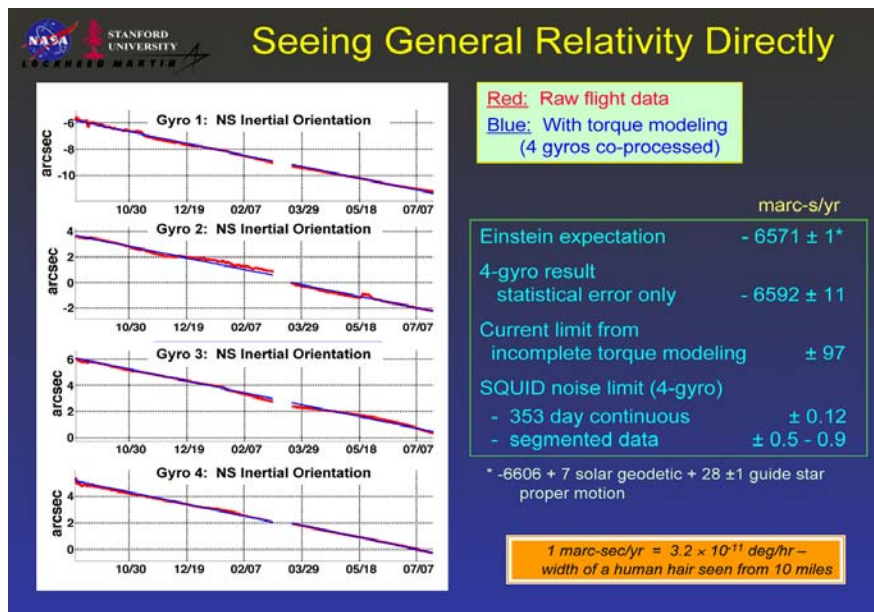


**Figure 15-3.** A slide from the GP-B plenary talk that Francis Everitt will deliver at the APS meeting on April 14, 2007. The plots on the left side of this slide clearly show the predicted geodetic effect in the unprocessed gyro data to an accuracy level of ~1%. A copy of this talk will be available on the APS page of the GP-B Web site: [http://einstein.stanford.edu/content/aps\\_posters#talks](http://einstein.stanford.edu/content/aps_posters#talks).

The graph in [Figure 15-3](#) above shows that the geodetic effect is clearly visible even in the raw data (prior to processing) from the GP-B gyroscopes, confirming Einstein's predictions to a precision of better than 1 percent. As Professor Francis Everitt, GP-B Principal Investigator, recently remarked: "It's fascinating to be able to watch the Einstein warping of spacetime directly in the tilting of these GP-B gyroscopes—more than a million times better than the best inertial navigation gyroscopes."

We have also seen indications of the frame-dragging effect, which is 170 times smaller than the geodetic effect. GP-B scientists are still in the process of extracting its signature from the spacecraft data.

## 15.3 A First Peek at the Results

After 18 months of rigorous, ground-breaking data analysis, our science is preparing to present a first public peek at the results summarized above during the April meeting of the American Physical Society (APS) in Jacksonville, Florida. Professor Francis Everitt will kick off the April APS meeting with a plenary talk entitled: Gravity Probe B Interim Report and First Results. In addition, GP-B team members are scheduled to give three invited talks, two submitted papers, and the team will present 22 poster papers on various aspects of GP-B.

The preliminary results to be announced at the April APS meeting for the geodetic effect are consistent with the prediction of general relativity to an accuracy of  $\sim 1.0$  percent. This is on par with the only other measurement of this effect that was performed using the Earth-Moon system orbiting the Sun, but seen in a different and much more direct way. Moreover, the indications of frame-dragging measured thus far are also highly encouraging. However, for both measurements, the current level of experimental error must be significantly reduced and the measurements thoroughly cross-checked before being announced as final results.

The inherent noise in the GP-B SQUID readout system imposes a natural physical limitation on the experimental accuracy that it is possible to achieve with the GP-B instrument. For the geodetic effect, this limit is  $\sim 0.01$  percent, and for the much smaller frame-dragging effect, the limit is  $\sim 1.0$  percent. The goal of GP-B is to achieve the highest possible experimental accuracy, approaching the physical limitations of the instrument readout.

The GP-B science instrument has sufficient resolution and we have collected ample data to obtain results approaching these limits. However, early in the data analysis, our science team uncovered surprising torque and sensor effects (from polhode motion of the gyros) that must be separated and removed from the relativity effects in order to obtain the desired level of accuracy. Addressing these torque and sensor effects has been our science team's dominant focus in recent months, and this has led to a longer and more sophisticated data analysis process than was originally anticipated.

On Friday-Saturday, March 23-24, 2007, just prior to the final edit of this report, our GP-B science team reviewed the progress with the independent GP-B Science Advisory Committee (SAC) that has been consulting with us on every aspect of the program for the past decade. Summarizing the committee's findings and recommendations, SAC Chairman, Professor Clifford Will of Washington University in St. Louis, MO. and author of the classic text, *Theory & Experiment in Gravitational Physics*, reported: "The GP-B science team is continuing to make good progress on a number of fronts... We strongly support the [Stanford] proposal for funding through December 2007 to complete the data analysis and prepare publication of the final GP-B result." NASA has committed to extending support for GP-B at the required level.

In the press release we have prepared for the APS meeting, GP-B Program Manager, William Bencze, summarized the situation: "Understanding the details of this science data is a bit like an archeological dig: a scientist starts with a bulldozer, follows with a shovel, and then he finally uses dental picks and toothbrushes to clear the dust away from the treasure. We are passing out the toothbrushes now."



## 15.4 The Two Surprises and Their Impact On The Experiment

Francis Everitt is fond of telling the story that in the months leading up to the GP-B launch, several people who had deep experience with other space missions told him that all the things he knew were likely to go wrong would work perfectly, but other things that couldn't possibly cause any difficulty would keep the team up at night.

These turned out to be prophetic words. Our science team made two significant discoveries about the science instrument that have lengthened the data analysis process:

1. Shortly after the gyros were spun up in August 2004, we discovered that the polhode motion of the gyro rotors, which was expected to exhibit a constant pattern throughout the experimental period, was changing over time, significantly complicating the calibration of the gyroscope readout angles.

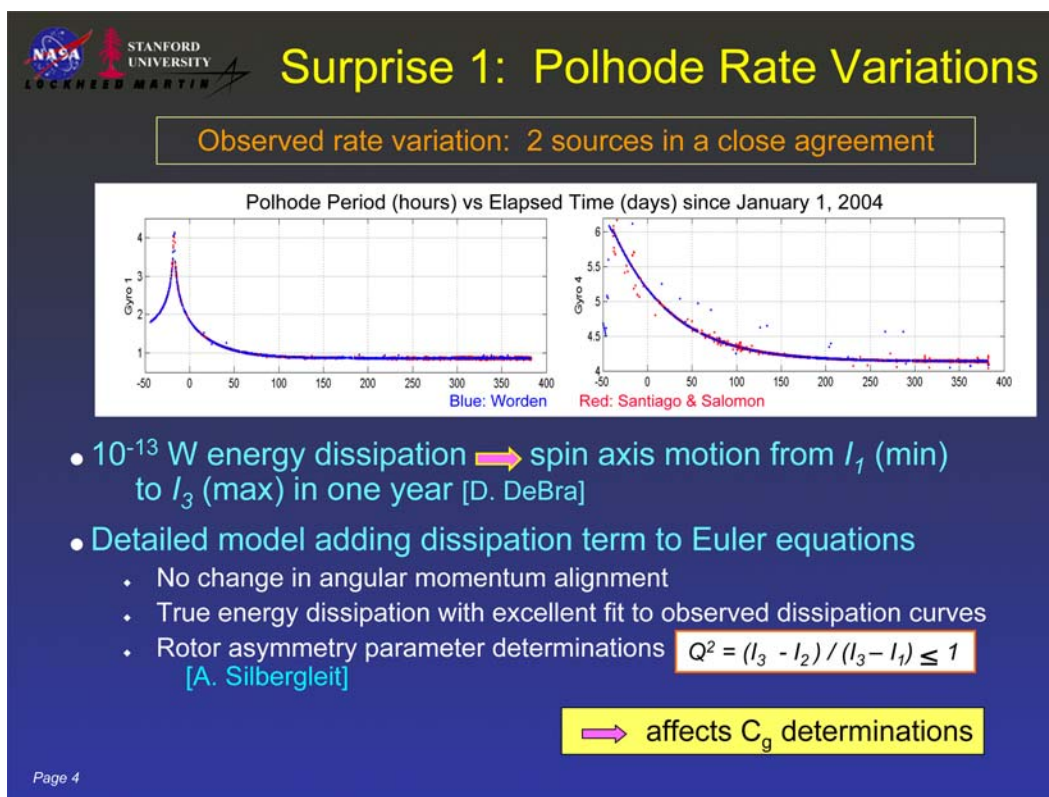


**Figure 15-4.** A slide from the GP-B plenary talk that Francis Everitt will deliver at the APS meeting on April 14, 2007. This slide shows the changing polhode paths of gyros #1 and #4 and summarizes the issues of polhode rate variations in the gyros.

2. During the post-experiment instrument calibration testing in August-September 2005, the spin axes of the gyroscopes were found to be affected by certain class of small classical torques, known as “misalignment torques,” whose effects must be rigorously separated from the relativity measurements.

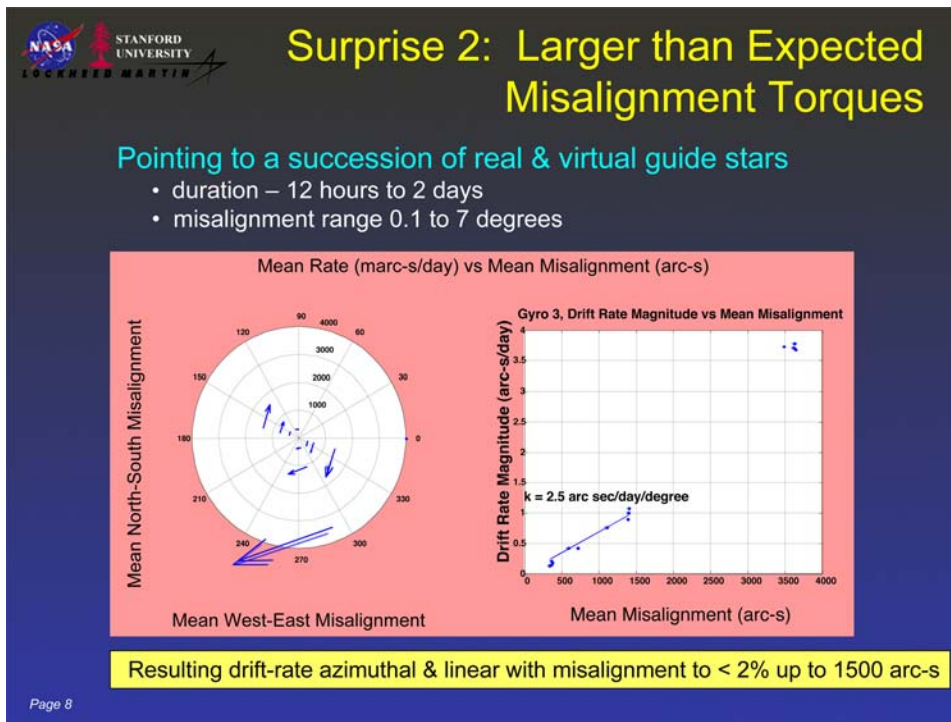


**Figure 15-5.** A slide from the GP-B plenary talk that Francis Everitt will deliver at the APS meeting on April 14, 2007. This slide shows the misalignment torques discovered during a series of instrument calibration tests performed during the last six weeks of the mission, prior to depletion of helium in the dewar.

However, the team was prepared for such an eventuality. In fact, the GP-B experiment was carefully designed to enable us to discover such unexpected sources of error. As Francis Everitt notes: “When trying to do an experiment that goes seven orders of magnitude beyond where anyone has gone before, some extraordinary planning is necessary. First, you design the experiment to make all the errors as close to zero as possible. Next, you average everything you can—for example, you roll the spacecraft throughout the experiment. Finally, you purposely look for things that were not expected.”

During one of many NASA program reviews prior to launch, experienced investigators from other NASA missions asked us what processes we had put in place to discover systematic sources of error that might crop up in the data. Our answer was that we would follow a principle set forth by the 18th century scientist, Henry Cavendish—namely, if you are worried that something in an experiment might be a potential source of error, you take the step of deliberately exaggerating the error sources to determine how bad they can get. This process enables you to quantify the magnitude of the problem and determine a way to deal with it. (For a thorough discussion of the “Cavendish” principle, see the 1977 paper by Francis Everitt entitled **Gravitation, Relativity and Precise Experimentation**, which is available in Adobe Acrobat PDF format on our GP-B Web site at [http://einstein.stanford.edu/content/sci\\_papers/papers/Everitt\\_Gravitation-Precise-Expt-1977.pdf](http://einstein.stanford.edu/content/sci_papers/papers/Everitt_Gravitation-Precise-Expt-1977.pdf).)

From mid-August through September 2005, after collecting 50 weeks of science data and before the liquid helium was exhausted from the dewar, we followed Cavendish's principle by performing a barrage of calibration tests on all parts of our science instrument. These tests, along with other tests that we performed throughout the mission, enabled us to confirm that all of the known and expected sources of error—with one exception—were, in fact, negligible as expected. As William Bencze put it: “Without the extensive calibration tests, we would have been looking for a needle in a haystack; instead, we only had to look for a needle on the floor.”

Specifically, these tests confirmed that six of the seven extrinsic “near zero” design specifications of the experiment had been met or exceeded, and we were able to eliminate each of these factors as sources of error in the final results. (For an explanation of GP-B’s seven near-zero specifications, see [Section 3.1.1, GP-B’s Seven](#)

**Near Zeroes.)** The exception that we could not eliminate as a source of error was the seventh extrinsic design constraint that the electric dipole moment of the gyro rotors be “near zero.” In other words, the gyro rotors must be highly electrically spherical as well as mechanically spherical.

The electrical out-of-roundness is due to larger than anticipated electrostatic patches (regions of electrical charge) on the rotor’s surface. These patches interact with similar ones on the housing’s inner surface to give rise to small “misalignment torques” that occur when the spin axes of the gyros are not aligned with the roll axis of the spacecraft. These patches also provide a subtle damping mechanism that extracts small amounts of energy from the spinning rotor, and this causes the polhode path to change. The potential existence of these patches was known prior to launch, but was believed to be negligible, based on careful physical analysis and laboratory measurements.

Nature is full of surprises, and it is common for physics experiments, particularly a ground-breaking experiment such as GP-B, to uncover unexpected phenomena. Because we anticipated this situation and were actively looking for surprises in the data, we were prepared to deal with them. Consequently, the team has been able to model precisely the polhode motion of all four gyroscopes, as well as the classical torques imparted by patch effects on the rotors and housings. This painstaking work, which is still in progress, has lengthened the data analysis phase of the mission by more than a year—such is the nature of scientific inquiry. Ultimately, the time spent isolating and removing these confounding effects from the final results will reduce the current margin of experimental error to the desired level.

Our goal in GP-B has always been to perform the best possible experiment and to use great care and redundancy to ensure the validity of the results. Every experiment has its share of unknowns or challenges that no one could have anticipated. But once such challenges surface, it is incumbent on the investigators to spend time addressing them and accounting for them in the process of determining the final outcome.

### 15.4.1 Time-Varying Motion in the Gyro Rotors

The gyroscope’s polhode motion is akin to the common “wobble” seen on a poorly thrown (American) football, though it shows up in a much different form for the ultra-spherical GP-B gyroscopes. While it was expected that this wobble would exhibit a constant pattern over the mission, it was found to slowly change due to minute energy dissipation in the spinning gyro rotors, caused by interactions of electrostatic patches on the rotor’s surfaces and patches on the metallic surfaces inside the housings. For example, [Figure 15-6](#) below shows “snapshots” of the changing polhode path of gyro #1 at various times during the mission.

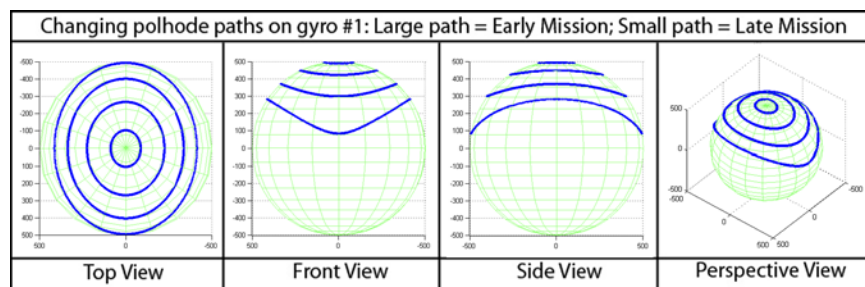


**Figure 15-6.** Plots from different viewing angles showing the changing polhode path of gyro #1 over the life of the experiment.

The polhode wobble complicates the measurement of the relativity effects by putting a time-varying wobble signal into the data.

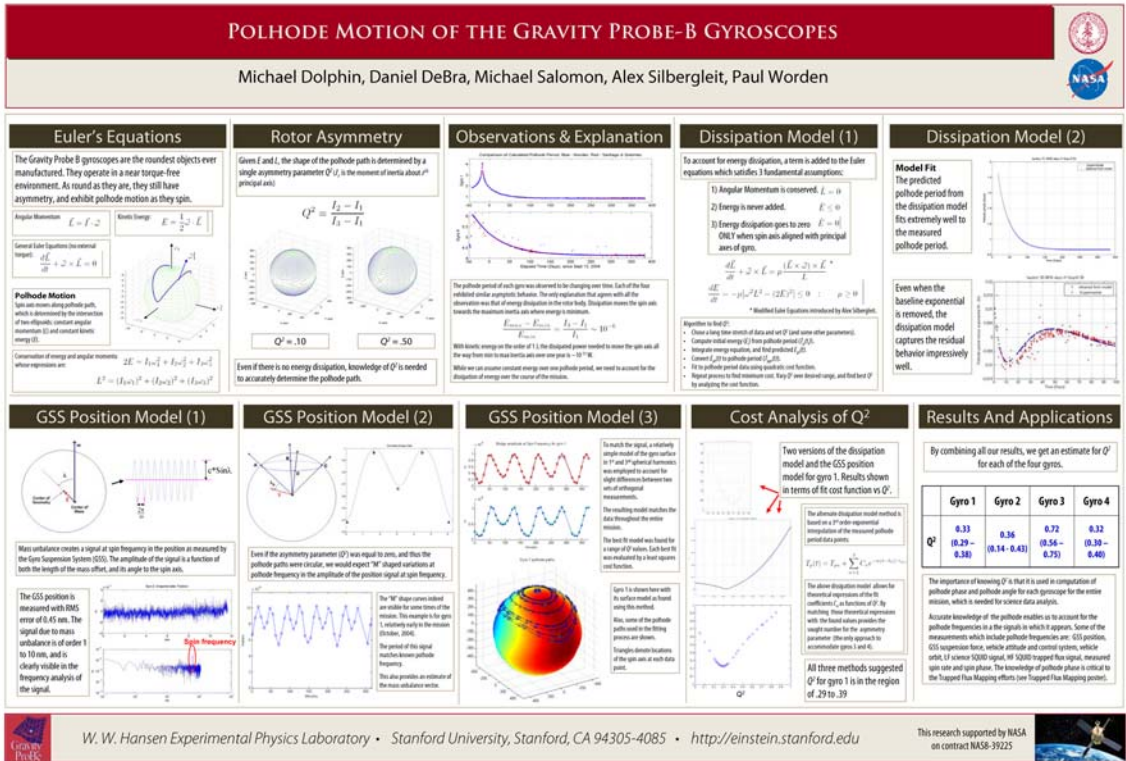


**Figure 15-7.** A poster on gyro polhode motion to be presented at the APS meeting in April 2007. You can view/download a larger and more readable PDF version of this poster on our GP-B APS Web page: [http://einstein.stanford.edu/content/aps\\_posters#posters](http://einstein.stanford.edu/content/aps_posters#posters).

For a complete discussion of polhode motion, see the GP-B Mission News story entitled: Polhode Motion in the GP-B Gyroscopes in the 20 November 2006 GP-B update on our Web site at: [http://einstein.stanford.edu/highlights/hl\\_polhode\\_story.html](http://einstein.stanford.edu/highlights/hl_polhode_story.html).

## 15.4.2 The Effects of Time-Varying Polhode Motion on the Experiment

As noted in Section 15.5, Next Steps—Moving Towards a Final Result below, both the SQUID-based magnetic measurement (London moment) of the gyro spin axes and the telescope measurement of the spacecraft pointing direction with respect to the guide star produce electrical signals that represent angular measurements. Because these two systems are independent of each other, it is necessary to cross-calibrate these instruments to ensure that both systems are measuring the same relative angle when the orientation of the spacecraft changes.



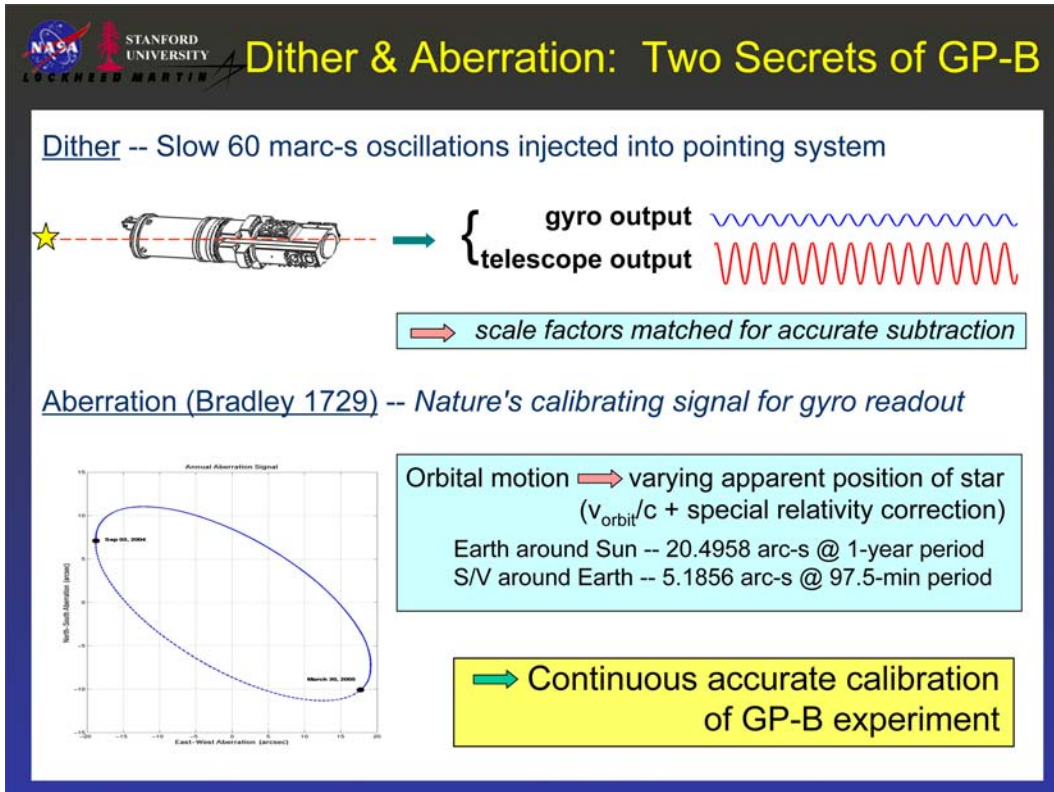


**Figure 15-8.** A slide from the GP-B plenary talk that Francis Everitt will deliver at the APS meeting on April 14, 2007. This slide shows how dither and aberration of starlight are used as calibrating signals in determining the gyro-telescope scale factor,  $C_g$ .

Fortunately, the GP-B experimental data includes natural calibrating signals in the form of the aberration of starlight—both orbital and annual. (For a discussion of how the aberration of starlight is used as calibrating signal in the GP-B data, see [Section 14.1.5, Aberration of Starlight—Nature’s Calibrating Signal](#).) Our goal is to perform this calibration to a precision of 1 part in 100,000 (0.001 percent), but our measurements are limited by the noise in our SQUID readout system. If there were no variation in the polhode period of the gyros, we could simply string together the data taken during the Guide Star Valid (GSV) portion of each orbit (when the spacecraft has a direct line of sight to the Guide Star) from a sequence of orbits until we have reached the desired 0.001 percent precision. (We must string together data from ~15 orbits to reach this level of precision.) However, the polhode periods for the gyros did vary over the data collection period, and this makes it much more difficult to connect the data from successive orbits.

The complication is due to the presence of a residual magnetic flux that becomes trapped on the gyro rotors when they are cooled to superconductive temperatures. Whereas a constant polhode period can easily be removed, a varying polhode period must be precisely modeled for each orbit before it can be removed. Consider three cases:

1. London moment with varying polhode rates and no trapped magnetic flux—In this case, there is no problem; the data from successive orbits can easily be strung together to yield the desired precision since the London Moment is independent of rotor polhode dynamics to the levels we hope to measure.
2. London moment with 1% trapped magnetic flux, but constant polhode period (no variation)—Again, in this case there is no problem; the data from successive orbits can still be strung together because the constant polhode period clearly stands out from other signals as the data analysis proceeds. Thus, it can be precisely separated and removed.
3. London moment with both trapped magnetic flux and time-varying polhode rates—This situation, which we have determined is the case for the GP-B gyros, requires very precise modeling of the polhode motion for each gyro. Initial modeling that was based on information from the primary science readout gave reasonable results, but it lacked a detailed dynamic model of the polhode motion. Now, some GP-B graduate students are working on a method that uses high-rate SQUID data “snapshots” to map out the trapped flux patterns on each gyro. Using this map, together with a rotor dynamic model, we can more accurately predict the effect of rotor trapped flux on the gyro readout calibrations. Moreover, with accurate trapped flux maps, we can string together relativity data from successive orbits to achieve the desired experimental precision. Once we have the trapped flux modeling, the fitting process becomes much easier.

### 15.4.3 Classical Misalignment Torques on the Gyros

After months of research and analysis, our GP-B science team has determined that electrostatic patches are also the cause of the small torques we have observed on the gyroscopes when the spacecraft's axis of symmetry is not aligned with the gyroscope spin axes. Torques cause the spin axis of a gyroscope to change orientation, and in certain circumstances, this effect can look like the relativity signal GP-B measures.

Fortunately, the change in gyro spin axis orientation due to these torques has a precise geometrical relationship to the misalignment of the gyro spin/vehicle symmetry axis, and thus effects of these so-called misalignment torques can be removed from the data without directly affecting the relativity measurement.

Important data that has enabled us to understand and model these torques was collected during a series of planned instrument calibration tests that we conducted during the final six weeks of the flight mission, from mid-August through the end of September 2005, when the helium in the dewar was finally exhausted. During these calibration tests, we purposely slewed the spacecraft and telescope from the guide star, IM Pegasi, to observe other stars nearby for 12 to 24 hours, and then returned to IM Pegasi. These exaggerated mis-pointing maneuvers produced measurable torques on the gyros. From the results of these tests, the team has been able to determine the nature and limits of these torques and has devised methods for modeling and removing them during the data analysis phase. To learn more about these instrument calibration tests, see [Section C.5, Instrument Calibration Phase: 8/19/05 – 9/30/05](#).





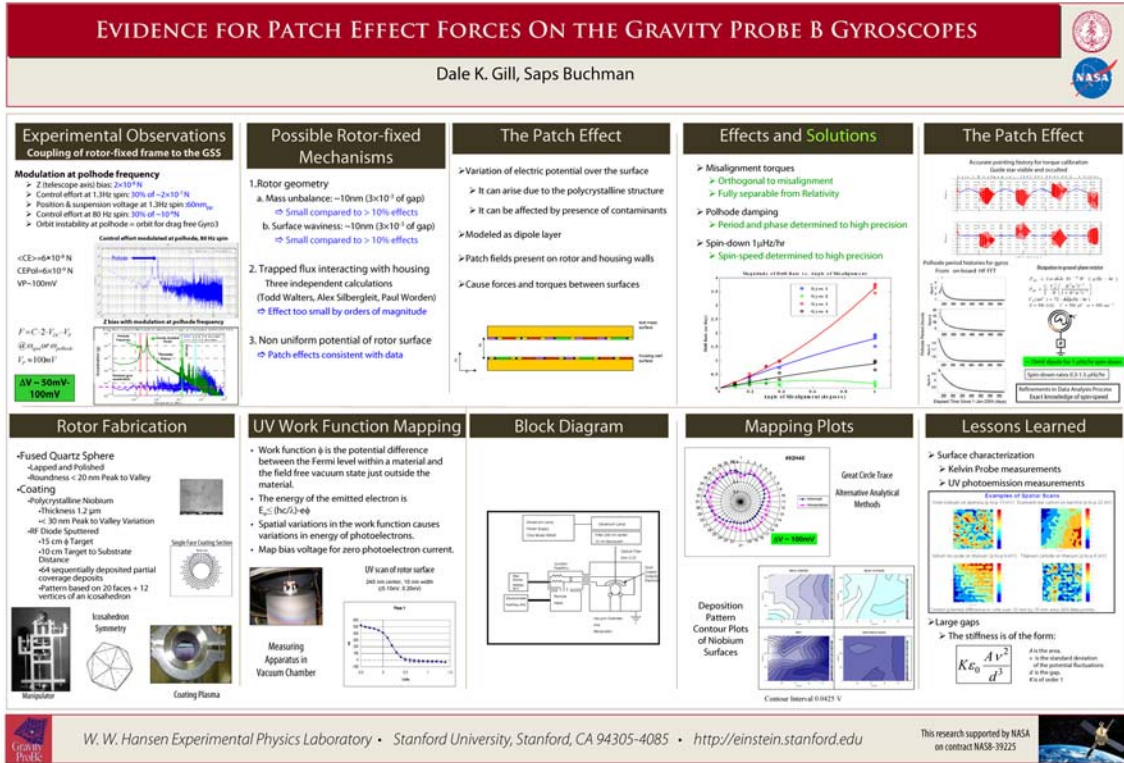


**Figure 15-10.** A poster on the evidence for patch effects to be presented at the APS meeting in April 2007. You can view/download a larger and more readable PDF version of this poster on our GP-B APS Web page: [http://einstein.stanford.edu/content/aps\\_posters#posters](http://einstein.stanford.edu/content/aps_posters#posters).

Given the almost perfectly spherical and homogeneous nature of the GP-B gyro rotors, there are two possibilities:

1. Internal energy dissipation in the gyro rotors
2. External torques with just the right frequency

Early in the data analysis phase, we thought that some kind of internal energy dissipation was the cause. However, adding the variation in spin-down rates to the analysis, we currently believe that both mechanisms listed above are involved and that the underlying cause is “patch effect charges” on the gyro rotors and on the inside surfaces of their housings. Patch charges arise from varying surface electrical potentials in polycrystalline materials from regions of changing crystal orientations over the surface of the metal, or due to non-uniform distribution of constituent elements in a metal alloy, or can arise due to the presence of contaminants on the metal surface.

The sputtered niobium coatings on GP-B gyro rotors are naturally polycrystalline and thus inherently exhibit patch charge effects. These charges impart some potential on the six electrodes that suspend each gyro in its housing which causes a minute dissipation of energy as the rotor spins. This produces a small torque on the rotor as the energy is dissipated into the gyro housing, causing the spin rate of the gyro to slow down slightly, and also causing the polhode motion to be damped out over the mission.

We were well aware of the possible ramifications of electrostatic patches on the gyro rotors prior to launch, and we made a thorough investigation of them. In fact, a GP-B post-doctoral student carefully studied the effects of electrostatic patches on the gyro rotors and concluded that if the niobium coatings produced just two large

electrostatic patches, located at opposite poles of the rotors, this would create a significant, classical torque problem in our gyros. To address this issue and determine the sizes of the patches, we performed two types of tests:

1. a visual inspection,
2. a laboratory measurement of the size and magnitude of the patches.

The visual testing measured the grain size of the sputtered niobium coating, and found that the patches on the GP-B gyros were very small (less than 1 micrometer in size) and were scattered about the entire surface of each rotor. With such small patches randomly distributed, it was our expectation that the patch effects would average out and not be of any consequence to the experiment.

To ensure this was the case, we performed a laboratory test. We sent flat samples of niobium-coated surfaces (produced in our same Stanford lab where the gyro rotors were coated) to a lab in France where they scanned the samples with a Kelvin probe and showed that there was no problem with patches in the flat samples. (The lab in France could not handle spherical objects in their scanner, so we created flat samples using our same gyro coating machinery.)

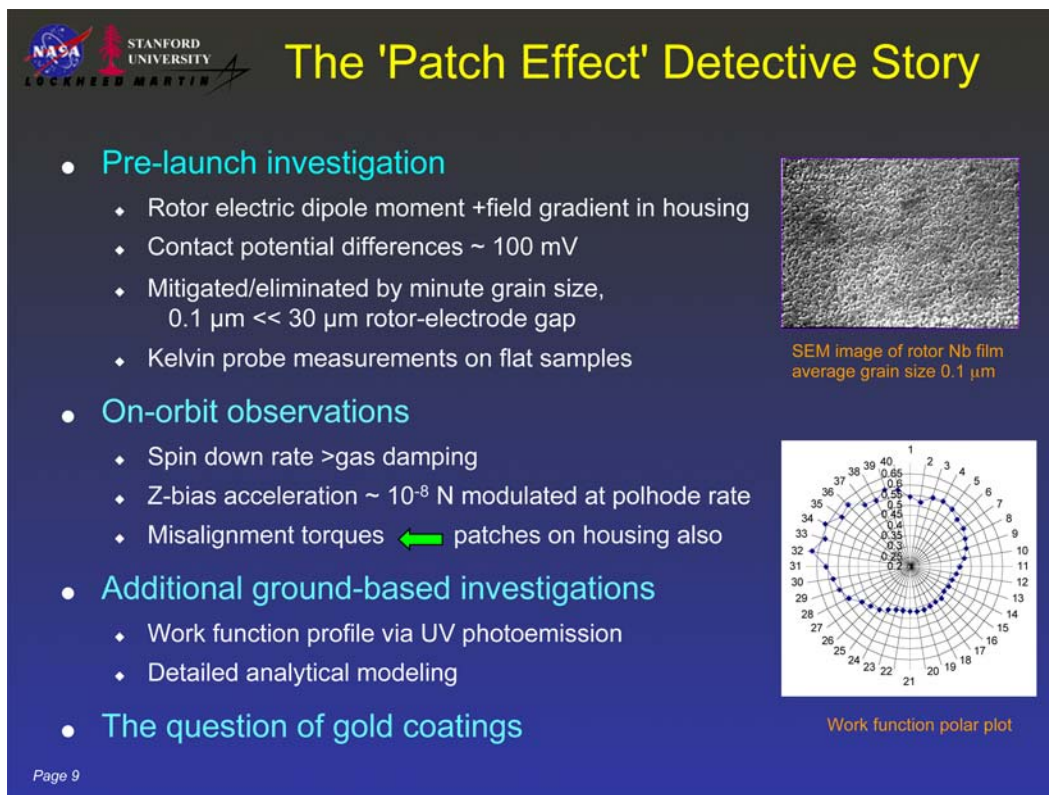


**Figure 15-11.** A slide from the GP-B plenary talk that Francis Everitt will deliver at the APS meeting on April 14, 2007. This slide shows the succession of investigative steps and observations that led to the determination that patch effects are the root cause of both the polhode variation and misalignment torques on the gyros.

Thus, once the spacecraft was in orbit and we began observing the changing polhode periods of the gyros and the misalignment torques, we did not initially suspect that patch effects might be the underlying cause. However, having eliminated other causes through all of the tests and calibrations performed during the mission, we have determined that patch effects are, indeed, the underlying cause of our two surprises. Furthermore, through recent gyro coating tests performed in our labs here at Stanford, we now know that we overlooked a critical issue in our method of coating the gyro rotors.

The niobium coatings on the rotors were sputtered on in a series of 64 stages, turning the rotor to a new position for each new coating. This process created a very uniform niobium coating on each rotor. However, it turns out that the final, 64th layer effectively created two large patches on the rotors, defined by its edge. In other words, the edge of the final coating essentially divides the rotor into two halves, each of which is, in fact, a large electrostatic patch at opposite poles of the rotor—the very situation that we had tested for pre-launch and had determined was “not going to be an issue.”

Knowing that this unprecedented experiment would likely uncover some surprises, we purposely collected copious spacecraft and instrument status data in addition to the scientific data and we thoroughly tested and calibrated the science instrument throughout the flight mission. This meticulous planning has paid off in many ways. For example, it has enabled our science team to develop a methodology for precisely modeling the polhode motion and trapped magnetic flux on each gyro. Most important, in the final months of the data analysis, our scientists will be able to use this modeled data to separate and remove the misalignment torques caused by these patch effects, thereby significantly improving the accuracy of the final results.

## 15.5 Next Steps—Moving Towards a Final Result

Our GP-B data analysis team comprises 34 people, including Principal Investigator, Francis Everitt. Program Manager, William Bencze, manages the team, and Chief Scientist, Mac Keiser, is ultimately responsible for the data analysis and results. The remainder of the team includes 22 scientists (physicists, mathematicians, engineers, and computer scientists), plus 9 physics and engineering graduate students. The entire data analysis team, except for Francis Everitt, is pictured in [Figure 15-12](#) below.

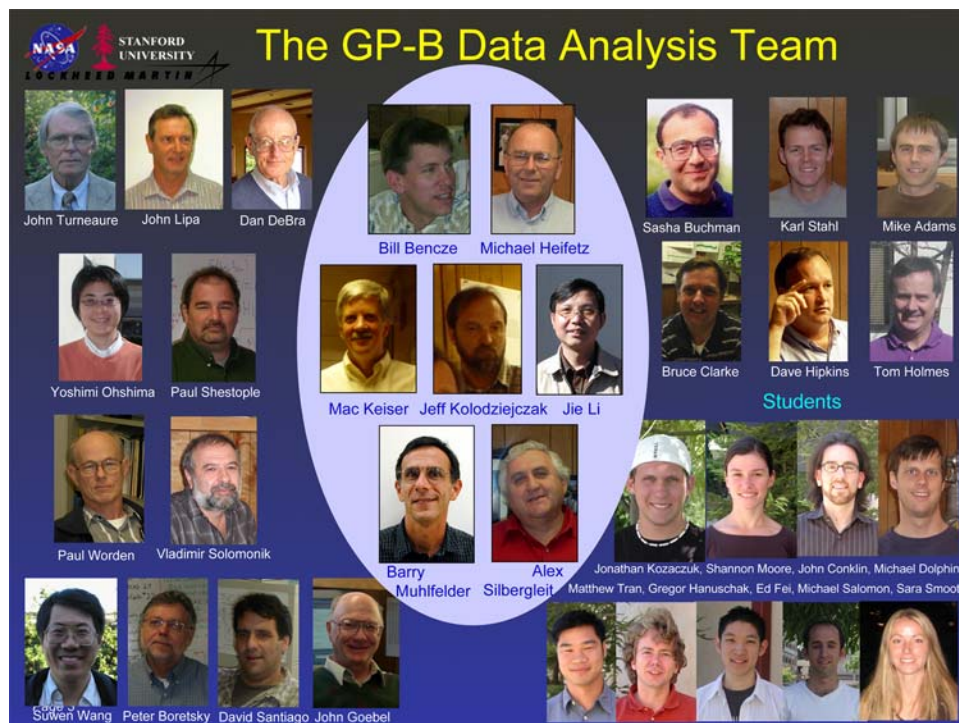


**Figure 15-12.** A slide from the GP-B plenary talk that Francis Everitt will deliver at the APS meeting on April 14, 2007. This slide shows the GP-B data analysis team, except for Principal Investigator, Francis Everitt. A copy of this talk will be available on our APS Web site: [http://einstein.stanford.edu/content/aps\\_posters#talks](http://einstein.stanford.edu/content/aps_posters#talks).



Last summer (2006), Mac Keiser devised a model-based, geometric method for separating the disturbance (misalignment) torques from the relativity signals. Over the past year, the team has been pursuing a combination of this geometric method and a model-based, algebraic estimation method formulated by mathematician Michael Heifetz. Recently, physicist Alex Silbergleit, following a line of inquiry first suggested by physicist Jeff Kolodziejczak (a collaborator from NASA's Marshall Space Flight Center), has found a way to combine the advantages of both the geometric and algebraic methods into a unified, integral data analysis approach. This integral approach eliminates the drawbacks of both previous methods, allows for iterative improvement of the results, and relies less on modeling than either of the previous methods. Thus, we will be continuing to employ this integral approach through the end of the analysis.

Specifically, our science team is focusing on two main issues:

1. Fine calibration of the gyroscope/telescope scale factor

Both the SQUID-based magnetic measurement of the gyro spin axes and the telescope measurement of the spacecraft pointing direction with respect to the guide star produce electrical signals that represent angular measurements. Because these two systems are independent of each other, it is necessary to cross-calibrate these instruments to ensure that both systems are measuring the same relative angle when the orientation of the spacecraft changes.

Because of trapped magnetic flux on the gyro rotors, the calibration—conversion from electrical signals to angles—of the gyro readout can vary in a complex, but computable way. Specifically, it is affected by the polhode period of the gyros, which was found to change during the flight mission, rather than remaining constant as originally expected.

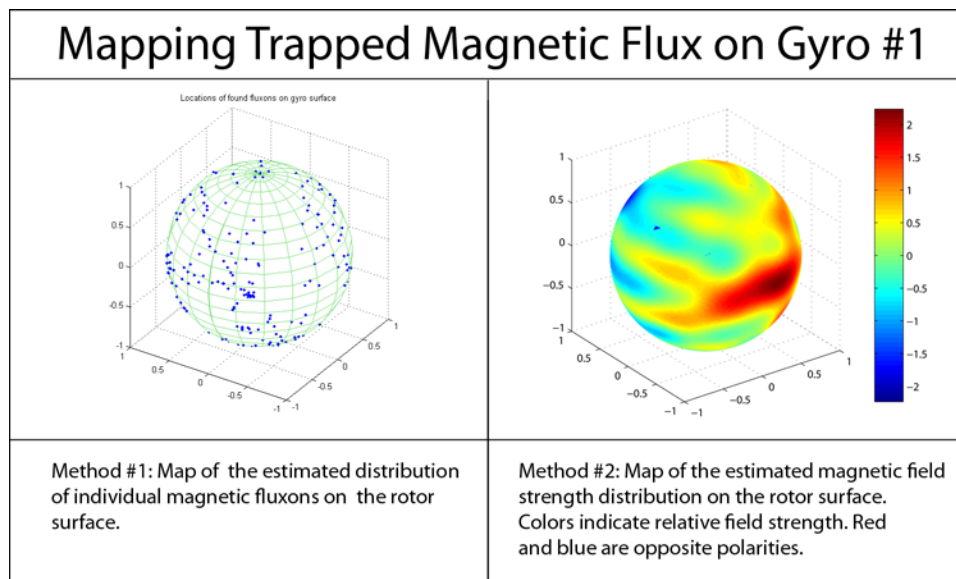


**Figure 15-13.** Map of the estimated magnetic flux trapped on the surface of the gyro rotors. Two methods are currently being employed—one mapping individual fluxons and the other mapping magnetic field strength.

To address these issues and determine the correct scale factor, the team is in the process of precisely modeling the time-varying polhode periods of each gyro for each orbit as well as creating precise mappings of the trapped magnetic flux on the surface of each gyro rotor.

2. Refining the analysis of the misalignment torques

The team is in the process of refining the data analysis techniques being used to separate and remove these classical misalignment torques from the relativity effects. To do this, it is necessary to take into account many variables, including vehicle motion and polhode paths of the gyros.

The refinement of the misalignment torques and the mapping of the trapped magnetic flux on the gyro rotors interact such that if one is incorrect, the other becomes harder. There is also a symbiotic relationship between these two activities so that as one improves, it facilitates calculating the other.

In addition to these two activities, the GP-B guide star (IM Pegasi) proper motion data is being held by Irwin Shapiro and his group at the Harvard Smithsonian Center for Astrophysics (CfA). Upon completion of the data analysis endeavor here at Stanford, this extremely precise VLBI measurement data will be substituted for the current placeholder values for the proper motion of IM Pegasi, taken from the 1997 Hipparcos [star] Catalogue, in order to obtain the greatest possible accuracy in the final GP-B result.

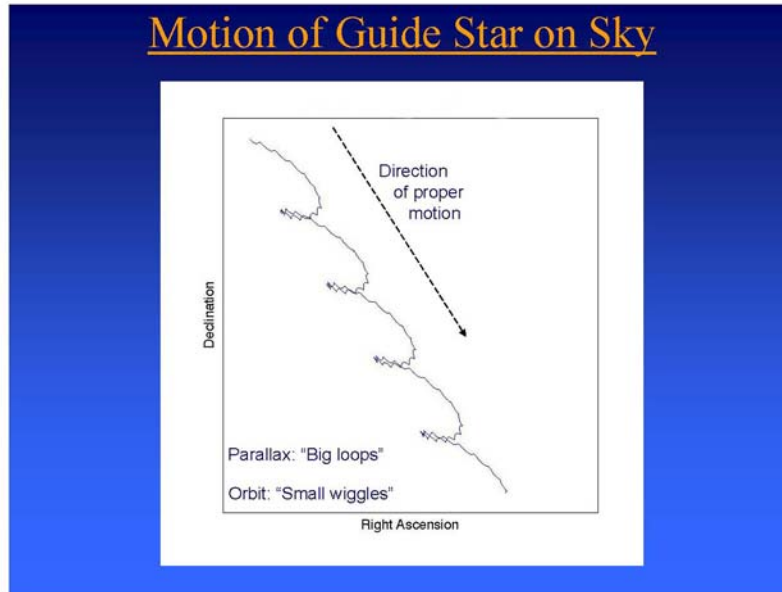


**Figure 15-14.** A slide from a talk that Irwin Shapiro will deliver at the APS meeting on April 14, 2007, entitled: **Proper Motion of the GP-B guide star.**

Irwin Shapiro is scheduled to give a talk about the GP-B Guide Star astrometry at the April APS meeting. In addition, two poster papers on the GP-B Guide Star Astrometry Project at the CfA. An audio recording of his talk, along with a PDF copy of his slides, as well as copies of both CfA astrometry poster papers will be available on the APS Meeting page of our GP-B Web site shortly after the conference:

[http://einstein.stanford.edu/content/aps\\_posters#talk.s](http://einstein.stanford.edu/content/aps_posters#talk.s)

## 15.6 GP-B Data Archive to be Available Through the NSSDC

During the past few weeks, while our science team continues to analyze the data, our GP-B data processing team has also been quite busy, compiling an archive of the GP-B raw data—both science data and spacecraft/payload status data, as well as an archive of associated documents, drawings, photos and other information about the GP-B mission. We are preparing to begin the process of transferring this entire archive to the National Space Science Data Center (NSSDC), located at the NASA Goddard Space Flight Center in Greenbelt, Maryland. Transfer of this archive is expected to be completed in late June, and the GP-B archive will then become publicly available sometime thereafter.





# 16

## Lessons Learned and Best Practices

---





This chapter summarizes some valuable lessons that were learned during the GP-B mission, selected best practices employed during this time that helped to make mission operations effective and efficient, and finally, some lessons about the GP-B Management Experiment, summarized from **Gravity Probe B: A Management Study**, an independent report presented to NASA by Edward S. Calder and Bradley T. Jones in April 2006.

## 16.1 Lessons Learned

Gravity Probe B logged 23 anomalies of various levels of severity and 170 observations during the 17-month flight mission. Most of these are specific to the Gravity Probe B vehicle and mission, and thus do not have significant applicability outside of the project. However, the following lessons have been identified that have broad applicability across other spaceflight projects. Included in this list are also significant lessons learned from the vehicle development and testing period preceding launch that also may be beneficial to other spaceflight programs.

Throughout the development and operation of the satellite, Gravity Probe B has also attempted to adopt “best practices” from lessons learned from other programs as well as the combined wisdom and experience of the team at Stanford, Lockheed-Martin, and NASA Marshall. We would like to affirm a number of practices as especially effective and worthy of continued adoption by the community.

### 16.1.1 Pre-launch lessons learned

The following subsections summarize lessons learned prior to launch of the GP-B spacecraft on April 20, 2004.

#### 16.1.1.1 Power system monitoring

*Issue Summary:* Extensive, detailed power system monitoring is beneficial.

*Description of the GP-B experience:*

Both during pre-launch testing and on orbit, it has been useful to carefully monitor the performance of the power system throughout the space vehicle. Many of the spacecraft and payload subsystems provide some level of power system monitoring, however, in some important instances, no explicit pre and post regulation power monitoring was provided. The engineering team, thus, had to rely on some of ancillary monitors to infer the performance of some box power systems.

*Lesson:*

- Include voltage and current monitoring for the primary and secondary sides of all power conversion systems as a standard design requirement for all custom designed power supplies.

#### 16.1.1.2 Early engineer involvement

*Issue Summary:* Involve subsystem engineers early in display page development.

*Description of the GP-B experience:*

Formatting and design of operations console display pages (numeric data displays and graphs) were many times put together without RE input. There wasn't enough time spent to ensure presentation of data was sufficient.

*Lessons:*

1. Involve the users early enough to allow them to have input into the monitors that they will need to use. Many displays pages have monitors that were useful for testing, but not for operations.
2. The display page should allow the user to easily modify the display.

### 16.1.1.3 Flight science downlink database

*Issue Summary:* Use flight science downlink database for system functional testing.

*Description of the GP-B experience:*

During system and vehicle functional testing prior to launch, a custom engineering data analysis package was used to evaluate system performance. This package was incompatible with the flight data system and was only available at Lockheed-Martin, the system integrator. A separate database was to be used to manage data from the vehicle once on orbit.

A lack of load-testing of this science database, especially using the science data reduction applications, long access times. Lack of system administrator resources slowed the development and deployment of hardware and software solutions to the data bottlenecks.

*Lessons:*

1. Dedicate personnel resources to develop flight database infrastructure early in the program.
2. Performance test database with high user loads to identify and rectify bottlenecks prior to launch.
3. Establish one master database for both vehicle test and operations.

### 16.1.1.4 Early integrated vehicle testing

*Issue Summary:* Perform early integrated tests of the space vehicle.

*Description of the GP-B experience:*

A system level test was performed late in the program. This test determined that the ECU was generating noise adversely impacting the SRE. Removing the ECU from the space vehicle for rework resulted in a program delay.

*Lessons:*

1. Perform perceptive system level tests as early as possible in during the integration of the vehicle.
2. Allow significant spans of time to perform integrated vehicle tests; plan time in the schedule to perform system rework if necessary. Hold tight to this contingency time – do not trade it off for schedule relief elsewhere in the program.

### 16.1.1.5 Configuration verification prior to vehicle power-on

*Issue Summary:* Verify vehicle configuration prior to power-on to avoid blowing fuses.

*Description of the GP-B experience:*

Power distribution fuses were blown during in-process testing of the space vehicle. The most likely cause was an in-work power harness with non-terminated wires touching the spacecraft structure when power was applied.

*Lesson:*

- Verify configuration of vehicle, especially un-terminated cables, to ensure that power can safely be applied without the risk of a short circuit.

### 16.1.1.6 Customer-contractor information exchange

*Issue Summary:* Establish customer-to-contractor information exchange protocols early.

### ***Description of the GP-B experience:***

The formal (contractual) relationship between NASA and Stanford, as well as Stanford's prime subcontractor, Lockheed-Martin, evolved over time as NASA Marshall worked to gain more technical and programmatic insight into the operations of the project. This led to difficulties with information exchange and peer-to-peer interaction while new protocols were established.

### ***Lessons:***

1. Establish and maintain open peer-to-peer communications and clear technical visibility between the customer (NASA) and contractors, including sub-contractors, from the beginning of the project.
2. Establish a secure information exchange vehicle, such as the internet-based MSFC Virtual Research Center (VRC) to allow unfettered access to program information to all authorized team members.
3. Create and maintain all program documentation in common electronically readable and searchable format (not image format).
4. Establish protocols to access and keep secure flight data between the Principal Investigator and the sponsoring organization (NASA), possibly including off-site tools for data viewing and analysis.

### **16.1.1.7 Disturbance from sunshade shutter**

***Issue Summary:*** Reduce the dynamic disturbance from sunshade shutter activations.

### ***Description of the GP-B experience:***

Large science gyro position excursions were observed during science telescope shutter activation. It was decided to leave the shutter open continuously to avoid these dynamic disturbances on the science gyroscopes. The primary root cause of this situation was insufficient testing and analysis of the off-the-shelf design for mechanical disturbances.

### ***Lessons:***

1. Perform detailed tests to determine the magnitude of mechanical disturbances on the integrated vehicle.
2. Minimize dynamic disturbances caused by mechanisms.

### **16.1.1.8 Telemetry data rates**

***Issue Summary:*** Add Capability to Dwell Telemetry on Payload Units for Higher Rate Data.

### ***Description of the GP-B experience:***

On GP-B there are four identical GSS units, and two SRE units. Obtaining continuous data for each of the 4 units at a high sample rate is not possible due to bandwidth limitations on the downlink. However, short-duration (10-20 second) full data rate snapshots have been effective in providing focused high rate telemetry.

### ***Lesson:***

- Consider a function in Flight Software to dwell telemetry on a subset of the high data rate telemetry via ground command. Create a "payload-checkout" downlink format that would contain a minimal number of monitors for all payload units, and a high sample rate for the one selected unit.

### **16.1.1.9 Command Database improvements**

***Issue Summary:*** Improvements to Command Database.

***Description of the GP-B experience:***

The command database contains a binary flag regarding the hazardous nature of each command. The Constraints and Restrictions database (CARD) contains text regards the reasons that certain commands might be hazardous. Since there was no relationship between the 2 databases manual effort was required to try and relate the 2 databases in text documentation.

***Lesson:***

- Integrate such databases as described above to automate manually intensive and time-consuming functions.

### **16.1.1.10 Software command and telemetry flexibility**

***Issue Summary:*** Create more flexible flight software command and telemetry data

***Description of the GP-B experience:***

We have limited space in telemetry processor interface tables (PITs) and telemetry downlink. Furthermore, the number of commands are limited, and we had an unclear understanding of everything that we are going to need to look at and/or change early in the design effort. Once the software is built there is not much flexibility to look at or change things that were not anticipated.

***Lesson:***

- Provide a set of monitors that can be commanded to look at any Flight Software (FSW) variable, provide a command that can change any FSW variable, as addressed by memory location.

### **16.1.1.11 Real-time displays and plots**

***Issue Summary:*** Capability to Build Telemetry Displays and Plots In Real-time.

***Description of the GP-B experience:***

Ground software displays and plots had to be defined and delivered with a ground software delivery. If they needed to be changed or new ones added the ground software had to be re-delivered with the new displays/plots.

***Lesson:***

- Build in the capability for the user to build displays/plots in real time.

### **16.1.1.12 Meteorite and orbital debris issues**

***Issue Summary:*** Meteorite and orbital debris mitigation should be part of core space vehicle design.

***Description of the GP-B experience:***

The GP-B M/OD (meteorite and orbital debris) study/analysis was a qualitative, comparative risk assessment, allowing the relative high-risk items to be addressed, as needed.



### **Lessons:**

1. M/OD design and analysis must be considered and evaluated early in the program/project life cycle from a complete system level approach, integrated with other systems such as structures, radiation shielding and thermal protection materials, and not on component by component comparison.
2. M/OD critical item lists may be different from failure effects mode critical items.
3. Several items were omitted from the “critical items” list, since they were functionally redundant, or impossible to shield at the point M/OD analysis was done in the program design (i.e., the dewar). For M/OD impacts, if items are located adjacent to each other, they may not always be considered redundant. For example, critical damage to the first item can generate debris, which could easily damage the second. Thorough assessments should be performed for every item on the spacecraft, considering location, redundancy, inherent shielding in the design, for the entire spectrum of environmental parameters (particle density, velocity, direction, size, shape, etc.). This kind of assessment must begin at the beginning of a program, not at the end, to assure items such as the dewar are, in fact, not high-risk items.
4. Some items were omitted from the list, such as the aft thruster plumbing. These lines are protected only by the MLI blanket surrounding them, and may cause mission failure if punctured and pressure is lost.
5. For a better understanding of the quantitative risk of GP-B, and similar spacecraft, hypervelocity impact data of flight-like items is required.

## **16.1.2 Lessons Learned from On-orbit Operations**

The following subsections summarized various lessons that the GP-B team learned from operations of the spacecraft on orbit.

### **16.1.2.1 Validation of pre-launch vehicle testing**

**Issue Summary:** Ensure that testing is backed-up by thorough data analysis & review.

#### **Description of the GP-B experience:**

One of two transponders (4<sup>th</sup> generation TDRSS transponder, GFE from NASA/General Dynamics) experienced low link margins immediately following launch, and this resulted in degraded performance on the GP-B forward omni antenna. This particular transponder was retrofitted to GP-B’s frequency prior to launch; it replaced a transponder with a low power output anomaly found during system testing.

The root cause was determined to be a low-level, out-of band oscillation in the second LNA stage that results in interference inside the transponder. The unit level test data suggests that the cause of the problem was induced during the retrofit but was not observed during retrofit testing. Thermal cycle testing was performed, but a thermal vacuum test was omitted with the rationale that a thermal cycle test in atmosphere would provide larger thermal stresses on the vehicle, and thus provide a more thorough test. Current data indicates that crystal oscillator performance and center frequency is sensitive to the pressure environment—this was not evident to the team at the time of the rework. Vehicle level testing did not find the problem because RF signal levels were unrealistically high, thus masking the link margin problem. At the vehicle level, the program review of the transponder test data was not able to uncover the problem, though there was evidence of the issue upon further, detailed review.

**Lessons:**

1. Perform all tests with a realistic signal levels as possible.
2. Review test data with manufacturer to ensure as-installed performance matches manufacturer's specifications. Projects with existing 4th Generation TDRSS transponders should review their test data before launch to ensure they do not have the same or similar problems.
3. Thermal-Vac unit testing is advisable when reworking frequency characteristics of a unit, given new understanding of crystal oscillator performance / frequency variation with pressure environment.
4. When testing a unit, a manufacturer should verify that the unit's performance is both within specifications and within family – once a design has been manufactured and tested multiple times, out of family test results are a good indication of possible manufacturing flaws. Additionally, requirements need to be evaluated to determine if they should be tightened to assure adequate on-orbit performance.
5. Test configurations should be optimized to monitor RF system performance at all times – the ability to flag anomalous telemetry and compare prime/redundant strings in real time is preferable.
6. Each test should have a set of objectives and success criteria (preferably measurable in the test data) defined prior to the test, and a post-test review should clearly establish that the test objectives and success criteria were met.

### **16.1.2.2 Independent configurability of redundant equipment**

**Issue Summary:** Independent configurability of redundant equipment is required.

**Description of the GP-B experience:**

GP-B's flight computer consists of two separate processors and is designed to be cold-redundant: only one computer may be powered at a time. Each processor holds an independent default parameter and macro set, identical at launch, but is modified as part of vehicle tuning operations. In the event of a major vehicle fault, the primary processor is shut down and the backup is cold-booted which then starts to execute to its default parameter set.

In this architecture, the only way to update the parameter and macro set on the backup processor is to perform a "fail-over" to the backup side, allow the processor to boot-up and run with the default parameters and macros, and then perform an update. This process is very disruptive to the mission, so much so in GP-B's case that we have elected not to update the backup-side configuration if and when some other event forces the vehicle to the backup system.

**Lesson:**

- Design the computer system so that all configurable elements for both processors (code, parameters, macros, etc.) may be loadable when either processor is running. This will ensure that, in the event of a processor failure, the backup system will control the vehicle with the same parameter set as the primary system.

### **16.1.2.3 Computer memory design, monitoring and error correction**

**Issue Summary:** Design of digital systems for single event upset (SEU) monitoring and correction.

**Description of the GP-B experience:**

GP-B has noted 34 separate anomalies relating to radiation induced single or multi-bit errors in its flight processor set. To a large extent, such events are unavoidable for spacecraft operating in a radiation environment. It has been noted that the multi-bit error rate (errors that are not correctable using the in-

processor EDAC parity word) is higher than originally predicted from pre-launch analyses. Any multi-bit error in the central processor has the potential of forcing a fail-over to the backup processor; this event seriously degrades the science data taken by the space vehicle.

**Lessons:**

1. Develop and test patch procedures to rapidly correct multi-bit errors via ground command. Develop detailed memory maps sufficient to allow the operations team to identify the potential criticality of any multi-bit error.
2. Design into the codes detailed SEU multi-bit error reporting schemes. The GP-B flight computer needs to use a software debug interface to read out the locations of multi-bit errors.
3. Choose memory and processor components based on on-orbit performance data when possible. The GP-B spacecraft suffered 34 multi-bit errors when pre-launch estimates for the susceptibility of the processor memory predicted only one during the mission. Detailed re-analysis during the mission brought to light flight data from another mission that agreed with our experience, but was not used by the team during processor memory selection (the data was published, but was not identified at that time). In lieu of this data, the team should have chosen memory with an established performance record.

#### **16.1.2.4 Ground simulator fidelity**

**Issue Summary:** Flight projects should pay careful attention to ground simulator fidelity.

**Description of the GP-B experience:**

GP-B uses an Integrated Test Facility (ITF) to test and verify flight codes and command sequences for use on orbit. The ITF is a combination of flight-like hardware, hardware dynamics simulators, and software simulators to model the operation of the vehicle as a whole in its on-orbit environment. This is a critical development and debugging tool for the project. While a good model for much of the spacecraft, not all interfaces are included and some that are provide only static values (they are not dynamic and thus do not respond to spacecraft operation as one would expect)

A number of anomalies have been identified that relate to issues generated due to lack of fidelity of the ITF. Command sequences operated differently on the vehicle because the ITF did not have sufficient fidelity to show response, or that the interfaces were incomplete and thus did not respond where the vehicle did.

**Lessons:**

1. Manage the simulation facility like the vehicle; devote significant program resources and use aerospace best practices to maintain the design and configuration of the system.
2. Carefully define and broadly communicate the scope of any vehicle or subsystem simulator. Simulators, by their nature, cannot be perfect and including all vehicle features may be prohibitive. However, a careful plan managed by a dedicated team of simulation supervisors – independent from the team developing the spacecraft – would improve fidelity.
3. Include as many interfaces as possible in the model. Wherever possible, use flight-like hardware rather than software models of systems. This includes cables built to flight prints.

#### **16.1.2.5 Gas thruster contamination**

**Issue Summary:** Gas thrusters are vulnerable to contamination.

### ***Description of the GP-B experience:***

Two of GP-B's gas thrusters were taken off line after failing; the identified root cause for both was foreign object contamination in thruster body which prevents the thruster from turning off properly. This observation has also been made by numerous other projects with a variety of gas thruster designs.

### ***Lesson:***

- Pay particular attention to contamination control and cleanliness of all systems which interface with the cold gas thruster system. Use ultra-high-vacuum and optics procedures to maintain cleanliness. Design in as much filtering as possible to limit migration of potentially damaging particles.

## **16.1.2.6 Attitude Reference Platform Stability**

***Issue Summary:*** The alignment sensitivity of the space vehicle's Attitude Reference Platform (ARP) was found to be significantly more sensitive to the vehicle's thermal environment than originally calculated.

### ***Description of the GP-B experience:***

The space vehicle was unable to maintain the required wide-band and roll-frequency pointing requirements due to a out of spec thermal sensitivity of the ARP to the space vehicle thermal environment. This effect significantly complicated the GP-B data analysis by requiring careful modelling of the effect during both guide star valid and invalid periods.

### ***Lesson:***

- For such a mission critical piece of hardware, do not rely solely on analysis-only methods of verification, but place the vehicle in a thermal environment (in thermal vacuum testing, for example) in excess of what is expected in orbit and verify the stability of the platform by direct testing. Formally require the vehicle subcontractor to perform this verification by test, in addition to analysis.

## **16.1.2.7 Formal anomaly resolution process**

***Issue Summary:*** A formal anomaly resolution process proved to be very effective.

### ***Description of the GP-B experience:***

GP-B developed, simulated, and practiced an Anomaly Resolution process during pre-launch preparations. The system developed (described elsewhere in this report) was very effective, and a number of lessons were learned and re-affirmed during the mission:

### ***Lessons:***

1. A formalized anomaly resolution process is very helpful to focus and guide investigations. Each anomaly was evaluated with a checklist to ensure all key issues were addressed. Recording of anomaly data and closure information was enforced with this process. It provided a framework in which to develop fault trees and form root cause investigations and assists in the rapid assimilation of new team members via clear processes and standards.
2. Leadership of the anomaly review board by senior, mission-cognizant technical staff critical for effective anomaly resolution. Senior technical staff, especially at the managerial level, have a deep understanding of the operation of the space vehicle and can effectively direct investigations in "high yield" directions. They have the broadest knowledge of the skills of the team members and are most effective in forming anomaly teams. ARB members that are senior managers from core subcontractors and technical

oversight groups (e.g. NASA) are able to draw on their organizations for expertise as needed. This leadership is distinct from program management; it is primarily focused on the technical issues surrounding the anomaly.

3. Employ flexible and easy-to-use record keeping tools. This provides flexibility in the method of recording anomalies and attacking problems, it does not significantly limit the team, and it requires minimal training required. They provide for easy dissemination of data by using popular, established file formats. Does not (generally) require special software applications installed on each users' system. A formal investigation process provides the structure needed to ensure relatively uniform record keeping.
4. Develop "custom" computer tools only after true mission needs are known. Experience in pre-launch simulations with tools developed a-priori found the tools lacking or utterly useless; they did not address the practical needs of anomaly investigation. Tools developed following detailed simulations with realistic anomalies fall closer to the mark. Some of the tools' features address large time intervals, features not generally brought out during a typical 1 to 3 day simulation; this should be taken into account during tool development. The ops, engineering, and analysis teams should recognize that some of their true needs will be clear only after launch. Ensure that the tools are flexible enough to be modified in short order.

### 16.1.2.8 Complexities of a 9-DOF satellite

**Issue Summary:** Design, test, and operation of a 9-DOF satellite must take into account the additional complexities and challenges that are inherent in such a system.

**Description of the GP-B experience:**

The Gravity Probe B satellite actively monitors and controls 9 interacting degrees of freedom during normal operation:

- 3 in orientation of the space vehicle to keep the tracking telescope pointed at the guide star and maintain a constant roll rate and fixed roll phase with respect to the orbital plane
- 3 in translation of the space vehicle to keep the vehicle in a drag-free orbit about the geometric center of the one of the science gyro's housing cavities (nominally Gyro 3)
- 3 in translation of the housing cavity with respect to the gyroscope rotor (nominally Gyro 3)

The other 9 degrees of translation freedom of the remaining 3 gyroscopes are slaved to the first 9 described above and do not significantly interact with the dynamics of the vehicle as a whole. Note that by design, the rotational degrees of freedom of the gyroscopes are not controlled.

Gyro 3 serves as the drag-free sensor (accelerometer) for the satellite. The three control efforts required to keep the housing centered around the gyroscope rotor are fed to the spacecraft. The spacecraft, in turn, applies compensating forces via its thruster set to null the forces felt by the gyroscope rotor, as shown in [Figure 16-1](#). These six degrees of freedom significantly interact. The gyroscope position control loop bandwidth (GSS) is made small to minimize disturbance torques on the rotor, and is on the order of 2 Hz. The spacecraft translation and pointing (ATC) bandwidth is of the same order and is limited by thruster authority and ATC processing. These two control loops interact significantly during operation.

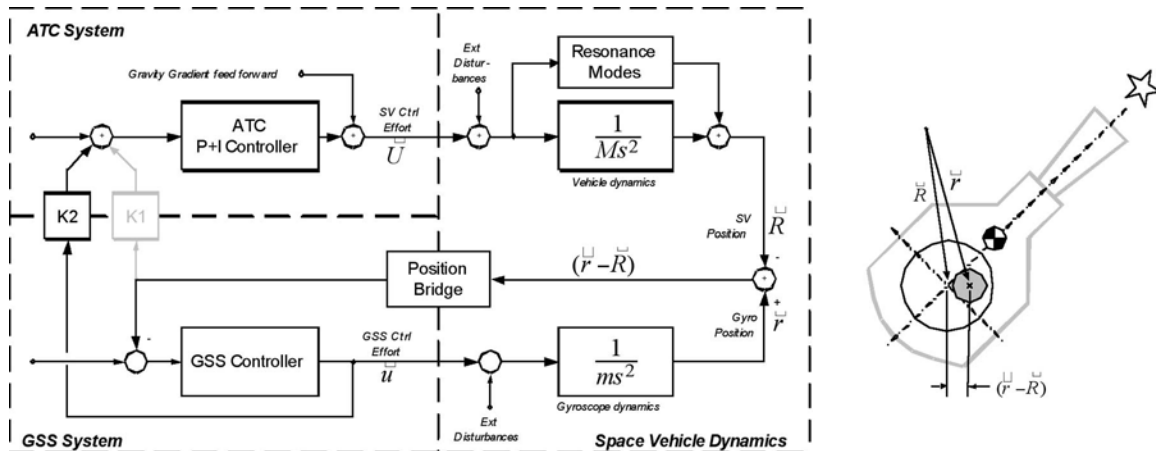


**Figure 16-1.** Six interacting translational degrees of freedom

Additional coupling between the translational DOF comes from orientation changes. The center of mass of the spacecraft is about 20 centimeters from the center of the drag-free sensor's housing. Thus, any change in orientation tends to be about the center of mass of the vehicle. The drag-free action nulls these orientation induced forces and thus moves the effective center of mass of the vehicle to the center of the drag-free sensor's housing. Again, the orientation control loop bandwidth is the same as the translation control bandwidth and thus this control loop, as well, interacts significantly with the gyro suspension control loop.

This brief overview shows, in outline form, that the 9 degrees of freedom are strongly coupled in normal operation and thus cannot be easily separated into simpler and isolated control subsystems.

**Lessons:**

Gravity Probe B has learned a number of important lessons about the design, test, and operation of a sophisticated 9 DOF space vehicle, and these can be extended to other similarly complex missions (ST7/GRS, STEP, LISA, ConX)

1. Interacting control systems must be tested together. While design is done using best engineering practices, often the full performance and complexity of the instrument can be assessed only through a joint test of the equipment. For missions such as GP-B, a representative ground test is not possible. Thus, final performance is assessed and adjusted on orbit. This was proven out on GP-B with the drag-free system, the attitude control system, and the gyro charge management systems.
2. Complex mission operations. Tuning up the space vehicle pointing and translation control loops required significantly more time than originally expected (4 months actual vs. an estimated two weeks), though significant effort was expended prior to launch to develop and test in simulation the on-orbit operations plan. Unmodelled vehicle dynamics required in-place system identification to allow the vehicle to perform to science-compatible levels while both the translation and orientation control was in operation. This mission complexity stems directly from the coupled nature of the 9 degrees of freedom.
3. Prepare for unanticipated behavior. The GP-B gyroscopes exhibited some unexpected behavior once on orbit, significantly: 1) the initial rotor charge was 450mV rather than the expected 100mV or less, 2) the polhode period of the rotor changed over time when it was expected to be constant, 3) patch charge



effects appear greater than ground testing would indicate. Though all of these subjects were studied extensively before launch, our best knowledge about how the instrument operated was not as accurate as anticipated. Only on-orbit operation made it possible to identify and mitigate these issues.

4. Invest in high fidelity simulations. Hardware in the loop simulators are critical to validate the overall effectiveness of a complicated scientific instrument and satellite system. Where the instrument cannot be operated on the ground, suitable high fidelity simulations with flight compatible interfaces must be developed. These simulators, however, must be vetted against flight data and updated once actual performance data are known. This is required to be able to resolve operational anomalies

### **16.1.3 IOC Observations by Lewis Wooten of NASA MSFC**

The GPB Operations team has done an exceptional job conducting the Launch and the IOC phases of the mission. The team is very intelligent, extremely dedicated, and has an unprecedented commitment to mission success. Plus, they are just a wonderful group of individuals to work with. I measure an operations team performance on its ability to learn from mistakes, and adapt quickly to change, and make the right subsequent decisions. On this basis, the GP-B team is one of the best in the business, and it is a team that will continue to make adjustments and improve along the way. With that being said, I have very little to offer in terms of suggestions for improvements at this phase of the mission. However, if I am pressed to come up with something, I have provided the following two observations for consideration.

#### **16.1.3.1 Execution of Pass Plan Change Request**

**Issue Summary:** The PPCR screening, approval, and execution process work extremely well for the majority of the cases, however it was not always consistent

**Description of the GP-B experience:**

Given the dynamic approach used in troubleshooting some of the ATC sub-system problems, many of their Pass Plan Change Requests (PPCR's) was executed without a through review with the flight team. There were times when they were pressed to send the commands before a specific communication pass expired, without being given the opportunity to participate in the screening process. The flight team are not "just button pushers", they should be aware of what, why, when, the expected results, and fallback plans before they given "a clear to execute." I did see this as a significant problem and it should not be an issue during the science mission phase.

**Lesson:**

Take the time necessary to get the flight team completely onboard before they are asked to execute a PPCR. Stanford modified the PPCR process to address this issue, which improved the process for a group that had a large number of issues. It allowed them to work the problems yet it maintained discipline while not becoming administratively difficult.

### **16.1.3.2 Training and certification of new flight controller**

*Issue Summary:* Stanford University has an excellent source of bright and “Gung Ho” young people to support the mission as flight controllers. As capable as these people are, there is no substitute for their preparation.

*Description of the GP-B experience:*

In fairness to the team, not enough time was allowed for them to be mentored and coached by the spacecraft lead subsystem engineers before these knowledgeable engineers rolled off the program. However, the mission controllers did a good job. The training and certification requirements for the initial team was much more structured and rigorous than it was for the latter team. This not a major concern during this phase since a vast majority of the high risk commanding and activities have been retired.

*Lesson:*

Make sure that the lead subsystem engineers meet at least once weekly for a 3-4 months period for mentoring and information exchange with their Stanford replacements. This was implemented at Stanford and worked well.

## **16.2 Selected Best Practices**

The following items were adopted by GP-B as “best practices” and we would like to affirm their effectiveness. In addition to a broad set of best practices brought forth from the collective wisdom of NASA, Lockheed-Martin, and the Stanford teams, these selected best practices are were particularly significant in day-to-day operations:

### **16.2.1 Design team transition to mission operations**

*Issue Summary:* Test and engineering team transition to mission operations ensured ownership.

*Description of the GP-B experience:*

The GP-B development and test teams transitioned to work on the mission operations team after launch. This reduced risk of mishaps and improved anomaly resolution efficiency. Expert knowledge was immediately available to efficiently resolve anomalies. Individuals had strong sense ownership, dedication, and responsibility for their components and subsystems.

*Best Practices:*

Retain and train design team for mission operations. Encourage a sense of “ownership” and continuity of responsibility for all individuals involved in the program. Provide long-term team stability. Take into account the conflict of hardware development versus mission operations development and manage it effectively

### **16.2.2 Mission planning flexibility**

*Issue Summary:* Mission planning flexibility provided needed timeline adjustments.

*Description of the GP-B experience:*

On-orbit anomalies and calibrations required mission planning to be flexible and responsive to changing program priorities. The mission operations team was extremely responsive to changes.

*Best Practices:*

Mission planning needs to be flexible and responsive to mission needs.

### 16.2.3 Control and communication of spacecraft configuration

*Issue Summary:* Maintain thorough configuration control and communicate changes.

*Description of the GP-B experience:*

Important documents are maintained on secure web pages for access by all team members. Baseline configuration was established and successfully managed.

*Best Practices:*

Establish and document program baselines for schedules, databases, timelines and technical information. Thoroughly review all changes and communicate changes as appropriate to team members

### 16.2.4 Effective use of databases

*Issue Summary:* Make good use of databases for requirement, test tracking and change control.

*Description of the GP-B experience:*

A Filemaker Pro database was used on GP-B for requirements/test tracking, change requests and many other operational information uses. This allowed quick cross-referencing of open items, requirements to test case information and many other uses. It was very useful to quickly generate different matrices for tracking purposes.

*Best Practices:*

This type of relational database is very useful for program management and control.

### 16.2.5 Inclusion of operations experts in hardware development

*Issue Summary:* Early insertion of operations experience into hardware development positively affects on-orbit operations.

*Description of the GP-B experience:*

Early insertion of skilled operations personnel into the hardware development process, notably the Experiment Control Unit (ECU), allowed the experience of what both procedure and hardware failures looked like, how to tell the difference between the two and the best way to recover from them. Experiences during development made functional test development more intuitive. The increased understanding allowed for more coherent test procedures and simpler code.

*Best Practices:*

Apply operations experience into development process for:

1. an intuitive set of flight procedures
2. experience in recognizing and efficiently resolving anomalies

### 16.2.6 Team member cross-training

*Issue Summary:* Team member cross training is effective.

***Description of the GP-B experience:***

Cross training of operations team members is being implemented and is effective. Observed cross training benefits include:

1. more people to provide gap coverage for planned and unplanned gaps in schedule coverage,
2. broadened team member knowledge and provides systems approach,
3. avoids single string team members,
4. minimizes team member fatigue caused by long work hours,
5. shared workload improves teamwork,
6. improves individual professional development

***Best Practices:***

Start cross training early and practice in mission simulations to ensure team is ready and flexible to handle changing mission needs.

## **16.2.7 Peer reviews in software development**

***Issue Summary:*** Including peer reviews during software development was effective in finding errors and saving time and money.

***Description of the GP-B experience:***

Peer reviews were introduced after several years of work as part of the U.S. Defense Department's Software Engineering Institute (SEI), based at Carnegie Mellon University, Level-3 certification. The peer reviews were preceded by formal training, which was beneficial. Also, we were careful not to include management in these reviews, as recommend by the process. As a result, code that was properly reviewed was very stable and experienced fewer test errors. Software peer reviews should be provided priority

***Best Practices:***

Peer reviews have shown their worth in finding errors early in the development cycle, which save time and money.

## **16.2.8 Minimizing program risks with formal risk management plan**

***Issue Summary:*** IA formal, regular risk review is effective at early identification and control of program risks.

***Description of the GP-B experience:***

GP-B instituted a high visibility risk steering committee, which program management used to evaluate and set overall program priorities. Risk groups met on a monthly basis; both Stanford and MSFC had independent risk evaluation teams that met regularly to share their assessments.

Hardware risks were evaluated using probability and impact of potential failure using a complete FMEA process; other program risks (budget, schedule, personnel) were evaluated using a similar method. The committees solicited advice from independent councils of experts to ensure our evaluations were correct. [Table 16-1](#) summarizes the five risk categories and definitions used by GP-B.

**Table 16-1.** GP-B Risk categories and definitions

Event	Likelihood	Consequences—Impact to Program if Event Occurs		
Risk Value	Chance of Occurrence	Program Cost Increase	Critical Path Impact	Technical Impact
5	Near certainty: (90%)	> \$8 M	> 60 days	Loss of mission.
4	Highly likely: (75%)	>\$4M but < 8M	31 - 60 days	Mission performance requirements degraded.
3	Moderate: (50%)	>\$1M but < 4M	8 - 30 days	Loss of some system level redundancy; no compromise of mission requirements
2	Low: (25%)	1M	1 - 7 days	Technical impact without loss of system level performance or redundancy.
1	Not likely: (10%)	\$100K	None	No compromise in mission performance or redundancy.

Based on potential impact to the program, each risk was evaluated using [Table 16-1](#) above as a guideline and assigned to one of three categories:

- **Mitigate.** Eliminate or reduce the risk by reducing the impact, reducing the probability or shifting the time frame. If a risk is marked as “mitigate” the user will input a summary of the mitigation plan in the Mitigation Strategy Summary field and a detailed plan if necessary.
- **Watch.** Monitor the risks and their attributes for early warning of critical changes in impact, probability, time frame, or other aspects. If a risk is marked as “watch”, the user will input triggers for changing that approach in the Contingency plan/trigger field and any other appropriate/applicable plans.
- **Accept.** Do nothing. The risk will be handled as a problem if it occurs. No further resources are expended managing the risk. If a risk is marked as “accept”, the user will be prompted to input a mandatory acceptance rationale along with any plans for handling the risk if it does occur.

Risks were promoted or demoted as program need or technical understanding evolved.

**Best Practices:**

A formal risk management process with strong management support significantly improves the efficiency and technical understanding of the project team.

## 16.3 Management Lessons from the Calder-Jones Report

Because some aspects of GP-B program management were unique among NASA programs, and because GP-B was viewed as a management experiment as well as a scientific experiment—as described in [Chapter 6, The GP-B Management Experiment](#)—in 2005, NASA Headquarters commissioned two former GP-B team members, Ned Calder from the Engineering Systems Division at MIT and Brad Jones, from the Aeronautics & Astronautics Department at Stanford University to research and prepare an independent study on the management of GP-B. Calder and Jones presented their finished report, entitled: **Gravity Probe B: A Management Study** to NASA in April 2006. A PDF copy of the complete Calder-Jones Report is available for downloading from the GP-B Web server at: [http://einstein.stanford.edu/pao/pfar/cj\\_report-apr2006.pdf](http://einstein.stanford.edu/pao/pfar/cj_report-apr2006.pdf).

Below is an edited summary of six areas of the GP-B Management Experiment, described on page 24 of the Calder-Jones Report, from which NASA can glean some lessons for management of other missions. The full report includes a more complete discussion of these six management areas.

### **16.3.1 Working With Organizational Asymmetries**

Each of the institutions involved in the development of GP-B—a research university, an aerospace company, and NASA—have different strengths and different cultures. These entities should be managed to leverage their unique strengths in a team context, while respecting their cultural differences. In a university environment, the goal is typically knowledge-driven; a university researcher will pursue a problem until it has been solved...no matter how long it takes. In aerospace companies, schedule and budget are typically the important management factors; product development is always constrained by time and budget, and this often leads to trade-offs. At NASA, risk management is often of greatest concern. The management lesson for a program like GP-B is the importance of leveraging these asymmetries to best advantage. For example, unique hardware such as the GSS could only be developed in a university environment, whereas more common flight hardware that resides on the critical path for a satellite launch—e.g. the Gas Management Assembly on the GP-B spacecraft—is best developed by a knowledgeable and experienced aerospace company.

### **16.3.2 Recognizing and Managing Critical Transition Points**

All NASA program progress through various stages or transitions where management requirements and styles need to change and/or adapt. Recognizing and planning for these transitional periods ahead of time can significantly streamline the program development process. This may include planning ahead for a management change at future transition point. For example, a program like GP-B was bound to reach a point where it was necessary to transition from an R&D program to a tightly-scheduled, minimal risk flight program. Planning for this transition ahead of time, including anticipated management changes from an R&D-oriented program manager to an aerospace-operations-oriented program manager, can facilitate making this transition more smoothly.

### **16.3.3 Adaptive Program Management.**

This is a corollary to Lesson #2 above. It is important to recognize that management styles and competencies must adapt as a program progresses through different stages in its life cycle. For example, in the case of GP-B, the operations management skills of Gaylord Green, which were very well suited for the flight program, were less germane when the program transitioned to the data analysis phase. GP-B senior management adapted to this phase shift in the program by changing program managers.

### **16.3.4 Maintaining Aerospace Knowledge at Universities**

Universities working on NASA programs need to acquire some degree of institutionalized aerospace system knowledge—that is, procedures, best practices, and lessons learned that have evolved in the aerospace industry and in government agencies from developing, launching, and operating spacecraft for over 50 years. This type of knowledge is essential to the success of any NASA mission, regardless of management structure, and when applied appropriately, it can reduce risk and facilitate progress. However, if such knowledge is applied by rote, without proper contextual forethought, it can actually impair progress. By definition, this type of knowledge is experiential, rather than academic; it cannot be taught in a classroom, but rather it must be learned in the process of actually building flight hardware and software. For this reason, once staff and/or students have been through the process of building flight hardware or working on a spacecraft, it behooves NASA and universities to value these trained individuals as an investment for future aerospace programs, rather than as sunk costs for a single project.

### **16.3.5 Managing Risk**

In a program such as GP-B, there is no such thing as zero risk. Rather, at any given phase of the program, it is important for NASA to determine what level of risk is acceptable and manage program risks accordingly. The creation of a formal risk-based management program, such as the one instituted jointly by MSFC, Stanford, and LMMS during the latter years of GP-B, allowed managers to take a high level look at overall program risks and to monitor the rate at which those risks were changing. This risk management plan included a graphic display that was easy to review at a glance, and it also defined a timeline for mitigating risks. Moreover, it provided guidance to NASA for determining the appropriate approach in mitigating program risks. Thus, a predictable process was developed whereby NASA support was scaled, based on the level of risk—i.e., the higher the risk the more support imparted by NASA. This not only enabled the GP-B team to receive an appropriate amount of support, but it also enabled the team to have reasonable expectations as to the level of support to expect from NASA for any given issue.

### **16.3.6 Funding Predictability**

To ensure the health and success of any program, NASA must strive to maintain funding commitments that have been specified and agreed to. In the case of GP-B, NASA's actual level of funding was substantially less than the agreed upon funding commitment for the years 1999-2002. Scheduling the development of flight hardware is intimately tied to expectations regarding available funds. Because funding expectations were not met during the critical years leading up to launch, the GP-B management team was forced either to unexpectedly cut or to restructure investments in technology development and support activities during this period. In turn, these trade-off decisions that were based on insufficient funding ultimately contributed to some of the technical and scheduling problems that emerged near the end of the program.





# A

## Gravity Probe B Quick Facts

---





## Gravity Probe B Quick Facts

<b>Spacecraft</b>	
Length	6.43 meters (21 feet)
Diameter	2.64 meters (8.65 feet)
Weight	3,100 kg (3 tons)
Power	Total Power: 606 Watts (Spacecraft: 293 W, Payload: 313 W)
Batteries (2)	35 Amp Hour
<b>Dewar</b>	
Size	2.74 meters (9 feet) tall, 2.64 meters (8.65 feet) diameter
Contents	2,441 liters (645 gallons) superfluid helium @ 1.8 Kelvin (-271.4°C)
<b>Telescope</b>	
Composition	Homogeneous fused quartz
Length	35.56 centimeters (14 inches)
Aperture	13.97 centimeter (5.5-inch)
Focal length	3.81 meters (12.5 feet)
Mirror diameter	14.2 centimeters (5.6 inches)
Guide Star	HR 8703 (IM Pegasi)
<b>Gyroscopes (4)</b>	
Shape	Spherical (Sphericity < 40 atomic layers from perfect)
Size	3.81 centimeter (1.5-inch) diameter
Composition	Homogeneous fused quartz (Purity within 2 parts per million)
Coating	Niobium (uniform layer 1,270 nanometers thick)
Spin Rate	Between 5,000 – 10,000 RPM
Drift Rate	Less than $10^{-11}$ degrees/hour
<b>Launch Vehicle</b>	
Manufacturer & Type	Boeing Delta II, Model 7920-10
Length	38.6 meters (126.2 feet)
Diameter	3 meters (10 feet)
Weight	231,821 kg (511,077 lbs or 255.5 tons)
Stages	2
Fuel	9 strap-on solid rocket motors; kerosene and liquid oxygen in first stage; hydrazine and nitrogen tetroxide in second stage
<b>Mission</b>	
Launch Date	April 20, 2004
Site	Vandenberg Air Force Base, Lompoc, CA
Duration	12-14 months, following 60-90 days of checkout and start-up after launch
<b>Orbit</b>	
Characteristics	Polar orbit at 640 kilometers (400 miles), passing over each pole every 48.75 min.
Semi-major axis	7027.4 km (4,366.8 miles)
Eccentricity	0.0014

---

**Gravity Probe B Quick Facts**

---

Apogee altitude	659.1 km (409.6 miles)
Perigee altitude	639.5 km (397.4 miles)
Inclination	90.007°
Perigee Arg.	71.3°
Right Ascension of asc. node	163.26°
<b>Measurements</b>	
Predicted Drift- Geodetic Effect	6,606 milliarcseconds or 6.6 arcseconds ( $1.8 \times 10^{-3}$ degrees)
Predicted Drift - Frame-Dragging	39 milliarcseconds ( $1.1 \times 10^{-5}$ degrees)
Required Accuracy	Better than 0.5 milliarcseconds ( $1.39 \times 10^{-7}$ degrees)
<b>Program</b>	
Duration	43 years from original conception; 40 years of NASA funding
Cost	\$750 million dollars

---

# B

## Spacecraft Data Chart

---



Photo by Russ Underwood, Lockheed Martin Corporation





# Space Vehicle Characteristics

## Mass Properties

Space vehicle mass w/ cont	3236.9	kg	
Space vehicle contingency	127.9	kg	4.0%
Space vehicle margin	88.9	kg	
Spacecraft mass w/cont	1271.7	kg	
Spacecraft contingency	57.5	kg	4.7%
Ballast	64.1	kg	
CM in z (fwd of point midway between SG 1 and PM)	69	mm	
Payload mass w/cont	1901.1	kg	
Payload contingency	70.4	kg	4.8%
Ix (at launch)	5003	kg-m <sup>2</sup>	
Iy (at launch)	4907	kg-m <sup>2</sup>	
Iz (at launch)	2253	kg-m <sup>2</sup>	

## Mass Trim Mechanism

Product of inertia (20 kg masses)	8.35	kg-m <sup>2</sup>	
Radial COM (20 kg masses)	3.69	mm	

## Flight Software

(32 bit RISC processor)

CPU throughput	70%		
EEPROM	44%		
RAM (Op system)	27-49	%	
ATC	10	Hz	
Science data	1	Hz	

## Solid State Recorder

Memory (EOL)	1.5	Gbits	
Record rate	26,400	bps	

## Thruster System

Operates over porous plug 2 to 16 mg/sec range at nominal 6.5 mg/sec from dewar

Force, x	6.3	mN	
Force, y and z	8.3	mN	
Torque, x	18	mNm	
Torque, y	14	mNm	
Torque, z (roll)	8.5	mNm	

At 8 mg/sec from dewar:

Force per thruster	8.3	mN	
Bandwidth	100	Hz	

## Disturbance Forces

Gravity gradient	0.98E-3	N peak (rss)	
	1.26E-3	N rms (rss)	
Aero (1 sigma density)	1.5E-3	N peak (rss)	
	1.3E-3	N rms (rss)	
Center of Mass offset force	0.15E-3	N rms (0.3 rpm)	

## Electrical Power

Payload power (unregulated)	254	W	(11%)	cont. included
Spacecraft power (unregld.)	293	W	(6%)	cont. included
SV power required (normal Science)	547	W		
Load power margin (GaAs)	156	W	(29%)	best/worst case season
Batteries	2-35	AH		
Eclipse DOD not to exceed:	40%			

## Communication

(750km; 3dB link margin Rqmt)		FWD	AFT	link	Margin	
TDRSS MA forward link	125	bps	3.9	dB	3.9	dB (75 deg)
TDRSS MA return link	1024	bps	3.0	dB	3.0	dB (50 deg)
TDRSS SA forward link	2000	bps	3.5	dB	3.5	dB (70 deg)
TDRSS SA return link	2048	bps	3.9	dB	3.9	dB (70 deg)
GN downlink (11.3 meter)	2.5	Mbps	9.7	dB	6.1	dB (90 deg)
EGSE (system test)	30.696	kbps				

## Attitude and Translational Control System

### Attitude

Pitch/yaw pointing (GV)	12	marcsec rms	
Pitch/yaw pointing (GI)	4	arcsec rms	
Roll pointing error	7	arcsec rms	
Roll rate error	0.3E-5	rpm rms	
Roll rate range	0 - 1	rpm	
Roll rate range (nominally)	0.3-0.5	rpm	
Attitude BW w/ control gyro	0.15	Hz	
Attitude BW w/o control gyro	0.05	Hz	
Attitude BW Roll	0.066	Hz	

### Translational

Proof mass error	15	nm rms	
Translational BW	0.5	Hz	

## Disturbance Torques

Gravity gradient	2.2E-3	Nm peak (rss)	
	1.3E-3	NM rms (rss)	
Magnetic	2.4E-3	Nm peak (rss)	
	1.0E-3	NM rms (rss)	
Aero (1 sigma density)	1.1E-3	Nm peak (rss)	
	0.6E-3	NM rms (rss)	
Cross product torque	0.26E-3	Nm rms (0.3 rpm)	

## Structure

All margins of safety positive

Factor of 2 for spacecraft truss

Fundamental lateral frequency	9	Hz	
Fundamental lateral freq. (axial)	25.3	Hz	
Lowest solar array deployed freq.	1	Hz	
Lowest SV structure freq. on orbit	>10	Hz	

## Dewar Control

Pressure accuracy (sensor spec)	0.02	Torr	
Orbit mass flow (67% worst atm)	4.48	mg/s	
Worst case temperature variation			
(3 sigma density, 1% ullage)	±1	mK	

## Orbit

Polar inclination

Altitude is 646 km ±3 km

Eccentricity (circular) 0.001

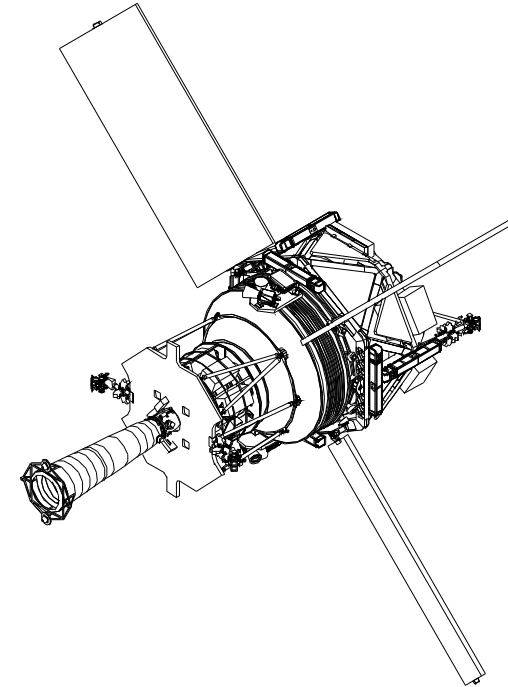
## Thermal

Avg. dewar shell temp. 227 K

## Reliability

At 18 months: 0.966  
At 3 years: 0.922

Mean mission duration 2.95 yrs





# C

## Weekly Chronicle of the GP-B Mission

---





This appendix contains a complete compilation of all the GP-B weekly highlights/email updates posted from three weeks prior to launch on April 2, 2004, through the end of the Post-Science Instrument Recalibration Phase of the mission on September 30, 2005.

## C.1 Pre-Launch Mission Phase: 4/2/04 – 4/18/04

---

### 2 April 2004—Pre-Launch Briefing at NASA Headquarters

The official pre-launch Gravity Probe B mission and science briefing was held this past Friday, April 2, 2004 at 1:00 PM Eastern Daylight Time at NASA Headquarters in Washington, D.C. The participants in the briefing (pictured from left to right in the photo) were Anne Kinney, Director of Astronomy/Physics Division, NASA Headquarters; Rex Geveden, Program Manager, GP-B and Deputy Director, NASA's Marshall Space Flight Center in Huntsville, Alabama; Francis Everitt, GP-B Principal Investigator at Stanford University, Stanford, California; Bradford Parkinson, GP-B Co-Principal Investigator at Stanford University, Stanford California; Kip Thorne, Feynman Professor of Theoretical Physics, California Institute of Technology, Pasadena, California



Following this press briefing, stories about Gravity Probe B appeared in a number of newspapers around the country. For example, the Boston Globe carried a front-page story. On the Internet, a story about GP-B, written by Associated Press science writer Andrew Bridges, became one of Saturday's most popular stories on Yahoo News.

The official Gravity Probe B launch date is Saturday, April 17, 2004 at 10:09 AM Pacific Daylight Time, from Vandenberg Air Force Base in Southern California.

Early Thursday morning, the Gravity Probe B Program reached a major milestone: the GP-B space vehicle was moved on a trailer from the clean room, where it has resided since last summer, to the launch pad at Space Launch Complex 2 (SLC-2). At the launch pad, the space vehicle was hoisted up the side of the Mobile Service Tower (MST) to the "White Room" at the top, where it was mated to the 2nd stage booster rocket. Current dewar temperatures are not available this week, but the dewar is 95.5% full. Last Friday, the temperature of the dewar's main tank was 1.7525K, and the Guard Tank level was 48.5%. All launch preparations are currently proceeding on schedule, and we are "Go" for launch on April 17th.

---

### 7 April 2004—GP-B Launch Postponed Two Days

The official Gravity Probe B launch date has been postponed by two days to Monday, April 19, 2004 at 10:01 AM Pacific Daylight Time, from Vandenberg Air Force Base in Southern California. The additional time is necessary to allow engineers to troubleshoot an apparent short in launch pad ground support equipment. This equipment is needed for a safe and secure launch of the GP-B spacecraft.

Today, the temperature of the dewar's main tank was 1.7744K, and the dewar is 95.5% full. The Guard Tank level was 88.6%. Problems with the connection between the ground service equipment and the booster have caused a two-day delay in the launch countdown.

---

### 12 April 2004—Ground Support Problems Fixed, Launch is "Go" for April 19 Launch

The problems which delayed the April 17th launch date by two days were closed out, and technicians worked through the Easter holiday weekend to keep GP-B on track for launch on Monday, April 19th. Today, the temperature of the dewar's main tank was 1.787K, and the dewar is 95.5% full. The Guard Tank level was 66.5%. On Saturday, ordnance was installed on the solid rocket boosters, and compatibility testing between the boosters and the space vehicle was carried out. Tonight, a visual inspection is in process to ensure that all items unnecessary for launch have been removed from the launch vehicle premises.

---

### 14 April 2004—Technicians Begin Installation of Payload Fairing

Today, technicians began installing the payload fairing—the "nose cone" at the top of the launch vehicle that surrounds the spacecraft during launch. Four minutes and 41 seconds after launch, the fairing will split apart and be jettisoned into space, in preparation for the second stage rocket to position the spacecraft in its circular polar orbit and proper orientation towards the guide star, IM Pegasi.

The official Gravity Probe B launch date is Monday, April 19, 2004 at 10:01 AM Pacific Daylight Time, from Vandenberg Air Force Base in Southern California.

Yesterday, Gravity Probe B was the lead story in the Science section of the New York Times, (you'll need to register on the NY Times site to view the story on their Web site), and it was one of the front page stories in the San Jose Mercury News. In addition, a story about GP-B appeared on the New Scientist Web site yesterday.

---

## 16 April 2004—Vehicle is Prepared for April 19 Launch

Installation of the payload fairing—the “nose cone” at the top of the launch vehicle that surrounds and protects the spacecraft during launch has been completed. Four minutes and 41 seconds after launch, the fairing will split apart and be jettisoned into space, in preparation for the second stage rocket to position the spacecraft in its circular polar orbit and proper orientation towards the guide star, IM Pegasi.



The launch vehicle, with its payload and fairing at the top, are still surrounded by the Mobile Service Tower (MST). Very early Monday morning, the MST will be rolled away, leaving the launch vehicle standing in readiness as the launch countdown begins.

Yesterday, the temperature of the dewar's main tank was 1.797K, and the dewar was 95.5% full. The Guard Tank level was 76.6%.

A Flight Readiness Review (FRR) was successfully conducted yesterday, and Gravity Probe B is “Go” for launch.

Today, Gravity Probe B Co-Principal Investigator, John Turneaure, was interviewed by Ira Flatow on NPR Talk of the Nation—Science Friday. This Sunday evening, April 18th, a feature story about Gravity Probe B and principal investigator, Francis Everitt, is scheduled to air on ABC World News Tonight.

## C.2 GP-B Launch: 4/19/04 – 4/20/04

---

### 19 APRIL 2004—GRAVITY PROBE B LAUNCH POSTPONED FOR 24 HOURS

A launch hold was called three minutes before the scheduled liftoff of the Gravity Probe B spacecraft. Marginal upper level wind conditions had been observed throughout the countdown, and there was insufficient time to confirm that the Delta II rocket had the correct wind profile loaded for the data from the final weather balloon. The launch of Gravity Probe B has been re-scheduled for tomorrow (Tuesday), April 20, 2004 at 9:57 AM Pacific Daylight Time, from Vandenberg Air Force Base in South-central California. The GP-B satellite has only a one-second launch window. Why a one-second launch window? Find out on our FAQ Page.

---

### 20 APRIL 2004—GRAVITY PROBE B LAUNCHED SUCCESSFULLY TODAY AT 9:57:24 AM PDT!

At 9:57:24 AM PDT today, the Gravity Probe B spacecraft was successfully launched from Vandenberg Air Force Base in South-central California. The countdown went smoothly, and at the moment of launch, a packed auditorium here at Stanford University broke into cheers and applause.

The launch is proceeding perfectly, exceeding all of our expectations. The initial visual images from the various tracking stations were heart-warming and beautiful to behold—surpassed perhaps only by the extraordinary images from the two cameras on-board the second stage, which showed the separation of the spacecraft from the launch vehicle more than 300 miles above the Earth.

**Following the launch on the Internet:** The launch was Webcast on NASA Direct, as well as on NASA TV on the Web. To view NASA Direct, see <http://www.ksc.nasa.gov/nasadirect/index.htm>. For information about viewing NASA TV on the Web, using either the Real Player or Windows Media Player, see <http://www.nasa.gov/multimedia/nasatv/index.html>. You'll find a list of alternate sources of NASA TV on the Web at [http://www.nasa.gov/multimedia/nasatv/MM\\_NTV\\_Web.html](http://www.nasa.gov/multimedia/nasatv/MM_NTV_Web.html). Another very comprehensive source of information is the Spaceflight Now Web site: <http://www.spaceflightnow.com/delta/d304/status.html>.

We will send out more updates as new information becomes available.







## C.3 IOC Mission Phase: 4/21/04 – 8/26/04

---

### 24 APRIL 2004—MISSION UPDATE: DAY 4

At 9:57:24 am Pacific Daylight Time on Tuesday, April 20, 2004, the Gravity Probe B spacecraft had a picture-perfect launch from Vandenberg Air Force Base in South-central California. The Boeing Delta II rocket hit the exact center of the bull's eye in placing the spacecraft in its target polar orbit, 400 miles above the Earth.

At approximately one hour eleven minutes, the spacecraft's solar arrays deployed, and shortly thereafter, the on-board cameras treated all viewers, via NASA TV, to the extraordinary sight of the separation of the spacecraft from the second stage rocket, with a portion of the Earth illuminated in the background.

After three days in orbit, all Gravity Probe B systems are performing as planned. The solar arrays are generating power, and all electrical systems are powered on. The spacecraft is communicating well with the Tracking and Data Relay Satellite System (TDRSS) and supporting ground stations.

All four Gyro Suspension Systems have now been activated. In addition, a lift check was successfully accomplished for gyros #2 and #3. This was the first ever levitation of a Gravity Probe B gyro on "orbit."

The spacecraft's Attitude Control System is maintaining initial attitude control. Fine attitude control should be achieved when thruster calibrations have been completed. After that, the ultra-precise science telescope will be locked onto the Gravity Probe B guide star, IM Pegasi, to within a range of 1/100,000th of a degree.

The spacecraft is being controlled from the Gravity Probe B Mission Operations Center, located here at Stanford University. The Initialization & Orbit Checkout (IOC) phase of the Gravity Probe B mission is planned to last 45-60 days, after which the 12-month science data collection will begin.

---

### 30 APRIL 2004—MISSION UPDATE: DAY 10

Gravity Probe B's many successes in its first week on orbit will ensure a smooth transition into the science phase of the mission and the best possible experimental accuracy.

The spacecraft has already achieved a science mission orbit, within the plane of the Guide Star, IM Pegasi, and its inclination error is one sixth of that expected.

In the quiet environment of space, the gyro readout system is performing significantly better than it did during any ground testing. All four SQUIDs (Super-conducting Quantum Interference Devices) are fully functional and have detected calibration signals with high precision. Noise levels are below the allowable mission requirements.



The electrical power system is fully functional and is providing adequate power for all operating conditions. Eclipse operation (when the spacecraft is in the shadow of the Earth) meets all requirements. There is no evidence of solar array motion that might disturb the experiment.

All other spacecraft subsystems are fully functional. All four gyros have been checked out and are performing well. They have all been electrically suspended in analog mode; digital suspension activities will commence shortly. The team is in the process of updating data tables for the Gyro Suspension System (GSS) to aid in achieving digital suspension of the gyros.

The spacecraft's Attitude Control System (ATC) is maintaining a stable attitude (relative position in orbit—pitch, yaw and roll). We expect to lock onto the Guide Star, IM Pegasi, within a few days, after completing on-orbit re-calibration of the spacecraft's 16 micro thrusters. During thruster re-calibration, it was observed that one of the redundant micro thrusters was stuck partially open. It was isolated and removed from the system, and the flow of helium to the remaining micro thrusters has been adjusted to compensate for its removal.

Overall, one week after launch, it appears that all of the spacecraft's subsystems are functioning well—meeting or exceeding mission requirements, in preparation for beginning the science experiment.

---

#### **7 MAY 2004—MISSION UPDATE: DAY 17**

As of Mission Day #17, the Gravity Probe B spacecraft continues to perform well, and we are expecting a smooth and successful transition into the science phase of the mission.

The spacecraft remains in a science mission orbit, within the plane of the Guide Star, IM Pegasi. The gyro readout system performance continues to exceed expectations, and all four SQUIDs (Superconducting Quantum Interference Devices) are functional and calibrated, with very low noise levels. Power and thermal systems meet all of our mission requirements. All spacecraft subsystems continue to perform nominally.

All four gyros have been electrically suspended in analog mode, and gyros #1, #2 and #4 are now digitally suspended; we expect gyro #3 to transition from analog to digital suspension shortly.

Last weekend, the spacecraft was hit by radiation while passing over the Earth's south magnetic pole. This radiation caused data errors in the spacecraft's primary (A-side) computer, which exceeded its capacity for self-correction. Thus, by design, the spacecraft automatically switched over to the backup (B-side) computer, placed the spacecraft in a "safe" mode, and put the planned timeline of events on hold.

The automatic switch over from primary to backup computer worked flawlessly. The GP-B mission operations team has since re-booted the primary computer, restored its data parameters, and then commanded the spacecraft to switch back to the primary computer, which is once again in control. During this incident, the GP-B science instrument continued to function perfectly—as expected—with all four gyros remaining suspended in their assigned modes.

The spacecraft's Attitude Control System (ATC) is continuing to maintain a stable attitude (relative position in orbit—pitch, yaw and roll). However, the process of locking onto the Guide Star, IM Pegasi, has been delayed a few days by the South Pole radiation incident.

---

#### **14 MAY 2004—MISSION UPDATE: DAY 24**

As of Day #24 of the mission, all spacecraft subsystems are functioning properly. The orbit is stable and meets our requirements for next month's transition into the science phase of the mission, upon completion of the spacecraft initialization and orbit checkout. Furthermore, Gravity Probe B has successfully achieved several important milestones over the past week.

All four gyroscopes have now been digitally suspended for over a week. At launch, the gyros were unsuspected. Once on orbit, each gyro was first suspended in analog mode, which provides coarse control of the gyro's suspended position within its housing. Analog mode is used primarily as a backup or safe mode for suspending the gyros. Each gyro was then suspended digitally. The digital suspension mode is computer-controlled; it puts less torque on the gyros than analog mode and enables their position to be controlled with extremely high precision.

At the end of last week, the Gravity Probe B team practiced Low Temperature Bakeout (LTB), in which discs of sintered titanium (very tiny titanium balls, smaller than cake sprinkles) are "warmed up" a few Kelvin, thereby attracting helium molecules to them. This process will remove any remaining helium from the gyro housings after full gyro spin-up. Last week's practice LTB procedure had the added benefit of imparting a very small amount of spin-up helium gas to the gyros. Following the practice LTB, the SQUID gyro read-out data revealed that gyro #1, gyro #3, and gyro #4 were slowly spinning at 0.001, 0.002, and 0.010 Hz, respectively (1 Hz = 60 rpm). Amazingly, the Gyro Suspension Systems (GSS) were able to measure gas spin-up forces at the level of approximately 10 nano-newton (10<sup>-8</sup> N). This means that the GP-B science team is able to interpret data from gyro spin rates four to five orders of magnitude smaller than what was planned for the GP-B science experiment.

Earlier this week, the GP-B spacecraft flew "drag-free" around gyro #1, maintaining translation control of the spacecraft to less than 500 nanometers. The term, "drag-free," means that the entire spacecraft literally floats in its orbit—without any friction or drag—around one of the gyros. Pairs of proportional micro thrusters put out a steady and finely controlled stream of helium gas, supplied by the dewar, through its porous plug. Signals from the Gyro Suspension System (GSS) control the output of the micro thrusters, balancing the spacecraft around the selected gyro. The initial drag-free Control (DFC) checkout lasted 20 minutes, as planned. Then, a two-hour DFC session was tested, during which the spacecraft roll rate was increased and then returned to its initial rate, maintaining drag-free status throughout the test. Achieving DFC indicates that we are on track to meet the science mission control requirements.

Last, but not least, early this week, the Attitude & Translation Control system (ATC) successfully used data from the on-board star sensors to point the spacecraft towards the guide star, IM Pegasi. This was the final step before initiating the dwell scan process, a series of increasingly accurate scans with the on-board telescope that enable the ATC to lock onto the guide star. Two days ago, the telescope's shutter was opened, and a first dwell scan was completed. We are now in the final stages of repeating the dwell scan to home in on the guide star and lock onto it. Photo: ATC Engineers with the Attitude Control system before it was placed on the spacecraft, circa May 2001.

---

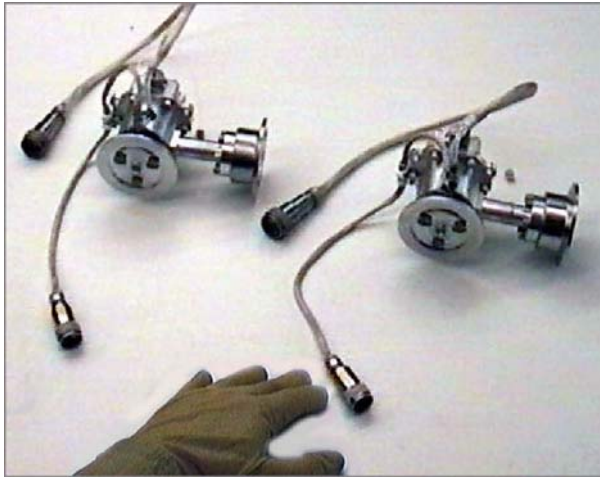
## 21 MAY 2004—MISSION UPDATE: DAY 31

One month into the mission, all spacecraft subsystems are continuing to perform well. The spacecraft's orbit remains stable and meets our requirements for next month's transition into the science phase of the mission, upon completion of the spacecraft initialization and orbit checkout. The four gyroscopes are suspended, and we have indications that they are rotating slightly in their housings.

Last weekend, the team successfully performed a procedure to reduce magnetic flux that had built up around the gyroscope rotors (spheres). Magnetic flux is a measure of the number of magnetic field lines penetrating a surface. To ensure that the SQUID readouts receive clean signals from the gyroscopes and to provide the highest possible degree of accuracy during the GP-B science experiment, any magnetic flux around the gyroscope rotors must be minimized.

We reduce magnetic flux by turning on heaters and flowing helium gas, warmed to 10 Kelvin, through the Probe. This process also drives off any residual helium remaining in the well of the dewar, where the Probe sits. The flux reduction procedure went smoothly, and when it was completed, the level of trapped flux remaining within the gyros was almost imperceptible. In fact, gyroscope #4, which previously had the highest amount of trapped magnetic flux of all the gyros now has the lowest level.

The flux reduction procedure added heat to the dewar, thereby increasing the pressure inside to its maximum allowable level. The increased pressure during this stress period caused some of the spacecraft's micro thrusters to become unstable, resulting in the spacecraft pointing in the wrong direction and triggering a "safemode."



The 16 micro thrusters are arranged in clusters of four, and local feedback loops within each cluster enable the thrusters to communicate with each other and automatically adjust their flow rates. Ground commands were issued to isolate the unstable thrusters, which resolved the thruster cross-talk issue and enabled the spacecraft to re-orient itself. The thrusters are now functioning properly, the spacecraft's attitude has been corrected, and it is once again pointing towards the guide star.

The flux reduction operation and subsequent thruster instability and attitude problems has delayed locking the spacecraft onto the guide star, which will be our next major activity. While we have used up some of the contingency days built into the Initialization & Orbit Checkout (IOC) schedule, this phase of the Gravity Probe B mission is

still on track for completion within 60 days after launch, at which time the 13-month science data collection will begin. This will be followed by a two-month final calibration of the science instrument assembly.

---

## 28 MAY 2004—MISSION UPDATE: DAY 38

At five weeks past launch, the Gravity Probe B team is now about half way through the Initialization and Orbit Checkout (IOC) phase of the mission. Thus far, the team has successfully transmitted over 5,000 commands to the spacecraft, which remains healthy on orbit. All spacecraft subsystems are continuing to perform well. The spacecraft's orbit is stable, meeting our requirements for next month's transition into the science phase of the mission. All four gyros are now digitally suspended, and the team is in the process of locking the on-board telescope onto the guide star, IM Pegasi.

This past week, the team began spinning up the gyros. During this complex and delicate process, which spans the entire second half of IOC, each of the four gyros undergoes a series of spin-up and testing sequences, the first of which gets the gyros spinning—but at a very slow speed. Because the correct performance of the gyros is critical to the success of the experiment, the team is proceeding through the spin-up process slowly, painstakingly monitoring and checking the performance of the gyros throughout the process.

In preparation for spin-up, the digital suspension system for each gyro was first tested. This was accomplished by suspending each gyro in the center of its housing, electrically "nudging" it slightly off center in one of eight directions (the corners of a cube), and monitoring its automatic re-centering. This checkout was first performed under low voltage conditions (fine control) and then under high voltage conditions (secure hold). Photo: The Forward GSS unit prior to installation and flight, circa May 2001.

To begin the actual spin-up process, ultra-pure helium gas was flowed over gyro #1 and gyro #4 for 15 seconds, which started them spinning at approximately 0.125 Hz (7.5 rpm). While these gyros were slowly spinning, the suspension test was repeated under high voltage conditions on gyros #2 and #3. During this high voltage suspension test on gyro #3, the team discovered an error in its command template, which turned off the high voltage amplifier to gyro #1 and caused it to lose suspension. There was no damage to gyro#1.

More than 1,000 commands have now been sent to the Gyro Suspension System (GSS), and this was the first error found. Discovering an error in these numerous, intricate command templates was exactly the kind of situation that the painstaking gyro spin-up process was designed to identify; it enabled the team to correct the command template for gyro #3 without serious consequences. Also, as a further precaution, the team has thoroughly reviewed the command templates for the remaining three gyros. Gyros #2 and #3 have now been spun-up to 0.26 Hz (15 rpm) and 0.125 Hz (7.5 rpm) respectively without incident, and gyro #1 is currently being spun-up, as well.

Over the past week, much progress has been made towards the goal of locking the spacecraft's on-board telescope onto the guide star. The pointing error of the spacecraft has been reduced to within 385 arc-seconds (0.11 degrees). This allows the on-board telescope to see the guide star over a portion of a spacecraft roll cycle. The team is in the process of fine-tuning the spacecraft's attitude by adjusting the navigational gyroscope in the Attitude and Translation Control (ATC) system, so that the telescope will be able to see the guide star throughout the entire spacecraft roll cycle, and the team hopes to lock onto the guide star by the beginning of next week.

---

#### 4 JUNE 2004—MISSION UPDATE: DAY 45

After six weeks in orbit, the spacecraft continues to be healthy, with all subsystems performing well. Over the past two weeks, with the arrival of summer in the Northern Hemisphere, the spacecraft emerged from being partially eclipsed by the Earth each orbit to being in full sunlight continuously. The spacecraft's orbit is stable and meets our requirements for transition into the science phase of the mission. All four gyros remain digitally suspended, and all are spinning very slowly. Progress in locking the on-board telescope onto the guide star, IM Pegasi, has been slower than anticipated, but this afternoon, as these highlights were being posted, we achieved this important milestone.

This past week, the team started performing a highly methodical and painstaking series of calibration tests on the four science gyroscopes. These tests begin at very low gyro spin rates of 0.333 Hz (20 rpm) or less. This enables the team to exercise and check out the software command templates that control the tests, without risk of damage to the gyro rotors or housings, which could occur at higher speeds. We accomplish these calibration tests by briefly applying voltages asymmetrically to the suspension electrodes on a given gyro, causing that gyro rotor (sphere) to move off center by a few micrometers (10-6 meters) or less, and then re-centering it. Photo: A backlit housing half of a gyroscope. The three oval shapes (at 1 o'clock, 5 o'clock and 9 o'clock, on the picture) are where the electrodes are placed.

During these initial calibration tests, the team discovered that the performance characteristics of the gyros on orbit are slightly different from the simulator predictions on which the original command templates were based. As a result of these differences, during one of the initial tests, gyro #4 touched one of its electrodes and stopped spinning. A simple modification to the spin-up command templates is now in process. Once the on-orbit performance characteristics of each gyro is well understood, the team will repeat these tests at gradually increasing spin rates.

The team also exercised the Ultraviolet Discharge procedure to reduce the electrostatic charge, which builds up on the gyro rotors over time. The rotors build up a charge in two ways: first, the process of suspending the rotors electrically deposits some charged particles on them, and second, protons from the sun are constantly bombarding the spacecraft, especially over the South Atlantic Ocean—the so-called “South Atlantic Anomaly”—and some of these protons strike the rotors and leave a residual charge on them.

We use ultraviolet light to remove the build-up of electrostatic charge from the gyro rotors. Each gyro housing is fitted with fiber optic cables that run from the gyro housings, up through the top hat of the Probe and out to an ultraviolet light source in the Experiment Control Unit (ECU) box, mounted on the spacecraft frame. UV light is beamed through the fiber optics onto the gyro rotors to discharge them. Reducing the level of charge is important because it increases the sensitivity and accuracy of the Gyroscopic Suspension System (GSS).

---

#### 11 JUNE 2004—MISSION UPDATE: DAY 52

On its 52nd day in orbit, the spacecraft continues to be in good health, with all subsystems performing very well. The spacecraft's orbit, which will remain in full sunlight through August, is stable and meets our requirements for transition into the science phase of the mission. All four gyros are digitally suspended and have passed several very slow-

speed calibration tests. Furthermore, the science telescope is locked onto the guide star, IM Pegasi, and we have verified that it is locked onto the correct star

Over the past two weeks, through a combination of software modifications, revised procedures, and commands sent directly to the spacecraft, considerable progress has been made in adjusting the Attitude and Translation Control system (ATC) to properly maintain the spacecraft's attitude (pitch, yaw, and roll) in orbit. The ATC system accomplishes this important job by controlling the flow of helium gas, continually venting from the dewar, through the spacecraft's micro thrusters. This system is critical to the success of the mission because it maintains the required roll rate of the spacecraft, it keeps the spacecraft and science telescope pointed at the guide star, and it keeps the spacecraft in a drag-free orbit. Thus, the team is particularly gratified to now have the ATC functioning reliably, with the science telescope locked onto IM Pegasi.

The process of locking the science telescope onto IM Pegasi started with star trackers on either side of the spacecraft locating familiar patterns of stars. Feedback from the star trackers was used to adjust the spacecraft's attitude so that it was pointing to within a few degrees of the guide star. The telescope's shutter was then opened, and a series of increasingly accurate “dwell scans” was performed to home in on the star. Since the spacecraft is rotating along the axis of the telescope, imbalance in the rotation axis can cause the guide star to move in and out of the telescope's field of view. Feedback from the telescope was sent to the ATC system, which adjusted the spacecraft's attitude until the guide star remained focused in the telescope throughout multiple spacecraft roll cycles. The ATC was then commanded to “lock” onto the guide star. Photo: The GP-B Star Tracker before installation onto the spacecraft, circa April 1999.

Finally, to verify that the telescope was locked onto the correct guide star, the micro thrusters were used to point the spacecraft/telescope at a known neighboring star, HD 216635 (SAO 108242), 1.0047 degrees above IM Pegasi. When the telescope was pointed at this location, the neighboring star appeared with anticipated brightness, and there were no other stars in the immediate vicinity. Thus, the sighting of the star, HD 216635, confirmed the correct relationship between the locations of the two stars, ensuring that the telescope is indeed locked onto the correct guide star. In addition, the telescope has also seen the star HR Peg (HR 8714), a brighter and redder star, located less than half a degree to the left of IM Pegasi.

This past week the team continued performing calibration tests of all gyros, spinning at less than 1 Hz (60 rpm). In addition, the team successfully tested a back-up drag-free mode of the spacecraft with three of the gyros for an entire orbit, and, more significantly, the team completed its first successful test of the primary drag-free mode since re-configuring the micro thrusters, using gyro #3.

In primary drag-free mode, the Gyro Suspension System (GSS) is turned off on one of the gyros, so that no forces are applied to it. The ATC uses feedback from the position of this gyro in its housing to “steer” the spacecraft, keeping the gyro centered. Back-up drag-free mode is similar, but in this case the GSS applies very light forces on the gyro to keep it suspended and centered in its housing. The ATC uses feedback from the GSS to “steer” the spacecraft so that the GSS forces are nullified or canceled, thereby keeping the gyro centered. Applying forces with the GSS to suspend the drag-free gyro adds a very small, but acceptable, amount of noise to the gyro signal, and thus, either primary or back-up drag-free mode can be employed during the science experiment. Upcoming milestones include maintaining the spacecraft in a drag-free orbit, and beginning gyro calibration tests at spin rates of up to 5 Hz (300 rpm).

## 18 JUNE 2004—MISSION UPDATE: DAY 59

Just under two months into the mission, the spacecraft is in good health, and all subsystems are performing well. The spacecraft's orbit continues to be stable, meeting our requirements for transition into the science phase of the mission. All four gyros remain digitally suspended, and we are completing the planned series of calibration tests at very low gyro spin rates. The science telescope remains locked onto the guide star, IM Pegasi, and we are beginning the process of distributing and balancing the mass of the spacecraft at increased roll rates, as required for the science mission. For reasons discussed below, the Initialization and Orbit Checkout (IOC) phase of the mission has been extended to 90 days.

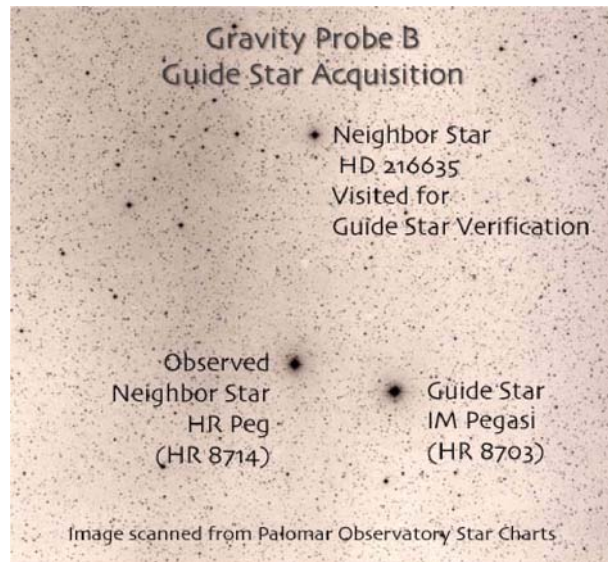


Last Saturday, the team was honored to have NASA Administrator Sean O'Keefe, Alaska Senator Ted Stevens, and some of their staff members visit the GP-B facilities here at Stanford University. The visit began with brief presentations by GP-B NASA Program Manager, Rex Geveden from Marshall Space Flight Center, Principal Investigator Francis Everitt, and Stanford Program Manager Gaylord Green. Next, the group viewed a display of spare flight gyroscopes, the flight telescope, and other hardware and then toured the Mission Operations Center (MOC), talking with members of the GP-B Operations team who were on duty and observing them in action. While the visitors were watching, the MOC received data relayed from the spacecraft through the Tracking Data Relay Satellite System (TDRSS) to the ground tracking station at White Sands, New Mexico, as the guide star returned to view in the telescope during a validation check.



This past week, the team increased the roll rate of the spacecraft from 0.1 rpm to 0.3 rpm, in preparation for “mass trim” and “bubble wrap.” These procedures are used to bring the entire spacecraft into balance so that it rolls smoothly about its main axis, while continuing to focus on the guide star through the telescope. The mass trim operation is similar to dynamically spin balancing a tire, using movable weights on the spacecraft frame under computer control to adjust the spacecraft's center of mass. Bubble wrap is the process of uniformly distributing the liquid helium around the dewar's outer shell. We will accomplish this by increasing the roll rate of the spacecraft in steps, from 0.3 rpm to 0.6 rpm.

Also during this past week, the spacecraft/telescope re-visited guide star neighbor HD 216635 (SAO 108242) as well as guide star neighbor HR Peg (HR 8714), for further testing and brightness calibration.



Another important event this past week was using the results of prior gyro calibration tests to fine-tune the Gyro Suspension System (GSS) for each gyro. This significantly improved the suspension performance of all the gyros, especially gyro #2. Parameters are now in place for spinning up the gyros to 5 Hz (300 rpm).

We have received several email inquiries about how the spin rate of the gyroscopes is determined in orbit. It is determined using the SQUIDS. Even though the gyros are currently spinning very slowly, there is enough trapped magnetic flux on the gyro rotors for the



SQUIDs to detect their rotation speed to an accuracy of 10 millionths of a Hertz. Because the measurement is made between the gyro rotors and their housings, and because the gyro housings are connected to the spacecraft itself, the roll rate of the spacecraft was also measured using the gyros. In fact, two of the gyros spin in the same direction as the spacecraft roll, and two spin against the roll. Thus, as the roll rate of the spacecraft was increased, two of the gyros appeared to spin faster, and two appeared to slow down in accordance with the increased roll rate. Photo: The gyro housing and SQUID lines under inspection during repairs of the Science Instrument Assembly, circa August 2000.

As chronicled in previous weekly updates, two difficulties—now both overcome—have made the task of locking onto the guide star take longer than anticipated, and as a result, the IOC phase of the mission has been extended from 60 to 90 days. First, the side-facing star trackers on the spacecraft required an extended search period to properly identify the known field of stars. Feedback from these star trackers is used to orient the spacecraft in the vicinity of the guide star, similar to using a spotting telescope to position a high-powered telescope on a particular part of the sky. The second is from malfunction of two of the spacecraft's 16 ultra-sensitive micro thrusters. Redundancy built into the system enables the spacecraft to fly without the two problematic thrusters, but to optimize performance with 14 instead of 16 thrusters, it was necessary to revise the control software. This software change has now been implemented, and after a Flight Readiness Review on June 25, 2004, it will be uploaded to the spacecraft. At a later stage, we will explore partial re-activation of the two problematic thrusters.

## 25 JUNE 2004—MISSION UPDATE: DAY 66

On Day# 66 of the mission, the spacecraft continues to be in good health, with all subsystems performing well. The spacecraft's orbit remains stable, ready for transition into the science phase of the mission. All four gyros remain digitally suspended, and final calibration tests at very slow gyro spin rates of up to 1 Hz (60 rpm) have been completed. The spacecraft's roll rate has been incrementally increased from 0.3 to 0.9 rpm, as part of the process of uniformly distributing and balancing the mass of the spacecraft. Following a Flight Readiness Review currently in progress, we will begin uploading revised drag-free thruster-control software to the Attitude and Translation Control system (ATC) on-board the spacecraft over the weekend.

This past week, we completed the last of a series of very low spin rate calibration tests on the gyros and the gyro suspension system (GSS). As described in previous highlights, these tests involve briefly applying voltages asymmetrically to the suspension electrodes on a given gyro, causing that gyro rotor (sphere) to move off center by a few millionths of a meter and then re-centering it. We also tested the GSS by measuring the level of electrostatic charge on each gyro rotor after applying 20% higher than normal suspension voltages to the suspension electrodes, with the gyro rotors in spin-up position. None of the rotors showed a significant charge build-up after this procedure, which indicates that the GSS is functioning as anticipated.

Additionally this past week, we continued with two procedures designed to bring the entire spacecraft into balance, rolling smoothly about its main axis while the telescope focuses on the guide star. In the first procedure, called "bubble wrap," the spacecraft's roll rate was increased in incremental steps, from 0.3 rpm to 0.9 rpm. The increased roll rate begins to rotate the liquid helium, effectively pushing it outwards as it tries to move in a straight line with its inertia. The dewar walls hold it in with a centripetal force. This wraps the helium

uniformly around the outer shell. Distributing the liquid helium uniformly along the spacecraft's roll axis helps to ensure that the science telescope can remain locked on the guide star while the spacecraft is rolling.

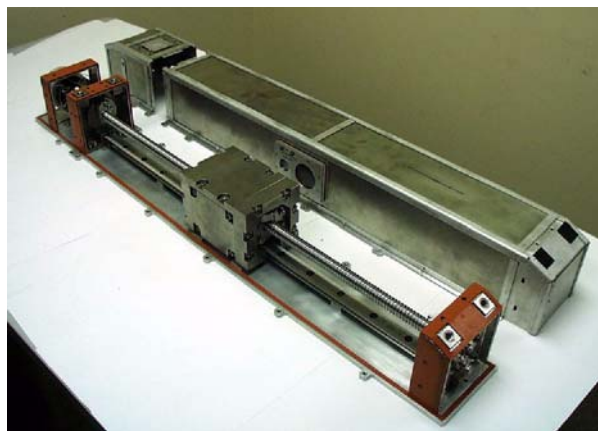


Some people might think this is centrifugal force. One might ask, what is the difference between centripetal and centrifugal force, anyway? The words centripetal and centrifugal are in fact antonyms defined as follows:

centrifugal: tending to move away from a center.

centripetal: tending to move toward a center.

In the second procedure, called "mass trim," weights mounted on long screw shafts are attached in strategic locations around the spacecraft frame. Small motors, under control of the spacecraft's ATC, can turn these screw shafts in either direction, causing the weights to move back and forth by a specified amount. Thus, based on feedback from the GSS, the spacecraft's center of mass can be precisely centered, both forward to back, and side to side, around the designated "drag-free gyro."



Finally, revisions to the spacecraft's drag-free thruster-control software that will optimize the spacecraft's performance, using 14 instead of 16 micro thrusters, passed a design review last week. A Flight Readiness Review is currently in progress to approve the uploading of this updated software to the spacecraft this weekend. Next week, the ATC will be re-started using the new software. The 16 micro thrusters are arranged 4 clusters, with each cluster having two pairs of thrusters. Redundancy built into the thruster system enables the spacecraft to meet the attitude control requirements for the science mission with only 12 functioning micro thrusters. In the event of a thruster problem, the original thruster-control software was designed to isolate both the malfunctioning thruster and its paired partner. The revised software now enables individual micro thrusters to be isolated in any thruster pair, without affecting the paired partner. Of the 14 micro thrusters currently functioning, only two are critically located,

and if these two were both to malfunction, it is still possible to operate the thruster system by partially opening the valves in the isolated thrusters.

Once the revised thruster-control software is up and running, the helium bubble is wrapped, and the spacecraft's mass has been trimmed, we will lock onto the guide star, IM Pegasi, in a drag-free orbit, in preparation for the science mission.

---

## 2 JULY 2004—MISSION UPDATE: DAY 73

At a little over ten weeks into the mission, the spacecraft is in excellent health, with all subsystems performing well. The spacecraft's orbit remains stable, ready for the transition into the Science Phase. All four gyros are digitally suspended and have completed calibration testing at approximately 0.3 Hz (18 rpm) spin rates. Two problematic micro thrusters, which were preventing the spacecraft from sustaining a drag-free orbit, have been isolated, and the thruster-control software was modified to optimize Attitude and Translation Control system (ATC) functionality without them. Over the past two weeks, the spacecraft's roll rate was increased from 0.3 rpm to 0.9 rpm as part of the process of uniformly distributing and balancing the mass of the spacecraft.

During this past week, we completed the mass trim procedure at 0.9 rpm, using movable weights on long screw shafts to alter the spacecraft's center of mass from front to back and from side to side. The mass trim operation is necessary to precisely align the spacecraft's roll axis so that it passes through the centers of the gyros and the telescope's line of sight. The mass trim procedure also balances the mass of the spacecraft so that it rolls smoothly around this axis.

Also, this past week, we decreased the spacecraft's roll rate incrementally from 0.9 rpm back to 0.5 rpm. During the first roll-down decrement to 0.7 rpm, we discovered that the distribution of the liquid helium in the dewar is less predictable during roll-down than it is during roll-up. When the spacecraft's roll rate is slowed too quickly, the liquid helium begins to slosh around. The resulting displacement of the center of mass from the sloshing helium affects the micro thrusters, resulting in a significant increase in the time required to complete the roll-down.

Last weekend, in preparation for optimizing ATC performance with 14 instead of 16 micro thrusters, we uploaded revised drag-free thruster-control software to the on-board computer. After completing the mass trim maneuver and stabilizing the spacecraft at the 0.5 rpm roll rate, we re-booted the on-board computer with the revised software. The re-boot went very smoothly, and a checkout of the new software confirms that the two problematic thrusters are isolated and receiving no helium, while the remaining 14 thrusters are responding to commands as expected. With the new software up and running, we have begun successfully testing both primary and backup drag-free modes around gyro #1.

Meanwhile, gyro #1 and gyro #3 are currently in the process of being spun up to 3 Hz (180 rpm), and likewise, gyros #2 and #4 will be spun up to 3 Hz next week. Over this weekend, the team will also re-lock the science telescope on the guide star, IM Pegasi, with the spacecraft rolling at 0.5 rpm and balanced along the telescope's axis of sight. Before we begin calibration testing of the gyros at a spin rate of 3 Hz next week, our goal is to have the spacecraft rolling smoothly at 0.5 rpm, locked onto the guide star, and in a drag-free orbit around one of the gyros. Photo: A picture of a gyro rotor before coating, being measured for roundness many years ago.

---

## 9 JULY 2004—MISSION UPDATE: DAY 80

After 80 days in orbit, the spacecraft remains in excellent health, and all subsystems are continuing to perform well. All four gyros are digitally suspended and are currently spinning at approximately 3 Hz (180 rpm). Two weeks ago, the on-board computer was re-booted with a new version of the drag-free thruster-control software to work around two problematic micro thrusters that were isolated and taken out of service shortly after launch. The new software optimizes the performance of the Attitude and Translation Control system (ATC) using 14, instead of 16 micro thrusters, and it has been performing as expected since the re-boot. The spacecraft is flying drag-free around gyro #1, at a roll rate of 0.52 rpm, with the science telescope locked onto the guide star, IM Pegasi. We are now entering the home stretch of the Initialization and Orbit Checkout (IOC) phase of the mission.

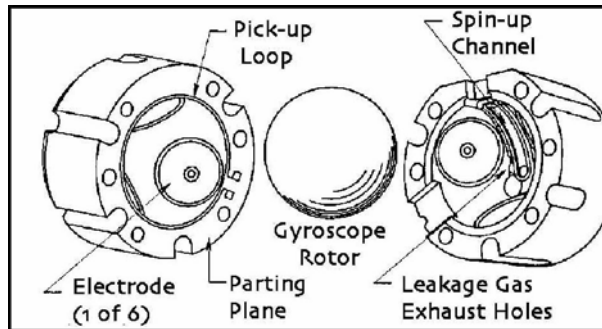
On Saturday, July 3rd, we re-locked the science telescope on the guide star, IM Pegasi, with the spacecraft rolling at 0.5 rpm. The spacecraft remained locked on the guide star throughout the 4th of July weekend.

This past week, we continued testing and optimizing ATC performance in both primary and backup drag-free modes. Based on this testing, we have selected back-up drag-free as the nominal mode for the science phase of the mission. In back-up drag-free mode, the Gyro Suspension System (GSS) applies very light forces on the gyro to keep it suspended and centered in its housing. The ATC uses feedback from the GSS to "steer" the spacecraft so that the GSS forces are nullified or canceled, thereby keeping the gyro centered. Applying forces with the GSS to suspend the drag-free gyro adds a very small amount of noise to the gyro signal, but this noise is negligible, and it is outweighed by the added stability that has been demonstrated in our tests over the past few weeks. This increased stability is due to the fact that the back-up mode uses both the micro thrusters and the GSS to counteract drag on the spacecraft, whereas the primary mode relies solely on the micro thrusters to create a drag-free orbit.

Yesterday, the roll rate of the spacecraft was slightly increased from 0.50 to 0.52 rpm, in preparation for the transition into the science phase of the mission. This slightly higher roll rate was chosen based on ATC and SQUID readout performance, as well as the requirement that the science phase roll rate should not be a harmonic of either orbit or calibration frequencies. We are in the process of evaluating whether or not further mass trim operations will be needed for the science phase of the mission.

On Friday, July 2nd, we successfully spun-up gyros #1 and #3 to 3 Hz (180 rpm), by streaming ultra-pure helium gas through their spin-up channels for 90 seconds each. This past Tuesday and Wednesday, July 6th and 7th, we followed suit with gyros # 2 and #4. Note that we cannot control the exact spin rate of the gyro rotors (spheres). Rather, we control the length of time that ultra-pure helium gas flows through the spin-up channel for each gyro, and then the SQUID readouts tell us the resulting spin rates—which may differ slightly from one gyro to another. Pending a final review meeting this afternoon, tomorrow morning, we are planning to stream helium gas over the gyro #4 rotor for another 90 seconds, thereby increasing its spin rate to approximately 6 Hz (360 rpm). Then, after performing a number of tests to ensure that gyro #4 and its suspension system are functioning properly, tomorrow afternoon, we plan to spin up this gyro to full speed by streaming ultra-pure helium over its rotor for approximately 90 minutes. We anticipate that the final spin rate of the gyro #4 rotor will be between 120 Hz (7,200 rpm) and 170 Hz (10,200 rpm). We will then monitor the performance of gyro #4 for several days before spinning up the remaining gyros to full speed.

## 17 JULY 2004—MISSION UPDATE: DAY 88



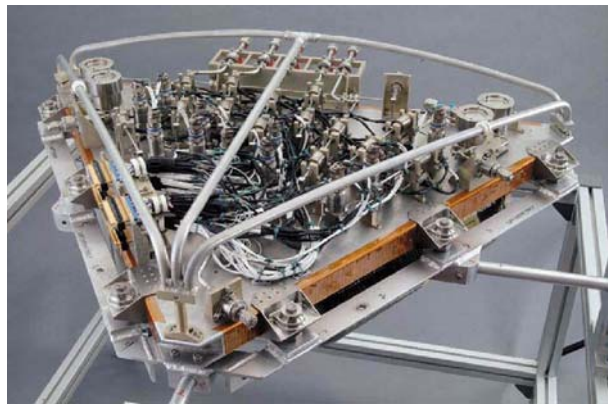
At just under 3 months in orbit, Gravity Probe B is nearing the end of the Initialization and Orbit Checkout (IOC) phase of the mission. The spacecraft remains in excellent health, and all subsystems are continuing to perform well. All four gyros are digitally suspended, with gyros #2 and #4 spinning at science mission speed—greater than 80 Hz (4,800 rpm)—and gyros #1 and #3 spinning at approximately 1.5 Hz (90 rpm), ready for full-speed spin-up. The updated drag-free thruster control software that was uploaded to the spacecraft three weeks ago to optimize performance of the Attitude and Translation Control system (ATC) is continuing to perform nominally. The spacecraft's roll rate is 0.52 rpm, and the science telescope is being relocked onto the guide star, IM Pegasi, following the full-speed spin-up of gyro #2 yesterday.

This past Tuesday, July 13th, Gravity Probe B achieved a major milestone with the successful spin-up of gyro #4 to a science-ready speed of 105.8 Hz (6,348 rpm). Second to the launch, the full-speed spin-up of the gyros has been the next most long-awaited event in the history of GP-B. Members of the team were very attentive at their stations in the Mission Operations Center (MOC) here at Stanford for 3 hours and broke into applause when the final announcement boomed over the MOC intercom that the gyro #4 full spin-up had been completed successfully.



Yesterday, July 16th, gyro #2 underwent the same spin-up procedure, reaching a final spin rate of 87 Hz (5,220 rpm). Spinning up the gyros to science-ready speed is a complex and dynamic operation that exercises the full capabilities of the Gyro Suspension System (GSS) and requires a high level of concentration and coordination on the part of the GP-B Team. Following is an overview of the process.

First, commands are sent to the GSS to move the gyro rotor (sphere) very close to the spin-up channel (about 1/100th of the edge of a sheet of paper) in one half of the gyro's housing. Ultra-pure (99.99999%) helium gas is streamed from the Gas Management Assembly (GMA), mounted in a bay on the spacecraft frame, through tubing that enters the "top hat" (the thermal interface at the top of the Probe) and travels down to the gyro housings in the Science Instrument Assembly (SIA) at the bottom of the Probe. As the helium gas descends into the Probe, which is at a temperature of approximately 1.8 Kelvin, the gas cools down from 273 Kelvin to around 12 Kelvin.



Before entering the spin-up channel in one of the gyro housings, the gas is passed through a combination filter/heater. The filter, which is made of sintered titanium, removes any impurities that may have been imparted to the helium on its journey into the Probe. The heater enables the helium to be warmed slightly, which increases its adhesion to the ultra-smooth surface of the gyro rotor. The filtered and warmed helium then passes through the spin-up channel in one half of the gyro housing, and most of the gas evacuates into space through an exhaust system. However, some of the helium leaks into the housings of the other gyros, causing their spin rates to decrease up to 20% over a full spin-up period of 2-3 hours.



For this reason, the order in which the gyros are spun up is very important. Earlier in the IOC phase, the 3 Hz (180 rpm) spin-up provided information on the helium leakage rate of each gyro. Gyro #4, which had the highest leakage rate, was spun-up to full speed first, so that helium leaked from its spin-up would not affect other gyros that were already at science mission speed. The remaining gyros are then spun-up in decreasing order of their helium leakage rates—gyro #2, gyro #1, and finally, gyro #3.

Each full-speed spin-up takes most of a day. In the morning, helium gas is flowed over the gyro for 90 seconds, and tests are run to ensure that the helium leakage rate for that gyro corresponds to previous measurements. If everything checks out, the full-speed spin-up, in which helium gas is flowed over the rotors for 2-3 hours, commences early in the afternoon. The GP-B team controls the spin-up process by sending commands from the Mission Operations Center (MOC) here at Stanford to the spacecraft in real-time. For example, they send commands to open or close the GMA valves to flow helium through the gyro's spin-up channel. They also control the amount of heat applied to the gas before it enters the gyro spin-up channel, and they control opening and closing of exhaust valves. Real-time telemetry provides immediate feedback on the progress of the spin-up so that various parameters can be adjusted as necessary.

The successful spin-up of gyro #4 to full speed enabled us to spin-up gyro #2. Gyro #2 topped out at 87 Hz (5,220 rpm), which is only slightly above the minimum spin rate of 80 Hz (4,800 rpm) required for the science experiment. Also, the helium gas leakage from the Gyro 2 spin-up slowed gyro #4 down to 91Hz (5,460 rpm). We are taking some time to evaluate the data from the first two spin-up procedures and to perform some ground-based tests before spinning up gyros #1 and #3 to full speed.

Meanwhile, we are fine-tuning the drag-free software used by the Attitude and Translation Control system (ATC) to optimize its performance at the current and final spacecraft roll rate of 0.52 rpm. For part of each orbit, the spacecraft passes behind the Earth, causing the telescope to lose visual contact with the guide star. During this "eclipse" period, two standard external rate gyroscopes, plus the star trackers on either side of the spacecraft, enable the ATC to keep the spacecraft/telescope pointed towards the guide star. When the spacecraft emerges over the North Pole and the guide star becomes visible again, the telescope must be re-locked onto it. This re-locking has been taking up to 15 minutes, and the fine-tuning will speed up this process considerably.

---

## **23 JULY 2004—GRAVITY PROBE B MISSION UPDATE: Day 94**

One day #94 of the mission, Gravity Probe B is poised to enter the home stretch of the Initialization and Orbit Checkout (IOC) phase of the mission. The spacecraft is in excellent health, and all subsystems are continuing to perform well. All four gyros are digitally suspended, with gyros #2 and #4 spinning at science mission speed—greater than 80Hz (4,800 rpm). Gyros #1 and #3 are spinning at less than 1.5 Hz (90 rpm) and are ready for full-speed spin-up next week. Fine-tuning of the Attitude and Translation Control system (ATC) is still in progress, and the ATC is performing well. The spacecraft's roll rate is 0.52 rpm, and the science telescope is locked onto the guide star, IM Pegasi.

Last Friday, the full-speed spin-up of gyro#2 went smoothly, with a final spin rate of 87 Hz (5,220 rpm). Helium gas leakage from the spin-up of gyro #2 caused gyro #4 to slow down from 105.8 Hz (6,348 rpm) to 91 Hz (5,460 rpm). We had hoped that gyro #2 would achieve a spin rate above 100 Hz (6,000 rpm), with less leakage effect on gyro #4.

Thus, rather than spinning up gyros #1 and #3 as originally planned, we spent the past week doing analysis and running tests—both on the spacecraft and here at Stanford—in order to ensure that the upcoming spin-up of gyros #1 and #3 will result in higher speeds, with less leakage effect on the remaining gyros.

The spin rate of the gyros during the Science Phase of the mission affects the signal-to-noise ratio in the SQUID readouts of the experimental data. The noise level is quite small, but constant. The higher the gyro spin rate, the larger the London moment (magnetic field created by a spinning superconductor), and thus, the greater the signal-to-noise ratio. In ground testing prior to launch, we determined that a spin rate of 80 Hz (4,800 rpm) or greater for each gyro would provide a good signal-to-noise ratio for the science mission. However, the threshold of 80 Hz (4,800) rpm is not a hard and fast limit, so if the final spin rate of one or more gyros falls slightly below this value, this will not appreciably compromise the science data.

One way to potentially increase the spin-up rate of the remaining two gyros, while reducing the amount of helium gas leakage during spin-up is to use the Gyro Suspension System to position the gyro rotors closer to the spin-up channel in the gyro housing. Tests and analysis performed this past week indicate that we can move the rotors of gyros #1 and #3 up to 30% closer to the spin-up channels than gyros #2 and #4, and still have a safe margin of clearance from the suspension electrodes and the gyro housings. We have also determined that opening a second exhaust valve during spin-up may help to reduce the pressure in the Probe caused by helium leakage, thereby reducing the spin-down effects on the remaining gyros. Both of these changes will be implemented in the spin-up of gyros #1 and #3 next week.

Also, this past week, we continued fine-tuning the drag-free software used by the Attitude and Translation Control system (ATC) to optimize its performance at the current and final spacecraft roll rate of 0.52 rpm. Tests from parameter changes we made to the ATC system indicate that we have reduced the time it takes to re-lock onto the guide star from as much as 15 minutes to less than 2 minutes.

---

## **31 JULY 2004—GRAVITY PROBE B MISSION UPDATE: Day 102**

Gravity Probe B successfully accomplished a major milestone this week as the final two gyroscopes were spun up to high spin speed. All four gyros are now spinning at high spin speed. The spacecraft is in excellent health, and all subsystems are continuing to perform well. With this major accomplishment behind us the Program is entering the home stretch of the Initialization and Orbit Checkout (IOC) phase of the mission.

This week's high speed spin-up operations were performed on gyro #3 (Tuesday) and gyro #1 (Friday). There were no anomalies during the spin up. The SQUID readout FFT tracked the spin up in real-time. As expected, the other gyros spun down approximately 15% with each high speed spin-up operation due to pressurization of the Probe caused by gas leakage during the spin-up. Final spin speeds of the gyros are now: gyro #1 (80.0 Hz - 4800 rpm), gyro #2 (62.3 Hz - 3738 rpm), gyro #3 (82.7 Hz - 4962 rpm) and gyro #4 (65.5 Hz - 3930 rpm). At these spin speeds, GP-B's relativity measurement is expected to be significantly better than specification. Therefore, no further gyro high speed spin-up operations are planned.

Fine-tuning of the Attitude and Translation Control system (ATC) is nearly complete, and the ATC is performing well. This past week, we continued fine-tuning the drag-free software used by the ATC to optimize its performance at the current spacecraft roll rate of 0.52 rpm. Tests from parameter changes we made to the ATC system

indicate that we have reduced the time it takes to re-lock onto the guide star from as much as 15 minutes to less than a minute. We have also increased the number of reference stars seen by the star tracker from 3 to 8.

Next week we will be performing a few final operations prior to beginning taking science data. The most significant operation left to be performed is the spin axis alignment of each gyro. This is performed using the Gyro Suspension System in a special oscillation mode to slowly align each gyro spin axis to be in nearly perfect alignment with the guide star. Having the gyros aligned at the beginning of the mission makes any precession caused by general relativity simpler to measure. We are nearly complete aligning the spin axis of gyros #2 and #4 and plan to align #3 and #1 next week. Another operation for next week is to perform a final bake-out operation to remove any residual helium molecules from around the gyros. This operation is performed by heating up the instrument area slightly (to approximately 6 degrees Kelvin), which will cause residual helium to migrate to a collector device in the Probe. And finally, the final operation prior to science is to command the spacecraft to begin drag-free operations.

---

### **6 AUGUST 2004—GRAVITY PROBE B MISSION UPDATE: DAY 108**

Gravity Probe B has nearly completed the Initial On-Orbit Calibration Phase of the Mission. Last week we completed the fast speed spin-up of all four gyros. This week we completed the low temperature bakeout of the Probe and expect to complete spin axis alignment of the final two gyroscopes this weekend. Prior to starting the Science Phase of the Mission, we decided to increase the roll rate of the spacecraft from .52rpm to .75rpm which will improve the accuracy of the experiment and minimize the risk of achieving a good measurement in the event of a shortened mission. We plan to increase the roll rate early next week. At that point we will transition to the Science Phase of the mission.

The low temperature bakeout operation was done in order to minimize the pressure inside the vacuum probe. The resulting low pressure, or ultra-high vacuum, is required to minimize the spindown rate and torques on the gyroscopes. The low temperature bakeout process involved heating the Probe to approximately 6-7 degrees Kelvin while the Probe was open to the vacuum of space. This allowed excess helium gas to escape to space. The probe was then closed to space and the heaters turned off. The probe temperature then returned to its nominal value and the remaining helium was adsorbed into the cryopump. The cryopump is a passive device made of sintered titanium, which has a very large adsorbing area. GP-B's low temperature bakeout process created pressure inside the vacuum probe less than one thousandth that of space.

We continued to perform spin axis alignment of the gyroscopes this week. This is performed using the Gyro Suspension System in a special oscillation mode to slowly align each gyro spin axis to be in nearly perfect alignment with the guide star. Having the gyros aligned at the beginning of the mission makes any precession caused by general relativity simpler to measure. Thus far, we've completed the alignment of gyro #1 and #2. Gyro's #3 and #4 should be completed this weekend.

After much analysis and discussion this week we decided to increase spacecraft roll rate during the science mission from .52 rpm to .75 rpm. A .75 rpm roll rate minimizes the risk of events which might occur that could cause degradation to the accuracy of the mission. In addition, by combining the factors that influence gyro accuracy and guide star acquisition, this relatively small increase in roll rate should

produce a ~20% improvement in the overall accuracy of the experiment. We expect to perform this operation beginning Monday. Assuming success, we then will begin drag-free operation with the start of the Science Mission Phase later next week.

---

### **13 AUGUST 2004—GRAVITY PROBE B MISSION UPDATE: DAY 115**

On day #115 of the mission, Gravity Probe B is within a week of completing Initialization and Orbit Checkout (IOC) and making the transition into the Science Phase of the mission. The spacecraft is in excellent health, and all subsystems are performing well. The spacecraft's roll rate is stable at 0.75 rpm, and final testing of drag-free orbital flight and fine-tuning of the Attitude and Translation Control system (ATC) is nearing completion. All four gyros are digitally suspended and spinning at science mission speeds, ranging from 61.8Hz (3,708 rpm) to 82.1 Hz (4,926 rpm). The spin axes of Gyros #1 and #3 have been aligned with the science telescope's sighting axis, which is locked onto the guide star, IM Pegasi, and these gyros have completed the transition to science data collection mode. Spin axis alignment is continuing on Gyros #2 and #4, which are expected to transition to science mode over the next few days.

This past Monday, August 9, 2004, we successfully increased the spacecraft's roll rate from 0.52 rpm to 0.75 rpm. In last week's highlights, we noted that the decision to do this was made "after much analysis and discussion," triggering a number of email inquiries about the risks of increasing the roll rate. Three main issues influenced this decision: First, increasing the roll rate requires more fine-tuning of the ATC system, which would delay the transition into Science mode by a few more days. Second, because the star trackers used by the ATC are mounted on the sides of the spacecraft, an increase in roll rate means that the star trackers must perform their pattern-matching on a faster moving field of stars. Third, there was a concern that any effects of mass imbalances in the spacecraft might be exaggerated at a faster roll rate. In the end, we decided that the ~20% improvement in experimental accuracy outweighed these risks. All systems are performing correctly at the increased roll rate, and the only downside was a small delay in our transition to the Science phase of the mission.

Also this past week, we have flown the spacecraft in both primary and back-up drag-free modes, using Gyro #1 as the proof mass (spacecraft's center of mass). Primary drag-free mode relies solely on the micro thrusters to create a drag-free orbit around the proof mass gyro, whereas in back-up drag-free mode, the ATC uses suspension force data from the Gyro Suspension System (GSS) of the proof mass gyro to "steer" the spacecraft so that residual GSS forces are nullified or canceled on this gyroscope. Either primary or back-up drag-free mode can be used in the Science Phase of the mission. However, the residual voltages applied by the GSS to suspend the drag-free gyro add a very small, but acceptable, amount of noise to the gyro signal in back-up drag-free mode, so the primary mode is preferable, all other things being equal.

In fact, early in July, we had selected back-up drag-free mode as the nominal mode for the Science Phase of the mission because at that time, when the gyros were spinning very slowly, back-up mode was yielding better results than the primary mode. However, now that the gyros are spinning at full speed, primary drag-free mode is yielding the best results, as originally anticipated, so it will be the nominal mode for drag-free operation during the Science Phase of the mission. The reason for this performance difference is that while the GP-B gyro rotors (spheres) are the roundest objects ever manufactured, they are not perfectly spherical. The GSS is capable of controlling the position of the gyros to a level of one nanometer. However, some of the

“bumps” or deviations on the rotor surfaces are as large as 20 nanometers. When the rotors are spinning slowly, these larger “bumps” are detected by the GSS, and they decrease its positioning accuracy. However, when the rotors are spinning fast, these deviations average out. Thus, at full speed, the average surface deviation on the gyro rotors is less than the one-nanometer precision of the GSS, so there is no degradation in positioning the gyro rotors.

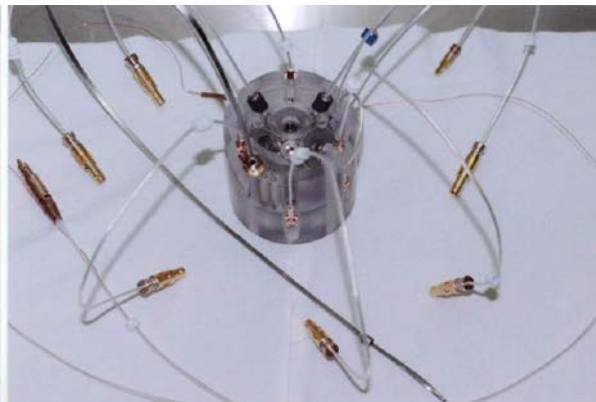
The final steps in the IOC, prior to beginning data collection, involve the transition of each gyro into science mode. There are three main steps in this transition. First, the spin axis of each gyro is aligned with the science telescope/spacecraft roll axis. Then, ultraviolet light, beamed from lamps on the spacecraft frame through fiber optic cables into the gyro housings, are used to remove any residual static charge from the gyro rotor surfaces. Finally, the GSS voltage is reduced, in order to obtain the best signal on the SQUID readouts. Currently, Gyros #1 and #3 have completed this transition to science mode. Gyros #2 and #4 are finishing spin axis alignment, and they are expected to complete the transition to science mode over the next few days.

---

## 20 AUGUST 2004—GRAVITY PROBE B MISSION UPDATE: DAY 122

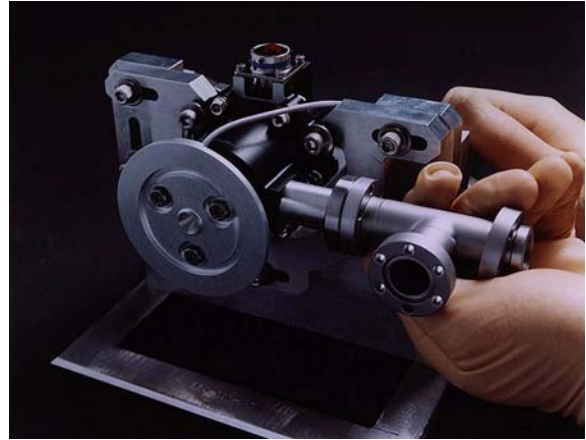
A little over four months into the mission, the spacecraft remains in excellent health, and all subsystems continue to perform well. The spacecraft’s roll rate remains stable at 0.75 rpm, and final testing of drag-free orbital flight and fine-tuning of the Attitude and Translation Control system (ATC) is continuing. All four gyros are now suspended in low-voltage science mode. All of their spin axes have been aligned with the science telescope’s sighting axis, which is locked onto the guide star, IM Pegasi. These alignments are in the process of being fine-tuned.

Last weekend, we completed coarse spin axis alignment on gyros #2 and #4. On Monday, August 16th, ultraviolet light was beamed through fiber optic cables into the housing of gyro #2 to remove excess static charge on the gyro #2 rotor (sphere). Then, the suspension voltage for gyro #2 was reduced to 200 millivolts, the level required for science data collection. The following day, the same procedures were completed on gyro #4. Thus, by the middle of this past week, all four gyros were in the science mode configuration.



About ten days ago, we began to notice that while in primary drag-free mode, the ATC was requiring more helium propellant than planned to counter an unexpected force along the spacecraft’s roll axis—that is, in the direction of the guide star. This past weekend, we switched to back-up drag-free mode on gyro#3, which gave a similar result. Over the past two days, we have completed two tests that have provided a

solution for ensuring that the helium mass flow through the ATC system remains within required levels. By adjusting thruster biases, and by reducing the commanded helium flow, the amount of helium consumed by the ATC system is now less than the helium boiled away by the natural heat in the dewar. As a result, the helium requirements of the ATC system will have no impact on the mission lifetime, thereby maximizing the science performance.



Furthermore, in the process of performing these tests, we have determined that back-up drag-free mode is working very reliably, and thus we have re-selected back-up drag-free operation as the baseline mode for the Science Phase of the mission. We anticipate that our investigation and problem-solving efforts around this roll-axis force will take a few more days. During that time, we will continue testing back-up drag-free mode around gyro #3, as well as further fine-tuning the spin axis alignment of the four gyros.

In addition this past week, while optimizing the performance of the telescope system, we have found a small source of bias noise in the telescope detector output signal. Although it would probably have no effect on the science outcome, it seems prudent to eliminate this bias noise, especially since a simple adjustment will take care of it. We are planning to make this adjustment over the next two days.

Finally, analysis of the gyroscope spin-down rate performance over this past week has shown that, under low-voltage, science mode suspension, the spin-down rate for all four gyros is less than 0.000001 Hz (0.00006 rpm) per hour. This means that it would take more than 7,000 years for one of our gyros to completely spin down. On Earth, we could only test the spin-down rates of the gyros in a high-voltage suspension mode, and based on these ground tests, the orbital spin-down requirement for the gyros was set at 2,300 years. We now see that the spin-down performance of the GP-B gyros in science mode is more than three times better than this requirement.

## C.4 Science Mission Phase: 8/27/04 - 8/12/05

---

### 27 AUGUST 2004—GRAVITY PROBE B MISSION UPDATE: DAY 129

On Day #129, we have arrived at the second major milestone of the mission—the completion of the Initialization and Orbit Checkout (IOC) Phase and transition into the Science Phase. The spacecraft continues to be in excellent health, with all subsystems performing well. The telescope is properly tracking the guide star, IM Pegasi, during the portion of each orbit when the guide star is visible. Fine precision spin axis alignment has been completed on gyros #1, #2, and #3, and after the suspension voltages on these gyros were reduced from 10 volts to 200 millivolts in preparation for data collection, a final electrostatic discharge was performed on the gyro rotors using ultraviolet light. Gyro #4 is further behind its fellow gyros and will continue undergoing spin axis alignment awhile longer. Today, the spacecraft was placed in a drag-free mode around gyro #3, and it will remain in this mode for the duration of the Science Phase of the mission, which has now officially begun.

Over the course of this past week, we completed a number of final adjustments to the spacecraft and the gyros, in preparation for the transition to the Science phase. For example, on Wednesday, August 25th, we increased the spacecraft's roll rate very slightly from 0.75 rpm to 0.7742 rpm. This moved the signal frequencies from the gyros out of the range of telemetry sample rate harmonics, thus improving the signal to noise ratio of the experimental data.

Throughout most of this past week, we continued fine precision alignment of the gyro spin axes to the telescope axis. Conceptually, this is a straightforward process. Our SQUID magnetometers, in conjunction with the Gyro Suspension System (GSS), can detect very slight imperfections in the gyro rotors, and they utilize these imbalances, enhanced by a suspension force of 10 volts (50 times higher than the science suspension voltage of 200 millivolts) to torque the rotors ever so slightly, causing their spin axes to spiral in towards the target alignment position. However, our success in creating gyro rotors that are almost perfect spheres actually hinders this process. The smaller the level of imperfections in the rotors, the longer it takes the GSS to complete the alignment.

Today, we completed the final preparations, prior to beginning data collection. First, we reduced the suspension voltages on gyros #1, #2, and #3 from the 10 volt level used for spin axis alignment to 200 millivolts (0.2 volts), which is the level that will be used for data collection throughout the Science Phase of the mission. We use higher voltage in the GSS whenever we are controlling the position of the gyro rotors. However, during the data collection phase, we use the lowest voltage required to maintain proper suspension, so that only the effects of relativity will be influencing the spin axis deflections of the gyros.

After lowering the suspension voltages, we used ultraviolet light, shining through fiber optic cables as we have done previously, to remove any excess electrical charge that has built up on the rotors. When ultraviolet light shines on certain metals, it liberates electrons. Two fiber optic cables are embedded in each gyro housing—one at each end—and each fiber optic cable terminates at an electrode, located just above the rotor surface. When the ultraviolet lamps are turned on, electrons form between the electrode and the rotor surface, and by changing the bias on these electrodes, we can control the direction of electron flow, either towards or away from the surfaces of the rotors.

Finally, this morning, we commanded the spacecraft into back-up drag-free mode, balanced around gyro #3. After testing the spacecraft in both primary and back-up drag-free modes over the past few weeks, we have determined that back-up drag-free mode has yielded the most reliable and efficient performance, and thus, the spacecraft will remain in this mode for the duration of the Science Phase. We will continue tuning the drag-free performance of the Attitude and Translation Control (ATC) system in the early portion of the Science Phase to correct for a previously reported, unknown force, which is causing excess helium flow from the dewar through the micro thrusters. The current science configuration of the spacecraft has very little margin for increased helium flow.

In next week's highlights, we will look back over the IOC period and put it into the perspective of the whole mission. In the process of doing this, we will hopefully answer a number of email inquiries we have received recently regarding the health, longevity, and success of the GP-B mission.

---

### 3 SEPTEMBER 2004—GRAVITY PROBE B MISSION UPDATE: DAY 136

As of Day #136, GP-B has successfully completed its first full week in the Science Phase of the mission, with gyros #1, #2, and #3 in science mode. Gyro #4 is still undergoing alignment of its spin axis, which we expect to be completed in about a week. For the past week, the spacecraft has been in drag-free mode around gyro #3.

The spacecraft remains in excellent health, rolling at a rate of 0.7742 rpm, with all subsystems performing well. The telescope continues properly tracking the guide star, IM Pegasi, during the portion of each orbit when the guide star is visible. We are still investigating a small force or bias along the roll axis of the spacecraft, but this bias has no effect on science data collection. Moreover, during the past two weeks, we have tuned the spacecraft's Attitude and Translation Control (ATC) system to compensate for this bias, with no excess expenditure of helium through the micro thrusters.

Having just achieved the major milestone of transitioning into the Science Phase of the mission, this is a good time to pause and look back over the Initialization and Orbit Checkout (IOC) phase of the mission. During this 19-week period, the GP-B mission has already achieved a number of extraordinary accomplishments:

- The orbit injection of the spacecraft was so close to perfect (within 6 meters of the target orbit plane) that none of the planned orbit trim operations were necessary.
- We've communicated with the spacecraft over 3,000 times during the IOC phase, and the Mission Planning team has successfully transmitted over 70,000 commands to the spacecraft without an error.
- GP-B is the first satellite ever to achieve both 3-axis attitude control (pitch, yaw, and roll), and 3-axis drag-free control. Essentially, while orbiting the Earth, the whole spacecraft flies around one of the science gyros.
- The GP-B gyros, which are performing perfectly in orbit, will be listed in the forthcoming edition of the Guinness Book of World Records as being the roundest objects ever manufactured.

- The spin-down rates of all four gyros are considerably better than expected. GP-B's conservative requirement was a characteristic spin-down period (time required to slow down to ~37% of its initial speed) of 2,300 years. Recent measurements show that the actual characteristic spin-down period of the GP-B gyros exceeds 10,000 years—well beyond the requirement.
- Once tuned up, the spacecraft's Attitude and Translation Control (ATC) system has been able to function at a spacecraft roll rate of 0.7742 rpm—more than twice the roll rate of 0.3 rpm initially specified.
- The magnetic field surrounding the gyros and SQUIDs (Superconducting QUantum Interference Device) has been reduced to 0.0000001 gauss, less than one millionth of the Earth's magnetic field—the lowest ever achieved in space.
- The gyro readout measurements from the SQUID magnetometers have unprecedented precision, detecting fields to 0.0000000000001 gauss, less than one trillionth of the strength of Earth's magnetic field.
- The science telescope on board the spacecraft is tracking the guide star, IM Pegasi (HR 8703), to superb accuracy, and it is also collecting long-term brightness data on that star.

A number of people have asked the following two-part question about GP-B: "Given that our gyros are spinning about half as fast as we originally anticipated, and that the IOC phase took about twice as long as originally anticipated, how will these two situations affect the success of the GP-B experiment?"

Regarding the gyros, several of the accomplishments above—especially the extremely low SQUID noise and higher than planned spacecraft roll rate—have effectively reduced the error factor in the GP-B science experiment, thereby partially compensating for the reduced spin rates of the gyros.

Regarding the extended length of the IOC phase, the GP-B mission is unique because it is truly a physics experiment in space. As such, there are trade-offs that can be made. The primary trade-off we had to wrestle with was: More optimization/calibration of the instrument prior to entering science, with a shorter data collection period; or, less optimization/calibration, with a longer data collection period. We concluded that the best overall accuracy would be achieved by ensuring that the science instrument was optimally calibrated from the start, even if this meant collecting data for a shorter period than we had hoped. And, in fact, we now have a considerably better understanding of the instrument than originally anticipated at this stage of the mission.

The original ideal duration of the experiment was 13 months of relativity data gathering, but this is not essential, especially in view of the work we have now done on the optimization/calibration phase. After two months of science data collection, we can make a very good measurement of the geodetic effect and a significant measurement of the frame-dragging effect. The data improves as the 3/2 power of the time (i.e. double the time, and the result will improve by a factor of ~3). In the near future, we will make another measurement of the residual helium in the dewar, which will provide an accurate determination of its cryogenic lifetime. This, in combination with the observed instrument performance, will indicate the final expected accuracy of the experiment.

The GP-B program will not release the scientific results obtained during the mission until after the science phase has concluded. It is critically important to thoroughly analyze the data to ensure its

accuracy and integrity prior to releasing the results. After more than 40 years of development, we have learned the value of thoroughness and patience.

---

## 10 SEPTEMBER 2004—GRAVITY PROBE B MISSION UPDATE: Day 143

Just over 20 weeks in orbit, GP-B remains in the Science Phase of the mission. Gyros #1, #2, and #3 are in science mode, generating relativity data. Alignment of the spin axis of gyro #4 with the guide star, IM Pegasi, is continuing and will be completed by early next week.

The spacecraft remains in excellent health, rolling at a rate of 0.7742 rpm (one revolution every 77.5 seconds). The Attitude and Translation Control (ATC) system is maintaining a drag-free orbit around gyro #3, and it is properly tracking the guide star, IM Pegasi, during the portion of each orbit when the guide star is visible. The dewar temperature is nominal, and the flow of helium, venting from the dewar through the micro thrusters to maintain the drag-free orbit has remained within expected limits. All other spacecraft subsystems are continuing to perform well.

On Tuesday, September 7, a double-bit error occurred in a non-critical memory location of the spacecraft's main (A-side) computer due to a proton hit. This type of error is likely to occur from time to time during the mission. The necessary correction was prepared and uploaded to the proper memory location of the computer. This incident had no effect on science data collection or spacecraft subsystems.

Our statement in last week's highlights that the GP-B program will not be releasing any scientific data or results until after the completion of the science and instrument re-calibration phases of the mission prompted several inquiries that essentially boil down to two questions: 1) What steps have we taken to ensure the integrity of the raw data and the accuracy of the results? And, 2) Why is it necessary to wait so long before releasing any results?

GP-B's principal investigator, Professor Francis Everitt, has been quoted on several occasions as saying: "I don't care whether Einstein was right or wrong; what I want is the experimental truth." This is our guiding philosophy here at GP-B. The results of the GP-B experiment will be invaluable to science whether or not they agree with Einstein's predictions. Also, given that this experiment is unlikely to ever be repeated, everyone on the GP-B team feels a great sense of personal responsibility to be as careful and thorough as possible in collecting the data and cross checking our instruments and procedures for accuracy.

More specifically, in answer to the first question above, many safeguards are built into the GP-B experiment to ensure the integrity of the raw data, the correctness of the data analysis, and the accuracy of the results. These safeguards include:

- GP-B is a joint effort between NASA, Stanford, and Lockheed Martin. People from NASA and Lockheed Martin work on site here in the GP-B facilities at Stanford, and NASA managers review all GP-B mission activities.
- GP-B has an external Science Advisory Committee, comprised of renowned physicists and space scientists. That committee has overseen the preparations for data collection, and it will review all of the data and analysis before the results are published.

- GP-B also has an independent data analysis team that will be analyzing the data in parallel with the GP-B science team to corroborate our results. Any differences in the results of these two teams will be reconciled before the results are announced.
- The incoming raw data is fed directly into a database and is only available on a “read-only” basis to the scientists who will be analyzing it.
- Multiple cross checks are performed to identify any potential systematic experimental errors. For example, the results of all four gyros are compared and correlated for consistency.
- During the GP-B experiment, the spin axis deflections of the gyroscopes are measured relative to the guide star, IM Pegasi. But, in order to determine the actual relativistic drift rate of the gyros, we must also measure the proper motion of IM Pegasi relative to quasars (the most distant objects in the universe). The Harvard-Smithsonian Center for Astrophysics (CfA) is measuring the proper motion of IM Pegasi with respect to quasars to an unprecedented level of precision. However, by design, the CfA will not release this proper motion data to the GP-B science team until after the scientific data collection, post-science instrument calibrations, and the data analysis have all been completed. In other words, the relativistic drift rates of the gyros may only be determined once the GP-B gyro drift results and CfA proper motion results are combined.

Regarding the second question of why it is necessary to wait so long before releasing any results, one reason is now apparent: the guide star proper motion safeguard requires that all the GP-B data analysis be completed before we can receive and combine the CfA proper motion data and release/publish the final result. A related technical reason is that while we should have a very good measure of gyro drift after 2-3 months of data collection, it is essential that this data be cross checked and calibrated to ensure its accuracy. We use the annual aberration of our guide star signal (the difference between the actual position of IM Pegasi and its apparent position due to the Earth’s revolution around the Sun) as one means of calibrating the telescope/gyro readout scale factor. Collecting this aberration data over a substantial portion of a year will ensure the greatest accuracy of this calibration.

In summary, we are using utmost care and rigor in our experimental methods and analysis, and only after the analysis has been completed and thoroughly checked will we announce and publish the results. At that time, all of the GP-B data will become available to the public through the National Space Sciences Data Center (NSSDC), located at NASA’s Goddard Space Flight Center in Greenbelt, MD.

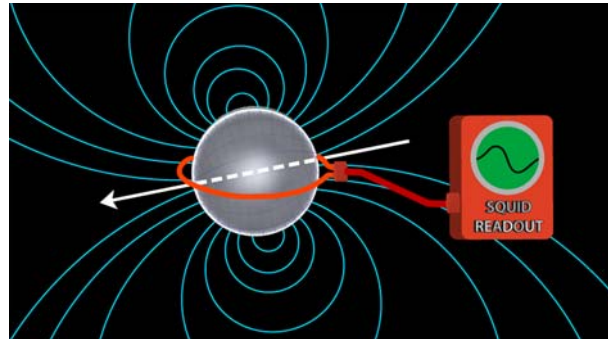
---

## 17 SEPTEMBER 2004—GRAVITY PROBE B MISSION UPDATE: Day 150

After 22 weeks in orbit, GP-B finally has all four gyroscopes generating relativity data. Gyro #4 joined Gyro’s #1, #2, and #3 in science mode this week after its spin axis was successfully aligned with the guide star, IM Pegasi, on Tuesday. The official transition occurred on Thursday morning (PDT), marking the first time that GP-B is conducting science on all four gyros.

The spacecraft continues to be in excellent health, rolling at a rate of 0.7742 rpm (one revolution every 77.5 seconds). The Attitude and Translation Control (ATC) system is maintaining a drag-free orbit around gyro #3, and it is properly tracking the guide star, IM Pegasi. The dewar temperature is nominal (1.82 Kelvin), and the flow of helium, venting from the dewar through the micro thrusters has remained within expected limits.

During the week, GP-B continued to tune-up the ATC system by improving the quality of “roll phase data” of the spacecraft. This data increases the precision with which we can monitor the alignment of the gyroscopes. The “roll phase data” refers to the precise orientation of the spacecraft as it rolls around its axis (360 every 77.5 seconds).



When the spacecraft rolls, so do the pickup loops encircling each gyroscope. These superconducting wire loops are used to monitor the orientation of the magnetic field around each gyroscope. They are located in the same plane as the spacecraft’s roll axis, so when the spacecraft rolls the loops turn with it. As a result, the loops perceive a “change” in each gyroscope’s orientation as the wire turns through the gyroscope’s magnetic field.

If GP-B knows the exact orientation of the spacecraft (and, in turn, the pickup loops) at each moment in time, we can better determine the orientation of each gyroscope. The spacecraft’s orientation is determined primarily through the two star trackers located on the forward portion of the spacecraft on opposite sides. These star trackers image the starry sky through an 8x8 field, providing the spacecraft with a reference map to measure its orientation. If the stars in each tracker’s field of view are in the right location, then the spacecraft is pointing in the right direction.

In last week’s highlights, we noted that a double-bit error in computer memory was caused by “a proton hit”. An astute reader asked, “How do we know that the spacecraft was hit by proton?”

Onboard the spacecraft is a proton detector, specially made for the GP-B mission. Its purpose is to monitor the high-energy particles that impact the spacecraft and the science instrument. This proton flux can lead to the accumulation of charge on the gyroscopes, which in turn could lead to unacceptable torques on the gyroscopes. So far, the charge accumulated on the gyroscopes is much less than expected.

One ancillary benefit of GP-B’s proton monitor has been its ability to accurately locate the South Atlantic Anomaly, a region above the South Atlantic Ocean where the fluxes of particles trapped in the Earth’s geomagnetic field are much greater than anywhere else. GP-B’s orbit takes it through this region regularly, allowing it to produce a more precise map of this magnetic anomaly.

---

## 24 SEPTEMBER 2004—GRAVITY PROBE B MISSION UPDATE: Day 157

GP-B had an eventful week. We began the 4th week of science with all four gyroscopes in the science mode. Then on Thursday we had an anomaly with gyro #3.

At 8:30 PM local time on Thursday, the drag-free gyro #3 transitioned to analog mode resulting in safemode that stopped the timeline. The GP-B vehicle and science gyros were safe. Gyro’s #1, #2 and #4



remained in the digital suspension science mode. A preliminary assessment by the science team indicated minimal impact to any experiment accuracy. An investigation is under way to determine the cause of the drag-free gyro #3 transition to analog mode and safemode activation. The operations and engineering teams did an excellent job working through the night to safe the vehicle and quickly develop a recovery plan.

By Friday afternoon the spacecraft was back in science collecting mode with gyro #1 performing the drag-free operation. On Saturday the operations team successfully transitioned Gyro #3 from analog suspension to the digital suspension science mode. All other spacecraft systems are in excellent health. The spacecraft is rolling at a rate of 0.77419 rpm (one revolution every 77.5 seconds). The Attitude and Translation Control (ATC) system is maintaining a drag-free orbit around gyro #1, and it is properly tracking the guide star, IM Pegasi. The dewar temperature is nominal (1.82 Kelvin), and the flow of helium, venting from the dewar through the micro thrusters has remained within expected limits.

During the week the team performed a heat pulse test on the spacecraft dewar to obtain further information to help predict lifetime. Early indications are that the helium in the dewar will last another 10 months, which should be sufficient to satisfy the mission requirements.

---

## 1 OCTOBER 2004—GRAVITY PROBE B MISSION UPDATE: Day 164

The spacecraft is in good health, flying drag-free around gyro #1. All four gyros are digitally suspended, and their SQUID readouts are collecting relativity data during the portion of each orbit when the science telescope is locked onto the guide star, IM Pegasi. The spacecraft's roll rate remains at 0.7742 rpm (one revolution every 77.5 seconds). The dewar temperature is nominal (1.82 Kelvin), and the flow of helium, venting from the dewar through the micro thrusters is within expected limits.



At this time of year in North America, at around 8:30 PM Pacific Daylight Time, the constellation Pegasus, in which the guide star IM Pegasi resides, is clearly visible above the Eastern horizon. With a magnitude ranging from 5.6 – 5.85, IM Pegasi is too dim to see with the naked eye, but in a good viewing location, it should be visible with binoculars.

In last week's update, we reported that at 8:30 PM local time on Thursday, 23 September 2004, gyro #3—which was then serving as the drag-free gyro—suddenly transitioned to analog backup suspension mode, automatically triggering a safemode that stopped the mission timeline. The GP-B operations and engineering teams quickly developed a recovery plan, and by the following afternoon, the

spacecraft was back in science mode, with gyro #1 performing the drag-free operation. The effect of this event on the science experiment was insignificant. The most likely cause of this event was a data spike in the Gyro Suspension System (GSS) position sensor for gyro #3. Gyro #3 was returned to digital suspension as part of the recovery plan, and it has remained digitally suspended, with no further problems, since that time. However, we are continuing to monitor its performance and investigate the root cause. Thus, for the foreseeable future, the spacecraft will continue to fly drag-free around gyro #1.



Also last week, we reported that the team had performed a heat pulse test on the spacecraft dewar in order to determine the mass of liquid helium remaining inside, which determines the remaining lifetime of the mission. The heat pulse test works in the following way: The amount of heat that it takes to warm an object by a specified amount depends on the type of material, its temperature, and its mass. Thus, if the “specific heat” (the amount of heat needed to warm a kilogram of material by one degree kelvin) is known, it is a simple matter to measure the mass by applying a known amount of heat (usually with an electric heater) and measuring the resultant temperature rise. In the case of the GP-B dewar, the situation is simplified by the fact that heat distributes itself virtually instantaneously throughout superfluid helium. The amount of heat used in the test must be large enough to cause a measurable temperature change (approximately 10 millikelvin) but not so large as to appreciably shorten the mission lifetime. The heat pulse test yielded a remaining superfluid helium mass of 216 kg, which translates into a remaining mission lifetime of 9.9 months. This means that the science (data collection) phase of the mission will continue for a little over 8 more months, and then we will spend the final month re-calibrating the science instrument.

Finally, this past Tuesday, 28 September 2004, we observed a slight increase in the helium required by the micro thrusters to maintain drag-free flight around gyro #1. To be conservative, we decided to turn off drag-free mode and evaluate the situation. Over a period of 4-6 hours, the oscillations that were causing the ATC to require excess helium died out and have not returned. After some analysis and discussion, we have determined these oscillations were caused by a sympathetic resonance between the ATC drag-free control efforts and a sloshing wave on the surface of the now reduced superfluid helium in the dewar. This situation is somewhat analogous to placing a vibrating tuning fork on the body of a guitar, which then causes guitar strings tuned to harmonics of the same frequency to start vibrating. This is a transient situation, and the team has adjusted the ATC drag-



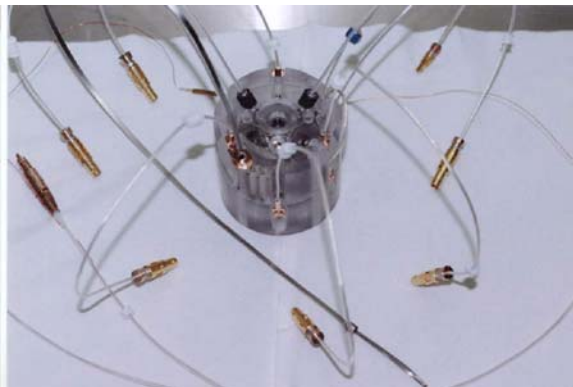
free suspension parameters to de-tune this harmonic coupling. We have since returned the spacecraft to drag-free operation around gyro #1, and it is performing nominally.

---

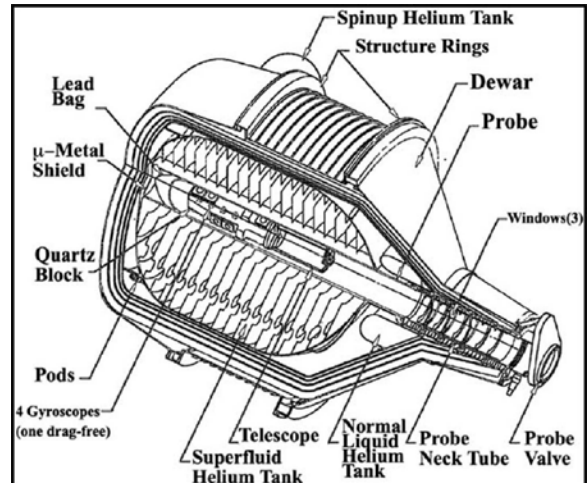
## 8 OCTOBER 2004—GRAVITY PROBE B MISSION UPDATE: Day 171

At the end of Mission Week #25, GP-B is in its sixth week of science data collection. The spacecraft continues to be in good health, flying drag-free around gyro #1. All four gyros are digitally suspended and performing nominally. The spacecraft's roll rate remains at 0.7742 rpm (one revolution every 77.5 seconds). The dewar temperature is nominal (1.82 Kelvin), and the flow of helium, venting from the dewar through the micro thrusters remains within expected limits.

As noted in last week's update, we have continued to monitor the performance of gyro #3, which had been serving as the drag-free gyro until it suddenly transitioned to analog backup suspension mode two weeks ago. At that time, we quickly implemented a recovery plan, switching drag-free flight operations to gyro #1 and reinstating digital suspension on gyro #3. It remained digitally suspended all last week until last Friday, 1 October 2004, when it once again transitioned into analog backup mode. This past Monday, 4 October 2004, we re-suspended gyro #3. Subsequently, we changed the Gyro Suspension System (GSS) bridge setting for this gyro to the high-level excitation mode used during gyro spin-up to increase the signal-to-noise ratio of this gyro's position readout. The GSS team will continue to monitor the performance of this gyro, and they are preparing to test several hypotheses regarding the root cause of this gyro's loss of digital suspension.



Last week, we also reported detecting oscillations in the drag-free control force, which we suspect were caused by a sympathetic resonance between the ATC drag-free control efforts and a sloshing wave on the surface of the now reduced superfluid helium in the dewar. We adjusted the ATC drag-free suspension parameters to de-tune this harmonic coupling, and the oscillations disappeared for most of last week, but last Friday, they began to re-appear. We have since reduced the gain in the drag-free controller to its initial level, prior to the appearance of these oscillations, and this seems to have mitigated these oscillations. Following is a more detailed explanation of this suspected harmonic resonance phenomenon, provided by our GP-B cryogenic expert, Mike Taber.



GP-B recently experienced a minor instability, characterized by excessive thruster venting and a slowly rotating force transverse to the roll direction. This force oscillation was observed by the suspension system of all four gyros and had a period of approximately 220 seconds (3.7 minutes). At the time this occurred, the system was in "drag-free" mode, where the control effort needed to center gyro #1 was being minimized by the helium thrusters. This is normal operation in science mode, wherein the space vehicle is being flown in such a way as to minimize the suspension forces and torques that can perturb the gyro spin direction. As a precautionary measure, in response to this oscillation, the drag-free control system was commanded off. The oscillation was then observed to slowly decay over a period of about six hours.

The initial assessment of this phenomenon was that it was due to a slosh instability in the liquid helium. The helium in the main tank exists in two phases: liquid and vapor. Since the space vehicle is slowly rolling, centrifugal force causes the denser liquid to reside near the outer wall of the main tank with the vapor forming a bubble at the center. Normally, the liquid rotates as a solid body with the rest of the vehicle. However, if excited, it is dynamically possible for a surface wave to form at the liquid-vapor interface that can propagate circumferentially. The fact that the oscillation persisted, but then slowly decayed after the drag-free control was turned off, supports this scenario. The energy to build up and sustain the wave was supplied by the drag-free system reacting to the force of the propagating wave with an appropriate phase shift. A subsequent examination of telemetry data indicated that this phenomenon actually started when the gain of the drag-free controller was doubled some time ago, but the amplitude was too small for it to be readily apparent. Ten days (and a number of events) actually passed before the oscillation grew sufficiently large that it was noted in the Attitude and Translation Control (ATC) system and dewar data. The drag-free controller gain has since been reduced back to its original value. There is no indication that any of these events had any adverse impact on the GP-B experiment.

---

## 15 OCTOBER 2004—GRAVITY PROBE B MISSION UPDATE: Day 178

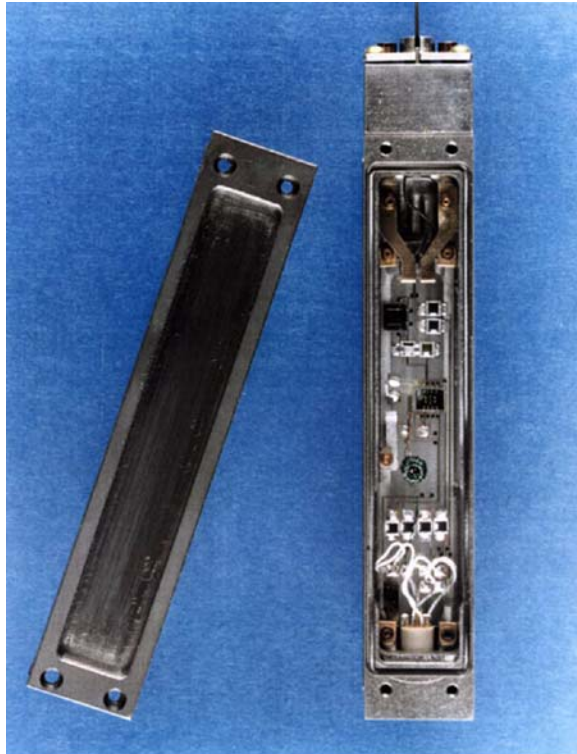
Six months into the mission, GP-B is performing remarkably well. The spacecraft is in fine health, flying drag-free around gyro #1. All four gyros remain digitally suspended, and they are all generating science data. The spacecraft is rolling at 0.7742 rpm (77.5 seconds per revolution), and all subsystems are performing well. The dewar temperature remains nominal at 1.82 kelvin, and the flow of helium

from the dewar through the micro thrusters continues to be within expected limits. We are now in our seventh week of data collection, which is going very smoothly, and a recent test on the dewar indicates that we have enough helium to continue collecting data for approximately eight more months. The quality of the data gathered thus far is excellent.

This past week has been a relatively quiet one for the GP-B spacecraft. The oscillations in the drag-free control force, which we have been reporting on for the past two weeks, have diminished to an insignificant level. Adjustments that we made to the drag-free suspension parameters to de-tune a harmonic coupling between the drag-free control system and helium sloshing in the dewar, combined with reducing the gain in the drag-free controller to its initial level, seem to have mitigated this instability. To be certain, we are continuing to monitor the drag-free control system with regards to this issue.

Furthermore, gyro #3, which we have been monitoring over the past three weeks, since it unexpectedly transitioned from digital to analog back-up suspension, has remained digitally suspended, without further incident this past week. We suspect that the issue with gyro #3 is not related to the gyro rotor (sphere) itself, but rather with some noise spikes in its suspension system that have exceeded pre-set limits, automatically triggering a transition into analog back-up suspension mode. Increasing the signal-to-noise ratio of this gyro's position readout seems to have mitigated this problem. However, we are continuing to monitor gyro #3, and we are still analyzing the root cause of this behavior.

The two issues mentioned above have prompted several inquiries about the effects of such events on the health of our data and the ultimate results of the experiment.



A SQUID (Superconducting Quantum Interference Device)

The short answer is that neither of these events has had any significant effect on the data or the experimental results. The SQUID readouts for each gyro continue to provide spin axis orientation data in both digital and analog suspension modes, so no data was lost when gyro #3 transitioned to analog mode. Also, even in those few moments when the spacecraft is not in drag-free mode, we continue to collect data, but in this case, we must carefully evaluate any potential torques (forces) placed on the gyros to ensure that they did not alter the gyro's spin axis alignment.

---

## 22 OCTOBER 2004—GRAVITY PROBE B MISSION UPDATE: Day 185

GP-B continues to perform well. We have switched back to flying the spacecraft drag-free around gyro #3, and all four gyros are digitally suspended and generating science data. The spacecraft's roll rate remains constant at 0.7742 rpm (77.5 seconds per revolution), and all subsystems are continuing to perform well. As we near two months of data collection, the flow of helium from the dewar through the micro thrusters remains within expected limits, and the dewar temperature is stable at 1.82 Kelvin. We have approximately seven months of data collection remaining, and the quality of the data received thus far continues to be excellent.



This past Tuesday, October 19th, gyro #1, which has been serving as the "drag-free" gyro for the past few weeks, transitioned into analog backup suspension mode. Having already worked through this same scenario with gyro #3 last month, we were able to smoothly switch drag-free operations back to gyro #3 and restore digital suspension to gyro #1 within three hours of this event. Because gyro #3 has been performing well after we increased the signal to noise ratio in its Gyro Suspension System (GSS) position readout, we have made the same adjustment to gyro #1. We are now monitoring the performance of both gyros #3 and #1 to determine if the analog suspension transition will recur, or if this issue has been resolved.

The oscillations in the drag-free control force, which we have been reporting on in previous highlights, have remained at an insignificant level over the past week. We are performing further analysis and adjustments on the drag-free suspension parameters to ensure the de-tuning of any harmonic coupling between the drag-free control system and helium sloshing in the dewar. We are continuing to monitor the drag-free control system with regard to this issue.



We have received inquiries about a recent letter to *Nature* by Ignazio Ciufolini and Erico Pavlis claiming to have verified the Lense-Thirring frame-dragging effect of general relativity through laser ranging data observations of the LAGEOS I & II spacecraft. In their measurement, the frame-dragging effect needs to be separated by an extremely elaborate modeling process from Newtonian effects more than 10,000,000 times larger than the effect to be measured. The letter does not provide enough detail of the methods of verification and validation to allow a critical evaluation. We and other members of the relativity community look forward to a more complete account. If verified, their result will be of considerable interest.



The GP-B science instrument and spacecraft were specifically designed to create a pristine environment to perform direct measurements of both the frame-dragging and geodetic effects of general relativity with all Newtonian disturbances several orders of magnitude smaller than the effects to be measured. Theoretically, only one gyroscope is needed to make GP-B's measurements, but we use four gyroscopes to give highly accurate independent checks of the two effects. As a further validation, throughout the whole GP-B mission we conduct a continuing series of verification/calibration tests. In particular, during our final month-long instrument re-calibration following data collection, we will perform a series of tests in which certain classes of potential disturbances are deliberately increased in order to uncover any previously unknown effects. Tests of this kind, where possible disturbances are enhanced in order to calibrate and remove them, are a vital part of good experimental physics practice.

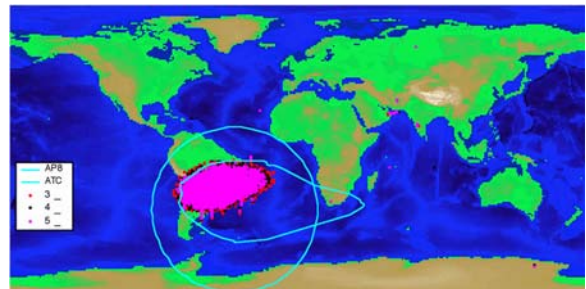
## 29 OCTOBER 2004—GRAVITY PROBE B MISSION UPDATE: Day 192

In its 28th week in orbit, GP-B is continuing to perform well. We have completed two months of data collection, and the quality of the data received thus far is excellent. The spacecraft is maintaining a constant roll rate of 0.7742 rpm (77.5 seconds per revolution) and flying drag-free around gyro #3. The dewar temperature remains stable at 1.82 kelvin, and the flow of helium from the dewar through the micro thrusters is nominal. All other spacecraft subsystems are continuing to perform well.

This past Wednesday evening, for the first time since 1918, when Austrian physicists, Josef Lense and Hans Thirring published their important paper on the gravitomagnetic or “frame-dragging” effect, the Boston Red Sox swept the World Series. Some say the heavens responded with a glorious total eclipse of the moon—or perhaps, it was the eclipsed moon that enabled the Red Sox to achieve this stunning victory. Whatever the case, these cosmic events had absolutely no effect on the GP-B spacecraft.



However, in preparation for solar events that could have an effect on our spacecraft, yesterday, the GP-B Mission Operations team performed an all-day simulation of the recovery process we will need to go through in the unlikely event that proton radiation from the sun temporarily disables our main, A-side computer, triggering an automatic switch-over to our backup, B-side computer. Chances of such a switch-over increase slightly whenever our spacecraft passes through the region over the South Atlantic Ocean, called the “South Atlantic Anomaly,” where the fluxes of particles trapped in the earth's geomagnetic field are greater than anywhere else.



In fact, this may have been the cause of the B-Side switch-over we experienced during the second week of the mission. At that time, we were just beginning to adjust various parameters on the spacecraft, and switching back to the A-side computer went smoothly and quickly. Now that we are well into the science phase of the mission, flight-control parameters have changed, so it is prudent to rehearse the recovery procedures in order to minimize down time and loss of data in the event of a switch-over. To this end, we were pleased with the team's excellent performance during yesterday's simulation.

Again, this past week, oscillations in the drag-free control force that we have reported on in previous updates remained insignificant. We are continuing to perform analysis and adjustments on the drag-free suspension parameters to ensure that no harmonic coupling occurs between the drag-free control system and helium sloshing in the dewar, and we continue to monitor this situation.

Likewise, increasing the signal to noise ratio in the Gyro Suspension System (GSS) position readouts of gyros #3 and #1 appears to have mitigated the problems we experienced with these gyros unexpectedly transitioning to analog suspension mode. Both gyros #3 and #1 have both remained digitally suspended this past week, and we are continuing to monitor the performance of their suspension systems.

On Thursday, 21 October 2004, our GP-B external Science Advisory Committee, chaired by Professor Clifford M. Will of Washington University in St. Louis, met here at Stanford and conducted a valuable review of our science data processing approach.

## 5 NOVEMBER 2004—GRAVITY PROBE B MISSION UPDATE: Day 199

As of mission Day #199, all vehicle and payload systems remain in good health. We have now completed nine weeks of data collection, and the quality of the data continues to be excellent. The spacecraft is maintaining a constant roll rate of 0.7742 rpm (77.5 seconds per revolution) and flying drag-free around gyro #3. The flow of helium from the dewar through the micro thrusters is nominal, and the dewar temperature is stable at 1.82 Kelvin.

Once again, this past week has been a relatively quiet one for the GP-B spacecraft. Adjustments that we made to the drag-free suspension parameters have prevented any further harmonic coupling between the drag-free control system and helium sloshing in the dewar. As a result, the previously reported oscillations in the drag-free control force have completely disappeared. We will continue to monitor the drag-free control system and any motion of helium in the dewar, but this is no longer considered to be an issue.

Likewise, increasing the signal to noise ratio in the Gyro Suspension System (GSS) position readouts of gyros #3 and #1 has mitigated the problems we experienced with these gyros unexpectedly transitioning to analog suspension mode. Both gyros #1 and #3 have remained digitally suspended since we made these adjustments, so we also consider this issue to be closed.



Close-up of GP-B telescope specialist, Ken Bower, adjusting the wires on the GP-B pre-flight telescope.

This past week, we moved our pre-flight prototype science telescope into a clean room to photograph it, before returning it to its sealed display case in our GP-B lobby here at Stanford. The science telescope is both a beautifully crafted instrument and a marvel of engineering.

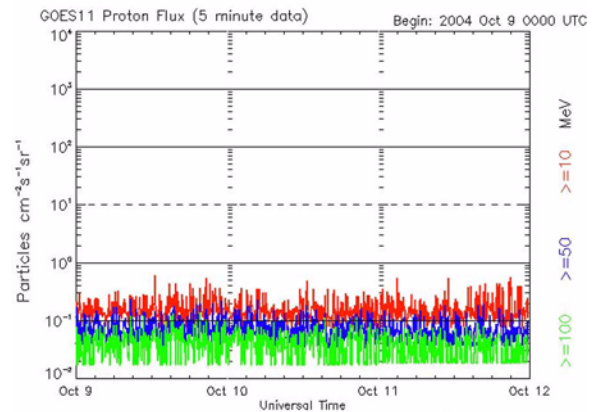


Side view of the pre-flight prototype Gp-B telescope. The actual flight version has clear sides.

## 12 NOVEMBER 2004—GRAVITY PROBE B MISSION UPDATE: Day 206

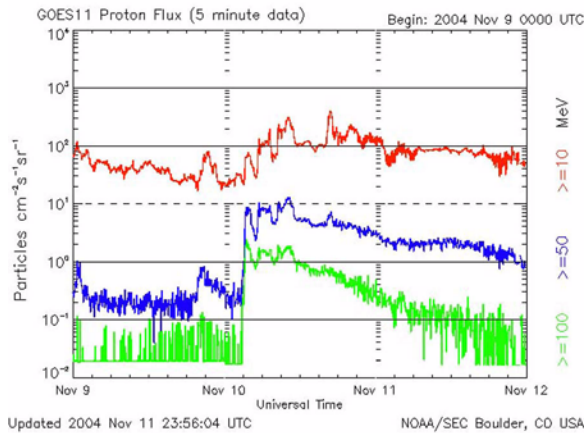
In its 30th week in orbit, the GP-B spacecraft is in good health and is performing well. We have completed 2.5 months of data collection, and the quality of the data continues to be excellent. The spacecraft is flying drag-free around gyro #3, while maintaining a constant roll rate of 0.7742 rpm (77.5 seconds per revolution). As we enter the second portion of the year when the spacecraft remains in full sunlight for approximately a month, the shell of the dewar is warming up slightly, and thus rate of helium boiling off from the dewar has increased slightly, resulting in a uniform increase of helium flow through the micro thrusters, in order to maintain the appropriate pressure inside the dewar to keep its temperature stabilized at 1.82 kelvin.

The two plots to the right show a side-by-side comparison of normal solar activity from one month ago versus the activity during the geomagnetic storm this past Wednesday and Thursday. The difference is dramatic. Note especially the large increase in highest-level (green) proton flux on November 10th. The increase in these particles rarely rises above the 0.1 (first) level on this plot.



Updated 2004 Oct 11 23:56:03 UTC NOAA/SEC Boulder, CO USA

NOAA/SEC plot of solar proton activity during a quiet period one month ago.



NOAA/SEC plot of heightened proton bombardment from this week's solar flares and geomagnetic storm. In particular, note the increase of high-energy protons (green) on November 10th.

One of the effects of geomagnetic storming is a significant increase in high-energy proton bombardment in any part of the Earth facing the Sun, and especially in the region known as the South Atlantic Anomaly, which normally experiences heightened levels of solar particle bombardment. Thus, it was not surprising that at 4:58 PM PST on 10 November 2004, as the GP-B spacecraft was entering the South Atlantic Anomaly region, a proton hit a critical memory location in the SQUID Readout Electronics (SRE). This event triggered a chain reaction of safemodes that, among other things, halted the GP-B mission time line, caused the SRE computer to reboot, and transitioned all four gyros to analog backup suspension mode.

Over the past few weeks, the SRE electronics had sustained two proton hits to non-critical memory locations, and we were already in the process of planning the necessary steps to manually reboot it, but as it happens, nature apparently took care of this issue for us. Fortunately, the effects of this event were limited to the SRE electronics, and the spacecraft's main (A-side) computer was not affected. Our team worked through the night this past Wednesday and most of Thursday, sending commands to the spacecraft to reset affected systems and restore all four gyros to digital suspension modes. As of this afternoon, the spacecraft has returned to normal operation. The effect of this event on the experimental data is not yet known. A few data points from this period may have to be omitted, but such an omission will have no significant effect on the overall experimental results.

### 19 NOVEMBER 2004 – GRAVITY PROBE B MISSION UPDATE: DAY 213

The GP-B spacecraft remains in good health and is continuing to perform well. We have been collecting science data for 83 days, and data acquisition process is proceeding as expected. The spacecraft is maintaining a constant roll rate of 0.7742 rpm (77.5 seconds per revolution), and it is flying drag-free around gyro #3. The dewar's internal temperature remains steady at just under 1.82 Kelvin.



At this time of year, the spacecraft is entering a 6-week period where it remains in full sunlight—that is, light from the Sun shines broadside on the spacecraft. As a result, the dewar's outer shell has been warming up, and some of this heat is transferred to the liquid helium inside. Because the temperature and pressure inside the dewar are maintained at constant levels, this expected seasonal warming of the dewar causes the helium inside to boil off at a faster rate. To compensate for this increased helium flow and maintain the correct pointing position, the spacecraft's Attitude and Translation Control system (ATC) has been “null dumping” (uniformly venting) the excess helium out through the micro thruster system.

Last week, we reported that on 10 November 2004, the SQUID Readout (SRE) computer failed a fundamental “health check,” which resulted in its rebooting itself and triggering six protective safemodes that, among other things, halted the spacecraft's on-board timeline, unlocked the telescope from the guide star, closed the telescope shutter, and transitioned all four gyros into analog backup suspension. On first analysis, it appeared that the root cause of this anomalous event was that a high-energy proton had struck a critical memory location in the SRE computer during the severe geomagnetic storm that was raging all last week.

However, further analysis now suggests that the spacecraft did not suffer a new proton hit after all. Rather, the SRE computer had previously suffered high-energy proton hits resulting in multi-bit (not self-correctable) errors in two of its memory locations. These memory locations were thought to be non-critical, but it now appears that one of these affected memory locations was accessed during a routine maintenance procedure.

This caused a health check of the SRE computer to fail, which in turn, automatically triggered the safemodes and re-booted the computer. For precautionary purposes, our team had already prepared a procedure to manually reboot the SRE computer and clear out any multi-bit errors, but this will no longer be necessary, since the computer's self-reboot last week cleared and reset all of the computer's memory locations. The fact that this event happened while the spacecraft was entering the South Atlantic Anomaly region of the Earth (where protection from proton bombardment is significantly reduced) during a severe geomagnetic storm, was apparently a coincidence.

Events such as the one that occurred last week always prompt a number of inquiries about whether such glitches cause any loss of scientific data or detriment to the experimental results. The short answer to this question is “no.” Such events typically do not—and have not—had any significant effect on the GP-B experimental data or the results.



---

**26 NOVEMBER 2004—GRAVITY PROBE B MISSION  
UPDATE: Day 220**

On the eve of the 2004 Thanksgiving holiday weekend—mission week #32—the GP-B spacecraft is in good health, with all subsystems performing well. We have now been collecting data for three months. Data collection is proceeding smoothly, and the quality of the data is excellent. The spacecraft continues to fly drag-free around gyro #3, maintaining a constant roll rate of 0.7742 rpm (77.5 seconds per revolution.) The temperature inside the dewar remains steady at just under 1.82 Kelvin.

---

**3 DECEMBER 2004—GRAVITY PROBE B MISSION  
UPDATE: Day 227**

The GP-B spacecraft continues to be in good health, with all subsystems performing well. As of tomorrow, we will have been collecting relativity data for 100 days. The data collection process is proceeding smoothly, and the quality of the data remains excellent. All four gyros are digitally suspended in science mode, and the spacecraft is flying drag-free around gyro #3, maintaining a constant roll rate of 0.7742 rpm (77.5 seconds per revolution.) The temperature inside the dewar is holding steady at just under 1.82 kelvin.

It has been relatively quiet here in the GP-B Mission Operations Center, since the strong solar flares and geomagnetic storm three weeks ago. Our team continues to adjust the flow rate of the excess helium from the dewar during the present a 6-week “hot” season, where the spacecraft is continually in sunlight throughout each orbit. (See last week’s highlights for a discussion of the spacecraft’s seasons.)

Furthermore, seasonal warming of the spacecraft has resulted in the Attitude Reference Platform (ARP) on the outside of the spacecraft producing data that slightly diminishes the pointing accuracy of the Attitude and Translation Control system (ATC). To address this issue, the ATC team installed a modified data filter, and tests performed this past week indicate that spacecraft pointing accuracy has now improved.

Finally, the team has been adjusting controls on the navigational gyroscopes that are used by the ATC to keep the telescope pointed towards the guide star, IM Pegasi (HR 8703), during periods when the spacecraft moves behind the Earth, eclipsing the telescope’s view of the guide star. These adjustments have reduced the time required for the telescope to re-lock onto the guide star—when the spacecraft emerges over the North Pole—to less than one minute.

---

**10 DECEMBER 2004—GRAVITY PROBE B MISSION  
UPDATE: Day 234**

Now, almost 34 weeks in orbit, the GP-B spacecraft is in fine health, with all subsystems continuing to perform well. The spacecraft, which is in the middle of a 6-week un-eclipsed (full sun) period, is flying drag-free around gyro #3, maintaining a constant roll rate of 0.7742 rpm (77.5 seconds per revolution.) The temperature inside the dewar is holding steady at just under 1.82 kelvin. All four gyros are digitally suspended in science mode. We have been collecting relativity data for 15 weeks. The data collection process is continuing to proceed smoothly, and the quality of the data continues to be excellent.

For much of the month of December, our Mission Planning staff has scheduled minimal spacecraft activity, outside routine monitoring of spacecraft functionality and downloading of science data. However, lest we become complacent, Mother Nature seems to have a way of stirring up the pot—as was the case last Saturday afternoon.

**The Spacecraft’s Tale**

Last Saturday began as a rather “ho-hum” California winter’s day. Orbiting the Earth every 97.5 minutes, the GP-B spacecraft passed directly over California around 6:30AM PST, but the Sun was already up, and the sky was too bright to see the satellite. In the GP-B Mission Operations Center (MOC), a skeleton crew consisting of the on-duty Mission and Flight directors and one or two resident engineers monitored several telemetry passes (communications sessions) during the morning hours. Most were 25-minute satellite passes, during which the spacecraft relays status information to the MOC through the NASA TDRS (Tracking and Data Relay Satellite) communications satellite system. And, during a 12-minute ground pass at 1:15PM PST, the spacecraft’s solid-state recorder relayed relativity data to the GP-B science database through a high-speed telemetry connection with the Svalbard ground tracking station, on the island of Spitzbergen in Norway. All in all, it was a normal Saturday, and the atmosphere in the MOC was quite relaxed.



Svalbard Ground Station, Longyearbyen, Spitzbergen, Norway

Following the successful ground pass with Svalbard, the spacecraft continued on its southward route. At around 1:30 PM PST, Pacific time, the spacecraft was flying over South America—heading towards the South Pole—when it entered the South Atlantic Anomaly (SAA). This is a region above the Earth where the fluxes of trapped protons and other particles, emitted by the Sun, are much greater than anywhere else on Earth, due to the asymmetry of the Earth’s protective Van Allen Radiation Belts. Thus, spacecraft are more vulnerable to being struck by protons when flying through this region.

At 1:48PM, Pacific Time, an odd event silently occurred on-board the spacecraft, triggering four safemodes (pre-programmed command sequences designed to automatically place the spacecraft, its gyros, telescope, and other systems and instruments, in a stable and safe configuration in response to anomalous or out-of-limits feedback from various on-board sensors).

Back in the MOC, the next telemetry pass was not scheduled until 3:16 PM, so the operations staff was completely unaware of this change in the spacecraft’s condition—for the time being. At 3:15PM, the MOC staff settled into their seats for the upcoming satellite status telemetry pass. As the spacecraft’s antenna locked into the TDRSS satellite and



began transmitting, one-by-one, status monitors around the MOC began turning red, signaling the spacecraft had triggered its safemodes. There is a problem on-board.

During the next 20 minutes, phones rang, pagers beeped, and soon, the MOC was teeming with activity. An assessment of the safemodes that were triggered indicated that an error—never seen before—had occurred in a module of the Attitude and Translation Control (ATC) computer system. The spacecraft's GPS had registered an off-the-scale velocity spike, which if correct, indicated that, for one brief moment, the spacecraft had traveled faster than the speed of light—or to use Star Trek terminology, it had “warped into hyperspace.” In fact, the GPS system had reported a single data point with an erroneously high velocity, which when squared, caused a computer overflow. The ATC computer module took exception to this data overflow and triggered a safemode test, which in turn activated a chain reaction response sequence.



The MOC staff immediately scheduled several extra satellite communication passes so they could communicate with the spacecraft more frequently. Then, over the ensuing 24 hours, they methodically worked through a series of tests and command sequences to return the spacecraft to its normal science operation mode. We initially assumed that the GPS receiver had suffered a proton hit in the SAA region, but further analysis suggests that this was not the case. Rather, this anomaly was apparently caused by one of the four accessible GPS satellites being in the wrong position for proper GPS triangulation. The ATC system usually catches situations of this kind and disallows the data; but, this one slipped through the filter.

The spacecraft has returned to normal operations. This incident was not detrimental to the GP-B experimental data. And, once again, the fact that an anomalous event occurred while the spacecraft was flying through the SAA region appears to be a coincidence—or is it?

---

## 17 DECEMBER 2004—GRAVITY PROBE B MISSION UPDATE: Day 241

As we near the end of 2004, the GP-B spacecraft has been in orbit for just under eight months and collecting science data for almost four months. It remains in fine health, and all subsystems are continuing to perform well. The spacecraft is beginning to experience brief periods of being eclipsed from sunlight by the Earth during each orbit, signaling that its recent full-sun season is waning. It is flying drag-free around gyro #3, maintaining a constant roll rate of 0.7742 rpm (77.5 seconds per revolution.) The temperature inside the dewar is holding steady at just under 1.82 Kelvin. Recent measurements indicate that approximately half of the superfluid has now been expended from the dewar. All four gyros are digitally suspended in science mode. We are now approximately 40% of the way through the science phase of the mission. The data collection process is continuing to proceed smoothly, and the quality of the data remains excellent.

### A GP-B RETROSPECTIVE ON 2004

Looking back, 2004 has been a year of monumental triumph for GP-B. The year began with a re-work of the Experiment Control Unit (ECU), and its subsequent reinstallation into the space vehicle.

At the beginning of April, as the space vehicle was being readied for launch, the official GP-B pre-launch press conference was held at NASA headquarters in Washington DC. (You can view a streaming video of this press conference, which includes many technical details about the GP-B science experiment and technology, on NASA's Kennedy Space Center ELV Web page.)

Three weeks following the press conference, at 9:57 am PST on 20 April 2004, a Boeing Delta II rocket carried the GP-B spacecraft, embodying over 40 years of dogged persistence in science and engineering, into a perfect orbit. That emotionally overwhelming day, culminating with the extraordinary live video of the spacecraft separating from the second stage booster meant, as GP-B Program Manager Gaylord Green put it, “that 10,000 things went right.” The GP-B launch will long be remembered—not only by GP-B Principal Investigator, Francis Everitt, and the GP-B team, but also by thousands of people who have been associated with GP-B in one way or another over the years and countless others who have been following it.

The launch was the “end of the beginning” for GP-B. The ensuing 4-month IOC period demonstrated the exceptional preparedness and dedication of the GP-B team, from dealing with anomalies in orbit to spinning up the four gyros last August, which following the launch, was the second greatest milestone in the program.

Now, four months into the 10-month science phase of the mission, our whole GP-B team can reflect back on the past year with an enormous sense of pride and accomplishment. And, as we look forward to the coming year, we are keenly aware of our continued responsibility to see this once-in-a-lifetime experiment through to its final conclusion.

---

## 7 JANUARY 2005—GRAVITY PROBE B WEEKLY UPDATE: Day 262

Throughout the holiday season, the GP-B spacecraft has remained in excellent health, with all subsystems performing well and no anomalous events. The GP-B spacecraft has now completed more than 3,870 orbits over 8.5 months, and on average, the four gyros have each made approximately one billion revolutions.

The spacecraft's full-sun season has ended, and it is now experiencing longer periods of being eclipsed from sunlight by the Earth during each orbit. It is flying drag-free around gyro #3, maintaining a constant roll rate of 0.7742 rpm (77.5 seconds per revolution.) All four gyros are digitally suspended in science mode. The temperature inside the dewar is holding steady at 1.82 Kelvin, and it is now less than half full of superfluid helium. We have been collecting science data for 19 weeks, and we are now approximately 45% of the way through the science phase of the mission. The data collection process is continuing to proceed smoothly, and the quality of the data remains excellent.

---

### 14 JANUARY 2005—GRAVITY PROBE B WEEKLY UPDATE: Day 269

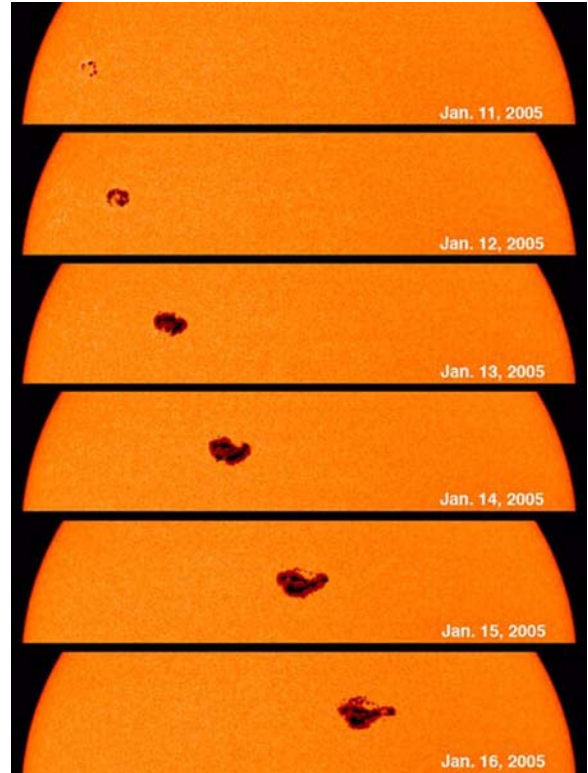
The spacecraft is in excellent health, with all subsystems performing well. The GP-B spacecraft is flying drag-free around gyro #3, maintaining a constant roll rate of 0.7742 rpm (77.5 seconds per revolution.) All four gyros are digitally suspended in science mode. The temperature inside the dewar is holding steady at 1.82 Kelvin. We have been collecting science data for 20 weeks, just under halfway through the science phase of the mission. The data collection process continues to proceed smoothly, and the quality of the data remains excellent.

---

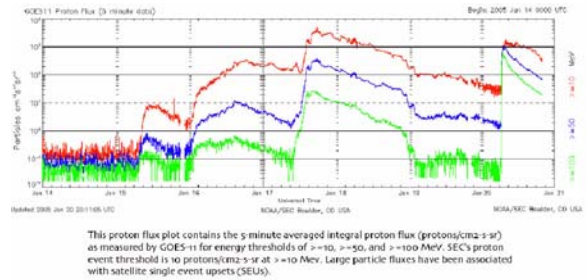
### 21 JANUARY 2005—GRAVITY PROBE B WEEKLY UPDATE

**Mission Elapsed Time:** 276 days (39 weeks/9 months)  
**Current Orbit #:** 4,075 as of 4:30PM PST  
**Spacecraft General Health:** Good  
**Roll Rate:** Normal at 0.7742 rpm (77.5 seconds per revolution)  
**dewar Temperature:** 1.82 Kelvin, holding steady

We are in the process of recovering from the effects of 7 major solar flares that have erupted from the Sun's surface since 15 January 2005. These flares have resulted in extremely high levels of proton radiation and two multi-bit errors (MBE) in our SRE electronics.



In addition, these high levels of solar radiation saturated the GP-B telescope detectors, causing the telescope to lose track of the guide star (IM Pegasi). We have now re-locked the telescope onto the guide star. We have determined that one of the MBEs in the SRE electronics is in a non-critical location, but the second one is in a location that is used for SQUID calibration.



We are in the process of creating a work-around for the second MBE location. Our science team reports that the loss of data from these events has been minimal, and that it will have no significant effect on the experimental results.

---

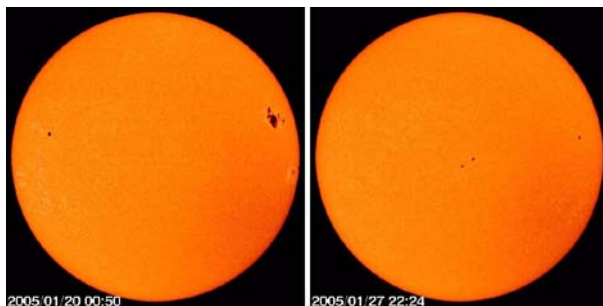
## 28 JANUARY 2005—GRAVITY PROBE B MISSION UPDATE

Mission Elapsed Time: 283 days (40 weeks/9.25 months)  
Current Orbit #: 4,178 as of 4:00 PM PST  
Spacecraft General Health: Good  
Roll Rate: Normal at 0.7742 rpm (77.5 seconds per revolution)  
Dewar Temperature: 1.82 Kelvin, holding steady  
Command & Data Handling (CDH): Multi-bit errors (MBE): 0, Single-bit errors (SBE): 8.5 (daily avg.)

Last Thursday morning (20 January 2005), GP-B entered Safemode 2A (gyro hold), due to the loss of the guide star. Analysis of this safemode indicated that the telescope detectors were saturated by a large solar flare (X-7 class) that occurred Wednesday night.

The solar flare had fluxes spiking several orders of magnitude above nominal in the > 100MeV proton energy range. Less than a day later (16:27 PST), GP-B successfully re-locked onto the guide star and the Attitude and Translation Control (ATC) system returned to its nominal configuration. During this event, the attitude error of the spacecraft and telescope remained within 800 arcseconds of the guide star. A preliminary assessment suggests that this event had minimal impact on the GP-B data or experiment.

One issue currently being investigated is the spacecraft's proton monitor, which had been yielding spurious values before last week's solar storm. The proton monitor was power cycled this Tuesday night (25 January). After reboot, it provided two hours of meaningless data followed by zeros. The proton monitor team is examining the data for additional clues, and a review of this issue will be forthcoming.



Last week's intense solar storm has died down, and solar proton activity, as reported by the National Oceanic & Atmospheric Administration's (NOAA) Space Environment Center (SEC), has returned to normal levels. (The left solar photo and graph are from last week; the solar photo and graph on the right are from today.) Likewise, the GP-B spacecraft has returned to normal functioning, with the ATC system locking normally on the guide star each orbit and the telescope detectors returning normal values. GP-B was not the only satellite affected by last week's solar storm; other satellites fared worse from the ordeal. In fact, given that last week's solar storm was the worst one since October, 2003, the GP-B spacecraft performed remarkably well, with a very swift recovery and no significant impact to the experiment.

---

## 4 FEBRUARY 2005—GRAVITY PROBE B MISSION UPDATE

Mission Elapsed Time: 290 days (41 weeks/9.5 months)  
Science Data Collection: 161 days (23 weeks/5.25 months)  
Current Orbit #: 4,281 as of 4:00 PM PST  
Spacecraft General Health: Good  
Roll Rate: Normal at 0.7742 rpm (77.5 seconds per revolution)  
Dewar Temperature: 1.82 kelvin, holding steady  
Command & Data Handling (CDH): Multi-bit errors (MBE): 1 (See MD Summary below), Single-bit errors (SBE): See MD Summary below)

Last weekend, on both Saturday and Sunday, the spacecraft's main computer (CCCA) erroneously displayed a dramatic increase in single-bit errors (SBE). We observed similar SBE increases in July 2004 and one other time since then. In both previous cases, the SBE count quickly returned to normal, and we were unable to determine the root cause of the erroneous increase. SBEs are self-correcting, so no particular action is required, but we are monitoring this situation. Also, this past Tuesday, a new multi-bit error (MBE) was discovered in a memory location of the CCCA computer. A command was subsequently sent to reload this memory location, clearing the MBE.

The health of the spacecraft's Proton Monitor is still under investigation. Telemetry indicates that it is powered on, but the data appears to be corrupt. Note that the science mission is NOT affected by the loss of the Proton Monitor. The Proton Monitor Engineering unit is continuing to investigate this failure.

We have been notified that the sun spot which caused the GP-B science telescope to lose track of the guide star two weeks ago, will be coming around to the front side of the sun on 5 February 2005. Geomagnetic activity around the Earth tends to increase after the appearance of sun spots. Thus, we have added extra telemetry passes and increased sensitivity to this issue during the next two weeks.

---

## 11 FEBRUARY 2005—GRAVITY PROBE B MISSION UPDATE

Mission Elapsed Time: 297 days (42 weeks/9.75 months)  
Science Data Collection: 168 days (24 weeks/5.5 months)  
Current Orbit #: 4,384 as of 4:00 PM PST  
Spacecraft General Health: Good  
Roll Rate: Normal at 0.7742 rpm (77.5 seconds per revolution)  
Dewar Temperature: 1.82 Kelvin, holding steady  
Command & Data Handling (CDH): Multi-bit errors (MBE): 0, Single-bit errors (SBE): 1,731 (daily average)

This past week was a quiet one for GP-B, with very few activities scheduled. The solar flares that caused us to lose the guide star three weeks ago came around to the front of the Sun, facing towards Earth, again this past week. We took extra precautions and scheduled extra telemetry passes to deal with possible effects of these solar flares on the spacecraft. However, this time, the solar flares produced no substantial geomagnetic activity around the Earth. This may be a sign that the Sun has moved into a quieter part of the solar cycle.



---

## 18 FEBRUARY 2005—GRAVITY PROBE B MISSION UPDATE

Mission Elapsed Time: 304 days (43 weeks/10.0 months)  
Science Data Collection: 175 days (25 weeks/5.75 months)  
Current Orbit #: 4,486 as of 2:00 PM PST  
Spacecraft General Health: Good  
Roll Rate: Normal at 0.7742 rpm (77.5 seconds per revolution)  
Dewar Temperature: 1.82 Kelvin, holding steady  
Command & Data Handling (CDH): Multi-bit errors (MBE): 0, Single-bit errors (SBE): 4,704 (daily average)

This past week was again a relatively quiet one for GP-B. Solar flare activity is low, and solar radiation levels are normal. Guide star capture times (time required to re-lock the telescope onto the guide star as the spacecraft emerges from behind the Earth each orbit) are averaging approximately one minute, which is excellent. The brightness table was updated for two of the stars that are monitored by the spacecraft's star trackers, and this significantly improved the star tracker's performance. Brightness tables for other stars in the star tracker catalog will be updated next week.

To determine how much helium is currently left in the dewar, the GP-B dewar team is in the process of performing another heat pulse meter operation. The heat pulse test works in the following way: The amount of heat that it takes to warm an object by a specified amount depends on the type of material, its temperature, and its mass. Thus, if the "specific heat" (the amount of heat needed to warm a kilogram of material by one degree Kelvin) is known, it is a simple matter to measure the mass by applying a known amount of heat (usually with an electric heater) and measuring the resultant temperature rise.

In the case of the GP-B dewar, the situation is simplified by the fact that heat distributes itself virtually instantaneously throughout superfluid helium. The amount of heat used in the test must be large enough to cause a measurable temperature change (approximately 10 millikelvin) but not so large as to appreciably shorten the mission lifetime.

The dewar team expects to complete their analysis of the heat pulse data next week, and we will report the results in next week's update. Our current expectation is that the science phase of the mission will conclude towards the end of June, and the results of the heat pulse meter operation will help us determine whether or not the current mission time line is correct.

---

## 25 FEBRUARY 2005—GRAVITY PROBE B MISSION UPDATE

Mission Elapsed Time: 311 days (44 weeks/10.25 months)  
Science Data Collection: 182 days (26 weeks/6.0 months)  
Current Orbit #: 4,589 as of 2:00 PM PST  
Spacecraft General Health: Good  
Roll Rate: Normal at 0.7742 rpm (77.5 seconds per revolution)  
Dewar Temperature: 1.82 kelvin, holding steady  
Command & Data Handling (CDH): Multi-bit errors (MBE): 0, Single-bit errors (SBE): 9,937 (daily average)

Three activities occupied our attention this past week:

The Heat Pulse Meter Operation (HPMO), used to determine helium in the dewar, occurred as scheduled on Wednesday night, 16-February. Preliminary analysis has been concluded and a sub-system level review is in progress.

Star Sensor Magnitude Update was run Thursday to adjust the cataloged magnitude of star 173. As of Tuesday, updates of observed magnitude of stars 50 and 173 were successful. Other stars' magnitudes may be updated.

Two separate communications issues at Poker Flat, AK (2hr40m) and Wallops Ground Station (2hr50m) caused brief outages of data. All the data was recovered from Alaska; Wallops data was unrecoverable. Since the start of the mission, the GP-B team has successfully collected 99.0% of the data (requirement is 90%).

---

## 4 MARCH 2005—GRAVITY PROBE B MISSION UPDATE

Mission Elapsed Time: 318 days (45 weeks/10.5 months)  
Science Data Collection: 189 days (27 weeks/6.25 months)  
Current Orbit #: 4,694 as of 2:00 PM PST  
Spacecraft General Health: Good  
Roll Rate: Normal at 0.7742 rpm (77.5 seconds per revolution)  
Dewar Temperature: 1.82 Kelvin, holding steady  
Command & Data Handling (CDH): Multi-bit errors (MBE): 0, Single-bit errors (SBE): 8,198 (daily average)



Guide star capture times have improved to the one-minute range after gyro biases were updated on all three axes. This is a typical adjustment of the positioning gyroscopes on the satellite (which are different than the science gyros) that is required due to the influence of the Sun as GP-B orbits the Earth. These adjustments allow the satellite to more quickly re-focus, or "capture", the guide star as it emerges from the Earth's eclipse on each orbit.

---

## 11 MARCH 2005—GRAVITY PROBE B MISSION UPDATE

Mission Elapsed Time: 325 days (46 weeks/10.75 months)  
Science Data Collection: 196 days (28 weeks/6.50 months)  
Current Orbit #: 4,767 as of 2:00 PM PST  
Spacecraft General Health: Good  
Roll Rate: Normal at 0.7742 rpm (77.5 seconds per revolution)  
Dewar Temperature: 1.83 kelvin, decreasing slowly  
Command & Data Handling (CDH): Now using B-side (backup) computer & guidance systems  
Multi-bit errors (MBE): 0, Single-bit errors (SBE): 7 (daily average)

The switch-over to the backup systems occurred automatically at 7:17 am PST last Friday morning, 4 March 2005, due to two or more multi-bit errors (MBE's) in the flight computer, occurring within a 0.2 second interval. The MBEs were caused by radiation hits in the south

magnetic pole. This event triggered pre-programmed safemodes, which in turn resulted in the automatic switch-over. We have provided a more complete description of this anomalous event and the ensuing recovery efforts in the Mission News Section below.

The possibility of a B-side switch during the science phase of the mission was anticipated, and the team had recently rehearsed the procedures for dealing with such an event. As a result, much of the recovery process—which otherwise might have taken two weeks or longer—was accomplished last weekend. This event has caused us to lose about a week's worth of science data. Our data collection rate has been running above 99% up to this point in the science phase of the mission, and the loss of a week's data will only reduce that level by about 2%, which is still well within the mission requirement of 90%. Assuming that this event did not place any non-relativistic torques (forces) on the gyros, the loss of this small amount of data will not have any significant effect on the outcome of the experiment. Analysis to ensure that this is the case is underway.



The GP-B Anomaly Room, where spacecraft issues are resolved by members of the GP-B Anomaly Review Board (ARB).

This week, the team is still in the process of fine-tuning the backup control systems in order to provide the same level of response and quality of science data that we had been obtaining from the main (A-side) systems prior to this event. These fine-tuning efforts are proceeding well, and we have already resumed science data collection.

## 18 MARCH 2005—GRAVITY PROBE B MISSION UPDATE

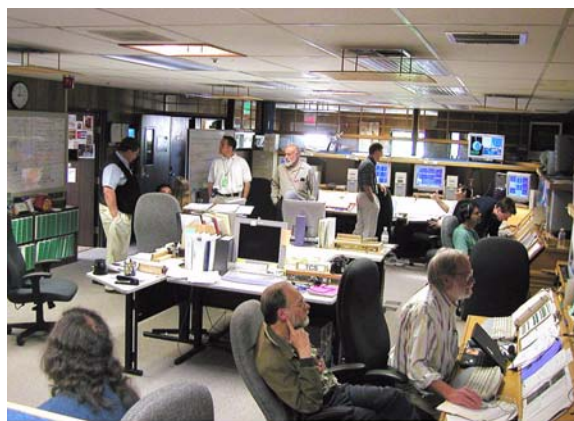
Mission Elapsed Time: 331 days (47 weeks/11.00 months) as of 3/17/05  
 Science Data Collection: 202 days (29 weeks/6.75 months) as of 3/17/05  
 Current Orbit #: 4,883 as of 2:00 PM PST on 3/17/05  
 Spacecraft General Health: Good  
 Roll Rate: Normal at 0.7742 rpm (77.5 seconds per revolution)  
 Dewar Temperature: 1.80 kelvin, rising slowly  
 Command & Data Handling (CDH): B-side (backup) computer in control, Multi-bit errors (MBE): 3 as of 3/17/05, Single-bit errors (SBE): 7 (daily average) as of 3/17/05



"There is a problem on-board the spacecraft..." Normally, all the indicators in the left column of this status screen are green. (This data on this screen was pixelated intentionally.)

On Monday evening, 14 March 2005 at 11:38PM PST, the spacecraft's safemode system triggered another computer reboot—the second flight computer reboot within the past two weeks. Telemetry indicated that this most recent safemode response was activated when a memory checkout procedure detected at least three multi-bit errors (MBE's) within a 0.2 second interval in the B-side computer.

Since the switchover from the A-Side (main) computer two weeks ago, the spacecraft has remained in control of the B-Side (backup) flight computer. In this configuration, if a new series of MBEs occurs, the spacecraft does not automatically switch back to the A-side computer. Rather, the B-side computer reboots itself, and the mission operations team follows a pre-defined set of procedures to restore the normal systems configuration for science data collection—as was the case this past Tuesday and Wednesday.



Members of the GP-B team communicating with the spacecraft from the Mission Operations Center (MOC) here at Stanford.

In response to the reboot, the mission operations team uploaded and ran a set of pre-approved recovery commands on the B-side computer. The spacecraft's roll rate, which had automatically decreased during the reboot, was quickly restored to the science value of 0.7742 rpm. The team also sent commands to reboot the SQUID Readout Electronics (SRE) as part of the initial recovery response, prior to re-acquisition of the guide star and return to drag-free flight. This accelerated the overall recovery process by a full day. We returned to drag-free operation on Gyro #3 at 5:34PM PST on Tuesday, less than 18 hours after the B-side reboot event. After several guide star search maneuvers Tuesday night, the guide star was successfully acquired at 4:41AM PST on Wednesday, 29 hours after the reboot event.

Because this is the second MBE-triggered event in a two-week period, we have changed the action response of the sequential MBE safemode test from “rebooting the B-side computer” to “stopping the mission timeline.” We have made this configuration change because we believe that the reboot response overreacts to the reporting of sequential MBEs. This change will minimize unnecessary adverse impact to science data collection that occurs when the GP-B flight computer reboots. The cause of the last two safemode response activations is under investigation, and a fault tree is being developed to identify the root cause of these events.

Each time we experience a switchover or reboot of the on-board flight computer, a small amount of science data is lost. If the reboot events of the past two weeks have not placed any non-relativistic torques (forces) on the gyros, this small data loss will not have any significant effect on the outcome of the experiment. Analysis to determine whether this is the case is in progress.

---

## 25 MARCH 2005—GRAVITY PROBE B MISSION UPDATE

Mission Elapsed Time: 339 days (48 weeks/11.25 months)  
Science Data Collection: 210 days (30 weeks/7.00 months)  
Current Orbit #: 5,004 as of 5:00 PM PST  
Spacecraft General Health: Good  
Roll Rate: Normal at 0.7742 rpm (77.5 seconds per revolution)  
Dewar Temperature: 1.82 kelvin, holding steady  
Command & Data Handling (CDH): B-side (backup) computer in control, Multi-bit errors (MBE): 1 (on 3/18), Single-bit errors (SBE): 8 (daily average)

Once again last Friday, 18 March 2005 at 7:20AM PST, as the spacecraft was passing over the western edge of the South Atlantic Anomaly (SAA), the B-Side flight computer, which has been controlling the spacecraft for the past three weeks, suffered a multi-bit error (MBE) and rebooted. Although last week’s reboot was triggered by an MBE, it was a different situation from the reboots of the previous two weeks. In the previous two weeks, multiple multi-bit errors occurring within a 0.2 second interval caused a safemode test to fail, which then triggered the reboot response. After the reboot last Monday, we re-programmed the multiple MBE safemode response to be less sensitive, and the reboot last Friday was not triggered by a failure of this safemode test. Rather, it was apparently triggered by an MBE striking a critical memory location in the B-side flight control computer, causing the computer to “hang.” A reboot command was then executed automatically when a “watchdog timer” in the computer’s interface module expired without receiving an expected signal from the computer. For a more detailed explanation of the flight computer’s error detection system, see this week’s GP-B Mission News below.



In the GP-B Anomaly Room, team members discuss a set of recovery commands that are about to be sent to the spacecraft.

Because of the reboot, the vehicle roll rate automatically decreased from its normal level of 0.77 rpm to 0.66 rpm, and the telescope became unlocked from the guide star, IM Pegasi. However, the spacecraft’s Attitude and Translation Control system (ATC) kept the spacecraft and telescope pointed to within 3,000 arcseconds of the guide star using the on-board navigational control gyroscopes.

Our mission operations team quickly swung into action, preparing a set of pre-planned recovery commands. The team uploaded these commands to the spacecraft, and they were executed at 3:20PM PST on Friday. The team then commanded the spacecraft to return to drag-free operation at 7:30 PM—just 12 hours after the flight computer reboot. The guide star was re-captured at 8:40 PM on Friday evening, concluding a swift and flawless execution of the recovery procedure.

On Saturday, the team sent real-time commands to optimize the attitude control performance, including enabling both roll and rate filters, powering on the A-side navigation control gyro, and enabling the science dither (an error reduction technique). We also switched back to the A-side (main) navigation control gyroscopes, and by Wednesday, 23 March, the spacecraft’s ATC pointing performance had improved to the pre-anomaly level. Finally, the team re-programmed a section of the ACT’s stored commands, so that in the event of a future computer reboot, the vehicle will not roll down. This should result in better pointing accuracy during the anomaly period and faster recovery.

Last Friday’s reboot anomaly presented yet another challenge to our mission operations team—a challenge that they faced and overcame with professionalism and teamwork. Congratulations to the team for their continued outstanding performance.





Uploading commands to the spacecraft from the MOC during recovery procedures following the B-side computer reboot.

## 1 APRIL 2005—GRAVITY PROBE B MISSION UPDATE

Mission Elapsed Time: 346 days (49 weeks/11.50 months)  
 Science Data Collection: 217 days (31 weeks/7.11 months)  
 Current Orbit #: 5,10 as of 4:00 PM PST  
 Spacecraft General Health: Good  
 Roll Rate: Normal at 0.7742 rpm (77.5 seconds per revolution)  
 Dewar Temperature: 1.82 kelvin, holding steady  
 Command & Data Handling (CDH): B-side (backup) computer in control, Multi-bit errors (MBE): 1 (on 3/26), Single-bit errors (SBE): 9 (daily average)

Last Saturday, the Gyro Suspension (GSS) computer for gyro #4 reported a multi-bit error (MBE). Upon investigation of this MBE, the GSS team determined that it was in a memory location that would soon be accessed by a program command sequence. To avert the computer reboot problems that the spacecraft has been experiencing for the past three weeks, the team sent commands to the flight computer halting the mission timeline. Then, as described in last week's Mission News, computer specialists used the Integrated Test Facility (ITF) simulator at Lockheed Martin to determine the correct value for the afflicted memory location and uploaded a patch to repair that location. After this repair, the team sent a revised command timeline to the GSS computer and resumed normal operations.

Because of the team's intervention, the guide star lock was not lost and the spacecraft remained in drag-free flight throughout this period. Also, gyro #4 remained digitally suspended in science (data collection) mode. Complete recovery from this MBE took only a few hours, thanks to the diligence of the team.

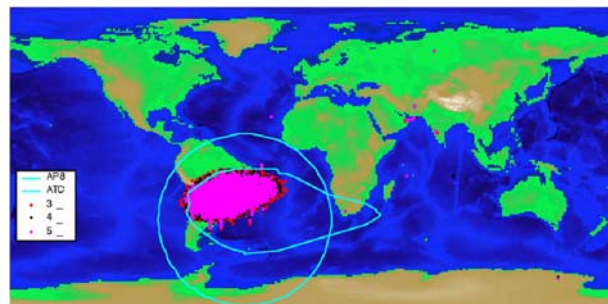
Investigations into the root causes of the recent spate of MBEs suggests the possibility that the scrub routine which is checking the memory cells of the on-board Command & Control Computer Assembly (CCCA) could trigger a safemode response on a single MBE if that error occurs in certain locations. As a result, the team has reprogrammed the safemode response for the MBE test to automatically stop the mission timeline, rather than rebooting the computer.

Also this past week, the GP-B team continued work on the Attitude and Translation Control system (ATC) and the telescope detectors. The purpose of these adjustments is to enable the spacecraft to remain under control of the science gyros (rather than the navigation control gyros) in all orbits through the South Atlantic Anomaly (SAA) region.

## 8 APRIL 2005—GRAVITY PROBE B MISSION UPDATE

Mission Elapsed Time: 353 days (50 weeks/11.57 months)  
 Science Data Collection: 224 days (32 weeks/7.34 months)  
 Current Orbit #: 5,210 as of 4:00 PM PST  
 Spacecraft General Health: Good  
 Roll Rate: Normal at 0.7742 rpm (77.5 seconds per revolution)  
 Dewar Temperature: 1.82 kelvin, holding steady  
 Command & Data Handling (CDH): B-side (backup) computer in control, Multi-bit errors (MBE): 0, Single-bit errors (SBE): 7 (daily average)

For a number of weeks now, the spacecraft has been experiencing degraded attitude performance in the South Atlantic Anomaly (SAA) region. As a short-term fix for this problem, we have been commanding the Attitude and Translation Control system (ATC) to switch from the science telescope to the spacecraft's navigational gyroscopes for controlling the spacecraft's attitude while in the SAA region. This has increased the spacecraft's stability in the SAA, but since we only use relativity data collected when the science telescope is in control of the ATC, we have effectively been losing science data in those orbits where the spacecraft passes through the SAA under navigational gyro control.



Over these past few weeks, our Attitude and Translation Control (ATC) group has been working very hard to fine tune the ATC system so that the science telescope can remain in control of the spacecraft's attitude in the SAA region. Three weeks ago, we made some progress on this issue by shrinking our defined boundaries of the SAA region, thus reducing the number of orbits affected. Two weeks ago, the ATC group made further progress by changing the ATC gain settings (similar to adjusting the volume control on a radio). Finally, this past week, the ATC group adjusted the gain settings on the Telescope Readout Electronics (TRE). This past week's adjustments, in combination with those previously made, have mitigated this issue. The science telescope is now able to remain locked on the guide star in all passes through the SAA, and we are once again collecting science data in all orbits.

Also this past week, we started making detailed plans for the post-science instrument re-calibration phase, estimated to begin early in July.

## 15 APRIL 2005—GRAVITY PROBE B MISSION UPDATE

Mission Elapsed Time: 360 days (51 weeks/11.80 months)  
 Science Data Collection: 231 days (33 weeks/7.57 months)  
 Current Orbit #: 5,316 as of 9:00 PM PST  
 Spacecraft General Health: Good  
 Roll Rate: Normal at 0.7742 rpm (77.5 seconds per revolution)  
 Dewar Temperature: 1.82 kelvin, holding steady

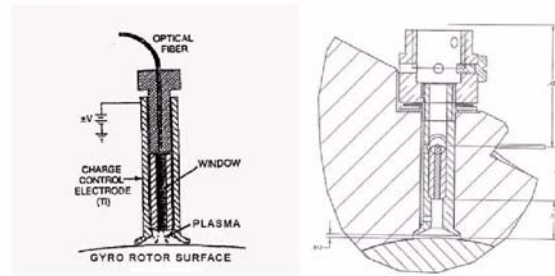
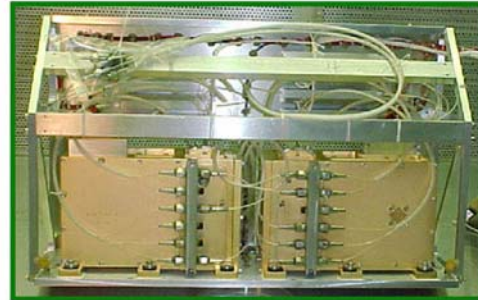
Command & Data Handling (CDH): B-side (backup) computer in control, Multi-bit errors (MBE): 0, Single-bit errors (SBE): 6 (daily average)

Around February of this year, we entered a GP-B “season” where the front of the spacecraft is pointing towards the sun. Many of the electronics boxes on-board the spacecraft are located in the Forward Equipment Enclosure (FEE), and we are in the process of investigating the possibility that the spacecraft’s sunward orientation may be a contributing factor to the increase in multi-bit errors (MBEs) we experienced a few weeks ago, as well as some of the attitude control issues we have experienced recently—especially in the South Atlantic Anomaly (SAA) region.



This past week, we made further progress operating the spacecraft through the SAA region. In analyzing the SAA attitude data we have collected recently, our ATC group noticed some interesting patterns. They have now investigated these patterns and determined that a data type conversion routine was causing data values exceeding a certain threshold to become corrupted. This situation was greatly exacerbated in the SAA region, where the telescope’s detectors were being flooded with stray protons, which causes a noticeable increase in these corrupted data values.

As reported in last week’s update, we addressed these SAA attitude problems by shrinking our defined size of the SAA region and reducing the gains on both the ATC system and the telescope detectors. These gain reductions have provided a work-around for this data corruption problem by re-scaling the data values so that they no longer exceed the threshold in the SAA region. As a result, our spacecraft can now point at the guide star throughout the SAA region with the same precision as it does outside the SAA.



(Top) Gyro Suspension System (GSS) computer & fiber optics  
(Bottom) Drawing & Schematic of Gyro UV Discharge System

Also last week, we exercised the Ultraviolet Discharge procedure on science gyros #1, #2, and #4, followed later by drag-free gyro #3. This procedure reduces the electrostatic charge that builds up on the gyro rotors over time. The rotors build up a charge in two ways: first, the process of suspending the rotors electrically deposits some charged particles on them, and second, protons from the sun are constantly bombarding the spacecraft, especially over the SAA region, and some of these protons strike the rotors and leave a residual charge on them.

Finally, this past week, we began planning for another heat pulse test to determine the level of liquid helium remaining in the dewar. We also continued our detailed planning for the post-science instrument re-calibration phase, estimated to begin early in July.

## 22 APRIL 2005—GRAVITY PROBE B MISSION UPDATE

Mission Elapsed Time: 367 days (52 weeks/12.00 months)  
 Science Data Collection: 238 days (34 weeks/7.80 months)  
 Current Orbit #: 5,419 as of 9:00 PM PST  
 Spacecraft General Health: Good  
 Roll Rate: Normal at 0.7742 rpm (77.5 seconds per revolution)  
 Dewar Temperature: 1.82 kelvin, holding steady  
 Command & Data Handling (CDH): B-side (backup) computer in control, Multi-bit errors (MBE): 0, Single-bit errors (SBE): 9 (daily average)

Our mission operations team performed routine tasks over this past week related to the electrostatic discharge of Gyro #3 (the “drag-free” gyro) and minor dewar pressure oscillations. After performing a number of tests on Gyro #3 early in the week, it was discharged on Thursday to -3.0 mV, using ultraviolet light, as explained in last week’s update.

The Attitude and Translation Control (ATC) group reports that the time required to re-lock onto the guide star as the spacecraft emerges from behind the Earth each orbit continues to be excellent, including one guide-star capture (re-locking) this weekend that took only 20 seconds.



On Tuesday afternoon (19-April), GP-B Principal Investigator, Francis Everitt, delivered a Physics Colloquium to a packed auditorium at Stanford entitled: "The Gravity Probe B Flight Mission: A Stanford Physics-Engineering Partnership". In this lecture, Professor Everitt explained some of the finer points of GP-B's various technologies, emphasizing in each case the interdisciplinary collaborations required to produce these extraordinary technological innovations.

---

## 29 APRIL 2005—GRAVITY PROBE B MISSION UPDATE

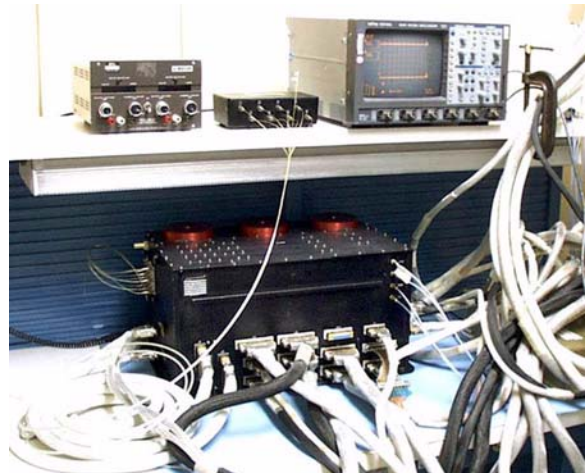
Mission Elapsed Time: 374 days (53 weeks/12.26 months)  
Science Data Collection: 245 days (35 weeks/8.03 months)  
Current Orbit #: 5,523 as of 5:00 PM PST  
Spacecraft General Health: Good  
Roll Rate: Normal at 0.7742 rpm (77.5 seconds per revolution)  
Dewar Temperature: 1.82 kelvin, holding steady  
Command & Data Handling (CDH): B-side (backup) computer in control, Multi-bit errors (MBE): 0, Single-bit errors (SBE): 8 (daily average)

This past Tuesday, 26 April 2005, the GP-B dewar team ran another heat pulse meter test to get an update on the amount of liquid helium remaining in the dewar. Their preliminary results suggest that we have about two weeks more helium than anticipated. Further analysis is in process, and if these results are correct, the helium will be depleted around the end of August or beginning of September. This means that we will be able to continue collecting science data into the first two weeks in July, before beginning a very important series of instrument calibration tests that must be completed before the helium runs out.



Also this past week, we continued fine-tuning our SQUID readout system, analyzing potential sources of noise. To this end, we turned off the telescope dithering motion all day on Wednesday, 27 April 2005 to determine its contribution to experimental noise.

Likewise, for the same reason, on Thursday, we turned off the Experiment Control Unit (ECU) for several days. We are in the process of analyzing the results of these noise experiments, which may lead to further fine-tuning of various spacecraft systems.



The Experiment Control Unit (ECU) box on a test bench at Lockheed Martin Corp.

---

## 6 MAY 2005—GRAVITY PROBE B MISSION UPDATE

Mission Elapsed Time: 381 days (54 weeks/12.49 months)  
Science Data Collection: 252 days (36 weeks/8.26 months)  
Current Orbit #: 5,627 as of 5:00 PM PST  
Spacecraft General Health: Good  
Roll Rate: Normal at 0.7742 rpm (77.5 seconds per revolution)  
Dewar Temperature: 1.82 kelvin, holding steady  
Command & Data Handling (CDH): B-side (backup) computer in control, Multi-bit errors (MBE): 1, Single-bit errors (SBE): 9 (daily average)

Further analysis of the results of the heat pulse test run on Tuesday, 26 April 2005, to determine the amount of liquid helium remaining in the dewar, confirms the preliminary prediction that the helium in the dewar will be depleted in late August or early September. Based on these results, the GP-B mission operations team is planning to complete readout calibrations, some of which can be done while we are still collecting science data, by the beginning of August. Gyro torque calibrations, which cannot be done during the science phase of the mission because they involve placing small torques (forces) on the gyro rotors, will commence early in August and continue until the helium runs out.

Our telescope pointing and guide star capture times continue to be excellent, thanks to recent fine-tuning of the spacecraft's Attitude and Translation Control system (ATC) parameters. We have also determined that we can reduce some noise in the SQUID Readout Electronics system (SRE) by turning off the Experiment Control Unit. However, we will now periodically power on the ECU for about 6 hours in order to obtain certain readouts that require information from the ECU.

Finally, a memory location in the B-side (backup) flight computer that is now controlling the spacecraft sustained a multi-bit error (MBE) last Saturday, 30 April 2005. The memory location affected is not currently being used. Following new procedures developed a few weeks ago, when we were experiencing an increased level of MBEs, our computer operations team quickly uploaded a patch to correct the contents of the affected memory location.

Also this past week, the GP-B Anomaly Review Board met to determine whether or not to change the pre-programmed safemode trigger and response to MBEs detected in the main flight computer. After a lengthy discussion, it was decided to change the safemode trigger condition from 3 to 9 MBEs and the response actions from

simply stopping the timeline (halting execution of the command set currently loaded into the computer) to automatically rebooting the computer. These changes ensure that if the error occurs in a memory location that increments the error counter at 10 Hz, the computer will automatically reboot immediately, rather than possibly freezing up and waiting for up to 8 hours for an “aliveness” test to trigger a reboot.

---

### 13 MAY 2005—GRAVITY PROBE B MISSION UPDATE

Mission Elapsed Time: 388 days (55 weeks/12.72 months)  
Science Data Collection: 259 days (37 weeks/8.49 months)  
Current Orbit #: 5,726 as of 5:00 PM PST  
Spacecraft General Health: Good  
Roll Rate: Normal at 0.7742 rpm (77.5 seconds per revolution)  
Dewar Temperature: 1.82 kelvin, holding steady  
Command & Data Handling (CDH): B-side (backup) computer in control, Multi-bit errors (MBE): 0, Single-bit errors (SBE): 9 (daily average)

Our telescope pointing and guide star capture times continue to be excellent. The Experiment Control Unit continues to remain off during most orbits, resulting in reduced noise in the SQUID Readout Electronics system (SRE). Once a week, we power the ECU back on for a few hours in order to obtain and check certain readouts, such as the dewar temperature, that are provided by the ECU.

Because the spacecraft has been in orbit for over a year now, we are able to conduct an analysis of the external temperature and solar array efficiencies by comparing current data from these systems with data collected a year ago.

In preparation for the end of the GP-B mission, which is fast approaching, we have begun delegating tasks to complete our final mission report, which we will deliver to NASA in July.

GP-B PRINCIPAL INVESTIGATOR FRANCIS EVERITT HONORED BY NASA

Following is a copy of the press release we sent out earlier this week, announcing this award.

Stanford experimental physicist Francis Everitt has been awarded a NASA Distinguished Public Service Medal. NASA Deputy Director Fred Gregory presented the medal to Everitt on April 27 at an awards ceremony at NASA Headquarters in Washington, D.C. Everitt is principal investigator of the Gravity Probe B (GP-B) experiment, a collaboration between Stanford University, NASA and Lockheed Martin Corp. that is testing predictions of Albert Einstein's 1916 general theory of relativity (his theory of gravitation) by means of four ultra-precise gyroscopes that have been orbiting the Earth in a satellite for just over a year.



GP-B Principal Investigator Francis Everitt at the NASA 2005 Awards Ceremony at NASA Headquarters in Washington, D.C. on 27 April, 2005. From left to right: Fred Gregory, NASA Deputy Administrator, Francis Everitt, James Jennings, NASA Associate Administrator for Institutions and Management.

The NASA Distinguished Public Service Medal is awarded to an individual whose distinguished accomplishments contributed substantially to NASA's mission. Contributions must be so extraordinary that other forms of recognition by NASA would be inadequate. This is the highest honor that NASA confers to an individual who is not a government employee.



Everitt obtained his doctorate at the University of London (Imperial College) in 1959 for research under Nobel laureate P. M. S. Blackett. He then spent two years at the University of Pennsylvania working on liquid helium. In 1962, Everitt joined William Fairbank and Leonard Schiff in the Stanford Physics Department as the first full-time research worker on the GP-B experiment. His efforts advanced the state of the art in the areas of cryogenics, magnetics, quantum devices, telescope design, control systems, quartz fabrication techniques, metrology and, most of all, gyroscope technology. His leadership as the principal investigator for GP-B advanced the GP-B program from the concept and technology development stages to the experiment's launch on April 20, 2004, and its ensuing orbital operations.

“None of us at the beginning had any idea how long it would take for the GP-B spacecraft to fly and take the science data,” Everitt said when asked about the long life of the project. “But speaking for myself, I have never been bored.”

Gravity Probe B was developed on the Stanford campus in the W. W. Hansen Experimental Physics Laboratory (HEPL). The current on-orbit GP-B mission operations center (MOC) is located in HEPL, where the science data is currently processed as well. From the MOC, the GP-B spacecraft is commanded with ground antennas in Alaska or



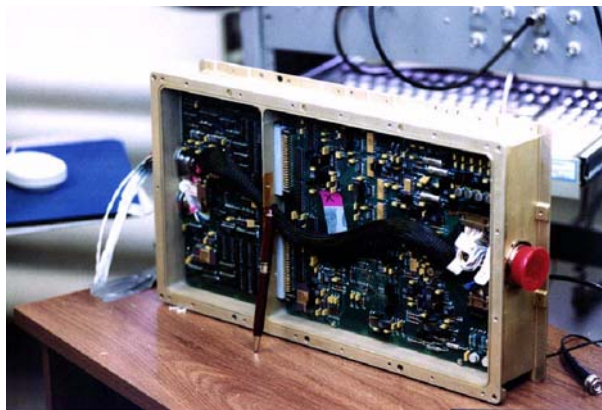
Norway or through the NASA space net. HEPL supports a number of collaborative scientific research programs that cross traditional university departmental boundaries. The GP-B space mission itself was a successful interdepartmental collaboration of the Stanford Physics and Engineering departments.

“HEPL is one of the few places in the United States where an interdisciplinary experiment such as Gravity Probe B could be successfully carried out,” said HEPL Director Robert Byer, a professor of applied physics.

## 20 MAY 2005—GRAVITY PROBE B MISSION UPDATE

Mission Elapsed Time: 395 days (56 weeks/12.95 months)  
 Science Data Collection: 266 days (38 weeks/8.72 months)  
 Current Orbit #: 5,830 as of 5:00 PM PST  
 Spacecraft General Health: Good  
 Roll Rate: Normal at 0.7742 rpm (77.5 seconds per revolution)  
 Dewar Temperature: 1.82 kelvin, holding steady  
 Command & Data Handling (CDH): B-side (backup) computer in control, Multi-bit errors (MBE): 1 (Gyro Suspension System on 5/20/05), Single-bit errors (SBE): 8 (daily average)

At the most recent weekly review of all spacecraft subsystems, one of our GP-B mission directors remarked that this past week has been one of the quietest and smoothest since launch. Our telescope pointing and guide star capture times continue to be excellent. To minimize noise in the SQUID Readout Electronics (SRE), the Experiment Control Unit (ECU) is now only being powered on for a few hours each week in order to obtain a set of readouts, such as the dewar temperature, that are provided. We have also begun some preliminary SQUID calibration signal tests. These tests involve turning on calibration signals on one pair of SQUIDS for one day, while turning these signals off on the other pair of SQUIDS. The next day, we reverse the procedure, turning off the calibration signals on the first pair of SQUIDS and vice versa. At the end of the test, we will compare the results. These tests do not in any way affect the science data collection, but they help us evaluate the performance of the four SQUIDS relative to each other by the ECU.



A SQUID Readout Electronics (SRE) box. Each SRE box controls four SQUID magnetometers.

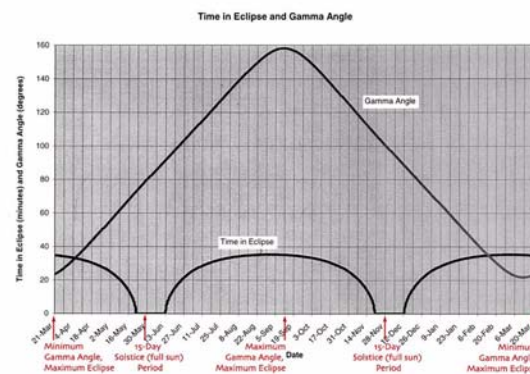
Preparations for the end of the GP-B mission are now in full swing. Various chapters of our final mission report, which we will deliver to NASA late this summer, are currently being drafted. Procedures for the final set of instrument calibration tests, which will occur in August, just before the liquid helium in the dewar is exhausted, are now being created. The mission operations team will practice using these procedures during two upcoming calibration phase simulations.

Because these final instrument calibration tests place controlled torques (forces) on the gyros, they cannot be performed until after the data collection has been completed.

## 27 MAY 2005—GRAVITY PROBE B MISSION UPDATE

Mission Elapsed Time: 402 days (57 weeks/13.18 months)  
 Science Data Collection: 273 days (39 weeks/8.95 months)  
 Current Orbit #: 5,933 as of 5:00 PM PST  
 Spacecraft General Health: Good  
 Roll Rate: Normal at 0.7742 rpm (77.5 seconds per revolution)  
 Dewar Temperature: 1.82 kelvin, holding steady  
 Command & Data Handling (CDH): B-side (backup) computer in control, Multi-bit errors (MBE): 0, Single-bit errors (SBE): 15 (daily average)

The spacecraft has entered its third solstice or full-sun period of the mission. During these periods, the plane of the spacecraft's orbit is perpendicular with respect to the sun's position for about two weeks. Thus, the sun shines broadside on the spacecraft throughout each orbit around the Earth. As in previous full-sun periods, some fine tuning of various spacecraft systems is required to counter the effects of temperature increases in the dewar shell and the electronics boxes mounted in the bays of the spacecraft frame.



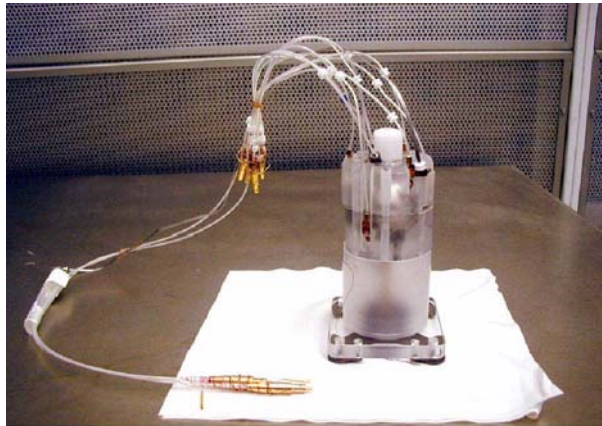
Preliminary SQUID calibration signal tests, described in last week's Mission Director's Summary, are continuing. These tests do not affect the science data collection, but they help us evaluate the performance of the four SQUIDS relative to each other.

Also, development of procedures for the final set of instrument calibration tests that will occur in August, just before the liquid helium in the dewar is exhausted, are continuing. Likewise, the plans for two full-day simulations, during which the Mission Operations Team will rehearse executing these procedures and work through any issues or problems, are being finalized.

## 3 JUNE 2005—GRAVITY PROBE B MISSION UPDATE

Mission Elapsed Time: 409 days (58 weeks/13.40 months)  
 Science Data Collection: 280 days (40 weeks/9.18 months)  
 Current Orbit #: 6,036 as of 5:00 PM PST  
 Spacecraft General Health: Good  
 Roll Rate: Normal at 0.7742 rpm (77.5 seconds per revolution)  
 Dewar Temperature: 1.82 kelvin, holding steady  
 Command & Data Handling (CDH): B-side (backup) computer in control, Multi-bit errors (MBE): 2 (in SRE computer on 5/30), Single-bit errors (SBE): 7 (daily average)

Late last Thursday, Gyro #2 transitioned from its normal digital suspension to analog backup suspension mode. This gyro was re-suspended in digital mode last Saturday, 28 May 2005, and it has remained digitally suspended since that time. The root cause of this transition is still under investigation.



An assembled gyroscope housing, ready for insertion into one of the four gyro cavities in the quartz block.

Last Sunday, 20 May 2005, the SQUID Readout Electronics (SRE) computer experienced two multi-bit errors (MBEs). One of these errors was located in a data buffer location that cleared itself, thus removing the error. The second error was located in a section of program code that is not planned for use. In response, the Mission Operations team has since removed this code module from the computer's database, so that it cannot be accessed inadvertently.

Various planned preliminary calibration tests are continuing, including some tests of Gyro #3 and the drag-free system. Such tests are standard operating procedure on experimental missions. During these tests, we purposely vary certain parameters that would not be expected to change greatly during the experimental portion of the mission for the purpose of characterizing instrument component performance. In order to maximize the length of the science data collection phase of the GP-B mission, we are currently running some preliminary calibrations that can safely be performed while we are still collecting science data. Our final calibration tests, which must be completed before the helium in the dewar is depleted, involve placing torques (forces) on the gyros, so we can only perform these tests after data collection is finished—early in August.

## 10 JUNE 2005—GRAVITY PROBE B MISSION UPDATE

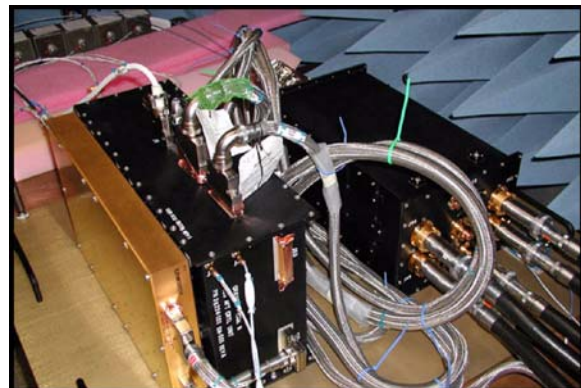
Mission Elapsed Time: 416 days (59 weeks/13.64 months)  
 Science Data Collection: 287 days (41 weeks/9.41 months)  
 Current Orbit #: 6,139 as of 4:30 PM PST  
 Spacecraft General Health: Good  
 Roll Rate: Normal at 0.7742 rpm (77.5 seconds per revolution)  
 Dewar Temperature: 1.82 kelvin, holding steady  
 Command & Data Handling (CDH): B-side (backup) computer in control, Multi-bit errors (MBE): 1 (in SRE computer on 6/6), Single-bit errors (SBE): 8 (daily average)

Over the past two weeks, we have performed several routine adjustments to various systems on the spacecraft and continued our preliminary calibration tests. These included:

- Updating the feed-forward term of the backup drag-free controller. The spacecraft is flying drag-free around Gyro #3, which means that this gyro is treated as its center of mass. Since the other three

gyros are located in slightly different positions on the quartz block, we must apply small voltages to their suspension systems to fly them drag-free around Gyro #3's position. The feed-forward term is an adjustment factor for anticipating the position of the other gyros in order to prevent error build-up. Our initial calculation of the feed-forward term prior to launch was fairly accurate, and we've been using it thus far in the mission. However, based on 13 months of flight data, we are able to update this term to be even more accurate, which we did this past week. We will now use the updated feed-forward term for the duration of the science (data collection) phase.

- Increasing the preload voltage on science gyro #3 to 1.5V for a brief time. The Gyro Suspension System (GSS) for each gyro has a "preload voltage" and a "control voltage." You can think of the preload voltage as coarse positioning and the control voltage as fine positioning. Generally, we like to keep these voltages about equal. However, right now as part of our calibration tests, we are purposely changing the preload voltage for a brief time to see the effect of this asymmetry. Note that we can perform this calibration test while remaining in drag-free flight.



The Gyro Suspension System (GSS)

- Starting a new readout calibration cycling plan where we operate the calibration signal on either SQUID's #1 and #2, or SQUIDs #3 and #4, with the other pair off. (We toggle the pairs every 24 hours.) This is another of the preliminary calibration tests that we are currently conducting.

On Monday 6 June 2005, a multi-bit error (MBE) occurred in the SQUID Readout Electronics (SRE) computer. A preliminary analysis of this error suggests that the memory location in which the error occurred is not being used, and most likely, this MBE is benign. However, if after further investigation, this is not the case, we will reboot the SRE computer to clear the error.

Finally, another Heat Pulse meter test to re-check the level of the helium remaining in the dewar is scheduled for Monday, 13 June 2005. If the results of this test correlate well with previous results, this will be the last heat pulse test of the mission.

## 17 JUNE 2005—GRAVITY PROBE B MISSION UPDATE

Mission Elapsed Time: 423 days (60 weeks/13.87 months)  
 Science Data Collection: 294 days (42 weeks/9.64 months)  
 Current Orbit #: 6,242 as of 4:30 PM PST  
 Spacecraft General Health: Good  
 Roll Rate: Normal at 0.7742 rpm (77.5 seconds per revolution)



Dewar Temperature: 1.82 kelvin, holding steady  
Command & Data Handling (CDH): B-side (backup) computer in control, Multi-bit errors (MBE): 0, Single-bit errors (SBE): 8 (daily average)

The GP-B spacecraft is beginning to move out its full-sun "season," and it is once again being eclipsed from sunlight by the Earth for a portion of each orbit. Because of the geometry of the spacecraft's polar orbit around the Earth, and the Earth's orbit around the sun, the spacecraft experiences two "seasons" when the plane of the spacecraft's orbit is perpendicular with respect to the sun's position for about two weeks. Thus, the sun shines broadside on the spacecraft throughout each orbit around the Earth. During these full-sun periods, the Attitude Reference Platform (ARP) containing the star trackers and other equipment heats up, causing it to move slightly, and consequently we must adjust certain parameters to counteract this motion. Then, as the full-sun season comes to an end, we re-adjust these parameters back to their normal settings.

A final heat pulse test was run on the dewar this past Monday, 13 June 2005. The results of this test indicate that the liquid helium in the dewar will run out towards the beginning of September. This result is consistent with previous heat pulse measurements, so this was the last heat pulse measurement we will perform.

Preliminary SQUID calibration signal tests described in previous Mission Director's Summaries are continuing. These tests do not affect the science data collection, but they help us evaluate the performance of the four SQUIDS relative to each other.

---

## 24 JUNE 2005—GRAVITY PROBE B MISSION UPDATE

Mission Elapsed Time: 430 days (61 weeks/14.01 months)  
Science Data Collection: 301 days (43 weeks/9.87 months)  
Current Orbit #: 6,345 as of 3:00 PM PST  
Spacecraft General Health: Good  
Roll Rate: Normal at 0.7742 rpm (77.5 seconds per revolution)  
Dewar Temperature: 1.82 kelvin, holding steady  
Command & Data Handling (CDH): B-side (backup) computer in control, Multi-bit errors (MBE): 1 (in main CCCA computer on 6/20), Single-bit errors (SBE): 9 (daily average)



GP-B micro-thruster module.

Last Monday, 20 June 2005, a multi-bit error (MBE) occurred in the B-Side (backup) main computer (CCCA). Our resident computer expert traced the location of this error to a thruster initialization routine that

is currently not in use. Thus, a memory patch was prepared and uploaded to the spacecraft, and this event had no further impact on the mission.

On Wednesday, 22 June 2005, as part of our ongoing instrument calibration tests, we switched the spacecraft's drag-free control from gyro #3 to gyro #1. The purpose of this switch is to determine whether or not certain gyro control data values that have been uniquely observed on gyro #3 are a function of the drag-free system or gyro #3 itself. The process of moving drag-free operation from gyro #3 to gyro #1 went very smoothly, and we intend to continue drag-free operation around gyro #1 for the remainder of the science phase of the mission.

---

## 1 JULY 2005—GRAVITY PROBE B MISSION UPDATE

Mission Elapsed Time: 437 days (62 weeks/14.32 months)  
Science Data Collection: 308 days (44 weeks/10.10 months)  
Current Orbit #: 6,449 as of 3:00 PM PST  
Spacecraft General Health: Good  
Roll Rate: Normal at 0.7742 rpm (77.5 seconds per revolution)  
Dewar Temperature: 1.82 kelvin, holding steady  
Command & Data Handling (CDH): B-side (backup) computer in control, Multi-bit errors (MBE): 1 (in GSS computer on 6/30), Single-bit errors (SBE): 15 (daily average)

This past week was relatively quiet for GP-B mission operations. Several routine adjustments were made in various spacecraft systems, and preliminary instrument calibration tests are continuing.



Aft SQUID Readout Electronics (SRE) box

During the mission up to this point, we have been cycling certain applications on and off in the SQUID Readout Electronics (SRE) and Telescope Readout Electronics (TRE) computers during Guide Star Valid (GSV) and Guide Star Invalid (GSI) periods to ensure that these computers have adequate margin for memory scrubbing, which automatically corrects single-bit errors (SBEs). Based on recent engineering tests, we have determined that leaving these applications on all the time, instead of cycling them on and off, doubles the length of the memory scrub period, which doubles the likelihood of these computers sustaining a multi-bit error (MBE) composed of two SBEs in a single memory word during a scrub cycle. However, based on the engineering tests and on-orbit experience, we have determined that the probability of sustaining an MBE composed of two SBEs was deemed to be an acceptable level of risk. The advantage of keeping these applications enabled all the time is that it provides simultaneous data on trapped flux and the London moment, in addition to the science pointing (relativity) data.

On Wednesday 29 June 2005, members of our Anomaly Review Board presented information about our GP-B anomaly review process to a NASA group studying anomaly resolution best practices at NASA's Ames Research Center here in Mountain View, CA.

On Thursday, 30 June 2005, a multi-bit error (MBE) occurred in a benign location in the Gyro Suspension (GSS) computer for gyro #2. This memory location was subsequently patched, restoring its proper value.

## 8 JULY 2005—GRAVITY PROBE B MISSION UPDATE

Mission Elapsed Time: 444 days (63 weeks/14.56 months)  
Science Data Collection: 315 days (45 weeks/10.33 months)  
Current Orbit #: 6,553 as of 5:30 PM PST  
Spacecraft General Health: Good  
Roll Rate: Normal at 0.7742 rpm (77.5 seconds per revolution)  
Dewar Temperature: 1.82 kelvin, holding steady  
Command & Data Handling (CDH): B-side (backup) computer in control, Multi-bit errors (MBE): 0, Single-bit errors (SBE): 6 (daily average)

As of Mission Day 444, the Gravity Probe B vehicle and payload are in good health. All four gyros are digitally suspended in science mode. The spacecraft is flying drag-free around Gyro #1.

Last Saturday, 2 July 2005, a GPS channel alignment error flag was triggered in the spacecraft's B-side (backup) Global Positioning System (GPS) as it passed over the Earth's north magnetic pole. We have seen this same behavior twice before with the A-side (main) GPS receiver, and in both previous cases there was no discernible effect on the GPS system performance. An analysis of this latest event is in progress, and if necessary, we will reboot the GPS system.

Otherwise, all was quiet and nominal on-board the GP-B spacecraft during this year's 4th of July holiday weekend. Because its orbit did not pass over North America last Monday evening, the telescope detectors on-board the spacecraft did not register any brilliant bursts of pyrotechnics in the skies over U.S. cities.

Yesterday, we performed a calibration test on gyro #3 (formerly the drag-free gyro) in which the gyro rotor was electrically "nudged" to various pre-defined positions within its housing. About 45 minutes into this test, the Gyro Suspension System (GSS) for gyro #3 automatically switched from digital to analog suspension mode. Analog suspension is used primarily as a backup mode that holds a gyro rotor securely to keep it from striking the housing wall and allows only coarse positioning of the rotor. By contrast, digital suspension mode is computer-controlled; it puts less torque on the rotor and enables its position within the housing to be controlled with extremely high precision. Yesterday evening, we sent commands to re-suspend gyro #3 in digital mode, and the calibration tests are continuing today and into the weekend. Due to the nature of this calibration test and the performance history of gyro #3, we will not be surprised if it transitions to analog mode again during the second phase of this calibration test.

### ANALYZING END OF MISSION TRADE-OFFS

Towards the beginning of June, the spacecraft transitioned out of its two-week full sun season to once again being eclipsed from the Sun for part of each orbit. Furthermore, the position of the Earth relative to the Sun has been changing so that the Sun's light is now moving towards the rear of the spacecraft, and this orientation will continue through August and September. During this period, the spacecraft's Attitude and Translation Control (ATC) performance will be the most stable, giving us the "cleanest" data of the entire mission. The pointing

performance stabilizes during this period because the Sun is no longer heating up the spacecraft's attitude reference platform (ARP), where the navigational rate gyros and star trackers are mounted, on the forward dome of the dewar.

As we have reported recently, our measurements indicate that the superfluid helium in the dewar will be exhausted in approximately eight weeks—during the period of maximum ATC stabilization. This situation has raised some questions about how to proceed through the final two months of the mission. Our original plan was to stop collecting relativity data 3-5 weeks before the helium runs out and to spend those final weeks of the mission exclusively running calibration tests of the science instruments. Some of these tests involve placing torques (forces) on the gyros, and we cannot use the science data collected from a gyro while it is undergoing such a test. Another calibration test involves purposely moving the telescope's pointing axis away from our guide star, IM Pegasi, to a different star and then back again. Clearly, we cannot collect any science data during this telescope pointing test.

However, our plan for spending the final 3-5 weeks of the mission exclusively running calibration tests is not cast in stone, and we are currently at a point of making some trade-off decisions in this regard. For example, we have determined that it is possible to perform the gyro torquing calibration tests on an individual gyro, while the other gyros continue to collect science data. (We are performing such a calibration test on gyro #3 right now.) To address these issues and trade-offs, our GP-B management and science teams spent the entire day today at an off-site meeting. The decisions resulting from this off-site meeting will determine our course of action for the remainder of the mission, and we will report on these decisions in an upcoming Mission News story.

In conjunction with today's off-site meeting, yesterday we had a visit from Tony Lyons, our NASA Program Manager at NASA's Marshall Space Flight Center (MSFC) in Huntsville, Alabama and his boss, Tony Lavoie, Director of Space Systems Programs at MSFC. Tony Lavoie assumed his current role at the Marshall Center last October, and he had never before visited GP-B. So, instead of our usual daily all-hands meeting yesterday, we began the day with a brief presentation to both of our MSFC visitors by GP-B Principal Investigator, Francis Everitt, GP-B Program Manager, Gaylord Green, and several GP-B staff members.



GP-B Principal investigator, Francis Everitt (right) answers a question from NASA Marshall Center's Tony Lavoie (center), as GP-B Co-Principal Investigator, Brad Parkinson (left) looks on.

The presentation included an overview of the program for the benefit of Tony Lavoie, followed by a status update on the spacecraft and data collection. Following the presentations, Francis Everitt, Gaylord Green, and GP-B co-founder Bob Cannon took both of our MSFC



visitors on a tour of the GP-B facilities, including our Mission Operations Center (MOC), the Anomaly Resolution Board Room (ARB), and the display of GP-B technology in the lobby of our building.



In the GP-B Anomaly Resolution Room. Left to Right: Tony Lavole (NASA Marshall Space Flight Center), Francis Everitt (GP-B), Paul Shestopole (GP-B), Tony Lyons (NASA MSFC), Gaylord Green (GP-B).

## 15 JULY 2005—GRAVITY PROBE B MISSION UPDATE

Mission Elapsed Time: 451 days (64 weeks/14.79 months)  
 Science Data Collection: 322 days (46 weeks/10.56 months)  
 Current Orbit #: 6,655 as of 4:30 PM PST  
 Spacecraft General Health: Good  
 Roll Rate: Normal at 0.7742 rpm (77.5 seconds per revolution)  
 Dewar Temperature: 1.82 kelvin, holding steady  
 Command & Data Handling (CDH): B-side (backup) computer in control, Multi-bit errors (MBE): 0, Single-bit errors (SBE): 8 (daily average)

As of Mission Day 451, the Gravity Probe B vehicle and payload are in good health. All four gyros are digitally suspended in science mode. The spacecraft is flying drag-free around Gyro #1.

As reported last week, gyro #3 transitioned into analog backup suspension mode during the first phase of a calibration test that began on Thursday, 7 July 2005, that involves electrically “nudging” the gyro rotor to various pre-defined positions within its housing. We restored gyro #3 to digital suspension last Thursday evening and continued phase 2 of the test last Friday. We suspected that the root cause of the transition to analog mode was likely due to a known “race” condition, which occurs when the gyro rotor reaches a low threshold, set by the hardware. For this reason, we suspected that gyro #3 would transition to analog mode again during the second phase of the calibration test, and this was the case last Friday. We again returned gyro #3 to digital suspension and completed the test successfully.

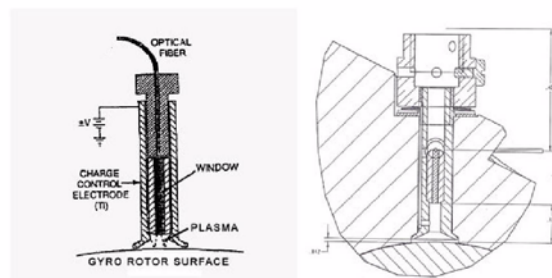
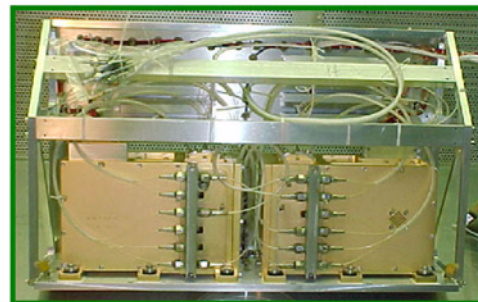


NASA Ground Station at Poker Flats, Alaska



The Poker Flats ground station in Alaska has been experiencing hardware problems, and for this reason, we have had to re-schedule some of our data telemetry sessions at other NASA TDRSS ground station facilities. We have recently run tests at the McMurdo station in Antarctica, and we successfully completed a data capture session from McMurdo this past Monday, 11 July 2005, after some last-minute scrambling to get the connection properly set up. We have also been using the Wallops ground station in Virginia.

On Wednesday, 12 July 2005, we completed a paper simulation of the calibration procedures we will be performing towards the very end of the mission, just before the helium runs out, to move our telescope from our guide star, IM Pegasi, to a nearby star and back to IM Pegasi.



(Top) Gyro Suspension System (GSS) computer & fiber optics  
 (Bottom) Drawing & Schematic of Gyro UV Discharge System

Yesterday, 13 July 2005, marks the one-year anniversary of our full-speed gyro spin-up in space (gyro #4 was spun up to 105 Hz/6,300 rpm). That was a very tense and exciting time in the Mission Operations Center (MOC) here at GP-B. Also yesterday, we used ultraviolet light to reduce the electrostatic charge on all four gyros.

Very small amounts of charge continually build up on the gyro rotors throughout the mission. When the charge build-up reaches a sufficiently high level, we use ultraviolet light to reduce the charge. We last performed this procedure on during the week of 15 April 2005.

---

## 22 JULY 2005—GRAVITY PROBE B MISSION UPDATE

Mission Elapsed Time: 458 days (65 weeks/15.02 months)  
Science Data Collection: 329 days (48 weeks/10.79 months)  
Current Orbit #: 6,757 as of 4:00 PM PST  
Spacecraft General Health: Good  
Roll Rate: Normal at 0.7742 rpm (77.5 seconds per revolution)  
Dewar Temperature: 1.82 kelvin, holding steady  
Command & Data Handling (CDH): B-side (backup) computer in control, Multi-bit errors (MBE): 0, Single-bit errors (SBE): 8 (daily average)

As of Mission Day 458, the Gravity Probe B vehicle and payload are in good health. All four gyros are digitally suspended in science mode. The spacecraft is flying drag-free around Gyro #1.

Preliminary calibration testing of gyros #1, #2, and #4, which does not place torques (forces) on the gyros, continued this past week. Also, we continued calibration testing of gyro #3, which involved electrically “nudging” the gyro #3 rotor to various pre-defined positions within its housing. During this test, gyro #3 transitioned into analog suspension mode. However, anticipating this condition, we automatically re-suspended the gyro rotor and increased the gyro bridge excitation voltage during the calibration test. Based on the performance of gyro #3, we will now include the auto-suspension and increased excitation voltages when running this test on the other three gyros.



Touring the GP-B Anomaly Resolution Board Room. From left to right: Anne Kinney (NASA), Gaylord Green, Dave Hipkins, and Holly Matthews (GP-B).

On Wednesday, 20 July 2005, Dr. Anne Kinney, Director of the Universe Division in NASA's Science Mission Directorate, spent the day here at Stanford, meeting with various research teams and reviewing the status of GP-B and several other joint Stanford-NASA missions/experiments that fall under her jurisdiction at NASA Headquarters. This was Dr. Kinney's first on-site visit to GP-B, so the day began with a brief tour of the GP-B facilities, followed by a series of briefings and discussions. At the end of the day, Dr. Kinney gave a very interesting lecture to a standing room only audience from the Stanford physics and aerospace community on the topic of “Blue Planets, Black Holes.”



GP-B co-principal investigator, Brad Parkinson (left), Anne Kinney (center) from NASA Headquarters, and GP-B Principal Investigator, Francis Everitt (right), tour the GP-B lobby display.

---

## 29 JULY 2005—GRAVITY PROBE B MISSION UPDATE

Mission Elapsed Time: 465 days (66 weeks/15.29 months)  
Science Data Collection: 329 days (49 weeks/11.05 months)  
Current Orbit #: 6,860 as of 1:00 PM PST  
Spacecraft General Health: Good  
Roll Rate: Normal at 0.7742 rpm (77.5 seconds per revolution)  
Dewar Temperature: 1.82 kelvin, holding steady  
Command & Data Handling (CDH): B-side (backup) computer in control, Multi-bit errors (MBE): 2, Single-bit errors (SBE): 8 (daily average)

Preliminary calibration testing of gyros #2, #3, and #4 continued this week and will be completed by Monday. These calibrations do not impact science data collection, but they do help us learn more about the characteristics of these gyros. These tests included a modulation of the Gyroscope Suspension System (GSS) preloads at roll rate, a SQUID configuration test, and a SQUID off test.

On Thursday, we performed the final heat pulse meter to determine the amount of liquid helium remaining in the dewar. Preliminary analysis supports previous estimates for the helium lifetime. Final results of this test are pending analysis.

---

## 5 AUGUST 2005—GRAVITY PROBE B MISSION UPDATE

Mission Elapsed Time: 472 days (67 weeks/15.53 months)  
Science Data Collection: 343 days (50 weeks/11.28 months)  
Current Orbit #: 6,962 as of 1:00 PM PST  
Spacecraft General Health: Good  
Roll Rate: Normal at 0.7742 rpm (77.5 seconds per revolution)  
Dewar Temperature: 1.82 kelvin, holding steady  
Command & Data Handling (CDH): B-side (backup) computer in control, Multi-bit errors (MBE): 0, Single-bit errors (SBE): 8 (daily average)

With more than eleven months of science data captured, the mission is proceeding well. Over the past week, we completed preliminary calibration tests and prepared for the final calibration phase in late August. Preliminary calibration testing of gyros #2, #3, and #4 included a modulation of the Gyroscope Suspension System (GSS) preloads at roll rate, a SQUID configuration test, and a SQUID off test.

On July 28, we performed the final heat pulse meter test to determine the amount of liquid helium remaining in the dewar. The results support previous estimates for the helium lifetime. Based on this final

test, we are planning on running final calibrations from August 15 to September 1, 2005. If any time remains after that, further calibrations will be performed at a different roll rate.

---

## **12 AUGUST 2005—GRAVITY PROBE B MISSION UPDATE**

Mission Elapsed Time: 479 days (68 weeks/1.31 years)  
Science Data Collection: 350 days (51 weeks/11.51 months)  
Current Orbit #: 7,006 as of 1:00 PM PST  
Spacecraft General Health: Good  
Roll Rate: Normal at 0.7742 rpm (77.5 seconds per revolution)  
Dewar Temperature: 1.82 kelvin, holding steady  
Command & Data Handling (CDH): B-side (backup) computer in control, Multi-bit errors (MBE): 0, Single-bit errors (SBE): 7 (daily average)

With nearly a full year of science data captured, the mission is proceeding well. This past week, we made some routine adjustments during our final week of nominal science data collection. These adjustments included updating the star tracker star magnitudes, running an SRE calibration (SQUID Readout Electronics), updating the control gyro z-bias, and power cycling the ECU (Electronics Control Unit).

On Monday, August 15th, we will begin the final calibration phase of the mission. In this phase, we will be maneuvering the spacecraft to nearby stars and then back to the guide star to calibrate the Gyroscope Suspension System (GSS). This phase will last two weeks, ending around August 29th. If any helium remains, further calibrations will be performed at a different vehicle roll rate. Because of the nature of these calibrations, the science (data gathering) phase of the mission will end as soon as we begin these calibrations. By that point, we will have collected 352 days (or 11.5 months) of science data—a great success!

Note: During this final calibration phase, our weekly updates will be limited to the Mission Director's Summary, as our communications and public affairs team members will be concentrating their efforts on our End-of-Mission activities and our final report to NASA.



## C.5 Instrument Calibration Phase: 8/19/05 – 9/30/05

### 19 AUGUST 2005—GRAVITY PROBE B MISSION UPDATE

Mission Elapsed Time: 486 days (69 weeks/ 16 months)  
IOC Phase: 129 days (4.2 months)  
Science Phase: 352 days (11.6 months)  
Final Calibration Phase: 5 days  
Current Orbit #: 7,169 as of 1:00PM PST  
Spacecraft General Health: Good  
Roll Rate: Normal at 0.7742 rpm (77.5 seconds per revolution)  
Gyro Suspension System (GSS): Drag-free off during calibration phase  
Dewar Temperature: 1.82 kelvin, holding steady  
Global Positioning System (GPS) lock: Greater than 98.0%  
Attitude & Translation Control (ATC): X-axis attitude error: 166.9 marcs rms  
Y-axis error: 254.5 marcs rms  
Command & Data Handling (CDH): B-side (backup) computer in control  
Multi-bit errors (MBE): 1 (in GSS#1 Computer on 8/17/05)  
Single-bit errors (SBE): 10 (daily avg.)  
As of Mission Day 486, the Gravity Probe B vehicle and payload are in good health and all subsystems are performing nominally.

The final calibration phase officially began at 6:26am (PST) on Monday when the drag-free gyro (Gyro #1) was transitioned to “drag-free off.” After setting the gyro preloads to the IOC levels of 10V (Initialization & Orbit Checkout Phase), we maneuvered the space vehicle to point at HD216235, a star one degree away from the guide star. On Tuesday, we returned to the guide star and resumed drag-free operation. On Wednesday and Friday, we are repeating these maneuvers to the neighboring star (HD216235). The aim of these calibrations is to place tight constraints on potential systematic errors.

The calibrations are scheduled to be completed by 31 August. With any remaining helium, further calibrations will be performed at a different spacecraft roll rate.



On Monday, 15 August 2005, the Gravity Probe B mission concluded the science phase of the mission and transitioned to the final calibration phase of the mission. In total, the mission collected science data for 352 days (11.6 months) during its 7,000+ orbits around the Earth with an extremely high data capture rate for that time (99.0%).

### DR. NANCY ROMAN VISITS GP-B

Two notable events related to GP-B occurred this past week. First, this past Tuesday and Wednesday, we were honored with a visit from Dr. Nancy Roman, one of the nation's leading scientists in the space program.



NASA Photo of Dr. Nancy Roman with a model of the Orbiting Solar Observatory

Roman received her Ph.D. in astronomy from the University of Chicago in 1949. She began her career doing astronomy research in stellar distances and motions at the University of Chicago's Yerkes Observatory and also teaching graduate courses there. In 1959, Roman joined NASA, and from 1960-1979, she served as Chief of the Astronomy and Relativity Programs in the NASA Office of Space Science. In her position at NASA, Roman was very influential in creating astronomical research satellites such as the Cosmic Background Explorer (COBE) and the Hubble Space Telescope (HST).



Left to right: Francis Everitt, Dan DeBra, Nancy Roman, Bob Cannon, Gaylord Green, and Barry Muhlfelder

She also oversaw the development of a number of ground and space research programs, including Gravity Probe B. In fact, Roman helped organize a NASA-sponsored two-day seminar, held at Stanford in July 1961, in which over 30 distinguished physicists, engineers, and aerospace experts from all over the U.S. gathered to discuss the possibilities of testing Einstein's theories of relativity in space. Some of the ideas discussed at that seminar—most notably the concept of a drag-free satellite—are currently being used in the GP-B mission. After retiring from NASA in 1979, Dr. Roman continued working as a



contractor at the Goddard Space Flight Center. Throughout her career, Dr. Roman has been a spokesperson and advocate of women in the sciences.

This past week was Dr. Roman's first trip to Stanford since 1979, but she has been following the progress of Gravity Probe B through our weekly updates. During her visit, she sat in on several mission status briefings, she met with scientists and engineers on the GP-B team, she attended a student presentation session and had lunch with the students and staff, and she toured the GP-B development labs and Mission Operations Center. We've included some photos from Dr. Roman's GP-B visit, plus a black and white NASA photo taken early in her career, in this week's highlights on our Web site. You can read more about Dr. Nancy Roman at <http://solarsystem.nasa.gov/people/profile.cfm?Code=RomanN>.

REX GEVEDEN APPOINTED ASSOCIATE NASA ADMINISTRATOR

Also in the news this past week, NASA Administrator Michael Griffin named Rex Geveden as the agency's associate administrator. In this capacity, Geveden has oversight for all the agency's technical missions' areas and field center operations. He will be responsible for programmatic integration between NASA's mission directorates and field centers. In November 2004, Geveden moved from NASA's Marshall Space Flight Center (MSFC) in Huntsville, AL to NASA Headquarters in Washington DC to become NASA Chief Engineer. He has been serving as acting associate administrator since June 2005.



Rex Geveden gives a pre-launch briefing to visitors at a hotel near Vandenberg Air Force Base in California on 19 April 2004, the day before the GP-B launch.

Prior to moving to NASA Headquarters, Geveden held various leadership positions at MSFC. He served as deputy director of the Marshall Center from July 2003-November 2004. Prior to that, he was deputy director of the MSFC Science Directorate, leading research and development projects in space science, materials science, biotechnology, earth science and space optics. Geveden was project manager for several successful efforts, including the Optical Transient Detector and Lightning Imaging Sensor satellites, which produced data for the world's first global map of lightning.

However, we here at GP-B have a special connection with Rex Geveden. From 1995-2003, Geveden was the NASA MSFC Program Manager overseeing GP-B's final development and testing, and readying the spacecraft for launch. Geveden has long been a staunch supporter of GP-B, and we wish him every success in his new position at NASA. You can read the NASA press release announcing Geveden's appointment last week at: [http://www.nasa.gov/home/hqnews/2005/aug/HQ\\_05227\\_geveden.html](http://www.nasa.gov/home/hqnews/2005/aug/HQ_05227_geveden.html)

## 26 AUGUST 2005—GRAVITY PROBE B MISSION UPDATE

Mission Elapsed Time: 493 days (70 weeks/ 16.2 months)  
—IOC Phase: 129 days (4.2 months)  
—Science Phase: 352 days (11.6 months)  
—Final Calibration Phase: 12 days  
Current Orbit #: 7,272 as of 1:00PM PST  
Spacecraft General Health: Good  
Roll Rate: Normal at 0.7742 rpm (77.5 seconds per revolution)  
Gyro Suspension System (GSS): Drag-free off during calibration phase  
Dewar Temperature: 1.82 kelvin, holding steady  
Global Positioning System (GPS) lock: Greater than 98.0%  
Attitude & Translation Control (ATC): X-axis attitude error: 127.7 marcs rms  
Y-axis error: 181.5 marcs rms  
Command & Data Handling (CDH): B-side (backup) computer in control  
Multi-bit errors (MBE): 1 (in GSS#2 computer on 8/26)  
Single-bit errors (SBE): 10 (daily avg.)  
Gyro #1 Drag-free Status: Backup Drag-free mode (OFF during calibration maneuvers)

As of Mission Day 493, the Gravity Probe B vehicle and payload are in good health and all subsystems are performing nominally.

The Gravity Probe B mission has continued with the final calibration phase this week, which it began ten days ago. Last Friday, the space vehicle was pointed toward HD216635 (the one-degree star) for the third time in five days and then returned to IM Pegasi for the weekend. On Monday, we maneuvered the space vehicle towards Zeta Pegasi (aka Homam or HD 214923/ HR 8634), which is our seven-degree star.

On Wednesday, the space vehicle was returned to the guide star (IM Peg) after spending ~30 hours on Zeta Pegasi. Later this week, we will perform DC mis-centering on Gyros #1, #2 and #4, and GSS torque calibrations on Gyros #1 and #4 with five hours of nominal science between the two tests. Three additional visits to the one-degree star have been added to the schedule starting August 26.

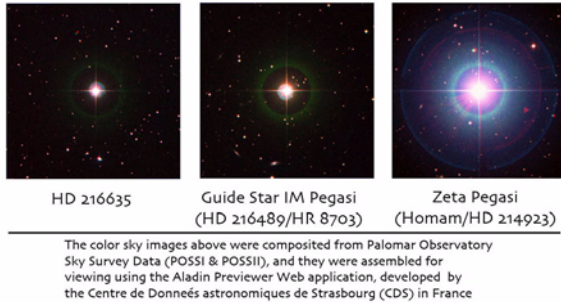
The calibrations are scheduled to be complete by next Wednesday (August 31). The projected helium depletion date remains Friday, September 2. With any remaining helium, further calibrations will be performed at a different spacecraft roll rate (0.5 rpm).

### POINTING AT A LUCKY STAR



As noted in the Mission Director's summary above, we are now in the final days of our instrument calibration testing. Last week, we slewed the on-board telescope (and the spacecraft) away from the guide star, IM Pegasi, to point at a neighboring star about one degree away. The

neighbor star we chose has no proper name, only catalog numbers such as HD 216635, and with an average V magnitude of 6.61 it is somewhat fainter than IM Pegasi (V magnitude 5.89). We kept the telescope pointed at HD 216635 for about half an hour and then slewed the telescope back to IM Pegasi. Over the course of last week, we repeated this procedure a total of five times. Then, this past Monday, 22 August 2005, we slewed the telescope and spacecraft to the star named Homam (aka Zeta Pegasi or HD 214923), which is about seven degrees away from IM Pegasi and considerably brighter (average V magnitude 3.40). This time, we kept the telescope and spacecraft pointed at Homam for about 30 hours before returning to IM Pegasi.



The reason we are performing these slewing tests is to measure and calibrate the amount of torque (force) placed on the science gyroscopes by intentionally mis-aligning the telescope axis from the gyroscope spin axes by relatively large factors of first one, and then seven degrees. At the beginning of the science phase of the mission, we aligned both the telescope and the spin axes of all four gyroscope with the guide star, IM Pegasi to an accuracy level of a few arcseconds. During the science phase of the mission, we kept the telescope aligned with the guide star to within 100-150 milliarcseconds. (an arcsecond is 1/3600th of a degree, and a milliarcsecond is 1/1000th of an arcsecond). By design, the spin axes of the gyroscopes are aligned with the axis of the telescope, which is also the roll axis of the spacecraft, and as long as these alignments are maintained, the non-relativistic torques on the gyros average out. However, during these final calibrations, we intentionally break these alignments, forcing the telescope first one degree and then seven degrees away from the gyro spin axis alignments, and we can then determine the extent to which these misalignments place torques on the gyro spin axes. Clearly, given the nature of these final calibration tests, they could not be performed while we were still collecting science data, which is why they were left to be performed at the very end of the experiment.

The star, Homam or Zeta Pegasi, was not one of our initial candidates to be used in the final calibrations, but it was selected by our telescope team because it emits light in the blue range of the spectrum, whereas IM Pegasi emits light in the red range of the spectrum. Homam is also much brighter than IM Pegasi, as noted above, and thus this latest calibration test was not only useful for examining torques on the gyros, but also for evaluating the telescope performance on a brighter star with a different color of light.

Burnham's Celestial Handbook (a three-volume compendium of astronomical information), gives the following information about the name Homam, by which Zeta Pegasi is also known:

*Homam, probably comes from the Arabic phrase Sa'd al Humam, the "Lucky Star of the Hero," though Thomas Hyde derived it from Al Hammam, which seems to mean "The Whispering One." According to R. H. Allen, the names Sa'd al Na'amah, "The Lucky Star of the*

*Ostriches" and Na'ir Sa'd al Bahaim, "The Bright Fortunate One of the Two Beasts" were also in use among the Arabs. The Chinese, for some unknown reason, connected the star with thunder.*

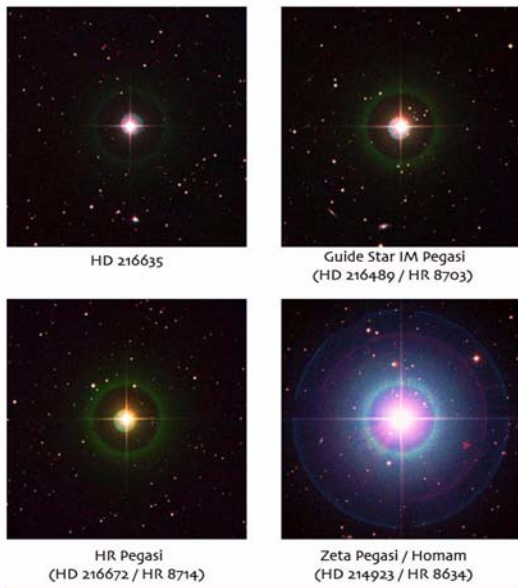
Zeta Pegasi is computed to be about 210 light years away, with an actual luminosity about 145 times brighter than our Sun. On our Web site this week, we have posted photos of HD 216635, IM Pegasi, and Zeta Pegasi, along with sky charts produced by the Voyager III Sky Simulator from Carina Software (<http://www.carinasoft.com>) that shows the locations of these stars. The star photos, as well as much of the information about these stars came from the various Web pages of the Centre de Données astronomiques de Strasbourg—CDS (<http://cdsweb.u-strasbg.fr/>), including the Simbad astronomical database (<http://simbad.u-strasbg.fr/sim-fid.pl>) and the Aladin interactive sky atlas (<http://aladin.u-strasbg.fr/aladin.gml>).

## 2 SEPTEMBER 2005—GRAVITY PROBE B MISSION UPDATE

Mission Elapsed Time: 500 days (71 weeks/ 16.4 months)  
 —IOC Phase: 129 days (4.2 months)  
 —Science Phase: 352 days (11.6 months)  
 —Final Calibration Phase: 19 days  
 Current Orbit #: 7,376 as of 1:30PM PST  
 Spacecraft General Health: Good  
 Roll Rate: Normal at 0.7742 rpm (77.5 seconds per revolution)  
 Gyro Suspension System (GSS): All 4 gyros digitally suspended  
 Dewar Temperature: 1.82 kelvin, holding steady  
 Global Positioning System (GPS) lock: Greater than 98.5%  
 Attitude & Translation Control (ATC): X-axis attitude error: 140.0 marcs rms  
 Y-axis error: 186.4 marcs rms  
 Command & Data Handling (CDH): B-side (backup) computer in control  
 Multi-bit errors (MBE): 0  
 Single-bit errors (SBE): 8 (daily avg.)  
 Gyro #1 Drag-free Status: Backup Drag-free mode (OFF during some calibration maneuvers)

On Mission Day 500, the Gravity Probe B vehicle and payload are in good health and all subsystems are performing nominally.

As of today, there is still an ever-thinning film of superfluid helium in the dewar, and thus calibration tests, which began 19 days ago, continued throughout this past week. Over the course of last weekend and early this week, we thrice slewed the telescope (and spacecraft) to "visit" the star HD 216635, which is about one degree northwest of IM Pegasi, and then back to IM Pegasi.



The colored sky images above were composited from Palomar Observatory Sky Survey Data (POSS1 and POSS2), and they were assembled for viewing using the Aladin Previewer Web application, developed by the Centre de Données astronomiques de Strasbourg (CDS) in France.

On Wednesday, we visited the star HR Pegasi (HD 216672), which is about 0.4 degrees west of IM Pegasi. We had previously visited this star during the Initialization and Orbit Checkout (IOC) phase of the mission in June 2004, as a test to confirm that the star we were using as the guide star was, in fact, IM Pegasi. (You can read about our previous visit to HR Pegasi in our 11 June 2004 update.

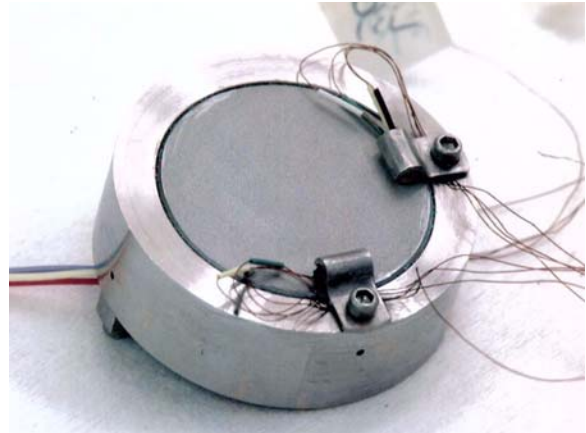
Thus far during these final calibration tests, our visits to HD 216635 and to Zeta Pegasi were predominately in a north-south plane, relative to IM Pegasi. Our visit to HR Pegasi this past Wednesday was our first calibration test with a star located in the east-west plane, with respect to IM Pegasi. Continuing this line of exploration, yesterday and today we completed several visits to locations less than one degree west, and less than one degree east of IM Pegasi. No stars visible to the on-board telescope exist in these recently visited locations, so we used data from our star trackers and our standard navigational gyroscopes, which are accurate to within 20 arcseconds, to determine the positions of these “virtual stars.” Since the purpose of these calibrations is to evaluate the effects of telescope mis-alignments on the science gyros, greater pointing accuracy is not required for these excursions.

We have postponed our previous plans to slow down the spacecraft’s roll rate until after the helium in the dewar is fully depleted. Over this weekend, we will continue making calibration tests similar to those we have been performing, and if the helium lasts into next week, we will perform other types of calibration tests. Once the helium is depleted, the GP-B flight mission will officially end.

Tony Lyons, NASA’s program manager for GP-B from Marshall Space Flight Center in Huntsville, AL, has been here at Stanford all week, participating with our team in these final days of the mission.

**GP-B MISSION NEWS—THE FINAL DAYS**

This past week marks a major transition point in the GP-B program. Exactly 16.4 months after a picture-perfect launch on 20 April 2004, we have come to the end of the GP-B flight mission. Literally any day now, the supply of superfluid helium—the coolant that has maintained the cryogenic temperatures necessary for our SQUID gyro readouts to function—will be exhausted.



Right now, there is an ever-thinning layer of superfluid liquid helium lining the dewar, and there will come a point where the last of this liquid helium has “sweated” out through the porous plug, leaving only helium gas inside the dewar. (See our Mission News story of 29 July 2005 for a description of the porous plug <http://einstein.stanford.edu/highlights/hlindex.html>.) As this final helium gas begins to pas through the porous plug, the pressure in the dewar will begin to drop, causing the temperature in the Probe to rise. We don’t know whether this transition will happen gradually or suddenly (as was the case with NASA’s COBE spacecraft), but we will know that we have reached this point when our telemetry data shows a rise in the temperature sensors on the bracket that houses the SQUID gyro readout controllers and the temperature sensors on the telescope detector packages. When the temperature in the Probe reaches about 7 kelvin, we will begin to lose superconductivity in the niobium gyro rotor coatings, and the SQUID gyro readouts will gradually cease to detect the London moments in the gyros. At this point, it be no longer be possible to determine the spin axis orientation of the science gyroscopes, although the Gyro Suspension Systems (GSS) will continue to indicate the position of each gyro rotor within its housing to great precision. Also, with no helium propellant left, the spacecraft will no longer be able to maintain a drag-free orbit.

The 650 gallons of helium that filled the dewar at launch has lasted exactly the length of time planned. We collected 50 weeks of science data—just two weeks short of the year’s worth of data we had hoped to collect. Furthermore, we lost less than 1% of the data collected to telemetry and/or spacecraft hardware problems. We have now completed all of the vital planned calibration tests that needed to be done with the gyro readouts still functioning, and we are using these final days of helium to perform additional tests that will be valuable to the data analysis now in process. In short, GP-B has been a remarkably successful mission.

There is an air of triumph here at Stanford, but there is also a note of sadness. Having become a very tight-knit team, we are saddened that today is the last day of work on GP-B for a number of our colleagues, especially those from Lockheed Martin Corporation. Thus, this afternoon, we all gathered in the conference room where we’ve been holding daily status meetings since before launch, and we spent a few minutes raising toasts to our successful mission and to the future endeavors of our colleagues who will be moving on to new jobs next week.

Regarding the GP-B spacecraft, the experiment, and the remaining members of the team, following is a brief overview of what’s in store. Next Tuesday, when we return from the Labor Day holiday, GP-B will be a much quieter place. Our science team is already well into the long, painstaking process of analyzing the data. A small spacecraft



operations crew, including several GP-B graduate students who are being cross-trained for these duties, will continue to monitor the spacecraft's system status, send commands to it when necessary, and regularly, though much less frequently, download various types of data via NASA telemetry satellites and ground stations.

We will use magnetic torquers—long electromagnets mounted on the spacecraft frame—to slow down the spacecraft's roll rate from 0.7742 rpm to 0.5 rpm or less and to control the spacecraft's orientation in orbit. For about two weeks, we will perform a number of tests on various electronic systems in the spacecraft. For example, we want to compare various performance characteristics of the GSS system after it has “warmed up” to its performance in a cryogenic superconductive state. Finally, in about a month, we will spin down all four science gyros to speeds slow enough that they will not be in danger of shattering, should they lose suspension and touch their housing walls. At this point, the spacecraft could be used by other scientists to make various non-relativistic measurements. For example, it could be used for experiments in geodesy (measuring the shape of Earth's gravitational field) and aeronomy (measuring atmospheric density). We are in the process of exploring the interest in further use of the GP-B spacecraft for such experiments with a number of scientists.

One last note: All of us on the GP-B team are deeply saddened by the horrific disaster and unfathomable human tragedy that has been unfolding in Gulf Coast this past week. Our hearts and prayers go out to the countless victims.



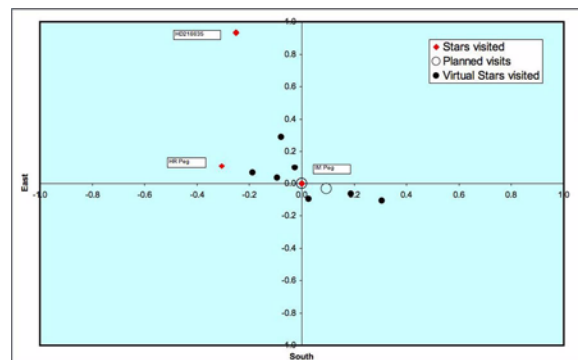
A spare GP-B magnetic torque rod. These rods are basically electromagnets located on the spacecraft frame that interact with Earth's magnetic field to control the spacecraft's orientation in orbit.

## 9 SEPTEMBER 2005—GRAVITY PROBE B MISSION UPDATE

Mission Elapsed Time: 507 days (72 weeks/ 16.6 months)  
 —IOC Phase: 129 days (4.2 months)  
 —Science Phase: 352 days (11.6 months)  
 —Final Calibration Phase: 26 days  
 Current Orbit #: 7,482 as of 4:30PM PST  
 Spacecraft General Health: Good  
 Roll Rate: Normal at 0.7742 rpm (77.5 seconds per revolution)  
 Gyro Suspension System (GSS): All 4 gyros digitally suspended  
 Dewar Temperature: 1.82 kelvin, holding steady  
 Global Positioning System (GPS) lock: Greater than 96.5%  
 Attitude & Translation Control (ATC): X-axis attitude error: 149.7 marcs rms  
 Y-axis error: 179.9 marcs rms  
 Command & Data Handling (CDH): B-side (backup) computer in control  
 Multi-bit errors (MBE): 0  
 Single-bit errors (SBE): 8 (daily avg.)  
 Gyro #1 Drag-free Status: Backup Drag-free mode (OFF during some calibration maneuvers)

On Mission Day 507, the Gravity Probe B vehicle and payload are in good health and all subsystems are performing nominally.

The helium in the dewar has lasted throughout this past week, and thus we have continued with the calibration tests that we began over three weeks ago. These tests involve slewing the telescope (and spacecraft) to “visit” stars (both real and virtual) in the neighborhood around the guide star, IM Pegasi. In each case, we visit a neighboring location for a period of time and then lock back onto IM Pegasi for several hours. The purpose of these tests is to calibrate, in detail, the torques imparted onto the science gyroscopes by purposely misaligning the telescope (and spacecraft roll axis) from the direction of the gyro spin axes.



Last weekend, we visited a “virtual star” (location where no stars visible to the telescope exist) located 0.1 degree in the direction of neighboring star HD 216635, northwest of IM Pegasi. We remained at this location for 24 hours and then returned to IM Pegasi for 16 hours. We then repeated this procedure, visiting a location 0.1 degrees in the opposite direction. Then, this past Tuesday we visited a virtual star location halfway to the Star HR Pegasi (HD 216672), which is located to the west of IM Pegasi. After dwelling in that location for 24 hours, we again returned to IM Pegasi. And, on Thursday, we visited a virtual location 0.3 degrees towards HD 216635, remained there for 24 hours and then returned to IM Pegasi.





Members of the GP-B team monitor telemetry data during the spacecraft's visit to Alpha Pegasi.

Last Tuesday, 13 September, we visited the very bright (magnitude 2.45) neighboring star Alpha Pegasi (also known as Markab or HD 218045), located about 3.25 degrees south of IM Pegasi. We remained locked on Alpha Pegasi for 12 hours. Upon returning to returning to IM Pegasi. We switched drag-free control back to gyro #1.

Then, last Wednesday, we sent commands to the spacecraft to decrease its roll rate from 0.7742 rpm (77.5 seconds per revolution) to 0.4898 rpm (122.5 seconds per revolution). This resulted in some interference with a SQUID calibration signal, and the frequency of the calibration signal was subsequently changed, eliminating this issue. The spacecraft has since been performing nominally at the slower roll rate.

Finally, today, we initiated procedures to de-fluxing the SQUIDS—that is, removing electromagnetic flux from the SQUIDS by heating them up a few kelvins, and then allowing them to cool back down to their normal cryogenic operating temperature of 1.8 kelvin. Assuming that we still have helium remaining this weekend and next week, this process is a prelude to performing several gyro housing exploration tests, followed by a switch from backup to primary drag-free mode.

#### GP-B MISSION NEWS—RUNNING ON EMPTY, AND VISITING THE BRIGHTEST STAR IN THE CONSTELLATION PEGASUS

If you drive a car, you have likely experienced—at least once—the situation where the needle on your car's gas gage moves into the red zone, and the light comes on indicating that the gas tank is nearly empty. But, unless you've been in this situation a few times with any particular car, you don't know for sure how much farther you can drive before the engine finally sputters and stops running. This is essentially the situation with our GP-B spacecraft right now. We know that we're in the "red zone" with our helium very nearly depleted, but how many more orbits will actually be sustained is basically anyone's guess.

And so, continuing our prioritized calibration tests, last week we visited the star Alpha Pegasi (aka Markab/HD 218045/ HR 8781), located about 3.25 degrees southward of IM Pegasi. Alpha Pegasi is one of the defining stars in the constellation Pegasus, the flying horse. It is approximately 110 light years away, and its luminosity is about 95 times greater than our Sun. In fact, the designation of "Alpha" Pegasi means that it is the brightest star in the constellation Pegasus. A set of composite photos from the Palomar Observatory Sky Surveys (POSSI and POSSII) accompanying this week's Mission News story on our Web site clearly show the comparative luminosity or brightness of

Alpha Pegasi, Zeta Pegasi, HR Pegasi, IM Pegasi, and HD 216635—all the stars in the neighborhood of IM Pegasi that we have visited recently.



The colored sky images above were composited from Palomar Observatory Sky Survey Data (POSSI and POSSII), and they were assembled for viewing using the Aladin Previewer Web application, developed by the Centre de Données astronomiques de Strasbourg (CDS) in France.

At this time of year in North America, the constellation Pegasus is clearly visible above the Eastern horizon during the evening hours, as shown in the sky charts accompanying this week's Mission News on our GP-B Web site.

As we noted last week, as long as we still have helium in the dewar, we will continue working our way through our prioritized list of calibration tests. When the helium actually does run out, we will post a notice on our Web site and send out a message to the subscribers of our GP-B Update email list. NASA will also issue a news release, and we will then post the content of that release on our Web site and send it to our email subscribers.

## 23 SEPTEMBER 2005—GRAVITY PROBE B MISSION UPDATE

Mission Elapsed Time: 521 days (74 weeks/ 17.08 months)  
 —IOC Phase: 129 days (4.2 months)  
 —Science Phase: 352 days (11.6 months)  
 —Final Calibration Phase: 40 days  
 Current Orbit #: 7,688 as of 4:00PM PST  
 Spacecraft General Health: Good  
 Roll Rate: Normal at 0.4898 rpm (2.04 minutes per revolution)  
 Gyro Suspension System (GSS): All 4 gyros digitally suspended  
 Dewar Temperature: Not Available  
 Global Positioning System (GPS) lock: Greater than 99.4%  
 Attitude & Translation Control (ATC): 128.0 marcs  
 Y-axis error: 170.8 marcs  
 Command & Data Handling (CDH): B-side (backup) computer in control  
 Multi-bit errors (MBE): 1 (in GSS#3 computer on 9/23)  
 Single-bit errors (SBE): 7 (daily average)  
 Telescope Readout (TRE): Nominal  
 Gyro #1 Drag-free Status: Backup Drag-free mode (OFF during some calibration maneuvers)

On Mission Day 521, the Gravity Probe B vehicle and payload remain in good health, with all subsystems performing nominally. We still have some helium in the dewar, and the spacecraft is flying drag-free around Gyro #1.



The helium in the dewar has now surpassed its estimated lifetime by more than three weeks, and thus, our dewar team has been analyzing the calculations and underlying assumptions on which their helium lifetime predictions were originally made. (See the Mission News story below for more information about this.)

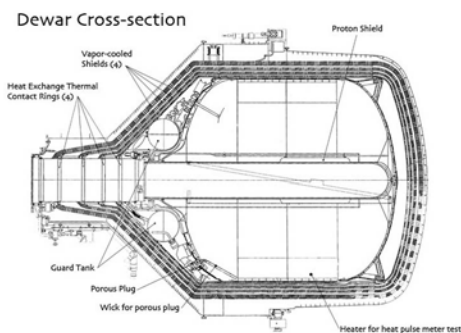
Meanwhile, we have continued working our way through our prioritized list of calibration tests. Last weekend, we completed the process of de-fluxing the SQUIDS—that is, removing electromagnetic flux from the SQUIDS by heating them up a few kelvins, and then allowing them to cool back down to their normal cryogenic operating temperature of 1.8 kelvin.

On Monday, we attempted to switch from backup to primary drag-free operation on gyro #1. For various reasons, including a mis-configuration of the ATC system prior to the mode switch, the attempt failed, and we reverted to backup drag-free mode on gyro #1.

On Tuesday, we visited a virtual star 0.1 degrees east of IM Pegasi, in the opposite direction from HR Pegasi. We remained locked in the position for 48 hours, while the telescope team performed some dark current calibration tests, and then we returned and re-locked the telescope onto IM Pegasi on Thursday. We then attempted again to switch from backup to primary drag-free mode on gyro #1, and again the attempt failed. We are currently investigating the possible causes of this failure, and we plan to try this switch again next week...assuming that we still have helium in the dewar.

#### GP-B MISSION NEWS—REVISING THE HELIUM LIFETIME PREDICTIONS

Our dewar team made its initial helium lifetime predictions by making calculations based on the results of several heat pulse meter tests that were performed at various points throughout the mission and some assumptions derived from the scientific literature and experience of other spacecraft that used a helium-based cryogenic system.



The dewar team's initial calculations suggested that the helium in the dewar should have been depleted sometime around Labor Day (5 September 2005). Because the helium has now lasted three weeks longer than the initial predictions, the dewar team has been re-examining their calculations and the underlying assumptions used to make them. The team has checked and re-checked their calculations, and it appears that no errors were made. This has led them to re-evaluate the assumptions underlying these calculations.

Inside the dewar, there is some amount of superfluid liquid helium and some amount of helium vapor (gas). The initial longevity calculations were based on the assumption, as suggested by the literature and performance of other spacecraft, that the helium liquid

and the helium gas inside the dewar are in a state of thermal equilibrium. That is, they are both maintaining the same temperature due to close thermal contact between the liquid and gas.

An alternative assumption is that there is poor thermal contact between the helium liquid and gas in the dewar, due to the low thermal conductivity of the vapor. If this is the case, the temperatures of the liquid and gas are not necessarily in equilibrium over the time scale of the measurement. That is, over short time scales, a temperature increase in the liquid helium does not necessarily result in a corresponding temperature increase in the helium vapor bubble. (Equilibration does ultimately occur, but over a longer time scale.)

Taken to their extremes, these two assumptions result in two limiting cases for the helium depletion:

- 1) Strong thermal contact between the two helium phases (the thin layer of liquid helium coating the dewar wall and the bubble of helium vapor in the center of the dewar are in thermal equilibrium over the short time frame of the measurement—the initial assumption)
- 2) Weak thermal contact between the two helium phases (a change in temperature in the liquid phase has little effect on the temperature of the gas bubble over the time scale of the measurement; rather, it takes many hours for the helium vapor bubble to reach equilibrium with the liquid helium).

The dewar team's initial predictions for the helium longevity were based on the first assumption, which yielded the 5 September helium depletion date. However, if the second assumption is used, the longevity of the helium increases by 5-6 weeks. In other words, the upper bound on the helium longevity, based on the second assumption, places the helium depletion date around mid October. It is most likely that the actual conditions inside the dewar lie somewhere between these two bounding assumptions. And, judging from the dewar's performance thus far, it appears that the thermal contact between the helium phases is weaker than was originally assumed.

As we have noted these past few weeks, as long as we still have helium in the dewar, we will continue working our way through our prioritized list of calibration tests. When the helium actually does run out, we will post a notice on our Web site and send out a message to the subscribers of our GP-B Update email list. NASA will also issue a news release, and we will then post the content of that release on our Web site and send it to our email subscribers.

### 30 SEPTEMBER 2005—GRAVITY PROBE B MISSION UPDATE

Mission Elapsed Time: 528 days (75 weeks/ 17.3 months)  
 —IOC Phase: 129 days (4.2 months)  
 —Science Phase: 352 days (11.6 months)  
 —Final Calibration Phase: 43 days (1.3 months)  
 —Science II Phase: 4 days  
 Current Orbit #: 7,792 as of 4:00PM PST  
 Spacecraft General Health: Good  
 Roll Rate: Normal at 0.4898 rpm (2.04 minutes per revolution)  
 Gyro Suspension System (GSS): All 4 gyros digitally suspended  
 Dewar Temperature: 5.632 kelvin and rising  
 Global Positioning System (GPS) lock: Greater than 95.0%  
 Attitude & Translation Control (ATC): N/A  
 Y-axis error: N/A  
 Command & Data Handling (CDH): B-side (backup) computer in control  
 Multi-bit errors (MBE): 0  
 Single-bit errors (SBE): 7 (daily average)  
 Gyro #1 Drag-free Status: OFF

On Mission Day 528, the Gravity Probe B vehicle and payload are in good health, with all subsystems performing nominally. The dewar is now depleted of liquid helium, and this has affected various subsystems, as summarized below. Drag-free mode has been turned off.



In the Mission Operations Center, GP-B operations team members communicate with a NASA ground station to retrieve data confirming helium depletion.

Yesterday at 1:55 pm Pacific Daylight Time, the last of the liquid helium in our dewar transitioned to the gas phase, and the science instrument began to warm. The team correctly assessed the status of the dewar, based on a set of pre-approved indicators, and they began running our planned Helium Depletion Procedure.

As of 9:30 am PDT this morning, the temperature in the dewar had risen from 1.8 to 5.6 kelvin, and it is slowly continuing to rise. Likewise, the temperature in SQUID Readout Electronics (SRE) had risen to 7 kelvin, but as of our 10:00 am PDT status meeting this morning, the dewar was still cold enough for the SRE to provide readouts of the gyros' spin axes. As the SRE temperature continues to rise, we will gradually lose these readouts.

This past Monday, 26 September 2005, we made a third attempt to switch from backup drag-free mode to primary drag-free mode on gyro #1. This latest attempt also failed, but for a different reason. Configuration issues were determined to be the root cause in each of the first two failures, and these issues were addressed prior to making this 3rd attempt on Monday. Analysis later this week showed that Monday's failed attempt was consistent with similar failures we had seen during the Initialization and Orbit Checkout (IOC) phase of the mission in July and August, 2004, and it was likely due to un-modeled forces between the gyro rotor and its housing.

As was the case during IOC, these issues could have been resolved with further experimentation and fine tuning the Attitude and Translation Control system (ATC). However, given the imminent depletion of the dewar's helium supply, we decided to return the spacecraft to its stable science configuration (backup drag-free mode, locked on the guide star) and remain in this configuration until the helium ran out—which as it turned out, happened three days later.

Our science team is interested in comparing the data collected in science configuration during this past week with the science data they collected prior to beginning gyro torque calibrations in mid August.

#### GP-B MISSION NEWS—THE DAY THE DEWAR DIED

As we have been anticipating for some time now, the moment finally arrived yesterday when the liquid helium in the dewar ran out. I was sitting in my office, thinking about what I was going to write in this

week's Mission News section when a colleague stopped by and said, "It appears that we've run out of helium." Suddenly, my dilemma of what to write about this week was a non-issue.



GP-B Dewar experts examine data received from the spacecraft, following indications that the liquid helium in the Dewar had run out.

I grabbed my camera and dashed off to our Mission Operations Center (MOC). In recent weeks, our MOC has been relatively quiet, and typically there have only been a handful of people there at any given time. But, yesterday afternoon, the MOC was teeming with activity, reminiscent of the days when we spun up the gyros in the summer of 2004.

The evidence was clearly visible on the dewar monitor screen. The pressure display had suddenly taken a nose-dive. Elsewhere in the MOC, GP-B scientists and engineers were clustered around the status monitors representing their respective areas of expertise, engaged in animated conversations. Meanwhile, our mission operations team members, headphones and microphones in place, were communicating with a NASA ground station, arranging for extra telemetry time.



Following indications of helium depletion in the Dewar, three GP-B team members monitor gyro and SQUID performance while others discuss Dewar readout data.

There were some tense moments when all were patiently awaiting the download of more data that would confirm, unequivocally, that the liquid helium was depleted. We were also attempting to turn on the Experiment Control Unit (ECU) on the spacecraft so that we could receive some important data, such as the current temperature in the dewar. It took several hours to arrange all the necessary telemetry passes, send the required commands to the spacecraft, and download

the all the spacecraft status data. By late evening, it was clear that the liquid helium in the dewar had run out, and that the dewar and SQUIDs were slowly beginning to warm up.

This morning, at our daily all hands meeting-the last of our daily spacecraft status meetings-the room was packed. The word was out that we had run out of helium, and everyone came to hear the details. At the end of the meeting, GP-B program manager, Gaylord Green, and GP-B principal investigator, Francis Everitt, each congratulated the team on their superb performance in working with one of the most complex spacecraft ever launched. We then assembled in front of the GP-B building for a group photo, and the next to last chapter in the long and colorful history of GP-B came to a close.



GP-B team members present at the last daily spacecraft status meeting on September 30, 2005, following depletion of the liquid helium in the spacecraft's Dewar the previous evening.

We will continue to post these weekly updates for another week or so, while we perform some final tests as the spacecraft warms up. We will then transition to less frequent updates-either bi-weekly or monthly-as there will be little news to report from week to week during the coming year of data analysis.

For now, we leave you with a song, written by Rob Brumley (our former gyro expert), Greg Gutt (one of our former SQUID experts), with help from Bill Bencze (our deputy program manager for engineering).

---

## AMERICAN PIE—GYRO STYLE (With apologies to Don McLean)

A long, long time ago....  
I can still remember how that dewar used to make me smile  
And I knew if I had my chance  
That I could make those gyros dance  
And Francis would be happy for a while.  
But September 1st had come and gone  
The helium went on and on  
No time for celebration  
Another calibration....

I can't remember if I cried  
Remembering how hard we'd tried  
And I was filled with a sense of pride  
The day the dewar died....

### REFRAIN

So, bye-bye, our friend in the sky  
Tied my SQUID to the dewar,  
But the dewar was dry,  
And the good ol' boys, drinking coffee and wine,  
Singing this'll be the day that I die,  
This'll be the day that I die....

The gyros spun a little slow,  
So Gaylord said increase the roll.  
And gyro drift was truly low,  
The day the dewar died...



# D

## Summary Table of Flight Anomalies

---





This appendix contains a table summarizing the complete set of 193 anomalies/observations that the GP-B Anomaly Review Board (ARB) worked through during the IOC period from 20 April 2004 through 13 October 2005. In the table, all formal anomalies are shown in boldface type.

These anomalies have been divided in the four ARB categories as follows:

1. **5 Major Anomalies** (2 in IOC) These anomalies had the potential to endanger the safety of the spacecraft and/or the payload.
2. **12 Medium Anomalies** (9 in IOC) These anomalies did not endanger the safety of the space vehicle but did impact the execution of planned timeline
3. **6 Minor Anomalies.** (3 in IOC) These anomalies did not endanger the safety of the space vehicle and did not stop the execution of the timeline. However, they did require actions to mitigate or correct the issue.
4. **170 Observations.** (94 in IOC) Observations are off-nominal or unexpected behavior of the space vehicle that was not an operational or functional issue and does not violate any limits, but did warrant attention over time. These can be considered vehicle “squawks”.

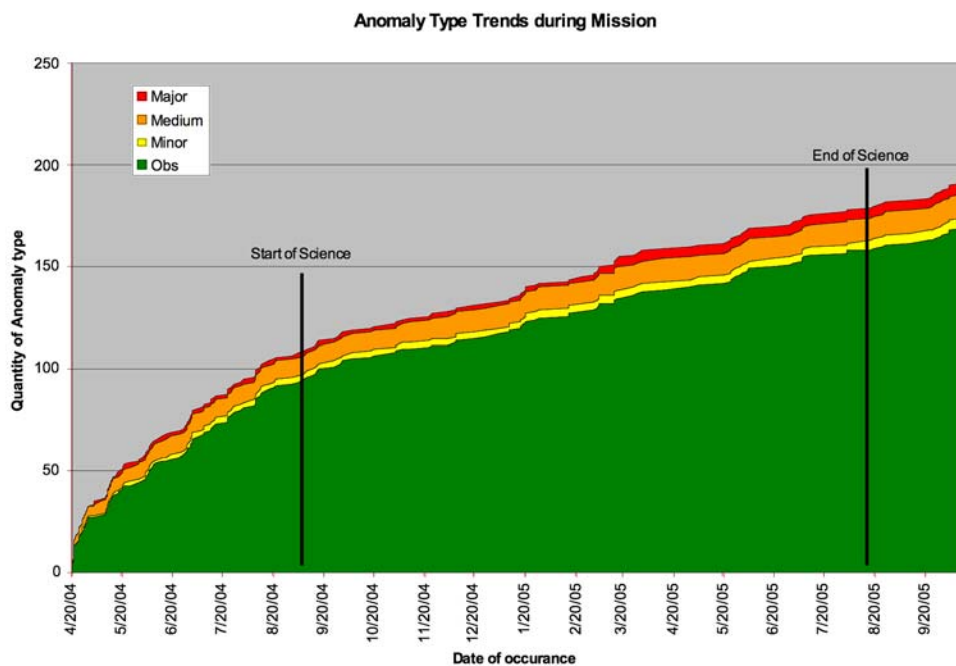


**Figure D-1.** Anomaly Type Trends during the mission

The large table that comprises the bulk of this appendix presents a summary of all identified anomalies: description, root cause, and corrective action taken. The observations listed there—essentially very small and easy to resolve anomalies—may be further categorized as follows:

- (A) Analysis items—Items still in work to understand the root cause (for open items only).
- (T) Tune items—Out of spec features resolved with on-orbit tuning of the spacecraft or payload.
- (O) Ops issues—Unexpected behavior due to an operations, mission planning, or other “human” error.
- (F) Features—Unexpected functionality that has no long term effect on the mission. This category also includes routine issues, such as correcting double bit errors in processor memory.
- (N) Non-issues—Expected behavior not initially understood by the individual making the observation.



Figure D-2 below shows the distribution of these categories across the major space vehicle subsystems. Because the vehicle is a system, not a collection of independent components, an observation may span more than one subsystem.

	ATC	GSS	TRE	SRE	CDH	COM	Dewar	GMA	GPS	EPS	Gyro	PM	TCS	ECU	Sum
<b>Tune Items</b>	29	14	7	2			6			1				1	60
<b>Analysis items</b>	2	4					1								7
<b>Features</b>	6	28	2	10	19	2	3		6		1	2	2	5	86
<b>Non-issues</b>	5	2	1	3	1		3	1					1	2	19
<b>Ops issues</b>	5	4			1	2								1	13
<b>Sum</b>	47	52	10	15	21	4	13	1	6	1	1	2	3	9	

**Figure D-2.** Observation categories by subsystem

The key observation that can be made is that the two systems that could not be completely tested on the ground – the GSS and ATC systems – gathered a disproportionately large number of observation items. The other systems had the advantage of being nearly fully testable in the lab and thus the operational bugs could be worked out prior to launch. Since the ATC and GSS require the space environment to function completely, they required the most adjustment once on orbit.

	Date	Severity	Sub-type	Title	Description	Root cause	Corrective Action
1	20-Apr-04	Obs	F	RAV4 Status	RAV4 does not indicate "open".	Known issue with RAV valves (CARD 255).	None; valve confirmed open once thrusters began working.
2	20-Apr-04	Obs	F	SS1 Aliveness Test Activated	SS1 aliveness test activated, but mapped to no-op macro 64.	Result of bright object detection and subsequent internal reset of star sensor electronics.	Disable this safemode test.
3	20-Apr-04	Obs	T	Thruster 2 & 14 shows low pressure	Thrusters 2 & 14 – very low pressures (most are 4-5 mV, 2 & 14 at -.1) (Saturated.)	Thruster bias	Adjust thruster biases sa part of item 005.
4	20-Apr-04	Obs	F	Vatterfly temp sensor noisy reading	Vatterfly temp sensor noisy reading	Noise in ECU seen during ground testing.	None
5	20-Apr-04	Medium		Star sensor lack of acquisition	Star sensor not properly identifying reference stars; attitude solution form star sensor processing erratic	Vehicle initial conditions (mass imbalance, alignments, star sensor settings) generated data that the star sensor processing algorithm was unable process successfully.	Switch to magnetometer-based attitude determination algorithm, adjust magnitude and error gate thresholds, tune control gyro biases and cross products of inertia, update star sensor alignment matrices. Reacquisition procedure updated based on-orbit performance.
6	20-Apr-04	Obs	T	Orbit modeling mismatch.	Hard to fit orbit modeling with TDRS GSFC data.	Residual venting of guard tank after launch	None; wait for guard tank to complete venting.
7	21-Apr-04	Obs	T	Various star tracks that are not aligned with roll	Various star tracks that are not aligned with roll	ATC off-tune after initial orbit insertion.	Tune ATC system (gyro biases, thruster biases)
8	21-Apr-04	Obs	F	SEU observation	Multi-bit and single bit errors seen on Flight computers; caused Anomaly #034 C&DH B side switch	Radiation events	Increase frequency of SEU monitoring of CCCA.

	Date	Severity	Sub-type	Title	Description	Root cause	Corrective Action
9	21-Apr-04	Medium		Bias torque observed on vehicle	Bias torque on vehicle seen in telemetry data; large mass flow from dewar through thruster system.	Thruster 6 malfunctioning; producing excessive, uncontrollable thrust. Likely root cause: foreign object contamination of thruster	Isolate thruster 6 (via TIV), adjust other thruster biases and control modes (do not use pressure feedback), update pseudo-inverse matrix between ATC controller and thrusters.
10	21-Apr-04	Obs	N	SRE Supplemental Heater on; SRE at 30 deg C	Forward SRE Supplemental Heater on; AFT SRE at 30 deg C	Heater on per plan	None
11	21-Apr-04	Medium		Dropouts on forward antenna to TDRSS	Poor link margins when operating on transponder A (forward) that caused poor command links, delayed TDRSS lockup.	Most likely: (Mfgr assessment) low level out-of-band oscillation in the second LNA stage of the receiver input. Hardware problem with transponder as provided by manufacturer, not detected at unit or system level testing. Limited to this unit only.	All forward transponder contacts are 125/1K, transmitter commanded on/off in SV load, not by ground command
12	21-Apr-04	Obs	T	SPRU inrush current exceed the red limit after eclipse.	SPRU inrush current exceed the red limit after eclipse.	Limits set too tight to "fresh" batteries	Adjust the limits and monitor performance
13	21-Apr-04	Obs	N	Battery heater control authority lower than expected	~half the battery heaters are on full time, the other half always off - resulting in less TCS authority than expected	N/A - further analysis showed pallet heaters working properly after vehicle temps stabilized	None
14	21-Apr-04	Obs	N	GSS3 Load defaults compare may have load error	GSS3 Load defaults compare may have load error	N/A - data dump showed no error.	None

	Date	Severity	Sub-type	Title	Description	Root cause	Corrective Action
15	21-Apr-04	Obs	F	SRE Bracket temperature trending upward	Should have gone to 4K, instead, not decreasing. New set point 2.5 and is stable at 2.5K.	Feature of algorithm; does not affect overall operation	Document feature for ops team.
16	21-Apr-04	Obs	F	P9B SM Test Activated	P9B safe mode test triggered shortly after P9A test was activated (value went negative).	Likely cause: data spike in gauge.	Disable P9 safemode and manually monitor valve during spinup.
17	22-Apr-04	Obs	T	TRE -XA channel limit violation	-XA channel at 9.99 V	Detectors have not yet been balanced on orbit.	Run balance algorithm per timeline plan.
18	22-Apr-04	Medium		Backup to digital failed on gyros 2 & 3	Gyros 2, 3 failed to make transition to science level digital control after initial levitation in backup mode.	High gyro charge from initial levitation off wall (300 mV)	Increase control authority in digital mode via parameter update, discharge gyroscopes, switch back to nominal science level preloads.
19	23-Apr-04	Obs	T	OD in track thrusting observed	Estimate of drag (Cd) from a value of 2.2 to about 1.2.	Thruster biases	Adjust thruster biases.
20	24-Apr-04	Obs	F	Spikes in ECU Data (GMA SDTs)	Spurious spikes in some of ECU data / open Obs 20 (GMA SDTs?) No change in thermal control of GMA from SDT spikes.	Noise in ECU seen during ground testing.	None
21	24-Apr-04	Obs	N	Zone 5 Pressure Increase	Increased pressure on Zone 5 GMA pressure sensor	Gas leakage through GMA valves; expected	None
22	24-Apr-04	Obs	T	GS Valid too early	GS invalid flag start late end early; extraneous light in scope --> Ops change. (former Obs 22)	Guide star valid widow too big to exclude all earthshine	Tighten guide star valid window.
23	25-Apr-04	Obs	N	SQUID 2 railed during SRE temperature roll mod test	SQUID 2 railed during SRE temperature roll mod test	Thermal transient pushed SQUID limits	Re-set base temperature and re-run test.

	Date	Severity	Sub-type	Title	Description	Root cause	Corrective Action
24	26-Apr-04	Obs	F	Noise on GSS FSU mux monitors	"hair" like data seen on all GSS health monitors; not on position data	Low level cross coupling of monitors in GSS forward box.	None. Data is useable as is.
25	26-Apr-04	Obs	F	Transient temperature increase on the porous plug temperature differential	Temperatures have been consistently 4 mK apart. A severe transient occurred 2 to 3 mK apart. Corresponding GT tremendous drop of 0.3 K.	Calibration of temperature sensor	Use independent means to verify a suspected breakthrough condition.
26	26-Apr-04	Minor		LPS voltage trending down	Liquid point sensor, which indicates possible porous plug breakthrough, was trending toward yellow region after TIV6 closure.	Small bias in liquid point sensor data giving erroneous indication.	Use two independent methods to identify breakthrough conditions.
27	27-Apr-04	Medium		LV1 Neither Indicates open or closed	After leakage vatterfly valve 1 (LV1) initial opening, telemetry indicates that the valve is in an intermediate state, neither fully opened or closed	Insufficient duration specified in valve command template to open valve completely.	Increase duration to open and close the valve in command templates.
28	27-Apr-04	Obs	N	SAA Flag only set on half of passes	SAA Flag only getting set half the time it is expected to be set.	Flag only valid during guide star valid per design	None
29	28-Apr-04	Obs	F	Station 200 Temperature Variation	Temperature oscillation seen in SQUID bracket	Gas in dewar well	Flux flux will drive off residual gas.
30	28-Apr-04	Obs	T	SQUID 1, 3, 4 railed during transition to gain level 5	SQUID 1, 3, 4 railed during transition to gain level 5	Tune-up issue with minimize low pass filter algorithm	Adjust algorithm parameters and re-deliver
31	29-Apr-04	Obs	F	TRE Data Spikes	There are intermittent data spikes in the TRE current telemetry.	Radiation events in telescope detector.	None
32	29-Apr-04	Obs	N	SRE bus current jump	SRE bus current jump	Known issue with current sensor used in SRE	None

	Date	Severity	Sub-type	Title	Description	Root cause	Corrective Action
33	30-Apr-04	Obs	F	Delta in 32 K and 2 K data values	The 32 K and the 2 K data for the same mnemonics are not matching up exactly in TCAD.	Feature of timing of ECU sample table.	Watch.
34	3-May-04	Major		SV switched to B-side	Spacecraft autonomously switched to B-side C&DH (CCCA, ACE, IU, CTU, SSR).	Multiple unrecoverable double bit errors (DBE) in CCCA memory. DBE most likely due to a radiation event.	Recover spacecraft and payload to A-side systems. Review DBE safemode entry criteria.
35	3-May-04	Medium		Possible porous plug choking - high thruster flow	High thruster flow rates and potential porous plug breakthrough indications noted after a CSTOL command to reconfigure the ATC system after the A-034, "SV switch to B-side)	Mis-configuration of ATC system; SW set for gyro low mode, but control gyro hardware is in high mode and resulted in large commanded thrust. CSTOL template was in error; ITF testing of template had insufficient fidelity to catch error.	Analysis and correction of CSTOL procedures to properly configure the hardware and software systems.
36	7-May-04	Obs	T	Prime drag-free performance	Failed first attempt at drag-free on Gyro4 This item tracking all open drag-free issues	Insufficient ATC control authority to maintain drag-free suspension on gyro 4.	Use backup drag-free as program baseline
37	10-May-04	Obs	N	Observer on following spin up	Observer on following roll up	Part of roll up template	None
38	10-May-04	Obs	F	Spurious noise on Proton Detector V channel	Spurious noise on Proton Detector V channel	None at this time	Watch
39	11-May-04	Obs	N	Snapshots not being processed or missing per timeline needs	Some GSS snapshots not being processed or missing per timeline needs	Corrupted data from ground station	Re-deliver and process clean data.



	Date	Severity	Sub-type	Title	Description	Root cause	Corrective Action
40	11-May-04	Obs	T	Dwell scan aborted	Dwell scan aborted due to ATC mis-configuration of roll rate	Abort due to momentarily exceeding commanded mass flow with combination of drag-free and roll-down maneuver.	Adjust mass flow limits to allow for sufficient mass flow or separate dwell scan and drag-free maneuvers.
41	11-May-04	Obs	T	High He Mass Flow during drag-free	High He Mass Flow during drag-free (as observed by dewar telem)	Thruster biases.	Update thruster biases to eliminate excess mass flow.
42	12-May-04	Obs	T	TRE +XA Ch Clipping/ATC dwell Scan issue	TRE +XA channel clipping.	DMA balance algorithm not generating a good balance solution.	Update algorithm and redeliver.
43	12-May-04	Obs	T	Change of rotor charge after high-voltage checkout	Change of rotor charge after high-voltage checkout on gyros 4 & 1	Field emission of electrons in HV configuration with rotor off-center.	Discharge rotor and continue tests.
44	13-May-04	Medium		CSS reasonableness safemode activated	Coarse Sun Sensor reasonableness test triggered safemode: stopped timeline, switched to ACE B, safed GMA valves, reconfigured COM to 125/1K.	CSS reasonableness algorithm misinterpreted sun sensor data as SV went from full sun to eclipse period.	Disable SM response; modify VMS macros to only use/look at CSS in ATC backup modes. VMS macros updated following FSW 3.4.3 upload.
45	13-May-04	Obs	O	Misconfiguration AFT versus FWD antenna	Following A-044, AFT and FWD transmitters were misconfigured.	Operations mis-configuration of transponders	Explicit commands in load are now used to command the transponders on and off.
46	14-May-04	Obs	F	Double-bit error tracking	No automatic method of tracking double bit errors.	Templates not available as part of pre-launch set.	Develop and deliver templates to perform DBE monitoring.
47	14-May-04	Obs	F	Science Gyro 2 Large position excursion seen with shutter activation	Science Gyro2 Large position excursion seen with shutter activation	Shutter generating larger than anticipated mechanical transient.	Do not use shutter; abandon in place.
48	16-May-04	Obs	T	Dewar main Tank temp rising faster than expected during flux flush	Dewar main Tank temp rising faster than expected during flux flush	Larger than expected gas in well between probe and dewar.	Increase null dump to maintain dewar temperature.

	Date	Severity	Sub-type	Title	Description	Root cause	Corrective Action
49	17-May-04	MAJOR		SM activated - High body rates	High body rates observed (pointing) that activated safemode following flux flush. Significant attitude excursions observed over a number of days, degrading communications.	Thruster 8 failed during high flow conditions following flux flush. Failed open thruster caused porous plug to choke prior to thruster 8 isolation. Most likely root cause is foreign object contamination of thruster 8.	Disable Thruster 8 (via TIV). Rebuild and reload ATC controller (FSW) to thruster selection algorithm to compensate for loss of thrusters 6, 8. Update and install related VMS macros.
50	18-May-04	Obs	N	Vatterfly valve state upon SM (Anomaly #49) entry changed to closed, but we believe the valve remained open	Vatterfly valve state upon SM (Anomaly #49) entry changed to closed, but we believe the valve remained open	Feature of ECU telemetry sampling scheme.	Non-issue
51	20-May-04	Obs	T	GSS low voltage checkout failed to complete on Gyros 2 & 3	Preliminary analysis of telemetry indicates GSS low voltage checkout failed to complete	High gyro charge from initial levitation off wall (300 mV)	Discharge rotor and continue tests.
52	20-May-04	Obs	T	Dewar micro-temp variation at orbital and roll period	Dewar micro-temp variation at orbital and roll period	Residual thermal coupling to probe from environment	Adjust tank temperature and watch.
53	21-May-04	Obs	T	GSS2 reduced stability margins during uncaged checkout	Indications of reduced stability margins of science gyro 2 during uncaged checkout	Insufficient stability margin for gyro 2 at original modulation frequency, possibly due to disconnected ground plane	Increase frequency of drive voltage from 20 to 30 Hz.
54	25-May-04	Minor		Unexpected turn off of gyro1 High Voltage	Gyro1 de-levitated unexpectedly during Gyro2 suspension operation. The gyroscope was not spinning at a significant rate at this point in the mission.	Template error; a template cloning error left the Gyro 1 HV off commands in all four gyro's "science mission pre-suspend" templates. ITF had insufficient fidelity to detect this error when tested.	100% review of all GSS templates (~250 items) for cloning errors or misplaced commands. Correct any errors found, retest.

	Date	Severity	Sub-type	Title	Description	Root cause	Corrective Action
55	30-May-04	Obs	F	UV Bias Setting Template Failure	After 2 attempts, UV Bias for Gyro 3 set to 0 instead of the desired -3 resulting in slow discharge rate.	Interface issue between FSW and GSW; exact cause unknown	Directly send commands to GSS rather than routing them through CCCA.
56	30-May-04	Medium		Gyro 1 and 4 unexpected change to analog backup	Gyros 1, 4 transitioned autonomously to analog backup control during gyro torque calibration (1Hz cal) dry-runs. Gyro 4 touched wall during transition at low spin speed.	Overly aggressive preload imbalances used during dry runs, causing the digital controller to lose control of the rotor. Tested OK in ITF, but ITF had insufficient fidelity to model on-orbit forces and biases.	Rewrite and test templates based on ground experience and conservative estimates of controller stability margins. Retest and verify functionality.
57	1-Jun-04	Obs	F	High Dewar Shell Temperature	Dewar shell temperature 20 deg higher than prediction.	Thermal model analysis indicated earth shine (albedo) is 10x greater than originally modeled and accounts for most of the effect. Root cause: insufficient or detached insulation around cone section of the dewar.	Correlate info with thermal model and use for lifetime predictions.
58	3-Jun-04	Obs	N	Bright Object Events	Sun Bright Object Test has been generating events since it was enabled for SG4 spinup	Star sensor naturally identifies bright objects (sun, earth, moon) and generates such events	none.
59	3-Jun-04	Obs	F	Science Gyro oscillations	Science Gyro oscillations occurred during thruster oscillation that occurred prior to anomaly 49.	Excessive and erratic thrust generated during thruster 8 failure	Isolate thruster 8 (per anomaly 49)
60	4-Jun-04	Obs	T	Spin Ax align preload in phase	Preloads on all three axes move in phase during the initial spin axis alignment test; should move differentially on X, Y only	Error in setup of spin axis alignment algorithm	Correct parameters and redeliver templates.

	Date	Severity	Sub-type	Title	Description	Root cause	Corrective Action
61	6-Jun-04	Obs	F	CCCA 10Hz Timeouts	3 CCCA 10Hz timeout events have been counted	CCCA under high workload at start of guide star valid. Occasional single instance of 10 Hz interrupt overrun detected due to stackup of CCCA processing tasks. Not and issue if overrun occurs infrequently.	Watch
62	6-Jun-04	Obs	T	Lost Star from Science Telescope	Lost Star from Science Telescope in mode 1B	Root cause: bug with gyro bias averaging algorithm.	Correct and re-deliver gyro bias algorithm (loaded with FSW 3.4.3)
63	7-Jun-04	obs	T	Telescope star tracking not adequate for science during initial mode 1B checkout	Telescope star tracking not adequate for science	ATC off-tune after initial guide star acquisition	Optimize ATC parameters
64	8-Jun-04	obs	F	DC offset in SQUID observed during GS valid/GS Invalid transition	Small SQUID output shifts occurred at shutter open/close events only when GSS is HV mode.	Electromechanical interaction of suspension with SQUID.	Watch; does not occur in GSS low voltage modes.
65	9-Jun-04	obs	F	Delay in fwd acquisition, transponder yellow temp limit	Delay in fwd acquisition, transponder yellow temp limit	Most probable cause of delayed acquisition on fwd transponder was frequency shift caused by high transponder temperature.	None; temporary condition developed during item 11 root cause investigation.
66	11-Jun-04	Obs	A	GSS1 C axis control effort noise	GSS1 Z axis control effort shows 10 nm "digital" type noise occasionally seen; position spikes on Z correlate.	Probable root cause: thermal issues on GSS suspension cables. Does not show up in science configuration.	Watch.
67	14-Jun-04	Obs	F	Gyro 2 dropped out of digital	Gyro 2 dropped out of digital	Likely root cause: race conditions in the analog arbiter state machine due to holding the gyro for extended periods near the low backup threshold.	when positioning gyro off-center, stay 1um away from backup threshold.

	Date	Severity	Sub-type	Title	Description	Root cause	Corrective Action
68	16-Jun-04	Medium		Decline in GPS lock	GPS lock time ratio decreased from a nominal 98% to 35% over a few day period, roughly 60 days into mission.	Likely cause: SEU or long-period software error/overrun.	Reboot of unit cleared the problem; GPS continues to perform as expected following reboot.
69	19-Jun-04	Obs	T	GSS Cal14 Sequence	Gyros 1-4 did not re-center at conclusion of Cal Sequence	Template scheduling error.	Schedule templates in correct order.
70	24-Jun-04	Obs	T	Thruster 12 bottoming out during roll-up to 0.6 rpm	Thruster 12 commanded completely closed during roll-up to 0.6 rpm. May reduce ATC dynamic range.	Thruster pressure sensor bias	Adjust pressure sensor bias to eliminate bottom-out
71	27-Jun-04	Obs	T	Loss of Star Sensor IDs at higher roll rates	At 0.6 and 0.9 rpm, initial star identifications decreased resulting in attitude errors	Most probable causes are: 1) Gyro Bias errors, 2) sensor gate strategy, 3) star attitude correction weighting gain.	Remaining actions: Update procedure for re-ID and lock on after possible future loss of stars (in work)
72	28-Jun-04	Obs	F	GPS First Failure Test Activated	GPS First Failure Test Activated	Insufficient time allowed in safemode test for receiver to lock onto GPS constellation	Increase first failure test timeout duration.
73	29-Jun-04	Obs	O	SSR not in playback mode during playback pass	SSR not in playback mode during playback pass	Template scheduling error.	Shedule templates in correct order.
74	29-Jun-04	Obs	T	Roll down is less than expected	SV roll down only to 0.7 rpm, 0.5 rpm expected.	The excess mass flow went negative for substantial portions of the roll down period, causing the vehicle to abort the roll down during those times. Sensed rates on X and Y were larger than expected.	Command slower roll down rates.

	Date	Severity	Sub-type	Title	Description	Root cause	Corrective Action
75	1-Jul-04	Minor		Magnetometer test triggered safemode	Magnetometer reasonableness test triggered safemode macro; switched to B-side magnetometer.	Recovery load for the FSW 3.4.3 reboot mis-configured the magnetometer safemodes. Should have been "off" in recovery load.	Audit future recovery loads for proper management of magnetometer safemodes.
76	30-Jun-04	Obs		Corruption of Science (L2) database	Corruption of Science (L2) database	Internal database error	Reprocess L2 data from L1 data.
77	1-Jul-04	Obs	A	ATC Massflow/Dewar massflow determination disagreement	Dewar temperature (MT and HEX) indicates higher massflow estimated greater than 10 mg/s.	Differing calibration of measuring methods for mass flow. Time character of results are consistent.	Continue of cross calibration/correlation of ATC and Dewar measurements
78	2-Jul-04	Obs	N	High gyro charge in spinup mode	Indicated gyro charge of ~1.5 V in Spin Up	User interpretation error; procedure was correct.	None.
79	2-Jul-04	Obs	N	GMA heater thermostat variability	GMA heater and BE_Htr coming on same time	Gradual change in thermal character of SV as sun angle changes over the mission	Expected behavior.
80	2-Jul-04	Obs	T	GSS2 multi-bit error	Double bit error in snapshot section of SRAM (non-executable)	Radiation event	Upload patch to correct memory
81	7-Jul-04	Obs	F	High single bit error count and rate in CCCA-A	High single bit error count and rate in CCCA-A	Radiation event, watch item.	Watch
82	9-Jul-04	Obs	T	Lost guide star	Guide star was lost in during a pass in the South Atlantic Anomaly	Radiation events in telescope detector.	Increase size of SAA keepout window; adjust telescope sanity check parameters to exclude bad data points.
83	9-Jul-04	Obs	O	G1x3x transition to low backup	G1x3x transition to low backup	Template scheduling issue; transitioned from DC preload config to charge measurement config without going through the AC preload configuration.	Update GSS standard transition sequences with proper sequence



	Date	Severity	Sub-type	Title	Description	Root cause	Corrective Action
84	13-Jul-04	Obs	F	Slightly elevated solar radiation	Slightly elevated solar radiation. Greater than 10 MEV particle count.	Sun spot activity.	Level below danger limits outlined in Solar Flare contingency procedure. Wathc
85	13-Jul-04	Obs	F	Gyro 2 possible floating ground plane	Gyro 2 possible floating ground plane	Likely cause: disconnect of ground wire to one half of ground plane.	None at this time; still under investigation.
86	15-Jul-04	Obs	O	Control Gyro A switched to "High" mode	Control Gyro A to "High" mode when previously commanded "Low" mode	Template coding error; ITF has insufficient fidelity to detect error.	Correct error and re-deliver template.
87	16-Jul-04	Obs	F	High Gyro4 Spindown during Gyro2 Spinup	Gyro4 spun down from 105.8 to 90.77 Hz during Gyro2 spinup	Larger than expected gas leakage from spinup channel of gyro 2 during gyro 4 spinup.	Tune position of to be spun up subsequently (1, 3) to minimize leakage flow.
88	23-Jul-04	Obs	F	ATC Cross Coupling	Pitch/yaw appears to have some cross-coupling	Cross coupling due to removal of gyro bias errors when transitioning out of gyro hold.	No action required.
89	23-Jul-04	Obs	T	Spin Axis Alignment rates less than expected	Observed rates about 25% of expected rates	Insignificant centrifugal bulge due to low spin speed.	Manually tune algorithm to produce alignment in desired direction.
90	23-Jul-04	Obs	O	Anomalous spin down of gyro 1	Gyro 1 spun down during cavity exploration activities while scouting new location for full spinup.	Positioning gyroscope too close to housing wall during cavity exploration.	Do not command gyro position to within 2 um of the spindown position during spinup operations.
91	25-Jul-04	Obs	O	Gyro 1 switched to analog backup mode	Gyro 1 switched to spinup analog backup mode during HV qualification of spinup position.	Likely root causes: 1) computer heartbeat glitch due to high processor loading, 2) radiation event in GSS analog electronics, 3) race-mode condition in GSS arbiter.	Recover gyro to digital suspension and watch performance.
92	26-Jul-04	Obs	F	Large solar flare	Large solar flare, >10 MeV protons peaked at 2000 PFU at 26Jul04 2200Z	Solar activity in Sun.	Safe vehicle per solar flare contingency procedure.

	Date	Severity	Sub-type	Title	Description	Root cause	Corrective Action
93	27-Jul-04	Obs	F	MSS 10Hz timing spike	MSS 10Hz timing spike from 91% to 97%	CCCA under high workload at start of guide star valid. Occasional single instance of 10 Hz interrupt overrun detected due to stackup of CCCA processing tasks. Not and issue if overrun occurs infrequently.	Watch
94	31-Jul-04	Obs	T	Telescope Signals Saturated	3 of 8 detectors are saturated	Thermal changes in the Probe and/or warm electronics generated slight drift. Corrected via regular detector balancing operations	Watch and balance as required. Adjust TRE gain to avoid saturation.
95	2-Aug-04	Obs	F	Multibit Error in GSS 4	Multibit Error in GSS 4	Radiation event.	Correct error with software patch.
96	9-Aug-04	Obs	T	Gyro4 spin axis motion erratic	Gyro 4 spin axis motion not consistent with spin axis alignment theory; shows polhode modulated sensitivity	Insignificant centrifugal bulge due to low spin speed.	Manually tune algorithm to produce alignment in desired direction.
97	9-Aug-04	Obs	F	Star Sensor SM test activation	Star Sensor Aliveness safemode test 1 activated; mapped to 64 (no-op)	Bright object data overwhelming star sensor processor	Feature of star sensor; no action required.
98	9-Aug-04	Obs	T	High mass flow during drag-free ops	Higher mass flow (8 mg/s est) seen during prime compared to BU drag-free ops on Gyro1	Thruster biases and GSS control effort biases.	Tune out thruster biases; continue root cause on GSS control efforts.
99	10-Aug-04	Obs	O	Vehicle attitude excursion after gyro bias updates	Vehicle attitude excursion after gyro bias per PPCR # 133	Incorrect gyro bias updates	Install correct bias updates.

	<b>Date</b>	<b>Severity</b>	<b>Sub-type</b>	<b>Title</b>	<b>Description</b>	<b>Root cause</b>	<b>Corrective Action</b>
100	13-Aug-04	Obs	F	CCCA 10 Hz timeout	CCCA 10 Hz processing timeout occurs occasionally at start of guid star valid.	CCCA under high workload at start of guide star valid. Occasional single instance of 10 Hz interrupt overrun detected due to stackup of CCCA processing tasks. Not and issue if overrun occurs infrequently.	Watch.
101	12-Aug-04	Obs	T	Common mode signal observed on telescope detectors	Common mode signal observed on telescope detectors.	Sub-optimal detector gains (balance); Improvements gained via tuning of on orbit parameters.	ATC parameter optimization
102	12-Aug-04	Obs	F	GPS channel alignment error bit = true	GPS channel alignment error bit = true	Radiation event.	Reset GPS receiver.
103	20-Aug-04	Obs	T	Desire to improve rms pointing performance for science	Desire to improve pointing performance for science	Sub-optimal gains in the ATC control loop; Improvements gained via tuning of on orbit parameters.	ATC parameter optimization
104	21-Aug-04	Obs	T	SQUID Bracket Temperature Out of Limits	Should be within +/- 5 Volts, but is going as high as +/- 10 Volts	Probe thermal variations while moving to a new setpoint	Reset bracket temperature setpoint.
105	17-Aug-04	Obs	T	Roll Phase Variation	Since roll up from 0.52 to 0.75, roll phase variation has increased.	Still under investigation	ATC parameter optimization
106	8-Aug-04	Obs	O	Forward link mutual interference	Receiver B (aft antenna) indicated momentary detector lock and two other occasions the same receiver did not acquire the forward signal apparently due to some interference.	Mutual interference with AURA or AQUA spacecraft operating in our transponder band (scheduling issue)	Work with SN (GSFC) group to identify points of interference and apply schedule keepout times.

	Date	Severity	Sub-type	Title	Description	Root cause	Corrective Action
107	31-Aug-04	Obs	F	Double Bit Error in CCCA Memory	There was a double bit error (DBE) at 244/00:41Z while in South Atlantic Anomaly (SAA).	Radiation event.	Watch.
108	<b>Insert Time</b>	Obs	F	GPS Fwd +Y antenna shows temperature dropouts	TL_GPSfwdant_pY shows dropouts to -65C from -16 to -25C when warming.	(Preliminary) intermittent failure of space vehicle temperature sensor.	Watch; look for changes as vehicle comes out of eclipse season
109	8-Sep-04	Obs	F	Double Bit Error in CCCA Memory	There was a double bit error (DBE) at 252/02:16Z while in South Atlantic Anomaly (SAA).	Radiation event. MBE occurred in noncritical Rational function calls.	Dumped area of CCCA memory containing MBE. Ran patch procedure to clear from memory.
110	10-Sep-04	Obs	T	Backup drag-free performance	Performance of backup drag-free is marginal at roll rate.	GSS bias	Drag-free gain was increased and updates in gyro biases improved performance.
111	13-Sep-04	Obs	F	Elevated solar radiation levels	100pfu (>10MeV) exceeded	Radiation event	Closely monitored solar activity. Radiation levels returned to nominal.
112	15-Sep-04	Obs	F	SRE Multi-Bit Error	MBE detected to have occurred in SRE code on 9/1/04 @ 10:22:28; no immediate impact	Radiation event	No effect on mission. MBE location is in Science Slope default values and will not affect function.
113	16-Sep-04	Obs	F	MBE in the SRE	MBE detected to have occurred on 9/16/04 @ ~20:00Z; no immediate impact	Radiation event	SRE rebooted as part of Obs #122 recovery.
114	17-Sep-04	Obs	F	Excessive PB Data Seq. Errors	Alaska and Wallops GN contacts indicated excessive sequence errors.	GN antenna pointing	Scheduled more playback passes. SSR pointer reset if excessive sequence errors.
115	24-Sep	Medium		Gyro3 in low backup; drag-free terminated.	Safe Modes 2, 7, 11, 59 triggered, causing the vehicle to roll down to 0.6 rpm.	Most probable cause is some vehicle motion created a large control effort on gyro 3, causing it to go into backup.	Vehicle commanded back to drag-free on SG#1 and roll rate commanded back to nominal value.

	Date	Severity	Sub-type	Title	Description	Root cause	Corrective Action
116	26-Sep-04	Obs	F	SG3 to LB1	Gyro3 transitioned to low backup due to position spike on a single gyro axis.	Radiation event	Gyro 3 resuspended in digital mode and excitation voltage was increased.
117	28-Sep-04	minor		Oscillation in DF1 total force	A 3.7 minute period, 1.5E-6 m/s <sup>2</sup> oscillations seen in GS1 control efforts during drag-free. After drag-free mode terminated, effect decayed over ~6 hours.	Most probable cause is the drag-free system pumping at the natural resonance frequency of the helium in dewar.	Updated DFS loop gain to the launch value and oscillation is damping out.
118	30-Sep-04	Obs	T	Star tracker jumps	Jumps in Star tracker Z-error monitor at roll frequency, ~30-40arc-sec	ARP/star sensor motion	Decreased star sensor FOV to 0.4 degrees to reduce likelihood of future large spikes.
119	1-Oct-04	Obs	F	GS3 DBE Counter incrementing	Multi-bit error flagged in benign portion of GSS3 payload processor	Radiation event	Memory patch procedure built and implemented.
120	7-Oct-04	Obs	T	Long GS Acquisition times	Acquisition times at start of Guide_Star_Valid have been ten minutes or longer; two minutes is nominal	Gyro biases needed updating due to ARP motion caused by thermal variations.	Gyro bias updated on the X and Y axes.
121	18-Oct-04	Obs	F	Gyro 1 Transitioned to LB1	Drag-free Gyro 1 Transitioned to Analog Back Up. Safemode Macro 7 activated	Position spike on a single gyro axis.	Went to backup drag-free for Gyro 3. Gyro 1 resuspended in digital mode.
122	20-Oct-04	Obs	F	Multiple MBEs in SRE	2 MBEs detected to have occurred in SRE at 10/8/04 at 1:13:25 in FFT and at 10/13/04 at 00:18:35 in SQ_Bracket_Temp_Ctrl	Radiation event	Rebooted SRE to clear MBEs.
123	2-Nov-04	Obs	F	MBE in GSS4	MBE detected to have occurred in GSS4 in Snapshot buffer 10, a non-critical area	Radiation event	Normal overnight dumping of snapshots cleared the MBE

	Date	Severity	Sub-type	Title	Description	Root cause	Corrective Action
124	2-Nov-04	Obs	T	ATC Pointing variation	Pointing varies when in eclipse vs. when in sun	Most probable cause is thermally induced ARP motion	Implemented roll notch filter in rate gyro path during GV.
125	6-Nov-04	Obs	T	TRE channel railed	TRE MX-A channel railed	Most probable cause is temperature change in TRE box	Readjusted 2 TRE clamp voltages
126	11-Nov-04	Medium		SRE 1Hz Aliveness test activated	Safemodes 2, 3, 7, 11, 15, 59, and 60 activated	Most probable cause is interaction between the SQUID bracket temp control algorithm and the MBE in the BTC area	Macro 60 updated to prevent dropping out of drag-free if safemode activates.
127	22-Nov-04	Obs	F	Ratio of MBE to SBE is approx 10x higher than pre-launch prediction	Higher than expected SBE and MBE rates in SRE and GSS	Radiation induced MBE errors resulting from component selection of non rad-hard computer memory.	No known method to reduce the SBE/MBE rates now that GPB in orbit.
128	24-Nov-04	Obs	N	Star tracker A temperature trending up	SS-A TE cooler and lens temperature showing a 1-2 degree rise over the last few days	As SS warms, the temp approaches the 10 degree setpoint from the cold side	No issue – temp below 10 degree setpoint. Seen in weekly ATC trend plots.
129	4-Dec-04	Medium		ADA unrecoverable exception in ATC ephemeris	Safemodes 2, 5, 7, and 59 activated	Poor satellite geometry caused large DOPs combined with only 4 satellites in view generated a spurious velocity solution.	Recovered to drag-free within 7 hours of event and captured guide star within 23 hours of event.
130	9-Dec-04	Obs	N	Spurious CCCA MBE indicated in RTWorks	BC_TImDiag06 changed state, causing RTWorks to go red	Diagnostic test was run during a 2k pass and left the TImDiag06 pointing at a different memory location than expected by RTWorks.	Red limit cleared by itself when another diagnostic test was run during a 32k pass. Ops procedure being updated.
131	9-Dec-04	Obs	O	Loss of guide star after roll notch filter parameter load	Loss of guide star after roll notch filter parameter load	Overly aggressive ATC notch on rate gyros during GSV	Reacquired guide star



	Date	Severity	Sub-type	Title	Description	Root cause	Corrective Action
132	20-Dec-04	Obs	F	Uncorrelated elevated proton monitor activity	Proton monitor shows elevated activity	Failure appears to be digital in nature, possibly thermal related	Proton monitor commanding and rebooting proved unsuccessful, however loss of Proton Monitor poses no threat to mission
133	27-Dec-04	Obs	N	Higher than expected flow rate	SF_P_IntErrSp shows decreasing trend	Seasonal issue, in eclipse with less sunlight when telescope looks at Earth	Increased mdot_out
134	4-Jan-05	Obs	F	GSS1 Double bit error	DBE indicated in GSS1 telemetry	Radiation event	Identified to be in a spinup parameter set location, which is not being used at this time. Corrected via patch procedure.
135	10-Jan-05	Obs	F	GPS Alignment Bit Set	GPS alignment bit indicates telemetry issue	Single event upset during passage over South Pole	GPS operating nominally with this fault. No reboot required.
136	10-Jan-05	Obs	F	GSS1 DBE	DBE indicated in "VecFromPartofArray" function GSS1	Radiation event	Peek procedure run to determine exact location of DBE. Patch procedure run to clear the DBE.
137	17-Jan-05	Obs	F	MBE in SRE	MBE in SRE detected on 2005/017-14:53	Radiation event	Code analysis verified MBE is in unused part of table.
138	17-Jan-05	Obs	T	Charge Measurement on drag-free gyro	Charge rate significantly lower on gyro 3 (drag-free gyro) than other gyros	ATC was taking out the control effort modulations on gyro 3.	Turned off charge measurement on gyro 3. Went to new 14 sec instance D02 on gyros 1,2,4. Turned charge measurement on gyro 3 back on at 23 sec.
139	19-Jan-05	Obs	F	ITF UPS failed	UPS connected to some workstations in the ITF failed after a building power failure. ITF shut down.	Possible computer circuit board failure in UPS.	Replaced PC boards in UPS unit. Pod G not affected.

	Date	Severity	Sub-type	Title	Description	Root cause	Corrective Action
140	20-Jan-05	Minor		Large solar flare	Large solar event and loss of guide star	Solar event blinded science telescope	Space vehicle reconfigured to science configuration. No long term issues remain.
141	20-Jan-05	Obs	F	MBE in SRE	MBE detected at 159501296	Radiation event	SRE rebooted
142	26-Jan-05	Obs	F	Increase in CCCA SBE error rate for 4 minutes	Increase in CCCA SBE error rate occurring during subsequent scrub cycles	1 Stuck bit in the A-side flight computer	After the B-side switch, the plan is to stay on the B-side flight computer for the rest of the mission.
143	28-Jan-05	obs	F	MBE in CCCA	MBE in CCCA detected at 2005/028-17:30	Radiation event	MBE found to be in used area of Ping buffer. Cleared by patch procedure.
144	15-Feb-05	Obs	F	TRE thermal disturbance after DAS switch	Decaying oscillation in A-side detector high signal observed for 15 consecutive orbits 2005/43-09:05 to 2005/44-09:20	Switching of SRE-A DAS boards caused thermal transient in TRE-A, resulting in oscillatory Detector High signals.	No more SRE-A DAS board switches are planned. If a switch is planned, schedule all switch templates during GSI, >15 min before GSV.
145	15-Feb-05	Obs	T	Reduction of excess mass flow when gyro B turned on	Excess mass flow reduced seconds after gyro B turned on	Extra ATC control effort required to counteract gyro B torque accounts for excess mass flow decrease.	Gyro B turned off. A-side performs better at roll than B-side, and A-side gyro to stay on for control.
146	23-Feb-05	Ground Obs	F	ITF SRE-A time-out	1Hz and 10Hz timeouts in the ITF SRE-A	Payload processor control block was corrupted.	Swap Aft SRE-A with SRE-B and attempt transition.
147	2-Mar-05	Obs	T	Poor pointing performance due to SAA	Poor pointing performance during and after SAA passage	If TRE gain is too high, ATC pointing slopes roll over.	Reduced SAA circle from 43 to 35 deg and notch filter to 45 deg circle. Reduced A-side gains to 9.
148	2-Mar-05	Major		B-Side Safemode Recovery	B-side Safemode recovery. Scrub rate failed	2 simultaneous MBEs.	Followed B-side recovery procedure. Recovery activities for this anomaly rolled over to Anomaly 152 (CCCA-B Reboot)

	Date	Severity	Sub-type	Title	Description	Root cause	Corrective Action
149	5-Mar-05	Obs	T	Few stars being tracked on star tracker B	Never acquired roll stars with B-side tracker after the B-side switch on 2005/63.	Operator error; telemetry monitor was providing stale telemetry which was mistaken to be updated.	Set feedforward command and wait 1 orbit to confirm.
150	6-Mar-05	Obs	F	MBE in CCCA	MBE in B-side of CCCA detected at 2005/65-00:36Z	Radiation event	MBE found to be in the sysinit of the CCCA. Cleared by patch procedure.
151	6-Mar-05	Obs	F	MBE in GSS4	MBE in GSS4 detected at 2005/65-19:15	Radiation event	Cleared by patch procedure.
152	15-Mar-05	Major		CCCA-B Reboot	CCCA Reboot at 2005/74-7:38:27 caused by MBE in CCCA	Radiation event	Followed B-side recovery procedure. Recovery activities for this anomaly rolled into Anomaly 156 (CCCA-B Reboot)
153	15-Mar-05	Obs	F	MBE in CCCA Side B	MBE in CCCA-B detected at 2005/74-07:10	Radiation event	MBE cleared by Anomaly 152 (CCCA-B Reboot).
154	15-Mar-05	Obs	O	Loss of ECU telemetry after B-side reboot (Anomaly 152)	Received no ECU telemetry after the B-side reboot (Anomaly 152) on 2005/74-7:38:27	When the CCCA reboots, it comes up on RT7. The ECU was on RT8 after the Mar-4-05 reboot.	ECU switched back to RT7. Plan is to not go back to RT8.
155	17-Mar-05	Obs	F	4 MBEs in GSS2	4 MBEs in GSS2 detected at 2005/76-05:15	Radiation event	Cleared by patch procedure
156	18-Mar-05	Major		CCCA-B Reboot	CCCA Rebooted to B-side at 2005/77-15:20:49	Radiation event	Followed B-side recovery procedure. Vehicle returned to science configuration
157	27-Mar-05	Obs	F	MBE in GSS4	MBE in GSS4 detected at 2005/86-06:00	Radiation event	Timeline stopped, patch procedure ran to clear MBE.
158	29-Mar-05	Obs	F	MBE in GSS2	MBE in GSS2 detected at 2005/88-13:50	Radiation event	MBE in benign area, cleared by patch procedure
159	1-Apr-05	Obs	T	Underdamped dewar pressure oscillations	Main tank pressure is oscillating 3uK peak to peak with a period of 120hrs.	Heat exchanger's efficiency causing underdamped condition	Reduced dewar gain by 20x to improve performance.

	Date	Severity	Sub-type	Title	Description	Root cause	Corrective Action
160	14-Apr-05	Obs	F	Mdot change after gyro discharge	Using more mass flow for control after 4/13/05 gyro discharge. Observed in all three axes.	Change in gyro potential causing bias changes which may correlate to Mdot out change.	Adjusted z-bias to examine effect on X and Y.
161	30-Apr-05	Obs	F	MBE in CCCA	MBE in CCCA detected on 2005/120-12:21	Radiation event	MBE in a benign area, cleared by patch procedure.
162	5-May-05	Obs	O	Elevated cross-track residuals	High cross-track residuals in a pattern not seen before. Unknown force on the spacecraft could be modifying the orbit plane	Incorrect OD solution	Cross track residuals returned to nominal.
163	20-May-05	Obs	F	DBE in GSS2	DBE in GSS2 observed at 2005/140-10:47Z	Radiation event	The DBE is in the benign GSS2 snapshot buffer and will clear itself after snapshots are taken as part of the timeline.
164	24-May-05	Obs	F	DBE in CCCA	DBE detected via TImDiag6 in CCCA location 0x36E50	Radiation event	Patch affected area of GSS memory.
165	24-May-05	Obs	N	Data processing detected non-existent clock reset	Data processing detected a clock reset in data stream; no clock reset happened on SV.	SKS sent ASCII file instead of binary. Auto data processing algorithms mis-identified a clock reset on SV.	Request SKS to resend file in proper format.
166	27-May-05	Obs	F	Gyro 2 in analog backup	Gyro 2 in analog backup	Radiation event	Resuspend using contingency templates in timeline.
167	30-May-05	Obs	F	2 MBEs in SRE	2 MBEs in SRE	Radiation event	None; MBEs will clear only SRE is power cycled. Found to be benign
168	31-May-05	Obs	T	Loss of Guide Star	Loss of Guide Star	Large radiation signature on ATC telescope slopes corrupted data in ATC roll notch filter	Notch filter to be turned off prior to SAA passes

	<b>Date</b>	<b>Severity</b>	<b>Sub-type</b>	<b>Title</b>	<b>Description</b>	<b>Root cause</b>	<b>Corrective Action</b>
169	04-Jun-05	Obs	F	MBE in SRE	MBE in SRE detected on DOY 155	Radiation event	None; MBEs will clear only SRE is power cycled. Found to be benign
170	05-Jun-05	Obs	N	Spike in TRE Science Slopes	Unexpected light spike in TRE Science Slopes; consistent with seeing a bright object.	Most likely cause is another satellite passed into the field of view.	None
171	20-Jun-05	Obs	F	MBE in CCCA	MBE in thruster current data	Radiation event	MBE cleared by patch procedure.
172	30-Jun-05	Obs	F	MBE in GSS-2	MBE in benign area of GSS-2 code.	MBE cleared by patch procedure.	MBE cleared by patch procedure.
173	02-Jul-05	Obs	F	GPS channel alignment error	GPS channel alignment error flags toggled true	Radiation event	No impact to vehicle health or GPS data; flag would be cleared by GPS receiver reset (not executed)
174	07-Jul-05	Obs	F	Gyro 3 in low backup	Gyro 3 in low backup. Likely causes: Radiation induced arbiter or known race condition.	Radiation event	Resuspend using contingency templates in timeline.
175	07-Jul-05	Obs	O	Drag-free safemode	Drag-free safemode triggered on attempted drag-free entry to Gyro 1	Mis-configured drag-free safemodes	Update templates for proper configuration
176	08-Jul-05	Ground Obs	N	ITF GSS 4 AFT Unable to do external sync	GSS 4 in the ITF does not do 10Hz sync on external clock but does sync to 1553.	Sync cable damaged	Cable repaired during move to Stanford
177	12-Jul-05	Obs	A	GP-B Roll Error Phase	Develop an improved model and better understanding of the roll phase error	ATC roll phase affected by ARP motion	Post-process star tracker information on the ground.
178			N	(number skipped in database)			
179	03-Aug-05	Obs	F	MBE in CCCA	MBE in CCCA	Radiation event	MBE cleared by patch procedure.

	Date	Severity	Sub-type	Title	Description	Root cause	Corrective Action
180	03-Aug-05	Obs	N	Aft SRE-A in ITF	Negative transition in the aft SRE-A in the ITF	Sync cable damaged	Cable repaired during move to Stanford
181	17-Aug-05	Obs		MBE's in GSS_1	MBE's in Mission Critical areas	Radiation event	MBE cleared by patch procedure.
182	19-Aug-05	Obs	N	Excess Mass Flow violates yellow limit.	Excess mass flow violated yellow limit.	Expected condition based on day's operations	Update RTWorks with new limits to prevent errant limit flags.
183	26-Aug-05	Obs	F	MBE in GSS-2	MBE in benign area of GSS2	Radiation event	MBE cleared by patch procedure.
184	24-Aug-05	Obs	F	Channel Alignment Error in GPS	Channel Alignment Error in GPS	Radiation event	MBE cleared by patch procedure.
185	11-Sep-05	Obs	N	Pressure Drop in Dewar	Dewar Pressure dropped, Z bias railed and thrusters 16 and 10 went unstable.	High dewar pressure and flow rates generated conditions similar to Anom 59.	Command open loop on all thrusters.
186	22-Sep-05	Obs	F	MBE in GSS 3	MBE in GSS 3	Radiation event	MBE cleared by patch procedure.
187	26-Sep-05	Obs	O	ATC drag-free did not shut down on GSS DF termination	Following an attempt at Prime DF, the ATC did not shut down properly when the GSS resumed control after Prime DF attempt. Thrusters randomly fired up to 5mN limit until manually shut down	Root casue found to be that the response to SMACRO7 was disabled.	Re-enable SMACRO7 for all prime DF operation
188	29-Sep-05	Minor		END OF HELIUM	END OF HELIUM		
189	30-Sep-05	Obs	A	GSS2 transitioned to backup	GSS2 transitioned to backup during dewar/probe warmup	Position spikes on GSS bridge due to warming probe	None; wait for dewar to warm
190	04-Oct-05	Obs	A	GSS 1 and GSS 3 transitioned to analog backup	GSS 1 and GSS 3 transitioned to analog backup	Position spikes on GSS bridge due to warming probe	None; wait for dewar to warm



	<b>Date</b>	<b>Severity</b>	<b>Sub-type</b>	<b>Title</b>	<b>Description</b>	<b>Root cause</b>	<b>Corrective Action</b>
191	04-Oct-05	Obs	A	GSS1-4 rotors held against wall	GSS1-4 rotors held against wall	Potential root cause: actuation of mechanical caging system by warming probe	None.
192	16-Oct-05	Obs	F	MBE in GSS1	MBE in GSS1; GSS1 already in HBU	Radiation event	MBE cleared by patch procedure.
193	13-Oct-05	Obs	O	MOC server performance degradation	Moc server performance degraded to the point where the system was unusable	Process overloaded due to too many applications running at once during post-mission code development ops.	Conform to MOC/MCR process and monitor system health during all test runs of new code

# E

## Flight Software Applications SLOC

---





Table E-1 below lists the source lines of code (SLOC) for the various GP-B flight software applications and their sub-components. 59,000 lines of ADA and 2.3 MB of memory were required to implement the FSW features required by GP-B. At run time, the FSW expands to 3.5 MB in the CCCA SRAM after heap, stack, an other dynamic storage is allocated.

Detailed requirements and functional descriptions of the FSW components can be found in Lockheed Martin Document #P086580: SCSE-15, Gravity Probe B Flight Software Requirements Specification.

**Table E-1.** Mission Support Software (MSS) Software Lines Of Code (SLOC) Detail

Req ID	Level 1 CSC	Level 2 CSC	Level 3 CSC	Level 4 CSC	Unit Source Name	SLOC	Memory Size
FSW	58989	2.3 MB					
Net							
Statistics							
MSS	Mission Support SW				debug_io.1.ada	81	
MSS	Mission Support SW				debug_io.2.ada	74	
MSS	Mission Support SW				generic_datatypes.1.ada	100	200
MSS	Mission Support SW				generic_datatypes.2.ada	99	176
MSS	Mission Support SW				int_io.1.ada	3	128
MSS	Mission Support SW				stack_class.1.ada	34	
MSS	Mission Support SW				stack_class.2.ada	93	
MSS	Mission Support SW				time_io.1.ada	8	24
MSS	Mission Support SW				time_io.2.ada	14	144
DMP		Data Mgmt Processing			application_process_id.1.ada	20	
DMP		Data Mgmt Processing			application_process_id.2.ada	4	

Req ID	Level 1 CSC	Level 2 CSC	Level 3 CSC	Level 4 CSC	Unit Source Name	SLOC	Memory Size
DMP		Data Mgmt Processing			memory_access.1.ada	12	
DMP		Data Mgmt Processing			memory_access.2.ada	96	1476
SCH			Scheduler Processing		binary_semaphore.1.ada	19	48
SCH			Scheduler Processing		binary_semaphore.2.ada	38	760
SCH			Scheduler Processing		ccsds_time.1.ada	71	32
SCH			Scheduler Processing		ccsds_time.2.ada	193	2556
SCH			Scheduler Processing		counting_semaphore.1.ada	20	48
SCH			Scheduler Processing		counting_semaphore.2.ada	37	740
SCH			Scheduler Processing		discretes.1.ada	16	
SCH			Scheduler Processing		discretes.2.ada	47	800
SCH			Scheduler Processing		external_interrupts.1.ada	8	24
SCH			Scheduler Processing		external_interrupts.2.ada	50	1032
SCH			Scheduler Processing		hss_sequence_01.2.ada	31	200
SCH			Scheduler Processing		hss_sequence_02.2.ada	27	288
SCH			Scheduler Processing		hss_sequence_03.2.ada	2	
SCH			Scheduler Processing		hss_sequence_04.2.ada	39	476
SCH			Scheduler Processing		mss_status.1.ada	68	320
SCH			Scheduler Processing		mss_status.2.ada	58	2304
SCH			Scheduler Processing		mutual_exclusion_semaphore.1.ada	15	
SCH			Scheduler Processing		mutual_exclusion_semaphore.2.ada	30	412
SCH			Scheduler Processing		onboard_timer.1.ada	11	

<b>Req ID</b>	<b>Level 1 CSC</b>	<b>Level 2 CSC</b>	<b>Level 3 CSC</b>	<b>Level 4 CSC</b>	<b>Unit Source Name</b>	<b>SLOC</b>	<b>Memory Size</b>
SCH			Scheduler Processing		onboard_timer.2.ada	22	380
SCH			Scheduler Processing		p10hz_sequence_01.2.ada	47	404
SCH			Scheduler Processing		p10hz_sequence_02.2.ada	72	628
SCH			Scheduler Processing		p10hz_sequence_03.2.ada	250	1700
SCH			Scheduler Processing		p10hz_sequence_04.2.ada	75	556
SCH			Scheduler Processing		p1hz.2.ada	171	1084
SCH			Scheduler Processing		protected_fifo.1.ada	19	
SCH			Scheduler Processing		protected_fifo.2.ada	35	
SCH			Scheduler Processing		scheduler.1.ada	2	24
SCH			Scheduler Processing		scheduler.2.ada	225	3244
SCH			Scheduler Processing		task_priorities.1.ada	12	
SCH			Scheduler Processing		tlm_status.1.ada	16	32
SCH			Scheduler Processing		vehicle_time.1.ada	24	56
SCH			Scheduler Processing		vehicle_time.2.ada	60	2208
IOP			Input Output Processing		io_directive.1.ada	203	484
IOP			Input Output Processing		io_directive.2.ada	193	15756
IOP			Input Output Processing		io_telemetry.1.ada	12	32
IOP			Input Output Processing		level_discrete_fifo.1.ada	4	2244
IOP			Input Output Processing		packet_identifier.1.ada	25	112
IOP			Input Output Processing		packet_identifier.2.ada	14	200
IOP			Input Output Processing		uplink.1.ada	21	32
IOP			Input Output Processing		uplink.2.ada	165	7584



Req ID	Level 1 CSC	Level 2 CSC	Level 3 CSC	Level 4 CSC	Unit Source Name	SLOC	Memory Size
IOP			Input Output Processing		uplink.display_buffer.2.ada	2	8
IOP			Input Output Processing		uplink_check.1.ada	16	24
IOP			Input Output Processing		uplink_check.2.ada	211	10812
HSS				High Speed Serial	cdhs_protocol.1.ada	21	
HSS				High Speed Serial	cdhs_protocol.2.ada	23	
HSS				High Speed Serial	downlink.1.ada	10	24
HSS				High Speed Serial	downlink.2.ada	54	460
HSS				High Speed Serial	hss_interface.1.ada	18	
HSS				High Speed Serial	hss_interface.2.ada	76	964
HSS				High Speed Serial	hss_interface.check_errors.2.ada	11	320
HSS				High Speed Serial	cdhs.1.ada	98	2016
HSS				High Speed Serial	cdhs.2.ada	121	7260
HSS				High Speed Serial	cdhs_command_type.1.ada	231	448
HSS				High Speed Serial	gps_cdhs.1.ada	42	472
HSS				High Speed Serial	gps_cdhs.2.ada	48	2220
HSS				High Speed Serial	gps_io.1.ada	2	
HSS				High Speed Serial	gps_io.2.ada	449	9280
HSS				High Speed Serial	high_level_discrete.1.ada	34	248
HSS				High Speed Serial	high_level_discrete.2.ada	53	1736
HSS				High Speed Serial	low_level_discrete.1.ada	34	248
HSS				High Speed Serial	low_level_discrete.2.ada	65	1880
BCP				Bus 1553 Protocol	bus1553.1.ada	117	32
BCP				Bus 1553 Protocol	bus1553.2.ada	416	25868
BCP				Bus 1553 Protocol	hw_buffer.1.ada	101	952
BCP				Bus 1553 Protocol	hw_buffer.2.ada	272	14316
BCP				Bus 1553 Protocol	hw_command_type.1.ada	124	256
BCP				Bus 1553 Protocol	hw_telemetry_type.1.ada	212	1708
BCP				Bus 1553 Protocol	ace_buffer.1.ada	76	868
BCP				Bus 1553 Protocol	ace_buffer.2.ada	73	4420
BCP				Bus 1553 Protocol	ace_command_type.1.ada	125	336
BCP				Bus 1553 Protocol	ace_host.1.ada	42	24
BCP				Bus 1553 Protocol	ace_host.2.ada	87	4356
BCP				Bus 1553 Protocol	ace_telemetry_type.1.ada	81	
BCP				Bus 1553 Protocol	ss_buffer.1.ada	83	2024
BCP				Bus 1553 Protocol	ss_buffer.2.ada	181	2580
BCP				Bus 1553 Protocol	ss_command_type.1.ada	97	680
BCP				Bus 1553 Protocol	ss_host.1.ada	72	176

Req ID	Level 1 CSC	Level 2 CSC	Level 3 CSC	Level 4 CSC	Unit Source Name	SLOC	Memory Size
BCP				Bus 1553 Protocol	ss_host.2.ada	267	9264
BCP				Bus 1553 Protocol	ss_telemetry_type.1.ada	183	96
BCP				Bus 1553 Protocol	transponder_buffer.1.ada	81	2104
BCP				Bus 1553 Protocol	transponder_buffer.2.ada	63	1104
BCP				Bus 1553 Protocol	transponder_command_type.1.ada	100	
BCP				Bus 1553 Protocol	transponder_host.1.ada	94	88
BCP				Bus 1553 Protocol	transponder_host.2.ada	430	23724
BCP				Bus 1553 Protocol	transponder_telemetry_type.1.ada	127	
CID				Computer And Interface Diagnostics			
TMP			Telemetry Processing		telemetry.1.ada	36	24
TMP			Telemetry Processing		telemetry.2.ada	503	12692
TMP			Telemetry Processing		commlink.1.ada	4	24
TMP			Telemetry Processing		commlink.2.ada	12	304
PFT				Programmable Format Telemetry	format_table.1.ada	48	24
PFT				Programmable Format Telemetry	format_table.2.ada	89	108388
PFT				Programmable Format Telemetry	monitor_set.1.ada	15	
PFT				Programmable Format Telemetry	monitor_set.2.ada	506	38752
PFT				Programmable Format Telemetry	primary_programmable_telemetry.1.ada	4	2904
PFT				Programmable Format Telemetry	programmable_telemetry.1.ada	13	
PFT				Programmable Format Telemetry	programmable_telemetry.2.ada	65	
PFT				Programmable Format Telemetry	secondary_programmable_telemetry.1.ada	4	3064
MDP				Memory Dump Processing	ccca_memory_dump.1.ada	24	276
MDP				Memory Dump Processing	ccca_memory_dump.2.ada	112	3992
TTE				Record Time Tagged Events	event_log.1.ada	38	
TTE				Record Time Tagged Events	event_log.2.ada	91	

<b>Req ID</b>	<b>Level 1 CSC</b>	<b>Level 2 CSC</b>	<b>Level 3 CSC</b>	<b>Level 4 CSC</b>	<b>Unit Source Name</b>	<b>SLOC</b>	<b>Memory Size</b>
TTE				Record Time Tagged Events	event_supervisor.1.ad	34	
TTE				Record Time Tagged Events	event_supervisor.2.ad	219	
TTE				Record Time Tagged Events	primary_event_supervisor.1.ad	3	7500
TTE				Record Time Tagged Events	secondary_event_supervisor.1.ad	3	7508
TTE				Record Time Tagged Events	system_event_log.1.ad	2	4316
ADB				Application Database Readout	database_dump.1.ad	31	64
ADB				Application Database Readout	database_dump.2.ad	86	6288
TFB				Transfer Frame Builder	fifo_queue.1.ad	32	
TFB				Transfer Frame Builder	fifo_queue.2.ad	32	
TFB				Transfer Frame Builder	frame_header.1.ad	51	128
TFB				Transfer Frame Builder	frame_header.2.ad	17	144
TFB				Transfer Frame Builder	primary_channel.1.ad	3	6324
TFB				Transfer Frame Builder	recorder.1.ad	5	
TFB				Transfer Frame Builder	recorder.2.ad	22	408
TFB				Transfer Frame Builder	regular_packet.1.ad	4	11312
TFB				Transfer Frame Builder	rolling_buffer.1.ad	7	
TFB				Transfer Frame Builder	rolling_buffer.2.ad	40	
TFB				Transfer Frame Builder	secondary_channel.1.ad	3	6396
TFB				Transfer Frame Builder	source_packet_class.1.ad	49	
TFB				Transfer Frame Builder	source_packet_class.2.ad	116	
TFB				Transfer Frame Builder	special_packet.1.ad	4	3656
TFB				Transfer Frame Builder	telemetry_channel.1.ad	12	

<b>Req ID</b>	<b>Level 1 CSC</b>	<b>Level 2 CSC</b>	<b>Level 3 CSC</b>	<b>Level 4 CSC</b>	<b>Unit Source Name</b>	<b>SLOC</b>	<b>Memory Size</b>
TFB				Transfer Frame Builder	telemetry_channel.2.ada	46	
TFB				Transfer Frame Builder	telemetry_data.1.ada	16	
TFB				Transfer Frame Builder	telemetry_data.2.ada	16	52
TFB				Transfer Frame Builder	transfer_frame.1.ada	29	48
CHP			Command Handler Processing		command_class.1.ada	210	1368
CHP			Command Handler Processing		command_class.2.ada	434	11172
CHP			Command Handler Processing		command_dataset_class.1.ada	41	444
CHP			Command Handler Processing		command_dataset_class.2.ada	299	7988
CHP			Command Handler Processing		command_envelope_class.1.ada	32	268
CHP			Command Handler Processing		command_envelope_class.2.ada	23	
CHP			Command Handler Processing		sw_mailbox_class.1.ada	64	104
CHP			Command Handler Processing		sw_mailbox_class.2.ada	182	6600
CHP			Command Handler Processing		telecommand_packet.1.ada	36	176
CHP			Command Handler Processing		telecommand_packet.2.ada	123	6884
RTC				Real Time Commands	rtc_processor.1.ada	16	112
RTC				Real Time Commands	rtc_processor.2.ada	153	3904
SPC				Stored Program Commands	general_spcp_a.1.ada	2	14732
SPC				Stored Program Commands	general_spcp_b.1.ada	2	14732
SPC				Stored Program Commands	general_spcp_c.1.ada	2	14732
SPC				Stored Program Commands	general_spcp_d.1.ada	2	14732
SPC				Stored Program Commands	general_spcp_e.1.ada	2	14732
SPC				Stored Program Commands	general_spcp_f.1.ada	2	14732

<b>Req ID</b>	<b>Level 1 CSC</b>	<b>Level 2 CSC</b>	<b>Level 3 CSC</b>	<b>Level 4 CSC</b>	<b>Unit Source Name</b>	<b>SLOC</b>	<b>Memory Size</b>
SPC				Stored Program Commands	global_variables.1.ada	21	632
SPC				Stored Program Commands	global_variables.2.ada	45	1492
SPC				Stored Program Commands	max_spcs.1.ada	2	
SPC				Stored Program Commands	mission_spcp.1.ada	2	14732
SPC				Stored Program Commands	safemode_spcp_1.1.ada	2	14732
SPC				Stored Program Commands	safemode_spcp_2.1.ada	2	14732
SPC				Stored Program Commands	spc_data_array.1.ada	4	150000
SPC				Stored Program Commands	spc_data_array.2.ada	6	256
SPC				Stored Program Commands	spc_data_index_array.1.ada	6	60000
SPC				Stored Program Commands	spc_data_index_array.2.ada	6	256
SPC				Stored Program Commands	spc_list.1.ada	17	200
SPC				Stored Program Commands	spc_list.2.ada	210	5388
SPC				Stored Program Commands	spc_processor.1.ada	66	
SPC				Stored Program Commands	spc_processor.2.ada	458	
SPC				Stored Program Commands	spc_tag_array.1.ada	14	168
SPC				Stored Program Commands	spc_tag_array.2.ada	47	928
SPC				Stored Program Commands	spc_time_indicator_array.1.ada	6	2504
SPC				Stored Program Commands	spc_time_indicator_array.2.ada	6	256
SPC				Stored Program Commands	spc_time_value_array.1.ada	5	100000
SPC				Stored Program Commands	spc_time_value_array.2.ada	6	256
SPC				Stored Program Commands	vms_spcp.1.ada	2	14732
MBL				Memory Block Loads	cca_memory_load.1.ada	10	80

<b>Req ID</b>	<b>Level 1 CSC</b>	<b>Level 2 CSC</b>	<b>Level 3 CSC</b>	<b>Level 4 CSC</b>	<b>Unit Source Name</b>	<b>SLOC</b>	<b>Memory Size</b>
MBL				Memory Block Loads	ccca_memory_load.2.ada	90	4644
IMP			Initial MSS Processing		initialize_mailboxes.2.ada	194	1048
IMP			Initial MSS Processing		eprom_tables.1.ada	10	
IMP			Initial MSS Processing		fsw.2.ada	9	56
IMP			Initial MSS Processing		initialize_fsw.2.ada	6	56
IMP			Initial MSS Processing		initialize_mss.2.ada	57	976
IMP			Initial MSS Processing		load_spc_tables.2.ada	25	
SRM			Solid State Recorder Management		epoch_block_type.1.ada	184	1724
SRM			Solid State Recorder Management		epoch_host.1.ada	19	64
SRM			Solid State Recorder Management		epoch_host.2.ada	281	7376
SRM			Solid State Recorder Management		srm_dram.1.ada	89	1744
SRM			Solid State Recorder Management		srm_dram.2.ada	417	19004
SRM			Solid State Recorder Management		srm_eprom.1.ada	89	160
SRM			Solid State Recorder Management		srm_eprom.2.ada	640	22652
SRM			Solid State Recorder Management		srm_processing.1.ada	130	176
SRM			Solid State Recorder Management		srm_processing.2.ada	967	22368
SRM			Solid State Recorder Management		ssr_controller.1.ada	25	24
SRM			Solid State Recorder Management		ssr_controller.2.ada	41	476



Req ID	Level 1 CSC	Level 2 CSC	Level 3 CSC	Level 4 CSC	Unit Source Name	SLOC	Memory Size
SRM			Solid State Recorder Management		ssr_management.1.ada	284	680
SRM			Solid State Recorder Management		ssr_management.2.ada	270	4020
VMS			Vehicle Mode Select		vehicle_mode_select.1.ada	18	92
VMS			Vehicle Mode Select		vehicle_mode_select.2.ada	72	2996
MFU			Mathematical Functions		generic_utilities.1.ada	124	24
MFU			Mathematical Functions		generic_utilities.2.ada	162	
MFU			Mathematical Functions		gnc.1.ada	63	160
MFU			Mathematical Functions		gnc.2.ada	97	3264
MFU			Mathematical Functions		leap_utilities.1.ada	280	
MFU			Mathematical Functions		leap_utilities.2.ada	325	152
MFU			Mathematical Functions		utility.1.ada	75	
MFU			Mathematical Functions		utility.2.ada	122	244
MFU			Mathematical Functions		utility_atc.1.ada	69	
MFU			Mathematical Functions		utility_atc.2.ada	404	10416
ATP		Attitude And Translation Control Proc			transfer_1hz_10hz.1.ada	49	4528
ATP		Attitude And Translation Control Proc			transfer_1hz_10hz.2.ada	62	2360
			Actuator And Sensor Processing				
SCP				Spacecraft Sensor Processing	gyro_processing.1.ada	54	232
SCP				Spacecraft Sensor Processing	gyro_processing.2.ada	141	7756

Req ID	Level 1 CSC	Level 2 CSC	Level 3 CSC	Level 4 CSC	Unit Source Name	SLOC	Memory Size
PLP				Payload Sensor Processing	dfs_processing.1.ada	92	408
PLP				Payload Sensor Processing	dfs_processing.2.ada	256	16148
ACC				Actuator Commands	thruster_cmd_gen.1.ada	102	656
ACC				Actuator Commands	thruster_cmd_gen.2.ada	344	22820
Attitude Control Processing							
ACL				Attitude Control Law	att_control.1.ada	78	480
ACL				Attitude Control Law	att_control.2.ada	306	19620
ACG				Attitude Command Generator	cmd_generator.1.ada	134	440
ACG				Attitude Command Generator	cmd_generator.2.ada	562	27416
ASA				Attitude Star Acquisition			
ARC				Attitude Reference And Correction	att_propagation.1.ada	23	88
ARC				Attitude Reference And Correction	att_propagation.2.ada	90	4060
ARC				Attitude Reference And Correction	css_processing.1.ada	75	264
ARC				Attitude Reference And Correction	css_processing.2.ada	286	16456
ARC				Attitude Reference And Correction	mss_processing.1.ada	65	264
ARC				Attitude Reference And Correction	mss_processing.2.ada	146	8908
ARC				Attitude Reference And Correction	sensor_select.1.ada	25	112
ARC				Attitude Reference And Correction	sensor_select.2.ada	148	6708
ARC				Attitude Reference And Correction	squid_processing.1.ada	81	536
ARC				Attitude Reference And Correction	squid_processing.2.ada	461	22360
ARC				Attitude Reference And Correction	st_processing.1.ada	70	128
ARC				Attitude Reference And Correction	st_processing.2.ada	255	13436

Req ID	Level 1 CSC	Level 2 CSC	Level 3 CSC	Level 4 CSC	Unit Source Name	SLOC	Memory Size
ARC				Attitude Reference And Correction	star_proc.1.ada	277	816
ARC				Attitude Reference And Correction	star_proc.2.ada	735	51804
TQC				Torque Calculation	torque_est.1.ada	43	120
TQC				Torque Calculation	torque_est.2.ada	106	6544
OBS				Observer Control Law	observer.1.ada	46	144
OBS				Observer Control Law	observer.2.ada	213	19528
			Translation Control Processing				
TCL				Translation Control Law	trans_control.1.ada	77	896
TCL				Translation Control Law	trans_control.2.ada	232	19608
TCG				Translation Command Generator	trans_cmd_gen.1.ada	21	48
TCG				Translation Command Generator	trans_cmd_gen.2.ada	79	3992
TRF				Translation Reference			
TFC				Total Force Command	force_sum.1.ada	30	96
TFC				Total Force Command	force_sum.2.ada	130	9560
GGF				GG Force Estimate	force_est.1.ada	50	536
GGF				GG Force Estimate	force_est.2.ada	135	12372
THC			Thruster Command Processing		dewar_processing.1.ada	157	112
THC			Thruster Command Processing		dewar_processing.2.ada	611	25964
THC			Thruster Command Processing		mts_distribution.1.ada	43	104
THC			Thruster Command Processing		mts_distribution.2.ada	154	10952
THC			Thruster Command Processing		pseudo_inverse.1.ada	17	56
THC			Thruster Command Processing		pseudo_inverse.2.ada	65	4904
THC			Thruster Command Processing		thruster_curve_fit.1.ada	121	4400
THC			Thruster Command Processing		thruster_curve_fit.2.ada	11461	325348

<b>Req ID</b>	<b>Level 1 CSC</b>	<b>Level 2 CSC</b>	<b>Level 3 CSC</b>	<b>Level 4 CSC</b>	<b>Unit Source Name</b>	<b>SLOC</b>	<b>Memory Size</b>
OTC			Orbit Trim Control Law		orbit_trim.1.ada	42	48
OTC			Orbit Trim Control Law		orbit_trim.2.ada	137	5820
MBP			Mass Balance Processing				
		Ephemeris And GPS Processing					
EMP			Ephemeris Model Processing		common_ephemeris_db.1.ada	14	48
EMP			Ephemeris Model Processing		common_ephemeris_db.2.ada	53	1868
EMP			Ephemeris Model Processing		ephemeris.1.ada	143	448
EMP			Ephemeris Model Processing		ephemeris.2.ada	732	31228
EMP			Ephemeris Model Processing		moon.1.ada	50	40
EMP			Ephemeris Model Processing		moon.2.ada	308	10384
EMP			Ephemeris Model Processing		sun.1.ada	29	48
EMP			Ephemeris Model Processing		sun.2.ada	190	6748
MFP			Magnetic Field Processing		magmodel.1.ada	20	56
MFP			Magnetic Field Processing		magmodel.2.ada	96	5968
OEP			Orbital Event Processing		orbital_events.1.ada	210	368
OEP			Orbital Event Processing		orbital_events.2.ada	643	28728
VAP			Velocity Aberration		velocity_aberration.1.ada	48	248
VAP			Velocity Aberration		velocity_aberration.2.ada	147	8360
TFM			Transformation Matrices		transforms.1.ada	117	824
TFM			Transformation Matrices		transforms.2.ada	432	19840
SMP		Safemode Processing			safemode_check_application.1.ada	32	
SMP		Safemode Processing			safemode_check_application.2.ada	95	

Req ID	Level 1 CSC	Level 2 CSC	Level 3 CSC	Level 4 CSC	Unit Source Name	SLOC	Memory Size
SMP		Safemode Processing			safemode_test.1.ada	21	
SMP		Safemode Processing			safemode_test.2.ada	40	1376
VSM			Vehicle Subsystem Monitoring				
DMM				Data Mgmt System Monitors	ccca_check.1.ada	32	216
DMM				Data Mgmt System Monitors	ccca_check.2.ada	163	5500
DMM				Data Mgmt System Monitors	cdhs_check.1.ada	34	200
DMM				Data Mgmt System Monitors	cdhs_check.2.ada	225	6764
DMM				Data Mgmt System Monitors	check_1553_errors.1.ada	2	
DMM				Data Mgmt System Monitors	check_1553_errors.2.ada	16	296
DMM				Data Mgmt System Monitors	data_input_10hz_check.1.ada	34	264
DMM				Data Mgmt System Monitors	data_input_10hz_check.2.ada	246	7496
DMM				Data Mgmt System Monitors	data_input_1hz_check.1.ada	16	520
DMM				Data Mgmt System Monitors	data_input_1hz_check.2.ada	14	4316
DMM				Data Mgmt System Monitors			
DMM				Data Mgmt System Monitors	error_messages.1.ada	30	256
DMM				Data Mgmt System Monitors	error_messages.2.ada	29	940
DMM				Data Mgmt System Monitors	gps_check.1.ada	33	192
DMM				Data Mgmt System Monitors	gps_check.2.ada	138	4884
DMM				Data Mgmt System Monitors	memory_scrub_interface.1.ada	2	24
DMM				Data Mgmt System Monitors	memory_scrub_interface.2.ada	41	744
DMM				Data Mgmt System Monitors	scrubfns.1.ada	33	
DMM				Data Mgmt System Monitors	uplink_safing_check.1.ada	41	136

<b>Req ID</b>	<b>Level 1 CSC</b>	<b>Level 2 CSC</b>	<b>Level 3 CSC</b>	<b>Level 4 CSC</b>	<b>Unit Source Name</b>	<b>SLOC</b>	<b>Memory Size</b>
DMM				Data Mgmt System Monitors	uplink_safing_check.2.ada	139	4668
EPM				Electrical Power System Monitors	eps_check.1.ada	32	136
EPM				Electrical Power System Monitors	eps_check.2.ada	119	4232
TSM				Thermal System Monitors	temperature_limits_check.1.ada	32	200
TSM				Thermal System Monitors	temperature_limits_check.2.ada	139	5284
ASM				ATC System Monitors	atc_10hz_check.1.ada	68	876
ASM				ATC System Monitors	atc_10hz_check.2.ada	506	16768
ASM				ATC System Monitors	atc_1hz_check.1.ada	42	144
ASM				ATC System Monitors	atc_1hz_check.2.ada	185	6764
ASM				ATC System Monitors	control_gyro_check.1.ada	49	240
ASM				ATC System Monitors	control_gyro_check.2.ada	228	6992
ASM				ATC System Monitors	sun_presence_detect.1.ada	29	168
ASM				ATC System Monitors	sun_presence_detect.2.ada	45	2088
PSM				Payload System Monitors	gyro_spinup_check.1.ada	48	360
PSM				Payload System Monitors	gyro_spinup_check.2.ada	333	12736
PSM				Payload System Monitors	payload_check.1.ada	37	376
PSM				Payload System Monitors	payload_check.2.ada	264	8788
PSM				Payload System Monitors	payload_temp_check.1.ada	42	392
PSM				Payload System Monitors	payload_temp_check.2.ada	351	10308
SRP			Safemode Response Processing		safemode_macros.1.ada	44	184
SRP			Safemode Response Processing		safemode_macros.2.ada	106	3852



Req ID	Level 1 CSC	Level 2 CSC	Level 3 CSC	Level 4 CSC	Unit Source Name	SLOC	Memory Size
SRP			Safemode Response Processing		safemode_response.1.ada	21	24
SRP			Safemode Response Processing		safemode_response.2.ada	149	3828
EPP		EPS Support Processing			eps_processing.1.ada	16	24
EPP		EPS Support Processing			eps_processing.2.ada	60	1768
BSP			Battery Support Processing		battery_processing.1.ada	194	256
BSP			Battery Support Processing		battery_processing.2.ada	927	38824
BSP			Battery Support Processing		charge_control.1.ada	179	520
BSP			Battery Support Processing		charge_control.2.ada	699	29584
TSP		Thermal Support Processing					
		Payload Support Processing					
STP			Snapshot Processing		gss_snapshot.1.ada	3	1072
STP			Snapshot Processing				
STP			Snapshot Processing		snapshot.1.ada	9	
STP			Snapshot Processing		snapshot.2.ada	31	
STP			Snapshot Processing		snapshot_data.1.ada	9	416
STP			Snapshot Processing		sre_snapshot.1.ada	3	1232
STP			Snapshot Processing				
SQP			SQUID Processing		ccca_pit.1.ada	86	112
SQP			SQUID Processing		ccca_pit_command.1.ada	42	96
SQP			SQUID Processing		ccca_pit_command.2.ada	146	3780
SQP			SQUID Processing		payload.1.ada	113	616
SQP			SQUID Processing		payload_host.1.ada	64	384

<b>Req ID</b>	<b>Level 1 CSC</b>	<b>Level 2 CSC</b>	<b>Level 3 CSC</b>	<b>Level 4 CSC</b>	<b>Unit Source Name</b>	<b>SLOC</b>	<b>Memory Size</b>
SQP			SQUID Processing		payload_host.2.ada	195	6564
SQP			SQUID Processing		payload_io.1.ada	44	3360
SQP			SQUID Processing		payload_io.2.ada	86	2112
SQP			SQUID Processing		router_command.1.ada	12	88
SQP			SQUID Processing		router_command.2.ada	41	712
SQP			SQUID Processing		squid.1.ada	128	328
SQP			SQUID Processing		squid_health_checks.1.ada	55	384
SQP			SQUID Processing		squid_health_checks.2.ada	568	14080
SQP			SQUID Processing		squid_init.1.ada	157	268
SQP			SQUID Processing		squid_init.2.ada	1744	54096
SQP			SQUID Processing		squid_offset.1.ada	39	368
SQP			SQUID Processing		squid_offset.2.ada	285	6836
SQP			SQUID Processing		squid_tlm.1.ada	37	1916
SQP			SQUID Processing		sre.1.ada	188	448
SQP			SQUID Processing		sre_host.1.ada	15	88
SQP			SQUID Processing		sre_host.2.ada	113	2768
SQP			SQUID Processing		sre_pit_distributor.1.ada	2	
SQP			SQUID Processing		sre_pit_distributor.2.ada	555	14476
SQP			SQUID Processing		sre_pit_format.1.ada	402	
SQP			SQUID Processing		sre_tlm.1.ada	113	2744
SQP			SQUID Processing		sre_tlm.2.ada	56	1792
SQP			SQUID Processing		tre.1.ada	68	232
SQP			SQUID Processing		tre.2.ada	42	
SQP			SQUID Processing		tre_tlm.1.ada	57	1280
SQP			SQUID Processing		tre_tlm.2.ada	28	48
PSU			Payload Processor Mgmt		interprocessor.1.ada	8	24
PSU			Payload Processor Mgmt		interprocessor.2.ada	35	452
PSU			Payload Processor Mgmt		pp_buffer.1.ada	99	2340
PSU			Payload Processor Mgmt		pp_buffer.2.ada	275	9908
PSU			Payload Processor Mgmt		pp_command_		
type.1.ada	59	304					
PSU			Payload Processor Mgmt		pp_host.1.ada	55	48
PSU			Payload Processor Mgmt		pp_host.2.ada	292	9704

Req ID	Level 1 CSC	Level 2 CSC	Level 3 CSC	Level 4 CSC	Unit Source Name	SLOC	Memory Size
GUP			GSS Processing		gss.1.ada	155	
GUP			GSS Processing		gss_host.1.ada	52	
GUP			GSS Processing		gss_host.2.ada	257	
GUP			GSS Processing		gss_pit.1.ada	43	
GUP			GSS Processing		gss_pit_command.1.ada	20	288
GUP			GSS Processing		gss_pit_command.2.ada	38	932
GUP			GSS Processing		gss_pit_distributor.1.ada	2	24
GUP			GSS Processing		gss_pit_distributor.2.ada	220	6064
GUP			GSS Processing		gss_pit_format.1.ada	203	
GUP			GSS Processing		gss_tlm.1.ada	103	4224
GUP			GSS Processing		gss1_host.1.ada	3	7860
GUP			GSS Processing		gss2_host.1.ada	3	7860
GUP			GSS Processing		gss3_host.1.ada	3	7860
GUP			GSS Processing		gss4_host.1.ada	3	7860
GUP			GSS Processing		roll_angle_data_filter.1.ada	55	1224
GUP			GSS Processing		roll_angle_data_filter.2.ada	117	5452
GUP			GSS Processing		spin_axis_allignment.1.ada	63	
GUP			GSS Processing		spin_axis_allignment.2.ada	275	
EUP			ECU Processing		ecu_command_type.1.ada	133	80
EUP			ECU Processing		ecu_interface.1.ada	204	24
EUP			ECU Processing		ecu_interface.2.ada	1423	58588
EUP			ECU Processing		ecu_io.1.ada	155	2756
EUP			ECU Processing		ecu_io.2.ada	459	19748
EUP			ECU Processing		ecu_pid.1.ada	89	4888
EUP			ECU Processing		ecu_pid.2.ada	677	41856
EUP			ECU Processing		ecu_telemetry_type.1.ada	115	88
OSS	Operating System SW				biccfns.1.ada	51	
OSS	Operating System SW				bus_1553_device_driver_interface.1.ada	209	
OSS	Operating System SW				hssfns.1.ada	21	
OSS	Operating System SW				rscfns.1.ada	55	
OSS	Operating System SW				sysio.1.ada	45	

# F

## Acronyms & Abbreviations

---





<b>Acronym</b>	<b>Definition</b>
A	analysis
A/D	Analog/Digital
A/T	Acceptance Test
Aberr.	Aberration
ABP	Aft Backplane
AC	Alternating Current
Ac	element - Actinium
ACE	Attitude Control Electronics
ACL	Aft Communication Link
ACO	Administrating Contracting Officer
ACS	Aft Clock Support
ACSL	Advance Continuous Simulation Language
ACU	Attitude Control Unit
ACU	Aft Control Unit
Ada	Ada Computer Programming Language
Ada	Computer software language
ADARTS	Ada-based Design Approach for Real Times Systems methodology
ADDA	Analog to Digital & Digital to Analog
ADP	Acceptance Data Package
ADR	Acceptance Data Review
AF	Air Force
AFB	Air Force Base
AFM	Air Force Manual
AFSCN	Air Force Satellite Control Network
AFSC DH	Air Force System Command Design Handbook
AFSD	Air Force Space Systems Division
AGS	GN station in Poker flats, Alaska
AGSU	Advanced Gyro Suspension Unit
Ah	Ampere Hour
AI	Action Items
AIPS	Astrological Image processing system
Al	element - Aluminum
ALRM	Attitude Reference Platform Launch Restraint Mechanism
Am	element - Americium
AMT	Aft Monitor/Timing
ANVO	Accept No Verbal Orders
AOS	Acquisition of Signal

<b>Acronym</b>	<b>Definition</b>
AP	Argument of Perigee
APC	Allocated Prime Cost
APC	Allocated pool charge
APID	Application Process Identification
APM	Aft Power Module
APPRO	Air Force Plant Representative Office
Aq	element - Silver
AR	Acceptance Review
Ar	element - Argon
ARAR	Accident Risk Assessment Report
ARB	Arbiter
ARC	Ames Research Center
ARCSEC	arcsecond
ARO	After Receipt of Order
ARP	Attitude Reference Platform
AS	Active Scheduler Scheduling Operator
AS	Artificial Star
As	element - Arsenic
ASCII	American Standard Code for Information Interchange
ASU	Aft Suspension Unit
AT	Acceptance Test
At	element - Astatine
ATC	Advanced Technology Center formerly RD&D
ATC	Aft Test Card
ATC	Attitude & Translation Control Subsystem
ATCS	Attitude & Translation Control System
ATM	Atmosphere
ATP	Automated Test Procedure
ATP	Automation Grnd. S/W Subsystem
ATP	Acceptance Test Procedure
ATP	ATC Processing
ATP	Authorization To Proceed
ATP	Automated Test Procedure
Au	element - Gold
AUT	Automation Grnd. S/W Subsystem
AVG	Average
AW	In Accordance with
B	element - Boron



<b>Acronym</b>	<b>Definition</b>
B&P	Bid and Proposal
B/Sec	Bits per Second
Ba	element - Barium
BBQ	Bar B Que
BCC	Battery Conditioning Console
BD	Board
Be	element - Beryllium
BER	Bit Error Rate
Bh	element - Bohrium
Bi	element - Bismuth
BIT	Built-In-Test
Bk	element - Berkelium
bldg	building
BOL	Beginning of Life
BOM	Bill of Materials
BPS	Belville Preload System
BPS	Bits Per Second
Br	element - Bromine
BS	Bootstrap Software
BSS	Boot Strap Software CSCI
BSS	Boot Strap Software S/W Subsystem
BTC	Binary Time Code
BUS	Backup Safemode Software
BW	Bandwith
C	Degrees Celsius
C	element - Carbon
C&DH	Command & Data Handling
C&DHS	Command & Data Handling System
C&DHU	Command & Data Handling Unit
C.G.	Center of Gravity
C/A	Corrective Action
CA	California
CA	Corrective Action
Ca	element - Calcium
CAD	Computer-Aided Design
CADAM	Computer-Aided Design and Manufacturing
CAL	Calibration Mission Phase [L+15 months to L+18 months]
CAL	California
Cal.	Calibration

<b>Acronym</b>	<b>Definition</b>
CALC	Calculate
CAM	Computer-Aided Manufacturing
CAM	Cost Account Manager
CAR	Corrective action request
CARD	Constraints and Restrictions Document
CASB	Cost account standard board
CASE	Computer Aided Software Engineering
CBS	CCCA Boot Strap Software S/W Subsystem
CCB	Change Control Board
CCB	LMMS Change Control Board
CCC	Command Control Computer Function Grnd. S/W Subsystem
CCCA	Command/Control Computer Assembly
CCSDS	Consultant Committee for Space Data Systems
CCT	Command & Control Trim Function Grnd. S/W Subsystem
CCW	Counter Clockwise
CD	Center Director
CD	Compact disc
CD	Center Director
CD	Change Directive
CD	Coefficient of Drag
Cd	Cd element - Cadmium
C&DHS	Command and data handling
CDHS	Command and data handling system
CDR	Critical Design Review
CDRL	CDRL Contractor Data Requirements List
Ce	Ce element - Cerium
CEI	Contract End Item
CET	Command Extraction Tools Grnd. S/W Subsystem
Cf	element - Californium
CfA	Harvard-Smithsonian Center for Astrophysics
CFE	Customer Furnished Equipment
CFG	Configuration Grnd. S/W Subsystem
cfm	Cubic Feet per Minute
CFP	Customer Furnished Property
CG	Center of Gravity
CG	Control Gyroscope on ARP

Acronym	Definition
CG	Control Gyros
CGN	Command Generation S/W Subsystem
CI	Continuous Improvement
CI	Configuration Item
CI	Configuration Inspection
CI	Configuration Item
CI	Continuous Improvement
CI	Critical Item
CIEM	Computer Integrated Engineering and Manufacturing
CIL	Critical Items List
CKT	Circuit
CLA	Coupled loads Analysis
Cl	element - Chlorine
CIL	Critical Items List
CM	Center of Mass
CM	Configuration Management
CM	Critical Milestone
Cm	element - Curium
Cmd	Command
CmdGen	Command Generator
CMM	Common Minor Material
CMM	Coordinate Measuring Machine
CMP	Configuration Management Plan
CMX	Commanding Grnd. S/W Subsystem
CNC	Computer Numerical Controlled
CNT	Composite Neck Tube
CR	configuration Register
Co	element - Cobalt
COBE	Cosmic Background Explorer
COM	Commanding Grnd. S/W Subsystem
COM	Computer Output Microfiche
COTS	Commercial-Off-The-Shelf
CPAF	Cost Plus Award Fee
CPI	Cost Performance Index
CPU	Central processing unit
Cr	element - Chromium
cryo.	Cryogenics
Cs	element - Cesium
CSC	Computer Software Component

Acronym	Definition
CSCI	Computer Software Configuration Item
CSE	Chief Systems Engineer
CSS	Coarse Sun Sensor
CSTOL	Colorado Spacecraft Test and Operations Languge
CTE	Coefficient of Thermal Expansion
CTS	Command and Telemetry Software CSCI
CTU	Command & Telemetry Unit
CTV	Compatiblility Test Van
CTV	Command and Telemetry Van
CU	Colorado University
CU	Command Unit
Cu	element - Copper
CW	Clockwise
D-log	Discrepancy Log
DA	Data Analysis
DAC as in SRE DAC	Digital to Analog Converter
DAC	Data Aquisition and Control
DAC	Digital to Analog Converter
DAS	Directory of Approved Suppliers
DAS as in SRE DAS	Digital to Analog Signal
DAS	Data Analysis Subsystem
DAS	Data Aquisiton System
dB	Decibel
Db	element - Dubnium
dB <sub>i</sub>	decibel isotropic Unit of power with respect to isotropic level
dB <sub>ic</sub>	decibel isotropic Unit of power with respect to isotropic level
dB <sub>m</sub>	decibel miliwatt unit of power with respect to one miliwatt
DB	Databas
DBR	Data Base Readout Grnd. S/W Subsystem
DBRO	Databae Readout
DBS	Data Base Grnd. S/W Subsystem
DBS	Database Grnd. S/W Subsystem
DC	Direct Current
DCAA	Defense Contract Audit Agency
DCD	Depth of discharge

<b>Acronym</b>	<b>Definition</b>
DCMA	Defense Contractor Management Agency
DCMC	Defense Contractor Management Command
Dec.	Declination
deg.	Degree
DEL	Deorbit, Entry, and Landing
Del.	Deliver
DEMUX	Demultiplexer
DES	Data Encryption Standard
DFD	Data Flow Diagram
DID	Data Item Description
DIFF	Differential
DIG	Digital Image Generation
Dig.	Digital
DIP	Designated Inspection Point
DIP	Display Input Processor
DIP	Dual Inline Package
DM	Data Management
DM	Disassembly Manual
DM	Docking Mechanism
DMA	Detector Mount Assembly
DMA	Direct Memory Access
DMP	Data Management Processing
DMR	Detailed Mission Requirement
DMS	Data Management System
DOC	Document
DOD	Department of Defense
DOD	Depth of discharge
DOF	Degrees of Freedom
DOT	Department of Transportation
DP	Data Processing
DPA	Detector Package Assembly
DPA	Destructive Physical Analysis
DPM	Deputy Program Manager
DPRO	Defense Plant Representative Office
DR	Discrepancy Report
DR	Data Requirement
DR	Data Resources Inc.
DR	Discrepancy Report
DRAM	Dynamic Random Access Memory

<b>Acronym</b>	<b>Definition</b>
DRD	Data Requirement Description
DRI	Data Resources Inc.
DSM	Data Systems Manager
DSMC	Direct Simulation Monte Carlo
DSN	Deep Space Network
DSP	Digital Signal Processor
DTA	Data Analysis grnd. S/W Subsystem
DTO	Detailed Test Objectives
DTO	Detailed Test Objectives
Dy	element - Dysprosium
E&PO	Education and Public Outreach
ECD	Expected Completion Date
ECEF	Earth Center Earth Fixed
ECI	Earth Center Inertial
ECIF	Earth Center Inertial Fixed
ECO	Engineering Change Order
ECP	Engineering Change Proposal
ECU	Experiment Control Unit
EDAC	Error detection and correction
EDD	Engineering Development Dewar
EDP	Event Data Processing Grnd. S/W Subsystem
EDR	Engineering Data Reduction software
EE	Electrical Engineer
E2E	End to End
EEE	Electrical, Electronic and Electromechanical Parts
EEPROM	Electrically Erasable Programmable Read out Only Memory
EFD	Engineering Flight Dewar
EGP	Ephemeris & GPS Processing S/W Subsystem
EGS	Engineering ground station
EGSE	Electronic Ground Support Equipment
EH&S	Environmental Health & Safety
EIRP	Effective Isotropic Radiated Power
EIRR	External Independent Readiness Review
ELEC	Electrical
ELEX	Electronics
ELV	Expendable Launch Vehicle
EM	Engineering Memo

Acronym	Definition
EM	Electrical Module
EMC	Electromagnetic Compatibility
EMI	Electromagnetic Interference
EMU	Electromagnetic unit
ESD	Electrostatic Discharge
EOL	End of Life
EOL	End Of Line
EOS	Earth Observing System
EOS	Earth Observation Satellite
EOS	Electrical Overstree
EOS	Emergency Oxygen Supply/System
EP	Electrical Power
E&PO	Education and Public Outreach
EPP	EPS Support Processing S/W Subsystem
EPS	Electrical Power Subsystem
Er	element - Erbium
ERR	External Independent Readiness Review
Es	element - Einsteinium
ESD	Electrostatic Discharge
ESD	Estimating System Description
ESD	Electrostatic Discharge
EST	Eastern Standard Time
EST	Estimate
ETE	End-to-End
EU	Engineering Unit Function
Eu	element - Europium
EU	Engineering Unit
EWR	Eastern and Western Range
F	Degrees Fahrenheit
F	element - Fluorine
FA	Failure Analysis
FA	Final Assembly
FA	Assymptotic Spend Speed
FA	Fully Automated
FAB	Forward Aft Bus
FBD	Functional Block Diagram
FBP	Forward Backplane
FC	Flight Computer
FCCM	Facilities capital cost of money
FCI	Final Configuration Item,

Acronym	Definition
FCI	Final Configuration Item
FCI	Functional Configuration Unit
FCL	Forward Communication Link Board
FCSR	Flexible elliptical solar reflector
FD	Flight Director
FDF	Flight Dynamics Facility
FDF	Flight Data File
Fe	element - Iron
FE	Flight Equivalent
FEE	Forward Equipment Enclosure
FEP	Front End Processor
FEP	Front end processor
FEP	Front end processor hardware
FEPI	Front End processor Interface Software
FET	Field Effect Transistor
FEU	Flight Equivalent Unit
FFT	Fast Fourier Transform
FH	Flex Hose
FIG	Figure
FIST	First Integrated System Test
FISTOP	First Integrated System Test Operation
FLL	Flux Locked Loop
FLT	Flight
FM	Frequency modulation
Fm	element - Fermium
FM	Failure Mode
FM	Frequency Modulation
FMECA	Failure modes, effects, and criticality analysis
FMR	Facility modification request
FMR	Forward Mode Register
FMX	Frame Extractor Grnd. S/W Subsystem
Fn	Function
FO	Failed Operation
FO	Fiber Optics
FO	Foreign Object
FOR	Flight Operations Review
FOSR	Flexible optical solar reflector
FP	Flight Prototype Form
FPDLRA	Forward Pricing Direct Labor Rate Agreement

<b>Acronym</b>	<b>Definition</b>
FPGA	Field Programable Gate Arrays
FPRA	Forward Pricing Rate Agreement
FQH	Flight Qualification Hardware
FQT	Formal Qualification Test
Fr	element - Francium
FR	Failure Rate
FRI	Friday
FRM	Forward Regulation Module
FRR	Flight Readiness Review
FSS	Flight Spin Speed
FS	Fail Safe
FS&S	Flight Systems and Servicing
FSU	Forward Suspension Unit
FSW	Flight Software
FT	Flight
FTP	File Transfer Protocol
FT	Full Time
FT	Full-Time Equivalent
ftp	file transfer protocol
FU	Flight Unit
FUT	Fixed Umbilical Tower atSLC-2W
FWD	Forward
G	Gauss
g	Grams
G	gravity constant
G	guide
Ga	element - Gallium
GaAs	Gallium Arsenide
gal.	Gallons
GB	Gigabyte
GBS	GPBPP Boot Strap Software S/W Subsystem
GCM	Ground Control Message at GSFC
GCR	GSE Control Room
GDS	Ground Data System
Ge	element - Germanium
Gen	Generation
GFE	Government Furnished Equipment
GFI	Government furnished Information
Ghe	Gaseous Helium

<b>Acronym</b>	<b>Definition</b>
GHz	Gigahertz
GI	Guide Star Invalid
GIDEP	Government Industry Data Exchange Program
GM	Gas Module
GMA	Gas Management Assembly
GMOCC	GP-B Mission Operations Center
GMT	Greenwich Mean Time same as UTC
GN	Ground network controlled by WFF
Gnd.	Ground
GndRT	Ground Real Time
GOP	Ground Operations Plan
GOWG	Ground Operation Working Group
GP-B	Gravity Probe B
GPBPP	GPB Payload Processor
GPS	Gallons Per Second
GPS	Global Positioning System
GPS-pp	GPB Payload Processor
GREAS	Generic resource, Event, & Activity Scheduler sw for mission planning, part of STK
GRGT	Guam Remote Ground station SN facility
Grms	Root Mean Square Acceleration g's
GRT	Germanium Resistance Thermocouple
GS	Guide Star
GSE	Ground Support Equipment
GSE	Ground Servicing Equipment
GSFC	Goddard Space Flight Center
GSI	Government Source Inspection
GSS	Gyro Suspension System
GSTDN	Goddard Space Flight Tracking and Data Network
GSU	Gyro Suspension Unit
GSV	Guide Star Valid
GSW	GSU / PMSU Support Software
GSW	Ground Software
GSW	GSS Support Software S/W Subsystem
GT	Ground Test
GT	Guard Tank
GTU	Ground Test Unit
GTU	Ground Test Unit

Acronym	Definition
GTU-2	Ground Test Unit #2
GUI	Graphical User Interface
GV	Guidestar Valid
GV	Global Variables
Gyro	Gyroscope
H	element - Hydrogen
HA	Hazard Analysis
HBK	Handbook
HBK	Hartebeesthoek, South Africa - CSNES Ground Station
HDOS	Hughes Danbury Optical Systems, Inc.
HDWE	Hardware
He	Helium
He	element - Helium
HEPL	Hansen Experimental Physics Labs at Stanford
HEX	Heat Exchanger, Hexadecimal
HEX	Heat Exchanger
HEX	Hexadecimal
Hf	element - Hafnium
Hg	element - Mercury
HHS	US Department of Health and Human Services
HIVOS	High-Vacuum Orbital Simulator
HLD	High Level Discrete
HLD	Hold
Ho	element - Holmium
HOL	Higher-Order Language
HPF	Hazardous Processing Facility
HQ	Headquarters
HR	Human Resources
Hr.	Hours
Hs	element - Hassium
HS	Heat Shield
HS	High Speed
HS	Horizon Sensor
HSC	Honeywell Space XComputer
HSIF	Hardware/Software Integration facility
HSS	High Speed Serial
HST	Hubble space Telescope
htr.	Heater

Acronym	Definition
HVA	High Voltage Amp/Bridge
HW	Hardware
Hz	Hertz
I	Electric current
I	element - Iodine
I/F	Interface
I/O	Input / Output
IAC	Inventory account code
IAR	Independent Annual Review
IAW	In Accordance with
ICD	Interface Control Document
ICN	Interfacility Communications Net
ICWG	Interface Control Working Group
ID	Identification
IDA	Image Divider Assembly
IDC	Inter-Departmental Communication
IDD	Interface Design Document
IDR	Internal Design Review
IE	Industrial Engineer
IERS	International Earth Rotation Service
IF	Interface
IIRV	Improved Inter-Range Vector
ILRS	International Laser Ranging Service
In	element - Indium
Ind.	Indicator
Ind.	Inductance
Ind.	Industrial
IOC	Initial Operations Capability
IOC	Indirect Operating Costs
IONet	NASA's IP Operational Network
IPDU	Internet Protocol Data Unit
IPT	Integrated Product Team
Ir	element - Iridium
IR	infrared
IR&D	Independent Research and Development
IRAS	Infrared Astronomy Satellite
IRD	Interface Requirements Document
IRR	Independent Readiness Review
IRS	Interface Requirements Specification



Acronym	Definition
IRU	Inertial Reference Unit
ISA	Instruction Set Architecture
I/O	Input/Output
lonet	lonet IP Operational Network
IT	Integrated Test
I & T	Integration and Testing
ITF	Integrated Test Facility
ITU	International Telecommunications Union
IU	Interface Unit
IV&V	Independent Verification & Validation
IWG	Interface Working Group
J	Joules
JACAC	Joint Audit Administration Committee
JFET	Junction Field Effect Transistor
JPA	Job Package Authorization
JPL	Jet Propulsion Laboratory
k	Notation for 1000
K	Kelvin temperature scale, notation for 1024 = 210
K	element - Potassium
K	Kelvin temperature scale
K	Kelvin
k	Notation for 1000
kbit	kilobits
Kbits	1024 bits
kg	Kilogram
kg-m	Kilogram*Meter
khps	Kilobits per Second
kHz	Kilohertz
KOLH	Potassium Hydroxide
Kr	element - Krypton
L	Launch
L	Left
L	Length
L	Level
L	Liter
L	Low
L	Lumen
La	element - Lanthanum
Lab	Laboratory

Acronym	Definition
LAD	Activate/Deactivate Grnd. S/W Subsystem
LAN	Local Area Network
LASP	Laboratory for Atmosphere and Space Physics
LB	Pounds
lbs.	Pounds
LD	Leak Detector
LDB	Load Builders Grnd. S/W Subsystem
LEAP	Lockheed Environment for Automatic Programming
LEO	Low Earth Orbit
LEU	Lab Engineering Unit
LHe	Liquid helium
LHSD	Liquid Helium Supply Dewars
Li	element - Lithium
LLD	Low Level Discrete
LM	Lockheed Martin
LM	Lockheed Martin
LMMS	Lockheed Martin Missiles & Space
LMTO	Lockheed Martin Technical Operations
LOCC	Launch Operations Control Center
LR	Laser Reflectometer
Lr	element - Lawrencium
LR	Laser Reflectometer
LSB	Launch Services Building
LTD	Lift To Drag
LTD	Limited
Lu	element - Lutetium
LV	Launch Vehicle
LVA	Low Voltage Amplifier
LWR	Long Wave Radiation
μ	Micro
M	Meter
MA	Multiple Access
MB	Mega Byte
M&P	Materials and processes
MGS	Mcmurdo Anartica Ground Station
M/S	Mainstage
M/S	Meters per Second
MA	Multiple Access on TDRSS

<b>Acronym</b>	<b>Definition</b>
MABE	Multiple Access Beamforming Equipment
MAF	Multiple Access Forward
MAR	Multiple Access Return
mas	milliarcseconds
mas	milliarcseconds
MB	Megabyte
Mbps	Mega-Bits per second
Mbps	Mega-Bits Per Second
MBRS	Integrated Product Team
MCB	Make or Buy
Md	element - Mendelevium
MDA	McDonnell Douglas Aerospace
ME	Mechanical Engineer
MECO	Main engine cut-off
MEDA	McIntyre Electronics Design Associates, Inc.
MELV	Medium Expendable Launch Vehicle
MET	Mission Elapsed Time
MeV	Mega Electron-Volts
mfgr.	manufacturing
MFR	Manufacture
mg	Milligrams
Mg	element - Magnesium
mg	Milligrams
Mgmt.	Management
Mgr.	Manager
MGSE	Mechanical Ground Support Equipment
MHF	Medium High Frequency
MHz	Megahertz
MIL	Military, as in military standard
MIL-HDBK	Military Handbook
MIL-STD	Military Standard
min.	minute
MIPS	Millions of Instructions per Second
MIS	Management Information System, used to track cost & schedule
MIWG	Mission Integration Working Group
mK	Millikelvin
Mk	Mark
MLI	Multi-Layer Insulation

<b>Acronym</b>	<b>Definition</b>
mm	Millimeter
MMA	Moving Mechanical Assembly
MMD	Mean Mission Duration
MMD	Mean Mission Duration
MMFD	Multi-Mission Flight Dynamics
Mn	element - Manganese
mNm	Milli Newton Newton-Meter
Mo	element - Molybdenum
MO	Mission Operations
MO&DA	Mission Operations & Data Acquisition
mo.	Month
MOB	Make or Buy
MOBLAS	Mobile Satellite Ranging Station
MO	Mission Operations
MOC	Mission Operation Center
MOCC	Mission Operations Control Center
MO&DA	Mission Operations & Data Acquisition
MOI	Moment of Inertia
MON	Monday
MOP	Mission Operations Plan
MOR	Mission Operations Review
MORR	Mission Operations Readiness Review
MORT	Mission Operations Team
MOSES	Mission Operations, Systems Engineering, and Software
MOSS	Mission Operations Support Software
MP	Mission Planning
MPB	Material Review Board
MPH	miles per hour
MPS	Mission Planning Software
MPT	Mission Planning Terminal at GSFC
MPT	Multiple Use Transporter
MRB	Material Review Board
MRD	Mission Requirements Document
MRO	Memory Readout- A type of data packet from the spacecraft
MRR	Mission Requirements Request
MS	Margin of Safety
MS	Mass Spectrometer
MS	Master Switch
MS	Material Science

<b>Acronym</b>	<b>Definition</b>
MS	Material Specification
MS	Milestone
MS	Military Standard
MS	Mission Specialist
MSB	Most Significant Bit
MSFC	Marshall Space Flight Center
MSM	Miscellaneous fabricating materials
MSP	Miscellaneous small parts
MSPSP	Missile System Prelaunch Safety Package
MSS	Magnetic Sensing System
MSS	Mission Support Software
MST	Mission Timeline Grnd. S/W Subsystem
MT	Main tank
Mt	element - Meitnerium
MT	Main Tank
MTM	Mass Trim Mechanism
MTR	Magnetic Tape Recorder
MTR	Motor
MTS	Magnetic Torquing System
MUA	Material Usage List
MUF	Model Uncertainty Factor
MUF	Model Uncertainty Factor
MUX	Multiplexer
mV	MilliVolt
mw	mw Milliwat
N	element - Nitrogen
N/A	Not Applicable
N/C	No Change
Na	element - Sodium
NARA	National Archives and Records Administration
NASA	National Aeronautics and Space Administration
NASCOM	NASA Communications Network System
NAVCEN	Naval Center
Nb	element - Niobium
NBP	Normal Boiling Point
NBPHe	Normal Boiling Point Helium
NCC	Network Control Center at GSFC
NCR	NonConformance Report

<b>Acronym</b>	<b>Definition</b>
Nd	element - Neodymium
NDI	Non Destructive Inspections
Ne	element - Neon
NEC	National Electrical Code
NEI	NonExplosive Initiator
NEI	NonExplosive Initiator
NFPA	National Fire Prevention Association
NGDC	National Geographic Data Center
NHB	NASA Handbook
Ni	element - Nickel
NiCD	Nickel Cadmium
NIST	National Institute of Standards & Technology
NM	NASA Milestone
nm	nanometer
NM	NASA Manual
NM	NASA Milestone
No	element - Nobelium
No.	Number
NOAA	National Oceanic and Atmospheric Administration
Np	element - Neptunium
NRAO	National Radion Astometric Observatory
NRT	Non-Real-Time
NSPAR	NonStandard Part Approval Request
NSSDC	National Space Sciences Data Center
NVR	Nonvolatile Residue
NSTS	National Space Transportation System
nW	NanoWatt
O	element - Oxygen
OAB	Operations Advisory Board
OASIS	Operations and Science Instrument Support
OASIS-CC	Operations & Science Instrument Support - Command & Control
OBE	Overcome By Events
OD	Orbit Determination
OD	Outer Diameter
OHA	Operational Hazards Analysis
ONR	Office of Naval Research
Ops.	Operations

<b>Acronym</b>	<b>Definition</b>
ORB	Operations Advisory Board
ORI	Operational Readiness Inspections
ORT	Operational Readiness Test
Os	element - Osmium
OS	Operating System
Osc.	Oscillator
OSCF	Operations Support Computing Facility at GSFC
OSHA	Occupational Safety and Health Act/Administration
OSS	Operating System Software
OSS	Operating System Software S/W Subsystem
OTD	Orbital Tracking Data
OTS	Off-The-Shelf
P	element - Phosphorus
P/cm <sup>2</sup>	Protons per Centimeter Squared
P/L	Payload
Pa	Pascal
PA	Product Assurance
Pa	element - Protactinium
Pa	Pascal
PA	Product Assurance
PA	Portable Antenna
PA	Public Affairs
PACO	Principal Administrative Contracting Officer
PAF	Payload Attachment Fitting
PAL	Product Assessment Laboratory
PAL	Product Assessment Laboratory
PAMPL	Program Approved Materials and Process List
PAPMR	Product Assurance Program Management Representative
PAPR	Product Assurance Program Representative
Para.	Paragraph
Parall.	Parallax
Parall.	Parallel
PASR	Product Assurance Supply Representative
Pb	element - Lead

<b>Acronym</b>	<b>Definition</b>
PBOM	Priced Bill of Materials
PC	Personal Computer
pC	PicoCoulomb
PCA	Program Commitment Agreement
PCB	Program Control Board
PCB	Printed Circuit Board
PCB	Product Change/Control Board
PCM	Pulse Coded Modulation
PCO	PCO Procurement Contracting Officer
PD	Proportional Plus Derivative
Pd	element - Palladium
PD	Proportional Plus Derivative
PDC	Program Data Center
PDF	Programmable Data Formatter
PDL	Program Design Language
PDR	Preliminary Design Review
PDT	Product Development Team
PDTL	Product Development Team Leader
PDU	Power Distribution Unit
PHA	Preliminary Hazard Analysis
PHSL	Program Hardware/Software List
PI	Principal Investigator
PID	Program Instruction Document
PIND	Particle Impact Noise Detection
PIND	Payload Integration Plan
PIP	Productivity Improvement Program
PIT	Processor Interface Table
PIT	Product Improvement Team
PK	Peak
PL	Payload
PLF	Payload Fairing
PSLA	Project Service Level Agreement
PM	Program Management
PM	Proof Mass
Pm	element - Promethium
PM	Program Management
PM	Program Manager
PM	Proof Mass
PM	Proton Monitor
PM	Pulse Modulation

Acronym	Definition
PM	Pump Module
PMA	Preliminary Mission Analysis
PMC	Program Management Council
PME	Proof Mass Electronics
PMET	Payload Mission Elapsed Time
PMS	Performance Management System
PMSU	Proof Mass Suspension Unit
PN	Part Number
Po	element - Polonium
PO	Purchase Order
POC	Point Of Contact
POCC	Program Operations Control Center at GSFC
POD	Not an acronym, its a cluster of computers
PODS	Passive Orbital Disconnect Struts
POI	Product of inertia
PPI	Producer price index
PPL	Preferred parts list
PPM	Parts Per Million
PPS	Pulse Per Second
PR	Planning for Radiation
PR	Purchase request
Pr	element - Praseodymium
PR	Planning for Radiation
PRD	Payload Requirements Documentation
Preproc.	Preprocessing
Preps.	Preparations
PROM	Programmable read-only memory
PRR	Preliminary Requirements Review
PRT	Platinum Resistance Thermometer
PSC	Payload Software and Computing
PSCN	Preliminary Specification Change Notice
PSI	Pounds per Square Inch
PSID	Pounds per square inch differential
psig	Pounds per square inch gauge
PSP	Payload Support Processing S/W Subsystem
PSLA	Project Service Level Agreement
Pt	element - Platinum
PT	Pacific Time

Acronym	Definition
PT	Part Time
PT	Part
PT	Point
PTS	Portable Test System
Pu	element - Plutonium
PV WAVE	Product which produces graphical data representations
PWA	Printed Wiring Assembly
PWB	Printed Wiring Board
PWH	Payload Wire Harness
QA	Quality Assurance
QB	Quartz Block
QBA	Quartz Block Assembly
QBS	Quartz Block Support
QE	Quality Engineer
QPSK	Quadri Phase shift keying
QUIKSCAT	Quick Scatterometer, a NASA Earth satellite
R	Radius
R	Range
R	Rankine
R	Ratio
R	Rear
R	Reliability
R	Resistance
R	Right
R	Roll
R&M	Repair and Maintenance
R&R	Remove and Replace
R&R	Rendezvous and Recovery
R/O	Readout
R/O	Rollout
R/T	Real Time
R/T	Receiver/Transmitter
Ra	element - Radium
RAAN	Right Ascension of Ascending Node
rads	Energy absorbed per unit mass 1 rad = 100 ergs/gram
RAM	Random Access Memory
RAM	Responsibility Assignment Matrix
RAV	Remote Actuating Valve

Acronym	Definition
Rb	element - Rubidium
RBD	Reliability Block Diagram
RCTU	Remote Command and Telemetry Unit
RCVR	Receiver
RD&D	Research & Development Division
RDBMS	Relational Data Base Management System
Re	element - Rhenium
RE	Responsible Engineer
Rearth	Radius of the Earth
REE	Responsible Equipment Engineer
Rev.	Review
RF	Radio Frequency
Rf	element - Rutherfordium
rf	radio frequency
RFP	Request For Proposal
RGA	Residual Gas Analyzer
Rh	element - Rhodium
RID	Review Item Disposition
RISE	Reusable Integrated Spacecraft Environment
RLCC	Remote Launch Control Center
RMS	Root Mean Square
Rn	element - Radon
ROM	Rough order of magnitude
RO	Read Only Memory
R/O	Readout
ROSAT	Roentgensatellite
rpm	Revolutions per minute
RR	Readiness Review
RSE	Responsible Software Engineer
RSS	Root Sum Squared
RT	real time
RT	room temperature
RTworks	Expert system and graphical display software
RtHz	root - hertz
RTI	RT SW Initialization Grnd. S/W Subsystem
RTOS	Real-Time Operating System CSCI
RTSA	Real-Time Structured Analysis

Acronym	Definition
RTworks	Real-Time monitoring, display, logging & cntrl sw by Talarian Corp
Ru	element - Ruthenium
S	Seconds
S	element - Sulfur
S	Seconds
S	similarity
SAA	South Atlantic Anomaly
S&MA	Safety & Mission Assurance
S/C	Spacecraft
SN	Space Network (TDRSS)
S/V	Space Vehicle
S/W	Software
SWSI	SN Web Service Interface
SA	Solar array
SAC	Science Advisory Committee
SACE	Sunshade Assembly Control Electronics
SADM	Solar Array Deployment Mechanism
SAE	System Acceptance Review
SAFE	Solar array flight experiment
SAFS	Standard Autonomous File Server
SAO	Smithsonian Astrophysical Observatory
SAR	System Acceptance Review
SARM	Solar Array Release Mechanism
SASN	Solar array switch network
SAT	SAT Saturday
Sb	element - Antimony
SC	Spacecraft, Sapphire Carrier Telescope
Sc	element - Scandium
SC	Sapphire Carrier
SC	Spacecraft
SCB	Software Change Board
SCC	Stress Corrosion Control
SC/PL	Software Payload
scc/s	Helium flow rate in cubic cm per sec at standard temp & pressure
sccHe/s	Helium flow rate in cubic cm per sec at standard temp & pressure
SCCS	Standard Cubic Centimeters Per Second
SCIT	Standard Change Integration and Tracking



<b>Acronym</b>	<b>Definition</b>
SCMO	Spacecraft Mission Operations
SCMT	Subcontract Management Team
SCN	Specification Change Notice
SCPA	Spacecraft Product Assurance
SCPM	Spacecraft Program Management
SCR	Software Change Request
SCSA	Spacecraft Safety
SCSE	Spacecraft Systems Engineering
SD	Silicon Diode
SDB	Small Disadvantaged Business
SDP	Software Development Plan
SDPF	Sensor Data Processing Facility at GSFC
SDR	Software Discrepancy Report
SDRL	Subcontractor Data Requirements List
SDRL	Supplier Data requirements List
SDT	Structural Dynamic Test
SE	Systems Engineering
Se	element - Selenium
SE	Support Equipment
SE	Systems Engineering
SEAKR	Company building solid state recorder Scott Eric Anderson Karen Ray
SEC	Second
SECO	Sustainer Engine Cut Off
SEER	System Evaluation and Estimation Resources
SEI	Support Equipment Installation
SFHe	Superfluid Helium
SEU	Single Event Upset
SFW	Software
SG	Science Gyroscope
Sg	element - Seaborgium
SG	Science Gyroscope
SGI	Silicon Graphics, Inc.
SGS	Stanford Science Ground Station
SHA	subsystem hazard analysis
SHS	Scheduler S/W Subsystem
Si	element - Silicon
SIM	Simulation
SIA	Science Instrument Assembly
SIC	specialized item control

<b>Acronym</b>	<b>Definition</b>
SIN	GPBPP Initialization S/W Subsystem
SINDA	Systems Improve Numerical Differencing Analyzer
SIO	GPBPP I/O Processing S/W Subsystem
SIRTF	Space Infrared Telescope Facility
SLC	Space Launch Complex
SLC-2	Space Launch Complex -2
SLR	Satellite Laser Ranging
SLVR	System Level Verification Review
SLVR	System Level Validation Review
SM	Science Mission
Sm	element - Samarium
SM	Science Mission
SMD	Science Mission Dewar
SMDN	Suspect Material Deficiency Notice
SME	Solar Mesosphere Explorer
SMON	Suspect Material Deficiency Notice
SMP	Software Management Plan
SMP	Safe Mode Processing S/W Subsystem
SMP	Software Management Plan
SMS	Structures and Mechanisms Subsystem
Sn	element - Tin
SN	Science Network
SN	Serial Number
SNOE	Student Nitric Oxide Explorer
SOC	Space Operations Center or Science Operations Cntr
SOPDT	Spacecraft Operations Product Development Team
SOW	Statement of Work
SPARC	SUN computer model type
SPARCS	Solar Pointing Attitude Rocket Control System
SPC	Statistical Process Control
SPC	Stored Program Commands
SPG	SV Parameter Generation Grnd. S/W Subsystem
SPRINT	Telephone Company
SPRU	Standard Power Regulator Unit
SQA	Software Quality Assurance
SQE	Software Quality Engineer

Acronym	Definition
SQS	SQUID Support Processing S/W Subsystem
SQUID	SQUID Superconducting Quantum Interference Device
Sr	element - Strontium
SRAM	Static Random Access Memory
SRB	Software Review Board
SRB	Solid Rocket Booster
SRE	SQUID Readout Electronics
SRI	Stanford Research Institute
SRR	Software Requirements Review
SRS	Software Requirements Specification
SS	Star Sensor
SS	Sun Shade
S/S	Subsystem
SSA	S-band Single Access
SSB	Source Selection Board
SSB	Station Status Block
SSD	Space System Division
SSE	Software Support Environment
SSE	Space Support Equipment
SSHA	Subsystem hazard analysis
SSM	Support systems module
SSP	System Safety Plan
SSR	Solid State Recorder
SSW	SQUID/Science Telescope Software
SSW	SQUID/ST Support Software S/W Subsystem
ST	Science Telescope
ST	Space Telescope
ST	Space Transport
ST	Station
ST	Sun Sensor/Tracker
STA	Station - z axis location on Probe
sta.	station
STAN	Stanford University
STAR	Scientific and Technical Report
STD	Standard, as in military standard
STD	Software Test Description
STDAN	Spaceflight Tracking and Data Acquisition Network

Acronym	Definition
STDN	Spaceflight Tracking and Data Network
STE	Special test equipment
STEP	Satellite Test of the Equivalence Principle
STK	Satellite Tool Kit
STOL	System Test and Operations Language
STP	Standard Temperature and pressure 293 K and 1 atm
STP	Software Test Plan
STP	Standard Temperature and pressure - 293 K and 1 atm
STS	Space Transportation System
STS	Space Transportation System
STS	ST Support Processing S/W Subsystem
STU	Shuttle Test Unit
SU	Stanford University
SUN	Stanford Unix Network
SUN	Stanford Unix Network
SUN	Sunday
SUS	Start-Up Software
SUS	Start Up Software S/W Subsystem
S/V	Space vehicle
SV	Space vehicle spacecraft and payload
SV	solenoid Valve
SV	Sunnyvale
SW	Software
SWAD	Shop work authorizing document
SWAR	Software Acceptance Review
SWCDR	Software Critical Design Review
SWCI	Software Customer Inspection
SWPDR	Software Preliminary Design Review
SWRI	Southwest Research Institute
SWSI	Station Status Block
SWSTR	Software System Test Review
SYBASE	Relational Data Base Management Software
T	Temperature
T	test
T	Time
T	Top
T/V	thermal vacuum

<b>Acronym</b>	<b>Definition</b>
Ta	element - Tantalum
TAG	Technical advisory group
TAO	Thermal Acoustic Oscillation
TAI	International Atomic Time
TAR	Telemetry Anomaly Report
Tb	element - Terbium
TBD	To Be Determined - Stanford will provide input
TBD-U	To Be Determined by Stanford University
TBD PL	To Be Determined - Lockheed Payload will provide input
TBR	To be resolved
TBS	To be Scheduled
Tc	element - Technetium
TCAD	Telemetry Checking, Analysis and Display
TCS	Thermal Control Subsystem
TCS	Temperature/Thermal Control System
TDP	Telemetry Data Processing Software
TDRS	Tracking and Data Relay Satellite
TDRSS	Tracking and Data Relay Satellite System
Te	element - Tellurium
TEL	Telemetry Grnd. S/W Subsystem
TEL	Telescope
TEM	Technical exchange meeting
Temp.	Temperature
TET	Telemetry Extraction Tools Grnd. S/W Subsystem
TFB	Telemetry Format Builder Grnd. S/W Subsystem
Th	element - Thorium
THU	Thursday
Ti	element - Titanium
TIM	Technical interchange meeting
TIV	Thruster Isolation Valve
Tl	element - Thallium
Tm	element - Thulium
TM	Telemetry
TM	Temperature Monitor
TM	Time Management
TM+A	Temperature Monitor and Alarm

<b>Acronym</b>	<b>Definition</b>
TML	Total Mass Loss
TOPEX	Topographical Explorer
TOPS	Terminal on-line pricing system
TQSM	Telemetry Quality and Status Monitoring
TPM	Technical performance measure
TMA	Temperature, moitor and alarm
TML	Total Mass Loss
TPOCC	Transportable Payload Operations Cntrl Center
TRE	Telescope Readout Electronics
TRR	Test Readiness Review
TSP	Thermal Support Processing S/W Subsystem
TSS	Thermal synthesizer system
TT&C	Telemetry, Tracking & Control
TT&C	Telemetry, Tracking & Command/Control
TU	Telemetry unit
TUE	Tuesday
TURFTS	TDRSS User RF Test Set
TV	Thermal Vacuum
TVAC	Thermal Vacuum
U	element - Uranium
U.S.	United States
UAZ	University of Arizona
UN	United Nations
UIS	Umbilical Interface System
UPS	Uninterruptible Power Supply/System
UPS	United Parcel Service
US	United States
USAF	United States Air Force
UT	Universal time
UT	University of Texas
UV	Ultraviolet
V	Electric Volt
V	element - Vanadium
V	Valve
V	Velocity
V	Volts
V&V	Verification & Validation

<b>Acronym</b>	<b>Definition</b>
Vac.	Vacuum
VAFB	Vandenberg Air Force Base
VCM	Volatile Condensable Material
VCO	Voltage-Controlled Oscillator
VCM	Volatile Condensable Material
VCS	Vapor Cooled Shields
VDD	Version Description Document
VES	Vehicle and Environment Simulator
verif.	Verified
VES	Vehicle and Environment Simulator
VIM	Vehicle Information Memo
VLBI	Very Long Baseline Interferometry
VM	Vacuum Module
VRCM	Verificate Request Compliance Matrix
VRIC	Vendor Request for Information or Change
VRSD	Verification Rqmt and Spec Document
W	Electric Watt
W	element - Wolfram
w/	with
WBS	Work Breakdown Structure
WDISC	WSC Data Interface Service Capability
WED	Wednesday
WFF	Wallops Flight Facility
WGS	Wallops Ground Station (Wallops island)
WIP	Work in Progress
WS	Work Station
WSC	White Sands Complex (TDRSS)
WSG	Wallops Scheduling Group (GN)
WSGT	White Sands Ground Terminal
w/o	without
WOTIS	Wallops Orbital Tracking Information System
WR	Western Range
WRR	Western Range Requirement
WSGS	White Sands Ground Station
WTR	Western Test Range
WWW	World Wide Web
Xe	element - Xenon
XPT	Real-Time Expert System Grnd. S/W Subsystem

<b>Acronym</b>	<b>Definition</b>
XTL	Flight SW Extraction Tools Grnd. S/W Subsystem
Y	element - Yttrium
Yb	element - Ytterbium
yr	year
YRS	years
Zn	element - Zinc
ZOE	Zone of Exclusion
Zr	element - Zirconium

